

Prashant M. Pawar · Babruvahan P. Ronge ·
Ranjitsinha R. Gidde · Meenakshi M. Pawar ·
Nitin D. Misal · Anupama S. Budhewar ·
Vrunal V. More · P. Venkata Reddy *Editors*

Techno-societal 2022

Proceedings of the 4th International
Conference on Advanced Technologies
for Societal Applications—Volume 1

Techno-societal 2022

Prashant M. Pawar · Babruvahan P. Ronge ·
Ranjitsinha R. Gidde · Meenakshi M. Pawar ·
Nitin D. Misal · Anupama S. Budhewar ·
Vrunal V. More · P. Venkata Reddy
Editors

Techno-societal 2022

Proceedings of the 4th International
Conference on Advanced Technologies for
Societal Applications—Volume 1

Editors

Prashant M. Pawar
SVERI's College of
Engineering, Pandharpur
Pandharpur, Maharashtra, India

Babruvahan P. Ronge
SVERI's College of
Engineering, Pandharpur
Pandharpur, Maharashtra, India

Ranjitsinha R. Gidde
SVERI's College of
Engineering, Pandharpur
Pandharpur, Maharashtra, India

Meenakshi M. Pawar
SVERI's College of
Engineering, Pandharpur
Pandharpur, Maharashtra, India

Nitin D. Misal
SVERI's College of Engineering
(Polytechnic), Pandharpur
Pandharpur, Maharashtra, India

Anupama S. Budhewar
SVERI's College of
Engineering, Pandharpur
Pandharpur, Maharashtra, India

Vrunal V. More
SVERI's College of Pharmacy, Pandharpur
Pandharpur, Maharashtra, India

P. Venkata Reddy
Amity University
Dubai, United Arab Emirates

ISBN 978-3-031-34643-9

ISBN 978-3-031-34644-6 (eBook)

<https://doi.org/10.1007/978-3-031-34644-6>

© The Editor(s) (if applicable) and The Author(s), under exclusive license to Springer Nature Switzerland AG 2024

This work is subject to copyright. All rights are solely and exclusively licensed by the Publisher, whether the whole or part of the material is concerned, specifically the rights of translation, reprinting, reuse of illustrations, recitation, broadcasting, reproduction on microfilms or in any other physical way, and transmission or information storage and retrieval, electronic adaptation, computer software, or by similar or dissimilar methodology now known or hereafter developed.

The use of general descriptive names, registered names, trademarks, service marks, etc. in this publication does not imply, even in the absence of a specific statement, that such names are exempt from the relevant protective laws and regulations and therefore free for general use.

The publisher, the authors, and the editors are safe to assume that the advice and information in this book are believed to be true and accurate at the date of publication. Neither the publisher nor the authors or the editors give a warranty, expressed or implied, with respect to the material contained herein or for any errors or omissions that may have been made. The publisher remains neutral with regard to jurisdictional claims in published maps and institutional affiliations.

This Springer imprint is published by the registered company Springer Nature Switzerland AG
The registered company address is: Gewerbestrasse 11, 6330 Cham, Switzerland

Preface

The technologies developed without consideration of social needs will not have a major impact on society. The useful societal technologies can only be developed through the interactions of an inspired and intellectual community having the background of science and engineering. The main goal of these interactions should be to develop techno-societal products, processes, and technologies. During these interactions, one may propose the technology for a particular domain or a region, which can be extended to other similar domains as well as regions. On the other hand, some of the theoretical researchers may have essential knowledge and theories, and through these interactions, applications of those technologies can be evolved. The applications developed through such interactions will not only create an impact by solving the societal problems but will also help in making these products sustainable. Some groups working closely for solving societal problems may be in need of technologies which can be identified through such multidisciplinary interactions. SVERI's College of Engineering has initiated these interactions under the series of International Conferences organized in alternate years with the title 'Techno-Societal.' Great response to the proceedings of our First International Conference 'Techno-Societal: 2016' was observed when articles of these proceedings were accessed more than 114,000 times. In the subsequent Second International Conference 'Techno-Societal: 2018,' the combined number of accesses for volume 1 and volume 2, was more than 139,000. In the Third International Conference 'Techno-Societal: 2020,' the accesses have crossed 87,000 till date for both the volumes. The editorial team has decided to publish the proceedings of the Fourth International Conference 'Techno-societal: 2022' in two volumes.

This book is a compendium of selected and best papers presented on December 9 and 10, 2022, during the International Conference 'Techno-societal: 2022' organized by SVERI's College of Engineering, Pandharpur, India. In this Fourth International Conference on Advanced Technologies for Societal Applications, more than 375 full papers of original works and 18 keynote addresses were presented from various areas of technology. The conference has offered various sessions under its name. Selected

208 papers are being published in the two volumes. Volume 1 is classified into the following seven topical areas:

1. Artificial Intelligence and Big Data
2. Commercially Successful Rural and Agricultural Technologies
3. Engineering for Rural Development
4. ICT-Based Societal Applications
5. Manufacturing and Fabrication Processes for Societal Applications
6. Material Science and Composites
7. Sensor, Image and Data-Driven Societal Technologies.

Pandharpur, India

Pandharpur, India

Pandharpur, India

Pandharpur, India

Pandharpur, India

Pandharpur, India

Pandharpur, India

Dubai, United Arab Emirates

Prashant M. Pawar

Babruvahan P. Ronge

Ranjitsinha R. Gidde

Meenakshi M. Pawar

Nitin D. Misal

Anupama S. Budhewar

Vrunal V. More

P. Venkata Reddy

Contents

Artificial Intelligence and Big Data

Health Mitra: Digital Diagnose Suggestion and Disease Prediction Using Machine Learning and Microsoft Azure	3
Vaishali V. Rajmane, Bhushan Deshmukh, Shubham Sakhare, Chinmay Halsikar, Pranoj Gonjari, and Shreyas Patil	
Cloud Based Intelligent Recommendation System for Company, Product and Service Selection	11
Amol C. Adamuthe, Amarjeet Kambale, and Vrushabh Kupwade	
Application of Artificial Intelligence and IoT to Membrane Bioreactor (MBR) and Sewage Treatment Plant	21
Manoj Wagh, Dnyaneshwar Vasant Wadkar, and Prakash Nangare	
Comparative Study of Machine Learning Techniques for Stock Market Price and Optimizing Its Cumulative Strategy Returns	29
Digambar Uphade and Aniket Muley	
Crop Leaf Disease Detection in Soybean Crop Using Deep Learning Technique	39
Vipul V. Bag, Mithun B. Patil, Shubham Shelke, Nagesh Birajdar, Aashutosh Sonkawade, and Rohit Rathod	
Severity Detection of COVID-19 Patient's Using Machine Learning Techniques	49
Digambar Uphade and Aniket Muley	
Fashion Classification Model	59
Sanika Rawate, Kuldeep Vayadande, Shivam Chaudhary, Sakshi Manmode, Resham Suryavanshi, and Kunal Chanda	

Implementation of Environmental Parameters Monitoring and Alert System for Underground Mining Using Internet of Things with LoRa Technology	69
Sandi Kumar Reddy, Anil S. Naik, and Mandela Govinda Raj	
Application of Artificial Intelligence in Geotechnical Engineering: A Review	77
Jitendra Khatti and Kamaldeep Singh Grover	
Commercially Successful Rural and Agricultural Technologies	
A Study of Role of It in Rural Development in India: Opportunities and Challenges	89
Pravin Pundlik Rajguru	
Development and Design of Min-T8 HP Power Weeder Back Rotor	97
Sumit R. Pawar and Mukund S. Kale	
Savonius Vertical Axis Wind Turbine for Effective Generation of Power—A Review	105
Vishal Patil, D. G. Kumbhar, and Kailasnath Sutar	
Hybrid Feature Extraction Method for Efficient Leaf Disease Detection and Grading	117
Rajendra Kanphade, Smita Desai, Rupali Deshmukh, and Smita Modi	
Development of an Innovative Ultrasound-Assisted Extraction Technique to Optimize Extraction on Phytoconstituents and Compared Conventional Extraction Method	127
Shankaraiah Pulipaka, Ashish Suttee, M. Ravi Kumar, Kalakotla Shanker, Ramesh Kasarla, and Swamy Kasarla	
Seasonal Impact Analysis Using Clay Pot Refrigerator on the Shelf Life of Tomatoes	135
Nishigandha Patel, V. K. Bhojwani, and Sachin Pawar	
Engineering for Rural Development	
Continuous 24*7 Water Supply System: A Review of Literature	147
Nitin P. Sonaje, Mukund M. Pawar, and Nitin D. More	
Performance of RCC Multistory Framed Structure in Different Geometric Shapes	155
Priyanka V. Padavale, Mukund M. Pawar, Mangesh S. Survase, Revnnath J. Salunke, Amruta L. Lugade, and Suraj R. Pawar	
A Study on Transfigure of Rural Agro Based Businesses Subsequent to COVID	165
Uday V. Hiremath and K. Shivashankar	

Analysis of Compressive Strength of Concrete Cubes Made from Different Sources of Water	173
Anil Shirgire, Nitin Shinde, Hemchandra Pawar, Satyawani Jagdale, and Ravikant Sathe	
By Using Ansys, Conduct a Free Vibration Analysis of a Cantilever Beam for Several Materials with Different Cross Sections	181
Prashant Mali and Swanand Kulkarni	
Optimization of Takali Zone in 24 × 7 Water Supply Network of Pandharpur City	189
Mukund Pawar and N. P. Sonaje	
Sustainable Development of Blended Cement by Using Colloidal Nano Alumina	197
Anirudh Harishchandra Shirke and Manish Patkar	
Anaerobic Digestion: Addressing the Problem of Food Waste by Converting it into Biogas	205
Chetan Patil and Kailasnath Sutar	
Survey on Trends in LPG Utilization Among Selected Rural Households in Western Maharashtra, India	217
Swapnil S. Shinde, Kailasnath B. Sutar, Dnyaneshwar G. Kumbhar, and Sandipraj Y. Salunkhe	
IOT-Based Monitoring and Control System for Greenhouses	225
Ranjana Khandebharad, Shraddha Garad, Ashutosh Garad, Shreya Moholkar, and Dhanraj Daphale	
Agri Tourism—A Means for Doubling Farmer’s Income—A Literature Review	233
Pratibha Galande and Abhijit Mancharkar	
Transfer Learning Using Convolutional Neural Network to Classify Leaf Diseases on Ridge Gourd Plant	241
Rohan U. Katare, Akash A. Mahajan, and Amol C. Adamuthe	
Optimal Sizing and Location of Distributed Generators in Distribution System for Loss Reduction	251
Nishant Thakkar, Khushali Bilare, Mukund Ghole, and Priyanka Paliwal	
Sustainable Development Assessment of South Asian Countries Using Fuzzy Logic	261
Abhishek Tripathi, Shafaque Shaikh, Elton Noronha, Sagar Kote, Pratibha Dumane, and Satishkumar Chavan	

Blockchain Based Supply Chain System: A Case Study of Agriculture	271
Pranav N. Shinde, Apoorvamegh A. Chechar, and Amol C. Adamuthe	
ICT-Based Societal Technologies	
Data Sharing and Privacy Preserving Access Policy of Cloud Computing Using Security	281
Dhanashri Kamble, Rajni Patel, and Prajakta Deshmukh	
Applications of Machine Learning in Automotive Verification and Validation: A Review	291
Shakti Chavan	
Teaching English Language in Rural Indian Classrooms: A Techno-Societal Approach	305
Santosh Pundalik Rajguru	
On Use of Various Leadership Styles for Implementation of Management Information System	313
Anil N. Barbole and Suraj B. Ronge	
Evaluating Students Mobile Gaming Approach Using Data Mining Technique	319
Aniket Muley and Sagar Joshi	
Amalgamation of Internet of Things (IoT) and Web Services for Advancement in the Tele-Medicine	329
Rajni Patel and Amarjit P. Kene	
Heart Disease Prediction Using Machine Learning Techniques: A Survey for Societal Care and Information	337
Kuldeep Vayadande, Arnav Dhiwar, Darpan Khadke, Rohan Golawar, Sarwesh Khairnar, Sarthak Wakchoure, and Sumeet Bhoite	
Stock Market Prediction Using Machine Learning	349
Reshma Patil and Swati P. Pawar	
Using RStudio to Analyze Big Data	361
Mohua Biswas, Papiya Biswas Datta, Tejas S. Joshi, and Suvarna D. Pujari	
Face Recognition Based Video Conferencing Add-On for Online Session Log Using Convolutional Neural Networks	371
Manish Jadhav, Ashwathy Marath, Rohan Jamuar, Kaustubh Sawant, and Satishkumar L. Varma	

The Influence of the Demography of Institutes on MIS-Based OBE Implementation 381
 Anil N. Barbole and Suraj B. Ronge

Optimization of Estimated Routing Paths in IoT Agriculture Applications 391
 Shreekant Salotagi and Jayashree D. Mallapur

Transformation of Project Management Process: An Influence of Industry 4.0 403
 Vijay Anant Athavale and Samprit Tanuj Patel

ICT Enabled Teaching for Transforming Rural Classrooms: A Reference to English Language and Teaching (ELT) for Betterment of Students from Rural Background 413
 Karan Babaso Patil and A. B. Nadaf

Manufacturing and Fabrication Processes for Societal Applications

Influence of Obstacles on the Mixing Performance of Serpentine Microchannels 425
 Kailas Malgonde, Babruvahan P. Ronge, and Sandeep S. Wangikar

Optimization of Finite Element Analysis and Natural Frequency for Engine Bracket 435
 Abhinav Shelar and Atul Aradhye

Multifunctional Solar Operated Agricultural Machine 445
 Vikram R. Chavan, Chetan C. Jadhav, Digambar T. Kashid, Avinash A. Mote, and Manoj A. Deshmukh

NACA 4415 Aerofoil: Numerical Analysis for Performance in Drag and Lift 461
 Digambar T. Kashid, Avinash K. Parkhe, Sachin M. Kale, Sandeep S. Wangikar, Chetan C. Jadhav, and Hrushikesh N. Paricharak

Prediction of Optimum Tool Life and Cutting Parameters by Comparative Study of Minimum Cost Criterion and Maximum Production Rate Criterion 475
 Amarjit P. Kene, Amitkumar A. Shinde, Pravin A. Dhawale, Ranjitsinha R. Gidde, Sandeep S. Wangikar, and Kuldip S. Pukale

Design and Fabrication of Hybrid Solar Dryer 489
 S. S. Gaikwad, Digambar T. Kashid, S. B. Bhosale, A. A. Mote, S. M. Shinde, and M. N. Gund

Design and Analysis of Compliant Macro Scale Gripper 495
 Jambhale Pooja and Deshmukh Bhagyesh

Designing and Optimization of Mechanical Gripper Finger Using Finite Element Analysis	505
Rohit Jadhav and Yogesh G. Kamble	
Mechanical Investigation of Naval Alloy in Spinodal Decomposition	513
S. C. Jirapure and A. B. Borade	
Filament Fabrication for 3D Printing Using Waste PET Material	521
Akshay R. Shah, Eshwar Paygude, Rohit Sonawne, Pradeep V. Jadhav, and Sachin M. Khomane	
Inventory Management for Power Tiller Using TOC Technique	531
Shubhankar R. Narwade and Mukund S. Kale	
Mathematical Modeling, Analysis and Simulation of MR Fluid Damper	539
Hanmant Salunkhe, Surendra Thikane, and Shivaji Sadale	
Improvement of Mechanical Properties of Banana Fiber Reinforced Composites	551
Swapnil Sawant, Aatish Chavan, Prashant Patil, and Sukhdev Waghmode	
Experimental Investigation and Micro Structural Variation in Friction Drilling on AISI 1015 Low Carbon Steel, AISI 1008 Aluminium and Copper by Using Tungsten Carbide Tool	561
Vinayak W. Bembrekar and Rahul N. Yerrawar	
Exploration into Tribological Behaviour of Graphite Reinforced Corn Cob Ash Epoxy Composites Utilizing Taguchi Approach	575
Pranav V. Swami and Vijaykumar B. Raka	
A Comparative Study of Nano—MQL and MQL on Chip Morphology and Shear Angle Under High Speed Turning of Inconel 718: For a Sustainable Machining	585
Pravin Mane, Anupama Kallol, Pravin Dhavale, and Avinash Khadtare	
Overview of Mechanics of Porous Dental Implants	599
Vasuudhaa Sonawane and Ratnakar R. Ghorpade	
Stress Concentration Studies for Crack Propagation Analysis of Spur Gear Using ABAQUS	609
Chetan C. Jadhav, Avinash K. Parkhe, Sachin M. Kale, Sandeep S. Wangikar, Digambar T. Kashid, and Vikram R. Chavan	
Development of Data Fusion Framework for Data-Driven Digital Twin in the Milling Process	621
A. D. Khandare, V. S. Jadhav, S. P. Deshmukh, and K. K. Rane	

Optimization While EDM of 304-H Stainless Steel by Super Ranking Concept 629
 S. A. Sonawane and B. P. Ronge

A Study on Simulation and Experimental Analysis of Gating System 637
 Avinash A. Mote, Sandeep S. Wangikar, Vikram R. Chavan, and Manoj A. Deshmukh

Fatigue Strength Evaluation During EDM Machining of Titanium Alloy 647
 Mahendra Uttam Gaikwad, Nitin Ambhore, and Shital S. Bhosale

Study of Structural Behavior of Beam with Middle 1/3rd Portion Replaced with Crushed Brick Aggregate 655
 S. A. Gosavi and Vishwajeet Surshetwar

Design and Optimization of Prosthetic Arm (Prototype Model) 663
 Devanshi Akshay Jhaveri, R. S. Motgi, S. K. Mohite, and N. P. Patil

Optimization of Ultrasonic Assisted Electro-discharge Machining Process Parameters Through Surface Response 671
 Atish Mane and Pradeep V. Jadhav

Robotic Joint Torque Sensors: A Review 679
 Shrikant C. Mahadik, Vikas R. Deulgaonkar, and Sachin M. Bhosle

Mathematical Modelling of Material Removal in Laser Assisted Electro-chemical Machining Process (LAECM) 685
 Amitkumar A. Shinde, Amarjit P. Kene, Kashfull Orra, and Karan B. Patil

Design and Development of a Metal Jet Print-Head 697
 Gurudev N. Mhetre, Vijay S. Jadhav, and Suhas P. Deshmukh

Innovative Design and Analysis of Plough for Vineyards 707
 Pratik Katkade, Nikhil Joshi, and Puskaraj D Sonawwanay

Experimental Investigation of Ball Bearing for Vibration Analysis 719
 Sunil Pondkule, Sachin Bhosle, and Pravin Dhandore

Material Science and Composites

A Study on Mechanical Properties and Tribological Behaviour of Jute Filler Composites 731
 Vijay Kumar Mahakur, Rajdeep Paul, Santosh Kumar, Promod Kumar Patowari, and Sumit Bhowmik

A Review on Epoxy Polymer Matrix Composite, Its Mechanical and Thermal Properties	741
Basavraj R. Birajdar and R. T. Vyavahare	
A Study on Mechanical Properties of Stainless Steel Welded Joints for Marine Applications	753
Kiran Lakkam, Chetankumar Jadhav, Sangamesh K. Sajjan, Ratan Patil, Anilkumar Shirahatti, and S. M. Kerur	
Formulation and Viscosity Evaluation of Copper Oxide Based Nanolubricants	763
Abhijeet G. Chavan and Y. P. Reddy	
Thermal Management of Electric Power Unit Using Phase Change Cooling Materials: Review, Classification, and Comparison	771
Roshan Mathew and Sateesh Patil	
Polyaniline Nanofibers Based Freestanding Electrode with High Electrochemical Performance for Supercapacitors	779
A. C. Molane, S. S. Gavande, A. S. Salunkhe, R. N. Dhanawade, R. N. Mulik, and V. B. Patil	
Dynamic Analysis of Rotating Composite Beam and Their Numerical Analysis Using COMSOL	787
Avinash K. Parkhe, Prashant M. Pawar, Sandeep S. Wangikar, Digambar T. Kashid, and Pradnya K. Patil	
Study of Mechanical Properties and Water Absorption Behavior of TiO₂ Nanofiller-Enhanced Glass Fiber-Reinforced Polymer Composites: A Review	799
Sandeep Kumar Singh and Thingujam Jackson Singh	
Strengthening and Retrofitting of Reinforced Concrete Beam by Using Composite Materials	811
Priyanka S. Mirajkar, P. M. Pawar, and Sonali P. Patil	
A Study on Effect of Severe Plastic Deformation Process on Hardness of Aluminum Alloys	823
Mansi Chavan, Mayuri Abhangrao, Kiran Lakkam, and Sandeep Wangikar	
Effect of Extrusion Process on Mechanical Properties of Al-MWCNT Composites Synthesized by Powder Metallurgy Route	829
Vijaykumar S. Jatti, Nitin K. Khedkar, Vinaykumar S. Jatti, Ashwini V. Jatti, and Ajay S. Athare	

Effect of Section Thickness on Solidification and Microstructure of Ductile Cast Iron 837
 Bahubali B. Sangame and Y. Prasannatha Reddy

Analysis of Progressive Collapse of Moment Resisting Steel Frames for Failure Performance Improvement 845
 Nishigandha Mahamuni, S. A. Gosavi, C. R. Abhangrao, S. P. Patil, and G. K. Koshti

Comparative Study of Seismic Analysis and Design of Different Types of Bridge Abutments 853
 Santosh K. Kumbar, Jyoti P. Bhusari, Anil Panjwani, and M. V. Bhogone

Different Approaches for Optimising the Micro-machining Quality Parameters of Composite Materials Using Electrochemical Discharge Machining (ECDM) for Societal Application—A Review 865
 Nikhil P. Ambole, Vijay K. Kurkute, and Mukund L. Harugade

Numerical Simulation of Reinforced Granular Blanket over Granular Pile Under Vertical Loading 877
 Himanshu Gupta, Jitendra Kumar Sharma, and Ravikant S. Sathe

Application of Modern Waste Materials for Stabilizing the Cohesive Soil 889
 Amit Kumar Jangid and Kamaldeep Singh Grover

Sensor, Image and Data-Driven Societal Technologies

Face Sketch to Image Generation and Verification Using Adversarial and Discrimination Network 901
 Mokshada S. Bhandare and Anup S. Vibhute

Touchless Fingerprint Recognition System 911
 Sujit A. Inamdar, Mahesh M. Zade, and Snehal Y. Abhangrao

Reducing Clock Power by Using the Clock Gating Technique 919
 Garad Ashutosh, Musale Jivan, Garad Shraddha, and Pawar Rahul

Generation of Isometric Projections in MATLAB 927
 Janhavi Saklecha, Swanand Pachpore, and Omkar Kulkarni

Non-intrusive Torque Measurement System 937
 Amruta V. Adwant, Suhas Dehmukh, and Vijay Kumar Singh

Development and Implementation of a Smart Agriculture System Based on LORA 951
 Manoj A. Deshmukh, Seema A. Atole, Avinash A. Mote, and Vikram R. Chavan

Fruit Weight Measurement and Categorization Using Convolution Neural Network 961
Amol Chounde, Anuja Lotake, and Satish Lendave

IOT-Based Waste Management for Smart Cities 971
Nirmala T. Pujari, Shital S. Pawar, and Vrushali V. Gore

Design of Narrow Band Pass Filter Using Open Loop Circular Resonator 979
Akhilesh Kumar Pandey, Meenakshi M. Pawar, and Mohammad Mushaib

Review of Obstacle Detection by Ultrasonic and Laser Sensor for Automated Guided Vehicles 985
Mahesh G. Sonawane and Nishigandha S. Patel

Establishing a Relationship Between Soil Erodibility and NDVI in the Urmodi River Watershed of Maharashtra Using GIS 993
Wasim Ayub Bagwan

Self-biased Cascade Current Mirror with Wide Range Level Shifter 1003
Tejas S. Joshi, Mohua Biswas, Smita Gawade, and Rahul B. Pawar

Free Vibration Analysis of Functionally Graded Skew Sandwiched Plates by Using a New Discrete Kirchhoff Quadrilateral Element 1013
G. A. Deshpande and R. S. Parekar

Wideband MIMO Antenna Design for Ku Band Application 1025
Aditi Bhardwaj, Mohammad Mushaib, Mohd. Gulman Siddiqui, and Poonam Tiwari

Electronic Shoe to Assist Visually Challenged People 1033
Salma S. Shahpur, Mahanthgouda Patil, Vikas Bandi, Kiran Patil, and Gopal Lamani

A Review of 6G Technologies and Its Advantages Over 5G Technology 1043
Suhas Khadake, Sagar Kawade, Shreya Moholkar, and Madhuri Pawar

Monitoring and Controlling of Field Pond Parameters Using an IOT 1053
Smita Gawade, Seema Atole, Snehal Marab, and Tejas Joshi

Development of Smart Strips in the House for Safety Monitoring	1061
Devyani Kadgaye, Rahul Chaudhari, and Manish Narkhede	
New Approaches for a Reconfigurable Microstrip Patch Antenna Using Inverse Artificial Neural Networks	1071
Mohammad Mushaib, Meenakshi Mukund Pawar, Akhilesh Kumar Pandey, and Mohd Gulman Siddiqui	

Artificial Intelligence and Big Data

Health Mitra: Digital Diagnose Suggestion and Disease Prediction Using Machine Learning and Microsoft Azure



Vaishali V. Rajmane, Bhushan Deshmukh, Shubham Sakhare,
Chinmay Halsikar, Pranoj Gonjari, and Shreyas Patil

Abstract Innovation has modified the wellbeing field generally in this period of IT. The objective of this exploration is to make a determination model for various illnesses in light of their clinical data. To make such a model, this framework system uses Random forest. The savvy specialist is prepared utilizing datasets containing abundant information in regards to patient sicknesses that have been accumulated, refined, ordered, and used. In the wake of arranging the dataset into preparing and testing we constructed a model utilizing a random forest classifier. Model can predict disease in view of clinical data of the patient. The patient could then contact the specialist for additional treatment in view of the outcomes by utilizing AI Chatbot.

Keywords Random forest classifier [3] · Medical data · Classification · Data mining · Microsoft azure · Microsoft cognitive service · Knowledge base · AI Bot

1 Introduction

Even in the age of the internet and machine learning, we still treat diseases in the same manner. We develop a complete Machine Learning based healthcare system called Health Mitra as our response. It is a web application with a fantastic user-friendly GUI that was created with the aid of streamlet, an open source Python app framework, and a core concept that utilizes Microsoft Azure and machine learning. The suggested methodology here offers a better and more efficient substitute for randomly Googling a diagnosis and more correctly predicting disease than the traditional method. By only enrolling on a network, one may diagnose himself, receive the diagnosis, and find physicians' contact information. Using machine learning algorithms, HealthMitra is able to forecast and assist in the diagnosis of several diseases. A method for improving disease prediction accuracy can be created with the development of machine learning.

V. V. Rajmane (✉) · B. Deshmukh · S. Sakhare · C. Halsikar · P. Gonjari · S. Patil
SVERI's College of Engineering, Pandharpur 413304, India
e-mail: vaishuavi1992@gmail.com

Using existing medical information and Random forest. The patient can get in touch with the closest or dearest disease specialist with the aid of an AI Chatbot [4] for any additional therapies. This method enables free disease prediction and doctor consultation.

2 Motivation

- Our innovation takes inspiration from ancient Indian civilization; We are living in a country where the medical field is far ahead at that time.
- Need of the user is an accurate diagnosis for a disease, cheaper cost, and ease of availability so as per the user requirement.
- Our innovation strictly follows the principle—high accuracy and cheap medical facility for everyone and also it can easily be accessible to everyone at no cost.
- With the help of this innovation we can make some positive changes in the medical field.

3 Methodology

The diseases are expected naturally in the system utilizing a model, which has been prepared on a clinical dataset. This method additionally shows the prediction's score. Following the conclusion of the expected disease, the system suggests experts who spend significant time in that disease, permitting the patient to talk with them on the web (Figs. 1 and 2).

When clients visit this application, they can register as a patient. after the user has successfully registered on the network. They can login in this application as a patient (Figs. 3 and 4).

After login as patient

- (A) On profile page users can see their ID, name, and email. They can also edit their information.
- (B) There are three choices to predict the disease and consultation from AI Bot.
- (C) At the point when they click on predict disease they will get a choice to multiple disease from the sidebar (Fig. 5).
- (D) Depending upon the medical information of the patient, the model will predict the disease with high accuracy (Fig. 6).
- (E) This application gives a connection that will guide the patient for better understanding of the predicted disease (Fig. 7).
- (F) Furthermore, the main element of the proposed model is that alongside the visualization the framework offers the chance to associate with the specialist representing considerable authority in that specific field to the client who is enrolled in the organization alongside their contact subtleties.

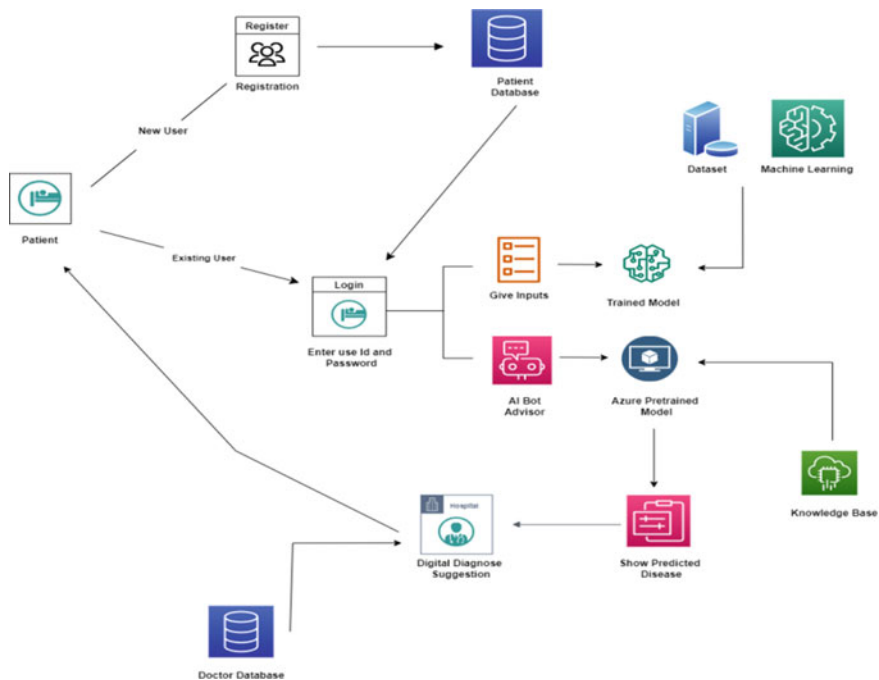


Fig. 1 Flow diagram

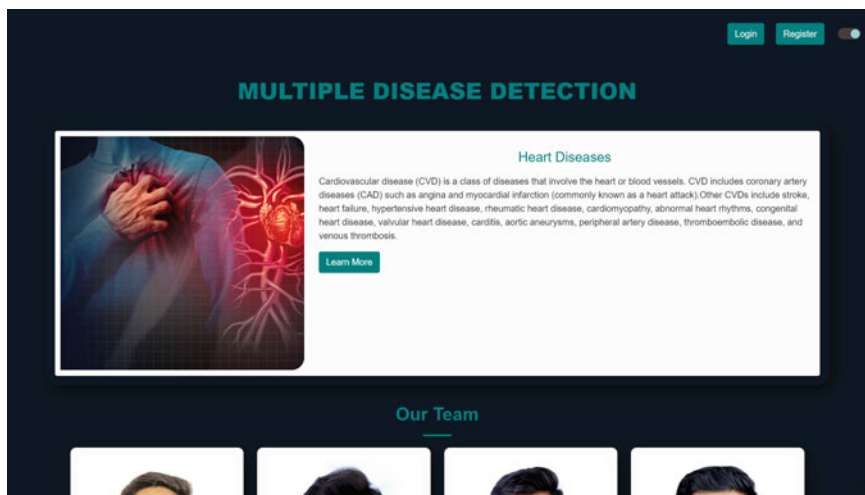


Fig. 2 Home page [1]

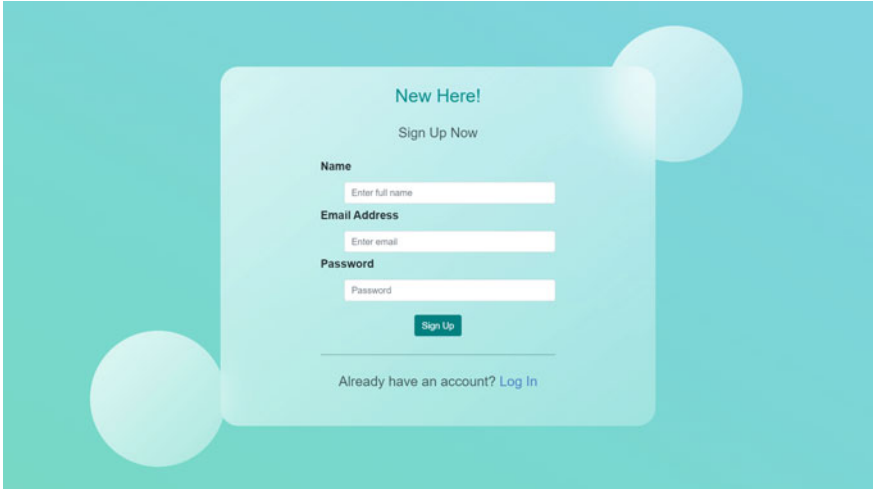


Fig. 3 Registration page [1]

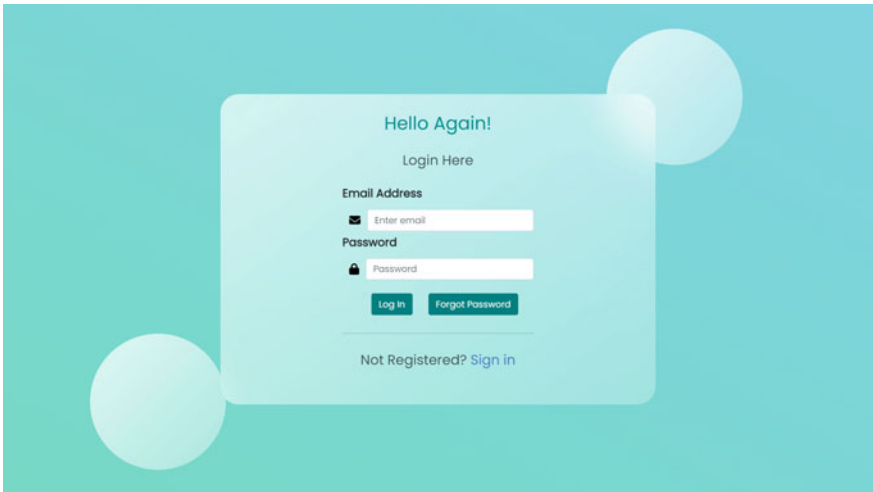


Fig. 4 Login page [1]

- (G) Patients can get to a rundown of specialists who have practical experience in their field with assistance of Azure [6] cognitive service based intelligence Chatbot, simulated intelligence Chatbot will assist patients to get specialist data with geographic area (Fig. 8).
- (H) User can contact us 24×7 for any kind of query (Fig. 9).

The screenshot shows a web application interface for a "Multiple Disease Prediction System". On the left is a sidebar with navigation options: "Diabetes Prediction" (highlighted in red), "Heart Disease Prediction", "Parkinsons Prediction", "Breast Cancer Prediction", and "Logout". The main content area is titled "Diabetes Prediction" and contains several input fields for user data: "Number of Pregnancies", "Glucose Level", "Blood Pressure", "Skin Thickness", "Insulin Level", "BMI", "Diabetes Prediction Function", and "Age". Below these fields is a "Diabetes Test Result" button. The interface is dark-themed with light-colored text and input boxes.

Fig. 5 Sidebar option [1]

This screenshot shows the same "Diabetes Prediction" interface as Figure 5, but with numerical values entered into the input fields. The "Diabetes Test Result" button is highlighted in red, and a green message box below it displays the result: "The person is Diabetic." The input values are: Number of Pregnancies: 1, Glucose Level: 148, Blood Pressure: 72, Skin Thickness: 35, Insulin Level: 0, BMI: 36.6, Diabetes Prediction Function: 0.627, and Age: 50.

Number of Pregnancies	Glucose Level	Blood Pressure
1	148	72
Skin Thickness	Insulin Level	BMI
35	0	36.6
Diabetes Prediction Function	Age	
0.627	50	

Diabetes Test Result

The person is Diabetic.

Fig. 6 Disease test result [1]

Data Preparation: The dataset is available on the Kaggle [5] website. The classification goal is to predict whether the patient has 10-years risk of multiple diseases. Dataset provides the information of the patient (Fig. 10).

Cleaning the Data: This is the most important stage in machine learning. Model quality of the model depends on the quality of the data. Data is cleaned before using it for the training of models. The sections in the dataset are all mathematical, with

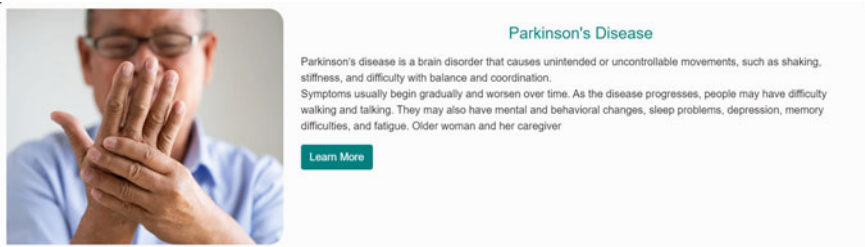


Fig. 7 Information about disease [2]

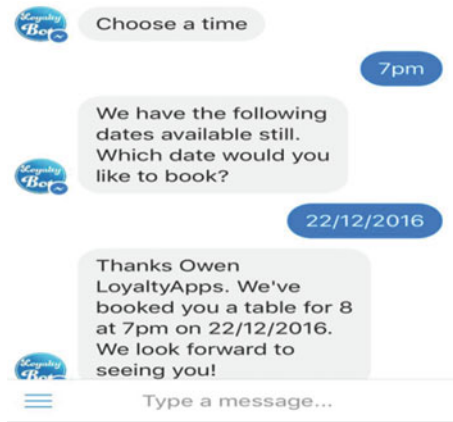


Fig. 8 AI Chatbot

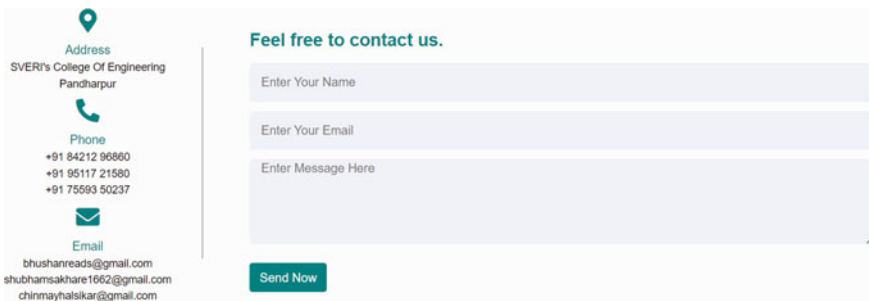


Fig. 9 Contact form

the exception of the objective segment, visualization, which is a literary sort that is encoded to mathematical structure utilizing a name encoder.

Dataset Splitting: Dataset is separated into two: Training dataset and Testing dataset.

Out[]:	Pregnancies	Glucose	BloodPressure	SkinThickness	Insulin	BMI	DiabetesPedigreeFunction	Age	Outcome
0	6	148	72	35	0	33.6	0.627	50	1
1	1	85	66	29	0	26.6	0.351	31	0
2	8	183	64	0	0	23.3	0.672	32	1
3	1	89	66	23	94	28.1	0.167	21	0
4	0	137	40	35	168	43.1	2.288	33	1

Fig. 10 Dataset

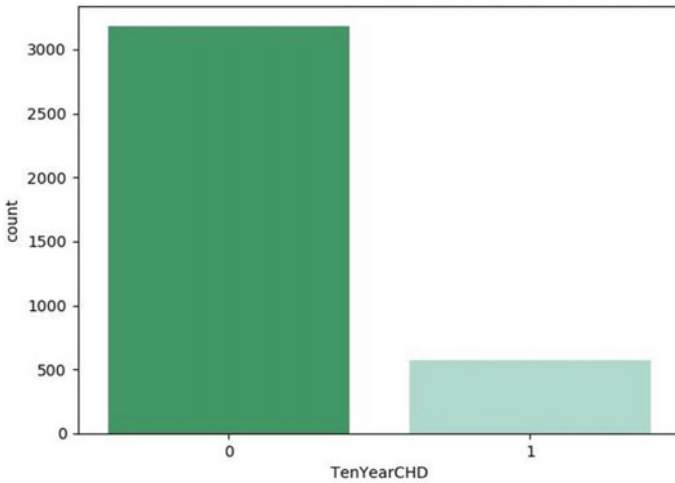


Fig. 11 Dataset splitting [2]

Data is divided into an 4:1 format, which means 80% of the information is utilized for training the model and remaining 20% is used to calculate the model’s performance (Fig. 11).

Random Forest Classifier: Random forest contains a large number of single decision trees which operate as an ensemble. Every tree in the random forest produces a hypothesis, to fabricate a far reaching model two different factors are combined.

4 Result

When the patient is signed in, they will be able to do prediction of disease. This guarantees consistent a single tick answer for get a correct prediction (Fig. 12).

The high precision results as well as this ensures that not one clinical data element is subsidiary to disease prediction and the result is not biased.

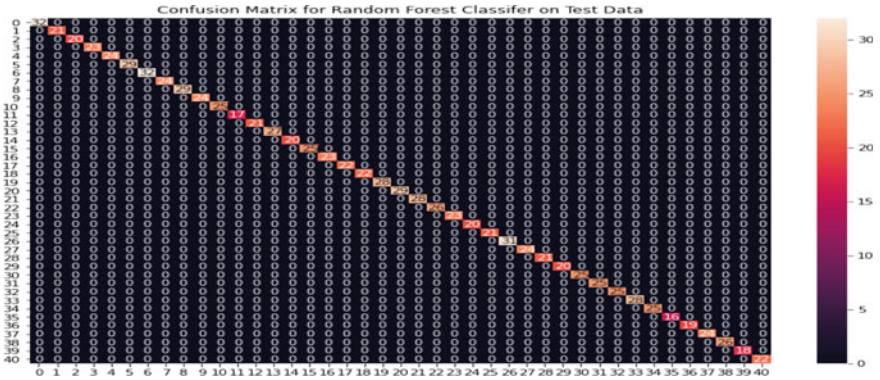


Fig. 12 Accuracy on the train data by random forest classifier

5 Future Scope

- Prime account option is available. We can add Video calling feature.
- The site’s record connecting highlight permits clients to connect their record with other internet based administrations like Gmail and web-based entertainment.
- Map element to the site, such as adding a Programming interface for it. E. Cooperate with a drug store and furthermore give limits on the medication.

6 Conclusion

The machine learning model we have assembled is around 90–97% exact. The diseases for which there are no diagnostics strategies. Machine learning models can anticipate regardless of whether the individual has illness. This is the power of machine learning technology by utilizing which a large number of present reality issues can be solved.

References

1. Visit our project at <http://healthmitra.live>. Access date: Nov. 12, 2022
2. Visit <https://www.github.com/8421296860>. Access date: Nov. 15, 2022
3. Visit <https://scikit-learn.org/stable/modules/generated/sklearn.ensemble.RandomForestClassifier.htm>. Access date: Nov. 18, 2022
4. Visit <https://www.qnamaker.ai/>. Access date: Nov. 25, 2022
5. Visit <https://www.kaggle.com/>. Access date: Nov. 27, 2022
6. Visit <https://azure.microsoft.com/en-in/>. Access date: Dec. 5, 2022

Cloud Based Intelligent Recommendation System for Company, Product and Service Selection



Amol C. Adamuthe, Amarjeet Kambale, and Vrushabh Kupwade

Abstract Identifying the right buyer and seller is a challenging problem for enterprises. To increase business profitability and efficiency there is need of solution, which create strong network so that companies can help/support each other. We have surveyed 65 small and medium scale industries from 5 MIDC/industrial estates in Maharashtra (India). Results shows that there is lack of connection between local industries in Maharashtra and outside Maharashtra. The main objective is to connect the industry on geological location for mutual benefit. It focuses on organizing the business information and leveraging technology to eliminate barriers between companies (provider/consumer). This paper presents a technological solution to the problem. Intelligent cloud computing-based solution is designed that recommends the suitable company, product and services. The system architecture, functional specifications, database design and working of recommendation engine is presented. The proposed keyword based recommendation system provides personalized service recommendation list and suggests the most appropriate services.

Keywords Business automation · Digital ecosystem · Recommendation system

1 Introduction and Related Work

In the current era, the number of products and information are increasing very rapidly. There is diversity in product and services available. It becomes challenging to provide right services/products to consumers. Many companies are spending their valuable time for finding better solutions for their requirements such as identifying expectations of buyers, buyer for their products, better vendor with good quality raw material, skilled labours, transportation facilities etc. In July 2015, the “Digital India

A. C. Adamuthe (✉) · V. Kupwade
Department of Information Technology, Rajarambapu Institute of Technology, Unun Islampur,
Sangli, MS, India
e-mail: amol.admuthe@gmail.com

A. Kambale
Amrta Technologies Pvt. Ltd., Pune, MS, India

© The Author(s), under exclusive license to Springer Nature Switzerland AG 2024
P. M. Pawar et al. (eds.), *Techno-societal 2022*,
https://doi.org/10.1007/978-3-031-34644-6_2

Campaign” launched by the Government of India has provided the much-needed push towards a digital ecosystem (<https://www.digitalindia.gov.in/>). According to Maharashtra State e-Governance Policy 2011, government is planning integrated environment for delivering seamless services which are Government to Business (G2B), Government to Citizen (G2C), Government to Employees (G2E) and Government to Government (G2G) services in a cost-effective manner. The state is looking into the possibility of using cloud computing as its preferred method for carrying out all of its governance tasks. To help the state’s decision support system, the state will put a priority on data warehousing and data mining (<https://www.maharashtra.gov.in/>). There is need for such B2B solutions for enterprises also.

Recommendation system is necessary in today’s era due to large number of options are available for any selection such as movie, product. The major hurdle for end user is to identify the best suitable option from available large pool [1–3]. These systems are used in different domains ranging from video services, product selections, content recommendations on social media, digital libraries, financial services [4–6]. Paper reported that recommendation systems research is popular and increasing from 1990 [7]. It is investigated in wide range of area. It is still evolving and developing. Different technology solutions are in development states. Current research is focusing of increasing the effectiveness of system with addressing wide range of challenges. Paper presented content-based product recommender systems. By comparing product descriptions from a catalogue with descriptions of client preferences and requirements, the system chooses products [8]. Paper presented review of different methods for fashion product recommendation [9]. Image based recommendation systems are investigated using different authors. The use of machine learning algorithms for classification, segmentation and parsing are increasing.

In present scenarios, small and medium scale companies are doing business in traditional way for getting raw material and selling product. They rely on fixed few companies for doing business from many years. Many times, they are unaware about better vendor and buyer.

Few reasons behind this problem are listed below:

- Non-existence of real-time geological data through which they can have details of those industries.
- Non-existence of global or generic communication, purchase and selling model through which they can do business (sending and receiving quotations and other product related information exchange between industries).

This paper provides digital ecosystem in the form of recommendation system. It is useful to providers and users of products/services in order to generate meaningful recommendations according to their requirements. Our proposed system provides strong network which helps industry for product/service-based marketing in cost effective way. It will help company to identify and focus on target audience. It helps industry to reach to clients in maximum possible way in minimum cost which increases its profit margin.

Main contributions of the paper are as follows.

1. Identified the real-world problem by surveying 65 small and medium scale industries in Maharashtra state India.
2. Front and backend design with recent technology stack.
3. Use and integration of cloud computing services in the proposed solution.
4. Novel recommendation system for company, product and service selection.

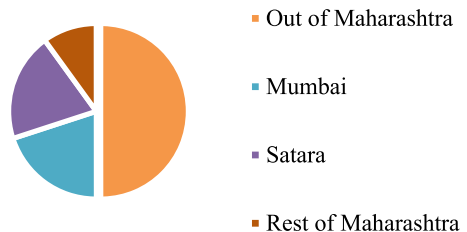
The rest of this paper is structured as follows. Section 2 is problem formulation. It presents the industry survey done in Maharashtra and features identification. Section 3 presents the design, implementation and working of proposed system. Section 4 presents conclusion.

2 Problem Formulation

2.1 Industry Survey in Maharashtra

The main purpose of preliminary survey is to identify the needs and problems of local industries for leveraging the profit. We have surveyed 65 small and medium scale industries from 5 MIDC/industrial estates in Maharashtra namely Kupwad MIDC, Miraj MIDC, Islampur industrial estate, Palus industrial estate and Ratnagiri MIDC. Types of industries visited are, agricultural equipment, food processing units, engineering job works and Fabricators, aluminium alloy manufacturers, foundry and dealers (submersible pump, solar panel, sewing machine, stone crusher, electrical goods, petrochemical, vehicle parts dealers, plywood dealers). Figures 1 and 2 shows statistical analysis of raw material purchase distribution chart and sell distribution chart of small scale packaging industry in Lote MIDC Dist. Ratnagiri, Maharashtra, India for year 2016–17 respectively. Purchase of raw material from out of Maharashtra is more due to lack of connectivity in local industries in state. Sell out of Maharashtra is less due to less connectivity outside Maharashtra.

Fig. 1 Raw material purchase distribution chart



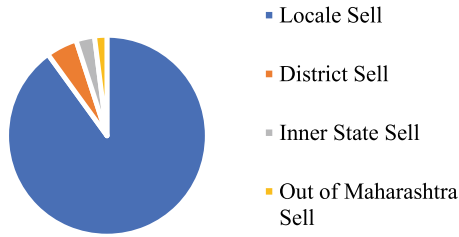


Fig. 2 Sell distribution chart

2.2 Feature Identification

Figures 3 and 4 shows the relationship between product-product and product-company respectively.

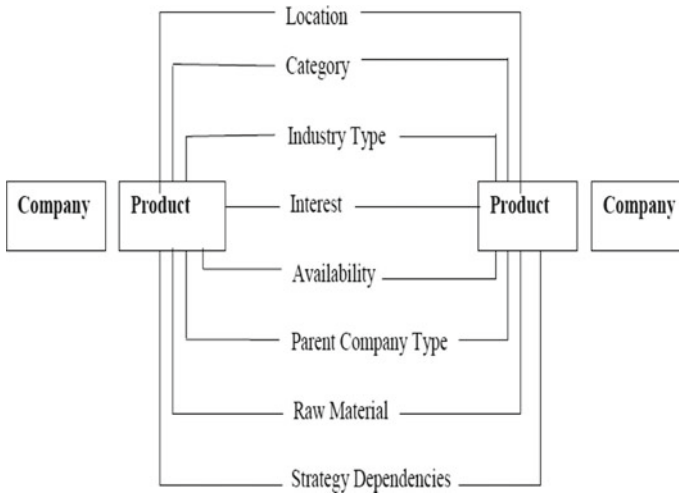


Fig. 3 Relationship between products

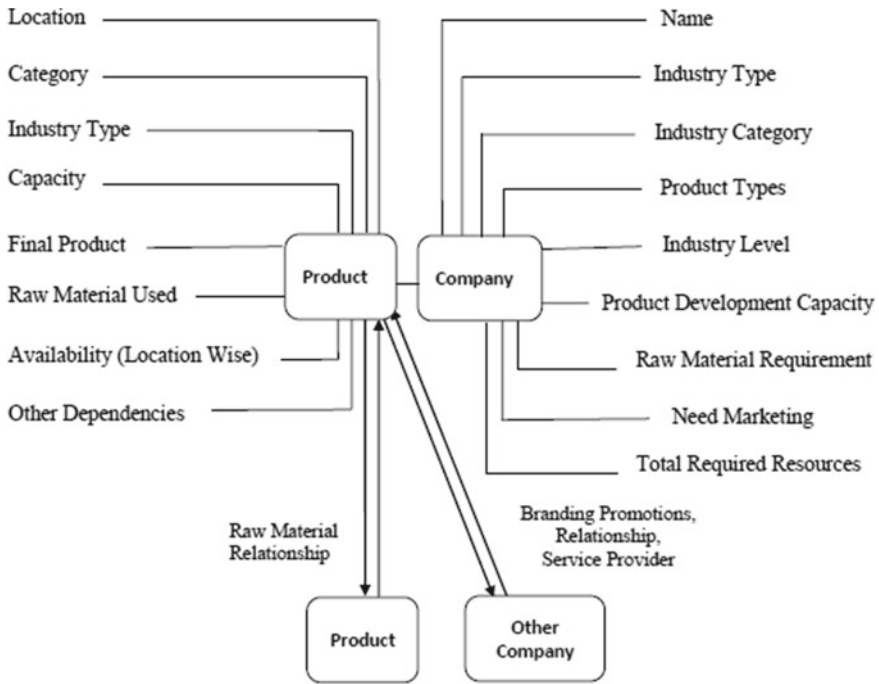


Fig. 4 Relationship between product and company

3 Design, Implementation and Working of Proposed System

3.1 Functional Specifications of the Project

The functional requirements of the project identified based on the customer interaction are create profile, create buyer profile, create seller profile, identify buyer interest, identify seller interest, add product according to interest, add company according to interest, create groups, post jobs, search job, search individual entity, search territory for available interest, notification, chat with seller or buyer, product listing, show all connections.

3.2 Recommendation Engine

The basic terminologies used in recommendation system is user and item. User is one to whom the entities are suggested. Item is the entity recommended to the user. The recommendation system work on historical data which involves the user and items in

one transaction. It is based on the interests shown on the item by user. A significant exception to this rule is the usage of knowledge-based recommender systems, which base their suggestions on user-specified requirements rather than the user’s prior experience.

We proposed a keyword-based recommendation system. In the proposed system, keywords are employed to denote users’ requirements and preferences about products or services. To generate appropriate recommendations for the user, user-based algorithm is used. The main aim of system is presenting a personalized service recommendation list and recommending the most appropriate services to her/him.

3.3 System Architecture of the Application

Company connect system is designed and developed using multiple technologies. Figure 3 shows the architecture using technology stack. The technologies used to design and develop the system are listed below.

1. Google cloud COMPUTE ENGINE, APP ENGINE, CLOUD Storage
2. Web Technology (J2EE, Spring, Struts, Hibernate)
3. Mobile Technology (Android, IOS)
4. Database (MySQL or most suitable according to data analytics) (Figs. 5 and 6)

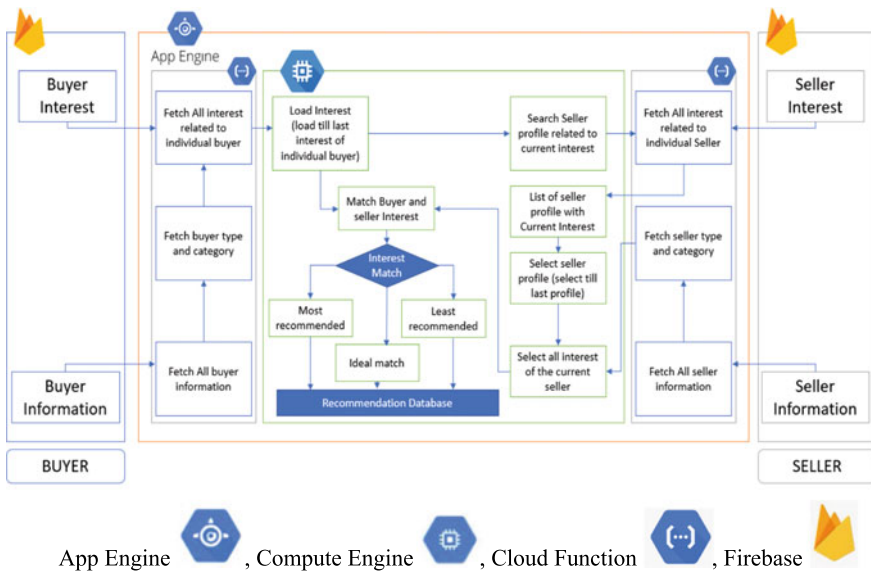


Fig. 5 Technology stack

Recommendation Database Building Flow- Step3

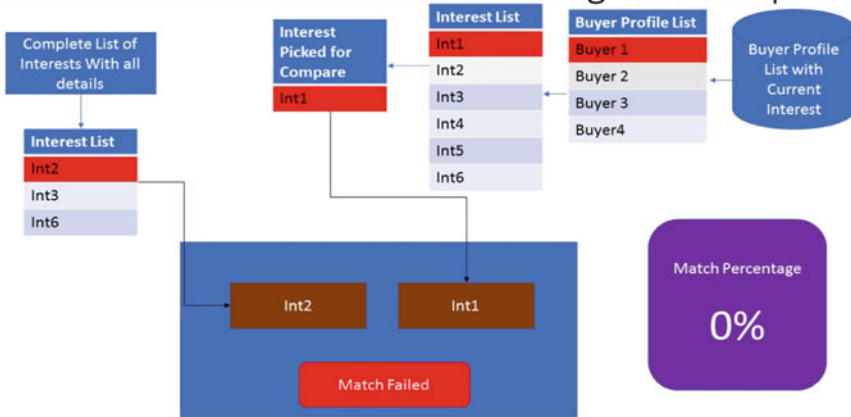


Fig. 6 Recommendation database building flow—step 3

3.4 Database Design

In this project we used NoSQL database. The reason behind using NoSQL databases is to manage heavy request loads which can be managed with ease. Here we are using firebase as a database.

1. **User table:** All the information that is related to user which is used further for user identification is stored. All the security related information is also stored.
2. **Company product profile table:** Company information with product information is stored. We are binding this information with the user table such that this information will be bounded with the user who is entering as a company or product.
3. **Interest purchase category table:** Stores all the interest of the user registered as per company or as a product with respect to their purchase interest from the portal, which will be later used to relate with seller request and create a recommendation.
4. **Interest seller category table:** Stores the interest of the user who are registered as company or product with respect to their seller interest from the portal, which will be later used to relate with the purchase request and create a recommendation.
5. **User company profile table:** Information about the company profile which is being entered by the user is stored. We are repeating all the parameters required for selling or purchasing with on behalf of the company. This information is used for creating a recommendation system.
6. **User product profile table:** It stores the information about the company profile which is being entered by the user and here only we are repeating all the parameters required for selling or purchasing with on behalf of the company. This information is used for creating a recommendation system.

3.5 *Application User Interface*

Application user interface is designed for web and mobile users. The application is designed similar to current social networking application. The important features of the application user interface are simple and easy to learn. These are, User account settings.

User profile view, Quick contact display card, Header Notifications, Header Messages, Main Page Groups, Main Page: Feed, Main Page Messages/Chat, Main page Market, Main page jobs.

- (a) **User account settings:** After user registration, account settings will be provided in which user can update his or her information according to the change in any. This section will give complete command to the user to play along with their information and associatively they can manage their own stuff personal plus whatever the business stuff they want to update.
- (b) **User profile view:** In this, user is able to see their own information along with the interest what they have shown as a seller or buyer into the portal. Recommendations will be appeared on their profile page which show that user can start doing business with their ease as per the location mentioned in the information panel.
- (c) **Header Notifications:** Provided on notification tab where user will be able to see all the notifications. These notifications are to identify whether next person is interested in their product or like their product or sent request or sent business proposal or the quotations. Business contact message is shown so that there is no need to search any user's profiles. User can directly get the key notification.
- (d) **Main Page Groups:** Provision to create groups according to the interest type or the business type is given. In each group there will be recommended users to which there will be complete provision to deal with the similar type of purchase or selling interest and directly you can connect to the group of purchases of similar category. With this they will be able to do direct business with their kind of companies which will give more value addition to their business and it will save their time.
- (e) **Main Page Messages/Chat:** In the main menu we are having a menu called message or chat in which user will be received the message from their direct buyer or purchasers. They will be able to directly have a communication with the buyer or seller and start doing business with them.
- (f) **Main page jobs:** In the application we are providing the option for recruitment. When company needs skilled employee then they can post their requirement on the portal. Any user with matching skillsets can apply for the job.
- (g) **Main Page Market:** All interested sellers can present their product and quote price.

This price will be based on negotiation (Figs 7 and 8).

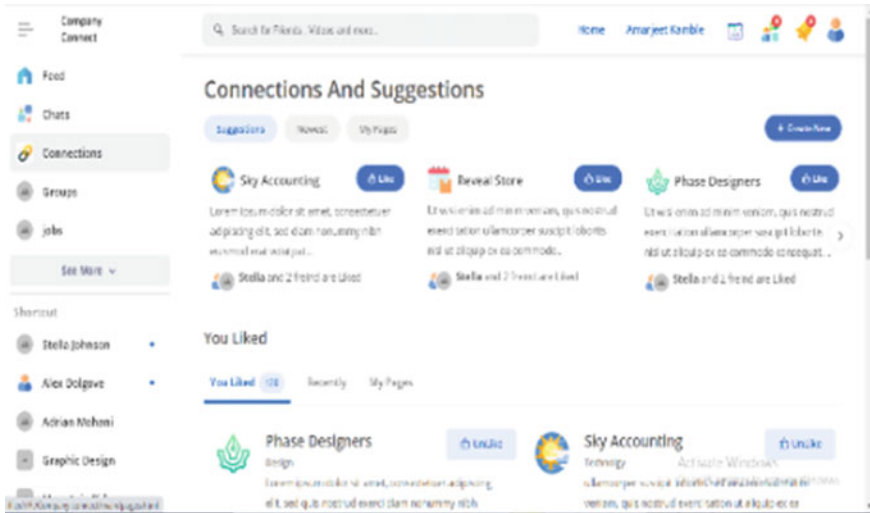


Fig. 7 Main page

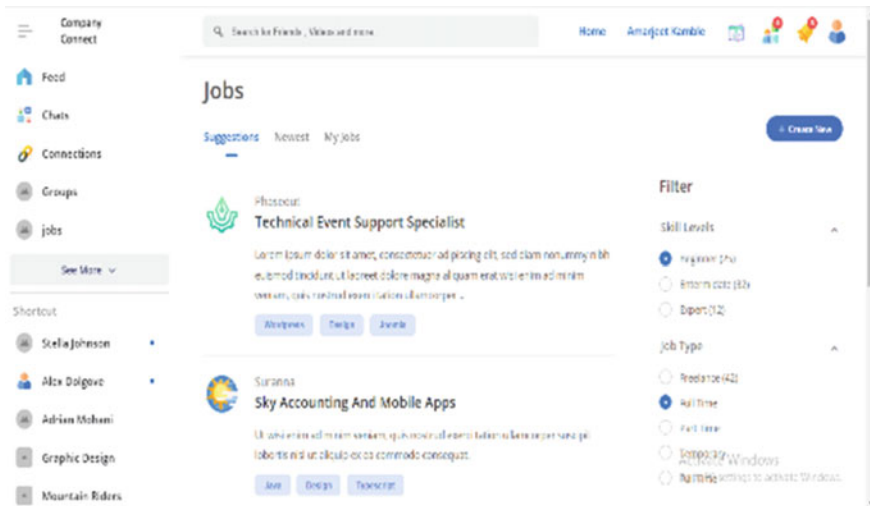


Fig. 8 Main page jobs

4 Conclusion

It is technological support system for companies to improving productivity. This study provides platform for linkage between different companies and digital ecosystem for promotion of products and purchase of raw materials. This research created global or generic communication model through which buyer and seller can

have conversation and exchange of quotation and finalize the deal in win-win situation and both the parties get benefited through model. As this project runs in real-time geological situations and through this seller will get maximum number of clients, cost will get reduced through the process so that profit margin will be increased. Due to the real-time values, buyer can compare the available data and will be in position to choose best fit seller in order to get expected product in most possible lower price. It provides quick, easy and cost-effective way for employee requirement process for skilled and unskilled man power. It provides strong network which helps industry for product-based marketing at affordable price. It helps to decide and focus on exact target-audience and helps industry to reach at clients in maximum possible way in minimum cost which increases its profit margin. Every industry will have real-time geological client and seller data through which they can get best deal and get benefited. By getting the knowledge of basic differentiation constraints of product, seller can make desired product available at affordable price to purchaser.

References

1. Resnick, P., & Varian, H. R. (1997). Recommender systems. *Communications of the ACM*, 40(3), 56–58.
2. Ricci, F., Rokach, L., & Shapira, B. (2022). Recommender systems: Techniques, applications, and challenges. In *Recommender systems handbook* (pp 1–35).
3. Bux, T. U., & Varshney, B. (2021). The movie buff: A movie recommendation system.
4. Felfernig, A., Isak, K., Szabo, K., & Zachar, P. (2007, July). The VITA financial services sales support environment. In *Proceedings of the National Conference on Artificial Intelligence* (Vol. 22(2), p. 1692). AAAI Press, MIT Press.
5. Chen, H. H., Ororbia II, A. G., & Giles, C. L. (2015). ExpertSeer: A keyphrase based expert recommender for digital libraries. arXiv preprint [arXiv:1511.02058](https://arxiv.org/abs/1511.02058)
6. Baran, R., Dziech, A., & Zeja, A. (2018). A capable multimedia content discovery platform based on visual content analysis and intelligent data enrichment. *Multimedia Tools and Applications*, 77(11), 14077–14091.
7. Kim, M. C., & Chen, C. (2015). A scientometric review of emerging trends and new developments in recommendation systems. *Scientometrics*, 104(1), 239–263.
8. Bridge, D. (2001, July). Product recommendation systems: A new direction. In *Proceedings of the Workshop Programme at the Fourth International Conference on Case-Based Reasoning* (pp 79–86).
9. Chakraborty, S., Hoque, M., Rahman Jeem, N., Biswas, M. C., Bardhan, D., & Lobaton, E. (2021, September). Fashion recommendation systems, models and methods: A review. *Informatics*, 8(3), 49. Multidisciplinary Digital Publishing Institute.

Application of Artificial Intelligence and IoT to Membrane Bioreactor (MBR) and Sewage Treatment Plant



Manoj Wagh, Dnyaneshwar Vasant Wadkar, and Prakash Nangare

Abstract A membrane bioreactor (MBR) is a capable treatment technology that consists of an activated sludge process (ASP) emerging with membrane filtration which retains the reduced biomass. MBR is an emerging treatment technology to treat sewage wastewater and reuse the water for various purposes like gardening, toilet flushing, farming, etc. In this paper, a design of the sewage treatment plant is proposed by using MBR technology. To achieve promising and effective results, the traditional design method has been replaced by modern techniques such as wireless sensor networks and the Internet of Things (IoT) software platform to carry out the analysis of sullage wastewater. It concludes that the traditional design system is influenced by the integration of IoT. Further, this paper gives insight into the application of Artificial intelligence (AI) for curtailing the complications in sewage treatment.

Keywords Artificial intelligence · Internet of Things · Membrane bioreactors · Sewage treatment plant · Wireless sensor networks · Wastewater

1 Introduction

Sewage is the wastewater generated by the community of human beings. Around 70% of freshwater consumption is converted into wastewater. Wastewater is contaminated by domestic, industrial, and commercial use that changes its parameters continuously such as COD, BOD, pH, hardness, TSS, etc. Water scarcity is a big challenge to fulfill the per capita demand of the city. Hence, there is an urgent need to treat wastewater and utilize it effectively so that the water demand can be fulfilled. It is observed

M. Wagh (✉)

Department of Civil Engineering, Dr. Vithalrao Vikhe Patil College of Engineering, Ahmednagar, Maharashtra, India

e-mail: profmpwagh@gmail.com

D. V. Wadkar · P. Nangare

Department of Civil Engineering, AISSM'S College of Engineering, Savitribai Phule Pune University, Pune, Maharashtra, India

© The Author(s), under exclusive license to Springer Nature Switzerland AG 2024

P. M. Pawar et al. (eds.), *Techno-societal 2022*,

https://doi.org/10.1007/978-3-031-34644-6_3

that 99% of water is characterized by the rate of flow of its biological, chemical, and physical factors (BOD, COD, pH, hardness, conductivity, turbidity, acidity, DO, TDS, TSS). The sewage wastewater systems can meet the demand for freshwater in smart cities by treating and managing wastewater with the help of Artificial intelligence (AI) and Internet of Things (IoT) sensors. AI and IoT have several influential and hands-on tools to overcome various complex problems related to wastewater treatment [1]. Nowadays, several researchers have implemented AI and IoT technologies because of convenient operation, high speed, high accuracy, and no issues related to the physical problem [2]. AI implemented for seed, crop, leaf, stem, fruit infection [3]. AI is also applicable for the financial sector to predict financial capital [4]. AI can resolve various practical issues related to various engineering disciplines such as civil engineering, environmental engineering, etc. To improve the quality of wastewater and drinking water AI was implemented [5]. The ground water contamination is detected using AI [6]. AI plays an important role to enhance the quality of water by assessing river water, wastewater recycling and water resource engineering [7]. Further, AI is used to find out the characteristics of saline water and to treat the saline water [6, 7]. To detect the machine fault, AI technology is convenient [8]. AI has application in an integrated vehicle health management (IVHM) for aerospace to identify the primary challenges related to paradigm [9]. The process of removing a contaminant from wastewater and household sewage both runoff and domestics are called Sewage treatment [8, 9]. The sewage wastewater treatment is the significant steps to reduce the pollution and promote the water quality [10]. Sewage is the complex waste affected by microbiological, physical and chemical factors variability which requires appropriate treatment technology to operate the sewage treatment plant [10, 11]. Membrane bioreactor (MBR) has made great attention owing to its very high efficacy and is a capable treatment technology which consists of activated sludge process (ASP) emerging with membrane filtration which retain the reduced biomass [11]. MBRs technology is observed as significant fundamentals of advanced effluent reposition and recycle technology and are comprised in a numeral of prominent schemes worldwide [12]. MBR having energy saving efficiency and footprint over conventional processes such as activated sludge process (ASP) oxidation pond, etc. MBR consists of ASP and a membrane detached method [13]. MBR functioning analogous to traditional ASP, and there is no requirement of sedimentation and filtration identical to slow sand filtration (SSF) [14]. Small pressure membrane purification whichever micro-filtration (MF) or ultra-filtration (UF) were implemented to distinct wastewater from ASP [15]. MBR configuration consists of submerged membrane or external circulation (side stream configuration) [16]. Submerged membrane often applied in municipal wastewater treatment [17]. Submerged membrane bioreactor consists of plate membrane module or hollow fibre [18]. Sufficient preliminary treatment was essential to avoid the clogging (Membrane fouling) [19]. 12–15 g/s is recommended for more concentration otherwise it will lead to the functioning problem and decreased oxygen transfer efficiency [20]. Hydrodynamic condition, type of membrane salient feature of module is highly responsible for the clogging of MBR. Due to the bacteriological digestion molecular weight of present substance may increase [21]. The emerging technology

interacts with active sludge and detached sludge and liquid wastewater [22]. ASP consist of screening aeration, clariflocculator and rapid sand filter but still sludge is generated on a large scale this problem can be solved easily using cutting-edge technology such as membrane bio technology which enhance organic treatment. This technology having scope to degrade the parameters of highly contaminated wastewater, dairy industry, sugar industries food processing industries etc. The technology becoming popular day-by-day due to less space is required for installation, instant operation, very less sludge generation and quality of treated parameters as per the central pollution control board norms.

This process involves physical, chemical, and biological methods that remove respective contaminants also produce clean and safe water. In this paper, IoT and Artificial Intelligence (AI) based prediction models were implemented to monitor the sewage treatment plant.

2 Preparation of Your Paper

Figure 1 shows the location of Imagica STP plant Khopoli-Pali Road, SH 92, Sangde-wadi, Maharashtra, India. The layout of the Imagica STP plant has been mentioned in Fig. 2. A row sample of sewage was collected in a container and kept in the refrigerator (Fig. 3). Analysis of sewage wastewater was carried out to find out the characteristics of sewage wastewater (Table 1).

Surrounding is extremely contaminated if industrial waste is discharged without treatment. Portable water is the basic need of human beings. The Maharashtra government treat 22% sewage collected. The remaining 78% row sewage predisposed into



Fig. 1 Site location of STP plant

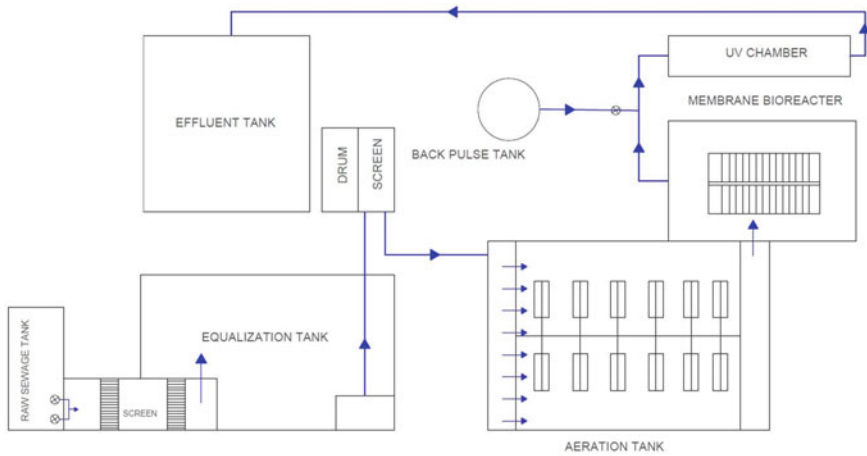


Fig. 2 Flow diagram of STP Imagica Water Park



Fig. 3 Row sewage collection

Table 1 Chemical characteristics of sewage wastewater

S. No	Test parameters of untreated sample	Laboratory result
1	pH value	7.12
2	Electrical conductivity, ds/m	0.631
3	Turbidity, NTU	9.0
4	TDS, ppm	321.4
5	COD, mg/lit	723
6	BOD (at 3 day), mg/lit	192
7	DO, mg/lit	1.42
8	Total hardness as CaCO ₃ , mg/lit	294
9	Total alkalinity as CaCO ₃ , mg/lit	148

waterways which creates chances of water-borne diseases. In India, the government and scientists are facing the problem due to habit of human being to handle the sewage water. To save the environment design, operation and treatment of sludge treatment plant (STP) is the solution.

2.1 Information of Imagica Water Park, Khopoli

See Fig. 4.

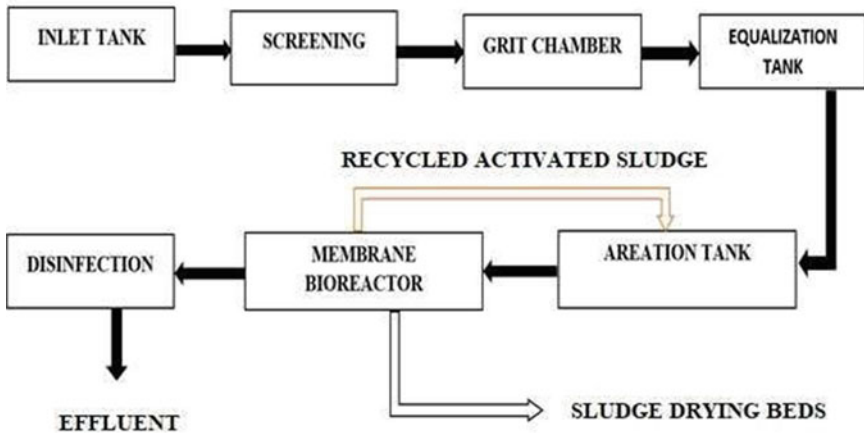


Fig. 4 Sewage treatment plant flow chart

3 Result and Discussions

Membrane bioreactor (MBR) is an advanced emerging technology that can curtail the parameters of sewage such as COD, BOD, TSS, etc. Table 2 illustrate parameter of sewage before and after the treatment. Which shows that treated effluent can be used for various purpose such as gardening, flushing of toilet, etc. The residual sludge can be used as manure for agricultural purposes. Figure 5 shows the quality of effluent and manure.

IoT plays a vital role in the operation, monitoring, and maintenance of sewage treatment plants. To achieve the sustainability of the sewage, plant digital innovations

Table 2 Parameters of sewage before and after treatment

Parameter	Influent (in mg/l except pH)	Effluent (in mg/l except pH)
pH	7.95	7.77
BOD	192	2.70
COD	720	8.18
TSS	321	3.51



Fig. 5 Water quality and manure after the MBR treatment

were carried out which sense the analysis of the collected data, and the operational treatment technology. The programmable logic controllers (PLC), process control station, and optical fiber sensor were implemented to control the operation. Supervisory Control and Data Acquisition (SCADA) method was executed to evaluate the overall functioning of the plant. PLC, remote terminal units (RTU) interpreted the gathered information about effluent characteristics, analyze the real-time data from the connected numerous sensors and transmit it to the field instrumentation. With the help of a real-time sensor and SCADA online monitoring of various parameters of sewage plant were carried out which includes monitoring of pH of effluent, total suspended solids variation during the process. The quality of effluent depends upon the amount of dissolved oxygen present in the effluent. Degradation of effluent is depending upon the microorganism such as aerobic bacteria which consume the oxygen and curtail the parameters of the effluent. Chemical oxygen demand (COD) is the crucial constraints which elaborate the sewage wastewater quality. SCADA application helps to monitor the parameters of COD.

References

1. Adeloje, A. J., & Dau, Q. V. (2019). Hedging as an adaptive measure for climate change induced water shortage at the Pong reservoir in the Indus Basin Beas River, India. *Science of the Total Environment*, 687, 554–566.
2. Ahmed, A. N., Othman, F. B., Afan, H. A., & Elsha, A. (2019). Machine learning methods for better water quality prediction. *Journal of Hydrology*, 578.
3. Al Aani, S., Bonny, T., Hasan, S. W., & Hilal, N. (2019). Can machine language and artificial intelligence revolutionize process automation for water treatment and desalination. *Desalination*, 458, 84–96.
4. Bozkurt, H., van Loosdrecht, M. C. M., Gernaey, K. V., & Sin, G. (2016). Optimal WWTP process selection for treatment of domestic wastewater—A realistic full-scale retrofitting study. *Chemical Engineering Journal*, 286, 447–458.
5. Bucci, V., Majed, N., Hellweger, F. L., & Gu, A. Z. (2012). Heterogeneity of intracellular polymer storage states in enhanced biological phosphorus removal (EBPR)—Observation and modeling. *Environmental Science and Technology*, 46, 3244–3252.
6. Carrasco, E. F., Rodríguez, J., Pual, A., Roca, E., & Lema, J. M. (2002). Rule-based diagnosis and supervision of a pilot-scale wastewater treatment plant using fuzzy logic techniques. *Expert Systems With Applications*, 22, 11–20.
7. Carrasco, E. F., Rodríguez, J., Punal, A., Roca, E., & Lema, J. M. (2004). Diagnosis of acidification states in an anaerobic wastewater treatment plant using a fuzzy based expert system. *Control Engineering Practice*, 12, 59–64.
8. Chakraborty, T., Chakraborty, A. K., & Chattopadhyay, S. (2019). A novel distribution free hybrid regression model for manufacturing process efficiency improvement. *Journal of Computational and Applied Mathematics*, 362, 130–142.
9. Dai, H., Chen, W., & Lu, X. (2016). The application of multi-objective optimization method for activated sludge process: A review. *Water Science and Technology*, 76, 223–235.
10. Dehghani, M., Seifi, A., & Riahi-Madvar, H. (2019). Novel forecasting models for immediate-short-term to long-term influent flow prediction by combining ANFIS and grey wolf optimization. *Journal of Hydrology*, 576, 698–725.
11. Jia, X., Li, Z., Tan, R., Foo, D. C. Y., Majozzi, T., & Wang, F. (2019). Interdisciplinary contributions to sustainable water management for industrial parks. 149, 646–648.

12. Han, H. G., Liu, Z., Guo, Y. N., & Qiao, J. F. (2018). An intelligent detection method for bulking sludge of wastewater treatment process. *Journal of Process Control*, *68*, 118–128.
13. Han, H. G., Zhang, L., Liu, H. X., & Qiao, J. F. (2018). Multiobjective design of fuzzy neural network controller for wastewater treatment process. *Applied Soft Computing Journal*, *67*, 467–478.
14. Hernández-Del-Olmo, F., Llanes, F. H., & Gaudioso, E. (2012). An emergent approach for the control of wastewater treatment plants by means of reinforcement learning techniques. *Expert Systems With Applications*, *39*, 2355–2360.
15. Huang, M., Han, W., Wan, J., Ma, Y., & Chen, X. (2016). Multi-objective optimisation for design and operation of anaerobic digestion using GA-ANN and NSGA-II. *Journal of Chemical Technology and Biotechnology*, *91*, 226–233.
16. Huang, M., Ma, Y., Wan, J., & Chen, X. (2015). A sensor-software based on a genetic algorithm-based neural fuzzy system for modeling and simulating a wastewater treatment process. *Applied Soft Computing Journal*, *27*, 1–10.
17. Podder, M. S., & Majumder, C. B. (2016). The use of artificial neural network for modelling of phycoremediation of toxic elements As(III) and As(V) from wastewater using *Botryococcus braunii*. *Spectrochimica Acta Part A: Molecular and Biomolecular Spectroscopy*, *155*, 130–145.
18. Zhang, X. P. S. (2017). To the victor go the spoils: AI in financial markets [perspectives]. *IEEE Signal Processing Magazine*, *34*, 176–176.
19. Zhang, Y., Gao, X., Smith, K., Inial, G., Liu, S., Conil, L. B., & Pan, B. (2019). Integrating water quality and operation into prediction of water production in drinking water treatment plants by genetic algorithm enhanced artificial neural network. *Water Research*, *164*, 114888.
20. Zhang, Y., & Pan, B. (2014). Modeling batch and column phosphate removal by hydrated ferric oxide-based nanocomposite using response surface methodology and artificial neural network. *Chemical Engineering Journal*, *249*, 111–120.
21. Zhang, Z., Kusiak, A., Zeng, Y., & Wei, X. (2016). Modeling and optimization of a wastewater pumping system with data-mining methods. *Applied Energy*, *164*, 303–311.
22. Zhao, L., Deng, J., Sun, P., Liu, J., Ji, Y., Nakada, N., Qiao, Z., Tanaka, H., & Yang, Y. (2018). Nanomaterials for treating emerging contaminants in water by adsorption and photocatalysis: Systematic review and bibliometric analysis. *Science of the Total Environment*, *627*, 1253–1263.

Comparative Study of Machine Learning Techniques for Stock Market Price and Optimizing Its Cumulative Strategy Returns



Digambar Uphade and Aniket Muley

Abstract In the present study our main focus is on the probable of making forecast of Facebook stock market prices by machine learning algorithms based on historical data. In recent years several tools and methods have been planned and used to check the accuracy of forecasting model. This paper presents a comparative study of machine learning techniques such as Support vector machine (SVM), artificial neural network (ANN) and logistic regression. Further, to optimize the buy or sell strategy we have evaluated cumulative returns and cumulative strategy returns with simulating train test data split. It has been observed that ANN model outperforming as compared to other models. Further, maximum cumulative returns with the cumulative strategy are obtained at split of 90:10. It gives the best performance of the stock with the 32.04% cumulative strategy return. The result suggests that, to optimize the performance of Facebook stock market one can predicted the stock price with proposed strategy in future.

Keywords Facebook · Stock · Machine learning · ANN · SVM · Logistic regression · Returns

1 Introduction

In real, performing stock market's forecast has constantly been a captivating and difficult trouble for financial sector as well as statistics experts. Stock market forecast is a tough task and researchers can also face challenges as increasing a predictive organization. Stock markets are also unpredictable, or unhinged. This unpredictability

D. Uphade (✉)

Department of Statistics, KRT Arts, BH Commerce and AM Science College, Nashik,
MS 422002, India
e-mail: dbuphade@gmail.com

A. Muley

School of Mathematical Sciences, Swami Ramanand Teerth Marathwada University, Nanded,
MS 431606, India
e-mail: aniket.muley@gmail.com

occurs while prices of fundamental securities ebb and flow. The main objective in this study is to carry out stock market forecast is to buy stocks that are probable to get higher in price in future and put up for sale those stocks which are probable to turn down. Conventionally, two approaches are applied for stock market guess. This paper aims to use the features viz., open price, close price, adjusted close price, high price, low price and volume as well in machine learning algorithms and forecast stock prices based on these attributes. Stock prices changes when the estimated cost of securities changes due to real national–international level actions; since these events are unforeseen, volatility also happened surprisingly. So, investors face challenges in forecasting the upcoming of stock markets. Machine learning (ML) techniques can be apply in stock market forecast systems to assist financial analysts and traders in their market decision-making. These algorithms aspire to mechanically study and identify patterns in huge amounts of data. Individual investors are very emotional and emotional factors can simply destroy the trading authority. Therefore, a ML approach is advantageous in increasing stock market forecast models. Ouahilal et al. [13] proposed a novel hybrid approach based on machine learning and filtering techniques. They combined Support Vector Regression and Hodrick–Prescott filter to optimize the forecast of stock price. They demonstrated the development in prognostic performance of stock market and verified the mechanism of their model and compared with additional optimized models and conclude that the planned algorithm constitutes a powerful model for predicting stock market prices. Bazrkar and Hosseini [1] presented a ML approach called SVM with existing data to predict future stock data. They compared proposed method with other methods viz., SVM, artificial neural network (ANN) and LSTM. Dash et al. [3] proposed a novel approach for predicting results. Das and Padhy [2] “proposed a hybrid model called USELM-SVR and is a combination of unsupervised extreme learning machine (US-ELM) based clustering and SVR forecasting. They assessed the feasibility and effectiveness of this hybrid model using a case study by predicting the one, two, and three-day ahead closing values.” Gong et al. [4] “constructed LS-SVM technique optimized by the customized PSO algorithm to enhance the returns volatility forecasting. They have compared the unpredictability forecasting performances of the planned model with other two comprehensive models using stock market data from wind database, namely the asymmetric GARCH models with non-Gaussian distributions hybridized with artificial neural network and the individual parametric asymmetric GARCH models.” Gowthul Alam and Baulkani [5] dealt with the use of multi-kernel SVM (MK SVM) parameter tuning approach with fruit fly optimization (FFO) on stock market trend forecast. They found that, MK SVM with greatest feature subset to predict stock market movement direction based upon historical data series optimal parameters are used. Hu et al. [6] proposed three profit guided models with the Sharpe Ratio evaluated based on diverse trading strategies and 3 statistical miscalculation guided models. Jenkins et al. [8] outlined a novel process for evaluating the human impact of ML applications. Khan et al. [10] studied inclusion of stock market features in ML algorithms and forecast stock prices using various attributes. They have developed this model by edge tweets from Twitter and political news from Wikipedia and further pre-processed the data for discovering the

sentiment and situation characteristics for stock market calculation. Khan et al. [9] used algorithms on public media and economic news data to discover the blow of this data on stock market forecast exactness for ten subsequent days. They execute experiments to find such stock markets that are not easy to forecast and those that are more inclined by social media and economic news. They compared results of different algorithms to find a reliable classifier. They also show that New York and Red Hat stock markets are tough to forecast, New York and IBM stocks are more influenced by societal media, while London and Microsoft stocks by economic news. Random forest classifier is found to be reliable and maximum correctness is achieved by its collection. Kurani et al. [11] focused on the financial risk management and stock prediction issues. They observed that SVM and ANN play prominent roles in tackling financial risk prediction issues. Li and Sun [12] established a prognostic model that combines kernel parameters and parameter optimization to model. They have used mesh search method, genetic algorithm, and particle swarm optimization algorithm for optimizing the parameters of the SVM in a variety of kernel functions. They have used well trained model for the stock smart investment perspective. Parray et al. [14] studied three machine learning algorithms for prediction of upcoming day stock. Saini and Sharma [15] performed relative basic approach and they compared predict stock price. Thenmozhi et al. [16] developed a global price transmission based model that showed that significantly outperforms. Also, they found that the US market is predisposed by Asian markets and there is maximum correlation among the Asian markets except China. Further they suggested that, a particular stock index can be predicted greatest using other stock market indices which open or close just before it. In this paper, main objectives of our study are, to find machine learning model which gives best performance for different train-test split. Also, based on the train-test proportion split, identify the optimal strategy that gives more returns. In the succeeding sections, methodology, result and discussion and finally conclusion is elaborated in detailed.

2 Methodology

In this mechanism, three machine learning techniques have been used viz., SVM, ANN and Logistic Regression model to find the optimal model for the Facebook-metadata analysis.

2.1 *Support Vector Machine (SVM)*

The SVM algorithm frequently applied to the labeled data and it helps to find the optimal hyperplane that can be used to classify new data points.

2.2 Artificial Neural Network (ANN)

It is copied from Biological neural networks that expand the arrangement of a human brain. Alike to the human brain that has neurons interrelated to one another; artificial neural networks also have neurons that are interrelated to one another in different layers of the networks. These neurons are identified as nodes. Artificial Neural Network mainly consists of 3 layers: Input Layer, hidden Layer and Output Layer.

2.3 Logistic Regression

It is a prognostic analysis algorithm and based on the idea of probability. The hypothesis of logistic regression tends it to boundary the cost function between zero and one. Logistic Regression uses a compound cost function and is defined as the sigmoid function or also known as the logistic function instead of a linear function. Here, Fig. 1 represents our workflow of this study. Initially, we have collected secondary Facebook dataset [17]. Afterwards, we have preprocessed our data and identified our study variables. Here, we have transformed our independent variables in the form of differentiation of the Open-close and High-low prices of stock. Further, we have set the target variable y and it is represented in the form 0 and 1 with special strategy explored in Fig. 1 and computed the following performance measures (Eqs. 1–4) to get the best machine learning model. The performance measures are:

$$Accuracy = \frac{TP + TN}{TP + TN + FP + FN} \quad (1)$$

$$Precision = \frac{TP}{(TP + FP)} \quad (2)$$

$$Recall = \frac{TP}{TP + FN} \quad (3)$$

$$F_1-Score = \frac{2(Precision * Recall)}{(Precision + Recall)} \quad (4)$$

where, True positive (TP), True Negative (TN), False Positive (FP), False Negative (FN).

Further, simulated the different train-test split to get the best returns through the cumulative strategy returns.

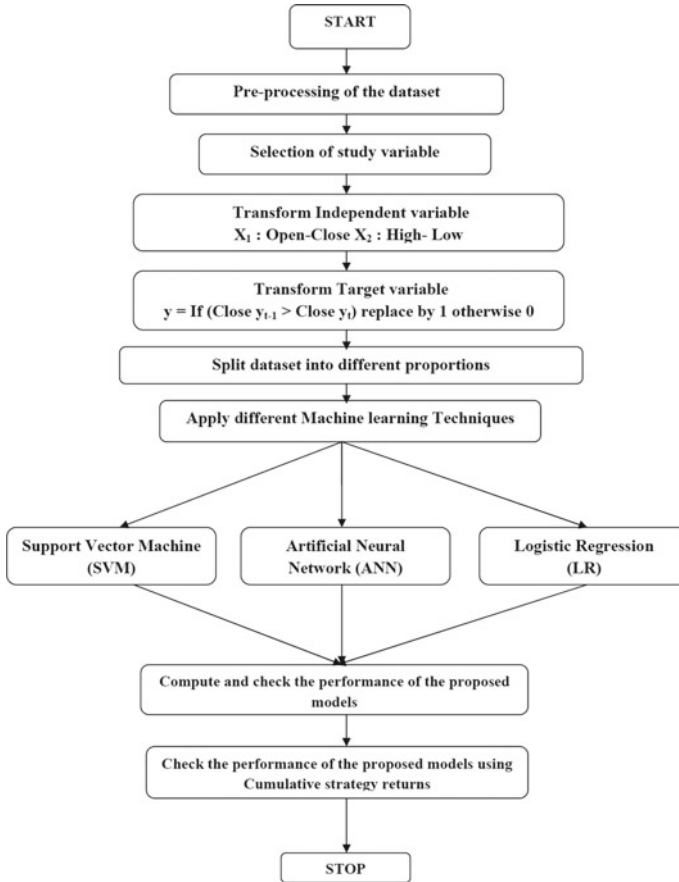


Fig. 1 Flowchart of the study

3 Result and Discussion

The result of the three machine learning techniques viz., SVM, ANN and Logistic Regression models are discussed in this section.

Table 1 represents the summary of the different machine learning methods. It covers their train-test split accuracy, precision, recall and F1-score. Based on various train-test split we observed that, the SVM model gives maximum accuracy 53.80% with split ratio 75:25. In ANN the split 75:25 gives the maximum accuracy 55.23% and in Logistic regression train-test split 70:30 gives maximum accuracy 51.45%. Table 2 represents the summary of cumulative returns and cumulative returns strategy returns analytical results. Figure 2 represents the graphical representation of cumulative return and cumulative strategy returns for 90:10 split. Further, it is compared with train-test data split ratio 50:50, 55:45, 60:40, 65:35, 70:30, 75:25, 80:20 and

Table 1 Summary of comparative results

Method	Train-test split	Accuracy	Classifier	Precision	Recall	F1-score	
Support vector machine (SVM)	50:50	0.4928	0	0.48	0.67	0.56	
			1	0.52	0.33	0.4	
	55:45	0.5105	0	0.5	0.37	0.42	
			1	0.52	0.64	0.57	
	60:40	0.4960	0	0.46	0.23	0.31	
			1	0.51	0.75	0.6	
	65:35	0.5000	0	0.48	0.43	0.45	
			1	0.52	0.56	0.54	
	70:30	0.5304	0	0.51	0.34	0.41	
			1	0.54	0.71	0.61	
	75:25	0.5380	0	0.54	0.32	0.40	
			1	0.54	0.75	0.63	
	80:20	0.5059	0	0.51	0.3	0.38	
			1	0.51	0.71	0.59	
	85:15	0.4894	0	0.5	0.29	0.37	
			1	0.48	0.7	0.57	
	90:10	0.5158	0	0.54	0.39	0.45	
			1	0.5	0.65	0.57	
	Artificial neural network (ANN)	50:50	0.5269	0	0.51	0.52	0.51
				1	0.55	0.54	0.54
55:45		0.5432	0	0.54	0.43	0.48	
			1	0.55	0.65	0.6	
60:40		0.5228	0	0.51	0.48	0.49	
			1	0.53	0.57	0.55	
65:35		0.5362	0	0.52	0.59	0.55	
			1	0.56	0.48	0.52	
70:30		0.5343	0	0.51	0.59	0.55	
			1	0.56	0.48	0.52	
75:25		0.5523	0	0.53	0.61	0.57	
			1	0.58	0.5	0.54	
80:20		0.5039	0	0.5	0.24	0.33	
			1	0.5	0.76	0.61	
85:15		0.5211	0	0.55	0.4	0.46	
			1	0.51	0.65	0.57	
90:10		0.5515	0	0.56	0.55	0.56	
			1	0.54	0.55	0.55	

(continued)

Table 1 (continued)

Method	Train-test split	Accuracy	Classifier	Precision	Recall	F1-score
Logistic regression	50:50	0.5103	0	0.48	0.27	0.35
			1	0.52	0.73	0.61
	55:45	0.4991	0	0.45	0.13	0.2
			1	0.51	0.85	0.63
	60:40	0.4940	0	0.45	0.19	0.27
			1	0.5	0.78	0.61
	65:35	0.5124	0	0.49	0.31	0.38
			1	0.52	0.7	0.6
	70:30	0.5145	0	0.49	0.28	0.36
			1	0.52	0.73	0.61
	75:25	0.5095	0	0.49	0.27	0.35
			1	0.52	0.73	0.61
	80:20	0.4940	0	0.48	0.17	0.25
			1	0.5	0.81	0.62
	85:15	0.4940	0	0.48	0.17	0.25
			1	0.5	0.81	0.62
	90:10	0.4940	0	0.45	0.19	0.27
			1	0.5	0.78	0.61

Table 2 Cumulative strategy returns results

Train-test split	Cumulative returns (%)	Cumulative strategy returns (%)
50:50	23.6	22.67
55:45		24.08
60:40		19.57
65:35		20.86
70:30		27.29
75:25		26.72
80:20		24.16
85:15		23.95
90:10		32.04

85:15. The result reveals that, maximum 32.04% of strategy returns are obtained for the split 90:10. Finally, it is recommended from our study the 90:10 split for the more accurate results for similar kinds of studies.

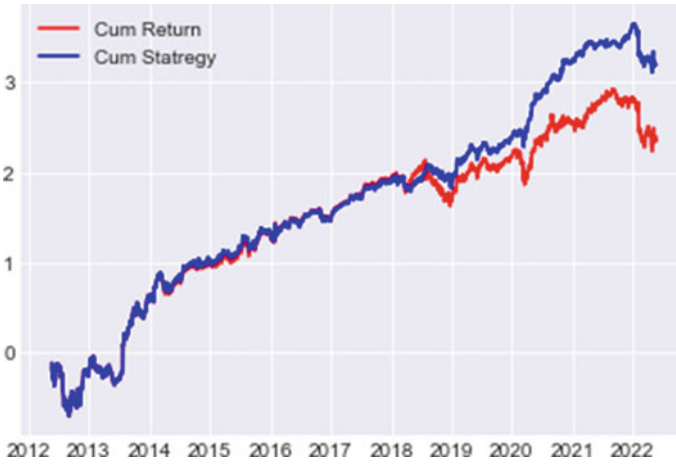


Fig. 2 Train-test data 90:10 dataset results of cumulative returns

4 Conclusion

In this study, we have dealt with Facebook-metadata of stock market secondary data. According to our objective we have implemented three different machine learning techniques. Also, we have used train test split through simulation perspective to judge the best split that gives us best optimal results to obtain the best model for the dataset. It is observed that, to achieve the maximum accuracy by SVM we can adopt the proportion of train-test split as 75:25. Further, if we uses ANN model it gives us maximum accuracy with train-test split 75:25. Thereafter, as we used Logistic Regression model it gives maximum accuracy for the spilt 70:30. Overall it is observed that, ANN gives maximum accuracy as compared to other. Later on, we have computed maximum cumulative returns with the cumulative strategy with different train-test split of the dataset; it is observed that, at 90:10 split model gives the best performance of the Stock returns i.e. our strategy provided the maximum return of **32.04%** whereas the stock provides the return of just **23.60%**. Table 2 simply elaborates the comparative results i.e. 23.60% of the cumulative returns are constant throughout different data split but the cumulative strategy of it matters for identifying the superiority of the model. In future, for buy or sell decision making perspective someone may adopt this method to optimize the cumulative returns.

References

1. Bazrkar, M. J., & Hosseini, S. (2022). Predict stock prices using supervised learning algorithms and particle swarm optimization algorithm. *Computational Economics*, 1–22.
2. Das, S. P., & Padhy, S. (2017). Unsupervised extreme learning machine and support vector regression hybrid model for predicting energy commodity futures index. *Memetic Computing*, 9(4), 333–346.
3. Dash, R. K., Nguyen, T. N., Cengiz, K., & Sharma, A. (2021). Fine-tuned support vector regression model for stock predictions. *Neural Computing and Applications*, 1–15.
4. Gong, X. L., Liu, X. H., Xiong, X., & Zhuang, X. T. (2019). Forecasting stock volatility process using improved least square support vector machine approach. *Soft Computing*, 23(22), 11867–11881.
5. Gowthul Alam, M. M., & Baulkani, S. (2019). Local and global characteristics-based kernel hybridization to increase optimal support vector machine performance for stock market prediction. *Knowledge and Information Systems*, 60(2), 971–1000 (2019)
6. Hu, Z., Bao, Y., Chiong, R., & Xiong, T. (2017). Profit guided or statistical error guided? A study of stock index forecasting using support vector regression. *Journal of Systems Science and Complexity*, 30(6), 1425–1442.
7. Huang, H. T., & Tserng, H. P. (2018). A study of integrating support-vector-machine (SVM) model and market-based model in predicting Taiwan construction contractor default. *KSCE Journal of Civil Engineering*, 22(12), 4750–4759.
8. Jenkins, R., Hammond, K., Spurlock, S., & Gilpin, L. (2022). Separating facts and evaluation: Motivation, account, and learnings from a novel approach to evaluating the human impacts of machine learning. *AI and Society*, 1–14.
9. Khan, W., Ghazanfar, M. A., Azam, M. A., Karami, A., Alyoubi, K. H., & Alfakeeh, A. S. (2020). Stock market prediction using machine learning classifiers and social media, news. *Journal of Ambient Intelligence and Humanized Computing*, 1–24.
10. Khan, W., Malik, U., Ghazanfar, M. A., Azam, M. A., Alyoubi, K. H., & Alfakeeh, A. S. (2020). Predicting stock market trends using machine learning algorithms via public sentiment and political situation analysis. *Soft Computing*, 24(15), 11019–11043.
11. Kurani, A., Doshi, P., Vakharia, A., & Shah, M. (2021). A comprehensive comparative study of artificial neural network (ANN) and support vector machines (SVM) on stock forecasting. *Annals of Data Science*, 1–26.
12. Li, X., & Sun, Y. (2020). Stock intelligent investment strategy based on support vector machine parameter optimization algorithm. *Neural Computing and Applications*, 32(6), 1765–1775.
13. Ouahilal, M., El Mohajir, M., Chahhou, M., & El Mohajir, B. E. (2017). A novel hybrid model based on Hodrick-Prescott filter and support vector regression algorithm for optimizing stock market price prediction. *Journal of Big Data*, 4(1), 1–22.
14. Parray, I. R., Khurana, S. S., Kumar, M., & Altalbe, A. A. (2020). Time series data analysis of stock price movement using machine learning techniques. *Soft Computing*, 24(21), 16509–16517.
15. Saini, A., & Sharma, A. (2019). Predicting the unpredictable: An application of machine learning algorithms in Indian stock market. *Annals of Data Science*, 1–9.
16. Thenmozhi, M., & Sarath Chand, G. (2016). Forecasting stock returns based on information transmission across global markets using support vector machines. *Neural Computing and Applications*, 27(4), 805–824.
17. <https://www.kaggle.com/datasets/ranugadisansagamage/facebookmeta-stocks>

Crop Leaf Disease Detection in Soybean Crop Using Deep Learning Technique



Vipul V. Bag, Mithun B. Patil, Shubham Shelke, Nagesh Birajdar, Aashutosh Sonkawade, and Rohit Rathod

Abstract Agriculture is the backbone of human life. The basic and essential needs of humans are fulfilled by agriculture. Soybean is grown on a large scale in the East Asia region. Now it is also grown in other parts of the world with modern methods. But it is affected by many unpredicted diseases which may lead to a reduction in yields. So, it is essential to identify soybean crop diseases and protect from unpredicted diseases at earlier stages. Most of the farmers are not able to find accurate diseases. Hence, we have developed a mobile application for soybean crop leaf disease detection using Deep Learning. The deep learning Model is built using a Deep Belief Network. We have built a model which can detect mainly three types of diseases of soybean. These diseases are frog eye leaf spots, powdery mildew, and septoria brown spot. After training the model using different CNN architectures, our model got a maximum accuracy of 99%. This application is user-friendly and can detect the disease and also suggest treatment for that disease. This will helpful to farmers save their soybean crops from diseases with minimum effort and maximum accuracy.

Keywords Convolutional neural networks (CNN) · Deep Learning · Frog eye leaf spot · Powdery mildew · Septoria brown spot

1 Introduction

In the agriculture field, the health of crops is very important. The yield production of a crop mostly depends on the health of the crop. Soybean is a major crop in many regions of the world. Predicting and doing treatment of diseases in the soybean plant is helpful to get more crop production. But the traditional way may get some errors while predicting the disease. In the soybean plant, most of the diseases are

V. V. Bag (✉) · M. B. Patil · S. Shelke · N. Birajdar · A. Sonkawade · R. Rathod
Department of CSE, N K Orchid College of Engineering and Technology, Solapur, MH, India
e-mail: vipulbag@gmail.com

M. B. Patil
e-mail: mithunbpatil2@gmail.com

caused and affected by leaves [11–13]. Identifying soybean crop leaf diseases by the human eye is not always accurate. There is a need to develop a user-friendly mobile application that will be able to detect soybean crop leaf diseases with high accuracy. After detecting the diseases there is a need of suggesting treatment for these diseases at the same time. Our research consist of a mobile application for soybean crop leaf disease detection which can identify three types of disease with 99% accuracy. This application is user-friendly. Farmers can select the image or click the photo using a mobile camera the image is sent to server for Deep belief network to get the name and treatment description of the disease. This will increase the accuracy of identifying diseases with minimum time. This will play an important role in soybean farming to maintain the health of the soybean crop.

2 Literature Review

Disease detection is a challenging task in the crop in which failure of the identification leads to an economical loss to the agriculturist. Some disease consultant systems and applications are available in the market, which can identify only common crop leaf diseases. In this Research, we have mainly focused on the Soybean crop as a sample crop identifying the disease based on the leaf of the soybean by applying Deep learning techniques. The identical few research work carried to identify the diseases in the crop are [1] presented a model that combines tomato leaf disease identification with classification by hybrid combination of CNN and learning vector quantization (LVQ) with data size of 500 images with four considered disease categories of tomato leaves in which extraction and classification of important attributes resulting accuracy 98.1% [2] conducted the feasibility of a convolutional neural network architecture for classifying various plant diseases based on leaf images captured. LeNet, one of most commonly CNN architectures for disease classification in soybean plants was used on 12,763 sample images of soybean leaves were taken from a standard database called Plant Village resulted in 99.32% accuracy and demonstrated the feasibility of CNN in classifying plant diseases from leaf images [3], have worked on generating new age models to identify different diseases of 13 plant diseases using leaf images of healthier plants with a deep learning architecture by name Caffe was used to train the data resulted in 91–98% accuracy. Fuentes [4] combined different architectures into a single meta architecture specific methods such as ResNet-50, VGG16, VGG-19, and included feature extraction from deeper depths and estimate the validity of these models resulting efficient model compared to others [5]. An automated deep learning-based framework for detecting and classifying various diseases of mango plants were proposed. The data set uses of 1200 images containing both diseased and healthy mango leaves resulting accuracy of 96.67% [10]. Current leaf disease detection solutions in soybeans do not provide accuracy for several rare crop diseases such as frog eye spot, powdery mildew and Septorioia brown spot, so to fill the research gap to improve accurate results in leaf

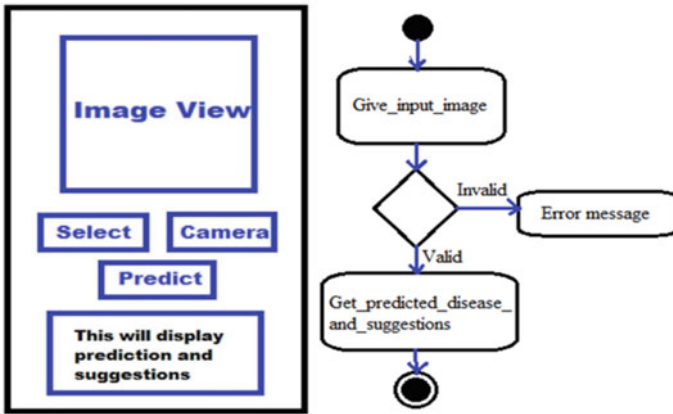


Fig. 1 GUI of mobile application and steps of predication

disease detection Deep belief network model of deep learning is used our research for better results.

2.1 Application for a User to Capture the Image

To enhance the application and make it user friendly an android mobile application is used for soybean crop leaf disease detection using Deep Learning and Image classification is Proposed system can detect three diseases such as frogeye leaf spot, powdery mildew, and septoria brown spot. The process of detection of disease in the mobile application is done as follows.

1. Capture the Image using the camera.
2. Click on the predict icon to preprocess and display the results of the prediction and suggestion.
3. Results in terms of suggestions and Predication are displayed in the text view as shown in Fig. 1.

2.2 Data Collection and Preprocessing

Data collection is an important and key step in developing deep learning models. In this study, he collected four different categorical data images of soybean crop foliage. The images include fresh images, toad leaf spot images, powdery mildew images, and septoria brown spot images [6–9]. In data preprocessing, the collected image data were rescaled to (224, 224, 3) format with a height of 224 pixels and a width of 224 pixels as a prerequisite for model building. Number 3 indicates the

RGB image format. We used data augmentation techniques to generate new images and increase the number of images. We split the entire image dataset into three parts: training dataset, validation dataset, and test dataset. We collected images from four different classes as shown in Fig. 2 and trained the overall data as shown in Table 1.

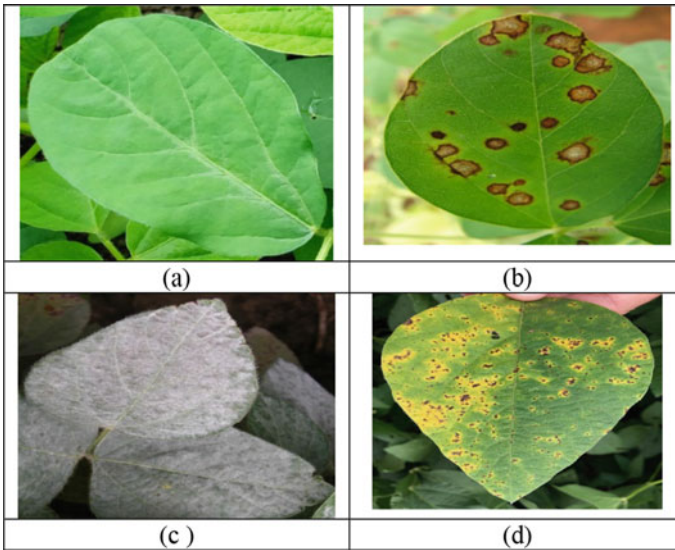


Fig. 2 Samples of Soybean leaf diseases **a** fresh leaf, **b** powdery mildew, **c** frog-eye leaf spot, **d** Septoria brown spot

Table 1 Image data details

	Training images	Validation images	Testing images	Total
Fresh	346	86	24	456
Frog-eye leaf spot	420	101	25	546
Powdery mildew	410	101	25	536
Septoria brown spot	420	100	25	545
Total	1596	388	99	2083

2.3 Deep Belief Network for Classification of Images and Identifying the Disease in Soybean Crops

A Deep belief network (DBN) is a Self generative deep learning algorithm with effective way to solve deep neural network problems using multilayer belief networks [14, 15]. DBN is a graphical neural network composed of several intermediate layers of Constrained Restricted Boltzmann Machines (RBMs) consisting of many visible and hidden layers mainly the last layer being a classifier as shown in Fig. 3 [16]. Unsupervised dimensionality reduction removes the classifier and uses a deep autoencoder network composed entirely of RBMs. Working with deep autoencoder networks involves two steps mainly pre-training and fine-tuning. In the pre-training phase each layer is processed and trained using the previous layer as the RBM. Low-dimensional features are captured from the input data by pre-training without losing information leading to accurate result convergence in the last layer. Here are the detailed steps:

1. Learn a layer of features from visible entities using a contrast divergence algorithm.
2. Treat previously trained feature activations as visible entities and learn feature by feature.
3. Finally, once the last hidden layer has been trained, the entire DBN is trained.

3 Results and Discussion

We used a transfer learning method to create an image classification model. Reusing a previously trained model for new problems is called transfer learning. To get accuracy, I worked on Deep Belief Network with about 1596 frames of training data. After training and evaluating the model, it showed good accuracy with a training loss of

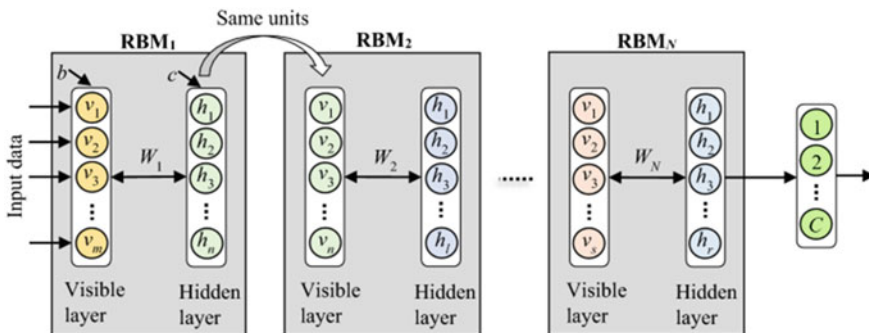
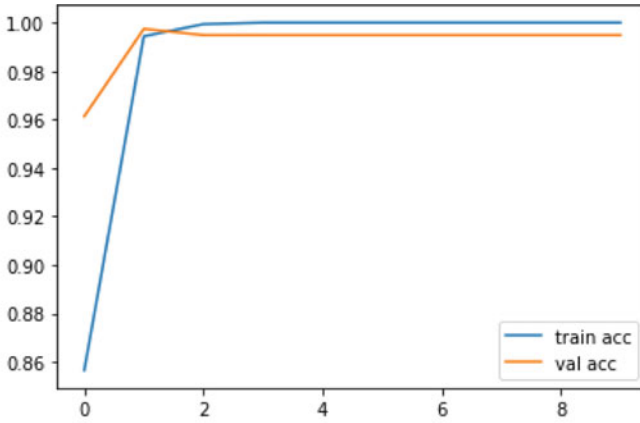
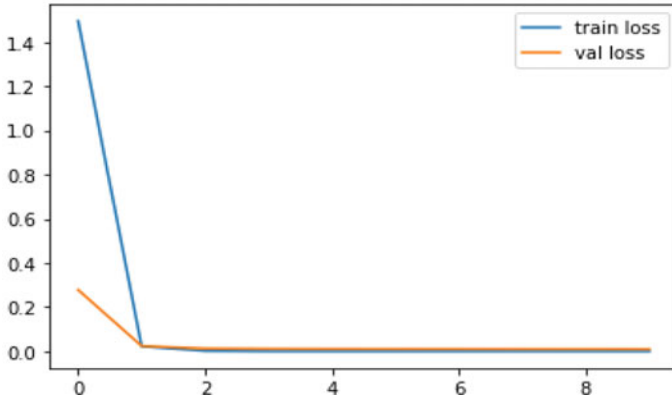


Fig. 3 Deep belief network

0.18%, a validation loss of 1.27%, a training accuracy of 99.82%, and a validation accuracy of 98.73%, as shown in Fig. 4.



(a)



(b)

Fig. 4 **a** Proposed method training and validation accuracy. **b** Proposed method training and validation loss

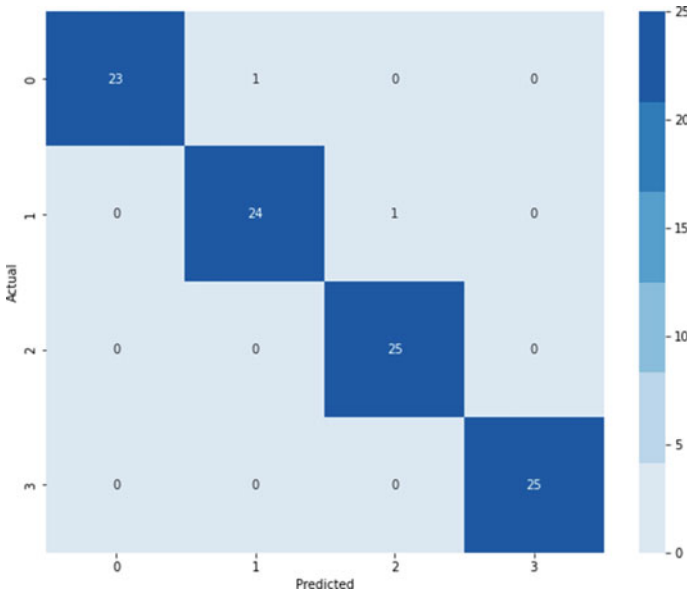


Fig. 5 Visualization of confusion matrix

3.1 Confusion Matrix

The confusion matrix [9, 10] describes the performance of the model. It is used to evaluate the model. Our need is to perform classification based on four different classes. Hence we have created a confusion matrix for multi-class classification. There are four classes as follows. 0: Fresh (Not a disease), 1: Frogeye Leaf Spot, 2: Powdery Mildew, 3: Septoria Brown Spot as shown in Fig. 5.

The confusion matrix [9, 10] represents the performance of the model. Used for model evaluation. What we need is to perform classification based on four different classes. Therefore, I created a confusion matrix for multiclass classification. There are four classes: 0: fresh (no disease), 1: frogeye leaf spots, 2: powdery mildew, 3: septoria brown spots, as shown in Fig. 5.

4 Conclusion

Agriculture is the economical backbone of our country and food is the basic need of all human beings due to the increase in population, there is a need for increasing agricultural food production. But due to environmental hazards maintaining Crop health and early detection of diseases is a challenging task. Soybean is a major crop in many regions. Which major source of food is grains and oil. So, it is important to identify soybean crop leaf diseases and protect the crop from these diseases at earlier

stages. Most farmers use traditional methods to identify crop diseases that may fail the prediction. In this paper a deep learning image classification model using DBN models by transfer learning technique is developed and to make the application user friendly we have built an android mobile application using android studio and the TensorFlow lite model. This application detects soybean crop leaf diseases such as frogeye leaf spots, powdery mildew, and septoria brown spot with an accuracy of 99.82%.

References

1. Krithika, P., & Veni, S. (2017). Leaf disease detection on cucumber leaves using multiclass support vector machine. In *2017 International Conference on Wireless Communications, Signal Processing and Networking (WiSPNET)*. <https://doi.org/10.1109/wispnet.2017.8299969>
2. Prakash, R. M., Saraswathy, G. P., Ramalakshmi, G., Mangaleswari, K. H., & Kaviya, T. (2017). Detection of leaf diseases and classification using Digital Image Processing. In *2017 International Conference on Innovations in Information, Embedded and Communication Systems (ICIIECS)*. <https://doi.org/10.1109/iciiecs.2017.8275915>
3. Mishra, B., Nema, S., Lambert, M., & Nema, S. (2017). Recent technologies of leaf disease detection using image processing approach—A review. In *2017 International Conference on Innovations in Information, Embedded and Communication Systems (ICIIECS)*. <https://doi.org/10.1109/iciiecs.2017.8275901>
4. Puttamadappa, C., & Parameshachari, B. D. (2019). Demand side management of small scale loads in a smart grid using glow-worm swarm optimization technique. *Microprocessors and Microsystems*, *71*, 102886. <https://doi.org/10.1016/j.micpro.2019.102886>
5. Pooja, V., Das, R., & Kanchana, V. (2017). Identification of plant leaf diseases using image processing techniques. In *2017 IEEE Technological Innovations in ICT for Agriculture and Rural Development (TIAR)*. <https://doi.org/10.1109/tiar.2017.8273700>
6. Fuentes, A., Yoon, S., & Park, D. S. (2020). Deep learning-based techniques for plant diseases recognition in real-field scenarios. In *Advanced concepts for intelligent vision systems* (pp. 3–14). https://doi.org/10.1007/978-3-030-40605-9_1
7. Thangaraj, R., Anandamurugan, S., & Kaliappan, V. K. (2020). Automated tomato leaf disease classification using transfer learning-based deep convolution neural network. *Journal of Plant Diseases and Protection*, *128*(1), 73–86. <https://doi.org/10.1007/s41348-020-00403-0>
8. Zhang, J., Yu, K., Wen, Z., Qi, X., & Kumar Paul, A. (2021). 3D reconstruction for motion blurred images using deep learning-based intelligent systems. *Computers, Materials and Continua*, *66*(2), 2087–2104. <https://doi.org/10.32604/cmc.2020.014220>
9. Wu, Y., & Xu, L. (2021). Image generation of tomato leaf disease identification based on adversarial-vae. *Agriculture*, *11*(10), 981. <https://doi.org/10.3390/agriculture11100981>
10. Sun, J., Yang, Y., He, X., & Wu, X. (2020). Northern maize leaf blight detection under complex field environment based on deep learning. *IEEE Access*, *8*, 33679–33688. <https://doi.org/10.1109/access.2020.2973658>
11. Kerkech, M., Hafiane, A., & Canals, R. (2020). Vine disease detection in UAV multispectral images using optimized image registration and deep learning segmentation approach. *Computers and Electronics in Agriculture*, *174*, 105446. <https://doi.org/10.1016/j.compag.2020.105446>
12. Harakannanavar, S. S., Rudagi, J. M., Puranikmath, V. I., Siddiqua, A., & Pramodhini, R. (2022). Plant leaf disease detection using computer vision and machine learning algorithms. *Global Transitions Proceedings*, *3*(1), 305–310. <https://doi.org/10.1016/j.gltp.2022.03.016>

13. Bag, V. V., & Kulkarni, U. V. (2017). Stock price trend prediction and recommendation using cognitive process. *International Journal of Rough Sets and Data Analysis*, 4(2), 36–48. <https://doi.org/10.4018/ijrdsda.2017040103>
14. Bag, V. V., Patil, M., Shinde, A., & Moulvi, S. (2022). Real-time detection of face mask and social distancing. *Applied Computer Technology*, 352–358. https://doi.org/10.1007/978-981-19-2719-5_33
15. Malage, R. N., & Patil, M. B. (2021). Location-based pomegranate diseases prediction using GPS. *International Journal of Innovative Computer Science and Engineering*, 375–383. https://doi.org/10.1007/978-981-33-4543-0_40
16. Ronoud, S., & Asadi, S. (2019). An evolutionary deep belief network extreme learning-based for breast cancer diagnosis. *Soft Computing*, 23(24), 13139–13159. Available at <https://doi.org/10.1007/s00500-019-03856-0>

Severity Detection of COVID-19 Patient's Using Machine Learning Techniques



Digambar Uphade and Aniket Muley

Abstract COVID-19 is a disease caused by a new corona virus called Severe acute respiratory syndrome corona virus 2 (SARS-CoV-2). Fever, dehydrated cough, tiredness, failure of flavor, overcrowding, painful throat and headache are the majority frequent symptoms of COVID-19. Due to the lack of useful information on the pathogenesis of COVID-19 and exact treatment, it highlights the significance of early diagnosis and suitable action. In this cram, our attention is to classify the patients as hospitalized and non-hospitalized. Statistical visualization plots were used to easily understand the concept. The machine learning (ML) classification algorithms were applied for performing this job. Further, proportional study is performed and finds the improved classification technique to categorize the respondents.

Keywords Classification · Machine learning · COVID · Performance

1 Introduction

A novel Covid (COVID-19) was famous in 2019 in Wuhan, China. Researchers all over the world are interested to find advance medicines for COVID-19. In the subsequent wave, there was disarray as per symptoms regardless of whether the patient ought to be confessed to the emergency clinic. Amongst the people who forward symptoms, the majority convalesce from the sickness without requiring health center treatment. Some genuinely unwell and have need of oxygen and scarcely any become basically sick and require escalated worry. Persons complete 60 years and over, and individuals with primary clinical evils like hypertension, heart and lung

D. Uphade (✉)

Department of Statistics, KRT Arts, BH Commerce and AM Science College, Nashik,
MS 422002, India
e-mail: dbuphade@gmail.com

A. Muley

School of Mathematical Sciences, Swami Ramanand Teerth Marathwada University, Nanded,
MS 431606, India
e-mail: aniket.muley@gmail.com

problems, diabetes, weight or malignant expansion, are at advanced risk of creating main disease. Difficulties prompting termination might include respiratory disappoointment, intense respiratory trouble condition (ARDS), sepsis and septic shock and additionally multiorgan disenchantment, together with damage of the heart, liver or kidneys. Notwithstanding, any person can become sick with COVID-19 and become really unwell or bite the dust at no matter what phase in life. According to our discernment we have zeroed in on COVID-19 patient's severity of hospitalized and non-hospitalized patients [1] "established that the XGBoost calculation performed with the most elevated precision ($> 85\%$) to anticipate and choose highlights that accurately show COVID-19 position for all age gatherings. Measurable examinations uncovered that the for the most part successive and critical prescient symptoms are fever (41.1%), hack (30.3%), lung contamination (13.1%) and runny nose (8.43%), while 54.4% of individuals analyzed fostered no symptoms". Debnath et al. [2] features the utility of proof based expectation devices in various medical settings, and how comparable models can be conveyed throughout the COVID-19 pandemic to direct emergency clinic bleeding edges and medical services heads to arrive at informed conclusions about understanding consideration and overseeing clinic volume. Guan et al. [3] "proposed the infection seriousness, age, serum levels of C-responsive protein hs-CRP, lactate dehydrogenase (LDH), ferritin, and interleukin-10 (IL-10) as huge indicators for death hazard of COVID-19, which might assist with recognizing the high gamble COVID-19 cases. Basic tree XGBoost model led by these highlights can foresee passing gamble precisely with greater than 90% precision and greater 85% awareness, as well as F1 scores greater than 0.90 in preparing and approval sets. Heldt et al. [4] have distinguished 15% patients that expected serious care, 7% patients requiring mechanical ventilation and 31% instances of in-emergency clinic mortality. The best model accomplishing region under the beneficiary working trademark (AUC-ROC) maximum scores of 0.76–0.87 (F1 scores of 0.42–0.60). Pan et al. [5] "Xtreme Gradient Boosting (XGBoost) model laid out with the 8 significant gamble factors showed the best acknowledgment capacity in the preparation set of 5-crease cross approval (AUC = 0.86) and the check line (AUC = 0.92). The alignment bend showed that the gamble anticipated by the model was in great concurrence with the real gamble. The 8-factor XGBoost model predicts hazard of death in ICU patients with COVID-19 well; it at first shows security and can be utilized really to anticipate COVID-19 guess in ICU patients." Roberts et al. [6] found that no papers in the writing at present have all of: (1) an adequately reported composition depicting a reproducible technique; (2) a strategy that follows greatest practice for fostering a machine learning model and (3) adequate outside approval to legitimize the more extensive materialness of the technique. Tezza et al. [7] noticed the Random Forest calculation beat the other MLTs in foreseeing in-medical clinic humanity, with a ROC of 0.84 (95% C.I. 0.78–0.9). Progress in years, along with crucial signs and lab boundaries (creatinine, AST, lymphocytes, platelets, and haemoglobin), were viewed as the most grounded indicators of in-emergency clinic mortality. Yan et al. [8] "have recognized three markers (LDH, hs-CRP, and lymphocytes) and, surprisingly, tracked down the early advance notice edges for COVID-19 prognostic expectation and fostered a XGBoost machine learning based

extrapolative model that can unequivocally foresee the endurance paces of extreme patients close over 90% exactness, empowering the premature identification, the near the beginning mediation and the decrease of mortality in high peril patients with COVID-19”.

The place of the survey is to perceive the classifier representation for the earnestness of COVID tolerant. In the following fragments framework, line of attack, result and explanation, and conclusions are discussed in feature.

2 Methodology

2.1 Data Collection

In this review, we have performed study through internet based survey Google structure to know the Covid-19 patients Symptoms. To gather the essential information, we have taken help of virtual entertainment sides' viz., WhatsApp, Facebook and email. This survey contained 33 inquiries connected with Covid-19 symptoms and diet. Generally, we have gotten 175 reactions. Here, we have played out a review based classification to distinguish the seriousness of hospitalized and non-hospitalized patients. To investigate this boundary we have applied ML calculations and assessed the exactness in light of huge boundaries. Clean and pre-process the gathered informational collection. Assess the informational collection with unaided learning strategies viz. graphical portrayal Identify the critical boundaries utilizing highlights determination method. Different classifier techniques applied on our dataset.

2.2 Feature Selection

Feature selection is a way of selecting the most relevant description from all features by removing irrelevant features. Here we used Chi square and an extra-trees classifier methods for feature selection.

2.3 Logistic Regression (LR)

LR is a Machine Learning categorization algorithm and is a particular case of linear regression in which the target variable is categorical in nature. It predicts the chance of incidence of a twofold outcome.

2.4 Decision Tree (DT)

DT is used to solve categorization problems this is supervised learning method. Decision tree mainly contains two nodes the Decision Node and Leaf Node. The conclusion is completed on the foundation of features of the specified dataset.

2.5 Random Forest

It is used to get better the presentation of the model. This method is based on the idea of ensemble learning, which is a procedure of combining manifold classifiers to resolve a compound difficulty.

2.6 Artificial Neural Network

It is copied from Biological neural networks that expand the arrangement of a human brain. Alike to the human brain that has neurons interrelated to one another; artificial neural networks also have neurons that are interrelated to one another in different layers of the networks. These neurons are identified as nodes. Artificial Neural Network mainly consists of 3 layers: Input Layer, hidden Layer and Output Layer.

2.7 Support Vector Machine (SVM)

It is simple classification method used for categorization problems in Machine Learning. The objective of the SVM algorithm is to produce the finest line or decision boundary.

2.8 K Nearest Neighbour Algorithm

This method is used for classification and regression problem. This algorithm comes under the Supervised Learning group. As the name suggests it considers K Nearest Neighbours to forecast the class of novel data point.

2.9 An Extra-Trees Classifier

This classifier fits a numeral of randomized decision trees on a variety of sub-samples of the dataset and uses mean to get better the prognostic correctness and manage over-fitting. The function is used to calculate the superiority of a split. To check the performance of the machine learning techniques the following measures are used (Eqs. 1–3):

$$\text{Accuracy} = \frac{(\text{TP} + \text{TN})}{(\text{TP} + \text{TN} + \text{FP} + \text{FN})} \quad (1)$$

$$\text{Precision} = \frac{\text{TP}}{(\text{TP} + \text{FP})} \quad (2)$$

$$\text{Recall} = \frac{\text{TP}}{(\text{TP} + \text{FN})} \quad (3)$$

where, True positive (TP), True Negative (TN), False Positive (FP), False Negative (FN).

Figure 1 represents our workflow of optimizing Severity detection of patient's via various ML tools. The flowchart is as follows.

3 Result and Discussion

3.1 Diagrammatic Representation

In this section, the results obtained through various learning are discussed in detailed.

Figure 2 gives details the HRCT scores of the COVID Patients it is observed that 69% of the cases having 0 HRCT score. Further, 21% of the COVID Patients having HRCT score between the range of 1–7 and 10% of respondent have HRCT scores above 8. Figure 3 represents place for Isolation 74% respondent use home for isolation, 20% use quarantine centre for isolation. Figure 4 explained that 45% respondent having symptoms dry cough. Figure 5 explores that 72% respondent blood oxygen level is normal and 28% having low. Figure 6 represents 85% respondent does not perform Neutrophil-Lymphocyte test and 12% having the score between 1 and 9 Fig. 7 Data reveal that 75% respondent does not required hospitalization and 25% required hospitalization.

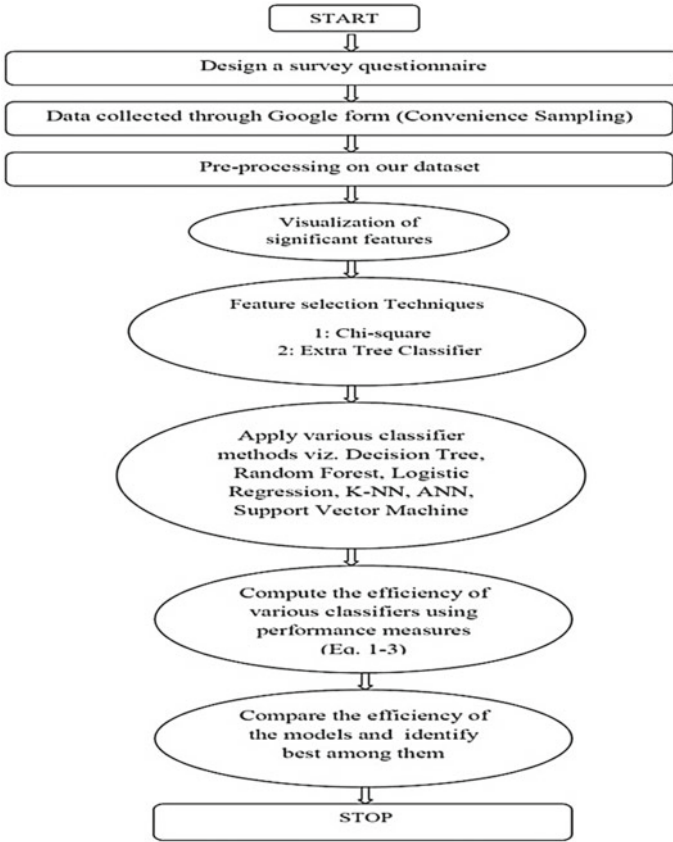


Fig. 1 Flowchart

Fig. 2 HRCT score test

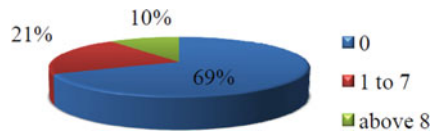


Fig. 3 Place for isolation

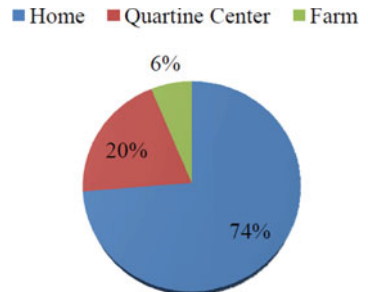


Fig. 4 Dry cough

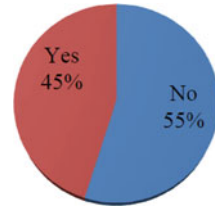


Fig. 5 Blood oxygen level

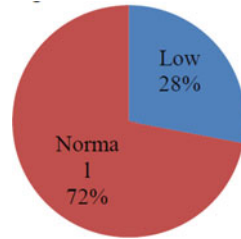


Fig. 6 N-L ratio (NLR)

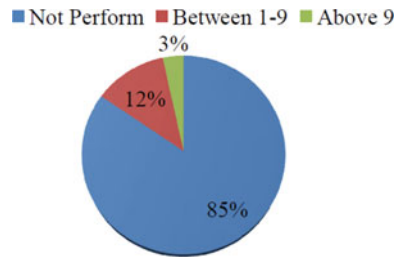
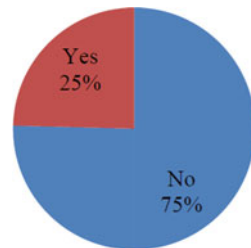


Fig. 7 Hospitalization



3.2 Feature Selection

It is necessary to classify the important features amongst overall parameters.

Table 1 give explanation the major features found by Chi-square test technique and observed that, HRCT Score, placed used for Isolation, N-L Ratio Dry Cough and Oxygen level are accumulating in data for additional investigation.

Table 1 Important features via Chi-square method

Feature	P-value
HRCT score	6.074997e-11
Placed used for isolation	1.665600e-05
N-L ratio	6.344384e-05
Dry cough	2.479871e-02
Oxygen level	4.372092e-02

Table 2 deals with the classification results obtained through various classifier techniques and it is observed that Logistic Regression and random forest gives high accuracy 87% as compared with other classifiers.

Table 3 explains the first five important features viz., HRCT Score, placed used for Isolation, N-L Ratio, Oxygen Level, and Number of Family Members are selected for further computation.

Table 2 Classification result by Chi-square method

Classifier	Accuracy score	Confusion matrix	Metrics classification report				
			Score	Precision	Recall	F1-score	Support
Decision tree	0.85	$\begin{bmatrix} 38 & 02 \\ 06 & 07 \end{bmatrix}$	0	0.86	0.95	0.90	40
			1	0.78	0.54	0.64	13
Random forest	0.87	$\begin{bmatrix} 37 & 03 \\ 04 & 09 \end{bmatrix}$	0	0.90	0.93	0.91	40
			1	0.75	0.69	0.72	13
Logistic regression	0.87	$\begin{bmatrix} 38 & 02 \\ 05 & 08 \end{bmatrix}$	0	0.88	0.95	0.92	40
			1	0.80	0.62	0.70	13
Neural network	0.85	$\begin{bmatrix} 40 & 00 \\ 08 & 05 \end{bmatrix}$	0	0.83	1.00	0.91	40
			1	1.00	0.38	0.56	13
SVM	0.85	$\begin{bmatrix} 39 & 01 \\ 07 & 06 \end{bmatrix}$	0	0.85	0.97	0.91	40
			1	0.86	0.46	0.60	13
K nearest neighbour	0.79	$\begin{bmatrix} 39 & 01 \\ 10 & 03 \end{bmatrix}$	0	0.80	0.97	0.88	40
			1	0.75	0.23	0.35	13

Table 3 Significant features through an extra-trees classifier

Feature	Value
HRCT score	0.12857702
Placed used for isolation	0.07816182
N-L ratio	0.05246101
Oxygen level	0.04902748
Number of family members	0.04176655

Table 4 Classification result by an extra-trees classifier

Classifier	Accuracy score	Confusion matrix	Metrics classification report				
			Score	Precision	Recall	F1-score	Support
Decision tree	0.80	$\begin{bmatrix} 30 & 03 \\ 06 & 05 \end{bmatrix}$	0	0.83	0.91	0.87	33
			1	0.62	0.45	0.53	11
Random forest	0.82	$\begin{bmatrix} 33 & 00 \\ 08 & 03 \end{bmatrix}$	0	0.80	1.00	0.89	33
			1	1.00	0.27	0.43	11
Logistic regression	0.82	$\begin{bmatrix} 32 & 01 \\ 07 & 04 \end{bmatrix}$	0	0.82	0.97	0.89	33
			1	0.80	0.36	0.50	11
Neural network MLP	0.86	$\begin{bmatrix} 32 & 01 \\ 05 & 06 \end{bmatrix}$	0	0.86	0.97	0.91	33
			1	0.86	0.55	0.67	11
SVM	0.75	$\begin{bmatrix} 30 & 03 \\ 08 & 03 \end{bmatrix}$	0	0.79	0.91	0.85	33
			1	0.50	0.27	0.35	11
K nearest neighbour	0.77	$\begin{bmatrix} 32 & 01 \\ 09 & 02 \end{bmatrix}$	0	0.78	0.97	0.86	33
			1	0.67	0.18	0.29	11

Table 4 reveals that, neural network gives high accuracy 86.36% as compared with other classifier techniques having high precision, recall and F-1 score.

4 Conclusion

Here in this case, our fundamental centre is to group patients to be hospitalized or not in view of different boundaries. That’s what this study uncovers, 58.48% of the persons having fever and intriguing truth is 12.50% of the general respondents have no symptoms except for they viewed as Covid-19 positive. Likewise, 75% of people don’t need hospitalization. At first, we have involved 33 boundaries for the review. Further, highlight determination procedures were utilized to recognize the critical boundaries. Here, two distinct methodologies were considered for highlight choice: Chi-square strategy and Extra tree classifier techniques. Our investigation communicated that Machine learning calculations reinforce the insightful precision and the discriminative viability of these arrangement. ML applications show expected output with maximum precision, awareness, and particularity utilizing various models. The likelihood of precision has been broke down from the qualities got from the enormous list of capabilities. The exploratory outcomes show the high precision for characterizing the patient’s hospitalization with extricated highlights. The near results in view of accuracy, precision, recall and F1-score measures are useful. Logistic Regression model and random forest gives high exactness 87% with high precision, recall and F-1 score by Chi-square technique. It is seen that, neural network gives high accuracy

86% when contrasted with other classifier procedures with high precision, recall and F-1 score by Extra tree classifier strategy.

References

1. Ahamad, M. M., Aktar, S., Rashed-Al-Mahfuz, M., Uddin, S., Liò, P., Xu, H., Summers, M. A., Quinn, J. M., & Moni, M. A. (2020). A machine learning model to identify early stage symptoms of SARS-Cov-2 infected patients. *Expert Systems with Applications*, *160*, 113661.
2. Debnath, S., Barnaby, D. P., Coppa, K., Makhnevich, A., Kim, E. J., Chatterjee, S., Tóth, V., Levy, T. J., Paradis, M. D., Cohen, S. L., & Hirsch, J. S. (2020). Machine learning to assist clinical decision-making during the COVID-19 pandemic. *Bioelectronic Medicine*, *6*(1), 1–8.
3. Guan, X., Zhang, B., Fu, M., Li, M., Yuan, X., Zhu, Y., Peng, J., Guo, H., & Lu, Y. (2021). Clinical and inflammatory features based machine learning model for fatal risk prediction of hospitalized COVID-19 patients: Results from a retrospective cohort study. *Annals of Medicine*, *53*(1), 257–266.
4. Heldt, F. S., Vizcaychipi, M. P., Peacock, S., Cinelli, M., McLachlan, L., Andreotti, F., Jovanović, S., Dürichen, R., Lipunova, N., Fletcher, R. A., & Hancock, A. (2021). Early risk assessment for COVID-19 patients from emergency department data using machine learning. *Scientific Reports*, *11*(1), 1–13.
5. Pan, P., Li, Y., Xiao, Y., Han, B., Su, L., Su, M., Li, Y., Zhang, S., Jiang, D., Chen, X., & Zhou, F. (2020). Prognostic assessment of COVID-19 in the intensive care unit by machine learning methods: Model development and validation. *Journal of Medical Internet Research*, *22*(11), e23128.
6. Roberts, M., Driggs, D., Thorpe, M., Gilbey, J., Yeung, M., Ursprung, S., Aviles-Rivero, A. I., Etmann, C., McCague, C., Beer, L., & Weir-McCall, J. R. (2021). Common pitfalls and recommendations for using machine learning to detect and prognosticate for COVID-19 using chest radiographs and CT scans. *Nature Machine Intelligence*, *3*(3), 199–217.
7. Tezza, F., Lorenzoni, G., Azzolina, D., Barbar, S., Leone, L. A. C., & Gregori, D. (2021). Predicting in-hospital mortality of patients with COVID-19 using machine learning techniques. *Journal of Personalized Medicine*, *11*(5), 343.
8. Yan, L., Zhang, H. T., Xiao, Y., Wang, M., Sun, C., Liang, J., Li, S., Zhang, M., Guo, Y., Xiao, Y., & Tang, X. (2020). Prediction of criticality in patients with severe Covid-19 infection using three clinical features: a machine learning-based prognostic model with clinical data in Wuhan (p. 27). MedRxiv

Fashion Classification Model



Sanika Rawate, Kuldeep Vayadande, Shivam Chaudhary, Sakshi Manmode, Resham Suryavanshi, and Kunal Chanda

Abstract These days there are two main problems which the ecommerce industry is facing, the first problem is where the sellers find it difficult to post a picture of a clothing item on their website or any platform for sale, sometimes it can lead to misclassifications of a any clothing item or can lead to absence from search results. Another problem which concerns is in placing an order when the customer is unaware of the product or doesn't know the name of the product but has the picture representation of it. Hence by allowing buyers to click a photograph of an object and then search for the related products without actually typing for the product name, an image-based search algorithm can help ecommerce reach its full potential. We have proposed a Fashion Classification Model which will classify the image and put them into that specific category.

Keywords Fashion · Classification model · Clothing · Product

1 Introduction

By delivering a hassle-free shopping experience as well as delivery to an individual, e-commerce has unleashed a bigger desire for products because of the number of consumers present globally. We discuss two difficulties facing the industry, one from the stand point of the seller and the other from the standpoint of the buyer [1].

Whenever the seller wants to sell his product online on a platform, seller has to click a picture and tag with the help of appropriate labels to make sure it reaches the buyer or appears in the search list. It becomes difficult for a human to process each and every image and put them into respective categories, so here machine learning comes to the rescue, the machine classifies the image and puts them into respective categories hence the problem of classification arises [2]. Therefore, a model is required to classify the images and put them into the right category. We

S. Rawate (✉) · K. Vayadande · S. Chaudhary · S. Manmode · R. Suryavanshi · K. Chanda
Department of Information Technology, Vishwakarma Institute of Technology, Pune,
Maharashtra, India
e-mail: sanika.rawate19@vit.edu

are creating model where we will be using “fashion_mnist” which will train the dataset and test the dataset. This dataset is more diverse as it enables us to learn complicated properties, to distinguish the images. Generally, the accuracy for these models is around 70–80% but we are able to get the accuracy of 93.1% by applying different layers to the model like dense, max pooling, convolutional layers etc. We have created such a model by which the error rate is low which will help the seller to upload their image and the model will classify the image and put them into that specific category and the buyers as well to search directly by the image rather than typing the name of that clothing item [4].

2 Literature Survey

2.1 VGGNet-16

VGGNet-16 contains 16 convolutional layers and is very different as it has a uniform architecture. Similar to Alexnet, it has 3×3 convolutions, but contains a lot of filters. Also, it can be train in 2–3 weeks on 4 GPUs. Nowadays, in the community this method is preferred for extracting features from the images [4]. It is possible to load a pre-trained version of the network trained model on more than a million images from the ImageNet database and pretrained model can classify the images as dog, cat, cow, calf etc. Hence, this network has learned rich feature representation from a vast variety of images. 224×224 is the input image size which is accepted by the network [3] (Fig. 1).

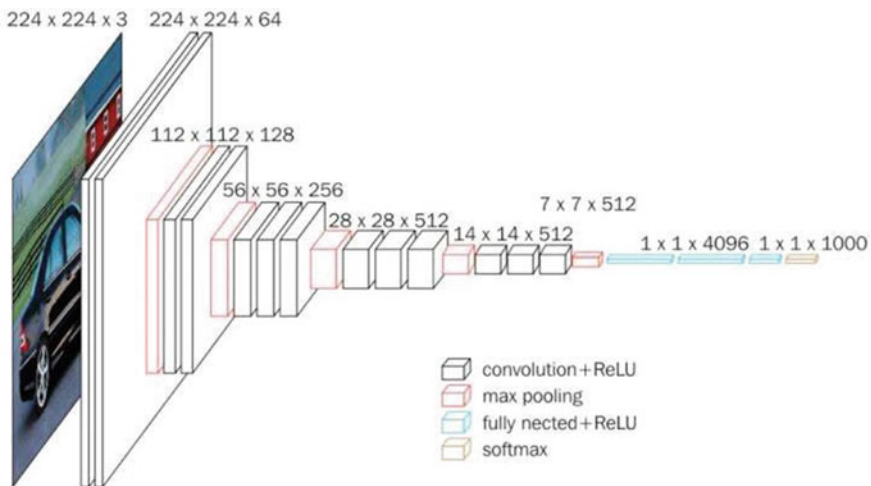


Fig. 1 VGG16—convolutional network for classification and detection [10]

2.2 Inception

Inception V3 is a deep learning model which is based on convolution neural networks generally used for image classification. Inception V3 is a superior model to inception V1 which was introduced back in 2014 by GoogleNet [3]. It is an image recognition model that gives an accuracy of more than 78.1% on ImageNet dataset. In a model when multiple amounts of deep layers of convolutions were used. It uses multiple filters of different sizes on the same level. Thus, in this model rather than having too deep layers we have parallel layers which makes the model wide instead of making it deeper.

2.3 ResNet 152 V2

Resnet is the short form for Residual Networks, it is a classic neural network mainly used for many computers vision tasks. Residual network is a CNN (convolutional neural network) architecture that overcomes the “vanishing gradient” problem. Deep ResNets are formed by stacking the residual blocks on top of each other and they go up to hundred layers per network. It is effective in deriving parameters from early activations further down the network [6]. On the other hand, the model ResNet deals with a very deep neural networks with 150+ layers. Resnet 152 V2 has a very deep network up to 152 layers in itself. Rather than of learning the signal representation directly the model learns the representation functions first [7].

3 Proposed Model

We have classified clothing items into 10 categories namely t-shirt, pullover, shirt, Trouser, dress, coat, bag, sandal, sneaker and ankle boot. We have achieved 93% accuracy for our model. Whenever a user uploads a picture. This model will classify the image of the clothing item then will put that image into its specific category. For gray level, color, motion, depth hidden Markov models are applied, few other models re supported by Bayesian belief model.

4 Methodology

4.1 Data Collection

The initial step to start a project is data collection wherein we select the subgroup of the data that we have and will be working with.

All the machine learning algorithms start with data which can consist of samples or the remarks for which we already are familiar with the target answer [5]. The data for which we already recognize the target answer is known as labeled data. Here for our model, we have used the “fashion_mnist” dataset.

4.2 Dataset Analysis

The dataset we are using is Fashion-MNIST of pictures Zalando’s dataset which consist of 60 K examples in the training set whereas approximately 10,000 examples in the test set. Every type in the dataset consists of a grayscale image which is attached to any 1 of the 10 classes mentioned and is of size 28×28 . For benchmarking machine learning techniques, the Fashion-MNIST dataset can easily be swapped in for the actual MNIST dataset [4].

There are some particular reasons as to why we rely the most on fashion_mnist dataset First reason is that we have a huge number of results to distinguish with, as some researchers use new methods and it has a decent level of accuracy and doubtfully any classifier can attain a perfect score on it, so there remains a scope for optimization. In short, the Fashion “MNIST” dataset is very much diverse, requiring machine learning (ML) methods to learn more complicated properties in order to consistently distinguish specific classes.

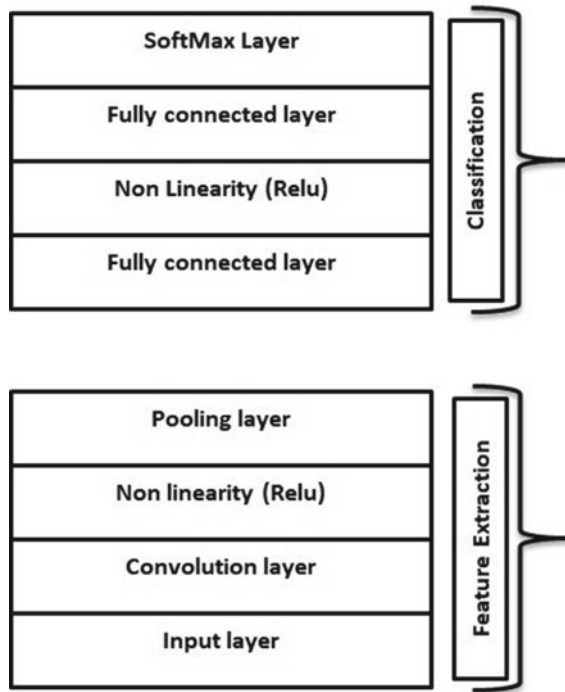
Deep neural networks have recently been applied to a wide range of problems to achieve remarkable results. Convolutional neural networks, in particular, have demonstrated outstanding results in image classification, image segmentation, laptop vision difficulties, and linguistic communication process problems [4]. Few probabilistic models, such as Bayesian Belief Networks (BBN) and Hidden Markov Models (HKM), have been used to categorize images with choices that comprise gray level, color, motion, depth, and texture. We have a propensity to examine the topic of categorizing Fashion “MNIST” images with convolutional neural network [2] (Fig. 2).

4.3 Machine Learning

The work on building software applications being accurate in predicting the results and outcomes which will not need any external programming help. Algorithms of machine learning use the data which is already present in the past as an input so that it can predict the new outcomes. Machine Learning can help industries and companies to understand as well as examine their customers and consumers subordinately.

In addition to this, predictive learning method can help in the formation of operating systems (OS) of self-driving cars, for example, Tesla [5]. Data of the consumers is collected and correlated with their behaviors all the time. Machine Learning is used

Fig. 2 Flow chart of the project



as an important as well as the primary driver for the business models of the companies such as Uber. They use certain ML algorithms which help in finding the driver to a rider (user). In search engine industries like Google, the algorithms of machine learning are used in the advertisement sector while surfing and searching. Machine Learning always focuses on making the prediction more accurate. The selection of approach, as well as algorithm, solely depends upon the type of data and information which is to be predicted [8].

4.4 CNN

4.4.1 Convolutional Neural Network

It is a deep learning neural network mainly used for processing the structured array of data such as portrayals. The main feature of CNN is that, it doesn't need any preprocessing; it can run directly on any underdone image [8]. Also, this algorithm is very competent in recognizing lines, circles, gradients or even face or eyes in an image. This characteristic makes this algorithm very strong (Fig. 3).

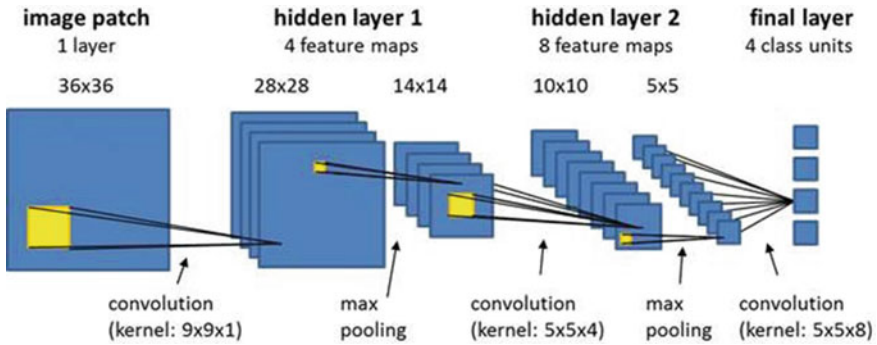


Fig. 3 CNN (convolutional neural network)

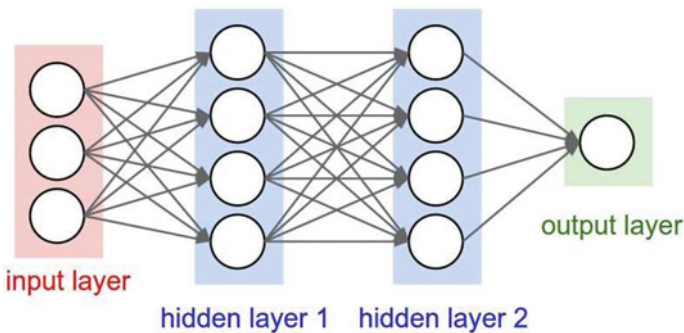


Fig. 4 Dropout layer [9]

4.4.2 Dropout

Dropout layer is a layer used in the CNN algorithm, mainly applied to the input vector where it nullifies some of its features or can be applied to the hidden layers, where it nullifies the hidden neurons [8]. The main reason why dropout layer is being used is, it prevents overfitting in the training dataset. Inputs which are not set to 0 are scaled up by $1/(1 - \text{rate})$ so that the total sum remains exact same [2] (Fig. 4).

4.4.3 Optimizer

Optimizers are methods or algorithms in neural networks which help to change the attributes such as weights etc. to reduce the losses and improves the accuracy. Optimizers help to get the results faster. They shape or mold the model to get the most accurate form [5].

4.4.4 Dense

Dense layer is a commonly used layer. It is a deeply connected neural network layer. It consists of a layer of neurons in which neurons receive input from the previous layer hence it is known as a dense layer. This layer classifies the images based on the output from convolutional layer. Here one layer contains multiple amounts of neurons.

5 Results

For excellent performance, deep neural networks are applied to various issues in deep neural networks. In image classification, image segmentation, laptop vision issues and linguistic communication process issues CNN has shown magnificent results [8]. Some probabilistic models supported by Bayesian Belief Networks and Hidden Markov Models have conjointly been applied to image classification issues with options supported gray level, color, motion, depth, and texture (Table 1; Fig. 5).

These are the graphs of model loss and model accuracy which we achieved in the research (Fig. 6).

Table 1 Accuracy versus loss

Product	Val accuracy	Val loss
Category	0.9324	0.4631

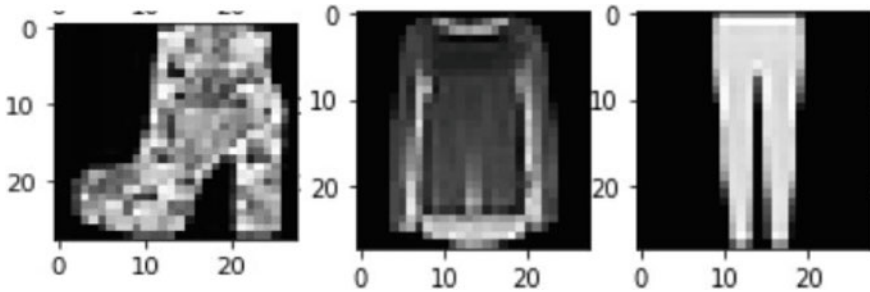


Fig. 5 Classification the class

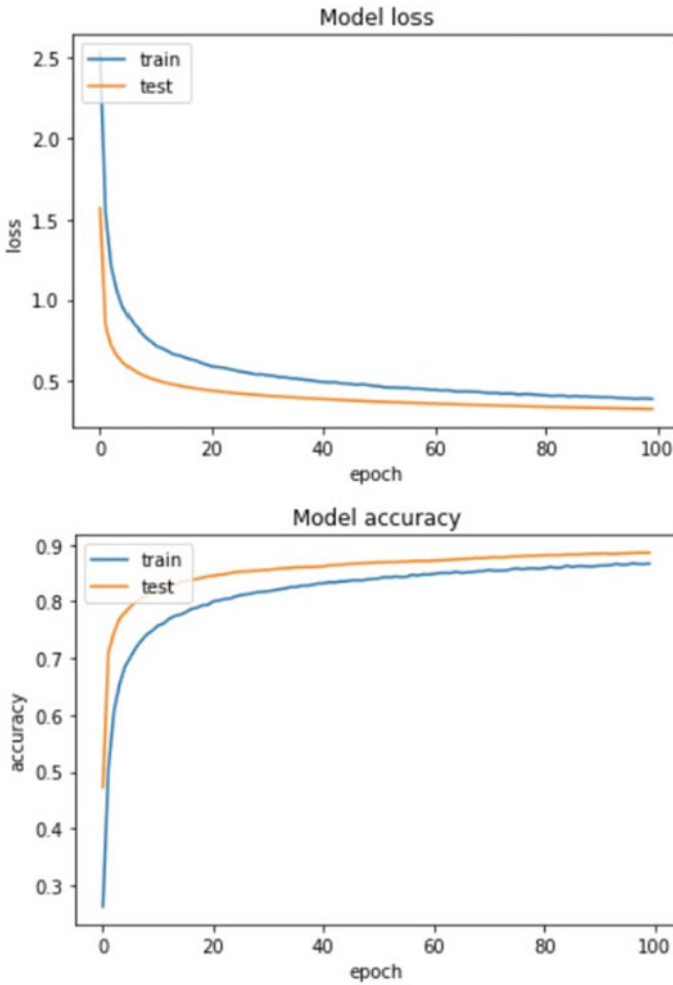


Fig. 6 Validation accuracy from classification

6 Conclusion and Future Scope

Deep neural networks have been used to solve a variety of problems in recent years. The potential application for picture classification is the detection of counterfeit goods (Nvidia 2018). An in-depth examination of a brand’s logo’s characteristics, such as design, colors, and placement, can aid in the detection of counterfeit goods. We may potentially use a generative adversarial network (GAN) to come up with new fashion accessory designs and reduce our reliance on human creativity, thanks to significant advances in processing power and machine learning methods.

References

1. Russakovsky O, Deng J, Su H, Krause J, Satheesh S, Ma S, Huang Z, Karpathy A, Khosla A, Bernstein M, Berg AC, Fei-Fei L (2015) ImageNet large scale visual recognition challenge. *IJCV*
2. Iwata T, Watanabe S, Sawada H (2011) Fashion coordinates recommender system using photographs from fashion magazines. In: *IJCAI*
3. Veit A, Kovacs B, Bell S, McAuley J, Bala K, Belongie SJ (2015) Learning visual clothing style with heterogeneous dyadic co-occurrences. In: *ICCV*. [Online]. Available <http://arxiv.org/abs/1509.07473>
4. Liu S, Feng J, Song Z, Zhang T, Lu H, Xu C, Yan S (2012) Hi, magic closet, tell me what to wear! In: *ACM Multimedia*, ser. MM' 12, pp 619–628
5. Chen K, Chen K, Cong P, Hsu WH, Luo J (2015) Who are the devils wearing Prada in New York city? In: *Proceedings of the 23rd ACM international conference on journal of information and computational science*, vol 10(3). ACM, pp 177–180. ISSN 1548-7741 250, www.joics.org *Multimedia*
6. Hidayati SC, Hua K-L, Cheng W-H, Sun S-W (2014) What are the fashion trends in New York? In: *Proceedings of the 22nd ACM international conference on multimedia*. ACM, pp 197–200
7. Liu S, Song Z, Liu G, Xu C, Lu H, Yan S (2012) Street-to-shop: cross-scenario clothing retrieval via parts alignment and auxiliary set. In: *CVPR*, pp 3330–3337
8. Kiapour MH, Han X, Lazebnik S, Berg AC, Berg TL (2015) Where to buy it: matching street clothing photos in online shops. In: *ICCV*, pp 3343–3351
9. <https://ai-pool.com/a/s/dropout-in-deep-learning>
10. <https://neurohive.io/en/popular-networks/vgg16>

Implementation of Environmental Parameters Monitoring and Alert System for Underground Mining Using Internet of Things with LoRa Technology



Sandi Kumar Reddy, Anil S. Naik, and Mandela Govinda Raj

Abstract Underground mines have a challenging environment and are affected by environmental factors such as toxic and flammable gases that affect productivity and safety. In response to the mining industry's challenges, wireless communication technology is widely adopted to monitor underground environmental parameters, track mine machinery, and workers, and establish remote communication systems between transmitter and receiver. Variation in mine environmental parameters leads to gas accidents and damage to the mine site structure. In this paper, Sx1278 LoRa 433 MHz transceiver module and ESP32/ESP8266 Wi-Fi Module are integrated with DHT 22 temperature sensor implemented to collect real-time temperature and humidity parameters. The system raises an early warning of any hazardous events. A mine safety and alert system are proposed for the underground mine site. The developed LoRa-based system can deploy in an underground mining area to monitor the real-time environmental parameters and to avoid dangerous gas accidents.

Keywords Internet of things · Lora · Gas sensors · Underground mine · Toxic gases · Environmental parameter monitoring · Blynk

1 Introduction

Underground mines working conditions are riskier and hazardous in nature compared to surface mining. Most of the accidents reported in underground mines are due to sudden increases in levels of gas concentrations such as carbon monoxide (CO), and methane (CH₄) in underground mine air. Reduction of oxygen (O₂) level and increase in carbon dioxide (CO₂) causes the death of mine workers [1]. Mine gases such as methane (CH₄), carbon monoxide (CO), carbon dioxide (CO₂), nitrogen (NO_x), and hydrogen sulfide (H₂S) are commonly found in underground mines. In general, 78% of nitrogen, 21% of oxygen, and 1% of other gases by volume are

S. K. Reddy · A. S. Naik (✉) · M. G. Raj
National Institute of Technology Karnataka, Surathakal 575025, India
e-mail: anilснаik.217mn001@nitk.edu.in

in the earth's atmosphere. However, the air composition in underground mines is completely changing due to the structure of mine strata, ventilation air streams, and chemical reactions. The strata gas that occurs in underground mines is methane and carbon dioxide. The use of heavy diesel-operated vehicles and the burning of fuels or explosives generate various gas pollutants [5].

Underground mine gas explosion is caused by toxic gases and more death rate is recorded in mines across the world. The effect of gases on mine workers' health is asphyxiation, headache, unconsciousness, skin burn, and also death if the gas concentrations exceed certain threshold limit values (TLV) [14]. Identification of hazardous areas in an underground mine is necessary so the mine workers should be alert or knowledgeable of hazardous areas to handle the situation in advance [3]. The gas hazards such as combustible gas hazards, where the atmosphere contains explosive gases, dust, or vapor, and toxic gas hazards, where the toxic gases are not visible and do not produce a smell. The toxic gases are inhaled or absorbed by the eyes and skin of mine workers in underground mines. It also affects living tissues and the nervous system, headaches, long-term health issues, and even death [11, 18].

The dynamic nature of gas is such that it spreads at any time in underground mine working areas or abandoned mine, which is not operational. As per the investigation report few gas accidents are recorded because of mine lamps and cables in underground mines. The wired monitoring system is not suitable as the wired system is a fixed network setup and any damage to the wired system will cost more for maintenance. The rapid development of wireless communication technology has benefitted many industries and can adapt to underground mines to monitor environmental parameters in a real-time scenario. To avoid gas accidents in underground mine areas, the integration of gas sensors into communication modules to monitor the gas level in a real-time is required. The monitoring system should generate an early warning if a gas level exceeds a certain threshold limit value to avoid hazards [4]. A safe working environment is required for mine workers to increase productivity and production by adapting wireless communication technology. ZigBee-based wireless safety monitoring system suitable to monitor the environmental parameters in underground mines [2, 3].

Underground mine disasters occur frequently causing loss of life and unsafe environmental effects on production and productivity. The disasters are due to mine working conditions and the dynamic and complex mine strata environment. It is necessary to monitor the mine condition in a real-time to avoid disasters or gas accidents [13]. The main aim of this paper is to describe the design and development of LoRa based IoT implementation of real-time monitoring of environmental parameters in underground mines.

2 System Architecture for Underground Mine Automation

2.1 Proposed LoRaWAN Based IoT System

The Proposed system consists of the LoRa shield node, sensors, and LoRaWAN gateway. Sensors CO, CH₄, H₂S, temperature, and humidity are connected to the Arduino board, which is connected to the LoRa node as shown in Fig. 1. The circuit schematic of the Arduino board with sensors and a LoRa interface to transmit data to the LoRaWAN cloud gateway [8] is represented as shown in Fig. 2. IoT kit based on LoRaWAN Gateway provides communication between LoRa nodes and LoRa gateway is 500 m to nearly 5 km distance in line of sight. The open-source IoT kit available in the market helps researchers to develop applications and it contains one multi-Channel gateway, two LoRa modules as per frequency configuration (865–868 MHz), two Arduino UNO boards to integrate sensors, and a few sensors with other electronics components to perform practical research work [7, 21]. The proposed reliable IoT with a LoRa-based system can deploy in underground mines to monitor the environmental parameters in real time.

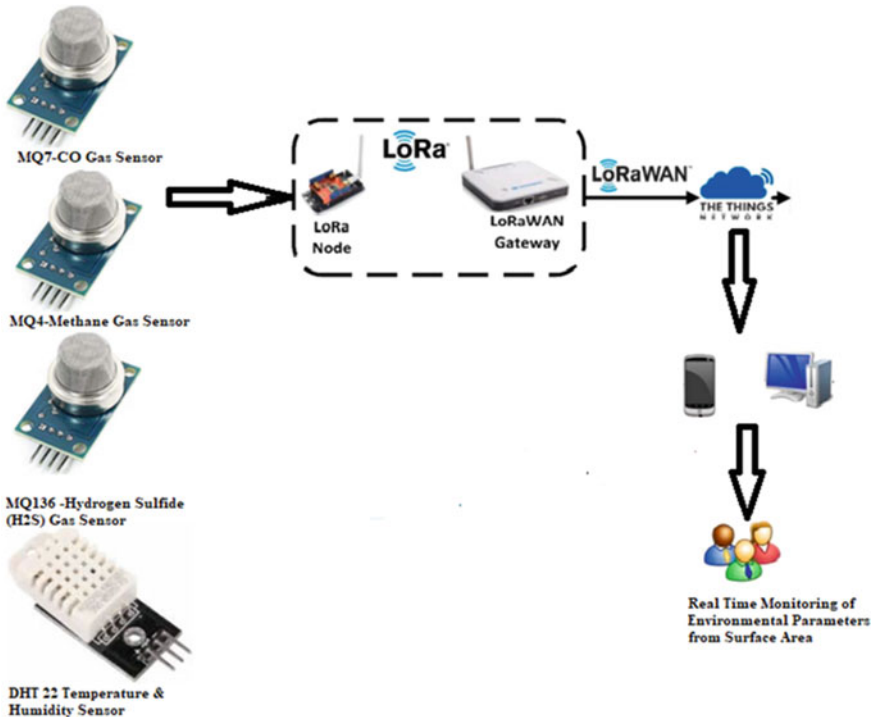


Fig. 1 Proposed LoRaWAN IoT system to monitor the environmental parameters in underground mining

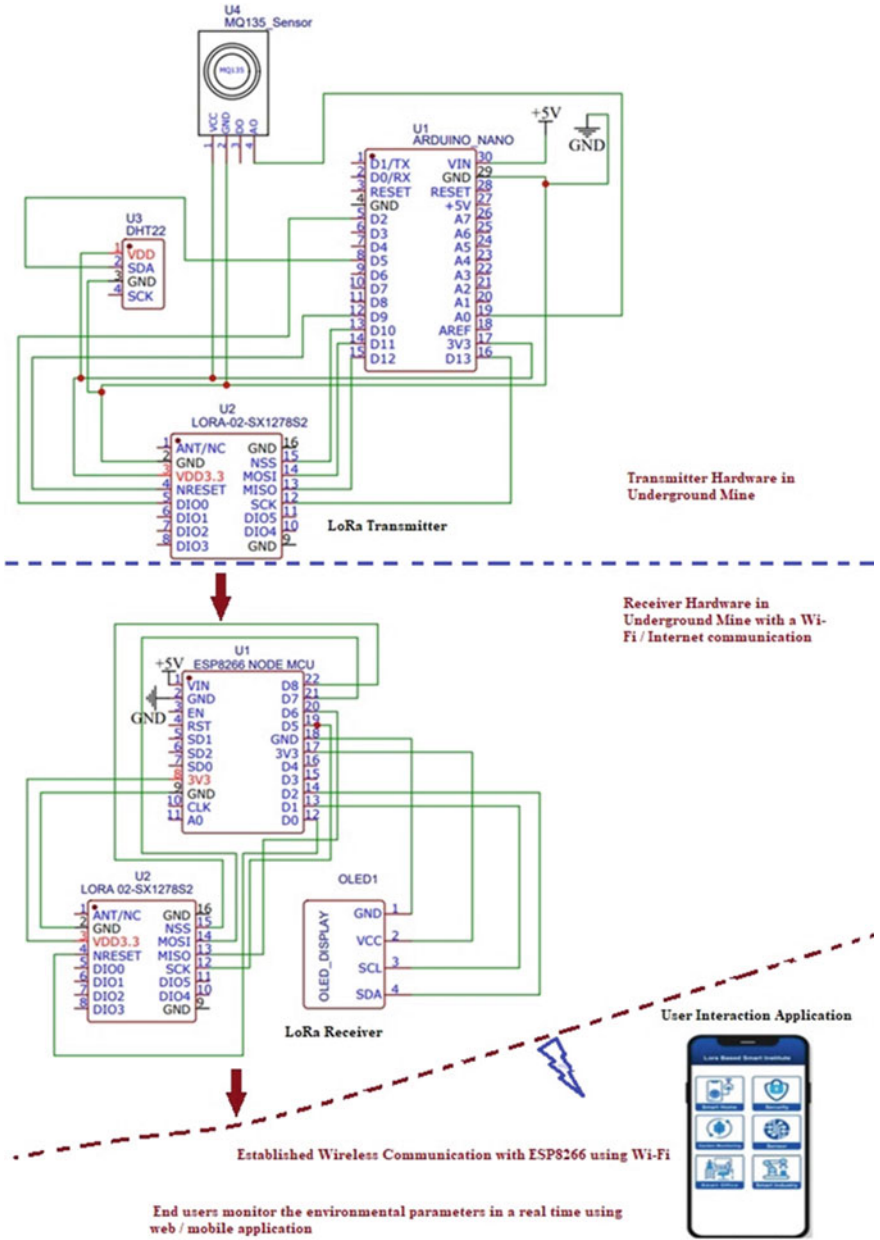


Fig. 2 Circuit diagram of the automation system for monitoring environmental parameters in a laboratory setup

2.2 Circuit Diagram of the Automation System at Laboratory Level Setup

The proposed system for smart automation is implemented by considering low-cost and reliable Sx1278 LoRa-02 (433 MHz) modules, NodeMCU ESP8266, an MQ-135 air quality sensor, and DHT 22 temperature and humidity sensor at the laboratory level setup. The circuit diagram is represented as shown in Fig. 2. The system has been divided into transmitter and receiver sections. The transmitter section consists of an Arduino NANO board and Sx1278 LoRa-02 transceiver module with the integration of a DHT 22 temperature and humidity sensor and MQ 135 air quality sensor [10] to measure the air quality in a surrounding environment at the surface level [6].





The LoRa transmitter will send the environmental parameter values such as temperature in degrees Celsius, humidity in percentage, and air quality level in a parts per million (PPM) to the LoRa receiver in a wireless mode of communication. The receiver side consists of the Sx1278 LoRa-02 transceiver module connected to the NodeMCU ESP8266 Wi-Fi-enabled module [15]. LoRa module receives the data from the transmitter section, ESP8266 Wi-Fi-enabled board uploads the sensed environmental parameters to the IoT-based server. The available open-source platform such as ThingSpeak [19] or Blynk IoT platform [20] is used to monitor the environmental data anywhere across the world in a web and mobile application dashboard.

Once the developed system is implemented successfully at a surface level and established communication then the system can be deployed in a selected underground mine to monitor the environmental parameters by enclosing hardware components in enclosures. The transmitter section hardware components are deployed in an underground mine working area to collect the environmental parameters. The receiver section hardware components are deployed in a location where an internet access facility is available through a Wi-Fi connection [9]. Once the network is established then NodeMCU ESP8266 sends data to the cloud server. The data stored in the cloud platform is processed for visualization and analysis as shown in Fig. 2. List of hardware components used to develop the system and their features are described in Table 1.

2.3 Hardware Setup and Experimental Results

The hardware implementation of LoRa based IoT system with the Blynk application at a laboratory level setup is shown in Fig. 3. The transmitter section integrated with LoRa modules with DHT 22 temperature sensor is connected to the Arduino NANO board. The receiver section consists of a NodeMCU ESP8266 Wi-Fi module connected to LoRa receiver and OLED display unit to display the sensed parameters and the same data is visualized in a Blynk IoT platform by users anywhere from the web or mobile application dashboard. The temperature and humidity values were

Table 1 Description of different sensors employed in the smart automation system

List of components	Description
 <p>Arduino NANO Development Board</p>	<p>Arduino NANO is an open-source development board based on an 8-bit microcontroller. It facilitates communication by connecting it to a computer and programming with Arduino IDE software [12]</p>
 <p>Sx-1278 LoRa-02</p>	<p>Sx1278 LoRa-02 Radio Frequency module is used for long-range wireless communication. Its low power (3.3 v) and high sensitivity is -148 dBm. In India, the unlicensed frequency range of the LoRa module is 865–867 MHz but the 433 MHz frequency-based LoRa modules can use for academic purposes [12]</p>
 <p>ESP8266 Node MCU Wi-Fi module</p>	<p>Development board ESP 8266 NodeMCU Wi-Fi module enables the microcontroller to load data to the IoT platform. It Supports UART or GPIO data communication interface [12, 16]</p>
 <p>DHT 22 Sensor</p>	<p>DHT 22 sensor to measure the temperature and humidity of an environment connected to an Arduino board. Its temperature measurement range is $(-40$ to $+125$ °C) with an operating voltage of 3–5 v. DHT 22 sensor contains a humidity sensing component and a thermistor temperature sensor. A semiconductor thermistor consists of a variable resistor. As the resistance changes with a change in the temperature [17]</p>

recorded as 20.10 °C and 61.40% respectively in the display unit as well as in the Blynk IoT mobile platform. The circuit connections are based on Fig. 2 with a consideration of only the DHT 22 sensor [8].

3 Conclusion and Future Work

An IoT with a LoRaWAN gateway system is proposed in this study and implemented IoT with LoRa based system at a laboratory scale to monitor the environmental parameters in real-time. Sx1278 LoRa-02, 433 MHz LoRa module is low-cost, long-range, low-power, and unlicensed radio frequency specification network architecture and is suitable for research purposes to develop applications. The receiver LoRa module is integrated with NodeMCU ESP8266 Wi-Fi microcontroller unit and Blynk cloud platform to monitor the values of the environmental parameters from anywhere and anytime. The temperature and humidity data can be easily accessed

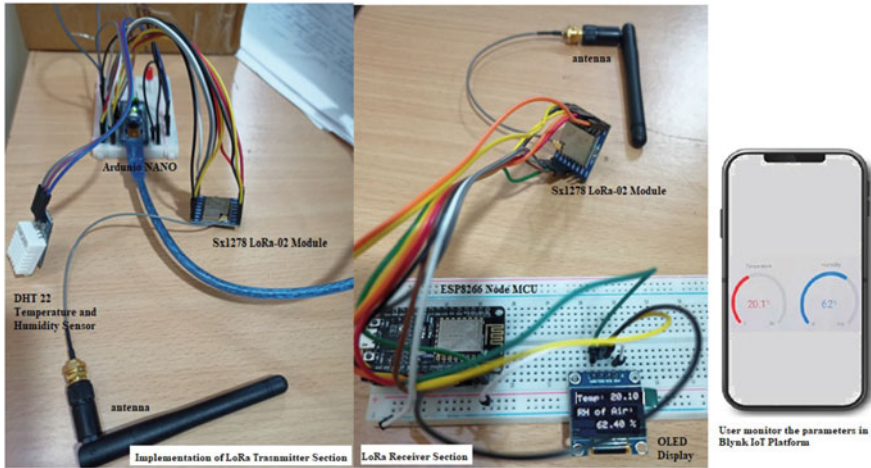


Fig. 3 Hardware implementation of environmental parameters monitoring with LoRa transceiver modules and IoT platform

from the Blynk mobile IoT platform. The system also configures to visualize the data from the web-based Blynk IoT platform. The system can be extended with an integration of multiple gas sensors as specified in a proposed system to monitor the environmental parameters and can deploy in underground mines. The sensor nodes acquire the environmental parameters and send the acquired data to the cloud to store and process. The system can also be configured to compare data with historic data or exceeds the threshold limit value and immediately send an alert or notification to the supervisor or concerned authority for requesting emergency assistance. In the Underground mining industry, the safety of mine workers is the main concern in the prevention of accidents. Establishing reliable communication in the underground mines by adopting IoT with wireless technology is challenging as the structure of the underground mine is different compared to surface-level open cast mines and radio signals drop due to mine strata and working conditions of mines. The reliable IoT-based system can design as per the mine structure and it will benefit mine workers and organizations in terms of safety and productivity.

References

1. Mandal, A., & Sengupta, D. (2000). The analysis of fatal accidents in Indian coal mines. *Calcutta Statistical Association Bulletin*, 50(1–2), 95–120.
2. Na, C., & Yi, M. (2011). Specific statistics and control method study on unsafe behavior in Chinese coal mines. *Procedia Engineering*, 26, 2222–2229.
3. Mu, L., & Ji, Y. (2012). Integrated coal mine safety monitoring system. In *Software engineering and knowledge engineering: Theory and practice* (pp. 365–371). Springer.

4. Debia, M., Couture, C., Njanga, P. E., Neesham Grenon, E., Lachapelle, G., Coulombe, H., & Aubin, S. (2017). Diesel engine exhaust exposures in two underground mines. *International Journal of Mining Science and Technology*, 27(4), 641–645.
5. Pranay, M., & Shrawankar, U. (2018). Monitoring and safety system for underground coal mines. In *Proceedings of the 1st IEEE International Conference on Power Energy, Environment & Intelligent Control (PEEIC2018)* (pp. 1–5).
6. Tripathy, D. P., & Ala, C. K. (2018). Identification of safety hazards in Indian underground coal mines. *Journal of Sustainable Mining*, 17(4), 175–183.
7. Zhu, Y., & You, G. (2019). Monitoring system for coal mine safety based on wireless sensor network. In *Cross Strait Quad-Regional Radio Science and Wireless Technology Conference (CSQRWC)* (pp. 1–2). IEEE.
8. Ali, N. A. A., Latiff, N. A. A., & Ismail, I. S. (2019). Performance of LoRa network for environmental monitoring system in Bidong island Terengganu, Malaysia. *International Journal of Advanced Computer Science and Applications*, 127–134.
9. Ali, N. A. A., & Latiff, N. A. A. (2019). Environmental monitoring system based on LoRa technology in island. In *IEEE International Conference on Signals and Systems (ICSigSys)* (pp. 160–166). IEEE.
10. Sai, K. B. K., Subbareddy, S. R., & Luhach, A. K. (2019). IOT based air quality monitoring system using MQ135 and MQ7 with machine learning analysis. *Scalable Computing: Practice and Experience*, 20(4), 599–606.
11. González, E., Casanova-Chafer, J., Romero, A., Vilanova, X., Mitrovics, J., & Llobet, E. (2020). LoRa sensor network development for air quality monitoring or detecting gas leakage events. *Sensors*, 20(21), 1–20.
12. Bhanu Priya, P., & Umamaheswara Reddy, G. (2020). Multi sensor IoT network system for safety applications based on LoRa technology. *JETIR*, 7(12), 347–352.
13. Ke, W., & Wang, K. (2020). Impact of gas control policy on the gas accidents in coal mine. *Processes*, 8(1405), 1–20.
14. Veeramanikandasamy, T., Gokul, R. S., Balamurugan, A., Ramesh, A. P., & Khadar, Y. S. (2020). IoT based real time air quality monitoring and control system to improve the health and safety of industrial workers. *International Journal of Innovative Technology and Exploring Engineering*, 9(4), 1879–1887.
15. Ahsan, M., Based, M. A., Haider, J., & Rodrigues, E. M. (2021). Smart monitoring and controlling of appliances using LoRa based IoT system. *Designs*, 5(1), 1–22.
16. Fan, Z., & Xu, F. (2021). Health risks of occupational exposure to toxic chemicals in coal mine workplaces based on risk assessment mathematical model based on deep learning. *Environmental Technology & Innovation*, 22(101500), 1–11.
17. Jabbar, W. A., Subramaniam, T., Ong, A. E., Shu'ib, M. I., Wu, W., & de Oliveira, M. A. (2022). LoRaWAN-based IoT system implementation for long-range outdoor air quality monitoring. *Internet of Things*, 19(100540), 1–25.
18. Ayaz, M., Jehan, N., Nakonieczny, J., & Mentel, U. (2022). Health costs of environmental pollution faced by underground coal miners: Evidence from Balochistan, Pakistan. *Resources Policy*, 76(102536), 1–10.
19. ThingSpeak for IoT Projects. <https://thingspeak.com/>
20. Blynk IoT platform: for businesses and developers. <https://blynk.io/>
21. IoT Kit v3 based on LoRaWAN. <https://www.enthutech.in/shop/product/lora-iot-kit-v3-iot-kit-v3-based-on-lorawan-3193?category=11>

Application of Artificial Intelligence in Geotechnical Engineering: A Review



Jitendra Khatti and Kamaldeep Singh Grover

Abstract In engineering, the soils are majorly classified as cohesive and non-cohesive soil. The cohesive soil changes its behavior in the presence of water. Each soil has different geotechnical properties, such as consistency limits, compaction parameters, strength parameters, and permeability, representing the soil's behavior. The laboratory procedures are time-consuming and cumbersome. Therefore, several researchers have used artificial intelligence techniques to compute the geotechnical properties of soil. The literature reveals that AI techniques give the most optimistic prediction of the engineering properties of soil. Also, the literature demonstrates that the effect of the quality and quantity of the database has not been analyzed in predicting the geotechnical properties of soil. The present study maps the future scope for determining the impact of the quality, quantity, and multicollinearity of the database in predicting the engineering properties of coarse and fine-grained soils.

Keywords Artificial intelligence · Deep learning · Hybrid learning · Machine learning · Geotechnical properties of soil

1 Introduction

Soil word is originated from the Latin word “Sodium,” which means the upper surface of the Earth. Several types of soils are available on this Earth. For the purpose of engineering, the soils are majorly classified as cohesive and non-cohesive soils. Each soil has different engineering properties, determined from laboratory experiments. The Atterberg's limits, compaction parameters, strength parameters, and permeability are the engineering properties of soil. The Atterberg's limits, such as liquid limit (LL), plasticity index (PI), and plastic limit (PL), are also known as the consistency limits

J. Khatti (✉) · K. S. Grover
Department of Civil Engineering, Rajasthan Technical University, Kota, Rajasthan, India
e-mail: jitendrakhatti197@gmail.com

K. S. Grover
e-mail: ksgrover@rtu.ac.in

of soil. The consistency limits are experimentally determined for the cohesive soils. On the other side, the California bearing ratio (CBR), optimum moisture content (OMC), maximum dry density (MDD), are the compaction parameters of cohesive and non-cohesive soils. The direct shear and unconfined compressive strength tests are used to determine the strength parameters of soil, i.e., the angle of internal friction and cohesion. However, the experimental procedures to assess these engineering properties are tedious and cumbersome. Also, it requires human resources to perform the engineering properties of soil. Therefore, several researchers and investigators have developed and employed different statistical and advanced computational tools to predict the geotechnical properties of cohesive and non-cohesive soils.

Williams and Ojuri [1] developed an artificial neural network and multiple linear regression models to predict the hydraulic conductivity of the soil. The authors selected PI, Sand, Fines, Clay, MDD, and OMC as input parameters to predict the hydraulic conductivity of soil in the published research work. The authors proposed two equations to predict the hydraulic conductivity of soil using the MLR method. The proposed equations are as follows

$$k = (-1.1416E-08) * PI + (3.2E-05) + (3.092E-08) * FI \\ + (1.413E-07) * S + (5.189E-10) * C + (-2.591E-07) * OMC \\ + (-1.909E-08) * MDD \quad (1)$$

$$k = (1.291E-07) * S + (1.858E-05) + (-1.198E-08) * MDD \\ + (-1.362E-08) * PI \quad (2)$$

The performance of Eqs. 1, and 2 based MLR models were 0.607 and 0.636, respectively. Similarly, the ANN model performance was 0.977, and it was compared with the MLR model and found that the ANN model has capability to predict the hydraulic conductivity of soil with better accuracy. Bouslihim et al. [2] evolved RF and MLR model to predict the Mean Weight Diameter (MWD) as an index of soil aggregate stability. In the published research work, the authors developed four models, (i) based on soil properties of 77 datasets—SP1, (ii) based on soil properties of 144 datasets—SP2, (iii) based on soil properties and remote sensing of 77 datasets—SPRS1, and (iv) based on soil properties and remote sensing of 144 datasets—SPRS2. The performance of SP1, SP2, SPRS1, and SPRS2 models of MLR was 0.768, 0.592, 0.721, and 0.600, respectively. Similarly, the performance of SP1, SP2, SPRS1, and SPRS2 models of MLR was 0.775, 0.600, 0.755, and 0.583, respectively. The authors stated that the performance of ML models is decreased because of SP1 and BR08. The authors also stated that the performance of ML models is not improved with the addition of soil data collected from remote sensing. The authors concluded that based on the results of the ML model, it is not possible to judge the best ML model to predict soil aggregate stability. The authors also concluded that the performance of ML models might be improved by increasing the datasets. Ly et al. [3] proposed SVM, GPR, and RF models using 145 soil specimens

to predict soil cohesion. The authors used void ratio, specific gravity, clay content, liquid limit, moisture content, and plastic limit to develop the ML models. SVM, GPR, and RF model performance were 0.27, 0.69, and 0.837, respectively. Based on the comparison of the performance of the ML models, the authors concluded that the RF model has the potential to predict the cohesion of soil.

Onyelowe et al. [4] applied gene expression programming to compute the strength of expansive soil treated with hydrated-lime-activated rice husk ash. The authors developed MLR and GEP models to predict the CBR, UCS, and resistance value (R_{value}) of treated soils. The GEP models performance was 0.9957, 0.9713, and 0.9957 for CBR, UCS, and R_{value} , respectively. Similarly, the performance of MLR models of CBR, UCS, and R_{value} was 0.9925, 0.9963, and 0.9925, respectively. The authors concluded that the performance and prediction accuracy of GEP models of CBR, UCS, and R_{value} is better than MLR models. The authors also concluded that the performance of models might be improved by increasing the datasets. Nwaiwu and Mezie [5] proposed empirical relationships to predict the compaction parameters using index properties of soil. The authors developed a relationship between compaction parameters and compaction energy (E) and fine to sand ratio (FC/S_dC). To develop the relationship between the compaction parameters and compaction energy and fine to sand ratio using linear regression analysis. The reported work was carried out for British Standard Light (BSL), West African Standard (WAS), and (British Standard Heavy (BSH) soils. From the prediction error, the author concluded that the fine-to-sand ratio (FC/S_dC) has a good relationship and can predict the compaction parameters with less than ± 1.0 error.

Zhang and Wang [6] developed ensemble models to predict soil liquefaction during an earthquake. The authors also developed backpropagation NN (BP), decision tree (DT), SVM, k-nearest neighbors (KNN), MLR, logistic regression (LR), and Naive Bayes (NB). The three different datasets were collected from the literature of Hanna et al. [7], Goh and Goh [8], and Juang and Chen [9]. The performance of BP, SVM, DT, KNN, NB, LR, MLR and ensemble models was 0.856, 0.875, 0.808, 0.856, 0.788, 0.788, 0.510, and 0.894, respectively for first datasets. The comparison of the performance of ML models for the first datasets shows that the ensemble model has a better performance than other models. Similarly, the performance of BP, SVM, DT, KNN, NB, LR, MLR, and ensemble models was 1.000, 0.920, 0.840, 0.880, 0.920, 0.800, 0.720, and 1.000. The performance of the BP and ensemble model was 1.00 and equal in both cases for the second dataset. Hence, BP and ensemble models' prediction accuracy was compared, and it was found that the ensemble models predicted soil liquefaction with 0.941 accuracy. For the third dataset, the performance of BP, SVM, DT, KNN, NB, LR, MLR, and ensemble models was 0.963, 0.926, 0.815, 1.000, 0.963, 0.935, 0.778, and 0.963, respectively. The KNN model achieved maximum performance. The authors concluded that the ensemble model outperforms in predicting soil liquefaction during an earthquake by comparing ML models' performance. The authors also concluded that the performance of the ensemble model is not stable when different datasets are used. The author also stated that the $(N_1)_{60}$, ϕ' , q_c , a_{max} , V_s play an essential role in predicting soil liquefaction during an earthquake.

Tenpe and Patel [10] developed SVM and GEP models to predict soil CBR. The particle size, compaction parameters, and Atterberg's limit were used as input parameters to develop the models. The authors developed various ML models with the following input parameters, (i) Model I—Input (G, S, γ_{dmax}), (ii) Model II—Input (G, S, I_p, w_{copt}), (iii) Model III—Input ($G, S, I_p, \gamma_{dmax}, w_{copt}$), (iv) Model IV—Input ($G, S, FC, I_p, \gamma_{dmax}, w_{copt}$), and (v) Model V—Input ($G, S, FC, W_L, I_p, \gamma_{dmax}, w_{copt}$). The performance of GEP models I, II, III, IV, and V was 0.807, 0.873, 0.879, 0.8833, and 0.880. Similarly, the performance of SVM models I, II, III, IV, and V was 0.844, 0.880, 0.880, 0.878, and 0.897, respectively. Based on the performance of the GEP and SVM models, the authors concluded that Model III (having five input variables) is the best prediction model. The authors also concluded that the SVM model's overfitting ratio (OR) was 0.630 calculated and shows better compatibility than GEP (OR = 1.02). The authors observed the percentage contribution in the prediction of CBR of soil as $S > G > I_p > \gamma_{dmax} > w_{copt}$ in both GEP and SVM models. John et al. [11] evolved the ANN, SVM, RF, Cubist, and MLR models to predict the organic carbon variability with environmental variables in alluvial soils. The performance of RF, Cubist, ANN, MLR and SVM models was 0.8246, 0.7141, 0.6000, 0.4123, and 0.6000, respectively. The random forest model achieved the maximum performance, and the authors concluded that a random forest is a useful tool for predicting organic carbon variability. Chen et al. [12] proposed models of Ridge regression, Lasso and LassoCV, RF, XGBoost, and MARS to predict soil liquefaction using the capacity energy concept. The performance of Ridge regression, Lasso and LassoCV, RF, XGBoost, and MARS models was 0.6180, 0.7622, 0.9055, 0.9121, and 0.9165, respectively. The performance of the MARS model was higher as compared to other ML models. The author concluded that soil liquefaction can be predicted using the MARS model considering the capacity energy concept on behalf of the performance. Lui et al. [13] suggested Gaussian process regression models predict soil moisture. The authors developed the GPR model using a Radially uniform (RU) algorithm. The results of the developed RU algorithm-based models compared with the results of generic GPR models. The authors proposed the following models, (i) GPR + full dataset, (ii) GPR + 100 datasets, (iii) GPR + 500 datasets, and (iv) ARMA. From the comparison of the performance of the proposed models, the GPR + 100 datasets achieved better performance compared to other models. The authors concluded that model II (GPR + 100 dataset) is able to predict soil moisture.

Ly and Pham [14] evolved the support vector machine model to predict soil shear strength parameters. The model was evolved using 500 datasets of soil properties such as moisture content, clay content, specific gravity, liquid limit, void ratio, and plastic limit. The authors concluded that the proposed SVM model has a performance of 0.90–0.95. The performance shows that the developed SVM models have the potential to predict the shear strength of soils. Wang et al. [15] developed random forest and genetic algorithm models to compute the permeability of the soil. The authors used 50 sets of Uniaxial compressive strength, effective stress, gas pressure, and temperature parameters to develop the models in the published research work. The authors compared the performance of RF and RF-GA models and reported that the RF-GA model is a robust model to predict soil permeability. The RF and RF-GA

model performance was 0.6753 and 0.9171, respectively. The authors also stated that the UCS, temperature, gas pressure, and effective stress have 0.054, 0.102, 0.102, and 0.742 correlations with permeability. The authors also suggested that the capabilities of the RF-GA model may be generalized by increasing the datasets. Najemalden et al. [16] proposed an artificial neural network to compute the collapse potential of gypseous sandy soil using soil parameters. The authors collected 180 samples from different regions in Iraq. The backpropagation neural network was developed to compute the collapse potential. The Levenberg–Marquardt algorithm was used in the neural network. The authors reported that the performance of the proposed ANN model was 0.998. The authors also determined the importance factor between input parameters and output. The importance factor was 4.99, 19.69, 17.35, 12.77, 14.57, 13.87, and 16.76% determined for $\%pass$, G_s , G_C , γ_d , ω_o , e_o , and S_r .

Wei et al. [17] developed an RNN model to predict pore-water pressure using time-series analysis. The authors developed standard RNN, LSTM, GRU, ANN, and MLP models to predict pore-water pressure. In the published study, the authors selected SP3 and SP8 measurement points to develop the RNN models to predict the pore-water pressure. The performance of GRU, LSTM, standard RNN, and MLP models for SP3 point was 0.9797, 0.9797, 0.9539, and 0.9539, respectively. The CPU training time (s) of GRU, LSTM, standard RNN, and MLP models was 39.68 s, 55.20 s, 28.77 s, and 23.01 s, respectively. The GRU and LSTM models performed better than standard RNN and MLP models. The performance of GRU, LSTM, standard RNN, and MLP models for SP8 point was 0.9434, 0.9381, 0.9327, and 0.8544, respectively. The CPU training time (s) of GRU, LSTM, standard RNN, and MLP models was 40.53 s, 52.64 s, 28.99 s, and 23.45 s, respectively. The authors also developed single and double layers GRU models to predict the pore-water pressure at the SP3 point. The single and double layers GRU model performance was 0.9797 for both models, but the training time of single and double layers GRU models was 43.23 s and 99.48 s, respectively. Based on the performance of RNNs and MLP models, the authors concluded that the performance of the MLP model varies with random training runs and also fluctuates with the length of the input dataset. The authors also concluded that the LSTM and GRU outperform the MLP and standard RNN because GRU and LSTM are able to mitigate the vanishing gradient problem. It was noted that the efficiency of GRUs is higher than LSTM because of a more straightforward structure. Based on the training time of the single and double-layer GRU models, the authors also stated that the single-layer GRU model can predict the pore-water pressure compared to the double-layer GRU model.

Wang and Yin [18] proposed multi expression programming approach to compute the MDD and OMC of soil. The authors developed linear models for OMC and MDD with gravel content (Cg), sand content (Cs), fine content (Fc), LL, PL, and energy (E). The OMC linear model performance with Cg, Cs, Fc, LL, PL, and E was 0.5128, 0.5692, 0.6928, 0.4049, 0.6943, and 0.1643, respectively. The maximum performance was 0.6943, determined for the linear model of OMC with PL. Similarly, the performance of the linear model of MDD with Cg, Cs, Fc, LL, PL, and E was 0.5514, 0.5148, 0.6686, 0.4329, 0.7355, and 0.1761, respectively. The maximum performance was 0.6686, determined for the linear model of MDD with Fc. The

OMC_PL and MDD_Fc models were validated by predicting the laboratory test data. The OMC_PL and MDD_Fc models predicted OMC and MDD with 0.9607, and 0.9263, respectively. The authors reported that the proposed OMC and MDD models have the potential to predict the OMC and MDD of soil. Male et al. [19] evolved gradient boosting regression, linear regression, and Carman-Kozeny models to compute the permeability of low and high porosity groups of cemented sandstone. The performance of gradient boosting regression, linear regression, and Carman-Kozeny models was 0.7211, 0.7000, and 0.6633, respectively, for the low porosity group of cemented sandstone. Similarly, the performance of gradient boosting regression, linear regression, and Carman-Kozeny models was 0.9110, 0.8185, and 0.9110, respectively, for the high porosity group of cemented sandstone. From the performance of gradient boosting regression, linear regression, and Carman-Kozeny models for low and high porosity groups of cemented sandstone, the authors concluded that machine learning shows a better correlation than advanced Carman-Kozeny models. The authors stated that the nonlinear effect of cementation may be identified by implementing linear regression in gradient boosting regression. The permeability prediction can be better if the porosity is more than 2.3%. The authors also concluded that porosity, cement, specific surface, and tortuosity are essential for high porosity. Similarly, pore-bridging cement, tortuosity, porosity, and pore-filling cement are essential for low porosity.

Sihag et al. [20] proposed SVM, GP, ANN, and RF models to predict soil infiltration. The proposed models were trained and tested by 272 and 120 datasets. The Polynomial and RBF kernels were used to develop the Gaussian process (GP) and SVM models. Kostikov and Philip's models were also developed to predict soil infiltration. The RMSE performance of RF, ANN, SVM_Poly, SVM_RBF, GP_Poly, GP_RBF, Philip's model, and Kostikov model was 50.8485, 78.7458, 67.7070, 132.5228, 40.3026, 84.5483, 198.0730, and 197.8236, respectively. The performance of GP_Poly was 0.9863, which was better as compared to other models. Boadu [21] developed electrical spectra with Jonscher fractal power model characterized by DC conductivity (σ_{dc}), exponent (n), and transition. The author developed the SVR model to predict the mechanical properties of soil. The mechanical properties K , γ_d , and E were predicted by SVR and MLR models. The performance of the SVR model of K , γ_d , and E was 0.9219, 0.9381, and 0.8718, respectively. Similarly, the performance of the MLR model of K , γ_d , and E was 0.7483, 0.826, and 0.7616, respectively. From the comparison of the performance of the SVR and MLR models, the authors concluded that the SVR model is a reliable model to predict the mechanical properties of soil such as K , γ_d , and E with better accuracy and performance. In last few years, Khatti and Grover have assessed different geotechnical properties of soil, such as modulus of subgrade reaction, permeability, soaked CBR, using different AI approaches [22–26].

2 Gaps in the Literature Survey

From the present study of the literature, it has been observed that several researchers have used different databases to develop and employ artificial intelligence techniques to compute the geotechnical properties of soil, presenting the best architectural approach and model that is still questionable. Also, it is well known that artificial intelligence techniques are data-driven, and the performance of the AI models is affected by the quality and quantity of the database. Still, the effect of the quality and quantity of the database on the performance and overfitting of AI models has not been analyzed in predicting the geotechnical properties of coarse and fine-grained soil.

However, the database also contains multicollinearity, affecting the AI models' performance, accuracy, and overfitting. The impact of the multicollinearity of the training database has not been determined in assessing the geotechnical properties of coarse and fine-grained soil. The literature survey also demonstrates that the hypothesis analysis has not been performed in computing the engineering properties of soils.

3 Conclusions and Future Scopes

Artificial intelligence techniques are the best predictive tools in the assessment of the geotechnical properties of soil. Several researchers and investigators have reported that the regression analysis gives a preliminary prediction of the engineering properties of soil with considerable errors. Artificial intelligence techniques, such as artificial neural network, Gaussian process regression, support vector machine, group method data handling neural network, decision tree, random forest, gene expression programming, and recurrent neural network, can predict the OMC, MDD, CBR, UCS, etc., soil properties with high accuracy and the least prediction error. To sum up, the present study maps the following futures scopes:

- The effect of the quality and quantity of the database on the performance and overfitting of the AI models may be analyzed in predicting the geotechnical properties of soil.
- The impact of the multicollinearity of the database may be studied for the performance and overfitting of the AI models.
- The parametric statistical analysis may be performed to identify the null and the research hypothesis.
- The cosine amplitude method may be used to perform the sensitivity analysis to determine the most influencing input parameters in predicting the engineering properties of soil.

References

1. Williams, C. G., & Ojuri, O. O. (2021). Predictive modelling of soils' hydraulic conductivity using artificial neural network and multiple linear regression. *SN Applied Sciences*, 3(2), 1–13.
2. Bouslihim, Y., Rochdi, A., & Paaza, N. E. A. (2021). Machine learning approaches for the prediction of soil aggregate stability. *Heliyon*, 7(3), e06480.
3. Ly, H. B., Nguyen, T. A., & Pham, B. T. (2021). Estimation of soil cohesion using machine learning method: A random forest approach. *Advances in civil engineering*, 2021, 1–14.
4. Onyelowe, K. C., Jalal, F. E., Onyia, M. E., Onuoha, I. C., & Alaneme, G. U. (2021). Application of gene expression programming to evaluate strength characteristics of hydrated-lime-activated rice husk ash-treated expansive soil. *Applied Computational Intelligence and Soft Computing*, 2021, 1–17.
5. Nwaiwu, C. M., & Mezie, E. O. (2021). Prediction of maximum dry unit weight and optimum moisture content for coarse-grained lateritic soils. *Soils and Rocks*, 44.
6. Zhang, J., & Wang, Y. (2021). An ensemble method to improve prediction of earthquake-induced soil liquefaction: A multi-dataset study. *Neural Computing and Applications*, 33, 1533–1546.
7. Hanna, A. M., Ural, D., & Saygili, G. (2007). Neural network model for liquefaction potential in soil deposits using Turkey and Taiwan earthquake data. *Soil Dynamics and Earthquake Engineering*, 27(6), 521–540. <https://doi.org/10.1016/j.soildyn.2006.11.001>
8. Goh, A. T., & Goh, S. H. (2007). Support vector machines: Their use in geotechnical engineering as illustrated using seismic liquefaction data. *Computers and Geotechnics*, 34(5), 410–421. <https://doi.org/10.1016/j.compgeo.2007.06.001>
9. Hsein Juang, C., & Chen, C. J. (2000). A rational method for development of limit state for liquefaction evaluation based on shear wave velocity measurements. *International Journal for Numerical and Analytical Methods in Geomechanics*, 24(1), 1–27. [https://doi.org/10.1002/\(SICI\)1096-9853\(200001\)24:1%3C1::AID-NAG49%3E3.0.CO;2-I](https://doi.org/10.1002/(SICI)1096-9853(200001)24:1%3C1::AID-NAG49%3E3.0.CO;2-I)
10. Tenpe, A. R., & Patel, A. (2020). Utilization of support vector models and gene expression programming for soil strength modeling. *Arabian Journal for Science and Engineering*, 45(5), 4301–4319.
11. John, K., Abraham Isong, I., Michael Kebonye, N., Okon Ayito, E., Chapman Agyeman, P., & Marcus Afu, S. (2020). Using machine learning algorithms to estimate soil organic carbon variability with environmental variables and soil nutrient indicators in an alluvial soil. *Land*, 9(12), 487.
12. Chen, Z., Li, H., Goh, A. T. C., Wu, C., & Zhang, W. (2020). Soil liquefaction assessment using soft computing approaches based on capacity energy concept. *Geosciences*, 10(9), 330.
13. Liu, M., Huang, C., Wang, L., Zhang, Y., & Luo, X. (2020). Short-term soil moisture forecasting via Gaussian process regression with sample selection. *Water*, 12(11), 3085.
14. Ly, H. B., & Pham, B. T. (2020). Prediction of shear strength of soil using direct shear test and support vector machine model. *The Open Construction & Building Technology Journal*, 14(1).
15. Wang, J., Yan, W., Wan, Z., Wang, Y., Lv, J., & Zhou, A. (2020). Prediction of permeability using random forest and genetic algorithm model. *Computer Modeling in Engineering and Sciences*, 125(3), 1135–1157.
16. Najemalden, A. M., Ibrahim, S. W., & Ahmed, M. D. (2020). Prediction of collapse potential for gypseous sandy soil using ANN technique. *Journal of Engineering Science and Technology*, 15(2), 1236–1253.
17. Wei, X., Zhang, L., Yang, H. Q., Zhang, L., & Yao, Y. P. (2021). Machine learning for pore-water pressure time-series prediction: Application of recurrent neural networks. *Geoscience Frontiers*, 12(1), 453–467.
18. Wang, H. L., & Yin, Z. Y. (2020). High performance prediction of soil compaction parameters using multi expression programming. *Engineering Geology*, 276, 105758.
19. Male, F., Jensen, J. L., & Lake, L. W. (2020). Comparison of permeability predictions on cemented sandstones with physics-based and machine learning approaches. *Journal of Natural Gas Science and Engineering*, 77, 103244.

20. Sihag, P., Kumar, M., & Singh, B. (2021). Assessment of infiltration models developed using soft computing techniques. *Geology, Ecology, and Landscapes*, 5(4), 241–251.
21. Boadu, F. K. (2020). A support vector regression approach to predict geotechnical properties of soils from electrical spectra based on Jonscher parameterization Soil electrical geotechnical properties. *Geophysics*, 85(3), EN39–EN48.
22. Khatti, J., & Grover, K. S. (2022). Prediction of soaked CBR of fine-grained soils using soft computing techniques. In *Multiscale and Multidisciplinary Modeling, Experiments and Design* (pp. 1–25).
23. Khatti, J., & Grover, K. S. (2022, December). Relationship between index properties and CBR of soil and prediction of CBR. In *Transportation and Environmental Geotechnics: Proceedings of the Indian Geotechnical Conference 2021* (Vol. 4, pp. 171–185). Springer Nature Singapore.
24. Grover, K. S., Khatti, J., & Jangid, A. K. (2021). Prediction of modulus of subgrade reaction using machine language framework. In *Communication and Intelligent Systems: Proceedings of ICCIS 2020* (pp. 375–393). Springer.
25. Khatti, J., & Grover, K. S. (2021). Determination of permeability of soil for indian soil classification system using artificial neural network technique. *Invertis Journal of Science & Technology*, 49.
26. Khatti, J., & Grover, K. S. (2021). Determination of Suitable Hyperparameters of Artificial Neural Network for the Best Prediction of Geotechnical Properties of Soil. *International Journal For Research in Applied Science and Engineering Technology*, 10(5), 4934–4961.

Commercially Successful Rural and Agricultural Technologies

A Study of Role of It in Rural Development in India: Opportunities and Challenges



Pravin Pundlik Rajguru

Abstract Information today is required in all areas that hinder growth and development. The many creative ways that communication technology can be used to help rural development. It is evident that increasing access to information technology supports rural development and empowers rural populations. Information and communication technology has made it possible to empower those who were left behind by the Industrial Revolution. While developing nations face the challenges of globalization brought on by free market privatization and liberalization. They must never lose sight of their disadvantaged rural and urban populations. Innovative approaches can reach the unreached and empower them with knowledge and skills. Cable operators, Public Communications Offices (PCOs), and now information centers use information. They would be able to meet their basic needs for food, shelter, education, health, and technology through innovative use for enhancing their productivity and facilitating their social and economic well-being. As a result, it significantly contributes to the achievement of rural development and progress.

Keywords People · Rural area · Development · It application · Challenges

1 Introduction

The term “Information Technology” (IT) is now commonly used in all contexts. Discussing the revolution in information technology in point of fact, the capacity of humans to collect, store, transmit, and retrieve data and information has significantly increased since the introduction of personal computers (PCs) and microprocessors. Information technology has evolved into a potent tool for managing information and communication, making it now possible to communicate more quickly and easily. The primary manifestations of information technologies, which are television, satellite, telephone, and computers, are rapidly altering our way of life, work, and leisure. In point of fact, what is new in the current revolution in information technology? With

P. P. Rajguru (✉)

Department of Economics, Sangameshwar College (Autonomous), Solapur, Maharashtra, India
e-mail: pravinrajguru@gmail.com

the advent of the ultra-fast Internet and information technologies, it is possible to refer to the convergence and integration of previously known communication and information technologies into a single system. It promises almost universal empowerment because it has greatly expanded the dissemination of knowledge and made sharing it simple. Additionally, it is contingent on our employing these “new” technologies in novel ways.

2 Objectives of the Study

The primary goal of this research is to investigate the role of information technology in rural development in India: opportunities and challenges in rural areas. The current study’s objectives are as follows:

- (1) To investigate the relationship between information technology and rural development.
- (2) Research IT opportunities for rural development.
- (3) Recognize the significance of information technology in rural area development.
- (4) To comprehend the IT challenges in the development of rural activities.

3 Hypothesis of Study

An application of Information and Technology (IT) are playing important role in field of rural development.

4 Research Methodology

In this paper, “researcher has adopted descriptive study methods and secondary data. The data and information which is used in the paper is drawn from reliable and creditable resources such as related books by various authors, related research papers, various journals and articles on the Rural Development, Application of IT for Rural Development which are available on online and offline” mode.

5 Literature Review

The book “E-Government: The Science of the Possible” examines and identifies significant e-government and ICT principles.

Bhatnagar [3] focused on e-government, e-commerce, and ICT for development. He is interested in how ICT can be used for rural development and corruption: In “e-government:” opportunities and challenges can help reduce it in service delivery from the vision to the execution.

Dwivedi and Bharti [7] look at governments and organizations in the public sector around the world to reform public administration organizations and offer services that are more cost-effective and efficient. E-governance is the efficient utilization of information and communication technology (ICT) to enhance the current governance system and enhance citizen services. E-Government is a top priority in India because it is the only way to teach information technology to the “common people” and talk about fundamental issues and whether or not E-Government is acceptable in the country.

This paper, by Ghosh, provides a succinct analysis of innovative ICT projects for rural development and their contribution. Reflecting on the successes and failures of information and communication technology in the process of sustainable development is the second objective. In addition, the analysis makes mention of C4D-related initiatives and projects both before and after media liberalization.

Boateng [4] the paper highlights the efforts made by Ghana’s previous and current governments to address the major obstacles to ICT development in Ghana. The study’s investigations revealed that ICT plays a crucial role in the socioeconomic development of Ghana’s rural areas, with enormous potential for accelerated development.

6 IT and Rural Development

The ICT revolution and the economic, social, cultural, and political responses to it, as previously mentioned. It has profound effects on how we work, live, and spend our free time. How will these changes in the IT industry affect India’s rural areas? Rural society is being profoundly altered by information and communication technologies like satellite, cable television, wireless telephony, computers, and the internet. In India as well as numerous other nations numerous exciting and promising experiments are being carried out in various regions of India, despite the fact that the actual access to and penetration of various information technologies in rural areas is still extremely limited. The impact of new communication technologies on rural development and social change lies in their capacity to consolidate a few qualities of the two individual’s to-individuals contact and the media.

7 The Role IT Plays in the Growth of Rural Areas

Information technology can be utilized in a variety of ways to exchange data. From one individual to another it offers expert groups effective communication as well as services for information exchange. Which help identify marketing information, fluctuations, better strategies for increasing agricultural productivity, and information on crop management in addition to providing basic information? There are numerous communication and informational tools, including the following:

SMS Portal for Kisan: Farmers in rural areas are less familiar with the most recent agricultural productivity-enhancing technologies. The farmer can find information about the language of his or her region through this portal.

Call Center of Kisan: It is a specialized advisory system that aids farmers in providing relevant information regarding agricultural activities. For expert advice on activities related to agriculture, farmers must call the toll-free number 1800-180-1551.

Kendras of Kisan Vikas: In India, it serves as the foundation for the dissemination of technology and information. Approximately 630 kV are currently operational, and several new ones are being built. By demonstrating cutting-edge technology at the district level, KVKs serve as a link between the scientific community and the Indian farmer. In order to reach the farthest farmers, the current government has instructed KVKs to use increasingly more ICT tools in their work. This is supported by plenty of money.

e-Nam: A huge online platform for selling agricultural products. This includes, among other services, the delivery of goods, their prices, trade offers, and responses to trade offers. In initially regulated markets, it provides transparency in sales transactions and price discovery.

E-governance: E-governance is another name. It is an application that makes use of ICT to provide citizens with government information. This will make it easier and more transparent for citizens to access government services or administration.

e-Choupal: e-Choupal is an Indian conglomerate's initiative to connect rural farmers directly with online retailers of agricultural goods. It addresses the difficulties posed by Indian agriculture, which is marked by the involvement of middlemen, poor infrastructure, and farm fragmentation. In order to provide farmers in rural India with up-to-date marketing and agricultural information, the software installs computers with internet access.

8 Opportunities for Using Information Technology for Rural Development

In rural development, there are numerous application opportunities that can be elaborated on as follows:

Social progress

Individuals and groups alike acknowledge the potential impact of information technology on social development. Education may play a significant role in social growth. Information technology and education have a clear connection. Access to substantial resources for higher education at minimal or no cost is perhaps the most tangible advantage of information technology for developing nations. However, distance education has been successful, particularly in rural areas where distance and lack of financial resources are major obstacles. As a result, through the provision of distance education, the advancement of information technology has the potential to foster social development for the poor and vulnerable in rural areas, particularly women and children.

9 Obstacles to IT Use in Rural Development

In recent times, IT has played a significant role in rural development; however, there are still numerous obstacles in this area, including the following:

Illiteracy: The rural population of India has a significantly lower literacy rate than the urban population. Although the rural population's literacy rate is significantly lower than that of the urban population, the government is making an effort to improve it. However, there is still a significant amount of work to be done.

Reluctance to transform: People don't want to change. Employees and the general public generally dislike e-governance because it involves moving the system from manual to computer-based. Most people don't like it because they have to learn new things, which take more time and effort.

Security and privacy: E-government stakeholders will have access at three fundamental levels: unable to access the web service; whether you want full or limited access to a web service, the process of creating a security access policy for sensitive personal data is more complicated and takes into account legal considerations. When e-government projects are put into action, effective measures need to be taken to safeguard the private information of the recipients. Projects containing sensitive data may be hampered by the absence of comprehensive security protocols and standards.

Language supremacy: Access for non-English-speaking people to the Internet is restricted by English's dominance. The majority of the population in India speaks Hindi. In Indian villages, computers and the Internet are practically non-existent due

to the English language's undeniable dominance over these channels of communication. Monetary issues: Various e-governance pilot projects, including public works, government services, and human resources, have received funding from governments all over the world. To achieve e-governance, the government faces the real challenge of continuing to finance a wide range of initiatives.

10 Conclusion

For any kind of growth in human settlements, whether they are in cities or the country. Any development activity can only be carried out if certain fundamental elements are either provided or developed. The study's overall conclusion demonstrates that, despite its proximity to a city, additionally, the fundamental technological and informational foundations for utilizing this technology were largely unsuccessful due to internal issues. Such as a lack of use and high Internet access costs. Social and cultural issues like a lack of specialized trainers, education, and illiteracy, as well as traditional conservative opposition to innovations, have all been impacted by technology. In the village, the development of ICT was only successful in achieving a few social and cultural objectives (primarily spreading the idea of using technology and making some public and private services' day-to-day operations easier). However, it is not in the economic aspects of electricity marketing and trading, job creation, or income growth. It is important to note that the public sector has not invested or provided financial support. ICT development in rural areas has failed as a result of a significant external obstacle.

References

1. Arulbalaji, P., Padmalal, D., & Sreelash, K. (2019). GIS and AHP techniques based delineation of groundwater potential zones: A case study from southern Western Ghats, India. *Scientific Reports*, 9(1), 1–17.
2. Bhatia, A., & Kiran, C. (2016). Rural development through E-Governance initiatives in India. *IOSR Journal of Business and Management (IOSR-JBM), Special Issue-AETM*, 16, 61–69.
3. Bhatnagar, S. C. (2004). *E-Government, from vision to implementation—A practical guide with case studies*. SAGE Publications Pvt. Ltd.
4. Boateng, M. S. (2012). The role of information and communication technologies in Ghana's rural development. *Library Philosophy and Practice (e-journal)*, 871, 8.
5. Cherupelly, N. K. (2022). Alternative agricultural extension functionaries in India: Substantive role of (ICTs)-study of e-Choupal. *Journal of Agricultural Extension and Rural Development*, 14(3), 132–139.
6. Chitla, A. (2012). Impact of information and communication technology on rural India. *IOSR Journal of Computer Engineering*, 3(2), 32–35.
7. Dwivedi, S. K., & Bharti, A. K. (2010). E-Governance in India—Problems and acceptability. *Journal of Theoretical and Applied Information Technology*.
8. Kaushik, P. D., & Singh, N. (2004). Information technology and broad-based development: Preliminary lessons from North India. *World Development*, 32(4), 591–607.

9. Kumar, A., Nayar, K. R., & Koya, S. F. (2020). COVID-19: Challenges and its consequences for rural health care in India. *Public Health in Practice, 1*, 100009.
10. MattooAsra. (2015). Role of information technology in Indian Agriculture. *Engineering Technology in India, 6*(2), 94–98.
11. Mittal, P., & Kaur, A. (2013). E-Governance—A challenge for India. *International Journal of Advanced Research in Computer Engineering and Technology (IJARCET), 2*(3), 1196–1199.
12. Navío-Marco, J., Ruiz-Gómez, L. M., & Sevilla-Sevilla, C. (2018). Progress in information technology and tourism management: 30 years on and 20 years after the Internet-Revisiting Buhalis and Law’s landmark study about e-Tourism. *Tourism Management, 69*, 460–470.
13. Sami, P., & Sayyed, I. U. (2014). Impact of information technology in agriculture sector. *International Journal of Food, Agriculture and Veterinary Sciences, 4*(2), 17–22. ISSN 2277-209X (Online).
14. Pramanik, J., Sarkar, B., & Kandar, S. (2017). Impact of ICT in rural development: Perspective of developing countries. *American Journal of Rural Development, 5*(4), 117–120.
15. Ranade, P., Londhe, S., & Mishra, A. (2015). Smart villages through information technology—Need of emerging India. *International Journal of Information Technology, 3*(7), 1–6.
16. Sai, S. S. T. (2016). Smart villages-need of emerging India. *International Journal of Innovative Research in Information Security (IJIRIS), 3*(09), 51–54.
17. Shanthi, P. J., & Bhuvaneshwari, G. (2021). Role of information technology in the agricultural sector with reference to rice cultivation in India. *Webology, 18*(6). ISSN 1735-188X.
18. Singh, K., & Shishodia, A. (2016). *Rural development: Principles, policies, and management*. SAGE Publishing India.
19. Singh, N. (2004). Information technology and rural development in India. In *Integrating the rural poor into markets* (pp. 221–246).

Development and Design of Min-T8 HP Power Weeder Back Rotor



Sumit R. Pawar and Mukund S. Kale

Abstract Since the 1960s, power tillers have been available in the nation. For forward motion as well as tillage operation, the majority of power tiller models produced in India are equipped with a front or rear mounted powered rotary unit. For wide-spaced row crops like sugarcane, cotton, etc., power tillers are employed for intercultural operations and seedbed preparation. The function of a power tiller and its various attachments are discussed in this essay. In a mechanised agricultural setting, a power weeder is frequently used to prepare the soil bed while saving time, labour, and fuel. However, in highly abrasive environments, weeder blades are particularly susceptible to excessive surface wear in dry sand, which significantly reduces their service life. Chain sprockets are used in the transmission system's operation in order to save money. Various machine components are modelled using the modelling programme Creo 4.0. The created approach is beneficial for the agriculture sector, particularly in emerging nations. According to the literature review, portable weeders are less flexible and substantially less expensive to operate. One of the most challenging duties on an agricultural field is weed management. There are three widely used weed management techniques in agriculture. Mechanical, chemical, and biological control are these. Chemical pest control methods contaminate the soil, which is bad for our health. These approaches are useless because they are less effective than other ways. Power tiller weeding reduces labour costs and saves time in addition to uprooting weeds that are growing in between crops. It also maintains soil particles loose, providing improved soil aeration and water intake capacity. Different kinds of mechanical weed have been created. Because human operation of marijuana requires muscular force, it cannot be operated for an extended period of time. This is the power weeder which is totally made in India. The power weeder back rotor given 336 rpm speed. Rotor speed is increased so it is the main advantage for farming this machine can be used for sugarcane, Ginger, onion and Turmeric etc. This works on different operating condition, creating bed for different crop.

Keywords Soil bed · Blades · Chain sprocket mechanism · Creo 4.0

S. R. Pawar (✉) · M. S. Kale
Government College of Engineering, Karad, India
e-mail: sumitpawar4198@gmail.com

1 Introduction

Indian agricultural has gone through different stages of power use pattern with time in twentieth century. Prior to Second War, the use of power machinery in Indian agricultural was almost nil. Appearance of large size tractors (70 hp and above) was seen for jungle clearance and rehabilitation of migrants from Pakistan to India. Use of tractors and power weeder in agricultural was introduced in early sixteen by importing few models and makes from Europe, America and Japan. However, the power tillers were imported from Japan only under some Yen credit assistance offered to India. Similar was story of the four-wheel tractors. Later, production and utilization of tractors took a major leap forward but the power tiller did not catch up to the desired level of expectations. The first batch of about 200 power tillers imported into the country were distributed in rice growing states of Eastern India during 1961. Subsequently, 100 more machines were received and distributed in southern rice growing states also. The main efforts were to assess the suitability of the single axle power source for Indian conditions. After 27 years of the introduction of power tillers i.e. in 1988 the analysis of the situation in respect of the power tiller as a source of power under Indian condition is being made. Critical review will be presented to highlight the successes and failure through case studies.

Agriculture, which directly employs roughly 70% of the working population, is the economic saviour of India. Agriculture and industries based on agricultural goods are extremely important to India's economy because it is a growing country. The majority of people in India depend on agriculture and agro-based companies and industries. Weeder is the name of a mechanical tool used to clear weeds from agricultural land.

Due to India's extensive agricultural industry, the necessity for contemporary technologies in agricultural practises is undeniable. An engine-powered, low-power tool called a power weeder is used to prepare beds. They are lightweight, portable, and medium-duty machines. Power tillers with 12–15 horsepower and a weight limit of 350 kg are now produced in large quantities all throughout the nation. This project's power tiller, an 8 hp power weeder with a focus on weeding, is appropriate for cultivation of sugarcane's rear soil. In order to adapt the engine speed to the power weeder's tilting speed, this project involves designing and developing several components, including a chain and sprocket, shafts, bearings, coupling shafts, gears, transmission case, and blades.

This machine is specifically for sugarcane, Onion, Turmeric and Ginger cultivation requirement and can be used for black soft soil. The trials performed showed considerable saving due to use of power weeder over men. Currently, the majority of power weeders made in the nation range in horsepower from 2 to 5 and weigh 100–125 kg. Due to their inability to operate on slopes, power tillers are not likely to be employed in hilly terrain. This is mostly caused by its weight, which has to be further improved. The development of a lightweight power weeder powered by two 4-hp engines is deemed required as a result. Taking into account all of these aspects, and as a tiny step toward mechanising agriculture and assisting the 60% of Indians

who depend on agriculture for a living, as well as to promote their contribution to the growth of our economy. This project's power weeder, an 8 hp machine with a focus on weeding, is appropriate for cultivation of ginger and turmeric in back soil. This power weeder is intended for use in farms growing sugarcane, ginger, and turmeric with minimum interrow distances of 2.5, 1, and 1.5 feet, respectively. This device is simple to use, inexpensive, portable, and straightforward to maintain using readily available spare parts.

2 Expérimentation

2.1 Power Weeder Information

Power weeder which are present nowadays are 8 HP takes input of 3000 rpm and give output of 200 rpm which is very less rpm due to which it use to take lot of time and addition to it also require additional adjustment to join the blade to power weeder i.e. first we need to remove tyre and then join the rotor blade which waste lot of time. In our new model of power weeder like the other power weeder it takes input of 3000 rpm but gives the output of 336 rpm which is compared more speed than the other power. We have added a new gearbox and back rotor which also enhance its performance. On other hand we do not need to do any additional adjustment to join the blade as rotor blades are directly connected. As a result, most of the time is saved (Fig. 1).

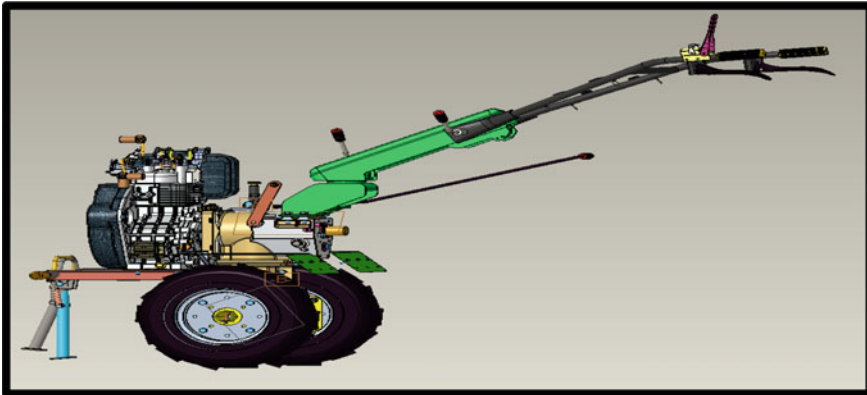


Fig. 1 Power weeder

2.2 *Operating Condition*

1. **Onion Field**

To grow seedlings that can be transplanted into the field, onion seeds are put in nursery beds. Prepared are raised beds with a 3×0.6 dimension and a height range of 10–15 cm. Two beds are separated by about 70 cm (2.5 ft) to allow for watering, weeding, etc. activities. The surface of beds should be levelled and smooth. A 3×0.6 -inch bed with a height of 10–15 cm is created for onions. Two beds are separated by about 70 cm (2.5 ft) to allow for watering, weeding, etc. activities (Fig. 2).

2. **Turmeric Field**

1. Minimum tillage operation should be adopted while preparing the land in Turmeric Forming (Fig. 3).



Fig. 2 Onion field



Fig. 3 Turmeric field



Fig. 4 Ginger field

2. To give least 50 cm (2 ft) spacing between beds, beds should be Prepared with a height of 15 cm, 1 m width and suitable length.
3. In case of irrigated crops, rhizomes should be planted in shallow pit on the top of the ridges and furrows should be prepared.
4. Solarization of beds is useful to check the multiplication of pests and diseases causing organisms.
5. After the work completed Polythene sheets which is used for soil solarisation should be kept away safely.

3. Ginger Field

Land Preparation: To get the soil to a fine tilth, the field must be ploughed four to five times or completely excavated while receiving early summer rains. The beds are set up with a 50 cm inter-bed distance and are approximately 1 m wide, 30 cm tall, and of a convenient length. For an irrigated crop, ridges are constructed at intervals of 40 cm. It is advised to solarize beds for 40 days using clear polythene sheeting in areas vulnerable to rhizome rot disease and nematode infestations (Fig. 4).

4. Sugarcane Field

1. This is the simplest and most affordable planting method, and it works best in low-rainfall locations (Fig. 5).
2. Local ploughs or cultivators are used to open shallow furrows (8–10 cm deep) at a distance of 75–90 cm.
3. The field should have enough moisture when planting takes place, and two blind hoeings are given to replace the setts that were destroyed by insects.
4. Plant the setts end to end, making sure that one set with three buds falls into each running 30 cm length of the furrow.
5. To suppress weeds and aid in tillering, two to five inter row cultivations may be administered at appropriate intervals after germination.
6. Earthing is often not done, but if it is essential, the crop may receive one earthing in the months of July and August to prevent lodging and to improve field drainage.



Fig. 5 Sugarcane field



Fig. 6 Developed Min T8 Power weeder machine

2.3 Final 3D Diagram

This is the power weeder which is totally made in India. The power weeder back rotor given 336 rpm speed. Rotor speed is increased so it is the main advantage for farming this machine can be used for sugarcane, Ginger, onion and Turmeric etc. This works on different operating condition, creating bed for different crop (Fig. 6).

3 Conclusion

Following are the conclusions under study of different agricultural category. We have improved the design of gear box housing and transmission housing so that our power weeder will be more efficient. Also our power wheeler is totally made in India which also one step toward our Indian government programmed of make in India. Roto speed is increased so it is the main advantage for farming this machine can be used

for sugarcane, Ginger, onion and Turmeric etc. This works on different operating condition, creating bed for different crop.e.g. For onion distance between two bed is 2.5 ft. For Sugarcane distance between two bed is 3.0 ft. For Ginger distance between two bed is 1.5 ft.

References

1. Swapnil Kadu, L., Ganesh Kadam, B., Kishor Jadhav, P., Vikas Gawade, S., Garje, A., & Gosavi, A. (2015). Design, development and operation of 3.5HP power tiller. *International Journal of Recent Research in Civil and Mechanical Engineering*, 2(1), 149–154.
2. Gavali, M., & Kulkarni, S. (2014). Comparative analysis of portable weeder and power tillers in the Indian market. *International Journal of Innovative Research in Science, Engineering and Technology*, 3(4), 11004–11013.
3. Krishi Vigyan Kendra, Sabour, Bhagalpur, Bihar. (2018). Different attachments of a power tiller: A review. *International Journal of Science, Environment*, 7(3), 1024–1035.
4. Zakariyan, A., El-Okene, A. M., Mohammed, U. S., Oji, N., Abubakar, I., Agunsoye, J. K., & Ahmad, K. (2021). Modification of portable power tiller for small scale weeding operation. *Journal of Engineering Research and Reports*, 54–56.
5. Ojha, T. P. Success and failures of power tiller in Indian agricultural (pp 30–33). Central Institute of Agricultural Engineering.
6. Yadav, R., & Pund, S. (2007). Development and ergonomic evaluation of manual weeder. *Agricultural Engineering International: The CIGR e-Journal*, 9, 1–9.
7. Okoko, P., Ajav, E. A., & Olosunde, W. A. (2018). Draft and power requirements for some tillage implements operating in clay loam soil. *AgricEngInt: CIGR Journal*, 20(1).
8. Omkar, Snehal, T., Akshay, U., Suchit, W., & Chandrashekhar, K. (2019). Design and fabrication of power operated tiller machine. *Journal of Emerging Technologies and Innovative Research Auti*, 6(2), 113–115.

Savonius Vertical Axis Wind Turbine for Effective Generation of Power—A Review



Vishal Patil, D. G. Kumbhar, and Kailasnath Sutar

Abstract In current scenario wind energy is the most favored nonconventional source of power generation due to several reasons. As per the International Renewable Energy Agency (IRENA), the global wind power generation in 2021 was 8.20×10^5 MW. However, India able to generate around 0.4×10^5 MW. The horizontal and vertical axis is the two main wind turbine types. The horizontal axis turbine is generally utilized to build a wind power plant. However, the vertical axis wind turbine (VAWT) can use to fulfill an individual power requirement. It can be installed at the top of the household building, too. Researchers are working on improving the performance of wind turbines. The vertical axis turbine has several types, like Darrieus, Savonius, Giromill wind turbines etc. As vertical axis turbine is for personal use, they can be commercialized in rural or remote villages where the population has relatively dense. Savonius VAWT is simple to construct and install. It can generate electrical power irrespective of conditional parameters such as wind velocity, direction etc. This article presents the utilization of Savonius VAWT to fulfill the need of the rural area.

Keywords Wind turbine · Vertical axis wind turbine · Savonius · Energy problem in a rural area · Renewable energy

1 Introduction

Inventions have continuously been developed as per the need of humans. Initially, the wind turbine was invented to pump water from a well. From that stage, it is now becoming a significant non-conventional source of energy [1]. Researchers are always looking for clean and efficient energy sources to fulfill the growing electricity demand. Solar power, biomass, ocean, and tidal energy are other alternative energy sources [2]. Most of these sources are in the developing stage. However, solar and

V. Patil · D. G. Kumbhar · K. Sutar (✉)

Department of Mechanical Engineering, Bharati Vidyapeeth (Deemed to be University), College of Engineering, Pune, MS, India

e-mail: kbsutar@bvcoep.edu.in

© The Author(s), under exclusive license to Springer Nature Switzerland AG 2024

P. M. Pawar et al. (eds.), *Techno-societal 2022*,

https://doi.org/10.1007/978-3-031-34644-6_12

wind power are coming into the actual application. The main advantage of a wind turbine is that it can be used on a mass level (wind power plant) and for personal use. Vertical axis turbine is always preferred for individual use. For the performance of the vertical axis turbine, several modifications have been made to the old models [3]. Savonius type wind turbine is the mile stone in the vertical axis turbine. The communities of researchers have contributed sincerely to reducing the noise level, operating velocity, and easiness of manufacturing [4]. Furthermore, the outcome is finally the Savonius type of turbine.

This type of turbine was used in 1922 first time. It is a drag-type turbine [3, 4]. There are some advantages of it over the Darrius rotor [4]. However, the main limitation is that it is less efficient than the Darrius rotor. Hence it is necessary to improve its efficiency of it. The following significant contributions have been made in that arena.

2 Wind Turbines and Power Generations

The hydropower and thermal power are the world's primary power generation sources. As the sources of the fuel will be exhausted in upcoming years, human is desperately looking for alternatives for power generation. However, the significant factors are capacity, cost, transmission, and technology. Currently, a wind turbine is considered a prominent alternative source of power generation, and wind turbine performance is being improved by researchers. This study is mainly focusing on Savonius vertical axis turbine. The parameters like types, number, shape, geometry of the blades, and ultimately types of deflectors are significant in the performance of VAWT.

2.1 The Effect of Blade Geometry and the Total Number of Blades

The geometrical shape of the blade plays a significant role in the turbine's performance. The research shows that the straight blade is less effective than the newly developed design blade. The twisted type of blade gives the best performance result over the curved and aero foil-type blades also [1]. Adding extra layers of blades also matters in the performance of VAWT. In the case of Savonius axis turbines, adding an end plate can create a huge difference. It has been observed that the starting torque of single and multiple-layer rotors is better than that of conventional turbines. We can obtain better results by varying the angle of multiple layers and overlap ratio [2]. The self-starting ability of Savonius axis turbines can be improved with the help of overlapping of blades. The tip speed ratio can be maintained at greater than one by adding a double-layer quarter blade [3]. The variation in the combination of layer

angles and the number of layers provides good results. The size and position of blades is the significant factor in the production of the highest fluid flow that causes the better value of Moment of Inertia. Both help develop positive torque and reduce negative torque [5]. The arrangement of blades or layers on the blades also affects the power coefficients (C_p). Different combinations of azimuths and twist blade angles can carry out the experiments. The CFD analysis can provide better results. The study of values of power coefficients for different values of TRS and Coefficient of torque (C_T) can be performed using CFD. For a twist angle greater than 90° , the torque coefficient remains constant. The maximum value of C_T is obtained at a twist of 45° . The importance of flow and surface pressure distribution are maximums for convex blades. The concave blade shows minimum values [6]. Using 2-dimensional flows in CFD analysis, the study of conventional semicircular blades and novel blades (blades with a combination of layers) has been performed. The role of blade geometry is being investigated in the performance parameters like dynamic torque and power coefficients. The most important thing is that the blades should have self-starting capacity from any angular position, and it can only be achieved with the help of the elimination of negative static torque. The performance parameters can be modified with the optimization of aspect ratio, overlap ratio, and Reynolds number [7]. The Maskell blockage correction method is beneficial for testing the wind turbine. The power output and torque coefficients can be maximized with the help of a circular end plate. Above 30% increase is there in the power coefficient [8]. The single-stage modified Savonius rotor has the highest coefficient of power. It also optimizes Reynolds's Number [9].

The style of the Savonius wind turbine has vital contribution in the performance. For a particular application, style is beneficial. The power coefficient is also affected by the rotor radius's value. Also, CFD analysis shows that researchers have to study steady flow, 2D flow, Laminar flow, and unsteady flow while doing the performance analysis [10]. The numerical simulation is an effective method to analyze the performance of the Savonius VAWT. Typically the commercial code COMSOL Metaphysic [11] is used to do the static analysis. It shows a negligible influence of slot angle on the torque and power coefficient [12]. Also, the aspect ratio should be considered an essential factor while designing the turbine. When the aspect ratio is higher performance coefficient is also higher [13] and in some cases, overlapping of the blades is necessary to achieve performance efficiency. Studies show that the highest power coefficient was performed with a baked overlap ratio of 15% [14]. While in two stages arrangement, no overlap of blades is required to achieve the highest efficiency [15] (Fig. 1).

The studies show that the performance of a turbine with three blades is lower than that of a turbine with two blades [16]. The rotational speed and TSR of three blades wind turbine is better than that of two of four blades turbine. Hence it can be said that rotation of the rotor and TRS does solely not depend on the number of blades. There is an opportunity to investigate this factor. Also, the number of blades influences in performance of wind turbines. Researcher outcomes show that wind turbine having four blades has good performance when the TSR is minimum, and the three-blade turbines display the best performance curve at a higher tip speed ratio [17]. Also,

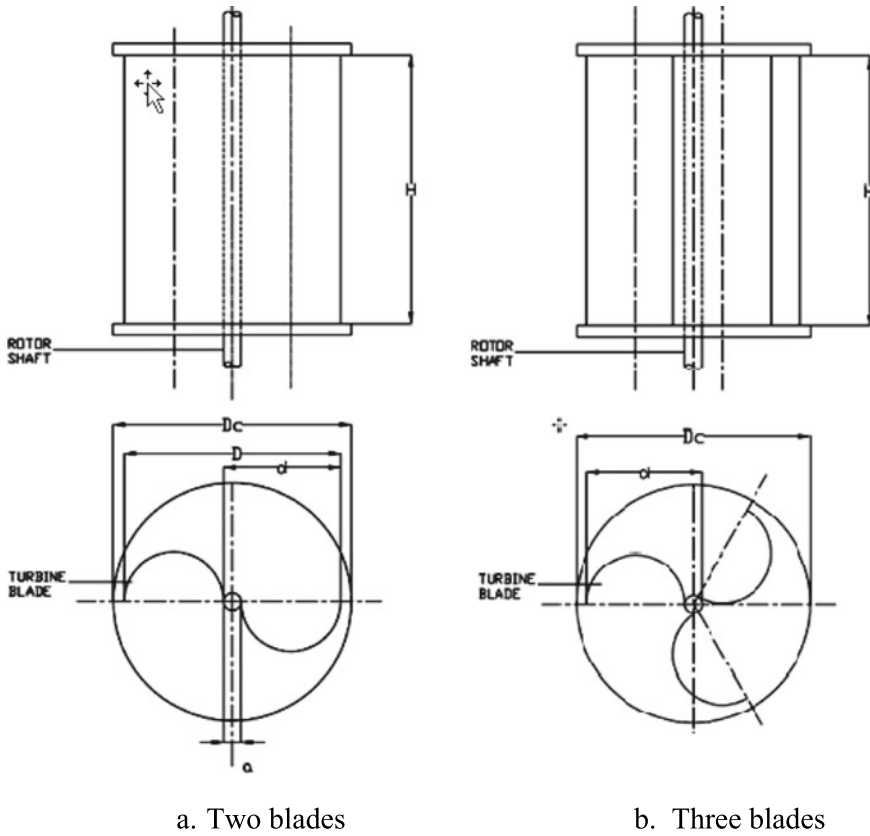


Fig. 1 Savonius vertical axis wind turbine [16, 17]

the researcher shows that if there is the typical incremental pattern in the number of blades, the power coefficient is also increases, because the drag increases on the blade's surface on which air flows are responsible for increasing the torque [18].

2.2 The Effect of Fin on the Performance of VAWT

Researchers found that the power output of VAWT with the fins is always more gathered than that of VAWT without fins because the change in the geometrical shapes of the surfaces and edges can impact the blade turbine due to the variation in lift and drag force [19]. The coefficients of the drag and drag forces contribute to the performance and power output. The blade with two fins has shown the highest drag coefficient and drag force. Pressure and velocity distribution are very critical factors. The results of the blade with two fins show the most elevated pressure and

Table 1 Effect of fins

Authors	Number of fins	Average wind speed (m/s)	Results	Remarks
Aher and Singh [19]	0	5	$P = 3.64 \times 10^4 \text{ kW}$, $T = 115,119 \text{ Nm}$	The addition of fins improves the power coefficient and the efficiency of VAWT
	1	5	$P = 5.46 \times 10^4 \text{ kW}$, $T = 173,708 \text{ Nm}$	
Setyawan [20]	0	5	$F_D = 2.7755 \text{ N}$, $C_D = 0.001724$	Adding fins improves the drag coefficient and produces the highest pressure and velocity distribution of VAWT
	1	5	$F_D = 4.1389 \text{ N}$, $C_D = 0.002571$	
	2	5	$F_D = 4.1468 \text{ N}$, $C_D = 0.002576$	
	0	7	$F_D = 5.4082 \text{ N}$, $C_D = 0.001714$	
	1	7	$F_D = 8.1223 \text{ N}$, $C_D = 0.002574$	
	2	7	$F_D = 8.1361 \text{ N}$, $C_D = 0.002578$	
Pamungkas et al. [21]	0	4.5	$TRS = 0.73$, $C_P = 0.135$	The addition of fins improves power generation, and the optimal configuration is the addition of 1 Fin
	1	4.5	$TRS = 0.81$, $C_P = 0.166$	
	2	4.5	$TRS = 0.76$, $C_P = 0.147$	
	3	4.5	$TRS = 0.74$, $C_P = 0.141$	
	4	4.5	$TRS = 0.73$, $C_P = 0.134$	
Anggara et al. [22]	1	4.5	$F_D = 21.0051 \text{ N}$, $T = 14,712 \text{ Nm}$	The addition of fins improves the power coefficient because greater torque and Drag forces are achieved by adding fins
	2	4.5	$F_D = 21.0001 \text{ N}$, $T = 146,658 \text{ Nm}$	

P = Power; T = Torque; F_D = Drag force; C_D = Drag coefficient; C_P = Power coefficient; TRS = Tip speed ratio

velocity distribution [20]. The selection of the geometrical shape of the fin can also affect the turbine’s power output. The low starting speed is always beneficial. At a wind speed of 4.5 m/s, the Savonius turbine with one s-shaped fin produced 13.4 W power [21]. The variation in the number of fins, the fin area, and the diameter of the fin show different results. The objective of the attachment of the fin is to boost positive drag force so that it can enhance power generation, power coefficient, and

torque coefficient. Increasing the fin area helps generate maximum drag force [22]. The Savonius type turbine with the modification of s shape always produces a batter effect; only adding one fin achieves the batter power coefficient value [23] (Table 1).

2.3 The Effect of the Addition of Dimples on the Performance of Wind Turbine

Dimples are small depressions on the highest point of the golf ball, and it helps maintain the distribution of rakish force and increase the amount of energy. In the case of a wind turbine, the dimples give the same effect. It helps to increase the efficiency and the power coefficient. It has been observed that the power generated by wind a turbine with dimples has always been superior to that caused by wind turbines with dimples [19]. The researchers created dimples only in those parts of the blade which displayed high pressure. The results show that adding dimples to the blade increased its performance [24]. There are different types of dimples according to the geometrical shapes, particularly in horizontal wind turbine researchers obtaining some conclusions with inwards and outward dimples. The aerodynamic parameters of the blades with inward dimples provided better results than those with outward dimples [25]. When we consider the dimples, the no. of dimples and diameter are always important because they decide their matrixes. Generally, the dimples on the suction sides of the wind turbine improve torque and power generation. The overall increase in torque generation is around 16% [26].

Generally, spherical and square dimples are used in wind turbines. Due to the dimples, the rate of heat transfer is considerably augmented. Also, the factors like drag, lift, and skin coefficient could be improved using square dimples. Reynolds number of 4.5×10^6 shows a gradual increase in a lift to drag coefficient [27]. It is also essential to investigate in detail about dimple shape. Previously we have seen the effect of spherical and square dimples. However, the researcher found that slight modifications in spherical or circular dimples will create a teardrop shape that can reduce the drag coefficient [28]. The aerodynamic performance of the blades can be improved with the help of dimples. It can decrease the drag pressure and increase the stall angle. Also, there is a considerable reduction in the blade sound, so it is helpful to reduce acoustic emissions. The different types of dimples, like semi-spherical hexagonal, cylindrical, and square, are analyzed using computational and actual experimentation later. The aerodynamic efficiency can be improved by increasing the length-to-diameter (L/D) ratio [29, 30].

2.4 Effect of Deflectors on the Performance of Wind Turbine

By optimizing the wind parameters, we can enhance the power and torque coefficients of VAWT. The deflectors are helpful in the processes of negative torque reduction. It also improves the efficiency and reliability of VAWT. Also, deflectors are easy to install accessories, and maintenance work is also to perform. A researcher has concluded that by using the flat plate deflector, the power coefficient can be improved by 27%. The aerodynamic shape can be altered for augmentation. We can achieve an average power coefficient up to 39% using [31] (Table 2).

A comparison between the performance parameter of the Savonius wind rotor with a deflector and without a deflector should be studied in detail because a deflector helps to boost the velocity of wind entering the rotor by minimizing the negative torque. The best result has been obtained in the Savonius turbine with the attachment of the deflectors. The static torque values are minimum when the deflector dimensions are minimum [32]. Research shows that the arrangement of deflectors or curtains impacts the performance of wind turbines. The length and curtain angle also constitutes the performance results. Overall improvement in the coefficient of the Savonius rotor

Table 2 Effect of types of deflectors on the VAWT [31]

Type of deflectors/curtain	Design parameters	Simulation techniques	Results (%)	Remarks
Flat plate	Savonius 2 blade	CFD simulation	27.3	At TSR, 0.7 leads to the highest power coefficient
Flat plate	Savonius 3 blade		27.55	
Flat plate	H-type NACA 0021Blade	Numerical simulation	47.1	Due to deflectors, the wind speed increase by 20% near the weak region
Airfoil shaped	Savonius	CFD simulation	50	At an angle of attack of 700, the maximum torque and power coefficient were obtained
Flat pate	Straight blade twin turbine	Experimentation	26	As a result of the deflectors, the power coefficient was changed from 0.031 to 0.101, and the TSR was changed from 0.98 to 0.123
Kite shaped	Straight blade twin turbine	CFD simulation and experimentation	38.6	Improvement in torque generation by changing the wind flow. The greater the wind speed and the larger the angle of attack on the rotor leads to improved output power generation

CFD = Computational fluid dynamics; TRS = Tip speed ratio

is around 15–38% using the different combinations of length and angles of curtains [33]. The Savonius rotor blade shape can be optimized by placing a deflector-type obstacle in front of the blade. It improves the blade’s self-starting capability, and the turbine’s overall performance can be improved by around 30% [34] (Table 3).

From the above literature study, the following factors are essential in designing the Savonius vertical axis wind turbine.

- The essential things are the wind turbines expected power output and string speed.
- According to that, the blade’s geometrical shape, number of blades, arrangement of the blades, and overlapping of the blades.
- The important measurable performance parameters are overlap ratio, coefficient of power, coefficient of torque, and tip speed ratio.
- Economic consideration is also important.

Table 3 Effect of deflector on the performance of VAWT

Type of deflectors/curtain	Wind speed	Design parameters	Experimental/numerical results	Remarks
Flat plate	7 m/s	$\theta = 45^\circ, 60^\circ, 90^\circ$ $\alpha = \text{between } 30^\circ \text{ and } 60^\circ$ $\beta = 10^\circ \text{ and } 15^\circ$ Curtain 1, $l_1 = 45 \text{ cm}, l_2 = 52 \text{ cm}$ Curtain 2, $l_1 = 34 \text{ cm}, l_2 = 39 \text{ cm}$ Curtain 3, $l_1 = 22 \text{ cm}, l_2 = 26 \text{ cm}$ Height = 32 cm Thickness = 2 mm	Curtain 1, $C_p = 0.38533$ Curtain 2, $C_p = 0.34154$ Curtain 3, $C_p = 0.26273$ The best performance is obtained with curtain no. 1 when $\theta = 60^\circ$, for $\beta = 150$ and $\alpha = 45^\circ$	The curtain lengths play a role in the result’s positive or negative effects on the torque. The heights torque obtained with Curtain 1 [33] The rotor with the curtains performs better than the one without curtains by increasing the velocity of air entering the rotor [34]

θ = rotor blade position; α = angle of a curtain plate; β = angle of b curtain plate; l_1 = length of a curtain plate; l_2 = length of b curtain plate; C_p = power coefficient

3 Conclusion

Non-conventional energy sources are gradually replacing conventional energy sources. The literature review has been conducted about the performance analysis of Savonius VAWT. However, the factor like geometrical shape, number of blades, fins, dimples, and deflectors are contributing in the performance.

- Due to the blade profiles and different geometrical shapes, significant change has been observed in the starting torque.
- Tip speed ratio (TSR) values are varying with respect to the number of blades.
- Addition of fins is helpful to improve the power output.
- Dimples are playing vital role in the overall performance, the factors like efficiency of VAWT and power coefficient are enhanced due addition of it.
- The deflectors are helpful for augmentation in power coefficient as well as make the functioning of VAWT more reliable.

As the Savonius vertical axis turbine is helpful for individual use, it can reduce the load on the grid if it works efficiently. An economical model of power generation can be developed with the help of Savonius VAWT.

References

1. Shah, S. R., Kumar, R., Raahemifar, K., & Fung, A. S. (2018). Design, modeling, and economic performance of a vertical axis wind turbine. *Energy Reports*, 4, 619–623. <https://doi.org/10.1016/j.egy.2018.09.007>
2. Kurniawan, Y., Tjahjana, D. D. D. P., & Santoso, B. (2020). Experimental study of savonius wind turbine performance with blade layer addition. *Journal of Advanced Research in Fluid Mechanics and Thermal Sciences*, 69(1), 23–33. <https://doi.org/10.37934/arfmts.69.1.2333>
3. Siregar, I., Effendy, M., & Rasyid, A. (2020, January). Experimental investigation of double layer blades as obstacle blades on Savonius wind turbine performance. In *International Conference on Research and Academic Community Services (ICRACOS 2019)* (pp. 46–50). Atlantis Press. <https://doi.org/10.2991/icracos-19.2020.9>
4. Adeyeye, K. A., Ijumba, N., & Colton, J. (2021, June). The effect of the number of blades on the efficiency of a wind turbine. *IOP Conference Series: Earth and Environmental Science*, 801(1), 012020. IOP Publishing. <https://doi.org/10.1088/1755-1315/801/1/012020>
5. Kurniawan, Y., Tjahjana, D. D. D. P., & Santoso, B. (2020, July). Experimental studies of performance savonius wind turbine with variation layered multiple blade. *IOP Conference Series: Earth and Environmental Science*, 541(1), 012006. IOP Publishing. <https://doi.org/10.1088/1755-1315/541/1/012006>
6. Lee, J. H., Lee, Y. T., & Lim, H. C. (2016). Effect of twist angle on the performance of Savonius wind turbine. *Renewable Energy*, 89, 231–244. <https://doi.org/10.1016/j.renene.2015.12.012>
7. Nilavarasan, T., & Dheenadhayalan, J. (2015). Numerical investigation of Savonius wind turbines with modified blade configurations. In *International Conference on Energy Systems and Developments (ISET 2015)*.
8. Jeon, K. S., Jeong, J. I., Pan, J. K., & Ryu, K. W. (2015). Effects of end plates with various shapes and sizes on helical Savonius wind turbines. *Renewable Energy*, 79, 167–176. <https://doi.org/10.1016/j.renene.2014.11.035>

9. Kamoji, M. A., Kedare, S. B., & Prabhu, S. V. (2009). Experimental investigations on single stage modified Savonius rotor. *Applied Energy*, 86(7–8), 1064–1073. <https://doi.org/10.1016/j.apenergy.2008.09.019>
10. Danesc, A., & Voinea, S. (2019). COMSOL model for simulating the mine natural ventilation to power a wind turbine. In *Proceedings of the 14th International Conference on Virtual Learning ICVL* (Vol. 32, pp. 452–458).
11. Abraham, J. P., Plourde, B. D., Mowry, G. S., Minkowycz, W. J., & Sparrow, E. M. (2012). Summary of Savonius wind turbine development and future applications for small-scale power generation. *Journal of Renewable and Sustainable Energy*, 4(4), 042703. <https://doi.org/10.1063/1.4747822>
12. Alaimo, A., Esposito, A., Milazzo, A., Orlando, C., & Trentacosti, F. (2013). Slotted blades savonius wind turbine analysis by CFD. *Energies*, 6(12), 6335–6351. <https://doi.org/10.3390/en6126335>
13. Akwa, J. V., da Silva Júnior, G. A., & Petry, A. P. (2012). Discussion on the verification of the overlap ratio influence on performance coefficients of a Savonius wind rotor using computational fluid dynamics. *Renewable Energy*, 38(1), 141–149. <https://doi.org/10.1016/j.renene.2011.07.013>
14. Mahmoud, N. H., El-Haroun, A. A., Wahba, E., & Nasef, M. H. (2012). An experimental study on improvement of Savonius rotor performance. *Alexandria Engineering Journal*, 51(1), 19–25. <https://doi.org/10.1016/j.aej.2012.07.003>
15. Gupta, R., Biswas, A., & Sharma, K. K. (2008). Comparative study of a three-bucket Savonius rotor with a combined three-bucket Savonius–three-bladed Darrieus rotor. *Renewable Energy*, 33(9), 1974–1981. <https://doi.org/10.1016/j.renene.2007.12.008>
16. Ali, M. H. (2013). Experimental comparison study for Savonius wind turbine of two and three blades at low wind speed. *International Journal of Modern Engineering Research (IJMER)*, 3(5), 2978–2986.
17. Wenehenubun, F., Saputra, A., & Sutanto, H. (2015). An experimental study on the performance of Savonius wind turbines related with the number of blades. *Energy Procedia*, 68, 297–304. <https://doi.org/10.1016/j.egypro.2015.03.259>
18. Chaichana, T., & Thongdee, S. (2019, November). Effect of blade number and angle on the characteristics of the savonius type wind turbine. *Journal of Physics: Conference Series*, 1380(1), 012110. IOP Publishing. <https://doi.org/10.1088/1742-6596/1380/1/012110>
19. Aher, S.S., Singh, N.P. (2021). Design and analysis of Savonius VAWT with dimples and fins. *IOSR Journal of Mechanical and Civil Engineering (IOSR-JMCE)*, 18–2. e-ISSN 2278-1684, p-ISSN 2320-334X, <https://doi.org/10.9790/1684-1806011824>
20. Setyawan, I. (2019, June). Performance of vertical axis Savonius wind turbines related to the fin number on the blade. *IOP Conference Series: Materials Science and Engineering*, 539(1), 012032. IOP Publishing. <https://doi.org/10.1088/1757-899X/539/1/012032>
21. Pamungkas, S. F., Wijayanto, D. S., Saputro, H., & Widiastuti, I. (2018). Performance ‘S’ type Savonius wind turbine with variation of fin addition on blade. *IOP Conference Series: Materials Science and Engineering*, 288(1), 012132. IOP Publishing. <https://doi.org/10.1088/1757-899X/288/1/012132>
22. Utomo, I. S., Tjahjana, D. D. P., & Hadi, S. (2018, February). Experimental studies of Savonius wind turbines with variations sizes and fin numbers towards performance. *AIP Conference Proceedings*, 1931(1), 030041. AIP Publishing LLC. <https://doi.org/10.1063/1.5024100>
23. Anggara, B., Widiastuti, I., & Saputro, H. (2018, November). Numerical study of Savonius wind turbine with additional fin blade using computational fluid dynamic. *IOP Conference Series: Materials Science and Engineering*, 434(1), 012172. IOP Publishing. <https://doi.org/10.1088/1757-899X/434/1/012172>
24. Arun, K. K., Navaneeth, V. R., Vimal, K. S., & Ajay, R. (2018). Analyzing the effect of dimples on wind turbine efficiency using CFD. *International Journal of Applied Engineering Research*, 13(6), 4484–4489. <https://doi.org/10.37622/IJAER/13.6.2018.4484-4489>
25. Fikadea, G., Bekeleb, A., Venkatachalam, C., & Parthiban, M. (2020). Effects of dimples on aerodynamic performance of horizontal axis wind turbine blades. *International Research Journal of Engineering and Technology (IRJET)*, 7(1), 525–529.

26. Sedighi, H., Akbarzadeh, P., & Salavatipour, A. (2020). Aerodynamic performance enhancement of horizontal axis wind turbines by dimples on blades: Numerical investigation. *Energy*, 195, 117056. <https://doi.org/10.1016/j.energy.2020.117056>
27. Joseph, D. R., Devi, P. B., & Gopalsamy, M. (2021). Investigation on effect of square dimples on NACA0012 airfoil with various Reynolds numbers. *International Journal of Ambient Energy*, 42(4), 397–402. <https://doi.org/10.1080/01430750.2018.1531267>
28. Tay, J., & Lim, T. T. (2018). Drag reduction with teardrop-shaped dimples. In *2018 Flow Control Conference* (p. 3528). <https://doi.org/10.2514/6.2018-3528>
29. Akwa, J. V., Vielmo, H. A., & Petry, A. P. (2012). A review on the performance of Savonius wind turbines. *Renewable and Sustainable Energy Reviews*, 16(5), 3054–3064. <https://doi.org/10.1016/j.rser.2012.02.056>
30. Livya, E., Anitha, G., & Valli, P. (2015). Aerodynamic analysis of dimple effect on aircraft wing. *International Journal of Aerospace and Mechanical Engineering*, 9(2), 350–353.
31. Rajpar, A. H., Ali, I., Eladwi, A. E., & Bashir, M. B. A. (2021). Recent development in the design of wind deflectors for vertical axis wind turbine: A review. *Energies*, 14(16), 5140. <https://doi.org/10.3390/en14165140>
32. Mohamed, M. H., Janiga, G., Pap, E., & Thévenin, D. (2011). Optimal blade shape of a modified Savonius turbine using an obstacle shielding the returning blade. *Energy Conversion and Management*, 52(1), 236–242. <https://doi.org/10.1016/j.enconman.2010.06.070>
33. Altan, B. D., Atılgan, M., & Özdamar, A. (2008). An experimental study on improvement of a Savonius rotor performance with curtaining. *Experimental Thermal and Fluid Science*, 32(8), 1673–1678. <https://doi.org/10.1016/j.expthermflusci.2008.06.006>
34. Altan, B. D., & Atılgan, M. (2008). An experimental and numerical study on the improvement of the performance of Savonius wind rotor. *Energy Conversion and Management*, 49(12), 3425–3432. <https://doi.org/10.1016/j.enconman.2008.08.021>

Hybrid Feature Extraction Method for Efficient Leaf Disease Detection and Grading



Rajendra Kanphade, Smita Desai, Rupali Deshmukh, and Smita Modi

Abstract Efficient feature Extraction Technique is a ablaze topic that how-to take-out prominent image structures with a sturdy representation from the processing image using brilliant technology. Since every disease has new symptoms, it is very difficult to process and train the algorithm. The proposed research steps consist of features extraction and classification. Histogram of gradient (HOG) method is used for colour feature extraction, Shape features are extracted using Edge histogram descriptor (EHD). In texture-based features, we extracted features using gray level co-occurrence matrix (GLCM). After combining all features it results in the high dimensional feature vector. Finally, the classification is performed using the artificial neural network (ANN) classifier and Support vector machine (SVM) classifier, MATLAB is software for simulation. Proposed approach achieved the significant improvement in performances with 95.12 and 93.30% accuracy with different training testing ratio with hybrid feature extraction method and ANN classifier.

Keywords Disease detection · Image processing · Hybrid feature extraction · ANN classifier · SVM classifier

1 Introduction

Agriculture is a significant economic sector; hence it plays a significant role. 50% of the workforce is employed by it, and it contributes 18% of the nation's GDP. However, plant diseases cause a decrease in farm productivity. Different plant diseases also have

R. Kanphade (✉)
JSCOE, Hadapsar, Pune, India
e-mail: kanphaderd2015@gmail.com

S. Desai · R. Deshmukh · S. Modi
DIT, Pimpri, Pune, India
e-mail: smita.desai@dypvp.edu.in

R. Deshmukh
e-mail: rupali.deshmukh@dypvp.edu.in

an impact on plant quality and quantity. Early detection is crucial to reducing plant disease damage, but the manual method is ineffective, time-consuming, unreliable, and expensive. The results of feature extraction are crucial for picture identification; incorrect feature extraction will lead to misclassification. Prior to extracting significant features from the image, distinguished features will be segmented, so dynamic region expanding segmentation is utilised, in which the threshold is set dynamically. To distinguish the disease based on shape, colour, and textures, feature extraction is a crucial processing step. Plants that have been afflicted by various diseases and pests will exhibit illness symptoms in the form of deformation. We can analyse and distinguish crop illnesses from one another based on the qualities of colour, texture, and shape using segmentation and retrieved features from the image. If we can use a computerised system to quickly diagnose the illness, we may be able to prevent and limit its spread. This is possible by correctly identifying the lesion area's properties based on a variety of factors, including colour, texture, and shape. Crop health monitoring and control should be handled automatically and brilliantly, as this will have a significant impact on the economic development of the nation. We take into account texture, colour, and shape features from the sorted or partitioned image for this study. We employed support vector machine (SVM) and artificial neural network (ANN) classifiers.

2 Related Works

We survey recent methods presented for plant disease detection using the computer vision methods since from last 10 years.

In [1], the author suggested employing fuzzy logic and image processing to detect orchid diseases. The main objective of the author in this research was to present a system that can identify an orchid disease by analysing an image of its leaf. The system consists of two components: fuzzy logic and image processing. Grayscale, threshold segmentation, and noise removal are some of the techniques utilised in leaf image processing. The centroid, area, and number of infected spots were the data that were gathered through the image processing. The output was then obtained by feeding these data or numbers into the fuzzy logic system, where they underwent fuzzification, fuzzy inference, and defuzzification.

In [2], author introduced method for colour forecast of disease in crop leaf of paddy using image processing. They designed the method in which there will be pre occupied leaf colour chart for particular crop and that will be compared with the diseased leaf image database and from comparison it will be find out deficiency well in advance, before enough to get the yield affected.

In [3], for detecting bacterial leaf scorch of shade trees novel algorithm using image processing concepts is proposed. The method of this paper uses a original method to find out the lesion areas of the crop. In this paper particular region of interest will be found by the K means segmentation technique, in which different clusters are formed based on image segmentation information.

In [4], author has proposed an efficient technique using hybrid technique which includes K means and NB classifier to find the disease severity in okra leaf named of Yellow Vein Mosaic Virus which shows satisfactory result also.

In [5], author suggested a different method based on image processing for identifying plant diseases. This essay covered the techniques for identifying plant diseases using photos of their leaves. The segmentation and feature extraction algorithms utilised in the identification of plant diseases were also covered in this research. This is merely the author's introduction to the research article.

In [6], author introduced a study for disease detection on different classes of horticulture or agricultural crops: vegetable crops, commercial crops, cereals and fruits crops. Many methods have been incorporated and studied in order to have robust method to find accurate disease on above crops.

In [7], in addition to a survey of several disease classification strategies that can be utilised for plant leaf disease detection, the author developed an algorithm for image segmentation technique that is used for automatic detection as well as classification of plant leaf illnesses. This paper gives a survey of the various diseases classification techniques that can be used for plant leaf disease detection, and a genetic algorithm for image segmentation technique used for automatic detection as well as classification of plant leaf diseases has been described later. Image segmentation is a crucial component of disease detection in plant leaf diseases. Some of the ten species on which the author's proposed algorithm was tested include bananas, beans, jackfruit, lemons, mangoes, potatoes, tomatoes, and sapotas.

In [8], research is divided in four stages in order to have desired result out of which a very first stage is colour transformation structure is created, for the input RGB image in next stage, a threshold has been set and using specific threshold value, masking of green pixels are done and then removed. In third stage by comparing a pre computed threshold values a green pixel will be removed and covering is done for the useful sections are extracted first in this stage, and in last or fourth main stage the final segmentation is done.

3 Work Done

3.1 Features Extraction

For features extraction we used different types of features such as colour, shape, structure and methods are Histogram of Gradient (Hog) as low level features, shape-based features like EHD and texture features like GLCM (Fig. 1).

Feature is used to represent a piece of data which is applicable for explaining the computational task related to a specific application. Major features are extracted and from specificity we can detect accurate features and also diagnose a correct disease. Each disease has different symptoms and accordingly it has different features on a



Fig. 1 Hybrid feature extraction

scale of colour, texture, and shape. Efficient feature extraction plays vital role leading to better accurate results.

A. Color Features

To extract colour, feature the colour histogram is the common and effective method. Colour is very distinct parameter in the image each disease has its own colour and characteristics. The colour feature is very efficient as its efficacy does not dependant on to zoom of the image, rotation and size we used the HOG method. We are condensing large image data in small specific size bean to form a standard feature vector. Magnitude and orientation is calculated using above formulas, and magnitudes we can put it in particular angle bins.

B. Texture Features

Texture feature extraction is very effective and robust technique for big size image. In many diseases like fungi and bacteria it mainly attacks on texture of leaves. Two main texture feature methods are (1) Spatial texture feature extraction, and (2) Spectral texture feature extraction.

The Gray Level Co-occurrence Matrix¹ is a type of texture feature extraction technique. We extracted total 5 features using GLCM technique. GLCM is second order statistical method used to find out the co-variance in pixels. We have extracted very unique 18 features using GLCM like contrast, correlation, homogeneity, mean, energy, standard deviation.

C. Shape Features

Classified as: Region based and contour based. Region methods compute the feature from the entire region. The contour methods compute the characteristic from the border and take no notice of its interior.

In this work we used EHD method for shape extraction. It works according to 5 Different types of edges over every image block. The segmented image is divided into 4*4 non overlapping blocks, from each image block, 5 edges such as horizontal, vertical, 135° diagonal, 45° diagonal, and non-directional are extracted. The histogram features then extracted of each edge to construct each block histogram representation. The features extracted in this method based on both global and local histograms.

4 Results

For accuracy, precision, and recall evaluations, we compared the performance of hybrid features extraction technique with existing methods of features extraction such as GLCM, EHD, and HOG using the classifier ANN. The proposed features extraction method along with segmentation shows the significant improvement in classification performance. We have considered hybrid approach and varied training/testing ratio compared to other methods as shown in Table 1, it gives the performance of ANN classifier considering the training and testing ratio 70–30% as well as 80–20%. Analysis shows 80–20% ratio gives better result than 70–30%.

Total DB Images used are = 1150

- Training Images (70%) = 805
- Testing Images (30%) = 345.

Classifier: ANN

All the parameters are calculated for the training and testing ration of 70 and 30% ratio. Also we found that accuracy can further increased by changing the Training and testing ratio 80 and 20%.

Figure 2 shows the graph of accuracy on four different parameters Texture, Shape, Visual, Hybrid and it shows the hybrid parameter gives good result considering 80–20% training testing images.

Figure 3 shows the outcome of Feature extraction it is visual analysis using ANN classifier. We found the performance parameters using confusion matrix and ROC curves Formulas for calculating parameters are given below.

1. Accuracy = $\frac{TP + TN}{\text{Total Images}}$
2. Precision = $\frac{TP}{\text{Predicted yes}}$
3. Recall = $\frac{TP}{\text{Actual yes}}$
4. Specificity = $\frac{TN}{TN + FP}$
5. F1 Score = $\frac{TP}{TP + FN}$.

Same experiment is done using two different datasets like DS-2 having 1152 images with two classes, and dataset DS-6 having 5152 images for six different classes (Table 2).

Table 1 Performance analysis of different feature extraction methods

Parameter TR/ TS ratio	Accuracy		F1 score		Precision		Recall		Specificity	
	20%	30%	20%	30%	20%	30%	20%	30%	20%	30%
Texture	82.51	82.32	82.24	82.05	81.01	80.82	83.52	83.32	81.56	81.38
Shape	86.46	89.88	86.26	89.73	84.96	88.38	87.54	91.11	85.40	88.72
Visual	89.10	83.09	88.94	82.83	87.60	81.59	90.3	84.11	87.96	82.12
Hybrid	95.12	93.30	95.19	93.40	93.81	92.04	96.62	94.80	93.62	91.80

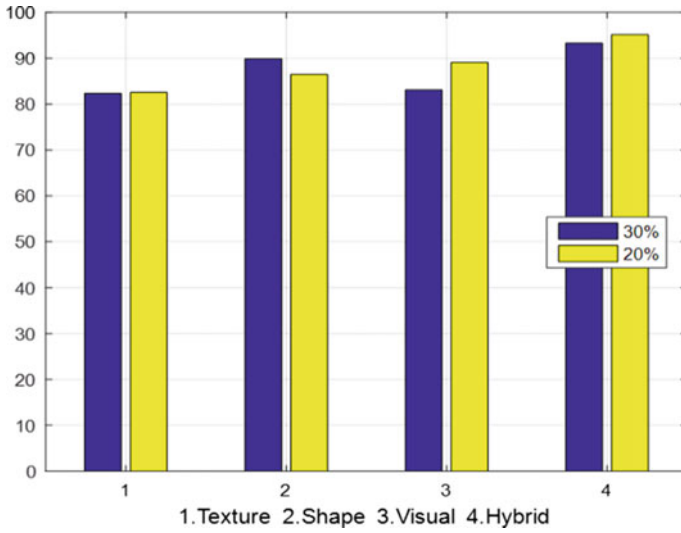


Fig. 2 Accuracy graph on 30–20% testing ratio

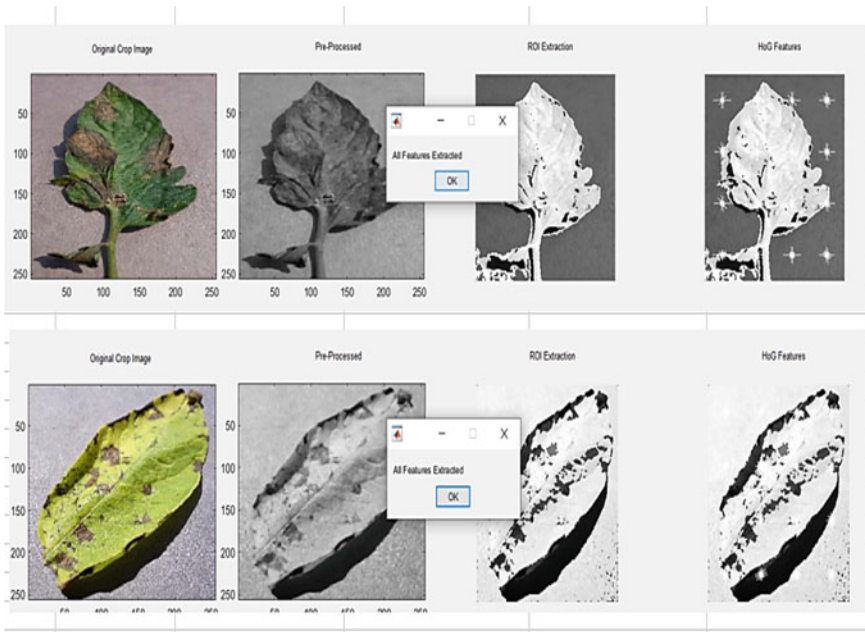


Fig. 3 Visual result

Table 2 Datasets used for implementation

Dataset	Total images	Bifurcation of total images	Crops	Accuracy	
				ANN	SVM
DS-2	1152	Late blight-1000 Healthy-152	Potato	95.12	82.75
DS-6	5152	Early blight-1000 Late blight-1000 Healthy-152	Tomato	92.12	83.14
		Early blight-1000 Late blight-1000 Healthy-152			

Simulation Tool: MATLAB is used for simulation.

Future Scope: We can develop a smart application wherein we can scan the image and tell the disease name with its grading to the farmer (Fig. 4).

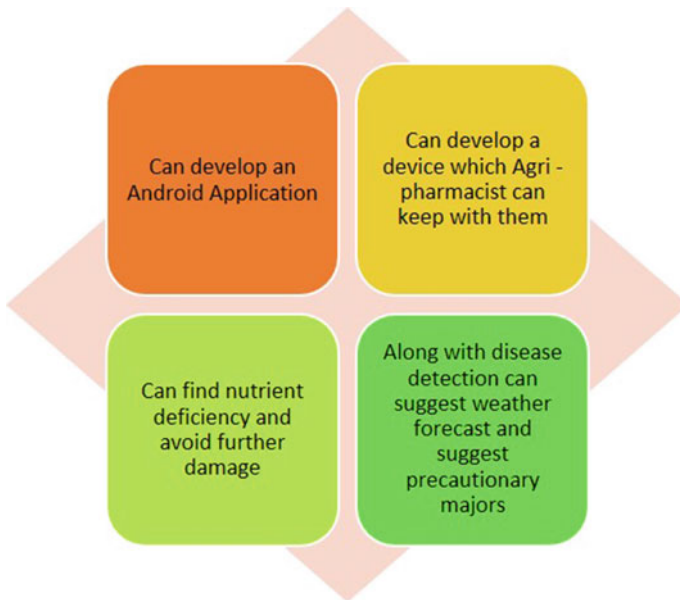


Fig. 4 Future scope

5 Conclusion

We focused on the performance analysis of proposed feature extraction technique in which the performances are evaluated in terms of accuracy rate, specificity and F1 Score, precision rate, recall rate. Among all the features extraction methods, the proposed approach achieved the significant improvement in performances with 95.12% accuracy for hybrid features using ANN classifier and 82.75% accuracy for SVM classifier using DS-2, similarly 92.12% accuracy for hybrid features using ANN classifier and 83.14% accuracy for SVM classifier using DS-6 dataset.

References

1. bin MohamadAzmi, M. T., & Isa, N. M. (2013). Orchid disease detection using image processing and fuzzy logic. In *2013 International Conference on Electrical, Electronics and System Engineering*. IEEE.
2. Singh, A., & Singh, M. L. (2015). Automated color prediction of paddy crop leaf using image processing. In *2015 IEEE International Conference on Technological Innovations in ICT for Agriculture and Rural Development (TIAR 2015)*.
3. Krishnan, M., & Sumithra, M. G. (2013). A novel algorithm for detecting bacterial leaf scorch (BLS) of shade trees using image processing. In *2013 IEEE 11th Malaysia International Conference on Communications*.
4. Mondal, D., & Kole, D. K. (2015). Detection and classification technique of yellow vein mosaic virus disease in okra leaf images using leaf vein extraction and Naive Bayesian classifier. In *2015 International Conference on Soft Computing Techniques and Implementations (ICSCIT)*. IEEE.
5. Khirade, S. D., & Patil, A. B. (2015). Plant disease detection using image processing. In *2015 International Conference on Computing Communication Control and Automation*. IEEE.
6. Pujari, J. D., Yakkundimath, R., & Byadgi, A. S. (2014). Identification and classification of fungal disease affected on agriculture/horticulture crops using image processing techniques. IEEE.
7. Singh, V., Varsha, & Misra, A. K. (2015). Detection of unhealthy region of plant leaves using image processing and genetic algorithm. In *2015 International Conference on Advances in Computer Engineering and Applications (ICACEA)*. IEEE.
8. Dhaygude, S. B., & Kumbhar, N. P. (2013). Classifical plant leaf disease detection using image processing. *International Journal of Advanced Research in Electrical, Electronics and Instrumentation Engineering*, 2(1).
9. Dubey, Y. K. (2018). Superpixel based roughness measure for cotton leaf diseases detection and classification. In *4th International IEEE Conference on Recent Advances in Information Technology (RAIT 2018)*.
10. Arya, M. S., & Anjali, K. (2018). Detection of unhealthy plant and genetic algorithm with Arduino. *IEEE Transactions*.
11. Jaiswal, H., & Choudhari, J. (2020). Plant leaf disease detection and classification using conventional machine learning and deep learning. *International Journal on Emerging Technologies*.
12. Zhang, X., Qiao, Y., Meng, F., Fan, C., & Zhang, M. (2018). Identification of maize leaf diseases using improved deep convolutional neural networks. *IEEE Access*, 6, 30370–30377.
13. Maniyath, S. R., Vinod, P. V., Niveditha, M., Pooja, R., Shashank, N., & Hebbar, R. (2018, April). Plant disease detection using machine learning. In *2018 International Conference on Design Innovations for 3Cs Compute Communicate Control (ICDI3C)* (pp. 41–45). IEEE.

14. Doh, B., Zhang, D., Shen, Y., Hussain, F., Doh, R. F., & Ayepah, K. (2019, September). Automatic citrus fruit disease detection by phenotyping using machine learning. In *2019 25th International Conference on Automation and Computing (ICAC)* (pp. 1–5). IEEE.
15. Balakrishna, K., & Rao, M. (2019). Tomato plant leaves disease classification using KNN and PNN. *International Journal of Computer Vision and Image Processing (IJCVIP)*, 9(1), 51–63.
16. Iqbal, Z., Khan, M. A., Sharif, M., Shah, J. H., urRehman, M. H., & Javed, K. (2018). An automated detection and classification of citrus plant diseases using image processing techniques: A review. *Computers and Electronics in Agriculture*, 153, 12–32.

Development of an Innovative Ultrasound-Assisted Extraction Technique to Optimize Extraction on Phytoconstituents and Compared Conventional Extraction Method



Shankaraiah Pulipaka, Ashish Suttee, M. Ravi Kumar, Kalakotla Shanker, Ramesh Kasarla, and Swamy Kasarla

Abstract In the past, people have relied on some methods like the Soxhlet and reflux device to extract plant matter. To address this problem, we use a cutting-edge extraction technique to remove the relevant plant material. There are several advantages of using ultrasonic-assisted extraction over the conventional approach, such as reduced solvent consumption, reduced extraction time, increased extraction purity, and an increased yield of bioactive phytoconstituents. The family Commelinaceae includes the Indian herb *Tradescantia spathacea* (T.S), which is used as a traditional medicine. It is the southeast Mexican region known as “Maguey Morado” are derived from *Tradescantia spathacea* (T.S) leaves extracted using traditional and ultrasonic-assisted extraction procedures using petroleum ether, ethyl acetate, methanol, hydroalcoholic, and aqueous solvents (Purple Maguey). Total phenolic

S. Pulipaka · A. Suttee (✉)

School of Pharmaceutical Sciences, Lovely Professional University, Phagwara, Punjab 144411, India

e-mail: ashish7manipal@gmail.com

S. Pulipaka · M. Ravi Kumar

Department of Pharmacognosy, Geethanjali College of Pharmacy, Cheeryal, Keesara, Medchal, Hyderabad, Telangana 501301, India

K. Shanker

Department of Pharmacognosy and Phyto-Pharmacy, JSS College of Pharmacy, JSS Academy of Higher Education and Research, Tamil Nadu, Ooty, Nilgiris, India

R. Kasarla

Lab of Molecular and Cellular Endocrinology, Division of Endocrinology, Diabetes, and Metabolism, Department of Medical Sciences, University of Turin Corso Dogliotti, 14 - 10126 Turin, Italy

S. Kasarla

Laboratory of Biomolecular Interactions Studies, Faculty of Chemistry, Warsaw University of Technology, 00-661 Warsaw, Poland

and flavonoid concentrations were also determined for extracts made using the two techniques. Results indicate that ultrasonic-assisted extraction technique produces a higher phytoconstituent yield compared to standard extraction methods.

Keywords *Tradescantia spathacea* · Ultrasonic assisted extraction technique · Optimization

1 Introduction

Medicinal plants used in alternative treatment are gaining more and more attention from the pharmaceutical, food, and nutraceutical businesses. Plants possess and used as the primary sources of treatments of diseases from olden days and till to date a number of plants are identified to have various activities [1]. From that the olden days plants were used by all cultures of the *world wide* with India that has one of the ancient, prosperous, and highly *multiple* cultures [2]. The analysis and standard jurisdiction *possessed* beneficial activity of plant drug in the cure of more illnesses [3]. Modern times need the use of cutting-edge extraction methods that may eliminate the drawbacks of the status quo. Ultrasonic-assisted extraction (UAE) is useful in this setting because it shortens extraction times while increasing extraction purity and minimising solvent use. Extraction of bioactive substances from plants is a typical practice in the Ultrasonic-assisted extraction (UAE) [4]. Because it uses less organic solvent than conventional methods, UAE is considered a “green” technique.

The vegetative plant *Tradescantia spathacea* (SW.) Stearn (T.S) had distinguished as a utilitarian nourishment, especially in the Southern part of U.S.A with the dehydrate leaves have the possibility to be expanded into a pekoe—similar to refreshment, the decoction is taken orally consistently as treatment for malignant growth [5]. It has been existed that individual in various pieces of the world routinely to utilize the equivalent or comparative plants for treating similar sicknesses *however, in* different mixes [6].

2 Materials and Techniques

2.1 Plant Specimens were Collected and Authenticated

In the months of May and June, local residents of Hyderabad, Telangana, India, gathered fresh (*Tradescantia spathacea*) plants from their own yards. These components have been validated as being of botanical origin by Scientist G. P.V. Prasanna, from the Deccan Regional Center of the Botanical Survey of India in Hyderabad, Telangana, India. The Department of Pharmacognosy, Geethanjali College of Pharmacy, Hyderabad, India, has contributed a sample voucher (BSI/DRC/2020-21/Identification/

Tech/66). A future reference may be made to this authenticated voucher. Every reagent in this analysis is of the highest possible quality.

2.2 Conventional Method

When the plants were collected, they were shade dried in a cool area and then finely pulverised in a pulverizer. Pet. ether, ethyl acetate, methanol, hydroalcoholic, and water solvents were used in a Soxhlet extraction to extricate the bioactive phyto-constituents from powdered plant. Distillation was then used to concentrate the solvent under vacuum in a rotating evaporator. The extracts were dried and stored in a desiccator [7].

2.3 Ultrasound Assisted Extraction Method

One gramme of dry ground plant was added to twenty millilitres of water in a 250 millilitre Erlenmeyer conical flask to make the concentrates. The ultrasonic shower was worked at 60 °C for 30 min at a recurrence of 35 kHz utilizing the greatest information force of 240 W. There were no additional preservatives used, and all recovered components were filtered after incubation and stored at 4 °C until analysis. The extraction was performed in triplicate and further the results for both the extraction process i.e. conventional method and UAE was compared with each other in Table 1 [8].

Table 1 *Tradescantia spathacea* extracts' shade, texture, and percentage yield sample of *Tradescantia spathacea*

Plant extract	Color observed in day light	Consistency	Conventional method yield (%w/w)	Ultrasound assisted extraction (%w/w)
Methanolic extract	Dark green	Semisolid	10.52	16.29
Ethyl acetate extract	Light green	Semisolid	6.23	8.56
Hydro alcoholic extract	Dark green	Semisolid	6.56	10.19
Petroleum ether extract	Light green	Semisolid	2.31	7.85
Aqueous extract	Light green	Semisolid	8.25	14.45

Estimation of total phenolic contents

3 Analysis of Plant Extracts for Their Phytochemical Content

3.1 Total Phenolic Content Approximation

3.1.1 Principle

The Folin-Ciocalteu method was used to determine the total phenolic content. To perform a colorimetric test of polyphenolic and phenolic antioxidants, scientists use a reagent that consists of phosphotungstate and phosphomolybdate. It aids in determining the quantity of testable material needed to prevent reagent oxidation. Dilutions of the sample extract were oxidised using the Folin Ciocalteu reagent, and the subsequent response blend was killed with sodium carbonate. The absorbance of the blue arrangement was estimated at 765 nm following 30 min.

3.1.2 Preparation of Sample

After extracting the leaves of *Tradescantia spathacea* (SW.) Stearn using ethyl acetate, methanol, hydroalcoholic, and water, filter the solution and bring it to a total volume of 50 ml in a volumetric flask. One millilitre of sample was added to ten millilitres of distilled water in a test tube. Following the expansion of 1.5 ml of Folin-reagents, the combination was left to hatch at room temperature for 5 min. Sodium carbonate (Ciocalteu's), 20% (w/v) (4 ml). At room temperature for 30 min, the solution was rapidly stirred and raised to a final volume of 25 ml using distilled water. The solution's highest absorbance was found to be at 765 nm [9] when measured using a UV spectrophotometer. In this case, we got a good, solid, triple-checked result. We utilised a Gallic corrosive standard bend to decide the mass of the example. The complete phenolic content of the concentrate is displayed in Table 2, and the Gallic corrosive standard bend is displayed in Fig. 1.

Calculation

$$C = c \times V/M$$

C —Phenolic acid content

c —gallic acid concentration (mg/ml) based on a standard curve.

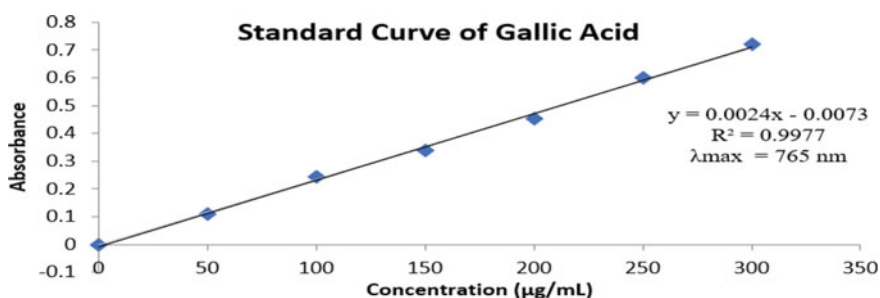
V —Volume extraction (ml).

M —Extract's Mass (g).

Table 2 Total phenolic contents of *Tradescantia spathacea*

S. No	Test sample (<i>Tradescantia spathacea</i>)	Gallic acid equivalent mg/g total phenolic content from conventional extraction	Gallic acid equivalent milligrammes per gramme of total phenolic content
1	Methanolic extract	1.29 ± 1.05	4.23 ± 1.70
2	Ethyl acetate extract	1.59 ± 0.71	1.80 ± 0.68
3	Hydro alcoholic extract	1.29 ± 1.05	1.53 ± 0.26
4	Petroleum ether extract	2.43 ± 0.17	3.33 ± 0.51
5	Aqueous extract	1.59 ± 0.7	2.22 ± 1.19

Estimation of total flavonoid content

**Fig. 1** Estimation of total phenolic content

3.2 Flavonoid Content in Plant Extracts: A Rough Approximation

3.2.1 Principle

This overhauled technique for aluminum chloride colorimetric test was uncovered by Woisky and Salatino. The complex was shaped because of associations between aluminum chloride and the C-4 place of keto gatherings or the C-3 and C-5 areas of hydroxyl bunches in flavonols and flavones (corrosive stable). In addition, flavonoids can be converted into an acid-labile compound via aluminum chloride's formation of orthodihydroxyl.

3.2.2 Preparation of Sample

After extracting the leaves of *Tradescantia spathacea* (SW.) Stearn (1 g), After filtering, we added numerous solvents until the volume in the volumetric carafe read 50 ml. (oil ether, ethyl acetic acid derivation, methanol, hydroalcoholic, and water). A 2% aluminium chloride/0.6 mL sample solution mixture (0.6 mL). The combination was then left alone for another hour at room temperature. Using a UV- spectrophotometer, we determined the absorbance of the reaction mixture to be 420 nm [10]. In this case, we got a good, solid, triple-checked result. All of the samples were quantified with the use of a quercetin standard curve. The total flavonoid content of the extract is shown in Table 3, and the quercetin standard curve is shown in Fig. 2.

Calculation

$$C = c \times V/M$$

Table 3 Total flavonoids contents of *Tradescantia spathacea*

S. No.	Test sample (<i>Tradescantia spathacea</i>)	Total phenolic content, expressed as the quercetin mg/g equivalent, after conventional extraction	Compare the amount of phenolic compounds present in milligrammes per gramme to the amount of quercetin
1	Methanolic extract	2.27 ± 0.81	10.60 ± 6.17
2	Ethyl acetate extract	2.40 ± 0.91	3.67 ± 0.38
3	Hydro alcoholic extract	1.79 ± 0.61	3.81 ± 0.47
4	Petroleum ether extract	1.66 ± 0.16	3.63 ± 0.52
5	Aqueous extract	2.40 ± 0.87	3.89 ± 0.69

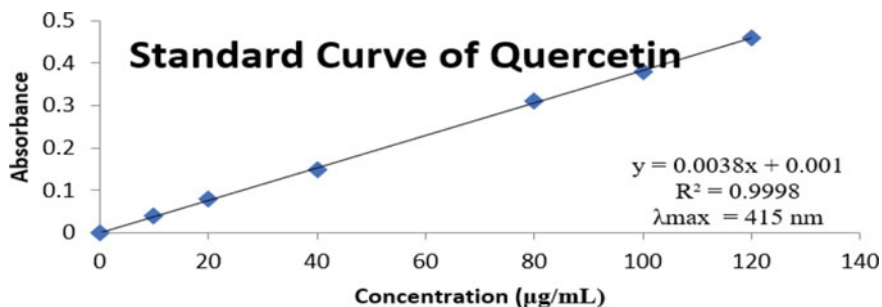


Fig. 2 Estimation of total flavonoid content

C —Total flavonoid content.

c —quercetin concentration (mg/ml) based on standard curve.

V —Total volume of extract (ml).

M —Mass extraction (g).

4 Results

4.1 Extraction

Ultrasound-assisted extraction has emerged as a promising technique to boost the efficiency and yield of *Tradescantia spathacea* plant extracts. UAE performed better than the conventional extraction approach, according to the findings.

5 Conclusion

This study aims to develop an innovative ultrasound-assisted extraction technique optimized for phytoconstituent extraction and compare its performance with a conventional extraction method. Researchers found that when comparing conventional and UAE techniques of extracting (*Tradescantia spathacea*), it was shown that the yield and level of phytoconstituents like phenolic and flavonoid content were significantly increased using the UAE technique.

Acknowledgements I am considerably thankful to Lovely Professional University, Jalandhar, Punjab, India, for their guidance, kind help, and constant encouragement at each step in my work progress

References

1. Kakkar, S., & Bais, S. (2014). A review on protocatechuic acid and its pharmacological potential. *ISRN Pharmacology*, 952943, 9 pp.
2. Tandon, V., Kapoor, B., & Gupta, B. M. (2004). Herbal drug research in India: A trend analysis using IJP as a marker. *Indian Journal of Pharmacology*, 36(2), 99–100.
3. Ehrlich, S. D. (2009). NMD. In *Solutions acupuncture, a private practice specializing in complementary and alternative medicine*. Steven D. Ehrlich, NMD, Healthcare Network.
4. Gadjalova, A. V., & Mihaylova, D. (2019). Sp, ultrasound-assisted extraction of medicinal plants and evaluation of their biological activity. *Food Research*, 3(5), 530–536.
5. Rosales-Reyes, T., de la Garza, M., Arias-Castro, C., Rodríguez-Mendiola, M., Fattel-Fazenda, S., Arce-Popoca, E., Hernández-García, S., & Villa-Trevino, S. (2008). Aqueous crude extract of *Rhoeo discolor*, a Mexican medicinal plant, decreases the formation of liver preneoplastic foci in rats. *Journal of Ethnopharmacology*, 115(3), 381–386.

6. Motaleb, M. A. (2011). *Selected medicinal plants of Chittagong hill tracts*, pp. 1–128
7. Choudhary, N., Bijjem, K. R. V., & Kalia, A. N. (2011). Antiepileptic potential of flavonoids fraction from the leaves of *Anisomeles malabarica*. *Journal of Ethnopharmacology*, *135*, 238–242.
8. Han, H., Wang, S., Rakita, M., Wang, Y., Han, Q., & Qin, X. (2018). Effect of ultrasound-assisted extraction of phenolic compounds on the characteristics of walnut shells. *Food and Nutrition Sciences*, *9*, 1034–1045.
9. Siddiqui, N., Rauf, A., Latif, A. et al. (2017). Spectrophotometric determination of the total phenolic content, spectral and fluorescence study of the herbal Unani drug Gul-e-Zoofa (*Nepeta bracteata* Benth). *Journal of Taibah University Medical Sciences*, 1–4.
10. Chandra, S., Khan, S., Avula, B., et al. (2014). Assessment of total phenolic and flavonoid content, antioxidant properties, and yield of aeroponically and conventionally grown leafy vegetables and fruit crops: A comparative study. *Evidence-Based Complementary and Alternative Medicine*, 1–9.

Seasonal Impact Analysis Using Clay Pot Refrigerator on the Shelf Life of Tomatoes



Nishigandha Patel, V. K. Bhojwani, and Sachin Pawar

Abstract This paper focuses on the evaporative cooling techniques for the preservation of farm produce like tomatoes. This investigation uses cost-effective passive evaporation enhancing technique with a wet jute bag and without a wet jute bag. Investigations have been done over seasons like winter, summer, and rainy. The suitable technique of clay pot refrigerator is used to reduce postharvest losses of farm produce (tomatoes). The effect of seasons on the clay pot refrigerator and its impact on the shelf life of tomatoes have been studied here. This paper gives the best possible solution for the storage of tomatoes in a clay pot refrigerator which works without electricity.

Keywords Evaporative cooling · Clay pot refrigerator · Relative humidity · Ambient temperature

1 Introduction

Evaporative cooling is an ancient and powerful technology for reducing temperature. Animals as well as plants also use evaporative cooling method to reduce their body temperature as compared to environment. Through the evapotranspiration, plants reduce their temperature and remain cooler than atmospheric condition. Indian economy is poor due to hunger management. Many people do not get food and majorly it affects farmers and their families. Post-harvest losses can be reduced and profit can be increased and it can serve many families in India.

In developed countries food losses occur majorly at a consumer level, but in under developing countries about 40% of the waste is due to post-harvest losses due to improper storage. In the villages of India, food losses burden falls on the smallholder like farmers and their families. A majority of people in rural areas are not privileged to have access to electricity. Economical and health problems are being created due to large amount of food spoilage for which refrigerated storage is presently an

N. Patel (✉) · V. K. Bhojwani · S. Pawar
MITSOE, MITADTU, Pune, India
e-mail: nishigandha.patel@mituniversity.edu.in

option. The clay pot refrigerators can be used in such a rural area for preserving the vegetables and fruits. Clay pot refrigerator does not require any electricity and they are available at cheaper rate. Use of toxic refrigerants is avoided in clay pots and also they are ecofriendly. The research work aims at performance investigation of clay pot refrigerator. Inside temperature variation with surrounding air condition and its dependency on various parameters like wind velocity, relative humidity, ambient temperature, exposure to sun light, wrapping of wet clothes have been studied [1]. Effective conversion of sensible heat to latent heat is a basic principle on which clay pot refrigerator works. Evaporative cooling is the ancient & most economical method for cooling effect [2]. There is an energy associated with phase change when evaporation takes place from surface this is called as latent heat of vaporization. Here the temperature is reduced but the relative humidity is increased in fruit and vegetables [3, 4]. Evaporative cooling works on the principle of total turning of sensible to latent heat. Dry and hot air of ambient flows over the wetted walls of clay pot where water is continuously dripping down from the water tank. In summer season due to low relative humidity water evaporates from the walls of the tank. Evaporation rate is less in winter and in rainy it's poor. Water is evaporated due to conversion of atmospheric air's sensible heat to latent heat. The latent heat follows the water vapor and diffuses into the air. Dry bulb temperature is decreased and Relative humidity is increased due to evaporation. Evaporation cooling is dependent on weather conditions or seasons.

2 Methodology

This experimentation focuses on the reduction of post-harvest losses of farm produce like tomatoes [5, 6]. Seasonal testing of clay pot refrigerator has been carried out for summer, winter and rainy season. It involves the number of parametric Investigation like Dry bulb temperature (DBT), Wet bulb temperature (WBT), Relative Humidity (RH) and ambient temperature. This experimentation has been carried out with and without Jute bag which is cost effective passive evaporation enhancing technique. The effect of listed parameters (DBT, WBT, RH, and Air Velocity) on clay pot refrigerator with farm produce has been tested over different seasons. This investigates the shelf life of tomatoes inside the clay pot refrigerator in terms of no of days (Fig. 1).

3 Results and Discussions

Relation between relative humidity (RH), ambient temperature (T_{amb}), defines the quality of the air as dry or hot or wet. T_{i1} is the wall with minimum temperature and top wall is on which we are keeping farm produce (tomatoes). Figure 2 shows the plot of temperature difference between ambient and T_{cold} where tomatoes has been kept is in the range of 3–5 °c for winter season without jute bag. This investigation

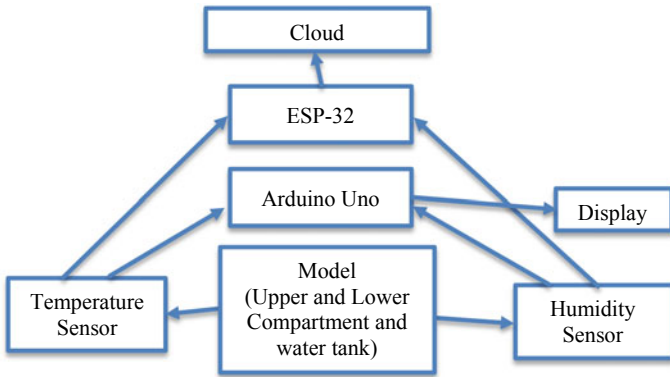


Fig. 1 Schematic diagram of clay pot refrigerator with jute bag and farm produce

says that in the winter season upper compartment of clay pot refrigerator keeps the tomatoes fresh for 3 days whereas lower compartment for 2 days without jute bag (Fig. 3).

Figure 4 shows the plot of temperature difference between ambient and T_{cold} where tomatoes has been kept is in the range of 4–7 °c for winter season with jute bag. This investigation says that in the winter season upper compartment of clay pot refrigerator keeps the tomatoes fresh for 3 days whereas lower compartment for 2 days with jute bag but with increase in moisture.

Figure 5 shows the plot of temperature difference between ambient and T_{cold} where tomatoes has been kept is in the range of 8–12 °c for summer season without jute bag. This investigation says that in the summer season upper compartment of

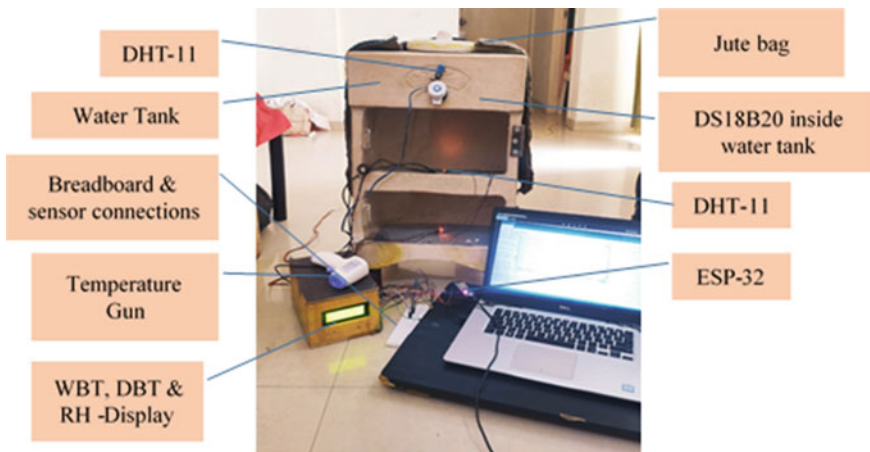


Fig. 2 Experimental setup of clay pot refrigerator with jute bag and farm produce

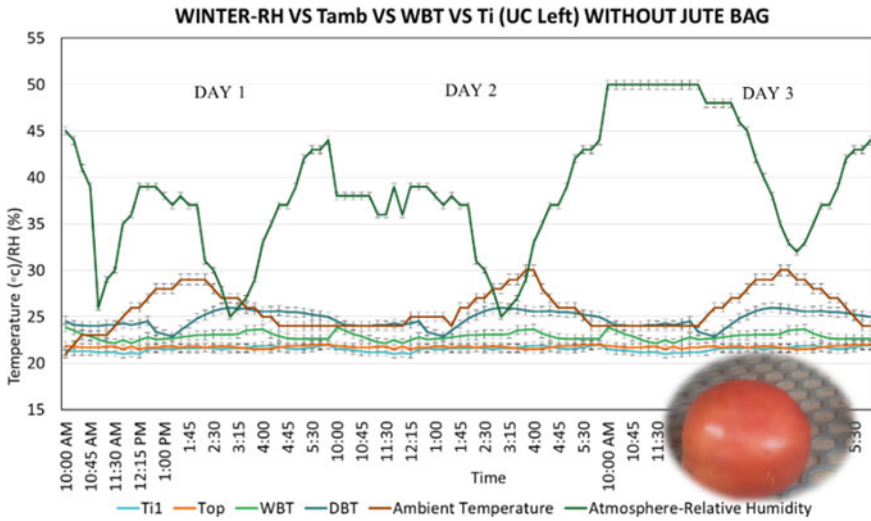


Fig. 3 Plot of Tamb, RH, WBT, DBT, Tcold versus time without jute bag for winter season

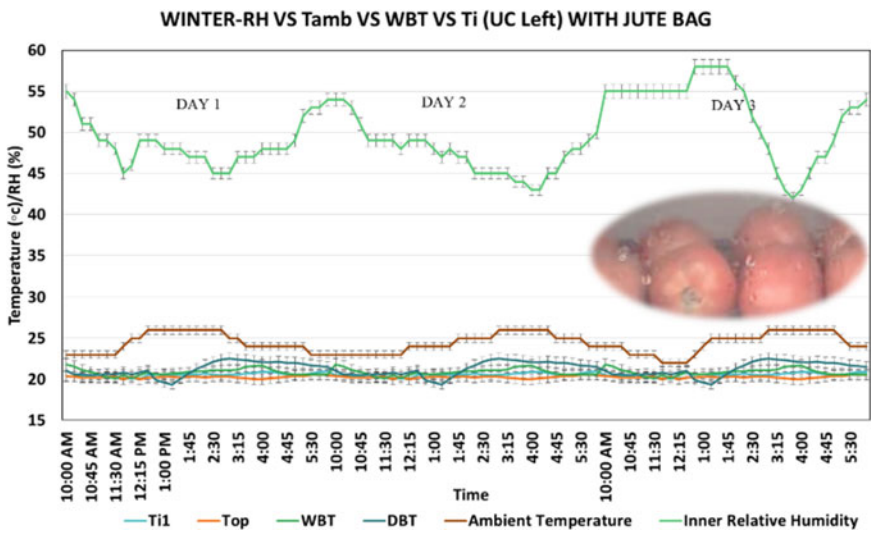


Fig. 4 Plot of Tamb, RH, WBT, DBT, Tcold versus time with jute bag for winter season

clay pot refrigerator keeps the tomatoes fresh for 4 days whereas lower compartment for 2 days without jute bag.

Figure 6 shows the plot of temperature difference between ambient and T_{cold} where tomatoes has been kept is in the range of 8–15 °C for summer season with jute bag. This investigation says that in the summer season upper compartment of clay pot refrigerator keeps the tomatoes fresh for 3 days whereas lower compartment

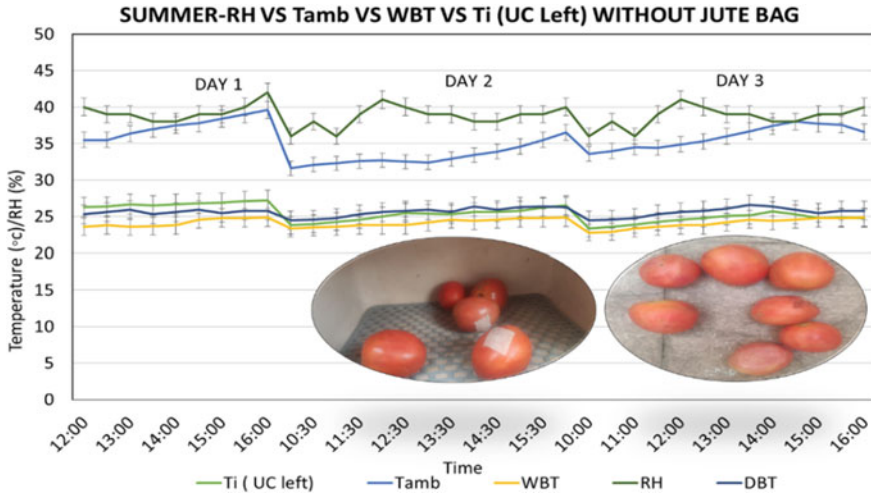


Fig. 5 Plot of Tamb, RH, WBT, DBT, Tcold versus time without jute bag for summer season

for 2 days with jute bag. It has been proved from the investigation that jute bag keeps tomatoes at lower temperature as compared to ambient and without jute bag experimentation but it increases inside relative humidity which is shown in Fig. 4 on the tomato skin in terms of water droplet which is condensate.

Figure 7 shows the plot of temperature difference between ambient and T_{cold} where tomatoes has been kept is in the range of 1–5 °c for rainy season with jute bag. This investigation says that in the summer season upper compartment of clay

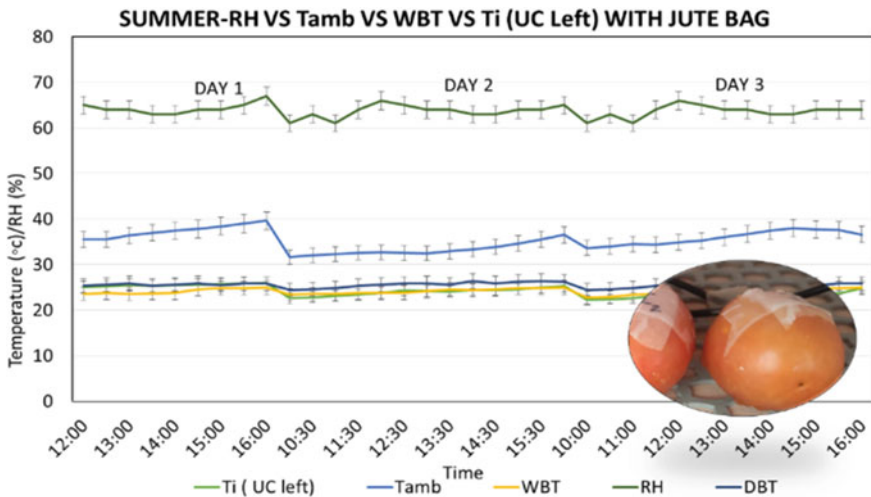


Fig. 6 Plot of Tamb, RH, WBT, DBT, Tcold versus time with jute bag for summer season

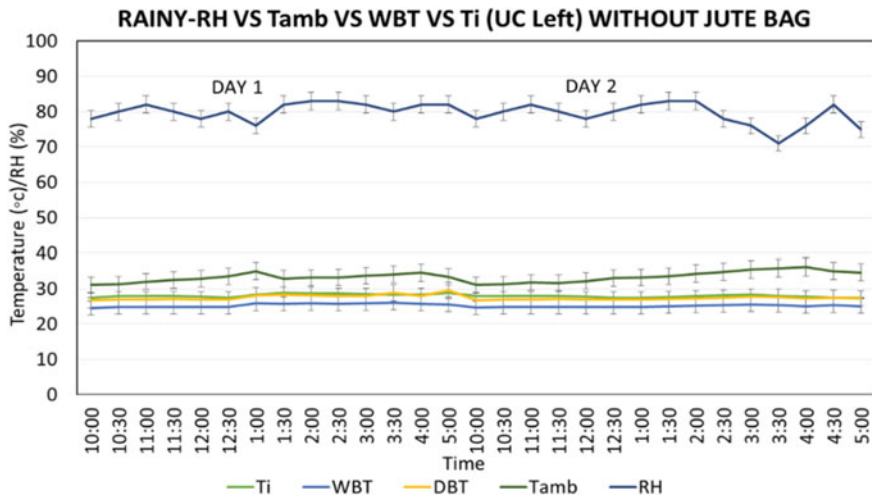


Fig. 7 Plot of Tamb, RH, WBT, DBT, Tcold versus time without jute bag for rainy season

pot refrigerator keeps the tomatoes fresh for 2 days whereas lower compartment for 2 days with jute bag. Figure 5 shows that tomatoes have got fungus due to excessive moisture present inside the clay pot experimentation with a jute bag.

Figure 8 shows the plot of temperature difference between ambient and T_{cold} where tomatoes has been kept is in the range of 1–5 °c for rainy season with jute bag. This investigation says that in the summer season upper compartment of clay pot refrigerator keeps the tomatoes fresh for 2 days whereas lower compartment for 2 days with jute bag. Figure 5 shows that tomatoes have got fungus due to excessive moisture present inside the clay pot experimentation with a jute bag.

Figure 9 shows the plot of temperature difference between ambient and T_{cold} for various seasons without jute bag. It is seen from Fig. 6 that the clay pot refrigerator works well in summer and gives poor performance in rainy season.

It can also be used to store tomatoes in winter season as it gives ΔT is in the range of 3–6 °c. In summer this ΔT is in the range of 11–13 °c where as in rainy season it is in the range of 1–3 °c. This is due to ambient relative humidity which affect the rate of evaporation from the walls of clay pot refrigerator.

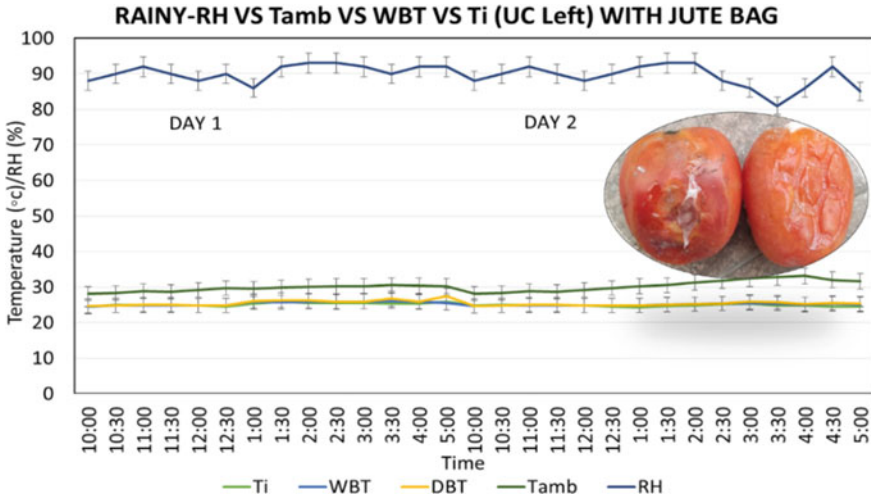


Fig. 8 Plot of Tamb, RH, WBT, DBT, Tcold versus time with jute bag for rainy season

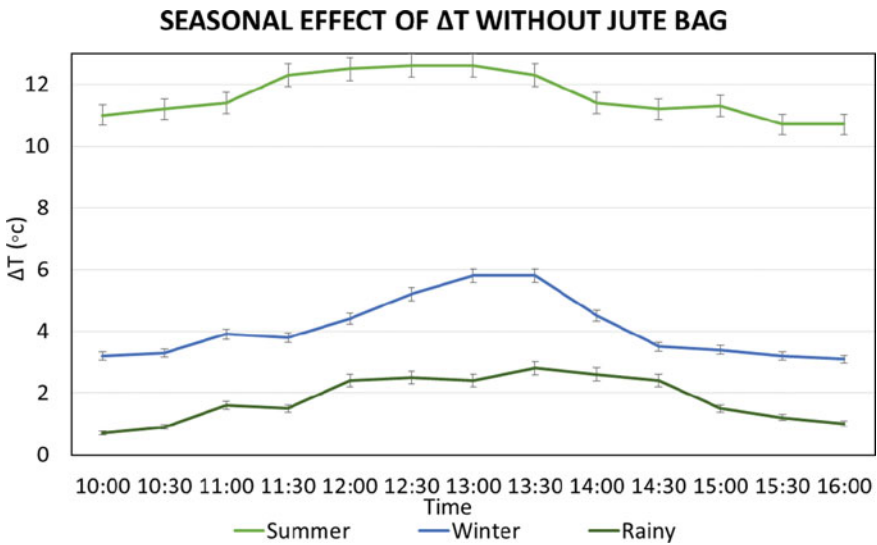


Fig. 9 Plot of temperature difference versus time over different seasons

4 Conclusion

This investigation proves that using a jute bag keeps tomatoes at lower temperature but increases inside relative humidity. This increase in inside clay pot relative humidity reduces the life of tomatoes. It is better to store tomatoes in the clay pot without jute bag over different seasons.

Clay pot refrigerator shows good results in storing the tomatoes in summer season where the ambient air is hot and dry. It also works well in winter season for storing tomatoes as compared to rainy season. In rainy season this clay pot refrigerator should not be recommended to store tomatoes.

References

1. Nishigandha Patel, O., Mindhe, M., Lonkar, D., Naikare, S., Pawar, V. K., & Bhojwani, S. P. (2021). Performance investigation of mitticool refrigerator. *Techno-Societal*, 1051–1106.
2. Anyanwu, E. E. (2004). Design and measured performance of a porous evaporative cooler for preservation of fruits and vegetables. *Energy Conversion and Management*, 45, 2187–2195.
3. Date, A. W. (2012). Heat and mass transfer analysis of a clay-pot refrigerator. *International Journal of Heat and Mass Transfer*, 55, 3977–3983.
4. Damle, R. M., & Date, A. W. (2015). Heat and mass transfer in a clay-pot refrigerator: Analysis revisited. *Journal of Energy, Heat and Mass Transfer*, 37, 11–25.
5. Harish. H. G., & Krishne Gowda, Y. T. (2014). Thermal analysis of clay pot in pot refrigerator. *IJMERE*, 4(9). ISSN: 2249–6645.
6. Harish, H. G., & Krishne Gowda, Y. T. (2014). Thermal analysis of clay pot. *International Journal of Engineering Research and Technology (IJERT)*, 2(10). ISSN: 2278-0181, IJERTV3IS100271.
7. Chinenye, N. M. (2011). Development of clay evaporative cooler for fruits and vegetables preservation. *Agriculture Engineering International: CIGR Journal*, 13(1).
8. Alami, A. H. (2014). Effects of evaporative cooling on efficiency of photovoltaic modules. *Energy Conversion and Management*, 77, 668–679.
9. Ndukwu, M. C., & Manuwa, S. I. (2014). Review of research and application of evaporative cooling in preservation of fresh agricultural produce. *International Journal Agriculture and Biology, Engineering*, 7(5), 85.
10. Amer, O., Boukhanouf, R., & Ibrahim, H. G. (2015). A review of evaporative cooling technologies. *International Journal of Environmental Science and Development*, 6(2).
11. Warke, D. A., & Deshmukh, S. J. (2017). Experimental analysis of cellulose cooling pads used in evaporative coolers. *International Journal of Energy Science and Engineering*, 3(4), 37–43, ISSN: 2381-7267 (Print); ISSN: 2381-7275 (Online).
12. Ndukwu, M. C., Manuwa, S. I., Bennamoun, L., Olukunle, O. J., & Abam, F. I. (2018). In-situ evolution of heat and mass transfer phenomena and evaporative water losses of three agro-waste evaporative cooling pads: An experimental and modeling study. *Waste and Biomass Valorization*.
13. Nolasco, C., Jácome, N. J., & Hurtado-Lugo, N. A. (2019). Solution by numerical methods of the heat equation in engineering applications. A case of study: Cooling without the use of electricity. In *5th International Week of Science, Technology and Innovation Journal of Physics: Conference Series 1388* (Vol. 012034).
14. Inamdar, S. J., & Kale, A. J. P. (2019). Performance enhancement of evaporative cooling by using bamboo. *International Journal of Engineering and Advanced Technology (IJEAT)*, 8(6S). ISSN: 2249-8958.

15. Ayomide, O. B., Ajayi, O. O., & Ajayi, A. A. (2019). Advances in the development of a tomato postharvest storage system: towards eradicating postharvest losses. In *International Conference on Engineering for Sustainable World Journal of Physics: Conference Series 1378* (Vol. 022064). <https://doi.org/10.1088/1742-6596/1378/2/022064>
16. Lahnizi, A., Mahdaoui, M., Abdellaha, A. B., Anoune, K., Bakhouyab, M., & Ezbakhed, H. (2019). Performance analysis and optimal parameters of a direct evaporative pad cooling system under the climate conditions of Morocco. *Case Studies in Thermal Engineering, 13*, 100362
17. Somwanshi, A., Mishra, P. R., & Gaba, V. Thermal analysis of a dual-purpose cooler used for air cooling and mild refrigeration, S2451-9049(19)30169-6.

Engineering for Rural Development

Continuous 24*7 Water Supply System: A Review of Literature



Nitin P. Sonaje, Mukund M. Pawar, and Nitin D. More

Abstract Modern improvements in water analysis methods have highlighted the many advantages of a continuous water distribution system over an intermittent water supply system. Early studies in this discipline mostly focused on case studies that described the difficulties and benefits of putting continuous water delivery systems in place. These studies gave important information about the process of implementation, budgetary considerations, and how people responded to the altered water supply system. In order to identify leaks and enhance water quality, the leakages were analysed using a representative sample of water from the end user's water tap that was tested for chlorine and turbidity monitoring.

Keywords 24*7 water supply systems · EPANET · CPHEEO · Non-revenue water

1 Introduction

Customarily, water supply systems are designed as continuous water supply systems. Because of insufficient funding and improper implementation coupled with impediment caused by un-projected urbanization and rise in water demand, the distribution systems are expanded without taking apprehension of the hydraulic design. Transforming this chaotic distribution system into a well-disciplined and properly designed system is the mission of 24*7 supply system. Continuous 24*7 water supply systems

N. P. Sonaje (✉)
Government Polytechnic, Miraj, Maharashtra, India
e-mail: nitinsonaje@yahoo.co.in

M. M. Pawar · N. D. More
SVRI's College of Engineering, Pandharpur, Maharashtra, India

are gaining popularity due to uninterrupted water supply to the consumers. The literature review discusses the following aspects of the continuous 24*7 water supply system.

- Water Supply System Design
- Operational Efficiency
- Consumer Behaviour
- Economic Considerations
- Case Studies.

2 Literature Review

With advancements in water analysis approaches, researchers brought out various advantages of a 24*7 water supply system over intermittent water supply systems. The initial studies in this domain were mainly case studies of implementing continuous water supply systems. They presented the experience of implementing continuous water supply systems, including the difficulties in implementation, cost approaches and people's behaviour over the modified water supply system.

Joshi et al. [1] evaluated the water supply systems that are intermittent and continuous, and a survey for opinions of consumers was undertaken for meticulous appraisal of both methods of operation. A door-to-door survey was undertaken in Ghaziabad and Jaipur's study area using predesigned questions related to different aspects of water supply and consumers' feedback regarding the degree of service. Consumers' feedback indicated a satisfying service where adequate water was supplied without considering the water supply mode. Many complaints about the quality of supplied water, duration of supply, lower water pressures and lapses in supply were brought to the surface during the intermittent water supply. Each family had stored water for domestic usages like drinking and other purposes. Almost all the families throw away stagnant drinking water as there is a freshwater supply the next day. The stale water was often used for the kitchen, washing clothes, and watering plants. The storage of water for other causes depends on financial conditions and the facility of an open well in the house premises. As there were no complaints about the water supply tariff, most residents preferred continuous water supply.

Dahasahasra [2] studied a 24*7 water supply scheme implemented in Maharashtra's Badlapur city. He presented the efficient management of existing water fields by restructuring the areas to enhance water distribution. The reframing included installing controllers for insulation for isolating areas of work. Effective Compliance of the valve for the outlet of the reservoir and the designation of crest demands.

Gohil [3] determined significant obstacles to effective reform and the provision of an urban pilot project. The author selected the city of Bhavnagar to design the network for water distribution. The author had split the small District Metering Area in the territory. The author used EPANET water management modelling tools for developing water distribution systems built by the US Environmental Protection Agency.

The guidelines of CPHEEO were followed to design the networks for distribution. The author suggested 27*7 water supply systems in place of the intermittent water supply system.

Patil and Deulkar [4] studied the Management of Water Supply Quality under 24*7 schemes of sector No. 21, PCMC, Pune. The authors stated that PCMC strives hard to provide a continuous water supply with better quality to all users. Before providing a continuous water supply, the authors assumed 'leakages' in the distribution points as prime parameters for impurities in water. A representative specimen of water through the end user's water tap was examined for chlorine and turbidity monitoring to identify leakages and provide better water quality. Water leaks were identified with the help of Helium. They observed that this methodology was secure and straightforward to use exact outcomes to identify leaks in water lines.

Rajeshwari and Kumar [5] undertook a study in order to assess the Intermittent Water Supply System and structure of the continuous water supply network for the domestic area in Mysore, Karnataka, India. As demand for water rises, groundwater supplies have been reduced, and capital costs have risen. They studied the quality of water for an intermittent water supply system. This paper incorporated the concept of a 24*7 water network to analyze water quality for current intermittent water supply systems. The configuration and evaluation of the network for water supply were based on LOOP and EPANET.

Vassiljev and Puust [6] developed an approach for optimizing water tank levels, estimating the impact of valve leakages and deciding on replacing old pipes. WaterGEMS had been brought into use for its simplified analysis to investigate the different alternatives.

Stokes et al. [7] introduced a Water distribution cost-emission nexus (WCEN) for consolidating computational tools to solve WDS optimization problems through a computational freeware framework. The simulation was carried out for cost calculations, GHG emissions, and MO heuristic optimization of hydraulic and pumping operations. Four functional scenarios were used: one represented standard practices, whereas the other 3 represented additional simulation complexity and flexibility, i.e., stable state simulation with the help of average emission factor, the tariff of electricity and the requirement of water. Taking into account the short-term and long-term variations in comparison with standard simulation practices, design, pumping operating management options, and their costs and emissions of GHG can have a significant impact.

Ghorpade and Vaidya [8] carried out an experiment-based study of the hydraulic water distribution model with a pressure-based approach. They stated that the water pressure on the consumer's side plays a crucial role in the water distribution system. The methodology driven by water pressure played a vital role in the design of the network. It was essential to hold the correct intensity of pressure at each node. The simulation of the network was done by using the Newton-Raphson method. They calculated the pressure using an experimental setup that consisted of a piezometer and verified it in WaterGEMS. The increase of percentage in each node's pressure heads is calculated in this experiment, and the outcomes generated an equation for pressure prediction.

Mallikarjun et al. [9] designed intake, jack well and pump house, water treatment units such as settling tanks, filters, disinfection units, and water distribution system for Ranebennur (Karnataka). The dead-end system was used for water distribution. They assessed the quality and quantity of supplied water. The quality and quantity of water supplied were satisfactory.

Mavi and Vaidya [10] conducted a study to build a 24 h water supply distribution system using the aid of WaterGEMS. They stated that given the cities' issues with erratic water supply, suitable zoning and distribution systems were required to meet the increased water demand. Water availability was inconsistent, which posed a serious health risk and rendered operations inefficient and expensive. The main goal of this study would be to make the current system operate continuously.

Varu and Shah [11] designed and builds a DPR for 24*7 water supply system at two wards of Ahmedabad city, Gujrat, India, viz., Sabarmati and old Wadaj wards. Its DPR includes a feasibility study, hydraulic design using WaterGEMS, a maintenance and operations plan, and economic viability. The state of the current intermittent water delivery network and the continuous water supply system of a few DMAs were compared. The study demonstrates that in order for the city to meet the service level criteria, it must switch from an intermittent to a 24-h water distribution system. indicates that in order to transform the intermittent water delivery system into a 24-h system, over 85% of the current network needed to be replaced.

Mallick et al. [12] focused on the simulation of the current and projected water distribution systems for the town of Jhunjhunu, Rajasthan, India, utilising Bentley's WaterGEMS V8i coupled with ArcGIS, AutoCAD, and SCADA software. The hydraulic model that was created helped to identify, locate, and characterise the main leakage sources with alarm systems, separate the network into district metre areas, establish operational protocols for pressure, optimise the network, implement real-time control, and analyse the water quality. According to CPHEEO, the hydraulic simulation model might reduce non-revenue water (NRW) by up to 7% within the DMA and by overall 12% with 12 m of water pressure at the consumer end.

Pawar and Sonaje [13] transformed the existing intermittent water distribution system to 24*7 for the Pandharpur city of Maharashtra, India by using WaterGEMS. A genetic algorithm with Darwin optimization approach was used for cost optimization of the 24*7 network. The effect on demand, head loss and pressure development of the forecasted population has been considered. It has been observed that the cost of the pipe network is reduced by 14 percent with the reduction of the pressure development by balancing it at different locations.

Jaiswal et al. [14] examined the reliability of the WDS in Dehradun city, Uttarakhand, India, by using a ground penetrating radar (GPR) survey and a GIS-based hydraulic model of WDN with EPANET software. Around three-quarters of the system's 564 km of water pipelines are antiquated, according to a map of the distribution network. The analysis confirmed that a hydraulically efficient distribution network is capable of supplying water continuously to all service points 24 h a day, seven days a week, within the acceptable pressure limits of 7 to 80 m at all nodes, and pipe velocity would not exceed 0.6 to 2 m/s as required by CPHEEO.

Tawalare and Balu [15] carried out two case studies in that they have given performance evaluation of implementing continuous water supply system. In an effort to provide 24*7 water supply in certain Indian cities, the government implemented projects using Public Private Partnership (PPP) or government funding. Unfortunately, many projects experienced failures during the later stages. To assess the performance of these projects and evaluate various risks involved, a case study was conducted, which selected two cases—one funded by PPP and the other by the government. The analysis indicated that the PPP project faced significant difficulties regarding consumers, revenue, finance, and socio-politics, while both projects failed to meet the initial expectations. Nonetheless, the study ultimately determined that government-funded continuous water supply projects had superior overall performance.

Mohapatra et al. [16] concluded that due to the infrastructure that was built during the previous two to three decades, the disadvantages of intermittent water delivery systems and the difficulty in switching to continuous supply mode present the biggest obstacle for developing countries. A pilot study using the EPANET software was conducted in Nagpur, India, to address this issue. The study modelled different scenarios using GIS maps, field survey data, remote sensing data, and in-situ measurements of pressure and water quality. The study found that in order to maintain desired head loss and pressure in the majority of the pipes prior to implementing a 24-h water supply, the existing network is insufficient, and issues with water age and quality in the central part necessitate the rehabilitation of distribution mains and critical pipes.

Kumpel and Nelson [17] conducted research comparing the water quality of intermittent and continuous water supply at Hubli-Dharwad, India,. According to the study, switching to a continuous supply of piped water had the potential to improve water quality while intermittent supply of piped water raised the danger of microbial contamination. During the course of a year, water samples were taken from reservoirs, consumer taps, and homes and examined for turbidity, total coliform, *Escherichia coli*, free chlorine, and combined chlorine. According to this study, water quality at service reservoirs serving the network's continuous and intermittent sections was comparable. In contrast to samples from continuously provided taps, those from intermittently supplied taps had higher amounts of indicator bacteria. Only 0.7% of tap samples from continuous water supplies tested positive for *E. coli*, compared to 31.7% of those from intermittent water supplies. In samples from both continuously supplied taps and intermittently supplied taps, higher total coliform concentrations were found following rainfall events, but only intermittently supplied tap water consistently contained significantly more indicator bacteria than continuously supplied tap water did.

The article by Taha et al. [18] investigated how the use of water tanks with float valves (FVs) affects the accuracy of water meters in situations of both intermittent and continuous water supply. The study utilized laboratory experiments, field measurements, and hydraulic modeling to explore this issue. The findings revealed that the inflow rates into the water tank are consistently lower than the outflow rates because of the tank's balancing mechanism. This discrepancy leads to greater

metering errors and more apparent losses when a water tank, FV, and continuous supply are combined. The hydraulic characteristics of different types of FVs vary, with larger FVs resulting in longer periods of low flows, worse meter performance, and more apparent losses because they maintain the water level close to the full level in the tank. In intermittent supply situations, higher intermittency levels result in better meter performance and reduced apparent losses. However, this also highlights the challenges of transitioning from intermittent to continuous supply globally, as water utilities may experience higher meter errors and revenue losses unless their meter replacement policies recognize the lower flows passing through the meter.

Chauhan and Belokar [19] have explored the difficulties and potential advantages of implementing a continuous water supply programme in India, where water is only occasionally supplied due to scarce resources. The case study of Chandigarh city is the main topic, and the objective is to change the city's intermittent water supply into a regular water supply. The research is based on information gathered from government organisations, fieldwork, experimental analyses, and pilot tests. The objective is to show how a pan city with a population of more than 1 million people may provide continuous water delivery.

3 Conclusion

Expanding the water distribution system by Genetic Algorithm (GA) Model for water distribution network optimization; Simulating the flow of water in various water supply system components for a qualitative description of the city's water supply system, simulations enabled a contemporary point of view examination of the water supply system related water flow rate, energy loss, and decanter efficiency; Online hydraulic state predictor (PC) model that forecasts potential hydraulic conditions utilizing a predictive data-driven algorithm (Predictor-corrector (PC) approach; Using EPANET software, flow rates, friction head losses, bent failure, and demand patterns are calculated to produce an effective pipe network distribution.

References

1. Joshi, M. W., Talkhande, A. V., Andey, S. P., & Kelkar, P. S. (2002). Urban community perception towards intermittent water supply system. *Indian Journal of Environmental Health*, 44(2), 118–123.
2. Dahasahasra, S. (2008). Transforming intermittent into continuous water supply system-badlapur case study. In *International Conference on Achieving 24 × 7 Continuous Water Supply*. Indian Water Works Association. Mumbai Repeated.
3. Gohil, R. N. (2013). Continuous water supply system against existing intermittent supply system. *IJSRD - International Journal for Scientific Research & Development*, 1, 109–110.
4. Patil, M. N. B., & Deulkar, W. N. Quality management of water supplies under 24 × 7 schemes. At sector NO. 21, PCMC, PUNE.

5. Rajeshwari, R., & Kumar, D. B. M. (2014). Evaluation of intermittent water supply system and design of 24x7 for a residential area in Mysore, Karnataka, India. *International Journal of Informative & Futuristic Research*, 1(11), 163–173.
6. Vassiljev, A., & Puust, R. (2016). Decreasing leakage and operational cost for BBLAWN. *Journal of Water Resources Planning and Management*, 142(5), C4015011.
7. Stokes, C. S., Simpson, A. R., & Maier, H. R. (2015). A computational software tool for the minimization of costs and greenhouse gas emissions associated with water distribution systems. *Environmental Modelling and Software*, 69, 452–467.
8. Ghorpade, A., & Vaidya, D. (2018). Experimental study of hydraulic modeling of water distribution network with pressure driven approach. *International Journal of Innovative Research in Science, Engineering and Technology*, 7(8), 9105–9246.
9. Mallikarjun, S., Jyothi, D., Manjureddy, K., Sandhya, H., & Anand, S. (2016). Design of 24x7 water supply system for Ranebennur Town. *International Journal of Innovative Research in Science, Engineering and Technology*, 5(6), 10051–10055.
10. Mavi, T., & Vaidya, D. R. (2018). Study and design of 24/7 water supply distribution system by watergems. *Journal Homepage* 7(3). <http://www.ijesm.co.in>
11. Varu, S., & Shah, D. (2018). Design of 24 × 7 water supply systems - a case study: Ahmedabad City. *Drink. Water Engineering Science Discuss.* [preprint], <https://doi.org/10.5194/dwes-2018-14>
12. Mallick, R. K., Choudhary, M., & Nagar, B. (2020). Study on efficient 24*7 water distribution systems – a case study of Jhunjhunu. *Tathapi (UGC Care Journal)*, 19(15), 142–152. ISSN: 2320-0693.
13. Pawar, M. M., & Sonaje, N. P. (2021). Converting traditional water supply network into 24*7, using water GEMS to optimize design. *International Journal of Recent Technology and Engineering*, 10(1). ISSN: 2277-3878.
14. Jaiswal, A. K., Thakur, P. K., Kumar, P., & Kannaujia, S. (2021). Geospatial modeling of water supply distribution system: A case study of Dehradun City, India. *H2Open Journal*, 4(1) 393–412. <https://doi.org/10.2166/h2oj.2021.118>
15. Tawalare, A., & Balu, Y. (2016). Performance evaluation of implementation of continuous water supply projects: Two case studies from India. *Procedia Engineering*, 161, 190–194.
16. Mohapatra, S., Sargaonkar, A., & Labhasetwar, P. K. (2014). Distribution network assessment using EPANET for intermittent and continuous water supply. *Water Resources Management*, 28, 3745–3759.
17. Kumpel, E., & Nelson, K. L. (2013). Comparing microbial water quality in an intermittent and continuous piped water supply. *Water Research*, 47(14), 5176–5188.
18. Taha, A. W., Mahardani, M., Sharma, S., Arregui, F., & Kennedy, M. (2020). Impact of float-valves on water meter performance under intermittent and continuous supply conditions. *Resources, Conservation and Recycling*, 163, 105091.
19. Chauhan, S., & Belokar, R. M. (2022). Conversion of intermittent water supply to continuous water supply of Chandigarh: A case study. In *Proceedings of Third International Conference on Computing, Communications, and Cyber-Security: IC4S 2021* (pp. 21–36). Singapore: Springer Nature Singapore.

Performance of RCC Multistory Framed Structure in Different Geometric Shapes



Priyanka V. Padavale, Mukund M. Pawar, Mangesh S. Survase,
Revnath J. Salunke, Amruta L. Lugade, and Suraj R. Pawar

Abstract Modern systems are safeguarded by engineering significance, making it extremely challenging to surpass with conventional shapes. This forces the structure to make accommodations for the irregularities there. These discrepancies are caused by a fundamental breakdown during an earthquake. It is evident in the common casing; nevertheless, due to symmetry, there might not be any torsional influence inside the casing. In any case, discontent happens when unforeseen systems emerge because of the torsional influence between the pillar segment joints. Weakening examination techniques are one of the various types of research because of its optimal precision, effectiveness, and comfort. The behaviour of G+10 storey R C outlines buildings with multiple geometrical anomalies exposed to seismic tremor load was examined in the current study, and the quantity of all systems was kept constant throughout all form building models. Additionally, the 33 m full stature was saved for all shape-building models. Using ETABS programming, situated in Seismic Area III is tested fast. The structure implements gravity loads and sidelong masses in accordance with IS 1893-2002, and its miles are planned using IS 456-2000. It is done to relocate manage to the weakening research.

Keywords Pushover analysis · Irregular plan · Irregular elevation · Same volume · ETABS

1 Introduction

One of the most dangerous, destructive, and life-threatening natural events that can cause the ground to tremble is an earthquake. We must build the homes to survive earthquakes, which may also happen at least once over the course of the structure's lifetime, or the systems will be harmed. When frames are configured abnormally, structures have significantly less stiffness and electricity [1]. To remedy this, lateral load resisting structures are added to the frames. It has been determined over the past

P. V. Padavale (✉) · M. M. Pawar · M. S. Survase · R. J. Salunke · A. L. Lugade · S. R. Pawar
SVERI's College of Engineering Pandharpur, Gopalpur, India
e-mail: padavale.priyanka@gmail.com

few years and more that damage control needs to be a more particular layout issue. The most effective method to do this is to include some sort of nonlinear evaluation in the seismic design process. Pushover evaluation has become the evaluation technique of choice for performance-based seismic design, PBSO, and assessment purposes as a result of decades of development. It is the procedure via which the remaining power and the restricted nation can be successfully researched following relinquishing. Until the shape reaches a limit state of crumble, the evaluation is performed by pressing a computerized replica of the shape while gradually increasing the horizontal masses, plotting the total applied shear force and related lateral displacement at each increment. Forces that cause earthquakes are equivalent static lateral hundreds around. The magnitude of the structural loading is incrementally accelerated in a static nonlinear system known as pushover evaluation. Mass, stiffness, and shape geometry discontinuities cause a shape's weakness. These discontinuous formations are referred to as irregular systems. These buildings' dynamic characteristics differ from "regular" buildings in a unique way due to height-sensitive stiffness and mass modifications [2–5]. The irregularity in the constructions may be caused by atypical distributions of their mass, electricity, and stiffness along the peak of the building. Any seismic occurrence that generates seismic waves, whether it is caused by a natural disaster or human activity, is referred to as a "earthquake." Although geological faults rupture most frequently to cause earthquakes, other phenomena including volcanic activity, mine blasts, landslides, and nuclear tests can also cause earthquakes. An earthquake is the result of a sudden release of energy in the Earth's crust, which causes seismic waves to be produced [6]. It is also referred to as a tremor, quake, or temblor. The frequency, nature, and magnitude of earthquakes that a region experiences over time determine its seismicity (seismic interest). Seismometer data are used to calculate earthquake magnitude. The size of instant importance is typically advised for earthquakes greater than five. The Richter scale, commonly known as the local magnitude scale, is used to assess most earthquakes less than magnitude five that are more frequent, as determined by the nation's seismological observatories. Even though many homes have the best structural systems, they do not meet contemporary seismic requirements, which causes extensive damage during the earthquake. Rourkela is situated in Zone II of the Seismic Zone Map of 2002, or in line with the Seismic Zoning Map of IS: 1893-2002, which indicates that the region is least likely to have earthquakes [7]. This is the explanation for it. As a result, key structural devices were used in the construction of the NIT Rourkela buildings. The institute building, a four-story building, was not built in accordance with IS: 1893-2002's architectural standards [8–11]. The techniques for evaluating structures that have been damaged by earthquakes or that are seismically unsound are still in their infancy [1]. A house that doesn't comply with seismic design rules may also experience significant damage or perhaps collapse in the event of a major earth movement. The seismic assessment underlines the buildings' future seismic utility as earthquake-prone structures. According to the Seismic Zoning Map of IS: 1893-2002, India is classified into four zones based on seismic activity. These territories are Zone II, Zone III, Zone IV, and Zone V.

2 Problem Statements

To identify performance level of RC multistory building by considering combination of different. Geometric shapes in plan and elevation. To achieve this objective different techniques will be used for design and analysis Of RCC framed structure Finite element method (FEM) model is to be developed to check the behaviour and performance level combination of irregularity in plan and elevation, pushover analysis is to be carried out and responses of building are to be studied by considering parameters like capacity spectrum, demand spectrum, performance point for an idea of the maximum base shear that the structure will capable of resisting at the time of earthquake.

3 Methodology

In this study the 11-story building is considered with each story height of 3 m and 6×6 bays in each floor as per the Indian Code, These buildings are analyzed and designed Finite element method (FEM) model is to be developed to check the behaviour and performance level combination of irregularity in plan and elevation, pushover analysis is to be carried out and responses of building are to be studied by considering parameters like capacity spectrum, demand spectrum, performance point for an idea of the maximum base shear that the structure will capable of resisting at the time of earthquake [12].

Building modelling: In this study, the behaviour of a building with shear walls in five distinct locations and shapes is examined across all zones [13]. The modelling was done using ETABS Ultimate 19, a general purpose programme. It is a more flexible and user-friendly tool that includes a wide range of capabilities like static and dynamic analysis, nonlinear static pushover analysis, and nonlinear dynamic analysis, among others [6] (Table 1).

The modulus of elasticity of reinforced concrete as per IS 456:2000 is given by

$$E_c = 5000\sqrt{f_{ck}}$$

The data needed for steel rebar includes yield stress, elastic modulus, and ultimate strength [14]. HYSDs, or high yield strength deformed bars, are frequently used in design practice and are used in the current work. Their yield strength is 415 N/mm² (Figs. 1 and 2).

Table 1 Building plan and dimension details of geometric data

S. No.	Component	Values
1	Model	G + 10
2	Floor height	3 m
3	Total Building height	33 m
4	Wall thickness-	Internal-150 mm, External-230 mm
5	Slab thickness-	150 mm
6	Beam-	350 × 600 mm
7	Column-	C1-450 × 450 mm, C2-430 × 430 mm, C3-410 × 410 mm
8	Material	M30, Fe415
9	Seismic data	Seismic zone III, importance factor = 1, soil = medium, RC frame, SMRF, poisson's ratio = 0.5, L.L. = 3 kN/m ² , F.F. = 1 kN/m ²

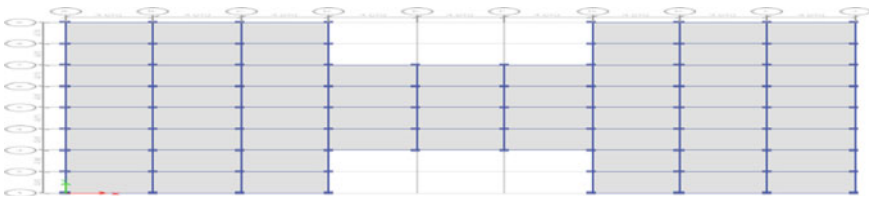


Fig. 1 Irregular building model combination of plan and elevation

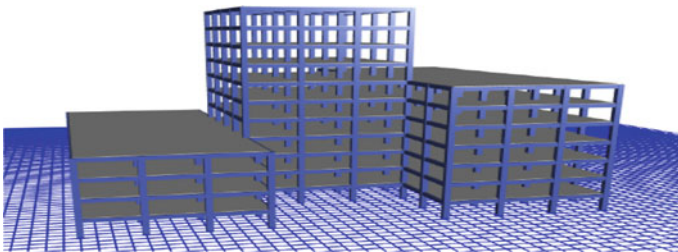
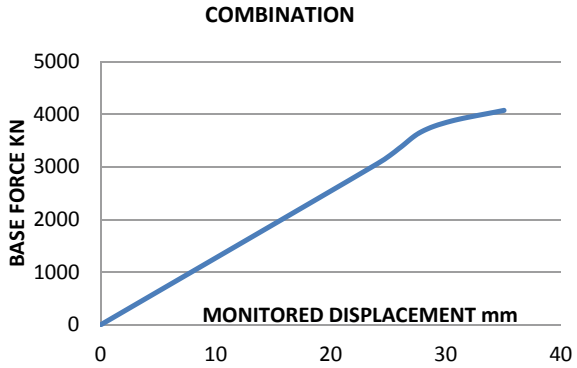


Fig. 2 3D model of irregular building combination of plan and elevation

Fig. 3 Graph of irregular building combination of plan and elevation



4 Results

This study takes into account both irregularities in the building model’s plan and elevation. The columns in this building model are 4 m apart in the center [15, 16]. A building with 3 m floor to floor height and the same building volume has 396 total rooms. The building’s overall height is 33 m. Depicts a plan for an atypical building model that combines an elevation and a plan, as well as a 3D representation of the same (Fig. 3; Table 2).

Results from a pushover analysis of an atypical model combination of plan and elevation are shown in the Fig. 3. Maximum monitored movement in this analysis is 35 mm, relative base force is 4074.71 KN, there are 5880 total hinges, and a total of 5 steps are obtained. Because it displays the building’s capacity, this graph is also known as a capacity spectrum curve (Figs. 4, 5 and 6; Tables 3 and 4).

Table 2 Pushover analysis results of irregular building combination of plan and elevation

Step	Monitored displacement (mm)	Base force (KN)	A-B	B-C	C-D-E	>E	A-IO	IO-LS	LS-CP	>CP	Total hinges
0	0	0	6028	0	0	0	6028	0	0	0	6028
1	24.085	3065.9	6021	7	0	0	6028	0	0	0	6028
2	25.961	3356.1	6016	12	0	0	6028	0	0	0	6028
3	27.852	3665.2	5992	36	0	0	6028	0	0	0	6028
4	30.513	3873.8	5970	58	0	0	6028	0	0	0	6028
5	35.054	4074.7	5900	128	0	0	6028	0	0	0	6028

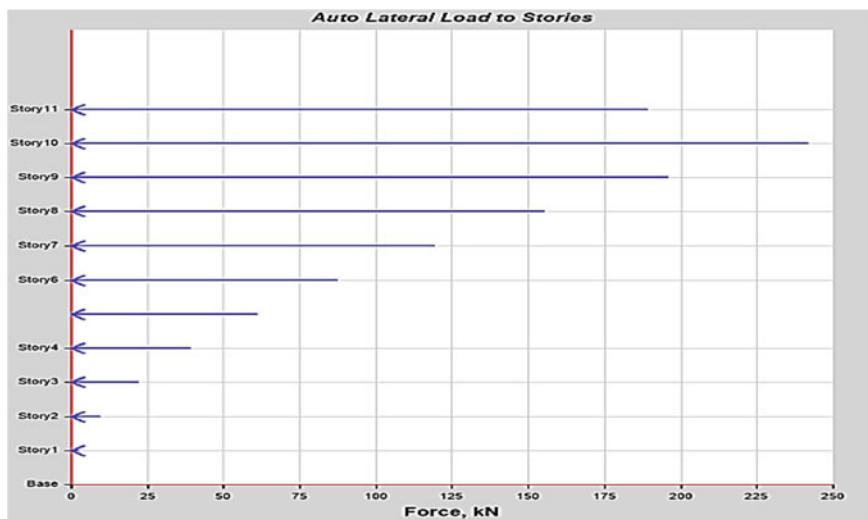


Fig. 4 Story wise earthquake force in X direction of combination

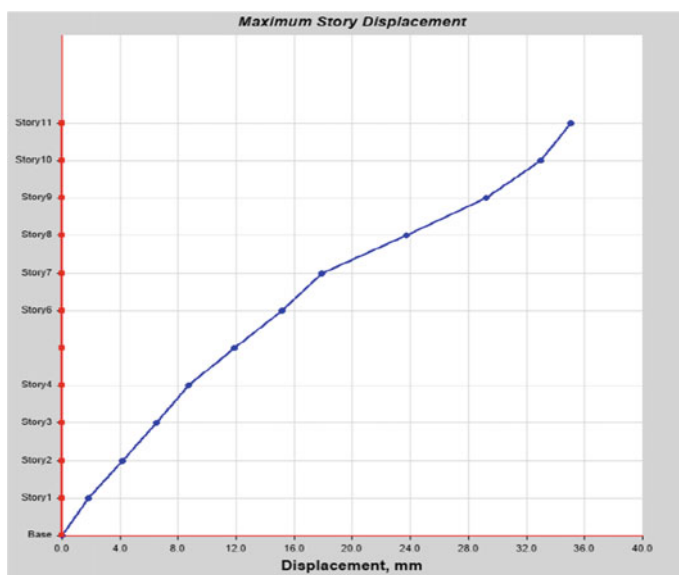


Fig. 5 Max. story displacement of combination

Fig. 6 Max. story drifts of combination

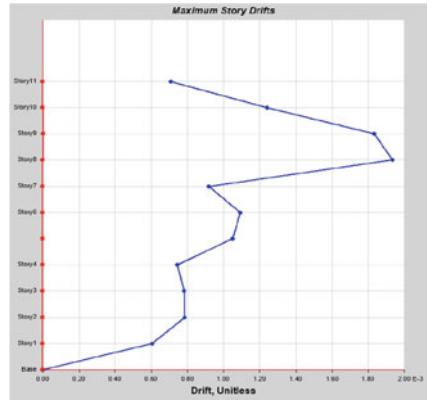


Table 3 Earthquake force results—X direction of combination

Story	Elevation (m)	Location	X-direction (mm)
Story11	33	Top	35.0
Story10	30	Top	32.9
Story9	27	Top	29.2
Story8	24	Top	23.7
Story7	21	Top	17.9
Story6	18	Top	15.1
Story5	15	Top	11.8
Story4	12	Top	8.7
Story3	9	Top	6.5
Story2	6	Top	4.1
Story1	3	Top	1.8
Base	0	Top	0

Table 4 Earthquake force in Y direction and displacement in X direction

Story	Elevation (m)	Location	Y-Dir (kN)	X-Dir (mm)
Story11	33	Top	254.09	35.0
Story10	30	Top	278.25	32.9
Story9	27	Top	225.38	29.2
Story8	24	Top	178.63	23.7
Story7	21	Top	318.89	17.9
Story6	18	Top	285.79	15.1
Story5	15	Top	199.03	11.8
Story4	12	Top	187.38	8.7
Story3	9	Top	118.44	6.5
Story2	6	Top	52.64	4.1
Story1	3	Top	13.16	1.8
Base	0	Top	0	0

5 Conclusion

Using non-linear static analysis, it was determined how well R.C. framed structures performed when abnormalities in elevation and plan were combined. The study's principal conclusions are listed below. H. The resistance to earthquake forces is 80.18% lower for an irregular building model combination (combination of irregularities in plan and irregularities in elevation) than for a regular building model. And before any other construction models, it will crumble. As a result, it may be concluded that a building's performance will decline if its irregularity increases while maintaining the same volume. From all of the findings, it can be inferred that the regular building model is more resistant to earthquake forces and is thus appropriate for earthquake zone III.

References

1. Hamraj, M. (2014). Performance based pushover analysis of R.C.C frames for plan irregularity 2(7). ISSN: 2348-4098.
2. Abhilash, R. A new procedure to include torsional effects in pushover analysis of torsional buildings. *Asian Journal of Engineering and Technology*, 03(04). ISSN: 2321-2462, Special issue for ICETTAS' 15.
3. Otani, S. (2000). *The second U.S.-Japan workshop on performance-based earthquake engineering methodology for reinforced concrete building structures*. Sapporo, Hokkaido, Japan. September 11-13, 2000.
4. Kadid, A. (2008). Pushover analysis of reinforced concrete frame structures. *Asian Journal Civil Engineering (Building and Housing)*, 9(1).

5. Khoshnoudian, F. (2008). A breakthrough in estimating the seismic demands of tall buildings. In *The 14th World Conference on Earthquake Engineering Beijing, China*. October 12–17, 2008.
6. Nachane, D. M. (2009). *Selected problems in the analysis of non-stationary and nonlinear time series*. Indian Institute of Management Bangalore (IIMB). August 9–12, 2009.
7. Himaja Sai, G. V., Ashwini, L. K., & Jayaramappa, N. (2015). Comparative study on non-linear analysis of infilled frames for vertically irregular buildings. *International Journal of Engineering Science Invention*, 4(6), 42–51. ISSN (Online): 2319–6734, ISSN (Print): 2319–6726.
8. Kumar, P., Naresh, A., Nagajyothi, M., & Rajasekhar, M. (2014). Earthquake analysis of multi storied residential building-a case study. *International Journal of Engineering Research and Application (IJERA)*, 4. ISSN:2248:9622.
9. Katti, G. B., & Balagol, B. S. (2014). Seismic analysis of multistoried RCC buildings due to mass irregularity by time history analysis. *International Journal of Engineering Research and Technology (IJERT)*, 3(7). ISSN: 22780181.
10. Balaji, K. V. G. D. (2013). Pushover analysis of a multi-storied frame with shear wall and Jacketed Columns. Department of Civil Engineering Gitam Institute of Technology Gitam University (Est. U/S 3 Of Ugc Act 1956) Visakhapatnam-530045 October, 2013.
11. Shah, M. D. (2011). Nonlinear static analysis of RCC frames (software implementation ETABS 9.7). In *National Conference on Recent Trends in Engineering and Technology-May 2011*.
12. Rana, N., & Rana, S. (2015). Non-linear static analysis (pushover analysis) a review. *International Journal of Engineering and Technical Research (IJETR)*, 3(7). ISSN: 2321-0869 (O) 2454-4698 (P).
13. Akhare, A., & Bhende, S. (2015). Modal pushover analysis to estimate the seismic demand of vertically irregular structures. *International Journal of Pure and Applied Research in Engineering and Technology, IJPRET*, 3(8), 40–50. ISSN: 2319-507X.
14. Anwaruddin M., Mohd. A., & Saleemuddin, M. Z. (2013). Pushover analysis of medium rise multi-story RCC frame with and without vertical irregularity. *International Journal of Engineering Research and Applications*, 3(5), 540–546.
15. Chore, H. S., Patil, S. B., & Pednekar, S. C. (2015). Pushover analysis of reinforced concrete structures. *International Journal of Computer Applications (0975 – 8887) (ICQUEST2015)*.
16. Srinivasu, P. R. (2013). Non-linear static analysis of multi-storied building. *International Journal of Engineering Trends and Technology (IJETT)*, 4(10).

A Study on Transfigure of Rural Agro Based Businesses Subsequent to COVID



Uday V. Hiremath and K. Shivashankar

Abstract The research is grounded on realistic study that will review literature of various authors after COVID period. Rural entrepreneurs make vital alms to money-spinning growth. Entrepreneurial aspect in discomfited areas is based on motivating original entrepreneurial aptitude and successive growth of home- grown companies. People who carry out entrepreneurial activities by incubating up industrial and business units in the rural sectors of the economy may be defined as rural entrepreneurs. Raising rural entrepreneurship is essential for disposal or reduction of poverty and helping in profitable growth of our country. Today Rural Entrepreneurship has get the big chance for those people who have shifted to municipal urban areas from rural or semi-urban areas. The study will concentrate on the changes transpired in the rural business after COVID which are inculcated by the rural entrepreneurs. The different aspect can be the rules for future rural business.

Keywords Rural challenges · Rural entrepreneur · COVID impact · Agro based business · Rural prospects · Rural development etc.

Abbreviations

COVID	Corona virus Disease
SME	Small and Medium-Sized Enterprises
DDM	District Development Manager
FSC	Food supply chain
FAO	Food and Agriculture Organization

U. V. Hiremath (✉)
ATS, Sanjay Bhokare Group of Institutes, Miraj, (MH), India
e-mail: prof.hiremath@gmail.com

K. Shivashankar
Visvesvaraya Technological University, Belgavi, (KA), India

1 Introduction

It's challenging to run a business during the COVID-19 epidemic, because the possessors and the small business leaders must be responsible for success. Top business people need to introduce and look for sources of invention, including practical inventions, similar as invention cloning. COVID-19 epidemic has been disastrous for nearly everything including the global frugality. Among numerous sectors, the husbandry sector was the worst megahit following the immediate lockdown and request shutdowns. Though some stability was current from force side till date, still, the severe restrictions put in place to check the spread of epidemic have risked the force of agrarian and food papers simultaneously across borders and from field to chopstick. While the income falls due to price fall and inventories chain dislocations due to epidemic have escalated the food dearths in several of developing and developed countries [1]. Now way the less the global demand for food particulars has remained more or less unchanged owing to their inelastic demand. Indeed, within the global position, the script of food security and force chain stability has been mainly deplorable for arising and lower developing countries due to their lack of sequestration to the global shocks or afflictions. Specially, the technological backwardness, inordinate knows- style dependence and denied availability on several grounds lead to poverty and food hunger in these countries. Utmost countries have designated the husbandry and agro-food sector as essential and pure from business check and restrictions on movement. For numerous countries, the direct impacts of the epidemic on primary husbandry should be limited, as the complaint doesn't affect the natural coffers upon which product is grounded. Still, the contagion poses a serious trouble to food security and livelihoods in the poorest countries, where agrarian product systems are more labour- ferocious and there's lower capacity to repel a severe macroeconomic shock. Because food is a introductory necessity, the position of food demand should be affected less by the extremity than the demand for other goods and services. Still, there has been a major shift in the structure of demand, with a collapse in demand from hospital and catering, the check of open requests, and a swell in demand from supermarkets.

2 Literature Review

The analysis of literature in the threat- vulnerability and adaptability of husbandry systems in the face of COVID-19 showed that the adaptability of food systems needs to be enhanced by enforcing specialized, profitable and measures. All these programs and measures first of all need to guard the health and food force security of world population [2]. Specialized measures aiming to ameliorate the functional performance position of the structure in husbandry sector are necessary to enhance physical adaptability. Organizations and institutions in husbandry sector need to

take necessary recovery sweats, considering the absorptive, adaptive, and restorative capabilities of the agrarian systems. It's egregious that the request forces via price mechanisms inevitably reduce the demand of rare agrarian goods and match force with demand during epidemic and the banning on similar price increases has negative impact on adaptability of husbandry systems by decreasing their absorptive and adaptive capabilities of adaptability handed by the request price system. Still, profitable support and subventions in face of profitable losses of growers allows them to recover briskly after disaster. The strong communities developed in pastoral areas can enhance the social adaptability capacities of agrarian systems as strong communities pool their coffers and survive during epidemic more fluently and start rebuilding as government aid always come with detention [2]. Studies have shown that SMEs are brazened with colorful difficulties and challenges due to the COVID-19 epidemic. The period of check and movement forestallment programs espoused by governments in numerous countries have greatly affected SMEs, paralyzing their operations, weakening their fiscal positions, and exposing them to fiscal threat. SMEs have suffered from a deficit of workers and product inputs because of deformations that marred force chains, which negatively affected their deals and their capability to fulfill their fiscal scores and pay workers' hires. This problem has coincided with a drop in consumer spending because of the reduction in consumers' income and wide passions of query. As a result, numerous SMEs set up themselves unable of dealing with the situation. Some businesses have stopped their conditioning and remained unrestricted since the first months of the outbreak. Published exploration has indicated that SMEs have failed to repel the consequences of profitable heads. This disfigurement can be attributed to a lack of fiscal coffers and the high cost of business capital as well as limited executive and specialized capacities. Experimenters have emphasized that SMEs are frequently the enterprises most affected by profitable heads. Thus, a socioeconomic extremity related to people's health similar as the COVID-19 epidemic can be anticipated to have dire goods on s because these businesses bear strong connections with people, whether they're guests or suppliers.

Studies have shown that SMEs are brazened with colorful difficulties and challenges due to the COVID-19 epidemic. The period of check and movement forestallment programs espoused by governments in numerous countries have greatly affected SMEs, paralyzing their operations, weakening their fiscal positions, and exposing them to fiscal threat. SMEs have suffered from a deficit of workers and product inputs because of deformations that marred force chains, which negatively affected their deals and their capability to fulfill their fiscal scores and pay workers' hires. This problem has coincided with a drop in consumer spending because of the reduction in consumers' income and wide passions of query. As a result, numerous SMEs set up themselves unable of dealing with the situation. Some businesses have stopped their conditioning and remained unrestricted since the first months of the outbreak. Published exploration has indicated that SMEs have failed to repel the consequences of profitable heads. This disfigurement can be attributed to a lack of fiscal coffers and the high cost of business capital as well as limited executive and specialized capacities. Experimenters have emphasized that SMEs are frequently the enterprises most affected by profitable heads. Thus, a socioeconomic extremity related to people's

health similar as the COVID-19 epidemic can be anticipated to have dire goods on s because these businesses bear strong connections with people, whether they're guests or suppliers [3]. NABARD had decided to collect and assay quick feedback through our quarter position field officers i.e. District Development directors (DDMs) posted in colorful sections on the effect of COVID-19 on husbandry, horticulture, dairy, flesh and colorful other sectors of the frugality. The gathered information may be useful in understanding the ground- position situation so as to concoct suitable policy responses. Agrarian product, postharvest handling, recycling, distribution/retail/service, and consumption i.e., field to chopstick are the 5 phases of Food force chain (FSC). In the food force chain, two mechanisms girding food thickness and protection are used. The first is concentrated on rules and legislation that use mandatory conditions that are reviewed by state departments. The alternate is concentrated on voluntary principles established by business laws or transnational associations. The COVID-19 epidemic doesn't specifically impact development, unlike bottom and mouth complaint, raspberry flu, since it doesn't propagate directly to creatures or agrarian products. Still as a result of the epidemic, policymakers around the world have placed major limits on the inflow of goods (land, ocean and air transport) as well as on labor mobility. Temporary or seasonal kind of employment is common in developing and underdeveloped countries, particularly when planting, sorting, harvesting, refining, or transporting crops to requests. Thus, due to the lack of original or temporary workers due to illness or travel restrictions executed by the lockdown, the force chain is greatly impacted. In situations where the illness specifically impacts their health or exertion, it also weakens not only the processing capability of others but also their own food protection. The lack of labor due to the epidemic extremity has led to significant disturbances in certain diligence, similar as beast product, horticulture, planting, harvesting and crop processing, which are fairly labor ferocious. Ranch worker dearth's, still, were formerly a significant concern long before the COVID-19 epidemic. The "Pick for Britain" crusade in Britain was planned to detect, British working in the field and through the crop. Still, owing to the lack of labor due to sickness and the physical distance to be sustained during product, the extremity is weakening the occasion to work for granges and agrarian undertakings. These conditions delayed the delivery of grain and agrarian inputs and produced difficulties with the continued force of food to markets.

3 Data and Methodology

The all data is collected is from secondary sources. There is the big scope and hi-reach of the study. It is not limited to the urban area it spread over the rural area too. So that the data at that extend not possible to collect on the stipulated time period. The following information collected and studied and evaluated. The following table shows the total COVID cases which are confirmed on the time line.

From the Fig. 1, it is clear that, The Food and Agriculture Organization states that COVID-2019 is affecting husbandry in two significant aspects the force and demand

for food. These two aspects are directly related to food security, so food security is also at threat. It can understand the connections between these rudiments, as well as the impact of COVID-19 [4]. The advents of social insulation made people go to the force centers and induce a deficit of some products, despite this, the food force has stabilized because it's one of the systems that must be maintained to insure food security. One of FAO's places is to promote that food value chains aren't intruded and continue to operate. Therefore, despite the restrictions those governments have assessed on the mobility of labor in agrarian systems, although with some problems, the force of introductory musts is typically assured. The situation is different when it comes to goods that are imported or exported; due to the check of borders, transnational trade was intruded, although after having defined security protocols to avoid the spread of the contagion, trade stabilized. This may be temporary; it depends on what countries are doing to stop the spread of the contagion. Interruptions to food transfers are minimum, so the food force remains stable; although observing China's experience in this epidemic, there's a lesser impact on the beast sector due to difficulties in penetrating beast feed and, on the other hand, the deficit of labor. Although it depends on the country and the measures that each one has espoused, encyclopedically the prices have remained stable, thus, no harpoons in the prices of introductory musts are anticipated, although it's more likely to do for high-value products, especially meat and perishables. The demand for food has dropped due to uncertainty and the reduction of people's spending capacity, although this drop is still slight; the situation could worsen if the epidemic continues for a long time, due to reduced income and job losses. In situations like these, where a contagion spreads on contact, contactless delivery services come preferred by consumers. There's a extremity in the husbandry sector over the once two decades. In India, the maturity of growers are small lodgers facing the problem of falling productivity, water failure etc. maturity of the returnees were borderline growers in the history. The rear migration will increase pressure on husbandry which is formerly overburdened. The rear migration will further affect in to fall in the patron price of crops which will reduce ranch stipend and income. On the other hand, due to low productivity and hoarding of food papers, there will be a rise in the prices of food particulars which will majorly affect poor people. Rear migration, fall in patron price and adding pressure on the agrarian sector will lead to an increase in pastoral severance and poverty.

4 Results and Discussion

One of the major enterprises of the review papers was related to food force. Numerous papers expressed concern that growers would stop producing because of the epidemic (as they get sick) and lower food will be available, if at each, at advanced prices. This is presumably the first and most common husbandry-related issue raised in times of a global extremity. Another concern regarding food force was related to the corrupt capability of the products a planter is on strict planting and harvesting schedule and cannot modify product at will. numerous growers face similar problems as fresh

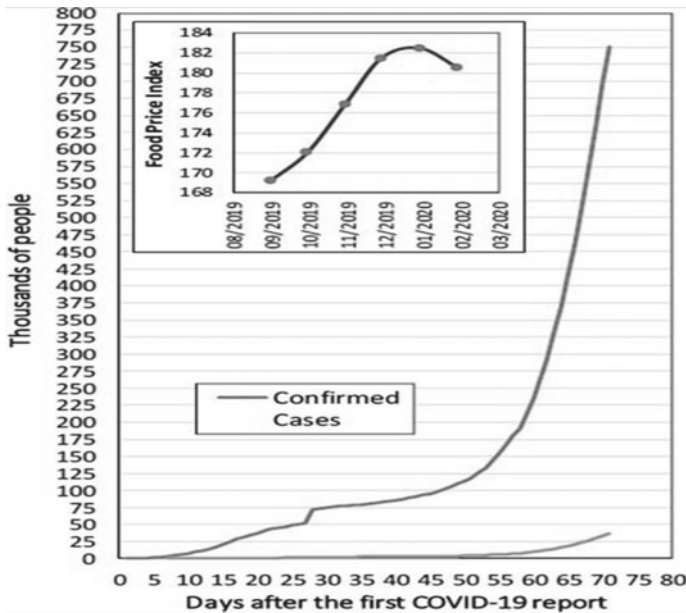


Fig. 1 Chart of data analysis during the COVID

days of storehouse make their products empty. Springtime is a critical planting and harvesting time for numerous growers around the globe, and the epidemic has made agrarian requests indeed more changeable. As to demand- related impacts, presumably the most important impact described by the papers was fear shopping and stockpiling. In the fear of being locked down for a longer period, people have started to buy up huge stocks of durable food in a fairly short time period, thereby causing difficulties for supermarkets. The most mentioned food and produce include sap, rice, firmid (UHT) milk, chuck, eggs, dried food, nuts and canned food, as well as colorful set and reused foodstuffs. Seasonal goods made this indeed worse, as was apparent in numerous places with eggs around Easter. Another major effect of the epidemic stressed in the papers was agrarian labor [5]. However, a part of their yield will be lost, and hence, If growers cannot find enough workers. As the world is globalised, this also means less or more expensive significances for countries depending on external food inventories. As people are instructed and anticipated to stay at home, the whole force chain can witness dislocations in addition to those impacting the normal husbandry processes. Critical workers along the force chain like truck motorists or boat wharf workers can get sick, quarantined or forced to stay at home, enlarging the original impacts. Short timeframes and the corrupt capability of agrarian yield also put serious constraints on non-agricultural labor. Food Security and Safety Impacts- Food security issues are also covered by certain papers grounded on the simple fact that roughly a third of the global population is on lockdown. In the first months of the epidemic, numerous target measures were taken by China and

also Italy to maintain food security. One of the issues covered the n's related to the shutting down of seminaries. As academy lunch programmers each over the world give low- cost and free lunches to millions of children, numerous parents face now real challenges to feed their hungry children.

The Food and Agriculture Organization (FAO) is suggesting specific strategies like expanding exigency food backing programs and furnishing immediate backing to smallholders by fastening on logistics and boosting e-commerce. As there's no substantiation so far that COVID-19 is food borne or food service-driven, food service isn't likely driving the epidemic. Of course, food packages can also be contagion transmitters, but as utmost papers suggest, the chances that these could carry the contagion are veritably low. The threat is presumably the loftiest in crowded super-markets, and numerous papers argue for proper preventative measures this content, still, leads far down from profitable impacts. How to eat healthy food during the epidemic is also an issue mentioned constantly indeed in the profitable news, which also leads veritably far from our main story. Trade and Other Impacts-On the one hand, the corona virus seems to help liberalize agro-food trade. China, for case, has formerly blazoned a significant reduction of tariffs for US- grounded products, thereby continuing to step back from a times-long trade war hurting both husbandries. Products concerned include agrarian goods like soybeans, pork, cotton and wheat. Although coming from a different sector, masks and gloves are also of critical significance for husbandry as keys to decelerate down the epidemic locally [6]. Another intriguing angle of the epidemic is the rapid-fire increase ecommerce, as reported by some papers. At the time of jotting, direct deals from growers to consumers were on the rise, together with the increase of ménage food consumption. The issue on everyone's minds was how to get their businesses through the current extremity caused by the health pitfalls associated with the COVID-19 epidemic and by the counter blockade that has forced them to close their businesses. With the option of delivery or take-away service still allowed in the country, the entrepreneurs sharing in the discussion participated their answers to some important questions like, how are they facing the extremity? How are they continuing to add value to their brands? And how are they preparing for the day when they can renew their businesses? Some strategies come in front of result to hand with the critical situation.

5 Conclusion and Recommendations

The epidemic called COVID-19 complaint has a great impact on the conduct and conditioning of humanity, husbandry isn't outdoors this impact. Food demand and therefore food security are greatly affected due to mobility restrictions, reduced coping power, and with a lesser impact on the most vulnerable population groups. As cases of contagion increase, governments take further drastic measures to stop the spread of the contagion, also impacting the global food system. The premise of any measure espoused should be to cover the health and food security of the population, to the detriment of profitable growth, although some governments go in the contrary

direction Everyone around the world likely knows that husbandry is one of the most changeable sectors. This principle seems to come indeed nay now. Farmers, food processors, retailers and nearly all stakeholders of the sector now wonder what's coming next. Everything depends on the length of the epidemic. Still, these first responses led to stockpiling gets at the manageable level. However, these sweats will surely not be enough, if the epidemic lasts for numerous further months. It's apparent that the COVID-19 epidemic turned the world upside down, including husbandry. Much further work is now demanded from colorful scientists working in different fields to assay the goods. In the current situation when long-term data aren't yet available, this abstract paper might serve as a background for unborn exploration in pressing the fields of global interest in husbandry and related sectors. As a limitation of the study, note that our analyses are grounded on English-language results only, which, on the one hand is accessible and, on the other hand, poses some bias. It would have been an endless exercise to probe papers in all languages of the world. Although original issues can also be important, we suppose that all major global issues raised in the period analyzed are covered by our hunt and results.

References

1. Adnan, N., & Nordin, S. M. (2020). How COVID 19 effect Malaysian paddy industry? Adoption of green fertilizer a potential resolution. *Environment, Development and Sustainability*. <https://doi.org/10.1007/s10668-020-00978-6>
2. Adhikari, J., Timsina, J., Khadka, S. R., Ghale, Y., & Ojha, H. (2021). COVID-19 impacts on agriculture and food systems in Nepal: Implications for SDGs. *Agricultural Systems*, 186, 102990. <https://doi.org/10.1016/j.agsy.2020.102990>
3. Dandekar, A., & Ghai, R. (2020). Migration and reverse migration in the age of COVID19. *Economics and Politics Weekly* 55(19).
4. Bhavani, R. V., & Gopinath, R. (2020). The COVID19 pandemic crisis and the relevance of a farm-system-for-nutrition approach. *Food Security*, 12(4), 881–884. <https://doi.org/10.1007/s12571-020-01071-6>
5. Singh, B. P. (2014). PDS: a review of its functioning and effectiveness, since independence.
6. Jambor, A., Czine, P., & Balogh, P. (2020). The impact of the coronavirus on agriculture: First evidence based on global newspapers. *Sustainability*, 12(11), 4535. <https://doi.org/10.3390/su12114535>
7. Source <http://www.scielo.org.pe/img/revistas/agro/v11n1//2077-9917-agro-11-01-00003-gf1.jpg>
8. Ahmed, F., Ahmed, N., Pissarides, C., & Stiglitz, J. (2020). Why inequality could spread COVID-19. *The Lancet. Public Health*, 5(5), e240. [https://doi.org/10.1016/S2468-2667\(20\)30085-2](https://doi.org/10.1016/S2468-2667(20)30085-2)
9. Singh, B. P. (2017). The political economy of Indigo farming in India and Champaran Satyagraha. Retrieved at: <https://mpr.ub.uni-muenchen.de/100408/>
10. International Organisation of Migration. (2011). *International migration law: Glossary on migration* (2nd ed.). IOM.
11. <https://datascience.nih.gov/covid-19-open-access-resources>

Analysis of Compressive Strength of Concrete Cubes Made from Different Sources of Water



Anil Shirgire, Nitin Shinde, Hemchandra Pawar, Satyawhan Jagdale, and Ravikant Sathe

Abstract The current study was carried out to find the effect of different sources of water on compressive strength of concrete cubes. The concrete mix with M20 grade and water to cement (W/C) ratio of 0.5 were used for this current study. Water samples like well water, waste water, tap water, Tube well water and packed drinking water were collected from various sources at Pimpri area and were used for casting of $150 \times 150 \times 150$ mm concrete cube sizes. The curing was done for 28 days. The cubes were crushed for determining compressive strength after 7 and 28 days. The results obtained showed that the concrete cubes -compressive strengths of made with well water, tap water, mineral water and waste water with increasing days were increased and too much variation in their compressive strength was not found.

Keywords Concrete testing · Compressive strength · Water Parameters · Sources of water

1 Introduction

Concrete made from cement is mixture of water, pebbles, sand, cement and crushed rock when it is properly moulded it became hard like hard stones. The major component of concrete is aggregate. The quality of aggregate and concrete always find out and that qualities being maintained whereas quality of water not properly maintained

A. Shirgire (✉) · N. Shinde
Dr D Y Patil Institute of Technology, Pimpri, Pune, India
e-mail: anil.shirgire@gmail.com

H. Pawar · S. Jagdale · R. Sathe
SVERI's College of Engineering, Pandharpur, India

or that much controlled [1, 2]. Now water quality is also essential parameter in determining strength of concrete, it is exercised to determine quality and purity of water. The mix proportion calculation is done and its design is also done properly for M20 grade of concrete as per IS 10262 standard. In present study bore well water, well water, tap water, waste water and tap water are tested and is used in concrete. The cubes of concrete are made by all this type concrete are tested in this study. The sizes used for making blocks were $150 \times 150 \times 150$ mm. The compressive strengths were calculated at 7 and 28 days.

2 Objective

1. To determine effective concrete strength by comparing different type of water.
2. To recommendation on basis for this study.
3. Find out alternate option for tap water by waste water.

3 Methodology

3.1 Water

The drinking water which was available is used for study. The IS 3025-1986- BIS-1986 having PH value 7.0 of water is preferred for addition in concrete. The Water to cement ratio used was 0.5 with M20 grade of concrete as Bore water, well water, bore well water, Bisleri water (mineral water) (various qualities of water) were used to cast 150 mm cube of concrete [3–6] (Fig. 1).

Fig. 1 Collection of waste water





Fig. 2 Mineral water sample was being used to mix the concrete

3.2 *Mixing*

See Fig. 2.

3.3 *Experimental Set up of Concrete Compression Test*

See Fig. 3.



Fig. 3 Compression testing machine

Fig. 4 Machine indicator needle (point of failure)



3.4 Compression Test

Compression test is the most common test conducted on hardened concrete, partly because it is an easy test to perform, and partly because most of the desirable characteristic properties of concrete are qualitatively related to its compressive strength [7–9].

The cube specimen is of the size $15 \times 15 \times 15$ cm. If the largest nominal size of the aggregate does not exceed 20 mm, 10 cm size cube may also be used as an alternative. Cylindrical test specimens (Fig. 4) have a length equal to twice the diameter. They are 15 cm in diameter and 30 cm long. Smaller test specimens may be used but ratio of diameter of the specimen to maximum size of aggregate, not less than 3–1 is maintained. This Compression testing Machine (Fig. 4) was used on the seven day, and twenty eight day cured concrete specimens. For each test day, the cubes were placed in the loading apparatus, and the load was actuated at a controlled loading rate [10, 11].

4 Result and Discussion

4.1 Result of Concrete Mix Design

See Tables 1, 2, 3, 4, 5 and 6.

Table 1 Trial mix results of concrete cube M-20

Test details	Unit	Compressive strength of concrete cubes		
Sample No.	–	1	2	3
Specimen ID	–	A-1	A-2	A-3
Date of casting	–	05/05/2022	05/05/2022	05/05/2022
Age. of specimen	Days	7	7	7
Date of test	–	12/05/2022	12/05/2022	12/05/2022
Maximum failure load	Tonnes	60	61	60
Compressive strength	N/mm ²	26.16	26.596	26.16

Table 2 Mix proportion of concrete

Proportion	Water	Cement	Sand	Coarse aggregate
By weight (kg/m ³)	191	382	705	1155
Weight (kg)	0.5	1	1.85	3.02
Volume (liters)	0.5	1	2.16	3.52

For 1 bag of cement, the quantities of material are

By weight (kg/bag)	25	51	92	150
--------------------	----	----	----	-----

Table 3 Weights of cubes (Kg) for 7 days of different water samples

Type of water sample	Sizes of cube (mm)	Age of cubes (days)	Weights of cube in kg	Avg. weights (Kg)
Well water	150 × 150 × 150	7	8.7	8.8
			9.0	
			8.8	
Tap water	150 × 150 × 150	7	8.8	8.8
			8.9	
			8.8	
Mineral water (Bisleri)	150 × 150 × 150	7	9.2	9.1
			9.1	
			9.1	
Waste water	150 × 150 × 150	7	9.2	9.1
			9.1	
			9.1	
Borewell water	150 × 150 × 150	7	8.8	8.9
			9.0	
			8.9	

Table 4 7 days compressive strength

Type of water sample	Cube size (mm)	Age of cubes (days)	Compressive strength (Tone)	Compressive strength (N/mm ²)	Average strength (N/mm ²)
Well water	150 × 150 × 150	7	51	22.2	23.0
			55	23.1	
			52	23.5	
Tap water	150 × 150 × 150	7	60	26.2	26.3
			60	26.2	
			61	26.6	
Mineral water (Bisleri)	150 × 150 × 150	7	62	27.5	27.2
			64	27.5	
			61	26.6	
waste Water	150 × 150 × 150	7	47	20.5	20.6
			47	20.5	
			48	20.9	
Borewell water	150 × 150 × 150	7	60	26.2	24.9
			60	25.7	
			52	22.7	

Table 5 Weights of cubes (Kg) for 28 days of different water samples

Type of water sample	Cube sizes (mm)	Age of cubes (days)	Weights of cube in kg	Average weights (Kg)
Well water	150 × 150 × 150	28	8.6	8.9
			8.9	
			9.1	
Tap water	150 × 150 × 150	28	8.9	8.9
			8.9	
			8.9	
Mineral water (Bisleri)	150 × 150 × 150	28	8.8	8.8
			8.9	
			8.8	
Waste water	150 × 150 × 150	28	9.1	8.8
			9.1	
			8.7	
Bore well water	150 × 150 × 150	28	8.8	8.8
			8.8	
			8.9	

Table 6 28 days compressive strength

Type of water sample	Cube size (mm)	Age of cubes (days)	Compressive strength (N/mm ²)	Avg. strength (N/mm ²)
Well water	150 × 150 × 150	28	32.7	30.2
			30.5	
			27.5	
Tap water	150 × 150 × 150	28	28.3	29.6
			29.6	
			31.0	
Mineral water (bottled)	150 × 150 × 150	28	36.6	34.2
			34.9	
			31.8	
Waste water	150 × 150 × 150	28	31.4	31.8
			32.3	
Tube well water	150 × 150 × 150	28	25.7	28.5
			28.8	
			31.0	

5 Result and Discussion

- (i) The final findings gives favorable results. Final results showed that concrete made with different types of water samples such as ground water, packed drinking water, waste water, ground water etc. had 7 days and 28 days compressive strength equal to or at least 85% of the strength of reference specimens made with fresh clean water for M20 grade of concrete.
- (ii) From the analysis of test carried out, it was revealed that, the concrete made with doubtful water sample i.e. waste water sample with constant water cement (W/C) ratio of 0.5, there was about 15% less 7-day compressive strength compared to reference specimen.
- (iii) The compressive strength obtained for concrete made by mineral bottled water was 14% more strength than the cubes prepared from tap water.
- (iv) The concrete cubes prepared with Tube well water (underground water) having slightly less 28-day compressive strength, compared to other cube specimens. (It was less by 5% compared to reference cube specimens).
- (v) It was recommended from this study slightly salty, alkaline, acidic, colored or smelling water should be used for concrete making regularly, as there is water scarcity in many part of world.

References

1. Al-Manaseer, A. A., Haug, M. D., & Naseer, K. W. (1988). Compressive strength of concrete containing fly ash, brine and admixture, American concrete institute. *Material Journal*, 85(2), 109–116.
2. Akinkulore, et al. (2007). The influence of salt water on the compressive and engineering and applied science, 2(2), 412–415
3. Cement Concrete & Aggregates Australia. (2007). Use of recycled water in concrete production
4. Griffin, D. F., & Henry, R. L. (2020). The effect of salt in concrete on compressive strength, water vapor transmission, and corrosion of reinforcing steel. Y-R007-05-01 -012.
5. I.S. 10262-2009: Recommended guidelines for concrete mix design. Bureau of Indian Standards, New Delhi.
6. I.S. 456: 2000 Code of practice for plain and reinforce concrete Bureau of Indian Standards, New Delhi. (third revision).
7. Islam-Ul-Haque, Baig, M. A., & Mir, M. Use of municipal waste water for plain cement concrete construction. *Electronic Journal of Environmental, Agricultural & Food Chemistry*. ISSN: 1579-4377.
8. Alawode, O., Dip, P. G., & Idowu, O. I. *Effect of water- cement ratios on the compressive strength and workability of concrete and lateritic concrete mixes*. MC Bauchemie (Ind) Pvt. Ltd.
9. Shetty, M. S. *Technical advisor*. MC Bauchemie (Ind) Pvt. Ltd. “Concrete Technology. Theory & Practice”
10. Saravanakumar, P., & Dhinakaran, G. (2010). Effect of acidic water on strength, durability and corrosion of concrete. *Journal of Civil Engineering Research and Practice*, 7(2), 1–10.
11. Richard, P., Cegrezy, M. H. Reactive powder concretes with high ductility & 200–800Mpa compressive strength. In *Proceedings of V. M. Malhotra Symposium*, Sp-144 ACI-1994.

By Using Ansys, Conduct a Free Vibration Analysis of a Cantilever Beam for Several Materials with Different Cross Sections



Prashant Mali and Swanand Kulkarni

Abstract The analysis of vibration in a cantilever beam is crucial for many mechanical applications, including machinery, building construction, propeller shafts and areophane wings. A thorough analysis was conducted to assess the effects of changing the cantilever beam's length, width, and thickness. In this paper, study is done. This is done by keeping an eye on the beam's native frequency as this sways freely there are two distinct phases to the study. The first stage is hypothetically carried out by figuring out the inherent frequency of a specimen with different lengths, widths, and thicknesses while attempting to change the specimen's material. This indicates how the specimen's measurements and substance have the greatest impact on minimizing resonance frequencies. The outcomes of the second phase are used to validate the outcomes of the first phase. In order to achieve this, the experimental phase conditions are modelled into ANSYS Workbench 14.5 while taking into in adjusting the specimen material, take into account the cantilever beam with different lengths, thicknesses, and widths. The theoretically derived findings are then compared to all of the data from the ANSYS workbench package. It was calculated that 1.655% was the highest conceivable percentage of natural frequency inaccuracy.

Keywords Cantilever beam · Ansys · Natural frequency · Mode shape · Vibration

P. Mali (✉)

M-Tech. Department of Mechanical Engineering, SKNCOE, Korti, Pandharpur, India
e-mail: pbmali2020@gmail.com

S. Kulkarni

Associate Professor, Department of Mechanical Engineering, SKN Sinhgad College of Engineering, Korti, Pandharpur, Maharashtra, India
e-mail: swanand293@gmail.com

1 Introduction

Vibration is indeed the displacement of a body or system of related bodies from its equilibrium position or its recurrence after a predetermined period of time. The associated with excessive vibration include the failure of components to balance, misalignment, wear, looseness, and damage to the equipment, an increase in the load on the bearing, among many other items. Such impacts also involve the manufacturing of unfriendly noise and excessive energy consumption even by machine [1]. A large piece of machinery or something comparable to an aircraft's engine are likewise subject by vibration. Fatigue and excessive vibration are generated as a result of this resonance. Machine performances are decreasing. Each vibrating body is supposed to vibrate with a specific frequency or larger amplitude in general. This frequency is considered as the resonance frequency, which is also referred as the natural frequency. In order to prevent resonance, it is therefore necessary to study these natural frequencies and create a solution [2]. According this description, the body is considered to vibrate freely or naturally when no external force imposes any force on it after an initial displacement. Free or natural frequency is the frequency of a vibration that really is free or natural. The amplitude keeps continuously decreasing with time. An examination of a cantilever beam's free vibration for various structural elements, modifications in beam length, and variations in beam material are the subjects of this paper. It illustrates that the natural frequency of varying properties differs, helping us in choosing the material which will work the best for our application. Using ANSYS Workbench 14.5, the value of natural frequency is calculated theoretically for the free vibration analysis and cross-checked [3].

2 Scope of Work

In this analysis, we measured the frequencies of beams for different cross-sectional areas comprised of three different types of materials: mild steel, aluminium alloy, and copper alloy with cantilever support. With Euler Bernoulli's beam theory and ANSYS 14.5 software, we attempt to perform a comparative analysis of the actions of different sections under different cross section areas based on the natural frequency with an initial displacement. The main goal of the research was to investigate whether various cross-sections of beams and materials respond while vibrated.

3 Principal Goal

As every fixed beam utilized in the manufacturing of vehicles, industrial machinery, aircraft, and home appliances has one end left open, it is essential to comprehend how well these beams vibration. The following is indeed the yoke's main objective.

1. A deep understanding of the way a beam configuration with a fixed end and a free end with a changing cross section behaves.
2. to analyses a beam with such a fixed end and a free end using FEA.
3. Are using a numerical method to analyses a beam including one end fixed and the other free.

3.1 *An Advantage of Vibration Investigation*

- (1) Understanding whether machine sections respond dynamic.
- (2) Understanding the machine's mechanical condition.
- (3) Understanding whether such a hypothetical capacity increase is possible.
- (4) Performing rebuilds the most inexpensive manner feasible.
- (5) Trying to anticipate future mechanical problems and avoiding unplanned shutdowns
- (6) Knows how to fix for problems such as gear train failures and barring.

4 Information

To perform the analysis, mild steel, aluminium alloy, and copper alloy beams are taken into consideration. By changing the geometries of the beam, the cross sections of materials are assumed to be rectangular and also have different support conditions. Following the analysis of a materials, methods includes theoretical analysis and FE analysis are used. The application of Euler's beam theory simplifies theoretical analysis. With both the assistance from ANSYS Workbench 14.5, finite element analysis (FEA) is accomplished. For a first mode of vibration, the theoretical part results are supported by a numerical approach.

The cantilever beam, with a fixed end and a free end, was used for free vibration analysis and was decided to make of different materials, such as copper alloy, mild steel, and aluminium alloy [4] (Fig. 1; Tables 1 and 2)

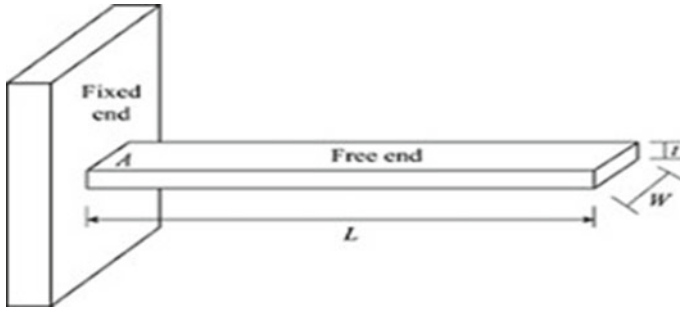


Fig. 1 Cantilever beam

Table 1 Specification of beam

Dimension	
Length	500 mm
Width	50 mm
Thickness	5 mm

Table 2 Properties of beam

	Mild steel	Aluminium alloy	Copper alloy
Density (kg/m ³)	7850	2770	8300
Young's modulus (G pa)	205	71	110
Poisson ratio	0.303	0.33	0.34

5 Theoretical Analysis

It was assumed in the theoretical calculation, which was done using Bernoulli's Beam Theory by Euler that the change in frequency was caused by changes in the moment of inertia and beam length. Equation (1) can be used to calculate the frequency of a uniform cantilever beam with a rectangular cross section area.

$$F_n = \frac{1}{2\pi} \left[(\beta_n)^2 \right] \sqrt{\frac{EI}{\rho A l^4}} \tag{1}$$

where

A = the area of the beam's cross section.

L is the beam's length. = material density.

E = elasticity modulus.

I = is the moment of inertia.

l = Bending mode value.

The initial bending mode's value for l is 1.875104.

Table 3 Calculation of mild steel

Condition of beam	Fn in Hz
Long condition	13.644
Short condition	20.383
Thick condition	23.114
Thin condition	9.906
Wide condition	16.510
Narrow condition	16.510
Long and narrow condition	13.644

It is feasible to determine the frequency of homogeneous cantilever beams made of various materials using this formula [5, 6].

5.1 Calculations of First Mode for Mild Steel

For Cantilever Beam (Table 3),

(1) Original Condition-

$$L = 500 \text{ mm} = 0.5 \text{ m}, A = 0.05 \times 0.005 = 2.5 \times 10^{-4} \text{ m}^2,$$

$$\rho = 7850 \text{ kg/m}^3,$$

$$I = (bd^3)/12 = 5.208 \times 10^{-10} \text{ m}^4.$$

5.2 Calculations of First Mode for Aluminium Alloy

For Cantilever beam,

(1) Original Condition-

$$L = 500 \text{ mm} = 0.5 \text{ m}, A = 0.05 \times 0.005 = 2.5 \times 10^{-4} \text{ m}^2,$$

$$\rho = 2770 \text{ kg/m}^3,$$

$$I = (bd^3)/12 = 5.208 \times 10^{-10} \text{ m}^4.$$

Table 4 and 5 shows calculation of first mode for Aluminium alloy and for copper alloy.

Table 4 Calculation of first mode for aluminium alloy

Condition of beam	Fn in Hz
Long condition	13.518
Short condition	20.193
Thick condition	22.899
Thin condition	9.814
Wide condition	16.356
Narrow condition	16.356
Long and narrow condition	13.518

Table 5 Calculation of first mode for aluminium alloy

Condition of beam	Fn in Hz
Long condition	9.720
Short condition	14.520
Thick condition	16.466
Thin condition	7.057
Wide condition	11.761
Narrow condition	11.761
Long and narrow condition	9.720

5.3 Calculations of First Mode for Copper Alloy

For Cantilever Beam,

(1) Original Condition-

$$L = 500 \text{ mm} = 0.5 \text{ m}, A = 0.05 \times 0.005 = 2.5 \times 10^{-4} \text{ m}^2,$$

$$\rho = 8300 \text{ kg/m}^3,$$

$$I = (bd^3)/12 = 5.208 \times 10^{-10} \text{ m}^4.$$

6 Discussion

The free vibration analysis of a cantilever beam is conducted in the current work utilising a theoretical method and a numerical technique using Ansys. Between 0.6135 and 1.6555% is the range of the error between the theoretical approach and the numerical approach. The accuracy of the model is demonstrated by the discovery that the relative error between the two approaches is extremely small. The highest possible percentage of natural frequency inaccuracy was discovered to be 1.655%.

Distinct materials combined exhibit different natural frequencies for the first mode form. Here, we can see that several materials, such as mild steel, aluminium alloy,

and copper alloy, have been compared for various cross sections. As seen in the above data, copper alloy has a lower frequency than mild steel and aluminium alloy.

7 Conclusions

After obtaining results utilising a theoretical strategy and a numerical technique, the following conclusions are drawn. This is accomplished by incorporating the experimental phase conditions for a variety of materials, such as copper alloy, mild steel, and aluminium alloy, into the ANSYS technique.

1. The length of the beam grew by 50 mm at the same cross section area (50v5), while the frequency of the beam fell by between 2.0535 and 2.8792 Hz.
2. After altering the cross section area of the beam, the frequency of the beam increased by between 4.7153 and 6.6160 Hz, and the thickness of the beam increased by 2 mm ($500 \times 50 \times 7$).
3. It has been noted that a change in beam width has no effect on frequency.
4. Taking into account the dimensions ($550 \times 50 \times 5$), which saw an increase in length of 50 mm and a drop in width of 5 mm, the frequency of the beam reduced by 2.0574–2.8837 Hz when compared to the original beam ($500 \times 50 \times 5$).

References

1. Chopade, J. P., & Barjibhe, R. B. (2013). Free vibration analysis of fixed free beam with theoretical and numerical approach method. *International Journal of Innovations in Engineering and Technology*, *II*(1), 352–356.
2. Duruik, O. C., & Ubulom, U.-A. Designing and manufacturing of a modal analysis test bench.
3. Chaphalkar, S. P., Khetre, S. N., & Meshram, A. M. Modal analysis of cantilever beam structure using finite element analysis and experimental analysis. *American Journal of Engineering Research*, *4*(10), 178–185.
4. Ghodge, V., Bhatu, A. P., & Patil, S. B. (2018). Vibration analysis of beam. *International Journal of Engineering Trends and Technology*, *55*(2).
5. Dive, V., Bhosale, M., Chavan, V., & Durugkar, N. (2017). Analysis of natural frequencies of cantilever beam using ansys. *International Research Journal of Engineering and Technology (IRJET)*, *04*(05).
6. Nirmal, T., & Vimala, S. (2016). Free vibration analysis of cantilever beam of different materials. *International Journal of Science and Research (IJSR)*, *5*(4).

Optimization of Takali Zone in 24×7 Water Supply Network of Pandharpur City



Mukund Pawar and N. P. Sonaje

Abstract The natural driving force is water. The entire globe fights to protect it. Water wasting is a serious problem for us because India is one of the top 12 countries that lack access to clean water. India's population is growing, and as a result, so is the country's need for water. An effective water distribution network, which may be created using cutting-edge hydraulic software like Water GEMS, can satisfy this expanding need. Pandharpur city has been chosen to transform the current water supply system into a continuous 24-h system using the Water GEMS software. The pipes utilized in the water distribution system represent the biggest investment. From an economic perspective, the design, modelling, and optimization of pipes in the water delivery system are crucial. As a result, this article uses WaterGEM software to carry out optimal pipe network design for turning current networks into 24×7 water supply system networks. The Pandharpur region is where the initial study of the current water supply network system for one zone, Ambedkar Nagar ESR, is conducted.

Keywords 24×7 water supply system · Optimal design · Darwin designer · Water GEMS software

1 Introduction

With the increasing cost of pipes and related accessories, it is important to develop a suitable pipe network optimization approach. Under-design issues can result in undesirable and costly pipe failures, and over-design can result in wasted resources [1]. Issues arising from both over-design and under-design can be minimized by incorporating an efficient search for an optimum design with the lowest life cycle cost.

M. Pawar (✉)
WIT, Solapur, India
e-mail: pawarmm@coe.sveri.ac.in

N. P. Sonaje
Government Polytechnic, Miraj, India

This chapter aims to optimize the water distribution system in Pandharpur city using the Darwin Designer optimization tool in Water GEMS [2]. The optimization process is applied to find the optimal pipe diameter to supply adequate water quantities at satisfactory pressures to the end-users. Darwin design approach is suitable for solving the optimization problems with very large solution spaces, which cannot be solved using conventional optimization methods [3].

2 Optimization Problem Formulation

For designing or rehabilitating a wide range of optimization performance parameter issues must be taken into account while designing a water distribution system. Costs associated with construction, operation, and maintenance are likely to be the main focus. In the pipe network design, the highest cost contribution comes from the pipes' cost, and hence proper pipe selection needs to be given the highest priority [4]. The main restrictions result from the need to maintain sufficient pressure heads at the client end while yet meeting the desired demands. Additionally, the nodal pressure heads and water flow in a distribution system must adhere to the fundamental rules of mass and energy conservation. Therefore, the formal optimization problem becomes with minimization of capital investment plus pipe costs, subject to:

Meeting hydraulic constraints,
Fulfilling water demands, and
Satisfying pressure requirements.

By optimizing the pipe diameter, the research's design difficulties for pipeline systems are resolved. By optimizing pipe diameter, the cost of the system can be reduced. By maximizing pipe diameter under steady-state flow circumstances, the primary goal of cost minimization is accomplished.

Total Network cost is given by:
Subjected to

$$Tc = \sum_{i=1}^n LiCi(di) \quad (1)$$

Pressure head requirements $P_j \geq P_{j\text{and}}$ Pipe diameters available $di = dA$.

Where, Tc = total cost of network

Li = Length of i th pipe in meter

$Ci(di)$ = Cost per unit length for that diameter of i th pipe in Rs.

n = total no. of pipes in network α = penalty parameter in Rs.

$P_j(A)$ = Pressure Head available at j th node in meter

$P_j(B)$ = Pressure Head required at j th node in meter

f = Friction constant

Q^i = Discharge required in i th outlet in l_{ps} d_i = diameter of i th pipe in meter

d^A = commercially available diameter in meter.

3 Methodology for Solving Optimal Design Problem

With the choice of pipe sizes as the decision variables, the water distribution system (WDS) design problem is described and solved here as a single-objective optimization problem. The network's cost reduction is a consideration for the primary parameter. The goal of the best design approach described here is to reduce overall design expenses while maintaining steady-state minimum head requirements. The processes for designing the distribution network in the best possible way using waterGEMS's Darwin Designer technique are listed below.

- i. **Setting the Darwin Designer Problem:** Using the Darwin Designer option from the waterGEMS a "New Designer Research" is created. For solving the optimization problem, a "New Optimized Run" option is selected.
- ii. **Creating a pipe network:** This step is similar to adding pipes to a new design or rehabilitation culture as explained earlier in Chap. 3. A new pipe group mark has been developed. A selection field can be found under the 'Factor IDs' tab. First pressed the cell, then the ellipsis button ('...'). This will open a new dialog box where you can choose the elements that should be included in the design optimization
- iii. **Adding Cost data:** There is a tab for Cost / Property. We may enter cost data here for a specific pipe size or rehabilitation action. Select the New Icon and either 'Group Design Options' to build a new entity. For Design Option Group, the material, diameter, Hazen Williams C factor, and unit cost are all added.
- iv. **Optimized Design Run:** The optimized design analysis employs a genetic algorithm to find the best possible solution within a set of parameters. The optimized design analysis has no true optimality; it simply knows the best solution in comparison to other solutions found during computation. The optimized design analysis, on the other hand, goes through a large number of potential solutions and can still find a good match for the model.

Once the optimization setup is created, the Darwin designer performs various combinations of experiments with different pipe sizes or recovery activities that fall within the constraints entered on the Design Event tab before determining the best solution for the target type. Darwin Designer keeps working until the right solution is obtained, meeting the convergence criteria. The results are presented similarly to the single run steady-state simulation, but there is the option to view up to ten solutions.

4 Optimally Designed Pipe Network

Figure 1 shows the length comparison between pipe lengths from manual design and pipe lengths obtained in Darwin optimization with respective diameters from zone-1 Ambedkar Nagar ESR. The optimization solution provides the lesser diameter

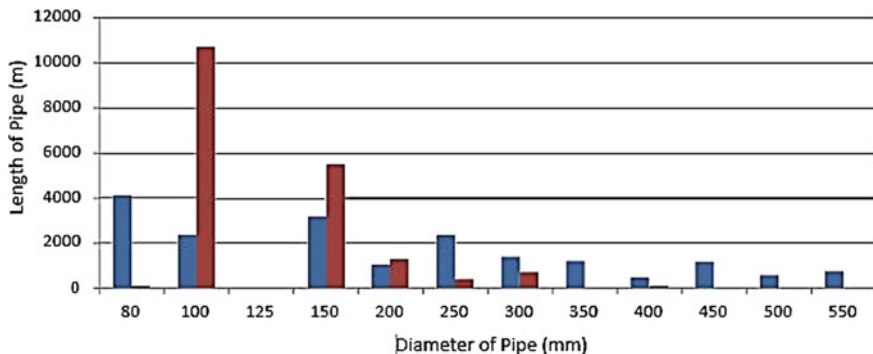


Fig. 1 Zone-1 pipe length comparisons

requirements by giving minimum pipe diameter of size 80 mm which results reducing the lengths of pipes of diameters 100, 150 and 200 mm. Therefore, overall pipe cost reduction as compared to the steady state analysis.

5 Cost Analysis of Optimal Network

The cost analysis of the pipes used in the steady state analysis has been carried out in Chap. 5. Total pipe lengths of Pandharpur city network is about 262,197 m. To construct this network total estimated expenditure based on the pipe costs per meter given in the Detailed Schedule Rate (DSR) of Pune region is Rs. 11,086,476. This cost is just for the piping of the network without considering excavation charges. The summary of this cost analysis is shown in the Table 1. The table shows that the Darwin optimization is able to reduce the cost of the network in each zone by about 8–29% and overall cost that can be saved by the Darwin Optimization is about 16.11%.

6 Design Criterion Validation of the Optimal Network

To check the optimally designed network satisfy the pressure and head loss criterion as per CPHEEO [4], steady state analysis of the optimally designed network has been carried out for the three stages of the water demands. Figure 2 shows the pressure values at each junction of the 13 zones of the network for the ultimate stage of water demand. Tables 2 and 3 shows the pressure and head loss summary of the optimally designed network for the all the zones for the three stages of demand. From the steady state analysis summary data, it can be seen that the optimally designed network not

Table 1 Cost analysis summary of pipe network by steady state analysis

Zone	Length of respective pipe diameter in (m)										Total length of the pipes for the zone	Total cost piping in Rs. without excavation cost	
	80 (mm)	100 (mm)	125 (mm)	150 (mm)	200 (mm)	250 (mm)	300 (mm)	350 (mm)	400 (mm)	450 (mm)			500 (mm)
Ambika Nagar	0	337	0	280	169	26	41	22	0	30	0	9091	1,108,647
ESR		5		1	8	9	7	4		7			6

Fig. 2 Darwin pressure in zone 1

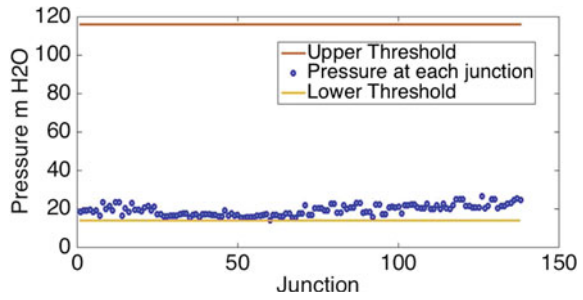


Table 2 Zone-wise pressure summary of the optimally designed network

Zone No.	Immediate stage		Intermediate stage		Ultimate stage	
	Minimum (m)	Maximum (m)	Minimum (m)	Maximum (m)	Minimum (m)	Maximum (m)
Ambekar Nagar	12	21	12	23	12	24

Table 3 Zone-wise head loss summary of the optimally designed network

Zone No.	Immediate stage		Intermediate stage		Ultimate stage	
	Minimum (m/km)	Maximum (m/km)	Minimum (m/km)	Maximum (m/km)	Minimum (m/km)	Maximum (m/km)
Ambekar Nagar	0	0.41	0	0.52	0	0.71

only satisfied the pressure head loss criterion for the ultimate stage of water demand but also satisfies it for immediate and intermediate stage of water demands.

7 Conclusions

In this research paper the proposed network suggested for Pandharpur city which will cater water supply for 24×7 is optimized using Darwin optimization approach. The pipe diameters required for the network has been optimized for the cost reduction of network keeping the constraints as pressure at each junction and the pipe diameters available in the market. The optimally designed network could save a piping cost by about 16.11% by satisfying the pressure and head criterion for all the three stages of water demands.

References

1. Kanakoudis, V. K. (2004). Vulnerability based management of water resources systems. *Journal of Hydroinformatics*, 6(2), 133–156.
2. Bentley Team, Bentley WaterGEMS V8i User's Guide, 2020.
3. Djebedjian, B., Abdel-Gawad, H. A., & Ezzeldin, R. M. (2021). Global performance of meta-heuristic optimization tools for water distribution networks. *Ain Shams Engineering Journal*, 12(1), 223–239.
4. Boulos, P. F., & Altman, T. (1993). Explicit calculation of water quality parameters in pipe distribution systems. *Civil Engineering Systems*, 10(3), 187–206.

Sustainable Development of Blended Cement by Using Colloidal Nano Alumina



Anirudh Harishchandra Shirke and Manish Patkar

Abstract Nanotechnology is the current cutting-edge technology used in the construction industry. Day by day cost of cement is increasing enormously. One ton use of cement in concrete produces around 1 ton of carbon dioxide. Hence it is essential to replace the cement partially in the preparation of concrete. In the paper, cement is replaced by fly ash and colloidal nano-alumina. This task plans to create nano concrete and concentrate on the impacts of nano alumina on the properties of cement. In this examination, the concrete is supplanted by 10% Fly-ash and Al₂O₃ nanoparticles of various percentages such as 0.5, 1, 1.5, 2.0, 2.5, and 3% in M 40 grade of cement. From the result, it is revealed that by the addition of fly ash and colloidal nano alumina compressive strength, split tensile strength, and flexural strength enhances by 4.1%, 10.75%, and 23.92% respectively.

Keywords Colloidal nano alumina · Compressive strength · Flexural strength · Nondestructive test

1 Introduction

The use of cement concrete in the construction industry has undergone amazing developments over the last ten years [1]. Concrete is a crucial part of building work when it comes to construction materials [2]. Without concrete, the engineering work cannot be finished [3]. In order to correctly bind the material, concrete is the lifeblood of civil engineers [4]. Cement, coarse aggregate, and fine aggregate are combined to create concrete [5]. The high compressive strength of the concrete is crucial for construction activity [6]. Concrete determines the construction's key characteristics, distinctive shape, and structural strength [7]. Concrete can lengthen the useful life of

A. H. Shirke (✉)

Research Scholar, Department of Civil Engineering, Oriental University, Indore, India
e-mail: anirudhshirke55@gmail.com

M. Patkar

Professor, Department of Civil Engineering, Oriental University, Indore, India
e-mail: manish.patkar@gmail.com

the building and increase its toughness [8]. Construction of bridges, docks, harbors, roads, tunnels, conduits, sewage systems, marine structures, monuments, etc. all benefit greatly from the use of concrete [9]. Around 450 million cubic meters of concrete were consumed nationwide in India in 2012, and that number is expected to increase to 800 million cubic meters by 2020 [10]. Universally concrete is a significant construction material used due to its durability and versatility [11, 12]. One ton use of cement in concrete produces around 1 ton of carbon dioxide hence having a bad impact on global warming directly or indirectly. So, it is essential to replace the cement partly to reduce the overburden on the environment. As nanomaterials are significant because of their unique properties, for example, high surface-to-volume proportions, as the surface region per mass of material, expands, which leads to a bigger measure of the material can show up in contact with adjoining materials, hence the nanomaterial are more reactive. Application of Nanomaterial in construction work is an innovative technology, as nanomaterial applies the science, and engineering technology for monitoring and enhancing the performance of material on a nanoscale. Nanomaterial can build the block at a molecular scale and hence nanomaterial is area investigated and examined on a large scale [13]. In the last two decades, the application of nanomaterial in the construction industry become popular as nanomaterial having unique salient features. The construction activities were accelerated by the application of nanomaterial.

2 Methodology

As per the Indian Standard method (IS-10262) mix designs for M -40 grade of concrete was prepared. The specific Gravity of cement is 3.15, Coarse Aggregate of size 20 mm was used. As per the IS 456-2000, the water-cement ratio is considered in the range of 0.35–0.45. The calculation has been mentioned in Table 1 as per the IS 10262.

Table 2 shows the concrete mix with different proportions of colloidal Nano Alumina (CNA) and Fly ash. Casting was carried out for 3, 7, and 28 days. Compressive strength, Flexural Strength, and Split tensile strength of the mix were carried.

In this paper replacement of OPC by P-60 grade of fly ash was used at 10% and colloidal nano alumina was used at 0%, 0.5%, 1%, 1.5%, 2%, 2.5% and 3% respectively. The strength of concrete depends upon the optimum workability of concrete. Hence maximum workability is kept while preparing the concrete. The workability of concrete depends upon the properties of the construction material used for the construction. The colloidal nano alumina has an influence on the water-binder ratio. Due to the application of nano alumina workability of concrete will be regarded as surface area increases by the application of colloidal nano alumina. Hence superplasticizer was used to obtain the optimum workability of concrete. Table 3 illustrate the slump cone value in mm and the replacement proportion of Nano alumina and fly ash.

Table 1 Observation and calculations

S. No.	Property of material	Value
1	Characteristic compressive strength	40 N/mm ²
2	Standard deviation (S)	5
3	Target mean compressive strength, $F_t = f_{ck} + 1.65X_s$	48.25 N/mm ²
4	W/C ratio	0.38
5	Type of cement	OPC(53 Grade)
6	Coarse aggregate size	20 mm
7	Cement specific gravity (S_c)	3.15
8	Fine aggregate specific gravity (S_{fa})	2.6
9	Coarse aggregate specific gravity (S_{ca})	2.825
10	Per m ³ of concrete water content	140 kg/m ³
11	Cement content	375 kg/m ³
12	Total fine aggregate	858 kg
13	Total coarse aggregate	1186.5 kg

Table 2 Concrete mix with different proportion of CNA, and FA

Materials in %				Quantities in Kg					
Concrete mix No.	Cement	Fly ash	CNA	Cement	Fly ash	CNA	Water	C.A	F.A
A1	100	0	0	375	0	0	140	1186.5	858
B1	90	10	0	337.5	37.5	0	140	1186.5	858
C1	89.5	10	0.5	335.81	37.5	1.67	140	1186.5	858
C2	89	10	1	334.125	37.5	3.375	140	1186.5	858
C3	88.5	10	1.5	332.43	37.5	5.06	140	1186.5	858
C4	88	10	2	330.75	37.5	6.75	140	1186.5	858
C5	87.5	10	2.5	329.06	37.5	8.43	140	1186.5	858
C6	87	10	3	327.37	37.5	10.12	140	1186.5	858

Table 3 Replacement of nano alumina and fly ash

S. No.	Replacement of cement		Slump (mm)
	Fly ash	Nano alumina	
1	00	00	74
2	10	00	67
3	10	0.5	62
4	10	1	59
5	10	1.5	54
6	10	2.0	53
7	10	2.5	51
8	10	3.0	49

3 Results and Discussion

To analyze the effect of the replacement of nano alumina and fly ash on the preparation of concrete compressive strength was carried out for 3, 7, and 28 days. The result obtained were summarized in the Table. 4. From the results it is concluded that by the addition of fly ash alone the compressive strength of concrete is reduced reason may be fly ash has fewer bind properties as compared to cement. Optimum strength achieved with the combination of 10% fly ash and 2% CNA was 21.73, 30.51, and 45. 73% for 3 days, 7 days, and 28 days respectively. The compressive strength of concrete going to be reduced by 2.5 and 3% colloidal nano alumina reason may be the high rate of water absorption. Similar results were reported by author Gowda et al. [9].

3.1 Split Tensile Strength

To determine the tensile strength of concrete split tensile strength, need to be calculate. After 28 days generally split tensile strength was carried out. Maximum split tensile strength obtained was 3.81 N/mm for 10% Fly ash and 2% Colloidal nano alumina. Similar result was reported by researcher Gerges et al. [11]. Table 5 shows the split tensile strength of concrete for various proportion of fly ash and colloidal nano alumina.

3.2 Flexural Strength

Flexural strength of the concrete was carried to find the yield of the concrete. This test is carried out to check the resistivity of concrete. Flexural strength is also known

Table 4 Compressive strength of concrete by the addition of fly ash and nano alumina

Replacement of fly ash and CNA	Avg. compressive strength N/mm ²		
	3 days	7 days	28 days
0% FA + 0% CNA	18.04	27.07	43.90
10% FA + 0% CNA	18.41	26.66	43.54
10% FA + 0.5% CNA	19.77	27.56	44.32
10% FA + 1% CNA	20.06	27.70	44.64
10% FA + 1.5% CNA	20.23	28.89	45.21
10% FA + 2% CNA	21.73	30.51	45.73
10% FA + 2.5% CNA	21.04	30.12	44.81
10% FA + 3% CNA	19.58	28.02	44.17

Table 5 Split Tensile strength of concrete of different proportion (28 Days)

Replacement of fly ash and CNA	Avg. split tensile strength after 28 days (N/mm ²)
0% FA + 0% CNA	3.44
10% FA + 0% CNA	3.49
10% FA + 0.5% CNA	3.47
10% FA + 1% CNA	3.52
10% FA + 1.5% CNA	3.69
10% FA + 2% CNA	3.81
10% FA + 2.5% CNA	3.34
10% FA + 3% CNA	3.12

Table 6 Flexural strength of concrete of different proportion (28 days)

Replacement of fly ash and CNA	Avg. split tensile strength after 28 days in MPa (N/mm ²)
0% FA + 0% CNA	5.16
10% FA + 0% CNA	5.44
10% FA + 0.5% CNA	5.25
10% FA + 1% CNA	5.47
10% FA + 1.5% CNA	5.98
10% FA + 2% CNA	6.89
10% FA + 2.5% CNA	6.42
10% FA + 3% CNA	6.28

as modulus of rupture. To check and analyze which type of material is suitable for the construction and having optimum strength and rupture. Flexural test is essential. Table 6 represents the flexural strength for various proportion of fly ash and colloidal nano alumina. Maximum strength obtained is 6.89 MPa for proportion 10% FA, and 2.5. % CNA.

3.3 Non-Destructive Test

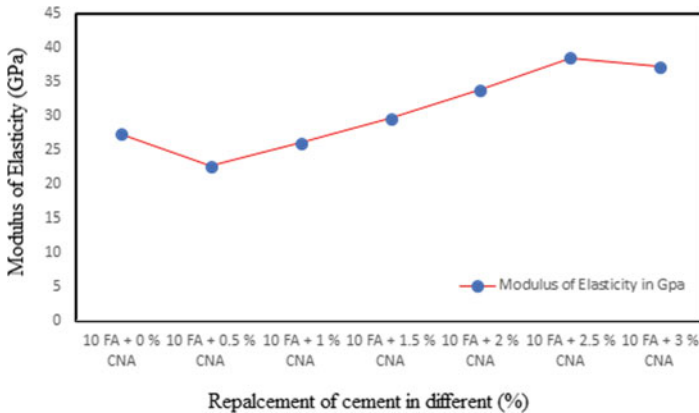
Nondestructive test is the special test carried out to check the quality of cement concrete. Test is performed by passing a pulse of ultrasound through concrete then measured the time required for the pulse. Highest velocity designates excellent quality of concrete. Highest velocity required is 10 km/sec it indicates combination of 10% FA, CNA 2.5% having good quality as compared to other combination. Similar report has been reported by author Rahman et al. (2020).

Table 7 Non-destructive test

Replacement of cement in (%)		Non-destructive test (ultrasonic pulse velocity)	
Fly ash	Nano alumina	Time in microsec	UPV in km/Sec
00	00	33	4.54
10	00	37	4.05
10	0.5	30	5
10	1	27	5.56
10	1.5	5.76	7.6
10	2	6.25	10
10	2.5	6.55	8.8
10	3	7.30	8.5

3.4 Test Results of Modulus of Elasticity

Optimum modulus of elasticity recorded for the combination of 10% Fly ash and 2% Colloidal nano alumina was 38.58 GPa. Modulus of elasticity determine the concrete hardness, and its abrasion resistance. Modulus of elasticity increases by the addition of 10% fly ash, 2% CNA (Colloidal nano alumina) (Table 7).



4 Conclusion

The maximum compressive strength, split tensile strength, and flexural strength of the concrete produced by the addition of 10% fly ash and 2% colloidal nano alumina are observed as 45.73, 3.81, and 6.89 N/mm² accordingly. The standard concrete typically has flexural strength of 5.56 N/mm², split tensile strength of 3.44 N/mm²,

and compressive strength of 43.90 N/mm². By adding fly ash and colloidal nano alumina, compressive strength, split tensile strength, and flexural strength are all increased by 4.1%, 10.75%, and 23.92%, respectively, according to the results.

References

1. Mohammed, R. K., Abdel-Hamead, A. A., & Othman, F. M. (2018). Effect of nano-alumina on microstructure and mechanical properties of recycled concrete. *Journal of Engineering and Sustainable Development*, 22(2), 90–103.
2. Alqamish, H. H., & Al-Tamimi, A. K. (2021). Development and evaluation of nano-silica sustainable concrete. *Applied Sciences*, 11, 3041. <https://doi.org/10.3390/app11073041>
3. Olafusi, O. S., Sadiku, E. R., Snyman, J., Ndambuki, J. M., & Kupolati, W. K. (2019). Application of nanotechnology in concrete and supplementary cementitious materials: A review for sustainable construction. *SN Applied Sciences*, 1, 580. <https://doi.org/10.1007/s42452-019-0600-7>
4. Ashok, K., Kameswara Rao, B., & Sarath Chandra Kumar, B. (2021). Experimental study on metakaolin and nano alumina-based concrete. *IOP Conference Series: Materials Science and Engineering*, 1091, 012055. <https://doi.org/10.1088/1757-899X/1091/1/012055>
5. Shaikh, F. U. A., & Hosan, A. (2019). *Effect of nano alumina on compressive strength and microstructure of high-volume slag and slag-fly ash blended pastes*.
6. Fayed, E. K., El-Hosiny, F. I., El-Kattan, I. M., Al-kroom, H., Elrahman, M. A., & Abdel-Gawwad, H. A. (2021). *An Innovative Method for Sustainable Utilization of Blast-Furnace Slag in the Cleaner Production of One-Part Hybrid Cement Mortar*, 14(19), 5669. <https://doi.org/10.3390/ma14195669>
7. Hosseini, P., Mohamad, M. I., Nekooie, M. A., Taherkhani, R., & Booshehrian, A. (2011). Toward green revolution in concrete industry: The role of nanotechnology (a review). *Australian Journal of Basic and Applied Sciences*, 5(12), 2768–2782.
8. Ashok, K., & Kumar, S. C. (2020). Influence of nano particles in concrete – a review. *International Journal of Advanced Research in Engineering and Technology*, 11(6), 248–263.
9. Gowda, R., Narendra, H., Rangappa, D., & Prabhakar, R. (2017). Effect of nano-alumina on workability, compressive strength, and residual strength at elevated temperature of cement mortar. *Materials Today Proceedings*, 4(11), 12152–12156.
10. Rahman, I., & Nano, N. D. (2020). Alumina based high strength concrete. *International Journal of Innovative Technology and Exploring Engineering*, 9(4), 356–363.
11. Gerges, N. N., Issa, C. A., & Fawaz, S. (2015). Effect of construction joints on the splitting tensile strength of concrete. *Case Studies in Construction Materials*, 3, 83–91.
12. Norhasri, M. S., Hamidah, M. S., & Mohd Fadzil, A. (2017). Applications of using nano material in concrete: a review. *Construction Building Material*, 133, 91–97.
13. Rahim, A., & Nair, S. R. (2016). Influence of nano-materials in high strength concrete. *Journal of Chemical and Pharmaceutical Sciences*, 3, 15–22.

Anaerobic Digestion: Addressing the Problem of Food Waste by Converting it into Biogas



Chetan Patil and Kailasnath Sutar

Abstract In some parts of rural India, biogas production is a crucial energy source. The statistics show that it is equivalent to 5% of total LPG production. It is a promising renewable source of energy. The resources required for biogas production are easily available in rural and urban areas. Biogas is mostly generated by using degradable wastes such as animal dung, agro-waste, industrial waste, poultry waste, vegetable, and food waste (FW), in addition to a combination of a majority of these wastes. The boost in the production of biogas can be helpful in reducing the load on traditional energy resources. Biogas production can be boosted by using various techniques, such as adding different additives, different pretreatment methods, and using the appropriate co-digestion technique. The present article discusses how biogas production can be boosted by using various techniques.

Keywords Biogas · Food waste · Anaerobic digestion · Co-digestion

1 Introduction

Due to the increasing population, industrialization, and urbanization in India, waste generation is increasing day by day. Control of solid organic waste is a main environmental trouble in India. Biomass, which may be solid or liquid wastes such as organically loaded wastewater, municipal solid waste, sewerage, animal waste, agricultural waste, seaweed, food, and vegetable wastes, can produce biogas via anaerobic digestion (AD) [1]. Organic waste is the mainstream for biogas production. Also, another advantage is to prevent the release of odour and decreases pathogens that do the degradation of organic waste through AD. Moreover, digested residues are nutrient-rich and can be utilized as a fertilizer [2]. According to Food and Agricultural Organization (FAO), approximately 30% of the food produced for human intake around the world is wasted in food supply chain control [3]. In many countries,

C. Patil · K. Sutar (✉)

Department of Mechanical Engineering, Bharati Vidyapeeth (Deemed to be University) College of Engineering, Pune, Maharashtra 411043, India
e-mail: kbsutar@bvucoep.edu.in

wasted food is currently dumped or burned along with other types of combustible waste. As food waste (FW) is organic and rich in nutrients, it is a promising supply for biogas generation and fertilizers via specific degradation processes. As yet, control of food waste has built increasing interest, with biogas, hydrogen, ethanol, and biodiesel as final merchandise. Food wasted worldwide and in Asia–Pacific countries are cereal, rice, sugar, pulses, oil crops, vegetable oil, veggies, beans, onions, peas, fruits, poultry meat, animal fats, and many others [3, 4]. There are different sources of FW such as the commercial food processing plants, kitchens, cafeterias, big restaurants, and domestic kitchens. However, food wastes are classified as grains, green vegetables, husks, vegetable oils, catering wastes, etc. The catering wastes generally contain egg shells, fats, skins, residues from the intestine, undigested gas, and dairy waste [5–7]. AD comes off as the most prominent method for the treatment of organic waste in comparison to other strategies [8]. It is critical to produce biomass from different degradable sources because alteration in properties is challenging [1]. Various approaches have been considered such as: (i) Performance Parameters, (ii) Pretreatment methods [9], (iii) Co-digestion [10] and (iv) Application of different additives [1] to overcome physical and chemical boundaries of the biomass. Figure 1 reports different approaches to convert FW to biogas [11].

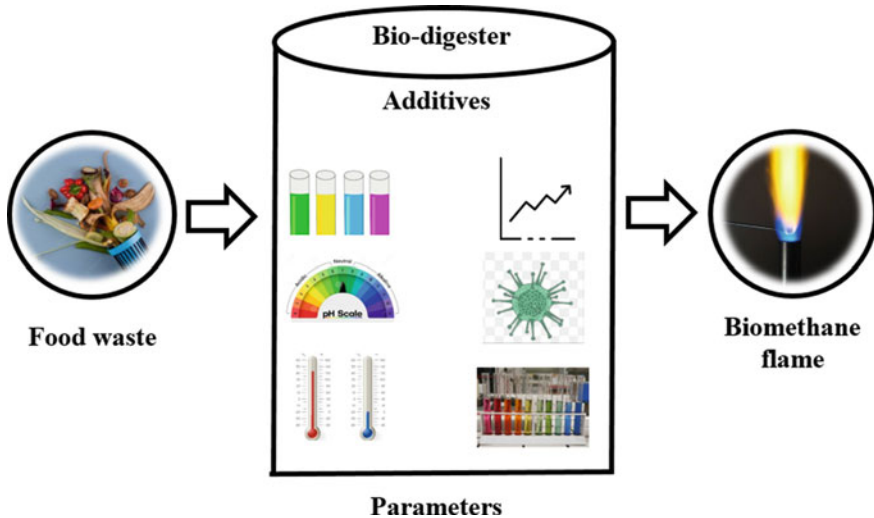


Fig. 1 Different approaches to convert FW to biogas

2 Anaerobic Digestion

AD is a good alternative for recycling degradable waste. The AD process follows a sequence of metabolic reactions, hydrolysis, acidogenesis, acetogenesis, and methanogenesis [8, 12]. The first step that is, hydrolysis, depends on the size and shape of the waste particles, surface area, biomass, enzyme production, and surface assimilation. Glucose is the end product of hydrolysis. In the acidogenic stage, propionic acid, butyric acid, acetic acid, formic acid, lactic acid, ethanol, and methanol are the major products that can be transformed from glucose. Among these principal products, acetic acid is seen to be an important organic acid because it makes use as waste to form methane organisms during the process. In acetogenesis, hydrogen plays an important role. In methanogenesis, the step needs to avoid the accumulation of volatile fatty acids (VFAs) and need to avoid a drop in pH that slows down the methanogenesis reaction [13].

In the AD process, practically any organic waste can be biologically converted into another useful end product in the absence of oxygen. The different microbes together biodegrade solid organic waste, that results in biogas and other energy-rich organic compounds as a useful product that is used as fertilizer [8]. In the design and operation of anaerobic digesters attention is given to the quality of feedstock compositions, various pretreatment methods, and reactor design and operation. For example, to get steady biogas, multi-stage anaerobic digesters are superior. They are well known to enhance biogas production as in these digesters, the acidogenic phase and methanogenic phase of the AD process are separated. Moreover, single-stage anaerobic reactors have their advantage, such as low installation as well as running cost, and are well accepted with advantages. To overcome the failure of single -stage anaerobic reactors due to their low acid buffering capacities at high organic loading rates, new strategies have been developed, such as optimizing reactor quality, co-digested feed for long-term and high organic loading rate to improve reactor performance and to get steady biogas [14]. The complicated construction of the digester's increased investment and maintenance costs has bucked up to accept the simple structure and cheaper anaerobic systems. Considering these elements, prefabricated digesters, low-cost biogas digesters, and composite material digesters have been developed for FW and used in many countries to manage the problems of constructed digesters. Constructed digesters have disadvantages such as required long construction periods, comparatively short life spans, high material costs, and maintenance and transportation cost. Prefabricated digesters have advantages such as low price, easily portable, relatively long-lasting, better insulation, corrosion resistance body, etc. It can balance and optimize the operational status of prefabricated biogas digesters. Prefabricated digesters provide an affordable, safer, more long-lasting, and well-organized system to produce energy in many countries [15]. BioPhantom software (Belach Bioteknik, Sweden) is used to monitor and record various parameters consisting of temperature, pH, the quantity of biogas, and the stirrer speed of the digester [16] (Fig. 2).

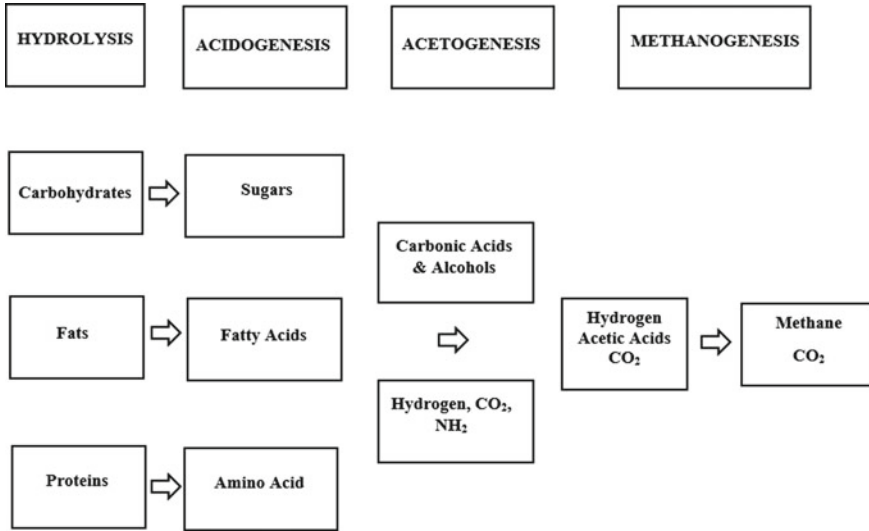


Fig. 2 Successive stages of the anaerobic digestion process [13]

2.1 Necessary Parameters for Anaerobic Digestion

Key parameters such as temperature range, pH range, carbon–nitrogen ratio, particle size, inoculum, mixing, and water content play a vital role in AD processes [17]. Biogas production rate is different at different temperatures. Metabolic activities involved in the AD process get affected by the temperature at successive stages of AD; hence it is an important parameter for biogas production. To maintain the required temperature of the reactor, there is a need for external heating and insulation to avoid inside temperature fluctuations [13]. Maintaining thermophilic (50–70 °C) or mesophilic (35–45 °C) temperature is necessary for the AD process. To maintain higher stability in the process, maintaining mesophilic conditions is necessary, which is easy compared to the thermophilic condition. But the thermophilic condition has the advantage of acclimatization, improves the growth of methanogenic bacteria, reduces retention time, avoids harm to pathogens, improves the digestibility of bacteria, and degradability of solid substrate [10, 18]. The heating approach can also be easily applied to small-size household biodigesters. Insulation and substrate heating are required to maintain a stable digester temperature. Homogeneous heat transfer and uniform heating of the substrate are possible with the in-vessel method [19]. The pH range is different at different AD stages. Hydrolysis is 6.0, methanogenesis is 6.0–7.0, and acetogenesis is 6.5–7.5 [13, 18, 20]. A comprehensive pH range required by fermentative bacteria is 4.0–8.5, and maintaining 6.5–7.2 is favourable for methanogenesis [9]. Factors that affect the pH during the AD process are alkalinity, volatile fatty acid (VFA), Carbon dioxide (CO₂) production, and bicarbonate

(HCO₃) [18]. pH is measured using Hach HQ440d pH meter, Thermo Orion, Model 550A pH meter, and WTW Inolab 7110 model pH meter [10, 21].

A carbon Nitrogen ratio in the range of 20–30 was advised to be convenient during the AD process. The C/N ratio of some waste products is Duck dung 8, Water hyacinth 25, cow dung 24, elephant dung 43, sheep dung 19, goat manure 12, pig manure 18, poultry manure 10, straw from maize 60, straw from rice 70, sawdust is above 200 [9, 13, 22]. LECO (TruMac) analyzer was used to determine the C/ N ratio [10].

TS and VFA affect the performance of the acetogens and methanogens. To monitor and control VFAs, different methods such as gas chromatography, liquid chromatography or titration, and back titration was developed, which are cost-effective, speedy, and simple to overcome the defects of traditional methods [9, 16]. TS and VFAs are measured by a TitraLab AT1000 Series Potentiometric Titrator, and analysis was carried out according to SM 2540 D and SM 2540 [10, 21].

The best Inoculum for kitchen waste (KW) will enhance methane yield. Healthy Inoculum collected affects the methane yield [23]. Hence it is necessary to concentrate on the Inoculum to substrate ratio [24]. Additions of active inoculums to biogas digesters that are preferable to low temperatures have an advantage for the AD process [13]. Combining different active inoculums with different proportions can reportedly improve biogas production [25]. To maintain uniformity of fluid in the digester and stability in the reactor, mixing/agitation is necessary. Mixing improves the AD process and biological process [13, 20, 26]. Agitator helps to avoid Scum formation and stratification in the anaerobic digester by combining the biomass with microorganisms [27]. Water Content-Activities of microorganisms get affected by water content in the AD process [13]. Research conducted by Demetriades reported that water content in the range of 60–95% is optimum in the biogas digester [28].

2.2 *Pretreatment Methods*

There are various pretreatment methods, such as Mechanical, Ultrasound, Thermal, Pressure-de-pressure, Chemical, etc. The particle size of 0.6 mm was considered optimum for maximum methane production. Still, the immoderate reduction of the particle size of less than 0.6 mm of the FW lowers methane production [9, 29]. With experimentation of the Ultrasonic pretreatment method on FW and Cardboard samples, the adequate time of ultrasonic pretreatment is 45 min for a ratio of 100:0 and 80:20, while for 60:40 and 50:50, the ultrasonic pretreatment time is 60 min. It is observed that ultrasound pretreatment enhances the biogas yield [25]. Mechanical pretreatment is completed using a Hollander beater to cut down large size particles of waste food into smaller size particles of waste food to enhance biogas production by increasing the expanse of feedstock. The result shows the pretreatment of waste food for 1800s beating time; the biogas yield is 610.3 ml/g TS at 39 °C,

Table 1 Experimental results of mechanical pretreatment

Experiment number	Beating time (sec)	Temperature (°C)	Biogas yield (ml/g TS)
1	0	35	114.2
2	900	35	365.5
3	1800	35	580.00
4	0	37	115.23
5	900	37	384.42
6	900	37	405.52
7	900	37	415.53
8	900	37	425.01
9	1800	37	590.80
10	0	39	125.21
11	900	39	440.23
12	1800	39	610.33

which is the maximum. It far determined that mechanical pretreatment enhances the biogas yield. The results of the experimentation are shown in Table 1 [30]. In alkali pretreatment, FW is pretreated with NaOH, KOH, and CaO used to degrade the complex organic matter, and it improves the solubilization of FW. It enhances the degradation process during AD, whereas adding 1% CaO to FW showed a better result of methane production as compared to NaOH and KOH [31]. Hydrothermal pretreatment (HTP) on co-digested FW and Sewage Sludge alters the physical structure of FW and sewage sludge, which in turn increases the soluble chemical oxygen demand, solubilization rate, and VFAs. The capillary suction time, time to filter, and decrease in particle size which is beneficial for fermentation. HTP temperature of 140° achieved an increase in biogas production by 50% [32]. Hybrid ultrasonic and alkaline (Na OH) pretreatments were applied on co-digested waste FW and Municipal sewage sludge. Production gets enhanced by 49% by hybrid pretreatment as compared to untreated waste [33]. Agricultural waste such as soybean waste, papaya skin, sugarcane bagasse, rice straw, and blue ginger was used, and they were finely chopped and ground into small particles less than 5 mm in size and mixed with Inoculum by mixing co w manure and distilled water in one: one ratio. As soybean residues contain 40% of total digestible nutrients and other components, it showed the highest biogas production rate [34].

2.3 Co-digestion Technique

In an AD system, varieties of organic wastes are processed with each other in a co-digestion technique. The necessity of the co-digestion technique is to stimulate the breakdown of organic matter, digestion time, and stabilization [35, 36]. Co-digestion

enhances biogas production, and factors that affect co-digestion are low pH, accumulation of volatile fatty acids (VFAs), i.e. controlled acidogenesis, and methanogenesis process is necessary to enhance the biogas production [5]. co-digestion of FW and wood chips showed an optimal increase in production yield by 640%. The favorable ratio of FW to wood chips is found to be 0.5. Properties such as moisture content, total solids, volatile solids, and density of FW and wood chips are summarized in Table 2 [37]. Co-digestion of chicken manure and straw in a ratio of three: three and chicken manure and goat manure in a ratio of four: two gives better results [10]. Also, experiments were conducted by processing FW with Low Fruit Vegetable and FW with High Fruit Vegetable waste. FW with High Fruit vegetables showed a stable performance in comparison with Low Fruit Vegetables due to ammonia inhibition and VFAs, which results in low biogas yield and an increase in solid removals [38]. Comparisons on biogas production from KW, from cattle manure (CM), and co-digested KW with CM at room temperature and co-digested KW with CM at 37 °C show the better result, which is summarized in Table 3 [39–41]. At Olive mill wastewater treatment plants, wastewater co-digested with dried FW, chees showed an increasing synergistic effect on methane production. Sewage Sludge with a 5% FCO (Olive mill waste water) mixture resulted in a 170% higher biogas production rate [42].

Hydrothermal pretreatment is effective on lignocellulosic waste biomass by destroying the effect on the lignocellulose structure and decreasing crystallinity in corn cob, which facilitates better co-digestion. When the FW and corn cob were mixed with anaerobic co-digestion at a Volatile Solid ratio of one: three at 150 °C achieved the maximum Cumulative Biogas yield of 4660 mL and the maximum specific methane yield of 316.91 mL/g [43]. As water hyacinth like yams, cassavas, plantains, and tubers which are easily available in Nigeria, contains indigestible recalcitrant complex molecules hence the co-digestion of water hyacinth with FW

Table 2 Properties of food waste and wood chips

Parameter	Food waste	Wood chips
Moisture content (wt %)	87.2	2.7
Total solids (wt %)	12.8	97.3
Volatile solids (wt %)	11.5	64.8
Density (g ml ⁻¹)	1.1	0.4

Table 3 Composition of biogas of different sample types with different proportions

Sample type	Proportion	CH ₄ (%)	H ₂ S (%)	CO ₂ %	Other%
KW and water	1:1	68.63	10.97	20.31	0.09
KW, water, and cow dung	4:5:1	71.08	7.59	21.32	0.01
KW, water, and slurry	5:4:1	74.52	7.70	17.66	0.12

decreases the biogas production [44]. Co-digestion of coconut copra and cow urine as co-substrate under the thermophilic condition at 45 °C improved the AD and increased the performance of the digester. Spent coconut obtained from coconut palm is highly degradable, and the addition of cow urine increases the waste's bioconversion faster [45]. Co-digestion of banana peels waste and cow manure where inoculum ratio was maintained at 2. Cow manure improved the AD process as expected due to the presence of active microorganisms required for biogas production [46]. In the domestic wastewater treatment plant, FW is co-digested in the ratio of 2% FW, and 98% domestic sewage sludge rich in organic matter was found appropriate. The current strategy maintained the pH range inside the digester [47]. An Experimentation was conducted on two different 1 m³ capacity anaerobic digesters for producing biogas from cow dung and kitchen waste in the ratio of one: one with water, and the results obtained turned into an average according per day gas yield of 0.35 m³ for cow dung and 0.20 m³ for the kitchen waste at a median substrate temperature of 32 °C and a pH of 6.5– 7.4 for the cow dung and 4.91–7.10 for the kitchen waste [48].

2.4 Addition of Different Additives/Trace Elements

The addition of different additives or trace elements favours the AD process. As the trace elements or additives in kitchen wastes are insufficient, their addition favours the process, which can enhance the biogas yield. The AD process is enhanced by the addition of metal-rich substrates or various metal elements as an additive to

Table 4 Overview of the addition of additives or trace elements

Author and year	Additives/ trace elements	Stimulation concentration	General function
Zhang et al. [9]	Sodium (N a)	350 mg/L	Enhances performance at the mesophilic condition
Zhang et al. [9]	Potassium (k)	> 400 mg/L	Enhances performance at both thermophilic and mesophilic conditions
Muratçobanoğlu et al. [21]	Graphite	1–1.5 g/L	It makes possible DIET among distinct microorganisms and enhances biogas production
Xiao et al. [49]	Granular Activated Carbon (GAC)	2.5×10^4 kg	Promotes the degradation of Organic matter, which accelerates the consumption of VFAs
Shamurad et al. [14] Liu et al. [50]	Cobalt(Co)	0.24–10 mg/L	Anaerobic digesters operating at high ammonia concentration activates to stable operation condition

the biomass; only the inhibition from sodium and potassium is avoided. Also, care should be taken to avoid inhibition caused due to high concentrations of light and heavy metal elements [9]. Synergistic effects are observed after graphite addition to FW, cow manure, and co-digested FW and cow manure. The production rate of methane increased by 28%, 67%, and 49.6% respectively [21]. Continuously stirred tank reactors of FW and co-digested wheat straw as co-substrate with or without trace elements enhance methane production. The addition of trace elements such as Co, Mo, Ni, Se, and W to the inoculated digestate fed in batch reactors of FW increased the methane by 45% to 65% [14]. The addition of iron as a trace element affects microbial metabolism; the deficiency of seven enzymes provided by eight microorganisms is fulfilled by adding iron as an additive. For enhancing methane production, these enzymes are necessary during the AD process [41]. In a dry anaerobic digester along with swine manure, granular activated carbon and assimilated sludge were employed, which increased the biogas rate by 10.6% [49]. During the AD process, the addition of different additives such as metal elements, carbon-based accelerants, biological additives, and alkali addition offered remarkable improvement in the AD process. Their dosage and different additives showed a remarkable influence on the improvement of the efficiency of biogas generation [11, 50] (Table 4).

3 Conclusions

The existing review makes evident that AD is one of the useful biological processes for the treatment of a different variety of biodegradable waste. AD is a multi-stage process; involving four degradation steps. For each degradation step, microorganisms are particular and thus could have different environmental requirements which help the AD process. Hence need to concentrate on the necessary parameters. Breaking down the particle size of organic waste increases biogas yield, which is attained using the proper pretreatment method. Inadequate nutrients in the waste inhibit the biogas yield. Co-digestion technique and the addition of trace elements assist in a stable AD process that enhances the biogas yield by reducing the H₂S and CO₂.

References

1. Rasapoor, M., Young, B., Brar, R., Sarmah, A., Zhuang, W. Q., & Baroutian, S. (2020). Recognizing the challenges of anaerobic digestion: Critical steps toward improving biogas generation. *Fuel*, 261, 116497.
2. Gupta, N., Yadav, K. K., & Kumar, V. (2015). A review on current status of municipal solid waste management in India. *Journal of Environmental Sciences*, 37, 206–217.
3. Kiran, E. U., Trzcinski, A. P., Ng, W. J., & Liu, Y. (2014). Bioconversion of food waste to energy: A review. *Fuel*, 134, 389–399.

4. Jenó, J. G. A., Viveka, R., Varjani, S., Nagappan, S., & Nakkeeran, E. (2021). Current trends and prospects of transforming food waste to biofuels in India. In *Waste biorefinery* (pp. 391–419). Elsevier.
5. Jeevahan, J., Anderson, A., Sriram, V., Durairaj, R. B., Britto Joseph, G., & Mageshwaran, G. (2021). Waste into energy conversion technologies and conversion of food wastes into the potential products: A review. *International Journal of Ambient Energy*, 42(9), 1083–1101.
6. Ajay, C. M., Mohan, S., & Dinesha, P. (2021). Decentralized energy from portable biogas digesters using domestic kitchen waste: A review. *Waste Management*, 125, 10–26.
7. Sinha, S., & Tripathi, P. (2021). Trends and challenges in valorisation of food waste in developing economies: A case study of India. *Case Studies in Chemical and Environmental Engineering*, 4, 100162.
8. Khalid, A., Arshad, M., Anjum, M., Mahmood, T., & Dawson, L. (2011). The anaerobic digestion of solid organic waste. *Waste Management*, 31(8), 1737–1744.
9. Zhang, C., Su, H., Baeyens, J., & Tan, T. (2014). Reviewing the anaerobic digestion of food waste for biogas production. *Renewable and Sustainable Energy Reviews*, 38, 383–392.
10. Bedoić, R., Špehar, A., Puljko, J., Čuček, L., Čosić, B., Pukšec, T., & Duić, N. (2020). Opportunities and challenges: Experimental and kinetic analysis of anaerobic co-digestion of food waste and rendering industry streams for biogas production. *Renewable and Sustainable Energy Reviews*, 130, 109951.
11. Vijayakumar, P., Ayyadurai, S., Arunachalam, K. D., Mishra, G., Chen, W. H., Juan, J. C., & Naqvi, S. R. (2022). Current technologies of biochemical conversion of food waste into biogas production: A review. *Fuel*, 323, 124321.
12. Kinyua, M. N., Rowse, L. E., & Ergas, S. J. (2016). Review of small-scale tubular anaerobic digesters treating livestock waste in the developing world. *Renewable and Sustainable Energy Reviews*, 58, 896–910.
13. Obileke, K., Nwokolo, N., Makaka, G., Mukumba, P., & Onyeaka, H. (2021). Anaerobic digestion: Technology for biogas production as a source of renewable energy—A review. *Energy and Environment*, 32(2), 191–225.
14. Shamurad, B., Sallis, P., Petropoulos, E., Tabraiz, S., Ospina, C., Leary, P., & Gray, N. (2020). Stable biogas production from single-stage anaerobic digestion of food waste. *Applied Energy*, 263, 114609.
15. Cheng, S., Li, Z., Mang, H. P., Huba, E. M., Gao, R., & Wang, X. (2014). Development and application of prefabricated biogas digesters in developing countries. *Renewable and Sustainable Energy Reviews*, 34, 387–400.
16. Zamanzadeh, M., Hagen, L. H., Svensson, K., Linjordet, R., & Horn, S. J. (2017). Biogas production from food waste via co-digestion and digestion-effects on performance and microbial ecology. *Scientific Reports*, 7(1), 1–12.
17. Rowse, L. E. (2011). *Design of small scale anaerobic digesters for application in rural developing countries*. University of South Florida.
18. Pramanik, S. K., Suja, F. B., Zain, S. M., & Pramanik, B. K. (2019). The anaerobic digestion process of biogas production from food waste: Prospects and constraints. *Bioresource Technology Reports*, 8, 100310.
19. Makamure, F., Mukumba, P., & Makaka, G. (2021). An analysis of bio-digester substrate heating methods: A review. *Renewable and Sustainable Energy Reviews*, 137, 110432.
20. Mirmohamadsadeghi, S., Karimi, K., Tabatabaei, M., & Aghbashlo, M. (2019). Biogas production from food wastes: A review on recent developments and future perspectives. *Bioresource Technology Reports*, 7, 100202.
21. Muratçobanoğlu, H., Gökçek, Ö. B., Mert, R. A., Zan, R., & Demirel, S. (2020). Simultaneous synergistic effects of graphite addition and co-digestion of food waste and cow manure: Biogas production and microbial community. *Bioresource Technology*, 309, 123365.
22. Dadaser-Celik, F., Azgin, S. T., & Yildiz, Y. S. (2016). Optimization of solid content, carbon/nitrogen ratio and food/inoculum ratio for biogas production from food waste. *Waste Management & Research*, 34(12), 1241–1248.

23. Miller, K. E., Grossman, E., Stuart, B. J., & Davis, S. C. (2020). Pilot-scale biogas production in a temperate climate using variable food waste. *Biomass and Bioenergy*, *138*, 105568.
24. Kong, X., Xu, S., Liu, J., Li, H., Zhao, K., & He, L. (2016). Enhancing anaerobic digestion of high-pressure extruded food waste by inoculum optimization. *Journal of environmental management*, *166*, 31–37.
25. Begum, S., Anupoju, G. R., & Eshtiaghi, N. (2021). Anaerobic co-digestion of food waste and cardboard in different mixing ratios: Impact of ultrasound pre-treatment on soluble organic matter and biogas generation potential at varying food to inoculum ratios. *Biochemical Engineering Journal*, *166*, 107853.
26. Abbasi, T., Tauseef, S. M., & Abbasi, S. A. (2012). Biogas capture from solid waste. In *Biogas energy* (pp. 105–143). Springer.
27. Kumar, A., & Ramanathan, A. (2021). Design of an agitator in the anaerobic digester for mixing of biomass slurry. *Materials Today: Proceedings*, *46*, 9678–9682.
28. Demetriades, P. (2009). Thermal pre-treatment of cellulose rich biomass for biogas production.
29. Montgomery, L. F., & Bochmann, G. (2014). *Pretreatment of feedstock for enhanced biogas production* (pp. 1–20). IEA Bioenergy.
30. Sawyerr, N., Trois, C., Workneh, T. S., Oyebode, O., & Babatunde, O. M. (2020). Design of a household biogas digester using co-digested cassava, vegetable and fruit waste. *Energy Reports*, *6*, 1476–1482.
31. Linyi, C., Yujie, Q., Buqing, C., Chenglong, W., Shaohong, Z., Renglu, C., & Zhiju, L. (2020). Enhancing degradation and biogas production during anaerobic digestion of food waste using alkali pretreatment. *Environmental Research*, *188*, 109743.
32. Park, S., Han, S. K., Song, E., Kim, H., Kim, M., & Lee, W. (2020). Effect of hydrothermal pre-treatment on physical properties and co-digestion from food waste and sewage sludge mixture. *Waste Management and Research*, *38*(5), 546–553.
33. Akbay, H. E. G., Dizge, N., & Kumbur, H. (2021). Enhancing biogas production of anaerobic co-digestion of industrial waste and municipal sewage sludge with mechanical, chemical, thermal, and hybrid pretreatment. *Bioresource Technology*, *340*, 125688.
34. Onthong, U., & Juntarachat, N. (2017). Evaluation of biogas production potential from raw and processed agricultural wastes. *Energy Procedia*, *138*, 205–210.
35. Shin, S. G., Han, G., Lee, J., Cho, K., Jeon, E. J., Lee, C., & Hwang, S. (2015). Characterization of food waste-recycling wastewater as biogas feedstock. *Bioresource Technology*, *196*, 200–208.
36. Okwu, M. O., Samuel, O. D., Otanocha, O. B., Balogun, P. P., Tega, O. J., & Ojo, E. (2020). Design and development of a bio-digester for production of biogas from dual waste. *World Journal of Engineering*.
37. Oh, J. I., Lee, J., Lin, K. Y. A., Kwon, E. E., & Fai Tsang, Y. (2018). Biogas production from food waste via anaerobic digestion with wood chips. *Energy and Environment*, *29*(8), 1365–1372.
38. Ghanimeh, S., Abou Khalil, C., & Ibrahim, E. (2018). Anaerobic digestion of food waste with aerobic post-treatment: Effect of fruit and vegetable content. *Waste Management and Research*, *36*(10), 965–974.
39. Iqbal, S. A., Rahaman, S., Rahman, M., & Yousuf, A. (2014). Anaerobic digestion of kitchen waste to produce biogas. *Procedia Engineering*, *90*, 657–662.
40. Das, A. K., & Panda, A. K. (2020). Effective utilisation of kitchen waste to biogas by anaerobic co-digestion. In *Recent developments in waste management* (pp. 1–10). Springer.
41. Dhungana, S., Adhikari, B., Shrestha, S. D., & Shrestha, B. P. (2019). Enhanced biogas production from fecal sludge by iron metal supplementation: Iron enriched fertiliser as a byproduct. In *IOP Conference Series: Earth and Environmental Science* (Vol. 301, No. 1, p. 012028). IOP Publishing.
42. Maragkaki, A. E., Vasileiadis, I., Fountoulakis, M., Kyriakou, A., Lasaridi, K., & Manios, T. (2018). Improving biogas production from anaerobic co-digestion of sewage sludge with a thermal dried mixture of food waste, cheese whey and olive mill wastewater. *Waste Management*, *71*, 644–651.

43. Gao, M., Zou, H., Tian, W., Shi, D., Chai, H., Gu, L., & Tang, W. Z. (2021). Co-digestive performance of food waste and hydrothermal pretreated corn cob. *Science of The Total Environment*, 768, 144448.
44. Longjan, G. G., & Dehouche, Z. (2020). Biogas production potential of co-digested food waste and water hyacinth common to the Niger Delta. *Biofuels*, 11(3), 277–287.
45. Ndubuisi-Nnaji, U. U., Ofon, U. A., & Offiong, N. A. O. (2021). Anaerobic co-digestion of spent coconut copra with cow urine for enhanced biogas production. *Waste Management and Research*, 39(4), 594–600.
46. Achinas, S., Krooneman, J., & Euverink, G. J. W. (2019). Enhanced biogas production from the anaerobic batch treatment of banana peels. *Engineering*, 5(5), 970–978.
47. Thakur, H., Dhar, A., & Powar, S. (2022). Biogas production from anaerobic co-digestion of sewage sludge and food waste in continuously stirred tank reactor. *Results in Engineering*, 16, 100617.
48. Glivin, G., Mariappan, V., Premalatha, M., Krishnan, H. H., & Sekhar, S. J. (2022). Comparative study of biogas production with cow dung and kitchen waste in Fiber - Reinforced Plastic (FRP) biodigesters. *Materials Today: Proceedings*, 52, 2264–2267.
49. Xiao, Y., Yang, H., Yang, H., Wang, H., Zheng, D., Liu, Y., & Deng, L. (2019). Improved biogas production of dry anaerobic digestion of swine manure. *Bioresource technology*, 294, 122188.
50. Liu, M., Wei, Y., & Leng, X. (2021). Improving biogas production using additives in anaerobic digestion: A review. *Journal of Cleaner Production*, 297, 126666.

Survey on Trends in LPG Utilization Among Selected Rural Households in Western Maharashtra, India



Swapnil S. Shinde, Kailasnath B. Sutar, Dnyaneshwar G. Kumbhar, and Sandipraj Y. Salunkhe

Abstract According to data from Ministry of Petroleum and Natural Gas, as on 1st July, 2021, there are about 29.11 crore LPG consumers. 99.5% households in India use LPG now for domestic cooking purpose. Net consumption of the gas of our country is about 145 million standard cubic meters every day. As on 5th March, 2022, cost of a 14.2 kg cylinder is Rs. 902.0 in Maharashtra. The cost of LPG has increased by 220% from March 2014 (Rs. 410.0) to March 2022 (Rs. 902.0). This trend shows that the cost of LPG is going to increase day by day. To control the expenses on LPG, individual LPG user needs to use it efficiently. A survey of 507 LPG using households was conducted in 10 villages of Western Maharashtra, India to know the trends of LPG utilization and to know awareness of people about conservation of LPG. The results of survey shown that family size of about 45% households was 4 members. The duration of refill of LPG cylinders was about 30 to 40 days in 47% households. In most of the households, smaller burner of LPG stove was used for performing common cooking cycles such as making of tea and boiling of milk. Most of the households prefer pre-soaking of dal and rice prior to cooking. About 78% of the households still use biomass cookstoves for cooking purpose in addition to LPG stoves. Only 20% of the LPG using households were found to be the beneficiaries of the Pradhan Mantri Ujjwala Yojana which was launched by Prime Minister of India Mr. Narendra Modiji on 1st May 2016 to distribute LPG connections to women of Below Poverty Line (BPL) families.

Keywords LPG cylinder · Efficiency · Burner · Household · BPL

S. S. Shinde (✉) · K. B. Sutar · D. G. Kumbhar
Bharati Vidyapeeth (Deemed to Be University) College of Engineering, Pune, India
e-mail: swapnil9510@gmail.com

K. B. Sutar
e-mail: kbsutar@bvucoep.edu.in

D. G. Kumbhar
e-mail: dgkumbhar@bvucoep.edu.in

S. Y. Salunkhe
SVERI's College of Engineering, Pandharpur, India
e-mail: sysalunkhe@coe.sveri.ac.in

1 Introduction

While 97% of Indian households have access to cleaner cooking fuel in the form of LPG, its exclusive use for cooking needs continue to remain low in rural areas. A key factor underlying low usage of LPG among economically poor households is the high recurring cost of the fuel. The Pradhan Mantri Ujjwala Yojana (PMUY) was started by the Centre in 2016 to provide clean cooking fuel to poor households. Its target to provide 8 crore deposit- free LPG connections had already been achieved in September, 2019. Liquefied Petroleum Gas (LPG) is increasing their popularity as a day by day. As on April 2016, there were total 16.62 crore LPG customers in the country which has increased to 29.11 crore as on July 2021. This research seeks to assess LPG utilization in western Maharashtra.

2 Survey Background

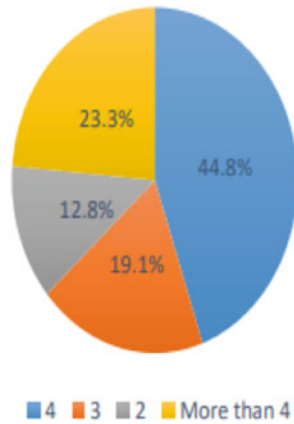
Surveys are useful in describing the characteristics of a large population. No other research method can provide this broad capability, which ensures a more accurate sample to gather targeted results in which to draw conclusions and make important decisions. Surveys can be administered in many modes, including: online surveys, email surveys, social media surveys, paper surveys, mobile surveys, telephone surveys, and face-to-face interview surveys. For remote or hard-to-reach respondents, using a mixed mode of survey research may be necessary (e.g. administer both online surveys and paper surveys to collect responses and compile survey results into one data set, ready for analysis). Different households in a specific region give us different trends of LPG consumption. LPG utilization trends are different in different regions of India. For LPG utilization trends we have conducted survey in LPG using households. The main purpose of this survey is to know the LPG utilization trends in WESTERN MAHARASHTRA region. For this survey we have prepared some questionnaires. These questionnaires are helpful in analyzing different trends of LPG in different households. We have distributed these questionnaires among the different households.

2.1 Survey Questionnaires

The questions for the survey were prepared in such a way that the information on family size, LPG consumption period, use of pressure cooker, presoaking of rice, frequency of servicing of gas stove, devices used other than LPG stove type of burner, pot sizes for boiling of milk, making of rice and making of tea, quantity of milk, consumer is beneficiary of UJJWALA YOJNA etc. can be known.

Fig. 1 Member in surveyed family

Member in Surveyed Family



3 Survey Results for Family Size and LPG Consumption

3.1 Family Size and Number of Families

After surveying Five Hundred Seven families we have obtained different results which are useful for our further research work. There are two hundred twenty-seven families having family size four and ninety-six families having family size three. Also, there are one hundred eighteen having more than four and sixty-four families having two family size respectively. In the further study we have also come know that there are few families having family size one and six respectively. So, we have concentrated our further study on the family size four. From this result we have concluded that as compared to other there are maximum numbers of families having family size four (Fig. 1).

3.2 LPG Consumption Variation for Same Family Size

After surveying several households, we are retrieved some results which are useful in our further work. This graph is about number of families for four members and LPG consumption days. In this pie diagram we can see LPG consumption days for the same family size. There are One Hundred Forty four families which consumes there LPG within thirty five days and Forty One families within twenty five days. From the above plot we can conclude that though there is a same family size (4) but the LPG consumption days are different. Though the family size is same the cooking

No. of families same size & LPG consumption days.

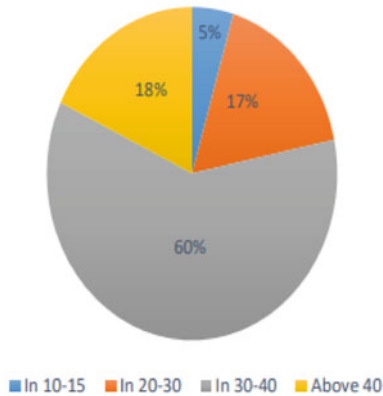


Fig. 2 Same family size and LPG consumption days. *Source* Survey form

practices in different households are different. That's why the LPG consumption days are different for the same family size (Fig. 2).

3.3 Rice Making Using Pressure Cooker

It is well known that huge research is done by leading home appliances manufacturers on development of pressure cooker. This reflects in Fig. 3 independent of manufacturers of the pressure cooker. This reflects in Fig. 3 independent of manufacturers of the pressure cooker, their capacities etc. the H/D ratios for all of them were in between 1.21 and 1.50.

3.4 Boiling of Milk (Milk Pots)

As stated earlier pot manufacturer enjoy lot of freedom in manufacturing of normal pots due to which, for boiling of milk two ranges of H/D ratio were prominently observed viz. 0.2–1 that is the H/D ratio for the milk pots in most of the households from 0.2 to 1 (Fig. 4).

RATIO OF PRESSURE COOKERS & NUMBER OF FAMILIES FOR FOUR MEMBERS

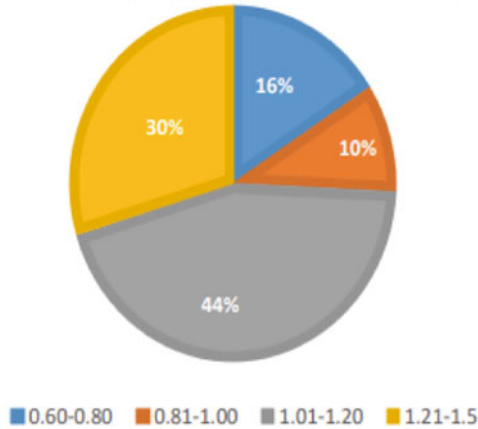
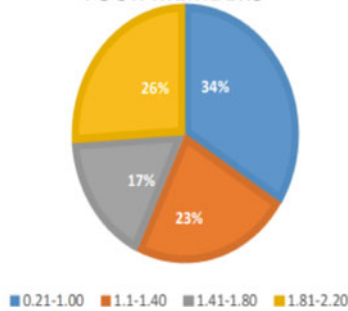


Fig. 3 Shows plot of H/D ratio of pressure cookers and number of families with four members

Fig. 4 Shows plot of H/D ratio of milk pots and number of families with four members

RATIO OF MILK POTS VS. NUMBER OF FAMILIES FOR FOUR MEMBERS



4 Limitations of Improved Wood Burning Stove

Today, one-third of the world’s population still relies on solid fuels, whose combustion in turn is the leading cause of death for children under the age of 5 and the greatest global environmental health threat. As a result, there has been much attention drawn towards finding a solution to lower exposure to HAP term the two central choices making the available clean and making the clean available. Determining the best path has not been straightforward. Until recently, most interventions have focused on the adoption and sustained use of improved wood-burning cookstoves—making stoves that burn the widely available, free-of-cost wood fuels in such a way that it reduces exposure to HAP. However, considering a focus on health, improved

cookstoves have not demonstrated sufficient reductions in personal exposure to air pollution.

5 Adoption and Use of Clean Cooking Fuel

Since solid fuel use and HAP exposure affects one-third of the world's population, there are significant demands for widespread and scalable solutions. While improved cookstoves, despite still burning solid fuels, have offered benefits and do reduce HAP under certain circumstances and will likely continue to improve, it is becoming increasingly clear that clean fuels are required to bring HAP levels below the WHO standard for air pollution in the long term. While there are a number of clean fuels—gas (LPG, biogas), electricity (coil, induction, solar), and ethanol—LPG is widely used around the world and regularly the first clean fuel to reach rural communities, making it the most poised to deliver substantial health, economic, and social benefits by lowering HAP around the world. In addition, LPG faces some specific barriers to adoption and sustained use: Cost, Availability, Heating Safety concern.

5.1 Clean Cooking Fuel in India

Although LPG has had a presence in India since 1950, From 2009 to 2012, the Rajiv Gandhi Gramin LPG Vitaran Yojana (RGGLVY) provided 1.5 million new LPG connections to rural areas. Since 2015, the Government of India, along with three large oil companies, has begun three major programs to promote LPG to poor and rural households: (i) Pahal moves fuel subsidies directly to individuals' bank accounts, to reduce illicit use of subsidized LPG outside the non-household sector; (ii) Give it Up enables middle class households to transfer their subsidies to poor households; and (iii) Pradhan Mantri Ujjwala Yojana (Ujjwala) will provide free connections to 80 million poor households by 2019). Already 10 million households have participated in "Give it Up" and 20 million households have received a free connection through Ujjwala. there is demand for this type of analysis in the literature and beyond as India and other countries heavily invest in promoting LPG cooking. [1].

6 Data and Method

6.1 Clean Cooking Fuel in India

Conducted in 2014–2015, ACCESS is the largest survey of energy access to this date. It covers the energy access patterns of 8,568 households in 714 villages across six energy-poor, contiguous states of Maharashtra. The survey was conducted in the local language, which is Marathi. The 45-min survey instrument contains information on lighting fuels, electricity use, and cooking arrangements. We use data from the modules on cooking. The survey contains sampling weights that we use to obtain descriptive statistics that are representative at the population level.

6.2 Adoption Variable

We asked non-adopting households, “why don’t you have LPG?” Responses were coded into four options, mirroring much of the central factors limiting clean fuel adoption in the literature: (i) “Is it not available or too far from your village?”, (ii) “Is it too expensive to install an LPG connection?”, (iii) “Is the monthly expense of LPG too expensive?”, and (iv) “Do you not know how to get an LPG stove or whom to ask?” We support this analysis by describing two central barriers to LPG use: (i) cost: the cost of LPG cylinders (small and large cylinders from the market and authorized distributors) and (ii) access: self-reported one-way distance to acquire LPG cylinders. In addition, we show when the connection was made (years with LPG) in the study sample.

7 Result and Discussion

This cross-sectional survey of households in rural and peri-urban communities of Maharashtra has identified current cooking fuel use practices and associated factors in a region with a relatively well-established LPG market, lower levels of poverty and national picture. The proportion of households using LPG as a primary cooking fuel is well below the national target set by the Maharashtra government (58% by 2030). In addition, the problem of fuel stacking is clear with less than 10% of LPG using households in urban areas reporting they do so exclusively (only 1% of rural households). Household-level factors identified to be associated with adoption and sustained/exclusive use of LPG, including household wealth and level of education, have been well documented as both important potential barriers (lower levels) and enablers (higher levels) in using cleaner fuels and technologies. However, to develop programs and policies to support their scaled transition, switching from polluting traditional fuels, it is necessary to consider factors across the whole LPG ecosystem.

With assistance from the Global LPG Partnership, the Maharashtra government launched an LPG Masterplan in 2025 to help achieve its stated aspirational LPG adoption goal.

8 Conclusion

LPG has carved out a dignified position in India's energy ecosystem. It is racing on fast lane in the direction of green energy and clean environment. The momentum of last three years will certainly continue for next two years, when there will be a need for consolidation. However, there are challenges to overcome in the short and medium term. Strengthening the infrastructure along the supply chain is a stupendous job. Keeping the supply chain clicking all the time requires a demanding managerial attention. Sound operating practice and inbuilt safety culture, which has been the hallmark of OMCs so far, needs to be passed on through generations. Rising up to customer's expectation of prompt delivery, refined service, customer feedback redressal and emergency preparedness are going to be mammoth tasks to be delivered through LPG Distributors' network. One can perhaps be justified in saying, it is time, Indian LPG expertise looks across the shore.

References

1. Dickinson, L., Kanyomse, E., Aliriga, R., Hagar, Y., Rivera, I., et al. (2016). Assessment of cookstove stacking in Northern Ghana using surveys and stove use monitors. *Energy for Sustainable Development*, 34, 67–76. <https://doi.org/10.1016/j.esd.2016.07.007>. [CrossRef][Google Scholar]

IOT-Based Monitoring and Control System for Greenhouses



Ranjana Khandebharad, Shraddha Garad, Ashutosh Garad, Shreya Moholkar, and Dhanraj Daphale

Abstract This endeavor's major objective is to employ modern technology to improve current farming practices in order to boost productivity. This work's notion of a smart greenhouse enables farmers to run farm operations automatically with minimal manual inspection. A greenhouse protects plants from dangerous weather conditions like wind, hail, UV radiation, and insect and pest infestations because it is a closed building. Automatic drip inundation is used to water agricultural areas, and it works depending on the dampness of the soil and irrigating equitable proportion of water. By using drip inundation ways depends upon the soil examine review, the equitable quantity of N₂, P₄, K, along with this supplementary veined to be given to soil. To compute the ongoing proportion of water supersonic inaudible detector is used. To growth of plants need to dispense right wavelength of light as well as growing lights are utilized at night. Climate as well as water vapor in air is supervised using water vapor and degrees detectors as well as an obscuring.

Keywords Greenhouses · Temperature control · Fuzzy controllers · IOT

1 Introduction

In recent trends United Nations envisions that foodstuff proffering need to rises by 60% due to supplying feeds to spreading community, which is predicted to cross 9 billion communities in 2050. There were 7 billion people on the earth between 1800 and 2012. At the wrap up of centurial the community is predicted outstretched to 11 billion communities. Due to growing composting and energy costs as well as irrigation bans, agriculturist is in pressure to avail their assets more efficiently. To

R. Khandebharad (✉) · S. Garad · S. Moholkar · D. Daphale
Department of Electrical Engineering, SVERI's College of Engineering, Pandharpur, Pandharpur, Maharashtra, India
e-mail: mkhandebharad@cod.sveri.ac.in

A. Garad
Department of Electronics and Telecommunication, SVERI's College of Engineering, Pandharpur, Pandharpur, Maharashtra, India

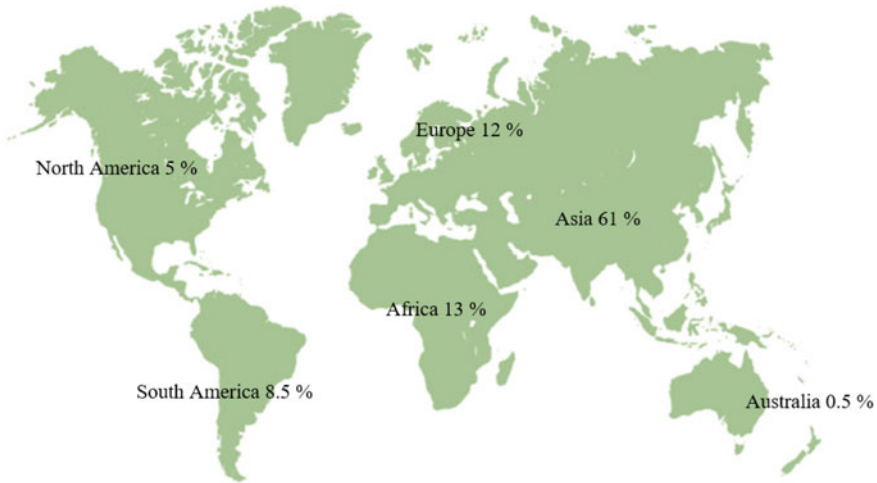


Fig. 1 Agriculture's percentage of the population

lessen food loss and spoilage, preferable ward surveillance is mandatory. Community with shortage of awareness as well as provocation occurred due to space need to contend with time restraints. Now a day's tremendous growth in agriculture sectors with the help of automation that is GPS guided harvesters. It is a sector that lacks access to data. Depending on changes in market pricing or rainfall, profits might rise or fall rapidly. Historically, it has been challenging to find up-to-date, accurate data about operations. Tomatoes cannot be mass produced in the same way as cars or microprocessors. Businesses like Clean Glow and Slum have begun to integrate big data to the actual environment through the development of devices that can dynamically calibrate moisture and other variables. Due to campaigns to eat more food grown locally, a younger generation of farmers, and less expensive component, agriculture is experiencing a flood of data and technology. As the concept of the "Internet of Things" gains more and more traction, numerous technologies are being created to make it possible to collect, analyze, and control devices across wireless data networks. The world of agriculture offers a significant opportunity for the Internet of Things. While connected devices like smart lights and thermostats are becoming more common in homes, there may be additional applications for them (Fig. 1).

2 Literature Survey

Only one-third of India's entire agricultural area is interconnected with an irrigation canal system, despite the country having multiple large river systems and receiving a lot of precipitation. The monsoon or tube wells are primarily responsible for the remaining percent. Locations where there is an excess of water, [1]. Water logging

and excessive irrigation have caused a problem with land sanity. In addition, surface water kills beneficial microbes by blocking soil pores [2]. Due to traditional irrigation methods like sprinklers or situations where water is simply allowed to irrigate the field directly from water drainage lines, the demand for water frequently exceeds the supply. Consequently, regions with scarce water resources are unable to irrigate throughout the growth season. The following are the effects of irregular and excessive irrigation on soil.

- Enhances sediment
- Tabulating of water
- Obstruction in plant roots through air
- A decrease in soil degrees
- The land turns swampy
- Increased soil nitrate formation
- PH of the soil.

Consequently, the foundation of the issue is the abuse of water [3]. Our drip irrigation method utilizes water most effectively. By directing water to plant roots, this irrigation method utilizes less water. Before it can be utilized to irrigate fields, all water from canals, tube wells, rainwater gathering systems, and other sources must first be stored in an underground tank. A tank-integrated ultrasonic sensor continuously checks the water level and sends the user an SMS message any time the level falls below the preset limit [4]. Leaf growth, pollination rates, photosynthesis, and crop yield are all impacted by relative humidity (RH). The delicate sepals may dry up quickly due to prolonged dryness or high temperatures, which could result in the flower dying before it reaches maturity. It is crucial to regulate the temperature and humidity of the air. Within the smart greenhouse, we attach sensors to measure temperature and humidity. When the degrees reach a peak point then microprocessor will activate an automatic switch linked with fogger, which will scatter microscopic water droplets that throws in an air likes fogs and will maintain the climates. If the dampness of airdropped in the predetermined level, a same process will engage, and the minute water plop will keep the relational dampness constant.

3 Methodology and Implementation

3.1 Schematic Diagram

Figure 2 displays the fundamental block diagram of the greenhouse system. The greenhouse-style setup has four sensors. The input for the microcontroller system is provided by these sensors. The input feed provided to the microcontroller is analogue data. This data is converted into a digital representation by the controller. Both the Android phone and the LCD display transmit the data over Bluetooth for display.

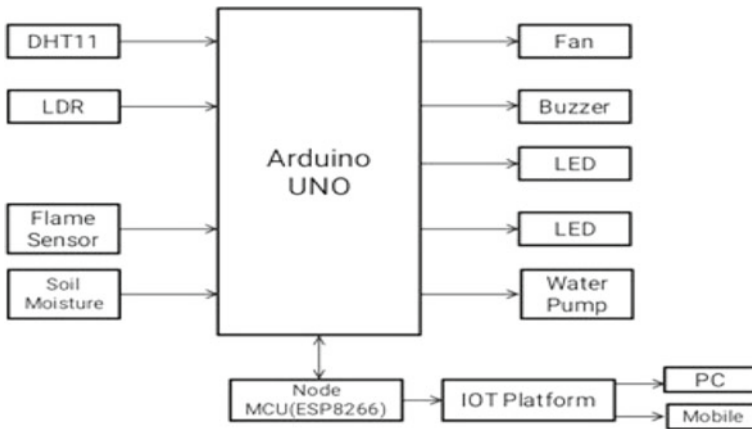


Fig. 2 Block diagram proposed methodology

As a result, characteristics like temperature, moisture, and others are automatically tracked. Once the parameter values have been tracked by the embedded system, which is developed using code, they can be changed. This is an automated control mechanism. The Android phone is controlled by the user.

The followed methodology is

- The owner is kept constantly informed by the IOT greenhouse monitoring system using a phone or PC base system.
- This microcontroller-based circuit continuously logs the degrees, stuffiness, soil dampness, and sunshine values of the spontaneous circumstances in order to optimize them for the greatest possible plant growth and yield.
- The system continuously tracks the various sensors' digital parameters. Sensing changes inside a greenhouse that may affect the rate of plant growth is a necessary step in monitoring and maintaining the environment there.
- The temperature inside the greenhouse, which has an impact on the transpiration and photosynthetic processes, humidity, soil moisture content, illumination, and other factors are crucial.

4 Components

4.1 *Arduino UNO*

Open-source The Arduino gadget depends on simple rigging and preparation. Before turning on a motor that triggers an LED that is visible to everyone on the Internet, an Arduino sheet will analyze inputs from a light sensor, finger capture, or twitter message. Various commands can be sent to the microcontroller to track the board. To

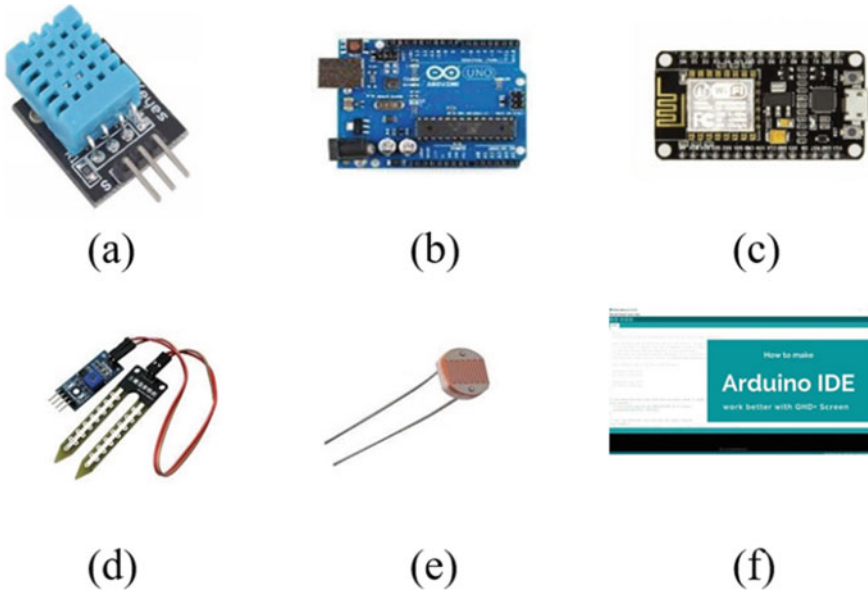


Fig. 3 a DHT11. b Arduino UNO. c Nod MCU(ESP8266). d Soil moisture sensor. e LDR sensor. f Arduino IDE

accomplish your objectives, you make advantage of the Arduino’s apps and programming language (IDE). Arduino controlled a variety of operations employing both conventional and sophisticated and logical instruments. It contains a power jack, an ICSP header, a 16 MHz crystal oscillator, 6 input analogue pins, and 14 input or output optical pins. The operating voltage is 5 V, and the recommended input voltage range is 7–12 V, according to Fig. 3b).

4.2 Light Dependent Resistor Sensor

The frequency of the sun is determined by the LDR sensor module. Both the digital output pin and the analogue output pin are accessible. As light intensity rises, the LDR’s resistance falls. Figure 6 shows that LDR resistance rises as light intensity decreases. A potentiometer button on the sensor allows the user to adjust the LDR sensitivity. The strength of a typical LDR is as follows: Nighttime: 20,000,000, daytime: 5000.

4.3 Soil Moisture Sensor

The two copper leads are what make up the sensor probes. They are buried into the soil sample while the moisture content is being measured. The soil's conductivity is determined by how much moisture is present. It expands when the soil's moisture content rises, forming a narrow path between two sensor probes that permits electricity to pass through.

4.4 Node MCU

Node MCU is an open source Internet of Things framework. It produces firmware for ESP-12 compatible devices including Expressive Systems' ESP8266 Wi-Fi SOC. The often used technique define "Node MCU" as firmware as opposed to changes. The firmware makes use of the Lua script. Utilizing Fig. 3's Expressive Non-OS SDK for ESP8266, it was created and built.

5 Result and Discussion

Each greenhouse parameter's sensing component is monitored using the appropriate sensors. The sensed data is entered into the database using the Thing Speak programmed, and a comparison of the parameters based on the sensor data is also carried out.

Mobile alerts are occasionally sent to the parties concerned to keep them updated on the state of the greenhouse environment. When environmental factors from the sensor exceed the threshold, the Greenhouse Monitoring System senses, monitors, and stabilizes the situation.

Actuators are used to control the parameters based on sensor input. There are automated and manual options offered. The user controls the actuators in the manual mode, which is not utilized in our project, depending on inputs received by SMS. Automatic actuator operation is performed using a database of the previous event.

The images from the agricultural surveillance in Thing Speak (Figs. 4, 5 and 6).

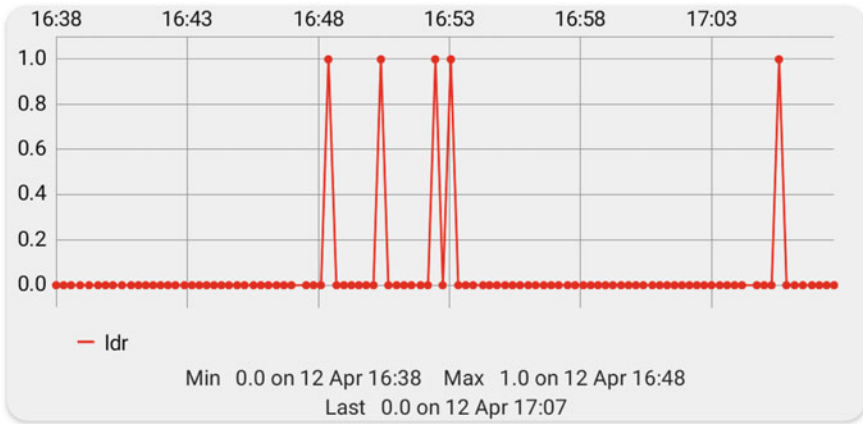


Fig. 4 Temperature and humidity information

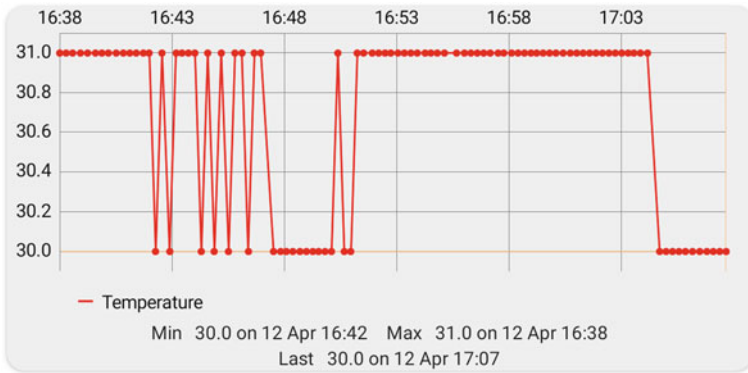


Fig. 5 Agriculture monitoring results-1

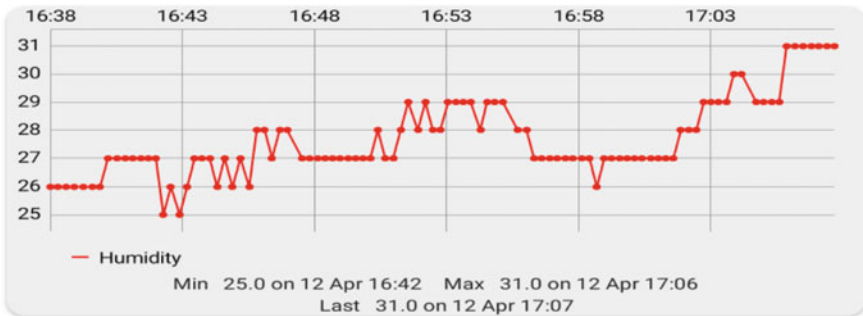


Fig. 6 Agriculture monitoring results-2

6 Conclusion

The benefits of Smart Greenhouse as compared to conventional cultivation are that we are able to produce crops without the use of pesticides and insecticides and create an environment that promoted healthy plant growth. Even the sale of tube well water is one of the alternative agricultural income sources that Smart Greenhouse provides. Furthermore, someone may use this kind of methods instead of rooftop shed net, we can grow any kind of crops because of sustaining any kind weather conditions. For a result orientation we enlarge the tropical plants like sorrel. As per need we provide seventy to eighty percent of water. There is a tremendous improvement in yield with biotic artifact using IoTs it is possible to connect the farmer with end customers. There are many methods to enhance the intelligent greenhouse and apply it in different agricultural applications. It may be used to grow any kind of plant in any setting and under any combination of circumstances. The Pettier effect is used to cool the independent greenhouse apparatus, which is fueled by unconventional vivacity provenance like solar and wind turbines. Without employing soil, it is still possible to cultivate and boost the nutritional value. The efficiency and profitability of farming can be dramatically increased by integrating IoT. Smart Greenhouse, which would transform Indian agriculture, has a promising future in the agricultural industry.

References

1. Kangralka, M. S., Nadaf, M. A., Jinabade, M. S., & Kudale, C. *Design and development of IoT based low-cost greenhouse monitoring system.*
2. Khandelwal, S. A. (2012). Automated green house management using GMS modem. *International Journal of Computer Science and Information Technologies*, 3(1), 3099–3102.
3. Sahu, K., & MazumdarS, G. (2012). Digitally greenhouse monitoring and controlling of system based on embedded system. *International Journal of Scientific and Engineering Research*, 3(1), 41–48.
4. Naseri, R. A. S. (2019). *Design and implementation intelligent greenhouse system with less power consumption* (Master's thesis, Altunbaş Universities).

Agri Tourism—A Means for Doubling Farmer’s Income—A Literature Review



Pratibha Galande and Abhijit Mancharkar

Abstract Agri tourism has incredible potential for inspiring the development of a vibrant, varied rural economy. In many advanced countries, Agri tourism has developed as an important part of the tourism industry. Agri tourism started to develop significantly in India and specifically in Maharashtra mostly due to its favorable climatic conditions if we consider the last decade’s scenario. It is being pursued as allied agriculture activities that enable farmers to harness the optimal profit of the multi-functional nature of agriculture. This tendency also offered rise to more demand for visitor accommodations and created tremendous opportunities for home-stays. The main objective is to discuss and provides a broad overview of Agri tourism. This paper has as its purpose to highlight the Benefits of Agri tourism for Increasing Rural Financial status, Tradition, Education, and Viable Agriculture practices. The sub-purpose is to know the major challenges related to Agri tourism growth.

Keywords Agri tourism · Allied agriculture activities · Farm income · Rural economy · Viable agriculture practices

1 Introduction of the Study

Ideas of presenting Agri tourism as a tourism activity on agricultural fields and farms started roughly two decades ago as an effect of the growing demand for tourism that costs not as much but could give tourists a satisfying experience with nature. Since that time, agri-tourism has become one of the fastest-growing tourism models worldwide. The concept of Agri tourism starts from various activities carried out on the working agricultural farms for pleasure, education, and natural and cultural heritage. Agri-tourism’s primary goal is to preserve the environment, history, and

P. Galande (✉)
Savitribai Phule Pune University (SPPU), Pune, India
e-mail: pratibha.galande@gmail.com

A. Mancharkar
AISSM’s, Institute of Management, Kennedy Road, Pune, India
e-mail: abhijitmancharkar@aissmsiom.org

© The Author(s), under exclusive license to Springer Nature Switzerland AG 2024
P. M. Pawar et al. (eds.), *Techno-societal 2022*,
https://doi.org/10.1007/978-3-031-34644-6_26

233

culture of rural areas, where it originally gained attractiveness while ensuring viable agriculture expansion.

The progress of Agri tourism in rural agricultural communities is mainly aimed at growing the monetary gains of the farmers. Agri tourism is a great educational means because it helps tourists to learn together the traditional agriculture, production of agricultural commodities, and cultural heritage of the rural area through direct involvement. India is known as the “Land of villages”. The majority of the population of India still rests on agriculture and its allied activities hence agriculture is not a mere business, but is still the “True Culture of India”. Agri tourism is an activity that interlinks the social, economic, and environmental components of sustainability, strongly related to local groups and their attitudes towards tourism, so one of the solutions for rural areas can undeniably be Agri tourism. Agri tourism’s impact on farmers’ living standards is major in terms of profit, so the rural areas where Agri tourism will be adopted will become the places where all components of local viable growth will be gathered.

2 Objectives of the Study

The purpose of the study was to systematically evaluate existing empirical data and theoretical literature on agri-tourism by considering the following objectives: -

1. To discuss and provide a broad overview of Agri tourism.
2. To highlight the benefits of Agri tourism for increasing rural financial status, tradition, education, and viable agriculture practices.
3. To know the major challenges related to Agri tourism growth.

3 The Analysis and Summary of the Review of the Literature

The researcher has reviewed district, state, national and international level research papers written by foreign and Indian authors related to Agri tourism centers. The following Table 1 indicates the paper inclusion criteria selected by the researcher.

“Assessment of Agro-Tourism Potential in Junnar Tehsil, Maharashtra, India”, Researchers found various potential zones Agro –tourism in Junner tehsil. The local folk art or different cultural forms will also prove helpful for developing agro-tourism centers. For e.g. Tamasha is a traditional folk dance of Maharashtra and Narayan-gaon is one of the famous centers for this art [1]. “Agro-tourism: An Alternative for Development of Agricultural Farmers in Kolhapur District (M.S.)” The focus of the research study was on developmental challenges in the Kolhapur district. Kolhapur district has the potential to establish enterprises of Agro-tourism on a large scale [2]. “A Study on Development of Agriculture Tourism Business in Baramati

Table 1 Paper inclusion criteria

Parameters	Inclusion criteria
Keywords/ phrases	Includes keywords agritourism, allied agriculture activities, farm incomes, rural economy, Viable Agriculture practices
Language	English
Publication year	2008–2020
Types of papers	Papers published in peer-reviewed journals and conference proceedings
Paper’s topics	Papers on agritourism, agriculture, and tourism
Written criteria	Written in clarity, sound data collection procedures as well as scholarly discussions and conclusions
Methodologies	Qualitative method, quantitative method, and mixed methods

District (Maharashtra).” This research helps to understand the chances for the development of agricultural tourism in the Baramati District and the domestic profile of the farming community. Researchers recommended that farmers must be educated in managing business, interpersonal, and communication skills to manage their business [3]. “Agro-Tourism: A Sustainable Tourism Development in Maharashtra—A Case Study of Village Inn Agro Tourism (Wardha)”. The development of agro-tourism in the village has encouraged other farmers to start the project. Employment generation for local people is seen and skill development is enhanced at the local level [4].

“Agro tourism: a sustainable development for rural Areas of India; with special reference to Maharashtra”. Attention was given to the importance of agro-tourism development in Maharashtra. Maharashtra has a high potential for the development of agro-tourism, because of environmental conditions and various types of agro-products as well as a variety of rural traditions, and festivals [5]. “Agritourism: for sustainable tourism development in Konkan region of Maharashtra”, the objective of the study was to understand the concept of Agro-Tourism as a specialized form of rural tourism. Agro-Tourism is emerging as an important instrument for sustainable human development including poverty alleviation, employment generation, environmental regeneration and development of remote areas, and advancement of women and other disadvantaged groups in the country apart from promoting social integration and international understanding [6]. “Agro tourism an economic option”. Small farmers with small holdings can form a cooperative society to establish an agro-tourism center, Give wide publicity in the media print, and electronically to get more tourists [7].

“Agro-Tourism: A Cash Crop for Farmers in Maharashtra (India)”. Maharashtra has great potential for the development of agro-tourism, because of natural conditions and different types of Agri products as well as a variety of rural traditions, and festivals. The agriculture departments of the districts, Agriculture Universities should try to give orientation about it. Union of agro-tourism service providers is also another need of these farmers which helps the agricultural tourism network in India including Maharashtra [8].

“Agritourism: A catalyst for rural development—A review paper”. This research paper provides information on the basic Principles of Agri tourism and the Role of Agri tourism in Rural Development, the Benefits of Agri tourism for Farmers, and the Benefits for communities. It creates a win-win situation for farmers as well as tourists. Not only are those, but the villages also benefited due to the development of agro-tourism. Some cases of agro-tourism in Maharashtra have proved that agro-tourism not only brings the development of farmers but to the village as a whole from a social and economic angle [9].

“Agritourism as a Local Economic Development Tool for Rural Hill Regions”. This paper highlights how Agritourism can be used as a strategic tool for boosting the agrarian economy. Farming communities are challenged due to disproportionate development across the state which has resulted in rural outmigration and farm abandonment. There is a strong need to revitalize village-based economies in the state to preserve culture, traditions, and the rural way of life [10]. “Identifying the potential of agri-tourism in India: overriding challenges and recommend strategies”. Agritourism is a supportive system for agricultural activities in India. It is an Innovative practice that can be utilized by the farmer to harvest this opportunity, through a diversified approach. It is the best platform for the socioeconomic development of rural areas. Thus the government has to provide a full fledged policy support system for the rooting and strengthening of Agri-tourism in India [11].

“A study on Agritourism in India: an inception”. In today’s era of liberalization and globalization travel and tourism is extensively recognized as an important civil industry worldwide that provides a major potential for economic growth and development. For many developing countries it is one of the main sources of foreign exchange income and the number one export category, creating much-needed employment and opportunities for development. In over 150 countries tourism is one of the five top export earners, and in 60 it is the number one export category. The agritourism industry in India has a lot of potential to develop rural India [12]. “A Study on Catalyzing Rural Economic Development through Agrotourism”. This research paper helps to understand the Catalyzing Rural Economic Development through Agrotourism. Concluded by the researcher that Mahatma Gandhi once said “the future of India lies in its villages”. Thus, integrating a successful sector called tourism with agriculture will always prove to be beneficial. Something new to see, do and buy will automatically promote a place as a tourist destination. [13]. “The economic impact of diversification into agritourism.” In both cases, researchers evaluated the impact of agritourism on the economic performance of the farm. The results of our simulation scenarios show that Diversification into more areas represents risk mitigation when some diversification strategy faces undesirable conditions. A case study shows how agritourism improves the economic output of the beef cattle farm more than the farm-to-table strategy. Even under conditions of one season lockdown, agritourism brings long-term benefits [14].

“Perceived Impact of Agritourism on Farm Economic Standing, Sales, and Profits.” The purpose of this study is to examine the economic gains of agritourism development on Missouri farms as perceived by farm operators. Future studies should explore a wide range of economic benefits agritourism may bring to farms [15].

“An Empirical Analysis of sustainable Rural Agro Tourism marketing practices in Kolhapur District”. The major focus is on studying the factors responsible for sustainable rural tourism in Kolhapur district, along with the researcher also studied the customer expectations from rural tourism, the problems involved in rural tourism, and various tourist activities conducted by tourism centers [16]. “Agro-Tourism: Opportunities and Challenges for Farmers in Ratnagiri District”. Researchers suggested that despite the gradually growing agro-tourism, the fact remains that the farmers should follow a commercial approach; government support through appropriate and conducive policies for development should give priority to the Agro-tourism business in rural India [17]. “Agritourism and Rural Development in North-East India: Prospects and Challenges”. Agritourism activities can provide the additional income necessary to allow for the preservation of small and mid-scale farms and rural communities. Agriculture coupled with the tourism business is a relevant and futuristic strategy to attain sustainable growth. It also helps in maintaining cultural diversity and provides sustainable job opportunities for rural people. In the northeast, agritourism provides great possibilities as an alternative development strategy [18].

“Overview of Agritourism in India and world”. This research paper helps to understand and explain the overview of agritourism in India and the world. Data is collected through Secondary data sources. Agritourism which has seen global outreach needs an overhaul policy for encouraging new generation agri entrepreneurs who wish to transform a portion of their farm into a tourism hotspot for learners and holiday seekers. Agrotourism is helping in boosting the local economy and motivation to maintain the same lifelong. To promote these public-private partnerships and convergence approaches are required [19]. “The Scenario of Agri-Tourism in India: An Overview”. Agri-tourism is an instrument for the generation of rural employment and poverty alleviation. Today it is emerging as a growing market in the rural economy. The government of India is trying to develop infrastructure for the development of agri-tourism in different parts of the country. Agro-tourism is a leisurely activity in rural areas that helps to discover rural destinations for tourists and helps to go back to nature [20].

4 Results and Discussion

4.1 *The Concept of Agri Tourism*

- A. **Agri tourism World Tourism Organization (1998)** defines Agri tourism as “involves accommodation being offered in the farmhouse or a separate guest-house, providing meals and organizing guests’ activities in the observation and participation in the farming operations.”

B. Definition of Agri Tourism Definitions of agri-tourism are wide-ranging in the literature. The discrepancies found among the various agri-tourism definitions relate to three issues:

- (1) The type of location (e.g., farm, any agricultural setting);
- (2) The authenticity of the agricultural facility (Benefits offered to visitors or the experience);
- (3) The types of activities involved (e.g., lodging, education, entertainment, and adventure activities).

Kolhapur district can potentially establish Agro-tourism enterprises on a large scale. An experiment of Tea plantation in Shahuwadi, Cashew and Ragi (Finger millet) Farming in Chandgad, and Jaggery farming in the surrounding area of Kolhapur are the most suitable sites to be developed as an Agro-tourism site in Kolhapur District. Mahatma Gandhi once said, "The future of India lies in its villages". In relevance to this statement, villages contribute on a higher scale to the nation's economy. Thus, integrating a successful sector called tourism with agriculture will always prove to be beneficial. Something new to see, do and buy will automatically promote a place as a tourist destination. Employment generation for local people is seen and skill development is enhanced at the local level. Agro-tourism puts less pressure on the local amenities and infrastructure as it is not on a large scale. Also, local culture is preserved as the guest becomes a part of the host family for a short duration of his stay. Agro-Tourism is emerging as an important instrument for sustainable human development including poverty alleviation, employment generation, environmental regeneration and development of remote areas, and advancement of women and other disadvantaged groups in the country apart from promoting social integration and international understanding. The government should promote Agro-Tourism to ensure sustainable economic development and positive social change.

Benefits of Agri tourism for Increasing Rural Financial status, Tradition, Education, and Viable Agriculture practices The local folk art or different cultural forms will also prove helpful for developing agro-tourism centers e.g. Tamasha is a traditional folk dance of Maharashtra and Narayangaon is one of the famous centers for this art. Small farmers with small holdings can form a cooperative society to establish agro-tourism centers. Develop contacts with schools, colleges, NGOs clubs, unions etc., Train your staff or family members for receptions and hospitality, and assess the needs of customers and what they want and expect from visitors. Agri-tourism is a supportive system of agricultural activities in India. It is an Innovative practice that can be utilized by farmers and farm owners to harvest this opportunity, through a diversified approach. It will be a beneficial Model for both farmer and the tourist, as farmers have an extra edge for earning and employment whereas the tourist gets the privilege to relive a smooth, calm, and rejuvenating atmosphere and culture of our agricultural heritage. It is the best platform for the socioeconomic development of rural areas. For many developing countries it is one of the main sources of foreign exchange income and the number one export category, creating much-needed

employment and opportunities for development. In over 150 countries tourism is one of the five top export earners, and in 60 it is the number one export category. The agritourism industry in India has a lot of potentials to develop rural India. Results also show that agritourism is perceived as having a positive impact on farm profits, with the majority reporting at least some increase after adding agritourism activities and nearly one-fourth reporting a two-fold or more profit increase. Those results are especially important considering the exponential growth of agritourism in the U.S. and Missouri during the past five years.

4.2 Challenges Related to Agri Tourism Growth

Farmers must be educated in managing a business, interpersonal and communication skills to manage their businesses. If they want to come out from their boundary line proper training and necessary education must be provided to farmers. It is a good opportunity to develop an Agro-tourism business in Maharashtra. Despite growing agro-tourism, the fact remains that government supports through appropriate and conducive policies for agro-tourism development is lacking and government should give priority to agro-tourism business in Maharashtra through appropriate policy measures. The agriculture departments of the districts, Agriculture Universities should try to give orientation about it and provide some innovative ideas regarding Agro Tourism. Union of agro-tourism service providers is also another need of these farmers which helps the agricultural tourism network in India including Maharashtra.

5 Conclusion

India’s growing economy is mainly supported by the existing “rich natural and cultural resources”. Capitalizing on that, our tourism sector has perceived one of the fastest development rates worldwide. The travel and tourism industry has established its significance as an economic “growth engine” for the world economy. The purpose of the study was to systematically evaluate existing empirical data and theoretical literature on agri-tourism. The study has revealed the tremendous benefits of Agri tourism in inspiring rural economies, endorsing local craft industries, and conserving the esteemed cultural heritage of rural areas. The Ministry of Food and Agriculture in countries must support farmers and offer them the required training program for them to acquire the skills in operating Agri tourism center. The majority of farmers in rural areas who own these farms are underprivileged and would require financial packages to start Agri tourism centers. Governments must provide such assistance to rural farmers through their entrepreneurship development programs and schemes. This initiative would help rural farmers to grab the inventive and sustainable means of starting Agri tourism centers on their farms.

References

1. Thorat, S. D., & Suryawanshi, R. S. (2017). Assessment of agro-tourism potential in Junnar Tehsil, Maharashtra, India. *Scholarly Research Journal for Interdisciplinary Studies*, 4(36), 6872–6881.
2. Bhandare, D. J., & Potdar, M. B. (2016). Agro-tourism: An alternative for development of agricultural farmers in Kolhapur District (M.S.). *Agricultural Transformation in India Since Independence*, 69–80.
3. Chande, K., Verma, R., & Ekka, B. K. (2020). A study on development of agriculture tourism business in Baramati District (Maharashtra). *Journal of Critical Reviews*, 618–623
4. Sathe, S., & Randhave, M. (2019). Agro-tourism: A sustainable tourism development in Maharashtra—a case study of village inn agro tourism (Wardha). *GE-International Journal of Management Research*, 7(6), 45–58. ISSN (O): (2321-1709), ISSN (P): (2394-4226).
5. Kanse, B. T., & Kanse, T. (2017). Agro tourism: A sustainable development for rural areas of India; with special reference to Maharashtra. *International Journal of Researches in Social Sciences and Information Studies*.
6. Joshi, M. P. V. (2016). Agritourism: for sustainable tourism development in Konkan region of Maharashtra. *International Multidisciplinary Research Journal*, 6(3), 1–9.
7. Sandeep, & Shelar, R. (2016). Agro tourism an economic option. *International Journal of Technical Research and Applications*, 4(6), 146–150.
8. Kumbhar, V. (2009). Agro-tourism: a cash crop for farmers in Maharashtra (India). *Munich Personal RePEc Archive (MPRA)*, 1–13.
9. Vasanthi, C., & Padmaja, B. (2019). Agritourism: A catalyst for rural development—A review paper. *Journal of Pharmacognosy and Phytochemistry*, 416–418.
10. Shah, C., Shah, S., & Shah, G. L. (2020). Agritourism as a local economic development tool for rural hill regions. *Extension Strategies for Doubling Farmer Income*, 19–28.
11. Priyanka, S., & Kumar, M. M. (2016). Identifying the potential of agri-tourism in India: Overriding challenges and recommend strategies. *International Journal of Core Engineering and Management (IJCEM)*, 3(3), 7–14.
12. Swain, N. R., Pati, M. R., & Nayak, Y. D. (2018). A study on agritourism in India: An inception. *International Journal of Engineering Science Invention (IJESI)*, 7(5 Ver VII), 85–89.
13. S. S. (2020). A study on catalyzing rural economic development through agrotourism. *Agri Mirror: Future India*, 1(7), 1–3.
14. Pitrova, J., Krejčí, I., Rydvald, J., Hlavatý, R., Horáková, T., & Tichác, I. (2020). The economic impact of diversification into agritourism. *International Food and Agribusiness Management Review*, 23(5), 713–734.
15. Barbieri, C., & Tew, C. (2008). Perceived impact of agritourism on farm economic standing, sales, and profits. *Sustainable Tourism Marketing: Doing Justice to Place, People and Pasts*, 1–9.
16. Mali, D. C. (2015). An empirical analysis of sustainable rural agro tourism marketing practices in Kolhapur District. *ETHOS A Journal of Research Articles in Management*, 8(1), 38–53.
17. Sawant, D. R. G. (2019). Agro-tourism: Opportunities and challenges for farmers in Ratnagiri District. *Think India Journal*, 22(33), 54–60.
18. Deka, T., & Sarma, A. (2019). Agritourism and rural development in north-east India: Prospects and challenges. *Advances in Economics and Business Management (AEBM)*, 6(5), 415–417.
19. Krishna, D. K., & Sahoo, A. K. (2020). Overview of agritourism in India and world. *Food and Scientific Reports*, 1(7), 56–59.
20. Sandeep, M. (2018). The scenario of agri-tourism In India: An overview. *International Journal of Creative Research Thoughts (IJCRT)*, 6(2), 136–140.

Transfer Learning Using Convolutional Neural Network to Classify Leaf Diseases on Ridge Gourd Plant



Rohan U. Katare, Akash A. Mahajan, and Amol C. Adamuthe

Abstract Leaf disease can have a long-term effect on vegetable growth. If proper care is not taken, it may have adverse effects on vegetable production. The disease on the leaf should be identified on time to avoid further deterioration and reduction in the yield of plants. In this study, we compare various image classification models created using Convolutional Neural Networks for the leaf diseases classification of a ridge gourd plant. Along with healthy leaf images, the dataset contains images of leaves affected by Larvae, Anthracnose, and Downy Mildew. Pre-trained image classification models like VGG16, VGG19, ResNet50, and MobileNetV1 are compared. Best fitted CNN model is designed by tuning the hyperparameters namely the number of filters, kernel size, activation function, and the optimizer. Results obtained with the proposed CNN model are compared against pre-trained models based on accuracy and training time. Results show that the proposed CNN model takes less training time and gives better accuracy compared to other pre-trained models.

Keywords Convolutional neural network · Disease classification · MobileNet · ResNet · VGGNet

1 Introduction

India is the second largest democracy in the world and around 70% of the population living in Indian rural areas is dependent on agriculture and farming [1]. Almost 21% of the GDP is covered by farming. Vegetable farming is an important as well as profitable business in India, carried out differently in each state. In the early stage of development, vegetable products are highly fragile and need special care from the farmers. Many uncertain events such as high winds, extreme sunlight, and precipitation are the main factor influencing the production rate of the land. In many cases, pests such as larvae and caterpillars attack the farm and consume the leaves,

R. U. Katare · A. A. Mahajan · A. C. Adamuthe (✉)

Department of Information Technology, Rajarambapu Institute of Technology, Urun Islampur, Sangli, Maharashtra, India

e-mail: amol.admuthe@gmail.com

vegetables, and other products. Some common fungal infections like anthracnose and downy mildew are notorious problems for farmers. In past years, along with the farm mechanization [2], machine learning and deep learning have been implemented for farming and agriculture [3–7], and most of them are based on Convolutional Neural Networks (CNN) [8]. By introducing machine learning techniques for farming, many authors have proved the efficiency of artificial intelligence for solving agricultural issues such as saving costs and human efforts. Most of the machine learning and deep learning models implemented for agricultural tasks are primarily image processing and classification. Besides agriculture, image classification models based on CNN are proven to be efficient in various tasks such as fashion image classification [9], medical image analysis [10], optical character recognition [11], and hand gesture recognition [12]. Many authors have reportedly applied convolutional neural networks and deep learning techniques to leaf disease and plant disease classification [13–19]. With a special organization of convolutional layers and other types of layers, a CNN-based deep learning architecture can be built. There are a few popular pre-trained architectures of CNN such as VGGNet [20], ResNet [21], and MobileNet [22] are discussed and used for various tasks related to image classification.

In this study, the common leaf diseases on ridge gourd plants are classified using the convolutional neural network models. The common diseases are namely larvae, anthracnose, and downy mildew. Those leaves which are not affected by any disease mentioned above are classified as “healthy” leaves. A CNN-based image classification model is built by hyper parameter tunings such as tuning the number of filters, size of the kernel, activation function, and the optimizer. The performance of this model is compared against pre-trained CNN architectures namely VGG16, VGG19, ResNet50, and MobileNetV1. The models are compared based on accuracy and training time. The following are the objectives of this paper.

- Designing best fitted CNN model through various hyper parameter tuning for plant disease image classification.
- Using pre-trained CNN architectures such as VGG16, VGG19, ResNet50, and MobileNetV1 plant disease image classification.

The rest of this paper is outlined as follows: Sect. 2 discusses the previous work related to leaf disease classification. Section 3 outlines the methods and tools used for experiments. Section 4 presents the results. The study is concluded in Sect. 5.

2 Literature Review

Precision agriculture [23, 24] techniques optimize the usage of resources such as water and fertilizers to improve productivity and reduce the cost required for farming. Machine Learning and neural networks can dramatically reduce the manual tasks to identify the diseases in crops and saves the associated procurements. Leaf disease classification is among the popular research topics under the innovation in precision

agriculture. This section discusses various studies conducted for leaf disease classification using deep learning and machine learning. Table 1 shows a comprehensive review of various studies comprising of leaf disease classification.

Transfer learning is a method of training a new model based on an existing model. This will ensure that the new model will have previously learnt features along with new features learnt during training [25]. Many existing CNN models are used for transfer learning. The study in [26] uses InceptionV3 and fine-tunes it for face mask detection, [27] compares the VGG16, ResNet50, and InceptionV3 for COVID-19 detection using chest X-ray images. Transfer learning technique is also used for agriculture applications of CNN [28, 29] to classify the type of crop and rice plant disease, respectively. Nowakowski et al. [28] uses VGG16 and GoogleNet to fine-tune model for crop type detection. In some cases, pre-trained models are hybridized with machine learning classifier. Shrivastava et al. [29] used AlexNet CNN to extract features and support vector machines to classify rice diseases.

In this study, pre-trained image classifiers VGG16, VGG19, ResNet50, and MobileNetV1 are used to classify the leaf diseases on ridge gourd. A CNN model is proposed and compared against the pre-trained models.

3 Methodology

3.1 Proposed CNN Model and Transfer Learning

Convolutional Neural Network uses a special type of layer called a Convolution Layer. This layer carries out a specialized function called the convolution function. Each convolution layer generates feature maps that are images generated by applying the filters on the input image. The feature maps are used to identify patterns in images and update weights accordingly. We propose a CNN model to classify leaf diseases. The proposed CNN model architecture is shown in Fig. 1.

A classifier based on CNN usually has the following types of layers along with the convolution layer. The input layer adjusts the input provided for classification into a fixed dimension. The image can be either grayscale, black and white, or RGB color image. A pooling layer extracts the most important features from the input. Max pooling is the commonly used pooling mechanism. In rare cases, Min pooling and average pooling are also used. A fully-connected layer connects all neurons in a single layer to the following layer. The classification is carried out in this layer. However, hybridized models may have different types of classification methods e.g., Support Vector Machine.

Transfer learning can be achieved by changing the number of ways a classifier can classify an image. The dataset images have 4 classes. For each pre-trained model, the final fully connected layer gives 4 outputs.

Table 1 Review of leaf disease classification

Refs.	Problem statement	Dataset	Contribution
[13]	A convolutional neural network (CNN) that effectively classifies diseases in three crops, namely pepper, potato, and strawberry using transfer learning methods	A plant village data set consisting of three crops: peppers, strawberries, and potatoes	VGG19 is used for the transfer learning method. The Deep CNN model was implemented with minor modifications. The system can detect diseases with 95% accuracy
[14]	Investigation of key factors affecting the design and effectiveness of deep neural networks applied to plant pathology	103 out of 171 diseases affecting 21 plant species with about 50,000 images	Learn more about the quantitative factors that influence deep learning models used to predict plant diseases. The author listed a total of 9 factors with descriptions of a strong correlation between the data and the model
[15]	Compared and analyzed multiple methods of data augmentation in the task of image classification including the image transformation techniques like cropping, rotating, and zooming etc.	No standard dataset was used. Few sample datasets were used for illustration purposes	Proposals to improve the efficiency of deep learning models for image processing tasks using modern augmented algorithms. Primarily author suggests combining the methods and generating new algorithms that could train a deep learning model even on more variations of an image dataset
[16]	Discussion of a new approach to develop a plant disease detection model based on leaf image classification using deep convolutional networks	Dataset build upon the images downloaded from the internet	This paper examines possible approaches for training deep learning models for detecting plant diseases. To provide support to the hypothesis, the author has generated a dataset of plant disease images and predicted the disease using novel methods
[17]	A real-time method based on deep convolutional neural networks for detecting maize leaf disease	Created from several images taken from corn plantations in the Raebareli and Sultanpur districts	A hardware framework was proposed which includes IoT components and processing devices. To process large data on mobile devices, cloud solutions are used. The proposed framework, once run in real-time gives 88.46% accuracy for corn disease prediction
[18]	A Raspberry Pi-based IoT device has been proposed to send images of plants to classify diseases and update real-time environmental parameters such as temperature, humidity, soil moisture, and pH in a MySQL database	Acquire images with required environmental parameters via a Raspberry Pi 3-enabled IoT-based device	Properly set up IoT components to gain images from the camera and classify it using the underlying deep learning model. Promisingly, the model gives an accuracy of around 98%

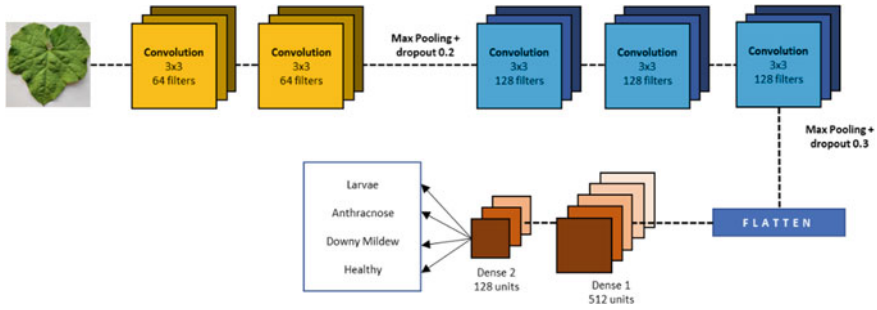


Fig. 1 Proposed CNN model

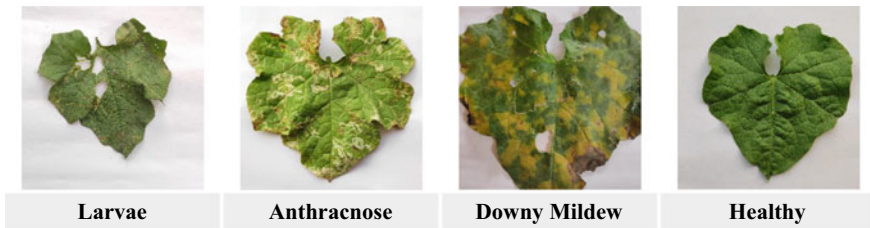


Fig. 2 Sample leaves from the dataset

3.2 Dataset

The original size of the images is 325×578 pixels, but it is cropped in the input layer of models during training to a specific size. Figure 2 shows the sample for each type of leaf in the dataset. The number of each type of leaf is as follows: Healthy—378, Downy Mildew—488, Anthracnose—211, and Larvae—70.

3.3 Experimental Setup

The Keras and Tensorflow library is used for implementing the deep learning models. Each model is trained for 100 epochs with a fixed batch size of 5. The pre-trained models are imported from the Keras applications package in Python. All experiments are carried out on Google Collaboratory with standard GPU settings.

Table 2 The results of tuning the number of filters

Accuracy	Filter size			
	32	64	128	256
Train	0.88	0.68	0.91	0.58
Test	0.67	0.73	0.85	0.67

Table 3 The results of tuning the activation function

Accuracy	Activation function		
	Elu	ReLU	Tanh
Train	0.91	0.96	0.90
Test	0.83	0.88	0.78

4 Result and Discussion

This section briefly describes the results of all experiments. CNN model hyper parameter tuning is done. The final CNN model is compared with the performance of VGG16, VGG19, ResNet50, and MobileNetV1.

4.1 Tuning the Number of Filters

Table 2 shows the results of tuning the number of filters. The filter sizes 32, 64, 128, and 256 are compared. The filters with size 128 worked best.

4.2 Tuning the Activation Function

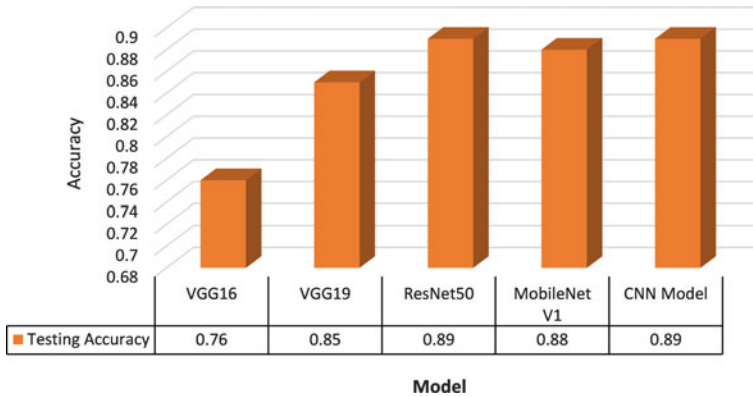
Table 3 shows the results of the tuning activation function. The ELu, ReLU, and Tanh activation functions are compared. The ReLU outperformed other activation functions and significantly improved the training and testing accuracy.

4.3 Tuning the Optimizer

Table 4 shows the results of tuning the optimizer. The optimizers such as AdaGrad, Adam, RMSProp, and SGD are compared. Adam optimizer outperforms other optimizers and improves the testing accuracy by 2%.

Table 4 The results of tuning the optimizer

Accuracy	Optimizer			
	AdaGrad	Adam	RMSProp	SGD
Training	0.90	0.97	0.86	0.83
Testing	0.82	0.89	0.75	0.76



Model name	VGG16	VGG19	ResNet50	MobileNet50	CNN Model
Training time (in mins)	56	186	210	126	45

Fig. 3 Comparison of pre-trained models and the CNN model

The original number of outputs on pre-trained models is 1000. It was changed to 4 during the training process. Along with training and testing accuracy, the training time in minutes is also indicated. Figure 3 shows the comparison chart of the models.

5 Conclusion

The diseases such as Larvae, Anthracnose, and Downy Mildew adversely affect the growth of ridge gourd and similar vegetables. The deterioration of plants’ growth and nutritional values directly affects the production of these vegetables. In this study, we created a CNN model to classify the diseased leaves of ridge gourd plants and compared it with the pre-trained models namely VGG16, VGG19, ResNet50, and MobileNetV1. The CNN model is created by hyper parameter tunings namely tuning the number of filters, the activation function, and the optimizer function. Model comparison is based on training and testing accuracy. ResNet50 achieves training and testing accuracy similar to CNN models, but at the expense of training time. The training time for ResNet50 is 210 min and the training time for the CNN

model is 45 min. The CNN model outperforms other pre-trained models by training and testing accuracy of 97.0% and 89.0% respectively.

References

1. Sah, S., Johar, V., & Karthi, J. S. (2022) Status and marketing of fruits and vegetables in India: A review.
2. Rajkhowa, P., & Kubik, Z. (2021). Revisiting the relationship between farm mechanization and labour requirement in India. *Indian Economic Review*, 56(2), 487–513.
3. Bazame, H. C., Molin, J. P., Althoff, D., & Martello, M. (2022). Detection of coffee fruits on tree branches using computer vision. *Scientia Agricola*, 80.
4. Rodríguez, J. P., Corrales, D. C., Aubertot, J. N., & Corrales, J. C. (2020). A computer vision system for automatic cherry beans detection on coffee trees. *Pattern Recognition Letters*, 136, 142–153.
5. Muro, J., Linstädter, A., Magdon, P., Wöllauer, S., Männer, F. A., Schwarz, L. M., Ghazaryan, G., Schultz, J., Malenovsky, Z. & Dubovyk, O. (2022). Predicting plant biomass and species richness in temperate grasslands across regions, time, and land management with remote sensing and deep learning. *Remote Sensing of Environment*, 282, 113262.
6. Pantazi, X. E., Moshou, D., Alexandridis, T., Whetton, R. L., & Mouazen, A. M. (2016). Wheat yield prediction using machine learning and advanced sensing techniques. *Computers and Electronics in Agriculture*, 121, 57–65.
7. Ebrahimi, M. A., Khoshtaghaza, M. H., Minaei, S., & Jamshidi, B. (2017). Vision-based pest detection based on SVM classification method. *Computers and Electronics in Agriculture*, 137, 52–58.
8. Chen, L., Li, S., Bai, Q., Yang, J., Jiang, S., & Miao, Y. (2021). Review of image classification algorithms based on convolutional neural networks. *Remote Sensing*, 13(22), 4712.
9. Eithardt, V. (2021). Classifying garments from fashion-MNIST dataset through CNN. *Advances in Science, Technology and Engineering Systems Journal*, 6(1), 989–994.
10. Yadav, S. S., & Jadhav, S. M. (2019). Deep convolutional neural network-based medical image classification for disease diagnosis. *Journal of Big Data*, 6(1), 1–18.
11. Wei, T. C., Sheikh, U. U., & Ab Rahman, A. A. H. (2018, March). Improved optical character recognition with deep neural network. In *2018 IEEE 14th international colloquium on signal processing & its applications (CSPA)* (pp. 245–249). IEEE.
12. Bhavana, D., Kumar, K. K., Chandra, M. B., Bhargav, P. S. K., Sanjana, D. J., & Gopi, G. M. (2021). Hand sign recognition using CNN. *International Journal of Performability Engineering*, 17(3), 314–321.
13. Smithashree, K. P., & Rao, B. M. (2020). Plant leaf disease detection. *International Journal for Technological Research in Engineering*, 7(11)
14. Hasan, M. A., Riana, D., Swasono, S., Priyatna, A., Pudjiarti, E., & Prahartiwi, L. I. (2020, November). Identification of grape leaf diseases using convolutional neural network. In *Journal of physics: conference series* (Vol. 1641, No. 1, p. 012007). IOP Publishing.
15. Barbedo, J. G. (2018). Factors influencing the use of deep learning for plant disease recognition. *Biosystems Engineering*, 172, 84–91.
16. Mikołajczyk, A., & Grochowski, M. (2018, May). Data augmentation for improving deep learning in image classification problems. In *2018 International interdisciplinary Ph.D. workshop (IIPhDW)* (pp. 117–122). IEEE.
17. Sladojevic, S., Arsenovic, M., Anderla, A., Culibrk, D., & Stefanovic, D. (2016). Deep neural networks-based recognition of plant diseases by leaf image classification. *Computational Intelligence and Neuroscience*, 2016.
18. Mishra, S., Sachan, R., & Rajpal, D. (2020). Deep convolutional neural network-based detection system for real-time corn plant disease recognition. *Procedia Computer Science*, 167, 2003–2010.

19. Pavel, M. I., Kamruzzaman, S. M., Hasan, S. S., & Sabuj, S. R. (2019, February). An IoT-based plant health monitoring system implementing image processing. In *2019 IEEE 4th international conference on computer and communication systems (ICCCS)* (pp. 299–303). IEEE.
20. Simonyan, K., & Zisserman, A. (2014). Very deep convolutional networks for large-scale image recognition. *arXiv preprint arXiv:1409.1556*.
21. He, K., Zhang, X., Ren, S., & Sun, J. (2016). Deep residual learning for image recognition. In *Proceedings of the IEEE conference on computer vision and pattern recognition* (pp. 770–778).
22. Harjoseputro, Y., Yuda, I., & Danukusumo, K. P. (2020). MobileNets: Efficient convolutional neural network for identification of protected birds. *IJASEIT (International Journal on Advanced Science, Engineering and Information Technology)*, 10(6), 2290–2296.
23. Sharma, A., Jain, A., Gupta, P., & Chowdary, V. (2020). Machine learning applications for precision agriculture: A comprehensive review. *IEEE Access*, 9, 4843–4873.
24. Treboux, J., & Genoud, D. (2018, June). Improved machine learning methodology for high precision agriculture. In *2018 Global internet of things summit (GloTS)* (pp. 1–6). IEEE.
25. Hussain, M., Bird, J. J., & Faria, D. R. (2018, September). A study on CNN transfer learning for image classification. In *UK workshop on computational Intelligence* (pp. 191–202). Springer, Cham.
26. Jignesh Chowdary, G., Punn, N. S., Sonbhadra, S. K., & Agarwal, S. (2020, December). Face mask detection using transfer learning of inceptionv3. In *International conference on big data analytics* (pp. 81–90). Springer, Cham.
27. Perumal, V., Narayanan, V., & Rajasekar, S. J. S. (2021). Detection of COVID-19 using CXR and CT images using transfer learning and Haralick features. *Applied Intelligence*, 51(1), 341–358.
28. Nowakowski, A., Mrziglod, J., Spiller, D., Bonifacio, R., Ferrari, I., Mathieu, P. P., Garcia-Herranz M., & Kim, D. H. (2021). Crop type mapping by using transfer learning. *International Journal of Applied Earth Observation and Geoinformation*, 98, 102313
29. Shrivastava, V. K., Pradhan, M. K., Minz, S., & Thakur, M. P. (2019). Rice plant disease classification using transfer learning of deep convolution neural network. *International Archives of the Photogrammetry, Remote Sensing & Spatial Information Sciences*, 3(6), 631–635.

Optimal Sizing and Location of Distributed Generators in Distribution System for Loss Reduction



Nishant Thakkar, Khushali Bilare, Mukund Ghole, and Priyanka Paliwal

Abstract The optimal planning process of distributed generation (DG) involves its sizing and placement and has large potential for power loss decrease and voltage profile enhancement. Therefore, this present paper, an analysis on IEEE 14 bus system has been carried out to determine the effect of DG unit sizing and their location on the power loss in distribution system. The proposed model utilizes backward-forward sweep (BFS) method for load flow analysis and PSO for finest DG sizing and placement. In proposed work, two different cases viz. single DG and multiple DG have been analysed and compared with the no DG based case. The result of case analysis reveals that the placement of multiple DG at PSO-derived sites in distribution system can reduce the total power loss by 75.78% and improve the voltage profile by 18.56% in comparison of base case.

Keywords Backward forward sweep · Distributed generation · Loss reduction · Optimum placement · Voltage profile

1 Introduction

The growth in load demand has led to tremendous expansion in distribution systems [1]. This unplanned expansion may growth the system power loss, and degrade the voltage profile along the feeder. This causes inefficient operation of distribution

N. Thakkar (✉) · K. Bilare · M. Ghole · P. Paliwal
Department of Electrical Engineering, Maulana Azad National Institute of Technology, Bhopal,
India
e-mail: nishanthakkar1109@gmail.com

K. Bilare
e-mail: khushalibilare@gmail.com

M. Ghole
e-mail: mukundghole@gmail.com

P. Paliwal
e-mail: priyankapaliwal@manit.ac.in

system and may also lead to stability problems [2]. To overcome such problems, Distributed Generators (DGs) have emerged as a viable solution [3]. DGs are basically power generation systems which generate power locally unlike central grid structure. The power produced by DGs is not meant for long distance transmission, rather they are positioned at the point of usage [4]. The locally available renewable energy technologies (RET) are the most preferable DGs due to their modularity and compactness. RETs like solar photovoltaic and solar thermal systems harness the solar energy of sun and transform it into heat and electricity which are the prime applicants for distributed energy generation [5]. Some other major RETs in DG systems are wind turbines, biothermal, small hydropower systems and biomass. The RETs have ability to reduce harmful effects of fossil fuel use in the environment viz. greenhouse effect and global warming [6]. However, the finest placement and sizing of DG in distribution system are very significant components of adequate planning. When sized and placed inappropriately, it may lead to increase in power loss and voltage issues [7]. In various literature, many approaches have been used for finest DG sizing and placement comprising of heuristic and meta-heuristic optimization techniques. In ref. [8], author addressed a dynamic reliability-based model in DG planning for profit maximization in a distributed network. Reference [9] presents a time-varying model of load for the demand response analysis of DG-based distribution network. In ref. [10], authors present optimal sizing of different DGs by using PSO. In ref. [11] authors discussed the analysis of DG penetration and placement by using probabilistic model. In ref. [12], authors utilized the Satin bower bird algorithm for DG sizing. In this paper, the optimal planning problem of DGs wrt. sizing and location have been addressed using PSO. The objectives of planning formulation are loss reduction and voltage profile improvement. The proposed methodology utilizes BFS for load flow analysis. In this paper, two different cases comprising of a single DG unit and second one with multiple DGs have been used for the analysis with the discrete location and sizing. The case study has been carried out on IEEE 14 bus radial distribution feeder. The paper organization is as follows: Sect. 2 discusses about the problem objective and constraints. Section 3 describes the proposed methodology along with brief description of backward-forward sweep and PSO techniques which have been used in the methodological framework. Section 4 provides system description. Section 5 presents the results obtained for different cases. The conclusion of the paper is deliberated in Sect. 6.

2 Problem Design

2.1 Objective Function

The objective function involves two objectives: minimization of power loss and voltage deviation (VD). In this paper, the objective function has been formulated as the average of sum of square of VD and power loss.

$$\text{Objective Function} = \min\{(\text{Power loss})^2 + VD^2\}/2 \quad (1)$$

2.2 Constraints

The objective function is subjected to following constraints:

(i) Voltage magnitude constraints:

To improve the power quality, voltage magnitude at each node must be between minimum and maximum allowable range as follows:

$$|v_{\min}| \leq v_n \leq |v_{\max}|; n \in 1, 2, 3, \dots, N \quad (2)$$

where, v_{\min} : Minimum acceptable value of voltage limit, v_{\max} : Maximum allowable value of voltage limit, v_n : Voltage at n^{th} node.

(b) DG constraints:

The active power generation from DGs must be less than the total active power network demand as follows:

$$0 \leq \sum P_{DG} \leq \sum P_{\text{load}} \quad (3)$$

where, P_{DG} : Injected active power of DG, P_{load} : Load active power demand.

3 Methodology

The proposed model can provide a more efficient solution of DG integration. In this study initially random solutions for DG sizing and location are being generated. The objective function (Eq. (1)) is evaluated through the load flow analysis of the system using BFS. The optimal solution is being obtained through PSO. A brief discussion on BFS and PSO has been discussed in following subsections.

3.1 Backward-Forward Sweep (BFS)

The BFS method is being widely used for load flow analysis in distribution system [13, 14]. In each iteration, BFS method comprises of two computational processes. The forward sweep process involves the calculation of voltage at each node (from reference to end node), backward process calculates power or current flow solutions (from end node to reference node) [15]. The process is repeated until convergence is obtained. The flow chart of BSF method is presented in Fig. 1. This method involves the following steps:

- Step 1—Calculation of bus injection current using Eq. (4).

$$i_j^k = \text{conj} \left(\frac{S_j}{v_j^{(k-1)}} \right) \quad (4)$$

where i_j^k presents injection current at j^{th} node in k^{th} iteration, S_j presents power injection at j^{th} node and $v_j^{(k-1)}$ presents voltage at j^{th} node at $(k-1)^{\text{th}}$ iteration.

- Step 2—In this stage backward sweep is executed using Eq. (5).

$$I_{j-1,j}^k = i_j^k + \sum (I_{j,j+1}^k) \quad (5)$$

where $I_{j-1,j}^k$ presents the current of branch connecting j^{th} node to $(j-1)^{\text{th}}$ node and $\sum I_{j,j+1}^k$ presents current of all branch coming from j^{th} node.

- Step 3—In this stage forward sweep is executed using Eq. (6).

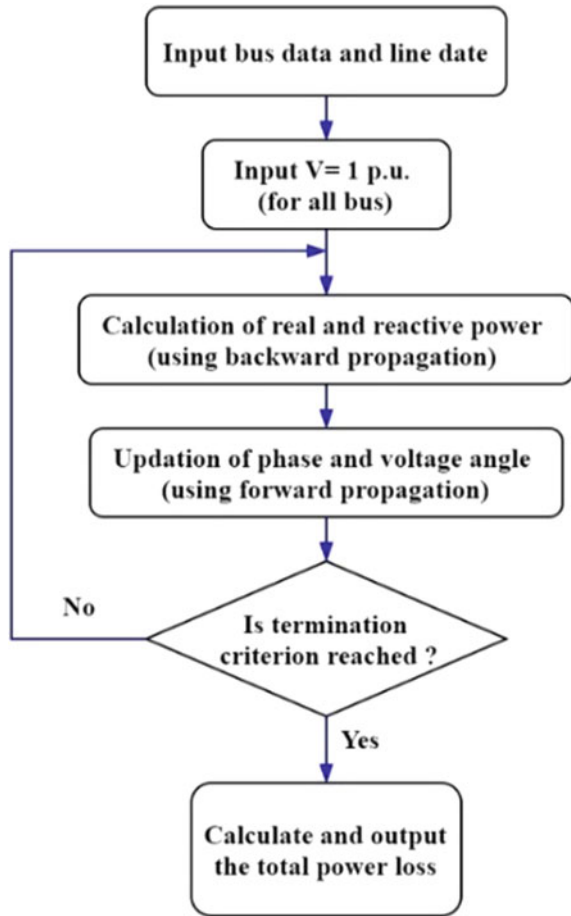
$$v_j^k = v_{j-1}^k - I_{j-1,j}^k Z_{j-1,j} \quad (6)$$

where v_j^k presents voltage of j^{th} node at k^{th} iteration, v_{j-1}^k presents voltage of upstream node of j^{th} node and $Z_{j-1,j}$ presents impedance of branch involving j^{th} node to its upstream node.

- Step 4—Voltage magnitude obtained by tracking variances of two succeeding iterations, by using Eq. (7).

$$\max(v^{k-1} - v^k) < \alpha \quad (7)$$

Fig. 1 Flow chart of backward forward sweep



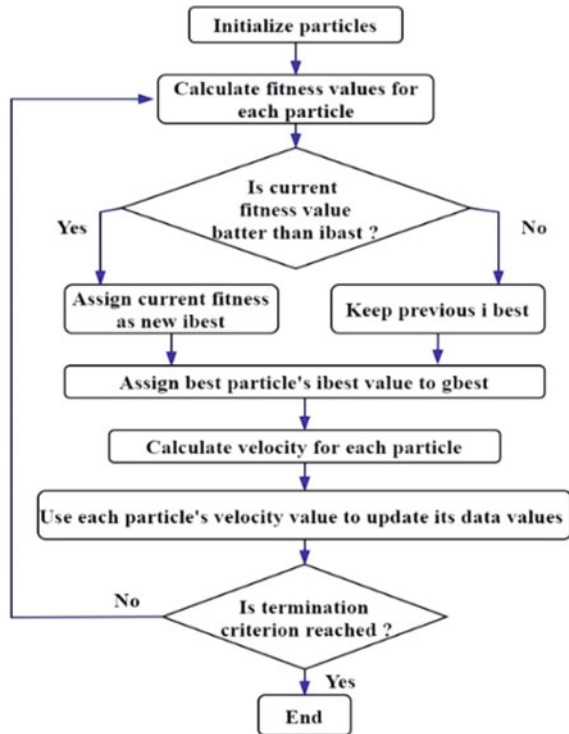
3.2 PSO

PSO is a swarm intelligence-based algorithms, which emulates the social behaviour of bird flowing [16]. The general procedure of PSO algorithm is presented in Fig. 2. The algorithm involves following equation for updation of velocity and position-

$$v_{pq}^{t+1} = w \cdot v_{pq}^t + c_1 r_1 (i_{pq}^t - x_{pq}^t) + c_2 r_2 (g_{pq}^t - x_{pq}^t) \tag{8}$$

$$x_{pq}^{t+1} = x_{pq}^t + v_{pq}^{t+1} \tag{9}$$

Fig. 2 Flow chart of PSO algorithm



where, v_{pq} : new velocity of p^{th} particle in q^{th} dimension, x_{pq} : Position of p^{th} particle in q^{th} dimension, w : Inertia weight, i_{pq} : Individual best position of p^{th} particle in q^{th} iteration, g_{pq} : Global position of p^{th} particle in q^{th} iteration, c_1 and c_2 : Acceleration co-efficient, r_1 and r_2 : Random variables.

4 System Description

As discussed in introduction section that the system analysis is configured on IEEE-14 bus system. The IEEE-14 bus test system is a standard IEEE system which involves several load points, generators and line parameters [17]. IEEE 14 bus system shows easy data and parameter availability [18, 19]. The used IEEE 14 bus system is illustrated in Fig. 3. The results are derived for a complete day considering an average load pattern of an area. In this study it is expected that load remain constant for each time segment and each time segment is considered as one hour. The load profile is present in Fig. 4.

Fig. 3 IEEE-14 bus system

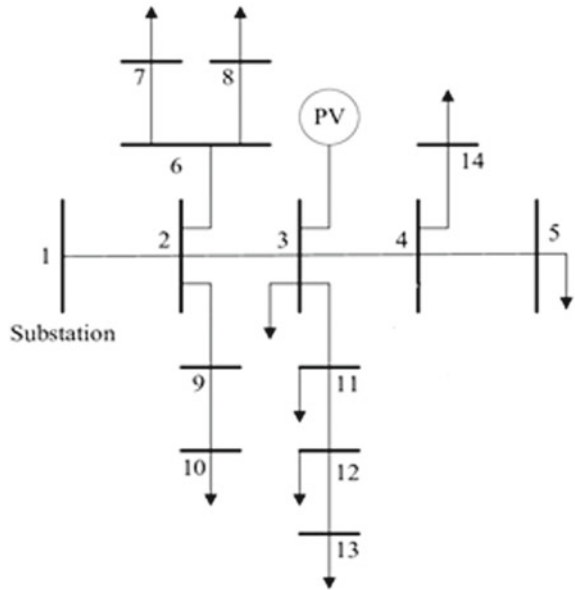
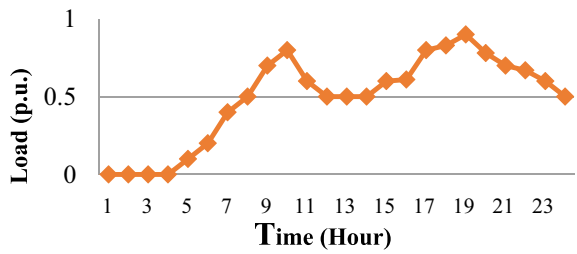


Fig. 4 Load profile for 24 h



5 Result and Discussion

The parameter of optimization problem is presented in Table 1.

Table 1 Parameter of PSO

Parameter	Value
Population size	15
C1 and C2	2
Number of iterations	25
Inertia weight	0.4–0.9

This routine of PSO is programmed in MATLAB M-File program on AMD Ryzen-5, 3200U with Radeon-Vega Mobile Gfx 2.10 GHz, 8 GB RAM. The result of optimal size and location of different cases are as follows:

- Case I (No DG-Base case)—In this case no additional DG is connected. Here the result exhibits the system power loss as 25.2367 kW and 0.2586 VD.
- Case II (Single DG)—The result of single DG placement is presented in Table 2. As shown from Table 2 that after 120 iterations the algorithm converges. Hence, we infer that we require at least 120 iterations to get the optimal results.
- Case III (Multiple DG)—The result of multiple DG placement is presented in Table 3.

As seen from Table 3 that, the optimal location for installing two DGs in the system are bus number 3 and 9. The optimal size for both the DGs is 40 kW. The total loss in the system after placing the two DGs is 6.1124 kW while the voltage deviation is coming out to be 0.2106. The power loss and voltage deviation result of all three case is presented in Fig. 5a and b respectively.

As observed from Fig. 5a, the variation in power loss for all three case presents that single DG based case shows 49.19% lower and multiple DG based case shows

Table 2 Finest location and size of single DG

S. No.	No. of iterations	Bus no.	Size (DG)	Power loss (kW)	Final VD (p.u.)
1	80	14	7.9022	14.6354	0.2563
2	100	14	8.9554	13.8743	0.24871
3	120	14	10	12.8225	0.2256
4	150	14	10	12.8225	0.2256

Table 3 Optimal location and size of multiple DG

S. No.	Location (Bus no.)	Size (DG)	Final power loss (kW)	Final VD (p.u.)
1	3	40	6.1124	0.2106
2	9	40		

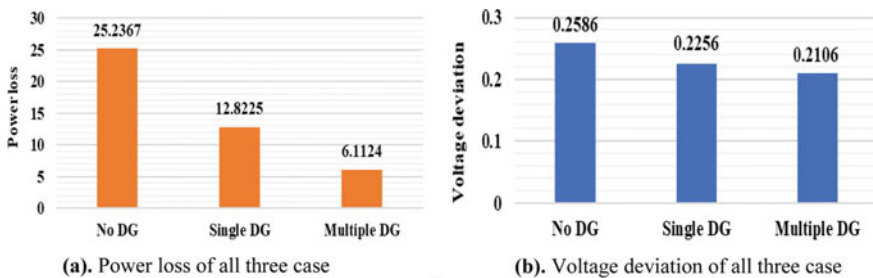


Fig. 5 a Power loss of all three case, b Voltage deviation of all three case

75.78% lower power loss in comparison to base case. As observed from Fig. 5b, the voltage deviation of all case presents that multiple DG based case show lowest voltage deviation, this case shows 18.56% lower voltage deviation in comparison of base case and single DG based case shows second lowest voltage deviation.

6 Conclusion

The sizing and placement of DGs in distribution system is very dynamic and involves different multiple objectives and constraints. In this study, a planning framework, for size–location planning of DG in distribution systems has been presented. BFS and PSO have been used for multi and single DG sizing and placement for loss minimization and voltage profile improvement. The analysis presents that, appropriate DG placement and sizing in a power distribution system plays important role in total power loss reduction and system voltage profile improvement. The proposed methodology is verified on 14 bus system by connecting DG at all probable locations. The results exhibited that the proposed methodology has ability for voltage profile improvement, power losses reduction and efficient DG planning in distribution system. The comparative result of single and multiple DG size and placement presents that the integration of multiple DG on different buses shows more improved voltage profile with less power loss.

References

1. Nixon, J. D., et al. (2012). The feasibility of hybrid solar-biomass power plants in India. *Energy*.
2. Paliwal, P., Patidar, N., & Nema, R. (2014). A novel method for reliability assessment of autonomous PV-wind-storage system using probabilistic storage model. *International Journal of Electrical Power & Energy Systems*, 55, 692–703.
3. Prakash, D., & Lakshminarayana, C. (2016). Multiple DG placements in distribution system for power loss reduction using PSO algorithm. *Procedia Technology*, 25, 785–792.
4. El-Zonkoly, A. (2011). Optimal placement of multi-distributed generation units including different load models using particle swarm optimization. *Swarm and Evolutionary Computation*, 1, 50–59.
5. Thakkar, N., Paliwal, P., & Ghole, M. (2021). Selection of power generation technology using a combination of CRITIC and TOPSIS. In *ICEPES*.
6. Thakkar, N., & Paliwal, P. (2022). Hydrogen storage based micro-grid: A comprehensive review on technology, energy management and planning techniques. *International Journal of Green Energy*, pp. 1–19.
7. Paliwal, P., Patidar, N., & Nema, R. (2012). A comprehensive survey of optimization techniques used for Distributed Generator siting and sizing. In *2012 Proceeding of IEEE Southeastcon*.
8. Wankhede, S., et al. (2022). Bi-level multi-objective planning model of solar PV-battery storage-based DERs in smart grid distribution system. *IEEE Access*.
9. Khoubseresht, O., & Shayanfar, H. (2020). The role of demand response in optimal sizing and siting of distribution energy resources in distribution network with time-varying load: An analytical approach. *Electric Power Systems Research*, 180, 106100.

10. Paliwal, P., Patidar, N., & Nema, R. (2014). Determination of reliability constrained optimal resource mix for an autonomous hybrid power system using particle swarm optimization. *Renewable Energy*, 63, 194–204.
11. Paliwal, P. (2021). Comprehensive analysis of distributed energy resource penetration and placement using probabilistic framework. *IET Renewable Power Generation*, 15.
12. Thakkar, N., & Paliwal, P. (2021). Application of satin bowerbird algorithm for optimal sizing of a solar-biomass based microgrid. In: *2021 13th IEEE PES Asia Pacific Power & Energy Engineering Conference (APPEEC)*.
13. Issicaba, D., & Coelho, J. (2016). Evaluation of the forward-backward sweep load flow method using the contraction mapping principle. *International Journal of Electrical and Computer Engineering*, 6, 3229.
14. Eminoglu, U., & Hocaoglu, M. (2008). Distribution systems forward/backward sweep-based power flow algorithms: A review and comparison study. *Electric Power Components and Systems*, 37, 91–110.
15. Kawambwa, S., Mwifunyi, R., Mnyanghwalo, D., Hamisi, N., Kalinga, E., & Mvungi, N. (2021). An improved backward/forward sweep power flow method based on network tree depth for radial distribution systems. *Journal of Electrical Systems and Information Technology*, 8.
16. Paliwal, P. (2021). Determining optimal component sizes for an isolated solar-battery microgrid using Butterfly PSO. In: *2021 1st International conference on power electronics and energy*.
17. Yadav, S. et al. (2014). Determination of appropriate location of superconducting fault current limiter in the smart grid. In: *2014 International conference on smart electric grid (ISEG)*.
18. Tiwari, S., Ansari, M., Kumar, K., Chaturvedi, S., Singh, M., & Kumar, S. (2018). Load flow analysis of IEEE 14 bus system using ANN technique. In: *2018 International conference on sustainable energy, electronics, and computing systems (SEEMS)*.
19. Javaid, B., et al. (2019). Analysis techniques for performance evaluation. In: *Conference on iCoMET 2019*. IEEE.

Sustainable Development Assessment of South Asian Countries Using Fuzzy Logic



Abhishek Tripathi, Shafaque Shaikh, Elton Noronha, Sagar Kote, Pratibha Dumane, and Satishkumar Chavan

Abstract The United Nations has given a blueprint for all the countries through the 17 Sustainability Development Goals for a more sustainable future. Sustainable Development Group publishes the sustainable development indicators for countries the world over. These indicators are complex in nature and highly interdependent. In this paper, the fuzzy inference system is used to assess the sustainable development based on economic, ecological, and societal sustainability indicators for South Asian countries. Fuzzy System, being the best approach to work with ambiguous data, provides a good degree of flexibility in assessment of SDG indicators for recommendations in achieving sustainable goals by countries under this study. The proposed work links human expectations about development with measurements of the sustainability indicators. It provides some good insights that can help these countries focus on their efforts in coming together in creating an inclusive, sustainable and a resilient future for all the beings and the planet.

Keywords Sustainable development goals · Fuzzy logic · Mamdani fuzzy inference system · South Asian countries · Sustainable policy decisions

1 Introduction

The Sustainable Development Goals or Global Goals are designed to be a blueprint to realize a far better and more sustainable future for all. In 2015, the 193-member states of the United Nations (UN) adopted the Agenda 2030. This is a universal agenda that contains the 17 goals for sustainable development [1] that integrate the social, environmental and economic aspects of sustainable development. All nations need to mobilize their efforts towards ending all forms of poverty, fight inequalities

A. Tripathi · S. Shaikh · E. Noronha · S. Kote · P. Dumane · S. Chavan (✉)
Department of Electronics and Telecommunication Engineering, Don Bosco Institute of Technology, Kurla (W), Mumbai, Maharashtra 400070, India
e-mail: satish@dbit.in

and also tackle problems arising due to climate change. It is important for each nation to be aware of its own issues so that there is optimum utilization and mobilization of its resources. In this regard, assessment of the sustainability parameters of every nation becomes a crucial factor.

The members of the South Asian countries comprise India, Nepal, Sri Lanka, Maldives, Bhutan, Bangladesh, Afghanistan, and Pakistan. These countries suffer due to poverty, sub-standard life style of people, limited growth in industrial development, etc. 21% of the world's population belongs to these countries [2]. In view of this, the global SDGs cannot be achieved if these countries do not achieve their SDGs. Although all South Asian countries consented to sustainable development, it is necessary to recommend the focus areas that each of these nations must focus on to achieve the 17 SDGs. This paper recommends various objectives derived using certain sustainable indicators with the help of fuzzy logic inference for each of the South Asian countries for a sustainable future. Fuzzy logic comes in handy for assessment of sustainability parameters as these parameters are highly inter-dependent and sometimes ambiguous.

In fuzzy mathematics, symbolic logic could also be a sort of many-valued logic in which the reality values of variables may be any real number between 0 and 1. Symbolic logic is employed in uncertain environments. The sustainability goals which are chosen have not just parameters which are not easily quantifiable but also time uncertain. The Mamdani Fuzzy Inference System is used to perform the sustainability assessment. The remaining sections of the paper are organized as: Section 2 gives various applications of the Fuzzy Inference System. Section 3 briefs about the Mamdani Fuzzy Inference Model and Sect. 4 provides the analysis of the results along with recommendations for South Asian countries. Section 5 concludes the work presented in this paper.

2 Literature Survey

A study of methodological framework for sustainability assessment is presented by Sala et al. [3] in order to address critical issues like development of novel methodologies/models, multi-geographical and temporal issues, accounting for assessment of extreme complexity and non-linearity of data, and achieving the sustainability goals. It is observed that appropriate methods are not employed by decision-makers due to the lack of systematic analysis of a problem and understanding of the available data and methods for sustainability assessment.

Zijp et al. [4] proposed an approach for selection of methods based on question articulation. The society is facing severe challenges due to global warming and climate change. These environmental issues are due to carbon emission through poorly managed manufacturing processes [5]. Pabuccu presented fuzzy logic-based approach for measurement of poverty index of households and in turn for countries. In this approach, the weighted determinants of poverty are estimated to identify the factors influencing poverty and recommendations are provided for the researchers and

policy makers [6]. Raman et al. [7] used a fuzzy inference system to estimate water quality index which was useful to classify the water-quality of rivers for public consideration. Wulf et al. [8] provided an extensive review of Life Cycle Sustainability Assessment (LCSA) with algorithmic developments and its implementation guidelines. Bottani et al. [9] presented sustainability assessment using monotonic fuzzy inference models for economic, environmental and social perspectives of industrial case study.

Sustainability assessment using fuzzy logic was proposed by Phillis and Andriantiatsaholiniaina [10] and further refined by Andriantiatsaholiniaina et al. [11], and Kouloumpis et al. [12]. This approach gives assessment of sustainability using various indicators defined for ecological, environmental and overall sustainability.

Multi-criteria fuzzy based approach was proposed by Raut et al. [13] to improve the food loss due to third party logistics providers. Permatasari et al. [14] presented classification of nutritional status for toddlers based on weight and height using Mamdani fuzzy inference system and the centroid method for defuzzification. To measure water quality and to advise water treatment for meeting the different demands, a fuzzy inference model was proposed by Raman et al. [7]. Fuzzy logic-based assessment of the urban sustainability is useful in the planning of the city's future development. Jaderi et al. [15] measured fuzzy sustainability index useful for Mahshahr, an industrialized coastal city in Iran. Dumane et al. [16] gave an overview of fuzzy based sustainability assessment tool for social, economic, and environmental parameter assessment.

Based on the literature survey of sustainability parameters and the methods used, Mamdani Model for the sustainability assessment is preferred in this work.

3 Mamdani Fuzzy Model for Sustainability Assessment of South Asian Countries

Mamdani Fuzzy Model which was proposed by Mamdani [17] is used in this paper for the sustainability assessment of south Asian countries. It has linguistic variables used as inputs to regulate the fuzzy rules based on membership functions defined for connected Key Perspective Indices (KPIs). The crisp input variables are connected with the crisp output variables with fuzzy membership functions defined using the linguistic variables.

The system consists of a fuzzification unit, knowledge domain with its inference system, and defuzzification unit as shown in Fig. 1. Crisp inputs are fed to the fuzzification unit. The fuzzification unit is responsible for converting crisp sets into fuzzy sets. The decision-making unit is responsible for the inference. The inference engine (decision making unit) makes decisions or infers with the help of a knowledge base. The knowledge base consists of a data base and a rule base. The data base includes fuzzy set definitions and parameters of membership functions and the rule base is

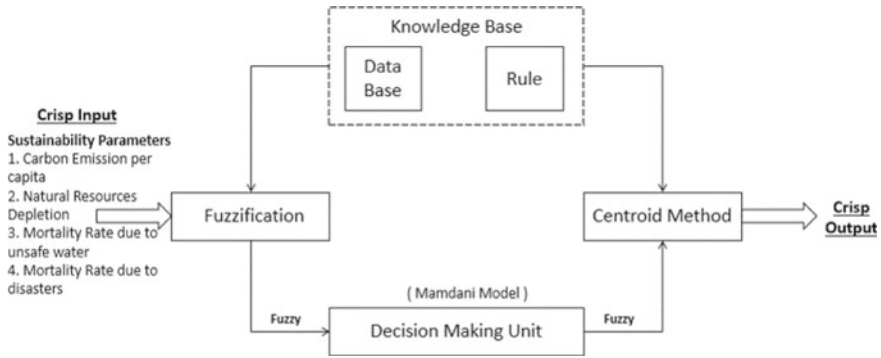


Fig. 1 Mamdani fuzzy inference system

basically a set of ‘if-else’ conditions. Here one or more antecedents eventually imply a certain number of consequents. The centroid method is used for the defuzzification. The process is summarized as follows:

1. The Fuzzification process begins with the introduction of input values and their interpretation as linguistic values which are the determined membership functions of the system variables within the fuzzy sets. Every variable is decided by the linguistic components like “Bad”, “Very Bad”, “Extremely Bad”, “Manageable”, “Good”, “Best” and “Excellent” for the inputs and output.
2. The knowledge domain consists of fuzzy rules defined with the assistance of the experts. Each row of membership functions constitutes an “IF–THEN” rule along with the “AND” operator. The inference function takes the membership degrees of the fuzzification, supported within the rule base to get the output of the fuzzy system. The output from each rule reflects these and obtains a fuzzified output by superposition of individual outputs.
3. The defuzzification process is employed to get an output from the fuzzy sets. Generally, the centroid method is commonly used for defuzzification.

4 Results and Analysis

The experimental analysis is obtained by considering four inputs viz. carbon emission per capita, natural resource depletion, mortality rate due to unsafe water and mortality rate due to natural disasters. In each case, total seven descriptors are preferred as presented in Fig. 2. In this paper, the sample set is limited to 8 South Asian countries. For a given country, there are 2041 possible outcomes. After entering a country’s name, it’s corresponding descriptors and membership value will be generated as shown in Fig. 3. Max–min inference method is used for deriving scaled membership

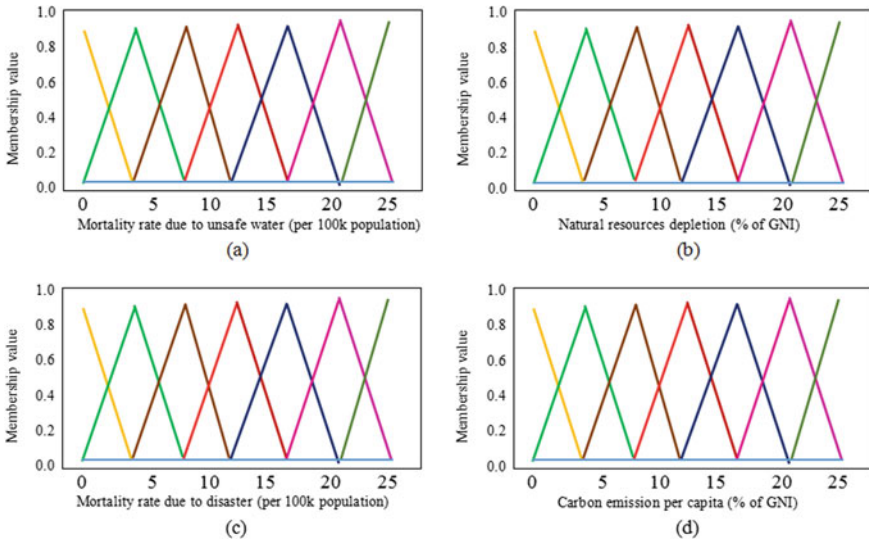


Fig. 2 Membership Functions, **a** Mortality rate due to unsafe water, **b** Natural resources depletion, **c** Mortality rate due to disaster, **d** Carbon emission per capita

function. The area obtained is used to generate a crisp value using the centroid method.

4.1 Data Used for Experimentation

The data for the selected four sustainable parameters from South Asian countries was taken directly from The UN Development Report published in 2019 [18]. The details of the used data are presented in Table 1.

4.2 Defuzzification Output

The greater the defuzzified output, the worse is the environmental sustainability. Table 2 gives the defuzzification output values generated from the proposed system for the South Asian Countries. Using these crisp values, we have recommended corrective measures leading to better sustainability of the South Asian Countries.

For example, the outputs with respect to the parameters for a country like Sri Lanka are ‘good’ Carbon Emission, ‘best’ Natural Resources Depletion, ‘best’ Mortality rate due to water, and ‘excellent’ Mortality rate due to Natural Disasters. The defuzzified value in this case comes out to be 1.29 which indicates the environmental sustainability of Sri Lanka is much better than most of the South Asian Countries.

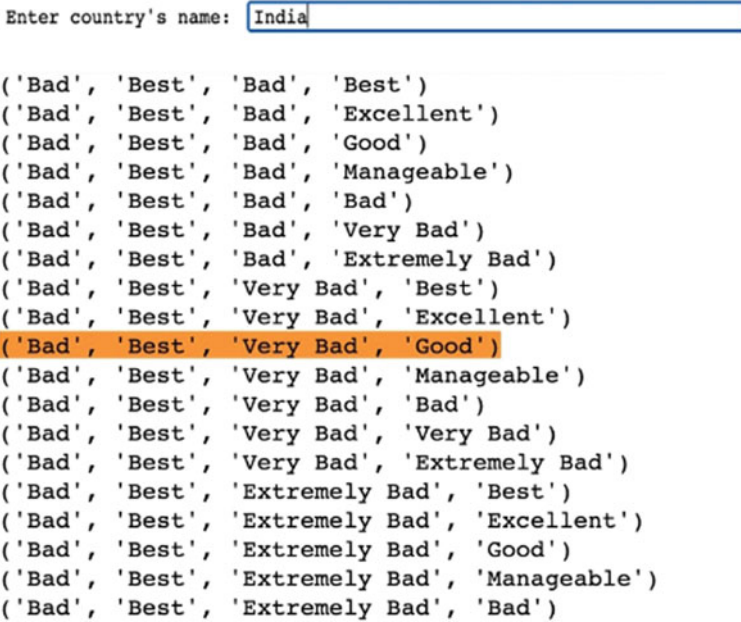


Fig. 3 Sustainable indicators for India

Table 1 Data from UNDP report 2019 used for assessment [18]

Countries/ parameter	Carbon emission per capita	Natural resources depletion	Mortality rate due to unsafe water	Mortality rate due to disasters
India	2.0	0.0	18.6	0.8
Nepal	0.3	0.3	19.8	1.9
Afghanistan	0.3	0.3	13.9	1.2
Bangladesh	0.5	0.6	11.9	0.2
Sri Lanka	1.1	0.0	1.2	0.5
Maldives	3.0	0.0	0.3	0.2
Bhutan	1.6	1.3	3.9	3.7
Pakistan	1.1	1.0	19.6	0.1

Table 2 Defuzzification output deciding sustainability index of country

Country	Maldives	Sri Lanka	Bangladesh	Afghanistan	Bhutan	India	Pakistan	Nepal
Output	00.6265	01.2936	09.3012	11.0400	13.4250	14.2800	15.3255	15.3235

Also, using the defuzzified values of various countries, we can quantify the sustainable development of a country.

4.3 Recommendations to Achieve SDGs in South Asian Countries

The experiment helped us arrive at certain recommendations for the selected 8 South Asian Countries. The country-wise recommendations are as follows:

Recommendations for INDIA

- Plant more trees and replace 30% of coal and oil usage with natural gas.
- Avoid animal farming, encourage use of public transport and reusable water bottles, use low-cost water filtration units, install water treatment plants and water wheels.
- Speak to the consumers and raise awareness.

Recommendations for NEPAL

- Encourage Rain Water Harvesting.
- Install wastewater treatment plants.
- Employ advanced techniques in structural engineering.
- Maintain vegetation on the slopes for soil retention.

Recommendations for AFGHANISTAN

- The country needs to raise education or awareness among its residents.
- Use rain water harvesting techniques and recycle waste water.
- Employ data analysis tools, develop advanced warning systems and disaster preparedness and building structures that can sustain earthquakes.

Recommendations for BANGLADESH

- Improved water sectors are needed so that people do not feel the need to directly access arsenic poisoned ground water by digging wells.
- Installation of Arsenic Removal technologies.

Recommendations for SRI LANKA

- Sri Lanka seems to be doing well in terms of environmental sustainability; it may work on minimizing its carbon footprint.

Recommendations for MALDIVES

- Maldives seems to be doing wonders in terms of environmental sustainability.
- It needs to work on its carbon emission as it falls in the 'bad' range by employing use of renewable energies.

Recommendations for BHUTAN

- Tools and technologies should be introduced for (Glacial Lake Outburst Flood) GLOF management.
- Radar imaging is an extremely valuable tool for GLOF.
- Natural Disasters cannot be avoided completely, however, awareness and education with respect to natural disaster management, better anti-earthquake architecture can be implemented.

Recommendations for PAKISTAN

- Very few industries in the country have their own water treatment plants to treat waste-water and many more industries must install them.
- The Government must take stringent action against industrial effluent disposal by the factories.
- Public awareness campaigns should be started at the college, university, and community level to increase awareness about the importance of clean water.
- The rural communities must be taught how to adopt safe control methods for protecting the stored water in houses and techniques on how to disinfect water.

5 Conclusion

The new approach presented in this paper will support decisions regarding sustainable development and can be very useful for policy makers to decide on the measures to be taken in the coming years for a sustainable future for life on planet Earth. Some goals may be more urgent and important for some countries as compared to others and hence, this approach will help in assessing the sustainable development parameters using Fuzzy logic. The assessment can also help in analyzing the efforts towards sustainability and give a direction so there is a structured and focused efforts towards achieving the SDGs by 2030 as collectively decided by the UN member nations.

References

1. Division Sustainable Development. (2015, October). *17 sustainable development goals 17 partnerships*.
2. Giri, P., Karinje, P., Verma, R., JSSATE, N., & Noida, I. J. (2015). A study and analysis of challenges, achievements and hurdles faced by SAARC nations in trade integration and growth. *International Journal of Engineering Technology, Management and Applied Sciences*, 3(1), 204–215.
3. Sala, S., Ciuffo, B., & Nijkamp, P. (2015). A systemic framework for sustainability assessment. *Ecological Economics*, 119, 314–325.
4. Zijp, M. C., Heijungs, R., Van der Voet, E., Van de Meent, D., Huijbregts, M. A., Hollander, A., & Posthuma, L. (2015). An identification key for selecting methods for sustainability assessments. *Sustainability*, 7(3), 2490–2512.

5. Shi, X., & Meier, H. (2012). Carbon emission assessment to support planning and operation of low-carbon production systems. *Procedia CIRP*, 3, 329–334.
6. Pabuccu, H. (2017). Measuring poverty level of households by using fuzzy logic. *Economics and Business*, 5(9), 510–517.
7. Raman, B. V., Bouwmeester, R., & Mohan, S. (2009). Fuzzy logic water quality index and importance of water quality parameters. *Air, Soil and Water Research*, 2, ASWR–S2156.
8. Wulf, C., Werker, J., Ball, C., Zapp, P., & Kuckshinrichs, W. (2019). Review of sustainability assessment approaches based on life cycles. *Sustainability*, 11(20), 5717.
9. Bottani, E., Gentilotti, M. C., & Rinaldi, M. (2017). A fuzzy logic-based tool for the assessment of corporate sustainability: A case study in the food machinery industry. *Sustainability*, 9(4), 583.
10. Phillis, Y. A., & Andriantiatsaholiniaina, L. A. (2001). Sustainability: An ill-defined concept and its assessment using fuzzy logic. *Ecological Economics*, 37(3), 435–456.
11. Andriantiatsaholiniaina, L. A., Kouikoglou, V. S., & Phillis, Y. A. (2004). Evaluating strategies for sustainable development: Fuzzy logic reasoning and sensitivity analysis. *Ecological Economics*, 48(2), 149–172.
12. Kouloumpis, V. D., Kouikoglou, V. S., & Phillis, Y. A. (2008). Sustainability assessment of nations and related decision making using fuzzy logic. *IEEE Systems Journal*, 2(2), 224–236.
13. Raut, R. D., Gardas, B. B., Narwane, V. S., & Narkhede, B. E. (2019). Improvement in the food losses in fruits and vegetable supply chain—a perspective of cold third-party logistics approach. *Operations Research Perspectives*, 6, 100117.
14. Permatasari, D., Azizah, I. N., Hadiat, H. L., & Abadi, A. M. (2017). Classification of toddler nutritional status using fuzzy inference system (FIS). In *AIP Conference Proceedings* (vol. 1868, p. 040007). AIP Publishing LLC.
15. Jaderi, F., Ibrahim, Z., Jaafarzadeh, N., Abdullah, R., Shamsudin, M., Yavari, A., & Nabavi, S. (2014). Methodology for modeling of city sustainable development based on fuzzy logic: A practical case. *Journal of Integrative Environmental Sciences*, 11(1), 71–91.
16. Dumane, P. R., Sarate, A. D., & Chavan, S. S. (2019). Sustainability assessment by use of fuzzy logic—A review. In *Computing, communication and signal processing* (pp. 363–370).
17. Mamdani, E. H., & Assilian, S. (1975). An experiment in linguistic synthesis with a fuzzy logic controller. *International Journal of Man-Machine Studies*, 7(1), 1–13.
18. Conceicao, P. (2019). Human development and the SDGs.

Blockchain Based Supply Chain System: A Case Study of Agriculture



Pranav N. Shinde, Apoorvamegh A. Chechar, and Amol C. Adamuthe

Abstract Effective supply chain is important for all the stake holders. In recent years use of ICT based solutions have increased rapidly. Cloud based systems improved the working and are a cost-effective solution. Still, the whole supply chain with multiple intermediaries being in play is affected by the problem of introducing counterfeit agriculture products which have been of major concern. There is a need for a technology-based solution to prevent such issues and identify culprits. This paper proposed a blockchain based agriculture supply chain assimilated with decentralized application into the various nodes of the supply chain. To perform actions on a product or raw material, certain conditions associated with these products should be met. The actions performed on a product will be redirected to smart contracts associated with these products and transactions of this product will be stored in respective transaction contract. The data consisting of different product details and the backtracking of ownership records correspond to an improvement in dependability, responsibility, and better traceability. This improvement is made possible by using a signature-based event, request-response verification mechanism, and mandatory data updates every time significant computer in the agriculture supply chain.

Keywords Supply chain · Blockchain · Smart contract · Transaction · Traceability

1 Introduction

In the Indian economy, agriculture plays an important role and it affects us on a big scale. In previous years there is an increment in GDP to 20.2% and it provides employment to around 58% of the population [1]. There are many problems related

P. N. Shinde (✉) · A. C. Adamuthe
Department of Information Technology, Rajarambapu Institute of Technology, Shivaji University,
Sakharale 415414, Maharashtra, India
e-mail: shindepranav780@gmail.com

A. A. Chechar
Department of Mechanical Engineering, Rajarambapu Institute of Technology, Shivaji University,
Sakharale 415414, Maharashtra, India

to the agriculture sector such as agriculture product quality, weather forecasting, crop yield improvement, and the gap between farmer and customer. Focusing on supply chain management as it is a key area with various intermediaries and complex working where the mode of failure is more and has a lot of grey space which can be improved upon. To guarantee product safety, it is required to make a system that monitors the rise of products from the agriculture supply chain.

The emphasis on improved traceability throughout the supply chain has been refocused in light of the rising worries about contamination hazards and food safety. The series of procedures used in the manufacture and delivery of a good or service to a customer is referred to as the supply chain. Important data must be obtained, exchanged, and managed in order for items to be traceable in the agricultural supply chain and vital information must be gathered, shared, and managed. This needs accurate origin identification and multiple information exchanges that use numerous intermediaries, making them challenging to track and trace. The emergence of counterfeit products into the supply chain and the consequences for public health highlight the need for traceability as a tool for authorities to use to monitor the quality and safety of products. The existing traceability approach in the agricultural supply chain struggles greatly as administrative controls and data fragmentation makes the data susceptible to management and modification. Immediately identifying the source of contamination and removing the contaminated product from the agricultural supply chain, requires extensive cooperation between a number of parties (see Fig. 1).

As we can see, this supply chain is highly convoluted and is made up of a number of intermediates with poor traceability and no method to pinpoint the company in charge in the event of significant errors. The current agricultural supply chain is cloud-based [2]. SaaS and PaaS are used in cloud computing to suit customer needs and store all relevant data in a central location. Data is obtained by end users from an inaccessible central authority. Cloud computing’s centralized architecture alienates the supply chain by reducing product transparency and traceability. Customers or buyers find it difficult to confirm that the product complies with the standard because most aspects of the current system lack transparency. Investigating supply chain tampering when there is a suspicion of illegal or unethical behavior can be difficult, but this problem can be handled by using blockchain technology.

Blockchain being a revolutionizing solution provides a compelling and viable solution ensuring the tracing and monitoring of agriculture products with no need of centralized authority over the system. Each transaction into the blockchain is immutable, which means there is no way sensitive product information and ownership transfer data can tamper. Blockchain provides complete transparency, which also



Fig. 1 Supply chain in agriculture

brings trust between the various main entities of the supply chain, such as, producers, the processing industry, intermediaries like distributors and suppliers, and the end-users as customers. Each product within the chain can be transferred between the different authenticated entities of the chain using an event request-response mechanism. The ‘Web 3.0’ based DApp (Decentralized App) provides a sophisticated medium for the nodes in the supply chain with an ease-of-use system and highly transparent database. The React Framework is used in the development of the DApp. The smart contracts are implemented on a publicly accessible local blockchain that ‘Ganache’ offers. The Truffle framework and Web3.js are used to connect the DApp to the blockchain.

The objectives of the proposed system are

- To enable greater traceability, and safety and prevent the counterfeiting of agricultural products.
- Design a decentralized and secured system for the agriculture supply chain to identify culprits.

This paper is organized as follows: In Sect. 2 presents a literature review. Section 3 is about the practical framework for the blockchain-based tracking process. Finally, Sect. 4 is conclusion.

2 Literature Review

Numerous academics and businesspeople have conducted extensive research and conversations over the years on how to use distributed ledger technology to enhance and supervise the existing state of the supply chain.

In [3–5], authors presented a full-fledged blockchain solution, including a design plan and a common method for integrating it into corporate strategies. The suggested solution is built on the Ethereum blockchain network.

In [6–9], authors proposed a blockchain-based product monitoring system. Smart contracts are in charge of storing histories and transactions in a distributed ledger, which is then converted into a chain of blocks from which product information can be verified. Traceability is enabled by deploying example use cases on two separate blockchain systems, namely ‘Ethereum’ and ‘Hyperledger Sawtooth.’ The performance of both installations was then evaluated and compared in terms of latency, CPU use, and network utilization, with emphasis placed on their primary benefits and shortcomings.

In [10], authors developed an application-based permissioned blockchain in which only legitimate parties can participate and enroll in the blockchain network.

In [11, 12], authors developed a system linking the product deletion decision-making process with blockchain technology. It boosted communication and collaboration across diverse supply chain actors, as well as information efficiency, efficacy, and dispute resolution. The proposed Possession of Products mechanism detects if any entity is unable to demonstrate possession of a certain product.

In [13, 14], the author created a double-layer structured permission blockchain that provides better product monitoring. Introduced the double-layer structure and detailed its benefits in the efficiency of agricultural supply chain systems.

In [15], authors extended research on the study of utilization and development situation of RFID (Radio-Frequency Identification) and distributed ledger technology is being utilized to construct the agri-food supply chain monitoring system.

In [16, 17], authors worked on the analysis of recent trends and applications in distributed ledger technology. Utilize cases, constraints, and research perspectives for a translucent agri-food supply chain.

3 Practical Framework for the Blockchain-Based Tracking Process

Cloud-Based System

Cloud-based supply chain management has less traceability and accountability. The main issue that exists in an existing system is product counterfeiting. The prevalence of counterfeit agricultural goods in Indian markets reduces input quality, reducing agricultural productivity. Poor data accessibility and tamper-proofing are the faults of the centralized architecture of the current system.

Proposed System

This section mainly focuses on product traceability and system implementation. Any node can be responsible for both functions such as demand and supply. This system suggested a request-response event mechanism to guarantee that both parties to the transaction consent to accepting and delivering the product.

3.1 Smart Contract Design

Certain conditions should be met for the execution of a smart contract. There is no need for a third party for the execution of the contract.

The smart contracts written below represent roles for each entity associated with certain conditions. The actions performed directly on a product or raw material will be redirected to 'Raw Material Contract' and 'Agri Product Contract'. The transaction associated with these actions will be stored in respective 'Transaction Contract'.

Supply chain Contract: All entities are bound by this contract. This contract is deployed by the supply chain owner. A function in a smart contract can be accessed by the respective role assigned to it, helping to increase data security and availability.

Raw Material Contract: When a raw material is created, the farmer deploys the raw material contract and the resource is added to the chain. From the farmer, the

address of the farmer, date, time, address of the carrier and address of the transaction contract are required.

Agri Product Contract: This contract is deployed by the processing industry the address of the product’s raw material, the day and time, the transporter’s address, and the address of the transaction contract must all be provided by the farmer.

Transaction Contract: The deployment of the transaction contract is done axiomatically when raw material and agricultural products are initialized. The transaction hash value is 32 bytes.

The smart contract mentioned above works in the same way for use cases with different raw materials, suppliers, transporter, and distributor. The supply chain is expanded with the addition of any new entity below it and its corresponding transaction contract.

3.2 Process Flow

See Fig. 2 for the process flow in agriculture supply chain.

1. The owner deploys smart contracts on the Ethereum blockchain.
2. The chain’s entities are authenticated and registered by the owner.
3. A new raw material is registered by a farmer.
4. For a new raw material respective raw material contract is deployed.
5. For a new raw material, transaction contract will be deployed.
6. The raw material was successfully registered.

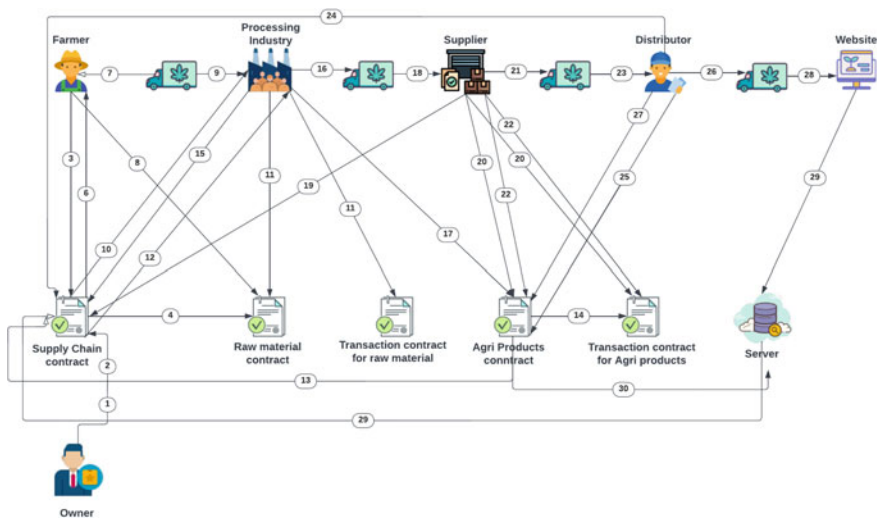


Fig. 2 Process flow in agriculture supply chain

7. The farmer delivers the raw materials to the transporter.
8. Farmer changes the status of the product and adds a transaction to the transaction contract.
9. The raw material is transported to the manufacturer by a transporter.
10. The processing industry verifies the raw materials origin.
11. The processing industry modifies the product status and adds a transaction to the transaction contract.
12. A new product is registered by the processing industry.
13. For a new product, “Agri Product Contract” will be deployed.
14. For a new product respective transaction contract will be deployed
15. The product was successfully registered.
16. The raw material is transferred to the transporter by the processing industry.
17. The processing industry modifies the product status and adds a transaction to the transaction contract.
18. The product is delivered to the supplier by the transporter.
19. The supplier verifies the product’s origin.
20. The supplier modifies the product status and adds a transaction to the transaction contract.
21. The product is delivered to the transporter by the supplier.
22. The supplier modifies the product status and adds a transaction to the transaction contract.
23. The product is delivered to the distributor by the transporter.
24. The distributor verifies the product origin.
25. The distributor modifies the product status and adds a transaction to the transaction contract.
26. The product is delivered to the transporter by the distributor.
27. The distributor modifies the product status and adds a transaction to the transaction contract.
28. The product is delivered to the customer by the distributor.
29. The customer confirms the product’s origin.
30. The customer updates the product’s status.

3.3 Product Traceability and Source Verification

Step 1: After the buyer initiates a purchase request, the supply chain contract’s buy () function is called. This function takes important inputs namely buyer address, seller address, address of the raw material to be purchased and a signature that is signed with the private key (Fig. 3).

Step 2: The viability of the signature is verified by the seller. If the verification is successful, the seller calls the respond () function, which responds to the buyer’s request along with a signature. The signature must be signed with private key of seller.

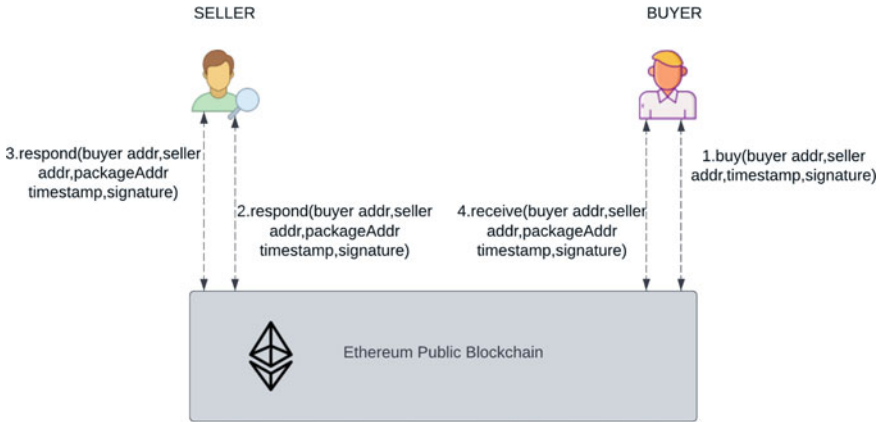


Fig. 3 Event request-response mechanism

Transactions List						
View all transactions for this Crop						
TxnHash	From	To	Previous TxnHash	Lat	Lng	Timestamp
0x0ea8b413aa7155a27ce0fa89a61d62344fa7cf160b12d4f37f128a8c8a845765	0x295f4a000518E532E807f98c85b860074cb16E07	0x60698E2D33d54534171DFFDbC0386B386eCB3833	0x0ea8b413aa7155a27ce0fa89a61d62344fa7cf160b12d4f37f128a8c8a845765	10	10	Tue Sep 27 2022 20:35:00 GMT+0530 (India Standard Time)
0xf08c3c5619b6c914ba135dc302ceef421af1f075cc35c939e933feb4b55a1f85	0x295f4a000518E532E807f98c85b860074cb16E07	0x295f4a000518E532E807f98c85b860074cb16E07	0x0ea8b413aa7155a27ce0fa89a61d62344fa7cf160b12d4f37f128a8c8a845765	10	10	Tue Sep 27 2022 21:13:26 GMT+0530 (India Standard Time)

Fig. 4 Transaction list

Step 3: The seller will hand over the goods to the buyer via a transporter. The transfer() function is called to prove that the raw material/product has been shipped.

Step 4: Finally, after the buyer receives the goods, the received () function is called to confirm that the goods have been received (Fig. 4).

4 Conclusions

Technology adoption is important to remain competitive and improve the productivity of any enterprise. Recent IT technologies such as cloud computing and blockchain have provided efficient supply chain processes. This paper presents improved blockchain based system for agricultural supply chain. The proposed system uses an event request-response verification system mechanism that increased

the transparency in the system. The proposed system is decentralized, improved data accessibility, tamper-proofing, and resistance to product counterfeiting.

References

1. <https://www.pib.gov.in/PressReleasePage.aspx?PRID=1741942>. Last accessed on 11 am, October 30, 2022.
2. Srivastava, H. S., & Wood, L. (2015). Cloud computing to improve agri-supply chains in developing countries.
3. Perboli, G., Musso, S., & Rosano, M. (2018). Blockchain in logistics and supply chain: A lean approach for designing real-world use cases. *IEEE Access*, 6, 62018–62028.
4. Shahid, A., Almogren, A., Javaid, N., Al-Zahrani, F. A., Zuair, M., & Alam, M. (2020). Blockchain-based agri-food supply chain: A complete solution. *IEEE Access*, 8, 69230–69243.
5. Borah, M. D., Naik, V. B., Patgiri, R., Bhargav, A., Phukan, B., & Basani, S. G. M. (2020). Supply chain management in agriculture using blockchain and IoT. In S. Kim, & G. Deka (Eds.), *Advanced applications of blockchain technology. Studies in big data* (vol 60). Springer.
6. Wang, S., Li, D., Zhang, Y., & Chen, J. (2019). Smart contract-based product traceability system in the supply chain scenario. *IEEE Access*, 7, 115122–115133.
7. Sivaganesan, D. (2020). Smart contract based industrial data preservation on block chain. *Journal of Ubiquitous Computing and Communication Technologies (UCCT)*, 2(01), 39–47.
8. Caro, M. P., Ali, M. S., Vecchio, M., & Giaffreda, R. (2018). Blockchain-based traceability in agri-food supply chain management: A practical implementation. *IoT Vertical and Topical Summit on Agriculture—Tuscany (IOT Tuscany)*, 2018, 1–4.
9. Alkahtani, M., Khalid, Q. S., Jalees, M., Omair, M., Hussain, G., & Pruncu, C. I. (2021). E-agricultural supply chain management coupled with blockchain effect and cooperative strategies. *Sustainability*, 13(2), 816.
10. Shrikant, P., Machhindra, P. P., & Baban, P. M. (2019). Traceability and detection of the counterfeit medicine supply chain through blockchain. Department of Computer Engineering Jaihind College of Engineering. Kuran. Vol. 21, Issue 8, November 2019.
11. Zhu, Q., & Kouhizadeh, M. (2019). Blockchain technology, supply chain information, and strategic product deletion management. *IEEE Engineering Management Review*, 47(1), 36–44.
12. Toyoda, K., Mathiopoulous, P. T., Sasase, I., & Ohtsuki, T. (2017). A novel blockchain-based product ownership management system (POMS) for anticounterfeits in the post supply chain. *IEEE Access*, 5, 17465–17477.
13. Ding, Q., Gao, S., Zhu, J., & Yuan, C. (2020). Permissioned blockchain-based double-layer framework for product traceability system. *IEEE Access*, 8, 6209–6225.
14. Leng, K., Bi, Y., Jing, L., Fu, H. C., & Van Nieuwenhuyse, I. (2018). Research on agricultural supply chain system with double chain architecture based on blockchain technology. *Future Generation Computer Systems*, 86, 641–649.
15. Tian, F. (2016). An agri-food supply chain traceability system for China based on RFID & blockchain technology. In *2016 13th International conference on service systems and service management (ICSSSM)* (pp. 1–6).
16. Vivekanadam, B. (2020). Analysis of recent trend and applications in block chain technology. *Journal of ISMAC*, 2(04), 200–206.
17. Menon, S., & Jain, K. (2021). Blockchain technology for transparency in agri-food supply chain: Use cases, limitations, and future directions. *IEEE Transactions on Engineering Management*.

ICT-Based Societal Technologies

Data Sharing and Privacy Preserving Access Policy of Cloud Computing Using Security



Dhanashri Kamble, Rajni Patel, and Prajakta Deshmukh

Abstract People admire the incredible power of cloud computing but cannot fully trust on cloud providers due to the absence of user-to-cloud controllability. The Attribute Encryption Standard (AES) is used to share and secure the encrypted file with different users. On cloud the user stores their sensitive data without direct control, so there is less security over the data. There are many chances for the hacker to consume the resources, modify the data or to corrupt the data. So, the proposed system overcomes all these issues; to keep data secure from hacker (insider/outside). We use a privacy-preserving access policy for secure communication and maintaining confidentiality for secure data access and transfer. SHA 512 is used for generating the hash function and authentication in the system. Therefore, providing security for the data sent over the internet is necessary. The owner and user of the server raise many issues without direct control. In this work, we take one middleware, the authority that verifies the user's request and gives the encryption key directly to the user via mail to obtain resources from the cloud. No one can modify data without user permission. This empowers every user and each authority specialist to claim and control their data associated with the user's documents inside a protected situation. The proposed system state that, for secret communication with the cloud. The data is given to the owner, and the hash is given to the authority. The user gets the encryption key to access the cipher text.

Keywords Cloud computing · Error localization · Erasure code · AES · Steganography · Encryption

1 Introduction

Cloud computing is used through the internet, which enables the distribution of services. Today, cloud computing is the most important concept that people advocate for the incredible power of cloud computing, but the lack of control from the user to

D. Kamble · R. Patel (✉) · P. Deshmukh
SVERI's College of Engineering, Pandharpur, India
e-mail: rpatel@coe.sveri.ac.in

© The Author(s), under exclusive license to Springer Nature Switzerland AG 2024
P. M. Pawar et al. (eds.), *Techno-societal 2022*,
https://doi.org/10.1007/978-3-031-34644-6_31

281

the cloud makes it impossible to fully trust the cloud provider. To share encrypted files with others, you can use Ciphertext-Policy Attribute-Based Encryption (CP-ABE) to enforce fine-grained, owner-centric access control. However, this is not secure enough against other attacks [1]. Malicious attackers can download thousands of files and launch EDoS (Economic Denial of Sustainability) attacks that consume a lot of cloud resources. Cloud computing concepts also include general terms such as data-as-a-service and everything-as-a-service [2, 3]. Attribute-based encryption (ABE) [4] is considered one of the most appropriate techniques for enforcing and managing data usage rights in public clouds, as it allows data owners to commit to direct control over their data. Many kinds of his ABE algorithms are currently proposed, divided into two categories: key policy attribute-based encryption (KP-ABE) [4] and ciphertext policy attribute-based encryption (CP-ABE). The benefits of cloud computing are immense, but security and privacy concerns remain major barriers to widespread adoption. While CSP infrastructure and management capabilities are far more powerful and reliable than personal computing devices, cloud platforms are still prone to media failures, software bugs, malware, administrator error, and malicious insider attacks [5, 6]. The cloud brings many advances in hardware and software applications for data management, seen in precise accessibility. However, cloud computing has many issues in terms of data security, which is one of the biggest problems in adopting data in cloud environment. Therefore, the work proposed here relinquishes data and security controls and employs several mitigation techniques against attacks. Focus on cloud data security, storage, protect system and data. We propose a strict distributed scheme against attacks.

2 Literature Survey

Combining Data Owner-Side and Cloud-Side Access Controls for Encrypted Cloud Storage [1, 7, 8]. In this paper, People recognize the incredible power of cloud computing, but the lack of user-to-cloud control prevents them from completely trusting cloud providers. To ensure confidentiality, data owners should upload data, not in plain text. To share encrypted files with others, you can use attribute-based ciphertext policy (CP-ABE) encryption algorithms to enforce fine-grained, owner-centric access control. However, this is not very secure against attackers. Here, a malicious attacker attacks the cloud, downloads thousands of files from the cloud, and launches her EDOS (denial of economic sustainability) attack that heavily consumes the cloud resources. Cloud server providers are the main players in providing services, accountants and payees for resource consumption fees and ensuring billing to owners. This work applied security to cloud storage using the CP-ABE algorithm to mitigate EDOS attacks [1]. Application of Digital Signatures with User-Authenticated Cryptographic Algorithms for Data Security in Cloud Computing [2, 9]. Cloud computing is used over the Internet to share software information and resources with the world [2]. Share resources for all servers and all users independently. This digital signature uses user authentication of secure data using the cloud computing digital signature

encryption algorithm. This allows you to keep your information in the cloud, handle all your sensitive data, and keep all your documents safe with digital signatures, as all important documents that are signed are not physically secure. You can do this by using a cryptographic algorithm that shares a key with both the sender and receiver. We have applied security to your data based on the internet using encryption algorithms RSA, AES, SHA. To protect against attackers, use encryption and encryption algorithms [2, 10].

TMACS: A Robust and Verifiable Threshold Multi-Authority Access Control System in Public Cloud Storages [4]. In this work, Attribute-Based Encryption (ABE) was used as the best algorithm and performed directly by the data owner. We guarantee the tools to You are promised control over your data in public cloud storage. TMACS (Training and Management Access Control) is a system that is not only proven to be secure, but also robust when permissions are active within the system. It uses the ABE and CP-ABE encryption algorithms to maintain the entire attribute set, creating a single bottleneck in both security and performance. After that, several systems with some powers have been proposed. In this system, permissions manage separate sets of disjoint attributes. TMACS is a system that satisfies attribute schemas from various agencies and provides robustness at the security and system level [4]. DDoS/EDoS Attacks in the Cloud: It Affects Everyone [11, 12]—DDoS attacks have recently become malicious attacks. This is a direct attack on the cloud, consuming all resources and causing economic loss. Her next DDOS attack is the EDoS (denial of economic sustainability) attack. Direct impacts of these attacks on other stakeholders include service disruption, web service performance, resource contention, indirect EDoS, downtime, and business loss [11]. A distributed denial of service (DDoS) attack is a targeted attack against a victim server being attacked cooperatively or uncooperatively by a large number of service requests from a group of distributed clients/bots. This is typically achieved by targeting one or more basic server resources such as CPU, memory, disk, and bandwidth.

For example, the number of TCP connections. It was used to understand the impact of DDoS/EDoS attacks in the cloud [11]. E. Public Cloud Security Challenges [5] Cloud computing is the latest term for the long-awaited vision of computing as a utility [13]. The cloud offers flexible on-demand access control, policy and security. Cloud computing has many security issues. Identifying the attacker is very difficult. The attacker's location could be an insider, an outsider, or a malicious attacker. It attacks the cloud, subverts all security and consumes resources without permission. CSP also grants access without knowledge of existing users. While this is a critical security challenge, here the authors outline some critical security challenges to motivate further exploration of security solutions for trusted public cloud environments. There are many problems with cloud computing in data security, one of the biggest problems in adopting data from the cloud. Since the storage takes place on the cloud service provider's servers, it poses security concerns. This means less control over stored data. Therefore, several applications are used in this document, including computational outsourcing security, access control, data service outsourcing security, multi-tenancy security and privacy, and security overhead. Security and privacy are fundamental obstacles to the success of cloud computing [5, 14, 15].

3 Proposed Methodology

3.1 Architecture

Our hypothesis is that huge numbers of these issues are because of an absence of direct control by owner and user over the innovation that serves them. Using Registration form user register in a system to login, Select file for uploading into a cloud (Private/Public) encrypt file using AES Check Authority Permission for uploading a file or not. If authority given permission to user for uploading then enters the encryption key which is sent by authority and upload a file on selected cloud data owner can download his own file without authority permission. If user is not data owner and he want to download the other user uploaded file then he must be give the authority permission first. If authority given permission to user for downloading the file, then user enters the decryption key which is sent by authority and download a file (Here we use AES Decryption Technique). User also checks the server or cloud is misbehaved with his uploaded file or not. Every time after logout the user account password will change using random password generation technique.

User: Want access from cloud for that user need to take permission from owner, if owner give permission authority generate encryption and decryption key and give access to user.

Cloud Service Provider (CSP): Provide the resources/data to the user who satisfies all the policies of cloud.

Authority: View users files encryption request verify that request and send encryption key to user for upload the file, view users decryption request send encryption key and OTP to user for download the data/file.

Cloud data storage: User store their data by cloud server provider on public/private cloud so less control on their data. But we cannot fully trust on CSP for that we apply strong security and without the authorities and data owner's permission no one can modify, download, or upload data on cloud.

Adversary section: Cloud data storage security alerts can come from two different sources. On the one hand, cloud service providers (CSPs) can be selfish, trustworthy, and sometimes repugnant. It can also try to cover data loss due to administrative errors, Byzantine failures, etc. On the one hand, the economic motivation of being able to compromise multiple cloud data storage servers at different time intervals and subsequently modify or delete user data There may also be enemies with There are two types of opponents with special abilities.

(a) Weak

An adversary that destroys a user's original data stored on individual servers. Once a server is hijacked, an attacker can modify or insert their own malformed

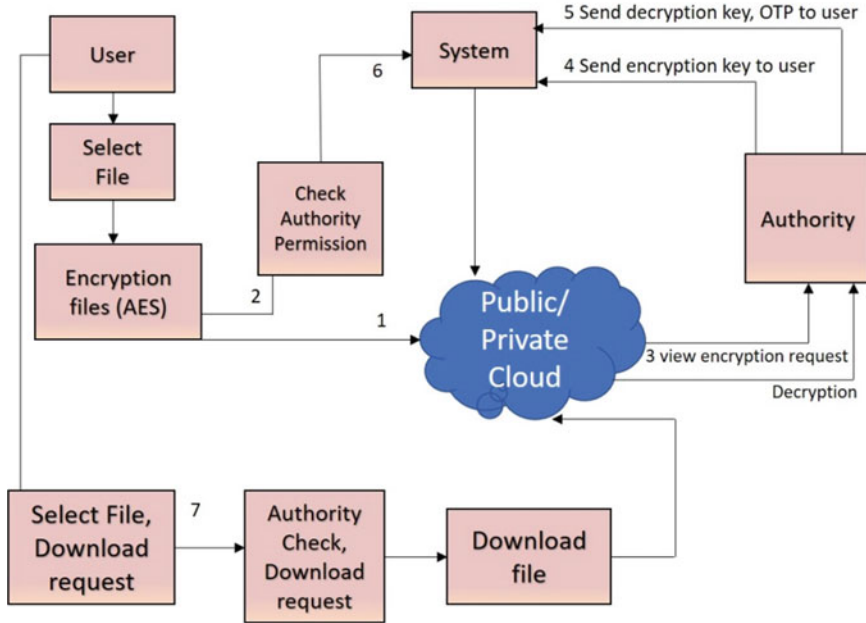


Fig. 1 Proposed architecture

data to corrupt the original file and prevent users from retrieving the original data.

(b) Strong

Attackers (strong versus weak). An attacker has compromised all storage her servers and assumes that they can deliberately modify data files as long as they are internally consistent. This addresses cases where all servers work together to cover up data loss and fraud incidents (Fig. 1).

3.2 Flow Chart for Login

In Fig. 2 if user want the access from cloud they must be register with server. when user register on system he gets the access permission from authority. For upload and download the data authority give the encryption key on users mail, so here we mitigate the attack and if server get cheated with user we get the message from system that your file get corrupted or someone modify your documents. and if new user wants to resister, he gets access. If hacker want to hack data before that authority check/verify the user and if the user is valid, user get access and connect with server. If invalid he cannot proceed for the further process.

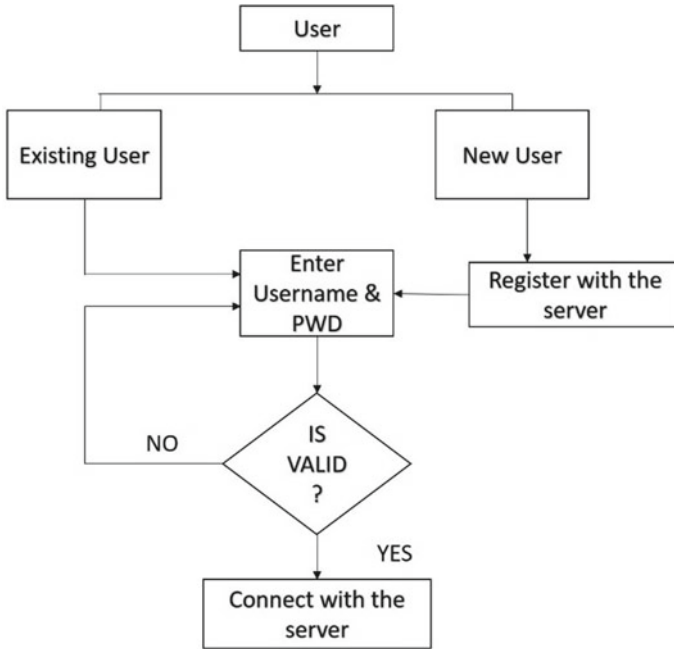


Fig. 2 System flow chart

3.3 Equation

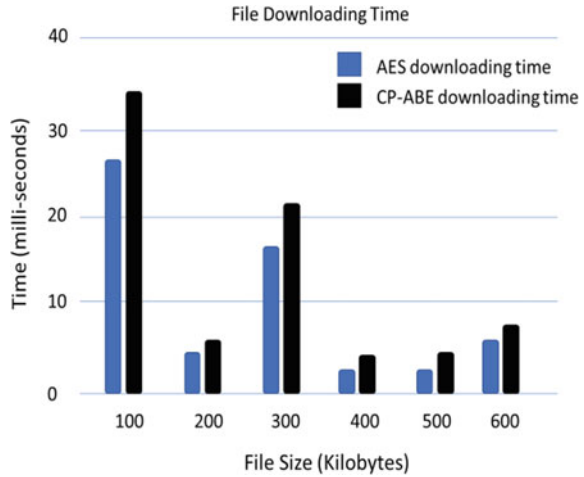
We use AES algorithm in that it generate a matrix and round made by parts: s-box, linear diffusion, sub key addition.

$$0 = W_0 + P + K_0$$

$$0 = W_i X_{i+1} \quad i \in \{0, 1 \dots 0.9\}$$

$$0 = M_B \cdot X_{i-1} + W_i + K_i \quad \text{for } i \in \{1, 2 \dots 0.9\}$$

$0 = M'_B \cdot X_i + C + K_i P$, $C \in B$ be the plaintext and cipher text, $W_i X_i$ be the state in round i before inversion, K_i be the round key assume each byte in X_i is never zero for each i .

Fig. 3 Upload time

4 Result and Discussions

In Fig. 3 The user uploads their documents in the form of text, doc or pdf on cloud three times. Time is shown in milliseconds (ms), and the file size is shown in a kilobyte(kb). The result shows the comparison of AES and CP-ABE. AES is faster than the Cp-ABE.

4.1 Download Time

Figure 4 the graph shows the downloading time. In this work, we can upload documents, files, sensitive data, and private data on the public/private cloud. So, the result changes the database's size, shown in (ms). Result changes with document length. In this proposed system users securely upload their documents in the form of text, doc or pdf on the cloud. The graph shows file downloaded by user three times. Time is shown in milliseconds (ms), and the file size is shown in a kilobyte(kb).

4.2 Communication of File Attack

In Fig. 5 we can see the uploaded text file and check the attacks on file. In this graph, we check the files and whether the file gets modified or not. If the file gets modified, the server sends the user that your file is not safe.

Fig. 4 Download time

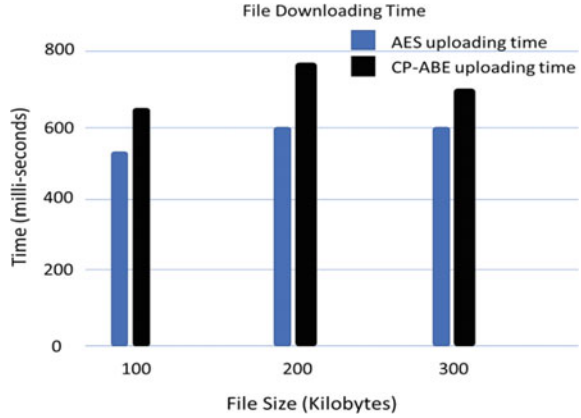
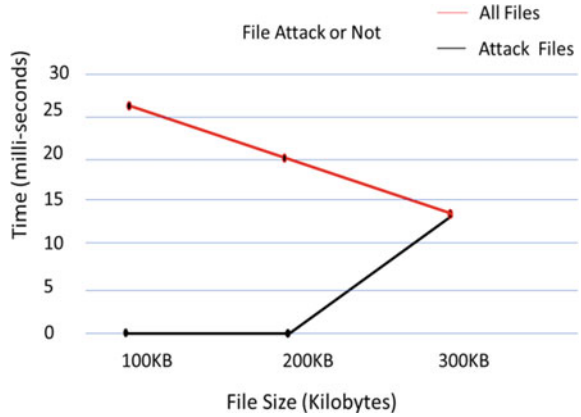


Fig. 5 File attack communication



5 Conclusion

In this paper, a new secure cloud system is presented. We have used encryption techniques and applied strong security against the attacker. We have used AES for encryption and decryption, which generates a random password for system security and SHA512 for key generation and authentication. In our attack mitigation, we check the attack on file and find the location of errors. No one can get access without the permission of the authority. The proposed system is faster, efficient as compared to the previous work.

References

1. Xue, K., Chen, W., Li, W., Hong, J., & Hong, P. (2018). Combining data owner-side and cloud-side access control for encrypted cloud storage. *IEEE Transactions on Information Forensics and Security*, 13(8), 2062–2074.
2. Sivasakthi, T., & Prabhakaran, D. N. (2014). Applying digital signature with encryption algorithm of user authentication for data security in cloud computing. *International Journal of Innovative Research in Computer and Communication Engineering*, 2(2), 456–459.
3. Zhang, Q., Cheng, L., & Boutaba, R. (2010). Cloud computing: State-of-the-art and research challenges. *Journal of Internet Services and Applications*, 1(1), 7–18.
4. Li, W., Xue, K., Xue, Y., & Hong, J. (2015). TMACS: A robust and verifiable threshold multi-authority access control system in public cloud storage. *IEEE Transactions on Parallel and Distributed Systems*, 27(5), 1484–1496.
5. Ren, K., Wang, C., & Wang, Q. (2012). Security challenges for the public cloud. *IEEE Internet Computing*, 16(1), 69–73.
6. Zhou, L., Zhu, Y., & Castiglione, A. (2017). Efficient k-NN query over encrypted data in cloud with limited key-disclosure and offline data owner. *Computers & Security*, 69, 84–96.
7. Hu, S., Wang, Q., Wang, J., Qin, Z., & Ren, K. (2016). Securing SIFT: Privacy-preserving outsourcing computation of feature extractions over encrypted image data. *IEEE Transactions on Image Processing*, 25(7), 3411–3425.
8. Sun, H. M., Chen, Y. H., & Lin, Y. H. (2011). oPass: A user authentication protocol resistant to password stealing and password reuse attacks. *IEEE Transactions on Information Forensics and Security*, 7(2), 651–663.
9. Waters, B. (2011, March). Ciphertext-policy attribute-based encryption: An expressive, efficient, and provably secure realization. In *International workshop on public key cryptography* (pp. 53–70). Springer, Berlin, Heidelberg.
10. Bhagyoday, R., Kamani, C., Bhojani, D., & Parmar, V. (2019). Comprehensive study of e-health security in cloud computing. *International Research Journal of Engineering and Technology (IRJET)*, pp. 1216–1228.
11. Somani, G., Gaur, M. S., & Sanghi, D. (2015). DDoS/EDoS attack in cloud: Affecting everyone out there! In *Proceedings of the 8th international conference on security of information and networks*. ACM.
12. Sqalli, M. H., Al-Haidari, F., & Salah, K. (2011, December). Edos-shield-a two-steps mitigation technique against edos attacks in cloud computing. In *2011 Fourth IEEE international conference on utility and cloud computing* (pp. 49–56). IEEE.
13. Chaitra, K. M., Tiwari, S., Bhardwaj, P., & Sharma, T. Authentication mechanisms for preventing cyber crime and providing security in cloud.
14. Yu, S., Wang, C., Ren, K., & Lou, W. (2010, March). Achieving secure, scalable, and fine-grained data access control in cloud computing. In *2010 Proceedings IEEE INFOCOM* (pp. 1–9). IEEE.
15. Feng, B., Ma, X., Guo, C., Shi, H., Fu, Z., & Qiu, T. (2016). An efficient protocol with bidirectional verification for storage security in cloud computing. *IEEE Access*, 4, 7899–7911.

Applications of Machine Learning in Automotive Verification and Validation: A Review



Shakti Chavan

Abstract In more aspects of daily life than one may think, the use of machine learning (ML) is widespread. More decisions are being made using solid evidence as a result of the use of ML in research, technology, and business. It is one of the technological sectors that is expanding the fastest right now in a variety of industries, for example manufacturing, health care, education, financial modelling, policing, and marketing. Data science, statistics, and computer science all converge in machine learning (ML) (Jordan and Mitchell in *Science* 349:255–260, 2015). ML's potential to transform Automotive Product Development Process (PDP) cannot be overlooked. Though ML in the automotive industry typically linked to self-driving or autonomous cars, there are many other applications behind the scenes. The use of ML techniques in PDP improves the effectiveness of numerical solutions by fusing them with human intelligence. The agility needed in the PDP due to ever changing customer expectations can be achieved with smart deployment of the ML systems. Automotive Verification and Validation (V&V) is a complex process involving a number of lengthy tasks requiring expertise. Human inaccuracy at any stage in the development could lead to flawed engineering decisions. ML tools could assist engineers to make accurate, robust and timely engineering decisions. In this paper the examples of ML implementation specific to V&V process are discussed. These examples should give a general though process for enthusiasts in this area. A concise summary of the fundamentals of Machine Learning concept and related terms is discussed in the beginning to make the readers familiar with the basic concept behind ML. The common stages needed to create a Machine Learning model through DNN beginning with scratch are listed in a typical ML workflow that is presented.

Keywords Automotive product development · Verification and validation · Machine learning · Artificial intelligence applications

S. Chavan (✉)
Wayne State University, Detroit, MI, US
e-mail: shakti@wayne.educom

1 Brief Overview of Machine Learning (ML)

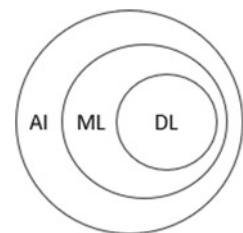
In this section, pertinent terms and concepts related to machine learning (ML) and its sub-disciplines are explained for the readers' familiarity [19]. More details can be found in [7].

Artificial Intelligence: AI is a sub-discipline belonging under computer science which emphasizes developing machines that can carry out responsibilities that typically call for human intellect. According to Jakhar and Kaur [17], it could be interpreted broadly like the human intelligence is incorporated into the hardware. Deep learning (DL), machine learning (ML), and deep neural networks (DNN) are terms that are frequently used interchangeably. The other two ideas are a subset of AI, which is typically thought of as a broader term (Fig. 1).

Machine Learning (ML): All methods that enable machines to infer information from data without explicit programming are referred to as machine learning (ML). It is a method for putting AI into practice [17]. By using the provided data, ML aims to give machines the ability to learn and make logical predictions. An output is produced by a traditional computer program by applying inputs and predetermined rules. However, the rules in ML are automatically created by the algorithm from the input data. For instance, using weather data from the previous week, the ML algorithm can predict the weather for the coming days or weeks with no any further information. An additional example is image identification program that uses a machine learning model that has been educated on a database of living thing images and can recognize images of different animals. There are numerous machine learning algorithms, and the number keeps growing every day. Various ML algorithms are described in detail in [4].

Deep Learning: DL is the branch of machine learning or method meant for applying ML. The subsequently stage of ML is DL. The information dispensation patterns established into human brain serve as the inspiration for DL algorithms. It uses algorithm & computational model with the aim of mimic the structure of the biological brain neural networks [17]. DL algorithms can be educated to carry out the similar tasks for machines similar to how our brains categorize various information's types and identifying patterns [13]. Since the majority of Deep Learning (DL) techniques make use of neural network architectures, they are frequently referred to like Deep Neural Networks. Additionally, they are referred to as Artificial Neural Networks

Fig. 1 AI, deep learning and ML scope



(ANN). The number of the network’s hidden layers is indicated by the term “deep.” A DNN model is made up of a network of artificial neurons that are connected together. The nodes connected by edges function similarly to the synapses in a biological brain that transmit signals to other neurons. Layers are collections of nodes. Every node analyzes signal it receive before sending them to other nodes it is connected to. Each link between the nodes has a weight attached to it. The significance of the input value is dictated by this weight. The output signal’s strength is altered by the weight. The term “activation function” refers to a threshold that nodes may have that prevents a signal from being sent unless the aggregate signal crosses it. In order to change the result, the activation function regulates how far the signal advances through the network. Different layers may transform their inputs in different ways. Signals move through the layers, possibly more than once, before moving through the output layer and into the input layer. Figure 2 depicts DNN architecture with two unseen layers, each with 5 nodes, plus an input layer, which has three nodes, output layer, and 1 node.

Supervised and Unsupervised Learning: Machine Learning, ML algorithms will be divided in two categories: supervised learning as well as unsupervised learning. With a datasets of feature values and corresponding target label, supervised learning algorithm is educated. Dataset with feature but no linked target label is used to train algorithms for unsupervised learning. According to Goodfellow et al. [13], such independently model the data’s underlying distribution or structure. The unsupervised learning form, for instance, can be educated using client purchase data to categorize them according to their purchase habits. According to Goodfellow et al. [13], supervised learning issues will be further divided into Regression and Classification types. While categorical response values are predicted for classification problems, continuous reaction values predict for regression-type problems (Fig. 3). The output

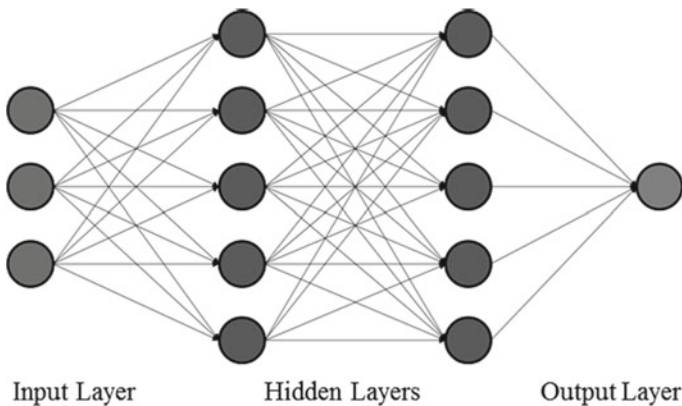


Fig. 2 An architecture for deep neural networks

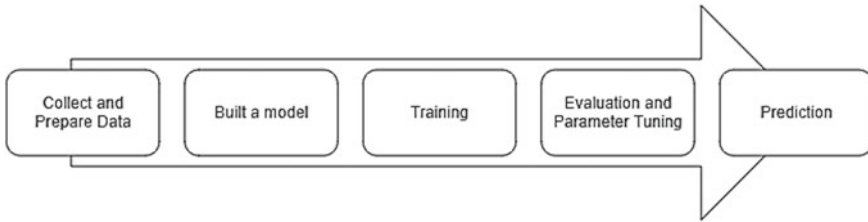


Fig. 3 A representation of ML model workflow

variable in a regression difficulty is a continuous or real value, for example forecasting a person's age. In contrast, the output variable in a classification problem is a category or else categories, like guessing whether the picture be of "a dog" or else "a cat."

AI Tools and Frameworks: There are several user-friendly, open-source DL frameworks that are available with the goal of making it easier to implement intricate and extensive DL models. Popular frameworks include Scikit-Learn, TensorFlow, and PyTorch, to forename a few. Because TensorFlow is adaptable and will be unaccustomed communicate a broad range of Machine Learning-ML algorithms, with data processing and investigation algorithms intended for DNN's model, it is chosen for this study. It offers a line for express Machine Learning-ML algorithms as well as an execution accomplishment. In numerous branches of computer science and further disciplines, such as speech recognition, robotics, geographic information extraction, information retrieval, computer vision, natural language processing, computational drug discovery, and TensorFlow have been used for research and for the deployment of machine learning systems into production [1].

2 Workflow for Machine Learning

Building mathematical models to study from the information and formulate predictions is a core of machine learning. The general steps needed to create a DNN-based ML model from scratch are listed in this section. A typical ML system outline is shown in Fig. 4. For further details readers can refer [7].

Gathering and preparing data: The effectiveness of ML systems is governed by the type and quantity of training data [12]. Data may be in any format, like pictures, comma-separated values, audio files, and many more, depending on the study's goals. To comprehend the relationships between the features, the input information must be further analyzed. Additionally, it needs to be cleaned to get rid of anomalies and unidentified entries. To prevent any learning bias, it be a high-quality idea to make the input data random. Depending on the type of data, additional form of adjusting

and management, like normalization and rectification of outliers, can moreover be carried out. Typically, the most of the data used as input are used to instruct a model (also known as education data) and the remaining data are used to estimate the model.

Selecting a model: The subsequently step is toward choose the suitable DNN architecture in favor of the difficulty. It is challenging to suggest a single kind of architecture which solves every kind of problem because the selection of a network varies on the issue at hand. An optimizer, a loss function, layers, and nodes make up the majority of a DNN model. In the section titled “DNN model setup,” these components are described. Usually, the best model for a particular problem requires some experimentation with various architectures.

Training: A significant component of the ML system is the training procedure. The model’s capacity for prediction is incrementally enhanced using the input data in this step. For some randomly initialized features, the model makes a prediction of the output before comparing it to the genuine values. Weights were afterward adjusted to reduce the prediction error. The cycle is repeated until the desired number of steps has been reached or an optimal solution has been found.

Assessment and parameter estimation: To see how the model would perform in practice, fresh or previously unexplored data can be used to test it. To determine the model’s performance, an estimate metric called Mean Absolute Errors were employed. By adjusting model parameters like the number of nodes, number of layers, loss function, learning rate, activation function, optimizer, and epoch, the model may be improved even further. These parameters, also known as hyper-parameters, control a model’s precision and training time. The problem determines the selection of evaluation metrics and hyper-parameter values.

Prediction: a computer algorithm’s result that has been educated on past data and then useful to fresh data to estimate the probability of result is referred to as a “prediction.” In the new dataset, the educated model will create likely values for target labels that are unknown. The value of the ML model is finally realized at this stage of the procedure. To produce the predictions, the evaluated model be retained and can be used again.

3 Automotive Product Development Process (PDP)

The management of the automotive PDP’s product development process is a complex process that calls for ongoing oversight and interaction based on the exchange of data and information [9, 26]. The high levels of design and process complexity leads to challenges within and between technical, organizational and process areas. The automotive PDP involves multiple simultaneous development phases referred as specific quality gates. Each phase provides the targets that must be met in order to enter the next gate. The process of developing a new program typically spans over three years from concept to launch. The development timeline depends on

scope of the program. For example, a completely new platform needs longer time over redesigning/refreshing a vehicle or a power train. Most product development process can be defined with five generic phases [8]. One or maybe more concepts are created and tested during concept development. The concept describes form, function, and characteristics of a product. The succeeding phase defines systems design and the overall automobile product architecture. The detail design phase complements system-level design phase. The vehicle's specifications are developed to production level during this phase. Testing and refinement phase is done in Verification and Validation (V&V) phase according to the set requirements. The start of production phase is the official product launch phase. Appendix A shows a generic development process with milestones and key activities in each phase [5].

4 Challenges of Product Development Process (PDP)

The automotive industry is undergoing the most profound change in its history after a century of gas-powered vehicle invention. Decarbonization, electrification, digital connectivity and a shift to sustainable fuels are changing the meaning of mobility [16]. The customer demands have been shifted to things such as autonomous-driving features, personalized experience, clean fuel from just fuel economy and luxury. The goal, according to Herlt and colleagues, is to incorporate digital services into an automotive ecosystem that goes far beyond the typical car and provides an experience similar to a smartphone. Additionally, Asia is continuing to gain importance in both global and local markets [20]. Globalization is a strong and undeniable economic force. It carries several unintended consequences but also benefits. The material availability, skilled workforces, technological innovation to meet the new trends is also crucial factors of global economic development. Globalization is must to build cars at a sustainable cost. It mandates that all market participants establish intricate engineering networks with partnerships and global and regional hubs. Hence, today the automotive business opportunities remain in creating efficient, sustainable, connected mobility solutions. Integrating more sustainability into business processes is becoming increasingly important for companies [27]. The car manufactures must do significant changes the way they innovate, develop and manufacture the product to remain competitive. The competence of companies to respond, however, is associated with adequate investments to research and development. Objective of an automotive development process is to build up the vehicle as speedily as likely, by utilizing the invested assets as capably as possible and to match or exceed the customers' expectations [2]. These objectives are linked to the timing and magnitude of the resulting cash flows, which are related to the efficiency of the automotive development process. These goals are neither independent nor inflexible. It is challenging to achieve high product reliability across the development processes due to the growing product complexity brought on by more product variants, sophisticated electronic systems, and complex distribution functionality. All of this could cause downstream disruptions to the development process at almost all the levels. Such unexpected disruptions

can have a major effect on the budgets and schedules of the PDP. For example, a disruption to a design and validation process is also one of the common causes for “Automotive Recalls” that are threatening profitability of the automotive industry. Tens of millions of vehicles are recalled every year in the U.S. to repair a wide range of issues, such as faulty headlights, windshield wipers, serious problems that could cause a fire or crash. The United States (U.S.) National Highway Traffic Safety Administration (NHTSA) have been issued 300 recalls for major car manufacturers in 2022, affecting millions of vehicles [10].

To meet the ever-increasing pressure to cut costs while enhancing efficiency, quality, and compliance with ever-stricter regulations, automakers must develop innovative new methods for designing and developing cars. Automakers anticipate that ML will enable them to overcome some of the new difficulties. ML can assist automakers in creating, producing, and selling vehicles more successfully and efficiently. By lowering accidents and enhancing driver safety, ML is becoming an increasingly significant factor in making cars safer. In order to identify and avoid potential road hazards, advanced driver assistance systems (ADAS) and fully autonomous driving systems use deep learning (DL) to process data from sensors and cameras. Connected cars, which help to increase vehicle performance, efficiency, and safety, are another example of how AI is being used in the automotive sector. ML can also lower the cost of creating and maintaining automobiles. For instance, Volkswagen is utilizing ML to create a system that can detect manufacturing flaws in auto parts. The objective is to up to 30% lower the cost of repairs [3]. Predictive maintenance can also benefit from the use of ML. Data from sensors is used in predictive maintenance to foretell when a car will require maintenance. After that, maintenance can be planned in advance of the issue [3].

Efficient V&V processes are for confirming that a product meets defined specifications and fulfills intended purpose. It is one of the time consuming and expensive phases in PDP. The development time signifies the efficiency, while the robust performance matrix signifies the effectiveness of V&V. ML technology can assist the engineers to establishing an efficient and powerful V&V process to meet the needs of new PDP. There are never-ending opportunities meant for the engineers to progress the conservative V&V by integrate ML techniques into the process. In the following examples of ML implementation specific to V&V process are discussed.

5 Machine Learning (ML) Application in V&V

The potential for ML systems to merge human intelligence through numerical solution could lead to extra reliable answers to a specific difficulty. They may lessen the need for human labor in a number of engineering development fields. The use of ML in V&V could reduce the need for human intervention, making simulations more accurate and quick. The PDP has demonstrated the potential of ML to support knowledge extraction, particularly in the early stages when important decisions need to be made. Then objective of this manuscript is to give readers a general overall

view of application of AI in PDP. More specifically ML implementations related to V&V are discussed. These examples provide the opportunity to assess the current state of ML implementation in V&V. They also show a general thought process of systematic deployment to solve some of the trivial problems in V&V.

For businesses to succeed, new product development (NPD) is essential, and it requires the right decision-making approach. To ensure that limited resources are allocated effectively, difficult choices must be made between incremental NPD strategy and radical NPD strategy, referred to as a binary NPD strategy [29]. An evaluating indicator system was created by Xie et al. [29] to determine the best approach for binary NPD forecasting. The empirical findings on actual OEM data show that the hybrid ensemble machine learning (HEML) method RS-Multi Boosting has exceptional forecasting performance with the small datasets.

Human imagination continues to be a key component of creative concepts and solutions. Machine learning-based concept generation research is still in its infancy. Text mining was used by Zhang et al. [31] to extract design concepts from design documentations and group them into sets of related designs. A framework that can design and potentially generate concept attributes based on the specified design objectives was proposed by Hein et al. [15]. The Gödel machine, a reinforced machine-learning framework, was integrated by the authors with a formal computational creativity framework.

Characterization of the mechanical properties is essential for Finite Element Analysis (FEM) which is one of the important tools used in V&V. The material properties are required to design and develop tools as well. Xie et al. [29] developed a DL model, to predict mechanical properties of industrial steel sheet including yield strength, ultimate tensile strength, elongation, and impact energy. The tuned DNN model was deployed in the real-steel plant for online monitoring and control of steel mechanical properties, and to guide the production of targeted steel plates with tailored mechanical properties. Convolutional Neural Network (CNN)-based methods to predict stress fields in solid material elastic deformation were presented by Nie et al. [22]. The precision of the constitutive material models determines how well forming operations can be simulated using FEM. The accuracy of a constitutive model is always constrained to its predefined mathematical formulation. ML techniques could be used to overcome FEM limitations. Gaspar & Andrade-Campos [11] discusses a concept that replaces the classical FEM formulations by ML techniques for the material behavior definition in forming simulations to improve the accuracy of a constitutive material model. The proposed model uses Artificial Neural Network (ANN), trained using virtual material simulations, whose behavior is reproduced by a classical Chaboche-type ‘elasto-viscoplasticity’ model. The ML model is introduced into a FEM tool as a user subroutine, to solve more complex strain states. Quan et al., [23] also used an ANN model to predict residual stress and distortion in the cast aluminum component. A multilayer feed-forward ANN model were trained and verified using FEA residual stress and distortion predictions together with part geometry information such as curvature, maximum dihedral angle, topologic features including node’s neighbors, as well as quench parameters like quench temperature and quench media.

To guarantee durable designs and avoid excessive product recalls vehicle durability testing is an integral part of V&V. Jang et al. [18] discusses feasibility of a machine-learning algorithm to strain-history prediction and durability evaluation of automotive components. The paper provides detailed information of the strain-history extraction process. It was suggested that the data ranges for ML training be larger than that in real application to minimize discrepancies around peaks. Additive materials could find applications in future vehicles. They have a unique property prediction challenge in the form of surface roughness effects on fatigue behavior of structural components. Hanlon et al. [14] employed a DNN model to predict low cycle fatigue life in additive materials to overcome computational resource challenges faced by traditional FEM.

Noise, Vibration, and Harshness (NVH) is the study of the noise and vibration characteristics of vehicles. NVH characteristics are crucial for a comfortable ride. Song et al. [25] proposed a process for NVH assessment of a vehicle by using data analysis and machine learning that utilizes long-term NVH driving data. The authors claim that proposed technique can accurately identify relationships between vehicle systems and NVH factors. This technique reflects the nonlinearity of dynamic characteristics using big data, which was not considered in existing methods. The proposed method claimed to quickly identify areas that need improvement, reduces vehicle development time, and improve efficiency. Mandal et al., [21] used ML approach to automate the vibration rating process of the engines equipped with Dynamic Skip Fire (DSF) calibration process delivering commercial NVH performance. Engines equipped with DSF technology generate low frequency and high amplitude excitations that could lower vehicles drive quality if not properly calibrated. A machine learning technique is utilized to accelerate the calibration effort. The automated vibration rating process can predict vibration rating for specific input power-train parameters coupled with driving conditions.

Crashworthiness simulations are very important during the development process to design a safe structure. Conventionally, dynamic nonlinear transient simulations are done using FEM which obtain an approximate solution to a group of problems governed by Partial Differential Equations (PDE). Chavan and Hor, [7] implemented an alternative or a supplemental tool to conventional FEA methods to accelerate and augment design decision making and briefed an overall process to set up the Machine Learning (ML) model using TensorFlow and Python libraries. Using machine learning (ML), a problem involving an elasto-plastic impact was solved. In order to predict the maximum axial displacement or the axial crush of a tube subject to impact loading, a DNN model was created using a dataset of 1000 records from an LS-DYNA-based FEA simulation. The DNN model was trained using 80% of the data, and the remaining 20% was used to test the model. The prediction accuracy of the trained model was then evaluated using a dataset that had not yet been seen. The results of the finite element simulation were contrasted with the output of the DNN model. The developed model displayed a respectable level of prediction accuracy.

Modern cars have advanced and developed significantly thanks to computational fluid dynamics (CFD). Engineers can predict and examine fluid flow around a vehicle or component using this computational technique. Use of ML in CFD enhances the

process of designing components, assemblies, and vehicles. The non-linear association between different vehicle design, operation, and aerodynamic performance parameters can be discovered and predicted using DNN [28]. DNN was used to create the mapping between the adjoint vectors and the local flow variables by Xu et al. [30]. A transonic drag reduction of the NACA0012 airfoil is used to test the generalizability of DNN's ability to predict adjoint vector with efficiency. The authors found that the proposed DNN-based adjoint vector method can achieve the same optimization results as the traditional adjoint method with insignificant computational cost. Uddin et al., [28] built a DNN with the back-propagation algorithm to establish a relationship between tire design parameters (groove depth and groove width), operational (temperature and velocity), and aerodynamic performance parameters (coefficient of drag and coefficient of lift). The authors used Reynolds-averaged Navier–Stokes equations-based Realizable K- ϵ model to analyze the variations in flow patterns around an isolated tire. The study found interaction of the groove depth and width is significant with respect to both coefficients of lifts and drag.

Prediction of lithium-ion batteries' State of Charge (SoC) plays a vital role in the battery management system of electric vehicle's performance. Forecasting the SoC is a tedious task as the process of battery degradation is usually non-linear and extremely time consuming. Chandran et al., [6] used different ML algorithms and statistical formulations which include ANN, Support Vector Machine (SVM), linear regression, Gaussian process regression, ensemble bagging and ensemble boosting algorithms for the non-linear mapping of battery input features (voltage and current) to SoC. The proposed ANN and GPR-based method uses probability distribution unlike the traditional point estimation which makes predictions robust and reliable. Besides, the GPR-linear model with the optimized hyper parameters can be used for real-time SoC estimations.

The DL models have a significant advantage and great potential in structural design and topology optimization due to their higher computational efficiency compared to traditional FEM models [22]. Because FEM performs so many fitness evaluations, topology optimization based on stochastic algorithms, particularly the Genetic Algorithm (GA), has a high computational cost. Sasaki and Igarashi [24] provided evidence of the effectiveness of DL in lowering computing complexity for topology optimization. The authors trained a CNN model that forecasts the motor's torque properties using cross-sectional RGB images of an Interior Permanent Magnet (IPM) motor. Furthermore, the cross-sectional shape of the motor is optimized using the trained CNN model. The authors provided quantitative evidence to support their claim that using ML techniques, the computational expenditure of topology optimization may be decreased with no sacrificing optimization superiority.

6 Discussion

The engineering development process will soon be significantly impacted by tools and systems based on machine learning (ML). Automotive V&V entails a number of labor-intensive tasks that call for knowledge. Any time during the V&V, a human error could result in poor engineering choices. Predictions would be more accurate and robust thanks to the strategic application of ML techniques in conjunction with the established V&V tools. By giving ML the repetitive, time-consuming tasks, engineers would have more time for innovative thinking. ML implementation in PDP would undoubtedly be a wise investment. By including ML techniques in the process, engineers can constantly find ways to enhance the traditional V&V. The examples discussed in this paper should provide interested parties with a general framework for the deployment of systematic machine learning. The literatures discussed can be used as a resource when creating applications for the V&V of future mobility that are based on ML, statistical methods, and advanced data analytics techniques.

Appendix A

Automotive product development process, the development milestone, and the measure activities in each phase [5].

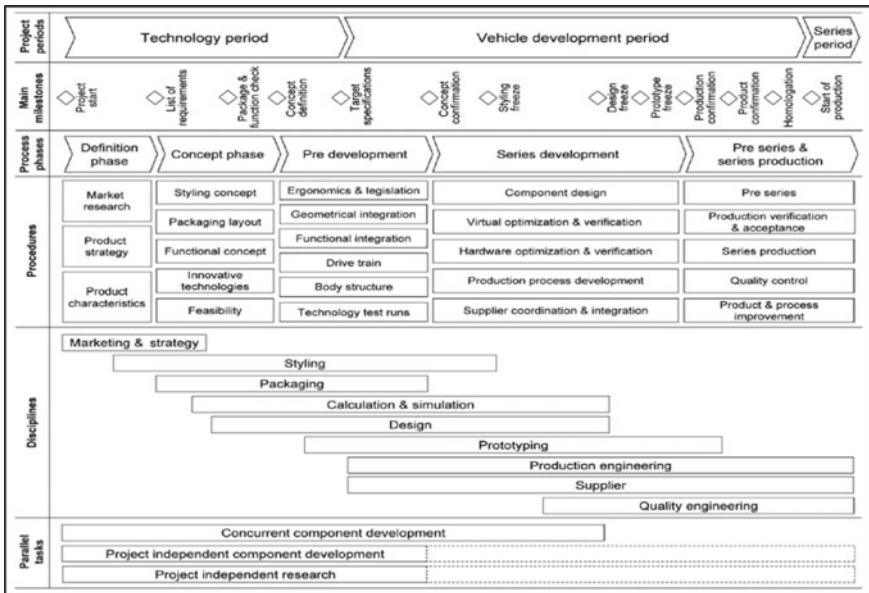


Fig. 4 Principal stages in a typical state-of-the-art full-vehicle development process [5]

References

1. Abadi, M., Barham, P., Chen, J., Chen, Z., Davis, A., Dean, J., & Isard, M. (2016). Tensorflow: A system for large-scale machine learning. In: *Proceedings of the 12th USENIX symposium on operating systems design and implementation (OSDI'16)* (pp. 265–283).
2. Herlt, A., Jana, P., & Kellner, M. (2022). *Smartphones on wheels: New rules for automotive-product development*. McKinsey's Automotive & Assembly Practice.
3. Bodendorf, F., & Franke, J. (2021). A machine learning approach to estimate product costs in the early product design phase: A use case from the automotive industry. *Procedia CIRP*, 100, 643–648.
4. Bonaccorso, G. (2018). *Machine learning algorithms: Popular algorithms for data science and machine learning*. Packt Publishing Ltd.
5. Brunner, H., Rossbacher, P., & Hirz, M. (2017). Sustainable product development: Provision of information in early automotive engineering phases. *Tehnički Glasnik*, 11(1–2), 29–34.
6. Chandran, V., Patil, C. K., Karthick, A., Ganeshaperumal, D., Rahim, R., & Ghosh, A. (2021). State of charge estimation of lithium-ion battery for electric vehicles using machine learning algorithms. *World Electric Vehicle Journal*, 12(1), 38.
7. Chavan, S., & Hor, H. (2021). *Application of artificial intelligence to solve an elasto-plastic impact problem*. SAE Technical Paper, 3, 2021-01-0249
8. Eppinger, S. D., & Ulrich, K. (1995). *Product design and development*.
9. Filipovic, E., & Großmann, A. (2014). NPD knowledge transfer via standards and patents? A case study. In *ISPIM Conference Proceedings* (p. 1).
10. FOX TV Digital Team: These carmakers had the most recalls in 2022: See if your car is on the list. (2022).
11. Gaspar, M., & Andrade-Campos, A. (2019). Implicit material modelling using artificial intelligence techniques. *AIP Conference Proceedings*, 2113(1), 120004.
12. Gonfalonieri, A. (2019). How to build a data set for your machine learning project. *Towards Data Science*.
13. Goodfellow, I., Bengio, Y., & Courville, A. (2016). *Deep learning*. MIT Press.
14. Hanlon, T., Reimann, J., Soare, M. A., Singhal, A., Grande, J., Edgar, M., & Vinciguerra, J. (2019). Artificial intelligence enabled material behavior prediction. arXiv Preprint [arXiv:1906.05270](https://arxiv.org/abs/1906.05270)
15. Hein, A. M., & Condat, H. (2018) Can machines design? An artificial general intelligence approach. In *Artificial general intelligence: 11th international conference, AGI 2018, Prague, Czech Republic, Proceedings 11* (pp. 87–99).
16. Hojdik, V. (2021). Current challenges of globalization in the automotive industry in European countries. In *SHS web of conferences*.
17. Jakhar, D., & Kaur, I. (2020). Artificial intelligence, machine learning and deep learning: Definitions and differences. *Clinical and Experimental Dermatology*, 45(1), 131–132.
18. Jang, D., Kang, J., & Lim, J. (2021). A feasible strain-history extraction method using machine learning for the durability evaluation of automotive parts. *Journal of Mechanical Science and Technology*, 35, 5117–5125.
19. Jordan, M. I., & Mitchell, T. M. (2015). Machine learning: Trends, perspectives, and prospects. *Science*, 349(6245), 255–260.
20. John, K. (2020). Column: China and the world economy's shifting centre of gravity.
21. Mandal, A., Arvanitis, A., Chen, S. K., Chien, L., Srinivasan, V., & Younkins, M. (2019). Vibration rating prediction using machine learning in a dynamic skip fire engine. *SAE International Journal of Advances and Current Practices in Mobility*, 1, 1491–1501.
22. Nie, Z., Jiang, H., & Kara, L. B. (2018). Deep learning for stress field prediction using convolutional neural networks. arXiv Preprint [arXiv:1808.08914](https://arxiv.org/abs/1808.08914)
23. Quan, Z., Gao, Z., Wang, Q., Wen, X., Wang, Y., & Xiao, B. (2014). *Rapid residual stress and distortion prediction in cast aluminum components using artificial neural network and part geometry characteristics*.

24. Sasaki, H., & Igarashi, H. (2019). Topology optimization accelerated by deep learning. *IEEE Transactions on Magnetics*, 55(6), 1–5.
25. Song, D., Hong, S., Seo, J., Lee, K., & Song, Y. (2022). Correlation analysis of noise, vibration, and harshness in a vehicle using driving data based on big data analysis technique. *Sensors*, 22(6), 2226.
26. Sörensen, D. (2007). *The automotive development process: A real options analysis*. Springer Science & Business Media.
27. Rafi, T. (2022). Why sustainability is crucial for corporate strategy.
28. Uddin, G. M., Arafat, S. M., Kazim, A. H., Farhan, M., Niazi, S. G., Hayat, N., & Kamarthi, S. (2019). Artificial intelligence-based Monte-Carlo numerical simulation of aerodynamics of tire grooves using computational fluid dynamics. *Ai Edam*, 33(3), 302–316.
29. Xie, Q., Suvarna, M., Li, J., Zhu, X., Cai, J., & Wang, X. (2021). Online prediction of mechanical properties of hot rolled steel plate using machine learning. *Materials & Design*, 197, 109201.
30. Xu, M., Song, S., Sun, X., Chen, W., & Zhang, W. (2021). Machine learning for adjoint vector in aerodynamic shape optimization. *Acta Mechanica Sinica*, 37(9), 1416–1432.
31. Zhang, C., Kwon, Y. P., Kramer, J., Kim, E., & Agogino, A. M. (2017). Concept clustering in design teams: A comparison of human and machine clustering. *Journal of Mechanical Design*, 139(11).

Teaching English Language in Rural Indian Classrooms: A Techno-Societal Approach



Santosh Pundalik Rajguru

Abstract Language is a basic pillar of communication, an effective way of conveying our ideas to one another. In the age of ICT and globalization, English has a very crucial part in the main area of communication at global level. It has an exceptional distinctiveness in the area of TLE, especially from the techno-societal point of view. When a teacher is teaching, he has to keep in mind the goals of the topic to be taught. Teaching needs some of the proper instructions, after all attainment of teaching relies upon its goals and outcomes. English is a global language and English is our major window on the world. It is a language of an opportunity. After the emergence of ICT, Indians have played a pivotal role in the development of ICT related industry, globally; there are lots of opportunities for the English-speaking Indians. Teaching English is a second level priority in India. While teaching English, it should be taught in such a manner that expected objectives should be achieved. So, the basic familiarity with English language is necessary for teaching it. This paper considers different approaches in the development of the ESL in the context of Indian English teaching.

Keywords ESL · ICT · Rural · Implication · Proficiency · Competence

1 Introduction

English language has received a special status in the academic and professional field of India. English is being used as a means of communication for explanation and instructions in school and colleges. In every walk of life and for getting success in the academic and professional examinations elementary level knowledge of English is required. Enough information of advanced areas of knowledge such as natural and artificial science and technology is only available in English. The value of English language can be compared with the passport like getting a good job not only in India

S. P. Rajguru (✉)

Rayat Shikshan Sanstha's, Arts and Commerce College, Department of English, Madha, Solapur, Maharashtra, India

e-mail: santosh.august@gmail.com

© The Author(s), under exclusive license to Springer Nature Switzerland AG 2024

P. M. Pawar et al. (eds.), *Techno-societal 2022*,

https://doi.org/10.1007/978-3-031-34644-6_33

305

but also abroad, one should clear the international tests of English like TOEFL and IELTS. Nowadays, computers are ubiquitous and occupied the fix place in every sphere of our life and simultaneously the English language has received a boost from it. According to recommendations of Radhakrishna Commission “English is a language which is rich in literature—humanistic, scientific and technical. If under sentimental urges we give up English, we would cut ourselves off from the living stream of ever-growing knowledge” [1]. The significance of English in competitive examination is increasing in comparison to the organized educational system. Almost all the professional entrance tests, job tests have emphasis on the English language. They are designed in such a way that student’s inclination towards English would be automatically tested.

1.1 Review of Literature

National Education Policy, 2020 insists on the “functionality and fluency” for imparting knowledge of English language in all spheres of education especially in schools [2]. Earlier, in NCERT-2012 survey, enough care was taken to address the issues of students regarding English communication skill amongst the school students where an imbalance was found in basic four skills such as reading, writing, listening and speaking. However, there is an absolute contrast at the ground level. According to the survey conducted by Clapham and Wall [3] “it has been observed that it is through this language that one can be refined with of advance knowledge in all fields of human activity and English can keep in touch with the world without leaving his own house.”

Endow [4] has drawn our attention towards the fact of how the demand of education in English language been increased for getting opportunities from the outbreak of service industry.

Mohan [5] noted that English should not be taught for the sake of good job but it should serve the purpose of a learner and get the good knowledge from other sources. It has been a thought that good jobs are only received by the elites but good knowledge of English can bring equal opportunities to all [5].

1.2 Essence and Objectives

The present study can help students to:

- (i) Deliver a modified and systematic learning atmosphere
- (ii) Emphasis on appropriate learning
- (iii) Shape the learners’ previous knowledge with technology
- (iv) Offer continuous review of societal approach
- (v) Simplify language in socio-cultural context

(vi) Build other skills while developing English.

This research paper tries to achieve the following objectives:

- (a) Study several tendencies of ELT;
- (b) Describe importance of English in rural Indian classrooms;
- (c) Examine technological developments of ELT in rural classroom;
- (d) An efficient beginning in the study of a foreign language can be made only with satisfactory basic materials and techno-societal approach.
- (e) The success of the class is judged by the amount of English which the students speak.

2 Social Implications of Language Learning

An overall development and to bring the desirable changes among its students is one of the main objective of every educational. In order to bring about those changes, the college and schools should implement the bilingual method of communication by simplifying in vernacular language. We must thank to the globalization in all the fields, which realized the learning of an English language at international level. By crossing to the native speakers English has become the world language where the numbers of the actual people who speak it as their mother tongue. Since, last two centuries, Indian educational system has been strongly influenced by the use of English language. Most of the study materials of STEM like subjects is only available in English.

Taking into consideration the above facts, learning English as a Second Language, becomes inevitable in Indian education system. The aims of an English language curriculum must at all times and at all stages be based on and conform with the principles of education in general. While English is a subject that may not in some circumstances lend itself too readily to correlation with other subjects, it would be educationally unsound to consider its aims apart from the aims of education in general. In English, too, as in the case of other subject, the course must contribute to

- (a) Individual competence
- (b) Social and civic competence, and
- (c) Vocational competence.

And it is only when all these factors are fully taken into consideration that it becomes possible to draw up a statement of aims that is scientifically sound. My object in this paper is not to trace the origin and development of the various principles and methods which are about to discuss. My main concern is with those features and problems which are of particular interest to teachers of English, especially to those engaged in teaching students to whom English is a non-cognate foreign

language. There are **three types** of methods to recognize the social circumstances of the students.

- (A) **Grammar-Translation Method-** This is the method which Palmer [6] calls 'The Classical Method'. This method considers that all languages are as if they were dead; as if each contained basically of a group of ancient forms to be interpreted and studied; thereby categorizing the term *linguistics* with the term *literary tradition*.
- (B) **Natural Method-** Little need be said of this method, which is seldom heard of these days. It was based on the manner in which a kid acquires its mother tongue without realizing that a child learning a foreign language is in a different position.
- (C) **Psychological Method-** It is based on its techniques and the association of ideas and the habit of mental visualization.

3 Common Factors Influencing English Teaching and Learning

There are several aspects that influence the teaching–learning process of English in India. We can categorize it in two parts i.e. one studying in regional language from primary level and second is having English as the medium of study from primary level. However, in Indian classrooms the problem of teaching English as a second language, begins from the pre-schooling. Further domestic background and surrounding atmosphere plays significant role in the development of learning skills of the students. In India, majority of the students belong to the agricultural and from the poor background and the parents are not interested in giving good education to their children. On the other hand, they think to involve them in some jobs in order to earn money. This approach is severely affecting the teaching learning of these students. Further, the basic infrastructural facilities are not adequate in the schools. Therefore, in order to resolve the issue of learning English, the following strategy should be framed in the pre-schooling stage itself.

- (i) *Use of the Mother Tongue*
- (ii) *Well-trained Teachers to teach Grammar*
- (iii) *Unmeasured Curriculum*
- (iv) *Lack of Oral communication*
- (v) *Pronunciation Problems*
- (vi) *Absence of the practice of Communicative Method in Teaching*
- (vii) *Lack of proper usage of Audio-Visual and ICT aids.*

4 Role of a Teacher

The teacher should have complete knowledge of the structure of the language i.e. English, to be taught and that of the students' vernacular. Structure is taught through giving several examples of the same pattern, and by only afterwards calling the students attention to the specific patterns that have been taught. The role of teacher working in rural areas is highly appreciative as compared to urban areas because in an urban situation a student has other models like culture, technology, and peers etc. to imitate. A teacher is the only option for rural student to imitate and learn from. The in rural educational campuses are used to be consider as temples of learning or an ideal place and it is the responsibility of the teachers to keep the places sacred with devotion towards teaching and educating the students. The classes may be over crowded, but the teacher should try the level best to attend each and every student and develop his or her language skills.

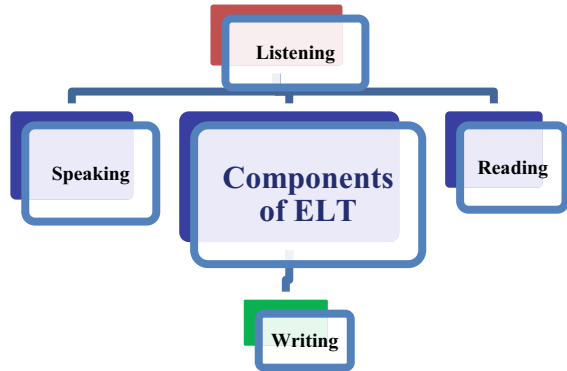
5 Teaching English as a Second Language

ELT has extremely transformed in the last few years. Teaching language in the present era has undergone numerous changes and improvements. The ELT methods has been laid emphasis on developing learners' communicative competencies and promoting learning strategies in language classrooms. A teacher has to develop strategies at every step. English has become an unnecessary fear. It is treated as elite over other languages. The teaching material is substandard, basic infrastructure is unavailable and the socio-cultural factors are hostile. Therefore, the role of teacher becomes more interesting in rural areas because in such areas it is the teacher who is the model, to whom a student looks for all learning needs. As far as teaching methodology is concerned, it is not easy to answer the question, 'how to teach?' In the era of Communicative Language Teaching (CLT), one cannot reject grammar and translation method. In this context, mother tongue is very useful tools for ELT. In order to simplify the meaning is translated into the mother tongue which helps a teacher to clear the concept. But at what extent it should be translated is to be decided by the teacher.

6 Language Proficiency Tests

According to the survey conducted in America about the aptitude of English language it has been observed that how student use English to ask questions, to expect the answer from faculties, and evaluation resources, to check the concepts and to revert what is being asked in the classroom. Following are the four skills which helps to bring proficiency of English (Fig. 1).

Fig. 1 Components of English teaching



1. Reading- a skill to understand and read text at appropriate level.
2. Listening- a skill to comprehend the language teacher and students.
3. Writing- a skill to create written text with content by fulfilling classroom assignments.
4. Speaking- an oral skill which helps to interpret language appropriately and effectively in learning activities inside the classroom.

Damico et al. [7] presents three schools of thoughts for language proficiency tests, the first one is, the distinct point method, was based on the hypothesis that language expertise consists of separate modules of phonology, morphology, lexicon, syntax, and so on, each of which could be further divided into different categories of components.

Next to the distinct point method, a trial could not be valid if it mixed numerous skills or fields of structure. Then, all the outcomes could be collected to form a total representation of language proficiency. The subject title is “Technical English”, a routine subject and “Communication Skills Lab”, an applied subject. The previous is taught at entry level students and the lab course is taken to 2nd and 3rd year students. The central objective of this course is to assist students to improve listening skills for professional and academic intentions.

7 Conclusion

As it is already mentioned that more than 70% students are from rural and semi-urban areas. Their medium of primary school is vernacular or in regional language. On the basis of such background, it is the duty of policymakers and the educational experts to design the syllabus and implement such methods to test their English language proficiency. Therefore, it is mandatory for us to discuss whether the current syllabus

is satisfying the prerequisites of the time and appropriate to the students in attaining their objectives, therefore proper feedback from the teaching faculties of the English language in technical institutions are to be taken.

The division of urban- rural in teaching of English has to be bridged. It is possible only if a proper approach is developed and methods adopted. In order to strengthen the rural student in English, a teacher has to develop some advanced approaches in the classroom. On the spot solution should be developed for action based research in the classrooms. At govt. level, necessary actions should be taken while appointing teachers their basic skills of language, integrity, ICT knowledge, research of English, innovative technological schemes, provision of minimum technological aids like LCD projectors, Online resources like MOOCs, SWAYAM, well configured computers, Audio-visual aids, student-friendly fresh ambience in schools and colleges, etc. should be established to amend the declining standards of teaching/ learning of English in rural areas.

References

1. Kohli, A. L. Techniques of teaching English. p. 12
2. New Education Policy. (2020). Point No. 4.14, 4.20, pp. 14–15.
3. Clapham, C., & Wall, D. (1995). *Language test construction and evaluation*. Cambridge University Press.
4. Endow, T. (2021). *Economic & political weekly EPW*, March 27, 2021. Vol. LVI, No. 13.
5. Mohan, P. (2014). The road to English—Slow migration of the economically weak child to elite. *Economic and Political Weekly*, 49(7), 19–24. <https://www.epw.in/journal/2014/7/commentary/road-english.html>
6. Palmer, H. (1922). *The principles of language study*. Oxford University Press.
7. Damico, J. S., Oller, J. W., Jr., & Tetnowski, J. A. (1999). Investigating the inter observer of a direct observational language assessment technique. *Advances in Speech Language Pathology*, 1, 77–94.

On Use of Various Leadership Styles for Implementation of Management Information System



Anil N. Barbole and Suraj B. Ronge

Abstract This paper presents the ways to implement Management Information System (MIS) successfully for Outcome-based Education (OBE) in an organization with different leadership styles used for different actions. Successful implementation of MIS in the organization is a big task for any organization. It includes lots of organizational changes. In this research, various leadership styles were studied and implemented in institute for various actions for successful implementation and adoption of MIS for Outcome-based Education. In that, different leadership styles which are helpful for the successful implementation of MIS were considered. Simply via instruction or compelled inducements, resistance to unwanted change is exceedingly difficult to overcome. Instead, creating the institutional and cultural circumstances that support transformation is essential.

Keywords Outcome-based Education · MIS · Organizational change · Management information system · Leadership style

1 Introduction

Successful implementation of the Management Information System (MIS) in the organization is a big task. This successful implementation and adoption of MIS in an organization depends upon many factors. The main factor affecting the implementation of the MIS is the management's leadership style. The efficiency of MIS implementation for evaluating the Outcome-based Education (OBE) system depends greatly upon the leadership style used in the organization. In this research work, the authors suggest different leadership styles which will be helpful during the

A. N. Barbole
Chhatrapati Shivaji Night College of Arts and Commerce, Solapur 413001, India

S. B. Ronge (✉)
SVERI's College of Engineering, Pandharpur 413304, India
e-mail: sbronge@coe.sveri.ac.in

successful implementation of MIS in an organization. A leader is a person who allocates resources or persuades people to perform certain activities. There are different styles of leadership that we need to apply for various activities while implementing new things in an institute or organization. So, leadership skills are beneficial for implementation of strategies for change.

Different styles of leadership exist in the organization, and they will be helpful for adopting MIS successfully. The management of any organizational change requires capable leaders who are aware of the complexity of the quickly evolving global environment. The effectiveness of employees will be high if the task is well-structured and the leader has a positive relationship with the team. According to the study, democratic leaders take great care to include every team member in discussions and work with a motivated workforce and democratic leadership approach also strongly supports the participation of employees and their unique ideas. Thoha and Avandana [1] state that affiliative leaders create a comfortable atmosphere and form emotional bonds with their team members, in contrast to pace-setting leaders who demand accuracy from their team members by setting high goals and setting examples. Ke and Wei [2] investigated effect of leadership on ERP implementation by fostering the desired organizational culture. They also relate the implementation of ERP with organizational culture along with development and dimension of learning and many other parameters.

2 Objective

The main objective of the study is to analyze various styles of leadership and identify the styles that are best for the successful implementation of MIS in organizations for the evaluation of the OBE system.

3 Methodology

For the implementation of MIS in organizational change, the management principle was used by Harrison et al. [3]. They found that Kotter's eight-step model or Lewin's three-stage model of change management is used in the majority of the research. Kavanagh and Ashkanasy [4] suggested that it is crucial to have open lines of communication and a clear change process since these factors frequently impact not just how a leader will be viewed, but also who will be recognized as a leader. For the process of transforming organizations leaders are supposed to be knowledgeable and competent enough for ensuring that individual within the organization accepts the change. The performance of organization can be improved by systematic implementation and adoption of MIS which helps in reducing the errors and required efforts for various processes. Eastman [5] suggested that simply via instruction or compelled inducements, resistance to unwanted change is exceedingly difficult to overcome. Instead,

creating the institutional and cultural circumstances that will support transformation is essential.

Bass [6] suggested that the top management must modify an organizational culture to become more transformational. The transformative leader motivates and challenges their thinking, shows them that they value individually, and involves their team member in making successful changes; this type of leadership is either participative or directive.

Commanding leadership is also popular in implementing any change in the organization. This commanding type of leader is demanding, straightforward and forceful. They will take command of any situation, even those fraught with ambiguity, and they don't hesitate to make challenging decisions. This leadership style focuses primarily on results and goals, and because they are willing to do whatever it takes to succeed, they roll over people in the process. This leadership style is effective when there is a corporate crisis, when there are problematic employees and when it is necessary to shock people out of old habits and into new ways of doing things. Still, it is not a dominant sustainable style.

Wachira et al. [7] found that affiliative leadership encourages teamwork and partnerships, boosting productivity, integrity, and commitment. By ensuring that followers feel connected, affiliative leadership can be utilized to resolve participants' issues or as a guiding principle to create a positive, inclusive work environment. The development of teams can benefit greatly from this approach. This kind of leadership focuses on the dynamics of the group. Their objective is to build capable teams that get along nicely. This approach focuses on reducing stress and fostering positive relationships among team members. This leadership style helps meet people's need to be understood and respected and is particularly helpful when there have been trust issues.

Democratic leadership is quite popular in decision-making. It is used when the leader still determines what direction to take and needs ideas from followers. In this type of leadership, leaders value their team members' feelings and suggestions. Due to democratic leadership, an employee feels involved, trusted, and respected. In this, less focus is given to results and goals than that of an employee's emotional needs. Still, democratic leadership is not used in times of crisis when urgent events demand a quick decision.

The pacesetter leaders are used to get quality results from a team which is highly motivated and competent with little direction. It is not used alone; along with it, visionary or affiliative leadership is used. These types of leaders are obsessive about doing things better and faster and ask the same of everyone. They quickly pinpoint poor performers and demand more if they don't rise to the occasion and rescue the situation personally. In this type of leadership, Pacesetters may get compliance and short-term improvements but will not create sustainable, high-performing teams.

Situational leadership is also used now-a-days. In this, leaders must recognize the need to use differing leadership approaches in different situations; for that, leaders have to adapt and use different leadership styles as required. In this leadership, there are four types of leading: telling, selling, participating, and delegating for different rolls in the organization.

4 Results and Discussion

Identifying strategies needed to maximize organizational performance, MIS is brought to evaluate OBE system. When OBE evaluation using MIS starts getting implemented, some faculty members in an institute resist to implement MIS system as they have fear of failure, mistrust and lack of confidence, poor communication, and unrealistic timelines about MIS. To overcome reluctance to change, top management and employees must effectively communicate the advantages and good results of utilizing MIS for OBE evaluation. For understanding the positive outcomes and benefits of MIS, Pre-implementation survey about existing outcomes' assessment process is carried out by preparing survey form. In this process, course instructor and academic and administrative leaders like class coordinator and HoD are deputed to collect the feedback forms. When feedback is collected, the critical points in improving the outcome assessment process are identified, and forms and processes are designed in departmental meetings using a democratic leadership style. In this case, the main emphasis is on group discussion and group meetings to consider everyone's thoughts and points.

Not everyone knows how to utilize MIS when it is used to analyses the OBE system in an organization. As a result, they have been trained for easy and quick handling. To instruct the faculty on the usage of the software (MIS) for carrying out the assessments and feeding the data for each assessment instrument, training sessions and user guides were created. Pacesetting leadership was used in this process because this kind of leader sets the pace for their teams with high standards and goals. After completing all the procedures for OBE evaluation, a post-implementation survey about usage of tools, observations, and time requirements was taken from the course instructor and various administrative levels like HoD and class coordinator. Positive outcomes of MIS implementation were discovered through the analysis of this survey. From this survey, the required time for OBE evaluation using manual and MIS processes is collected for different processes.

To know the impact of MIS implementation, comparison between manual and MIS processes is done on different parameters. The results of pre-and post-implementation of MIS for OBE evaluation were compared, and by identifying difficulties faced during MIS implementation, corrective actions were taken. For that, affiliative leadership style was preferred. After disciplinary action, the second level of testing with modification was implemented using pacesetting type leadership in the new semester. Table 1 shows action and leadership style used in implementation of MIS.

5 Conclusion

In this research paper, the authors have divided the implementation of MIS into seven actions. They have used a different leadership style and briefed about action measures and communication methods for implementing MIS in the organization.

Table 1 Actions and leadership styles used in implementation of MIS

Action	Action measure	Leadership style	Communication method
Conduct a pre-implementation survey about the existing Outcome Assessment Process	<ul style="list-style-type: none"> • Prepare question form • Conduct survey from Course Instructors, and Academic Administrators like Class Coordinators and HoD 	Commanding	Survey form
Defining outcome Assessment process improvement requirements	<ul style="list-style-type: none"> • Identify the points to be improved • Design the forms and processes 	Democratic	Department meeting, Focus group meeting
Training the processes and software	<ul style="list-style-type: none"> • Conduct the training for faculty members 	Pacesetting	Training sessions and Booklets
Performing the Assessment and feeding the data for each assessment tools	<ul style="list-style-type: none"> • Teachers will perform assessment of their course using set process • Compare the outcomes with the target 	Pacesetting	Use of software and access
Conduct post-implementation survey about usage of tools, observations, time requirement	<ul style="list-style-type: none"> • Survey of HOD and CC • Survey of teacher about effectiveness • Survey about time 	–	Survey form
Compare improvement of performance and identify best performing members	<ul style="list-style-type: none"> • Compare the pre and post implementation result • Identify and difficulties 	Affiliative	
Second levels of testing with modifications	<ul style="list-style-type: none"> • Corrective methods in process • Implementation of the process of the new semester 	Pacesetting	Use of software and assessment tools

Commanding type leadership was used to conduct a pre-implementation survey about the existing Outcome Assessment Process by preparing a survey form and collecting it from Course Instructors and Academic Administrators like Class Coordinators and HoD. Democratic leadership style was used for defining Outcome Assessment Process and requirements of improvement were discussed in departmental meetings by designing the survey forms and processes. The pacesetting leadership style was used to implement the training process and software, to perform the Assessment and feed the data for each assessment tool. The second level consists of testing with modifications to conduct the training for faculty members through training sessions by preparing booklets also, assessing their course using a set process by comparing the outcome with the target and taking corrective methods in the process, and implementing the process for the new semester by using software and assessment tools. The affiliative leadership style was used to compare improvement in

performance and identify the best-performing members. The pre-implementation and post-implementation results were compared by identifying the difficulties.

References

1. Toha, N., & Avandana, I. M. N. W. (2020). Project managers' leadership styles and their effects on project management performance. *Pertanika Journal of Social Sciences & Humanities*, 28(2).
2. Ke, W., & Wei, K. K. (2008). Organizational culture and leadership in ERP implementation. *Decision Support Systems*, 45(2), 208–218.
3. Harrison, R., Fischer, S., Walpolo, R. L., Chauhan, A., Babalola, T., Mears, S., & Le-Dao, H. (2021). Where do models for change management, improvement and implementation meet? A systematic review of the applications of change management models in healthcare. *Journal of Healthcare Leadership*, 13, 85.
4. Kavanagh, M. H., & Ashkanasy, N. M. (2006). The impact of leadership and change management strategy on organizational culture and individual acceptance of change during a merger. *British Journal of Management*, 17(S1), S81–S103.
5. Eastman, D. J. (1991). Improving cross-cultural communication during complex information systems development. *Journal of Management Systems*, 3(1), 19–31.
6. Bass, B. M. (1999). Two decades of research and development in transformational leadership. *European Journal of Work and Organizational Psychology*, 8(1), 9–32.
7. Wachira, J. G., Karanja, K., & Iravo, M. (2018). Influence of affiliative leadership style on organizational performance of commercial state corporations in Kenya. *European Journal of Business and Strategic Management*, 3(3), 17–28.

Evaluating Students Mobile Gaming Approach Using Data Mining Technique



Aniket Muley and Sagar Joshi

Abstract Nowadays, mobile gaming is one of the interesting issues for today's generation. It is part of entertainment for many people. Here, we have performed an online survey and collected 203 responses. The analysis is executed through the SPSS 22.0v software. Both unsupervised exploratory analysis and supervised learning is used to deal with the dataset. The result of the study gives emphasis on the human tendency to answer the questions. Here, gender-wise is significant with the sim users, the variety of features in mobile games, time of the playing games, their likings of playing the games, time spent on playing games, types of mobile game that they would like to play. Further, difference between location with types of mobile, mobile game that they would like to play, timings of playing mobile game, time spent on playing mobile games, searching features in mobile games, different types of mobile game that they would like to play, competing with friends to gain the highest score in a game contributes to playing more is observed. The obtained results are helpful in the development of the strategies regarding administrative as well as industry perspective.

Keywords Mobile game · Data mining · Play · Entertainment

1 Introduction

Nowadays, due to the Covid-19 pandemic crises, people were searching for entertainment and wanted to spend time with various activities. Mostly, mobile gaming is for entertainment and joy. Along with that, there might be some additional hidden aspects that might be present and one approach to find with the help of the data mining

A. Muley (✉)

School of Mathematical Sciences, Swami Ramanand Teerth Marathwada University,
Nanded 431606, Maharashtra, India
e-mail: aniket.muley@gmail.com

S. Joshi

Department of Electronics and Telecommunication, Nutan Maharashtra Institute of Engineering and Technology, Talegaon Dabhade 410507, Maharashtra, India

techniques. According to this perspective, we are interested to mine the information from the students pursuing their graduate or postgraduate degree. In this study, our special interest is to deal with the students' approach towards mobile gaming. As playing a game is somewhat refreshing the mind and fatigueness of the student. Some researchers performed studies with some different dimensions. Initially some review of the related studies has been taken here:

Hong et al. [6] performed the cross-sectional study on structural questionnaires focusing on the use of smartphones, behaviors and habitualness of college students. The structural equation model was adopted to predict behavior association. Fook et al. [4] studied the trend of mobile smart phones with various parameters. Exploratory methodology was proposed for the identification parameters. They have collected data with the help of Google form. The obtained result reveals that a moderate level of mobile phone addiction was identified among the students. They found gender-wise significance with mobile addiction, and attitude towards mobile phones.

Almalki et al. [1] investigated the study of medical girl students and observed that they are negatively associated with their academic score. De los Santos et al. [3] performed a study to investigate the impact of online mobile gaming comparative analysis. Random sampling was carried out and descriptive correlation thereafter correlation methods were applied which reveals that most were playing the games due to feeling bored. Tsai et al. [8] examined data students' aspects regarding playing games and time durations. Baharum et al. [2] investigated the impact of video games on university student's education performance with various parameters viz., time in hours, daily schedule, game type and their obtained grades were considered. Online survey was performed for data collection. Gandaputra et al. [5] performed a cross-sectional survey carried out of 315 students with a structured questionnaire. The demographic variables have been used to achieve their objectives. Tao et al. [7] examined the use of mobile, physical health activity and their negative mind aspect. 4624 students' data were considered with the age group of 17–25 years old students. The statistical tools used to check the significance viz., Chi square and logistic regression.

In this study, our main aim and objectives are: to perform unsupervised learning techniques as exploratory analysis of students' approach towards mobile gaming during the Covid-19 pandemic crises. Furthermore, supervised learning is to test gender-wise significant differences among the single or dual sim users, a variety of features in mobile games, about time of the playing games, their likings of playing the games, time spent on playing games, types of mobile game that they would like to play. Also, to test the significance location-wise difference between types of mobile game that they would like to play, mobile game that they would like to play, timings of playing mobile game, time spent on playing mobile games, searching features in mobile games, different types of mobile game that they would like to play, among respondents believes competing with friends to gain the highest score in a game contributes to respondents playing more. In the following subsequent sections methodology, result of study and conclusion is discussed in detail.

2 Methodology

In this study, we have designed a semi-structured survey questionnaire with the Google form and distributed it through online mode viz., email address, social media sites, WhatsApp and telegram. Overall 203 responses were recorded. Further, to explore the data first of all collected raw data is transformed into frequency data form. Afterwards, to identify the distribution of data exploratory i.e. unsupervised learning viz., exploration of data in the form of graphical manner and it is performed with MS-Excel. Furthermore, supervised learning view is dealt with SPSS 22.0v software and further analysis is performed.

3 Result and Discussion

In this section, analysis of the data has been performed in terms of unsupervised and supervised learning techniques.

Figure 1 represents the gender-wise distribution of the respondents. Figure 2 age-wise distribution of the respondents and it is observed that most of them have an age-group of 21–25. Figure 3 explores the distribution of responses from the rural and urban background. Figure 4 represents frequency distribution of the number of family members of the respondents. It is observed that, most of the respondents are from 4 to 6 members and range from 2 to 10 members in a family. Figure 5 explores the recharging plan of the respondents. 76% of the respondents monthly recharging their mobile phones, 9% of them prefer bi-month option, 8% used to select special plan, 4% denied to answer the question, 2% prefer daily and rest 1% recharging their mobile phones weekly basis. Figure 6 reveals that 63% of the respondents like to play a game, 3% of them do not like to play a game and 1% of them refuse to answer. Figure 7 explores the choices of the online, offline, free and paid type of the games preferences of the respondents and data reveals that respondents are not really to deal with purchasing the games. Figure 8 explores the liking of the games and it is observed that, most frequent of them are Candy crush, PubG, Ludo king. The interesting fact is that some of them have played some of the banned mobile games too. Figure 9 explores reasons regarding the playing of mobile phones by respondents. Figure 10 explores that, 42% plays mobile games when they are at home, 36% plays when they are outdoors and 22% denied to respond. Figure 11 explores the time spent by respondents on playing mobile phones. It is observed that, 89 of the respondents spent 30–60 min, 54 of them spent 1–2 h and so on. Figure 12 explains the respondents liking a variety of game type viz. action/adventure/platformer, shooting, racing, and casual. Most frequent is observed in action/adventure/plat-forming, casual, shooting, racing respectively. Figure 13 reveals that respondents have the number of games in their mobile. Figure 14 explains most of the respondents are competing with their friends (Table 1).

Fig. 1 Gender-wise distribution of response

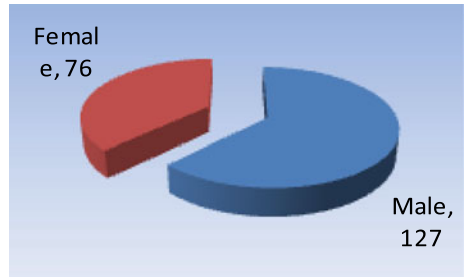


Fig. 2 Age-wise distribution of responses

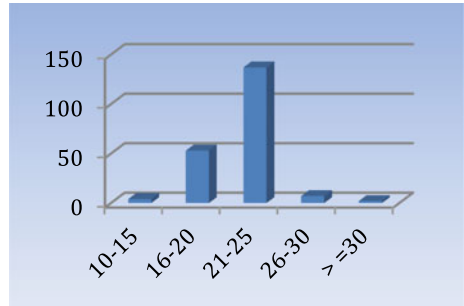


Fig. 3 Region-wise distribution of responses

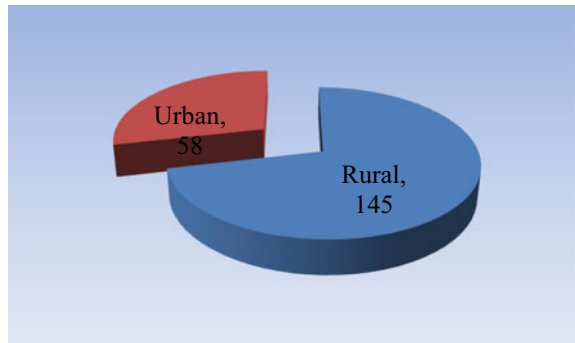
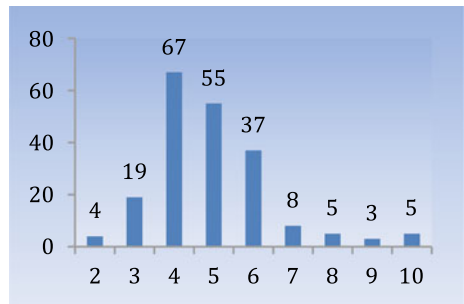


Fig. 4 Frequency of number of family members



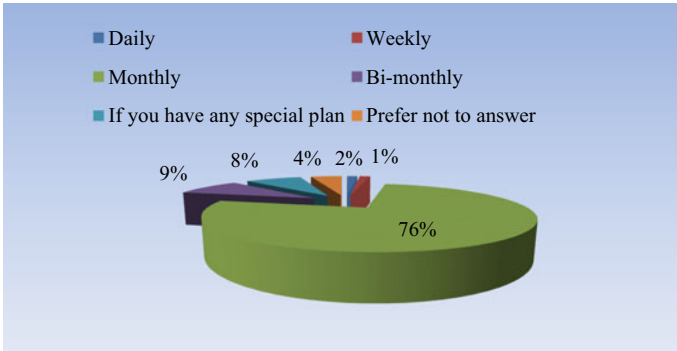
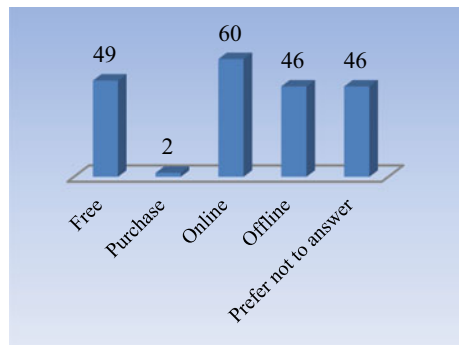


Fig. 5 Respondents type of recharge plan

Fig. 6 Number of respondents plays mobile games



Fig. 7 Choice of type of game to play



4 Conclusions

The result of this study explores some interesting results such as, some of the respondents played banned games. Most of the respondents like to play adventure types of games that are associated with their competing mindset with their friends. It simply

Fig. 8 Respondents like games to play

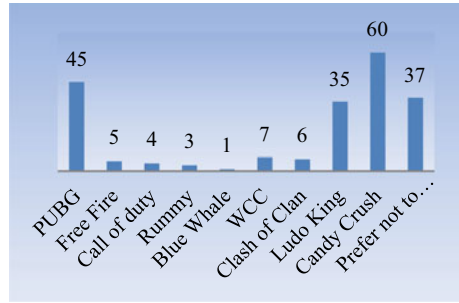


Fig. 9 Preferences like to play mobile games

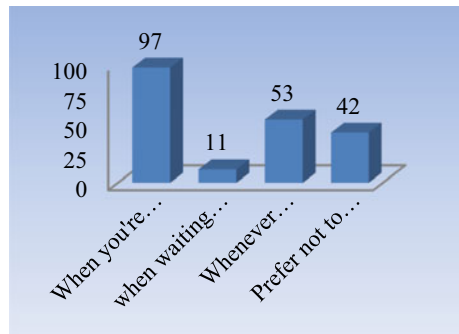


Fig. 10 Place where respondents would like to play a mobile game

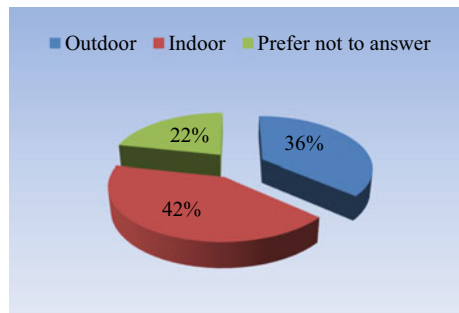
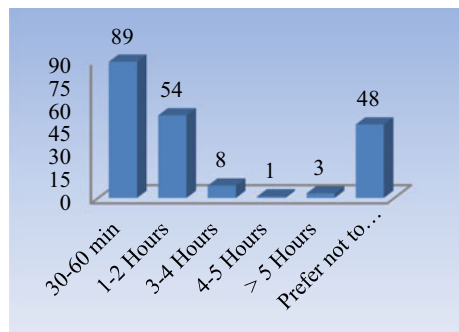


Fig. 11 Respondents spending time on playing mobile games



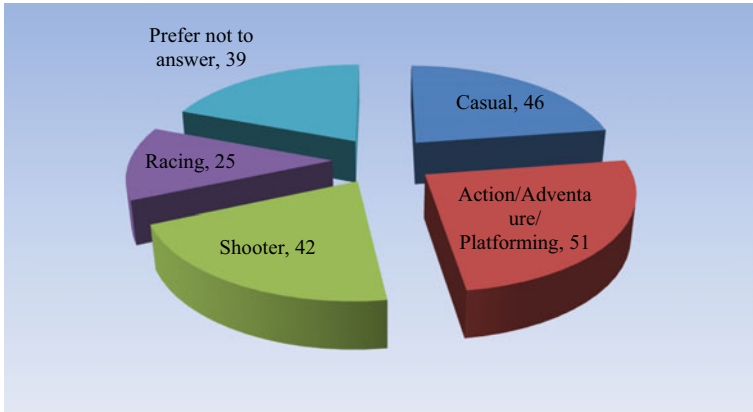


Fig. 12 Respondent likes to play types of mobile game

Fig. 13 Games available in respondents mobile

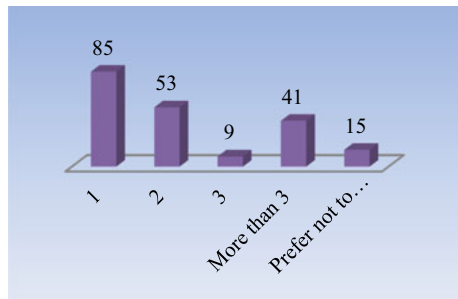
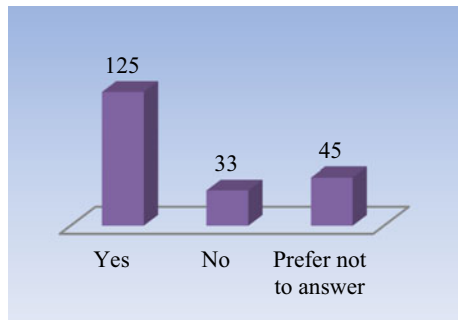


Fig. 14 Responds competing with friends



explains humans' natural tendency to compare with others. Most of the respondents like to play online, offline, free types of games but they are not interested in purchasing and playing the games. It is observed that, most frequently Candy crush, PubG and Ludo king mobiles frequency is more. Ludo king is more frequently used in rural regions. It is due to there being one traditional ludo game played in the rural

Table 1 Parameters significance with the type

Parameter	Type	Pearson chi square	Asymp. Sig. (2-sided)
Gender	Use of single or dual sim	6.942	0.031
	Features in mobile games	12.583	0.006
	Time when do you like to play mobile games	12.583	0.006
	Game like to play	76.445	0.000
	Time spending on playing mobile games	40.209	0.005
	Kind of mobile game	27.559	0.036
Location	Game like to play	14.771	0.005
	Type of game	17.907	0.036
	Time when do you like to play mobile games	10.642	0.014
	Time spending on playing mobile games	17.159	0.004
	Features in mobile games	17.622	0.001
	Kind of mobile	20.813	0.000
	Competing with your friends	7.949	0.019

part, so respondents might be preferred to deal with it. Also, found that, gender-wise significant between: the single or dual sim users, variety of features in mobile games, time of the playing games, their likings of playing the games, time spent on playing games, types of mobile game that they would like to play. There is location-wise difference observed for: types of mobile, mobile game that they would like to play, timings of playing mobile game, time spent on playing mobile games, searching features in mobile games, different types of mobile game that they would like to play, among respondents believes competing with friends to gain the highest score in a game contributes to respondents playing more. The obtained results are helpful in the development of the strategies for administrative as well as gaming industry.

Acknowledgements The authors gratefully acknowledge Mr. Govind Ebitdar for their help in the collection of data process.

References

1. Almalki, A. A., & Aldajani, H. M. (2021). Impact of playing video games on the social behavior and academic performance of medical student in Taif city. *International Journal of Progressive Sciences and Technologies*, 24(1), 572–585.
2. Baharum, A., Sabili, A. S., Benedict, H., Nazril, M. A. A. A., Razman, M. N. Z. D., Khan, R. Z. A., & Deris, F. D. (2021). Effect online game addiction in study grades among university students. *European Journal of Molecular & Clinical Medicine*, 7(8), 3852–3864.

3. De los Santos, J. R. N., Cornillez Jr, E. E. C., Carillo Jr, V. D., & De los Santos, G. N. (2020). Mobile games and academic performance of university students. *International Journal of Innovative Technology and Exploring Engineering*, 9(4), 720–726.
4. Fook, C. Y., Aziz, N. A., Narasuman, S., Mustafa, S. M. S., & Han, C. T. (2020). Mobile addiction, attitude and purpose of use among university students in a public university in Malaysia. *Journal of Critical Reviews*, 7(19), 4421–4428.
5. Gandaputra, S. A., Waluyo, I., Efendi, F., & Wang, J. Y. (2021). Insomnia status of middle school students in Indonesia and its association with playing games before sleep: Gender difference. *International Journal of Environmental Research and Public Health*, 18(2), 691.
6. Hong, F. Y., Lin, C. C., Lin, T. J., & Huang, D. H. (2021). The relationship among the social norms of college students, and their interpersonal relationships, smartphone use, and smartphone addiction. *Behaviour & Information Technology*, 40(4), 415–426.
7. Tao, S., Wu, X., Yang, Y., & Tao, F. (2020). The moderating effect of physical activity in the relation between problematic mobile phone use and depression among university students. *Journal of Affective Disorders*, 273, 167–172.
8. Tsai, S. M., Wang, Y. Y., & Weng, C. M. (2020). A study on digital games internet addiction, peer relationships and learning attitude of senior grade of children in elementary school of Chiayi County. *Journal of Education and Learning*, 9(3), 13–26.

Amalgamation of Internet of Things (IoT) and Web Services for Advancement in the Tele-Medicine



Rajni Patel and Amarjit P. Kene

Abstract Techniques and Technology have great prospects to address cost-effective, remote access and high-quality health care services. It gives birth to a rapidly expanding, diverse, and evolving field of medicine called Telemedicine. Rapidly growing Communication Technology and information involve fast internet services. It permits real-time data accessibility with proper authentication. IoT can undoubtedly significantly improve medical services, according to a variety of researchers and experts. In addition to its many advantages, Telemedicine is less widely used in developing nations because of the perceived high cost and lack of resources associated with its implementation. In this paper, through the introduction of Telemedicine and the Internet of Things (IoTs), we discuss the importance of IoT to enhance telemedicine services and facilities. Further, we will propose an architecture that provides a deep inside of the whole scenario. Telemedicine cannot exist without IoT and web services. It can also stretch its valuable benefits to improve the overall health scenario throughout the world.

Keywords Telemedicine · Internet of Things · Service oriented architecture

1 Introduction

The past era has observed the rapid development of Information and Communication Technologies (ICT) that enable Telemedicine to provide medical services from a remote distance. This is a strategic approach to breaking down geographical barriers and improving access to health services, especially in remote areas of the country. Very helpful in an emergency, providing emergency supplies.

R. Patel (✉)

Department of Computer Science and Engineering, SVERI's College of Engineering, Pandharpur, Maharashtra, India
e-mail: rpatel@coe.sveri.ac.in

A. P. Kene

Department of Mechanical Engineering, SVERI's College of Engineering, Pandharpur, Maharashtra, India

Home care has become convenient with the proliferation of technologies such as smartphones, tablets, video conferencing, and high-speed internet. Telemedicine services are available outside normal business hours, sometimes 24 h a day. Parents can avoid or shorten holidays by reducing travel time and increasing telemedicine availability. Staying indoors also reduces the risk of transmitting infections between patients. This is true for both mild and severe cases, from respiratory infections to more worrisome diseases such as Ebola.

However, telemedicine adoption continues to be hampered in developed and developing countries. There are many factors such as patient safety, quality, start-up, cost of ownership, payments, multi-state approvals, lack of system integration and technology [1]. According to the World Health Organization (WHO), it means that “distance is a key issue, with all health professionals using ICT to exchange correct information for the diagnosis, treatment and healing of illnesses and injuries. It is a methodology of providing medical services in case of, for research and evaluation, and continuing education of health care providers” [2]. Telemedicine is categorized into Static and Real-Time based on the transmission of information [3]. Static includes remote monitoring (also called self-monitoring/testing) and Store-and-forward telemedicine services (i.e., transmitting digital images like x-rays, MRIs, etc.). Real-Time includes interactive telemedicine services (i.e., live Videoconferencing, phone conversation, etc.) [4]. Telemedicine system implementations must consist of custom hardware and software on both the patient and professional sides. Diagnostic equipment such as ECG, x-ray, and pathology microscope/camera will be provided to the patient to generate reports.

2 Telemedicine in India

In India, state administration and the government are in charge of healthcare. According to a report by ASSOCHAM, India’s telemedicine sector, which has been expanding at a compound annual growth rate (CAGR) of over 20%, has the potential to surpass \$32 million by 2020 from its present level of over \$15 million [5, 6].

ISRO started the Pilot Project in 2001. It links Apollo Hospital in Chennai with the Apollo Hospital at Aragonda village (rural region) in the Chittoor district of Andhra Pradesh. Secondly, in March 2002, the Karnataka Telemedicine project linked the Narayana Hrudayalaya hospital for cardiac care at Bangalore with the district hospital, Chamarajanagar and the Vivekananda Memorial Trust Hospital at Saragur in Karnataka, as shown in Fig. 1 [2, 7].

Currently, the ISRO Telemedicine Network protects 384 hospitals, including 18 Mobile Telemedicine Units, 306 Remote/Rural/District/Medical College Hospitals, and 60 Specialty Hospitals [4]. The creation of “HEALTHSAT,” a high-end satellite designed to address the demands of the nation in terms of healthcare and medical education, has also been conceptualized by ISRO [4].

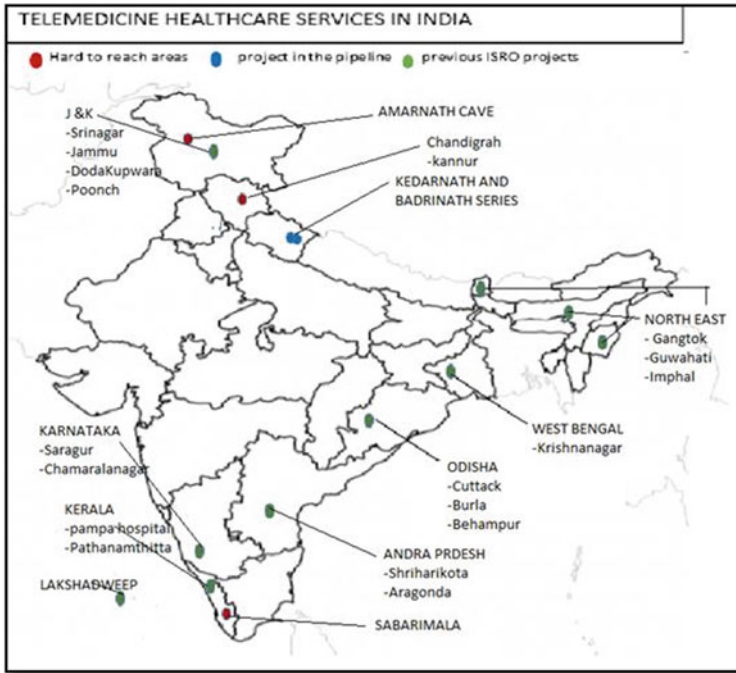


Fig. 1 Telemedicine healthcare services in India [7]

Indian Space Research Organization has provided satellite links to connect the telemedicine centres to hospitals in Delhi, Chandigarh, Srinagar, and Pondicherry. The Telemedicine units shield diverse areas of Ophthalmology, Cardiology, Radiology, Diabetology, General medicine, and Women and Child healthcare.

3 Internet of Things (IOT) in Telemedicine

The IOT concept came around 2008–2009. It is nothing but the integration of “Things”-oriented visions (i.e., RFID, UID, Smart items wire /wireless sensor and actuators), “Internet”-oriented Visions (i.e., IP for Smart object, Web of Things Objects, High-speed internet) and “Semantic”-oriented visions (i.e., Semantic Technologies Reasoning over data, Semantic execution environments) [8]. IoT provides sensing, tracking, identification and authentication and data collection of patients and specialists. It helps to evolve the Smart Telemedicine era, such as a smart city concept. It connects homes, streets, railways, offices, hospitals, etc. wireless technology plays a key role. Sensor devices enable continuous nursing and diagnosing, in particular patient conditions, providing real-time information about patients’ health indicators with medication regimen prescriptions. In this capacity, sensors can be

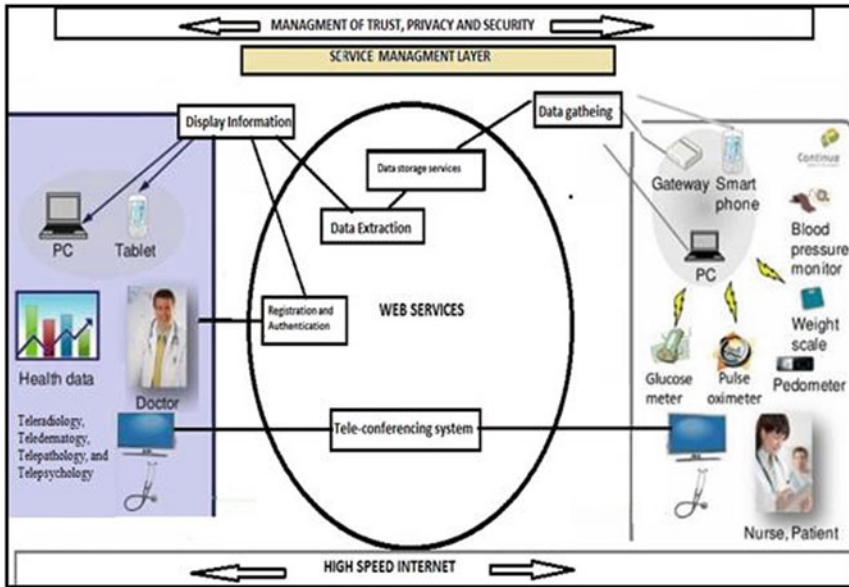


Fig. 2 Architecture of IoT and web services

applied in-patient and out-patient care. Diverse wireless access-based remote patient monitoring systems can be deployed to reach the patient everywhere, considering patient mobility [9].

IoT is enabled by technologies such as Real-Time Location Systems (RTLS), Global Positioning Systems (GPS), and Radio Frequency Identification (RFID). It supports many input/output devices and sensors, including cameras, microphones, keyboards, speakers, displays, Near Field Communication (NFC), and medical devices enabled with RFID tags and sensors.

The proposed architecture in Fig. 2 describes how the IoT combines with web services. It consists of three components.

3.1 Service Provider

It consists of doctors and hospitals and different types of telemedicine services like Teleradiology, Tele-dermatology, Telepathology, etc.

3.2 *Service Consumer*

It is any patient who requires a medical assistant. On this side, various equipment is installed glucose meter, pulse oximeter, blood pressure meter, x-rays machine, ECG machine, and many more.

3.3 *Web Services*

These are services provided by the Web. The interfaces provided for the registration of doctors and their authentication. Tele-conferencing and patient data storage at the database at the server are other services provided by this component. Besides these components, management of all these services is also required. So, the service management layer is introduced. The trust, privacy, and security of the patient and doctor's side must be maintained. This layer is maintained throughout the three components.

4 Merits of Telemedicine

The significant advantage of Telemedicine is its cost-effectiveness. Ongoing research and observation prove that Telemedicine is more cost-effective than traditional face-to-face testing. As technology advances, the cost of equipment is falling while the cost of skilled technicians is increasing [10]. An example of screening for diabetic retinopathy at a community health center, including the cost of his second in-person examination to confirm the need for treatment, would cost the patient 35% more Telemedicine than in person [11]. A few other advantages include ubiquitous, which facilitates specialist doctors anywhere, anytime, improving care efficiency, Telemedicine during natural disasters and remote monitoring.

5 Challenges and Issues in Telemedicine Hazards

5.1 *Trust, Privacy, and Security Management*

It could act as a surveillance mechanism that permeates most of our lives. Mediators, in turn, should include functionality related to managing the trust, privacy, and security of all data exchanged.

5.2 Third-Party Misuse

Nearly two-thirds of hospitals and radiology practices now use the remote interpretation of physician images. One concern is the temptation for insurers to require less-skilled personnel to review images as long as outsourcing “provides acceptable results at a significantly lower cost.”

5.3 Licensure and Liability

Physicians are very sensitive to getting licensed in the states where they practice. Some states require full domestic licenses for out-of-state consultants and interstates [12].

5.4 Reimbursement

Medicaid payments for Telemedicine are on the way, as is Medicare. Federal guidelines now urge states to “develop innovative payment methods” that: B. Reimbursement of interpreter fees for remote doctors and facility fees in their hometowns, and a uniform law has been enacted [12].

5.5 Implementation Issues

Training is needed at the grass-root level for technicians, IT staff, and local doctors to apply the Telemedicine concept.

5.6 Acceptance Issues

For village doctors and residents, using high-end technologies seems to be barricading. Still, once the benefits are understood, the agreement would be on the upper side, as seen with mobile telephony and rural internet services [13].

6 Future Trends

Remote Ambulance: In future cities, robotic ambulances will swarm together and travel to deliver services quickly and efficiently wherever needed. Rescue robots react in real-time.

City traffic regulations are standardized to reduce congestion during city closures and to serve the most frequently used pickup zones. It drives with or without a human driver, enters and exits traffic at optimal speed, and avoids accident situations with proximity sensors. The location of the user is robotically tracked via GPS, allowing the user to request an ambulance at a specific location at a specific time simply by pointing it out on a comprehensive map.

Automatized maintenance: On rare occasions when a vehicle not being used, it will head to a 'pit stop', where it automatically stacks into a narrow bay equipped with sensors, and actuators that trigger battery charging, perform simple maintenance tasks and clean the car.

Remote monitoring: doctors remotely observe the health conditions of patients via the internet.

7 Conclusion

The Internet of Things (IoT) technology has enormous potential in Telemedicine. It developed an intelligent infrastructure that connects far-to-reach areas into reach. In integration with IoT, Telemedicine has several advantages, including reduced cost, improved access, efficiency, urgent care, and efficiency. Besides having ethical, legal, and security concerns, it will be the future trend in the medical field. These challenges need to be addressed carefully for the continuous evolution of Telemedicine.

References

1. Raskas, M. D., Gali, K., Schinasi, D. A., & Vyas, S. (2017). Telemedicine and pediatric urgent care: A vision into the future. *Clinical Pediatric Emergency Medicine*, 18(4), 239–316.
2. Telemedicine: Healing touch through space, enabling specialty healthcare to the rural and remote population of India. <http://shiksha.isro.gov.in/pdf/brochures/4.pdf>. Retrieved March 1, 2017.
3. World Health Organization. (2010). *Telemedicine: Opportunities and developments in member states*. Report on the second global survey on ehealth. World Health Organization.
4. Bhatia, J. S., & Singh, C. (2020). Impact of usage of discrete networks on telemedicine capabilities especially in India.

5. <http://www.business-standard.com/content/b2b-pharma/indian-telemedicine-market-to-become-more-than-double-by>. In *IEEE international conference on medical imaging, m-health and emerging communication systems (Medcom)* (pp. 311–318), November 2014. <https://doi.org/10.1109/MedCom.2014.7006024>
6. <http://www.televital.com/>. (1989). Decade of telemedicine experience “Indian Telemedicine Company of the Year for 2009” by Frost and Sullivan M. Young, *The technical writer’s handbook*. University Science.
7. <http://www.hindustantimes.com/india-news/with-105-centres-govt-spreads-telemedicine-network-across-country/story-UDwyqZRniQOjzJg9MOzk8I.html>
8. Atzori, L., Iera, A., & Morabito, G. (2010). The internet of things: A survey. *Computer Networks, Computer Networks: The International Journal of Computer and Telecommunications Networking*, 54(15), 2787–2805. <https://doi.org/10.1016/j.comnet.2010.05.010>
9. Gómez, J., Oviedo, B., & Zhuma, E. (2016, December 31). Patient monitoring system based on Internet of things. In *Procedia computer science, the 7th international conference on ambient systems, networks and technologies* (Vol. 83, pp. 90–97).
10. Lamminen, J., Forsvik, H., Vopio, V., & Ruohonen, K. (2011). Teleconsultation: Changes in technology and costs over a 12-year period. *Journal of Telemedicine and Telecare*, 17(8), 412–416. <https://doi.org/10.1258/jtt.2011.110211>
11. Li, Z., Wu, C., Olayiwola, J. N., Hilaire, D. S., & Huang, J. J. (2012). Telemedicine-based digital retinal imaging vs. standard ophthalmologic evaluation for the assessment of diabetic retinopathy. *Connecticut Medicine*, 76(2), 85–90.
12. Newton, M. J. M. D. (2014). The promise of Telemedicine. *Survey of Ophthalmology*, 59(5), 559–567. <https://doi.org/10.1016/j.survophthal.2014.02.003>
13. Yuehong, Y. I. N., Zeng, Y., Chen, X., & Fan, Y. (2016). The internet of things in healthcare: An overview. *Journal of Industrial Information Integration*, 1, 3–13.

Heart Disease Prediction Using Machine Learning Techniques: A Survey for Societal Care and Information



Kuldeep Vayadande, Arnav Dhiwar, Darpan Khadke, Rohan Golawar, Sarwesh Khairnar, Sarthak Wakchoure, and Sumeet Bhoite

Abstract WHO reports states that nearly 1 crore 20 lakhs deaths happens due to heart diseases. In past years heart disease or cardiovascular disease cause large impact in medical industries, so they are really very dangerous and have a large impact worldwide. Although precious prediction of heart diseases or CD and also the 24 h monitoring on patient is not possible because it requires lots of knowledge and time. Heart disease treatment or diagnosis are very complicated, mainly in the poor countries or the countries which are not fully developed. Also, because of not having proper medical attention or timely cure of disease it can lead to death of the person. The medical industry has a large amount of data and is continuously used by researchers to develop new science and technology to minimize the number of deaths happens due to heart disease. This paper focuses on the various Machine Learning techniques used to predict heart disease from datasets.

Keywords Cardiovascular diseases · Heart disease · Heart disease prediction · Machine learning · Classification

1 Introduction

The heart being among our body's one of the most important parts, is the one that helps in pumping as well as being one of the most important elements of the cardiovascular system. It comprises various blood vessels network which includes arteries, capillaries and veins, let's not forget about the lymphatic vessels. With the help of blood vessels, the blood is delivered through our system. Multiple heart diseases including heart attacks, strokes, and coronary heart disease are caused by abnormal blood flow from the heart (CVD). If any kind of abnormalities are present in the heart, multiple diseases can occur such as Congenital heart disease, Arrhythmia, heart failure etc. also known as cardiovascular diseases. Over the years many biological research-oriented fields have observed that cardiovascular diseases have become

K. Vayadande · A. Dhiwar · D. Khadke · R. Golawar (✉) · S. Khairnar · S. Wakchoure · S. Bhoite
Vishwakarma Institute of Technology, Pune, Maharashtra 411037, India

the primary cause of death globally [1]. Cardiovascular diseases can be troublesome and bottleful and thus need immediate attention. Cardiovascular diseases of various types consist of Congenital Heart Disease, Arrhythmia, Coronary Artery Disease, Heart failure, Heart Muscle Disease and Heart Valve Disease. Such cardiovascular diseases are discussed below.

- (A) **Congenital Heart Disease**—It is a genetic defect that interferes with the structure of the heart since birth (Fig. 1).
- (B) **Arrhythmia**—Arrhythmia is occurring due to the changes in the normal heartbeat of the people (Fig. 2).
- (C) **Coronary Artery Disease**—Heart arteries are responsible for supplying nutrients and oxygen to the muscle of the heart. A high cholesterol level can damage or deteriorate the coronary arteries. Having high cholesterol limits the amount of oxygen and nutrients provided to the body by the coronary arteries (Fig. 3).
- (D) **Heart failure**—An alternative name for heart failure is congestive heart failure, which occurs when blood does not circulate efficiently and effectively throughout the human body (Fig. 4).
- (E) **Heart Muscle Disease (Cardiomyopathy)**—Similarly, Cardiomyopathy is the name given to the disease. Thickening of the human heart's walls or enlargement of the human heart leads to heart muscle disease. As a result of this condition, the body receives less blood supply, which results in the heart failing (Fig. 5).

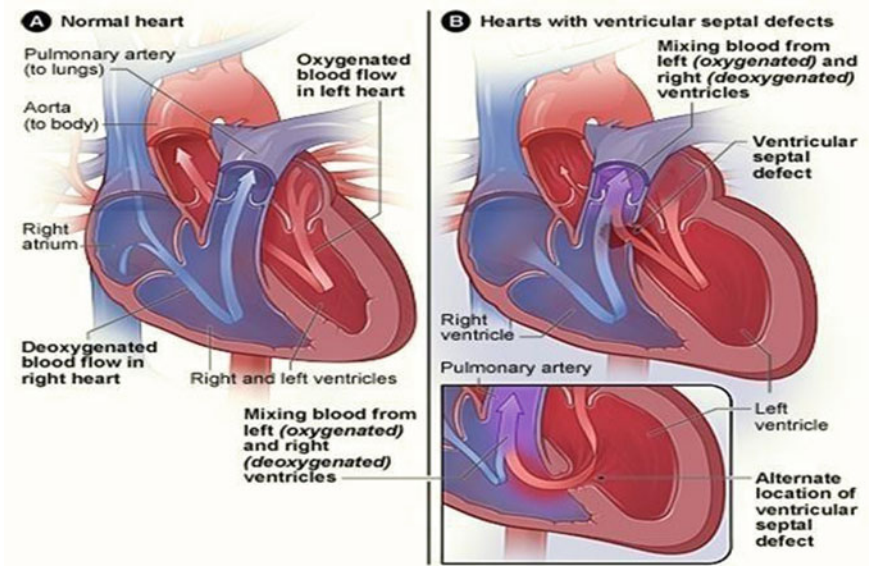


Fig. 1 Congenital heart disease [2]

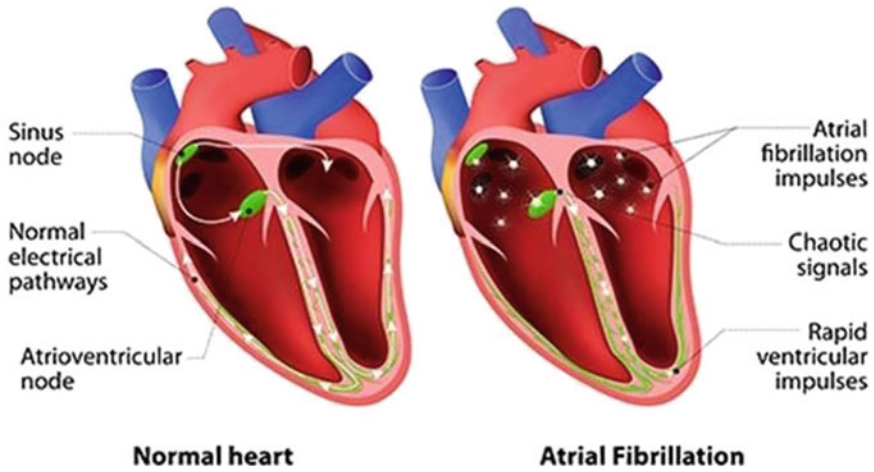


Fig. 2 Arrhythmia [3]

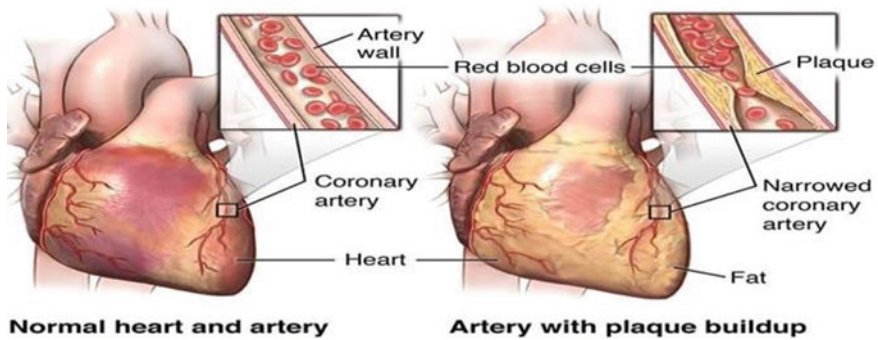


Fig. 3 Coronary artery disease [4]

(F) **Heart Valve Disease**—There are four valves for the Human heart. These four valves are responsible for pumping of the blood to the whole human body and to ensure that the heart keeps the forward flow of the blood in the human heart (Fig. 6).

Besides personal habits and professional activity, there are a number of other factors that become responsible for cardiovascular diseases such as heavy drinking, use of tobacco, intake of caffeine, being physically inactive and sitting for long periods of time. Not only these but other psychological factors too which include stress, depression, anxiety, obesity etc. [8]. Therefore, we must take preventive measures and steps to avoid such habits and also to capture the patients' symptoms and his day-to-day habits that lead to cardiovascular diseases. Before a diagnosis of CVD can be made, patients undergo various tests which include blood as well

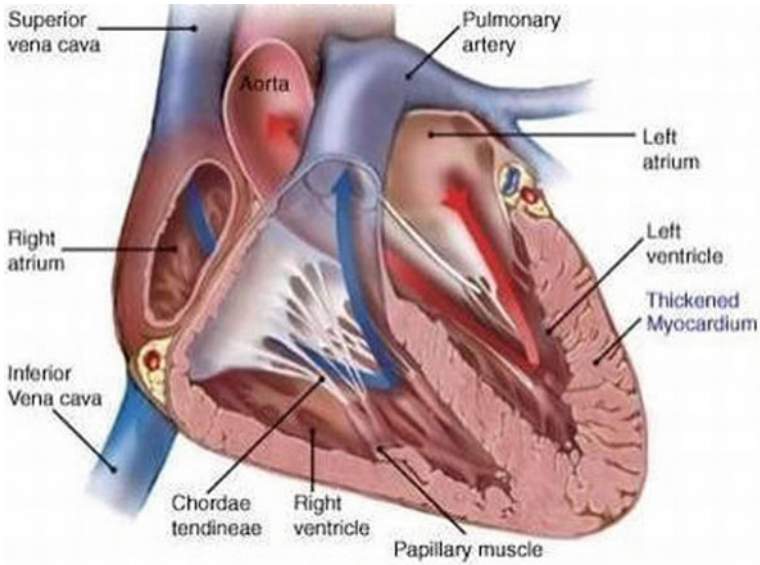


Fig. 4 Heart failure [5]

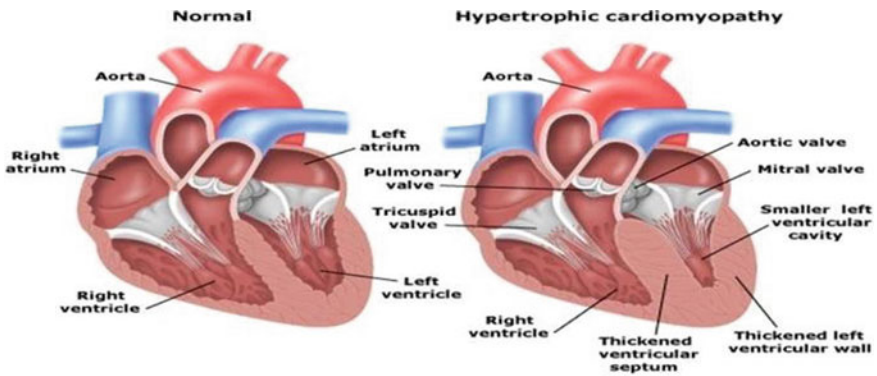


Fig. 5 Heart muscle disease (Cardiomyopathy) [6]

as blood sugar testing, ECG which records the rhythmic patterns of heart beats, measuring of blood pressure, checking of cholesterol levels, and auscultation. If a patient's condition is critical and medication is required right away, these tests tend to be long and complicated [3]. Taking preventive measures to avoid the complications of heart disease is dependent on making an accurate, efficient, and early medical diagnosis of the disease. Providing quality services and making accurate and efficient predictions is the chief challenge in the world of medical sciences today. Automation can be used to solve the last problem and provide opportunity for research within the healthcare sector, especially in early detection of diseases, such as cancer and CVD,

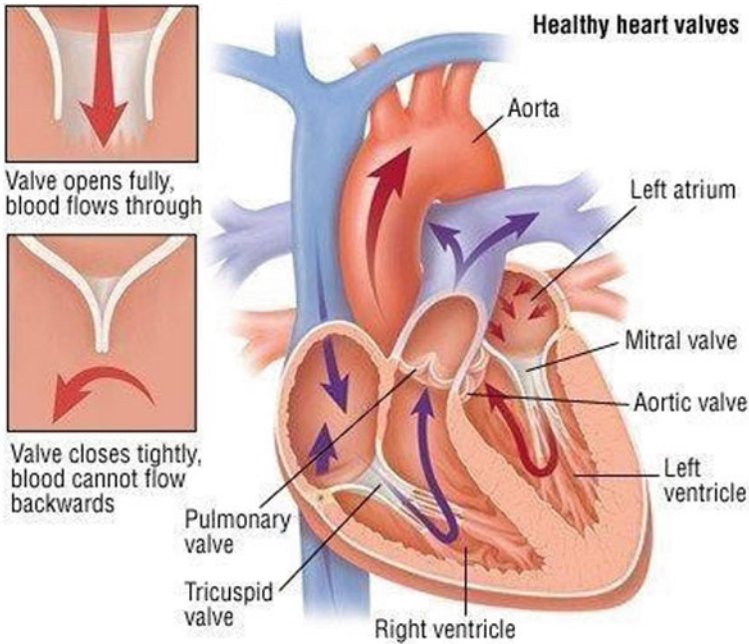


Fig. 6 Heart valve disease [7]

to enhance survival rates. We are constantly experimenting and observing the latest improvements in computing capabilities and programming capabilities and we found out that with the help of artificial intelligence and machine learning algorithms we can prove that these massive complications do have a solution [8]. Machine learning techniques such as classification are popular for predicting outcomes. When trained using adequate data, classification models are effective in identifying diseases [9]. This article will discuss various techniques that will be used for prediction and analysis of heart diseases.

2 Machine Learning

As Artificial Intelligence is growing rapidly it has made certain complex things look very easy with the help of Machine Learning. Machine Learning is one of the family of Artificial Intelligence which makes a computer machine smarter and gives an upper hand on taking precise decisions (Fig. 7).

Various Types of Classification Algorithms:

1. Logistic Regression
2. Naïve Bayes

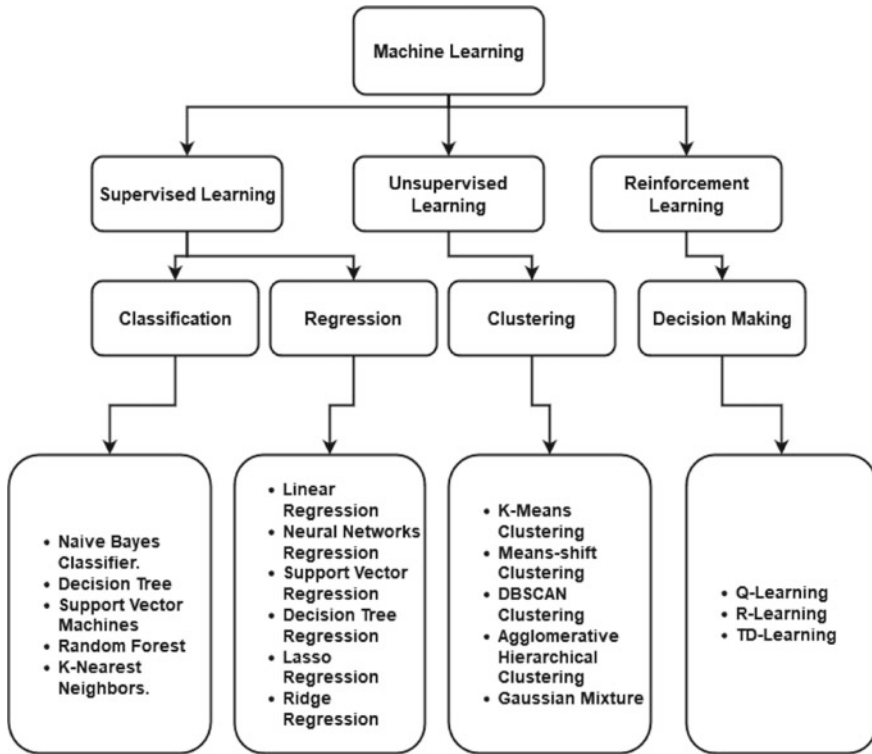


Fig. 7 Machine learning types

3. Stochastic Gradient Descent
4. K-Nearest Neighbors
5. Decision Tree
6. Random Forest
7. Support Vector Machine.

(A) **Supervised Learning**

The learning which is carried out by the service of a teacher, tutor or trainer is nothing but the Supervised Learning. It basically functions depending on the set of learning patterns based on guessing or predicting an instance and explaining the data along with input to output algorithms. Supervised learning is classified into ANN, SVM, Naive Bayes, neural network regression as linear and polynomials, decision trees, and arbitrary forests.

(B) **Unsupervised Learning**

The dataset in this learning is not supervised as the supervised learning and thus it's called unsupervised learning. Unsupervised learning generally focuses on grouping the similar type of data and making the dataset more compatible.

(C) **Semi Supervised Learning**

Semi Supervised learning was basically introduced to overcome the drawbacks of Supervised and unsupervised Learning techniques. Supervised learning needs to have datasets which are already labelled by the Data scientist which is a very tedious and time-consuming task in case of larger data sets. Whereas unsupervised learning does not have any prior knowledge about the data sets and learns from the raw data leading to consume more time.

(D) **Reinforcement Learning**

Reinforcement learning is all about taking an appropriate action in order to get the desired reward in a particular situation. So here the reinforcement agents come into action where they decide the instruction or the path with least obstacles to gain the reward.

3 Literature Review

Ramalingam and Dandapath [10], authors used three different input dataset that are Cleveland dataset, People's Hospital dataset and UCI heart disease dataset, after evaluation the People's Hospital dataset was better than the rest two dataset for all the different algorithm that were used. Based on performance the SVM, RF and Ensemble model gives better result. SVM gives 98.9%, RF gives 97% and Ensemble model gives 98% accuracy respectively.

Khourdifi and Bahaj [3], authors used two different dataset that are UCL Data set, Chennai Research Institute. The performance of K-NN, RF and MLP algorithm gives better result on both of dataset with Accuracy of KNN with 99.65%, Random Forest with 99.6% and MLP with 91.65% respectively.

Nashif et al. [1], in this paper two different dataset were used that are Cleveland dataset, Statlog dataset. The algorithms that are used on the dataset are NB, SVM, RB, SP and ANN. After the evaluation the result shows that SVM, RB, SP are gives more better result. Accuracy with SVM gives 97.53%, RB gives 95.76% and SP gives 95.05% respectively.

Abdeldjouad [11], with other two authors used two dataset that are UCI Repository Heart Disease Dataset, Cleveland database. The techniques used are MOEFC, LR and AdaBoostM1. From this AdaBoostM1 has the highest accuracy than MOEFC, LR. The accuracy of AdaBoostM1 was 80.01%.

Lakshmanarao [12], in this paper Kaggle Heart disease dataset is used. The algorithms Logistic Regression, KNN, AdaBoost, DT, NB, RF, SVM, Extra Tree Classifier and Gradient Boosting are used. Authors have used algorithm on three different methods. SVM gives best Accuracy with 99%. Random Forest and Extra tree Classifier give better accuracy with 91.3% and 91%. RF and Extra tree Classifier give best accuracy with 90.3%, 90.3%.

Table 1 Existing machine learning method comparison table

Sr. No.	Authors	Year	Disease	Machine learning algorithm	Dataset input	Remarks	Conclusion
1	Ramalingam et al. [10]	2018	Heart disease	K-Nearest Neighbor, Support Vector, Machine, decision Tree, Naïve Bayes, Random Forest, Ensemble Model	Cleveland dataset, People's Hospital dataset and UCI heart disease dataset	Naïve Bayes, SVM, K-NN, Decision tree, Random Forest, Ensemble Model has 83.49%, 98.9%, 83.16, 77.55%, 91.6%, 97%, 98% accuracy respectively	SVM, Random Forest, Ensemble Model are giving better result People's Hospital dataset are better than UCI heart disease dataset and Cleveland dataset
2	Khourdifi and Bahaj [3]	2019	Heart disease	K-NN, SVM, NB, RF, ANN, MLP, J48, Bayes Net	UCL Dataset, Chennai Research Institute	K-NN, SVM, NB, RF, ANN, MLP, J48, Bayes Net has 99.65%, 87.55%, 82.18%, 99.6%, 91.65%, 84.35%, 84.5% accuracy respectively	K-NN, SVM and MLP are giving better result
3	Nashif et al. [1]	2018	Heart disease	NB, SVM, RB, SP, ANN	Cleveland Heart Disease dataset, Stat logheart disease dataset	NB, SVM, RB, SP, ANN has 86.40%, 97.53%, 95.76%, 95.05%, 77.39% accuracy respectively	SVM, RB, SP are giving more better result
4	Abdeljoud et al. [11]	2020	Heart disease	MOEFC, LR, AdaBoostM1	UCI Repository Heart Disease Dataset, Cleveland database	MOEFC, LR, AdaBoostM1 has 79.42%, 78.77%, 80.01% accuracy respectively	AdaBoostM1 has the highest accuracy than MOEFC, LR

(continued)

Table 1 (continued)

Sr. No.	Authors	Year	Disease	Machine learning algorithm	Dataset input	Remarks	Conclusion
5	Lakshmanarao et al. [12]	2019	Heart disease	Logistic Regression, K-NN, AdaBoost, Decision Tree, Naive Bayes, Random Forest, SVM, Extra Tree Classifier, Gradient Boosting	Heart disease dataset from Kaggle	Results with Random over sampling:—67.5%, 79.4%, 66.6%, 91.5%, 60%, 97%, 99%, 97.8%, 94.6% accuracy respectively	Random oversampling:—SVM gives best Accuracy Synthetic Minority Oversampling:—RF and Extra tree Classifier gives best accuracy Adaptive synthetic sampling:—RF and Extra tree Classifier gives best accuracy
6	Anbuselvan [8]	2020	Heart disease	Logistic Regression, NB, SVM, K-NN, Decision Tree, RF, XGBoost	The Cleveland heart dataset from the UCI	Logistic Regression, NB, SVM, K-NN, Decision Tree, RF, XGBoost has 75.41%, 77.05%, 73.77%, 57.83%, 77.05%, 86.89%, 78.69% accuracy respectively	RF with 86.87% and XGBoost with 78.79% give more accuracy
7	Alotaibi [13]	2019	Heart disease	Decision Tree, Logistic Regression, RF, NB, SVM	Heart disease dataset from Kaggle	Decision Tree, Logistic Regression, RF, NB, SVM has 93.19%, 87.56%, 89.14%, 87.27%, 92.30% Accuracy respectively	Decision tree and SVM algorithm give more accuracy

Table 2 Comparison table of machine learning method on basis of accuracy, specificity and sensitivity

Method	Accuracy	Specificity	Sensitivity
NB	82.78	82.61	86.35
K-NN	81.43	85.17	85.93
SVM	87.39	80.12	91.75
RF	90.73	91.4	92.18
DT	83.83	83.76	89.73
ANN	87.91	63.42	77.40
MLP	83.53	78.21	85.31

Anbuselvan [8], author has used Cleveland heart dataset from the UCI. On this dataset the Logistic Regression, NB, SVM, K-NN, Decision Tree, RF, XGBoost algorithms are performed. The result after evaluation is RF with 86.89% and XGBoost with 78.69% give more accuracy (Tables 1 and 2).

4 Scope of Implementation

In this paper we have discussed about various Techniques that can be used for Predicting Heart Disease by considering various factors, so by performing analysis of these dataset one can predict possibility of Heart Disease. So, our Task in future would be Combining multiple Machine Learning algorithms and developing a robust system which can detect heart disease from the Human Beings and this system would be very useful for society for detecting heart disease from them.

5 Conclusion

As the mediums causing heart problems are increasing the demand for better health care is increasing now a days. However, to diagnose the heart disease it should be detected at early stage in order to ensure the patient's safety. The death rate could be reduced if appropriate actions are taken within right period of interval. This model will surely help the doctors to detect the heart problem at early stage and the treat the patient with appropriate treatment. Whereas the patients can use this model too. If the disease is detected at early stage by the patient, he can consult the doctors as soon as possible and can cure the disease. Furthermore, research can be performed for the betterment of model and more techniques can be implemented to get a precise and broader prediction of heart disease.

References

1. Nashif, S., Raihan, M., Islam, M., & Imam, M. (2018). Heart disease detection by using machine learning algorithms and a real- time cardiovascular health monitoring system. Scientific Research Publishing.
2. Congenital heart defect. https://en.wikipedia.org/wiki/Congenital_heart_defect
3. Khourdifi, Y., & Bahaj, M. (2018). Heart disease prediction and classification using machine learning algorithms optimized by particle swarm optimization and ant colony optimization. *The Intelligent Networks and Systems Society*.
4. Normal Heart Artery. <https://www.uchicagomedicine.org/conditions-services/heart-vascular/coronary-artery-disease>
5. Heart Failure. <https://www.havhrt.com/congestiveheartfailure>
6. Cardiomyopathy. <https://www.sujyoheartclinic.com/cardiomyopathy/>
7. Heart Valves. <https://www.drugs.com/health-guide/heart-valve-problems.html>
8. Anbuselvan, P. (2020). Heart disease prediction using machine learning techniques. *International Journal of Engineering Research & Technology*.
9. Reddy, K., Elamvazuthi, I., Aziz, A., Paramasivam, S., Chua, H., & Pranavananda, S. (2021). *Heart disease risk prediction using machine learning classifiers with attribute evaluators*. Multidisciplinary Digital Publishing Institute.
10. Ramalingam, V., Dandapath, A., & Raja, M. (2018). Heart disease prediction using machine learning techniques: A survey. *International Journal of Engineering & Technology*.
11. Abdeldjouad, F., Brahami, M., & Matta, N. (2020). A hybrid for heart disease diagnosis and prediction using machine learning techniques. Springer.
12. Lakshmanarao, A., Swathi, Y., & Sundareswarar, P. (2019). Machine learning techniques for heart disease prediction. *International Journal of Scientific & Technology Research*.
13. Alotaibi, F. (2019). Implementation of machine learning model to predict heart failure disease. *International Journal of Advanced Computer Science and Applications*.

Stock Market Prediction Using Machine Learning



Reshma Patil and Swati P. Pawar

Abstract To comprehend market behavior and develop effective investments and trades, investment organizations, hedge funds, and even individual investors must study financial models. Investors typically make accurate forecasts by researching past stock prices, corporate performance patterns, etc. The first round of theories emerging from the conjecture suggests that stock unit prices are completely arbitrary and unpredictable. Quantitative analysts are used to create predictive models to improve the guesses. The research focuses on improving models for enabling appropriate recommendations for financial investments by applying machine learning techniques.

Keywords Machine learning · Regression using a random forest · Stock price forecasting

1 Introduction

The stock markets around the world reflect huge wealth. Investors looked for ways to gather information on the companies listed on the market, just like they did during the extended market. Investors used to rely on their knowledge of market trends to identify trends, but this is no longer practicable. Simple mathematical study of financial data yields some insights. However, in recent years, a variety of artificial intelligence (AI) technologies have been employed by investing firms to search for patterns in massive volumes of real-time equities and financial information. These systems assist in the decision-making process for investments, and they have been in use for long enough that their features and performance will be examined and evaluated to find those systems, and enhance prophetic performance in comparison to other methods. The vendor and stock broker earn greatly if the prediction comes true. When a prognosis takes an unexpected turn, it is frequently predicted by looking at the history of many securities markets. Machine learning is cost-effective because

R. Patil (✉) · S. P. Pawar
SVERI College of Engineering, Pandharpur, Solapur, Maharashtra, India
e-mail: rkmalgonde@cod.sveri.ac.in

© The Author(s), under exclusive license to Springer Nature Switzerland AG 2024
P. M. Pawar et al. (eds.), *Techno-societal 2022*,
https://doi.org/10.1007/978-3-031-34644-6_38

349

it can represent these operations. With increasing accuracy, it forecasts a market price value that is close to the physical weight; the development of machine types of research is due to its accurate and economical value measurements.

The crucial component of machine learning utilized in education is the dataset. The data set should be as specific as it is possible to be, as any modification in the data would support significant changes in the output. The dataset for this project was collected from Yahoo Finance and used supervised machine learning. The five variables in this dataset are open, close, low, high, and volume. Airy, compact, soft, and increased area units indicate different bid costs at other times with nearly identical names. The basic measure involves the transfer of shares from one owner to another.

The development of a model is then done using the test data. This hypothesis is tested using an LSTM model and a regression model separately. Regression reduces errors while LSTM aids in information and result processing during working hours. Last but not least, graphs for the actual and anticipated price variations are planned for both the regression-based model and the LSTM-based model.

The goal of Stock Market Prediction is to forecast the price of a company's money stocks over the longer period. Machine learning is used in market prediction systems to create forecasts based on current exchange indices and coaching on prior values. Machine learning produces more precise and in-depth projections by using several models. Utilizing regression and LSTM machine learning algorithms and gaining a comprehensive grasp of stock values are our main goals. The size of the unit, the high, the low, and the volume of stock values are among the many variables taken into account. This paper introduces a number of pricing calculation methods, including the R factor and quantitative analysis.

R factor—The chance/praise ratio, also known as the “R/R ratio,” contrasts a change's capability income and loss. It is a calculation that uses the distinction between the income goal and the access factor to locate praise and the distinction between the difference between the stop-loss and the access factor to decide chance.

Quantitative Analysis—A technique known as quantitative analysis (QA) in finance emphasizes mathematical and statistical analysis to help determine the price of a financial asset, along with an inventory or option. Quantitative buying and selling analysts, also known as “quanta,” use a variety of data to improve buying and selling algorithms and computer models, including historical funding and inventory market data.

2 Problem Statement

Project focuses on development of Real time website—Share market prediction Investment firms, hedge funds and even individuals have been using financial models to better understand market behavior and make profitable investments and trades.

A wealth of information is available in the form of historical stock prices and company performance data, suitable for machine learning algorithms to process. Investors make educated guesses by analyzing data. For the purpose of accurate price prediction, we need a website which will give us correct and accurate prediction.

3 Objectives

The objective of the proposed system is given below.

- To study literature related to proposed system.
- Look into Stock Prices.
- Apply a simple linear regression model.
- Implement the LSTM model with the classification report and confusion matrix.

4 Literature Survey

AI and machine learning algorithms in the field of machine learning can be used to predict stock prices. In order to anticipate stock price, it employs the SVM model. Support vector machine that uses algorithms for classification. It is employed to produce a fresh text. Predicting the direction of the stock market using multiple linear regression with interactions [1].

Beginner's examines whether there are any abnormalities and whether the markets are efficient using data from stock markets around the world. Scholars always confirm any market anomalies they discover before looking for pre-existing models that could account for the anomaly. Let's say researchers are unable to estimate, assess, and predict any model to account for the anomaly. If so, academics will utilise modelling, quantitative analysis, or even a brand-new information theory to explain the anomaly that gave rise to behavioural finance. One might be able to take advantage of the monster to make money in the event of an inexplicable abnormality. This is one method by which investors can obtain helpful investing guidance [2].

The connection between the stock market and the economic activity of the five European nations—Germany, France, Italy, the Netherlands, and the United Kingdom—is reflected in the actual Gross Domestic Product. In addition to the usual variables employed in such assessments, this approach also takes into account stock market returns, actual economic activity, and interest rates. The authors have incorporated the composite leading indicator into the empirical VAR model [3].

The stochastic process behaviour and weak-form potency of the CIVETS stock markets from 2002 to 2012. We frequently use variance quantitative relation tests, serial autocorrelation tests, and unit root tests. Our unit root findings suggest that CIVETS are subject to a stochastic process [4].

The authors employ four-deciler architectures to forecast the stock value of the NSE and securities markets, two of the top stock markets in the world. With the stock

value of TATA MOTORS obtained from the NSE, we frequently train four networks: MLP, RNN, LSTM, and CNN. The models were used to forecast the stock values of MARUTI, HCL, and AXIS BANK from the NSE stock exchange and BANK OF AMERICA (BAC) and CHESAPEAKE ENERGY from the securities market. The models clearly have the ability to describe the patterns present in each stock market, as shown by the results [5].

Financial experts are aware of the significance of correctly estimating the price of a security because they need to know what kind of return they can expect on their investments. In order to estimate stock costs, specialist experts and intermediaries typically examine historical prices, volumes, value designs, and fundamental trends. Since the socio-economic situation of the country, the political climate, and major events all have an impact on stock prices, stock value predictions now are even more perplexing than they were in the past [6].

5 System Design

This study developed a stream-lit LSTM (Long Short Term Memory) model that forecasts values using historical data. High, Low, Open, and Close are the Prediction values. For those looking to trade who are students or newbies, it is a trustworthy application. They can immediately spot market trends, whether they are rising or downward; otherwise, the market would continue sideways. The confusion matrix for the classification report is generated by the model. The two regression and classification methods for stock market prediction were introduced in this research. The closing price of the firm shares is foreseen using the regression method. The classification approach will forecast whether the closing price of a company’s stocks will rise or fall in the next days (Fig. 1).

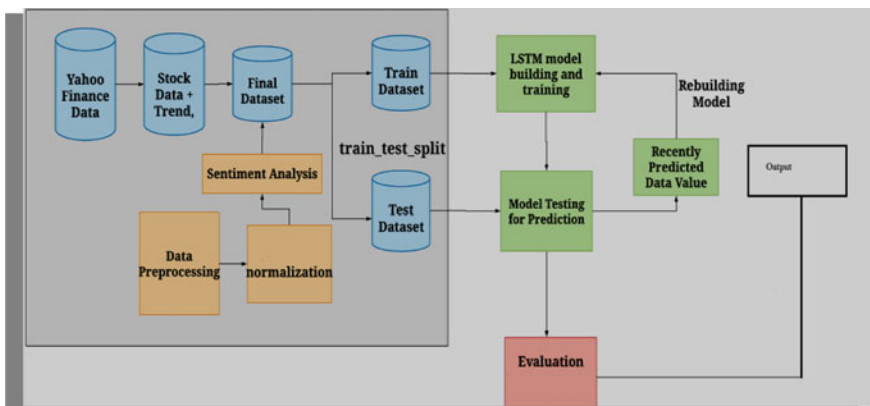


Fig. 1 Diagram of proposed system

6 Method of Proposed Work

6.1 *R Factor*

Equity market risks come in two flavors: systematic and non-systematic. Changing government policies, rising oil costs, and currency fluctuations are all well-known sources of frequent dangers. However, unsystematic risks are brought on by elements that are specific to a business or sector. Unsystematic risk is also influenced by factors like management and labor relations, increased competition, the entry of rival players, and customer preference for a company's products.

6.2 *Stock Analysis Candle Stick Chart*

The price changes of securities, derivatives, and currencies are displayed on candlestick charts. Each candle, like a graph, depicts the four key data points for that day: open and close in the thick body; high and low in the wick. Candlesticks can be used in two different ways to represent the buying and selling pressure.

6.3 *LSTM Model*

Long Short-Term Memory styles are incredibly efficient in gathering time. They can anticipate a random wide range of stages into their destiny. An LSTM module (or molecule) includes five necessary components that allow it to model both long- and short-term data. Cell nation (ct) is the term used to describe the molecular's internal memory, which stores both short-term and long-term memories.

Hidden nation (ht)—These output nation records are used to predict future stock market prices by taking into account current input, previous remote country, and current molecular input. Additionally, the hidden country can choose to only retrieve the short- or long-term or each type of memory stored inside the molecular country in order to make the subsequent prediction.

Determines how many records from the present entrance flow to the molecular nation is the input gate (it).

The number of data from the present that enter and flow into the previous molecular nation is determined by the forget gate (ft).

In order for the LSTM to easily choose out only long-term memories, or both short-term and long-term memories, the output gate (ot) determines how many records from the contemporary molecular nation go into the hidden government.

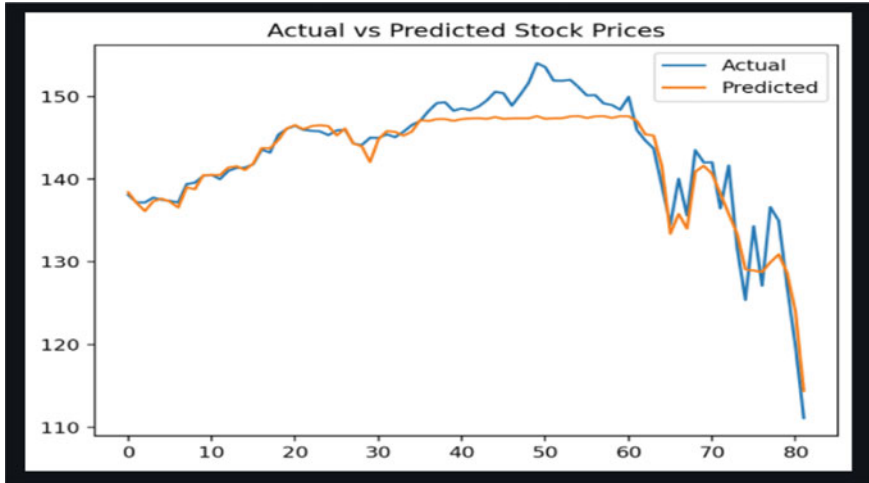


Fig. 2 Actual and predicted result

7 Expected Result

7.1 *New Actual Predicted Result*

See Fig. 2.

7.2 *R Factor*

Figure 3 the graph depicts the close price of the Nike (NKE) company, with the actual value indicated in green, and is contrasted with the MA (Moving Average), which has an MA53-day blue marker and an MA30-day red marker. The graph displays the firm NKE's (Nike's) total daily returns. The value is indicated on the y-axis, and the year is indicated on the x-axis.

7.3 *Stock Analysis Candle Stick Chart*

In Fig. 4 we can see the candlestick chart, which is contrasted with the Bollinger Band, which is indicated by the colour red, the RSI, which is indicated by the color blue, and the volume, which is indicated by the color gray. The stock price is indicated on the y-axis, and the month and year are indicated on the x-axis.



Fig. 3 R factor



Fig. 4 Stock analysis candle stick chart

7.4 Quantitative Analysis

The only person who creates a complex framework for financial institutions to help them charge and exchange securities on the financial market is a quantitative analyst.

Quants may be of types:

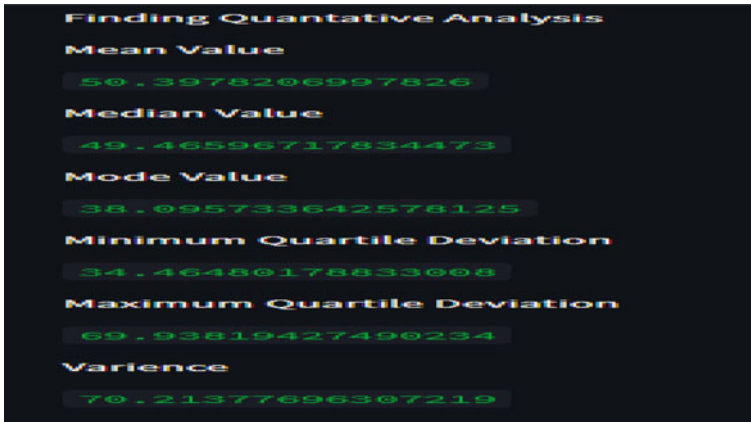


Fig. 5 Quantitative analysis

7.4.1 Front Workplace Quant

These are the people who offer the dealer the money or the tools for buying and selling securities right away.

Quants working in the back office—These quants are there to validate the framework and develop new methods following research.

The quantitative analysis of the NKE (Nike) company's contents is listed below (Fig. 5).

1. Mean
2. Median
3. Mode
4. Maximum
5. Minimum
6. Variance.

In Fig. 6 Variance value is shown by the colour blue, maximum value by the colour red, mean value by the colour green, median value by the colour violet, mode value by the colour orange, and minimum value by the colour light blue.

7.5 Forecasting of Values

The value of the stock is predicted using forecasting for time series in terms of the day, such as short term (5–10 days), medium term (20–100 days), and long term (200 days). NKE stock predictions on the testing set, with a 17.41% testing error. The predicted value for the prior data is displayed in the graph below.

The graph displays value through April 24, 2022.



Fig. 6 Quantitative analysis pie chart

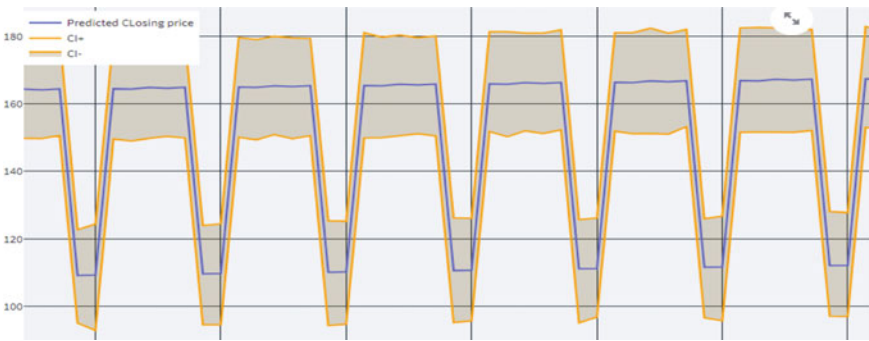


Fig. 7 Forecasting of values

In Fig. 7 Predicted closing price is denoted with a blue color line, CL+ (closing positive) fee, which is above the predicted price and denoted with orange color and also, we see CL- (closing negative) price, which is below the expected price and denoted with orange paint.

Confusion Matrix

See Fig. 8.

7.6 Advantages

- Predict Correct Prices
- Reduce Human Efforts.

```

Classification report :
      precision    recall  f1-score   support

     1         0.67     0.50     0.57         4
     0         0.71     0.83     0.77         6

 accuracy          0.70         10
 macro avg         0.69     0.67     0.67         10
 weighted avg     0.70     0.70     0.69         10

```

Fig. 8 Confusion matrix

8 Conclusion

This paper is aimed at helping stock brokers and investors to invest their money wisely and knowingly, in the stock market. The applicability of prediction in stock market business is immense, which is a very complex process owing to ever-changing facade of the stock market. This project aims at finding the best prediction model among a plethora of those existing today, and implementing the one with the highest empirical and/or real accuracy in order to predict stock prices. The purpose of this paper is to analyze the shortcomings of the current system and building a time-series prediction model that would mitigate most of them, by implementing more efficient algorithms. This would indeed make investment in the stock market, a safer bet.

References

1. Bhuriya, D., Kaushal, G., Sharma, A., & Singh, U. (2017, April). Stock market prediction using a linear regression. In *2017 International conference of electronics, communication and aerospace technology (ICECA)* (Vol. 2, pp. 510–513). IEEE.
2. Iacomin, R. (2015, October). Stock market prediction. In *2015 19th international conference on system theory, control and computing (ICSTCC)* (pp. 200–205). IEEE.
3. Nivetha, R. Y., & Dhaya, C. (2017, April). Developing a prediction model for stock analysis. In *2017 International conference on technical advancements in computers and communications (ICTACC)* (pp. 1–3). IEEE.
4. Xing, T., Sun, Y., Wang, Q., & Yu, G. (2013, December). The analysis and prediction of stock price. In *2013 IEEE international conference on granular computing (GrC)* (pp. 368–373). IEEE.
5. Rajput, V., & Bobde, S. (2016, April). Stock market prediction using hybrid approach. In *2016 International conference on computing, communication and automation (ICCCA)* (pp. 82–86). IEEE.
6. Parmar, I., Agarwal, N., Saxena, S., Arora, R., Gupta, S., Dhiman, H., & Chouhan, L. (2018, December). Stock market prediction using machine learning. In *2018 First international conference on secure cyber computing and communication (ICSCCC)* (pp. 574–576). IEEE.
7. Liu, S., Liao, G., & Ding, Y. (2018, May). Stock transaction prediction modeling and analysis based on LSTM. In *2018 13th IEEE conference on industrial electronics and applications (ICIEA)* (pp. 2787–2790). IEEE.
8. Shakva, A., Pokhrel, A., Bhattarai, A., Sitikhu, P., & Shakva, S. (2018, January). Real-time stock prediction using neural network. In *2018 8th International conference on cloud computing, data science & engineering (confluence)* (pp. 1–4). IEEE.

9. Abhishek, K., Khairwa, A., Pratap, T., & Prakash, S. (2012, July). A stock market prediction model using artificial neural network. In *2012 Third international conference on computing, communication and networking technologies (ICCCNT'12)* (pp. 1–5). IEEE.
10. Jinyu, T., & Xin, Z. (2009, August). Apply multiple linear regression model to predict the audit opinion. In *2009 ISECS international colloquium on computing, communication, control, and management* (Vol. 4, pp. 303–306). IEEE.
11. Internet Source. yourpriceinfo.blogspot.com
12. Internet Source. www.mafiadoc.com
13. Internet Source. <https://en.wikipedia.org/wiki/Regression>
14. Internet Source. https://en.wikipedia.org/wiki/Stock_market
15. Student Paper: Submitted to Wakefield College.
16. Student Paper: Submitted to University of Southampton.

Using RStudio to Analyze Big Data



Mohua Biswas, Papiya Biswas Datta, Tejas S. Joshi, and Suvarna D. Pujari

Abstract Online databases have replaced paper-based data sources. A greater amount of data is produced and used every day. Additionally, more and more data is being gathered from a wide variety of sources via robots, financial transactions, and sensors like security cameras. Data analytics, or simply “analytics,” is a burgeoning field that studies the processing of various data to derive such knowledge. Additionally, this procedure may involve gathering, organizing, pre-processing, transforming, modelling, and interpreting the data. R is a computer language designed specifically for data analysis. Additionally, it is a software environment used to examine graphical displays, reporting, and data modelling. Drawing graphs in R is simple and includes creating histograms, box plots, scatter plots, and pie charts.

Keywords R · Big data · Data analytics · Graphs

1 Introduction

Big data is a body of information that is enormous in volume and is always expanding exponentially. It is a data set that is so huge and complex that no data management solution can effectively store or process it. Some of the Big Data instances are as follows: One terabyte of brand-new transaction data is produced each day by the New York Stock Exchange, a prime example of big data. Also, through Social media: According to a statistic, Facebook’s databases receive more than 500 gigabytes of new data each day. This information is primarily produced by the uploading of images and videos, messaging, comments, etc. Data analysis is an essential component of successful business management. Effective data use helps organizations better

M. Biswas (✉) · T. S. Joshi · S. D. Pujari
SVERI’s College of Engineering, Pandharpur, India
e-mail: msbiswas@coe.sveri.ac.in

PAH Solapur University, Solapur, India

P. B. Datta
Devi Mahalaxmi College of Engineering, Titwala, Mumbai, India

understand their historical performance and make better decisions about their future operations. The amount of data generated by the many thousand flights per day can amount to many Petabytes. The R Development Core Team is presently responsible for developing R, which was developed by Ross Ihaka and Robert Gentleman at the University of Auckland in New Zealand. The names of both developers were used to create the name of this programming language. In 1992, the first project was under consideration. The first project was considered in 1992. The initial version was released in 1995, and in 2000, a stable beta version was released. Additionally, it is a software environment used to examine graphical displays, reporting, and data modelling.

2 Big Data Analytics

2.1 Types of Big Data

Essentially, there are three forms of big data [1] (Fig. 1).

- (a) **Structured Data:** Structured data refers to any data that can be accessed, processed, and stored in a fixed format. Because it is well-organized, structured data is the most straightforward to work with. Set parameters determine its dimensions. Similar to spreadsheets, every piece of data is organized into rows and columns. Examples of Structured Data: An “Employee” table in a database is an example of structured data. Structured data has quantitative data, such as age, contact address, billing, expenses, debit or credit card information, etc. (Table 1).
- (b) **Unstructured Data:** Unstructured data is any data whose shape is unknown. Unstructured data is any data that is not organized.
- (c) **Semi-Structured Data:** Both types of data can be found in semi-structured data. Semi-structured data examples include emails, webpages, graphs, tables, HTML code, and more.

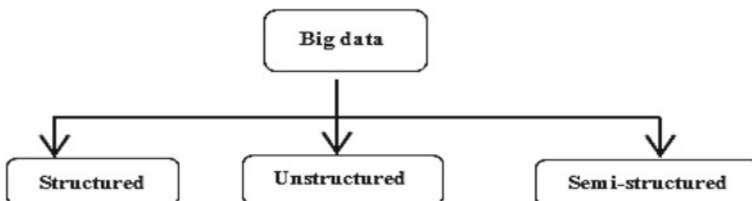


Fig. 1 Category of big data

Table 1 Employee’ table in a database

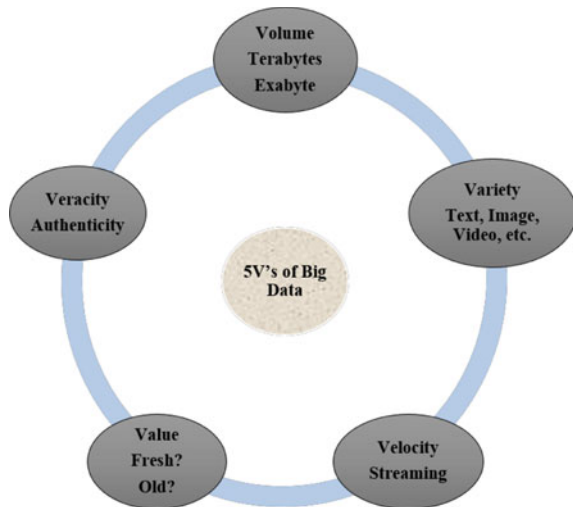
Employee_ID	Employee_Name	Gender	Department	Salary in lacs
2365	Pratibha Kulkarni	Female	Finance	650,000
2366	Rajesh Joshi	Male	Admin	650,000
2367	Shubhojit Roy	Male	Admin	500,000
2368	Shushil Das	Male	Finance	500,000
2369	Priyanka Sane	Female	Finance	550,000

2.2 Characteristics of Big Data

The characteristics of big data [2] are explained by the following five Vs (Fig. 2).

- (a) **Volume:** Big Data itself has a size-related concept. Big Data is the term used to describe the enormous “volumes” of data that are produced daily from numerous sources, including business, machines, social media, human interactions, etc.
- (b) **Variety:** Big Data, which is gathered from various sources, can be structured, unstructured, or semi-structured.
- (c) **Velocity:** The speed at which data is generated in real time is determined by velocity.
- (d) **Veracity:** Veracity refers to how trustworthy the data is. Veracity is the ability to effectively handle and manage data.
- (e) **Value:** Value is a crucial component of big data. We do not handle or store the data. We store, process, and also evaluate accurate and valuable data.

Fig. 2 Five V’s of big data



2.3 *Big Data Analysis*

Data analysis is an essential element of effective business management. Effective data use helps businesses understand their past performance and make better choices concerning their future business. There are four types of data analytics:

- (a) **Descriptive Analysis:** It is currently the most straightforward and typical use of data in business. By condensing historical data, descriptive analysis provides an explanation for “what happened.”
- (b) **Diagnostic Analysis:** Deeper analysis and “why did it happen?” are the next steps. Here, diagnostic analytic is useful. Descriptive analytics uncovers insights, and digs further to identify the root causes of those results.
- (c) **Predictive Analysis:** “What is likely to happen?” is a question that predictive analytics aims to resolve. This kind of analytics uses historical information to forecast future events.
- (d) **Prescriptive Analysis:** What is the optimum course of action, according to prescriptive analytics? This approach enables users to suggest numerous potential courses of action, which ultimately directs them toward a resolution.

3 Introduction to R

At the University of Auckland in New Zealand, Ross Ihaka and Robert Gentleman developed the interpreted programming language R. R is currently being created by the R Development Core Team. The names of both developers were used to create the name of this programming language. It is a software environment used to examine graphical displays, reporting, and data modelling. R and RStudio must be installed in order to work with the widely used R programming language. R and RStudio collaborate to build R project.

3.1 *Features of R*

- (a) R is a complete programming language that supports both object-oriented programming and procedural programming with functions.
- (b) The R programming package repository has almost 10,000 items.
- (c) R generates code that is portable and independent of any particular machine.
- (d) It simplifies the method of debugging coding bugs.
- (e) R makes it simple to perform complicated operations on vectors, arrays, data frames, and other data objects of various sizes.
- (f) Other programming languages including C, C++, Python, Java, FORTRAN, and JavaScript can be integrated with R.
- (g) R offers reliable tools for managing and storing data.
- (h) R works on various platforms.

3.2 GUI of R

An integrated development environment (IDE) for R is called R Studio [3, 4]. The following four windows or panes will be seen when you run RStudio (Fig. 3):

- (a) Source: You write and modify R Scripts—collections of code—in the Source Pane.
- (b) Console: The Console is the heart of R. Normally, it can be found in the bottom left corner of the window. The window where R executes code is also known as a command window. After the “>” character, we can also type code in the console.
- (c) Environment/History: Typically, this panel has the following two tabs:
 - (i) Environment—Shows all the data, variables, and user-defined functions you have entered.
 - (ii) History—A collection of all of your previous commands.
- (d) Files/Plots/Packages/Help: This may be found at the bottom right of the window. Here, you can browse major pages, install and load packages, examine charts, open files, and view markdown and other documents in the viewer tab.
 - (i) Files—A list of every file in the working directory you are currently in. On your computer, you can also go to several folders.
 - (ii) Plots—When your code generates plots, they will be shown here.
 - (iii) Packages—A list of the installed packages (or functional groupings) on your machine.

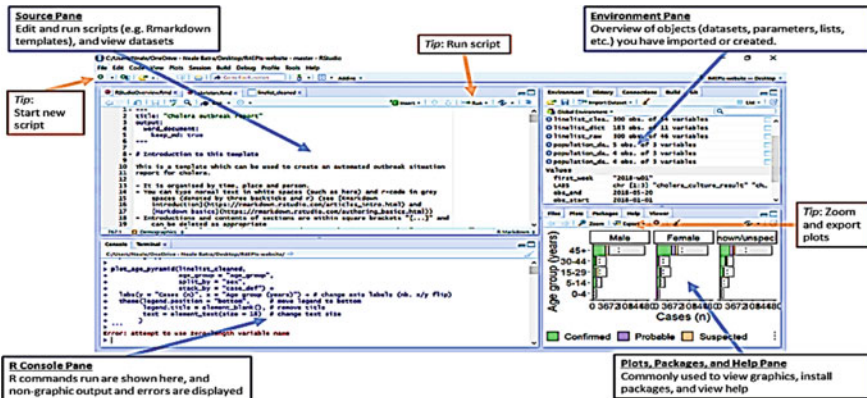
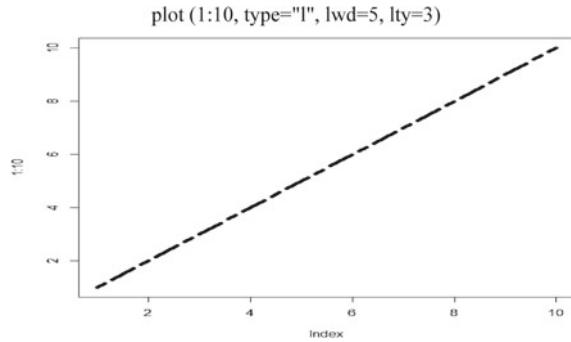


Fig. 3 GUI of R

Fig. 4 A simple line plot using plot () function



3.3 Data Visualization Using R

An approach for graphically representing data is data visualization. We make our data easier to grasp by using components like scatter plots, charts, graphs, histograms, maps, etc. It helps us to quickly and visually communicate information and results. Information given in a visual format is simpler for the human brain to comprehend and remember. Data visualization enables us to easily evaluate data, look at various variables to determine how they affect the patterns, and draw conclusions from our data. The graphics package in the R standard library has various functions that produce statistical graphs, including:

(a) Line Plots (b) Scatter plots (c) Pie Charts (d) Bar plots (e) Box plots [5].

In order to mark points on a chart, use the plot () function. The function accepts parameters to indicate diagram points. Points on the x-axis are specified in parameter. On the y-axis, parameter 2 specifies points. Use the lwd argument to modify the line's width (the default value is 1, while 0.5 indicates 50% smaller and 2 means 100% larger). The line is by default solid. To select the line format, use the lty option with a value between 0 and 6. 3 display a dotted line (Fig. 4).

```
plot (1:10, type = "l", lwd = 5, lty = 3)
```

One dot is plotted for each observation in a "scatter plot," a type of plot used to show the relationship between two numerical variables. It requires two identical-length vectors: one for the horizontal x-axis and one for the vertical y-axis (vertical) (Fig. 5).

```
x <- c(5,7,8,7,2,2,9,4,11,12,9,6)
y <- c(99,86,87,88,111,103,87,94,78,77,85,86)
plot(x, y)
```

A circular graphical representation of data is a pie chart. To create pie charts, use the pie() function. For each value in the vector, a pie is drawn in the pie chart. The first pie is plotted by default, moving counterclockwise from the x-axis (Fig. 6).

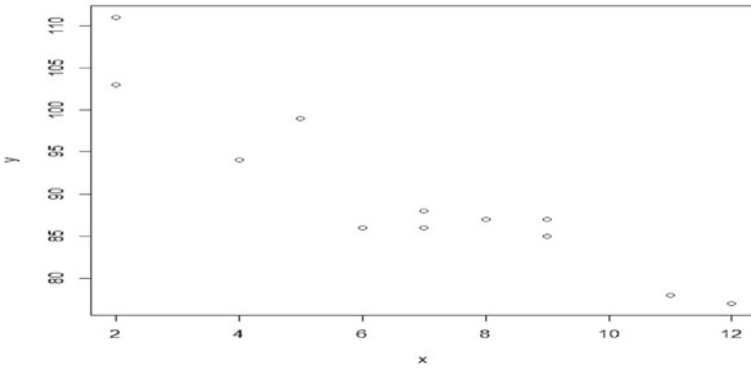


Fig. 5 Scatter plot

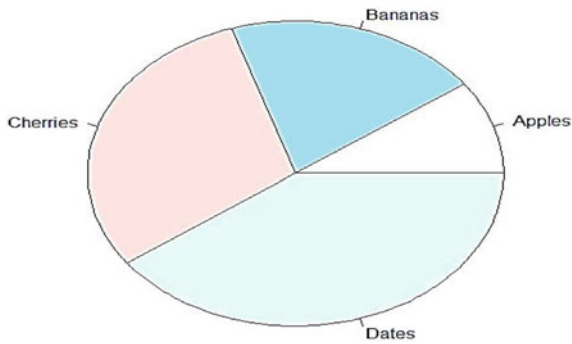


Fig. 6 Pie chart

```
x <- c(10,20,30,40)
mylabel <- c("Apples", "Bananas", "Cherries", "Dates")
pie(x, label = mylabel, main = "Fruits")
```

Rectangular bars are used in a bar chart to show data (Fig. 7).

```
x <- c("A", "B", "C", "D")
y <- c(2, 4, 6, 8)
barplot(y, names.arg = x)
```

Data distribution within a data collection is evaluated using boxplots. The data set is split into three quartiles as a result. The first quartile, third quartile, average,

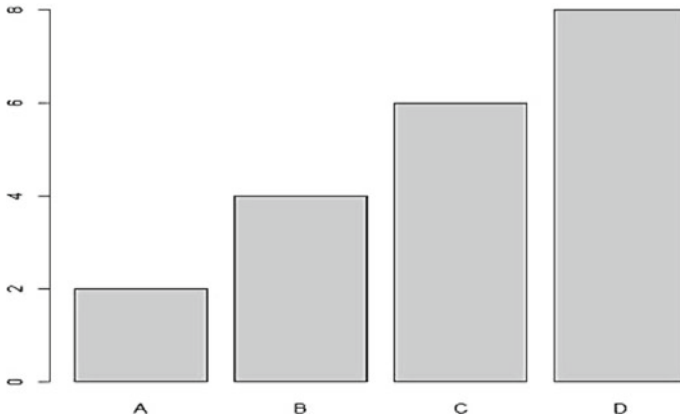


Fig. 7 Bar chart

lowest, and maximum of the data set is shown in this graph. To generate a boxplot, use the `boxplot()` function that R offers (Fig. 8).

```
vec <- c(3, 2, 5, 6, 4, 8, 1, 2, 3, 2, 4)
summary(vec)
boxplot(vec, xlab = "x-axis", ylab = "y-axis", main = "R Boxplot", varwidth = TRUE)
```

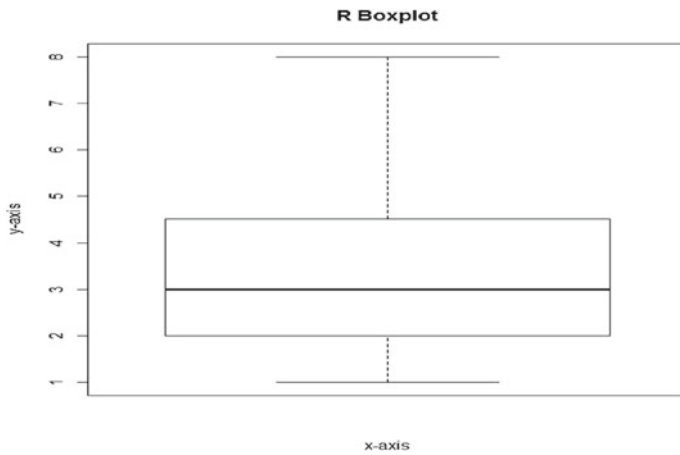


Fig. 8 Box plot

4 Conclusion

Data processing, comparison of several model possibilities, and result visualisation are crucial for developing a robust and trustworthy statistical model. The interactive nature of the R language encourages investigation, explanation, and presentation, which is why it has become so widely used.

References

1. Dehbi, S., Chakir, H., Belgnaoui, L. T. & Lafou, T. (2022). Big data analytics and management control. *Procedia Computer Science* 203.
2. Femi, A. G., & Samuel, I. O. (2022). The needs to embrace R programming language in every organizations that deals with statistical research and data analysis. *Iconic Research and Engineering Journals*, 5, 7, ISSN: 2456-8880.
3. Kumar, R., Kumar, S., & Tiwary, S. K. (2019). A case study on R: A powerful OSS and data analysis platform. *International Journal of Applied Engineering Research*, 14(9), 2260–2269.
4. Jatain, A., & Ranjan, A. (2017). A review study on big data analysis using R Studio. *International Journal of Computer Science and Mobile Computing, IJCSMC*, 6(6), 8–13.
5. Rajeswari, C., Basu, D., & Maurya, N. (2017). Comparative study of big data analytics tools: R and tableau. *IOP Conference Series: Materials Science and Engineering*, 263(4).

Face Recognition Based Video Conferencing Add-On for Online Session Log Using Convolutional Neural Networks



Manish Jadhav, Ashwathy Marath, Rohan Jamuar, Kaustubh Sawant, and Satishkumar L. Varma

Abstract Video conferencing is used to conduct sessions during pandemics and there is a need to maintain logs for assessment and evaluation purposes. In this work, an add-on tool for attendees data collection is developed. The system helps to mark session attendance of participants. The HOG and Face landmark estimation algorithms are used over SSVM, ANN, and CNN classifiers to assess the face recognition in real-time. The system captures faces from the video frames and compares them with the dataset images. System matches the face registered and marks the attendance in the datasheet. The system is initially trained and tested with the unique faces of the attendee, which in turn creates the database. A session log report is generated. This extension add-on tool is simple and useful for the education system to create logs without much effort and session time can be utilized for quality content delivery.

Keywords Face detection and recognition · Deep learning · Support vector machine · Artificial neural network · Convolutional neural network · Online session attendance

M. Jadhav · A. Marath · R. Jamuar · K. Sawant
Department of Computer Engineering, PCE New Panvel, Navi Mumbai, India
e-mail: jadhavmanki18ce@student.mes.ac.in

S. L. Varma (✉)
Department of Information Technology, PCE New Panvel, Navi Mumbai, India
e-mail: vsat2k@gmail.com

1 Introduction

Participation recording of an understudy is a significant job in the educational area which is tedious. Understudy enlistment builds each year and recording every understudy's participation assumes an indispensable part. Conventional understudy participation checking procedures are regularly confronting a great difficult situation particularly in the internet-based method of training. Accordingly, it is extremely important to examine the viable framework which records the participation of an understudy consequently. Such systems help to optimize the attendees' experience and the system is useful in other applications for authentication using face recognition.

2 Literature Survey

2.1 Face Recognition Rate Under Poor Illumination

Face Recognition Classifier. In [1] GF is applied (as shown in Table 1) all over to track down a facial fiducial point for each individual understudy. Subsequent to applying the GF technique, the PCA, LDA, and LBP calculations were utilized for face acknowledgment.

Dimensionality Reduction Using PCA and LDA. Patil et al. [2] utilized Voila Jones strategy for face location and for face acknowledgment, half breed approach of PCA and LDA as shown in Table 2.

In another review, [3] expressed that Mail Transfer Protocol (SMTP) is utilized to report the participation to the employees just as to the guardians. This concentrate

Table 1 Accuracy of face recognition rate under poor illumination with processing [1]

Exp.	Class	Student/Participant	Recognition	Accuracy (%)
1	A	64	55	85.90
2	A	64	52	81.20
3	B	55	45	81.80
4	B	55	46	83.60

Table 2 Face detection with respect to frame [2]

Frame#	# Students recognized	Student/Participant
1	9/19	4.36
2	14/20	70.00
3	5/12	41.67

likewise utilized the PCA strategy for face acknowledgment. Facial acknowledgment calculation was utilized for facial elements by extricating milestones from the understudy's picture. In [4], a review was completed that utilized RFID and IOT for the participation framework [5].

2.2 *Transformed Based Methods*

The discrete transform based methods are useful for feature extraction and face recognition which is reviewed in this section. In Lukas, Mitra [6] concentrated on the human face acknowledgment method that was utilized for understudy verification to stamp the participation in the information base. Discrete Wavelet Transforms (DWT) and Discrete Cosine Transform (DCT) were utilized to include extraction of the understudy's face. In another review [7], VJM was utilized for face identification while LBP and HOG were utilized for face acknowledgment.

In [8] study, foundation deduction was done after face location and afterward face crop was done and for face acknowledgment, the Eigenface strategy was utilized. In Sunaryono, Siswanto [9] observe, JVM has been used for face detection and LDA and k-nearest neighbor (k-NN) set of rules have been used for face popularity. This observation discarded the pix that have been now no longer clean because of the awful mild effect. VJM is turned [10, 11] into used for face detection and LBP turned into used for face recognition.

The framework utilized RFID [13] and face acknowledgment to check the understudy's participation. The RFID peruser is introduced on the entryway and the understudies are approached to filter their cards prior to going into the class. The aftereffects of this review featured that when the framework utilizes RFID [13] and IOT [4], naturally the course of face acknowledgment was worked with as opposed to doing it physically.

PCA and LDA algorithms [14] have been used for face detection and face reputation. Face reputation charge became 66% all through illumination the usage of PCA set of rules. Face reputation charge became 86% because of partial occlusion of the usage of LDA.

In [12] the single-face popularity technique is used for students' face popularity for marking their attendance using face detection. SVM is also used in [14] for facial expression recognition. A face recognition attendance system with GSM notification is developed by [15]. Face recognition attendance monitoring system is also developed for surveillance using deep learning technology and computer vision is used in [16]. The GUI is user friendly and flexible and achieved a maximum recognition accuracy of 74% using deep learning. The summary of literature review is shown in Table 3.

Table 3 Summary of literature survey

Method	PCA	LDA	LBP	KNN	RFID	IoT	SMTP	BJP
Sajid et al. [1]	✓	✓	✓					
Patil et al. [2]	✓	✓						
Nithya et al. [3]	✓						✓	
Sharma et al. [4]					✓	✓		
Shah et al. [5]	✓	✓						
Lukas et al. [6]	✓							
Mehta et al. [7]		✓						
Varadharajan et al. [8]								
Sunaryono et al. [9]		✓		✓				✓
Elias et al. [10]			✓					✓
Raghuwanshi et al. [11]		✓		✓				
Varadharajan et al. [12]	✓							

2.3 Challenges in Face Recognition

The goal is to expand a face reputation primarily based totally computerized pupil attendance gadget and to in addition use it as an add-directly to paintings with famous video conferencing packages like Google Meet, Zoom Meetings, etc. Expected achievements so that it will satisfy the following goals:

- To recognize the face fragment from the video outline.
- To remove the valuable elements from the face.
- To group the highlights to perceive the face recognized.
- To record the participation of the recognized understudy (Table 4).

Table 4 Summary of challenges in face recognition in the previous work done on attendance systems using face recognition

Method	Partial occlusion	Pose variance	Illumination
PCA, LDA, LBP, GF [1]		✓	
RFID, IOT [4]		✓	
DWT and DCT [5]		✓	
LBP, HOG [6]		✓	
Eigen face [7]			✓
PCA and LDA [8]	✓		✓

3 System Methodology

3.1 System Architecture

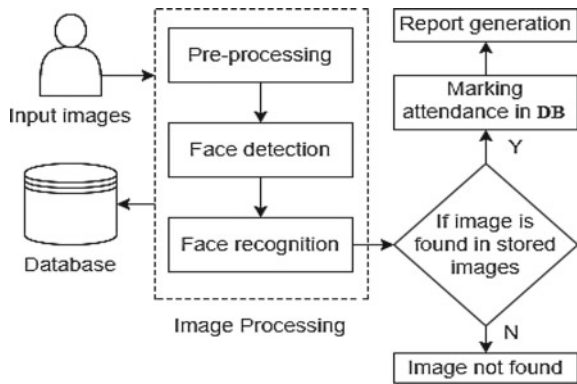
System architecture face recognition based video conferencing add-on for online session log using CNN. Each block is described separately in this Section. Under preprocessing, the face is detected by the use of the OpenCV face detector. Then the photo is cropped primarily based totally on the bounding field proposed through the face detector as shown in Fig. 1. In facial landmark detection, the HOG function is extracted inside a fixed-length area around every landmark.

Image Capturing. Images capture the usage of a virtual digital digicam whose hyperlink is included to the utility that evolved the usage of the proposed idea. After a photograph is captured, net offerings switch the photograph to the server for processing.

Face Detection. Because of the in-depth task of the face detection algorithm, this device is server-based. Detecting a face is in essence an item detection task, wherein the item of hobby in this situation is the face. Elements intervene with the face detection method by including face pose, scale, position, rotation, light, hues, etc.

Face Recognition. Face Recognition manner to perceive a specific face from a listing of faces on a database. The university, upon enrollment, takes snapshots from each pupil, and people’s pictures are saved in a database. Algorithms used for face identification. System uses a server primarily based totally module, programmed in Python which takes advantage of eigenfaces to perceive a face. The set of rules has drawbacks: it relies upon scale, poses, and the shade of the as compared pictures.

Fig. 1 Architecture for face recognition for online session log using CNN



3.2 Algorithms Used

Histogram of Oriented Gradients (HOG). HOG is used in this project to familiarize the program with the object we want to recognize. As explained in [11, 16], HOG is divided into 3 mandatory steps based on vector theory. First, the image of interest is roughly analyzed by separating the object from the background. This process looks for differences in size in the image. The size of the image is obtained from Eq. 1.

$$m(u, v) = \sqrt{fu(u, v)^2 + fv(u, v)^2} \quad (1)$$

According to Eq. 1, we get the magnitude m of a feature vector at the point. Adapted from [11] Copyright 2009, IEEE is a component in u -direction, and also $fv(u, v)$ is a component in v -direction. Object position in the image is estimated and trained to determine the object more precisely. This second process is to take the direction of the vector into account. This is comparable to the fine adjustment. Arctangent based on $fu(u, v)$ and $fv(u, v)$ are used to get an attitude as proven in Eq. 2.

$$\Theta(u, v) = \tan^{-1}(fv(u, v)/fu(u, v)) \quad (2)$$

Linear Support Vector Machine. Linear Support Vector Machine (SVM) [12, 14] is the principle assisting set of rules that software builders the world over agree with that it makes HOG paintings greater efficiently. The human detection software, which mixes HOG and SVM together, is now broadly time-honored at the moment [14]. w^T is weight vector and x_i is information vector from HOG.

$$f(x) = (w^T x_i + b) \quad (3)$$

4 System Implementation and Result Analysis

The system is developed using the Face Landmark Estimation algorithm. It is developed using Python, Dlib, and Django. To deal with lots of image data and the continuous nature of the environment, a system with 8 GB RAM, a web camera is used to capture the images of the attendees to receive their attendance.

4.1 Result Analysis

The result analysis is shown in Table 5 FEI_P1 and FEI_P2 of the FEI dataset are used in the experiment as shown in Fig. 2. FEI_P1 and FEI_P2 contain 700 images each [16, 13]. The dataset of the attendees i.e. face dataset, is made during the pre-registration phase. Approximately 30 images per attendee are recorded which are further used for training and testing purposes as shown in Fig. 3. The generated attendance log is shown in Fig. 4.

HOG as a facial image feature extractor with Linear SVM as the classifier is applied in this project to efficiently recognize attendees faces to eventually mark

Table 5 Performance evaluation of face recognition using HOG over different classifiers

Dataset	Method	Accuracy	Processing time	GPU utilization
FEI_P1 [15]	SVM	94.85	15.90	40.00
	CNN	97.64	20.39	48.00
	ANN	98.70	10.60	29.30
FEI_P2 [15]	SVM	95.63	16.02	35.00
	CNN	98.84	20.35	45.00
	ANN	99.00	11.19	30.00
Dataset (proposed)	SVM	96.45	14.09	31.00
	CNN	99.45	18.35	48.00
	ANN	94.00	08.00	30.00

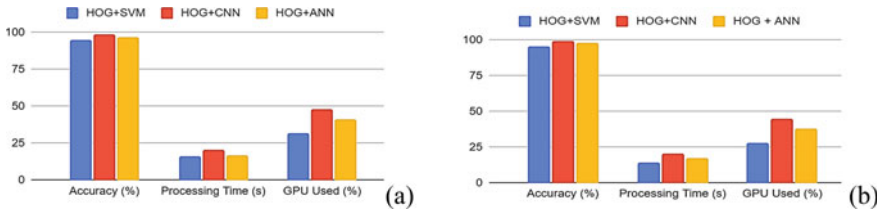


Fig. 2 Performance evaluation of over two datasets **a** FEI_P1 and **b** FEI_P2

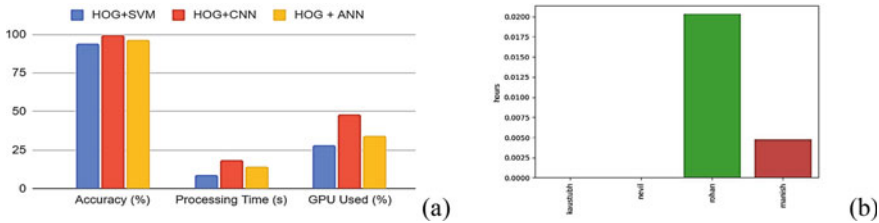


Fig. 3 Performance evaluation **a** using face dataset, **b** attendance visualization from the log

Date	Student	Present	Time in	Time out	Hours	Break Hours
March 3, 2022	kaustubh	A	-	-	0 hrs 0 mins	0 hrs 0 mins
March 3, 2022	nevil	A	-	-	0 hrs 0 mins	0 hrs 0 mins
March 3, 2022	rohan	P	March 3, 2022, 12:16 p.m.	March 3, 2022, 12:17 p.m.	0 hrs 2 mins	0 hrs 0 mins
March 3, 2022	manish	P	March 3, 2022, 12:21 p.m.	March 3, 2022, 12:21 p.m.	0 hrs 1 mins	0 hrs 0 mins

Fig. 4 Attendance log generated after the attendance is processed based on face recognition

their attendance. HOG with CNN as classifier was also studied during the project implementation and it was found that the HOG + Linear SVM face detector is faster than the HOG + CNN face detector but will also be less accurate as HOG + Linear SVM does not tolerate changes in the viewing angle rotation as shown in Table 5.

5 Conclusions

The face recognition based video conferencing add-on for online session log using CNN is developed and implemented using HOG as a facial image feature extractor and linear SVM as the classifier. The performance of the system is analyzed using accuracy. The HOG + SVM trained over 50 images per attendee and gave an average accuracy of 95%. System is useful for the education system to create logs without much effort and time can be utilized for quality content delivery. The proposed browser add-on tool is simple and effective for instructors to take attendance for online sessions.

References

1. Sajid, M., Hussain, R., & Usman, M. (2014). A conceptual model for automated attendance marking systems using facial recognition. In *IEEE Digital Information Management (ICDIM)*.
2. Patil, A., & Shukla, M. (2014). Implementation of classroom attendance system based on face recognition in class. *Journal of Advances in Engineering & Technology*, 7(3), 974.
3. Nithya, D. (2015). Automated class attendance system based on face recognition using PCA algorithm. *International Journal of Engineering Research & Technology (IJERT)*.
4. Sharma, T., & Aarthy, S. L. (2016). An automatic attendance monitoring system using RFID and IOT using cloud. In *IEEE Green Engineering and Technologies (IC-GET)*.
5. Vyas, R. A., & Shah, S. (2017). Comparison of PCA and LDA techniques for face recognition feature-based extraction with accuracy enhancement. *International Research Journal of Engineering and Technology*, 4(6), 3332–3336.
6. Lukas, S., Mitra, A., & Desanti, R. I. (2016). Student attendance system in the classroom using face recognition techniques. In *IEEE International Conference on Information and Communication Technology Convergence (ICTC)*.
7. Mehta, P., & Tomar, P. (2016). An efficient attendance management system based on face recognition using Matlab and Raspberry Pi 2. *International Journal of Engineering Technology Science and Research*.

8. Varadharajan, E., Dharani, R., Jeevitha, S., Kavinmathi, B., & Hemalatha, S. (2016). Automatic attendance management system using face detection. In *IEEE International Conference on Green Engineering and Technologies (ICGET)*.
9. Sunaryono, D., Siswanto, J., & Anggoro, R. (2019). An android based course attendance system using face recognition. *Journal of King Saud University, CIS*.
10. Elias, S. J., Hatim, S. M., Hassan, N. A., Latif, L. M. A., Badlishah Ahmad, R., Darus, M. Y., & Shahuddin, A. Z. (2019). Face recognition attendance system using local binary pattern (LBP). *Bulletin of Electrical Engineering Informatics* 8(1), 239–245.
11. Raghuvanshi, A., & Swami, P. D. (2017). An automated classroom attendance system using video based face recognition. In *2nd IEEE International Conference on Recent Trends in Electronics, Information & Communication Technology (RTEICT)*.
12. Varadharajan, E., Dharani, R., Jeevitha, S., Kavinmathi, B., & Hemalatha, S. (2016). Automatic attendance management system using face detection. In *IEEE International Conference on Green Engineering and Technologies (IC-GET)*, Coimbatore, India.
13. Fahmy, A., Altaf, H., Al Nabulsi, A., Al-Ali, A., & Aburukba, R. (2019). Role of RFID technology in smart city applications. In *International Conference on Communications, Signal Processing and Their Applications (ICCSPA)* (pp. 1–6).
14. Shinde, M., Varma, S., & Chavan, S. (2018). Analysis of PCA and LDA features for facial expression recognition using SVM and HMM classifiers. In *International Conference on Advanced Technologies for Societal Applications* (Vol. 1, pp. 109–119). Springer.
15. Okokpujie, K., Noma-Osaghae, E., John, S., Grace, K. A., & Okokpujie, I. (2017). A face recognition attendance system with GSM notification. In *IEEE 3rd International Conference on Electro-technology for National Development (NIGERCON)* (pp. 239–244).
16. Harikrishnan, J., Sudarsan, A., & Sadashiv, A. (2019). Vision-face recognition attendance monitoring system for surveillance using deep learning technology and computer vision. In *International Conference on Vision Towards Emerging Trends in Communication and Networking (ViTECoN)* (pp. 1–5).
17. Li, Y., Zheng, W. Cui, Z., & Zhang, T. (2018). Face recognition based on recurrent regression neural networks. *Neurocomputing*, 297, 50–58.

The Influence of the Demography of Institutes on MIS-Based OBE Implementation



Anil N. Barbole and Suraj B. Ronge

Abstract Now-a-days in India, there is more focus on implementing Outcome-based Education (OBE). For the evaluation of the OBE system, manual processes are very tedious and time-consuming. So, implementing a Management Information System (MIS) in the organization is essential for making the OBE process easy. In an organization, implementing MIS successfully is a challenging task. Successful implementation of MIS depends upon factors like the demographic characteristics of users. In this study, authors have studied different demographic variables such as gender, age, teaching experience, the highest level of education, knowledge about computer, and the nature of users' native places. For that purpose, responses from different users were collected from various institutes by distributing prepared questionnaires based on a 5-Point Likert Scale, and these collected responses were analyzed using descriptive statistics and frequency statistics for different demographic variables.

Keywords Outcome-based education · MIS · Demographic variables · Descriptive statistic · Frequency statistics

1 Introduction

In India, to improve the quality of education, more focus is given on implementing the OBE system; for this, evaluating the OBE system through a manual process is complex and time-consuming. To make the OBE system more accessible and time-saving, implementing MIS in the organization for evaluation of the OBE system is necessary. This successive implementation of MIS in the organization is complex. In this study, the authors have studied different demographic variables affecting the implementation of MIS in the educational organizations. In order to fully understand

A. N. Barbole
Chhatrapati Shivaji Night College of Arts & Commerce, Solapur 413001, India

S. B. Ronge (✉)
SVERI's College of Engineering, Pandharpur 413304, India
e-mail: sbronge@coe.sveri.ac.in

a user's population distribution of characteristics, prescribe appropriate policies for them, and forecast where a user or a group will be in the future, a demographic survey and analysis have to be done. Demography is helpful for any company and business as it predicts cultural and social trends related to users or stakeholders. All of us know that using MIS in organizations for rapid growth in this era is essential. In this research demographics, MIS users were examined from several perspectives such as gender, age, teaching experience, computer literacy, location of users, etc. For that, surveys from various institutions were taken to gather information about the users' demographics and their expectations from the MIS.

Tella and Mutula [1] conducted a survey at a university in Botswana to examine the gender gap in computer literacy. They subsequently performed a descriptive statistics analysis and concluded that students with higher computer literacy were more likely to access and use library resources. Zin et al. [2] conducted a survey to investigate the gender differences in computer literacy with 1570 respondents, compared the mean score of their answers as 2.62 for men and 2.34 for women, and concluded that men were more skilled in computer programming than women. Joo and Choi [3] investigated different factors affecting the use of online library resource as ease-of-use, individual differences, resource quality and usefulness. Teo et al. [4] discovered, in particular, that the demographic variables relate to PEOU, PU, and SN in distinct ways, while the constructs of SN, PU and PEOU were found to be positively significant with regard to intention to adopt m-banking. Majid and Abazova [5] found positive correlation between their utilization of electronic information and the age of academics. They also conceded that use of electronic information depends upon computer knowledge. Those who have more knowledge, use more electronic information. Furthermore, they also studied different aspects like user's age, gender and educational background and their effect on usage.

2 Objectives of the Study

The main objective of the study is to find out the demographic variables influencing the use of software in different institutes. The specific objectives are to:

1. Find out the easiness in handling MIS for different demographic variables.
2. Find out the minimal management efforts with MIS usage for different demographic variables.
3. Find out the minimal time required with MIS usage for different demographic variables.
4. Find out the correctness with MIS usage for different demographic variables.

3 Methodology

3.1 Data Collection

A survey form was prepared using questions which were further divided into four parameters: easiness in handling MIS, minimal management efforts with MIS usage, minimal time required with MIS usage, and correctness with MIS usage. These questionnaires were prepared by using the 5-Point Likert Scale. The forms for this survey were distributed to different institutes, and a total of 146 responses, along with their demographic variables, were collected.

3.2 Reliability Analysis

Reliability analysis of the questionnaire was done to measure internal consistency between questions, that is, the correctness of questions used in the survey. In reliability analysis, Cronbach’s Alpha was tested in SPSS software according to the standards of Cronbach’s Alpha. If the score is more than 0.7, it is acceptable; if it comes to be less than 0.7, then we have to revise the questionnaire. Different standard ranges of Cronbach’s Alpha values have been given in Table 1.

The formula for Cronbach Alpha is:

$$\alpha = \frac{N \cdot c}{v + (N - 1) \cdot c} \tag{1}$$

where

- c average covariance between item-pairs,
- N the number of Items and
- v average Variance.

In this research, the reliability analysis of questionnaire has been done using Cronbach’s Alpha in SPSS and it has been found to be 0.940 for 20 questions which denote excellent internal consistency of questions. Table 2 shows reliability statics of questionnaire through the SPSS software.

Table 1 Range for Cronbach’s Alpha

Cronbach’s Alpha	0.5 > α	0.6 > α ≥ 0.5	0.7 > α ≥ 0.6	0.8 > α ≥ 0.7	0.9 > α ≥ 0.8	α ≥ 0.9
Internal consistency	Unacceptable	Poor	Questionable	Acceptable	Good	Excellent

Table 2 Reliability statistics of questionnaire

Reliability statistics	
Cronbach's Alpha	No. of items
0.940	20

3.3 Descriptive Statistics

It gives simple summaries of the sample and the observations made. It is quantitative; it summarizes different statistical results: range, maximum, minimum mean, std. deviation, variance, and frequencies which is helpful for various types of analysis. The descriptive statistics of the demographic variable have been shown in Table 3.

Different demographic parameters were studied through survey and analysis of responses was studied on demographic variables and pie charts of the demographic variables have been shown in Fig. 1. Some of the demographic factors have also been explained below.

Table 3 Descriptive statistics of demographic variable

Descriptive statistics								
Demographic variable	N	Range	Min.	Max.	Mean		Std. deviation	Variance
	Statistic	Statistic	Statistic	Statistic	Statistic	Std. error	Statistic	Statistic
Gender	146	1.00	1.00	2.00	1.3973	0.0406	0.4910	0.241
Age	146	3.00	1.00	4.00	1.7329	0.0624	0.7546	0.570
Teaching experience	146	4.00	1.00	5.00	2.6438	0.1013	1.2246	1.500
Highest level of education	146	2.00	1.00	3.00	1.7808	0.0429	0.5185	0.269
Knowledge about computer	146	3.00	1.00	4.00	2.4247	0.0573	0.6931	0.480
Which of this best describes your native place?	146	1.00	1.00	2.00	1.2329	0.0351	0.4241	0.180
Valid N (list wise)	146	-	-	-	-	-	-	-

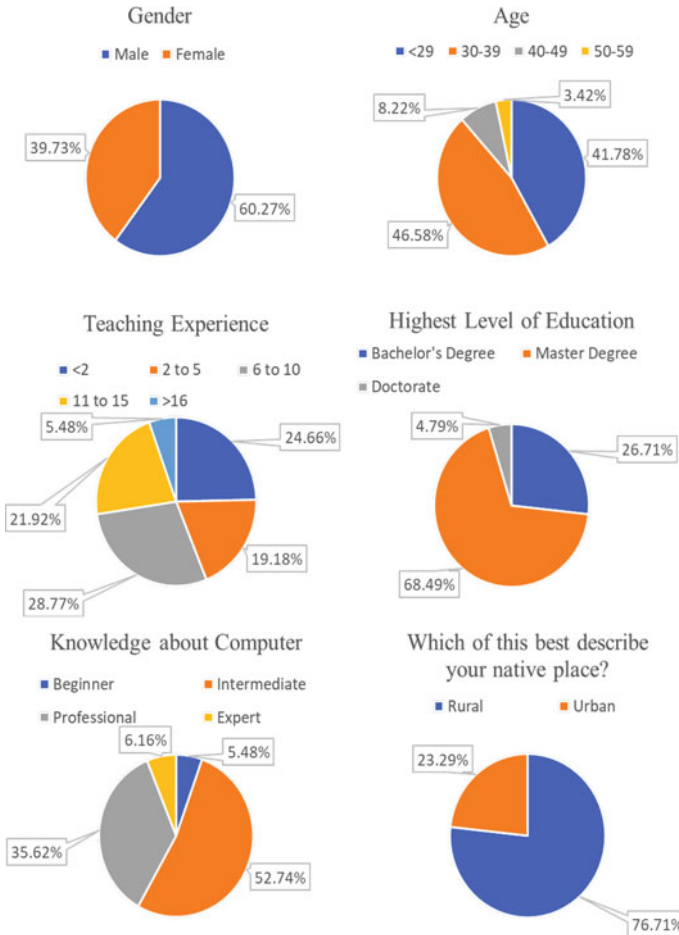


Fig. 1 Pie chart of demographic variables

3.3.1 Gender

The results obtained from the survey of various institutes has been presented in Fig. 1, which shows that 60.3% of the respondents are male and 39.7% are female. The results also show that there are more significant numbers of male users.

3.3.2 Age

For the current research, respondents were categorized into five different age groups, with the lowest age of the respondent is less than 29 years and the highest being above 60 years. In the age group of fewer than 29 years, there is a frequency of 61

(41.8%) respondents, and in the second age group, which is 30–39 years, there is a frequency of 68 (46.6%) respondents. The next age group of 40–49 years has the frequency of 12 (8.2%), while 5 (3.4%) respondents are between 50 and 59 years, and no respondent has an age greater than 60 years.

3.3.3 Teaching Experience

In this research, respondents were classified into five categories per their years of teaching experience. From the total number of responses received, 36 (24.7%) had < 2 years of teaching experience, and 28 (19.2%) had 2–5 years of teaching experience. There are 42 (28.8%) respondents with teaching experience between 6 and 10 years and 32 (21.9%) respondents with 11–15 years of teaching experience, while only 8 (5.5%) respondents have teaching experience above 16 years.

3.3.4 Highest Level of Education

For this survey, the level of education was subdivided into three types; all the respondents hold the minimum level of education as a bachelor's degree. Around 39 (26.7%) respondents have only a bachelor's degree, 100 (68.5%) respondents have a master's degree in their respective field, and 7 (4.8%) respondents have completed a doctorate as their highest level of education.

3.3.5 Knowledge About Computer/Knowledge About Microsoft Excel

Considering their knowledge of computer and Microsoft excel, the respondents were classified into four different groups, starting from beginners to experts. Regarding computer or knowledge of Microsoft excel, 8 (5.5%) of the 146 respondents are at the beginner level. In the following groups, there are 77 (52.7%) respondents with an intermediate level of knowledge about computer or Microsoft excel and 52 (35.6%) respondents are with a professional level of knowledge; only 9 (6.2%) respondents are experts in computer or Microsoft excel.

3.3.6 Nature of Native Place

From the collected 146 responses, it can be seen that 112 (76.7%) respondents belong to the rural areas, while 34 (23.3%) respondents belong to the urban areas.

4 Results

In this research, the data has been analyzed using SPSS software in which different demographic variables were tested with the mean of defined four parameters that is easiness in handling MIS, minimal management efforts with MIS usage, minimal time required with MIS usage, and correctness with MIS usage. The results of this study have been shown in Tables 4, 5 and 6.

Table 4 Mean comparison of parameters with gender and age

	Gender		Age				
	Male	Female	< 29	30–39	40–49	50–59	> 60
	Mean	Mean	Mean	Mean	Mean	Mean	Mean
Easiness in handling MIS	4.48	4.48	4.52	4.45	4.51	4.38	–
Minimal management efforts with MIS	4.49	4.50	4.56	4.46	4.48	4.18	–
Minimal time required with MIS	4.39	4.43	4.43	4.35	4.58	4.40	–
Correctness with MIS	4.45	4.45	4.54	4.38	4.42	4.40	–

Table 5 Mean comparison of parameters with teaching experience and highest level of education, demographic variable

	Teaching experience					Highest level of education		
	< 2	2–5	6–10	11–15	> 16	Bachelor's degree	Master degree	Doctorate
	Mean	Mean	Mean	Mean	Mean	Mean	Mean	Mean
Easiness in handling MIS	4.55	4.43	4.53	4.40	4.44	4.45	4.50	4.47
Minimal management efforts with MIS	4.53	4.55	4.54	4.36	4.39	4.51	4.48	4.57
Minimal time required with MIS	4.50	4.29	4.48	4.25	4.62	4.49	4.37	4.43
Correctness with MIS	4.56	4.43	4.43	4.38	4.50	4.44	4.47	4.29

Table 6 Mean comparison of parameters with knowledge about computer and description of native place

	Knowledge about computer				Which of this best describes your native place?	
	Beginner	Intermediate	Professional	Expert	Rural	Urban
	Mean	Mean	Mean	Mean	Mean	Mean
Easiness in handling MIS	4.40	4.46	4.53	4.43	4.46	4.56
Minimal management efforts with MIS	4.47	4.47	4.55	4.39	4.46	4.60
Minimal time required with MIS	4.63	4.40	4.37	4.44	4.37	4.50
Correctness with MIS	4.25	4.42	4.54	4.44	4.42	4.56

5 Conclusion

In this research paper, the demographic analysis of MIS users has been carried out. The demographic survey was carried out at different institutes, and a total of 146 responses have been collected from different users. In this study, the influence of institute demography on the implementation of MIS based OBE calculation has been studied, and it has been found that the users are attracted to MIS based OBE calculation due to its ease, minimal management efforts, minimal time requirement, and correctness. According to the findings, there is no significant effect of the institute's demographics on the use of MIS for the evaluation of OBE due to its ease of handling and learning.

References

1. Tella, A., & Mutula, S. M. (2008). Gender differences in computer literacy among undergraduate students at the University of Botswana: Implications for library use. *Malaysian Journal of Library & Information Science*, 13(1), 59–76.
2. Zin, N. A. M., Zaman, H. B., Judi, H. M., Mukti, N. A., Amin, H. M., Sahran, S., Ahmad, K., Ayob, M., Abdullah, S., & Abdullah, Z. (2000). Gender differences in computer literacy level among undergraduate students in Universiti Kebangsaan Malaysia (UKM). *The Electronic Journal of Information Systems in Developing Countries*, 1(1), 1–8.
3. Joo, S., & Choi, N. (2015). Factors affecting undergraduates' selection of online library resources in academic tasks: Usefulness, ease-of-use, resource quality, and individual differences. *Library Hi Tech*, 33(2), 272–291.

4. Teo, A. C., Tan, G. W. H., Cheah, C. M., Ooi, K. B., & Yew, K. T. (2012). Can the demographic and subjective norms influence the adoption of mobile banking? *International Journal of Mobile Communications*, 10(6), 578–597.
5. Majid, S., & Abazova, A. F. (1999). Computer literacy and use of electronic information sources by academics: A case study of International Islamic University Malaysia. *Asian Libraries*.

Optimization of Estimated Routing Paths in IoT Agriculture Applications



Shreekant Salotagi and Jayashree D. Mallapur

Abstract IoT application are now gaining high popularity in all walks of life to apply such as health monitoring, agriculture security system, home appliances etc., but they are having lot of challenges with respect to heterogeneity in the device connection environmental situation application requirement etc. The agriculture application is the most important and essentials application for India, because India depend on 67% on agriculture. In our proposed we have taken agriculture application with heterogeneous devices connected across. Because of this there are a lot of control signals exchange require to turn the application. We have proposed an optimistic estimated path request in IoT agriculture application simulation results shows there is a control commendable reduction in delay and latency and also overhead.

Keywords QoS · Estimated route · Heterogeneity · EREQLLN

1 Introduction

In India 67% of the people depend on the agriculture but because of underdevelopment technology in agriculture. The agriculture production has not achieved, it goes now is a time to relook the agriculture application with a new technology such as IoT automation etc. The IoT application in agriculture will make formers life very easy and there production to increase Multifood. IoT application such as automatic water supply, temperature control and humidity control are important issues that can be managed with an IoT application. IoT application in agriculture is having multiple challenges such as (1) Protection of electronic circuits of devices used in IoT agricultural system from natural environmental situations like heavy rain, fire,

S. Salotagi (✉)

Annasaheb Dange College of Engineering & Technology, Ashta, Sangli, Maharashtra, India
e-mail: shreekant2486@gmail.com

S. Salotagi · J. D. Mallapur

Basaveshwar Engineering College, Bagalkote, Karnataka, India
e-mail: bdmallapur@gmail.com

intolerable winds, extreme humidity, high/low temperature, etc. (2) Reliable energy-efficient network-based setup for the secure transmission of information to respective stakeholders in a secured manner. (3) Selection of suitable IoT end devices, tools, and technologies for implementing smart farming. (4) Design and implementation of highly scalable and reliable security mechanism for each IoT end devices used in Smart Agriculture. (5) Resource utilization in an optimized manner is a big challenge in IoT agriculture. (6) Cost- analysis and mobility are also huge challenges for smart farming. (7) Maintenance of Quality of Service (QoS) efficiently in IoT based Smart Agricultural System is also an unfolded issue. (8) A proper decision-making system to handle the natural disaster with the latest policies is a part of these open challenges in IoT agriculture. (9) Crop residue for a clean environment is still a major problem. (10) Software complexity for smart objects work with minimal resources, there is a need for software infrastructure to support the network.

The issues such as control overhead which intern increases the QoS parameters such as delay and latency will increase and intern them will increase the cost of the application. When the cost of application increases intern it becomes difficult to former to buy the product and utilize for their forms.

2 Literature Survey

In this paper the data's are analysed with the help of Big Data mining techniques [1]. The authors used the cloud based big data analytics and the IoT technology for feasibility study of smart agriculture. Smart agricultural systems are estimated to play an essential role in improving agriculture activities. Prediction is performed based on data mining technique which information reaches the farmer via mobile app. The author's proposed smart model for the agriculture field is to predict the crop yield and decide the better crop sequence based on the previous crop sequence in the same farmland with the soil nutrient current information. In this model also facilitates the estimate of total production and per crop region wise, total fertilizer requirements.

In this paper the author's explained about Smart farming management concept that use Internet of Things (IoT) to overcome the current challenges of food production [2]. There work uses the preferred reporting items for systematic review of existing literature on smart farming with IoT. There aims to identify the main devices, platforms, network protocols, processing data technologies and the applicability of smart farming with IoT to agriculture. There review shows an evolution in the way data is processed in recent years and more recent approaches, however, new technological developments allowed the use of data to prevent crop problems and to improve the accuracy of crop diagnosis. The author presented a systematic review of the state-of-the-art of IoT adoption in smart agriculture and identified the main components and applicability of IoT solutions.

In this paper they use wireless sensor network (WSN) as a major driver of smart agriculture to the use of IoT and DA [3]. The IoT integrates several existing technologies, such as WSN, radio frequency identification, cloud computing, middleware systems, and end-user applications. In this paper, several benefits and challenges of IoT have been identified. They present the IoT ecosystem and how the combination of IoT and DA is enabling smart agriculture. Their survey of literature shows that there are lots of work ongoing in development of IoT technology that can be used to increase operational efficiency and productivity of plant and livestock. The benefits of IoT and DA, and open challenges have been identified and discussed in this paper.

In this paper the author explained for Livestock monitoring, conservation monitoring and plant and soil monitoring are the challenges where IoT can be a solution [4]. They also worked on innovative IoT applications address the issues in agriculture and increase the quality, quantity, sustainability and cost effectiveness of agricultural production. Their project aims at monitoring the soil parameters like soil moisture, temperature and electrical conductivity and automates the irrigation process. Decision making is done through microcontroller. Their work presents the design of an IoT based automatic irrigation system. Their proposed system reduced the efforts of farmers and provides high yield. And also conserves water for irrigation by locating the sensor at the right position above the soil level.

In this paper the author works on Irrigation method to supply water and water wastage [5]. Their proposed used in various sensors like temperature, humidity, soil moisture sensors which senses the various parameters of the soil and based on soil moisture value land gets automatically irrigated by ON/OFF of the motor. These sensed parameters and motor status will be displayed on user android application. The internet of things to the highly effective and safe agricultural production has a significant impact on ensuring the efficient use of water resources as well as ensuring the efficiency and stability of the agricultural production.

In this paper the author presented and discussed at the SpliTech2019 IoT technologies on societies and their potential effects on sustainability in general [6]. They have been worked on introductory article contributed to the better understanding of current technological progress in IoT application areas as well as the environmental implications linked with the increased application of IoT products.

In this paper the author proposed the future of communication that has transformed things (objects) of the real-world into smart objects [7]. The functional aspect of IoT is to unite every object of the world under one common infrastructure in such a manner that humans not only have the ability to control those objects, but to provide regular and timely updates on the current status This research article presents a comprehensive literature survey on the concept of IoT. The term IoT has been broadly described keeping in view the current standings of IoT, its evolution from time to time along with various communication technologies used by various objects for interface and communications purposes. Open Issues, Challenges and Future Research Directions concerning IoT have also been discussed.

In this paper the author worked on improving farm productivity is essential for increasing farm profitability and meeting the rapidly growing demand for food that is fuelled by rapid population growth across the world [8]. They proposed crop recommendation is currently based on data collected in field-based agricultural studies that capture crop performance under a variety of conditions. They proposed an Emerging Internet of Things (IoT) technologies, such as IoT devices (e.g., wireless sensor networks, network-connected weather stations, cameras, and smart phones) used to collate vast amount of environmental and crop performance data, ranging from time series data from sensors, to spatial data from cameras, to human observations collected and recorded via mobile smart phone applications. In this paper, they present the design of SmartFarmNet, an IoT-based platform to automate the collection of environmental, soil, fertilisation, and irrigation data for any particular farm. The proposed SmartFarmNet uses a unique and novel real-time statistical analysis approach that enables near real-time responses to user queries.

In this paper worked on the potential of wireless sensors and IoT in agriculture, as well as the challenges expected to be faced when integrating the technology with the traditional farming practices [9]. They were analysed IoT devices and communication techniques associated with wireless sensors encountered in agriculture applications are in detail. Furthermore, they explained the use of unmanned aerial vehicles for crop surveillance and other favourable applications such as optimizing crop yield. The focus on smarter, better, and more efficient crop growing methodologies in order to meet the growing food demand of the increasing world population in the face of the ever-shrinking arable land. This paper presented the role of various technologies, especially IoT, in order to make the agriculture smarter and more efficient to meet future expectations.

In this paper, the author explained various potential IoT applications, and the specific issues and challenges associated with IoT deployment for improved farming [10]. To focus on the specific requirements the devices, and wireless communication technologies associated with IoT in agricultural and farming applications are analysed effectively. On smart services towards smart agriculture. Various case studies are presented to explore the existing IoT based solutions performed by various organizations and individuals and categories according to their deployment parameters. Related difficulties in these solutions, while identifying the factors for improvement and future road map of work using the IoT are also highlighted. They present the difficulties of the existing applications. For future research specifically, low cost, autonomous, energy efficient, interoperable, standardized, heterogeneous and robust solutions with features like artificial intelligence.

In this paper the author presented IOT modernization of get together data on conditions like atmosphere, protection, temperature and productivity of soil, Harvest online assessment enables disclosure of wild plant, level of water, cultivation area etc. [11]. They worked on IOT improvement to decrease the expense and update the efficiency of standard creating for farmers. To control the agriculture monitoring in fields where the human being not capable to provide security such system they are developing in the field where the crops are costly.

In this paper the author presented IoT is furnishing people with smart and remote approach, the remote applications such as smart agriculture, smart environment, smart security, and smart cities etc. [12]. They used main components of IoT are sensors, actuators, embedded system, and internet connection IoT application for smart agriculture. The paper proposed a remote sensing of agriculture parameters and control system to the greenhouse agriculture. They worked on to control CO₂, soil moisture, temperature, and light, based on the soil moisture the controlling action for the for the greenhouse agriculture. They designed system to remotely monitor the greenhouse parameters such as CO₂, soil moisture, temperature, and light.

In this paper the author presented emerging system increases the quantity and quality of agricultural products [13]. In this paper, an IoT based advanced solution for monitoring the soil conditions and atmosphere for efficient crop growth is presented and the developed system is capable of monitoring temperature, humidity, soil moisture level using NodeMCU and several sensors connected to it. In this paper, IoT technology is used to sense and analyse the temperature, humidity level, soil moisture level and the rain condition and DC motor is controlled using NodeMCU. In this system, adequate water is pumped and rain is also utilized efficiently.

In this paper the author presented about automatic irrigation system using the Arduino microcontroller with moisture sensor and water flow management [14]. They also used humidity sensor unit consists of an Arduino board, Wi-Fi unit, Humidity sensor and water flow control mechanism to collect data from Humidity sensor will be sending to data monitoring system by Arduino boards over a wireless network using WiFi. In their Monitoring system, the humidity levels are monitored and any decrease in humidity level below a limit is reported as requirement for water and signal is raised to the entire humidity sensor unit to open the water flow management. There developed system is beneficial and works in cost effective manner. That reduces the water consumption to a greater extent and it needs minimal maintenance with less power. The crop productivity increases and the wastage of crops is very much reduced in this irrigation system.

In this paper the author introduces the Internet-of-Things (IoT) and describes its evolution from a concept where IoT devices are available as off-the-shelf products from major manufacturers [15]. In this paper author have been reviewed the Internet-of-Things concept and its evolution since 1999 taking a smart device and user-centric perspective. They discussed some of the issues and ideas in the area of smart agriculture and user centred design and acceptance for the Internet-of-Things agriculture application.

3 Proposed work

See Fig. 1.

3.1 PREQ Processing

The receive PREQ is processed as follows:

Step 1: PREQ is validated using the immutable fields. If PREQ is not valid then it is dropped else it is further processed.

Step 2: The mutable fields update as follows:

- $Hop.cout = hop.count + 1$
- Validate the $path.metric$
- Update the $PREQ.sentlist$
- $PREQ.Hop-limit = PREQ.hop-limit - 1$
- $Next.Hop-addr = Pre.Hop-addr$

Step 3: $PREQ.sending-list$ is computed as explained in Sect. 3.1.

Step 4: The PREQ is forwarded to the neighbouring nodes (routing tuples) that are present in the $PREQ.sending-list$.

3.2 Working Procedure of EREQLLN

Step 1: The neighbour nodes are identified using HELLO packet broadcast and this process is referred as network topology identification.

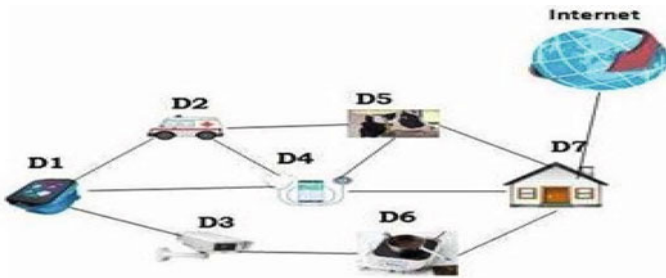


Fig. 1 Network scenario

Step 2: Source node initiates the Path Request (PREQ) to find the optimum path from source to destination. The PREQ construction is as follows:

- PREQ.addr-size set to the size of the address.
- PREQ.route-metric = 0
- PREQ.identifier = RREQ.identifier + 1
- PREQ.hop-count = 0
- PREQ.sending-limit = MAX_sending_LIMIT;
- PREQ-destination = the address of the receiving device or address of the device to which the receiving host attached.
- PREQ-sender = address of the source that generates the PREQ. If the device is generating PREQ on behalf of a host then the source address for the data packet will be generated by the host.

Step 3: The PREQ sent list is updated in PREQ.sentlist and multicasted to all the nodes.

Step 4: Whenever a node receives a PREQ, it will be validated and processed.

Step 5: Each node in topology maintains two tables, one contains its neighbour information and the other contains information about the nodes which receive PREQ.

Step 6: When the destination receives the PREQ, it constructs the PREP and forwards to the nodes if and only if the nodes are present in both neighboring table and PREQ table.

Step 7: The intermediate nodes which receive the RREP also forward it like the destination node.

Step 8: The source node receives the RREP from different paths. It finds the optimum path and establishes the path to the destination.

Step 9: The data is transferred in the established path.

Step 10: The path maintenance is initiated till the data transmission complete.

Algorithm: PREQ Processing Pseudo Code (Rout Discovery Algorithm)

```

Begin PREQ processing
    if <source node> holds active path to
    Destination then Initiate data transfer
    else
    For (i = 1 to n) // for all neighbour nodes
    if Node_Address != Destination_Address
        if PREQ_Lifetime < PREQ max lifetime
            if there is no reverse path
            available then Drop PREQ
            else
                insert the address of eligible nodes in
                PREQ sent list and forward PREQ
        if Routing Type != Node Routing-Type then \\ Metric matching
        if Control Msg-Type = PREP_TYPE and next-hop is blacklisted then \\ Invalid
node
            Drop PREP
    else
    for (i = 1 to n) \\ for all node in neighbour list
        for (j = 1 to m) \\ for all node in PREQ_received - list
            if (i_address = j_address) then
                PREQ_sent_listi Neighbour_listi –
                PREQ_sent_listj return PREQ processing false to node i
    else
    RREP processing
End

```

3.3 Simulation Results

EREQLLN is simulated using Cooja simulator with Contiki OS. Unit Disk Graph (UDG) Model with Distance Loss Communication is used as wireless channel model. In MAC layer, IEEE 802.11 protocol with 55 m transmission range and 80 m interference range are used for the simulation of route discovery process of EREQLLN as shown in Fig. 3. The sky motes (nodes) are deployed in simulation area of 1000×1000 m with 25 motes in linear distribution. The parameters that are used for this simulation is tabulated in Table 1. The average value is obtained from numerous simulations to reduce the estimation error. Two parameters viz. Node density and number of nodes are varied to measure the performance of EREQLLN and LOADng (Fig. 2).

Figure 3 shows 100 sky motes deployed in random distribution for simulation. The minimum distance between the motes is assigned as 40 m. The transmission range is 55 m and the interference range is 85 m. Performance of EREQLLN and LOADng are analyzed in varied node density. The node density has been varied as 25, 50, 100 and 150 nodes over fixed simulation area 1000×1000 m. The simulation

Table 1 Simulation parameters

Simulator	Cooja
OS	Contiki
Simulation area	1000 × 1000 and 1500 × 15,000 m
Number of nodes	25, 50, 100 and 150
Time to live	200 ms
Wireless channel model	UDG model with distance loss communication
Max-hop count	8
Transmission range	55 m

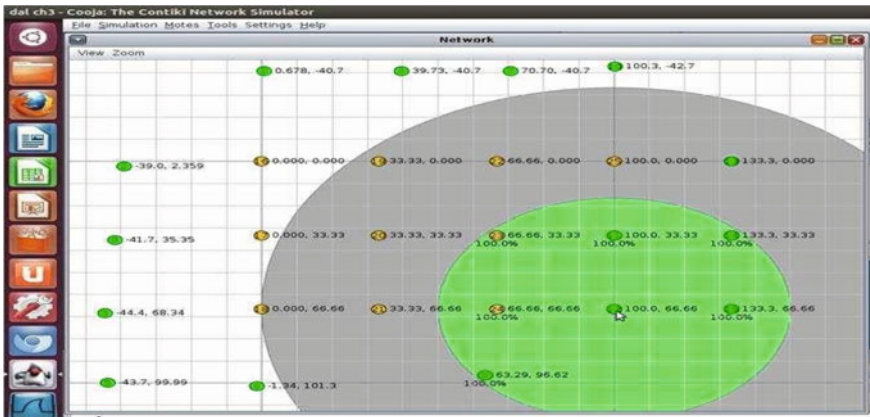


Fig. 2 Linear topology of 25 nodes in the simulation environment

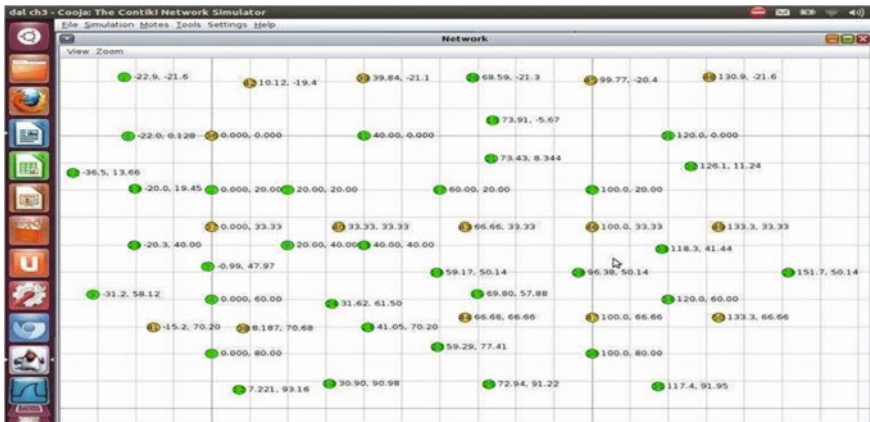


Fig. 3 Random topology of 100 nodes in the simulation environment

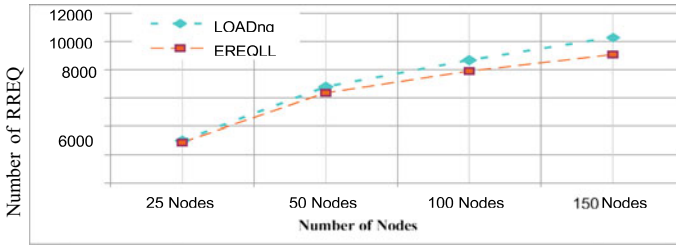


Fig. 4 Number of RREQs forwarded in 1500 × 1500 m simulation area

is carried out for 900 s with 10 different source and destination nodes (randomly selected). The maximum hop count is fixed as 8 and the minimum hop count is 4. It is observed that EREQLLN performs better when the node density decreases. When the distance between the nodes is reduced from $D = 40$ to 6.6 m^2 , the RREQ packet forwarding is increased from 4.5 to 59.5%

The performance of LOADng and EREQLLN is observed in $1500 \times 1500 \text{ m}$ ($22.5 \times 10^4 \text{ m}^2$) simulation area for 25, 50, 100 and 150 nodes with maximum possible distance between the nodes as 9000 m^2 , 4500 m^2 , 2250 m^2 and 1500 m^2 respectively. It is observed that in 900 s simulation, 578 times the route discovery initiated by 10 different source and destination nodes. The number of control packets is high when the simulation area is $1000 \times 1000 \text{ m}$ and it is low in $1500 \times 1500 \text{ m}$ as shown in Fig. 4. This is because the node density is high in $1000 \times 1000 \text{ m}$. When the neighbour degree is high then the number of RREQ forwarding is also high.

The impact of number of RREQ and probability of RREQ forwarding is shown in Fig. 5. Initially the forwarding probability is 0.25 and increased to 0.5, 0.75 and 1 for 50 nodes and 100 nodes respectively. It has been observed that there is increase in number of RREQ when the RREQ forwarding probability increases. The neighbour degree is high when the density is high. The simulation results show that the number of RREQ is decreased in EREQLLN while compared to LOADng.

The impact of control packet size is analyzed as shown in Fig. 6. The RREQ overhead is measured in terms of kilobits (kb) with different number of nodes. Though

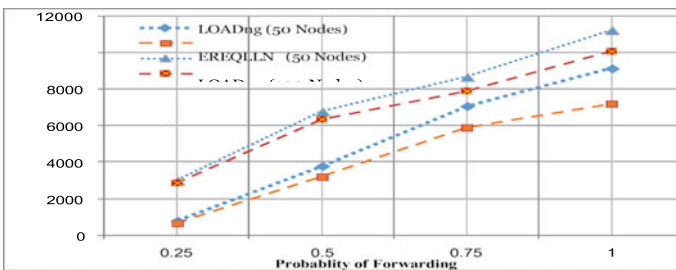
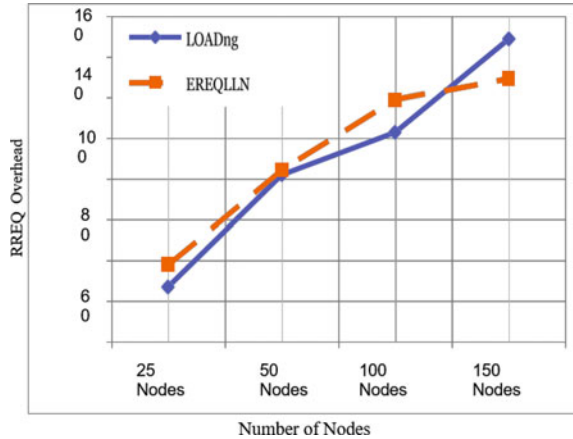


Fig. 5 Impact of RREQ forwarding probability

Fig. 6 RREQ forwarded in route discovery in 1000×1000 m simulation area



the number of RREQ is less in EREQLLN, the size of RREQ is high. This is because of the additional field added in the PREQ.

4 Conclusions

In this research work, an enhanced routing algorithm based on route request is proposed. The proposed algorithm enhances the reactive routing protocol LOADng with respect to route discovery delay and routing overhead. Forward chaining is an expert system used for RREQ processing to enhance the route discovery. The PREQ_sent-list is the new field added to the existing control packet. This algorithm reduces the number of RREQ by removing the identical from the RREQ sending list. The mathematical model is used to estimate the number of RREQ forwarded in the network. It is established that the EREQLLN provides better results than LOADng from the mathematical model.

The simulation is carried out using cooja simulator and Contiki OS. The impact of node density is analysed by increasing and decreasing the node distance. The RREQ control overhead is observed in terms of total number of RREQ forwarded and total size of forwarded RREQ. The results show that the number of RREQ in EREQLLN is reduced. Therefore, this algorithm improves the QoS in terms of route discovery control overhead. However, to achieve this enhancement, a new field RREQ sending list is added to the RREQ packets which introduces additional communication overhead. To overcome this problem EREQLLN algorithm has been proposed.

References

1. Rajeswari, S., Suthendran, K., & Rajakumar, K. (2017). A smart agricultural model by integrating IoT, mobile and cloud-based big data analytics. In *2017 International Conference on Intelligent Computing and Control (I2C2)* (pp. 1–5). <https://doi.org/10.1109/I2C2.2017.8321902>
2. Navarro, E., Costa, N., & Pereira, A. (2020). A systematic review of IoT solutions for smart farming. *Sensors*, *20*(15), 4231. <https://doi.org/10.3390/s20154231>
3. Elijah, O., Rahman, T. A., Orikumhi, I., Leow, C. Y., & Hindia, M. N. (2018). An overview of internet of things (IoT) and data analytics in agriculture: Benefits and challenges. *IEEE Internet of Things Journal*, *5*(5), 3758–3773. <https://doi.org/10.1109/JIOT.2018.2844296>
4. Priyadharsnee, K., & Rathi, S. (2017). An IoT based smart irrigation system. *International Journal of Scientific & Engineering Research*, *8*(5), 44. ISSN 2229-5518.
5. Naik, P., & Kumbi, A. (2018). Automation of irrigation system using IoT. *International Journal of Engineering and Manufacturing Science*, *8*(1), 77–88. <http://www.ripublication.com>
6. Nižetić, S., Šolić, P., López-de-Ipiña González-de-Artaza, D., & Patrono, L. (2020). Internet of things (IoT): Opportunities, issues and challenges towards a smart and sustainable future. *Journal of Cleaner Production*, *274*, 122877. ISSN 0959-6526, <https://doi.org/10.1016/j.jclepro.2020.122877>
7. Khanna, A., & Kaur, S. (2020). Internet of things (IoT), applications and challenges: A comprehensive review. *Wireless Personal Communications*, *114*, 1687–1762. <https://doi.org/10.1007/s11277-020-07446-4V>
8. Jayaraman, P. P., Yavari, A., Georgakopoulos, D., Morshed, A., & Zaslavsky, A. (1884). Internet of things platform for smart farming: Experiences and lessons learnt. *Sensors*, *2016*, 16. <https://doi.org/10.3390/s16111884>
9. Ayaz, M., Ammad-Uddin, M., Sharif, Z., Mansour, A., & Aggoune, E.-H.M. (2019). Internet-of-things (IoT)-based smart agriculture: Toward making the fields talk. *IEEE Access*, *7*, 129551–129583. <https://doi.org/10.1109/ACCESS.2019.2932609>
10. Ray, P. P. (2017). Internet of things for smart agriculture: Technologies, practices and future direction. *Journal of Ambient Intelligence and Smart Environments*, *9*, 395–420.
11. Swaraj, C. M., & Sowmyashree, K. M. (2020). IOT based smart agriculture monitoring and irrigation system. *International Journal of Engineering Research & Technology (IJERT) NCETESFT*, *8*(14).
12. Pallavi, S., Mallapur, J. D., & Bendigeri, K. Y. (2017). Remote sensing and controlling of greenhouse agriculture parameters based on IoT. In *2017 International Conference on Big Data, IoT and Data Science (BIG DATA, IoT and Data Science (BIG DATA))* (pp. 44–48). <https://doi.org/10.1109/BID.2017.8336571>
13. Abhiram, M. S. D., Kuppili, J., & Manga, N. A. (2020). Smart farming system using IoT for efficient crop growth. In *2020 IEEE International Students' Conference on Electrical, Electronics and Computer Science (SCEECS)* (pp. 1–4). <https://doi.org/10.1109/SCEECS48394.2020.147>
14. Jothi Muneeswari, S., Merlin Janet, E., Rajeshwari, Selvarani, G. (2017). Smart irrigation system using IoT approach. *International Journal of Engineering Research & Science (IJOER)*, *3*(3). ISSN: 2395-6992.
15. Chin, J., Callaghan, V., & Allouch, S. B. (2019). The internet-of-things: Reflections on the past, present and future from a user-centered and smart environment perspective. *Journal of Ambient Intelligence and Smart Environments*, *11*(1) 45–69.

Transformation of Project Management Process: An Influence of Industry 4.0



Vijay Anant Athavale and Samprit Tanuj Patel

Abstract Management has gone through many stages until it reaches its modern scientific understanding and has always existed in practice. The necessity for industrialisation has grown as a result of rising global population and urbanisation for economic, social, and environmental activities. Due to the uniqueness of each project in various industries, the significance of project management has increased day after day. An important research area in this field is the effect of Industry 4.0 on project management, which reflects an era full of ground-breaking technological applications in many industries. In this study, first of all, literature research was conducted on the transformations brought by Industry 4.0. The effects of these transformations on the project management elements were then revealed by elaborating on the management factors, and an analysis of the benefits of industry 4.0 was conducted. With the use of Industry 4.0 technologies, it is predicted that successful project management will be achieved by bringing real-time solutions to problems. It is aimed that the obtained data will guide the project stakeholders and contributes to the field.

Keywords Project management factors · Industry 4.0 · Big data · Project management · Cloud computing · IoT

1 Introduction

In the history of the economy, it is mentioned that the agricultural and industrial revolution provided the development and growth worldwide. The industrial revolution led to the development by changing the life of societies and increasing their economic standard (Fig. 1). The Fourth Industrial Revolution (Industry 4.0) began with the advent of the internet and automated systems at the beginning of the twenty-first

V. A. Athavale (✉) · S. T. Patel
Walchand Institute of Technology, Solapur, India
e-mail: vijay.athavale@gmail.com

S. T. Patel
e-mail: patelsamprit@gmail.com

century with the goal of reducing complexity in the various industries. It is possible with project management to complete the projects within the desired time, quality and cost. Project management uses digital technical principles to gather and analyze data in real-time, providing the production system with important information [1]. The actions and factors involved in project 4.0 includes “Big Data, Autonomous Robots, Simulation, management are related to each other, building production, System Integration, Industrial Internet of Things, Cyber” [2].

Hannover fair experts say that Industry 4.0 has introduced a new level of efficiency to production processes in the information age. Klaus Schwab, the founder and chairman of the World Economic Forum, stated that Industry 4.0 is not a prolongation of Industry 3.0. Industry 4.0 can be defined as the replacement of human power with machine power and the ability of machines to manage their production processes. By introducing standardized interfaces and compatible business processes to a product’s production, logistics, engineering, and planning processes, Industry 4.0 will positively impact the quality, adaptability, and robustness of products (Fig. 2).

i. **Big data:**

It is a system that includes high speed, large volume, complex and variable data, advanced techniques and technology to enable big data storage, distribution and management, and information analysis. Big data offers innovations in terms of volume, speed and diversity, unlike traditional data processes. With the use of big data system in Industry 4.0, real-time decision making will become standard by providing the collection and comprehensive evaluation of data obtained from many different sources and systems, as well as management systems. With the use of big data system in the building sector, it is thought that real-time and fast solutions will be produced for the problems that arise by bringing together data from different disciplines at different stages of building production. Thus, quality, time and cost losses in building production will be prevented.

ii. **Autonomous robots:**

Many manufacturers in the industrial system have long used robots to tackle complex tasks. With the start of Industry 4.0, autonomous robots have been developed so that robots can contribute more to the system. Autonomous robots

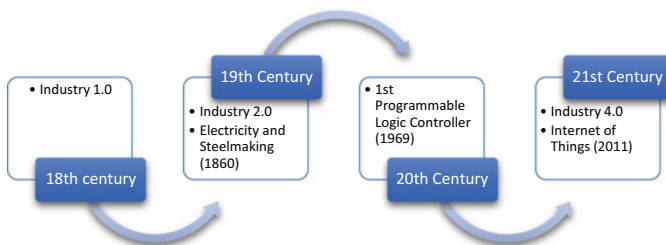


Fig. 1 Industrial revolution Industry 4.0

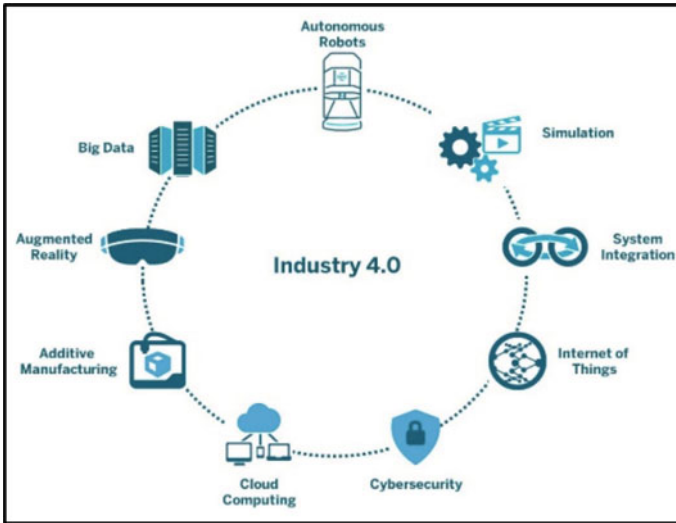


Fig. 2 Structure of Industry 4.0

are able to complete a given task precisely and intelligently in a given time, focusing on safety, flexibility, versatility, and collaboration. At the same time, it is foreseen that industrial applications that are dangerous in many sectors and that negatively affect human health and safety can be carried out by autonomous robots. For Example, the use of autonomous robots in the construction of buildings will reduce the loss of life and property in dangerous situations and enable real-time job follow-up. In addition, it is predicted that the materials used in the construction sector will be used in the production process and will positively affect both material companies and construction sites in terms of time, cost and quality [3].

iii. **Simulation:**

Simulations of products, materials and production processes are an indispensable and powerful tool for the successful implementation of digital manufacturing [4, 5]. The simulation system helps to better predict and understand the modeled systems and production process through behavioral analysis [3]. With the use of real-time simulations within Industry 4.0, simulations are able to analyze the behavior of the user and the system in milliseconds, allowing the manufacturer to develop and produce a “virtual” prototype for his service [4]. Cloud computing systems together with product and process flows can be visualized and monitored by relevant experts.

iv. **System integration:**

System integration is the coordination between multiple systems that enables more than one system to work as a single unit. In the Industry 4.0 organizational system, two separate mechanisms are used, namely integration and self-optimization. In the integration mechanism; there are three different dimensions: horizontal integration, vertical integration and networked production systems throughout the entire value creation network, and end-to-end digital integration throughout the entire product lifecycle. Horizontal integration; It is inter-company integration and forms the basis of close and high-level cooperation among many companies. Vertical integration with a networked production system, in-house integration, corporate planning, it forms the basis of knowledge exchange and collaboration between different levels of the hierarchy, such as pre-production scheduling or management. The end-to-end digital integration includes the flow of a permanent and interactive digital model by closing the gaps between product design, production, logistics and the customer [5]. With the use of integration systems in Industry 4.0, every physical object in production systems becomes a self-organized structure by connecting to each other through smart networks [6].

v. **Industrial internet of things (IIoT):**

The IIoT refers to a worldwide network of interconnected and uniformly addressed objects that communicate via standard protocols. The main task of the IIoT is to collect data from physical objects and connect them to the internet. IIoT technology provides real-time information about an object's location, physical or atmospheric conditions. With the use of the IIoTs, industrial activities become more complex and integrated, and at the same time, it provides a competitive advantage to the company that uses it.

vi. **Cloud computing:**

Cloud computing is the means to virtualize resources and services and consolidate server-based system. It includes resource pools of information technologies that provide storage and processing features in the virtual system by serving more than one user. The services of cloud computing systems are divided into three as software, platform and infrastructure service [6]. Access to cloud computing systems, on the other hand, can be done through public, private and multi-organization clouds [7, 8].

vii. **Cyber security:**

Data stored in the IIoT, remote access and cloud computing systems are connected to the global network via the internet [9]. It is thought that in the near future, the main data source will be completely inanimate objects. In order to ensure the security of this information on the Internet, a cyber-security system has been developed within the scope of Industry 4.0. The cyber security system is a technology based on protecting, detecting and responding to attacks that may come over the internet developed a three-layer and human-centered deep defense concept, including system, network and facility security, in accordance

with international standards. The use of cloud computing systems is related to the information and communication technologies paradigm and service control. It helps automate and integrate the mechanism. Cloud computing systems can be provided with portable devices which will reduce the cost of companies for information technology infrastructure [6].

viii. **Additive manufacturing:**

Additive manufacturing refers to producing customized products. With additive production, the traditional production system will leave its place to the technological production system [10]. Today, the continuous change in customer needs and the personalization of products negatively affect the time to market of companies. The additive production system developed to solve this problem has enabled products to be produced faster and cheaper [6]. With the additive production system, companies gain advantage by keeping less stock in their warehouses, reducing production volume and supply times. It is observed that the use of the additive production system in the construction sector in material production factories will positively affect both the manufacturer and the construction site process in terms of time, quality and cost.

ix. **Augmented reality:**

Augmented reality is a technology that enhances the virtual world by integrating digital content with two-dimensional and/or three-dimensional objects. The working principle of augmented reality entails electronically processing real life phenomena and incorporating them into the virtual environment. [11]. Augmented reality helps to bridge some gaps between manufacturing operation and product development, as it has the ability to reproduce and reuse digital information simultaneously [12]. The use of augmented reality in the early design, tender, construction, maintenance and repair phases of the buildings obtained by the construction sector and the harmony between the phases, persons and organizations, disciplines and machines in the building production problem is expected to be solved.

2 Influence of Industry 4.0 on Project Management Process

Project management is the use of all the knowledge, skills, tools, and methods necessary for the realization of the phases of the project [13]. Project management ensures that the investor's organization is kept updated on the progress of the project, as well as providing guidance to the project management team. In project management, scope means the amount and quality of work, budget means measurable cost, and schedule means the logical sequence and timing of the work. Today, the importance of effective project management has become a key factor in companies' competition, due to the presence of multiple disciplines within the projects and the fact that projects have evolved into something unique. Furthermore, because the projects tend to be large and original, managing them effectively has become increasingly important. The factors that provide optimization in project management are adapted to the

transformations and technologies brought by Industry 4.0. Based on the situation, the effect of Industry 4.0 on the project management is examined below.

i. **Organization:**

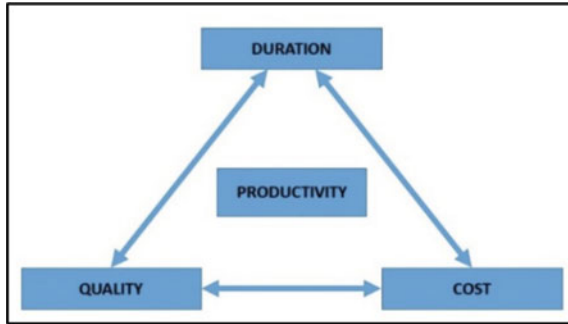
The activities included in the project are to ensure coordination and to establish the power system. Organization includes examining the project planning and objectives, determining and grouping the activities to be carried out, determining the teams that will take part in the activities and the relations between the teams, and preparing the tools and methods to be used in the activities [14]. There are four different types of organizations, depending on the nature of the projects, the disciplines involved, and interdisciplinary communication [8]. The internet and other technology advancements in people's lives have altered communication styles in addition to the traditional organizational forms. [14]. Communication problems have been prevented by the use of virtual organization, which emerged with the effect of current technology on the organization systems in the building industry.

ii. **Coordination:**

Coordination; is the management of communication between project managers, staff, and organizational units. A high degree of operational efficiency can be achieved by seeing coordination as a process of managing project resources. Modern technologies allow for the proficient and efficient use of simulations and computer-based tools, cloud computing bases that hold data on the product and the project, project coordination with authorized project managers, and the use of simulations and computer-based tools. In this direction, the coordination process will be more effective by using the IoT and AR technologies developed by Industry 4.0 and bringing together the data of the production process and personnel in the big data system is considered [15]. Throughout the production process, it is predicted that cloud computing platforms would enable real-time communication between project stakeholders.

iii. **Efficiency:**

It is the ratio of the product to the inputs or resources used in the production process [15]. Efficiency is achieved when the time spent in the process of producing quality products and the economic inputs consisting of capital, labor, energy, materials and services are suitable for the conditions [2, 16]. Productivity measurement in industrial production is divided into three as: total factor productivity, total productivity and labor productivity [17]. Since the productivity of machinery, materials cannot be changed, it has been determined that more importance is given to labor productivity in the direction of partial productivity measurement [15, 17]. Labor productivity is measured as output per unit labor input "in hours worked". The total productivity measurement, which includes equipment, materials, production techniques and management, gives more accurate results [17]. The use of material tracking technology is one of the potential areas where productivity gains can be achieved. With this technology, the time spent by workers searching for material at work space is reduced during the production processes [18] (Fig. 3).

Fig. 3 Productivity triangle

iv. **Standardization:**

The concept of standardization, which is one of the concepts affecting the quality of industrial products, is derived from the concept of standard. According to the definition of the International Organization for Standardization (ISO), the standard is a set of documents approved by relevant institutions, containing rules, guidelines or characteristics related to activities for common and repeated uses, aiming to establish the most appropriate order under current conditions [18]. Standardization is the process of establishing and applying certain rules with the assistance and cooperation of all interested parties in order to obtain economic benefits in relation to a particular activity [16]. Standardization provides quality reliability by determining the lower limit of the quality of the product obtained after the production process. Providing superiority in exports and imports, development of competition, helping to balance supply and demand, labor, eliminating the waste of time and raw materials are the benefits of standardization [18].

v. **Keeping pace with changing conditions and developing technology:**

Standards are compatible with technology, so they can be modified to reflect issues that develop during the production process. Today, as a result of the advancement of information and industrial technology, standards have emerged as the universal language of international trade. The way to compete in international markets is through the production of products in accordance with the standards [19]. In this direction, today's construction systems, materials, equipment and management standards technology needs to be updated. With the use of simulation and augmented reality technologies, the creation of standards, and the use of cloud computing systems.

vi. **Constraints:**

One of the aims of project management is to obtain a quality output despite time, budget and scope constraints in the production process. In order to reduce the negative impact of constraints on the production process, the project duration will be shortened and the corresponding indirect costs will decrease by ensuring the business continuity of the workers and management team working in the project. An algorithmic resource allocation and balancing stated that it can be

achieved by methods. With these methods, time/resource management, material management, cost planning and monitoring, time/cost balancing, making integrated project planning applications is required [2]. Today, ministries and municipalities frequently amend legal regulations. Therefore, the technology and legislative constraints included in the project management factors are not under the control of the project management team. System integration of the project management team that emerged with technological developments, cloud computing systems, and additive manufacturing system should be included in the management process. Thus, it is believed that by having external influences impact the management process as little as possible; time and expense issues can be avoided.

3 Conclusion

With the development of industrialization and technology, there is an increasing complexity of the projects. The factors of project management used in today's industry have been researched in the literature. Given that Industry 4.0's nine primary technologies would fundamentally alter the project management system, research has been done on how these changes will affect key project management elements, and predictions have been made based on the results. The analysis of the collected data reveals that Industry 4.0 technologies will offer real-time solutions to the issues with conventional project management. In this direction, it is crucial for Industry 4.0 technologies to incorporate all of the project management concepts. The effective utilisation of personnel and equipment, as well as the accurate assessment of material resources, will ensure successful project management in the construction industry with the application of these technologies in the project management system. Parallel to this, cost, quality and time parameters will be used at the optimum level in the project management process. Stakeholders are expected to contribute to its development. It has been tried to establish a basis for the developments that will occur in the construction sector in the future in the future.

References

1. Taner, Z. T. (2019). *Examination of construction management in the context of sustainable development in Çukurova region* (Master thesis). Erciyes University, Institute of Science and Technology.
2. Gültekin, T. (2007). *Project management pre-production process*. Palme Publishing House.
3. Weyer, S., Meyer, T., Ohmer, M., Gorecky, D., & Zühlke, D. (2016). Future modeling and simulation of CPS-based factories: An example from the automotive industry. *IFAC-Papers OnLine*, 49, 97–102.
4. Mourtzis, D., Doukas, M., & Bernidaki, D. (2014). Simulation in manufacturing: Review and challenges. *Procedia CIRP*, 25, 213–229.

5. Athavale, V. A., & Athavale, A. (2021). Digital twin—A key technology driver in industry 4.0. *Engineering Technology Open Access Journal*, 4(1). <https://doi.org/10.19080/ETOAJ.2021.04.555628>
6. Rennung, F., Luminosu, C. T., & Draghici, A. (2016). Service provision in the framework of Industry 4.0. *Procedia-Social and Behavioral Sciences*, 221, 372–377.
7. Athavale V. A., & Bansal A. (2022). Problems with the implementation of blockchain technology for decentralized IoT authentication. *Blockchain for Industry 4.0*, 91–119. CRC Press. <https://doi.org/10.1201/9781003282914-5>
8. Kumar, S., Athavale, V. A., & Kartikey, D. (2021). Security issues in cloud computing: A holistic view. *International Journal of Internet of Things and Web Services*, 6, 18–29. <https://www.iaras.org/iaras/home/caijitws/security-issues-in-cloud-computing-a-holistic-view>
9. Sharma, R., & Athavale, V. A. (2019). Survey of intrusion detection techniques and architectures in wireless sensor networks. *International Journal of Advanced Networking and Applications*. <https://doi.org/10.35444/IJANA.2019.10044>
10. Kim, H., Lin, Y., & Tseng, T. L. B. (2018). A review on quality control in additive manufacturing. *Rapid Prototyping Journal*, 645–669.
11. Hořejší, P. (2015). Augmented reality system for virtual training of parts assembly. *Procedia Engineering*, 100, 699–706.
12. Rentzos, L., Papanastasiou, S., Papakostas, N., & Chryssolouris, G. (2013). Augmented reality for human-based assembly: Using product and process semantics. *IFAC Proceedings*, 46, 98–101.
13. Mert, H., & Kucukkoglu, N. (2016). PMI methodology in project management and applicability in Turkey. *Press Academia Procedia*, 2, 564–569.
14. Harran University, Management and Organization (2020). <http://birecik.harran.edu.tr/assets/uploads/sites/21/files/yonetimveorganizasyon24032019-23032019.pdf>
15. Chauhan, D., Kumar, A., Bedi, P., Athavale, V. A., Veeraiah, D., & Boppuru, R. P. (2021). An effective face recognition system based on cloud based IoT with a deep learning model. *Microprocessors and Microsystems*, 81, 103726. ISSN 0141-9331, <https://doi.org/10.1016/j.micpro.2020.103726>
16. UNDP annual report. (2022). <https://annualreport.undp.org/>
17. Arora, S., Athavale, V. A., Maggu, H., & Agarwal, A. (2021). Artificial intelligence and virtual assistant—working model. In N. Marriwala, C. C. Tripathi, D. Kumar & S. Jain (Eds.), *Mobile radio communications and 5G networks. Lecture notes in networks and systems* (Vol. 140). Singapore: Springer. https://doi.org/10.1007/978-981-15-7130-5_12
18. Dalal, S., & Athavale, V. (2012). Challenging bullwhip effect of supply chain through case based multi agent system: A review. *International Journal of Advanced Research in Computer Science and Software Engineering*, 2(12), 267–272.
19. Technology and innovation report. (2021). https://unctad.org/system/files/official-document/tir2020_en.pdf

ICT Enabled Teaching for Transforming Rural Classrooms: A Reference to English Language and Teaching (ELT) for Betterment of Students from Rural Background



Karan Babaso Patil and A. B. Nadaf

Abstract Technology has become an essential component of learning both in and out of the classroom. Every language class makes use of technology. Technology has aided and enhanced language learning. Teachers can use technology to modify classroom activities, which improves the process of learning a language. Innovation continues to grow in importance as a tool to assist educators in working with language learning for their students. This research focuses on the task of incorporating new innovations in learning English as a second/unknown dialect. It discussed various perspectives that help English language students improve their learning abilities by utilizing advancements. In this paper, the specialist defined the terms innovation and innovation reconciliation, explained how innovation is used in language classrooms, reviewed previous studies on incorporating advances in further developing language acquiring abilities, and made specific recommendations for better utilizing these advances, which aid students in further developing their mastering abilities. The current review uncovered that the powerful utilization of new advancements further develops students' language mastering abilities.

Keywords ELT · ICT · CALL · Collaborative · Social networking

1 Introduction

In language educating and learning, we have a ton to look over the universe of innovation: Radio, television, Disc Rom, PCs, C.A.L.L., the Web, Electronic Word reference, Email, Web journals and Sound Tapes, Power Point, Recordings, DVD's

K. B. Patil (✉)
SVERI's College of Engineering, Pandharpur, India
e-mail: kbpatil@coe.sveri.ac.in

K. B. Patil · A. B. Nadaf
Abhijit Kadam Institute of Management & Social Sciences, Bharati Vidyapeeth (Deemed to Be University, Pune), Solapur, India

or alternately Vcd's. The most recent twenty years have seen unrest because of beginning of innovation, and has changed the elements of different enterprises, and has likewise impacted the ventures and the manner in which individuals cooperate and work in the general public. This rapid rise and development of data innovation has provided an excellent model for investigating the new educational model. As a result, innovation plays an important role in English education. Using sight and sound to create a setting to demonstrate English's interesting benefits. This paper attempts to deconstruct the importance of interactive media innovation in language instruction, as well as the issues addressed by utilizing these advances. It also implies making English educators aware of the methodologies for successfully incorporating it.

Web was first acquainted with understudies as a device to accumulate information; numerous students in India got into happiness by just discard their written words and exchanged their learning propensity into the new innovation. This peculiarity likewise gives large effect on the educating and learning of dialects and culture.

This paper attempts to take a gander at how to characterize a norm of advancing by utilizing the Web. What esteem understudies can gain from utilizing and how to make an extensive and successful web based learning framework without manhandling it?

2 Theory

2.1 Internet

Hill and Slater in *Network Technology and Language Learning*, mentioned that the Internet, which is part of network technology have certain characteristics such as the power to stimulate, excite and motivate learners in ways which are far beyond the reach of a teacher working alone in a traditional classroom. Notwithstanding, it is expected for the students to be imaginative by planning host of exercises that can be advanced which include students in working inventively and creatively. It is in some cases hard yet exceptionally surprising experience for the standard and ordinary data provider. The Web likewise offers various devices to clients. To begin, there is the possibility of remote access to assets, either credible (e.g., electronic papers) or reason composed, to aid language learning. The World Wide Web, which allows users to browse and search a vast array of hyperlinked materials ranging from text and images to video, is making these resources more widely available. The level of interactivity of web resources varies. Some limit students to simply turning pages, while others allow them to complete exercises and then receive feedback. Slater and Hill (2000) another important aspect of the Internet is the ability to communicate. This can be asynchronous communication, such as e-mail, news-groups, and computer conferencing, or synchronous communication, such as Internet

Relay Chat (IRC), Internet telephony, and video conferencing. Early Internet applications for language learning primarily made use of the Internet's single facilities. The projects that resulted tended to focus on either accessing Internet resources or enabling student-to-student communication.

2.2 *E-Learning*

E-Learning can be interpreted in many ways and few of the components of E-Learning are as follows:

1. Electronic learning
2. Effective learning
3. Extend the classroom
4. Exploration is an extraordinary experience
5. Extra efforts
6. Enrich knowledge
7. Enhance communication.

All of the aforementioned definitions are founded on the idea of "offering a new method of learning." However, it makes no mention of the requirement for costly equipment. Instead, it suggests that, thanks to the internet, learning may be done whenever, whenever, and without regard to place or time. In earlier research, Toe and Gay [1] acknowledged that e-learning has demonstrated tremendous promise for producing major changes in accessibility and learning opportunities. It combines improvements in information highway technology to remove barriers related to socioeconomic position, time, and location, creating an entirely new learning experience.

The main issue with e-learning is that there isn't a single uniform standard for online instruction and learning. Many enterprises, including institutes of higher learning, are thus entering the contest and asserting that their systems are "e-learning-compliant." They are only automating their services and offering their courses online, though, at these companies. The only enhancement to the educational learning process offered by online content is the absence of time and space restrictions. The majority of Higher Education Institutions (HEI) erred because they lacked a solid understanding of e-learning as a teaching strategy. E-learning should be more than just a collection of technological solutions because the majority of HEIs place more of an emphasis on demonstrating technology than on imparting knowledge. E-learning technology should only be used to offer educational materials. The goal of any e-learning solution, for instance, should be to enhance learning and intellectual interaction at the cognitive, behavioural, and physiological levels, regardless of how sophisticated the solution is. Any technology, according to Gardner (1999), is pedagogically neutral and can be used for a variety of pedagogical purposes.

The educational philosophy or approach is more crucial than the technology itself, and even the most basic technological pedagogical methods can be quite effective.

Second, despite how advanced its design, a machine will never be able to completely replace people. The development of instructionally sound e-learning should therefore take precedence over traditional classroom training. The subject matter expert (SME) needs to provide more details and be understandable enough to stand on their own without additional interpretation (Gardner 1999). It is crucial to remember that internet information is not always knowledge. The use that is made of this information will turn it into knowledge. Last but not least, the value of online learning is not in the knowledge. Information is plentiful, if not excessive, as a result of recent developments in information and communication technologies. Gay contends that the Meta data is where the real value lies. Specifically, knowing the many sorts of information, when to utilize them, how to reuse them, and what to do with them. As a result, the system defines and manages knowledge material, which is the core of electronic learning. Most importantly, e-learning should move away from a content-oriented strategy and towards a knowledge-synthesis approach in the future.

3 Methods and Processes

Some of the methods and process which are helpful for ICT enabled teaching learning process are as follows:

3.1 Integrating the Internet in the Teaching–Learning Process

E-mail, without a doubt, has altered the way people communicate. In higher education, e-mail could provide students with a direct channel to their tutor, regardless of time or location, to report on progress, ask questions, and discuss other course-related issues. This is now being used successfully in many higher education institutions.

3.2 Remote Learning

Users can now communicate visually in “real time” thanks to the high-speed internet connection. The streaming audio and video can be used to create a teleconferencing event, allowing teachers to facilitate a ‘long distance’ class room in which students can interact with their counterparts. The authentic image and sounds from the webcam could provide learners with an exciting learning experience. If privacy is such a concern, students could create a virtual chat room to discuss a specific topic and share ideas.

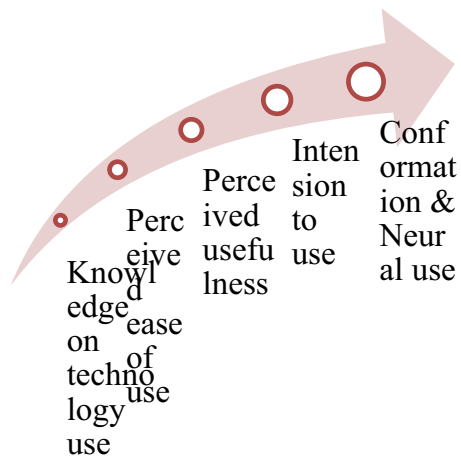
3.3 Data Terminal

The Internet is also used to disseminate administrative information. Learners can access timetables, module content and assessment information, staff information, and links to other (primarily textual) data sources at any time and from any location. As teaching staff create Web pages to help structure students’ data collection and provide access to a variety of other resources, HE institutions can improve this capability by linking to various multimedia data resources relevant to subject content. Links to other websites containing lecture notes, research papers, discussion documents, virtual environments, programmed code, images, sounds, icons, buttons, and so on, as well as other resources such as interactive tutorials, are examples of such pointers.

3.4 Shared Workspace

The Internet can also be used to create collaborative workspaces where students can help each other learn. Students can use interactive whiteboards and computer conferencing to collaborate on projects, as well as explore and create 3D worlds and multimedia presentations. Consider the user’s behavioral intentions as well as perceived usefulness and ease of use. While perceived usefulness refers to a person’s belief that using a particular technology will improve job performance, perceived ease of use refers to the importance of a technology in being user-friendly. TAM theory was developed in general to evaluate the effectiveness or success of a technology in aiding understanding of the value and efficacy of a specific system. It is also widely regarded as one of the most influential theories in contemporary information systems research. However, the theory has evolved over time, with more specific variables explaining how a user can accept a technology (Fig. 1).

Fig. 1 Conceptual framework of study



4 Learning Approaches

The vital approaches in respect of learning include collaborative learning, learning through online learning community and better and proper use of social network services, etc. (Fig. 2).

4.1 Collaborative Learning

The internet's most valuable feature is its networking capability, which allows users to collaborate on projects. Several researchers believe that this feature is critical for the learning experiences of students. "Collaborative working means that students will be able to perform at higher intellectual levels," says Gokhale. Cooperative learning methods, according to Bruner [2], "improve problem-solving strategies" [3]. Previous research by Johnson and Johnson (1997) found that collaborative learning had a positive impact on individual achievement when compared to individualistic learning. In these studies, cooperative learning was shown to promote higher individual achievement than competitive or individualistic learning. In the same article, they also stated that collaboration among learners promotes greater intrinsic motivation to learn as well as more frequent use of cognitive processes like re-conceptualization, higher-level reasoning, cognitive elaboration, and networking. The challenge is to find new ways to organize learning communities. Create a virtual discussion forum, mailing list, or web blog to accomplish this [4].

4.2 Learning Through Online Learning Community

An online learning community is a place on the Internet where members share their learning needs through proactive and collaborative partnerships. People collaborate as a group to achieve a common learning goal, which may be proposed by an instructor or emerge from discussions among participants about personal interests [5, 6].

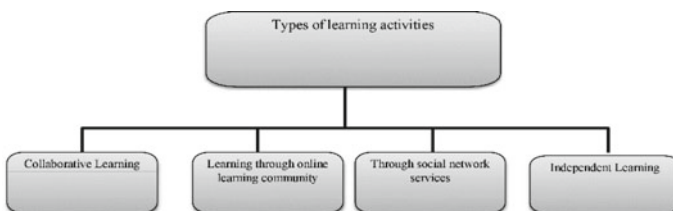


Fig. 2 Types of learning activities

4.3 Learning Through Social Network Service

People in an online community communicate using text (chat), audio, video, or other devices. According to Riel and Pollin (2004), intentional online learning communities are classified into three types: knowledge-based, practice-based, and task-based. Users create them in order to address their specific needs and interests.

In general, this community has divided itself into groups based on the mode of communication that they use, such as:

(a) **Content Management**

WebCT/Blackboard <http://www.blackboard.com/us/index.Bb>

Angel <http://www.angellearning.com/>

Desire2Learn <http://www.desire2learn.com/>

Moodle <http://moodle.org>

(b) **Social Networking**

Facebook <http://www.facebook.com/>

Second Life <http://secondlife.com/>

Friendster <http://www.friendster.com/>

Myspace <http://www.myspace.com/>

(c) **Learning Object Storage Area**

Merlot (Multimedia Educational Resources for Learning and Online Teaching) <http://www.merlot.org/merlot/index.htm>

Taking It Global <http://www.takingitglobal.org>

(d) **Blogs**

Blogger <https://www.blogger.com/start>

As compared to the other learning methods, social networking website such as Friendster and Facebook offers a very exciting learning tool based on the Circle of Friends (social network) and Web of Friends techniques for networking individuals in a huge number of virtual communities (Friendster® for example currently has 50 million users). Students can even interact with someone from another country by using a social network service in the internet. Students may find this very interesting and it will be very useful for learning culture from different country [7, 8].

4.4 Independent Learning

The Internet will be an excellent resource for independent learning. The vast amount of data can be a valuable resource for students. It can be used in a self-access language learning center to encourage students to study independently by selecting from a variety of available resources. However, before beginning to learn using this style of learning, students, particularly foreign language students, learn better if they understand how they learn. The learner-centered approach, learner autonomy, and self-directed learning are all closely related to the self-access language learning style

because they all emphasize student responsibility and active participation in his or her own learning.

The internet can be used in self-access language centers in a variety of ways, such as by placing digital centers in various corners of the center or by uploading self-access learning materials online. What resources are available and how students are guided to use them are determined by the financial resources available as well as the amount of learner autonomy an institution decides to grant students. The primary benefit is one of the benefits of combining internet and self-access learning is that students can, at the very least, set their own pace. Students can also set the level and content of their work and complete their assignments using the self-access center. Therefore, it supports flexibility, with the purpose of giving the students themselves the opportunity to tailor the course to fit their learning needs and styles than the conventional mode of teaching. Use of multiple technologies in a more independent setting has been shown to improve motivation and increase students' ability to work independently by taking more responsibility for their own learning. Students also report feeling more "empowered" by such modes of instruction.

5 Challenges of Applying Internet in the Rural HEI

The major disadvantages of this mode have basically deals with the ability of both students and teachers to adapt and integrate the technology into the classroom. Many students are not used to work independently, and creating the need. One study reports that some students do not want too much freedom in their use of technology. Recent study conducted at Bina Nusantara University, indicates that about 43% preferred a controlled learning environment with the presence of a teacher. On the other hand, teachers have to trust students by 'letting go' of their control. This can be equally disorienting for conservative teachers who might feel that it has depreciated teachers' skills and experience. For teachers who are used to being the center of student activity, he or she will find the internet quite disturbing. They have to change the role from being the center of the knowledge into the facilitator controlling how, when and why students do what they do. Teachers cannot rely only on textbooks that allow little variation. He or she has to be a knowledge resource more than he or she expected before, because student may contest the information from the teacher with what they have found in the internet. The use of self-access center and the internet will steer students' way from the rigidity and "security" of teachers as the "all-powerful" and "all-knowing" position into the secondary source of knowledge after the internet [9, 10].

6 Conclusion

Using the Internet to support learning and teaching necessitates a cultural shift for both teachers and students. Both faculty and students must see the Internet as having “added value” over other resources for course-related work, rather than simply viewing it as a source of entertainment. E-mail and the ability to communicate with others on a global scale can be extremely beneficial to the learning and teaching processes. Failure to use the internet, on the other hand, can be caused by both learner and teacher anxiety. This is due to a shift in the nature of learning as well as a shift in how both parties perceived technology as a component of the learning process. Overdependence on teachers toward technology can also bring failure. There should be a sense of balance among the teacher as facilitator in perceiving information technology as source of knowledge. Creativity of teachers in developing the course material is the key factor before integrating the internet inside the classroom. Teachers also should build a sense of trust and create a positive attitude between them. The biggest challenge for the conventional traditional teacher, however, is the willingness to ‘update’ the old conservative teaching style by diversifying their source of knowledge. The euphoria of learners while discovering information through the web can be considered as part of learning. This can be done by suggesting learners to access only the approved website when browsing for information. They are allowed to open search engine but they should be lead to open the specific web addresses. Our experience is suggesting users to open a ‘safer and much reliable’ URL such as those with the extension of: .org, .gov, .edu, and warn them about the .com (dot com) because of its commercial nature.

References

1. Teo, C. B., & Gay, R. K. L. (2006). A knowledge-driven model to personalize e-learning. *Journal on Educational Resources in Computing (JERIC)*, 6(1), 3-es.
2. Bruner, J. (1985). Vygotsky: An historical and conceptual perspective. In *Culture, communication, and cognition: Vygotskian perspectives*.
3. Gokhale, A. (1995). Collaborative learning enhances critical thinking. *Journal of Technology Education*, 7(1).
4. Venkatesh, V., Morris, M. G., Davis, G. B., & Davis, F. D. (2003). User acceptance of information technology: Toward a unified view. *MIS Quarterly*, 425–478.
5. Honey, M., Culp, K. M., & Carrigg, F. (2000). Perspectives on technology and education research: Lessons from the past and present. *Journal of Educational Computing Research*, 23(1), 5–14.
6. Mernit, S. (1995). Publishing on the WWW: What’s happening today and what may happen in the future.

7. Howard, R. (2004). Common ground and critical differences in designing technical environment.
8. Grattan, J., Brown, G. H., & Horgan, J. (1998). Student C&IT skills development and the learning environment: Evaluation and module evolution. *Education+ Training*, 40(8), 366–373.
9. Hill, B., & Slater, P. (1998). Network technology and language learning. *Education+ Training*.
10. Vygotsky, L. S., & Cole, M. (1978). *Mind in society: Development of higher psychological processes*. Harvard University Press.

Manufacturing and Fabrication Processes for Societal Applications

Influence of Obstacles on the Mixing Performance of Serpentine Microchannels



Kailas Malgonde, Babruvahan P. Ronge, and Sandeep S. Wangikar

Abstract The several Lab on a Chip devices depend largely on the microchannels. Each microchannel's performance is determined by its mixing properties and pressure drop. The performance evaluation for serpentine microchannels including obstacles is the main topic of this paper. The simulations based on computational fluid dynamics (CFD) were performed by employing COMSOL Multiphysics 5.0 software. The semicircular obstacles were introduced in the flow direction of serpentine microchannels. The two inlets' entrance velocities ranged between 0.5, 0.75 and 1 mm/s. The microchannels' width and height were 400 μm (for an aspect ratio of 1). Pressure changes (drops) and mixing in straight serpentine microchannels with no obstructions and semi-circular obstructions are discussed. Study is done on how inlet velocity affects pressure drop as well as mixing length.

Keywords Serpentine microchannel · Semicircular obstacles · Curved bend · Mixing length · Pressure drop

1 Introduction

Microfluidics is a concept that describes fluid control and actuation methods and components used for microscopic level fluid transport phenomena. The field of microfluidic systems is one that is rapidly developing, and research in this area is crucial to the implementation of lab-on-a chip (LOC). The LOC systems, also known as systems for micro total analysis (μTAS), are capable of carrying out the full range of biological and chemical processes [1, 2]. Numerous industries, such as cosmetics, medicine, pharmaceuticals, and biotechnology as well as the control systems using physical sciences and heat management, use microfluidics. One of the essential parts of microfluidic systems is a microchannel. The term "microchannel" refers to a channel with dimensions in the micrometer (μm) range. A micromixer is

K. Malgonde (✉) · B. P. Ronge · S. S. Wangikar
Department of Mechanical Engineering, SVERI's College of Engineering, Pandharpur,
Maharashtra, India
e-mail: kailas_mallu@yahoo.com

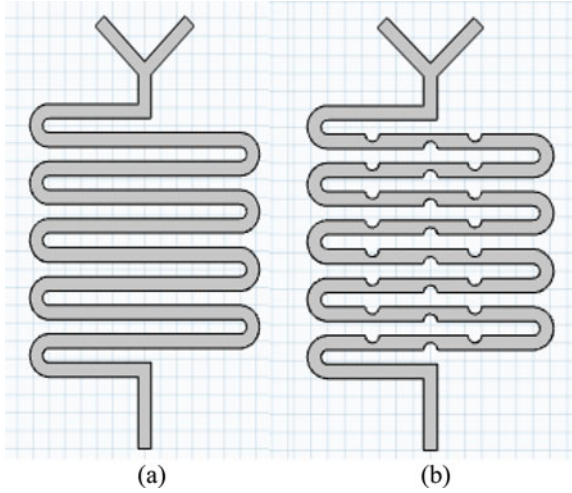
a microchannel only which is employed for mixing fluids. The microfluidic chips, which are circuits, already have the geometries in place. Since this technology provides a way to perform the crucial chemical evaluation processes in the biomedical field, it has been the subject of extensive research [1–3]. Micromixers can always be split into 2 groups: passive and active. These micromixers differ in terms of capacity, mixing speed, and operational needs. For instance, a power source is needed to enable mixing in an active micromixer.

A passive micromixer, in contrast, uses applied pressure meant for fluid motion to achieve mixing. As a result, several micromixers better suited than others for a given application. Although integration with other devices is challenging and fabrication is expensive, active micromixers typically offer accurate mixing. Because of this, passive micromixers are frequently preferred [4–6].

Numerous studies discuss the mixing capabilities of passive microchannels. Different researchers have used a variety of geometries, including wavy structures, curved shapes, static micromixers, square waves, straight microchannels, spiral-shaped microchannels, serpentine microchannels with non-aligned inputs, serpentine microchannels with cyclic L-shaped units, etc. to investigate impact of geometry along with profile on mixing performance [7–15]. The split-and-recombine (SAR) microchannel has also been a subject of extensive research. To improve the diffusion process, SAR splits and recombines the two fluids that need to be mixed. Planar SAR micromixers, P-SAR micromixers with cavities, modified P-SAR micromixers with dislocation sub-channels, two-layer crossing channels, 2D modified Tesla structures, ellipse-like micropillars, etc. are a few examples of the various configurations of passive micromixers created by a number of researchers. The split and recombining mechanism and the resulting chaotic advection have been observed to improve mixing performance [16–18]. Lots of studies using various varieties of grooves and obstacles across the mixing path to study the mixing behavior of microchannels have been published by different researchers. [19–24] and reported that performance of mixing was improved on account of the creation of recirculation zones downstream of these obstructions. A select group of researchers have created microchannels using a variety of techniques, including micro-milling, laser machining, and photochemical machining [25–35].

Based on the aforementioned studies, it can be deduced that the mixing index (also known as mixing length) and pressure drop are the two main factors that control the behavior of the microchannel. However, a comparison of microchannels that are serpentine and have both straight and curved bends is still possible. Also impressive is how width as well as height (i.e. aspect ratio) affects the analysis of mixing. The mixing performance analysis for microchannels with obstacles is presented in this paper. These simulations were done with the aid of COMSOL Multiphysics 5.0. Analysis is done on pressure change (drop) and combining in serpentine microchannels with and without semicircular obstructions.

Fig. 1 Serpentine microchannel **a** without obstruction **b** including semi-circular obstruction



2 Numerical Simulations as a Methodology

2.1 Microchannel Configuration

Inside this current study, a serpentine microchannel with no obstacles and a serpentine microchannel using semicircular obstacles have both been taken into consideration. COMSOL Multiphysics 5.0 was used to create the computational models, which are shown in Fig. 1a, b for serpentine microchannel with as well as without semicircular obstacles, in that order. In each configurations of aspect ratio 1, microchannel’s sizes (width and height) are 400 μm . Semicircular obstacles have a 200 μm radius. Inlet 1 and Inlet 2 were used for feeding the two fluids. For both inlets, it has been assumed that the velocity of fluid (u mm/s) is the same.

2.2 Boundary Criteria

COMSOL Multiphysics 5.0 has been used to run the various simulations for the created microchannels. Laminar flow and the transportation of diluted species are the physics used during COMSOL simulations. Governing equations or Eqs. 1–3, were solved by the software using appropriate boundary conditions. The used boundary conditions include no-slip conditions at the microchannel walls, equal velocities at the both the inlets, atmospheric pressure at the outlet, symmetry at the fluid-to-fluid interface, and equal velocities at the two inlets. Water and ethanol at a temperature of 25 °C have been assumed to be the fluids at the two inlets. The fluid concentrations

just at inlet boundaries have been calculated as 10 mol/m^3 for fluids and 0 mol/m^3 for fluid 2. It has been determined that ethanol's water diffusion coefficient is $1.0 \times 10^{-9} \text{ m}^2/\text{s}$. Inlet velocity is adjusted between 0.5 and 1 mm/s.

The steady state conditions used for fluid flow, as well as convection and species diffusion, have been considered for the established computational models. The Navier-Stokes as well as continuity equations are used to express the incompressible isothermal Newtonian fluids in microchannels' mass-momentum balance. These are the equations:

$$\nabla \cdot \mathbf{u} = 0 \quad (1)$$

$$\rho(\mathbf{u} \cdot \nabla)\mathbf{u} = \nabla \cdot [-p\mathbf{I} + \mu(\nabla\mathbf{u} + (\nabla\mathbf{u})^T) - 2/3\mu(\nabla \cdot \mathbf{u})\mathbf{I}] + \mathbf{F} \quad (2)$$

where \mathbf{I} is unit diagonal matrix, $\mathbf{u} = (u, v, w)$ is flow velocity field, μ is the fluid dynamic viscosity, p is fluid pressure, ρ is density of fluid, and $\mathbf{F} = (f_x, f_y, f_z)$ is a fluid-affecting volume force.

Diffusion and convection cause the fluid flow to mix as a result. Mass transportation has been governed by the formula:

$$\nabla \cdot (-D \cdot \nabla c) + \mathbf{u} \cdot \nabla c = R \quad (3)$$

2.3 Mesh Generation

Unstructured mesh was used for the computational analysis (CFD) of micro channel models. The simulations were run with various mesh sizes (domain elements) to prevent the impact of more meshing elements on the simulation results' quality. The pressure drop results at various domain elements are compared for both microchannel configurations. Figure 2a as well as b show the mesh-enclosed serpentine microchannel with parallel oblique bends, respectively.

3 The Study Results and Discussion

The COMSOL Multiphysics 5.0 tool was used to create the serpentine microchannel's three-dimensional models, which include both straight and curved bends, and then run simulations on them. By taking into account the conditions of the boundary, Eqs. 1 through 3 have been solved. The primary fluid is water, and the secondary fluid is ethanol, both at a temperature of $25 \text{ }^\circ\text{C}$.

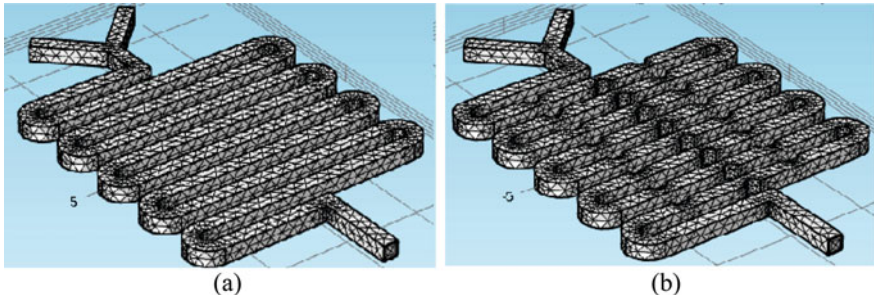


Fig. 2 Serpentine microchannel meshing **a** with no obstacles **b** with semicircular obstacles

3.1 Impact (in Pa) on the Drop in Pressure

Analysis is done on how the aspect ratio affects the pressure drop. There were three different inlet fluid velocities tested: 0.5, and 0.75, and 1 mm/s. Figure 3a, b respectively show the sample pictures for the pressure drop measurement for the Serpentine microchannel (a) without obstacles and (b) with semicircular obstacles.

The pressure drop was measured, and Fig. 4 illustrates how the aspect ratio affected the pressure drop for serpentine microchannels with and without semicircular obstacles. Figure 4 shows that the pressure drop increases as the velocity rises from 0.5 to 1 mm/s. The pressure drop for serpentine micro channels with semicircular obstacles is higher than it is for channels without obstacles, it is also noted. This is due to the fact that the cross-sectional area of the microchannel grows as the aspect ratio does. The pressure on a fluid will be greater in a smaller area and lower in a larger area. Due to the shape of the obstacles, the fluids are subjected to greater pressure there, which causes a greater pressure drop in a serpentine microchannel with semicircular obstacles.

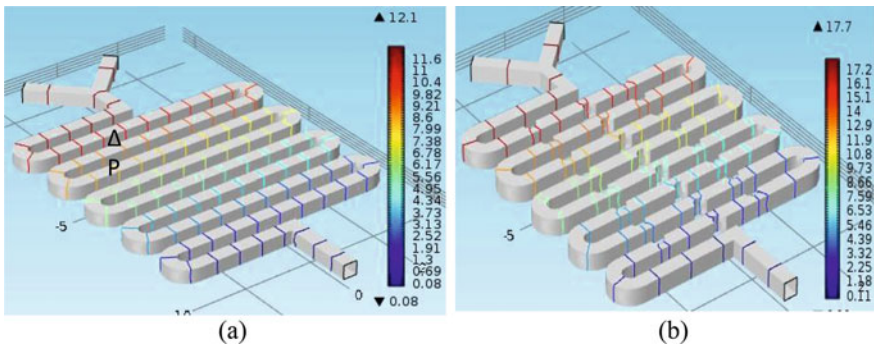


Fig. 3 Pressure drop for **a** serpentine microchannel with no obstacles **b** serpentine microchannel with semicircular obstacles

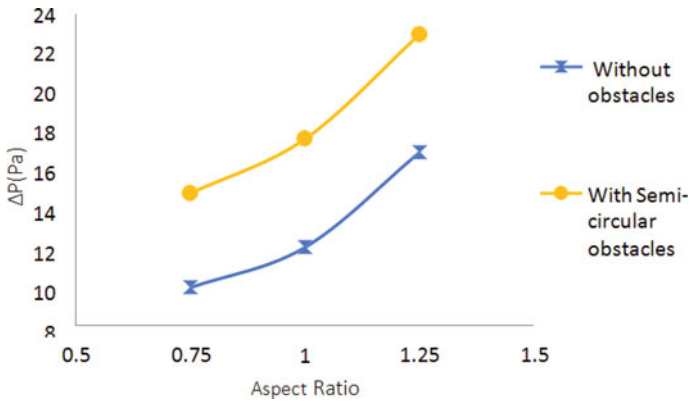


Fig. 4 Relationship between aspect ration and pressure drop

3.2 Impact on Mixing Length

The phrase “mixing length” refers to the length of the channel at which the two fluids are completely mixed, or when the mixing index is 1. In the COMSOL Multiphysics 5 program, the mixing duration is recorded. Figure 5 shows examples of the cross-sectional mixture images for a Serpentine microchannel (a) with no obstacles and (b) with semicircular obstacles.

Figure 6 shows that the mixing length is significantly shorter for microchannels with semicircular obstacles than it is for channels without obstacles. This increase results from the fact that the flow is laminar at lower fluid velocities and that diffusion causes mixing in the microchannels. This shorter mixing length results from chaotic advection and vortices that form near semicircular obstacles, which improve mixing and result in shorter mixing lengths than for situations without obstacles.

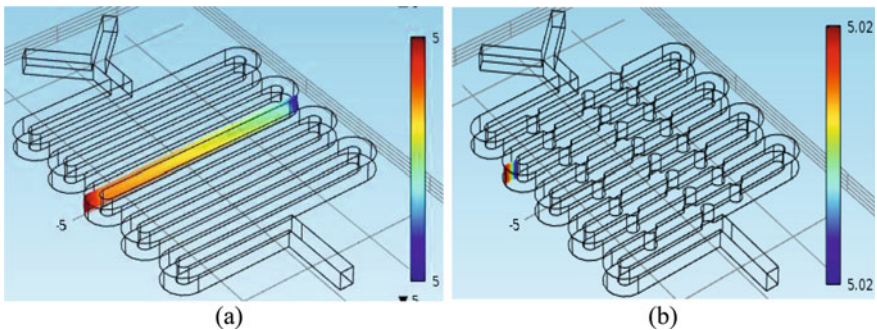


Fig. 5 Few images of mixing at the channel’s cross-section for a serpentine microchannel **a** without obstacles **b** with semicircular obstacles

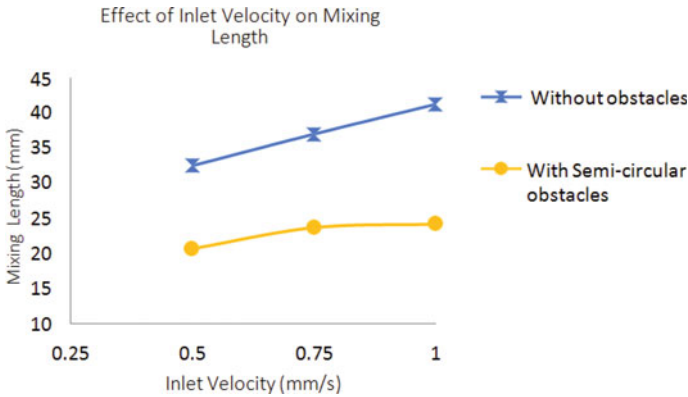


Fig. 6 Mixing length for Serpentine microchannel **a** with no obstacles **b** with semicircular obstacles

4 Conclusions

Using computational analysis by means of COMSOL Multiphysics 5.0 tool, the mixing performance analysis of a Serpentine microchannel (a) without obstacles and (b) with semicircular obstacles has been studied. Investigation is done into how inlet velocity affects the pressure drop as well as mixing length. The following conclusions have been drawn from the numerical analysis:

- As inlet velocity increases, the pressure drop also grows.
- In comparison to serpentine microchannels without obstacles, higher pressure drops are observed in serpentine microchannels with semicircular obstacles.
- In comparison to serpentine microchannels without obstacles, shorter mixing lengths are observed for semicircular obstacles.

References

1. Lee, C. Y., Wang, W. T., Liu, C. C., & Fu, L. M. (2016). Passive mixers in microfluidic systems: A review. *Chemical Engineering Journal*, 288, 146–160.
2. Lim, Y. C., Kouzani, A. Z., & Duan, W. (2010). Lab-on-a-chip: A component view. *Microsystem Technologies*, 16(12), 1995–2015.
3. Whitesides, G. M. (2006). The origins and the future of microfluidics. *Nature*, 442(7101), 368–373.
4. Bothe, D., Stemich, C., & Warnecke, H. J. (2006). Fluid mixing in a T-shaped micro-mixer. *Chemical Engineering Science*, 61(9), 2950–2958.
5. Bahrami, M., Yovanovich, M. M., & Culham, J. R. (2005). Pressure drop of fully-developed, laminar flow in microchannels of arbitrary cross-section. *International Conference on Nanochannels, Microchannels, and Minichannels*, 41855, 269–280.

6. Song, H., Wang, Y., & Pant, K. (2012). Cross-stream diffusion under pressure-driven flow in microchannels with arbitrary aspect ratios: A phase diagram study using a three-dimensional analytical model. *Microfluidics and Nanofluidics*, 12(1–4), 265–267.
7. Ansari, M. A., Kim, K. Y., & Kim, S. M. (2010). Numerical study of the effect on mixing of the position of fluid stream interfaces in a rectangular microchannel. *Microsystem Technologies*, 16(10), 1757–1763.
8. Gobby, D., Angeli, P., & Gavriilidis, A. (2001). Mixing characteristics of T-type microfluidic mixers. *Journal of Micromechanics and Microengineering*, 11(2), 126.
9. Cortes-Quiroz, C. A., Azarbadegan, A., & Zangeneh, M. (2014). Evaluation of flow characteristics that give higher mixing performance in the 3-D T-mixer versus the typical T-mixer. *Sensors and Actuators B: Chemical*, 31(202), 1209–1219.
10. Lü, Y., Zhu, S., Wang, K., & Luo, G. (2016). Simulation of the mixing process in a straight tube with sudden changed cross-section. *Chinese Journal of Chemical Engineering*, 24(6), 711–718.
11. Yang, I. D., Chen, Y. F., Tseng, F. G., Hsu, H. T., & Chieng, C. C. (2006). Surface tension driven and 3-D vortex enhanced rapid mixing microchamber. *Journal of Microelectromechanical Systems*, 15(3), 659–670.
12. Sudarsan, A. P., & Ugaz, V. M. (2006). Fluid mixing in planar spiral microchannels. *Lab on a Chip*, 6(1), 74–82.
13. Hossain, S., & Kim, K. Y. (2015). Mixing performance of a serpentine micromixer with non-aligned inputs. *Micromachines*, 6(7), 842–854.
14. Gidde, R. R., Pawar, P. M., Ronge, B. P., Shinde, A. B., Misal, N. D., & Wangikar, S. S. (2019). Flow field analysis of a passive wavy micromixer with CSAR and ESAR elements. *Microsystem Technologies*, 25(3), 1017–1030.
15. Das, S. S., Tilekar, S. D., Wangikar, S. S., & Patowari, P. K. (2017). Numerical and experimental study of passive fluids mixing in micro-channels of different configurations. *Microsystem Technologies*, 23(12), 5977–5988.
16. Hong, C. C., Choi, J. W., & Ahn, C. H. (2004). A novel in-plane passive microfluidic mixer with modified Tesla structures. *Lab on a Chip*, 4(2), 109–113.
17. Xia, G., Li, J., Tian, X., & Zhou, M. (2012). Analysis of flow and mixing characteristics of planar asymmetric split-and-recombine (P-SAR) micromixers with fan-shaped cavities. *Industrial & Engineering Chemistry Research*, 51(22), 7816–7827.
18. Li, J., Xia, G., & Li, Y. (2013). Numerical and experimental analyses of planar asymmetric split-and-recombine micromixer with dislocation sub-channels. *Journal of Chemical Technology & Biotechnology*, 88(9), 1757.
19. Tran-Minh, N., Dong, T., & Karlsen, F. (2014). An efficient passive planar micromixer with ellipse-like micropillars for continuous mixing of human blood. *Computer Methods and Programs in Biomedicine*, 117(1), 20–29.
20. Guo, L., Xu, H., & Gong, L. (2015). Influence of wall roughness models on fluid flow and heat transfer in microchannels. *Applied Thermal Engineering*, 84, 399–408.
21. Jain, M., Rao, A., & Nandakumar, K. (2013). Numerical study on shape optimization of groove micromixers. *Microfluidics and Nanofluidics*, 15(5), 689–699.
22. Kim, D. S., Lee, S. W., Kwon, T. H., & Lee, S. S. (2004). A barrier embedded chaotic micromixer. *Journal of Micromechanics and Microengineering*, 14(6), 798.
23. Wangikar, S. S., Patowari, P. K., & Misra, R. D. (2018). Numerical and experimental investigations on the performance of a serpentine microchannel with semicircular obstacles. *Microsystem Technologies*, 24(8), 3307–3320.
24. Jadhav, S. V., Pawar, P. M., Wangikar, S. S., Bhostekar, N. N., & Pawar, S. T. (2020). Thermal management materials for advanced heat sinks used in modern microelectronics. In *IOP Conference Series: Materials Science and Engineering* (Vol. 814, No. 1, p. 012044). IOP Publishing.
25. Wangikar, S. S., Patowari, P. K., & Misra, R. D. (2017). Effect of process parameters and optimization for photochemical machining of brass and German silver. *Materials and Manufacturing Processes*, 32(15), 1747–1755.

26. Wangikar, S. S., Patowari, P. K., & Misra, R. D. (2016). Parametric optimization for photochemical machining of copper using grey relational method. In *Techno-Societal 2016, International Conference on Advanced Technologies for Societal Applications* (pp. 933–943). Springer.
27. Wangikar, S. S., Patowari, P. K., & Misra, R. D. (2018). Parametric optimization for photochemical machining of copper using overall evaluation criteria. *Materials Today: Proceedings*, 5(2), 4736–4742.
28. Wangikar, S. S., Patowari, P. K., Misra, R. D., & Misal, N. D. (2019). Photochemical machining: a less explored non-conventional machining process. In *Non-conventional machining in modern manufacturing systems* (pp. 188–201). IGI Global.
29. Chavan, N. V., Bhagwat, R. M., Gaikwad, S. S., Shete, S. S., Kashid, D. T., & Wangikar S. S. (2019). Fabrication & characterization of microfeatures on PMMA using CO₂ laser machining. *International Journal for Trends in Engineering and Technology*, 136, 29–32.
30. Kulkarni, H. D., Rasal, A. B., Bidkar, O. H., Mali, V. H., Atkale, S. A., Wangikar, S. S., & Shinde, A. B. (2019). Fabrication of micro-textures on conical shape hydrodynamic journal bearing. *International Journal for Trends in Engineering and Technology*, 36(1), 37–41.
31. Raut, M. A., Kale, S. S., Pangavkar, P. V., Shinde, S. J., Wangikar, S. S., Jadhav, S. V., & Kashid, D. T. (2019). Fabrication of micro channel heat sink by using photo chemical machining. *International Journal of New Technology and Research*, 5(4), 72–75.
32. Jadhav, S.V., Pawar, P. M., Shinde, A. B., & Wangikar, S. S. (2018). Performance analysis of elliptical pin fins in the microchannels. In *Techno-Societal 2018* (pp. 295–304). Springer.
33. Bhagwat, R. M., Gaikwad, S. S., Shete, S. S., Chavan, N. V., & Wangikar, S. S. (2020). Study of etchant concentration effect on the edge deviation for photochemical machining of copper. *Novyi MIR Research Journal*, 5(9), 38–44.
34. Patil, P. K., Kulkarni, A. M., Bansode, A. A., Patil, M. K., Mulani, A. A., & Wangikar, S. S. (2020). Fabrication of logos on copper material employing photochemical machining. *Novyi MIR Research Journal*, 5(7), 70–73.
35. Kame, M. M., Sarvagod, M. V., Namde, P. A., Makar, S. C., Jadhav, S. V., & Wangikar, S. S. (2020). Fabrication of microchannels having different obstacles using photo chemical machining process *Novyi MIR Research Journal*, 5(6), 27–32.

Optimization of Finite Element Analysis and Natural Frequency for Engine Bracket



Abhinav Shelar and Atul Aradhya

Abstract The automotive engine mounting systems are crucial because of the many facets of a vehicle's performance. Without using a vehicle sample, the construction of the engine mounting system should be quickly and precisely examined early in the improvement process authorization. As a basis for maintaining support for this same engine bracket engine. Engine bracket fatigue and vibration have long been issues, particularly if the ensuing Extreme and unnecessary loads and vibration could lead to structural failure. To fully comprehend the structural and dynamic aspects of the investigations, additional there must be research. It will be discovered what the natural frequency of a typical automobile engine bracket. In this paper's Finite Element (FE) study.

Keywords FEA · Engine mounting bracket · Modal FEA

1 Introduction

One of a car's or any road vehicle's most crucial parts is the engine. Brackets support the engine in high-performance sports cars. It is necessary for enhancing the operating and comfortable conditions in a car. For a long time, improving engine bracket systems have attracted a lot of attention. For a car, a suitable engine bracket must be developed. The engine bracket was therefore created as a framework to support engines. One of the long-term problems of engine mounting vibrations and fatigue is the risk of structural collapse if the resulting vibrations and stresses are significant and excessive. Long-term exposure to whole-body vibration can wear you out and, in rare instances, have negative health effects. An automobile engine's vibration-relevant excitations typically include the following: combustion power, main bearing reaction forces, such as bulk forces, damper operation, and crankshaft whirling, piston side forces, including secondary motion, crankshaft bearing load applied, which

A. Shelar (✉) · A. Aradhya

Department of Mechanical Engineering, SKN Sinhgad College of Engineering, Korti, Pandharpur, Maharashtra, India

e-mail: shelarabhi1777@gmail.com

include bulk forces, open and closed impacts, and bearing affects, valve closing and opening affects, and valve train is doing by chain/belt. To better regulate vibration, it is possible to determine the engine bracket system's natural frequency, which should be substantially lower than the frequency range where excitation manifests the majority of the vibratory energy. Basic non-linear vibration theory reveals this. The construction of an engine bracket in this case may allow the engine to dampen vibration. A vehicle engine mounting mechanism should meet the requirements for fundamental engine displacement, rigid-body dynamic characteristics, and vibration isolation. To suit mounting system requirements, a mounting bracket was designed and developed using Ansys software. The creation using mounting systems is constrained due to NVH and drivability difficulties, which saves design resources. A key aspect of cars that contributes to overall consumer enjoyment is NVH. The engine mount plays a crucial role in determining the vibration characteristics of a vehicle once it has been installed. The engine is frequently attached to the primary sub frame. Early in the engine design process, the mounting system can be optimised using computer-aided engineering (CAE) methods. The acquisition of expensive prototypes is not necessary for the analysis of CAE data. The outcomes can be utilised to design a strategy for the vehicle mounting system as well as to optimise mount sites and rates. Because the engine vibration is isolated from the car's body, the driver is less sensitive to road inputs.

2 A Summary of Some Research

Zhang et al. [1] examined the vibrational and acoustical conduct of an IC engine made up of a number of parts and subjected to loads of various magnitudes and speeds. The introduction of CAE tools will significantly save the time needed to design engines while also guaranteeing a marked improvement in product quality. The relative benefits of modification and extensive structural/acoustic engine optimization are highlighted., as well as the creation of original low-noise designs, CAE capabilities in engine dynamic and acoustic behavior simulation are highlighted. Modern CAE technologies enable engine analysis, evaluation, and acoustic optimization.

Anton et al. [2] Investigations were made on the relationships between NVH test results and calculations, engine FE model updates, and vibration levels at body contact sites. This method's primary objective is to use an updated FE model to ascertain the absolute values of the vibration level (low and medium frequency range) on the interface points. We were able to comprehend the true vibratory behavior and acquire a new FE model that is more closely matched to reality thanks to the theoretical and practical research used in this study. Included are the results of the last update, test-calculation correlation and operating analysis.

Subbiah et al. [3] Durability testing on automobiles in the end-user enviro was established to reduce breakdowns as well as rework costs in the hands of the final user. Failure study of the three-wheeler muffler mounting brackets revealed during

the adsorption tests. After an aggregate of 10,000 km, all of the cars developed fractures at the weld site linking the engine chassis and brackets. The fishbone diagram is used to pinpoint a variety of potential failure causes. With the aid of the finite element method, additional research on the design was carried out. A FEM model of the engine and exhaust system was produced for the engine mounting assembly. The results show that the weld region has a high level of stress and strain and strain energy. The bracket was designed to act as cantilever beam including one's engine cradle welding. While the aforesaid failure was eliminated, the failure mode was shifted to the mountain region. Choia et al. [4] By expanding the 160,000 km, we examined the obtained acceleration signals and studied virtual damage and frequencies. The acceleration vibration test involves a six-DOF acceleration test in the time—frequency domain using MAST and a single-DOF acceleration test using single axis equipment in the frequency domain. The obtained PG acceleration signals, which correspond to the simulated damage of 160,000 km, are used for the six-DOF accelerated test. For the single-DOF test, the axis reflecting the maximum fictitious damages value from the real road test is used. After determining the frequencies, the testing is conducted out by enclosing and boosting real-world highway PSD lines. There are no failures in the six-DOF acceleration testing. However, the contact between both the battery as well as the brackets had been destroyed in single-DOF tests. This is why, when studying real roads, the selected test axis has to have the greatest virtual damage values. In terms of safety, the results are good; nevertheless, further study will enhance optimization. Loh et al. [5] have underlined the significance of various FE investigations, like frequency analysis, which evaluates how buildings react to harmonics stimulation over a variety of frequencies. The time frequency responses can be used to estimate the resonant frequency. The dynamic & static vibration studies also reveal the high structural stressful conditions during dynamic and static loading situations. The intrinsic yield strength of the material is compared to the projected maximum stresses. Elastic limit is not covered in the work since only the elastic attribute is defined. It has also been investigated how to use FE model and a fatigue damage criterion approach to anticipate fatigue failure of a present P- TAC motor bracket. The use of applied load curves using applied load and alternative stress has been used to anticipate the potential of fatigue occurrence in recognized fatigue damage criterion, including such Yield and also Fracture Criteria. For avoiding structural fatigue, this technique is regarded as a conservative prediction approach, and it is most suitable and secure for certain design applications. Different modifications to the motor brackets shape have been investigated in an effort to strengthen it, and the findings of each inquiry are compared. In order to examine the effects, they have on the total static and dynamic behaviour, the rib supports, edge radius, and thicknesses have all been modified or added. According to the investigations, raising edge radius and adding rib-supports can both greatly enhance structural performance. Irving et al. [6] the fatigue performance of two distinct bracket connectors for high-speed ocean vessels was examined. The weld quality inside the curved or nesting insert has a considerable influence on fatigue behavior, as shown by constant amplitude, cyclic testing. Under severe circumstances, a reduction in fatigue performance brought on by a subpar weld may offset the benefits of a more ideal bracket design. When a

good mark butt weld with depth of penetration is used, the nesting bracket improves the softer toe brackets in term of fatigue performance. Firat et al. [7] The suggested approach, which uses clear and specific and implicit-iterative FE approaches to analyses stamping processes mathematically, was investigated. Factor analysis is used to analyses the effects of a numerical model parameters, as well as the response surfaces produced by multi-linear regression are used to explain these effects. When the recommended approach is used, the forming process produces a spring back-critical channel shape. The implications of the modeling variables are established in order to offer a statistically calibrating simulation model by examining the impacts of the punching velocity and element size. Several response surfaces were created after taking into account the susceptibility of the spring back deflections to contact interfaces friction and blank holding force. Experimental data comparisons demonstrated the suitability of the recommended method for spring back predictions. The recommended method was used to stamp the high-strength steel engine suspension bracket.

3 Types of Brackets

3.1 Vehicle Engine Mounting Bracket

The bracket that maintains the engine from the rear side of the vehicle is the engine mounting bracket, as seen in Fig. 1. It has a stamped steel construction. To carry the weight and absorbs vibrations, it is linked to the engine with its bigger face and the vehicle frame with its smaller end. Because of the decreased vibrations rate and even lower engine knocking rate, it has a longer operating life. The engine mounting brackets is subject to breakdown, though, if the engine is old and the vehicle construction has other problems. The main reason for the engine mounting brackets to fail is cracking, which starts at a point where there is a lot of stress and spreads throughout the bracket's structure. Vehicle movement on an uneven road surface and engine vibrations are the main factors contributing to the stresses in the bracket's structural integrity [8].

Fig. 1 Engine mounting bracket of car



3.2 *Continental Engine Attachment Bracket for Aircraft Engines*

In this type of vehicle engine-supporting structure, a cut-out portion is created either have a bolt insertion-hole of an aided bracket or even a bolt insertion-hole of a holding bracket in order to allow the engine to be altered on an axis extension inside the perpendicular direction of a vehicle throughout proportion to affect loads. When two cars collide, the engine receives impact loads. The other section of the base is linked to the engine; it carries the bulk of the load, while the base is coupled to the structure of the aircraft. For efficiency and lightness, it is made in aluminum. In order to completely rule out the chance of serious mishaps, it is checked often. It must also tolerate sizable vibrations caused by the aviation engine, which runs at high velocities and produces a large amount of power. These limitations make it difficult to create the brackets for these kinds of engines. The continent engine mounting bracket for an aero plane engine is shown in Fig. 2 [8].

4 Bracket Installation Site

A support element that is intended to be secured to a portion of the car frame makes up the engine assembly. a support member, two engine mounting brackets mounted on the isolators and connected to an engine component, two polymeric engine vibration dampeners placed in relationship to each other on the frame, and two polymeric engine isolators. The engine mounting brackets are kept apart from the support member by the engine isolators, which reduce engine vibration and regulate engine movement in relation to the vehicle. An important noise conduit is typically the engine mounting system. Regarding sound transmission, durability, and crashworthiness, the construction of the vehicle at the mounting position is crucial. The top bracket is fastened to the gearbox using two horizontal bolts. The vertical space is constrained for both the plastic mount and the bracket. It is impossible to allow a rubber to be as smooth as necessary for the best vibration isolation with a limited rubber volume. Thus, the bracket needs to be as rigid as possible. Its stiffest, heaviest, and cheapest bracket design is designed using computer-aided engineering,

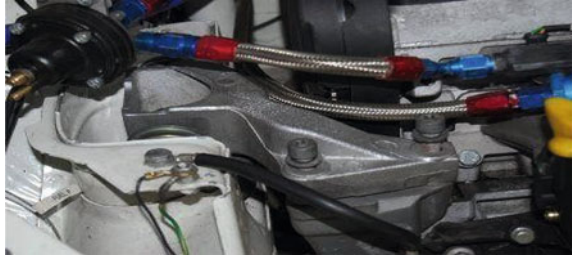
Fig. 2 Engine bracket



Fig. 3 Position of mounting bracket



Fig. 4 Mounting engine bracket



enabling a quicker development cycle. Engine mounting systems' primary duties include supporting and positioning the engine inside the vehicle, isolating vibrations caused by the engine, and controlling movement and vibration from outside the vehicle. Engine mount brackets must support the engine; meet first of mode resonance and stiffness criteria, and exhibit essential product qualities such as resistance to corrosion, stress, and temperature. A support component provided by the engine is held in the supporting bracket. The holding bracket is fastened to the body of the car. In this type of vehicle engine-supporting structure, a cut-out portion is created either have a bolt insertion-hole of an aided bracket or even a bolt insertion-hole of a holding bracket in order to allow the engine to be altered on an axis extension inside the perpendicular direction of a vehicle throughout proportion to affect loads. When two cars collide, the engine receives impact loads [8] (Figs. 3 and 4).

When a bracket is assembled, the bushes are brought in to contact with the cut-out parts made at the supportive arm sections of the bracket. The fixing bolt is then used to secure the bush in place between the components of the supporting arm [8].

4.1 Analytical Method to Figure Out Non-linear Vibration

Think about the conservation system that the equation describes.

$$(U + f(x)) = 0 \tag{1}$$

Acceleration is,

$$(U) = ((V dv)/dx) \tag{2}$$

Put Eq. 2 put Eq. 1 We get,

$$(V dv) = (-f(x)dx)$$

where,

$$(U = V) \text{ If } x = X$$

when $V = 0$,

The Integration is,

$$\begin{aligned} |V| &= |dx/dt| \\ |V| &= (\sqrt{x} \int Xf(\lambda)d\lambda) \end{aligned} \tag{3}$$

The 2nd integral yields are,

$$(t - t_0) = ((0 \int x(d/x \int Xf(\lambda)d\lambda))) \tag{4}$$

where, t_0 corresponds to $x = 0$, Eq. 4 describes the relationship between displacement and time is expressed in terms of displacement and its inverse.

When a motion has a periodicity of period T , A motion from $x = 0$ ($t = t_0$) to $x = X$ ($v = 0$) corresponds to a quarter period in time. Due to this,

$$T = (4x(dU/x \int Xf(\lambda)d\lambda)) \tag{5}$$

As a result, a period is now a function of amplitude is X .

4.2 FEM Model and Results

An important engineering analytical tool for nonlinear settings is FEA. As a geometric input, FEA needs a finite element mesh. A solid model can be used to construct a detail part of model in a 3-D CAD system. The detail solid model must be simplified using an appropriate idealization technique, such as changing the material and shrinking the model's mesh size in FE, to cut down on the needless calculation time. Grey C.I. aluminium alloy is used to make the engine mounting brackets. A specific sort of meshing method is needed for thin bodies. Using components

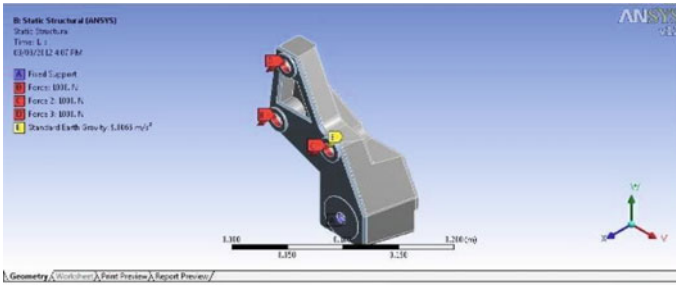


Fig. 5 FE model of mounted engine bracket

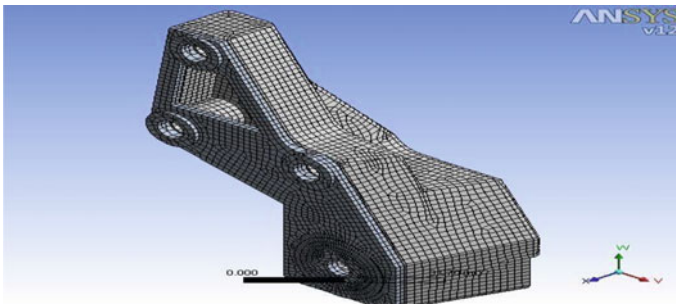


Fig. 6 FE mesh model of mounting engine

with hexadecimal dominance and triangles, the mid-surface of the engine mounting bracket was extracted and meshes [3].

The FEM model of the current design is shown in Fig. 5. Currently, the plan has four holes. Three holes have a force of 1000 N, and one hole is fixed. This force is created via thrust. Self-weight is another option (g). For FE Analysis, nonlinear materials are utilised. The six degrees of freedom in the FEM Model include rotations about the nodal x, y, and z-axes as well as translations in the nodal x, y, and z directions (Figs. 6, 7, 8 and 9).

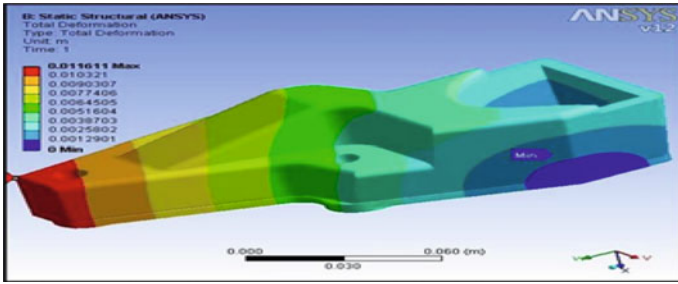


Fig. 7 Engine bracket with a 3 mm mesh size that has undergone total deformation

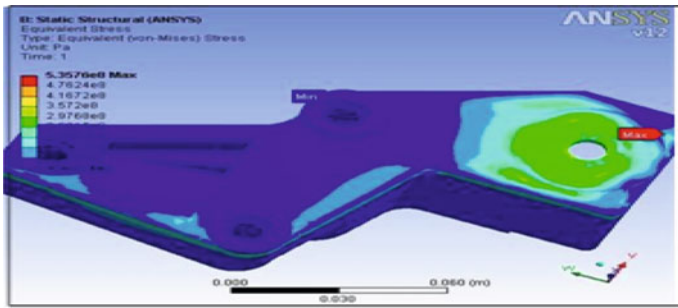


Fig. 8 Equivalent (von-misses) stresses of an engine bracket mounted on an 8 mm mesh of aluminum

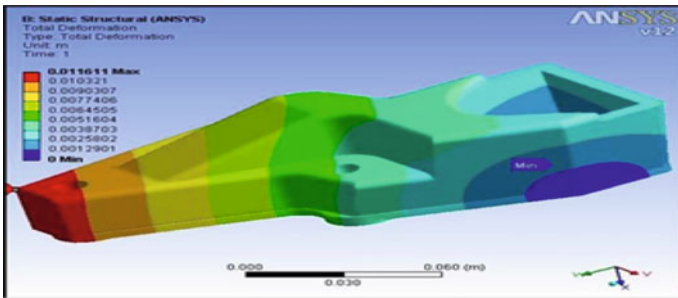


Fig. 9 Natural frequency of an engine bracket mounted on an 8 mm mesh size of aluminum

5 Results

S. No.	Materials	Maximum deformation (mm)	Maximum stress (MPa)	Natural frequency (Hz)
01	Aluminum alloy	1.38	228.5	151.44
02	Gray C.I	1.6854	227.15	146.41

6 Conclusion

In engine parts, vibration is particularly noticeable in the auxiliary bracket. The findings suggest that bracket low natural frequencies will serve as a vibrating barrier since grey cast iron is fragile. With regard to analysis, Al alloy has a higher natural frequency value than Grey Cast Iron, indicating that it is a better choice. However, one FEA shortcoming is that Modal FEA does not account for the influence of Damping. In use, Al alloy dampens more effectively than Grey Cast Iron alloy.

References

1. Zhang, J., & Jun, H. (2006). CAE process to simulate and optimise engine noise and vibration. *Mechanical Systems and Signal Processing*, 20, 1400–1409.
2. Anton, G.-P., Paval, M., & Sorel, F. (2011). Application on an updated finite element model of an engine in the automotive industry. In *SISOM 2011 and session of the commission of acoustics*, Bucharest 25–26 May.
3. Subbiah, S., & Singh, O. P. (2011). Effect of muffler mounting bracket designs on durability. *Engineering Failure Analysis*, 18, 1094–1107.
4. Choia, Y., Jungb, D., & Hamc, K. (2011). A study on the accelerated vibration endurance tests for battery fixing bracket in electrically driven vehicles. *Procedia Engineering*, 10, 851–856.
5. Loh, S. K., Chin, W. M., & Faris, W. F. (2009). Fatigue analysis of package terminal air conditioner motor bracket under dynamic loading. *Materials and Design*, 30, 3206–3216.
6. Irving, S., Ferguson-Smith, F., Hu, X. Z., & Liu, Y. (2005). Comparative fatigue assessment of soft toe and nested bracket welded aluminium structures. *Engineering Failure Analysis*, 12, 679–690.
7. Mehmet, F., Mete, O. H., Kocabicak, U., & Ozsoy, M. (2010). Stamping process design using FEA in conjunction with orthogonal regression. *Finite Elements in Analysis and Design*, 46, 992–1000.
8. Gaikwad, M. M. Bracket Document 112978. Coventry Engineers, UK.

Multifunctional Solar Operated Agricultural Machine



Vikram R. Chavan, Chetan C. Jadhav, Digambar T. Kashid,
Avinash A. Mote, and Manoj A. Deshmukh

Abstract India's population is largely dependent on agriculture and related industries. Approximately 70% of India's rural population is dependent on the agricultural sector. Fewer than two hectares of land are owned by 82% of farmers. Small landowners do not adopt modern agricultural techniques or equipment because it is too expensive, cumbersome, and difficult to obtain. The price of agricultural inputs is rising daily. Fertilizer, pesticides, insecticides, and labour costs are examples of agricultural inputs. We have addressed the problems in the farm and provided solution for listed problems in this paper. Seed sowing is done manually using traditional methods. After seeding, water should be sprayed over the seeds, however traditional methods call for a lot of water. In small farms, grass cutting is always done by laborers. Electricity is a problem for the farmer's different farm operations. The cultivator, crop cutting, seed sowing, and water or pesticides sprinkling are the four basic tasks performed by the multipurpose farming equipment. The machine's speed was 0.8 M/min, the rate of seed sowing was 50 g/min, the hopper's capacity was 1 kg, the water flow rate was 6 l/h, and as a result, the grass cutter spins at a speed of 1300 RPM, and the depth of the farm cultivator is 5 mm.

Keywords Solar operated · Cultivation · Seed sowing · Grass cutting · Pesticides sprinkling

V. R. Chavan (✉) · C. C. Jadhav · D. T. Kashid · A. A. Mote
Department of Mechanical Engineering, SVERI's College of Engineering, Pandharpur,
MH 413304, India
e-mail: vrchavan@coe.sveri.ac.in

M. A. Deshmukh
Department of Electronics and Telecommunication Engineering, SVERI's College of
Engineering, Pandharpur, MH 413304, India

1 Introduction

The demand for agricultural production per hectare is rising along with India's population, which calls for effective, high-capacity machinery. Therefore, mechanization in the agriculture sector is crucial to the Indian economy. Kshisagar and others [1] The main goal of sowing operations is to arrange the seed and fertilizer in rows at the correct depth and seed-to-seed spacing, cover the seeds with soil, and apply proper compaction over the seed. Modern farming equipment for seed planting is bulky and more expensive, according to Kannan et al. [2]. To avoid this, they created a multipurpose sowing machine with a hopper, seed distributor, ground wheel, power transmission system, and tiller. It was made using PRO-E programme. Mechanization in agriculture is necessary, and Mada et al. [3] proposed multifunctional single axle vehicle for pre and post harvesting. This has served as the foundation for our study and ongoing development of our multipurpose agricultural vehicle. The performance aspect of a power tiller is highlighted by Adamu [4]. Among them, the most popular demand was for a light-weight power tiller. These factors, together with fuel efficiency and field capacity, are also discussed. When creating a sustainable, multipurpose agricultural vehicle, we take these factors into account. According to Tewari [5], a case study on farm mechanization in west Bengal, which is a part of India, provides a clear position about availability and advancement in India. Compared to our present steps, this made sure we were taking the appropriate ones. Vipul et al. [6]'s study concentrated on methods for fertilizing plants, watering plants, and employing pumps that were powered by solar energy. Additionally, a basic explanation of the chassis frame design is made. Anvesh et al. [7] described how to operate a cultivator as a multipurpose device and indicated many attachments that could be swapped and used for various farming tasks. Sharath et al. [8] discussed using a traditional combustion engine and rubber tyre, which had some issues with getting stuck in the ground or dirt and also wasn't powered by the sun. According to Kumar [9], a brand-new kind of multipurpose mechanism has been created that differs from previous machines and uses an unconventional energy source that is entirely controlled by humans. Such systems are crucial in Asian nations as a result of the twelve to fourteen-hour load shedding that occurs in rural India and practically all other Asian nations due to electricity and power shortages.

Therefore, it is necessary to create locally manufactured, multifunctional agricultural equipment. To attain the best yields, Purosothaman et al. [10] advocate varying seed to seed spacing and depths for different crops and agro climatic situations. From this, we can infer that mechanical parameters, such as regularity of seed placement and dispersion along rows, have an impact on seed germination. Since the turn of the century, agriculture has steadily adapted mechanization. Farm machinery has seen a number of advancements. Both expensive and inexpensive machinery is offered. It is also evident how different multifunctional, practical tools are approached. Machines that are inexpensive and simple to operate have been developed.

2 Design Consideration

A proposed machine may execute multiple tasks at a low cost when compared to other agricultural machinery. For this idea, expertise is not required. The machine's mechanism should be fairly straightforward. This idea is intended for small-scale farming and gardening. The design of a solar-powered multipurpose agricultural machine is based on three key considerations: (1) the ease of manufacturing component parts; (2) the operator's safety; and (3) the machine's operation should be straightforward for small-scale or rural farmers.

Dimensions: Total Height—295 mm, Total Breadth—380 mm, Total Length—820 mm Ground Clearance—85 mm, Battery—80 × 75 × 40 mm, Wheel—170 mm, Water tank—180 × 120 × 80 mm, Hopper—200 × 200 × 200 mm, Cultivator—85 × 220 × 280 mm.

Material used- Frame—Gray Cast Iron, Gray Cast iron is a class of iron-carbon alloys with content C-3.04%, S-0.11%, P0.068%, SI-2.58%, Mn-0.42%, Cu-0.05%, Cr-0.07, Ni-0.02%, Mo-0.005%, Wheel—Gray Cast Iron ●Cultivator—Gray Cast Iron, Water tank—polycarbonate, Hopper—Plywood, Cutter—Mild Steel (AISI 1010) Mild steel contains carbon percentage upto 0.16–0.18%, Water PipeTransparent Pipe.

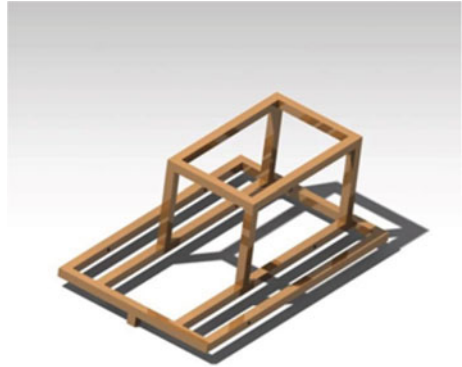
Solar & Battery Calculations—One solar panel is of 6v which generates 3amp currant Total current generated in parallel connection = $3 \times 6 = 18$ amp Which is used to charge battery Time taken by 12 V 16-A battery to full charge is 3.5 h. Battery Calculations Running rate of motor = 3.4 A Battery capacity = 16 Ah Battery life (at full motor output) = 2.2 h. So, the minimum battery life is 2.2 h.

The base frame, which is propelled by the DC motor, has four wheels attached to it. A cultivator that is powered by a DC motor is mounted at one end of the frame. The base frame has a seed sowing device attached to it. Crop cutter is fixed on the opposite end, and a water pump sprayer is fixed on the opposite side to spray water. The machine's top will be covered with a solar panel that will be used to charge the batteries. The solar panel and battery can thus use the sun's energy to its fullest potential. The system needs a 12-V battery to run the entire machine. The vehicle's functionality is managed using toggle switches.

3 Modeling

CATIA V15 Software is used to model parts of Multifunctional Solar Operated Machine. The main chassis frame is made of cast iron; all components of machine are placed on chassis frame. The wheels are also made of cast iron and the diameter of wheel is 170 mm as you can see they have small plates placed at outer side of wheels, there are total 8 small plates on one wheel which are placed at 45° to each

Fig. 1 CATIA model of chassis frame

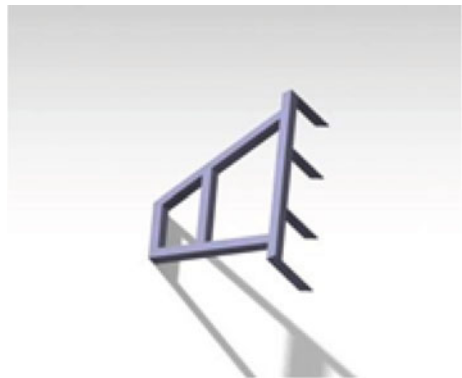


other. A cultivator is also made of cast iron and it is attached to the front side of the main body. Figure 4 shows the complete structural assembly of Chassis, wheels, cultivator. In CATIA Software under assembly section we have assembled different parts of the machine (Figs. 1, 2 and 3).

Fig. 2 CATIA model wheel



Fig. 3 CATIA model of cultivator



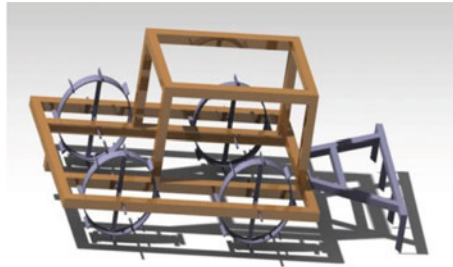


Fig. 4 Isometric view of machine

4 Construction Details

Multipurpose agricultural machine consists of the following components Figs. 5, 6, 7, 8, 9, 10, 11, 12, 13, 14, 15, 16, 17 and 18 as mentioned: Chassis frame, DC motors 12V, transparent pipe, cultivator, Hopper, Switch and controller, Mini-Submersible Water Pump, 2 V Batteries, water tank, Cutter, Wheels, Solar panels.

The components are mounted on a framework that makes up the chassis frame. The underside of a machine is called the chassis frame, and it is made up of the frame (on which everything is mounted). As seen in Fig. 5, the primary chassis structure is built of hollow cast iron bars. One of a machine's most important structural components is its chassis. It is the component that supports the machine's body on both sides. The chassis frame is where components like the wheels, motor, hopper, spraying systems, etc. are fixed. A 125 g DC motor has a 6 mm shaft diameter and an internal hole. similar-sized motors with a range of rpm torque of 0.5 kg-cm Load current

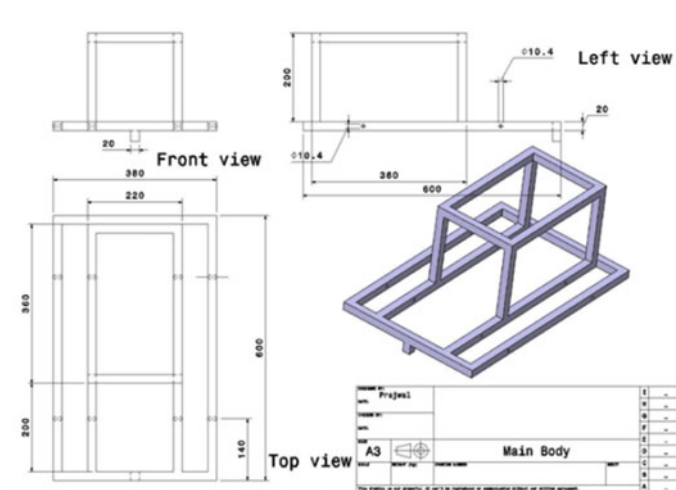


Fig. 5 Chassis frame in CATIA V15

Fig. 6 DC motor



Fig. 7 Transparent pipe

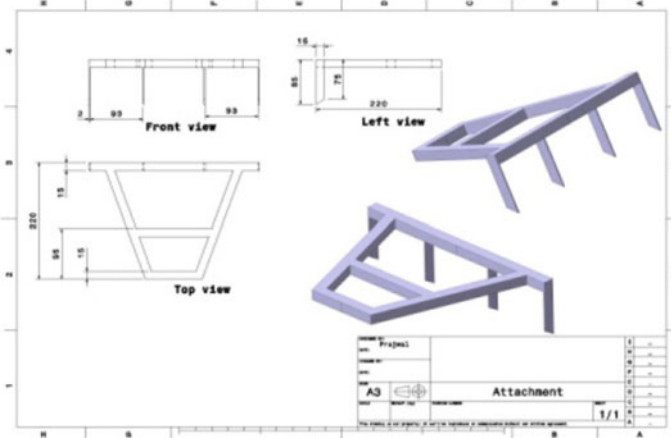


Fig. 8 Cultivator in CATIA V15

is 300 mA, with a maximum no-load current of 60 mA (Max). A transparent pipe may only continue to be transparent if it is both internally and outwardly clean. The former can be more challenging when a plastic pipe system is involved, but the latter can be easily controlled by washing off dust and debris.

Fig. 9 Top view of hopper



Fig. 10 Side view of hopper



Fig. 11 Toggle switches



Fig. 12 Control switches

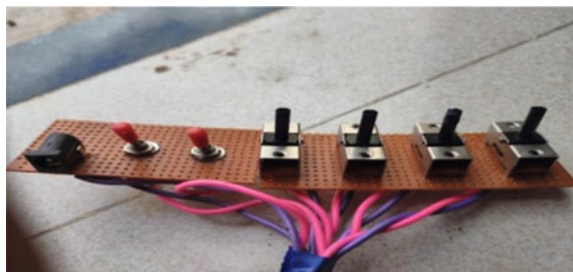


Fig. 13 Water pump**Fig. 14** 12 V battery**Fig. 15** Water tank

The front side of the main body is joined to a cultivator, which is likewise composed of cast iron. A piece of agricultural machinery used for secondary tillage is a cultivator. One meaning of the gardening tool is one that requires less physical effort than a manual instrument like a spade to mix and aerate soil, eliminate weeds, and generally provide the ideal seedbed for many plants. As they are dragged through

Fig. 16 Rotary cutter



Fig. 17 Wheels in CATIA V15

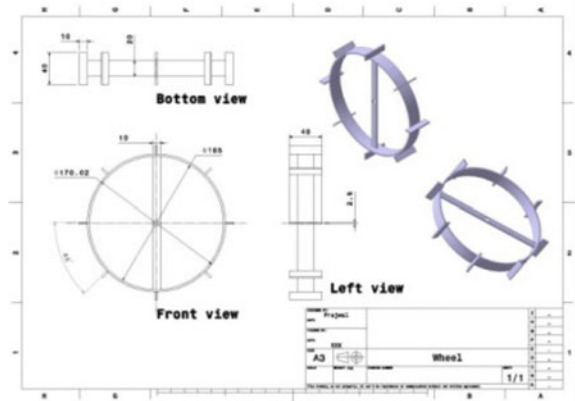
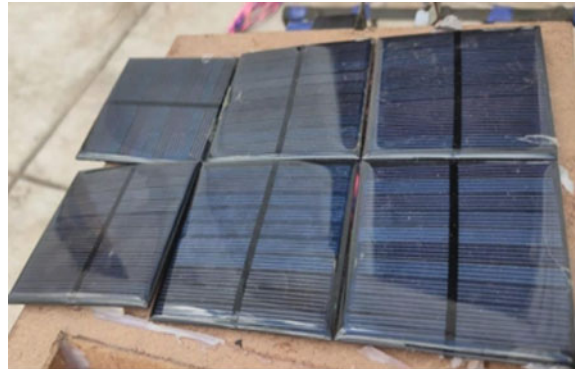


Fig. 18 Solar panels



the ground linearly, frames with teeth—also known as shanks—pierce the ground. In order to run, a DC motor is used.

In this solar operating multifunctional agricultural machine, hopper is used for seed sowing. Hopper is also made up of Medium-density fiberboard. Hopper maintains a uniform and continuous flow of seeds into the agricultural land through the holes at bottom of the hopper. It also has an open and close mechanism to do seed sowing whenever it is required. We can also change the rate of seed sowing by changing the bottom side of the hopper.

The toggle switch simulates a real switch, such as a light switch, that enables users to turn items on or off. Use toggle switch controls to provide users a choice between two mutually exclusive alternatives (like on/off), with the choice having an immediate impact. The Toggle Switch class is used to create toggle switch controls. The control panel has six toggle switches, the function of first switch is to control the movement of front side wheels forward and backward motion of wheels with the help of DC motors. The function of second switch is to control the motion of backside wheels. The function of third switch is to open and close the hopper for seed sowing. The function of fourth switch is to control the movement of cultivator up and down. The function of fifth switch is to supply water with the help of Mini Submersible Water Pump which is placed inside the tank. The function of sixth switch is to turn on and turn off the cutter. In addition to this there is one connector with help of this we run the system directly using AC supply. A 6 V Mini Submersible Water Pump is of submersible type. So, it can be put in water, and it will throw the water from the nozzle. It operates on 2.5–6 V DC. It has a connector for output nozzle. This pump sucks the water in from the front side, and throws the water out from the nozzle. And can be used with any other liquid. A 12-V battery is a rechargeable battery that has grown in popularity because of its many different uses. A battery pack supplies power by boosting the voltage of multiple batteries. A 12-V battery is split into six cells, each with an open-circuit voltage of approximately 2 V. As a result, this totals to about twelve volts. Connecting two batteries in series will increase their output voltage. But, batteries in series mean increased load on each cell, which is not what we want. Instead, what you should do is to parallel connect the cells. Therefore, this will decrease the load on each cell and increase your Amp-hour capacity simultaneously. Battery life calculation Running rate of motor = 3.4, A Battery capacity = 14 Ah, Battery life (at full motor output) = 2.2 h. So, the minimum battery life is 2.2 h.

The water tank of 1 L capacity is placed at centre of the machine, in which mini-submersible water pump is placed to supply water from tank to sprayer throw pipe. In order to aid control overgrowth of properties and pastures that have been swamped with brush or tall weeds, a rotary cutter is attached on the machine's back side. These tools are frequently mistaken for grooming mowers. The distinction between the two must be made clear. Rotary cutters can be adjusted to cut through tough plant material that is up to roughly an inch thick. The rotary cutter will leave the ground-level material behind after cutting the rough material. A tool that quilts frequently use to cut cloth is a rotary cutter. The rotating blade is attached to a handle, giving the tool its name. Rotary cutter blades come in a variety of diameters, are extremely sharp, and can be sharpened again. Typically, smaller blades are used to cut narrow

curves and straight lines, while bigger blades are used to cut large curves and straight lines. A sharp (fresh) blade may cut through multiple layers of cloth at once, making it simpler to create patchwork pieces that are the same size and form. Specially designed wheels for the machine, as you can see they have small plates placed at outer side of wheels, there are total 8 small plates on one wheel which are placed at 45° to each other and these wheels are made of cast iron. It is made for run smoothly on uneven surfaces, muddy and rough terrains.

A collection of photovoltaic cells arranged in a framework for installation is known as a solar cell panel, solar electric panel, photo-voltaic (PV) module, or solar panel. Solar energy is harnessed by solar panels to provide direct current power. A system of PV panels is known as an array, and a collection of PV modules is known as a PV panel. Electrical equipment is powered by solar energy from photovoltaic arrays. Even though our two solar panels have different wattages but the same voltage, there is no issue because they can be wired in parallel. However, if the two solar panels have different voltages and wattages, it is not viable to connect them in parallel since the panel with the lowest voltage would act like a load and start absorbing current rather than creating it, which would have a negative impact on the system as a whole. Solar Calculation—One solar panel is of 6v which generates 3amp currant. Total current generated in parallel connection = $3 \times 6 = 18\text{amp}$ which is used to charge battery. Time taken by battery to full charge is 3.5 h.

5 Working

In this device, solar energy is absorbed by a solar panel and transformed into electrical energy. A 12 V battery with a 7.5 Ah capacity stores the electrical energy, which is subsequently used to power a DC motor. The entire system then receives this power. The frames used for cultivating have teeth (sometimes referred to as shanks) that penetrate the soil as they are pulled over it. In order to run, a DC motor is used. Through the openings at the bottom of the hopper, the seed hopper maintains a consistent and continuous flow of seeds into the agricultural area. Additionally, it contains a system that allows seed sowing whenever necessary. Due to their own weight, seeds will fall from the holes and land on the ground. The primary goals of the sowing process are to place the seeds in rows at the required depth, maintain seed-to-seed spacing, cover the seeds with soil, and produce sufficient compaction over the seed. For each crop and for various agro-climatic conditions, the recommended row to row spacing, seed rate, seed to seed spacing, and depth of seed planting can change to get the best yields. Application of seed sowing commonly used for cereals, such as groundnuts, all varieties of seeds, oil seed crops, etc. An adjuster is used to move the soil toward the furrow the cutter made in order to reposition it over the seeds. Water is sprayed from the pipe for cultivation once the soil has been adjusted. For irrigation, a water tank-tap system is employed. In order to aid control overgrowth of properties and pastures that have been swamped with brush or tall weeds, a rotary cutter is attached on the machine's back side. Mild steel is cut and welded, solid

shafts are cut and welded, cutters are cut and welded, ball bearings are clamped, DC motors are bolted, slots are made for the motors to move laterally, batteries and solar panels are clamped, wiring is clamped, and seed sowing and adjusters are clamped, among other fabrication processes.

In Fig. 19, it is shown that how the power is transmitted through the whole system, as we can see first of all the power is generated by the solar panel then it is stored in battery then the power is supplied to remote and it is distributed to all components such as DC motor to provide motion and pump to supply water, to open and close the seed sowing mechanism in hopper and cultivator to lose the soil also it also supplies power to cutter to cut small crops. The seed filled in the hopper which is provided on the center part of the machine. As the machine is moved in the forward direction the cultivator at the front of the machine will dig the ground and create the channel for the seeds to be cultivated in the ground. It also has an open and close mechanism to do seed sowing whenever it is required. We can also change the rate of seed sowing by changing the bottom side of the hopper (Figs. 20 and 21).

The Cultivator is in the front of the machine. It is mostly used for the preparation of the land for seed sowing and making the land regular. And by doing this the plants/crop which is cultivated in the farms will come in regular pattern. This is usually to remove the bush and the waste plants coming in the farms which can destroy the crops and damage them. The cultivator is made of high carbon steel with low phosphorous & Sulphur cultivators because Cultivators are used for tilling and also for loosening the soil in the planting area of crops. The cultivator is also powered by the solar energy. On the prototype machine we have used the motor to drive the cultivator in upward and downward direction. In the actual model we can use the hydraulic or pneumatic type of setup depend on the type of soil as the black soil requires more energy as compared to red soil in the farms to cultivate the ground. As when we are moving forward the more force is induced on the cultivator so it should be strong to sustain more stress on it. And the operator should keep on the account that when he is operating the joystick, he should keep the cultivator in the

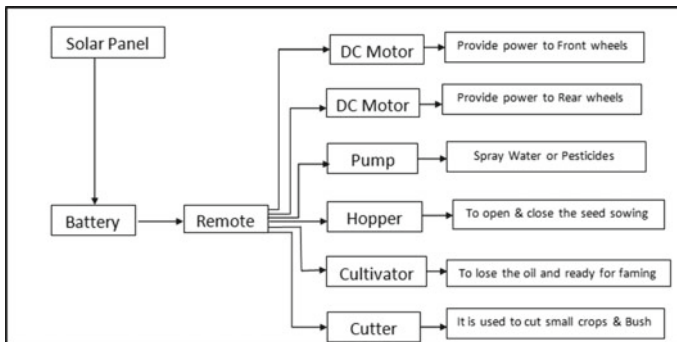


Fig. 19 Block diagram of power supply



Fig. 20 Cropcutting



Fig. 21 Fertilizer sprayer

right direction using the joystick. Otherwise, it will be raising upside because of the force on it (Fig. 22).

Crop Cutter is provided at the end of the machine. But the location of the machine changed according to the requirement it can be placed on the front and back of the machine in special condition it can be provided on the side also if required. This is provided for cutting of the crops and also the waste bush which grows along with the crops. In the traditional method more labor is required now less labor and machine work is introduced over here. The Cutter height can be adjusted according to the need of the cutting crops some crops need to be cut from the bottom and some need to be cut from the top this can be controlled from the height of the cutter.



Fig. 22 Actual pictures of multipurpose machine

And also, multi cutter can be used from increase the speed of the cutting and also using the cutter and the different location to cut the crops it can be used. The cutter can be place on or below the chassis of the machine. Depend on the type of crops we can decide with type of the cutter to be used. The prototype mode used a motor to drive the cutter which is also powered by the battery using the solar battery to charge it up.

Some of the crops need to be sprayed fertilizer neat the steam / at the time of sowing of the seed only at that time the pipes are provided near the cultivator only at the same time it can spray the fertilizers or supply the water and per the requirement. For the supplying of the water and fertilizers the pump is provided on the chassis and also the tank to hold it. This is also powered by the solar energy. This can be used at the time of cultivating the land and also after crops have grown to water them out. And also, by providing some of the nozzle and other set up we can spray the fertilizers also with are used in grapes, wheat and other crops.

6 Result and Discussion

After successful construction of the machine, we have taken a various trails and following results are observed: Speed of the machine is 0.8 M/min, Rate of seed sowing is 50 g/min, Capacity of the hopper (seed holding quantity) is 1 kg, Flow rate of water is 6 l/h, Speed of the grass cutter is 1300 RPM and Depth of cultivator for cultivation of frames is 5 mm.

7 Conclusion

Based on the machine's overall performance, it is observed that the proposed system will fulfill the needs of small-scale farmers who cannot afford to buy expensive agricultural machinery. The Multi-Purpose Agricultural machine is designed to carry out numerous agricultural tasks. In the proposed study the use of a solar panel, a centrifugal pump, a D.C. motor, and motion transmission mechanisms have been made. The various parts needed to fabricate the multifunctional agricultural machinery have been drafted using CATIA V-5 design software. This system is used for various agricultural operations such as seeding, watering, ploughing, and digging. Additionally, it can be utilised for material handling in local transit. For poor farmers, a multipurpose agricultural machine will lower external costs like fuel, electricity, etc. The equipment weighs between 8 and 10 kg, making rural transportation simple. The machinery can complete the tasks of four workers in a single day, which lowers the labour costs of farmers.

References

1. Hannure, A. O., Kshirsagar, S. P., Kodam, V. S., Patange, O. N., & Nakod, V. S. (2016). Literature review on auto matic seed feeder. *International Journal of Engineering Trend sand Technology (IJETT)*, 36(7), 333–336.
2. Kannan, A., Esakkiraja, K., & Thimmarayan, S. (2014). Design modifications in multipurpose sowing machine. *International Journal of Research in Aeronautical and Mechanical Engineering*, 2(1), 35–45.
3. Mada, D. A., & Mahai, S. (2015). The role of agricultural mechanization in the economic development for small scale farms in adamawa state. *The International Journal of Engineering And Science (IJES)*, 2(11), 91–96.
4. Adamu, F. A., Jahun, B. G., & Babangida, B. (2014). Performance evaluation of power tiller in Bauchi State Nigeria. *International Evaluation Sharing Platform*, 4, 2224–3208.
5. Tewari, V. K., Ashok, K. A., Kumar, S., & Nare, B. (2012). Farm mechanization status of West Bengal in India. *Basic Research Journal of Agricultural Science and Review*, 1(6), 139–146.
6. Saxena, V. (2018). Solar powered seed sowing machine. *International Journal of Applied Engineering Research*, 13(6), 259–262.
7. Anvesh, S., Sarfaraz, R., Akash, S., Taufiq, S., & Dilip, B. (2011). A research paper on multi-purpose agriculture cultivator. *International Journal of Scientific and Engineering Research*, 8(11).
8. Sharath, T. D., Sachin, R. K., & Dharmaveera, S. (2019). A review paper on multipurpose agriculture machine. *IJARIE*, 5(3).
9. Kumar, A., Kumar, A., Faridi, K., & Visen, A. (2018). Implementation and development of multi-purpose mechanical machine. *International Journal of Engineering Research & Technology (IJERT)*, 7(04).
10. Purushothaman, P. (2012). Development of working prototype for ragi harvesting and threshing operation. *International Journal of Scientific and Engineering Research*, 3(12).

NACA 4415 Aerofoil: Numerical Analysis for Performance in Drag and Lift



Digambar T. Kashid, Avinash K. Parkhe, Sachin M. Kale,
Sandeep S. Wangikar, Chetan C. Jadhav, and Hrushikesh N. Paricharak

Abstract The National Advisory Committee for Aerodynamics (NACA) 4415 aerofoil is the most widely used aerodynamic shape in wind turbine blade applications. In this study, a numerical analysis of NACA 4415 airfoil profile is done using ANSYS Software to investigate the performance of NACA 4415 airfoil profile in terms of drag and lift forces. Reynolds number (Re) and Angle of Attack (AOA) for the blade of a wind turbine are the performance parameters considered in this study. The different AOA values used in this analysis are 0° , 15° , 30° , 45° , and 60° . The Reynolds number (Re) values used are ranging from 10,000 to 200,000. The results are represented in terms of Drag coefficient (C_D), Lift coefficient (C_L), Drag force and Lift force. It is observed that drag and lift force increases with increase in Reynolds Number. Angle of attack is the most important parameter influencing the performance of the aerofoil shape. For 30° AOA the lift and drag is found to be maximum for all values of Reynolds numbers considered in this study. NACA 4415 gives maximum drag force of 209.2039 N and lift force of 777.25 N at 200,000 Reynolds Number for 30° Angle of Attack. A maximum percentage increment of 96.4 is observed in the drag force for Reynolds number value of 200,000 and 30° angle of attack. Similarly, in case of the lift force the maximum percentage increment observed is 70.2 for 50,000 Reynolds number and 30° AOA.

Keywords Airfoil · Angle of attack · NACA4415 · Reynolds number · Drag · Lift

D. T. Kashid (✉) · A. K. Parkhe · S. M. Kale · S. S. Wangikar · C. C. Jadhav
Department of Mechanical Engineering, SVERI's College of Engineering, Pandharpur,
Maharashtra, India
e-mail: dtkashid@coe.sveri.ac.in

H. N. Paricharak
Department of Mechanical Engineering, Dr. B. R. Ambedkar National Institute of Technology,
Jalandhar, Punjab, India

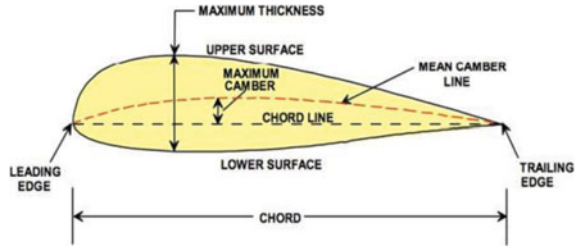
1 Introduction

The aerofoil shape of a blade of wind turbine is ultimately in charge for converting a kinetic energy into mechanical energy, and this is a reactionary part to develop a wind turbine. The ANSYS Fluent software is the most capable computational fluid dynamics (CFD) tool available, allowing you to optimize your product's performance further and quicker. NACA aerofoils are airplane wing aerofoil structures which were designed by NACA. The NACA 4415 aerofoil is the most widely used aerodynamic shape in wind turbine blade applications. However, for understanding influence of varying Reynolds numbers and the different angle of attack values on wind blade shapes, there are few analytical, numerical, or experimental researches available. Many experts have focused their efforts on the design of optimal blade geometry for the sake of produce the higher kinetic energy by using the wind.

Patil et al. [1] considered NACA 0012 Aerofoil for analysis of wind turbine blades using CFD for calculating lift and drag forces at different AOA and various Reynolds number. Rubel et al. [2] carried out numerical and experimental study of NACA 4415 and NACA 0015 to make a decision of their performance. For different values of the angle of attack, ranging from 50 to 200, drag and lift forces are estimated. Different studies presented works associated to CFD and experimental analyses employing airfoils such as NACA 0012, NACA 4412, NACA 2415, and others, suggesting that when the Reynolds number increases, both the lift force and the drag force increase [3–6]. Different aerofoil blades were used in experiments with varying blade pitch angles and varying wind speeds, and the power produced and wind turbine speed were calculated [7]. CFD was used to compare the coefficients of lift and drag at various angles of attack for constant air velocity for various airfoil sections [8]. Prediction of the aerodynamic study of upgraded NACA 4415 airfoil and comparison to that of NACA 4415 Standard is done [9]. The impact of surface groove characteristics on aerodynamic performance was investigated using parametric simulation [10]. Blades' airfoil and size effects of a miniature wind turbine were investigated. Various airfoils and rotor diameters are considered [11]. In order to comprehend the impact of rotational speed on the rudder and to establish its link with the Reynolds number, the NACA 0012 section analyzed the hydrodynamic features of a maritime rudder using CFD simulations [12]. Research was done on a wing with the NACA 4412 airfoil [13]. At various wind speeds and solidity ratios, the effectiveness of a Savonius types VAWT on a NACA 0020 aerofoil profile blade was assessed [14].

According to a review of the literature, the study of the forces of lift and drag on an aerofoil for quite low Reynolds numbers at AOA does not explode much further. As a result, the current work makes an attempt to investigate the both Drag and Lift forces on the blade of a windmill for different Reynolds number and different angles of attack. In this study, a numerical analysis of NACA 4415 aerofoil profile is done using ANSYS Software to investigate the performance of aerofoil profile in terms of drag and lift forces. Reynolds number (Re) and Angle of Attack (AOA) for the blade of a wind turbine are the performance parameters considered in this study. The different AOA values used in this analysis are 0°, 15°, 30°, 45°, and 60°. The

Fig. 1 Aerofoil terminology of wind turbine blade



Reynolds number (Re) values used are ranging from 10,000 to 200,000. Also, Lift coefficient (C_L) and Drag coefficient (C_D) are calculated regarding different Angle of Attacks and Reynolds Number values.

The terminology used for the designation of aerofoils used in wind turbine blades is as shown in Fig. 1 [6].

1.1 Geometry and Mesh Generation of NACA 4415 Aerofoil

The NACA 4415 aerofoil shape is the subject of the current research. The geometry of aerofoil NACA 4415 is drawn in ANSYS. According to NACA four-digit aerofoil nomenclatures, aerofoil dimensions are selected. The coordinates of NACA 4415 were imported and an aerofoil surface was generated in ANSYS Design Modular. The chord length of aerofoil used 100 mm for profile. A C-mesh domain was created around it for air enclosure with 1 m radius of semicircle and length of rectangle is also 1 m from trailing edge of the aerofoil. The aerofoil surface was subtracted from the enclosure. Figure 2 displays a 2-D model of an aerofoil that is submerged in fluid. The aerofoil is meshed using edge, face, and biasing in order to produce a fine mesh zone surrounding the aerofoil. Afterward, names were given to the outlet, inlet and aerofoil selections. The enclosure of an aerofoil mesh in a fluid domain is shown in Fig. 3.

2 Numerical Analysis of Aerofoil NACA 4415 Using ANSYS

In order to determine the impact of lift or drag on the wind turbine blade, the analysis of NACA 4415 using ANSYS software was performed for four angles of attack, namely 0° , 15° , 30° , 45° , and 60° at various Reynolds Numbers (Re) and fluid velocities. Table 1 indicates Drag and Lift force obtained by varying Reynolds Number (Re), Velocity and Angle of Attacks. Also, the numerical results obtained from ANSYS software are represented by the following figures.

Fig. 2 Geometric model

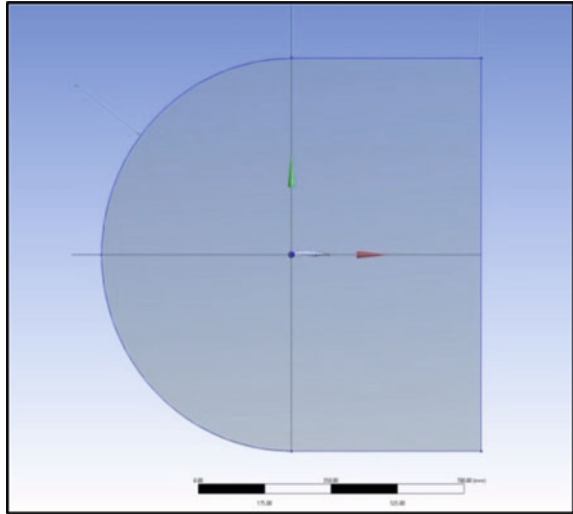
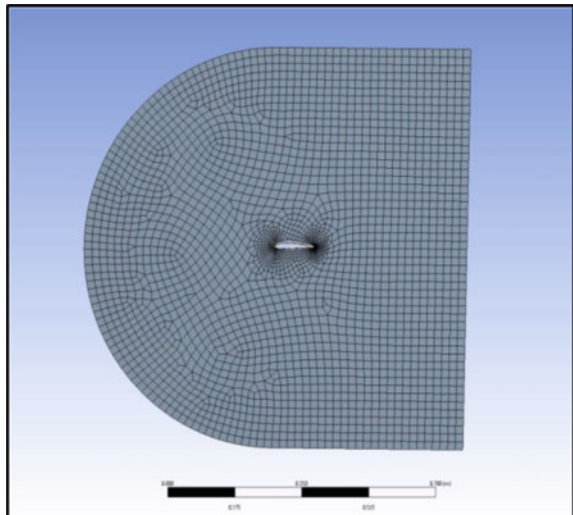


Fig. 3 Mesh generation



3 Result and Discussion

The analysis involves changing the Reynolds Number to simulate flow around an airfoil at different angles of attack (0, 15, 30, 45, and 60°).

Table 1 Drag and Lift force for various Reynolds number, velocities and angle of attack

S. No.	Reynolds number (Re)	Velocity (m/s)	Angles of attack in degree (°)	Drag force (N)	Lift force (N)
1	10,000	1.4770	0	0.1892	1.7477
			15	0.2714	1.4194
			30	0.4544	1.9552
			45	0.2367	1.4150
			60	0.5430	1.3563
2	50,000	7.3877	0	0.5750	14.4391
			15	4.1009	36.1056
			30	12.5322	48.5261
			45	8.2808	37.4073
			60	2.3359	35.1387
3	100,000	14.7755	0	2.0366	57.9351
			15	16.7303	145.3902
			30	32.3522	195.9259
			45	14.8984	94.2276
			60	10.3098	141.2990
4	150,000	22.1632	0	4.3082	130.7019
			15	38.0288	329.0228
			30	117.8332	437.9432
			45	61.0680	315.9920
			60	25.2634	327.6098
5	200,000	29.5510	0	7.3479	232.8
			15	68.0480	586.22
			30	209.2039	777.25
			45	110.8556	569.48
			60	41.8434	577.92

3.1 Contours for Pressure and Velocity Magnitudes

The sample of results obtained from ANSYS software for Reynolds Number 200,000 and velocity 29.5510 m/s are shown in the following figures (i.e. Figs. 4, 5, 6, 7, 8, 9, 10, 11, 12 and 13), pressure contours and velocity contours at various attack angles (0, 15, 30, 45, 60°) were obtained for NACA 4415 aerofoil, where CFD simulations are shown. The leading edge is where you can see the stagnation point, where each airfoil’s flow velocity is almost zero. As the airfoil’s upper surface experiences a rise in flow velocity, the lower surface of each airfoil experiences a full reversal in velocity. Also, we can observe that, Bernoulli’s principle states that the upper surface will have low pressure and the lower surface will have higher pressure. Therefore,

both the coefficient of lift and the coefficient of drag will rise, but the gain in lift will be greater, while the increase in drag will be less. The bottom surface of each aerofoil is under more pressure than the top surface. It is necessary to force each aerofoil into the entering flow stream from above.

Fig. 4 Pressure contour for 0° angle of attack

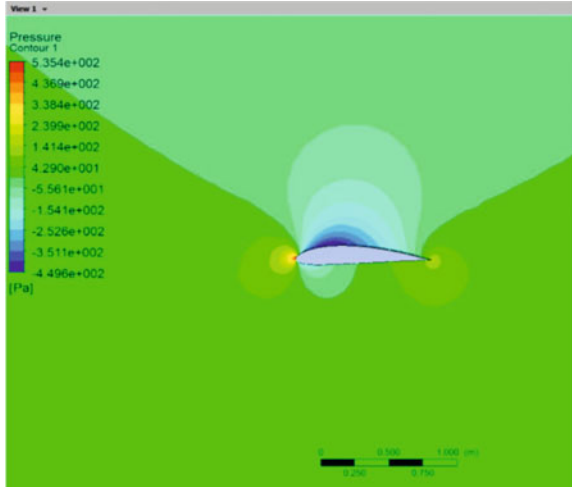


Fig. 5 Velocity contour for 0° angle of attack

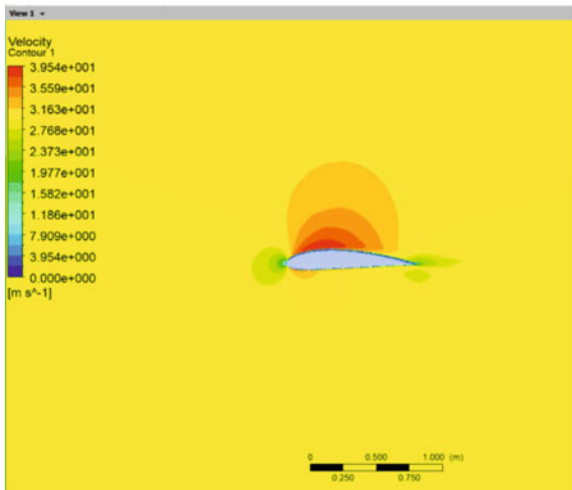


Fig. 6 Pressure contour for 15° angle of attack

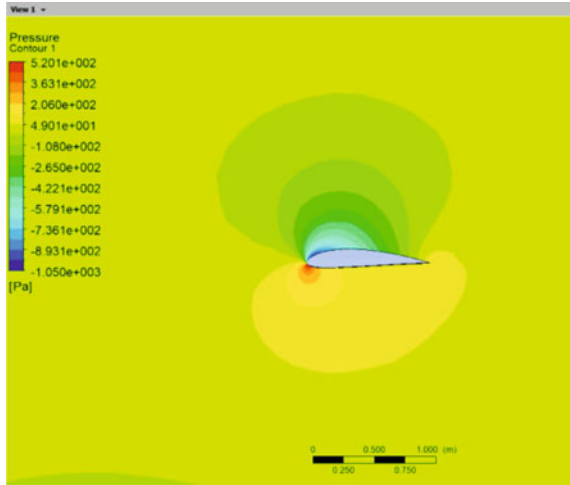
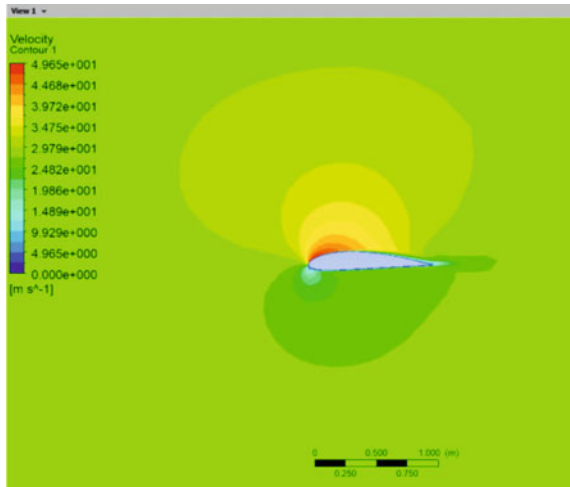


Fig. 7 Velocity contour for 15° angle of attack



3.2 Lift-and-Drag Curve

Different angles of attack are used to calculate the lift and drag curves for NACA 4415 to know the effect of different Reynolds Number (Re) and various Angles of Attack on Drag and Lift force is shown in Figs. 14, 15, 16 and 17. The lift coefficient and drag coefficient values show that C_L and C_D values rise as attack angles and Reynolds numbers increase. After looking at the C_L and C_D values, it has been observed that the optimum value of angle of attack is 30° for NACA 4415 aerofoil. NACA 4415 gives maximum drag force of 209.2039 N and lift force of 777.25 N at 200,000 Reynolds Number for 30° Angle of Attack.

Fig. 8 Pressure contour for 30° angle of attack

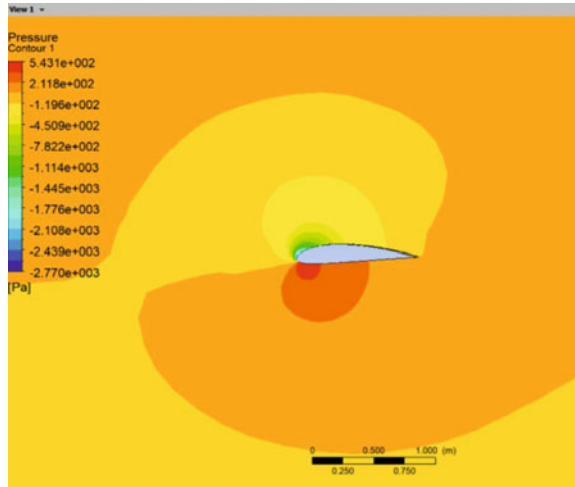
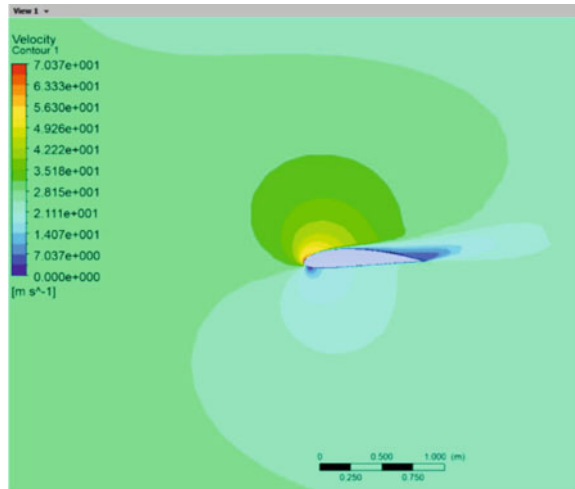


Fig. 9 Velocity contour for 30° angle of attack



A percentage Increment in Drag Force and lift force is shown in Tables 2 and 3. A maximum percentage increment of 96.4 is observed in the drag force for Reynolds number value of 200,000 and 30° angle of attack. Similarly, in case of the lift force the maximum percentage increment observed is 70.2 for 50,000 Reynolds number and 30° angle of attack.

Fig. 10 Pressure contour for 45° angle of attack

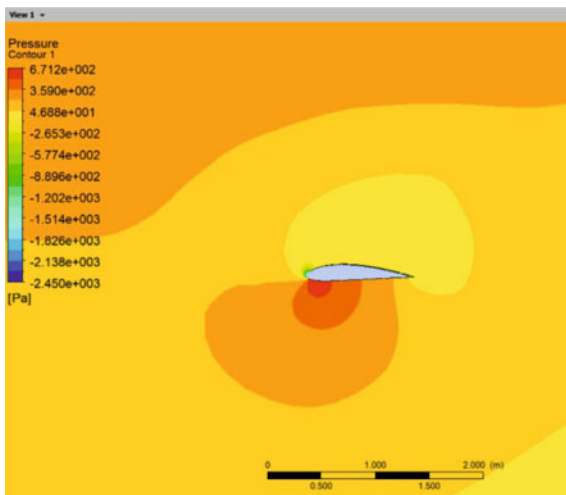
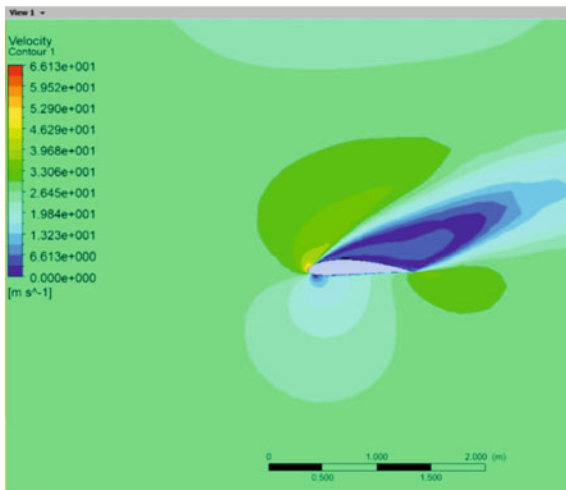


Fig. 11 Velocity contour for 45° angle of attack



4 Conclusions

The NACA 4415’s aerodynamic performance has been investigated at different attack angles (0°, 15°, 30°, 45°, 60°) and Reynolds numbers ranging from 10,000 to 200,000. The following are some key findings from the present study.

1. From the lift force and drag force values, it is clear that the lift force and drag force values rise as the attack angles and Reynolds numbers rise. Examining the lift force and drag force numbers reveals that the ideal angle of attack for the NACA 4415 aerofoil is 30°.

Fig. 12 Pressure contour for 60° angle of attack

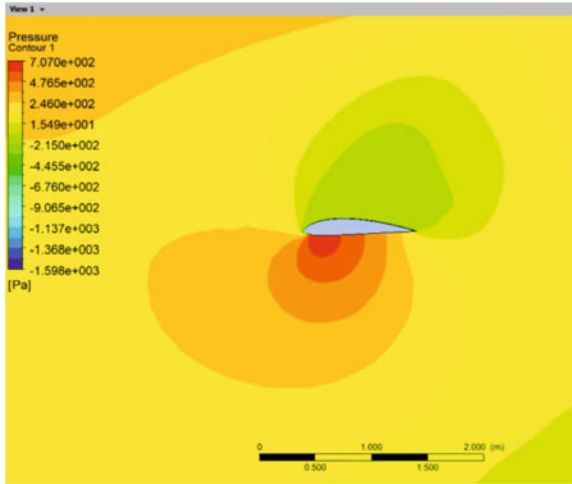
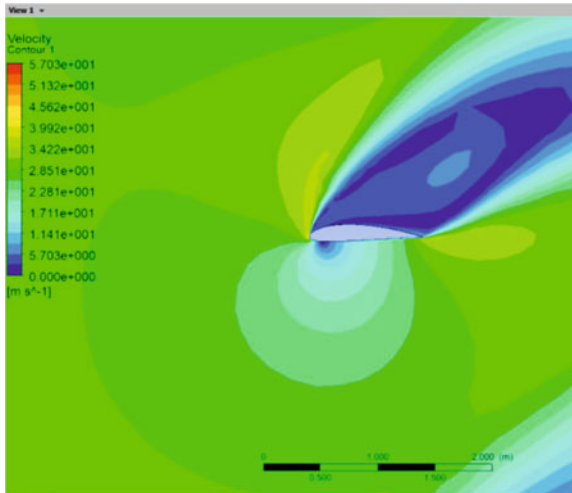


Fig. 13 Velocity contour for 60° angle of attack



2. NACA 4415 gives maximum drag force of 209.2039 N and lift force of 777.25 N at 200,000 Reynolds Number for 30° Angle of Attack.
3. As seen in the tables for CL and CD values, CL and CD values increase as attack angles increase. When CL and CD data are examined, it becomes clear that 30° is the ideal angle of attack for NACA 4415.

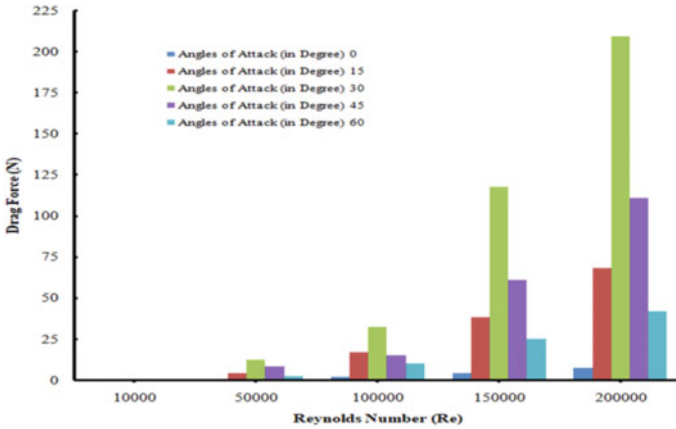


Fig. 14 Effect of different Reynolds number (Re) and various angles of attack on drag force

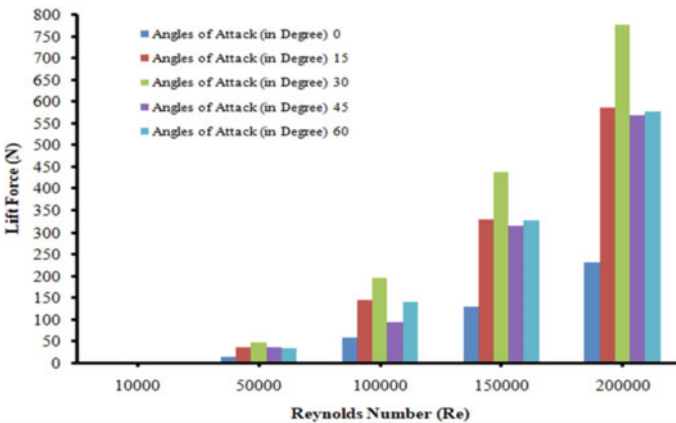


Fig. 15 Effect of different Reynolds number (Re) and various angles of attack on lift force

4. A maximum percentage increment of 96.4 is observed in the drag force for Reynolds number value of 200,000 and 30° angle of attack. Similarly, in case of the lift force the maximum percentage increment observed is 70.2 for 50,000 Reynolds number and 30° angle of attack.

It is advised to keep the mesh size as tiny as possible so that the computations can pick up even the tiniest variations in turbulence. Friction and turbulent behavior may be considered. The simulation and modeling only included the NACA 4415 aerofoil model, but it is recommended that all other series profiles be modeled as well. So that the lift and drag coefficients could be applied more easily and precisely, while bearing in mind that the computational grid shouldn't get too big because that would require a lot of computer power and processing time. Additionally, assuming

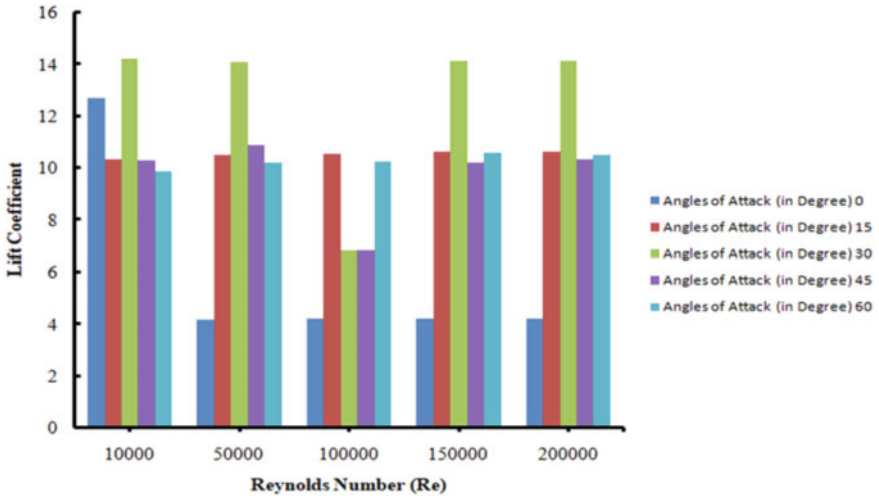


Fig. 16 Effect of different Reynolds number (Re) and various angles of attack on drag coefficient

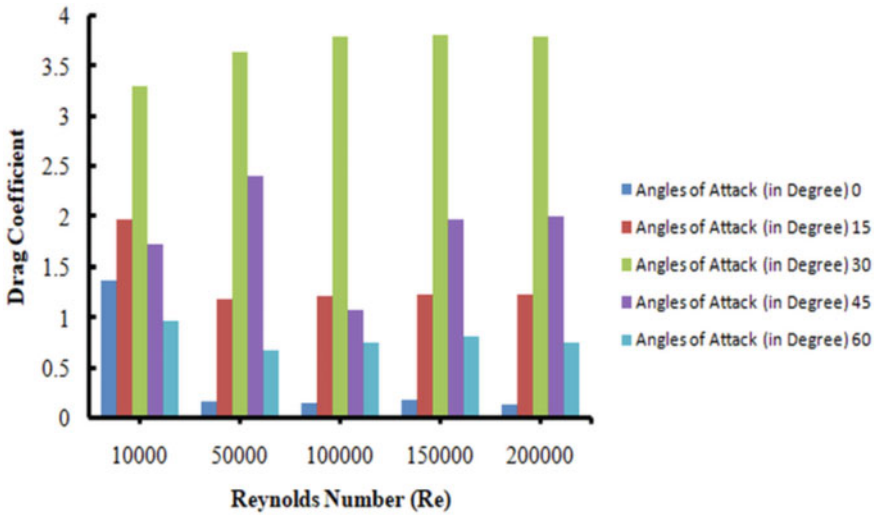


Fig. 17 Effect of different Reynolds number (Re) and various angles of attack on lift coefficient

laminar flow governed by the Navier–Stokes incompressible flow equations, a thorough experimental and numerical investigation of the aerodynamic behaviour of the NACA 4415 aerofoil profile can be successfully evaluated in a subsonic wind tunnel.

Table 2 Percentage increment in drag force

S. No.	Reynolds number (Re)	Max. drag force (N)	Percentage increment in drag force (%)
1	10,000	0.543	65.16
2	50,000	12.5322	95.41
3	100,000	32.3522	93.70
4	150,000	117.8332	96.34
5	200,000	209.2039	96.49

Table 3 Percentage increment in lift force

S. No.	Reynolds number (Re)	Max. lift force (N)	Percentage increment in lift force (%)
1	10,000	1.9552	30.63
2	50,000	48.5261	70.24
3	100,000	195.9259	70.43
4	150,000	437.9432	70.16
5	200,000	777.25	70.05

References

- Patil, B. S., & Thakare, H. R. (2015). Computational fluid dynamics analysis of wind turbine blade at various angles of attack and different Reynolds number. *International Conference on Computational Heat and Mass Transfer, Procedia Engineering, 127*, 1363–1369.
- Haque, M., Ali, M., & Ara, I. (2015). Experimental investigation on the performance of NACA 4412 aerofoil with curved leading edge planform. *Procedia Engineering, 105*, 232–240.
- Shah, S., & Pachapuri, M. (2015). NACA 2415-finding lift coefficient using CFD. *Theoretical and Javafoil, International Journal of Research in Engineering and Technology, 4*, 444–449.
- Rubel, R. I., Uddin, M. K., Islam, M. Z., & Rokunuzzaman, M. (2017). Comparison of aerodynamics characteristics of NACA 0015 & NACA 4415 aerofoil blade. *International Journal of Research Granthaalayah, 5*(11), 187–197.
- Yilmaz, M., & Koten, H. (2018). A comparative CFD analysis of NACA0012 and NACA4412 airfoils. *Journal of Energy Systems, 2*(4), 145–159.
- Kashid, D. T., Parkhe, A. K., Wangikar, S. S., Jadhav, S. V., Kale, S. M., & Chavan, V. R. (2020). Analysis of drag and lift forces with different angle of attacks on airfoil used in aircraft wings. *NOVI MIR Research Journal, 5*(6), 9–18.
- Avvad, M., Vishwanath, K. C., Kaladgi, A. R., Muneer, R., Kareemullah, M., & Navaneeth, I. M. (2021). Performance analysis of aerofoil blades at different pitch angles and wind speeds. *Materials Today: Proceedings, 47*(17), 6249–6256.
- Kulshreshtha, A., Gupta, S. K., & Singhal, P. (2020). FEM/CFD analysis of wings at different angle of attack. *Materials Today: Proceedings, 26*(2), 1638–1643.
- Sudarsono, H. S., & Rusianto, T. (2020). Prediction of aerodynamics coefficients of modified NACA 4415 airfoil using computational fluid dynamics. *E3S Web of Conferences, 202*, 11002.
- Liu, Y., Li, P., He, W., & Jiang, K. (2020). Numerical study of the effect of surface grooves on the aerodynamic performance of a NACA 4415 airfoil for small wind turbines. *Journal of Wind Engineering and Industrial Aerodynamics, 206*, 104263.

11. Yossri, W., Ayed, S. B., & Abdelkefi, A. (2021). Airfoil type and blade size effects on the aero dynamic performance of small-scale wind turbines: Computational fluid dynamics investigation. *Energy*, 229, 120739.
12. Sener, M. Z., & Aksu, E. (2022). The numerical investigation of the rotation speed and Reynolds number variations of a NACA 0012 airfoil. *Ocean Engineering*, 249, 110899.
13. Dwivedi, Y. D., Wahab, A., Pallay, A. D., & Shesham, A. (2022). Effect of surface roughness on aerodynamic performance of the wing with NACA 4412 airfoil at Reynolds number 1.7×10^5 . *Materials Today: Proceedings*, 56(1), 468–476.
14. Sadaq, S. I., Mehdi, S. N., Mehdi, S. D., & Yasear, S. (2022). Analysis of NACA 0020 aerofoil profile rotor blade using CFD approach. *Materials Today: Proceedings*, 64(1), 147–160.

Prediction of Optimum Tool Life and Cutting Parameters by Comparative Study of Minimum Cost Criterion and Maximum Production Rate Criterion



Amarjit P. Kene, Amitkumar A. Shinde, Pravin A. Dhawale, Ranjitsinha R. Gidde, Sandeep S. Wangikar, and Kuldip S. Pukale

Abstract In the Economics of machining three criteria are commonly used: Minimum cost criterion, Maximum production rate criterion and Maximum profit rate criterion. In this paper emphasis has been given to former two criteria as economics are highly related to cost of production and rate of production. The comparison has been made between these two criteria on the basis of tool life which has been calculated using optimum values of cutting speed and feed rate in extended Taylor's tool life equation with predetermined value of depth of cut.

1 Introduction

The art of metal cutting or removing the material from raw material to obtain a predetermined shape is perhaps as old as human civilization. As time passes and as requirement changes, many scientists worked to minimize many challenges in the developing cutting processes. Advancements have been done to increase the efficiency of the process with respect to cost of machining, production rate, quality of the product, energy and the profit rate. Further in machining, the parameters can be optimized which directly took part in machining process such as cutting speed, feed rate and depth of cut. Economics of machining have suggested the three different criteria to evaluate the optimum cutting process parameters which are minimum cost criterion, maximum production rate criterion and maximum profit rate criterion.

The depth of cut is often fixed. In certain machining operations specifically turning, the effect on tool life is normally very insignificant while in milling the radial depth of cut has a substantial outcome so that an optimal relation between cutter diameter and depth of cut can be evaluated. In end milling of difficult to machined materials the axial depth may affect the tool life. Therefore, for generalization these parameters should also be considered [1–4].

A. P. Kene (✉) · A. A. Shinde · P. A. Dhawale · R. R. Gidde · S. S. Wangikar · K. S. Pukale
SVRI's College of Engineering, Pandharpur 413304, India
e-mail: apkene@coe.sveri.ac.in

2 Formulation

As already discussed, there are three criterions from which the optimized values of cutting speed and feed rate can be calculated. The results obtained from these methods will be different for the same cutting conditions. In this section the formulation required for the calculation of the cutting speed and feed rate has been given considering the depth of cut as constant in case of both the criterions.

Let consider,

Total Cost = R, Row Material cost/piece = R1, Setting + Idle time cost/piece = R2, Machining cost/piece = R3, Tool changing time cost/piece = R4, Tool cost/piece = R5, Labor + Overhead cost = λ_1 , Tool cost/grinding = λ_2 , Tool life = T, Machining time/piece = t_m , Setting + Idle time/piece = t_s , Tool changing time (TCT) = t_{ct} . Therefore, Frequency of the tool changing (in producing one part)

$$freq = \left(\frac{t_m}{T} \right)$$

2.1 Minimum Cost Criterion

The main objective of the minimum cost criterion is to find the optimum value of cutting parameters against minimum cost of the machining process. The different costs prescribed in the above section have to be minimized without compromising the quality of product.

The total cost occurred in the machining operation is as follows,

$$R = R1 + R2 + R3 + R4 + R5 \quad (1)$$

$$R1 = \text{constant} \neq f(V, f, d) \quad (2)$$

$$R2 = t_s \times \lambda_1 \neq f(V, f, d) \quad (3)$$

$$R3 = t_m \times \lambda_1 = f(V, f, d).$$

Since as we know,

$$t_m = \frac{L}{f \cdot N} \text{ And } V = \frac{\pi \cdot D \cdot N}{1000}$$

where,

L length of the work piece.

N speed in RPM and
 D diameter of the work piece.

Therefore,

$$t_m = \frac{\pi \cdot D \cdot L}{1000 \cdot V \cdot f} \tag{4}$$

And machining time cost/piece will be,

$$\therefore R_3 = \frac{\pi \cdot D \cdot L}{1000 \cdot V \cdot f} \times \lambda_1 \tag{5}$$

$$R_4 = \left(\frac{t_m}{T} \right) \times t_{ct} \times \lambda_1$$

But as we already know Taylor’s tool life equation,

$$T = \left(\frac{K}{V^{\frac{1}{n}}} \right) \tag{6}$$

Therefore, tool changing time cost/piece will become,

$$\therefore R_4 = \frac{\pi \cdot D \cdot L}{1000 \cdot V \cdot f} \times \left(\frac{V^{\frac{1}{n}}}{K} \right) \times t_{ct} \times \lambda_1 \tag{7}$$

Now, $R_5 = \left(\frac{t_m}{T} \right) \times \lambda_2$

$$\therefore R_5 = \frac{\pi \cdot D \cdot L}{1000 \cdot V \cdot f} \times \left(\frac{V^{\frac{1}{n}}}{K} \right) \times \lambda_2 \tag{8}$$

From Eqs. (1), (2), (3), (5), (7) and (8),

$$\begin{aligned} R &= R_1 + (t_s \times \lambda_1) + \frac{\pi \cdot D \cdot L}{1000 \cdot V \cdot f} \times \lambda_1 \\ &+ \frac{\pi \cdot D \cdot L}{1000 \cdot V \cdot f} \times \left(\frac{V^{\frac{1}{n}}}{K} \right) \times t_{ct} \times \lambda_1 \\ &+ \frac{\pi \cdot D \cdot L}{1000 \cdot V \cdot f} \times \left(\frac{V^{\frac{1}{n}}}{K} \right) \times \lambda_2 \end{aligned} \tag{9}$$

Optimum Velocity

From Eqs. (2) and (3), it is clear that the values of R1 and R2 are independent of cutting speed. So neglecting that terms from Eq. (9) and differentiating it with respect to V will gives optimum value of Cutting speed.

Therefore, for R to be minimum,

$$\begin{aligned} \frac{dR}{dV}|_{V=V_{opt}} &= 0 \\ &- \lambda_1 + \left(\frac{1-n}{kn}\right) \times v_{opt}^{\frac{1}{n}} \times \lambda_1 \times t_{ct} \\ &+ \left(\frac{1-n}{kn}\right) \times v_{opt}^{\frac{1}{n}} \times \lambda_2 = 0 \\ V_{opt} &= \left[\frac{K.n.\lambda_1}{(1-n).(\lambda_1.t_{ct} + \lambda_2)} \right]^n \quad (a) \end{aligned}$$

Optimum Feed Rate

The values of R1, R2 and R3 will be same for calculation as given above but the values of R4 and R5 will get change because of the feed rate contribution in the Taylor's tool life equation.

The extended Taylor's tool life equation is given below:

$$T = \frac{K}{V^{\frac{1}{n}}.f^{\frac{1}{m}}} \quad (10)$$

Therefore, modified R4 and R5 will be,

$$\therefore R_4 = \frac{\pi.D.L}{1000.V.f} \times \left(\frac{V^{\frac{1}{n}}.f^{\frac{1}{m}}}{K}\right) \times t_{ct} \times \lambda_1 \quad (11)$$

And similarly,

$$R_5 = \frac{\pi.D.L}{1000.V.f} \times \left(\frac{V^{\frac{1}{n}}.f^{\frac{1}{m}}}{K}\right) \times \lambda_2 \quad (12)$$

Now Eq. (9) will become,

$$\begin{aligned} R &= R_1 + (t_s \times \lambda_1) + \frac{\pi.D.L}{1000.V.f} \times \lambda_1 \\ &+ \frac{\pi.D.L}{1000.V.f} \times \left(\frac{V^{\frac{1}{n}}.f^{\frac{1}{m}}}{K}\right) \times t_{ct} \times \lambda_1 \end{aligned}$$

$$+ \frac{\pi.D.L}{1000.V.f} \times \left(\frac{V^{\frac{1}{n}}.f^{\frac{1}{m}}}{K} \right) \times \lambda_2 \tag{13}$$

Differentiating (13) with respect to feed will results in optimum feed rate for minimum cost criterion,

$$\begin{aligned} \therefore \frac{dR}{df} |_{f=f_{opt}} &= 0 \\ &- \lambda_1 \times f^{-2} + \left(\frac{m}{n} - 1 \right) \times v^{\frac{1}{n}} \times f^{\left(\frac{m}{n}-2\right)} \times \lambda_1 \times t_{ct} \\ &+ \left(\frac{m}{n} - 1 \right) \times v^{\frac{1}{n}} \times f^{\left(\frac{m}{n}-2\right)} \times \lambda_2 = 0 \\ f_{opt} &= \left[\frac{K.n.\lambda_1}{(m-n).V^{\frac{1}{n}}(\lambda_1.t_{ct} + \lambda_2)} \right]^{\frac{n}{m}} \tag{b} \end{aligned}$$

2.2 Maximum Production Rate Criterion

Maximum production rate criterion is generally applied for higher production rate in the industries. Maximum production rate can be obtained by increasing the speed of the process. Increasing speed does not merely means cutting velocity but it indicates decrease in idle time, tool changing time and machining time. Though machining time is a direct function of the cutting velocity. In this section an attempt has been made to evaluate the expression for optimum velocity and feed rate for the certain machining condition.

$$Total\ time/piece = t = t_s + tm + \left(\frac{tm}{T} \right) \times t_{ct} \tag{14}$$

Using Eqs. (4) and (6) in (14) we get,

$$\therefore t = \frac{\pi.D.L}{1000.V.f} + \frac{\pi.D.L}{1000.V.f} \times \left(\frac{V^{\frac{1}{n}}}{K} \right) \times t_{ct} \tag{15}$$

$\therefore t_s$ has been neglected as $\neq f(v)$

Optimum Velocity:

$$\begin{aligned} \frac{dt}{dV} |_{V=V_{opt}} &= 0 \\ \frac{1-n}{K.n} . V^{\frac{1}{n}} . t_{ct} &= 1 \end{aligned}$$

$$\begin{aligned}
 V_{opt}^{\frac{1}{n}} &= \left[\frac{K.n}{t_{ct} \cdot (1-n)} \right] \\
 V_{opt} &= \left[\frac{K.n}{t_{ct} \cdot (1-n)} \right]^n \quad (c)
 \end{aligned}$$

Optimum Feed Rate

Using Eq. (10), the Eq. (15) can be modified to consider feed rate effect,

$$\therefore t = \frac{\pi.D.L}{1000.V.f} + \frac{\pi.D.L}{1000.V.f} \times \left(\frac{V^{\frac{1}{n}}.f^{\frac{1}{m}}}{K} \right) \times t_{ct} \quad (16)$$

Therefore, differentiating this equation with respect to feed rate we get,

$$\begin{aligned}
 \therefore \frac{dt}{df} |_{f=f_{opt}} &= 0 \\
 -f^{-2} + \left(\frac{m}{n} - 1 \right) \times \frac{v^{\frac{1}{n}}}{K} \times t_{ct} \times f^{\left(\frac{m}{n} - 2 \right)} &= 0 \\
 f_{opt}^{\frac{m}{n}} &= \left[\frac{K.n}{(m-n).V^{\frac{1}{n}}.t_{ct}} \right] \\
 f_{opt} &= \left[\frac{K.n}{(m-n).V^{\frac{1}{n}}.t_{ct}} \right]^{\frac{n}{m}} \quad (d)
 \end{aligned}$$

3 Case Study

To check the reliability of the process and the formulae given above, a case study has been done. In this section, the case study has been carried out to compare the tool life from both the minimum cost criterion as well as maximum production rate criterion.

3.1 Problem

A mild steel rod is being turned with an HSS tool with Extended Taylor’s tool life is given below.

$$T = \frac{70}{V^{\frac{1}{0.91}}.f^{\frac{1}{0.78}}}$$

Tool changing time is 2 min, the average cutting speed is 20 m/min, the overhead and labor cost is Rs. 1500/h and the tool cost per grinding is Rs. 150. Determine the Optimum values of the Cutting Speed and Feed assuming the predetermined value of the Depth of cut as 3 mm. Also find out for which criterion (maximum production rate or minimum cost) the tool life will be more?

Given:

$n = 0.78$, $m = 0.91$ and $K = 70$, $t_{ct} = 2$ min, $\lambda_1 = \text{Rs.}1500/\text{hr} = \text{Rs.} 25/\text{min}$, $\lambda_2 = \text{Rs.}150$, $d = 3$ mm.

Solution:

(A) Minimum Cost Criterion:

From Eq. (a),

$$V_{opt} = \left[\frac{K.n.\lambda_1}{(1-n).(\lambda_1.t_{ct} + \lambda_2)} \right]^n$$

$$V_{opt} = \left[\frac{70 \times 0.78 \times 25}{(1-0.78) \times (25 \times 2 + 150)} \right]^{0.78}$$

$$V_{opt} = [31.022]^{0.78}$$

$$V_{opt} = 14.571 \text{ m/min.}$$

From Eq. (b),

$$f_{opt} = \left[\frac{K.n.\lambda_1}{(m-n).V_{opt}^{\frac{1}{n}}.(\lambda_1.t_{ct} + \lambda_2)} \right]^{\frac{n}{m}}$$

$$f_{opt} = \left[\frac{70 \times 0.78 \times 25}{(0.91-0.78) \times 20^{\frac{1}{0.78}} \times (25 \times 2 + 150)} \right]^{\frac{0.78}{0.91}}$$

$$f_{opt} = [1.2412]^{0.8571}$$

$$f_{opt} = 1.2035 \text{ m/rev.}$$

(B) Maximum Production Rate Criterion

From Eq. (c),

$$V_{opt} = \left[\frac{K.n}{(1-n).t_{ct}} \right]^n$$

$$V_{opt} = \left[\frac{70 \times 0.78}{(1-0.78) \times 2} \right]^{0.78}$$

$$V_{opt} = [124.090]^{0.78}$$

$$V_{opt} = 42.9652 \text{ m/min.}$$

From Eq.(d),

$$f_{opt} = \left[\frac{K \cdot n}{(m - n) \cdot V^{\frac{1}{n}} \cdot t_{ct}} \right]^{\frac{n}{m}}$$

$$f_{opt} = \left[\frac{70 \times 0.78}{(0.91 - 0.78) \times 20^{\frac{1}{0.78}} \times 2} \right]^{\frac{0.78}{0.91}}$$

$$f_{opt} = [4.5150]^{0.8571}$$

$$f_{opt} = 3.63722 \text{ m/rev.}$$

Tool Life:

(A) Minimum Cost Criterion

$$T = \frac{K}{V^{\frac{1}{n}} \cdot f^{\frac{1}{m}}}$$

$$T = \frac{70}{14.571^{\frac{1}{0.78}} \times 1.2035^{\frac{1}{0.91}}}$$

$$T = 1.841 \text{ min.}$$

(B) Maximum Production Rate Criterion

$$T = \frac{K}{V^{\frac{1}{n}} \cdot f^{\frac{1}{m}}}$$

$$T = \frac{70}{42.9652^{\frac{1}{0.78}} \times 3.6372^{\frac{1}{0.91}}}$$

$$T = 0.1365 \text{ min.}$$

From the above case study, it can be seen that the tool life will be more for the Minimum Cost criterion than Maximum production rate criterion. This case study has been done for generalization of the results depends on the various tool-work piece combinations.

3.2 Optimization

The Optimum values of the Tool life has been calculated using both the criterions and compared on the basis of graphical results. Response surface method (RSM) has been employed for design of experiment of values of cutting speed and feed rate. RSM uses Centered composite design technique for obtaining different combinations of the input parameters. MINITAB 16 has been used to carry out the optimization. The experimental data has been manipulated (Shown in Tables 1 and 2) and an empirical formula for tool life has been generated on the basis of it for both minimum cost criterion and maximum tool life criterion respectively. The tool life has been calculated from the extended tool life Eq. (10), using same values.

Table 1 Experimental data for minimum cost criterion

S. No.	Cutting speed (m/min)	Feed rate (m/rev)	Tool life (min)
1	14.5710	1.20350	1.8409
2	33.0400	1.20350	0.6444
3	14.5710	2.95970	0.6848
4	33.0400	2.95970	0.2397
5	10.7459	2.08160	1.4897
6	36.8651	2.08160	0.3067
7	23.8055	0.83978	1.4570
8	23.8055	3.32342	0.3213
9	23.8055	2.08160	0.5373
10	23.8055	2.08160	0.5373
11	23.8055	2.08160	0.5373
12	23.8055	2.08160	0.5373
13	23.8055	2.08160	0.5373

Table 2 Experimental data for maximum production rate criterion

S. No.	Cutting speed (m/min)	Feed rate (m/rev)	Tool life (min)
1	42.965	3.6372	0.1365
2	153.261	3.6372	0.0267
3	42.965	12.8800	0.0340
4	153.261	12.8800	0.0067
5	20.122	8.2586	0.1466
6	176.104	8.2586	0.0091
7	98.113	1.7230	0.1076
8	98.113	14.7942	0.0101
9	98.113	8.2586	0.0192
10	98.113	8.2586	0.0192
11	98.113	8.2586	0.0192
12	98.113	8.2586	0.0192
13	98.113	8.2586	0.0192

4 Results and Discussion

The optimum value of cutting speed and the feed rate have been calculated from the derived expression for cutting speed and feed rate using analytical methods and formulae assuming the value of depth of cut as known. The tool life has been found out at the given cutting condition for both Minimum cost as well as for Maximum production rate criterion and later both the criterion have been compared to see

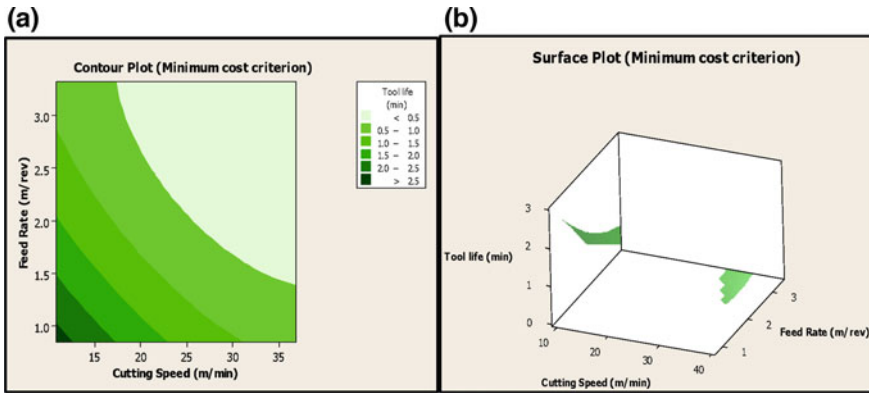


Fig. 1 a Contour plot, b surface plot generated by MINITAB 16 for minimum cost criterion

the optimum values of both cutting speed and feed rate along with the tool life. The minimum cost criterion has suggested the optimum values of the cutting speed and feed rate as 14.571 m/min and 1.2035 m/rev respectively. And the maximum production rate criterion has proclaimed that the optimum values of the cutting speed and feed rate as 42.9652 m/min and 3.6375 m/rev respectively. The tool life has been calculated on the basis of these optimum values of the cutting speed and feed rate using Extended Taylor’s tool life equation and it is found to be 1.8409 min and 0.1365 min for Minimum cost criterion and Maximum production rate criterion respectively.

4.1 Minimum Cost Criterion

The empirical tool life equation has been obtained as,

$$\begin{aligned}
 T = & 5.75318 - 0.188084 \times V - 1.89653 \times f \\
 & + 0.00199521 \times V^2 + 0.214794 \times f^2 \\
 & + 0.0231661 \times V.f. \quad (A)
 \end{aligned}$$

The optimum value of tool life is found to 2.73031 min at cutting speed 10.7459 m/min and feed rate 0.839779 m/rev for taken values (Figs. 1 and 2).

4.2 Maximum Production Rate Criterion

The empirical tool life equation has been obtained as,

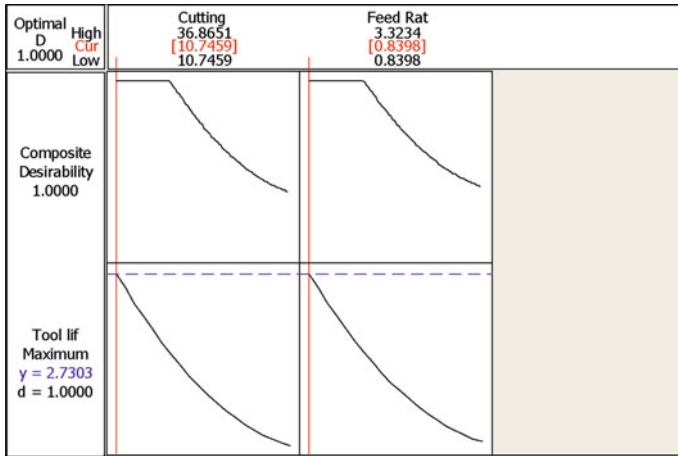


Fig. 2 Desirability plot for tool life against cutting speed and feed rate for minimum cost criterion

Tool Life,

$$T = 0.345181 - 0.00303166 \times V - 0.0269558 \times f + 8.21403 \times 10^{-6} \times V^2 + 0.00074871 \times f^2 + 8.09268 \times 10^{-5} \times V.f. \quad (B)$$

The optimum value of tool life is found to **0.246016 min** at cutting speed **20.1222 m/min** and feed rate **1.72298 m/rev** for taken values (Figs. 3 and 4).

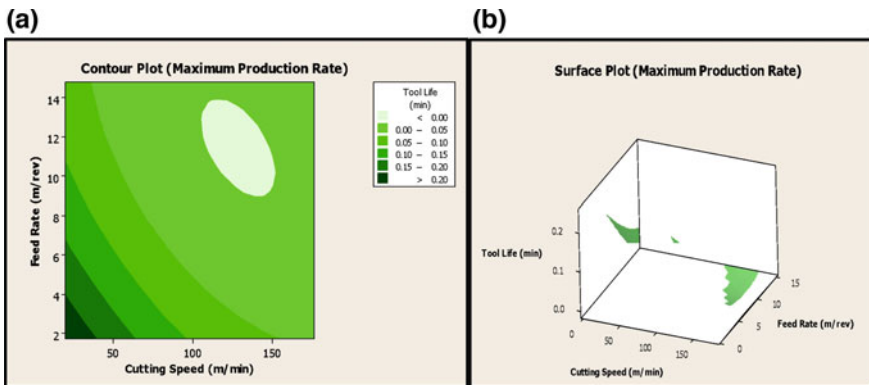


Fig. 3 a Contour plot, b surface plot generated by MINITAB 16 for maximum production rate criterion

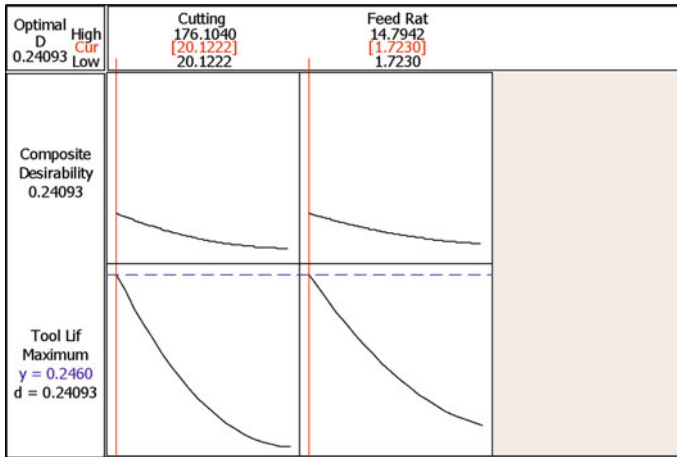


Fig. 4 Desirability plot for tool life against cutting speed and feed rate for maximum production rate criterion

5 Conclusions

As it is clear from the theory of Taylor’s tool life equation that as cutting speed and feed rate increases individually or simultaneously, the tool life is going to decrease. From the case study done in this paper, the tool life in case of minimum cost criterion has been found to be 2.73031 min and in case of maximum production rate criterion has been found to be 0.240634 min. The tool life was higher for minimum cost criterion and lower for maximum production rate criterion. So, it can be concluded that for better tool life in any machining operation, the minimum cost criterion can be applied. Further the optimum value of cutting velocity for both the criterion has been compared. From the results, it can be summarized that for maximum production rate criterion the cutting velocity is increasing drastically whereas there is very less change in the feed rate. This shows that the cutting velocity has higher effect on the economics of machining than other cutting parameters.

References

1. Ravnani, G. L. (1980). Economic analysis of machining including a consideration of tool life scatter. *Wear*, 62(1), 233–243. [https://doi.org/10.1016/0043-1648\(80\)90046-0](https://doi.org/10.1016/0043-1648(80)90046-0)
2. Nagasaka, K., & Hashimoto, F. (1988). Tool wear prediction and economics in machining stepped parts. *International Journal of Machine Tools and Manufacture*, 28(4), 569–576. [https://doi.org/10.1016/0890-6955\(88\)90068-5](https://doi.org/10.1016/0890-6955(88)90068-5)

3. Shabtay, D., & Kaspi, M. (2002). Optimization of the machining economics problem under the failure replacement strategy. *International Journal of Production Economics*, 80(3), 213–230. [https://doi.org/10.1016/S0925-5273\(02\)00255-4](https://doi.org/10.1016/S0925-5273(02)00255-4)
4. Egbelu, P. J., Davis, R. P., Wysk, R. A., & Tanchoco, J. M. A. (1982). An economic model for the machining of cast parts. *Journal of Manufacturing Systems*, 1(2), 207–213. [https://doi.org/10.1016/S0278-6125\(82\)80030-7](https://doi.org/10.1016/S0278-6125(82)80030-7)

Design and Fabrication of Hybrid Solar Dryer



S. S. Gaikwad, Digambar T. Kashid, S. B. Bhosale, A. A. Mote, S. M. Shinde, and M. N. Gund

Abstract There is want to layout a dryer that is beneficial for small scale framers to mills their crop into ready-made and tradable goods. Different forms of sun dryers are to be had and categorized however there are few taken into consideration neighborhood environmental conditions, cost, availability, etc. In this, paintings literature overview is carried to recognize sun drawing mechanism layout and modern kingdom of era the choice standards are diagnosed from literature for choice of sun dryer. Based at the evaluation, nice layout is hybrid sun layout for our diagnosed problem. While designing sun dryer for merchandise tomato, chilies, potato and onion it's taken into consideration this layout is primarily based totally at the graphical region Pandharpur. To be had fabric wherein used for the development and eventually checking out of the operating of sun dryer is performed.

Keywords Hybrid dryer · Sun electricity · Natural and compelled convection

1 Introduction

A simple feature of a sun dryer is the ability to warm air to a consistent temperature using sunlight, which aids in the extraction of humidity from plants within a drying chamber. Through defined air inlets and outlets, small sun ventilators, or a temperature difference caused by exposure or vertical height, ventilation is available at a regular cost. The meals are stored in containers with clear lids in direct solar dryers. Additionally, the greenhouse effect raises the temperature inside the dryer, regulating the air trade through the use of vents. Because the sparkling air is heated one at a time from the meals chamber, oblique solar dryers do not always expose the food to direct sunlight. When drying ingredients that lose their nutritional value when exposed to

S. S. Gaikwad (✉) · D. T. Kashid · S. B. Bhosale · A. A. Mote
SVERI's College of Engineering, Pandharpur, Maharashtra, India
e-mail: gaikwadss@coe.sveri.ac.in

S. M. Shinde · M. N. Gund
Karmayogi Institute of Technology, Shelve, Pandharpur, Maharashtra, India

direct sunlight, this method is preferable. The sun's energy is combined with gasoline from fossil fuels or biomass. The process of extending a product's garage length with preferred quality is referred to as maintenance. Solar dryers are used extensively in the agricultural and commercial sectors; Dryers are the most energy-efficient appliances, especially from an electricity standpoint. These have the ability to store a lot of time, a lot of electricity, take up little space, are beautiful, made of high-quality materials, and most importantly, they are good for the environment [1, 2].

2 Hybrid Solar Dryer

Hybrid sun dryer paintings on precept of warmth and mass transfer. Mass transfer consist of mass discount because of dehydration moisture to the warmth transfer process due to temperature difference. The hot air flowing from solar collectors and heat exchanger. A hybrid sun dryer turned into designed and built the use of direct solar energy and a warmness exchanger. The dryer includes sun collector, reflector, and warmth exchanger come warmness garage unit and drying chamber [3].

Hybrid sun drying structures are dryers in which solar power is just one of the additional resources of electricity used to heat the drying air. To ensure proper air circulation, they combine solar power with additional electric or fossil fuel-based complete heating systems and ventilators. In most cases, hybrid sun dryers operate in forced convection mode. If they have sufficient heat, the drying system will immediately utilize the sun-generated electricity-heated drying air; Otherwise, the dehydrator that runs on fossil fuel is used to achieve the required drying temperatures (for example, at night or during periods of low insulation, like wet seasons). According to Ekechukwu and Norton [4], the fossil gasoline device is frequently managed to provide the desired drying conditions. Hybrid sun dryers are extra preciously used for drying excessive mass product the use of sun electricity and electricity. It is extra efficient, having huge variety of drying temperature and is appropriate for warmness-touchy merchandise. Allow higher manage of drying, paintings on day time and night time also. It offers higher overall performance and it's far quicker than lively and passive sun dryer. Hybrid sun dryers are extra high priced examine to different sun dryer (Fig. 1).

3 Hybrid Solar Dryer

The hybrid dryers most important additives are; sun panel, sun battery, and manipulate panel, drying chamber, rack and trays, and fan/blower. The following materials were used in the development: (1) Mild steel, (2) Sheet steel, (3) Wire gauge (4) Plywood, (5) Solar panel with 12 W, (6) Battery and (7) Switch [5, 6].

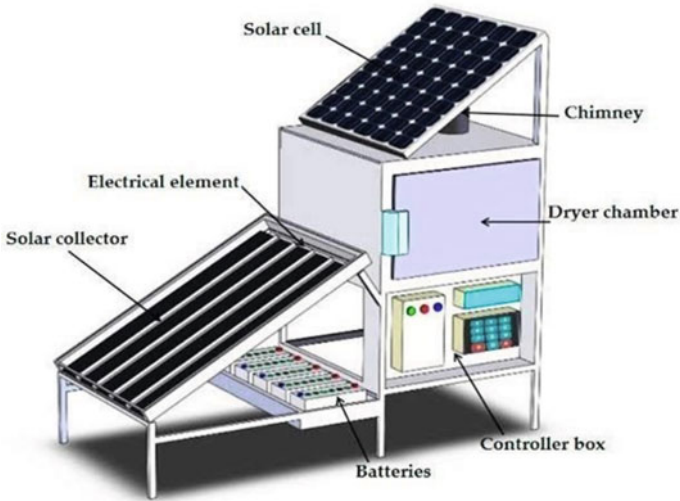


Fig. 1 Hybrid solar dryer [4]

3.1 Drying Chamber

It was painted a silver colour to reduce radiation heat loss. An external chamber also surrounded the inner chamber of 0.432 m³ volume (Made up of 20 mm skinny steel sheet and 1 × 1 Inch box pipe). Thick silver reflector for the insulating material (0.05 mm layer of silver reflector) to gain a minimum warmness lack of 5% from the drying chamber. It consists two holes one is mounted on top and another is at bottom [7–9]. (Having 3 Inch Diameter) (Fig. 2).



Fig. 2 Drying chamber

Fig. 3 Trays of drying chamber



3.2 Trays

Tray is made up for the storing the dried food product trays are used for storing it. It consists a tray holes on it for the travel hot air around the food product with his buoyancy Force. The trays are made up of metal wire gauge (15 × 20 Inch) consisting of holes on it [10, 11]. It is covered with steel plate (½ Inch) (Fig. 3).

4 Experimental Calculations

The drying time required for Potato and Onion products by forced and natural convection are as follows for plotting graph of Potato and Onion products are time versus moisture %.

$$\text{Moisture}\% = \frac{\text{Initial Mass} - \text{Final mass}}{\text{Initial mass}}$$

5 Results and Discussion

Compared to solar drying, the weight loss achieved by solar drying is shown in Table 1. From these figures, it can be concluded that the performance of solar dryer.

The removal of water content and removal of moisture in solar drying are shown in Fig. 4. Figure shows a comparison of time and percent moisture and Onion in the sun dryer after 100, 200 and 300 min. X-axis mentioned humidity % and Y-axis mentioned times in minutes are shown in Fig. 4.

Table 1 Drying product moisture and weight details

Time (h)	Particulars	Weight before drying in gm	Weight after drying in gm.	Moisture % removed in solar dryer
5	Onion	1000	258.3	74.17
5	Potato	1000	303.6	69.64

Fig. 4 Onion moisture % removal versus time

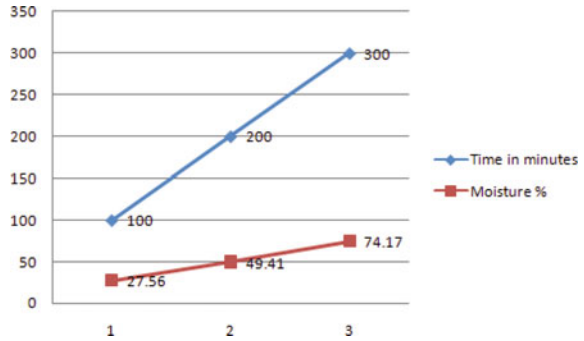
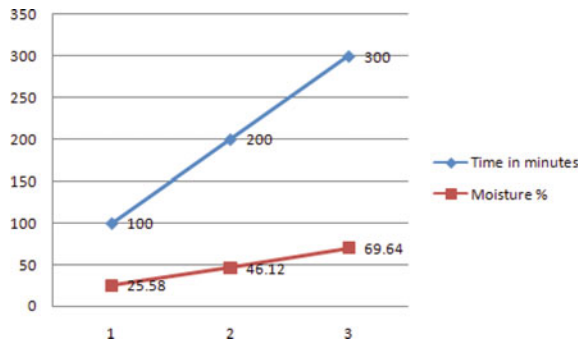


Fig. 5 Potato moisture % removal versus time



Water removal and moisture removal during solar drying are shown in Fig. 5. Figure 5 shows a comparison of time and percentage of moisture in the solar dryer for potatoes after 100, 200 and 300 min. X-axis represents humidity % and Y-axis represents times in minutes are shown in Fig. 5.

6 Conclusion

It was discovered that plants with high humidity prefer a hybrid dryer with forced convection or active mode, whereas plants, fruits, and vegetables with low humidity prefer a dryer with natural convection or passive mode. We concluded from the experimental analysis that the solar dryer dries agricultural products by raising the

ambient air temperature to maximum efficiency. For hybrid solar drying products like onions and potatoes, we removed water and moisture. Hybrid solar dryer at 100°, 200 and 300 min, the result is good compared to the open drying. Future scope is thermal performance evaluation in Ansys and exhaust air reuse.

References

1. Gaikwad, S. S., Wagaj, V. B., Kadam, R. H., Ghaytidak, V. M., & Kale, Y. B. (2021). Design and fabrication of solar tracking system. In *National conference on relevance of engineering and science for environment and society—R{ES}^2*.
2. Gaikwad, S. S., Shinde, A. B., Mote, A. A., & Kachare, P. S. (2016). Design and construction of briefcase type portable solar dryer. In *International conference techno-societal* (pp. 771–778). Springer International Publishing AG 2018.
3. Khalifa, A. J. N., Al-Dabagh, A. M., & Al-Mehemdi, W. M. (2012). An experimental study of vegetable solar drying systems with and without auxiliary heat. *International Scholarly Research Network ISRN Renewable Energy*, 2012.
4. Ekechukwu, O. V., & Norton, B. (1999). Review of solar-energy drying systems II: An overview of solar drying technology. *Energy Conversion and Management*, 40(6), 615–655.
5. Gaikwad, S. S., Devmare, A. D., Karvar, N. A., Chavan, K. H., & Gavali, S. A. (2021). Fabrication and performance analysis of wooden solar dryer. In *National conference on relevance of engineering and science for environment and society—R{ES}^2*.
6. Gaikwad, S. S., & Mote, A. A. (2015). Experimental analysis of cabinet solar dryer for food drying. *International Engineering Research Journal (IERJ)*, 169–174. ISSN 2395-1621.
7. Kumar, A., Singh, R., Prakash, O., & Ashutosh. (2014). Review on global solar drying status. *Agricultural Engineering International: CIGR Journal*, 16(4), 161–177.
8. Mohsin, A. S. M., Nasimul Islam Maruf, M., Sayem, A. H. M., Rejwanur Rashid Mojumdar, M., & Farhad, H. M. S. (2011). Prospect & future of solar dryer: Perspective Bangladesh. *IACSIT International Journal of Engineering and Technology*, 3(2).
9. Scalin, D. (1997). The design construction and use of an indirect through-pass solar food dryer. *Home Power Magazine*, 57, 62–72.
10. Vidya Sagar Raju, R., Meenakshi Reddy, R., & E. Siva Reddy. (2013). Design and fabrication of efficient solar dryer. *International Journal of Engineering Research and Applications*, 3(6), 1445–1458. ISSN: 2248-9622.
11. Whitfield, D. E. (2000). Solar dryer systems and the internet: Important resources to improve food preparation. In *Proceedings of international conference on solar cooking*, Kimberly, South Africa, November 26, 2000.

Design and Analysis of Compliant Macro Scale Gripper



Jambhale Pooja and Deshmukh Bhagyesh

Abstract At the present day, there is a need of creative and innovative designs. Compliant mechanisms have a huge contribution in the mechanical engineering field and become an important branch of modern mechanisms. Compliant macro grippers need to be precise, accurate, and automated in the field of medical, robotics, material science, and in the automotive industry for gripping, handling, and assembling of objects. A compliant mechanism offers a better and a precise solution. Flexure-based compliant mechanisms has various application in medical, robotics, MEMS, biomedical devices, aerospace industry, adaptive structures, and automotive industry for gripping handling and manipulation purpose. due to the excellent benefits of no friction, no backlash, no wear, and the least requirement of assembly. By applying Pseudo Rigid Body Model (PRBM) the compliant macro scale gripper is developed. The result obtained by PRBM model is verified by simulation. ANSYS software is used for analysis and simulation. This paper represents a study of flexure-based compliant mechanisms.

Keywords Compliant macro scale gripper · PRBM · Flexure hinge · FEA

1 Introduction

In the last few years, compliant mechanisms have become a significant branch of modern mechanisms. The conventional rigid-body grippers have a problem with accuracy due to the presence of joints. This paper introduces a compliant macro scale gripper. The compliant mechanism gains its mobility from deformation of flexible member, in most of the cases hinge is used as flexible member and the design of hinge is a very important part [1].

J. Pooja (✉) · D. Bhagyesh

Walchand Institute of Technology, Walchand-Hirachand Marg, Ashok Chowk, Solapur 413006, India

e-mail: poojasachink96@gmail.com

Compliant mechanisms has a major contribution in the field of the automotive industry, robotics industry, MEMS, biomedical devices, aerospace industry, components in transportation, and for adaptive structures. In a compliant mechanism at most of the time flexure hinge is used as a flexible member to gain mobility. Often notch-type flexure hinges used with different contours like circular contours, corner-filletted contours, or elliptical contours to design compliant mechanisms [2, 3]. Compliant mechanism offers several advantages like scalability, high reproducibility, no backlash, less wear and tear, eliminate friction, removing lubrication of monolithic structures, and no need for assembly. The mechanisms are constructed to gain flexibility from deformation in the flexure hinge or any other flexible part of that mechanism called as a compliant mechanism. The use of a compliant mechanism offers numerous benefits like as reduction in part count and due to flexible segment it gives more accurate motion. The motion and the force is transferred by rigid joints in conventional rigid body mechanisms. The compliant mechanism is designed by two methods kinematic synthesis approach and continuum synthesis approach. For lumped system analysis PRB modelling are most widely used [4, 5].

The objectives of current research are,

- To study various aspects of compliant mechanism and their advantages.
- To design and study the macro scale gripper.
- To carry out analysis and simulation of macro scale gripper.

2 Literature Review

The literature is carried out to study and understand various aspects of compliant mechanisms. However, compliant mechanism is very challenging to design and analyze. There are primarily three factors that affect the flexibility of compliant mechanisms which are Material properties, geometry, loading, and boundary conditions.

Albanesi et al. [6] explained design methods of compliant mechanisms. Mechanisms with distributed compliance, and mechanisms with concentrated compliance, these two are feasible categories of compliant mechanisms. While designing a compliant mechanism the PRBM is most accurate method because it approximate the performance of flexible link. inverse analysis model allows finding the initial shape of a beam. Structural optimization method are mostly used design to design compliant mechanism because it is not necessary or it is not required to start with known rigid links. However, Structural optimization techniques such as topology optimization are more costlier method when it is to be compared with pseudo-rigid-body-model.

Arumugam et al. [7] presented the different structural optimization method for designing compliant mechanisms. The author describes design methods, advantages, fabrication, disadvantages, and application of compliant mechanism. Author mainly concentrated on structural optimization techniques. sequential linear programming

(SLP), sequential quadratic programming (SQP), generalized convex approximation (GCA), convex linearization (CONLIN), Topology Optimization Method, and other the most prominent methods to solve optimization problems.

Ibrahim et al. [8] investigated the best suitable polymeric material for designing compliant mechanisms. The author carried out finite element analysis in Siemens NX 12 software. Analytically topology optimization technique is used to design the model of the plier. The author uses Acrylonitrile Butadiene Styrene, Thermoplastic polyurethane, and Polylactic Acid polymers for analysis of plier. From the result it observed that ABS was best material. Reduced inventory storage, ease of manufacturing, reduction in number of parts, eliminate the lubrication, due to single piece reduction in manufacturing and assembly time and cost are the merits of compliant plier. The model of compliant plier is 3D printed for testing.

Karaku et al. [9] designed a compliant wiper for car get more simpler design compared to traditional wiper mechanisms. A number of linkages and joints. The compliant wiper produced in single piece. Due this it reduced the number of parts. The wiper is constructed for L7e car. The material used for compliant wiper AISI 1080 steel. The FEA analysis is performed to verification of analytical calculation, and then the prototype is manufactured. After the demonstration of the model it offers advantages like reduction in number of parts and hence reduction in cost and assembly time, but it has issue with fatigue life of the wiper.

Jagtap et al. [10] studied the various application of compliant mechanisms communicated by various researchers in different fields like hand-held tools, MEMS, transportation, aerospace, micro-mechanism, biomedical, and robotics. The author study the detail study about compliant mechanism. In compliant mechanism due to compactness of the flexible parts it is to be used for precise application.

Kota et al. [11] introduced the design of a compliant kidney manipulator for surgical application. The compliant mechanism offers several advantages in the field of biomechanics and in surgical instruments over conventional devices. The author mainly concentrated on surgical application of compliant mechanism. The kidney manipulator is designed by using CAD model and then simulation has been done in ANSYS. The purpose of his work is to develop a compliant mechanism that can pick the object and is relatively stiffer to resist the reaction forces acting on gripping the object.

Lofroth et al. [12] developed a compliant gripper for the manipulation of multiple tiny objects. The micro gripper is operated by piezo actuator. The author aims to design compliant gripper with effortlessly replaceable gripper tip. The silicon material is used to design gripper tip. The kinematic analysis of micro gripper provided. The operating range of gripper in between 6 and 500 μm . while designing the compliant gripper, the author conducted an experiment with four different types of silicon tip for handling and manipulation of micro scale objects. The microgripper used for cell sorting and cell manipulation etc.

Sebastian et al. [13] presented a design of a flexure hinge-based compliant mechanism. The author looks over the methods of modelling for flexure hinges compliant mechanisms for different four hinge contours. Various specifications such as design

tools, design equations, design graphs, and geometric scaling approach is demonstrated. For analytical calculation topology optimization approach is used to design flexure hinge and the results are validated through simulation. The author mainly concentrated on notch type flexure hinge. Various types of flexure hinges have been established over the last decades.

3 Design Approaches

(a) Kinematic synthesis approach

This approach includes the pseudo-rigid body model method for modeling compliant mechanism for large deflection and non-linear behavior of compliant joints. Kinematic synthesis approach relay on conventional rigid body for solution. The pseudo-rigid body model aims to give an uncomplicated approach to solve problem. Pseudo Rigid Body modelling is applicable for analytical calculations of flexure based compliant mechanisms. PRBM can be approximate the performance of flexible link [14] (Fig. 1).

Small length flexural pivots the spring constant k is given in Eq. (1) by [14]

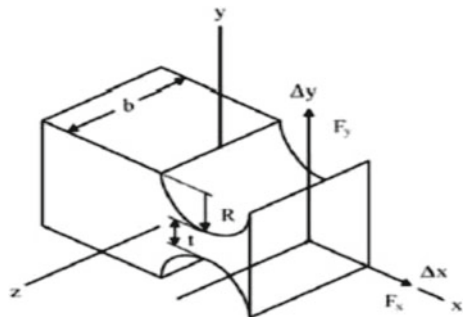
$$K = \frac{(EI)l}{l} \tag{1}$$

where,

- K Spring Constant
- E Young's Modulus
- l Length of Flexible segment and
- I Beam Moment of Inertia.

$$k_{\theta} = \frac{2Ebt^{2.5}}{9\pi r^{0.5}} \tag{2}$$

Fig. 1 Flexure hinge [4]



where,

- k_θ Torsional stiffness of the hinge,
- E Young's modulus of material
- b Thickness of plate
- t Thickness of hinge and
- r Flexure radius.

(b) Continuum synthesis approach

Structural optimization-based approach also referred as continuum synthesis approach. This approach is mainly concentrated on their solution of the geometry, size and topology of the mechanism. It is not necessary to start with known rigid links while designing. It is grounded on topology optimization. Topology optimization method most widely used to design compliant mechanism [4].

4 Modelling and Analysis

The input displacement and input force equation for a compliant macro gripper was developed. Using the PRBM method, calculations are carried out for displacement so as to validate the developed model. It is necessary to compare analytical model results with simulation for validation.

Analytical calculation of compliant macro gripper for displacement

Basic modelling of compliant macro gripper is carried out by using Pseudo Rigid Body Model (PRBM) concept. After the modelling theoretical calculation performed by using following formula,

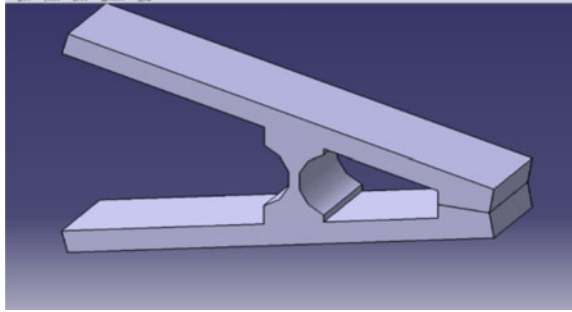
$$Y = \frac{Fl^2}{4k_\theta}. \quad (3)$$

Figure 2 shows the CATIA model of the compliant gripper and Eq. (3) provide a displacement of a compliant macro gripper. The dimensions taken into consideration for macro gripper are $L = 18.12$ mm, $b = 7$ mm, $r = 4.5$ mm, and $t = 1$ mm.

5 Numerical Simulation

After formulating relation between force and displacement analytically, the simulation is to be carried out by ANSYS software.

Fig. 2 Compliant macro gripper in CATIA



Steps in FEA

Following are the steps undertaken for analysis of a compliant macro gripper.

- (a) **Pre-processor:** Pre-processor comprises the generic steps noted below
- i. Constructing geometry of model
 - ii. Specifying materials and properties of that material
 - iii. Developing mesh of the model.

In this process the model of compliant macro gripper is constructed. The simulation process starts with this step.

- ii. Specifying materials and properties of that material

This process specifying the material of the model and properties of that material which are going to be used. Acrylonitrile butadiene styrene (ABS) plastic material is used to design compliant macro scale gripper. The Young's modulus for Acrylonitrile butadiene styrene is taken as 1628 N/mm^2 , and Poisson's ratio 0.3.

- iii. Developing mesh of the model

After defining the material for compliant macro gripper, next is to generate mesh which shown in Fig. 3.

- (b) **Solution—Application of Boundary Conditions**

In ANSYS the static structural analysis module is to be chosen for investigation. In this process the one end of the gripper is to be fixed and from the another end the force is to be applied on the gripper i.e. load and boundary conditions are applied on the gripper for the solution. After the defining boundary conditions next is post processor (Fig. 4).

- (c) **Post Processor—Display Result**

In this process result is displayed. We got the displacement plot in the form of total deformation for particular imposed force. Figure 5 shows the displacement plot. In ANSYS the simulation is carried out over the range 0.1–10 N i.e. the force is applied

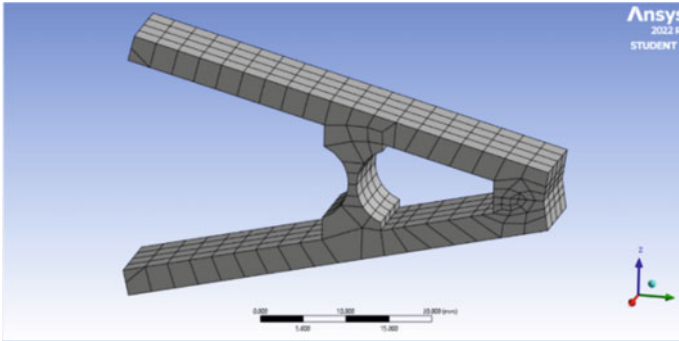


Fig. 3 Meshed model

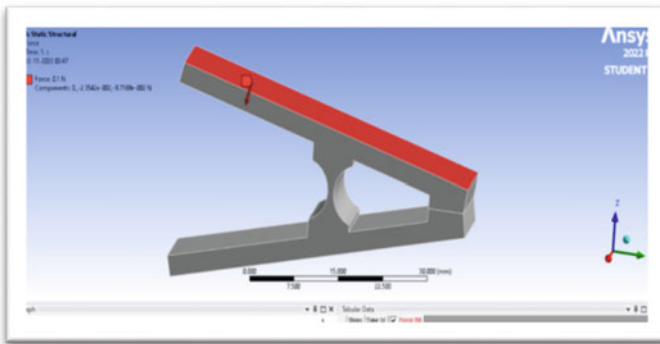


Fig. 4 Boundary conditions applied to the model

from 0.1 to 10 N, the results obtained from the analysis are shown in Table 2. Also the result calculated by PRBM and simulation is compared to each other and percentage of error displayed in Table 2.

Now from the Tables 1 and 2, Results obtained by PRBM technique, Analysis using ANSYS, and error percent are tabulated below.

These results show a minimum error, which can be proved to be smaller on further refinement of the model.

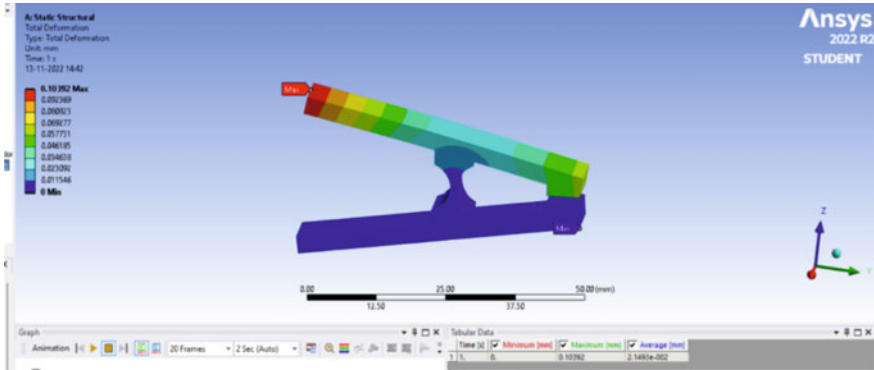


Fig. 5 Displacement plot

Table 1 Force versus displacement

Force (N)	Displacement by simulation (MM)	Force (N)	Displacement by simulation (MM)
0.1	0.02131	2	0.4263
0.2	0.04263	3	0.6394
0.3	0.06394	4	0.8526
0.4	0.08526	5	1.0657
0.5	0.10657	6	1.2789
0.6	0.1278	7	1.492
0.7	0.1492	8	1.7052
0.8	0.1705	9	1.9184
0.9	0.1918	10	2.1315
1	0.2131		

Table 2 Resulting displacement

Force (N)	Displacement (MM) by PRBM	Displacement (MM) by ANSYS	% error
0.1	0.02131	0.02078	2.5505
0.2	0.04263	0.04156	2.5745
0.3	0.06394	0.06234	2.5665
0.4	0.08526	0.08313	2.5622
0.5	0.10657	0.10392	2.5500
0.6	0.1278	0.1247	2.4859
0.7	0.1492	0.1454	2.6134
0.8	0.1705	0.1662	2.5872
0.9	0.1918	0.187	2.5668
1	0.2131	0.2078	2.5505
2	0.4263	0.4156	2.5745
3	0.6394	0.6234	2.5665
4	0.8526	0.8313	2.5622
5	1.0657	1.0392	2.5500
6	1.2789	1.247	2.5581
7	1.492	1.4548	2.5570
8	1.7052	1.6626	2.5622
9	1.9184	1.8705	2.5608
10	2.1315	2.0783	2.5597

6 Conclusion

Compliant mechanisms plays vital role modern mechanisms. While designing a compliant mechanism two approaches are taken into consideration first is the kinematic synthesis approach and the Continuum synthesis approach. Pseudo Rigid Body modelling is applicable for analytical calculations of flexure based compliant mechanisms. The results obtained via PRBM authenticate the importance of this technique in analysis for compliant mechanism. This compliant macro gripper can be used in the field of Robotics, automotive, medical, material science etc. for gripping, handling, and assembling of objects. By applying Pseudo Rigid Body Model (PRBM) the compliant macro scale gripper is developed. The result obtained by PRBM model is verified by simulation. ANSYS software is used for analysis and simulation.

Acknowledgements Authors are thankful to the authorities of Walchand Institute of Technology, Solapur to support this research work.

References

1. Deshmukh, B., et al. (2014). Development of a four bar compliant mechanism using pseudo rigid body model (PRBM). *Procedia Materials Science*, 6, 1034–1039.
2. Henning, S., et al. (2021). Analysis of planar compliant mechanisms based on non-linear analytical modelling including shear and lateral contraction. *Mechanism and Machine Theory*, 164, 1–23.
3. Late, D., et al. (2020). Compliant mechanisms in progress and development of modern technology. *International Journal of Engineering and Management Sciences*, 5(2), 186–189.
4. Vidap, A., et al. (2015). Modelling and analysis of compliant cantilever beam. *International Journal of Science and Research*, 4(7), 970–973.
5. Deshmukh, B., et al. (2012). Conceptual design of a compliant pantograph. *International Journal of Emerging Technology and Advanced Engineering*, 2(8), 270–275.
6. Albanesi, A. E., et al. (2010). A review on design methods for compliant mechanisms. *Mecánica Computacional*, 22, 59–72.
7. Arumugam, P., et al. (2016). Design methods for compliant mechanisms used in new age industries—A review. *14(2)*, 223–232.
8. Ibrahim, A., et al. (2020). Finite element (FE) assisted investigation of a compliant mechanism made of various polymeric materials. *Materials Today Proceedings*, 1–7.
9. Karaku, R., et al. (2018). Novel compliant wiper mechanism. *Mechanical Science*, 9, 327–336.
10. Jagtap, S. P., et al. (2021). Applications of compliant mechanism in today's world—A review. *Journal of Physics: Conference Series*, 1969, 012013, 1–10.
11. Kota, S., et al. (2005). Design and application of compliant mechanisms for surgical tools. *Journal of Biomechanical Engineering*, 127, 981–989.
12. Lofroth, M., et al. (2019). Development of a novel modular compliant gripper for manipulation of micro objects. *Micromachines*, 10(313), 1–22.
13. Sebastian, L., et al. (2019). Modelling and design of flexure hinge-based compliant mechanisms. *Intech Open*, 1–24.
14. Howell, L. L. (2001). *Compliant mechanisms* (1–18). Mechanical Engineering Department, Brigham Young University, Wiley.

Designing and Optimization of Mechanical Gripper Finger Using Finite Element Analysis



Rohit Jadhav and Yogesh G. Kamble

Abstract This study deals with design analysis of a pick and place six axis jointed robotic arm and its optimization. The available gripper design grasps the circular objects by angular movement. The movement is caused by effect of pressure exerted by double acting cylinder. The mechanical gripper has payload capacity of a 1 kg load that includes weight of gripper. The study focuses on optimizing payload capacity by reducing gripper finger thickness and by creating perforation on fingers. Simulation is done such as to study structural analysis by calculating equivalent stresses and total deformation. It is found that the weight of perforated finger is 10% less and weight of finger after reducing thickness is found 33% less than that of existing finger. Also the study includes the load bearing capacity of this mechanical gripper.

Keywords Robotic arm · Mechanical gripper · ANSYS · FEA · Weight optimization

1 Introduction

A robotic arm is a manipulator consists of the arm links and set of joints. Basic parts of robotic arm are base, joints, links and an end effector. Wrist assembly motions in an arm and body are Vertical transverse, Radial transverse and rotational transverse. And motions in wrist assembly are Pitch, roll and yaw. An end effector is connected to the wrist of the robot arm which enables robots to perform a particular task. Grippers may be two fingered or more designed to grasp a parts like human hands. Grippers in used in applications where pick and place operations required.

Characteristics of gripper:

1. It must be able to grasp, lift, and release the part or group of parts that the process requires.
2. Some grippers use their grasping motion to detect the part's presence.

R. Jadhav (✉) · Y. G. Kamble
D.Y. Patil College of Engineering, Akurdi, Pune, India
e-mail: rjadhav@dypcoeakurdi.ac.in

3. Keep the weight of the tooling to a minimum.
4. A good gripper should have a straightforward design, accurate performance, be affordable, and require no maintenance.
5. It must be equipped with a collision sensor to accommodate overload conditions and safeguarding

Mechanical gripper uses mechanical fingers to grasp an object actuated by a mechanism. The fingers are either replaceable or internal part of gripper. If fingers are attachable and replaceable, they can be attached and changed. Wear and interchangeability are made possible via replaceable fingertips. To suit various part models, alternative sets of fingers can be created for use with the same gripper mechanism. To hold an object firmly, the gripper needs to be able to open and close its fingers and provide enough force to the object achieved by roughly modelling the part geometry on the contacting surfaces of the fingers. The friction between the fingers and the work part is the second method of holding the part. A gripper's primary job is to hold and release work parts during a material transfer process. When the object is firmly grasped by the gripper, the system is statically definable. The relationship between the actuating forces is its resulting gripping force, as well as the reactional forces at each joint of the gripping mechanism, can be determined by the classical method of static force analysis.

The following force equations can be used to determine the required magnitude of gripper force to grasp & hold the object:

$$\mu \text{ nf } F_g = W$$

where,

μ = Coefficient of friction between the component surface and the fingers' contact surface.

nf = number of fingers in touch.

F_g = Gripping force.

W = weight of part.

Type of gripper according to its movement.

1. Rotation movement gripper (Angular gripper): the gripper is based on a rotation movement to take the objects.
2. Translation movement (Parallel gripper).

2 Literature Review

Sabnis [1] focuses on the use of robotic arms and finite element analysis in waste management applications. Finite Element Analysis is done on Ansys software. Robotic arm was designed using aluminum sheet which has high strength to density ratio for handling and separating wastes in waste management facility.

Samadikhoshkho et al. [2] designed pneumatic four jaw gripper for pick and place operation in soda can automation industry. Razali et al. [3] studied about 3D modelling and FEA of five finger robotic gripper. This gripper modeled in creo software and analyzed motion to determine angular velocity and angular momentum by applying angular displacement. The FEA static analysis done on Ansys by applying forces 45 kgf, 90 kgf and torques 17,640 Nmm, 35,280 Nmm to determine stresses. They analyze for 2 materials titanium and alloy steel and FEA results shows that stress values of alloy steel are slightly less than titanium. So they have finalized to use alloy steel for robotic arm. Velineni and Suresh [4] studied about design of a new type of impactive gripper. One component of this gripper mechanism is a 4-bar mechanism with a single flexible link, while the other is an inverted slider crank mechanism. They have done graphical, computational and FEA for simulation. Paramesh et al. [5] discussed about design and development of an advance weld gripper for aristo robot. This gripper carries out tasks including automatically altering the height and detecting electrode consumption while regulating the arc. A variety of sensors are employed, including proximity, load, temperature, and piezoelectric. Badadhe et al. [6] designed an advanced multi objective gripper to grasp, carry and assemble complex shapes objects and allows translation movement which gives strong and firm grip to grasp objects. Aluminium material selected considering factors like working condition, load bearing capacity and weight. Chatuvedi et al. [7] designed an articulated robotic arm which can be used for material handling tasks. Cad drawing of parts of robotic arm was created using SOLIDWORKS. This Robotic arm has Base, Shoulder, Arm, Forearm, Wrist, connectors and gripper. Simulation of robotic arm is done by using ANSYS software, Cad model is converted into STEP format. Then after meshing, analysis of robotic arm done by applying different loads on gripper of arm. Raut et al. [8] Using experimental methods and finite element analysis, the modal analysis of a two-finger robot hand was completed. Two finger robot hand was designed which is pneumatically operated. Theoretical modelling was carried out using stress and deflection equations derived from the robotic clamp's free body diagram.

3 Input Parameters

Inputs parameters for this analysis includes existing design specifications of mechanical gripper. 2D sketch of design created which has cover body, gripper jaws and the removable external fingers. This mechanical gripper's specifications as shown in Table 1.

Existing gripper specifications:

Mechanical two fingered robotic gripper shows in Fig. 4. This gripper jaws are opened and closed in an angular motion in relation to the gripper body (Fig. 1).

Material properties:

Table 1 Existing gripper specifications

Sr. No	Factor	Information
1.	Gripper type	Angular moment gripper
2.	Degree of freedom	6 DOF
3.	No of fingers	2 Fingers
4.	Opening angle	40°
5.	Configuration	Jointed arm
6.	Connection	Pneumatic
7.	Pay load capacity	1 kg
8.	Gripper jaw material	Steel
9.	Gripper weight	250 g

Fig. 1 Mechanical gripper



Structural steel selected as this is the material of gripper jaws. Properties are shown in Table 2.

Table 2 Material selected

Sr. No	Properties	Value
1.	Yield strength	250 Mpa
2.	Poisson's ratio	0.3
3.	Young's modulus	2e + 05 Mpa
4.	Bulk modulus	1.66e + 05 Mpa
5.	Shear modulus	76,923 Mpa

4 Design by Analysis (FEA)

3D Modelling was done on the design modeler of Ansys workbench 2021 R2 as shown in Fig. 3. Mechanical gripper has 2 external fingers attached on gripper by using screws. External finger dimensions are 50 mm × 9 mm × 3 mm (Fig. 2).

Fig. 2 3D CAD model of existing gripper

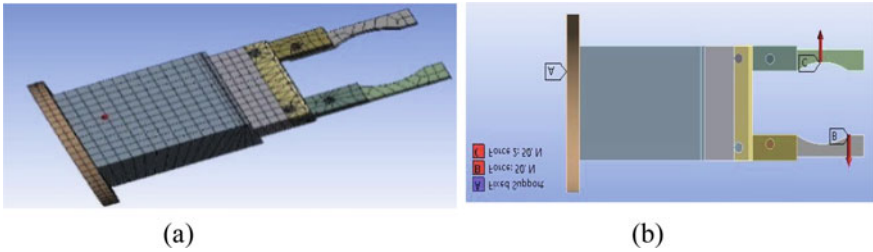
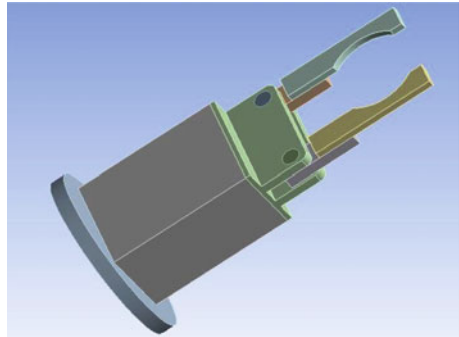


Fig. 3 a Meshed model, b boundary conditions

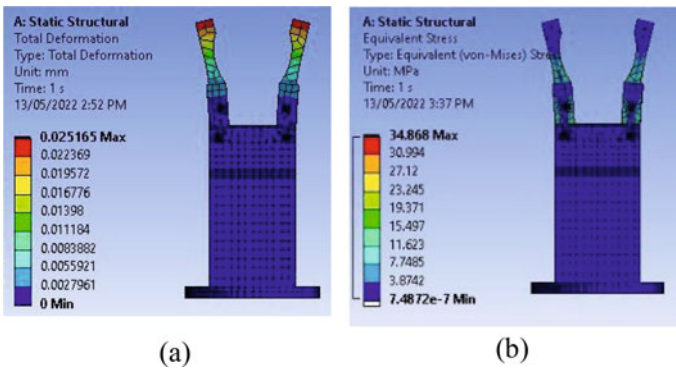


Fig. 4 a Total deformation, b equivalent stress for 40 N

Table 3 Load bearing capacity

Sr. No	Load (N)	Total deformation (mm)	Equivalent stress (MPa)	Factor of safety
1.	40	0.0251	34.86	7.16
2.	50	0.0314	43.58	5.73
3.	60	0.0377	52.30	4.77
4.	70	0.044	61.01	4.09
5.	80	0.05	69.73	3.58
6.	90	0.056	78.45	3.18
7.	100	0.062	87.17	2.86

Meshing is the technique of breaking the entire model down into a number of components so that when the load is applied to the model, the load is distributed evenly. Mesh types are Hex, Tet. For Hex dominant mesh, the face and targeted face should have same shape and elements are in quadrilateral shapes. In Tet mesh, tetrahedral shaped elements are there shown in Fig. 3a. Fixed support applied at the end of robot arm as shown in Fig. 3b at.

Point A and force of 50 N is applied on finger face as shown Fig. 3b. In processing stage, main solving process has been done. Boundary conditions applied that is one end of robotic gripper fixed. Load of 50 N applied on faces of gripper finger. For meshing Hex element type were selected because quadrilateral elements have high stiffness value and high accuracy than tetrahedral elements but hex dominant mesh not possible in every part of body. There is requirement that part should have same shape from object face to target face. So for remaining parts Tet mesh used having patch conforming method for. In this way, the mesh has generated. Then this problem solved by Ansys mechanical APDL solver.

Case I: Load bearing capacity of this gripper

For pick and place robot deformation should not exceeds 0.05, and factor of safety should be above 3. Load applied on the face of the finger (Fig. 4; Table 3).

5 Conclusion

- Structural analysis for load bearing capacity was done by applying different load conditions. Total deformation and equivalent stresses was calculated by applying load from 10 N to 100 N.
- It is found that at 80 N load, the fingers unable to do its operation of pick and place. So grippers load bearing capacity was found 80 N.
- Weight optimization has been done by creating perforation on fingers and by reducing 1 mm thickness of fingers.
- It is found that weight of perforated finger is 7.69 g that is 10% less than existing gripper finger.

- The weight after reducing thickness of finger is 5.59 that is 33% less than existing gripper finger weight.

References

1. Sabnis, N. V. (2018). A review: State of the art of robotic grippers. *International Journal of Engineering and Technology*, 5(5), 371–375.
2. Samadikhoshkho, Z., Farrokh, K. Z., Janabi-Sharifi, et al. (2019). A brief review on robotic grippers classifications. In *IEEE Canadian conference of electrical and computer engineering*.
3. Razali, Z. B., Daud, M. H., Datu Derin, N. A. (2015). *Finite element analysis on robotic arm for waste management application*, Conference paper
4. Velineni, P., Suresh, J., Naveen Kumar, C., & Suresh, M. (2020). Design of pneumatic gripper for pick and place operation (Four Jaw). *International Research Journal of Multidisciplinary Technovation*, 2(2), 1–8
5. Paramesh. J., Govindu, J., Purushotham, V. (2018). 3D modeling and finite element analysis of five finger robot. *International Journal of Creative Research Thoughts (IJCRT)*, 6(2), 2320–2882.
6. Badadhe, H. A., Singh, A. P., Roy, S., & Tiwari, M. (2018). *Fem based dynamic analysis of robot end gripper mechanism* (Vol. 7, Issue 11, Ver II, pp. 50–67). ISSN: 2319-6734
7. Chatuvedi, R., et al. (2020). Design and analysis of mechanical gripper of aristo-robot for welding. *Test Engineering and Management*, 83, 23202–23209.
8. Raut, V. A., Tambe, N. S., Li, Z. (2018). Optimal design and finite element analysis of robot gripper for industrial application. *International Journal of Engineering and Science*, 1–9.

Mechanical Investigation of Naval Alloy in Spinodal Decomposition



S. C. Jirapure and A. B. Borade

Abstract The present research mainly focuses on a formation of a new alloy called as Naval alloy, which is a combination of Copper, Nickel and Chromium. This alloy is spinodally decomposed and various mechanical tests and also corrosion tests are performed on this alloy in order to find out the optimized composition of this alloy, at which the alloy will provide maximum strength with minimum corrosion. As this alloy provides very high resistance to corrosion, so it has a large number of applications in the Naval environment and hence, it is called as the Naval alloy.

Keywords Cu–Ni–Cr spinodal alloy · Heat treatment · Corrosion · Marine environment

1 Introduction

Metals such as Copper, Nickel and Chromium are widely used engineering materials. In present investigation various hardening methods such as work hardening, solid solution hardening, grain boundary hardening, dual-phase hardening, precipitation hardening and order hardening are discussed. Along with the traditional hardening methods some of the recent approaches of hardening such as dispersion hardening, surface modification and Spinodal hardening are also discussed [1–5]. The main focus in this is spinodal hardening process and the Naval alloy. The Spinodal hardening process is studied in detail with its applications and advantages. From the comparative analysis it is found that, how the Spinodal decomposition is advantageous than Nucleation and Growth [6–10]. Basic introduction of the Naval alloy and where it is applicable is also mentioned. Properties of metals such as specific gravity,

S. C. Jirapure (✉)

Department of Mechanical Engineering, Dr. Rajendra Gode Institute of Technology and Research, Amravatil, Maharashtra, India

e-mail: sagarjirapure@rediffmail.com

A. B. Borade

Government Polytechnic, Gadchiroli, Maharashtra, India

Table 1 Composition of the alloys

Alloy No.	Atomic percent composition			Weight percent composition		
	Copper	Nickel	Chromium	Copper	Nickel	Chromium
13	80	10	10	82.12	9.48	8.40
14	70	20	10	72.43	19.12	8.45
15	60	30	10	62.58	28.89	8.53
16	50	40	10	52.57	38.83	8.60
23	70	10	20	73.22	9.66	17.12
24	60	20	20	63.28	19.47	17.25
25	50	30	20	53.16	29.44	17.40
26	40	40	20	42.88	39.58	17.54
33	50	20	30	53.77	19.85	26.38
34	40	30	30	43.37	30.02	26.61

hardness, ultimate tensile strength, modulus of elasticity, corrosion and castability are also studied [11–19]. Apart from this, the objectives of the present research work and the methodology to be followed is also discussed in this paper.

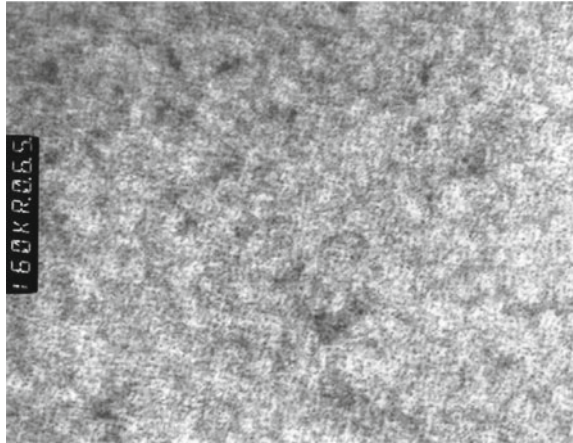
2 Preparation of Naval Alloy

The Naval alloy specimens of different compositions containing Copper, Nickel and Chromium as alloying elements are prepared by using Sand Casting technique. All the specimens are made identical i.e. same in shape and size. Further, these specimens will undergo various tests in order to find out the quality and usefulness of the resulting Naval alloy. An equal care must be taken while preparing this Naval alloy, that it should not be too expensive and hence, the use of Chromium must be less in the alloy as compared to Copper and Nickel, as Chromium is very costly. Some of the compositions of the alloys with minimum Chromium content as compared to others are Table 1.

3 Spinodal Decomposition

Spinodal decomposition of Copper–Nickel–Chromium alloy is done successfully resulting into a production of microstructures of Copper rich and Nickel rich regions, which are identical in structure but different in composition. FCC structure is obtained in both the resulting phases after the spinodal decomposition of this alloy. This spinodal structure is produced by ageing the alloy and it is observed that as

Fig. 1 Transmission electron micrograph showing the spinodal structure



ageing proceeds, coarsening of particles occurs. The aged specimens and spinodal structure of the alloy is observed under microscope. Figure 1 Shows the Spinodal microstructure of the alloy.

4 Mechanical Testing of the Alloy

The mechanical testing of the Copper–Nickel–Chromium alloy is done, which mainly includes tensile test, hardness test, specific gravity calculation and castability of the resulting alloy composition. As discussed the alloys containing minimum Chromium should be considered first for testing. So, the test results of only these alloys are shown in Tables 2, 3, 4 and 5.

From the tensile test, the ultimate tensile strength is found for all the specimens of the desired alloy and it is found that specimen no. 16 is having 58,399 lb per sq. in ultimate tensile strength which is maximum, whereas specimen no. 27 is having 11,353 lb per sq. in ultimate tensile strength which is minimum. Specific gravity is also calculated for all the specimens of the alloy and from the calculations it is seen that the specimen no 4 is having maximum specific gravity equals to 8.92, whereas the specimen no 61 is having minimum specific gravity equals to 7.28. Similarly, from the hardness test, it is found that the specimen no 55 is having the highest Brinell hardness number i.e. 228 and some of the specimens got broken while performing the hardness test. The quality of casting is also determined for all the specimens and it can be seen that some specimens are casted excellently while some are having the internal defects due to the poor castability of the particular alloy composition.

Table 2 Ultimate tensile strength of different specimens of alloy

Sample No.	Weight percent composition			Ultimate tensile strength in lb per sq. in
	Copper	Nickel	Chromium	
13	82.12	9.48	8.40	43,888
14	72.43	19.12	8.45	46,897
15	62.58	28.89	8.53	39,768
16	52.57	38.83	8.60	58,399
23	73.22	9.66	17.12	43,987
24	63.28	19.47	17.25	42,243
25	53.16	29.44	17.40	44,213
26	42.88	39.58	17.54	54,245
33	53.77	19.85	26.38	45,332
34	43.37	30.02	26.61	53,221

Table 3 Specific gravities of the different specimens of alloy

Sample No.	Weight percent composition			Specific gravities at 25 °C
	Copper	Nickel	Chromium	
13	82.12	9.48	8.40	8.57
14	72.43	19.12	8.45	8.81
15	62.58	28.89	8.53	8.72
16	52.57	38.83	8.60	8.75
23	73.22	9.66	17.12	8.71
24	63.28	19.47	17.25	8.34
25	53.16	29.44	17.40	8.62
26	42.88	39.58	17.54	8.52
33	53.77	19.85	26.38	8.49
34	43.37	30.02	26.61	8.42

5 Result and Comparison

The comparative analysis of the results of all the tests performed on the all specimens of the alloys is made. This analysis for the ternary alloys with minimum chromium content which are important for the economical point of view is shown in Table 6.

Table 4 Hardness of different specimens of alloy

Sample No.	Weight percent composition			Diameter of impression	Brinell hardness number
	Copper	Nickel	Chromium		
13	82.12	9.48	8.40	6.30	86
14	72.43	19.12	8.45	5.80	103
15	62.58	28.89	8.53	5.00	143
16	52.57	38.83	8.60	4.73	161
23	73.22	9.66	17.12	6.40	82
24	63.28	19.47	17.25	6.20	89
25	53.16	29.44	17.40	5.90	99
26	42.88	39.58	17.54	4.80	156
33	53.77	19.85	26.38	5.50	116
34	43.37	30.02	26.61	5.30	126

Table 5 Casting quality of different specimens of alloys

Sample No.	Weight percent composition			Kind of casting
	Copper	Nickel	Chromium	
13	82.12	9.48	8.40	Sound
14	72.43	19.12	8.45	Sound
15	62.58	28.89	8.53	Sound
16	52.57	38.83	8.60	Small but sound
23	73.22	9.66	17.12	Good
24	63.28	19.47	17.25	Good
25	53.16	29.44	17.40	Good
26	42.88	39.58	17.54	Very good
33	53.77	19.85	26.38	Excellent, there was some segregation of Cr at top of casting
34	43.37	30.02	26.61	Good

Table 6 Comparative analysis of mechanical testing of the alloy

Alloy No.	Ultimate tensile strength	Specific gravity	Brinell hardness no	Castability
13	43,888	8.57	86	Sound
14	46,897	8.81	103	Sound
15	39,768	8.72	143	Sound
16	58,399	8.75	161	Small but sound
23	43,987	8.71	82	Good
24	42,243	8.34	89	Good
25	44,213	8.62	99	Good
26	54,245	8.52	156	Very good
33	45,332	8.49	116	Excellent, there was some segregation of Cr at top of casting
34	53,221	8.42	126	Good

References

- Antonov, N. M., & Popov, I. Y. (1999). Model of spinodal decomposition of phases under hyperbolic diffusion. *Physics of the Solid State*, 41(5), 824–826.
- Barrett, C. S. (1952). Structure of metals (2nd Ed.). In *Metallurgy and metallurgical engineering series*. McGraw-Hill Book Co., Inc.
- Binder, K., Billotet, C., & Miold, P. (1978). On the theory of spinodal decomposition in solid and liquid binary mixtures. *Zeitschrift für Physik -Condensed Matter*, 30(2), 183–195.
- Cohen, A. (2006). Copper standards. In *ASTM standardization news* (pp. 34–43).
- Copper-nickel alloys, properties and applications*. Copper Development Association, British Standards Institution, London, W1A 2BS TN30 (1982).
- Copper—The vital metal*. Copper Development Association, British Standards Institution, London, W1A 2BS CDA Publication No. 121 (1998).
- Cost-effective manufacturing—Design for production*. Copper Development Association, British Standards Institution, London, W1A 2BS CDA Publication No. 97 (1993).
- Copper and copper alloys—Compositions, applications and properties*. Copper Development Association, British Standards Institution, London, W1A 2BS publication No. 120 (2004).
- Cribb, W. R., & Raka, J. (2002). Copper spinodal alloys. In *Advanced materials and processes, AP0056* (pp. 01–04).
- Erukhimovich, Y., & Prostormolotova, E. V. (1997). New approach to the theory of spinodal decomposition. *Journal of Experimental and Theoretical Physics*, 66(6), 463–469.
- Findik, F. (2013). Modulated (Spinodal) alloys. *Periodicals of Engineering And Natural Sciences*, 1(1), 47–55. ISSN 2303-4521.
- Harald, P. C., & Schaftenaar. (2008). *Theory and examples of spinodal decomposition in a variety of materials* (1–17). Utrecht University, Padualaan 8, 3584 CH Utrecht, The Netherlands.
- Kodgire, V. D., & Kodgire, S. V. (2011). *Material science and metallurgy for engineers* (30th Ed.). Everest Publishing House. ISBN: 8186314008.
- Kuksin, A. Y., Norman, G. E., & Stegailov, V. V. (2007). *The phase diagram and spinodal decomposition of metastable states of Lennard-Jones system* (Vol. 45, No. 1, pp. 37–48). High Temperature- Pleiades Publishing, Ltd.
- Petrishcheva, E., & Abart, R. (2012). Ex-solution by spinodal decomposition in multi-component mineral solutions. *Acta Materialia*, 60, 5481–5493.

16. Ramnarayan, H., & Abhinandan, T. A. (2003). Spinodal decomposition in fine grained materials. *Bulletin of Materials Science*, 26(1), 189–192.
17. Jirapure, S. C., & Borade, A. B. (2017). Measurement of mechanical properties and microstructure of Cu–Ni–Cr spinodal alloy. *International Journal of Advanced engineering and Management*, 2(3), 78–81.
18. Jirapure, S. C., & Borade, A. B. (2014). A new approach of strengthening-spinodal decomposition. *International Journal of Applied Sciences and Engineering Research*, 3(5), 1021–1029.
19. Jirapure, S. C., & Borade, A. B. (2014). Naval corrosion-causes and preventions. *International Journal of Engineering Science & Research Technology*, 263–268.

Filament Fabrication for 3D Printing Using Waste PET Material



Akshay R. Shah, Eshwar Paygude, Rohit Sonawne, Pradeep V. Jadhav, and Sachin M. Khomane

Abstract Disposal of plastics has lately developed into a critical concern in environmental protection and trash management. Polymer composites have found application in many parts of everyday life and many industries. Along with their expanded usage, the issue of plastic waste developed since the following withdrawal from use, they became tenacious and poisonous wastes. The potential of reusing polymeric materials affords a possibility of recycling them and permits efficient waste utilization to get the goods required. The market for 3D printing is growing quickly. A broad variety of thermoplastic materials, including recyclable materials, may be used to make printable filaments for 3D printers. The goal of this project is to create 1.75 mm-diameter PET filament for 3D printing using scrap PET material and inexpensive, readily accessible components. The filament manufacturing method and machine operation are described in this paper.

Keywords 3D printer filament · Recycling · PET bottles · Filament maker machine

1 Introduction

3D printing is becoming a frequently used technology of fast prototyping, creating fully working models and projects. Researchers are using 3D printing in a variety of applications where it is feasible; many components are tiny and must be tough, such as gears, motor mountings, and other components. Even now, researchers are searching

A. R. Shah · E. Paygude · R. Sonawne · P. V. Jadhav (✉)
Bharati Vidyapeeth (Deemed To be University) College of Engineering, Pune, India
e-mail: pvjadhav@bvucoep.edu.in

A. R. Shah
e-mail: arshah20-ra@bvucoep.edu.in

S. M. Khomane
SVERI's College of Engineering, Pandharpur, India

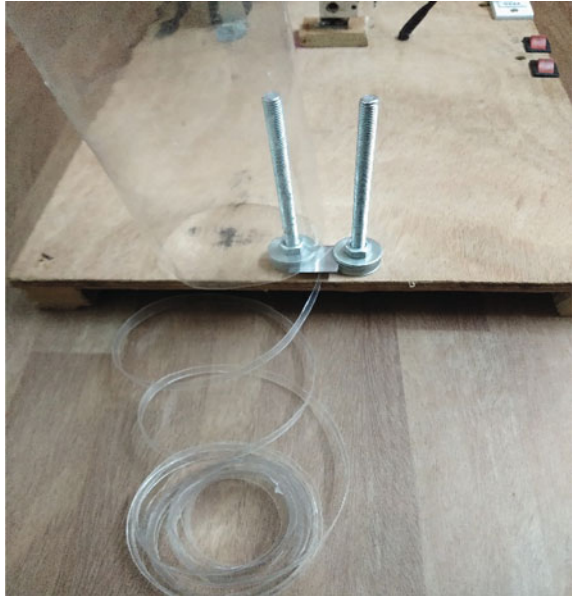
for ways to create composite filaments and improve prints' mechanical qualities [1–3]. The possibilities offered by 3D printing are irreplaceable, with extremely low costs and quick stages of computer model conversion into a real product. 3D printing enables us to manufacture components that are unattainable by other techniques. Many materials and components are wasted during the prototype process due to failed prints, poorly made models, or inadequate print optimization. There is a lot of waste material produced while making a totally satisfactory item that is discarded. Living in an era where lots of waste is created, including vast numbers of PET bottles, might relate this wasting procedure with enthusiasm and work [4]. The goal of this research, similar to that of other academics, is to lower the environmental impact and find ways to reuse recyclable waste materials for 3D printing. This article describes a simple mechanism that converts discarded PET bottles into 3D printer filaments. In addition to PET filament, which is particularly strong, chemically and thermally resistant, flexible, and simple to print, there are many alternative materials available in the market [5]. Recycling facilities have developed many ways to recover and reuse plastics, spurred by market demand and environmental laws. The process of extruding molten plastic into tiny pellets is sometimes referred to as mechanical recycling or conventional recycling in this sector. When using a single kind of material, like PET, mechanical recycling is most effective. The recycled plastic pellets are a more affordable and environmentally friendly alternative to virgin plastics since they are offered to producers as raw materials. The pellet shape enables the plastic to be readily disseminated and utilised in the creation of new components. Because recycled resin is often downcycled into less expensive goods because recycled pellets have inferior and irregular mechanical characteristics [6]. The stages of sorting, cleaning, resizing, compounding, and spooling are typically performed in all plastic recycling operations, regardless of their size.

2 Methodology

The methodology includes constructing a setup for cutting the bottles and manufacturing filament, which is necessary for 3D printing. The most common types of empty water or waste bottles are first required. It should be cleansed from dust, labels, and adhesive. The bottle's top is trimmed. Using the bottle cutter created specifically for this purpose, a long strip of 5 mm width is produced. Depending on the thickness of the material, the width of the strip may be altered.

Depending on the size of the bottle, the length of the generated strip might be up to 10 m. The next step is to wound the plastic string up on the spool. The loose end of the strip should be small to make it simpler to fit the bottle strip into the heating block element indicated in Fig. 1.

Fig. 1 A strip made out of a bottle



2.1 The Process of Creation

This machine has a basic design and mechanism. As a result, every component of the machine is completely interchangeable. Every part is fastened to the hardwood bottom by screws at properly designated locations. Figure 2 displays the machine's design.

The Spool has given rotational motion at a speed of 5 rpm by using a synchronous motor which is driven by a Direct Ac supply of 230 V. The motor delivers a torque

Fig. 2 Machine design

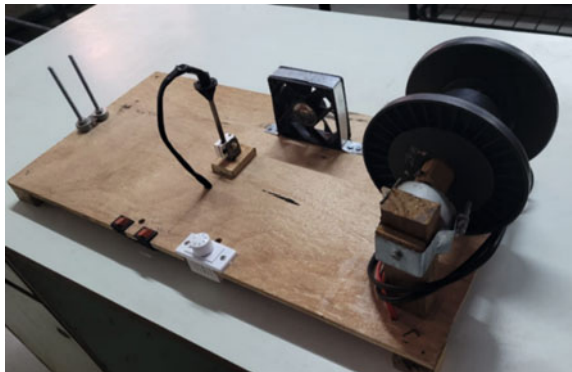


Fig. 3 Spool attached with motor for receiving the filament

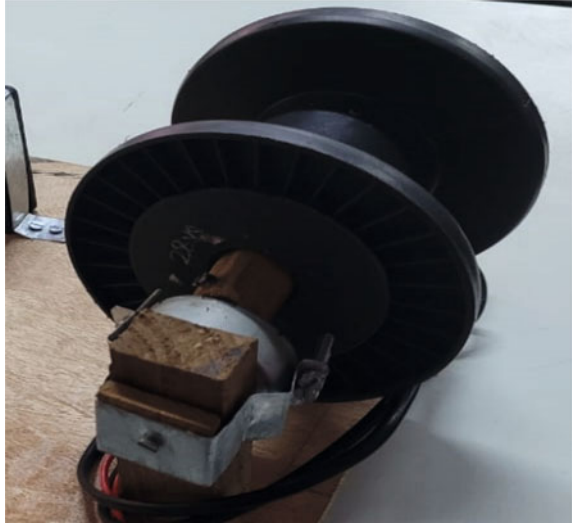
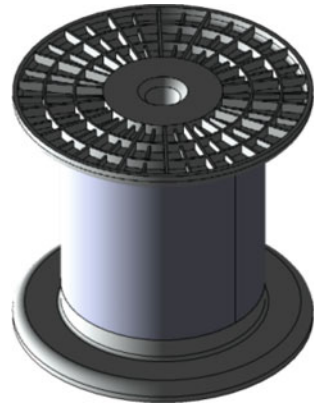


Fig. 4 CAD model of spool



of 4kgf.cm. The spool must have this level of torque in order to function effectively, since extracting the filament from the nozzle demands a specific amount of force. Specifications are shown in Figs. 3 and 4.

2.2 Design of the Heating Block

The heating block seen in Figs. 5 and 6 is a typical 3D printing heating block; however, a specifically drilled nozzle enables the extrusion of filaments with a 1.75 mm diameter. A plastic strip is drawn from a nozzle into a filament after being plasticized and passing through the heating block.

Fig. 5 Design of the heating block

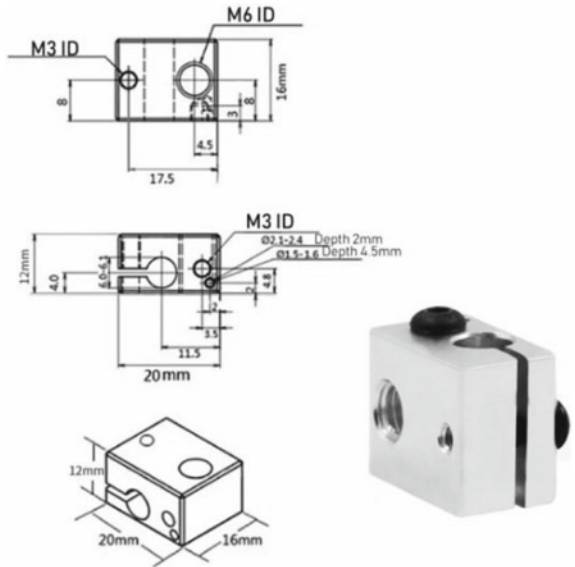
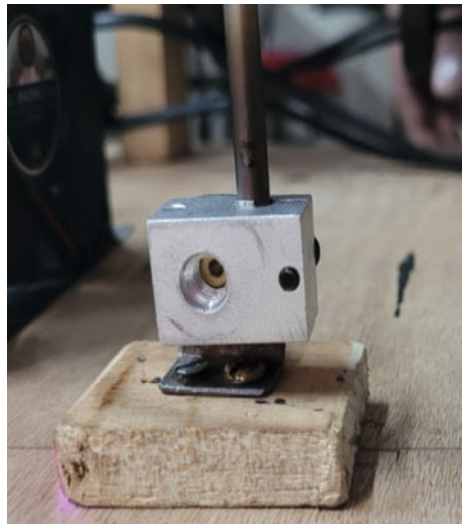


Fig. 6 Heating block with Heating element



There is an airflow at the end of the nozzle that cools and cures the newly formed filament. Cooling fans are used to cool the filament after it has been extruded from the nozzle, allowing for the production of flawless filament. Because wood is a poor conductor of heat, all pieces are assembled on it.

Fig. 7 Machine operation

2.3 Production of Filaments and Machine Operation

In order to considerably assist the first extrusion of the filament via the nozzle, a narrower plastic bottle strip should be put through the cold nozzle, which is the power supply/initial feed, before connecting the power supply. After that, switch on the power supply. The heating element now begins to transmit heat to the heating block, reaching a temperature of 260 °C. After a few minutes, when the heating block reaches the proper temperature, the plastic string must be manually dragged until it can be fastened to the spool. By turning on the motor, the spool begins to rotate, and the plastic strip is driven through the hothead nozzle, cooled by the airflow from the fan, hardened, and then wound directly on a spool, as shown in Fig. 7.

A spool is positioned in front of the heating block and head of the nozzle for accepting the filament and winding it on the spool; this is depicted in Fig. 8.

2.4 Use of PET MATERIAL

PET filament may be used to print calibration cubes, and certain 3D printer calibrations are also required; excellent results were obtained at temperatures as high as 260 °C, a bed temperature of 80 °C, and a printing speed of 35 mm/s. In the image below, the printing procedure is shown. Figures 9 and 10 depict the printing procedure.

Fig. 8 Filament creation process



Fig. 9 BPET-made filaments



Fig. 10 Shows BPET-made filaments steps (Bottle-strips-filaments)



The resulting material has a very high hardness in comparison to other materials, and the surface is lustrous. Due to the unusual width of the bottle strip, we can also see the bumps that were created as a consequence of some dirt that was not removed when the filament was produced in the finished piece. Plastic bottles have one major benefit over glass ones: they can be recycled endlessly. PET is a rare polymer because it can be recycled indefinitely into the same shape. Consider it a closed-loop recycling solution. Recycled PET, often known as “rPET” is widely used to create a variety of new products. This may include clothing, car components, food and non-food packaging, and bottles. Depending on the application, rPET will be blended with original PET.

3 Creating Filament from Plastic Bottles

Following are the methods used to test converting PET bottles into filament:

1. Waste water bottles were gathered, cleaned, and their exterior lids or seals were also taken off.
2. The bottles were heated to flatten their exterior surfaces.
3. After the bottles had cooled, they were split into smaller strips (i.e., 5 mm wide).
4. The acquired strips were then put on the spool.
5. After feeding the PET strips into the aluminium heating block and nozzle or filament extruder.
6. It is then extruded from the nozzle end and given the desired filament thickness.
7. The filament is then coiled on the spool.

3.1 List of Materials Used

Following is the list of materials used to develop the product.

1	Wooden board	9	On–Off switches
2	Brass Nozzle \approx 1.75 mm (output diameter)	10	Wire coating tube
3	Aluminum heating block	11	Voltage regulator box
4	Heating element—35w	12	Nut-bolts
5	Synchronous motor	13	Washers
6	Filament holder—Spool	14	Cutter blade
7	Filament holder nut	15	12 V DC FAN
8	Connecting wires	16	12 V DC power adapter

4 Conclusion

Plastics are difficult to biodegrade, and the process significantly pollutes the environment. Recycling was discovered to be the best way to preserve post-consumer plastics while adhering to the circular economy concept. Making complex plastic objects at home rather than in a factory is now feasible thanks to desktop 3D printing. The concept is that customers may use their old materials to directly produce goods. This offers various financial benefits: Environmental concerns and the purchase of commercial plastic items. Additionally, one must be aware that various plastics yield various filaments. High-density polyethylene shampoo bottles, are generally simple to turn into filament, but since they shrink more when they cool than other polymers, they are challenging to print with. The PET material, on the other hand, spools poorly as filament because it is brittle and prints cheaply. Though the use of recycled filament for 3D printing is becoming increasingly popular, Because of the development of 3D printing in recent years, greater attention is being focused on plastic recycling.

References

1. Mikula, K., et al. (2021). 3D printing filament as a second life of waste plastics—A review. *Environmental Science and Pollution Research*, 28(10), 12321–12333.
2. Jandyal, A., et al. (2022). 3D printing—A review of processes, materials, and applications in industry 4.0. *Sustainable Operations and Computers*, 3, 33–42.
3. Allouzi, R., Al-Azhari, W., & Allouzi, R. (2020). Conventional construction and 3D printing: A comparison study on material cost in Jordan. *Journal of Engineering*.
4. Tylman, I., & Dzierżek, K. (2020). Filament for a 3D printer from pet bottles-simple machine. *International Journal of Mechanical Engineering and Robotics Research*, 9(10), 1386–1392.
5. Raza, S. M., & Singh, D. (2020). Experimental investigation on filament extrusion using recycled materials.
6. Pakkanen, J., et al. (2017). About the use of recycled or biodegradable filaments for the sustainability of 3D printing. In *International conference on sustainable design and manufacturing*. Springer.

Inventory Management for Power Tiller Using TOC Technique



Shubhankar R. Narwade and Mukund S. Kale

Abstract The cost-effective management of spare parts is essential for manufacturing and service companies. Production and inventory management are crucial components in improving these manufacturing processes, and as a result, a variety of information systems, such as Material Requirements Planning (MRP) and Enterprise Resource Planning (ERP), have been developed. Goldratt developed a proposal for the management of operations and production in the latter part of 1984. The Theory of Constraints (TOC), as it is currently known, provides a consistent management approach for managing the organization. Theory of Constraints is a key to identify Constraints or Bottleneck and then eliminates or rejects. This study consists of implementation of TOC method, is done for inventory management through buffer penetration sheet. Buffer penetration sheet consists of colour coding scheme through which daily coverage of parts can be easily recognized. It is easy and simple to understand and operate.

Keywords MRP · ERP · ABC analysis · Theory of constraints · Microsoft excel

1 Introduction

Inventory management includes the entire inventory control process, including raw materials to finalized products. Inventory management is the process of streamlining stocks in almost any management system in order to manage surplus and shortage of raw materials, items work in progress (WIP), and finished products. Inventory control is critical to a company's health because it ensures that there are never too many or too few items on hand, reducing the chance of stock outs and errors in operations or data records. Just-in-time (JIT) and Materials Requirement Planning (MRP) are two most common inventory management techniques [1–3]. When there is a considerable inventory, the risk of waste, theft, damage, or demand fluctuations is increased. Inventory should be maintained, and if it isn't sold quickly, it may have

S. R. Narwade (✉) · M. S. Kale
Government College of Engineering, Karad, India
e-mail: shubhankarnarwade@gmail.com

to be destroyed or sold at a discount. Because of these factors, inventory management is vital for companies of all sizes. It can be straightforward to make challenging decisions regarding whether to replenish inventory, how much to purchase or produce, how much to buy, when to sell, and how much to sell for. Small businesses typically use spreadsheet formulas (Excel) to calculate recording points and amounts while manually tracking their inventory. Larger businesses will employ specialised enterprise resource planning (ERP) software. As a result, holding too much stock is costly and reduces cash flow [4]. One measure of efficient inventory control is the inventory turnover rate. Inventory turnover is an economic metric that measures the frequency with which stock is sold over a certain time period. A company does not want to have more inventory than sales. A poor inventory turnover rate may result in dead stock or unsold inventory. The Theory of Constraints was developed by Dr. Eliyahu M. Goldratt, an Israeli physicist (TOC). The Theory of Constraints is a management philosophy approach that focuses on identifying the system's weak points. When Goldratt and his colleagues were developing software to optimise manufacturing processes in the 1970s, they came up with the term "optimised production technology" (OPT). TOC's application programme has been extended to include marketing, supply chain management, and retail. The TOC philosophy considers all processes in a system as rings in the same chain, all of which are interdependent. The TOC philosophy focuses on the chain's weakest links (bottlenecks) and constraints in the chain (system). TOC's goal is to maximise throughput contribution while minimising investments and operational expenses.

2 ABC Categorization

ABC analysis is a prominent technique for categorising and understanding inventories. If you have handling inventory at a Power Tiller manufacturing plant, each Power Tiller requires various parts (almost 700) to assemble a machine, some of which are costly, while others are cheap. As a result, we have classified parts based on cost by ABC category as follows (Table 1).

After the categorization of parts into ABC categories, we are taking 10 parts of A category parts on the basis of commodities such as casting, proprietary, sheet metal.

Table 1 ABC Categorization

Class	Value	Units
A	70–80%	105
B	15–20%	130
C	5–10%	463

3 Buffer Management in Theory of Constraints (TOC)

Buffers are utilized in critical chain management to help with project management decisions. Some of the safety buffer will be used up if the critical chain is affected. The status of their projects must be meaningfully known by the project manager, and they must be aware of when to take corrective action [5, 6]. The required information is provided by the buffer utilization rate. Usually, buffers are divided into three equal time periods known as “expected variation,” “normal variation,” and “abnormal variation.” They have some similarities with the traffic signal control light’s green, yellow, and red colours. But in this system, we are using five colour codes with their status, which are as follows:

The figure shown with colour coding is as follows (Fig. 1).

White: The white colour coding indicates that we have an abundance of the parts. It is applicable when the coverage in days exceeds 8 days.

Green: Green colour coding indicates that we have a healthy stock of parts. It is suitable when the coverage in days is 7–8 days.

Yellow: The yellow colour coding indicates that we have a comfortable stock of parts. It is suitable when the coverage period is 4–6 days.

Red: The red colour coding indicates that we are almost out of stock. It is useful when the coverage in days is 2–3 days.

3.1 Buffer Penetration Sheet

The following Excel spreadsheet presents the one-day status of ten parts, with columns such as Part name, which represents the part name; commodity, which represents the part’s commodity; and so on. The monthly plan, which displays the monthly demand for each part, received from MRP, followed by stock (on hand), under inspection (UI), and in transit, acquired from the ERP software, and finally a sum of those three columns, determined from the total stock level. The next column

Coverage in Days	Colour code	Colour	Status
>8	White		Excessive Stock
7-8	Green		Health Stock
4-6	Yellow		Comfortable stock
3-2	Red		Near Stockout
0-1	Black		Stockout

Fig. 1 Colour coding status

represents lead time for each part, which is different for each part. The next column is the one-day requirements of the part that is determined by: in one month, there are 30 (working days). We may calculate by monthly plan to working days.

Summation of on hand stock, in transit stock and under inspection stock is done to calculate Total stock level.

$$\text{Total stock level} = \text{On hand quantity} + \text{Under inspection} + \text{In transit}$$

Lead time depends upon the time the supplier will require to supply the parts. One day requirement gives the required number of parts for one day.

$$\text{One day requirement} = \frac{\text{Monthly plan of part}}{\text{Monthly requirement of part}}$$

Coverage in days gives the data for count of the days the stock will be sufficient. Coverage in is calculated as the ratio of Total stock by One day requirement.

$$\text{Coverage (in days)} = \frac{\text{Total stock level of part}}{\text{one day requirement of part}}$$

Based on the colour coding scheme mentioned in pt. (i) the colour coding is defined on the bases of their status such as, Excessive stock, Healthy stock, Comfortable stock, Near stock out, stock out. Here, we are using colour coding like, White, Green, Yellow, Red and Black is used which is based on the coverage in days of the parts. When the coverage in days of parts changes automatically the colour coding will be changed, from that colour code the action taken will be different for each colour. The main concentration of parts buyer is on the Red and black colour code parts. When buyer will update the data taken from the ERP on the daily bases the colour code will automatically changes, and the action is triggered on the bases of colour code (Fig. 2).

The following actions are triggered on the basis of colour code:

For, White colour code, no action should be taken by the buyer of that part, as we have excessive stock of that part. White colour code means we have excessive stock of these parts, and this part is likely to be in stock for greater than 8 days. Here no action is required for purchasing as we have adequate stock. Taking corrective action at this stage when none is required can waste productive time and cause loss of target.

For, Green colour code also No action should be taken by the buyer of that part, as we have healthy stock of that part. Green colour code indicate that the stock of the part will exist for 7–8 days. In this no action is needed as we have sufficient stock. For, yellow colour code action taken is still watching and continuous monitoring part is necessary, we have comfortable stock. Yellow colour coding, that is the parts are in Comfortable stock zone. Which means it can last for not more than 4–6 days. In this case an action of plan must include monitoring for excess demand to avoid replenishment delays.

											Working Days=	30
Sr.No	Part Name	Commodity	Monthly plan June	Stock (On Hand)	Under Inspection	In Transit	Total Stock level	Lead Time in Day	One day Requirement	Coverage (In day)	Colour Code	
1	CRANKCASE FOR POWER TILLER	Casting	250	39	0	0	39	15	8	5	Yellow	
2	RADIATOR (4R) WITH COOLANT B	Proprietary	594	155	5	5	165	45	20	9	Green	
3	FLYWHEEL	Casting	625	111	24	0	135	15	21	7	Green	
4	CRANK SHAFT FOR POWER TILLER	Casting	666	271	0	0	271	15	22	13	Green	
5	MAIN GEAR BOX HOUSING, EXCLU	Casting	175	15	0	0	15	15	6	3	Red	
6	FUEL TANK FOR POWER TILLER	Sheet Metal	573	156	0	0	156	15	19	9	Green	
7	SHAFT ASSLY ROTARY EXCLUSIVELY	Sheet Metal	150	76	0	0	76	10	5	16	Green	
8	SILENCER WITH HEAT SHIELD	Sheet Metal	725	107	0	20	127	10	24	6	Yellow	
9	BLADE TILLING LH EXCLUSIVELY F	Proprietary	6500	1728	0	0	1728	30	217	8	Green	
10	BLADE TILLING RH EXCLUSIVELY F	Proprietary	6500	1728	0	0	1728	30	217	8	Green	
11	FAN ASSEMBLY	Proprietary	599	165	0	5	170	70	20	9	Green	

Fig. 2 Buffer penetration sheet

For, Red colour code, the immediate action should be taken by the buyer of that part, as we are near stock out zone. In this case as the parts will be out of stock within 2–3 days prompt action is required to be taken by the buyer to avoid replenishment of parts. In this case immediate action means a call or mail should be send to supplier so that the supplier can supply the required quantity of parts within the specified lead time.

For, Black colour code in rare case this colour code happens as immediate action is taken in red colour code, even though due to some reasons action is not taken by the buyer then black colour code is seen. Black colour code means that the part is out of stock and the production will nearly go to stop at that time the immediate action should be taken by the buyer and it is necessary [7, 8].

3.2 Case Study on Crankcase

A prototype developed using Microsoft excel based system by using TOC is shown in the point 3.1 The developed prototype model is used for trial run for a month. From the prototype developed summary of single part for 10 days is explained below. TOC method of inventory management is implemented for Crankcase for ten days. The below table shows change in colour code with respect to change in coverage days for crankcase. Monthly plan of Crankcase is 250 parts this data is taken from MRP. On hand stock, under inspection and in transit stock of parts data is taken from ERP.

Inventory management for crankcase is done as we have updated the on-hand stock, in transit, under inspection, with respect to changes in total stock level, coverage in days will changes using above mentioned formulas and colour code depends upon change in coverage in days. In order to avoid too much of excessive stock which will only take more place in store house and also will increase the cost of inventory. This method is very efficient as only required number of parts will be

stored. Also order for purchasing are placed before total stock out zone the chances for shortages is also eliminated hence with change in colour code this system helps us to take corrective action and also maintain the stocks (Table 2).

Table 2 Case study on crankcase

Day	Stock (On Hand)	Under Inspection	In Transit	Total Stock level	Lead Time (in Days)	One day Requirement	Coverage (In days)	Previous Colour code	Today's Colour code	Action Triggered
1	30	0	0	30	15	8	4	Yellow	Yellow	Still watching
2	35	5	0	35	15	8	5	Yellow	Yellow	Still watching
3	40	10	5	55	15	8	7	Yellow	Green	No action taken
4	40	10	10	60	15	8	8	Green	Green	No action taken
5	50	10	10	60	15	8	9	Green		No action taken
6	55	10	5	70	15	8	9			No action taken
7	20	10	0	30	15	8	4		Yellow	Still watching
8	15	5	0	20	15	8	3	Yellow	Red	Immediate action taken
9	5	0	0	5	15	8	1	Red	Green	No action taken
10	25	5	0	30	15	8	4	Green	Green	No action taken

4 Result and Discussion

TOC method applied is easy and simple to understand and operate. It can be used as an alternative method to ERP. From that study it is understood that as there is change in stock level of the parts colour code changes. Each stock level is associated with different colour from which we can easily determine in danger stock, stock that is in near stock out zone that is stock will finish, safe stock that is comfortable stock and health stock and excessive stock. This mechanism so made is self-regulating as in as the stock level changes automatically change in associated colour code is seen. This system is designed to avoid replenishment of parts. As immediately we see red colour code call or email is sent to supplier for ordering of parts to avoid replenishment delays. Next day we can see red colour code changes to yellow colour code, as per the lead time inventory level is restored hence, we can see a reverse order of colour code that is from near stockout zone to comfortable zone to healthy zone to excessive zone (white colour code). Black colour code (stockout) zone is seen very rarely as ordering of parts is done at red colour code (near stock out zone) This mechanism is a cheap alternative to very costly software. This concept has been explained by using Microsoft excel. This system can be implemented in software and various more facilities can be provided such as direct contact through the software to the supplier on entering of part stock level to red colour code, automatic generation of receipts and so on.

5 Conclusion

The new concept, Theory of Constraints is implemented based on daily data of inventory buffer management to predict and avoid the potential excessive stock of parts or stock outs of the part. TOC is advantageous to manufacturing organization which have streamline production.

The suggested inventory buffer management offered following benefits:

- It improves capacity: Manufacturing more products are achieved by the constraints being optimized.
- It increases the profit: For most companies, it is the TOC's primary goal.
- It reduces the lead time: optimizing the Constraint results in smoother and faster product flow.
- By eliminating bottlenecks, it reduces inventory and the amount of work in progress.

References

1. Chuanpeng, Z., & Yi, Z. (2021). Study on inventory management optimization of small and medium sized retail companies in the context of new retail: Based on AHP. *Asian Journal of Business and Management*, 9(5). ISSN: 2321-2802.
2. O. Alaskaria, R., Pinedo-Cuencab, M. M., & Ahmad, C. (2021). Framework for on flexible implementation of enterprise resource planning (ERP) systems in small and medium enterprises (SMEs): A case study. In *30th international conference automation and intelligent manufacturing*.
3. Madanhirea, I., & Mbohwb, H. (2016). Enterprise resource planning (ERP) in improving operational efficiency: Case study. In *13th global conference on sustainable manufacturing—Decoupling growth from resource use*.
4. Harish, U. C. (2019). Implementation of theory of constraints (TOC) in a manufacturing plant. *International Journal of Advanced Scientific Research and Management*, 4(5), 228–232, May 2019.
5. Goldratt, E. M., & Cox, J. (1993). *The goal*. Second Revised Edition, Productivity Press (India Private Limited).
6. Simsit, Z. T., et al. (2014). Theory of constraints: A literature review. *Social and Behavioral Science*, 150, 930–936, Elsevier
7. Izmailov, A., et al. (2016). Effective project management with theory of constraints. *Social and Behavioral Sciences*, 229, 96–103, Elsevier.
8. Yuan, K. -J., et al. (2014). Enhancement of theory of constraints replenishment using a novel generic buffer management procedure. *International Journal of Production Research*.

Mathematical Modeling, Analysis and Simulation of MR Fluid Damper



Hanmant Salunkhe, Surendra Thikane, and Shivaji Sadale

Abstract In recent years, magnetorheological fluid dampers have been paid more attention because of their smart nature and properties. This paper presents the mathematical background of magnetorheological fluid dampers and their use in advanced technological applications. The main objective of this paper is to delineate how to find equations of motion for dynamics of MR dampers for different degrees of freedom and how to find their responses for various damping forces. In this paper, the performance of a MR damper are compared by MATLAB simulation.

Keywords Magnetorheological fluid · Vibration control · Magnetorheological damper

1 Introduction

John Rabinow first discovered Magnetorheological fluids in the 1940's at the United States National Bureau of Standards. Recently, researchers have shown an increased interest in magnetorheological fluids due to their smart nature and properties. Lord Corporation has been creating magnetorheological fluids and magnetorheological fluid-based gadgets since the mid-1990s. In the mid-1990s, Lord Corporation started to develop and fabricate magnetorheological dampers. Magnetorheological dampers are among the most encouraging SAS system utilized these days in prosthetic legs and vehicle suspension systems [1]. In addition, Lord Corporation also creates a rotary magnetorheological brake system that has been used for various applications.

H. Salunkhe (✉) · S. Sadale
Department of Technology, Shivaji University, Kolhapur 416004, India
e-mail: hps_tech@unishivaji.ac.in

S. Sadale
e-mail: sbs_tech@unishivaji.ac.in

S. Thikane
Department of Mathematics, Shivaji University, Kolhapur 416004, India
e-mail: surendra.thikane@gmail.com

MR dampers are not, in any case, confined to vehicle applications. Recently, the U.S. military has indicated enthusiasm for utilizing magnetorheological dampers to adjust gun recoil on Naval gun turrets and field artillery. Magnetorheological dampers are also utilized in the stabilization of buildings during earthquakes [2].

We expect that the mechanical properties of magnetorheological fluids make them appropriate for some advanced engineering applications. Notwithstanding dampers and brakes, magnetorheological fluid can be utilized in a variety advanced applications, including clutches, prosthetic legs, polishing and controlling systems.

The damper is a system that reduces the amplitude of mechanical vibrations or oscillations. In a automotive industry the vehicle damper system is known as shock absorber. Vehicle damper system dissipate energy, where springs & tires absorb shocks in a vehicle suspension [1, 3–5]. Because of its secure, efficient, and cost-effective design, the damper system is more often used to manage structural vibration.

The magnetorheological damper system is one of the advanced semi-active framework device, which contains magnetorheological fluid and an electrical circuit for the magnetic field. The overall performance and damping force of the magnetorheological fluid damper is adjusted by changing the viscosity of the magnetorheological fluid. The main advantage of MR damper is that it is sensitive and guaranteed to work under heavy loads.

2 Magnetorheological (MR) Damper

A Magnetorheological damper is well known and common applications of magnetorheological fluids. MR damper commonly comprises a cylinder, piston, magnetic system, bearing, seal, and cylinder filled with magnetorheological fluid. In terms of construction, magnetorheological dampers are quite similar to conventional viscous fluid dampers; however, to regulate the magnetorheological fluid, an electrical circuit or magnet is used in place of the conventional damper valves system.

In science and engineering, magnetorheological dampers are employed in a wide range of applications. Due to their popularity, there has been a lot of research and development done to create highly adjustable dampers with long lifespans. The MR damper is one of the most crucial components of a car suspension system.

There are three types of MR dampers utilized in suspension and control systems [3]; Monotube, Twintube and Double-ended. Of the three kinds, the monotube damper is the most widely recognized it tends to be set in any direction and is compact in size.

The variable damping force of this damper may be continuously controlled and modified by adjusting the strength of the applied external magnetic force [6, 7].

In magnetorheological damper system the damping force can be represented as [8–12]:

$$F_d = KX + C_{MR}\dot{X} + F_{MR} \quad (1)$$

where F_{MR} is the damping force produced by the pressure drop due to the applied magnetic force.

3 Mechanical Model for MR Damper

Figure 3 shows the 1DOF mechanical configuration of the magnetorheological damper used in this study. In this damper system, a spring and damper are suspended vertically from fixed-point support. Let a mass m attached to the upper end A of the spring and damper and spring compress the spring by a length e and come to rest at B. This position is called a static equilibrium position.

Now mass m is set in motion from its main position. Let at any time t , the mass is at P such that $BP = x$. The mass m experience the following forces,

1. Gravitational force mg acting downwards
2. Restoring force $k(e + x)$ due to displacement of spring acting upwards
3. Damping (frictional or resistance) force $c \frac{dx}{dt}$ of the medium opposing the motion (acting upwards)
4. External force $F(t)$ considering downward direction

According to Newton’s 2nd law of motion, the differential equation for the motion of the mass m is;

$$m \frac{d^2x}{dt^2} = mg - k(e + x) - c \frac{dx}{dt} + F(t) \tag{2}$$

At equilibrium position B,

$$mg = ke \tag{3}$$

Hence,

$$m \frac{d^2x}{dt^2} = -kx - c \frac{dx}{dt} + F(t) \tag{4}$$

$$\frac{d^2x}{dt^2} + \frac{c}{m} \frac{dx}{dt} + \frac{k}{m}x = \frac{F(t)}{m} \tag{5}$$

Let

$$\frac{c}{m} = 2\lambda \text{ and } \frac{k}{m} = \omega^2 \tag{6}$$

Above equation becomes,

$$\frac{d^2x}{dt^2} + 2\lambda \frac{dx}{dt} + w^2x = \frac{F(t)}{m} \quad (7)$$

The Eq. (7) represents the equation of motion and its solution gives the movement x of the mass m at any instant t . This equation is a ordinary differential equation of order two.

4 Mathematical Modeling

Let $x_1, x_2, x_3, \dots, x_n$ be a system of generalised coordinates for n -DOF system. Then the motion of the system is governed by a system of n odes with the generalised coordinates as the dependent variables & time as the independent variable.

Let $V(x_1, x_2, x_3, \dots, x_n)$ be the sum of Potential Energy of the damper system at an arbitrary instant. Let $T(x_1, x_2, x_3, \dots, x_n)$ be sum of the Kinetic Energy of the damper system at the same arbitrary instant. Hence the Lagrangian $L(x_1, x_2, x_3, \dots, x_n, \dot{x}_1, \dot{x}_2, \dot{x}_3, \dots, \dot{x}_n)$ for given system is defined as,

$$L = T - V \quad (8)$$

The Lagrangian is viewed as a function of $2n$ independent variables, with the time derivatives of the generalised coordinates assumed to be independent of the generalised coordinates.

Let $\delta x_1, \delta x_2, \delta x_3, \dots, \delta x_n$ be variations of the generalised coordinates. The virtual work δW done by the non conservative forces in the system due to the variations of the generalised coordinates can be written as;

$$\delta W = \sum_{i=1}^n Q_i \delta x_i \quad (9)$$

And the Lagrange's equations for dynamic systems are,

$$\frac{d}{dt} \left(\frac{\partial L}{\partial \dot{x}_i} \right) - \frac{\partial L}{\partial x_i} = Q_i, \quad i = 1, 2, 3, \dots, n \quad (10)$$

Above Lagrange's equations provides a system of n independent differential equations.

In case of linear system, the potential and kinetic energies have quadratic forms;

$$V = \frac{1}{2} \sum_{i=1}^n \sum_{j=1}^n k_{ij} x_i x_j \quad (11)$$

$$T = \frac{1}{2} \sum_{i=1}^n \sum_{j=1}^n m_{ij} \dot{x}_i \dot{x}_j \tag{12}$$

If viscous damping force and externally applied forces, independent of the generalised coordinates, are the only non conservative forces, the virtual work presented as;

$$\delta W = \sum_{i=1}^n \sum_{j=1}^n c_{ij} \dot{x}_j \delta x_j + \sum_{i=1}^n F_i \delta x_i \tag{13}$$

Use of Lagrange’s equation to the Lagrangian developed using Eq. (11) and (12) and the virtual work of Eq. (13) leads to;

$$M \ddot{X} + C_{MR} \dot{X} + K X = F(t) \tag{14}$$

Hence general form of the differential governing the vibrations of a n -dof system is;

$$M \ddot{X} + C_{MR} \dot{X} + K X = F(t) \tag{15}$$

where M is the $n \times n$ mass matrix its elements are represented by m_{ij} , K is the $n \times n$ stiffness matrix its elements are represented by k_{ij} , C is the $n \times n$ viscous damping matrix its elements are represented by c_{ij} , X is the $n \times 1$ displacement vector its elements are represented by x_i , and F . is the $n \times 1$. force vector its elements are represented by F_i .

According to Bingham plastic equation, the damping force of the magnetorheological damper expressed as [7, 9];

$$F_d = K X + C_{MR} \dot{X} + F_{MR} \text{sgn}(X) \tag{16}$$

where F_{MR} is the damping force developed by the pressure drop due to the applied magnetic force strength.

5 Mathematical Solution

Let $F(s)$ be the Laplace transform of the applied forces $F(t)$ on a MR damper system, for a particular form of $F_{EQ}(t)$ which is determined from the transform definition and properties of Laplace Transform.

By taking the Laplace transform of $M \ddot{X} + C_{MR} \dot{X} + K X = F(t)$ and applying linearity property of the Laplace Transform;

$$M \mathcal{L}\{\ddot{X}\} + C_{MR} \mathcal{L}\{\dot{X}\} + K \mathcal{L}\{X\} = \mathcal{L}\{F(t)\} \tag{17}$$

$$\mathcal{L}\{\ddot{X}\} + \frac{C_{MR}}{M}\mathcal{L}\{\dot{X}\} + \frac{K}{M}\mathcal{L}\{X\} = \frac{F(s)}{M} \tag{18}$$

Let,

$$\begin{aligned} \frac{C_{MR}}{M} &= 2\lambda w \text{ and } \frac{K}{M} = w^2 \\ \mathcal{L}\{\ddot{X}\} + 2\lambda w\mathcal{L}\{\dot{X}\} + w^2\mathcal{L}\{X\} &= \frac{F(s)}{M} \end{aligned} \tag{19}$$

The Laplace transform of a derivative permits to transform of derivatives of $X(t)$ into algebraic equation $X'(s)$. By applying this property to Eq. (19) we get,

$$[s^2X'(s) - sX(0) - \dot{X}(0)] + 2\lambda w[sX'(s) - X(0)] + w^2X'(s) = \frac{F(s)}{M}$$

which rearranges to,

$$X'(s) = \frac{\frac{F(s)}{M} + (s + 2\lambda w)X(0) + \dot{X}(0)}{s^2 + 2\lambda ws + w^2} \tag{20}$$

Then the definition and linearity property of the inverse Laplace transform is applied to determine $X(t)$,

$$X(t) = \frac{1}{M}\mathcal{L}^{-1}\left\{\frac{F(s)}{s^2 + 2\lambda ws + w^2}\right\} + \mathcal{L}^{-1}\left\{\frac{(s + 2\lambda w)X(0) + \dot{X}(0)}{s^2 + 2\lambda ws + w^2}\right\} \tag{21}$$

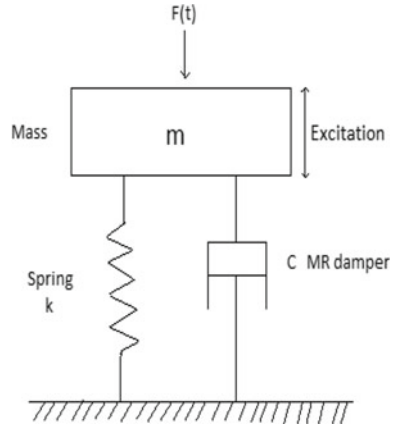
The inverse Laplace transform of RHS of Eq. (21) depends on the roots of the equation $s^2 + 2\lambda ws + w^2$, which, in turn, depend on the certain value of λ . For a given certain value of λ , the inverse Laplace transform of the term $\frac{(s+2\lambda w)X(0)+\dot{X}(0)}{s^2+2\lambda ws+w^2}$ of Eq. (21) is directly determined. The inverse Laplace transform of the term $\frac{F(s)}{s^2+2\lambda ws+w^2}$ is determined only after specifying $F_{EQ}(t)$ and taking its inverse Laplace transform.

In above mathematical solutions, the parameter λ is the damping coefficients related with the Bingham Plastic Model which is concerned with damping performance of the magnetorheological damper, it is controlled by changing intensity of external magnetic force, and overall performance of the damper system is improved.

6 Simulation

The first step in simulation of a magnetorheological damper is to draw the framework, demonstrating the required degrees of freedom, the mass matrix, stiffness matrix and damping control matrix, and showing applied external and internal forces. The 1-DOF MR damper framework to be followed throughout the simulation, appeared

Fig. 1 Mechanical model for MR damper



in Fig. 1, consists of mass m , fixed to a spring whose stiffness constant is k and magnetorheological damper with adjustable damping coefficient c_{MR} .

The equation for motion of 1-DOF MR damper is,

$$m\ddot{X} + c_{MR}\dot{X} + kX = F(t) \tag{22}$$

where, X = Vertical displacement of mass m , m = Mass of the body, c_{MR} = Viscous damping coefficient, k = Spring coefficient and $F(t)$ = Total force on the System.

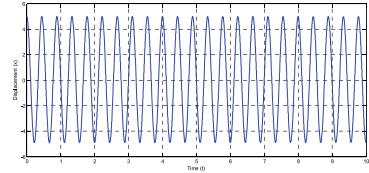
The differential Eq. (22) can be solved mathematically by using transfer function. Let us to simulate an ordinary differential Eq. (22) in simulink for the MR damper. The following parameters are used in the simulation. Body mass (m) = 10 kg, spring constant of spring (k) = 2000 N per metre, damping coefficient of damper (c_{MR}) = $10\sqrt{2}$ to $50\sqrt{2}$ Newton second per metre, control force $F(t)$ on system = 100Newton, initial position $X(0) = 5$, initial velocity $\dot{X}(0) = 0$.

MATLAB code of the above equation is written and a graph of displacement verses time and velocity verses time are drawn numerically as shown in Figs. 2 and 3 respectively. Simulation results demonstrate that both strategies equation modeling and state space modeling produce similar results. It shows that modeling is performed with great accuracy by understanding the dynamics of the MR damper system. Results are matching /validating with the historical data shown in renowned journals, books and literature [13–17].

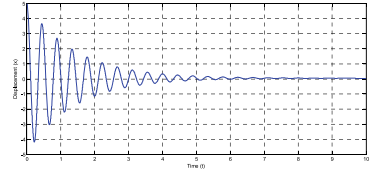
7 Conclusions

This paper gives the background information on MR fluids, MR dampers, types of MR damper, MR dampers modeling and simulations. In this paper, a differential equation has been modeled by using Newton’s laws of motion. The validation of the

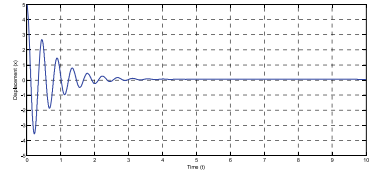
Fig. 2 Velocity verses time



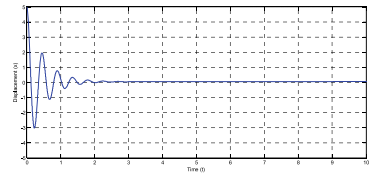
$$C_{MR} = 0$$



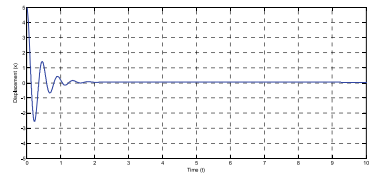
$$C_{MR} = 10\sqrt{2}$$



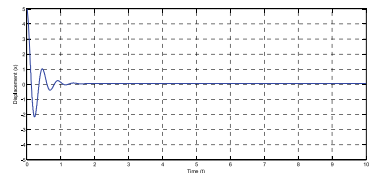
$$C_{MR} = 20\sqrt{2}$$



$$C_{MR} = 30\sqrt{2}$$

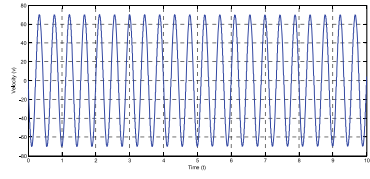


$$C_{MR} = 40\sqrt{2}$$

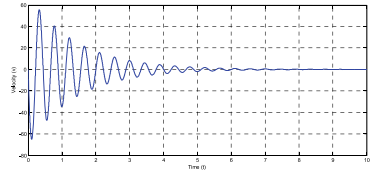


$$C_{MR} = 50\sqrt{2}$$

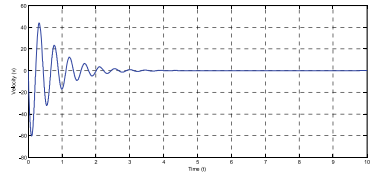
Fig. 3 Displacement verses time



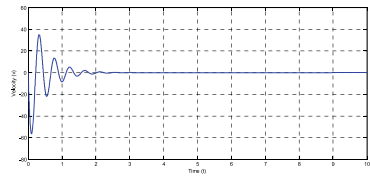
$$C_{MR} = 0$$



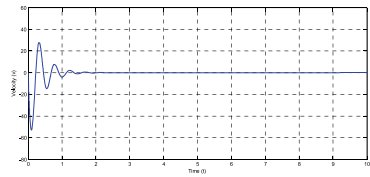
$$C_{MR} = 10\sqrt{2}$$



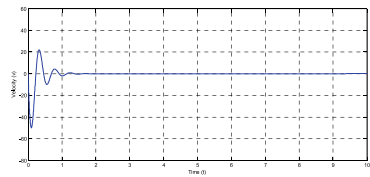
$$C_{MR} = 20\sqrt{2}$$



$$C_{MR} = 30\sqrt{2}$$



$$C_{MR} = 40\sqrt{2}$$



$$C_{MR} = 50\sqrt{2}$$

model gives a good accuracy, and it may be used for the calibration of the control strategies. These types of MR dampers are useful to control vibrations in the field of automobiles, trains and civil structures. The future applications of MR damper systems are to achieve a more stability and comfortable journeys in vehicle.

Acknowledgements This research was supported by the Department of Technology Shivaji University Kolhapur.

References

1. Choi, S. -B., & Han, Y. -M. (2013). Magnetorheological fluid technology: applications in vehicle systems: CRC press. <https://doi.org/10.1201/b13050>
2. Ding, Y., Zhang, L., Zhu, H. -T., & Li, Z. -X. (2013). A new magnetorheological damper for seismic control. *Smart Materials and Structures*, 22, 115003. <https://doi.org/10.1088/0964-1726/22/11/115003>
3. Gołdasz, J., & Sapiński, B. (2015). *Insight into magnetorheological shock absorbers*. Springer. <https://doi.org/10.1007/978-3-319-13233-4>
4. Vishwakarma, P. N., Mishra, P., & Sharma, S. K. (2022). Characterization of a magnetorheological fluid damper a review. *Materials Today: Proceedings*, 56, 2988–2994. <https://doi.org/10.1016/j.matpr.2021.11.143>
5. Umachagi, V., Venkataramana, K., Reddy, G. R., & Verma, R. (2013). Applications of dampers for vibration control of structures: An overview. *International Journal of Research in Engineering and Technology*, 02, 6–11. <https://doi.org/10.15623/IJRET.2013.0213002>
6. Seong, M. -S., Choi, S. -B., & Sung, K. -G. (2011). Control strategies for vehicle suspension system featuring magnetorheological (MR) damper. *Vibration Analysis and Control—New Trends and Development*, 97–114. ISBN 978-953-307-433-7. <https://doi.org/10.5772/24556>
7. Nguyen, Q. H., Choi, S. B., Oh, J. S., Seong, M. S., & Ha, S. H. (2011). Dynamic modelling of magnetorheological Damper using lumped parameter method. In *Proceeding of the 12th international conference on electro-rheological fluids and magneto-rheological suspensions: World scientific* (pp. 583–590). https://doi.org/10.1142/9789814340236_0080
8. Ha, S. H., Seong, M. S., Kim, H. S., & Choi, S. -B. (2011). Performance evaluation of railway secondary suspension utilising magnetorheological fluid Damper. In *Proceeding of the 12th international conference on electro-rheological fluids and magneto-rheological suspensions, world scientific* (pp. 142–148). https://doi.org/10.1142/9789814340236_0020
9. Viswanathan, K. K., Tang, J. S., Aziz, Z. A., & Sambath, P. (2019). Mathematical modeling of magneto rheological fluid damper in the semi-active suspension system. *AIP conference proceedings* (vol. 2112, no. 1, p. 020023). AIP Publishing LLC. <https://doi.org/10.1063/1.5112208>
10. Zhang, H. H., Liao, C. R., Chen, W. M., & Huang, S. L. (2005). Study on the design, test and simulation of a MR Damper with two-stage electromagnetic coil. In *Proceeding of the 9th international conference on electrorheological fluids and magnetorheological suspensions, world scientific* (pp. 728–734). https://doi.org/10.1142/9789812702197_0106
11. Seong, M. S., Choi, S. B., Cho, M. W., & Lee, H. G. (2009). Preview control of vehicle suspension system featuring MR shock absorber. *Journal of Physics: Conference Series*, 149, 012079. <https://doi.org/10.1088/1742-6596/149/1/012079>
12. Sohn, J. W., Choi, S. B., & Wereley, N. M. (2009). Discrete-time sliding mode control for MR vehicle suspension system. *Journal of Physics: Conference Series*, 149, 012080. <https://doi.org/10.1088/1742-6596/149/1/012080>

13. Zhang, X. Z., Wang, X. Y., Li, W. H., & Kostidis, K. (2009). Variable stiffness and damping MR isolator. *Journal of Physics: Conference Series*, 149, 012088. <https://doi.org/10.1088/1742-6596/149/1/012088>
14. Jung, H. J., Jang, D. D., Cho, S. W., & Koo, J. H. (2009). Experimental verification of sensing capability of an electromagnetic induction system for an MR fluid damper based control system. *Journal of Physics: Conference Series*, 149, 012058. <https://doi.org/10.1088/1742-6596/149/1/012058>
15. Berasategui, J., Elejabarrieta, M. J., & Bou-Ali, M. M. (2014). Characterization analysis of a MR damper. *Smart Materials and Structures*, 23, 045025. <https://doi.org/10.1088/0964-1726/23/4/045025>
16. Zayed, A. A. A., Assal, S. F. M., Khourshid, A. M., & Saber, E. (2014). Experimental investigation of the effect of magneto-rheological MR Damper on a rotating unbalance SDOF system. *International Journal of Engineering Research and Technology (IJERT)*, 3(12), 1087–1092. <https://doi.org/10.17577/IJERTV3IS120937>
17. Zhang, L., Hualin, T., Sun, T., Jianhui, Yu., Li, Z., & Wang, X. (2022). Vibration characteristics analysis of shaft system for bulb hydroelectric generating unit based on magnetorheological fluid damper: *Chaos, Solitons & Fractals*, 163, 112559. <https://doi.org/10.1016/j.chaos.2022.112559>

Improvement of Mechanical Properties of Banana Fiber Reinforced Composites



Swapnil Sawant, Aatish Chavan, Prashant Patil, and Sukhdev Waghmode

Abstract In the realm of engineering, composite materials are widely used. The requirement for more effective materials is crucial for the creation of new products in the current world. Due to its strong load-bearing material contained within the weaker element, this composite is crucial. The use of natural fiber as reinforcing components in polymer composites is the subject of numerous investigations. Almost the entire country of India is dedicated to banana farming. A system of materials made up of two or more components that are insoluble in one another and have various physical and chemical properties is referred to as a composite material. The stages that make up the majority of it are matrix and fiber. Metal or polymer fibers are both possible. Today, fibers made from jute, coir, and bananas are also used. Banana fibers are employed as fibers and epoxy is used as the matrix in the current effort to create composites.

Keywords Banana fiber · Mechanical properties · Tensile strength · Epoxy · Vinyl ester

1 Introduction

Due to increased environmental awareness and new regulations, businesses are looking for innovative, environmentally acceptable materials. Plant fibers have drawn a lot of interest as synthetic fiber replacements for reinforcing over the past 20 years. Lignocellulose fibers can give composites advantages such as minimal price, lightweight, specific strength, renewability, biocompatible, and a high level of processing freedom, in contrast to more traditional artificial fibers like glass and carbon. In other terms, a composite material is a material system composed of two

S. Sawant (✉) · A. Chavan · P. Patil
Mechanical Engineering Department, TKIET Warananagar, Kolhapur, India
e-mail: swapnilsawant1715@gmail.com

S. Waghmode
Mechanical Engineering Department, Government Polytechnic, Ratnagiri, India

or much more elements that are illiquid in one another and contrast in form and biochemical makeup. Composite materials have been synthesized by joining two or more components, most of which normally have different properties. Banana fibers are freely accessible, renewable, and have a lighter density than other fibers. When added to composite structures, banana fibers, which already have high tensile strength, can serve as reinforcement agents. Banana fiber is an attractive replacement for traditional airplane structural composite materials that are also environmentally sustainable [1].

2 Literature Review

To comprehend the study challenges involved, extensive research on natural fiber is conducted. Noticed that the epoxy resin can serve as a foundation for the production of laminate later on [2]. To compare wear rates of clean polypropylene matrix without fibers packed with red mud, the Taguchi method and artificial neural networks must be used. The ideal parameter is found using the grey Taguchi technique for different sliding velocities, red mud contents, and loads. Wear tests are carried out using connector-wearing analyzer equipment for various red mud mass fractions. Red mud is a potential filler that could be employed because it is discovered to have good wear resistance properties [3]. Researchers studied polyester composites reinforced with banana fiber and found that a banana fiber content of 40% is optimum. On the mechanical properties of composites made of banana fiber and cement, physical and mechanical investigations were done. It was claimed that banana fiber composite with Kraft pulp had a high flexural strength [4]. Sisal/banana hybrid composites were examined for their tensile properties, which were established via the hybrid mixture rule. When compared to experimental values, their levels are shown to be higher [5]. When the virgin epoxy composite was compared to a composite made from quasi-banana loom cloth reinforced with epoxy, it was discovered also that tensile strength rose by up to 90% [6]. The research was done for tensile tests of an epoxy matrix reinforced with different-sized banana fibers. Tensile strength has been proven to rise as the diameter of the fibers (size distribution) increases [7]. The mechanical characteristics of vinyl ester resin reinforced with varying weight percentages of 17 different natural fibers were investigated using mathematical modeling and ANSYS simulation. The results demonstrate that mechanical properties are significantly improved by a larger fiber content [8]. FEM and experimental techniques were used to study the characteristics of a hybrid composite comprised of banana coir. The hand lay-up technique was used to construct the epoxy composites reinforced with coir and banana, which were then chemically treated. The specimen's dimensions were within the parameters set forth by ASTM for flexural, impact, and tensile testing. The flexural strength of the composite was found to be reduced after alkali treatment, however, the impact and tensile strength of the fibers formed of coir and bananas rose [9].

Table 1 Controlled parameters

S. No	Resin	Banana fiber treatment
1	Epoxy	Treated
2	Epoxy	Untreated
3	Vinyl ester	Treated
4	Vinyl ester	Untreated

Table 2 Constant parameters

S. No	Resin	% Resin	% Banana fiber
1	Epoxy	30	70
2	Vinyl ester	30	70

3 Methodology

Using a universal testing machine, an experimental tensile strength investigation of composites made of banana fiber and various resins was performed. The regulated parameters for the current experiments are presented in Table 1, and composites are created using the hand layup technique. Table 2 lists the constant parameters as banana fiber (70%) and vinyl ester resin (30%) with epoxies (30%).

4 Experimental Details

4.1 Materials

The banana fiber is given a 5% NaOH treatment in the current study to make it more wet table. To create banana/epoxy composites and banana vinyl ester composites, banana fibers are added to epoxy and vinyl ester resins as reinforcement.

4.2 Extraction of Banana Fibers

The quasi of the banana plant is where banana fiber is extracted. These can grow up to 6–10 feeds, depending on the region and climatic conditions. The fibers are located in the stalk's outer sheath. The chosen plant stalk's external coat is scraped off and it is cut to an 80 cm length. These pieces are then squished between two roller cylinders with peeling blades at their edges to extract the pericarp material between the fibers. The banana fibers are then thoroughly cleaned with hot water to get rid of

Fig. 1 Rectangular shaped plastic frame



any impurities or contaminants that may have adhered to the surface. The fibers are then cleaned with distilled water and allowed to dry in the sun for a short period to remove any remaining moisture.

4.3 Mold Preparation

Proper mold preparation must be made before beginning the lay-up procedure. Figure 1 illustrates how this experiment's mold preparation involves just taping plastic sheets to the tabletop.

4.4 Banana Fiber Treatment

Following cutting into the necessary sizes, the dried textiles were treated with alkali in various batches. The alkaline content of the treatment fluids was used to determine the batches. An alkaline solution with 4.5% NaOH is employed. For four hours at room temperature, the textiles were submerged and steeped in a NaOH solution. Banana-derived fabrics were alkaline-treated for four hours, withdrawn from the solvent, and thoroughly rinsed with purified water to remove any NaOH that had remained on the fabric's surface. They are then prepared for the fabrication of the composite laminates needed to investigate drying at room temperature for 24 h.

4.5 Preparation of Resin

The mixing of the resin with the hardener is the initial step in the current study. The ratios are typically provided by the supplier and are printed on the resin or hardener container. The composite material is prepared using epoxy resin, which has a density

of 1.15 g/cm^3 . The hardener HY-951. Hardener is a highly viscous liquid with a density of 1.25 g/cm^3 that is added with resin in the proper proportions during the manufacturing of composites to aid in the solidification of the wet, smooth composite.

4.6 Preparation of Laminates (Hand Layup)

Start the lay-up procedure after all the materials are ready, the workstation is set up, and the mold preparation is complete. (1) Use a clean towel to clean the mold as part of this preparation. (2) Spread the release agent over the surface of the mold to prevent the resin from sticking. Wait to set up the release agent, for sure. Figure 2 illustrates how to lay the first layer of fiber reinforcement. The resin must be applied to this layer, and it must then be gently pressed with a brush or roller to allow the resin to flow up through the fiber cloth. Figure 3 illustrates how additional resin can be spread out and put on top of the fiber if it is not entirely saturated. At this point, the second layer of fiber is placed, and extreme care must be taken to remove any air bubbles that may still exist. You can do this by using a small hand-rolling tool to

Fig. 2 Addition of fiber



Fig. 3 Addition of epoxy resin



Fig. 4 Specimen of banana fiber treated epoxy composite



remove any air bubbles or by using a paintbrush to remove the air bubbles. Repeat this process until the required thickness is achieved.

4.7 Curing

The epoxy resin method used in this experiment and room temperature curing is both suitable. Later, the laminates were made utilizing a compression molding technique, where a 100 kg weight was applied to a wet fabric mat that was layered in between the mold plates. After the arrangement had roughly 8 h to cure, the specimens needed for mechanical characterization were cut per the standards, as illustrated in Fig. 4.

4.8 Tensile Test

According to ASTM D 638 test standard, a tensile test of a composite sample is performed. Figure 5 depicts the results of a tensile test that was performed in a UTM machine under ASTM D 638 to determine the tensile strength of the composites. All of the samples (composites) were rectangular, measuring 165 mm long, 19 mm wide, and 3.2 mm thick.

5 Result and Discussion

Table 3 displays the results of the measurements of the tensile properties of the treated and non-treated banana fiber epoxy and vinyl ester composites. There is a total of sixteen specimens that are prepared for the test. These samples have been divided

Fig. 5 Testing tensile strength of composite on UTM

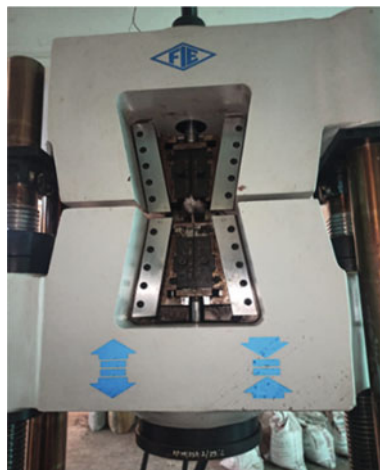


Table 3 Tensile test results from an experiment

S. No	Resin	Banana fiber treatment	First trail tensile strength MPa	Second trail tensile strength MPa	Third trail tensile strength MPa	Fourth trail tensile strength MPa	Average reading tensile strength MPa
1	Epoxy	Treated	83.02	78.23	81.15	80.89	80.625
2	Epoxy	Untreated	79.14	76.47	77.16	74.89	77.805
3	Vinyl ester	Treated	76.59	77.64	79.25	78.56	77.115
4	Vinyl ester	Untreated	74.29	71.87	75.12	74.23	73.08

into four groups, each of which has four samples. The treated banana fiber epoxy composite is the first group, with four specimens. The untreated banana fiber epoxy composite is the second group, with four specimens. The treated banana fiber vinyl ester composite is the third group, with four specimens. Figure 6 displays the composites' tensile strength comparison. The test results showed that the composites with treated banana fiber and epoxy resin reinforcement, which have a recorded tensile strength of 80.625 MPa, perform better than the other composite combinations.

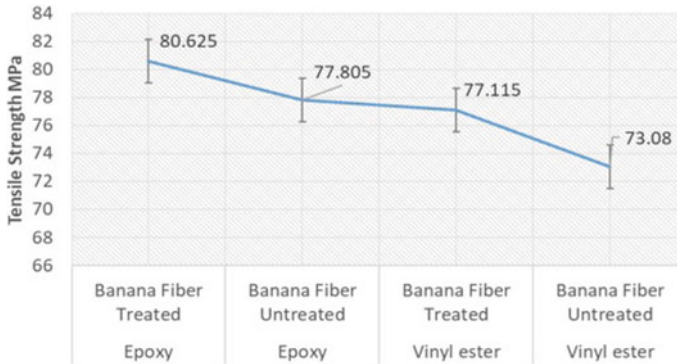


Fig. 6 Banana fiber reinforced composite tensile strength variation with different resins

6 Conclusion

Organic fiber-reinforced epoxy composites can be successfully made using the hand lay-up method. The treated composites of 70% banana fiber and 30% epoxy resin have a maximum tensile strength of 83.02 MPa, according to the experimental data. In this investigation, a composite material made of naturally occurring synthetic materials was used to replace plastic. According to the results, the composite of bananas has a high tensile strength, a low weight factor, and is easily biodegradable. As a result, this natural composite fiber can be used in place of polymer compounds.

References

1. Rao, Venkata, K., Babu, S., & Ratnakaram, Y. C. Laser analysis of HO³ doped different chlorophosphate glasses.
2. Pavanu Sai, J. (2014). Experimental investigation of effect of aluminium filler material on thermal properties of palmyra fiber reinforced Composite.
3. Mahapatra, S. S. & Data, S. (2011). *International Journal of Modeling and Optimization*, 1, 80.
4. Samivel, P., & Ramesh Babu, A. (2013). Mechanical behavior of stacking sequence in Kenaf and banana fiber reinforced-polyester laminate. *International Journal of Mechanical Engineering and Robotics Research*.
5. Venkateswaran, N., Elayaperumal, A., & Sathiya, G. K. (2012). Prediction of tensile properties of hybrid natural fiber composites. *Composites Part B: Engineering*, 43, 793–796.
6. Maleque, M. A., Belal, F. Y., & Sapuan, S. M. (2007). Mechanical properties study of pseudo-stem banana fiber reinforced epoxy composite. *Arabian Journal for Science and Engineering*, 32(2B), 359–364.
7. Khalifa, M., & Chapparr, S. S. (2014). Experimental investigation of tensile properties of banana reinforced epoxy composites. *International Journal of Science and Research*, 3(6), 832–836.

8. Ramakrishnan, S., Krishnamurthy, K., Mohan Prasath, M., Sarath Kumar, R., Dharmaraj, M., Gowthaman, K., Sathish Kumar, P., & Rajasekar, R. (2015). Theoretical prediction on the mechanical behavior of natural fiber reinforced vinyl ester composites. *Applied Science and Advanced Materials International*, 1(3), 85–92.
9. Hariprasad, T., Dharmalingam, G., & Raj, P. P. (2013). Study of mechanical properties of banana-coir hybrid composite using experimental and fem techniques. *Journal of MES*, 4, 518–531.

Experimental Investigation and Micro Structural Variation in Friction Drilling on AISI 1015 Low Carbon Steel, AISI 1008 Aluminium and Copper by Using Tungsten Carbide Tool



Vinayak W. Bembrekar and Rahul N. Yerrawar

Abstract Thermal drilling uses a tungsten carbide tool to conduct a comparative investigation of form-drilled holes on AISI1015 low carbon steel, AISI 1015 copper, and AISI 1008 Aluminium. By using friction drilling, which uses heat generated by friction between a revolving conical tool and the work material to soften and pierce the thin-walled work piece to make a hole with a bushing, holes have been drilled on AISI 1015 Copper, AISI 1008 Aluminum and Mild Steel square tubes. The bushing improves threading depth and clamp load capacity while being the most effective for threading. During friction drilling, naturally generated bush has a large variety of applications. Spindle speed and the t/d ratio of friction drilled holes have the biggest effects on the process. In tests, Taguchi's orthogonal array L9 has been employed. During the friction drilling process, temperature, bush length, hardness, and micro structural variation are measured and studied.

Keywords Micro structural variation · Bush length · Temperature · Surface roughness · Hardness

1 Introduction

Thermal drilling is an unconventional method of creating holes in which heat is generated between the tool and the work piece as a result of friction. Due to the speed, feed, friction that has created between the two, and the plastic deformation of the material, the tool and work piece are in a red-hot condition [1, 2]. Due to this plastic deformation, the work piece spontaneously developed collar and bush without chip formation. It is a bur-free operation since the material is removed by melting and

V. W. Bembrekar (✉)

G H Raisoni College of Engineering and Management, Pune 412207, India
e-mail: vinayak.bembrekar@gmail.com

R. N. Yerrawar

MES College of Engineering, Pune 411001, India

vaporizing without the use of coolant. These days, a wide range of applications for this activity include those in the manufacturing, thermal, design, aerodynamic, and biomedical fields. A naturally formed bush with numerous applications in the taping of sheet metal. The mechanical, surface, and metallurgical properties of the material are significantly influenced by the manufacturing methods [3, 4]. The manufacturing output parameters are, however, affected by the mechanical properties, such as impact strength, surface quality, as surface topography, surface roughness, and surface finish, as well as the metallurgical properties, such as grain size, grain orientation, surface hardness, residual stresses, and materials atomic structure [5–10].

2 Working Principal

Friction drilling, also known as thermal drilling, flow drilling, form drilling, or friction stir drilling, is a novel method of creating holes in the sheet metals. The heat generated by friction between a rotating conical tool and the work-piece causes the material to soften and allows for the penetration of a hole. The tool tip indentates into the workpiece and supports the drill in both radial and axial directions, much like the web centre in a twist drill. Axial force and relative angular velocity between the tool and the workpiece cause friction on the contact surface, which heats up and softens the workpiece's material. The first movement of the softened work material when the tool is extruded into the workpiece is side ways and upward. Once the tool has been heated and softened, the workpiece's material can be penetrated by it. Due to penetration naturally formed bush and boss formation take place.

3 Literature Survey

T. Prabhu et al. Took the different materials like Aluminium and copper for friction drilling experimentation. In this experimentation first they have explained working principle of friction drilling with required input and output parameters. Also they have told the maximum temperature which is generated is about $1/2$ – $2/3$ of the work piece melting temperature. This information is helped to us in selection of material, speed, feed, IR pyrometer and VMC machine. After that they have explained about application of materials used in various sector. Also as per their experimentation In friction drilling tool wear is very minimal in comparison with twist drill. They have noted the temperature values generated during the experimentation. Also the unwanted chips are not produced. During working with center drill and center tap they have given some safety rules [11].

Scott F. Miller et al. Presented the paper on friction drilling on cast metals. They have studied the Effects of work piece temperature, spindle speed, and feed rate on experimentally measured thrust force, torque, and bushing shape generated. For this experimentation they have selected 5.3 mm diameter tungsten carbide tool and two

materials used for experiments in this friction drilling study were 4.0 mm thick die cast Al380 and magnesium AZ91D alloy. They analyzed through this experimentation the petal formation of material so we studied that if the material is hard or brittle petal formation occurs. They have measured the temperature of material using thermocouple [12].

During experimentation high temperature is generated so we decided to select non-contact type temperature measuring device. Also they have measured torque and thrust force generated during experimentation with dynamometer. Then plotted the graph for thrust force and torque. As per their experimentation if the speed increases petal formation in material increases.

Cebeli Ozek et al. This study investigates the impact of heat conductivity on friction drilling of aluminium alloys. For the experimentation, a milling machine equipped with a tool with an 8 mm diameter is used. In this experiment, the feed rates were 25, 50, 75, and 100 mm/min, and the spindle speeds were 1200, 1800, 2400, 3000, 3600, and 4200 rpm. Materials for the workpiece included aluminium alloys A1050, A6061, A5083, and A7075-T651 with variable heat conductivity coefficients and a 4 mm thickness. With a 360 conical angle and a 16 mm cylindrical area length, the tool's material was HSS. They looked examined how spindle speeds, feed rates, and the thermal conductivity of the materials related to frictional heat produced, surface roughness, and bushing height. In the end, they found that when thermal conductivity coefficients increased, high spindle speeds and slow feed rates led to a large accumulation of frictional heat. Greater bushing heights were achieved with slower spindle speeds and higher feed rates, even if the best surface roughness data were at a certain spindle speed and feed rate [13].

V. V. Satyanarayana et al. Author selected material for experimentation is Aluminum (AA6351) of 1 mm thickness and they have designed proper experimental layout by Taguchi method. After Taguchi method they have selected L8 orthogonal array and torque and thrust force measured by using drill dynamometer. In this experiment they have used two tools with two different cone angles. They also created a regression model. The impact of cone angle on thrust force and torque is shown to be significant [14].

Pantawane P. D. et al. They presented a report on experimental research and multi-objective friction drilling process optimization on AISI 1015. In this work, the authors looked at the relationship between dimensional accuracy and bush surface roughness and the friction drilling input parameters of rotating speed, feed, and tool diameter [11].

They selected a number of AISI 1015 M8 and M10 tools. In this paper, dimensional error is used to evaluate the quality of the drilled holes (DE). Surface roughness was also the subject of an ANOVA. They get to the conclusion that the surface roughness falls from 0.536 to 0.341 μm with an increase in speed between 2500 and 4500 RPM.

Han-Ming Chowa et al. presented a paper on the research of friction drilling's machining characteristics on AISI 304 stainless steel. They chose to use AISI 304A with a modified feed rate and cone angle. Additionally, they created an orthogonal array using the L18 Taguchi method. In this experiment, they used the LMV-2000 micro-hardness tester to conduct a hardness test. A drilled hole is examined using

Table 1 Displays input parameters and their levels

Parameters	Level 1	Level 2	Level 3
Speed (RPM)	2500	3100	3700
Feed (mm/min)	80	120	160

SEM. In this paper, we examined how surface value increases along with feed rate. The hardness value gradually drops if the hardness test is conducted further from the drilled hole [12].

M. Boopathia et al. They have given a paper describing experimental research on friction drilling on brass, aluminium, and stainless steel. In addition to providing information on the thrust forces needed for drilling and the temperature distribution in the work piece, this paper describes the setup of the friction drilling process. According to our analysis, the temperature of the work piece rises as speed increases due to increased heat transfer and frictional heat flux. We observed that, for a fixed speed, the thrust force increases as the feed increases and that, in the heat-affected places on the work piece, the frictional heat generated by the drilling process is utilized to harden the materials [12].

4 Materials and Method

AISI 1015 Copper, AISI 1015 low carbon steel, and AISI 1008 aluminium were chosen as the materials for the current task. The substance is packaged in square tubes. Same-thickness material is used.

4.1 Methods

The following input and output variables are taken into account:

Input criteria: Spindle speed (rpm), material type, and feed rate (mm/min) the experiments' outputs (responses) were measured as follows: Drilling by friction Bush length (mm), Surface Roughness, and Hardness at 0 °C (Hv) (Table 1).

4.2 CATIA-Part

See Fig. 1.

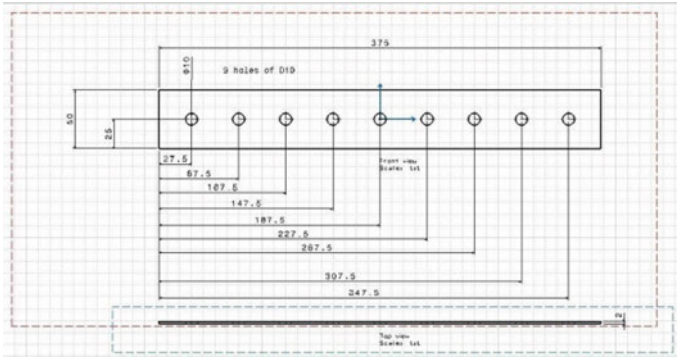


Fig. 1 Catia part of materials

4.3 Experimental Setup

See Figs. 2, 3 and 4.

Fig. 2 Experimental setup of friction drilling on VMC

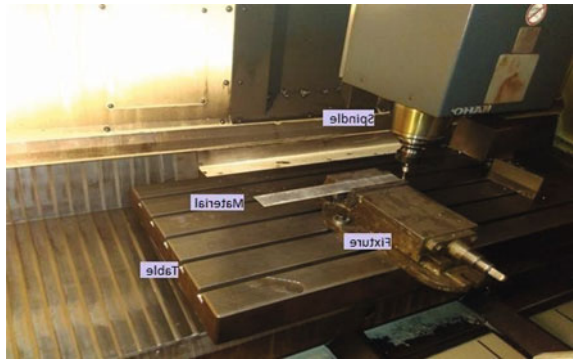


Fig. 3 Measurement of surface roughness of copper



Fig. 4 Measurement of bushing length of copper



5 Results

5.1 Response Measurement

See Tables 2, 3, 4 and 5.

Table 2 Temperature values of copper and aluminium

Observation No.	Copper	Aluminium
1	98.9	51.5
2	95.2	49.9
3	90.1	48
4	120.8	56.3
5	115.9	55.1
6	109.6	53.9
7	141.2	61.2
8	139.9	59.9
9	135.6	58.6

Table 3 Hardness values of copper

Observation No.	Copper
1	128.7
2	124.2
3	115.3
4	118.6
5	116.5
6	114.5
7	112.9
8	111.3
9	110.6

Table 4 Bushing height values of aluminium

Observation No.	At point 1	At point 2	Average
1	6.71	7.19	6.45
2	6.43	7.03	6.73
3	6.20	6.68	6.44
4	7.16	6.98	7.07
5	6.86	6.81	6.83
6	7.01	6.80	6.90
7	6.58	6.55	6.56
8	6.72	6.63	6.67
9	6.40	6.57	6.48

Table 5 Surface roughness values copper and aluminium

Observation No.	Copper (Rz)	Aluminium (Rz)
1	12.85	14.05
2	17.10	23.99
3	13.55	22.85
4	10.61	31.41
5	12.30	20.05
6	15.18	15.85
7	15.5	13.99
8	16.73	14.85
9	15.99	25.10

5.2 Result Graph

See Figs. 5, 6, 7 and 8; Graph 1.

5.3 Micro Structural Variation

See Figs. 9, 10, 11, 12, 13 and 14.

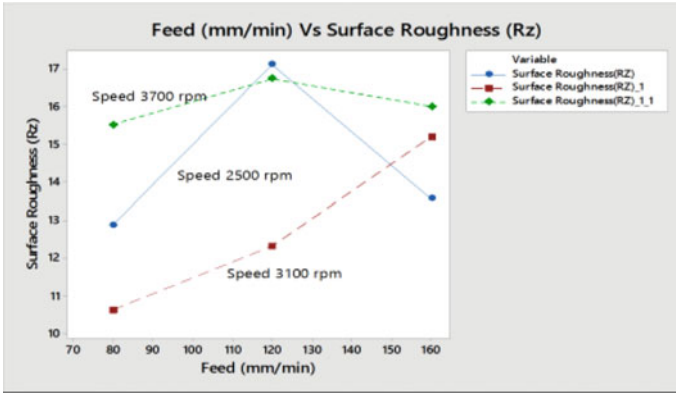


Fig. 5 Feed (mm/min) versus Bushing Height (mm) for copper

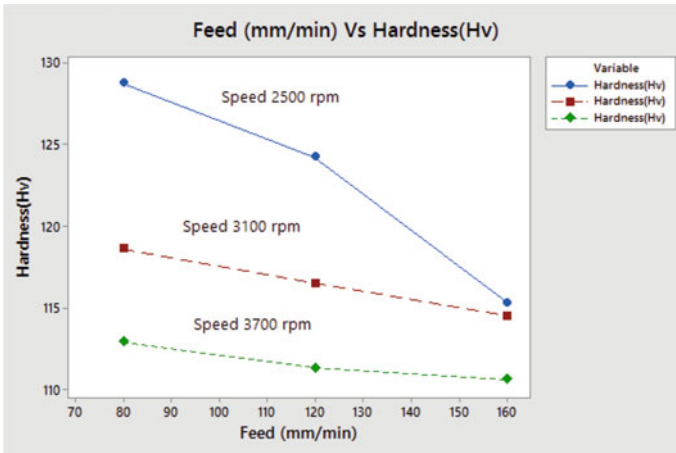


Fig. 6 Feed (mm/min) versus Hardness (Hv) for Copper

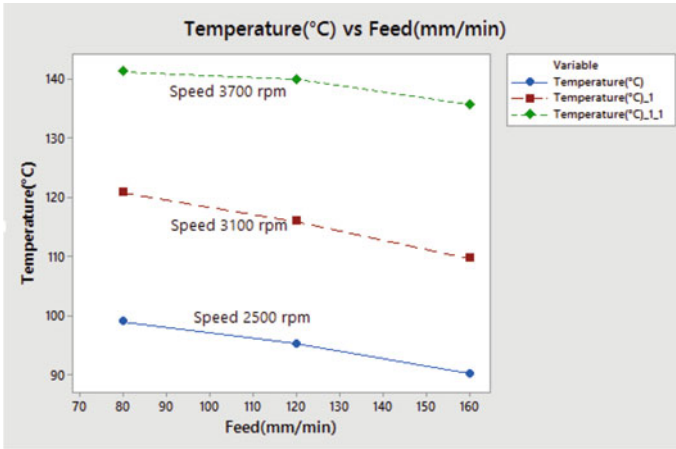


Fig. 7 Temperature (°C) versus Feed (mm/min) for copper

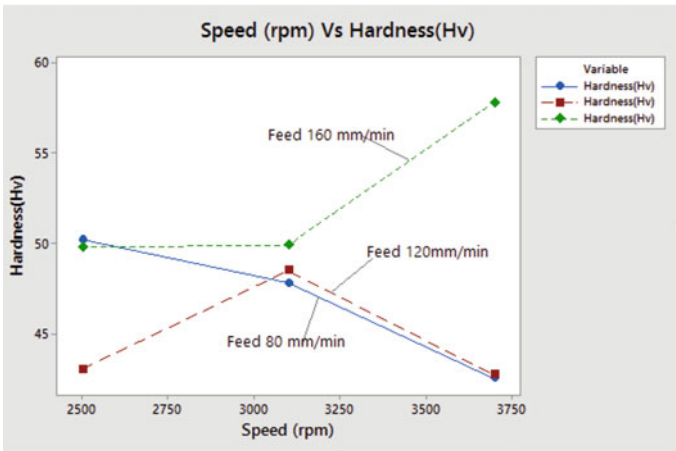
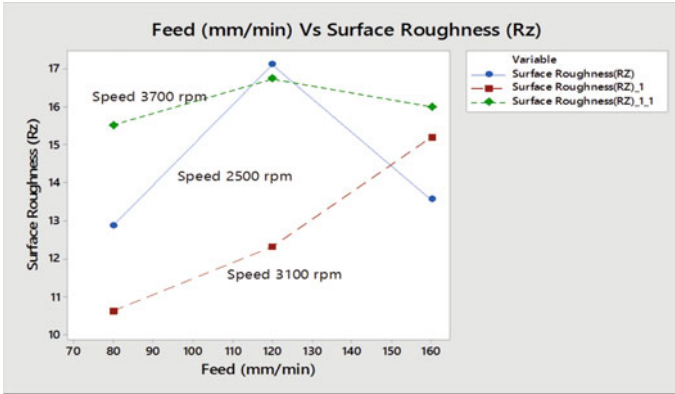


Fig. 8 Speed(rpm) versus Hardness (Hv) for Aluminium



Graph 1. Feed (mm/min) versus Surface Roughness (Rz) for Copper

Fig. 9 Aluminium

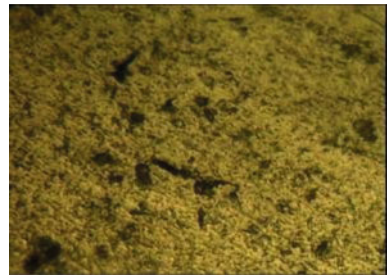


Fig. 10 Aluminium

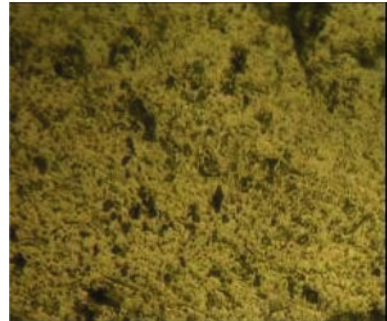


Fig. 11 Aluminium

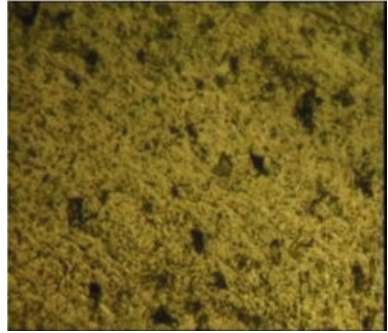


Fig. 12 Carbon steel

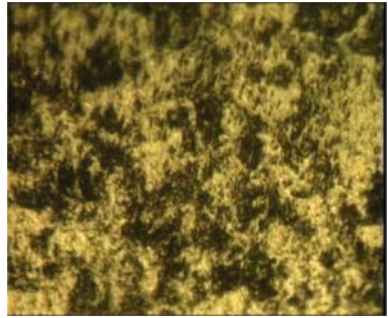


Fig. 13 Carbon steel

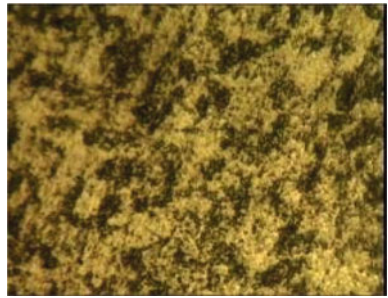
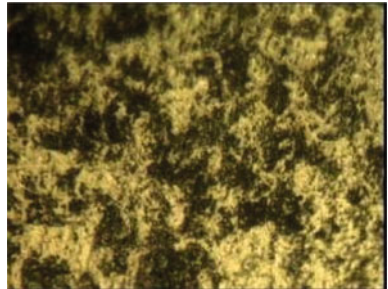


Fig. 14 Carbon steel



6 Conclusion

1. Evaluation of Traditional Drilling Method Compared to a twist drill, friction drilling tool wear is quite negligible. Additionally, no undesired chips are produced.
2. In order to generate a lot of frictional heat, copper, low carbon steel, and aluminium were all friction-drilled at high spindle speeds and low feed rates. As the feed rate increases, the temperature too does. Copper is more brittle than aluminium because it is heated to greater temperatures.
3. Aluminium did not reach the proper softening temperature, which caused the material to adhere to the drill and increase the hole's surface roughness. If you compare the twist drill's surface roughness to a friction drill, the difference is too great. In friction drilling, surface roughness values are therefore low.
4. The bushing height was progressively increased as the feed rates were raised, but occasionally it would fall because softened material was being pushed in the direction of tool motion. It also reduced often as spindle speed was raised due to the influence of the high momentum. Material qualities affect how petals form. The number of petals is significantly influenced by the t/d ratio. More petals are generated when the t/d ratio is minimal. Only in copper do petals develop.
5. A micro structural analysis of aluminium reveals that as speed increases, pure aluminium with insoluble FeAl impurities becomes the new phase, and as temperature rises, more pearlite is generated in the ferrite matrix of carbon steel.

References

1. Chow, H.-M., Lee, S.-M., & Yang, L.-D. (2008). Machining characteristic study of friction drilling on AISI304 stainless steel. *Journal of Materials Processing Technology*, 207, 180–186.
2. Gopal Krishna, P. V., Kishore, K., & Satyanarayana, V. V. (2010). Some investigation in friction drilling AA6351 Using high speed steel tools. *ARPN Journal of Engineering and Applied Sciences*, 5(3).
3. Huang, B. H. Y. (2016). Friction drilling of austenitic steel by uncoated and PVD AlCrN-TiAlN-coated tungsten carbide tools. *International Journal of Machine Tools and Manufacture*, 2 (1).
4. Ozek, C., & Demir, Z. (2013) Investigate the friction drilling of aluminium alloys according to the thermal conductivity. *TEM Journal*, 2(1).
5. Thorat, S. B., & Mudigonda, S. (2020). The relative influence of surface metallurgy and self-magnetization induced by different manufacturing processes on surface integrity of CoCr alloy using PCM. *Materials Characterization*, 167, 110526.
6. Thorat, S., Lonkar, V., Pailwan, A., Sargade, V., & Mudigonda, S. (2020). Effect of metallurgical parameters induced by manufacturing processes on photochemical machining of Co-Cr L605 alloy. *Procedia CIRP*, 95, 149–154.
7. Thorat, S., Dugad, R., & Mudigonda, S. (2017). Design, analysis and manufacturing of Bare Metal Coronary Stent using PCM. In *Proceedings of 10th International Conference on Precision, Meso, Micro and Nanoengineering*.
8. Thorat, S., & Sadaiah, M. (2019). Investigation on surface integrity of Co-Cr L605 alloy in photochemical machining. *Journal of Manufacturing Processes*, 38, 483–493.

9. Thorat, S., & Sadaiah, M. (2019). The effect of residual stresses, grain size, grain orientation, and hardness on the surface quality of Co-Cr L605 alloy in photochemical machining. *Journal of Alloys and Compounds*, *804*, 84–92.
10. Patil, D. H., Thorat, S. B., Khake, R. A., & Mudigonda, S. (2018). Comparative study of FeCl₃ and CuCl₂ on geometrical features using photochemical machining of monel 400. *Procedia CIRP*, *68*, 144–149.
11. (2020). The relative influence of surface metallurgy and self-magnetization induced by different manufacturing processes on surface integrity of CoCr alloy using PCM. *Materials Characterization*, *167*, 110526; Dehghana, S., Shah, Ismaila, M. I., & Sourib, E. (2020). A thermo-mechanical finite element simulation model to analyze bushing formation and drilling tool for friction drilling of difficult-to-machine materials. *Journal of Manufacturing Processes*, *57*, 1004–1018.
12. Srilatha, N., & Srinivasa, B. (2019). *A Novel Method of Friction Drilling Technique Review AIP Conference Proceedings 2200* (pp. 020052). <https://doi.org/10.1063/1.5141222> Published Online: 20 December 2019.
13. Dehghan, S., Ismail, M. I. S., Mohd Ari_n, M. K. A., & Baharudin, B. T. H. T. (2019). Friction drilling of difficult-to-machine materials: Workpiece microstructural alterations and tool wear. Received: July 3, 2019; Accepted: July 23, 2019; Published: August 29, 2019.
14. Shalamov, P. V., & Kazantseva, J. V. (2017). *Thermal Drilling with Force-Feed Tool Procedia Engineering*, *206*, 985–990

Exploration into Tribological Behaviour of Graphite Reinforced Corn Cob Ash Epoxy Composites Utilizing Taguchi Approach



Pranav V. Swami and Vijaykumar B. Raka

Abstract This work concentrates on the utilization of graphite particles as secondary reinforcement in the matrix of ash from corn cobs (CCA) epoxy resin in order to produce epoxy composites with low-friction and wear-resistant. The CCA weight percentage was set at 6%, graphite weight percentages were 3, 5, and 7%, and composites were tested for tribological performance using a pin-on-disc tribometer. The Taguchi approach was used for designing the experiment with a varying function of content of graphite, sliding speed, and normal load. The worn surfaces are examined using electron micrographs to gain a better understanding of the wear process faced by the composites. After going through all of the steps, it was discovered that employing graphite as a secondary reinforcement had a favorable effect on wear and friction, with friction and wear being decreased when compared to the CCA-reinforced epoxy composite.

Keywords Taguchi method · Graphite · Corn cob ash · Composite · Pin-on-disc

1 Introduction

Polymers and their composites have highlighted their potential to replace conventional engineering materials due to unique characteristics such as design flexibility, cheap price, ease of manufacture, and light in weight nature. Pure polymers have lower resistance to the wear but they'll be modified acceptable for the tribological applications by mixing with additives or reinforcements. The sticky wear mechanism dominates polymer wear when sliding over a clean metal surface. According to previous research, the wear of polymer material over the metal counter face may be reduced by lowering the adhesion phenomenon, improving the strength, and stiffness [1]. The stiffness and strength of the polymers can be increased by reinforcing them with micro or nano sized particles and with short fibers or long fibers. Which helps

P. V. Swami (✉) · V. B. Raka
Government College of Engineering, Karad, India
e-mail: pranavvswami@gmail.com

in reducing the genuine area of contact which results in adhesion of asperities of polymer-metal [2]. Increase in strength and handling the load (load bearing) property is achieved by the utilization of the soft and natural fibers [3]. In recent few years investigators have utilized reinforcing material such as silica(SiO_2), oxides of titanium(TiO_2), alumina(Al_2O_3) [4]. Controlled utilization of these material results in improvement in the resistance to the wear of the polymeric material. Generally, ceramics are found by the process of chemical synthesis but few of them like silica and alumina are present in good quantity in waste materials such as fly ash and ash of farming waste [5]. Onkar Mestry et al. [6] have utilized ash of corn cob as a reinforcing material in the epoxy's matrix. When kernels are removed from the corn cobs the bare cobs are utilized as food for the animals or they are termed as the farming waste. While utilizing as biomass bare cobs leaves ash behind which is termed as the corn cob ash(CCA). This ash of maze contains approximately 50–60% of silica and alumina of whole ash [7]. Due to such composition of the chemicals, it can be used as hard ceramic reinforcement. Alajmi et al. [8] have utilized graphite as a reinforcing material and studied properties of Graphite-Epoxy composite from tribological point of view. They found that the weight% of graphite has noticeable impact on effect the performance of the composite. This study uses graphite as secondary reinforcement with varying range of weight% (3, 5 and 7%) in the cca-epoxy composite with fixed weight% of ash of corn cob (6%CCA). Due to lamellar structure of graphite, it can be utilized for reducing the friction. It has minor coefficient of friction ranging from 0.1 to 0.2 when sliding over other cleaned metal surfaces. Furthermore, no research has been published in using graphite as secondary reinforcement in cca-epoxy composite for the aim of reducing the wear and friction.

In this current research, Taguchi's orthogonal array is employed for designing the of the experimentation and reducing experimental runs. Pin-on-disc tribometer is utilized in order to perform the experiments. Tribological results such as wear and friction are impacted not only by amount of the reinforcing material but also by factors of sliding such as applied load and speed of sliding. Grey analysis is used to access the wear behavior of the composite [9]. Regration analysis was used to estimate the effect of explanatory variable on the dependent variable.

2 Experimentation

2.1 Materials

The composites were produced using fixed weight% of ash of maze(6%), secondary reinforcement of graphite with changing weight% (3, 5 and 7%) and utilizing epoxy in the role of binder material. For production of epoxy resin(Bisphenol's eather-diglycidyl) and hardener(tri-ethylene tetra amine) were bought from ATUL polymers, Bangalore, India. For preparation of the ash of the maze fully developed maze were dried under the sun. The sundried maze was then burnt in the open air for the duration

Table 1 Sample nomenclature and composition

Notation	Composition
E6CCA	Epoxy + 6 wt% CCA
E6CCAG3	Epoxy + 6 wt% CCA + 3 wt% Graphite
E6CCAG5	Epoxy + 6 wt% CCA + 5 wt% Graphite
E6CCAG7	Epoxy + 6 wt% CCA + 7 wt% Graphite

of 6 h [10]. The charred maize cobs were smashed in to small sized particles and kept on heated plate. After some time at this point the colour of smashed particles began to change from black to grey which shows decrease in the content of carbon. The end product grey colored ash of corn cob was obtained after carrying the above process for 1 h. Then the powder was filtered through a 300 mesh size sieve. Further no any processes were performed on the resulted ash of corn cob. Graphite particle of 200 mesh size is utilized as a secondary reinforcement. Graphite is material formed by atoms of carbon stacked in layered pattern. It is having brilliant chemical stability in such a way that no chemicals can cause it for chemical reactions.

2.2 Manufacturing of Composite

Four variants with fixed content CCA(6%) and quirky weight% of graphite in the matrix of epoxy were fabricated as shown in Table 1. Graphite with weight% of 3, 5, and 7% were chosen and a product without graphite (neat cca-epoxy) were manufactured. Initially the weighted amount of ash of corn cob and graphite were added to the resin then the mixture was stirred for 20 min to obtain good mixture of graphite, epoxy and cca. After hardener was added in the above mixture and gently stirred once again. Then produced mixture was poured in the cylindrically shaped molds to get the final samples. Plastic molds were having 13 mm diameter and 25 mm height. Before pouring the mixture in the molds the internal part of them was sprayed with mold release spray of silicon. The specimens were allowed to cure for 24 h. at room temperature. Samples were post-cured in an oven at 55 °C for 30 min, then 70 °C for an extra 30 min.

2.3 Measurement of Hardness and Density

According to the procedure of ASTM D785 hardness of the samples were measured by utilizing Rockwell's hardness tester. Five reading were noted on surface of each sample and by taking average of each surface's reading hardness was recorded.

Density was measured cause it is required to measure the volume loss of the sample during the experimentation. ASTM-D792(Archimedes principle) was utilized for the measurement of the same. Density was evaluated using bellow Eq. 1 in which x, y represents the sample's weight in air and water respectively, ρ_{st} and ρ_w represent theoretical density and density of water respectively.

$$\rho_{st} = [a/(a - b)] * \rho_w \quad (1)$$

The above-mentioned method provides experimental density in which void available in the sample are also included. So, the theoretical density in which void are excluded was calculated by considering density of each and every component with help of following Eq. 2. in which ρ_{se} , ρ_{ep} and ρ_g represents experimental density, density of epoxy and graphite respectively and w_g and w_{ep} represents weight of graphite and epoxy respectively. In this research as weight% of CCA was kept constant so the epoxy will always be the mixture of resin, hardener and ash of corn cob.

$$\rho_{se} = [w_g/(w_{ep}/\rho_{ep}) + (w_g/\rho_g)] \quad (2)$$

So, the % difference of ρ_{st} and ρ_{se} was calculated using Eq. 3 which provides the void friction in the composite.

$$\text{Void friction} = [(\rho_{st} - \rho_{se})/\rho_{se}] * 100 \quad (3)$$

2.4 Pin-On-Disc Tribometer

Major of the experimentation included tribological testing, which was performed according to the ASTM-G99 procedure. The epoxy-cca-graphite composite specimens were fabricated in the form of flat-ended cylindrical pins with hight of 25 and 12 mm in diameter. The pins were employed to slide against the EN41 steel disc of hardness ranging from 58 to 62 HRC. Before starting the experiments, the disc and pins were cleaned by using acetone in order to remove the dust. Normal load(N) was set manually by placing weights on the loading portion. Frictional force(F) was observed using a load sensor throughout the complete process and noted as a function of sliding distance utilizing 'WINDUCOM' software. Evaluation of wear was made utilizing Eq. 4 for specific wear rate(K_s), in which Δm represents mass loss cause of wear and 'L' is the sliding distance.

$$K_s = [\Delta m/(\rho * N * L)] \quad (4)$$

To get the mass loss the samples were weighed before and after the experiments on the weighing device having an accuracy of ± 0.1 mg.

2.5 Designing of Experiment

Designing experiments using the Taguchi method avoids the need for extensive testing and results in saving time, material, and money. For performing the tests, the experimentation was designed using Taguchi’s orthogonal array(L-9). This work optimization parameter uses the grey relational analysis(GRA) method. This orthogonal array was obtained using ‘Minitab’ software in which three parameters with three levels were selected. Following Table 2 shows them (Table 3).

Where, %G = weight% of graphite, N = applied load(N), S = speed(rpm), μ = frictional coefficient, K_s = specific wear rate($\times 10^{-5}mm^3/N.m$).

Table 2 Level and parameters used in experimental work

Level	Parameter		
	% Graphite	Load (N)	Speed (rpm)
1	3	10	100
2	5	20	200
3	7	30	300

Table 3 Coefficient of friction and specific wear rate experimental findings using Taguchi’s L9 orthogonal array

Run No.	Process parameter			Experimental results	
	%G	N	S	μ	K_s
1	3	10	100	0.400005	3.76840
2	3	20	200	0.347241	0.77080
3	3	30	300	0.392118	1.54162
4	5	10	200	0.414913	0.61990
5	5	20	300	0.331114	3.09980
6	5	30	100	0.238289	1.61190
7	7	10	300	0.306922	0.66990
8	7	20	100	0.236954	0.40190
9	7	30	200	0.267845	0.29770

2.6 Grey Theory

The theory of the grey system was proposed by Deng and grey relational analysis (GRA) is part of the same [11]. This simplifies the initial issue to a single decision-making question [12].

Step 1. In this step the original data is transformed into the equivalent values using Eq. 5 in which $i = 1 \dots, m$; 'm' is number of experimental data, $k = 1 \dots, n$; 'n' number of replies, X_i = original data, $X_i^*(k)$ = pre-processed data, $X_i(k)_{\max}$ and $X_i(k)_{\min}$ represents largest and lowest value of X_i respectively and X = intended value.

$$X_i^*(k) = \left\{ \frac{[X_i(k)_{\max} - X_i(k)]}{[X_i(k)_{\max} - X_i(k)_{\min}]} \right\} \quad (5)$$

Step 2. By using normalized values grey relational coefficient is calculated using Eq. 6 in which Δ_{0i} = deviation sequence of $X_0(k)$ and $X_i(k)$ i.e. reference sequence and comparability sequence respectively, Δ_{\min} and Δ_{\max} = lowest and largest value of absolute difference respectively, $\xi = 0.5$ (identification coefficient);

$$\xi_i(k) = \left\{ \frac{[\Delta_{\min} + (\xi * \Delta_{\max})]}{[\Delta_{0i}(k) + (\xi * \Delta_{\max})]} \right\} \quad (6)$$

$$\Delta_{0i} = |X_0(k) - X_i(k)| \quad (7)$$

Step 3. In this, the grey relational grade (GRG) is obtained using Eq. 8 in which n = number of response characteristics and γ_i = required GRG for i th run.

$$\gamma_i = \frac{1}{n} \sum_{k=1}^n \xi_i(k) \quad (8)$$

Step 4. In this step, the rank of the results is obtained which helps to decide the optimal conditions of the experimentation. The findings of this process are mentioned in Table 4.

3 Result and Discussion

3.1 Characteristics of CCA and Graphite

The SEM images (Fig. 1a) of CCA revealed that it is amorphous and has agglomerated shape, from the results of EDS (Fig. 1b) it was seen that CCA contains a considerable amount of silica along with the presence of potassium and oxygen.

Table 4 Grey relational optimization values

Run No.	Evaluation of Δ_{oi}		Grey relational coefficient		GRG	Rank
	μ	K_s	μ	K_s		
1	0.0000	0.0000	0.2500	0.2500	0.2500	9
2	0.8449	0.8637	0.4329	0.4400	0.4364	4
3	0.7818	0.6416	0.4104	0.3681	0.3893	7
4	0.7498	0.9072	0.3999	0.4575	0.4287	6
5	0.8676	0.1926	0.4415	0.2766	0.3591	8
6	0.9981	0.6214	0.4991	0.3627	0.4309	5
7	0.9016	0.8928	0.4552	0.4516	0.4534	3
8	1.0000	0.9700	0.5000	0.4854	0.4927	1
9	0.9566	1.0000	0.4792	0.5000	0.4896	2

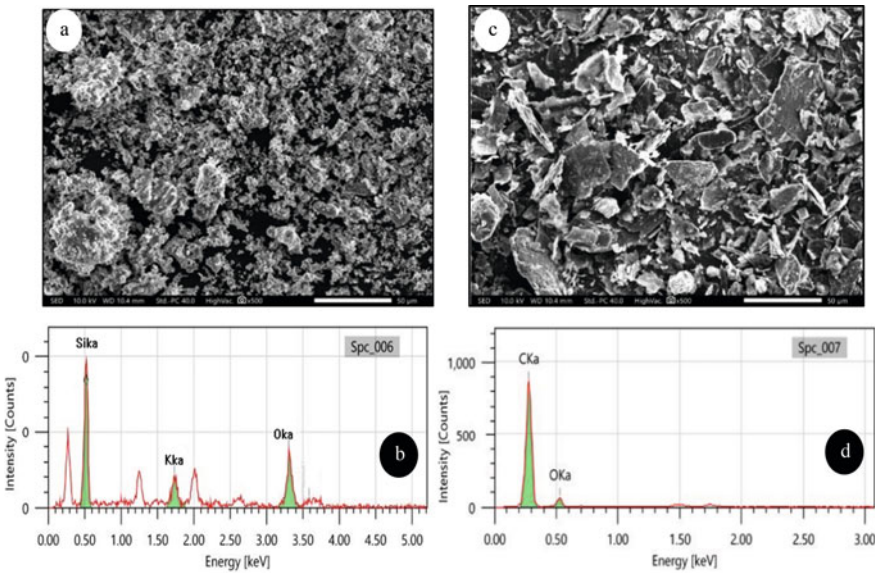


Fig. 1 a SEM of CCA, b EDS results of CCA, c SEM of graphite, d EDS results of graphite

Similarly, graphite went through the same procedure and it was noticed that graphite has a plate-like structure (Fig. 1c) and EDS (Fig. 1d) shows the presence of carbon and oxygen in it.

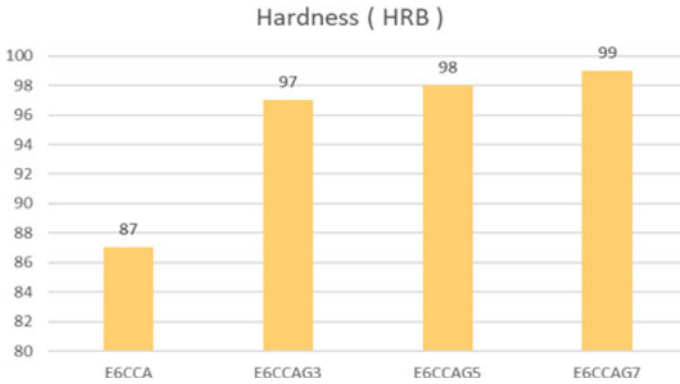


Fig. 2 Hardness of the composite

3.2 Hardness of Composite

Figure 2 shows the hardness of the developed specimens. The hardness of the composites was found to increasing as the content of the graphite was increased. Load bearing capacity of the composite was enhanced as the graphite filling was increased.

3.3 Arithmetical Analysis

Regression analysis was done on the results obtained by the experimentation for this purpose the MINITAB-19 statical software was utilized. Equations 9 and 10 are quadratic equations obtained for the response of the frictional coefficient and specific wear rate respectively. Using this regression analysis, we can plot the normal probability for μ and K_s as shown in Fig. 3a, b.

$$\mu = 0.4856 - [0.02730 * (\%G)] - [0.00373 * N] + [0.000258 * S] \tag{9}$$

$$K_s = 4.08 - [0.393 * (\%G)] - [0.0268 * N] - [0.00078 * S] \tag{10}$$

Figure 4a, b represent the main effect plot for ‘ μ ’ and ‘ K_s ’ from these it can be concluded that ‘ μ ’ get reduced as ‘ $\%G$ ’ and ‘ N ’ increases but it gets increased as ‘ S ’ gets increased. ‘ K_s ’ get reduced as ‘ $\%G$ ’ and ‘ N ’ increase but for an increase in ‘ S ’ firstly it gets reduced and then gets increased continuously.

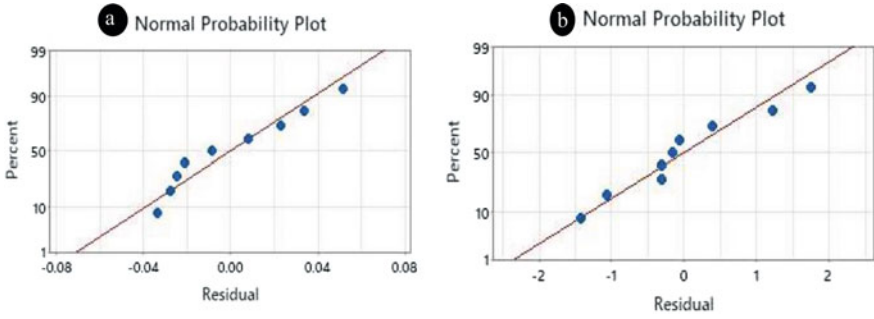


Fig. 3 Normal probability plot for: a coefficient of friction b specific wear rate

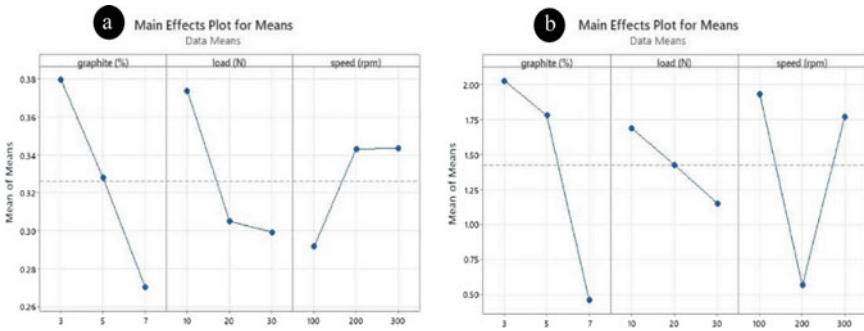


Fig. 4 Main effect plot for a coefficient of friction b specific wear rate

4 Conclusion

From the experimental work carried out for developing a wear-resistant, low friction polymer matrix composite using graphite as secondary reinforcement following conclusions are made.

- (1) With the addition of the graphite particle as a secondary reinforcement, in the epoxy-CCA, the hardness is increased by 13%, compared with the Epoxy-CCA composite (6% CCA).
- (2) Increase in graphite contain from 3 to 7% by wt resulted in lowering the coefficient of friction (up to 0.3629 to 0.2369) and specific wear rate $0.2977 \times 10^{-5} \text{ mm}^3/\text{Nm}$, as compared with Epoxy-CCA composite (6% CCA). This improvement can be attributed to an increase in hardness.
- (3) Frictional coefficient and specific wear rate decreased by 32% and 35% respectively compared with the epoxy-CCA composite (6% CCA).
- (4) The results for epoxy-CCA composite (6% CCA) were found in confirmation with the results obtained by Omkar et al. [6].

References

1. Alajmi, M., Alrashdan, K. R., Alsaeed, T., & Shalwan, A. (2020). Tribological characteristics of graphite epoxy composites using adhesive wear experiments. *Journal of Materials Research and Technology*, 9(6), 13671–13681. <https://doi.org/10.1016/j.jmrt.2020.09.106>
2. Baptista, R., Mendão, A., Guedes, M., & Marat-Mendes, R. (2016). An experimental study on mechanical properties of epoxy-matrix composites containing graphite filler. *Procedia Structural Integrity*, 1, 74–81. <https://doi.org/10.1016/j.prostr.2016.02.011>
3. Basavarajappa, S., Ellangovan, S., & Arun, K. V. (2009). Studies on dry sliding wear behaviour of Graphite filled glass-epoxy composites. *Materials & Design*, 30(7), 2670–2675. <https://doi.org/10.1016/j.matdes.2008.10.013>
4. Subbaya, K. M., Suresha, B., Rajendra, N., & Varadarajan, Y. S. (2012). Grey-based Taguchi approach for wear assessment of SiC filled carbon-epoxy composites. *Materials and Design*, 41, 124–130. <https://doi.org/10.1016/j.matdes.2012.04.051>
5. Zhu, Z., et al. (2015). Friction and wear behavior of resin/graphite composite under dry sliding. *Journal of Materials Science and Technology*, 31(3), 325–330. <https://doi.org/10.1016/j.jmst.2014.10.004>
6. Mestry, O., et al. (2022). Investigation into tribological performance of corn cob ash reinforced epoxy composites using RSM based TLBO algorithm. *Materials Today: Proceedings*, 60, 2076–2083. <https://doi.org/10.1016/j.matpr.2022.01.305>
7. Shankar, S., & Elango, S. (2017). Dry sliding wear behavior of palmyra shell ash-reinforced aluminum matrix (AlSi10Mg) composites. *Tribology Transactions*, 60(3), 469–478. <https://doi.org/10.1080/10402004.2016.1178362>
8. Friedrich, K., Chang, L., Hauptert, F. (2011). Current and future applications of polymer composites in the field of tribology. in *Composite materials* (pp. 129–167). Springer. https://doi.org/10.1007/978-0-85729-166-0_6
9. Srivastava, V. K., & Pathak, J. P. (1996). Friction and wear properties of bushing bearing of graphite filled short glass fibre composites in dry sliding.
10. Bagci, M., & Imrek, H. (2013). Application of Taguchi method on optimization of testing parameters for erosion of glass fiber reinforced epoxy composite materials. *Materials and Design*, 46, 706–712. <https://doi.org/10.1016/j.matdes.2012.11.024>
11. Peng Chang, B., Md Akil, H., Bt Nasir, R., & Khan, A. (2015). Optimization on wear performance of UHMWPE composites using response surface methodology. *Tribology International*, 88:252–262. <https://doi.org/10.1016/j.triboint.2015.03.028>
12. Biswas, S., & Satapathy, A. (2009). Tribo-performance analysis of red mud filled glass-epoxy composites using Taguchi experimental design. *Materials and Design*, 30(8), 2841–2853. <https://doi.org/10.1016/j.matdes.2009.01.018>

A Comparative Study of Nano—MQL and MQL on Chip Morphology and Shear Angle Under High Speed Turning of Inconel 718: For a Sustainable Machining



Pravin Mane, Anupama Kallol, Pravin Dhavale, and Avinash Khadtare

Abstract In this paper discussed the sustainable machining in terms of systematic utilization of Minimum Quantity Lubrication (MQL) and Nano MQL technique during high-speed turning of Inconel 718. The experimental study analyzed the effect of different cooling techniques, cutting speed, flow rate and weight percentage of nano particles on chip morphology and shear angle. Chip formation and its morphology provides in depth knowledge about the material deformation and cutting energy utilization whereas shear angle gives information about plastic deformation while cutting. There are four input parameters considered for the experimentations and experimental plan was designed based on the L_{18} orthogonal array. A triangular shaped WC based TiAlN coated inserts were selected for machining. Higher chip thickness ratio observed in case of MQL at lower cutting speed whereas as in NMQL at higher cutting speed. Short and snared chips are provided in case of nano MQL at higher cutting speed and whereas coil and continuous chips are produce at lower cutting speed in MQL environment. However, higher shear angle is observed in case of nano MQL than the MQL.

Keywords MQL · NMQL · Chip morphology · Shear angle · Sustainable machining

P. Mane (✉) · A. Khadtare
D Y Patil College of Engineering and Technology, Kolhapur 416006, India
e-mail: padhavale@coe.sveri.ac.in

A. Kallol
KLS Gogte College of Technology, Belgavi 590006, India

P. Dhavale
SVERI's College of Engineering, Pandharpur 413304, India

1 Introduction

In recent years the machining performance and productivity are improved through the utilization of cooling medium at the chip-tool interface. The main function of cutting fluids is to provide lubrication, reduction of friction between the tool-workpiece, minimize the cutting temperature at the tool-tip nose, and efficiently chip removal from the machining zone [1, 2]. The majority of cutting fluids used in metal cutting practices are mineral based. These cutting fluids continuously circulate during machining results difficult for disposal and repeated used if cutting fluids may changes the chemical structures. However, in practice, a large quantity (flood cooling) of cutting fluids are employed which leads to increasing the machining cost also large usage of cutting fluids generates mist which badly affects the respiratory system of the operator. Hence, to overcome this issue in the modern manufacturing era a sustainable system has to be implemented as a primary requirement and to provide effective solutions. The main aim of sustainability is to achieve better results from available resources through experimental studies with optimum utilization. Also, it will focus on the environmental, economic, and social points of view. Nowadays, researchers have tried to reduce cutting fluids consumption, also, cutting energy, cutting temperature, and reducing the environmental issues created by flood cooling. Hence, these issues can be minimized through alternative cooling techniques such as Minimum Quantity Lubrication (MQL) in the recent year. MQL is a novel technique in which is used a minimum quantity of cutting fluids is sprayed over the machining zone for reducing the usage of cutting fluid, improving the tool life, and reduce the machining forces and temperature [3, 4]. Besides, most of the authors mentioned that turning of Inconel 718 is a difficult. Because it is a precipitation hardening Ni-Cr based alloy, maintains its strength at high temperature working condition. Also, it is wrought form alloy that provides higher corrosion and creep resistance that it is primarily used in aircraft turbine engines parts and their associated parts. Besides, IN 718 has a low thermal conductivity; because of that large amount of heat is accumulated at toolworkpiece junction which results decreases the tool performance and subsequently affects the tool life. In addition to that higher strength of material and carbide presence in the microstructure generates higher cutting forces initiates the rapid tool wear and observed different tool wear mechanisms. Therefore, above difficulties are affects the material deformation characteristics as well as surface integrity of machined surface while turning. Hence, to improve the machining performance in turning of IN 718 cooling techniques are suggested. But turning of Inconel 718 superalloy with MQL is not an effectively cooling technique to remove high heat carry from the cutting zone. Therefore, to increases the heat carrying capacity and lubrication of MQL. The nano particles are mix with cutting fluids called as a Nano MQL. Therefore, these nano fluids have superior properties than MQL in term of thermal conductivity, high heat carrying capacity, good viscosity, and better lubrication provides a promising solution [5]. In the past literature various types of nano particles are used to prepare in nano MQL to improve the machining performance. In this context, Ali et al. [6] studied the effect of nano-fluid in turning of titanium alloys.

For uniform dispersion of nano particles in base oil they added surfactant in base fluid. Experimental results observed that feed rate and weight percentage of nano fluid were effective parameters for minimum tool wear and lower surface roughness. Venkatesan et al. [7] analyzed the machinability characteristics of Nimonic 90A using CuO nano fluid. Experimental results showed that lower concentration of nano particle and feed rate produces lower tool wear and cutting forces and surface roughness. Kumar et al. [8] investigated surface roughness of IN 718 under different machining environments. They observed that at MQL environment lower surface roughness was seen as compared to the dry and flood cooling due to effectively carried heat from machining zone and provides good lubrication between tool-workpiece. Vasu and Reddy [9] studied the effect of MQL on chip formation in machining of IN 600 alloy. They found that spiral and tightly coiled types of chips with brown in colour observed in case of dry turning whereas in MQL loose spring type chips and in case of NMQL loose spring type chips observed with metallic colour. Hegab et al. [10] analysed the effect of nano-fluids on tool performance and chip morphology during machining of Inconel 718. Lower tool wear was observed in case of nano MQL than MQL. Also, BUE formation was observed in case of higher speed and feed rate combination under pure MQL. Further, continuous but loose coiled chips were observed in case pure MQL but discontinuous with small arc chips found in case nano MQL. Duc et al. [11] studied the effect of alumina nano fluid concentration on minimum quantity lubrication hard machining. They suggested that as the increasing of nano particles concentrations in base of the oil thermal conductivity and viscosity of NMQL increases which helps to reduce cutting temperature. Das et al. [12] compared the machinability of AISI 4140 under MQL and Nano MQL environment. Experimental results showed that lower chip reduction coefficient was observed in case of NMQL as compared to the MQL. Khajehzadeh et al. [13] studied the effect of nano fluid on contact length in turning. They observed that contact length between tool-workpiece has been decreases when the using nanoparticles because, it provides lubrication as well as high thermal conductivity of nano particles reduce the machining temperature. Also, Ganesan et al. [14] and Babu et al. [15] studied the effect of nano MQL on machining performance such tool wear surface roughness and chip morphology. It was observed that using the nano particles in the MQL improve the machining performance. From the above mentioned literature reviewed it seen that the utilization of nano particles in MQL enhanced the machining performance. Also, various types of nano particles were used for preparation of nano fluid MQL in the past studies. But copper oxide nano particles were rarely discussed in high speed turning of superalloy. Also, few of the studies were carried on the superalloy but turning performance of cutting fluid at high speed region is not known. Therefore in this experimental study different cooling technique such as MQL and CuO based NMQL were employed for sustainable machining. Therefore, the outcome of this study is to analysis the effect of cooling technique on chip morphology and shear angle under high speed region.

2 Experimental Details

High speed turning was carried on cylindrical workpiece of IN 718 having dimensions of $\text{Ø} 30 \times 200$ mm (Fig. 1a) and it was received as a wrought form as shown in Fig. 1a. The nominal chemical composition of IN 718 was mentioned in Table 1. High speed turning were carried on CNC turning lathe make LMW Ltd India with maximum spindle speed was 3500 RPM (see Fig. 1). A TNMG 160408 MT TT 5080 type triangular shaped cutting inserts make Taegu Tac India was considered for both cutting environments experimental trials. These cutting inserts was coated TiAlN thin film coating and nose radius of cutting insert was 0.8 mm. Further, same cutting inserts were mounted on PCLNR 2525M 12 tool holder (make: Sandvik India) and tool holder clamped on hexagonal turret (see Fig. 1b). The level of cutting input parameters and their level for experiments were tabulated in Table 2 and it was selected based on the past literature. For sustainable machining environments MQL and Nano MQL were considered in this experimental study. For MQL cutting environment soybean oil was considered and it buys from the local market. Whereas, in case of NMQL copper oxide powder selected as a nano particles and supplied by Amnium Technology Pvt. Ltd. Pune. The size of CuO particles was measured using XRay Diffraction (XRD) technique which was available at D Y Patil Medical College, Kolhapur and two different sizes of nano particles were found such as 8 nm and 23 nm. For preparation of nano fluid soybean oil was considered. While the preparation of nano-fluid, initially pre-determined soybean oil poured into the flask then 0.1% of CuO powder was mix with base oil. After short time passes it was observed that a CuO particle agglomerates in the flask. For the better stability of nanoparticles in the base fluid SDBM surfactant has been added to base. When the surfactant added into the base oil the more surface area of nano-particle is contact with oil. Afterwards, the mixture oil and nano-particle was agitated by using magnetic stirrer for a period of 8 h. Then for uniform dispersion of nano-particles in the base oil magnetic stirrer was usage and an ultrasonic probe was made. It was discovered that nanoparticles begin to aggregate after 4 h. As a result, the magnetic stirrer was used for 3 h. CuO nanoparticles were uniformly distributed and stabilized using a 2-h ultrasonication bath procedure. Therefore, this nano-fluid preparation process is followed for different concentration of nano-fluid under the same time span (See Fig. 2). Initially cylindrical bar of Inconel 718 workpiece was clamped on a machine spindle using three jaws chuck and cutting inserts was mounted on tool holder further tool holder was fixed into the hexagonal turret. All the experimental runs were performed randomly according to the L18 orthogonal array using Taguchi method as shown in Table 3 for two separately cutting environment. In case of NMQL feed and depth of cut are kept constant and its magnitude mentioned in Table 2. Each experiment was used a new cutting edge and was carried out with a cutting length of 30 mm. MQL arrangement was employed to feed nano-fluid to the cutting zone (see Fig. 1c). However, there are two inlet ports and one port for oil-mist output in the MQL arrangement. Out of two inlets port one inlet used for compressed air supply at fixed pressure and another port for supply of nano particles for preparation of nano fluid. Further, the compressed air

and nano-particles are mixed together. Finally, this nano fluid was sprayed through a nozzle into the cutting zone. A knob on the MQL setup was used to control the flow rate of the nanofluid. However, in case of MQL only soyabean oil was passed through the input port instead of nano particles. After successfully completions of each experiment metal chips were collected for analysis of chip morphology and chip thickness using tool maker microscope. A small length of chip (5 mm) was considered for chip thickness measured from the respective experimental runs. Further, selected chips were fixed into the clay in such way that thickness of chip was exposed under the TMM. However, for chip thickness analysis five readings were taken along the length of chip at various location and considered average value for the chip thickness ratio analysis. Further, the chip morphology was analysed in terms of qualitatively and chip shape nature.



Fig. 1 Pictorial representation of experimental setup **a** Inconel 718 workpiece, **b** tool holder, and **c** enlarged view of experimental setup

Table 1 Experimental details

Turning work material	IN 718 cylindrical bar
Work material size	Ø 30 × 200 mm
Chemical composition	Ni 50.34%, Cr 17.30%, Mo 2.22, Nb 3.77, Ti 0.68%
Cutting inserts, geometry, and Tool holder specification	TNMG 160408 MT TT 5080, 0.8 nose radius coated by TiAlN, tool holder PCLNR 2525M 12
Machining environments	MQL and Nano MQL
MQL supply details	Pressure 1 Bar

Table 2 Cutting input parameters and their levels

Cutting parameters	Cutting environments	
	MQL	NMQL
Cutting speed (m/rev)	78.54, 117.81, 157.08	78.54, 117.81, 157.08
Feed (mm/rev)	0.12, 0.14, 0.16	0.1 constant
Depth of cut (mm)	0.1, 0.2, 0.3	0.2 constant
Flow rate (ml/hr)	80, 120, 160	80, 120, 160
Weight percentage (%)	–	0.1, 0.2, 0.3
Nano particle size (nm)	–	8, 23

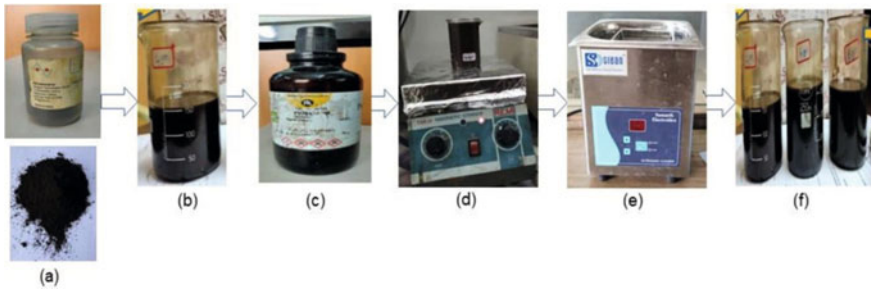


Fig. 2 Procedure of nano fluid preparation **a** CuO powder, **b** soyabean oil with cuo powder, **c** SDBM, **d** magnetic stirrer, **e** ultrasonic bath and **f** nanofluids at different concentration

3 Results and Discussion

In this section effect of cutting environments such and their cutting input parameters on chip thickness ratio and shear angle (plastic deformation) is discussed on the basis of experimental results and analytical calculation.

3.1 Analysis of Chip Thickness Ratio

Chip thickness ratio is a ratio of uncut chip thickness (t) to the chip thickness (t_c). It is denoted by (δ) and it is calculated by using in Eq. 1. It is a useful parameter provides insight information about the plastic deformation and shear angle analysis during machining. Also, it can correlate with machined surface quality with cutting input parameters. The schematic representation of uncut chip thickness and chip thickness

$$\delta = \frac{t}{t_c} \tag{1}$$

Table 3 L₁₈ experimental array

Minimum quantity lubrication (MQL)				Nano minimum quantity lubrication (NMQL)					
Exp. no	Cutting speed	Feed	Depth of cut	Flow rate	Exp. no	Cutting speed	Nano particle size	Weight percentage	Flow rate
1	78.54	0.12	0.1	80	1	78.54	8	0.1	80
2	117.81	0.14	0.2	80	2	117.81	8	0.2	80
3	157.08	0.16	0.3	80	3	157.08	8	0.3	80
4	78.54	0.12	0.1	120	4	78.54	8	0.1	120
5	117.81	0.14	0.2	120	5	117.81	8	0.2	120
6	157.08	0.16	0.3	120	6	157.08	8	0.3	120
7	78.54	0.12	0.2	160	7	78.54	8	0.2	160
8	117.81	0.14	0.3	160	8	117.81	8	0.3	160
9	157.08	0.16	0.1	160	9	157.08	8	0.1	160
10	78.54	0.12	0.3	80	10	78.54	23	0.3	80
11	117.81	0.14	0.1	80	11	117.81	23	0.1	80
12	157.08	0.16	0.2	80	12	157.08	23	0.2	80
13	78.54	0.12	0.2	120	13	78.54	23	0.2	120
14	117.81	0.14	0.3	120	14	117.81	23	0.3	120
15	157.08	0.16	0.1	120	15	157.08	23	0.1	120
16	78.54	0.12	0.3	160	16	78.54	23	0.3	160
17	117.81	0.14	0.1	160	17	117.81	23	0.1	160
18	157.08	0.16	0.2	160	18	157.08	23	0.2	160

is shown in Fig. 3. The chip thickness ratio for MQL and NMQL is tabulated in Table 4. However, to calculate the chip thickness ratio in the different cutting environment the uncut chip thickness was considered as a feed of respective experimental runs. The effect of cutting speed and flow rate on chip thickness ratio under MQL and NMQL cutting environment is as shown in Fig. 4. The continuous lines for MQL cutting environment whereas dotted lines for NMQL. In case of MQL higher chip thickness is observed at lower cutting speed and it decreases with number of points. This is due at lower cutting speed lower heat generation at machining zone and this heat effectively carried by MQL and provides lubrication between them. But at higher cutting speed the performance of cutting fluid decreases due to reduction of thermal conductivity and viscosity of oil hence heat is cannot removed effectively from the machining zone or may be at higher cutting speed oil may be evaporated due to high temperature generation. But in case of NMQL higher chip thickness ratio observed at higher cutting speed with respect to the MQL cutting speed. This is due to the addition of CuO nano particles maintains their thermal conductivity and viscosity of oil at higher cutting speed and removes heat effectively from the machining zone [16]. Besides, as the cutting speed increases material is elastically deformed than the plastically due to the thin types of chips (short and snarled) are observed. Whereas at lower cutting speed, thick chips (continuous snarled) are generated due to plastic deformation results lower chip thickness ratio. However, in case of NMQL at higher flow rate higher chip thickness is observed. This is due to higher flow rate small droplets easily placed between tool-workpiece because of that lower friction takes place. But opposite trend is observed in case of MQL. In addition to that it is seen in case of NMQL chip thickness ratio increases with particle size. The reason behind that as the particle size increases the lower numbers of nano particle available in between the tool- workpiece interaction. Hence, short and snarled chips are produced at 23 nm particle size. It can reflected that such kind of chips are easily removing from the machining zone or they cannot be in contact with machined surface which may results of high surface finish will be obtained. However in case of 8 nm particle size thick continuous type of chips are produced because of that lower chip thickness observed. Further, as weight percentage and flow rate increases the chip thickness also increases. This is due to the higher weight percentage results higher heat carrying capacity of nano fluid which leads to thin chips are formed. However in case MQL as the feed increases chip thickness reduces this is due to that as the feed increases larger chip area is available in front of cutting edge results thicker chips are produced. But at moderate feed higher chip thickness is observed the reason behind that at moderate feed, smaller chip area available therefore chances of thin chips will produced also at moderate feed also MQL can effectively reduce cutting temperature from the machining zone which result less plastic deformation take place during chip formation.

Fig. 3 Schematic representation of turning for chip thickness analysis

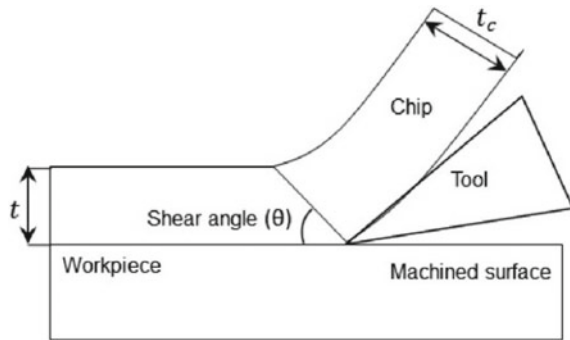


Table 4 Experimental results of MQL and NMQL

MQL			NMQL		
Exp. no	Chip thickness ratio	Chip type	Exp. no	Chip thickness ratio	Chip type
1	0.80	Continuous long	1	0.59	Straight chip
2	0.82	Curl chips	2	0.66	Coil spring
3	0.55	Continuous snarled	3	0.74	Coil spring
4	0.92	Continuous snarled	4	0.55	Helix type
5	0.93	Helix type	5	0.64	Short elemental
6	0.59	Coiled type	6	0.77	Helix type
7	0.75	Spring type	7	0.57	Helix type
8	0.70	Short elemental	8	0.66	Helix type
9	0.72	Tight coiled	9	0.69	Loose coiled
10	0.57	Continuous snarled	10	0.54	Straight chip
11	0.93	Continuous long	11	0.62	Coil spring
12	0.66	Curl chips	12	0.71	Straight chip
13	0.70	Helix type	13	0.59	Coil spring
14	0.73	Tight coiled	14	0.65	Straight chip
15	0.76	Short	15	0.68	Straight chip
16	0.63	Continuous long	16	0.77	Short elemental
17	0.82	Tight coiled	17	0.71	Helix type
18	0.72	Continuous long	18	0.74	Helix type

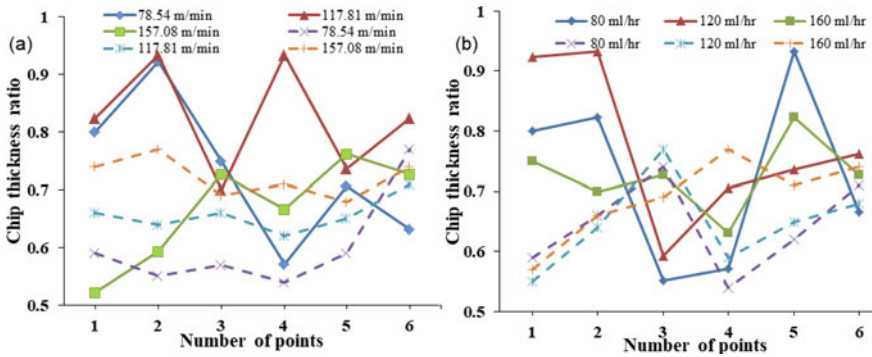


Fig. 4 Effect of a cutting speed and b flow rate on chip thickness ratio under MQL and NMQL cutting environment

3.2 Shear Angle Analysis

The analysis of shear angle for MQL and NMQL is depicted in Figs. 5 and 6 respectively. Shear angle provides a fundamental of machining aspects where chips are separated from machining zone in cutting mechanics also it provides toolworkpiece contact length. This shear is calculated from the chip thickness ratio and it is given in Eq. 2.

$$\theta = \frac{\delta \times \cos\gamma}{1 - \delta \times \sin\gamma} \tag{2}$$

From the Figs. 5 and 6 it is seen that higher shear angle is noticed in case of NMQL than MQL irrespective of input parameters. This is due to that CuO based nano fluid having low viscosity and more thermal conductivity because of that proper cooling is achieved during machining in NMQL as compared to the MQL. Also, Das et al. [16] mentioned that in case of nano fluids larger wetted area and proper cooling take place due to that shorter tool-chip contact take place hence larger shear angle observed. In addition to that in nano fluid machining, fluid film generated due to the presence of nano particles in the fluid. Fluid film reduces the friction leads to produces thin chips as well as small elemental or snared chips or continuous ribbon type see Table 4 and Fig. 8. Besides, in case of MQL shear angle is decreases with cutting speed and flow rate increases see Fig. 5. This is due to higher cutting speed cutting fluid may be evaporated and possibility high friction take place between tool-chip because of that chip will spread [16, 17]. Whereas in case of high flow rate higher amount of cutting fluid inefficient to provides lubrication as well as remove the heat. In case of MQL environment at higher cutting speed continuous ribbon type hips are produced whereas at lower and moderate cutting speed tight coiled or loose spring or elemental snarled chips are produced (see Fig. 7). Whereas in case NMQL as the cutting speed increases shear angle also increases (see Fig. 6a). It indicates that cutting work surface

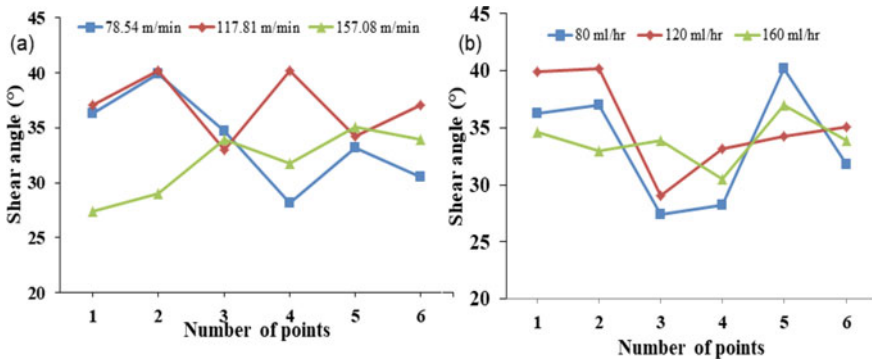


Fig. 5 Effect of a cutting speed and b flow rate on shear angle under MQL

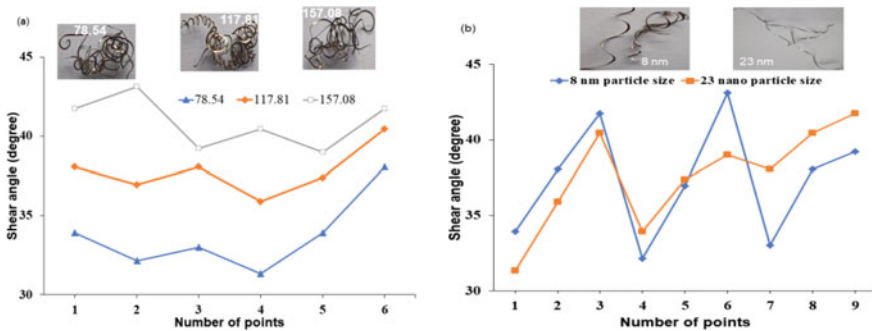


Fig. 6 Effect of a cutting speed and b nano particle size on shear angle under NMQL

deforms by elastically rather than plastically which leads ribbon (thin) types of chip are formed. Whereas at lower cutting speed thick chips (long snarled) are produced which indicates higher cutting energy utilised during turning or utilization of nano fluid in machining zone produces temperature difference between front and back surfaces of chips because of that long-snarled types of chips produced. A similarly results are observed by pawade et al. [18] Also higher shear angle is observed at lower cutting speed in case of 8 nm particle size (see Fig. 6b). It may be due to lower cutting speed generates lower temperature at machining zone also 8 nm particle produces protective film between tool and workpiece effectively because of that lower tool-chip contact take place hence ribbon type of chips are produced.

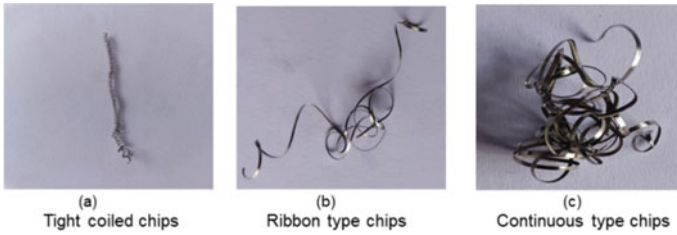


Fig. 7 Chip morphology of MQL environment at **a** 78.54 m/min, **b** 117.81 m/min and **c** 157.08 m/min

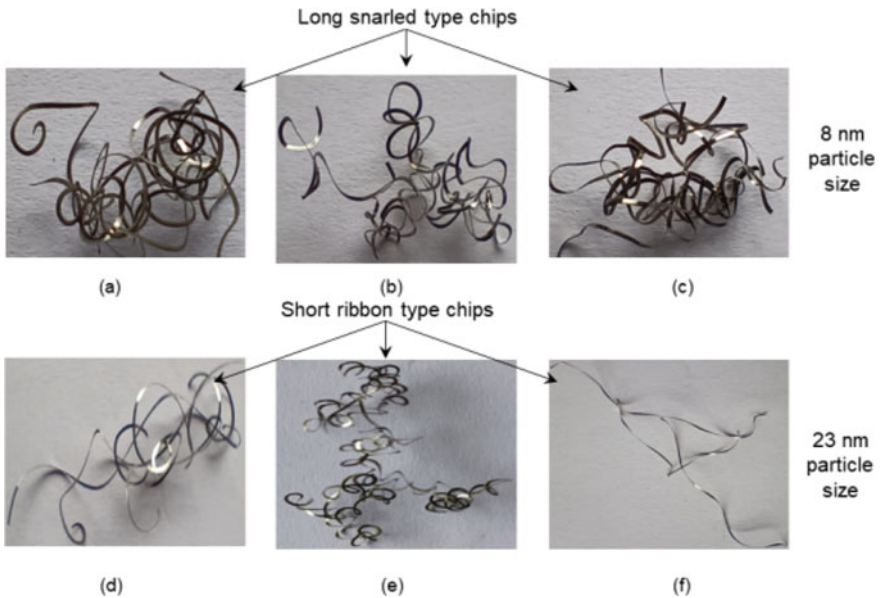


Fig. 8 Chip morphology of NMQL environment at **a, b, c** 8 nm and **d, e, f** 23 nm

4 Conclusions

From the experimental study and analytical calculation following conclusions are drawn.

1. Higher chip thickness ratio is observed in the MQL environment at moderate cutting speed but in case of NMQL higher chip thickness ratio observed at higher cutting speed and it increases with cutting due elastic deformation and better cooling and lubrication. Also, in case of MQL feed increases chip thickness ratio increases. Whereas in case of nano particle size increases chip thickness ratio also increases.

2. As cutting speed increases shear angle increases in case of NMQL and it reflect that short tool-chip contact length. Whereas in case of MQL at lower cutting speed and flow rate indicates the higher shear angle and decreases with cutting speed and flow rate respectively.
3. There are various type of chips type observed in MQL and NMQL cutting environment. But in case of NMQL most short, snarled and continuous chips are observed whereas in case of MQL tight coiled or helix type or spring type chips are observed.
4. From this study conclude that cutting performance at higher cutting speed can be improved by NMQL than MQL.

Acknowledgements The authors would like to acknowledge the support of D Y Patil Medical College Kolhapur for providing XRD facility. Besides, authors thank to Department of Mechanical Engineering D Y Patil College of Engineering and Technology Kolhapur, where this experimental analysis was carried out.

References

1. Srikant, P. N., & Rao, R. R. (2015). Sustainable machining utilizing vegetable oil based nanofluids. In *International conference on smart technologies and management for computing, communication, controls, energy and materials* (pp. 664–672).
2. Benedicto, E., Carou, D., & Rubio, E. M. (2017). Technical, economic and environmental review of the lubrication/cooling systems used in machining processes. *Procedia Engineering*, 184, 99–116.
3. Heinemann, R., Hinduja, S., Barrow, G., & Petuelli, G. (2006). Effect of MQL on the tool life of small twist drills in deep-hole drilling. *International Journal of Machine Tools and Manufacture*, 46(1), 1–6.
4. Kamata, Y., & Obikawa, T. (2007). High speed MQL finish-turning of Inconel 718 with different coated tools. *Journal of Materials Processing Technology*, 192, 281–286.
5. Amrita, M., Srikant, R. R., & Sitaramaraju, A. V. (2014). Performance evaluation of nanographite-based cutting fluid in machining process. *Materials and Manufacturing Processes*, 29(5), 600–605.
6. Mahboob Ali, M. A., Azmi, A. I., Mohd Khalil, A. N., & Leong, K. W. (2017). Experimental study on minimal nanolubrication with surfactant in the turning of titanium alloys. *The International Journal of Advanced Manufacturing Technology*, 92(1), 117–127.
7. Venkatesan, K., Devendiran, S., Thakur, A., Chauhan, V. A., & Pavan Kalyan, P.V. (2018). Study on influence of machinability characteristics in machining of nimonic 90A alloy using copper oxide nanofluid in MQL mode. *International Journal of Mechanical Engineering and Technology*, 9(3), 978–986.
8. Kumar, S., Singh, D., & Kalsi, N. S. (2017). Experimental investigations of surface roughness of Inconel 718 under different machining conditions. *Materials Today: Proceedings*, 4(2), 1179–1185.
9. Vasu, V., & Pradeep Kumar Reddy, G. (2011). Effect of minimum quantity lubrication with Al₂O₃ nanoparticles on surface roughness, tool wear and temperature dissipation in machining Inconel 600 alloy. *Proceedings of the IMechE Part N: Journal of Nanoengineering and Nanosystems*, 225(1), 3–16.

10. Hegab, H., Umer, U., Soliman, M., & Kishawy, H. A. (2018). Effects of nano-cutting fluids on tool performance and chip morphology during machining Inconel 718. *International Journal of Advanced Manufacturing Technology*, 96(9), 3449–3458.
11. Duc, T. M., Long, T. T., & Dong, P. Q. (2019). Effect of the alumina nanofluid concentration on minimum quantity lubrication hard machining for sustainable production. *Proceedings of the IMechE Part C: Journal of Mechanical Engineering Science*, 233(17), 5977–5988
12. Das, A., Das, S. R., Patel, S. K., & Biswal, B. B. (2020). Effect of MQL and nanofluid on the machinability aspects of hardened alloy steel. *Machining Science and Technology*, 24(2), 291–320.
13. Khajehzadeh, M., Moradpour, J., & Razfar, M. R. (2019). Influence of nanofluids application on contact length during hard turning. *Materials and Manufacturing Processes*, 34(1), 30–38.
14. Ganesan, K., Naresh Babu, M., Santhanakumar, M., & Muthukrishnan, N. (2018). Experimental investigation of copper nanofluid based minimum quantity lubrication in turning of H 11 steel. *Journal of the Brazilian Society of Mechanical Sciences and Engineering*, 40(3), 1–17.
15. Babu, M. N., Anandan, V., Muthukrishnan, N., & Gajendiran, M. (2018). Experimental process to evaluate the minimum quantity lubrication technique using copper nanofluids in turning process. *International Journal of Mechanics and Materials*, 20(6), 497–512.
16. Das, A., Patel, S. K., & Das, S. R. (2019). Performance comparison of vegetable oil based nanofluids towards machinability improvement in hard turning of HSLA steel using minimum quantity lubrication. *Mechanics & Industry*, 20(5), 506.
17. Muthuvel, S., Babu, M. N., & Muthukrishnan, N. (2018). Copper nanofluids under minimum quantity lubrication during drilling of AISI 4140 steel. *Australian Journal of Mechanical*, 18
18. Pawade, R., Khadtare, A., Dhumal, D., & Wankhede, V. (2019). Machinability assessment in high speed turning of high strength temperature resistant superalloys. *Journal of Advanced Manufacturing Systems*, 18(04), 595–623.

Overview of Mechanics of Porous Dental Implants



Vasuudhaa Sonawane and Ratnakar R. Ghorpade

Abstract The making of porous proposals for bone ingrowth into dental implant materials has undergone recent advances, which have been discussed. Due to the same design criteria for dental implants and different materials created for orthopedic implants in accumulation bone tissue engineering. Utilizing conventional techniques to produce porous titanium is difficult. To simulate the biological and mechanical characteristics of natural bone, a designer can now create more regular porous structures with varied pore sizes, shapes, percentages, and distributions. This is made possible by the advancement of additive manufacturing technology. The research in this field is encouraging and lays the groundwork for innovative advancements in dental implant proposal for patient role with lessened bone remedial.

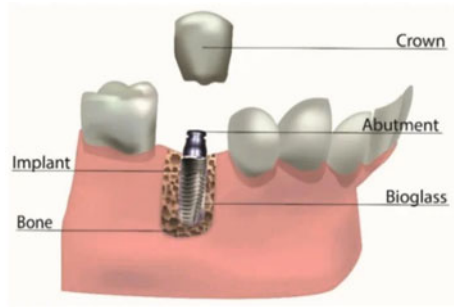
Keywords Dental · Implants · Porous · Biomechanics · Biomaterials · Titanium

1 Introduction

The importance of dental implantology has increased recently because to factors including the rising global population, longer life expectancies, and the pervasive preoccupation with our physical appearance [1]. Dental implants' material composition, geometry (which is typically guided to reduce stiffness), and contact with surrounding tissues have been the main areas of engineering solutions to surge the endurance amount of dental implants that have been thoroughly explored. Bone is a tremendously complex organ that constantly undergoes dynamic remodeling throughout its lifespan [2]. Osteoblasts and osteoclasts play two important roles in this process [3]. To maintain regular bone metastasis, osteoblasts produce new

V. Sonawane (✉) · R. R. Ghorpade
School of Mechanical Engineering, Dr. Vishwanath Karad MIT World Peace University, Pune,
India
e-mail: vasuudhaasonawane@gmail.com

Fig. 1 Modern implants usually implanted in the cecum [5]



bone while osteoclasts located older bone [4]. Mechanical, biological, and 20% peri-implantitis (caused by microbial plaque or bacterial infections), reasons account for the failures of the dental implant's long-term stability. A contemporary implant is schematically depicted in Fig. 1 [5].

2 Coatings in Dental Implants

2.1 Coatings

The most crucial elements aimed at the long-standing longevity of dental work have been recognized as biocompatibility, osseointegration, and the beneficial/sterile effect of the implant layer [6, 7].

Local drug delivery methods and a variety of bioactive materials have been investigated and are tabulated in Table 1. Organic and inorganic coatings are the two types of these novel coatings that have been classified according to the type of material used as shown in Fig. 2. Core bimetals coated with bioactive coatings combine a bioactive material's bone-healing properties with the biomechanical advantages of porous titanium as a matrix.

2.2 Inorganic Coatings

The most frequently utilized implant coatings have been nanostructured calcium, calcium phosphate, and HA). Hydrothermal deposition or plasma spraying are two methods that can be used to apply them to a metal implant. In order to promote bone healing and the mineralization of the interface tissues, these ingredients announcement calcium and phosphate ions [8].

Silver-based Coatings: Chemical stability, thermal resistance, then long-lasting activity are some of the better properties of inorganic-based coatings that work against

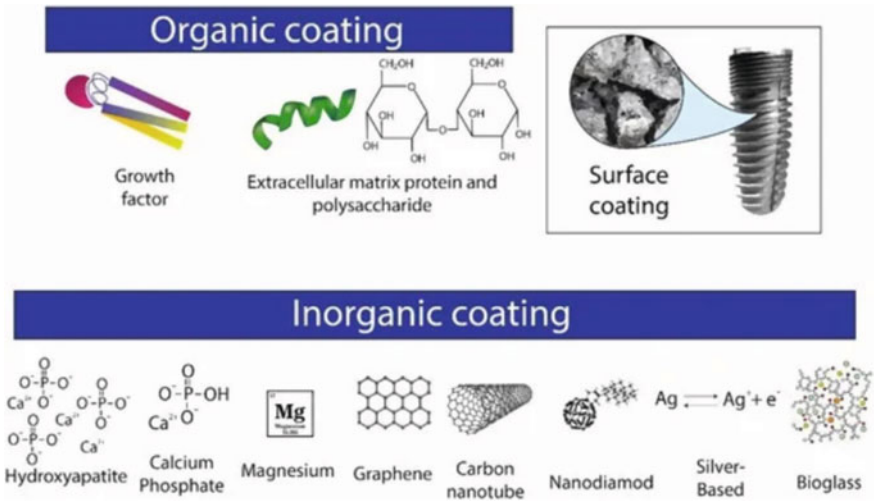


Fig. 2 Novel coatings in dental implantology [8]

microorganisms than mutual organic agents. In addition, silver has demonstrated bactericidal-bacteriostatic oligodynamic antimicrobial movement at extremely low concentrations [9].

Bioactive Glasses: In terms of osseointegration (stimulating bone regeneration) and a high Young’s modulus (averting stress-shielding phenomenon), BG coating for metallic substrates has been deemed more effective and efficient than other surface modifications [9]. The bioactivity of BG is influenced by its porosity and roughness, which can be altered by deposition methods (Fig. 3). The preliminary findings revealed a promising method for fabricating composite-coated porous titanium implants, which could be used to progress another treatments for illnesses in which unlike types of tissues must perfectly join together [10].

2.3 Organic Coatings

Coatings based on growth factors: A set of molecules called growth factors are complex in the process of cell division and tissue proliferation [12].

Coatings Antibacterial Strategies: As a postoperative difficulty of restoration, the presence of infections has frequently been linked to dental implant failure [12].

Coatings for Antifouling: Due to their excellent ability to repel microorganisms, antifouling coatings are gaining popularity in dental implantology. Hydrophilic polymers, zwitterionic materials, and superhydrophobic materials have stayed utilized aimed at this reason [12].

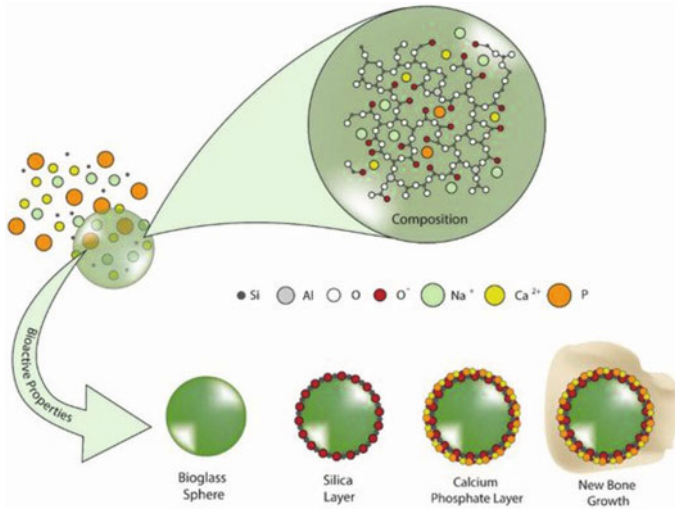


Fig. 3 Proceeding highest of the bioglass particle, a diagram of the various steps that result in the production of HA [11]

3 Dental Implants with a Porous Design

Implant porosity is a compromise between mechanical strength and sufficient tissue in growth-promoting pore size. The implant's pores make it possible for cells to drift, establish connections, thrive, in addition discern. At the same time, the scaffold's pores make room for vascularization in addition the development of new-fangled bone tissue. The shape of the openings, in addition to the pore size that was mentioned earlier, will have an effect on cell ingrowth. Goodman and examined the effect of the form of the cross-section of the pores on the ingrowth of tissue [13]. However, advances in medical care may result from the competition to produce implants that mimic natural tissues. In the process of tissue design, each cell should be represented because it performs particular functions within the body and has particular characteristics. Scientists typically favor one of two design approaches in order to shorten the tissue model and match its inner and outer features to the bone assembly in order to maximize its functionality: regular and irregular (random) structures [13].

The irregular porous structure design process was developed as a way to represent a variety of natural materials [14]. Biomaterials created on high-performance structures have received a lot of attention in recent years. Based on computed tomography and histological data, biomimetic scaffolds that exactly mimic the structure of a trabecular bone were developed as shown in Fig. 4 [15]. Imitating the functionality of matters thru adjusting the absorbency of several regions to achieve One way to simplify the design of biomimetic scaffolds is to mimic the structure of a natural bone [15].

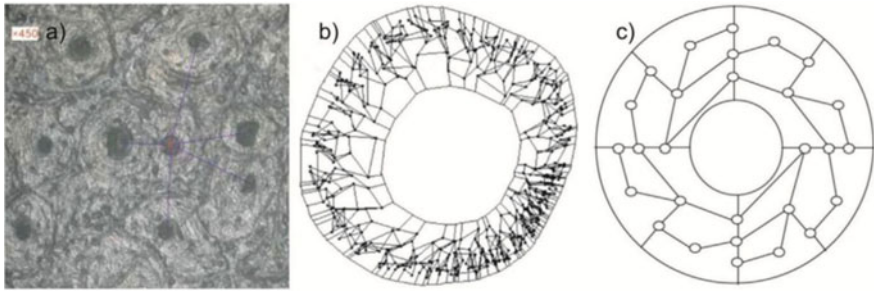


Fig. 4 A photograph of the femur's histological section, an irregular typical of the subject interior microarchitecture, and a simplified mathematical model (semiregular) that resembles the natural bone [15]

Scientists focused on creating abridged replicas that can imitator the functionality of the swapping tissue in order to fabricate scaffolds for tissue engineering. Different approaches have been used to design additively manufactured scaffolds.

Porous titanium or Ti alloys have not yet been manufactured using this method. Computer aided design put together plan is based mainly with respect to strong or surface displaying frameworks [16]. Constructive solid geometry and boundary representation are two examples of these systems as shown in Fig. 5 [17, 18].

The boundary representation design describes the solid through its boundaries, which contain sets of vertices, edges, and loops without clear relations [19].

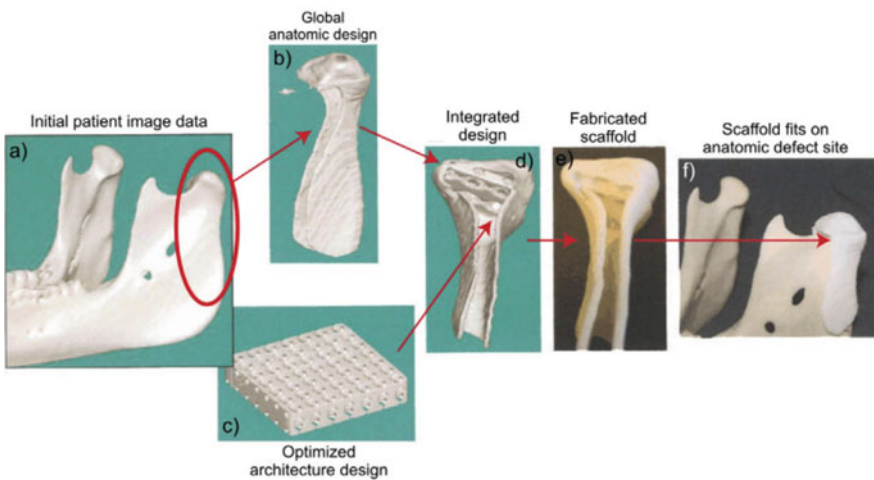


Fig. 5 a Using an image-based method, integrating the designed scaffold with the anatomical shape; a defect area CT or MRI scan. b shaping the scaffold's outer geometry; c designing the internal structure of the scaffold using images; d using Boolean image techniques to integrate scaffold and tissue; e fabricating the scaffold using an additive technique; and f putting the scaffold on the site of the anatomic reconstruction [18]

4 The Manufacturing of PPTM, or Porous Tantalum Trabecular Metal

Stainless steel, titanium alloys, and cobalt chromium have traditionally been the materials of choice for orthopedic implants. These materials have demonstrated high clinical efficacy with modifications and enhancements like porous designs and surface coatings [20].

Orthodontic, craniofacial, and dental implants that are more biocompatible can now be made stronger thanks to the discovery of porous Ta metal as shown in Fig. 6 [21]. Porous Ta metal has a structure with a high volumetric porosity, a low modulus of elasticity, and relatively high frictional characteristics [22]. Solid materials like titanium or porous materials like hydroxyapatite (HA) or tricalcium phosphate (TCP) are typically used to replace osseous structures. Some alloys, like chrome-cobalt or titanium alloy, had been coated with HA or TCP. As an orthopedic implant material, PTTM suggests that it is highly biocompatible, osteoconductive, and encourages bone growth [22]. The PTTM permits an enhancement of the implant surface for both bone ingrowth and bone on growth. Neovascularization and the formation of new bone can occur directly in the implant thanks to the PTTM structure. The term for this idea is “osseoincorporation.”

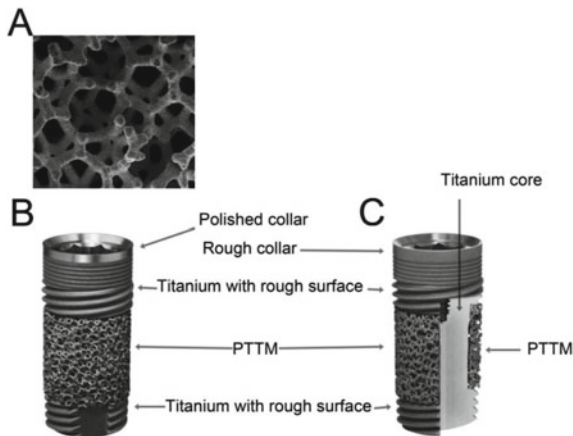


Fig. 6 Dental implants made of titanium with enhanced porous tantalum trabecular metal (PTTM) **a** the PTTM structure; **b** the overall structure of a PTTM-enhanced titanium dental implant with a cervical smooth titanium metal tissue collar; and **c** the structure of a PTTM-enhanced titanium dental implant with a total rough titanium surface displaying the cross-sectional cross-section of the middle-third of the implant with an outer layer of PTTM and a titanium core [21]

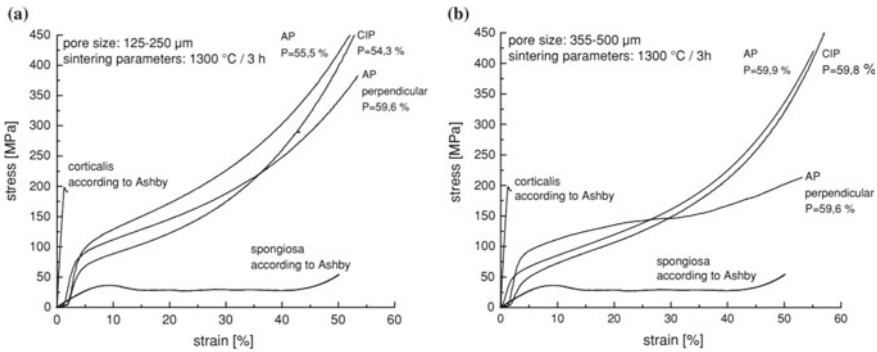


Fig. 7 **a** Comparison between the mechanical performance of human bone tissue and the stress–strain behavior of porous titanium with a pore size of 125–250 μm , as stated by Ashby. CIP stands for cold-isostatically pressed titanium, whereas AP stands for uniaxially pressed titanium. **b** According to Ashby, the mechanical behavior of human bone tissue was compared to the stress–strain behavior of porous titanium with a pore size of 355–500 μm . CIP stands for cold-isostatically pressed titanium, whereas AP stands for uniaxially pressed titanium [23]

4.1 Porous Titanium’s Mechanical Behavior

The stress–strain curve for porous titanium with a porosity of 54.3 to 59.6% and a pore size of 125–250 μm is depicted in Fig. 7. The porosity of the porous titanium samples can effectively adjust the stress–strain curve, which is located in the range of the corticalis and compacta curves. The same data are presented in Fig. 7 for porous titanium with pore sizes ranging from 355 to 500 μm [23].

It is surprising that all of the samples have a higher porosity because the same sintering parameters and quantity of space holder particles were used for all of them. If the application’s primary requirement is uniform deformation behavior in all spatial directions, smaller space holder particles are preferred [23, 24].

5 Conclusions

1. In conclusion, the surface adjustment behaviors augmented in earlier revisions (using porous discs) can be used to modify the surface of a real dental implant using the findings regarding the influence of porosity on dental implants.
2. In the case of immediate implant placement, PTTM-enhanced dental implants (TM implants) had a higher probability of bone gain besides a lower risk of bone loss.
3. The ideal implant should be biocompatible, have higher strength, fatigue, and fracture toughness behaviors, and be able to withstand the body’s reactive environment.

4. Additionally, it is important to take into account the modification of the porous metal surface and the construction of a useful porous metal compound system, both of which can boost cell proliferation and give the porous metal implant its antimicrobial and antineoplastic properties.
5. Similar to Ti implants, porous Ta implants are already available for clinical use and have produced positive outcomes.
6. Due to their excellent biocompatibility and biomechanical properties, tantalum and titanium are the most frequently utilized porous metals in orthopedics.

References

1. Han, Q., Wang, C., Chen, H., Zhao, X., & Wang, J. (2019). Porous tantalum and titanium in orthopedics: A review. *ACS Biomaterials Science & Engineering*, 5(11), 5798–5824.
2. Jemat, A., Ghazali, M. J., Razali, M., & Otsuka, Y. (2015). Surface modifications and their effects on titanium dental implants. *BioMed Research International*, 2015.
3. Pałka, K., & Pokrowiecki, R. (2018). Porous Titanium implants: A review. *Advanced Engineering Materials*, 20(5), 1–18.
4. Bencharit, S. et al. (2014). Development and applications of porous tantalum trabecular metal-enhanced titanium dental implants. *Clinical Implant Dentistry and Related Research*, 817–826.
5. Schiefer, H., Bram, M., Buchkremer, H. P., & Stöver, D. (2009). Mechanical examinations on dental implants with porous titanium coating. *Journal of Materials Science. Materials in Medicine*, 20(8), 1763–1770.
6. Asaoka, K., Kuwayama, N., Okuno, O., & Miura, I. (1985). Mechanical properties and biomechanical compatibility of porous titanium for dental implants. *Journal of Biomedical Materials Research*, 19(6), 699–713.
7. Saini, M. (2015). Implant biomaterials: A comprehensive review. *World Journal of Clinical Cases*, 3(1), 52.
8. Anitua, E., Tapia, R., & Luzuriaga, F (2009). The adaptation of implant osseointe.
9. Trueba, P., Navarro, C., Rodríguez-Ortiz, J. A., Beltrán, A. M., García-García, F. J., & Torres, Y. (2021) Fabrication and characterization of superficially modified porous dental implants. *Surface and Coatings Technology*, 408(January).
10. Keller, J. C., Young, F. A., & Hansel, B. (1985). Systemic effects of porous Ti dental implants. *Dental Materials*, 1(2), 41–42.
11. Xiong, Y., Gao, R., Zhang, H., & Li, X. (2019). Design and fabrication of a novel porous titanium dental implant with micro/nano surface. *International Journal of Applied Electromagnetics and Mechanics*, 59(3), 1097–1102.
12. Piglionico, S., Bousquet, J., Fatima, N., Renaud, M., Collart-dutilleul, P. Y., & Bousquet, P. (2020). Porous tantalum versus Titanium implants: Enhanced mineralized matrix formation after stem cells proliferation and differentiation. *Journal of Clinical Medicine*, 9(11), 1–15.
13. Fialho, L., Grenho, L., Fernandes, M. H., & Carvalho, S. (2021). Porous tantalum oxide with osteoconductive elements and antibacterial core-shell nanoparticles: A new generation of materials for dental implants. *Materials Science and Engineering C*, 120, 111761.
14. Edelmann, A. R., Patel, D., Allen, R. K., Gibson, C. J., Best, A. M., & Bencharit, S. (2019). Retrospective analysis of porous tantalum trabecular metal-enhanced titanium dental implants. *Journal of Prosthetic Dentistry*, 121(3), 404–410.
15. Revathi, A., Borrás, A. D., Muñoz, A. I., Richard, C., & Manivasagam, G. (2017). Degradation mechanisms and future challenges of titanium and its alloys for dental implant applications in oral environment, vol. 76. Elsevier B.V.
16. Menu, A. (1999). Search menu announcement thumb _ up textsms, 9.

17. Smith, T. M. (2014). Current trends in dental morphology research.
18. Topkaya, T., Solmaz, M. Y., Dündar, S., & Eltas, A. (2015). Numerical analysis of the effect of implant geometry to stress distributions of the three different commercial dental implant system. *Cumhuriyet Dental Journal*, *18*(1), 17–24.
19. Baggi, L., Cappelloni, I., Maceri, F., & Vairo, G. (2008). Stress-based performance evaluation of osseointegrated dental implants by finite-element simulation. *Simulation Modelling Practice and Theory*, *16*(8), 971–987.
20. “Published online by Cambridge University Press: 31 January 2011 Article contents”, (January), 9–10.
21. Menu, J. With interconnected 3D porous structures (I3D) a proof-of-concept, 1–10.
22. Weinstein, A. M., Klawitter, J. J., Anand, S. C., & Schuessler, R. (1977). Stress analysis of porous rooted dental implants. *Implantologist*, *1*(2), 104–109.
23. Franciosa, P., & Martorelli, M. (2012). Stress-based performance comparison of dental implants by finite element analysis. *International Journal on Interactive Design and Manufacturing*, *6*(2), 123–129. <https://doi.org/10.1007/s12008-012-0155-y>
24. Stability, E. (2008). Applied osseointegration, *6*(February).

Stress Concentration Studies for Crack Propagation Analysis of Spur Gear Using ABAQUS



Chetan C. Jadhav, Avinash K. Parkhe, Sachin M. Kale,
Sandeep S. Wangikar, Digambar T. Kashid, and Vikram R. Chavan

Abstract Gear failures are usually caused by gears, which are regularly utilised mechanical components in power transmission. Therefore, proper gear design implementation is crucial in light of the various problems that frequently occur during gear operation. The most dangerous failures are those caused by fracture initiation brought on by tensile stress in the tooth foot region, as they have the potential to cause irreparable harm. Utilizing ABAQUS' Extended Finite Element Method, this study's goal is to track the crack progression in a spur gear. Crack initiates where the tensile stress concentration is maximum. The prediction of stress concentration is applied considering the tooth behavior in bending fatigue. The parametric modeling of Spur gear is completed in CATIA to model gear based on Backup ratio. It is shown that the fields of maximum stress concentration are the tooth foot region.

Keywords Spur gear · Stress concentration · Parametric modelling · Backup ratio

1 Introduction

In power transmission, Gearbox failures are typically caused by gears, which are a common mechanical component. Due to their high level of durability and compactness, gears may become the predominant method of power transmission in future machines. A more sophisticated use of gear technology will also be required due to the industry's quick transition from heavy industries like shipbuilding and aviation to industries like auto manufacturing and automation tools.

Typically, gears are created in accordance with DIN and AGMA standards. The pitting of gear teeth sides and tooth fracture in the tooth root are two different types of tooth damage that can happen under repetitive loadings that lead to fatigue. The tooth foot fracture is the most unfavourable damage that may happen to gear units since it frequently renders the gear unit inoperable. A gear unit should always be

C. C. Jadhav (✉) · A. K. Parkhe · S. M. Kale · S. S. Wangikar · D. T. Kashid · V. R. Chavan
Mechanical Engineering Department, SVRI's College of Engineering, Pandharpur, Maharashtra, India
e-mail: ccjadhav@coe.sveri.ac.in

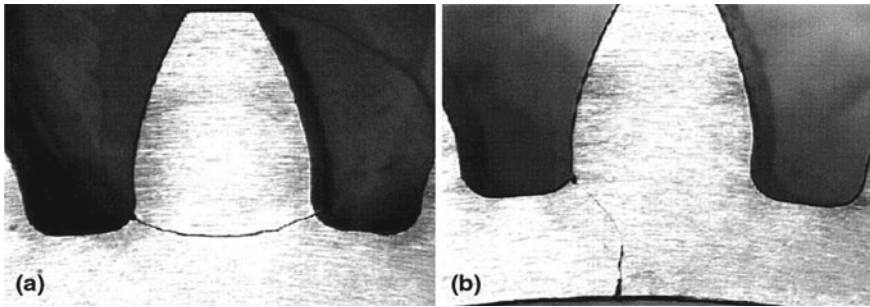


Fig. 1 (a and b): Crack Propagation in a Tooth, b Rim

maintained in the best possible operational condition in order to find, diagnose, anticipate, avoid, and/or remove damage [1]. Modern maintenance obviously serves to identify the gear degradation stage at which a sudden system operation failure may occur in addition to preventing breakdowns. It is vital to design components in particular industrial fields, like the aerospace sector, not only to prevent failures but also to control destructive behaviour in order to prevent catastrophic failure. The term “fail safe design” refers to this method of design [2]. As an illustration, because gears used in aircraft applications must be as light as possible, these components have thin rim and web thicknesses. In fact, if a fracture develops in a thin rim gear close to the tooth root, it may spread in the direction of tooth thickness by completely removing the tooth, or it may spread along the radial direction by completely destroying the gear, see Fig. 1 (respectively a and b).

The main focus of much research on the mechanical and dynamic behaviours of gears has been the phenomena of gear tooth crack propagation. As it relates to gear teeth, linear elastic fracture mechanics (LEFM) has gained popularity and evolved into a useful subject for predicting the behaviour of broken gear teeth.

Many published papers from national and international journals are studied and analyzed to understand the work of the authors which will be helpful to carry out this study. Rathore and Tiwari [3], Stated Fatigue-related gear tooth failure is a common occurrence. The results are catastrophic and occur with little or no warning if gear fails under tensile fatigue conditions. In this study, elliptical and circular stress relieving holes are used, and the outcomes of using circular stress relieving holes are superior. Lewicki and Ballarini [4], carried out experimental and analytical experiments to examine the impact of gear rim thickness on fracture propagation life. The simulation of crack propagation was done using the computer programme FRANC (Fracture Analysis Code). Based on the computed stress intensity variables, various fatigue crack development models were employed to estimate the crack propagation life. To verify anticipated fracture propagation results, experimental tests were carried out in a gear fatigue rig. Pandya and Parey [5], Since there is a tooth fault, the majority of the gear dynamic model depends on the analytical measurement of time-varying gear mesh stiffness. The cumulative reduction index (CRI), which this work presents, makes advantage of a changeable crack intersection angle to examine the impact of

various gear parameters on the overall time-varying mesh stiffness. Weicheng Cui (no. 4), The most frequently used material in engineering structures is stated metal, and fatigue failure is one of the most frequent failure types for metal structures. The most recent advancements in fatigue life prediction methods are highlighted in this paper's state-of-the-art review on metal fatigue. Cura et al. [6], indicates that the issue of crack propagation in gears is one that affects the idea of failsafe design as well as the lifespan of the components. The initial crack position has been numerically analysed in this work with respect to the backup ratio (the ratio between tooth height and rim thickness), and 3D models have been created using the Extended FEM (XFEM) approach. An efficient gear design, according to Eriki et al. [2], strikes a balance between strength, durability, dependability, size, weight, and cost. Even with an adequate gear tooth design, unexpected gear failure can still happen. For a range of gear tooth geometries at a number of crack start locations, crack propagation routes are projected. Consideration is given to the impacts of gear tooth thickness, pitch radius, and tooth pressure angle.

According to the literature study mentioned above, a significant amount of research has been done on the stress and crack propagation in spur gears, as well as the factors that influence these processes [9]. This study will be a great aid in carrying out the numerical analysis and future research on this subject. The purpose of this work is to anticipate the crack propagation path using geometrical gear parameters and the starting crack position, in order to prevent catastrophic failures and provide designers with a highly reliable gear design criterion. Using ABAQUS, the finite element approach is employed in this work to demonstrate that the region surrounding the tooth root fillet has the highest concentration of stress [7]. The fracture will start in the tooth fillet region because that is where the tensile stress is greatest and XFEM in ABAQUS will be used to track the crack's progression.

2 Fracture Mechanics

2.1 Introduction

The following techniques are provided by Abaqus/Standard for conducting fracture mechanics studies: beginning of cracking Contour integrals can be used to study the beginning of cracking in quasi-static issues. Abaqus/Standard computes the J-integral, Ct-integral (for creep), stress intensity factors for homogeneous materials and interfacial fractures, crack propagation direction, and T-stress. Problems in two or three dimensions can benefit from the use of contour integrals. Focused meshes are typically needed for these kinds of issues, and the crack's spread is not investigated.

Crack propagation: It is possible to study quasi-static crack formation along predetermined routes, including low-cycle fatigue. Cracks unbind along surfaces defined by the user. There are several fracture propagation criteria available, and the study can take into account multiple cracks. Crack propagation issues can be asked for contour integrals.

Extended finite element method (XFEM): By including degrees of freedom in elements with unique displacement functions, XFEM represents a fracture as an enriched feature. The mesh does not have to match the geometry of the discontinuities for XFEM to work. Without the need for re-mesh, it can be used to model the beginning and growth of a discrete crack along any given, solution-dependent path, without the requirement to fine-tune the mesh surrounding the crack tip.

2.2 Contour Integral

Contour Integral are output quantities that are only available during general analysis processes and have no bearing on the outcomes. There are two options for evaluating the contour integral in Abaqus/Standard. The first way is based on the traditional finite element method, which normally calls for you to explicitly define the crack front, conform the mesh to the cracked geometry, and designate the direction in which the virtual crack extension will take place. In general, highly detailed meshes are needed, and it can be difficult to produce precise contour integral values for a fracture in a three-dimensional curved surface. To understand crack studies using contour integral an edge crack problem is solved where a crack is defined using contour integral as shown in Fig. 2. Tensile load applied on upper and lower edges of plate which are allowed to move only in Y direction (Fig. 3).

Fig. 2 Seam and crack definition

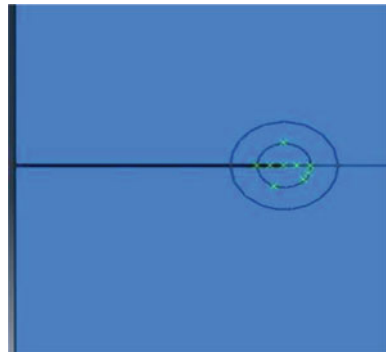
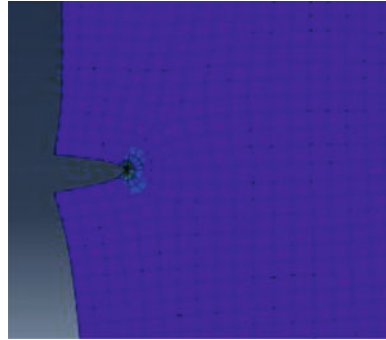


Fig. 3 Crack formation through mesh using contour integral



2.3 *Limitations of Contour Integral*

Using the traditional finite element method to model stationary discontinuities, such a crack, necessitates mesh conformance to the discontinuities' geometric properties. In order to accurately capture the singular asymptotic fields, a significant amount of mesh refinement is required in the area around the crack tip. It is significantly more difficult to model a fracture that is expanding because the mesh must be updated constantly to reflect the geometry of the discontinuity as the crack develops.

The flaws in meshing crack surfaces are fixed by the extended finite element technique (XFEM). Belytschko and Black are the authors who first introduced the extended finite element method (1999). It is an extension of the traditional finite element approach based on Melenk and Babuska's (1996) concept of partition of unity, which makes it simple to include local enrichment functions in a finite element approximation. The particular enriched functions in conjunction with additional degrees of freedom ensure the existence of discontinuities. The finite element framework and its attributes, such sparsity and symmetry, are still present (Fig. 4).

2.4 *Xfem*

The extended finite element approach, which is used to model discontinuities like cracks as enriched features (XFEM). It builds on the idea of partition of unity and is an extension of the traditional finite element method. By enhancing degrees of freedom with unique displacement functions, it permits the presence of discontinuities in an element and does not require that the mesh match the geometry of the discontinuities. Without the need for re-meshing in the bulk materials, XFEM is a very alluring and efficient technique to mimic the beginning and propagation of a discrete crack along an arbitrary, solution-dependent path. Similar edge crack plate problem is solved by defining a crack using XFEM with similar loading and boundary conditions. Two cases are used to show crack, first with no crack propagation as shown in Fig. 5 and second with propagating crack as shown in Fig. 6.

Fig. 4 Defining crack using XFEM

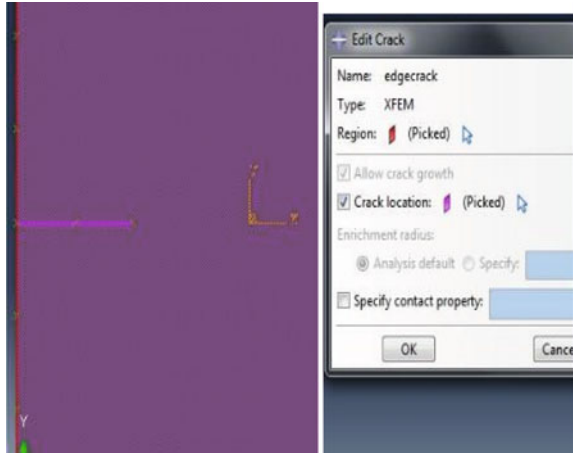
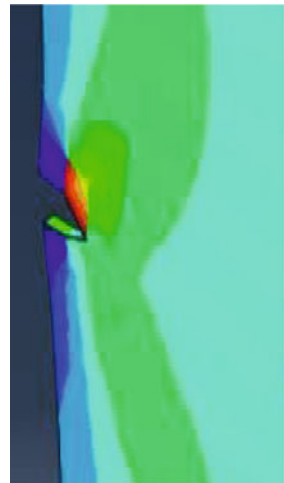


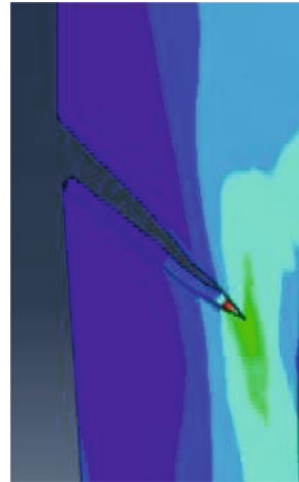
Fig. 5 With no crack growth



3 Gear Modeling

3.1 Introduction

In CATIA, parametric modelling is used to model gear. To define a model in parametric modelling, use parameters (dimensions, for example). Examples of parameters include: material density, formulas used to characterize sweep features, dimensions used to build model features, and imported data (that describe a reference surface, for example). Later, if the parameter is changed, the model will be updated to reflect the change. Usually, there is a connection between the drawings, assemblies, and parts.

Fig. 6 With crack growth

An assembly is made up of several components, and a part is made up of several characteristics. Parts and assemblies can both be used to create drawings.

In this investigation, fracture propagation will be monitored to see if it travels through the tooth, producing noise and vibration, or through the rim, stopping the entire system. The tooth height and rim thickness of the gear affect how far the crack spreads through the tooth or rim. The failure mode will be tooth root failure if the backup rim is thick enough; otherwise, root cracks may spread through the rim. Additionally, it appears that after a certain rim thickness, root failure becomes the failure mode and subsequent rim thickness increases do not increase the gear's basic load capability. Therefore, Backup ratio, which is referred to as the ratio of the rim thickness to the whole depth (height) of the tooth, must be used to model gears.

To study the crack propagation, it is necessary to follow crack for gear geometries with different backup ratio. For this, gears with different backup ratios are required to be modeled and subjected to crack propagation analysis. To overcome the difficulty of conventional modeling of gear with different backup ratios, parametric modeling of gear in CATIA is used so that there is no need to model gear every time when the backup ratio needs to be changed. Just by changing the value of backup ratio in the parameters specified, we get the desired gear geometry.

3.2 Spur Gear Parametric Modeling

The parameters that define the gear geometry are addendum circle, dedendum circle, pitch circle, base circle, module and number of teeth. As we are modelling gear based on backup ratio. Backup ratio is the parameter we are going to include in our modelling (Fig. 7).

Fig. 7 Gear tooth sketch

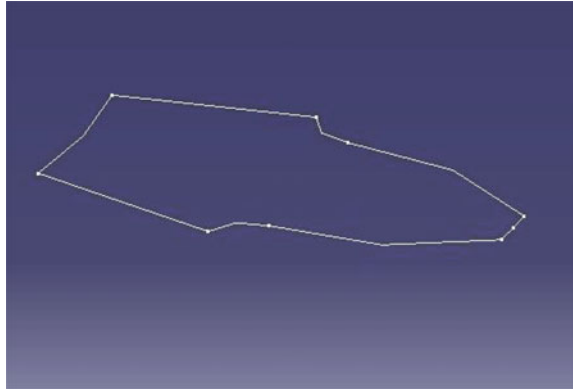


Table 1 Parameters entered in Formulas manager

Module (m)	3.175
Number of teeth (N)	14
Pressure angle	20
Degree Width of Gear in mm	10

<p>The geometric relations of all parameters are as below, $R_p = m * N/2$ $R_b = R_p + m$ $R_a = 0.94 * R_p$ $R_d = R_p - 1.25 * m$ Fillet radius = $0.39 * m$ $Br = R_t/Th$ $R_s = R_d - (R_a - R_d) * Br$ Pressure angle = 20 degree</p>	<p>Where, N—Number of teeth m—module R_p—Pitch circle radius R_b—Clearance or base circle radius R_a—Addendum circle radius R_d—Dedendum circle radius R_s = Slot radius R_t—Rim thickness = $(R_d - R_s)$ Th—tooth height = $(R_a - R_d)$</p>
---	---

This all relations are defined in the formulas manager in CATIA. Once all the relations are defined in formula manager, while modeling gear the parameters are assigned to its respective geometry. When the gear modeling is completed and the geometry needs to be changed, only the required parameters like number of teeth, module or backup ratio changed by entering the required value in the value tab, and all other parameters value gets changed accordingly as shown in Table 1.

The analysis is performed on single tooth of the spur gear to show the areas of stresses. Therefore, the gear sketch geometry of single tooth is modelled which is imported in ABAQUS to analysis. The Spur gear of following parameters will be used for analysis, The rest parameters will be calculated from the geometric relations mentioned above.

4 Gear Tooth Stress Analysis

4.1 Introduction

Two of the most crucial aspects to take into account when looking into real gears in use are the surface conditions and bending failure. When analysing the stress states of elastic bodies with complex geometries, such gears, the finite element approach is frequently used. Spur gears can fail in a number of different ways. Two of a transmission gearbox's primary failure modes are bending failure and tooth pitting. Surface failure is the common term used to describe tooth pitting. An further fascinating issue is the bending strains in a spur gear. Bending failure will happen under excessive loads.

4.2 2D Spur Gear Analysis

Two significant gear design considerations are wear or a gear tooth yielding from high bending loads. The maximum stresses on the compressive and tensile sides of the tooth, respectively, must be known in order to forecast fatigue and yielding [8]. Previously, photo elasticity or quite coarse FEM meshes were used to determine the bending stress sensitivity of a gear tooth. In contrast, we can significantly enhance FEM simulation accuracy using the state-of-the-art in computer technology.

The plane stress static analysis on the 2D model is performed in three ways by applying different kind of load as follows. Static analysis is preferred for analysis since only stress concentration zones are to be determined and not the actual dynamic stresses responsible for crack initiation.

4.3 Pressure Load

Loading—Pressure load is applied at highest point of contact by creating a small surface by partition.

4.4 Concentrated Force

Loading—Concentrated force is applied at highest point of contact in a new coordinate system.

4.5 Surface Traction

When a gear tooth's top edge is loaded, surface traction is applied.

In the direction of the applied load, tensile stress is on the left side of the gear tooth, and compressive stress is on the right side, as shown by Figs. 8, 9, 10, and 11. This region of the gear tooth has the highest concentration of stress. The start of a fracture occurs when the bending forces exceed the permissible fatigue strength.

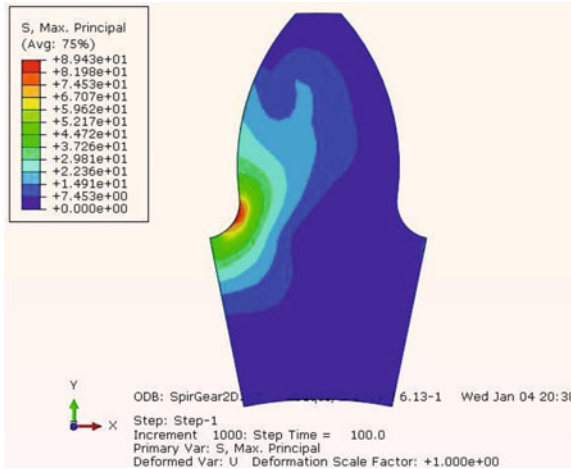


Fig. 8 Max Principal stress showing critical fields of stress concentration at the tooth root

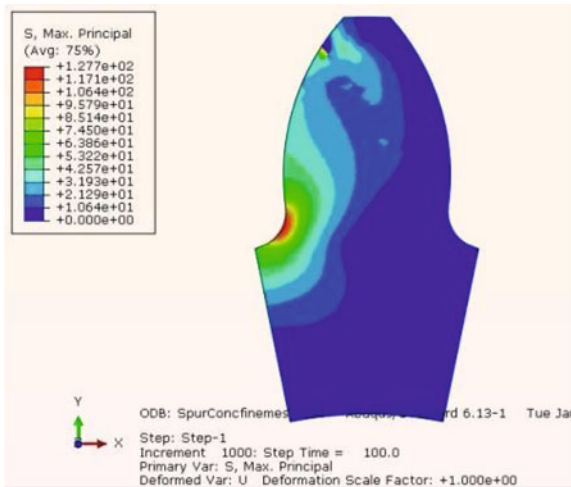


Fig. 9 Max Principal stress showing critical fields of stress concentration at the tooth root with increasing load

Fig. 10 Mises stress showing critical fields of tensile and compressive stress concentration at the tooth root

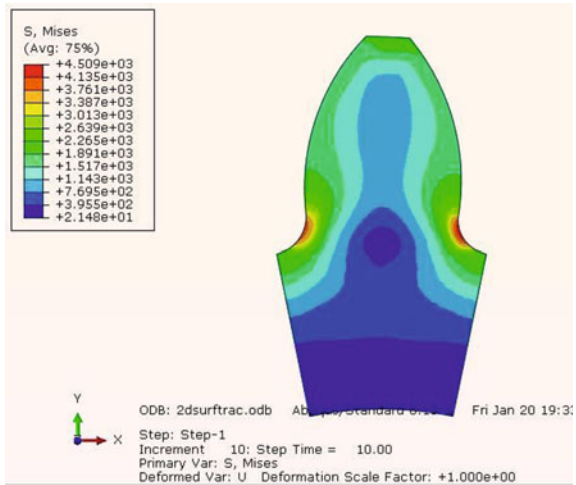
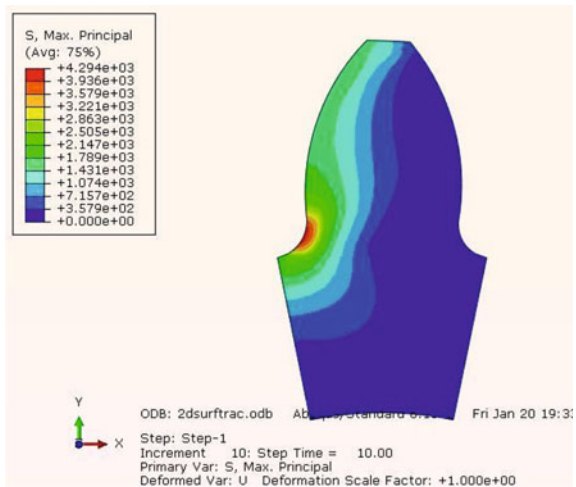


Fig. 11 Max Principal stress showing critical fields of tensile stress concentration at the tooth root



5 Conclusion

It is clear from the model's stress distributions that the tooth's root is subject to significant concentrated stresses. The substantial Von Mises and max primary stresses at the tooth root are depicted in Figs. 8, 9, 10, and 11. Additionally, it can be observed from the data that surface traction loading is most appropriate for bending stress analyses in gear. These bending stresses result in compressive tension on one side and tensile stress on the other. If the tensile stresses are large enough, crack initiation and failure due to crack propagation are primarily caused by them. Due to the shape of the gear, cracks typically start on the tensile side and spread in that direction.

Therefore, At the upcoming experiment, a crack will start in the tooth foot region, where tensile stresses are at their highest, and the fracture propagation for various gear designs will be explored.

References

1. Zouari, S., Maatar, M., & Fakhfakh, T. (2010). Following spur gear crack propagation in the tooth foot by finite element method. *ASM International*.
2. Eriki, A. K., & Ravichandra, R. (2012). Spur Gear crack propagation analysis using finite element method. *IMECS*.
3. Rathore, R. K., Tiwari, A. (2014). Bending stress analysis and optimization of spur gear. *International Journal of Engineering Research & Technology (IJERT)*.
4. Lewicki, D. G., & Ballarini, R. (1997). Effect of rim thickness on gear crack propagation path. *Journal of Mechanical Design, 119*(1), 88–95.
5. Pandya, Y., & Parey, A. (2013). Simulation of crack propagation in spur gear tooth for different gear parameter and its influence on mesh stiffness. *Engineering Failure Analysis, 30*.
6. Cura, F., Mura, A., Rosso, C. (2014). Investigation about crack propagation paths in thin rim gears. *Frattura ed Integrità Strutturale, 30*.
7. Sfakiotakis, V. G., Katsareas, D. E., & Anifantis, N. K. (1997). Boundary element analysis of gear teeth fracture. *Engineering Analysis with Boundary Elements, 20*(2), 169–175.
8. Cui, W. (2002). A state-of-the-art review on fatigue life prediction methods for metal structures. *Journal of Marine Science and Technology*.
9. Yu, W., Shao, Y., & Mechefske, C.K. (2015). The effects of spur gear tooth spatial crack propagation on gear mesh stiffness. *Engineering Failure Analysis*.

Development of Data Fusion Framework for Data-Driven Digital Twin in the Milling Process



A. D. Khandare, V. S. Jadhav, S. P. Deshmukh, and K. K. Rane

Abstract Digital Twin Technology is being considered to optimize the milling process with the least modification in machining to produce the best fit product per the market need and lower the overall production cost. As of now, the researchers are implementing digital twin technology by opting for the use of industrial-grade sensors to create a digital model of the physical model. As the cost of these sensors is sustainably high medium and small-size manufacturers are unable to adopt this technology. This research has developed a cost-efficient and easy-to-use multi-sensor data fuse framework for sensing vibration, acoustic emission, tool temperature, and workpiece temperature. This will be useful for the manufacturers to create a digital model for the optimization of the milling process using machine-learning-based algorithms. This developed framework can also be used on other machines to optimize the machine.

Keywords Digital twin technology · Digital model · Physical model · Milling process · Machine-learning

1 Introduction

Digital twin technology is being experimented with in various fields of engineering and has shown some outstanding results, especially in mechanical engineering helping in the overall improvement of the manufacturing of mechanical components in various machining processes [1], at present manufacturers are only focusing on either of the testing parameters on the machining process and not on all the

A. D. Khandare (✉) · V. S. Jadhav · S. P. Deshmukh
Department of Mechanical Engineering, Government College of Engineering, Karad
Maharashtra 415124, India
e-mail: anandkhandare36@gmail.com

K. K. Rane
National Institute of Manufacturing, Renfrewshire PA4 9LJ, Scotland, UK

parameters. Taking all the parameters in the count will help in further optimizing the machining process, resulting in a better-finished product in less reform, the present study is to optimize the CNC machining process by taking more parameters in the count [2].

Looking at the current state of manufacturing industrial milling operation is preferred for manufacturing mechanical components. As CNC milling can perform various operations on it such as face milling, surface milling, drilling, gear tooth, etc. with a good surface finish. But as of now, there is no real-time quality control, which lacks to optimize the manufacturing process leading to a waste of material and time [3]. the use of various sensors to sense various variable parameters such as spindle speed, tool, and workpiece temperature, vibration on the workpiece, and acoustic emission at the time of operation to fuse the data in a frame will help to monitor and optimize the operation in real-time through implementing a machine learning-based algorithm.

The rest of the paper is organized as follows. In Sect. 2, the data fusion framework of the system with an explanation of the working principles of the sensors employed. Section 3, shows the design of the experiment carried out to validate the designed framework. Discussing the results acquired from various sensors in Sect. 4, and drawing conclusions in Sect. 5.

2 Data Fusion Framework

To develop a low-cost, flexible, and easily implantable data fusion framework to create a digital model of the existing physical model of the CNC milling machine for the creation of Digital Twin for the CNC milling machine, a multiple-sensor setup that uses an Arduino board [4] connected to sensors via a Printed Circuit Board and PLX DAQ software for data acquisition is created for this research. The Arduino board is an open-source platform for connecting various sensors, whereas PLX DAQ is used to acquire data from the sensors through the Arduino board and fuse the data in an excel sheet format [5]. In this study, four types of sensors have been employed to monitor Acoustic Emission, Vibration in the workpiece, and Temperature of the Tool and Workpiece.

2.1 *Adxl335 Accelerometer*

A tri-axial adxl335(Datasheet in Table 1) accelerometer has been adopted to measure the vibration on the workpiece. Adxl335 uses only a single chip for measuring the acceleration in a tri-axle making it cheaper which is based on the principle of capacitance [6]. The conversation of ADC values to acceleration values is done by using the following formulae.

Table 1 Datasheet of the 3-axis accelerometer adxl335

Supply voltage (V)	Sensitivity (mV/g)	Operating temperature (°C)
1.8 to 3	330	- 40 to 85

$$A_{out} = \frac{\frac{ADC\ value * V_{ref}}{1024} - Voltage\ level\ at\ 0g}{Sensitivity\ scale\ factor} \quad (1)$$

where,

- A_{out} = Acceleration value
- ADC value = Raw value from sensor
- V_{ref} = Voltage supplied to the sensor

2.2 Sound Sensor

LM393 Sound sensor has been adopted to measure the Acoustic emission while machining. The sound sensor module provides an easy way to detect sound and is generally used for detecting sound intensity. This module can be used for security, switch, and monitoring applications. Its accuracy can be easily adjusted for the convenience of usage. It uses a microphone that supplies the input to an amplifier, peak detector, and buffer. When the sensor detects a sound, it processes an output signal voltage which is sent to a microcontroller and then performs necessary processing [7].

2.3 Thermal Sensors

To measure the temperature of the workpiece and tool MAX6675 K-type thermocouple (Datasheet in Table 2) and MLX90614 infrared temperature sensor (Datasheet in Table 3) are used respectively. The MAX6675 digitizes a Type-K thermocouple's signal and performs cold-junction correction. The data is produced in a read-only, 12-bit resolution format that is SPI compatible. This converter offers thermocouple accuracy of 8 LSBs for temperatures [8].

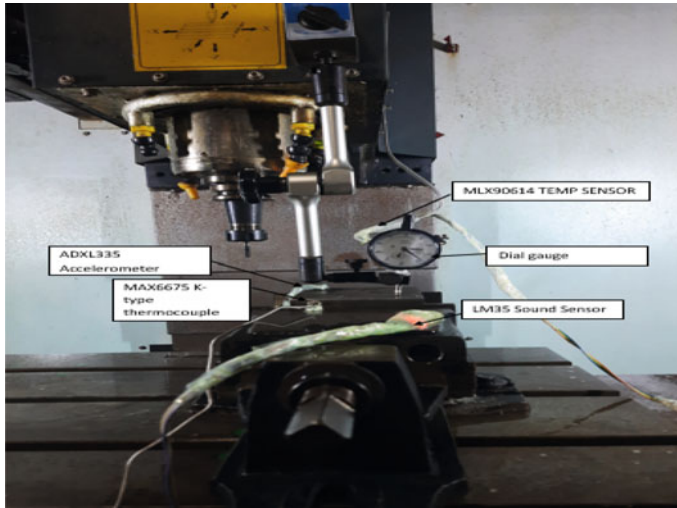
The MLX90614 is a Digital Temperature Sensor with Contactless Infrared (IR). The sensor connects with the microcontroller using the I2C protocol and measures the object's temperature using IR rays without making any physical contact [9].

Table 2 Datasheet of the MAX6675 K-type thermocouple

Supply voltage (V)	Operating temperature(°C)	Temperature resolution (°C)
1.8 to 3	0 to 700	0.25

Table 3 Datasheet of the MLX90614 infrared temperature sensor

Supply voltage (V)	Operating temperature (°C)	Temperature resolution (°C)
1.8 to 3	-70 to 382.2	0.02

**Fig. 1** Experimental setup

3 Design of Experiments

The system is shown in Fig. 1. All the experiments have been carried out on a CNC MAXMILL + 7055 by using 4 flutes 8 mm Solid Carbide TiAN coated milling cutter to machine MS blocks. Adxl335 to sense Vibration placed on the workpiece. LM35 Sound Sensors sense Acoustic Emissions [10], placed at different positions. K-type thermocouples for sensing Workpiece temperature are placed in different positions on the workpiece An Infrared thermocouple for sensing tool temperature is directed toward the cutting edge of the tool.

To validate the designed framework several slots were machined on an MS plate (Fig. 2) with variable Spindle speed, Feed, and Depth of cut. These experimental parameters used while machining is listed in Table 4.

4 Results and Discussion

Figure 3 shows the slot machined with different combinations of parameters. A huge no. of data was collected by the framework containing 7 different signals acquired from a 3 axes acceleration sensor, 2 sound sensors, and 2 thermal sensors in an excel

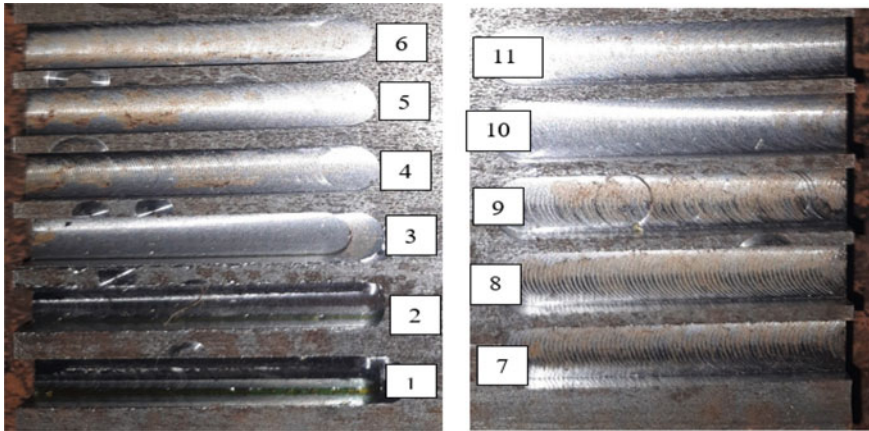


Fig. 2 Machined workpiece

Table 4 Experiment parameters

Slot No.	Spindle speed (rpm)	Feed (mm/rev)	Depth of cut (mm)
1	1000	0.2	0.2
2	1000	0.2	0.4
3	1000	0.2	0.6
4	1000	0.4	0.2
5	1000	0.4	0.4
6	1000	0.4	0.6
7	1000	0.6	0.2
8	1000	0.6	0.4
9	1000	0.6	0.6
10	1200	0.2	0.2
11	1200	0.4	0.2

sheet format by PLX DAQ software through Arduino mounted on PCB shown in Fig. 4.

The Raw Data Acquired from the framework is presented in a graphical format for a better understanding of the testing parameters viz. Vibration signals in the X, Y, and Z axis were obtained from adxl335, Sound Signals were obtained from the sound sensor, and Temperature values were obtained from the MAX6675 K-type Thermocouple and MLX90614 infrared temperature sensor.

Raw data acquired in an excel format has been filtered and graphically represented. Figure 4a represents frequency domain vibration in the X axis for slot no. 6 acquired from accelerometer adxl335 with Spindle Speed: 1000 rpm, Feed rate: 0.4 mm/rev,

start_time	sound_sensor1	sound_sensor2	v	f	workpiece_temp	ambient_temp	tool_temp
1.14375 07-08-2022	30.92	36.83 690 544 406			22.25	24.61	25.19
2.203975 07-08-2022	30.65	36.65 691 554 430			23.75	24.67	28.31
4.343251 07-08-2022	30.65	36.61 597 489 197			24.75	24.71	25.53
5.878906 07-08-2022	30.74	36.28 693 555 417			27.25	24.77	25.23
7.379906 07-08-2022	30.74	35.65 577 490 402			24.25	24.79	25.19
8.878906 07-08-2022	30.65	31.74 523 456 393			25.25	24.81	24.77
10.39453 07-08-2022	30.56	32.83 693 554 408			25.5	24.83	24.89
11.91018 07-08-2022	30.74	35.11 473 433 384			25	24.83	25.11
13.41018 07-08-2022	30.65	32.92 444 405 382			29	24.85	24.65
14.92578 07-08-2022	30.65	32.1 690 552 418			31.5	24.85	24.35
16.42578 07-08-2022	30.74	34.74 462 531 408			31.75	24.89	24.63
17.92578 07-08-2022	30.74	34.19 690 550 410			30	24.87	24.11
19.44441 07-08-2022	30.56	32.87 692 556 417			29.5	24.85	24.39
20.94441 07-08-2022	30.74	35.37 691 551 414			31	24.89	24.05
22.45703 07-08-2022	30.56	34.46 690 558 417			27.5	24.87	24.27
23.95703 07-08-2022	30.74	32.83 498 439 395			25.25	24.87	24.35
25.47266 07-08-2022	30.65	32.28 594 493 403			26.25	24.91	24.13
26.97266 07-08-2022	30.56	34.37 474 422 387			27.25	24.87	24.33
28.48828 07-08-2022	30.74	34.19 473 434 393			29.75	24.91	24.27
29.98828 07-08-2022	30.65	33.65 691 540 415			31.5	24.85	24.15
31.50391 07-08-2022	30.74	33.1 691 551 412			31.75	24.85	24.15
33.00391 07-08-2022	30.65	32.65 642 512 407			30.25	24.87	24.15
34.51393 07-08-2022	30.74	32.28 693 553 417			31	24.85	23.91
36.01393 07-08-2022	30.65	30.1 692 554 415			31	24.85	24.15
37.53516 07-08-2022	30.65	32.28 689 548 408			28	24.87	23.63
39.03516 07-08-2022	30.65	34.46 463 421 386			26	24.89	24.27

Fig. 3 Datasheet acquired from PLX DAQ

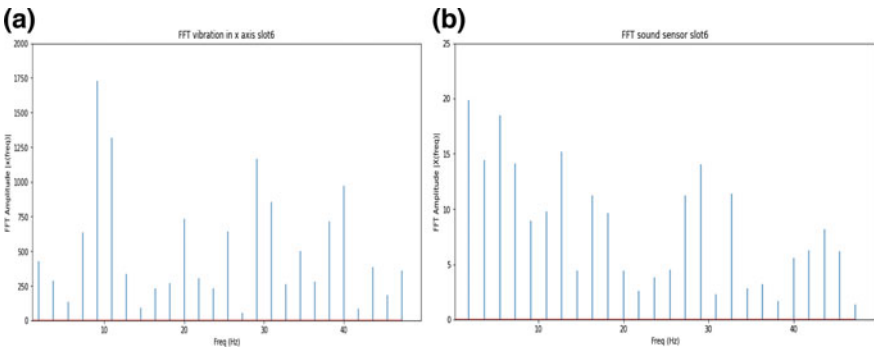


Fig. 4 a Vibration FFT b Acoustic emission

and Depth of cut: 0.6 mm to monitor the vibration level initial peak indicates the initial contact between the Tool and Workpiece where the vibration is high which is at 9 Hz. Figure 4b. Shows Acoustic emission.

Whereas Fig. 5a shows the variation of 8 °C in workpiece temperature for slot no. 6 during machining with the lowest temperature of 25 °C and the highest temperature of 33 °C. The workpiece temperature is quite low as the workpiece is under high-pressure coolant flow. Figure 5b. Shows the variation of 2 °C in Tool temperature for slot no. 6 with the lowest temperature of 23.6 °C and the highest temperature of 25.6 °C. The initial drop in tool temperature is because of the start in the coolant flow on the tool.

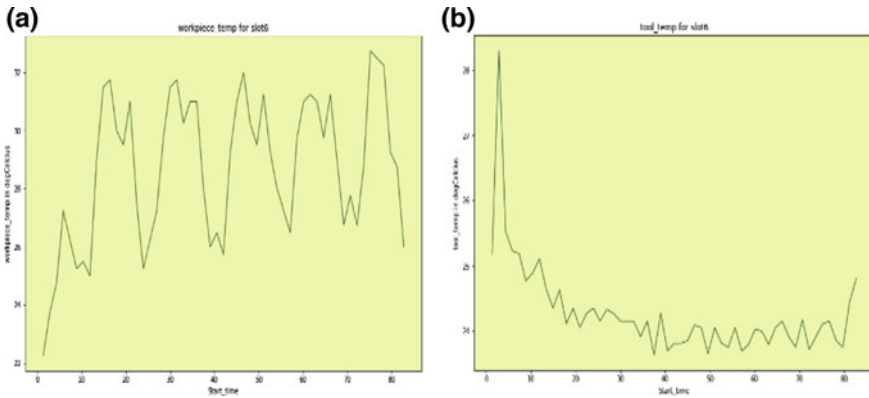


Fig. 5 **a** Workpiece temperature (°C) **b** Tool temperature (°C)

5 Conclusion

A low-cost data fusion framework for data-driven digital twin in the milling process has been developed to conduct an experimental study on various testing parameters such as Vibration, Acoustic Emission, Workpiece, and Tool Temperature while performing a machining operation on a CNC milling machine with variable input parameters such as Spindle Speed, Feed Rate, Depth of cut by using low-cost Arduino base multiple sensors for real-time process monitoring viz. Adxl335 for testing Vibration in the X, Y, and Z axis, LM35 sound sensor for testing acoustic emission, max6675 k-type thermocouple, and mlx90614 infrared temperature sensor for testing workpiece and tool temperature to understand the signature of processes for optimizing the manufacturing process. From this experimental observation following conclusions are drawn.

Adxl335 accelerometer for sensing vibration in the X, Y, and Z axis with the sensitivity scale factor of 330 mV/g, max6675 k-type thermocouple sensor for workpiece temperature ranging from 25 °C to + 80 °C, resolves temperatures to 0. 25 °C. Mlx90614 infrared sensor for tool temperature ranges from 22 to 32 °C. The designed framework fuses the data acquired from various sensors by using an intelligent architecture i.e. PLX DAQ software to understand the signature of processes for optimizing the manufacturing process. The designed framework can utilize to adapt digital twin in the manufacturing process.

Future research includes: conducting more trial run with variable input parameters as well as with different workpieces and tool materials will result in the creation of a highly efficient Digital twin. Experiments can also be conducted on different machines such as CNC Lathe, 3D printers, and Laser cutting machines using this setup to understand the signature of processes for optimizing the manufacturing process. Using a more efficient sensor can increase the accuracy of data, resulting in a more efficient digital twin model. And creating a Digital twin for CNC milling Machine.

Acknowledgements I am grateful to all of those with whom I have had the pleasure to work during this paper. Each of the members of my research committee has provided me with extensive personal and professional guidance and taught me a great deal about both scientific research and life in general.

References

1. Negri, E., Fumagalli, L., & Macchi, M. (2017). A review of the roles of digital twin in CPS-based production systems. *Procedia Manufacturing*, 11, 939–948. <https://doi.org/10.1016/j.promfg.2017.07.198>
2. Mawson, V. J., & Hughes, B. R. (2019). The development of modelling tools to improve energy efficiency in manufacturing processes and systems. *Journal of Manufacturing Systems*, 51, 95–105. Elsevier B.V., April 01, 2019. <https://doi.org/10.1016/j.jmsy.2019.04.008>.
3. Zhang, X. Y., Lu, X., Wang, S., Wang, W., & Li, W. D. (2018). A multi-sensor based online tool condition monitoring system for milling process. *Procedia CIRP*, 72, 1136–1141. <https://doi.org/10.1016/j.procir.2018.03.092>
4. Hoque, M. J., Ahmed, M. R., Uddin, M. J., & Faisal, M. M. A. (2020). Automation of traditional exam invigilation using CCTV and bio-metric. *International Journal of Advanced Computer Science and Applications*, 11(6), 392–399. <https://doi.org/10.14569/IJACSA.2020.0110651>
5. Jatakar, K. H., et al. (2022). Vibration monitoring system based on ADXL335 accelerometer and Arduino Mega2560 interface. *Journal of Algebraic Statistics*, 13(2), 2291–2301. [Online]. Available: <https://publishoa.com>
6. Mukhopadhyaya, S. (2016). Low cost sensor usability with Arduino UNO. <https://doi.org/10.13140/RG.2.1.2139.0327>
7. Nalavade, S. P., Patange, A. D., Prabhune, C. L., Mulik, S. S., & Shewale, M. S. (2019). Development of 12 channel temperature acquisition system for heat exchanger using MAX6675 and Arduino interface. *Lecture Notes in Mechanical Engineering, Pleiades Journals*, 119–125. https://doi.org/10.1007/978-981-13-2697-4_13.
8. Jin, G., Zhang, X., Fan, W., Liu, Y., & He, P. (2015). Design of non-contact infra-red thermometer based on the sensor of MLX90614. *Open Automation and Control Systems Journal*, 7(1), 8–20. <https://doi.org/10.2174/1874444301507010008>
9. Duro, J. A., Padget, J. A., Bowen, C. R., Kim, H. A., & Nassehi, A. (2016). Multi-sensor data fusion framework for CNC machining monitoring. *Mechanical Systems and Signal Processing*, 66–67, 505–520. <https://doi.org/10.1016/j.ymsp.2015.04.019>
10. Tao, F., Zhang, H., Liu, A., & Nee, A. Y. C. (2019). Digital twin in industry: State-of-the-Art. *IEEE Transactions on Industrial Informatics*, 15(4), 2405–2415. <https://doi.org/10.1109/TII.2018.2873186>

Optimization While EDM of 304-H Stainless Steel by Super Ranking Concept



S. A. Sonawane and B. P. Ronge

Abstract In this research work tests are conducted on 304-H stainless steel by electrical discharge machining process. Taguchi's L27 array is applied to conduct the experiments. Process factors chosen for the study are peak current (I_p), pulse on time (Ton), pulse off time (Toff) and tool lift time (TL) and the output characteristics are Material removal rate (MRR), surface unevenness (SR) and tool wear rate. The important process factors are analyzed by applying Taguchi based super ranking concept. The finest mixture of input course parameters started using Taguchi based super ranking concept are peak current 20 amp., pulse on time 60 μ s, pulse off time 90 μ s, and tool lift time 4 s.

Keywords Taguchi method · Super ranking concept · 304-H stainless steel · Material removal rate · Surface unevenness · Tool wear rate

1 Introduction

304-H is a squat carbon austenitic stainless steel alloy widely used in the built-up of shafts, valve trim, valve bodies, boilers, pans and catering tools for the food business, heat Exchangers, pipelines, steam exhausts, cooling towers, condensers and electric production plants. 304-H stainless steel has maintained its popularity due to the excellent properties it possess such as fine oxidation opposition in nonstop tune to 920 C, elevated tensile succumb strength, little and long time creep strength and resistance to rust from oxidation and natural acids.

In EDM incidence of sequence of electrical flashes connecting two electrodes eliminate the matter from work piece. These electrodes are splitted by a small gap and plunged in a dielectric fluid. Later spark occurs for a short time and is initiated at the crest between the assembly surfaces of tool and workpiece. Due to soaring heat of spark origin the localized melting and yet vaporization of material as of the workpiece. To improve surface quality and minimize fabrication cost optimization

S. A. Sonawane (✉) · B. P. Ronge
SVERI's College of Engineering, Pandharpur 413304, India
e-mail: sasonawane@coe.sveri.ac.in

© The Author(s), under exclusive license to Springer Nature Switzerland AG 2024
P. M. Pawar et al. (eds.), *Techno-societal 2022*,
https://doi.org/10.1007/978-3-031-34644-6_64

629

is requisite. Several of manufacturing study engineers to shell out attention into this course to advance process capabilities since its wide variety of applications in industry [1].

Mohanty et. al. [2] applied utility concept and particle swarm optimization (PSO) and quantum behaved particle swarm optimization (QPSO) algorithms to determine optimal parametric combination while EDM of Inconel-718 superalloy. Aliyu et. al. [3] carried out EDM of Siliconized Silicon Carbide and applied response surface tactic for the optimization of course parameters for MRR, TWR and SR. Singh [4] performed grey relational analysis during powder mixed EDM process on T1 grade high speed steel to study the effect of powder concentration, pulse on time, peak current, and tool electrode on MRR, TWR and SR. Faisal [5] applied evolutionary techniques such as biogeography based optimization (BBO) and particle swarm optimization (PSO) technique for the optimization of SR and MRR while EDM of EN-31 tool steel. Huo et. al. [6] conducted experiments on AISI 304 stainless steel on EDM considering input factors as voltage, current, duty factor and tool electrode and output. Das and Chakraborty [7] applied Taguchi based Super ranking concept for the optimization of various nontraditional machining practices such as EDM, WEDM and ECDD. Das et. al. [8] carried out optimization by using Taguchi based super ranking concept during PMEDM of H-11 die steel. Singh et al. [9] applied teaching learning based algorithm and particle swarm optimization algorithm during EDM of 316 L porous stainless steel. Chandrashekarappa et. al. [10] used hybrid Taguchi-Based PCA-Utility and CRITIC-Utility techniques while EDM of HcHr steel.

Thus, current paper incorporates Taguchi process next to with super ranking idea to resolve the desired grouping of EDM course through machining of 304-H stainless steel. This integrated move alters all responses into a solo grade and on additional computations finally ensuing in a lone non dimensional assessment termed as the super position answer.

2 Materials and Methods

In the current study, electrical discharge machining of 304-H stainless steel of dimension 30 mm × 20 mm × 5 mm has been carried out. The EDM machine used was ELEKTRA Punchcut 734. Each experiment was carried out for 10 min. The process factors chosen for the learning are pulse on time, peak current, pulse off time and tool lift time while the presentation procedures considered are tool wear rate (TWR), material removal rate (MRR) and surface roughness (SR). Copper material is used as a tool electrode of diameter 10 mm. The course limits and their heights are exposed in Table 1.

TWR and MRR were planned by using Eqs. (1) and (2).

$$\text{MRR} = \frac{(W_i - W_f)}{\rho \times t} \times 1000 \text{ mm}^3/\text{min} \quad (1)$$

Table 1 Course limits and their heights

Sr. No	Parameter	Symbol	Unit	Levels		
				1	2	3
1	Peak current	A	Amp	10	20	30
2	Pulse on time	B	μs	60	120	180
3	Pulse off time	C	μs	30	60	90
4	Tool lift time	D	s	2	4	6

$$TWR = \frac{(W_i - W_f)}{\rho \times t} \times 1000 \text{ mm}^3/\text{min} \tag{2}$$

where, W_i is the first weight; W_f is the last weight following machining; t is the instance taken in machining and ρ is the density of respective material.

Surface unevenness was deliberated in μm by using Talysurf exterior roughness tester with example span of 0.8 mm. Taguchi’s L_{27} orthogonal table is applied to perform the experiments. Each test was repeated thrice and by using randomization technique. The results of the experiments are indicated in Table 2. Along with the three responses, MRR is Larger-The-Better (LTB) criterion, whereas, the lasting two responses TWR and SR are of Smaller-The-Better (STB) criterion kind.

Dependent on the response kind, Eqs. (3)–(4) are currently utilized to alter the measured answer values into the matching S/N ratios, as offered in Table 3.

$$\text{For LTB response characteristic, } SN = -10 \log \left[\frac{1}{n} \sum \frac{1}{x_i(k)^2} \right] \tag{3}$$

$$\text{For STB response characteristic, } SN = -10 \log \left[\frac{1}{n} \sum x_i(k)^2 \right] \tag{4}$$

3 Optimization by Taguchi Scheme and Super Ranking Theory

The process of optimization by Taguchi based super ranking concept is explained as follows:

After estimation of the S/N ratios, positions are dispensed to all these S/N relations for all of the answers independently. This standing is completed in downward order based on the intended S/N ratio assessments, i.e. the biggest S/N ratio is consigned position 1, the second main position 2 and so on. After apt ranking of all the answers, the next pace engages squaring up of every those positions. The squared positions are

Table 2 Results of the experiments

Exp. No	A	B	C	D	MRR (mm ³ /min)	TWR (mm ³ /min)	SR (μm)
1	10	60	30	2	66.823	7.351	7.214
2	10	60	60	4	30.541	6.234	6.871
3	10	60	90	6	21.894	5.413	6.247
4	10	120	30	4	115.21	8.450	8.971
5	10	120	60	6	68.10	7.235	7.689
6	10	120	90	2	46.670	7.584	7.200
7	10	180	30	6	85.241	9.586	8.763
8	10	180	60	2	75.546	8.436	8.442
9	10	180	90	4	72.210	7.672	7.564
10	20	60	30	4	173.142	12.638	8.787
11	20	60	60	6	115.349	10.685	8.311
12	20	60	90	2	118.430	11.210	7.997
13	20	120	30	6	194.864	14.124	10.230
14	20	120	60	2	173.325	12.284	9.642
15	20	120	90	4	158.229	12.126	8.537
16	20	180	30	2	210.985	14.988	10.016
17	20	180	60	4	175.218	12.960	9.652
18	20	180	90	6	168.549	13.671	9.817
19	30	60	30	6	245.576	15.345	11.679
20	30	60	60	2	224.128	14.487	11.584
21	30	60	90	4	199.458	14.215	11.813
22	30	120	30	2	308.230	16.576	13.472
23	30	120	60	4	270.462	15.972	12.264
24	30	120	90	6	263.754	15.346	12.272
25	30	180	30	4	302.124	17.662	13.359
26	30	180	60	6	262.259	16.334	12.483
27	30	180	90	2	283.357	16.872	12.284

put in together to produce a particular answer which is named as sum of squared positions (SSP). Finally, these worked out SSP values are again positioned in mounting array (lowest being positioned 1), thus changing the multi-answer information into a position feature, phrased as super position answer (SUPA) (Table 4) [8].

Now, the math means of the weighed up SSP worths are figured out as the answer variables and are publicized in Table 5. Derived from these mean worths, the most excellent working levels of the EDM process limits (publicized in bold faced) are recognized. Thus, so as to arrive at the preferred presentation of the EDM course, the best parametric blend is to be place as peak current as 20 amp., pulse on time as 60 μs, pulse off time as 90 μs., and tool lift time 4 s, which can also be symbolized as

Table 3 S/N ratios

Exp. No	S/N ratios		
	MRR	TWR	SR
1	34.7406	-15.8188	-7.1924
2	27.0313	-13.2901	-6.6460
3	23.3403	-12.9394	-6.5599
4	39.8094	-17.0321	-7.5797
5	34.9239	-14.7623	-7.1971
6	31.4401	-15.1838	-7.1217
7	37.1211	-17.5505	-7.4878
8	36.0436	-16.5763	-7.4100
9	35.5599	-15.7627	-7.0776
10	43.4177	-20.2699	-7.5664
11	39.7906	-18.6394	-7.2852
12	40.0271	-18.992	-7.2277
13	44.5332	-21.2267	-7.9798
14	43.4810	-19.9781	-7.6986
15	42.6847	-19.7864	-7.5297
16	45.1952	-21.7994	-8.0050
17	43.5279	-20.48	-7.7218
18	43.1880	-20.9811	-7.6908
19	46.6103	-22.0737	-8.4742
20	45.7869	-21.4775	-8.4950
21	44.7006	-21.2595	-8.3735
22	48.6044	-22.7462	-8.9613
23	47.4440	-22.4609	-8.6933
24	47.2246	-22.0773	-8.7302
25	48.4309	-23.3278	-9.0088
26	47.1610	-22.6534	-8.7485
27	47.8739	-22.9342	-8.7530

A2B1C3D2. The delta value from Table 5 spots peak current as the mainly influencing course limit in purpose of SSP values. This can also be certified from the sharp slope for peak current from the answer graph developed rooted in response bench as illustrated in Fig. 1. The study of discrepancy (ANOVA) results as revealed in Table 6 also identifies peak current as the most important element influencing the process performance [8].

Table 4 Position Transformation

Exp. No	Position			Suqared position			SSP	SUPA
	MRR	TWR	SR	MRR	TWR	SR		
1	24	6	5	576	36	25	637	12
2	26	2	2	676	4	4	684	15
3	27	1	1	729	1	1	731	17
4	18	8	13	324	64	169	557	6
5	23	3	6	529	9	36	574	9
6	25	4	4	625	16	16	657	13
7	20	9	10	400	81	100	581	10
8	21	7	9	441	49	81	571	8
9	22	5	3	484	25	9	518	2
10	14	14	12	196	196	144	536	5
11	19	10	8	361	100	64	525	4
12	17	11	7	289	121	49	459	1
13	11	17	17	121	289	289	699	16
14	13	13	15	169	169	225	563	7
15	16	12	11	256	144	121	521	3
16	9	20	18	81	400	324	805	19
17	12	15	16	144	225	256	625	11
18	15	16	14	225	256	196	677	14
19	7	21	20	49	441	400	890	21
20	8	19	21	64	361	441	866	20
21	10	18	19	100	324	361	785	18
22	1	25	26	1	625	676	1302	25
23	4	23	22	16	529	484	1029	22
24	5	22	23	25	484	529	1038	23
25	2	27	27	4	729	729	1462	27
26	6	24	24	36	576	576	1188	24
27	3	26	25	9	676	625	1310	26

Table 5 Answer bench for means

Level	A	B	C	D
1	612.2	679.2	836.4	866.1
2	601.1	771.1	807.6	715.1
3	1096.7	859.7	666.0	728.8
Delta	495.6	180.4	170.4	151.0
Rank	1	2	3	4

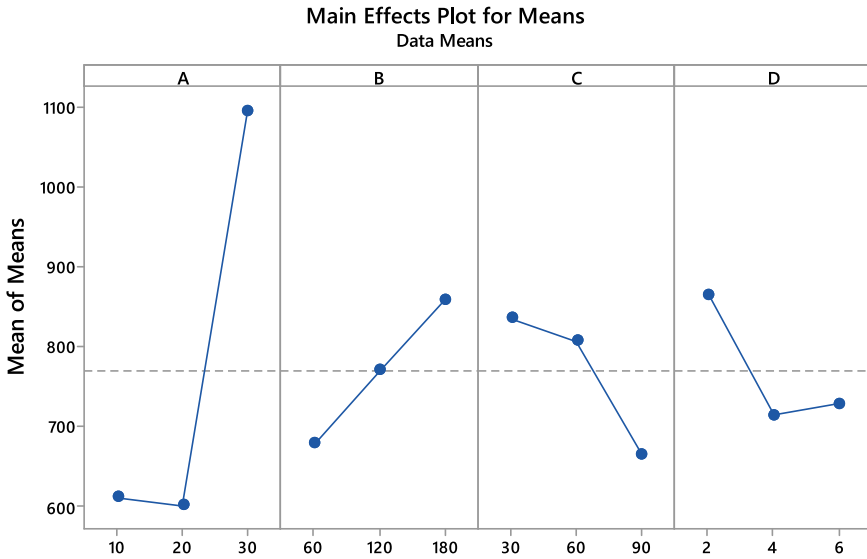


Fig. 1 Response chart for means

Table 6 Analysis of variance

Source	DF	Adj SS	Adj MS	F-value	P-value
A	2	1,441,156	720,578	91.20	0.000
B	2	146,538	73,269	9.27	0.002
C	2	149,772	74,886	9.48	0.002
D	2	125,545	62,772	7.94	0.003
Error	18	142,227	7901		
Total	26	2,005,236			

R-sq = 92.91%, R-sq (adj) = 89.75%

4 Conclusion

From the above scrutiny, it can thus be detected that for the lowest SSP, the optimum parametric grouping of input factors is A2B1C3D2 (peak current as 20 amp., pulse on time as 60 μs, pulse off time as 90 μs, tool lift time 4 s). From the ANOVA analysis it is found that peak current is the most influencing factor on the performance outputs. This technique is simpler, easier and has a smaller amount complex computation and also it does not require calculation of weights. It can be applied to other both conventional and non-conventional machining processes for determination of the desired optimal parametric combinations.

References

1. Vaddi, V. R., Reddy C., S., Pogaku, V. K., & Bushaboina, S. K. (2018). Optimization of electrical discharge machining of Titanium Alloy (Ti-6Al-4 V) using Taguchi-dear method. *SAE International*, 2018–28–0032, 1–5.
2. Mohanty, C. P., Mahapatra, S. S., & Singh, M. R. (2017). An intelligent approach to optimize EDM process parameters using utility concept and QPSO algorithm. *Engineering Science and Technology, an International Journal*, 20(2), 552–562.
3. Aliyu, A. A. A., Rohani, J. M., Rani, A. M. A., & Musa, H. (2017). Optimization of electrical discharge machining parameters of SISIC through response surface methodology. *Jurnal Teknologi*, 79(1), 119–129.
4. Singh, K. J. (2019). Powder mixed electric discharge machining of high-speed steel T1 grade: Optimize through grey relational analysis. *Multidiscipline Modeling in Materials and Structures*, 15(4), 699–713.
5. Faisal, N., & Kumar, K. (2018). Optimization of machine process parameters in EDM for EN 31 using evolutionary optimization techniques. *Technologies*, 6(54), 1–16.
6. Huo, J., Liu, S., Wang, Y., Muthuralingam, T., & Pi, Y. N. (2019). Influence of process factors on surface measures on electrical discharge machined stainless steel using TOPSIS. *Materials Research Express*, 6(8), 1–14.
7. Das, P. P., & Chakraborty, S. (2019). Parametric optimization of Non-traditional machining processes using Taguchi method and super ranking concept. *Yugoslav Journal of Operations Research*, 29(2), 249–271.
8. Das, P. P., Chatterjee, S., Singh, Y., Shivakoti, I., & Chakraborty, S. (2020). A Taguchi based super ranking method in parametric optimization of powder mixed electro-discharge machining processes. *AIP Conference Proceedings*, 2273(1), 050050, 1–6.
9. Singh, H., Patrange, P., Wang, Y., Saxena, P., & Puri, Y. M. (2022). Multi-objective optimization of the process parameters in electric discharge machining of 316l porous stainless steel using metaheuristic techniques. *Materials*, 15, 1–18.
10. Chandrashekarappa, M. P. G., Kumar, S., Jagdish, Pimenov, D. Y., & Giasin, K. (2019). Experimental analysis and optimization of EDM parameters on HcHcr steel in context with different electrodes and dielectric fluids using hybrid Taguchi-based PCA-utility and CRITIC-utility approaches. *Metals*, 11, 1–23.

A Study on Simulation and Experimental Analysis of Gating System



Avinash A. Mote, Sandeep S. Wangikar, Vikram R. Chavan,
and Manoj A. Deshmukh

Abstract In today's era foundry and casting units are aiming to develop components in the shortest possible lead time. The quality of the product is greatly influenced by the gating system's design. The effective position of the gating system and proper orientation of the component increases the performance of the gating system and ultimately helps to reduce the filling time and solidification time. AUTOCAST is one of the most economical casting simulation software which increases the quality of yield, develops casting quickly, and reduces the cost. Here gating systems have been designed with the help of AUTOCAST software by considering the orientation of the component and position of the gating system. Software for filling time, solidification time, and hotspot prediction is used to analyze the designed gating systems. Experimentation is carried out for the analysis of designed gating systems. Filling time and solidification time have been measured for respective gating systems. The comparison between the results obtained from simulation analysis and experimental analysis is carried out for the filling time and solidification time. Both results are found to be closer and more satisfactory.

Keyword Gating system · AUTOCAST · Filling time · Solidification time hotspot

1 Introduction

The gating system plays the role of transporting liquid material to mould by considering constraints of speed, turbulence, and shrinkage factor. The casting process is suitable for mass production. It requires a gating system. In industry gating system is prepared and then the analysis is done. An on-site video camera is recording flow patterns which are then analyzed by digital systems. Due to this time requirement for casting process is not optimum and ultimately productivity gets affected to overcome

A. A. Mote (✉) · S. S. Wangikar · V. R. Chavan · M. A. Deshmukh
SVERI's College of Engineering, Pandharpur, Solapur, Maharashtra 413304, India
e-mail: aamote@coe.sveri.ac.in

this drawback it is necessary to analyze the gating system before it is put into use and this is done by the use of AUTOCAS^T Software. The best and most optimized gating system can be made with the help of AUTOCAS^T Software. Ambekar and Jaju [1] explained the optimization of gating system for reducing defects. Foundry systems are aiming for defectless casting with the least production cost. Riser and gating design is the crucial part of casting which is made on a trial-and-error basis. Ultimately, the examination of simulation findings led to the creation of a more rational gating mechanism. Chavan et al. [2] had done recent work related to flow rates in multi-gate systems. Mold filling has most influence on cast quality though it requires the shortest possible time acting life cycle. An appropriate gating system ensures absolute, smooth and even filling of mold with clean metal, which consists of one or more pouring basins, sprues, runners, and gates. The flow rate of liquid metal into the mold cavity and sequence depends on the number, location, shape, and size of the gating elements. But there is a need for mathematics to decide the discharge and flow volume through each gate. The comparison of the acquired results with computer simulation then provides useful information for constructing multi-gate systems. Bryant et al. [3] demonstrated the use of tilting moulds in casting to lessen the severity of inclusions. Making use of tilting mold causes less turbulence and splashing & contact of less oxygen is made with the metal. A series of plate casting trials are made to investigate the utilization of tilting molds in steel casting to trim down inclusion severity. By using tilting molds for these casting trials and to allow reoxidation inclusions, metal is initially discharged into a holding basin in the mold and retained for several seconds. Carlos et al. [4] has developed an automatic optimization process with an optimum gating design to overcome the expensive trial-and-error approach. It leads to a velocity of flow that has been minimized with no trapped air in the main runner. The effect of gate geometry and size on flow pattern is studied by Masoumi and Hu [5] by discharging molten metal of aluminum alloy A413 into a sand mold. A video camera was utilized to record the different flow impressions left by different gating designs, and a computerized system was then used to analyze them. This method is known as direct inspection. The findings of the experiment show that the geometry, size, and ratio of the gating system have a significant influence on the pattern of mould filling. Ravi [6] also suggested the use of AUTOCAS^T casting software used to curtail the loss of resources required for trial production and lower production cost. Zero defect casting is also a potential way by casting simulation which can decrease the wastage of resources essential for trial production. Also, the optimization of quality and yield implies more value-addition and lesser production costs, enhancing the margins. Mohd et al. [7] studied the effects of gating design on the mechanical strength of thin section castings. Gating system design in the casting process is one of the important parameters to produce good quality casting products. The runner design preferred for this study is Radius bend shaped and L shape. Victor and Reyaz [8] Khan provided a gating system design for casting thin aluminum alloy plates. Improper gating leads to aluminum oxide films, entrapped gas, low casting yield, cuts and washes. In this study gating system design is described to produce thin Aluminium cast alloy plates of different sizes and thicknesses of 4, 6, 8, and 10 mm by using the non-pressurized gating green sand

moulding technique. The best gate the thin-walled part-bearing base was chosen by using Mold flow software carried out by Shen and Wang. The better gating system is determined by comparing factors like flow front temperature, shrinkage volume, weld lines, and filling analysis for point gate and disc-shaped gate.

2 Methodology

A study of casting materials and their various properties like isotropy and homogeneity and at the last cost of material will be carried out. A study related to the design of the gating system, in that, especially studying the design of the feeder and riser will be followed. For the design of the feeder, various parameters like fluidity, metallostatic head, viscosity, surface tension and turbulence will be considered. A detailed study of AUTOCAPT software for the design and analysis of the gating system will be carried out. By using AUTOCAPT software, the design of three different gating systems will be done by importing a pattern that is designed in CATIA. After the design of the gating systems, analysis of the gating systems for various parameters like filling time, solidification time and hotspot will be carried out by using AUTOCAPT software. The experimental analysis will be done to ensure solidification time and filling time. A comparison of filling time and solidification time by using AUTOCAPT software and experimentation will be carried out and the most suitable gating system for the given design consideration will be predicted.

3 Simulation of Casting on AUTOCAPT

3.1 Design of Component for Casting Analysis

For this, the 3D CAD model is the main input which is without drilled holes, and with draft, shrinkage and machining allowance. A local CAD agency or OEM firm will generate the model file required. Part models can be understood by various display options provided. Process and cast metal required can be obtained from the database. A thickness map is generated. Part manufacturability (compatibility with the selected process) is computed and pictorially displayed in Fig. 1.

3.2 Design of Gating System

The design methodology includes cores, feeders as well a gating system. Holes in the part model including complex holes are automatically recognized for core design by specifying their openings. Core diameter and length will help in computing the

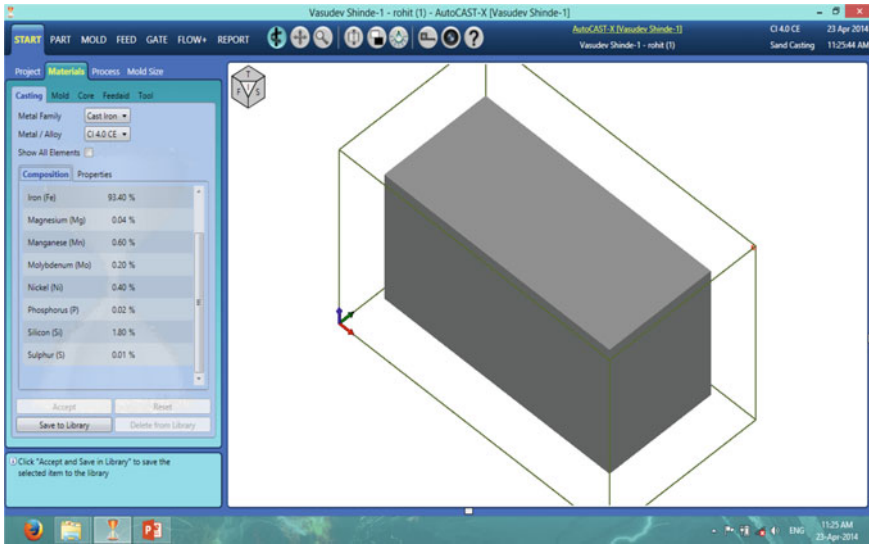


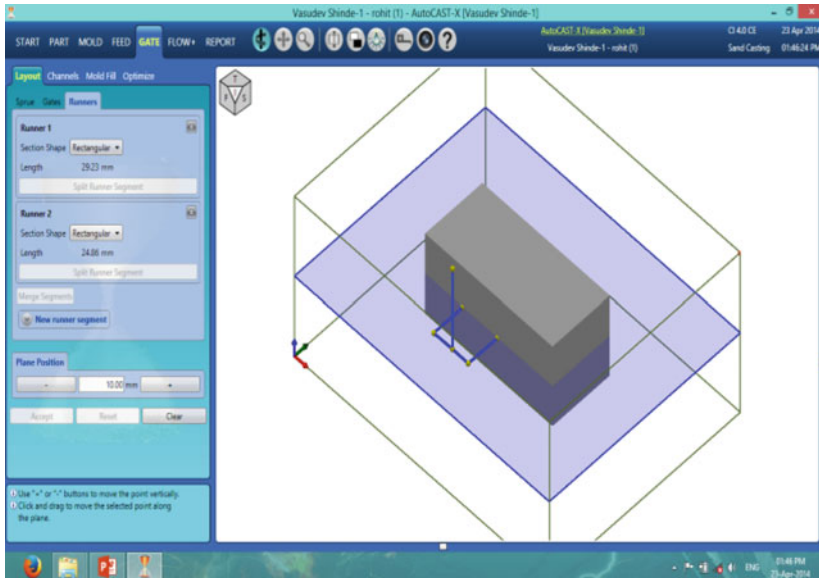
Fig. 1 Design of component

print length and then the entire core model is automatically created. By taking into consideration gaps between cavities and cavity and wall, the number of cavities can be determined based on the mold size (selected from a foundry-specific library). The part model is then automatically reproduced in the appropriate locations in accordance with the selected cavity pattern. The gating system consists of the layout of the ingates, runner and feeder, etc. as shown in Fig. 2a. Also, the positions of all parts from the reference plane are determined by the system. Again we can give the dimension i.e. the lengths for the ingates, runners, and feeders.

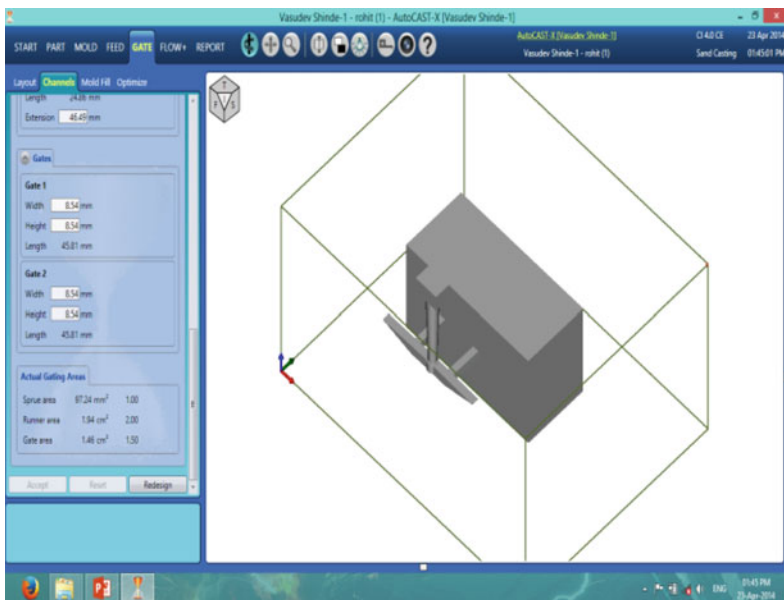
Also, Fig. 2b shows the actual gating parts. This fig. gives us the total dimension of the gating system i.e. length, width, and height of the pouring basin, feeder, runner, ingates, etc. Also, the Fig. 2b is the optimized design of gating system-1.

4 Analysis of Gating System by Using Autocast

In this chapter, the analysis of gating systems with Auto-cast software to find out solidification time, filling time and hot spots is carried out. The objective of selecting the best gating system can be achieved with the analyzed results of Auto-cast.



(a)



(b)

Figure 2 a Layout of Gating System. b Gating System

4.1 Analysis of the Gating System

The ideal mold filling time drives the gating design, which relies upon the cast metal, casting weight, and minimum wall thickness. Turbulence-related defects (such as mold erosion, air aspiration, and inclusions) are generated from fast filling. Mold filling simulation is then carried out and total fill time is calculated to optimize the gating design. The instantaneous velocity through the gates (considering backpressure, if applicable) and the local cross-section of the mould cavity are taken into account using a more straightforward layer-by-layer approach, which is preferred. It provides a precise estimation of filling times and is computationally effective. If the discrepancy between the ideal and simulated filling duration is greater than a set limit, the gating design will alter automatically. The solid model is then created, and the mould filling simulation is performed once more. The casting quality, which is the proportion of the casting volume free of shrinkage porosity, controls the feeder optimization. As the target quality is specified by the user the feeder dimensions are automatically changed by the program which then creates a solid model, solidification simulation, and determines casting quality. The Vector Element Method is used in the solidification simulation to calculate the temperature gradients (feed metal pathways) inside the casting and follow them back to locate and quantify shrinkage porosity. Also by using this software we can see the hotspot created in the product for a particular getting system. Hence by changing the place and orientation of the gating system and pattern we can minimize the hotspot created in the product.

4.2 Filling Time Analysis

The first need of any casting process is the complete filling without any defect after solidification. However, the pour gating system always leads to incomplete filling. Incorrect pouring and moulding temperature is also responsible for the same as shown in Fig. 3.

Gate filling takes place in 0.10 s, and cavity filling takes place in 11.14 s. Hence the total time required for the complete filling of mold in this gating system is 11.24 s. The time required for filling depends on the gating system, material, Hence for a particular material this software gives the optimum gating system. For this gating system, the maximum flow rate is 1.30 kg/s and the minimum flow rate is 0.98 kg/s. Also, the minimum vertex velocity is 7.29 mm/s and the maximum vertex velocity is 9.67 mm/s. The directional solidification starts from the casting and ends in the riser. This software analyses the solidification time. One can easily observe how the solidification takes place in the mold box.

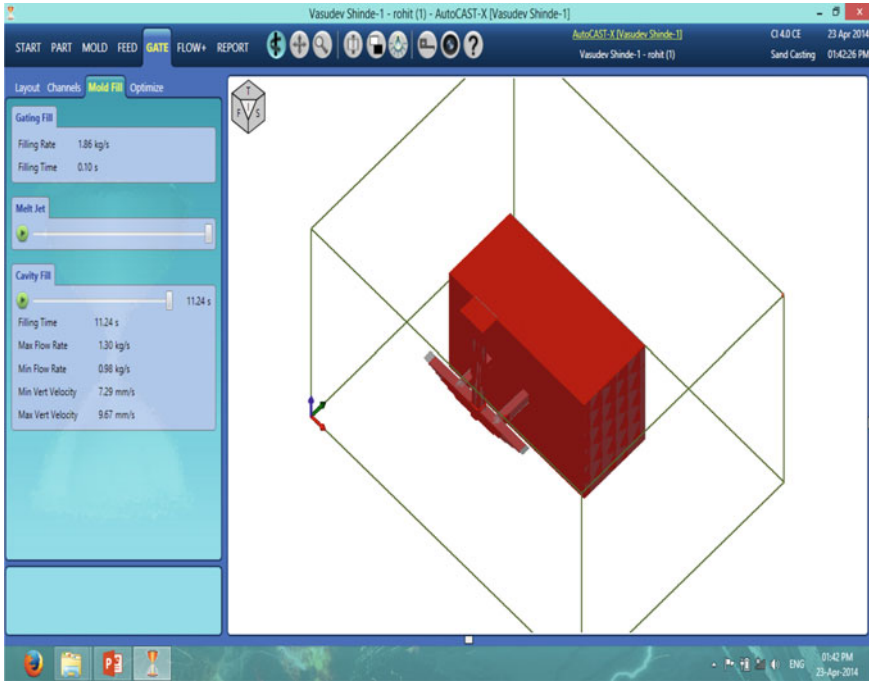


Fig. 3 Filling time for gating system

4.3 Gating System

For the gating system, the solidification time is 54.38 min. Also by using this software we can see the 3D simulation of the solidification which takes place layer by layer. Solidification starts from upper surface and end at inner side. Also, we come to know that the maximum temp. is 1110 °C and minimum temp is 213°C. this gives the solidification start temp. and solidification end temp. Also we can see the solidification for particular sections i.e. XY, YZ and XZ and their maximum and minimum temp shown in Fig. 4.

4.4 Hot Spot Analysis

The hotspot was created in the casting because of directionless solidification. The hot spot observed for the Gating System is shown in the above figure. The hot spots are observed at the center of mold cavity shown in Fig. 5. This software optimizes the gating system in such a way that the hotspot can minimize.

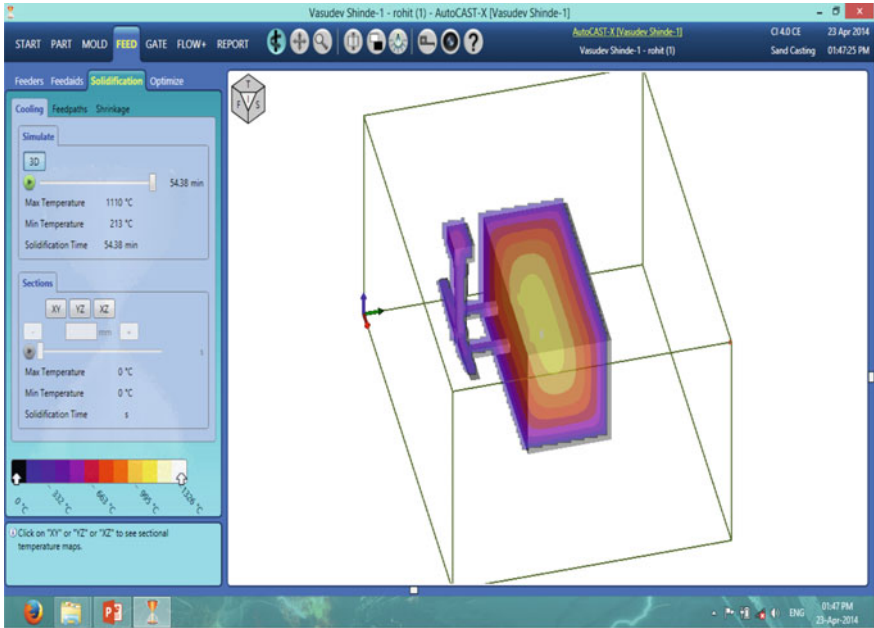


Fig. 4 Solidification time analysis for gating system

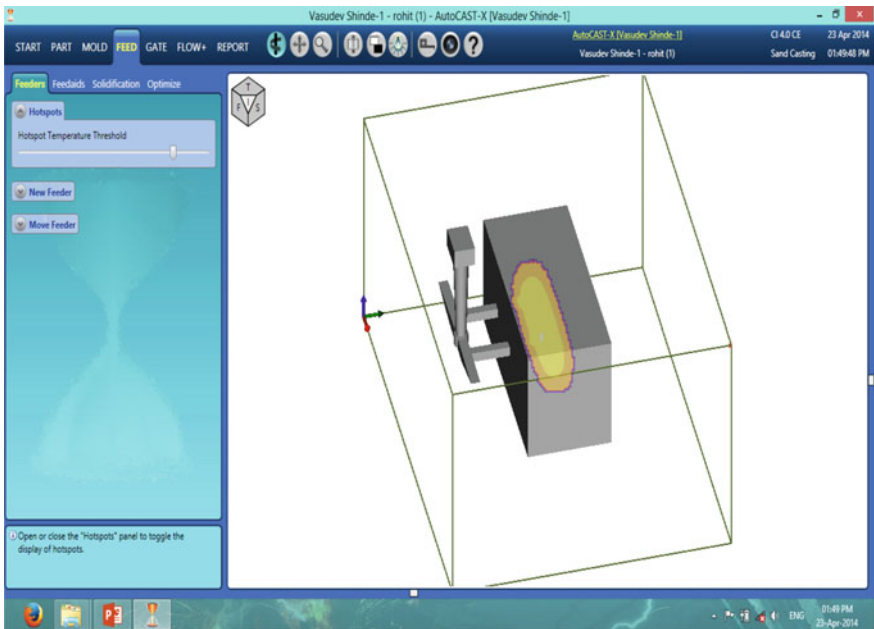


Fig. 5 Hotspot analysis for gating system

5 Experimental Analysis

This chapter consists of the experimental setup required for casting process. The process consists of pattern making, mould box preparation, melting of scrap in the furnace, actual pouring, pouring time estimation, solidification time estimation, fettling of the cast, shot blasting of the product. A pattern prepares space for molten metal during casting process. Patterns are generally made from wood, metal, plastics or other materials in case of sand casting. The Pattern used in the production of cast is a split pattern made up of wood. Sand casting is more affordable and adequately refractory for use in foundries. Sand is combined with clay or another suitable bonding agent in addition to the sand. To build up the strength and plasticity of the clay and to compose the aggregate it for molding, the mixture is moistened, typically with water, but sometimes with other substances. The system of frames or mold boxes is filled with sand. The mold cavities and gating system are set by compacting the sand around models, or patterns or impressing directly into the sand. Feeding of molten metal in the mold cavity via a gating system is called as pouring. The time required for the same is called as pouring time. The pouring time depends upon various factors such as fluidity, the temperature of molten metal, height of pouring, the structure of material, homogeneity, the velocity of flow, etc. The pouring time for the gating system had been measured to come out with an optimum gating system. The obtained pouring time was 12 s. Types of solidification inside castings are illustrated by directional solidification and progressive solidification. Solidification that begins at the casting's end and moves in a direction toward the sprue is known as directional solidification. Progressive solidification, also known as parallel solidification, is a process of solidification that starts at the casting's walls and moves perpendicularly away from them. The time required for the solidification is called solidification time and found 54.38 min. The prepared final casting has been shown in Fig. 6.

Fig. 6 Final prepared casting



6 Conclusion

From experimental analysis and software analysis, it will be clear that feeding time through the experimental method (12 s) and software analysis (11.24 s) is very closer. Also In the case of solidification time, experimental results (54.38 min) and software results (54.38) are nearly the same. Hot spot analysis is also not possible experimentally but it can be easily carried out through AUTOCAST. Hence use of AUTOCAST is proved beneficial.

References

1. Ambekar, A. S., & Jaju, S. B. (2014). A review on optimization of gating system for reducing defect. *International Journal of Engineering Research and Generic Science*, 2, 10–15.
2. Renukananda, K. H., Chavan, A., & Ravi, B. (2012). Flow rates in multi-gate systems: experimental and simulation studies. *Indian Foundry Journal*, 58(4).
3. Bryant, R., Carlson, K. D., Ou, S., & Beckermann, C. (2003). Tilt pour trials and analysis, SFSA, Paper No. 2.6, *Steel Founders' Society of America*.
4. Carlos, E., Esparza, A., Martha, P., Guerrero-Mata, B., Roger, Z., & Rí'os-Mercado, C. (2006). Optimal design of gating systems by gradient search methods. *Computational Materials Science*, 457–467.
5. Masoumi, M., & Hu, H. (2002). Effect of gating design on mold filling. *Indian Foundry Journal*, 152(02).
6. Ravi, B. (1999). Computer-aided casting design-past, present and future. *Indian Foundry Journal*.
7. Mohd, S., Mohd, H., & Mohd, S. (2009). Effects of gating design on the mechanical strength of thin section castings. *MUCEET*, 20–22.
8. Victor, A., & Reyaz, K. (2013). Gating system design for casting thin aluminium alloy (Al-Si) plates. *LEJPT*, 51–62.

Fatigue Strength Evaluation During EDM Machining of Titanium Alloy



Mahendra Uttam Gaikwad, Nitin Ambhore, and Shital S. Bhosale

Abstract Titanium alloy falls under the category of materials that are used for a wide range of engineering applications like spacecraft, missiles, and aircraft because of their excellent corrosive resistance, high strength, and low-density properties. Machining of such hard titanium (grade-5) material is suitable by adopting advanced machining processes like the Electrical Discharge Machining process this paper deals with the same. In the first part of the paper effect of EDM process parameters like current, voltage, pulse on time, and pulse off time on material removal rate were investigated while in the second part of the paper effect of these process parameters on the fatigue strength of titanium alloy has been investigated. The experiments were designed using the Taguchi optimization L9 orthogonal array method. The obtained results show that the material removal rate is a maximum of 0.068 mm³/min with a voltage of 40 V, current of 8 A, pulse on at 60 μs, and pulse off at 9 μs respectively. And it is also noted that increase in current and pulse-on time the fatigue strength of titanium alloy decreases.

Keywords Fatigue · Titanium · Process parameter

1 Introduction

Titanium alloys find a wide range of applications in aircraft, spacecraft, missiles, blades of steam turbines, etc. because of their low density and ability to withstand extreme levels of temperature. Under such applications, the reliability of the machined part is necessary to factor taken into consideration where the parts are subjected to cyclic load conditions. The reliability of the machined part is related to

M. U. Gaikwad (✉) · S. S. Bhosale
Mechanical Engineering Department, JSPM, Narhe Technical Campus, Savitribai Phule Pune University, Pune, Maharashtra, India
e-mail: mahendragaikwada1@gmail.com

N. Ambhore
Mechanical Engineering Department, Vishwakarma Institute of Information Technology, Savitribai Phule Pune University, Pune, Maharashtra, India

fatigue strength or fatigue life when the part is under working conditions. Parts are machined by traditional or by advanced machining processes where fatigue life is taken into consideration. In relation to this, some authors have carried their investigations out of which, Daud et al. [1] conducted comparative fatigue testing analysis for wire EDM machining and the polishing process by considering 14 KN load and frequency of 10 Hz followed by wire EDM machining and polishing process. They reported fatigue strength of wire EDM specimens is 20 Mpa which seems to be less than that of polished samples. Klock et al. [2] conducted a comparative analysis of fatigue analysis of wire EDM with the grinding process for titanium alloy ($\text{Ti}_6\text{Al}_4\text{V}$). They reported that tool marks are present on wire EDM machined specimens due to the process inabilities which can be overcome by setting proper parameters for a better surface and also reported that the fatigue life of the wire EDM process gives better results over the grinding process. Sherif et al. [3] focused on the necessity of fatigue strength in structural engineering for smart material alloys. They reported that structural analysis is related to cyclic loading conditions but functional fatigue is related to the loss of superelastic property of the material. After investigation, they found that smart material alloy has a fatigue capacity that can withstand hundreds of cycles without loss in the property. Deng et al. [4] investigated the fatigue strength of steel material during the heat treatment process normalized and carburized. They reported that carburized test samples have an abnormal surface microstructure of $20\ \mu\text{m}$ while normalized samples have surface roughness ranging from 1.13 to $0.04\ \mu\text{m}$ toward the surface of the notch. They stated that fatigue strength can be improved by 10% by the polishing process. Ghanem et al. [5] experimented the use of a finishing process after electro-machining of tool steel to improvising the fatigue life of the material. They reported a network of cracks formed in the region of white layer thickness that can be controlled by polishing operations. They achieved a 75% increment in fatigue life EDM machined specimens followed by polishing operations. Ali et al. [6] advised nitrogen ion implantation on fatigue life improvements in titanium alloy. They obtained results indicating improvements in fatigue strength for Cp-Ti (250 Mpa) and Ni-Ti (260 MPa) materials. Liu et al. [7] reported fatigue cracks that were initiated from microvoids in the thick white layer during the main cut operation of wire EDM machined NiTi alloy. They suggested conducting another trim cut operation to reduce fatigue crack growth is beneficial and they successfully achieved 48% more fatigue life than those by a main cut operation. Pramanik et al. [8] investigated titanium alloy ($\text{Ti-45Al-2Nb-2Mn-0.8\%TiB}_2$) by grinding, milling, and EDM process. They found the presence of tensile residual stresses on grinding specimens that cause reduced fatigue strength, compressive residual stresses present in milling process that causes increased fatigue strength of the material, and in EDM process tensile residual stresses in recast layers causing the formation of micro cracks on the machined surface that causes fatigue strength of material to reduce. Such kind of fatigue strength can be improved by electro-polishing of EDM machined specimens that remove the recast layers. Strasky et al. [9] estimated the fatigue strength of titanium alloy (Ti-6Al-4V) which can be used for biomedical applications by adopting a heat treatment process for EDM machined specimens. They reported low fatigue strength due to micro-cracks, brittle oxidized surface recast layer, internal tensile

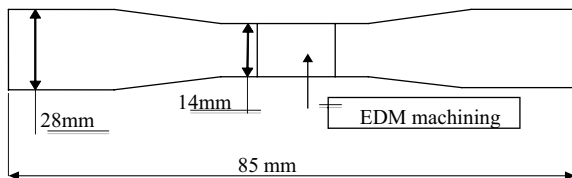
stresses and notch sensitivity of titanium alloys, such things can be overcome by using a heat treatment process. EDM samples followed by a heat treatment process give a better substrate for the adhesion and growth of human bone. Mehmood et al. [10] achieved good fatigue strength by selecting a low value of input current of about 3 A by keeping other EDM parameter constant. Ahmed Al-Khazraji et al. [11] fatigue stresses (284 MPa) at 106 cycles increases with the decrease of pulse current (8 A) and pulse on duration time (40 μ s) during EDM machined AISI D2 die Steel. Hence from the literature survey, it is understood that few authors have investigated studies on the fatigue strength of EDM machined parts. The current paper is focused on fatigue strength evaluation during EDM machining of titanium grade 5 alloy. In this paper, initially, the effects of EDM process parameters (current, voltage, pulse on time and pulse off time) on material removal rate (MRR) by designing the experiments with Taguchi orthogonal array L9 method was carried out and later on influence of EDM process parameters on fatigue strength of material was been investigated.

2 Methodology

2.1 Machine, Workpiece and Tool

In this investigation, a Die sink type EDM machine is used to conduct the experiments. ASTM titanium grade 5 is selected as a workpiece material which consists of 90% titanium, 6% aluminum and 4% vanadium in composition while and pure oxygen-free (99.9%) electrolytic copper material was selected as the electrode material. The dimension of a workpiece is shown in below Fig. 1. Initially, a tensile test was conducted on workpiece material whose yield and ultimate tensile strength was found to be 1100 and 1170 Mpa. The surface roughness effect was neglected for initially machining of electrode material on the workpiece. In order to determine the MRR weight of the workpiece was measured before and after the machining condition by using weight balance equipment [12].

Fig. 1 EDM workpiece



2.2 Design of Experiments (DOE)

By using the DOE method for hard materials like titanium grade 5, optimal machining parameters can be effectively determined [13]. Taguchi method (orthogonal array L9) is employed for DOE, which is one of the best methods for optimization [14]. During EDM machining, process parameter levels were maintained as shown in Table 1 below and the corresponding MRR for each trial was estimated by using Eq. 1 as mentioned below.

$$MRR = (W_a - W_b)/D \times Mt \quad (1)$$

where, W_a and W_b : Weight of workpiece before and after machining (mm^3), MRR: Material removal rate (mm^3/min), D : workpiece density (G/cc), Mt : time taken for machining (min) (Table 2).

After the EDM machining of the samples, fatigue testing was performed on the digital bending fatigue testing machine (model: MFT-8D) where the specimen was allowed to rotate at 4200 rpm speed, with bending moment of 200 kg cm, and the test was conducted for 106 cycles.

Table 1 EDM process parameter levels [12]

Parameters	Symbol	Unit	Levels		
			Level 1	Level 2	Level 3
Current	I	A	4	6	8
Voltage	V	V	40	55	80
Pulse on	Ton	μs	20	40	60
Pulse off	Toff	μs	5	7	9

Table 2 Experimental trials

Trials	Process variables			Performance variables	
	Voltage (V)	Current (A)	Ton (μs)	Toff (μs)	Experimental MRR (mm^3/min)
1	40	4	20	5	0.030
2	40	6	40	7	0.054
3	40	8	60	9	0.068
4	55	4	40	9	0.026
5	55	6	60	5	0.048
6	55	8	20	7	0.058
7	80	4	60	7	0.024
8	80	6	40	9	0.047
9	80	8	20	5	0.0059

Table 3 EDM process parameters and fatigue failure cycles

Trial No	Voltage (V)	Current (A)	Pulse on (μs)	Pulse off (μs)	Experimental MRR (mm ³ /min)	No. of cycles (10 ⁶)	Fatigue strength (MPa)
1	40	4	20	5	0.030	0.0032	937.54
2	40	6	40	7	0.054	0.0018	520.94
3	40	8	60	9	0.068	0.0030	870.19
4	55	4	40	9	0.026	0.0034	995.50
5	55	6	60	5	0.048	0.0028	780.10
6	55	8	20	7	0.058	0.00168	495.31
7	80	4	60	7	0.024	0.0024	645.82
8	80	6	40	9	0.047	0.0028	805.23
9	80	8	20	5	0.0059	0.0024	685.92

3 Result and Discussions

3.1 Influence of Process Parameters on Fatigue Strength

It is observed from the following Table 3 for trial 4, low value of current 4 A and pulse on time of 40 μs fatigue failure takes place at 0.0034 × 106 cycles where fatigue strength seems to be 995.50 Mpa maximum. While form trail 6, a high value of current 8 A and pulse on time of 20 μs fatigue failure takes place at 0.068 × 106 cycles where fatigue strength seems to be 495.31 Mpa which is minimum. Thus it can be concluded that a reduction in the fatigue strength of the material takes place because of an increase in current and pulse on time. The maximum fatigue strength calculated at 106 cycles was 995.50 Mpa which is less than the ultimate strength of 1170 Mpa for titanium grade-5 material.

3.2 Regression Analysis of Fatigue Strength

Linear regression analysis of fatigue strength is carried out and the following Eq. (2) is obtained. As the slope is negative indicates that an increase in MRR causes the fatigue strength to decrease and the corresponding R2 value obtained is 0.0714 (Tables 4 and 5). The coefficient values obtained in Table 6 match perfectly with the above Eq. (2) (Fig. 2).

$$y = -3E - 05x + 0.0652 \tag{2}$$

Table 4 Regression statistics

Regression statistics	Value
Multiple R	0.267196413
R square	0.071393923
Adjusted R square	− 0.061264088
Standard error	0.021574996
Observations	9

Table 5 ANOVA

	df	SS	MS	F	Significance F
Regression	1	0.000250512	0.000250512	0.53818	0.487025172
Residual	7	0.003258363	0.00046548		
Total	8	0.003508876			

Table 6 Coefficients

	Coefficients	Standard error	t Stat	P-value
Intercept	0.065202392	0.033336655	1.955876891	0.091373
X Variable 1	− 3.19038E−05	4.34889E−05	− 0.733607703	0.487025

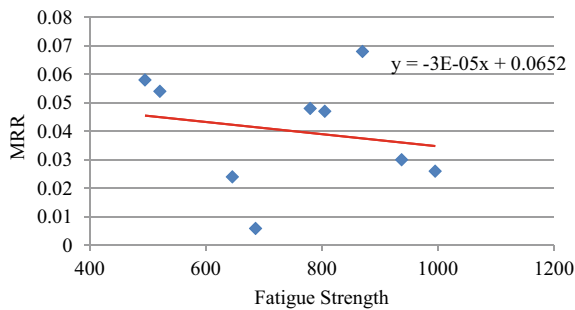


Fig. 2 Fatigue strength versus MRR

4 Conclusions

As concern with the MRR input current seems to be the dominating EDM parameter. It is observed during the investigation that MRR seems to be increased with an increase in current. The maximum MRR obtained was 0.068 mm³/min with process parameters of voltage—40 V, current—8 A, pulse on-time—60 μs, and pulse off time—9 μs respectively. Fatigue strength of titanium grade 5 alloy goes on reducing due to increments in current and pulse on time EDM parameter. The maximum

fatigue strength evaluated was 995.50 Mpa which is less than the ultimate strength of 1170 MPa workpiece material during an investigation.

Acknowledgements The authors would like to acknowledge Kakade lasers Industry, Pune, Maharashtra for providing an EDM machining facility. The authors would also like to acknowledge the Mechanical Engineering Dept. VJTI Mumbai, Maharashtra for providing a fatigue testing facility during this research work. Last but not least the authors like to thank Mr. Rushiraj T. Sawant, Trustee, JSPM, Narhe Technical Campus, Pune and Dr. S. A. Choudhari, Director JSPM, Narhe Technical Campus, Pune for their motivation and moral support to conduct this research.

References

1. Daud, M. A. M., Omar, M. Z., Syarif, J., & Sajuri, Z. (2010). Effect of wire-EDM cutting on fatigue strength of AZ61 magnesium alloy. *Jurnal Mekanikal*, 30, 68–76.
2. Klocke, F., Welling, D., & Dieckmann, J. (2011). Comparison of grinding and wire EDM concerning fatigue strength and surface integrity of machined Ti6Al4V components. *Procedia engineering*, 19, 184–189.
3. Sherif, M. M., & Ozbulut, O. E. (2017). Tensile and superelastic fatigue characterization of NiTi shape memory cables. *Smart Materials and Structures*, 27(1), 015007.
4. Deng, G., Suzuki, S., & Nakanishi, T. (2011). Effects of surface roughness and abnormal surface layer on fatigue strength. In *Applied mechanics and materials* (Vol. 86, pp. 867–870). Trans Tech Publications Ltd.
5. Ghanem, F., Fredj, N. B., Sidhom, H., & Braham, C. (2011). Effects of finishing processes on the fatigue life improvements of electro-machined surfaces of tool steel. *International Journal of Advanced Manufacturing Technology*, 52(5–8), 583–595.
6. Ali, N., Mustapa, M. S., Ghazali, M. I., Sujitno, T., & Ridha, M. (2013). Fatigue life prediction of commercially pure titanium after nitrogen ion implantation. *International Journal of Automotive and Mechanical Engineering*, 7, 1005–1013.
7. Liu, J. F., Li, C., Fang, X. Y., Jordon, J. B., & Guo, Y. B. (2018). Effect of wire-EDM on fatigue of nitinol shape memory alloy. *Materials and Manufacturing Processes*, 33(16), 1809–1814.
8. Pramanik, A., Dixit, A. R., Chattopadhyaya, S., Uddin, M. S., Dong, Y., Basak, A. K., & Littlefair, G. (2017). Fatigue life of machined components. *Advances in Manufacturing*, 5, 59–76.
9. Strasky, J., Janecek, M., & Harcuba, P. (2011). Electric discharge machining of Ti-6Al-4V alloy for biomedical use. In *Proceedings of the 20th annual conference of doctoral students—WDS*.
10. Mehmood, S., Shah, M., Pasha, R. A., Khushnood, S., & Sultan, A. (2017). Influence of electric discharge machining on fatigue limit of high strength aluminum alloy under finish machining. *Journal of the Chinese Institute of Engineers*, 40(2), 118–125.
11. Al-Khazraji, A., Amin, S. A., & Ali, S. M. (2016). Effect of electrical discharge machining and shot blast peening parameters on fatigue life of AISI D2 die steel. *Journal of Engineering*, 22(11), 111–135.
12. Gaikwad, M. U., Krishnamoorthy, A., & Jatti, V. S. (2019). Investigation and optimization of process parameters in electrical discharge machining (EDM) process for NiTi 60. *Materials Research Express*, 6(6), 065707.
13. Lingadurai, K., Nagasivamuni, B., Muthu Kamatchi, M., & Palavesam, J. (2012). Selection of wire electrical discharge machining process parameters on stainless steel AISI grade-304 using design of experiments approach. *Journal of the Institution of Engineers (India): Series C*, 93, 163–170.
14. Theisen, W., & Schuermann, A. (2004). Electro discharge machining of nickel–titanium shape memory alloys. *Materials Science and Engineering: A*, 378(1–2), 200–204.

Study of Structural Behavior of Beam with Middle 1/3rd Portion Replaced with Crushed Brick Aggregate



S. A. Gosavi and Vishwajeet Surshetwar

Abstract In this paper, we are striving to make the beam lighter, which automatically decreases the amount of reinforcing material needed in the components below the beam. This will reduce construction costs and increase the efficiency of the process, despite cutting costs; safety and durability are not sacrificed. As strain is linear and reaches its maximum at either the top or bottom, some distance above and below the neutral axis experience less strain than the extreme fiber strain. This means the tension created there is less than the ultimate stress at the fiber's extremes. As a result, the concrete there is not being used to its full potential in ways that maximize its strength. High strength materials are being used despite the fact that they are not necessary in that area. As a result, more expensive and high-strength material is wasted, raising the overall cost of building. And this is where our proposal enters the picture. And that's why middle third portion of the beam replaced with concrete produced from crushed brick aggregate. The results are compared with conventional beam same size and reinforcement.

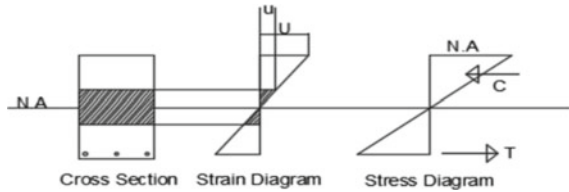
Keywords CBA—Crushed brick aggregate · NCA—Normal concrete aggregate · BM—bending moment · SF—shear force

1 Introduction

In the past, the fired clay bricks have successfully been used to produce the coarse aggregates for good quality concrete. The researchers investigate the use of fired clay bricks as coarse aggregate to produce the concrete [1–3]. They reported that fired clay brick aggregates can be effectively used to produce concrete with reasonable mechanical properties. They also studied the use of used crushed clinker bricks as coarse aggregated and replaced natural aggregates to produce concrete. We are aware of theory of flexure from strength of materials in which one of the assumptions is “plane section before bending remains plane after bending” [4, 5]. It means the

S. A. Gosavi · V. Surshetwar (✉)
SVERI's College of Engineering, Pandharpur, Pandharpur, Maharashtra 413304, India
e-mail: vbsurshetwar@coe.sveri.ac.in

Fig. 1 Stress strain diagram of concrete section



variation of bending strain is linear from zero at neutral axis to max at top or bottom surface. The high strength concrete material present nearby neutral axis is getting wasted its strength as the strain being very less compared to the extreme fiber stress [5, 6]. Which increase weight of beam unnecessarily without any significant addition to the strength. Hence replacing with crushed brick aggregate to reduce weight of beam. The density of the concrete made with brick aggregates is found lower than the concrete made with natural aggregates (Fig. 1).

2 Objectives and Methodology

2.1 To Find Flexural Behavior of Beam Partially Replaced by Crushed Brick Aggregate (CBA)

We are replacing the coarse aggregates with crushed brick clinker, we have to check the properties of materials and then design conventional beam of general specifications. After designing the conventional beam replace middle 1/3rd portion of beam depth with crushed brick clinker. Cast the beam and test its moment of resistance by flexure test. The results are being compared with conventional beam. The conventional beam constructed as same dimensions and using conventional material as cement, sand, coarse aggregate and water.

3 Material

3.1 Crushed Brick Aggregate

Bricks which are over burnt or brick which obtained from demolished construction waste are collected and smashed it to size of 10–20 mm such aggregates are known as crushed brick aggregate”[8]. Such aggregates used in our concrete making. We can see below that density of crushed brick aggregates is less than that of regular stone aggregate. Density of normal concrete aggregate (Stone) is 2300–2500 kg/m³. As

Fig. 2 Crushed brick aggregates



Table 1 Observation table

Description	Conventional Beam	CBA beam
Load carrying capacity (KN)	280	330
Weight of beam (kg)	540	470
Weight reduced (%)	–	12.96

compared with these aggregate crushed brick aggregate’s density is much less and this is the reason we are using it for weight reduction in beam. We found properties of crushed brick aggregate as follows (Fig. 2):

- Density: 1600–1800 kg/m³
- Water absorption: 20–25%

4 Observation

The main aim of this research is to reduce the weight of beam without losing its strength and durability. Hence we are comparing our different techniques with conventional in order to check how much weight is reduced by calculating % weight reduced with respect to conventional beam (Table 1).

$$\text{Weight of conventional beam} = 540 \text{ KN}$$

5 Result and Discussions

To understand the structural behavior of beam with different weight reduction techniques we are compared the results with conventional beam in respect to maximum bending moment, maximum shear force, maximum deflection and load carrying capacity. The graphs are plotted as above aspects of structure are thoroughly get compared with conventional beam and evaluate the weight reduction techniques in order to get future benefits and use in construction industry.

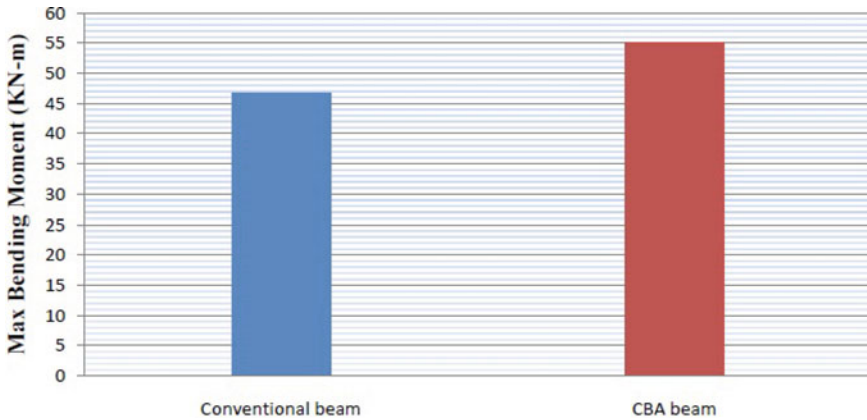


Fig. 3 Max bending moment comparison

In this chapter consist of results of consists results of conventional beam vs. Crushed Brick Aggregate beam. As higher density mass is at the top and the bottom edge hence increasing the moment of resistance of the CBA beam [7, 8]. The surface roughness of crushed brick aggregate is more than normal aggregates; increases shear strength of CBA beam. This together increases load bearing capacity of the CBA beam. As the CBA beam is taking more load till its breakdown; the deflection is more than conventional beam.

Figure 3 shows comparison of maximum bending moment (Moment resisting capacity) between conventional beam (46.67 KN-m) and CBA beam (55 KN-m) and CBA beam has higher final maximum bending moment than conventional beam 17.89%.

Figure 4 shows comparison of maximum shear force taken between conventional beam (140 KN) and CBA beam (165 KN) and CBA beam has far more shear strength than conventional beam with percentage variation of 17.85%.

Figure 5 shows comparison of maximum deflection at the time of failure between conventional beam (1.5 mm) and CBA beam (1.7 mm). The final deflection of CBA beam is higher than conventional beam with percentage variation of 13.33%.

Figure 6 shows comparison of load bearing capacities between conventional beam (280 KN) and CBA beam (330 KN) and CBA has higher load bearing capacity than conventional beam with percentage variation of 17.85% (Table 2).

6 Conclusions

1. Maximum bending moment (Moment resisting capacity) between conventional beam (46.67 KN-m) and CBA beam (55 KN-m) and CBA beam has higher final maximum bending moment than conventional beam 17.89%.

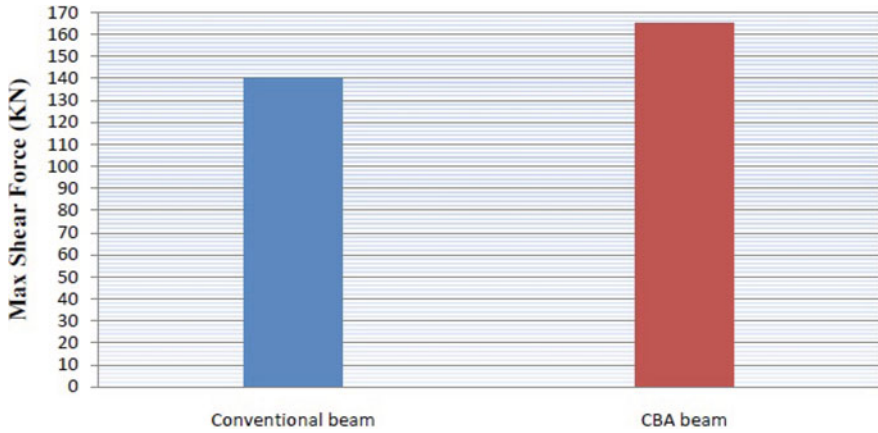


Fig. 4 Max shear force comparison

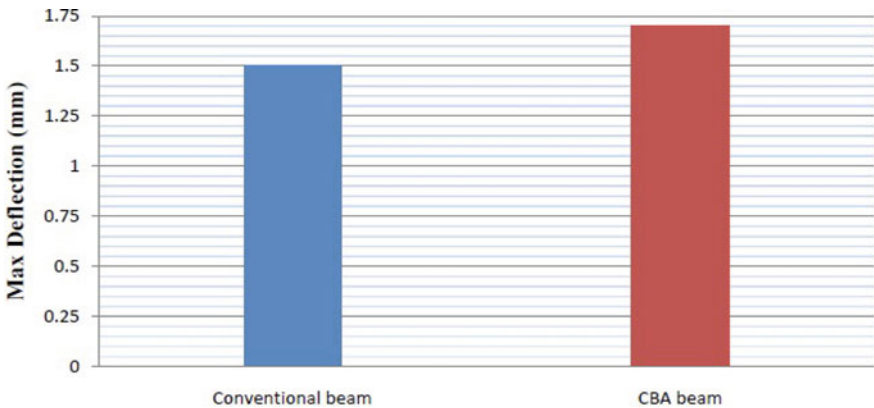


Fig. 5 Max deflection comparison

2. Maximum shear force taken between conventional beam (140 KN) and CBA beam (165 KN) and CBA beam has far more shear strength than conventional beam with percentage variation of 17.85%.
3. Maximum deflection at the time of failure between conventional beam (1.5 mm) and CBA beam (1.7). The final deflection of CBA beam is higher than conventional beam with percentage variation of 13.33%.
4. Load bearing capacities between conventional beam (280 KN) and CBA beam (330 KN) and CBA has higher load bearing capacity than conventional beam with percentage variation of 17.85%.
5. CBA can be efficiently used in structural elements by partial replacement with NCA. This will improve the strength of structural element and also reduce cost of the construction.

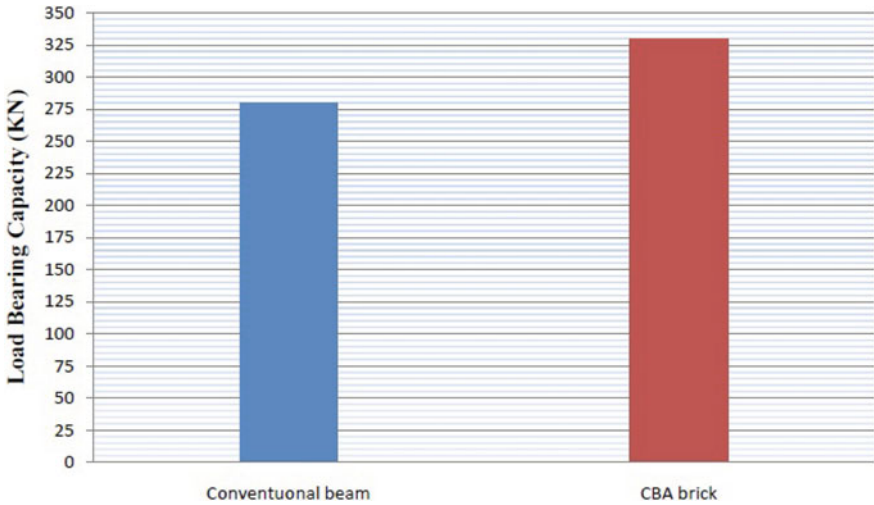


Fig. 6 Max load bearing capacity

Table 2 Result table

Types of beam	Conventional beam	Beam with CBC
Max BM (KN-m)	46.67	55
Max SF (KN)	140	165
Max Deflection (mm)	1.5	1.7
Moment of resistance (KN-m)	36.86	36.86
Load bearing capacity (KN)	280	330

6. Weight reduction of beam using CBA is approximately 13%. That reduces dead load on structure by 13% as moment resisting capacity is same as that of conventional beam with same cross section and same reinforcement details.

References

1. Xiong, B., Demartino, C., Xu, J., Simi, A., Marano, G. C., & Xiao, Y. (2021). High-strain rate compressive behavior of concrete made with substituted coarse aggregates: Recycled crushed concrete and clay bricks. Journal homepage: www.elsevier.com
2. Jankovic, K., Nikolic, D., & Bojovic, D. (2012). Concrete paving blocks and flags made with crushed brick as aggregate. Journal homepage: www.elsevier.com
3. Atyia, M. M., Mahdy, M. G., & Elrahman, M. A. (2021). Production and properties of lightweight concrete incorporating recycled waste crushed clay bricks. Journal homepage: www.elsevier.com

4. Noaman, A. T., Jameel, G. S., & Ahmed, S. K. (2020). Producing of workable structural lightweight concrete by partial replacement of aggregate with yellow and/or red crushed clay brick(CCB) aggregate. Journal homepage: www.sciencedirect.com
5. Ma, Z., Tang, Q., Wu, H., Xu, J., & Liang, C. (2020). Mechanical properties and water absorption of cement composites with various fineness and contents of waste brick powder from C&D waste. Journal homepage: <http://www.elsevier.com/locate/cemconcomp>
6. Vieira, T., Alves, A., de Brito, J., Correia, J. R., & Silva, R. V. (2015). Durability-related performance of concrete containing fine recycled aggregates from crushed bricks and sanitary ware. Journal homepage: www.elsevier.com/locate/matdes
7. Jagdale, S. D., & Kashid, S. S. (2020). Prediction of river basin-scale water yield using artificial neural networks. In *Techno-societal 2018: Proceedings of the 2nd international conference on advanced technologies for societal applications* (Vol. 1, pp. 289–298). Springer International Publishing.
8. Rodsin, K. (2021). Confinement effects of glass FRP on circular concrete columns made with crushed fired clay bricks as coarse aggregates. Journal homepage: www.elsevier.com/locate/cscm

Design and Optimization of Prosthetic Arm (Prototype Model)



Devanshi Akshay Jhaveri, R. S. Motgi, S. K. Mohite, and N. P. Patil

Abstract A G Patil Polytechnic Institute received LN4 Prosthetic Arm from Ellen Meadows Prosthetic Hand Foundation (USA) through Rotary Club Poona Downtown with kind imitative by Rotary E-club Of Solapur Elite. The club donated this arm for further research work and overcome the limitations of (LN4) with economic benefit. Our research work has been done on 3D printer unit which was received to our institute. LN4 hand has certain limitations to develop in new manner so it was at ask to work on it But, after many case studies in the society and practical example of a student from electrical department had the same issue and was not having her fingers in the hands since birth which was a case study for us too. After proper research and planning we were able to design a prototype model and tried to train our students to help and sustainability for social works.

Keywords LN4 arm · Rotary club · 3-D printers · Society · Prosthetic arm parts · Rubber hinges · Research work

1 Introduction

God has created human body in amazing way. Our body is a machine, each part of organ is developing for multipurpose use. Industrialization is boom in India now, our hands are our Karma to earn. Each fingers mechanism, their use and during covid situations work from home has given multipurpose use of our fingers mechanism and palms. If we think about our life without this natural mechanism, it is quite difficult to survive. So here in our research area we have accepted the challenge to design an arm for disabled and especially poor people, who lost their hands while working on machine, disability from childhood and lost their hands in conflicts as well as during accidents. The organization (AGPPI) works more for the students' development and demonstration many research work is going on by faculty members. Under CSR

D. A. Jhaveri (✉) · R. S. Motgi · S. K. Mohite · N. P. Patil
Mechanical Engineering Department, A. G. Patil Polytechnic Institute, Solapur, Solapur,
Maharashtra 413008, India
e-mail: devanshi.jhaveri6@gmail.com

policy, after receiving 3D printer from US and China research and development of mechanical devices and models have been started for students. With creative ideas of Mechanical Department. They got an idea to help poor people in society by using that 3-D printers, fortunately I, Mrs. Jhaveri, lecturer in Mechanical engineering department attended camp of LN4 always received from USA for needy people whose hands have been cut from an elbow and the same was received for LN4 for research purpose. However, it was found that it was not useful for the people whose hands cut from only wrist and above elbow. While designing arm many parameters, like mechanism, dimension of fingers, simple design, which should be affordable for people, many parameters have been considered. This research summarizes future scope of design of palm of people [1–4].

1.1 Objective

The person who doesn't have his/her second hand, they cannot operate LN4 easily. Whose arm cut only from palm and wrist area? LN4 doesn't fit and operate there. Fingers don't have proper mechanism, very hard for operating. The person must have second hand for operating LN4.

2 Materials and Methods

2.1 Structuring of Paper

Affiliations (Idea Generation and History of LN4)

In our organization, one girl student is learning whose fingers have not developed by birth. After observing her condition, we have generated one idea to design and developed one prosthetic arm. Many parameters were considered while designing this arm, first of all psychological impact of the person's mind while loss of hand or any organ of body part. Loosing arm during accident is a difficult challenge for them. Prosthetic arm replacement was a long sought technic from past so many years. Even palm has three different mechanisms, palms, fingers and even thumb.

In Rotary Pune downtown donated almost 5700 LN4 to needy people, in Solapur. With the help of PP. Rtn. Akshay Jhaveri catalyst person between Rotary and our organization, fortunately with his efforts, our institute received LN4 from Rotary Club Pune downtown with collaboration of Rotary E-club Solapur Elite (Fig. 2).

The motto of donation of LN4 is the Words joined by a line are subject to a superior law. If the first term can stand unaided, the second word should be exploited. Some have used the LN4 hand as a placeholder while they endure to move advancing on a 2-year intervening list that their country's therapeutic system has, hoping to

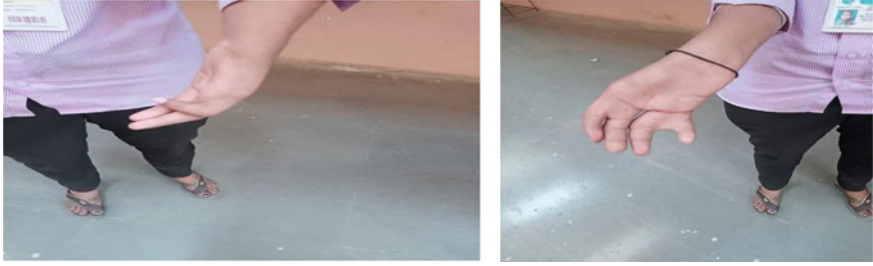


Fig. 1 Case study: permanent disablement student



Fig. 2 LN4 hand received from Rotary E-club of Solapur Elite

ultimately gain a more progressive prosthetic limb. For others, this hand will be the best occasion for salvaging flexibility and hand use they will always have [5].

2.2 Problem Definition

Several investigations have done by Ishikawa Diagram. There were certain limitations of LN4 arm [6, 7] (Fig. 3).

LN4 hand was designed for social cause. In LN4 arm, life of this hand is not too long. Sensors can't be fitted, in LN4 because poor people are not used to afford this.

3 Methodology

In above chart, the process regarding 3-D printer model has been explained. First 3D model has been designed by using cad on PC. It will be converted into STL file. In this file all design shaped is converted into triangular process. Again it has been sent to Slicing software where the design has converted into all appropriate for

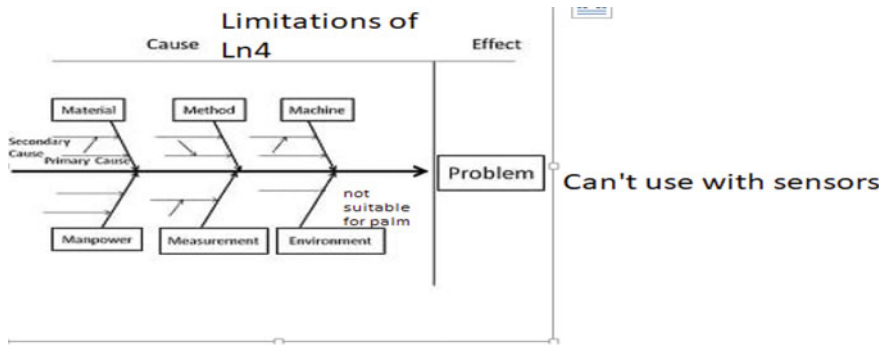


Fig. 3 Ishikawa diagram

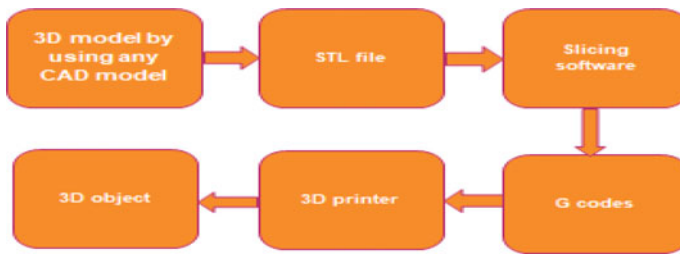


Fig. 4 Process chart

3D printer triangular shape. Then it is converted into special G Codes. Now data has been transferred by WIFI, Network or From Pan drive to 3-D Printer. Then 3-D object would be started on printer. On above process many parameters like speed, infill pattern, supports for overhanging are considered [8] (Fig. 4).

3.1 Process on 3-D Printer

In LN4, they use high-grade plastic. In our 3D printer, we will design demonstrating prosthetic arm by using material named as PLA. As we had some limitations of resources and the research, work has been started on FDM (Fused Deposition Modelling) 3-D printer. (FLASHFORGE) Filament Material PLA first step was to prepare a palm on 3-D printer and then work has been started step by step (palm without fingers) (Fig. 5).

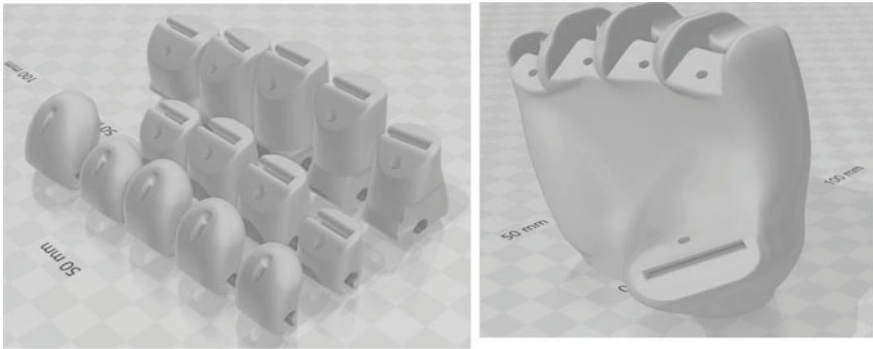


Fig. 5 Fingers and palm (courtesy: Thingiverse.com)

3.2 Process Steps on 3-D Printer

Then work has been started on different parts of fingers.14 parts of different fingers has been prepared separately. Now whole parts of prosthetic arm were in our hand (Figs. 6 and 7).

However, to make them assembled the mould has been found and designed then prepared at 3-D printer (Mould at 3-D Printer for making Rubber Hinges) Now we had everything Palm, Parts of fingers (Fig. 8).



Fig. 6 Palm prepared on 3-D printer



Fig. 7 Base of palm prepared on 3-D printer



Fig. 8 Mould with rubber hinges

Mould was also prepared on 3-D printer by using auto cad, but the question was how to prepare rubber hinges. Because to give movement of fingers silicon rubbers have been purchased from market and the original size was mould has to be reduced during design and manufacturing of mould. Then molten metal of rubber was poured inside the mould and final product was prepared. There are no. of holes in the finger parts so give the movement of those assemble part threads have been used to move whole fingers. In below images the process of making rubber hinges from mould have been seen [9].

3.3 *Demonstration with Hinges and Mould*

(Final Parts and demonstration of Prosthetic Arm) The movement of a single finger, assembled with thread and rubber hinges has been seen in above three images (Fig. 9).

Mechanism of arm is not so much easy to prepare on simple 3-d printer machine because, when it is fitted on a human body the questions arising of weight balance, temperature suitability, weight lifting of objects, typing, driving, fingers movement, elasticity etc....

So for preparing demo model of prosthetic arm, rubber hinges were used to give flexible movements of fingers, which is not available in LN4 arm mechanism [10] (Fig. 10).



Fig. 9 Rubber hinges



Fig. 10 Demonstration of palm and arm

4 Conclusion

With several researches on Prosthetic Arm Finally our team has decided to prepare one prototype model of this arm. It was a difficult task for us because already many researches have been done on this particular attachment. Then too seeing a problem of the girl, who studies in our organization and me with my team members have visited Jaipur Foot camp and LN4 camp. We got inspire to do really something for society. Finally, we could reach to our goal. Now our organization has collaboration with Rotary, which always helps to society in several areas so with the guidance of Rotarians and our higher Authorities, we will try to complete challenging task as well as innovation for society. After completion of this arm, the arm was again handed over to Rotary Elite club. District Governor was quite impressed for above research work, this news will be printed in weekly district magazine of club.

References

1. Peterson, N. G., Mumford, M. D., Borman, W. C., Jeanneret, P. R., Fleishman, E. A., Levin, K. Y., Champion, M. A., Mayfield, M. S., Morgeson, F. P., Pearlman, K., Gowing, M. K., Lancaster, A. R., Silver, M. B., & Dye, D. M. (2001). Understanding work using the occupational information network (o* net): Implications for practice and research. *Personnel Psychology*, *54*(2), 451–492 (Article Google Scholar).
2. Hoffer, J. A., & Loeb, G. E. (1980). Implantable electrical and mechanical interfaces with nerve and muscle. *Annals of Biomedical Engineering*. <https://doi.org/10.1007/BF02363438>
3. Kuiken, T. A., Dumanian, G. A., Lipschutz, R. D., Miller, L. A., & Stubblefield, K. A. (2004). The use of targeted muscle reinnervation for improved myoelectric prosthesis control in a bilateral shoulder disarticulation amputee. *Prosthetics and Orthotics International*. <https://doi.org/10.3109/03093640409167756>
4. Thali, M. J., & Egger, D. (2018). Case-study of a user-driven prosthetic arm design: Bionic hand versus customized body-powered technology in a highly demanding work environment. *Journal of Neuro Engineering and Rehabilitation*, *15*, 1–27. <https://doi.org/10.1186/s12984-017-0340-0>
5. Kuiken, T. A., Miller, L. A., Lipschutz, R. D., Lock, B. A., Stubblefield, K., Marasco, P. D., Zhou, P., & Dumanian, G. A. (2007). Targeted reinnervation for enhanced prosthetic arm

- function in a woman with a proximal amputation: a case study. *Lancet*. <https://www.sciencedirect.com/science/article/abs/pii/S0140673607601937>
6. Hijjawi, J. B., Kuiken, T. A., Lipschutz, R. D., Miller, L. A., Stubblefield, K. A., & Dumanian, G. A. (2006). Improved myoelectric prosthesis control accomplished using multiple nerve transfer. *Plastic and Reconstructive Surgery*. https://journals.lww.com/plasreconsurg/Abstract/2006/12000/Improved_Myoelectric_Prosthesis_Control.11.aspx
 7. Lipschutz, R. D., Kuiken, T. A., Miller, L. A., Dumanian, G. A., & Stubblefield, K. A. (2006). Shoulder disarticulation externally powered prosthetic fitting following targeted muscle reinnervation for improved myoelectric control. *Journal of Prosthetics and Orthotics*. https://journals.lww.com/jpojournal/Fulltext/2006/04000/Shoulder_Disarticulation_Externally_Powered.2.aspx
 8. O'Shaughnessy, K. D., Dumanian, G. A., Lipschutz, R. D., Miller, L. A., Stubblefield, K. A., & Kuiken, T. A. (2008). Targeted reinnervation to improve prosthesis control in transhumeral amputees: A report of three cases. *Journal of Bone and Joint Surgery*. https://journals.lww.com/jbjsjournal/Citation/2008/02000/Targeted_Reinnervation_to_Improve_Prosthesis.26.aspx
 9. Weir, R. F., & Grahn, E. C. (2005). Powered humeral rotator for persons with shoulder disarticulation amputations. In *Proceedings of the myoelectric control symposium*. Fredericton (Canada). https://dukespace.lib.duke.edu/dspace/bitstream/handle/10161/2754/weir_02.pdf?sequence=3
 10. Zhou, P., & Kuiken, T. A. (2006). Eliminating cardiac contamination from myoelectric control signals developed by targeted muscle reinnervation. *Physiological Measurement*, 27, 1311–1327. <https://doi.org/10.1088/0967-3334/27/12/005/meta>

Optimization of Ultrasonic Assisted Electro-discharge Machining Process Parameters Through Surface Response



Atish Mane and Pradeep V. Jadhav

Abstract This work aim to optimize the factors using the ultrasonic vibration generator for the EDM. The performance namely surface roughness, in the EDM, calls for a refined assessment of the input factors. In this study, the experiment was conducted with shape memory alloy with ultrasonic vibration. This paper describes an attempt to apply low-frequency vibration on a shape memory alloy (NiTi) workpiece during the EDM process. The workpiece was vibrated with low frequency and low amplitude fluctuations. The results suggest that using low-frequency vibration in the EDM process can decrease surface roughness. The experiment was carried out, and the outcomes were examined utilizing statistical approaches such as the response surface methodology. For analysis L_{32} orthogonal array was used. Finally, from the statistical technique, optimum process parameters are calculated and validated experimentally.

Keywords Ultrasonic assisted EDM · Shape memory alloy · Surface roughness · Metal removal rate · Response surface method

1 Introduction

In the unconventional electro-thermal machining technique known as EDM, electrical energy is used to create an electrical spark, and material removal results from the heat energy the spark produces. As a result, thousands of sparks are produced per second. each spark creates a tiny crater that erodes the tool. By heating and vaporizing material removed from work piece. The dielectric fluid contains the spark, which removes the removed material particles. To be machined by EDM, the work material must be electrically conductive. Patel et al. [1] found that the most important element influencing the grey relational grade is discharge current. Surface roughness rises as the discharge current rises. The MRR rises as the pulse rate. Mohamad et al. [2] used the Taguchi method to investigate and optimize EDM

A. Mane (✉) · P. V. Jadhav

Mechanical Engineering, Bharati Vidyapeeth Deemed University, College of Engineering, Pune, Maharashtra, India

e-mail: mane.atish@bharatividyaeeeth.edu

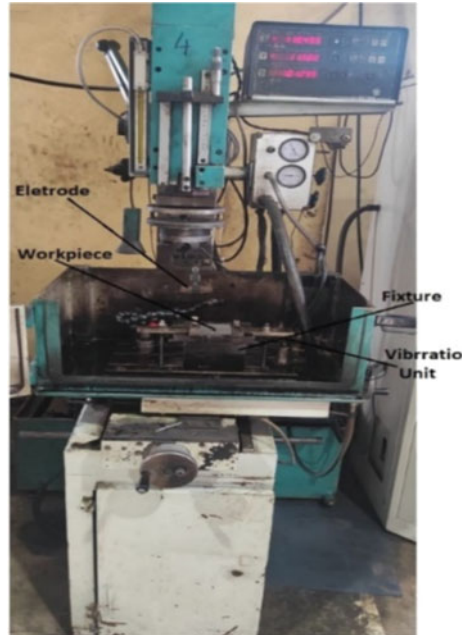
© The Author(s), under exclusive license to Springer Nature Switzerland AG 2024

P. M. Pawar et al. (eds.), *Techno-societal 2022*,

https://doi.org/10.1007/978-3-031-34644-6_69

671

parameters. They examined factors, such as discharge current and pulse on time, had the greatest impact on SR and the least impact on the quality of the machining process. Aliakbari et al. [3] discovered the ideal rotating process parameter setting. They deduced from this experiment that the most influential input parameters on MRR, EWR, and SR are current, pulse on time, electrode rotational speed, and electrode shape. Gopalswamy et al. [4] noticed that the parameters that have the most influence on rough machining are the cut width and depth. The most important factor in finish machining is cutting speed. Choudhary et al. [5] discuss the research that was done on die-sinking EDM, water-in EDM, dry EDM, and powdered mixed electric discharge machining from inspection through development. He deduced from this that the main advancement in research had improved tool wear and metal removal rate. Ho and Newman [6] presented a review on the electrical discharge machining process and discussed the parameters that are contributing to machining efficiency. EDM process involves many process parameters which can be broadly classified into two categories such as electrical and non-electrical process parameters. They stated that empirical modeling can be better described in the EDM process as it is stochastic in nature. Machado et al. [7] present a review on medical applications of shape memory alloys and the purpose of this review article is to present a brief discussion of the thermomechanical behavior of SMA and to describe their most promising applications in the biomedical area. These include cardiovascular and orthopedic uses and surgical instruments. Maeshima et al. [8] present a review shape memory properties of biomedical Ti-Mo-Ag and Ti-Mo-Sn alloys and in this Ti-Mo-Ag and Ti-Mo-Sn alloys for biomedical applications are developed and their shape memory properties are investigated. Hannula et al. [9] present a review paper on shape memory Alloys for biomedical applications and review the biomedical applications of shape memory alloys consisting of quite a broad field starting from dental and less-invasive surgery where they are mostly used today. The orthopedic applications were previously expected to become more numerous, but the development of new materials such as polymers resembling human bone has narrowed their field of use. Abbas et al. [10] reviewed the performance of EDM process variants and categorized them as ultrasonic-assisted EDM, dry EDM, powder-mixed EDM, and EDM in water. They also discussed the different modeling methods to predict EDM performance measures. Based on the performance ultrasonic-assisted EDM can be used in micromachining, dry EDM is economical, EDM in water is safe and has a conducive working environment, and powder-mixed EDM improves the surface finish, and material removal rate and reduces tool wear rate. The aim of this study is to investigate the effect of ultrasonic vibration on process parameters of EDM to improve the surface quality of shape memory.

Fig. 1 EDM setup

2 Experimental Setup

The Vinpak EDM machine was used for testing. The electrode or tool was made of Copper, which serves as the cathode, and the workpiece was made of a shape memory alloy (NiTi), which serves as the anode. Shape memory alloy pates measuring 20 mm × 20 mm × 15 mm were chosen for machining. As a dielectric fluid, kerosene was used. The EDM parameters provide for a spark gap of 10–120 μm, a frequency of 00–500 Hz, and a peak voltage across the gap of 25–250 V. The low-frequency vibration generator was linked to a workpiece, which controlled the frequency and amplitude. The experimental setup is depicted in Fig. 1. The workpiece was vibrated with low-frequency and low-amplitude variations.

3 Design of Experiments

Response surface methodology has numerous advantages such as its ability to accommodate many parameters, the arbitrary choice of its levels, and the smaller number of experiments. In addition, Response surface methodology is suitable for studying undefined machining methods or machining methods at an early stage. In this study, five input parameters, each with five levels, were utilized (Table 1).

Table 1 Initial USA-EDM parameter

EDM parameters	Unit	Level-1	Level-2	Level-3	Level-4	Level-5
Gap voltage	V	25	45	65	85	105
Discharge current	A	10	15	20	25	30
Pulse on time	us	30	45	60	75	90
Pulse off time	us	6	8	10	12	14
Frequency	Hz	200	250	300	350	400

4 Regression Models for SR USA EDM

Ultrasonic-assisted electrothermal machining of shape memory alloy experimental results are expressed in this section. In order to design the experiments, a central composite rotatable design was used, and the chosen process factors were varied up to five levels. The low-frequency vibration generator was connected to a workpiece that set the frequency and amplitude. The material was vibrated with low frequency and amplitude variation. Effect of ultrasonic vibration on process parameters (i) voltage (*V*), (ii) current (*I*), (iii) pulse on time (*ton*), (iv) pulse on time (*toff*), (v) frequency (*F*) on responses surface roughness was observed. A quadratic polynomial was fitted to experimental data and computed regression analysis and ANOVA using Minitab 19 software for USA EDM. Gap voltage, current, pulse on time, pulse off time, and frequency of ultrasonic vibration were varied and responses (SR) were noted. The results of regression analysis and ANOVA of surface roughness are presented in detail [11].

In Table 2 *X1 to X5* represents five controllable variables, while, *X1*X1 to X5*X5* are higher order terms, and *X1*X2 to X4*X5* are interaction terms of variables. Here * indicates multiplication of the two terms and magnitudes of the controllable variables should be taken as coded values while evaluating them from the corresponding equations. Regression analysis for SR model Table 2 indicates that the variables such as *V (X1)*, *I (X2)*, *ton (X3)*, *toff (X4)*, *F(X5)* are all higher order terms of variables except (*X2*X2*) *I*I*, and all interaction terms of variables except (*X1 * X3*) *V* ton*, (*X1 * X5*) *V* F*, (*X2*X5*) *I * F*, (*X3*X4*) *ton * toff*, have significant contribution in the SR model since 'P' values are less than 0.05. The value of surface roughness can be obtained by Eq. 1.

$$\begin{aligned}
 SR = & - 5.589 - 0.02704V + 0.2768 I - 0.05811 T_{ON} \\
 & + 0.7691T_{Off} + 0.02906 F + 0.000210V * V \\
 & - 0.000080 I * I + 0.000264T_{ON} * T_{ON} - 0.01615 T_{Off} * T_{Off} \\
 & - 0.000043 F * F - 0.001580V * I + 0.000009V * T_{ON} \\
 & + 0.002411V * T_{Off} + 0.000015V * F - 0.000565 I * T_{ON} \\
 & - 0.01022 I * T_{Off} + 0.000067 I * F - 0.000598T_{ON} * T_{Off} \\
 & + 0.000110T_{ON} * F - 0.001172T_{Off} * F
 \end{aligned}
 \tag{1}$$

Table 2 Regression analysis and ANOVA of NiTi for SR

Predictor	Coef	P	Predictor	Coef	P
Constant	3.0977	0.000*	–	–	–
X1	– 0.0859	0.042*	X1*X2	– 0.6322	0.000*
X2	0.5469	0.000*	X1*X3	0.0107	0.843
X3	– 0.3005	0.000*	X1*X4	0.3858	0.000*
X4	0.0434	0.036*	X1*X5	0.0606	0.276
X5	0.0708	0.029*	X2*X3	– 0.1696	0.008*
X1*X1	0.3362	0.000*	X2*X4	– 0.4089	0.000*
X2*X2	– 0.008	0.842	X2*X5	0.0666	0.233
X3*X3	0.2378	0.000*	X3*X4	– 0.0718	0.201
X4*X4	– 0.2585	0.000*	X3*X5	0.3309	0.000*
X5*X5	– 0.4261	0.000*	X4*X5	– 0.4687	0.000*
S = 0.211117		R-Sq = 98.80%		R-Sq (adj) = 97.13%	
Source	DF	SS	MS	F value	P value
Regression	20	40.4276	2.02138	45.35	0
Linear	5	9.688	1.93759	43.47	0
Square	5	13.3468	2.66936	59.89	0
Interaction	10	17.3928	1.73928	39.02	0
Residual error	11	0.4903	0.04457		
Lack-of-fit	6	0.0558	0.00931	0.11	0.992
Pure error	5	0.4344	0.08689		
Total	31	40.9178			

5 Conformity Experiments for Validating the Model

The conformity experiments were carried out utilizing the same experimental setup to determine the accuracy of produced mathematical models. The process parameters were allocated to intermediate values that were not in the design matrix, and validation test runs were performed. Table 3 shows the results of the computations and comparisons with the predicted values for SR models.

6 Conclusión

As the workpiece is vibrating, discharge energy is more intense as the tool electrode and the workpiece are brought closer more frequently, creating more discharges compare to when machining without vibration. The results of applying low-frequency

Table 3 Result of all 32 experiments using response surface methodology

SR (μm)		MRR (mm^3/min)	
Experimental	Predicted	Experimental	Predicted
1.241	1.252	12.344	12.457
1.542	1.545	7.122	7.118
1.864	1.977	9.914	10.081
1.055	1.006	16.088	15.948
2.964	2.956	8.222	8.144
1.525	1.535	9.077	8.973
2.326	2.357	10.031	10.107
1.987	1.986	12.375	12.303
5.524	5.463	8.555	8.542
3.923	3.961	8.291	8.372
3.012	3.022	10.531	10.532
3.623	3.098	11.425	11.251
3.524	3.511	12.666	12.720
1.987	1.972	11.674	11.823
3.325	3.322	11.375	11.503
2.883	3.098	10.375	11.251
1.423	1.403	9.375	9.315
4.522	4.614	11.764	11.784
4.342	4.271	10.062	10.051
3.221	3.098	11.675	11.251
2.883	3.098	11.146	11.251
2.873	3.098	11.064	11.251
4.654	4.650	10.375	10.259
3.124	3.098	11.831	11.251
2.012	1.971	8.675	8.649
5.244	5.190	10.395	10.387
3.223	3.274	11.375	11.438
3.654	3.698	9.375	9.324
4.124	4.160	12.831	12.691
3.011	3.001	15.965	15.979
2.243	2.151	9.831	9.673
3.423	3.448	9.777	9.902

vibration show that low-frequency vibration can be used to enhance surface roughness by 24%. Surface quality analysis revealed that surface response methodology could significantly improve the performance of low-frequency vibration assisted in the EDM process by improving the quality of performance of low-frequency vibration assisted in the EDM process by improving the quality of machining surfaces. Results of experiments and predicted values by regression model are compared and found in agreement with $\pm 10\%$.

References

1. Patel, K. M., Pandey, P. M., Venkateshwara Rao, P. (2010). Optimization of process parameters for multi-performance characteristics in EDM of AL2O3 ceramic composite. *International Journal of Advanced Manufacturing Technology*, 47, 1137–1147.
2. Mohamad, A. B., Noor, A., Siddiquee, Quadir, G. A., Khan, Z. A., & Saini, V. K. (2012). Optimization of EDM process parameters using Taguchi method. *International Conference on Applications and Design in Mechanical Engineering*.
3. Aliakbari, E., & Baseri, H. (2012). Optimization of machining parameters in rotary EDM process by using the Taguchi method. *The International Journal of Advanced Manufacturing Technology*, 62, 1041–1053.
4. Singh, S. (2012). Optimization of machining characteristics in electric discharge machining of 6061Al/Al2O3p/20P composites by grey relational analysis. *The International Journal of Advanced Manufacturing Technology*, 63, 1191–1202.
5. Choudhary, S. K., & Jadoun, R. S. (2014). Current advanced research development of electric discharge machining (EDM), a review. *International Journal of Research in Advent Technology*, 2(3), 273–297.
6. Ho, K. H., & Newman, S. T. (2003). State-of-the-art electrical discharge machining (EDM). *International Journal of Machine Tools and Manufacture*, 43, 1287–1300.
7. Machado, L. G. (2003). Medical applications of shape memory alloys. *Brazilian Journal of Medical and Biological Research*, 36, 683–691.
8. Maeshima, T. (2004). Shape memory properties of biomedical Ti-Mo-Ag and Ti-Mo-Sn alloys. *Materials Transactions*, 45(4), 1096–1100.
9. Hannula, S. P. (2006). Shape memory alloys for biomedical applications. *Advances in Science and Technology*, 49, 109–118.
10. Abbas, N. M., Solomon, D. G., & Bahari, M. F. (2007). A review on current research trends in electrical discharge machining (EDM). *International Journal of Machine Tools and Manufacture*, 47, 1214–1228.
11. Mane, A. B., & Jadhav, P. V. (2021). Optimization of response parameters of electrical discharge machine using shape memory alloy. *International Journal of Mechanical Engineering*, 6(3), 3386–3391.

Robotic Joint Torque Sensors: A Review



Shrikant C. Mahadik, Vikas R. Deulgaonkar, and Sachin M. Bhosle

Abstract The torque sensor is comparable to a mechanical fuse in design and ensures precise measurement. Since the torque sensor is one of the weakest parts of the driveline, choosing the proper one is crucial to preventing mechanical or unintentional failure in robots. At the same time, the accuracy of the torque sensor may be impacted by the uncertainty of the torque data. There are various types of torque sensors that can be used in robotic joints to measure torque between joints. This article compares various torque sensors and discusses them in detail. This study will help researchers choose the right torque sensors for robotic joints.

Keywords Joint sensors · Human-robotic collaboration · Perforated spoke structure

1 Introduction

Robots have been used in a variety of sectors that necessitate collaboration between the robot and humans majorly in medical sectors, where the dependability and safety of the robot must be assured first. As a result, a real-time interaction between a person and a robot is required. To detect the robot's collisions, many sensor-less approaches have been developed. The collision may be identified from the controller information by estimating the robot's location. Nonetheless, the technology described above is insufficient for detecting collisions between humans and robots in new surroundings. Measuring and estimating force and torque are essential components in the

S. C. Mahadik (✉)
VIIT, Kondhawa, Pune, India
e-mail: shrikantmahadik28@gmail.com

V. R. Deulgaonkar
Mechanical Engineering Department, Marathwada Mitra Mandal's College of Engineering, Pune, India

S. M. Bhosle
Mechanical Engineering Department, Vidya Pratishthan's Kamalnayan Bajaj Institute of Engineering and Technology Baramati, Baramati, India

development of collaborative robots. However, production feasibility, robustness, and cost must all be taken into account. There are numerous methods for detecting collisions. Sensor-less approaches, for example, use controller information like as position and velocity to estimate external forces. This strategy, however, is insufficient for identifying collisions in unknown situations. Furthermore, the accuracy of these approaches remains a concern. Vision-based solutions, on the other hand, are now gaining traction in robots. Vision cameras aid robots in detecting and avoiding obstacles, however delays and sophisticated computer vision processing with a high resolution computer are practical difficulties [1, 2].

The collision may be simulated using the friction model and the dynamic model of the robot by employing the electric current of each rotational actuator of the energy of the robot. The problem of adopting the robot model for estimate is that it is imprecise. Sensor-based collision detection systems have received lot of attention. Vision-based sensors can be used to avert a collision before it occurs [3]. The downsides of vision-based sensors are visionary problems as well as high manipulation costs. The sensitive sensor can detect impacts in various robot setups [3, 4].

An alternate approach is to use a multiple-axes force/torque sensor on the robot's end effector, however it is not sensitive enough to detect impacts that occur distant from the robot's end-effector [5]. The data-driven uniaxial torque sensor has lately piqued the curiosity of researchers. Normally, a uniaxial torque sensor is mounted to each manipulator joint. It can detect collisions on any section of the robot arm and improve detection performance [6]. The torque sensor is mounted on the gear head's outer rim, producing the friction values in the equation of motion.

To achieve collision detection with the uniaxial torque sensor, a high-performance torque sensor with a smart architectural integrated shape, extremely sensitive nature, and easy integration on the robot's joint is required. Torque sensors for robot collision detection may be divided into three subgroups depending on the collision recognition concept, namely optical, capacitive based, and strain gauge sensors. The optical-based torque sensor manipulates torque by establishing a link between torque load and optical deviation [7, 8].

The capacitive-based torque sensor can determine the load for a given applied torque by observing changes in capacitance. The benefits of using a capacitive-based torque sensor include contactless manipulation, a light construction, and a rapid dynamic changing response [9]. However, because of the thick form used in the manipulator's joints, its accuracy is limited. The torque sensor based on strain gauges employs the strain gauges to convert minor stresses into voltages in order to derive the torque signal [10]. The strain gauge-based torque sensor is further divided into three subgroups based on the positioning of the strain gauges [8].

To make certain signal processing for vigorous torque measurement, an adhesive type torque sensor is typically utilised in conjunction with a sliding ring [11]. In the case of the second kind, the torque sensor is made by stabbing strain gauges to the shear surface of a flexible support [9]. This type of sensor has the benefit of having an impenetrable construction and its signal operation unit may be enclosed within the

sensor assembly. It is difficult to paste strain gauges due to extreme tension around the spokes' ends. The third sort of torque sensor involves adhering strain gauges to the outside of an elastic support [12].

The sensor must respond quickly and be extremely sensitive during physical human robot interaction (p-HRI). The sensor must have small structure in order to enclose with joint construction. This article created and improved a novel form of torque sensor based on the third type of strain gauges [13].

2 Literature Survey

Dai-Dong Nguyen and Chung-Hsien Kuo, have studied the torque sensor for robots is created and refined utilising a strain gauge, according to research. The force measuring arm of this sensor was built using the ISS-based hole spoke type. This kind allowed for adjustment of the strain gauge insertion location, and its manufacturing enriched the strain gauge connexion. The DOE and RSM approaches were also used to improve the sensitivity and rigorousness of the torque sensor. The new proclivity surface reduced deformation by 22.8% while preserving the sensitivity, consistency level, and maximum stress design parameters [1].

Dewei Lai, Zhongxin Tang, Jianchang Zhao, Shuxin Wang, and Chaoyang Shi, have studied A new FBG-based torque sensor was designed and applied in this work to enable high-accuracy torque detection for MIS devices and multi-finger hands. In comparison to the present torque sensor, the suggested sensor design displayed an outstanding linear torque–strain relationship as well as high sensitivity in a tiny package. A generic technique for designing micro sensing a structure is provided by the torque-sensitive flexure design, which is based on the improvement and down-sizing of a hollow hexaform structure using the rigid-body replacement method. To study and confirm the sensor performances, both static calibration and dynamic experiments were carried out. To validate the anti-interference capability and stability under non-torsional loadings, bending moment and axial force crosstalk experiments were performed. Based on simulation, another design reached a resolution of 0.26 N mm inside [500, 500 N mm], exhibiting the easy modification capability to match varied applications. Future research will concentrate on sensor integration and the extension of the existing flexure architecture into multi-dimensional force/torque sensing [2].

Kang Han, Liheng Chen, Mingyi Xia, Qinwen Wu, Zhenbang Xu, Guoqiang Wang, have presented a joint torque sensor consisting of floating and supporting beams. The sensor measures 34 mm 4.2 mm and can accommodate the space requirements of finger joints. To increase sensor sensitivity, the structural properties of the sensor were adjusted using RSM. FEM was used to analyse the improved model and a prototype sensor was built and calibrated. The findings reveal that the sensor's sensitivity was 2.44 mV/V, which is greater than most torque sensors, that the linearity error was 0.62% F.S., that the hysteresis error was less than 1.48% F.S., and that the

repeatability error was less than 1.84% F.S. They confirmed that the torque measurement was not hampered by the force in the direction of the supporting beam [6] (Fig. 1).

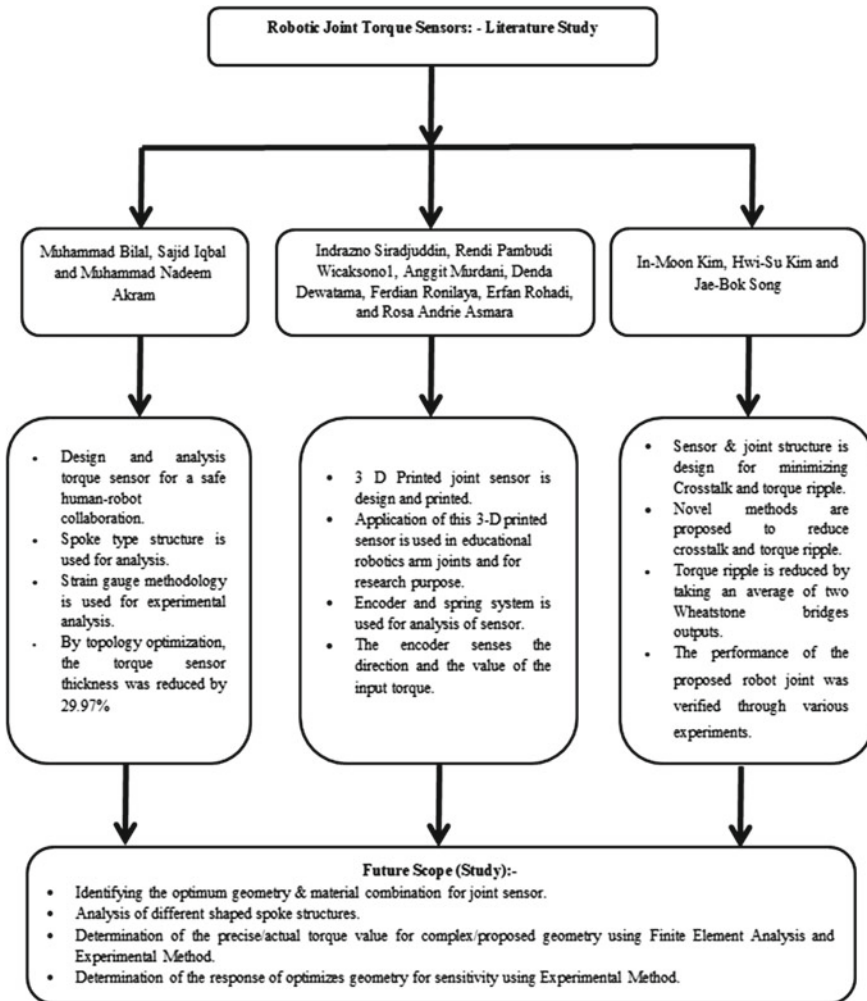


Fig. 1 Literature study and future scope of robotic joint sensor

Table 1 Comparative study of different types of torque sensor structures [1, 2, 4]

Geometry	Solid cylinder	Hollow cylinder	Hub sprocket	Hollow cruciform	Hollow hexaform	Spoke topology
<i>Parameter</i>						
1. Shape	Simple	Simple	Moderate	Moderate	Complex	Simple
2. Torsional Sensitivity	No	No	Moderate	Moderate	Good	High
3. Stiffness	High	High	High	Low	High	Moderate

2.1 Comparative Study of Different Types of Torque Sensor Structures

There are different types of sensors are available for torque and force measurement comparative study of all sensors is given in Table 1.

3 Conclusion

In this study different types of robotic joint sensor geometry and its evolution is discussed, comparative study of all joint sensor based on shape(structure), Torsional Sensitivity and Stiffness will help in future for researcher to select optimum torque sensor. Literature study describes that spoke topology geometry have optimum characteristics of all influencing parameters for optimum working of geometry.

References

1. Dai-Dong, N. (2021). Design and optimization of a joint torque sensor for lightweight robots. *IEEE Sensors Journal*, 21(8), 9788–9797. <https://doi.org/10.1109/JSEN.2021.3057920>
2. Lai, D., Tang, Z., Zhao, J., Wang, S., & Shi, C. (2021). Design and validation of a miniature fiber bragg grating-enabled high-sensitivity torque sensor. *IEEE Sensors Journal*, 21(18), 20027–20035
3. Muhammad, B., Sajid, I., & Muhammad, N. (2021). Design and analysis of joint torque sensor for safe human-robotic collaboration. In *11th annual international conference on industrial engineering and operations management, Singapore, conference proceeding*.
4. Yunjiang, L., Jiahao, W., & Shuang, S. (2019). Design and optimization of a joint torque sensor for robot collision detection. *IEEE Sensors Journal*, 19(16), 6618–6627. <https://doi.org/10.1109/JSEN.2019.2912810>
5. Farhad, A., Martin, B., & John, M. (2001). Design of a hollow hexaform torque sensor for robot joints. *The International Journal of Robotics Research*, 20(12), 967–976. <https://doi.org/10.1177/02783640122068227>
6. Kang, H., Liheng, C., Mingyi, X., Qinwen, W., Zhenbang, X., & Guoqiang, W. (2020). Design and optimization of a high sensitivity joint torque sensor for robot fingers. *Journal of*

- International Measurement Confederation*, 152. <https://doi.org/10.1016/j.measurement.2019.107328>
7. Siradjuddin, I., Wicaksono, R. P., Murdani, A., Dewatama, D., Ronilaya, F., Rohadi, E., & Asmara, R. A. (2018). A low cost 3D-printed robot joint torque sensor. *MATEC Web of Conferences*, 197, 11006. <https://doi.org/10.1051/mateconf/201819711006>
 8. Kim, I.-M., Kim, H.-S., & Song, J.-B. (2012). Design of joint torque sensor and joint structure of a robot arm to minimize crosstalk and torque ripple. In *9th international conference on ubiquitous robots and ambient intelligence (URAI) Daejeon, Korea* (pp. 404–407).
 9. Kim, B.-S., Yun, S.-K., Kang, S.-C., Hwang, C.-S., Kim, M.-S., & Song, J.-B. (2005). *Development of a joint torque sensor fully integrated with an actuator* (pp. 1679–1683). ICCAS2005 June 2–5, KINTEX.
 10. Chavan, D. K., Tasgaonkar, G. S., & Deulgaonkar, V. R. (2011). Mechatronics—A boon for technological development. *International Journal of Mechanical and Production Engineering Research and Development (IJMPERD)*, 1(2), 66–75.
 11. Mahadik, S., & Bhosle, S. M. (2020). Investigation of stress concentration in metallic plates with special shaped cutout and bluntness. *International Journal of Mechanical and Production Engineering Research and Development (IJMPERD)*, *Scopus Indexed Journal*, 10(3), 13477–13488. ISSN(P): 2249-6890; ISSN(E): 2249-8001 © TJPRC Pvt. Ltd. Paper Id.: IJMPERDJUN20201284. <https://doi.org/10.24247/ijmperdjun20201284>
 12. Pu, M., Luo, Q., Liang, Q., & Zhang, J. (2022). Modeling for elastomer displacement analysis of capacitive six-axis force/torque sensor. *IEEE Sensors Journal*, 22(2), 1356–1365.
 13. Devshete, M. V., Divase, P. D., Dhavale, A. D., Shinde, S. A., & Mahadik, S. C. (2016). E bike performance improvement. *International Research Journal of Engineering and Technology*, 06(12 Dec 2019), 585–588.

Mathematical Modelling of Material Removal in Laser Assisted Electro-chemical Machining Process (LAECM)



Amitkumar A. Shinde, Amarjit P. Kene, Kashfull Orra, and Karan B. Patil

Abstract Laser Assisted Electro Chemical Machining (LAECM) Process is a hybrid machining process, developed by combining the Electro Chemical Machining (ECM) and Laser Beam Machining (LBM) Processes from the different energy groups, i.e., electro chemical energy and thermal energy. The basic concept of these two parent processes has been explained and the mechanism of material removal of LAECM process has been discussed in detail, using the energy approach.

Keywords Laser beam machining · Electro-chemical machining · LAECM

1 Introduction

New and more advanced production techniques are being developed as a result of the usage of new engineering materials and the extremely high technological requirements for complicated micro components. High standards restrict the use of conventional production techniques to some extent, which leads to the development of unorthodox techniques and hybrid machining. Combining different physical and chemical processes into one machining process, or hybrid machining, is one of the most efficient ways to solve these issues and achieve excellent performance for micromachining. Combining several physicochemical actions on the material being machined might improve machining processes technologically. The motivation behind creating the hybrid machining technique was:

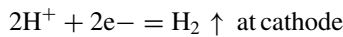
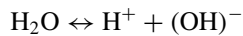
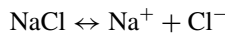
- To make use of the advantages that can be combined or improved by working together.
- To avoid or lessen some of the negative impacts that the various constituent processes can have.

A. A. Shinde (✉) · A. P. Kene · K. B. Patil
SVERI's College of Engineering, Pandharpur 413304, India
e-mail: aashinde@coe.sveri.ac.in

K. Orra
IIITDM Kanchipuram, Chennai, India

1.1 Electro-Chemical Machining

The non-traditional machining (NTM) process known as electrochemical machining (ECM) falls under the electrochemical category. The electrochemical or galvanic coating or deposition method is opposed to ECM. By flowing a high current at a low potential difference through an electrolyte, which is frequently a water-based neutral salt solution, ECM can be conceptualized as a controlled anodic dissolution of the work piece that is electrically conductive at the atomic level by a shaped tool. Reactions at the electrodes, i.e., the anode or work piece, the cathode or tool, as well as inside the electrolyte, will take place during ECM [1]. Let's use the machining of low carbon steel, which is essentially an iron-based ferrous alloy, as an example. Typically, sodium chloride (NaCl) neutral salt solution is used as the electrolyte for electrochemically machining steel. Ionic dissociation of the electrolyte and water occurs when a potential difference is introduced, as indicated below (Fig. 1).



Similar to this, the iron atoms will exit the work piece (anode) as:

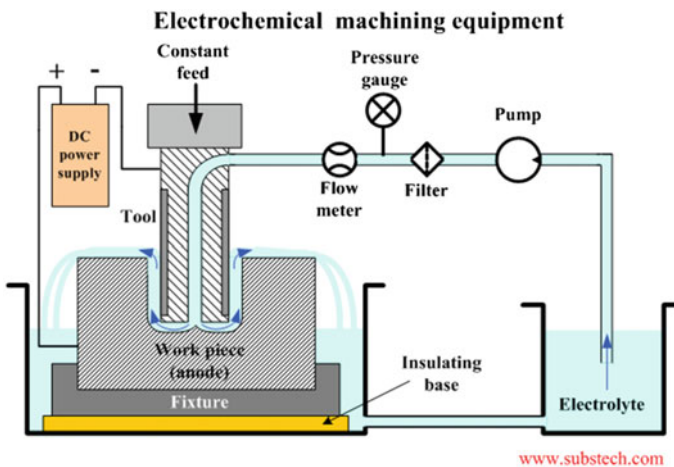
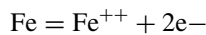


Fig. 1 Schematic of ECM process [2]

In the electrolyte, sodium ions and hydroxyl ions mix to make sodium hydroxide and Fe⁺⁺ ions combine with Cl⁻ ions to generate iron chloride.



1.2 Laser Beam Machining

One of the most popular thermal energy-based non-contact types of advanced machining processes, laser beam machining (LBM) can be utilized on a wide variety of materials. The laser beam is concentrated to melt and vaporize the undesired component from the parent component. It works well for cutting geometrically challenging profiles and punching tiny holes in sheet metal. The most well-known types of lasers for machining in industries are CO₂ and NdYAG lasers [3]. Melting, vaporization, and chemical degradation are a few of the processes that make up the mechanism of material removal during LBM (chemical bonds are broken which causes the materials to degrade). The work volume becomes heated and transformed into a molten, vaporized, or chemically altered condition that can be easily removed by flow of high pressure assist gas jet when a high energy density laser beam is focused on the work surface (Fig. 2).

2 LAECM

Laser drilling uses the energy of photons, which is combined with the energy of ions in LAECM. By decreasing the recast layer and spatter generated during laser drilling, the main goal of integrating a jet electrolyte and laser beam is to achieve good process quality. A noncontact tool-electrode is produced when the jet electrolyte is positioned

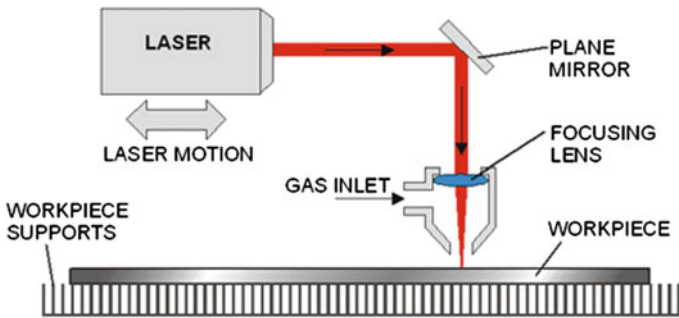


Fig. 2 Schematics of LBM [4]

coaxially with a concentrated laser beam. On the same surface of the work item, the concentrated laser beam and the jet electrolyte are operating simultaneously. Material is mostly removed during LAECM by pulse-width laser drilling. By effectively chilling the work piece, moving debris, and conducting an electrochemical reaction with the materials in between laser pulses, the jet electrolyte's effect eliminates the flaws (Fig. 3).

By combining an electrolyte jet and a relatively low power laser (375 mW), the hybrid method known as “Laser Assisted Jet Electrochemical Machining” makes it easier to remove metal. The laser's primary function is to improve the localization of electrochemical dissolution from the workpiece, which improves precision and machining effectiveness. The laser's thermal activation of the material surface where it makes contact raises the localized zone's electrochemical current density. The impacts of the localization of the electrochemical dissolution process are explained using a theoretical model. Laser aid can produce a volumetric rate that is up to 54% higher and an accuracy that is up to 38% better than electrolytic jet alone, according to experimental study on aluminum alloy and stainless steel. A novel hybrid process combining laser drilling with jet electrochemical machining (JECM-LD) has been developed to address these issues as well as improve the general quality of laser-drilled holes. Recast layers and spatters are two types of defects that frequently accompany laser-drilled holes and limit their potential applications in the aerospace and aircraft industries. Electrochemical dissolution is the most common method of

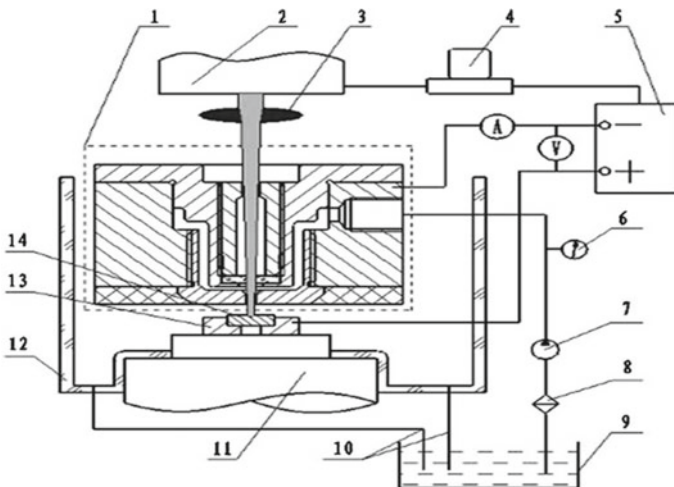


Fig. 3 Schematic Representation of the LAECM setup [5]. 1. The Jet cell, 2. system of LASER, 3. lens focusing, 4. the control unit system, 5. power supply DC system, 6. pressure sensors, 7. pump, 8. cleanse, 9. electrolyte storage tank, 10. reverse pipelines, 11. CNC desk, 12. the work cell, 13. holder, 14. work piece

material removal, and the laser's function is to support and focus electrochemical energy. The workpiece's ability to localize dissolution to a particular location is made possible by the thermal energy of the laser that is conveyed there. This energy improves the kinetics of electrochemical reactions.

3 Mechanism of Material Removal

The process combines two sources of energy simultaneously. Energy of photons (a laser beam) and energy of ions (ECM). The primary material removal method is the dissolving process, which is aided by the concurrent activity of the laser beam. The laser's heat activation promotes dissolution rather than removing any material. The significant heat stress, re-deposition, and evaporation or melting limits the precision of machining in laser machining. While the benefit of burr-free and stress-free processing is a feature of electrochemical machining techniques. Under typical circumstances, chemical reactions could be ineffective. Such processes can be accelerated using laser irradiation.

3.1 Law of Arrhenius

Elevating the electrolyte temperature causes it to have a higher conductivity and current density, eliminate surface passivation, and intensify the dissolution process by speeding up the pace at which materials are removed.

$$i_l = i_0 \exp\left(\frac{E_0 \Delta T_s}{RT_0(T_0 + \Delta T_s)}\right) \quad (*)$$

where T_0 and T_s are the surface temperature's initial and final values, i_0 is current density before heating, i_l is the current density after heating, E_0 is the activation energy, R is universal gas constant.

It is presumable that laser help can increase the efficiency and precision of electrochemical machining by locally heating the machined surface in a targeted location. It is crucial that the electrolyte boiling temperature is not exceeded as a result of the laser heating the machined surface. If not, the electrolyte would boil and the ECM process would stop.

4 Mathematical Modeling

Power from electrolyte jets E1: The energy is electrical. It is supplied by electrical charge flow and the following equation can describe it:

$$E_1 = \int_0^{t_n} U^2 \frac{K(t)A(t)}{g(t)} dt \quad (1)$$

where U represents the voltage, K represents conductivity, A represents specific area of machining, g represents inter-electrode gap, t represents machining time and t_n represents end machining time [6].

E2: The thermal energy that makes up a laser beam. The following equation, which provides this energy, can be obtained from the Gaussian distribution of the laser heat source:

$$E_2 = \int_0^{t_n} P_i f \exp(-kr^2)t dt \quad (2)$$

where P_1 represents impulse laser power, f represents pulse frequency of laser, t represents time, k represents concentration factor, r represents laser dot radius and t_n represents end machining time [6].

Energy from electrolyte flow, E3: It is the thermal energy that is being seized. It is seen negatively because it cools the surface of the outer substance. This energy loss can be interpreted as heat loss resulting from electrolyte overflow. It is assumed that the electrolyte's surface layer is laminar and that there is no surface pressure gradient. The equation is so as follows:

$$E_3 = \int_0^{t_n} \left\{ \int \int_A \rho c_p v T(A, t) dA dt \right. \quad (3)$$

where A represents specific machining area, ρ shows the material density, c_p represents material specific heat, v represents average flow velocity, T represents temperature of machining area, t represents machining time and t_n represents end machining time [6, 7].

$$MRR = \frac{i_1 \eta E}{F \rho_a} \quad (4)$$

where η represents the efficiency, E represents the electrochemical equivalent, $F = 96,500$ C and ρ_a represents the density of the anode.

Total Energy:

$$E = E_1 + E_2 + (-E_3) \tag{5}$$

From Eqs. (1), (2), (3) and (5);

$$E = \int_0^{t_n} U^2 \frac{K(t)A(t)}{g(t)} dt + \int_0^{t_n} P_i f \exp(-kr^2) t dt - \int_0^{t_n} \left\{ \int_A \rho c_p v T(A, t) dA \right\} dt \tag{6}$$

As we know that conductivity is inversely proportional to resistivity and therefore the conductance of the electrolyte will be inversely proportional to the resistance in the electrolyte for electric current to flow.

$$K = \frac{1}{\rho}$$

$$K = \frac{l}{R \cdot A_e} = \frac{G \cdot l}{A_e} \tag{7}$$

where G is the conductance, Ae is the Area of electrolyte and l = length. Also as we know that Inter electrode gap (IEG) at zero feed condition is,

$$g = y_o^2 + 2 \cdot C \cdot t$$

Here g is the IEG and at t = 0, y = yo, C is the constant and t is machining time [8–12].

Using (7) in (6) we get,

$$E = U^2 \int_0^{t_n} \frac{G \cdot l}{A_e} \times b \cdot h(t) \times \frac{1}{(y_o^2 + 2 \cdot C \cdot t)^{\frac{1}{2}}} dt + P_i f \exp(-kr^2) \int_0^{t_n} t dt - \int_0^{t_n} \left\{ \int_A \rho c_p v T(A, t) dA \right\} dt$$

Therefore, E

$$= \frac{U^2 \cdot G \cdot l \cdot b \cdot h}{A_e} \times \int_0^{t_n} \frac{t}{(y_o^2 + 2 \cdot C \cdot t)^{\frac{1}{2}}} dt + P_i f \exp(-kr^2) \int_0^{t_n} t dt - \int_0^{t_n} \left\{ \int_A \rho c_p v T(A, t) dA \right\} dt \tag{8}$$

Now, the first part of the Eq. (6) can be integrated as follows;

$$\frac{U^2 \cdot G \cdot l \cdot b \cdot h}{A_e} \times \int_0^{t_n} \frac{t}{(y_o^2 + 2 \cdot C \cdot t)^{\frac{1}{2}}} dt$$

Let $(y_o^2 + 2 \cdot C \cdot t)^{\frac{1}{2}} = X$

$$\therefore dt = 2X \cdot dX$$

$$t = \frac{X^2 - y_o^2}{2 \cdot C}$$

$$\begin{aligned} \therefore & \frac{U^2 \cdot G \cdot l \cdot b \cdot h}{A_e} \times \int_0^{t_n} \frac{X^2 - y_o^2}{2 \cdot C} dX \\ \therefore & \frac{U^2 \cdot G \cdot l \cdot b \cdot h}{A_e} \times \left\{ \int_0^{t_n} X \cdot dX - \int_0^{t_n} \frac{y_o^2}{X} dX \right\} \\ \therefore & \frac{U^2 \cdot G \cdot l \cdot b \cdot h}{A_e} \times \left\{ \left[\frac{X^2}{2} \right]_0^{t_n} - y_o^2 [\log X]_0^{t_n} \right\} \end{aligned} \tag{9}$$

Now substituting $(y_o^2 + 2 \cdot C \cdot t)^{\frac{1}{2}} = X$ in Eq. (9) we get,

$$\begin{aligned} & \frac{U^2 \cdot G \cdot l \cdot b \cdot h}{A_e} \times \left\{ \left[\frac{y_o^2 + 2 \cdot C \cdot t}{2} \right]_0^{t_n} - y_o^2 \left[\frac{1}{2} \log(y_o^2 + 2C \cdot t) \right]_0^{t_n} \right\} \\ & \frac{U^2 \cdot G \cdot l \cdot b \cdot h}{A_e} \times \left\{ \begin{aligned} & \left[\frac{y_o^2 + 2 \cdot C \cdot t_n}{2} - \frac{y_o^2}{2} \right] \\ & - \frac{y_o^2}{2} [\log(y_o^2 + 2C \cdot t_n) - \log y_o^2] \end{aligned} \right\} \end{aligned} \tag{10}$$

Now putting Eq. (8) in (6)

$$\begin{aligned} E = & \frac{U^2 \cdot G \cdot l \cdot b \cdot h}{A_e} \times \left\{ \begin{aligned} & \left[\frac{y_o^2 + 2 \cdot C \cdot t_n}{2} - \frac{y_o^2}{2} \right] \\ & - \frac{y_o^2}{2} [\log(y_o^2 + 2C \cdot t_n) - \log y_o^2] \end{aligned} \right\} \\ & + P_i f \exp(-kr^2) \int_0^{t_n} t dt - \int_0^{t_n} \left\{ \int_A \rho c_p v T(A, t) dA \right\} dt \end{aligned}$$

$$E = \frac{U^2 \cdot G \cdot l \cdot b \cdot h}{A_e} \times \left\{ \left[\frac{y_o^2 + 2 \cdot C \cdot t_n}{2} - \frac{y_o^2}{2} \right] - \frac{y_o^2}{2} \left[\log(y_o^2 + 2C \cdot t_n) - \log y_o^2 \right] \right\} + P_i f \exp(-kr^2) \frac{t_n^2}{2} - \int_0^{t_n} \left\{ \int_A \rho c_p v T(A, t) dA \right\} dt \tag{11}$$

As the value of electrolyte flow energy has been found to very small as compared to the electrolyte jet energy E1 and Laser beam heat energy E2, so it can be neglected from the Eq. (9)

The Eq. (9) transforms as,

$$E = \frac{U^2 \cdot G \cdot l \cdot b \cdot h}{A_e} \times \left\{ \left[\frac{y_o^2 + 2 \cdot C \cdot t_n}{2} - \frac{y_o^2}{2} \right] - \frac{y_o^2}{2} \left[\log(y_o^2 + 2C \cdot t_n) - \log y_o^2 \right] \right\} + P_i f \exp(-kr^2) \frac{t_n^2}{2}$$

After simplifying the final equation can be written as;

$$\therefore E = \frac{U^2 \cdot G \cdot l \cdot b \cdot h}{A_e} \times \left\{ \left[\frac{y_o^2 + 2 \cdot C \cdot t_n}{2} - \frac{y_o^2}{2} \right] - \frac{y_o^2}{2} \left[\log \left(\frac{y_o^2 + 2C \cdot t_n}{y_o^2} \right) \right] \right\} + P_i f \exp(-kr^2) \frac{t_n^2}{2} \tag{12}$$

Now this value of E can be substituted on the place of Eo in equation (*) to get the current density after heating due to laser;

$$i_l = i_o \exp \left(\frac{E_o \Delta T_s}{RT_o(T_o + \Delta T_s)} \right)$$

$$\therefore i_l = i_o \exp \left(\frac{\left\{ \frac{U^2 \cdot G \cdot l \cdot b \cdot h}{A_e} \times \left\{ \left[\frac{y_o^2 + 2 \cdot C \cdot t_n}{2} - \frac{y_o^2}{2} \right] - \frac{y_o^2}{2} \left[\log \left(\frac{y_o^2 + 2C \cdot t_n}{y_o^2} \right) \right] \right\} + P_i f \exp(-kr^2) \frac{t_n^2}{2} \right\} \Delta T_s}{RT_o(T_o + \Delta T_s)} \right) \tag{13}$$

As we know that Material removal rate is directly depends on the current density. So the Eq. (4) can be written as;

$$MRR = \frac{i_l \eta E}{F \rho_a}$$

$$MRR = \frac{i_0 \exp \left(\frac{\left\{ \frac{U^2 \cdot G \cdot l \cdot b \cdot h}{A_e} \times \left[-\frac{y_0^2}{2} \left[\log \left(\frac{y_0^2 + 2C \cdot t_n}{y_0^2} \right) \right] + P_i \cdot f \cdot \exp(-kr^2) \frac{y_0^2}{2} \right\} \Delta T_s}{RT_0(T_0 + \Delta T_s)} \right)}{F \rho_a} \cdot \eta \cdot E \tag{14}$$

Where,

y_0 —IEG at $t = 0$, t_n - End machining time, P_i - Laser power, $F = 96,500 \text{ C}$.

5 Results and Discussion

The Eq. (14) gives a mathematical model for material removal rate calculation in LAECM process. The energy approach has been used by us. The analytical results have been contrasted with the results of the experiments done by the different authors. From this comparison, it is clear that the MRR in LAECM is mostly depending on the IEG, machining time and the laser power. From the research done earlier, the same results have been confirmed in this paper. From the Eq. (14) and Fig. 4, the volumetric material rate is increases as voltage is increases and it will decrease as IEG increases.

The bar chart showed in Fig. 5 shows the contribution of energy in the LAECM process at particular sets of machining conditions. It shows that in LAECM process the most of the percentage of energy required is due to ECM as compared with LBM process which states that LBM is only a supporting process whereas ECM is acts as a parent process. The LBM is use for obtaining better surface finish which is not covered in this study.

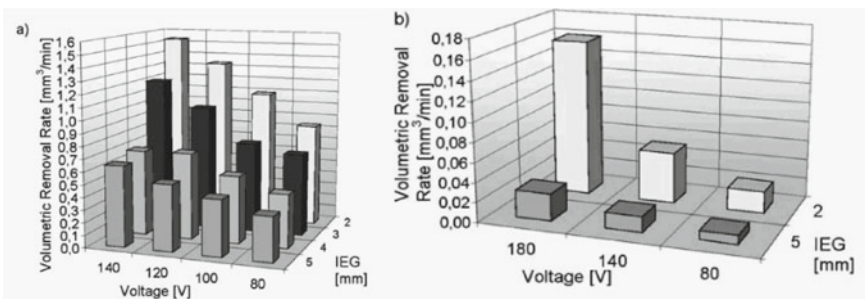


Fig. 4 For **a** aluminium alloy, **b** stainless steel LAJECM volumetric removal rate versus voltage and inter electrode gap [6, 13]

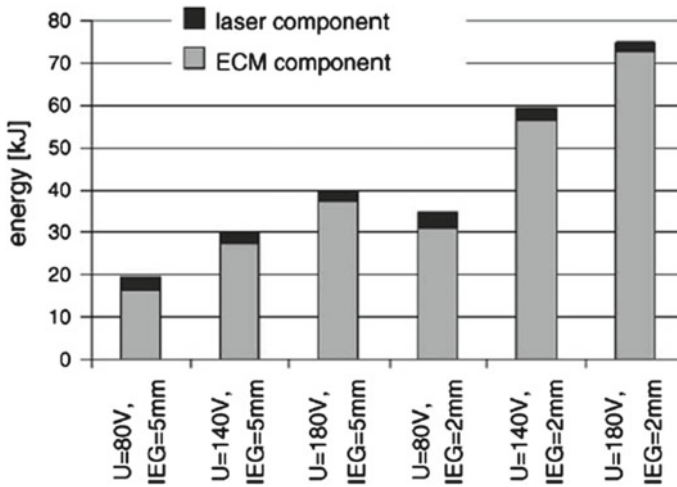


Fig. 5 Distribution of Energy components for different variable sets for stainless steel [14]

6 Conclusions

The study has been carried out on the basic principle of material removal in the ECM and LBM process. Both of them have been combined to form the LAECM process and it has been observed that ECM is the parent process by which material is removed and LBM is the assisting process which eases the material removal by the ECM process by increasing the surface temperature of the work piece. From the expression of MRR in ECM process, it is evident the material removal is a main function of current density (i) as all other parameters are usually constant.

There are many approaches given by various scientists to investigate the MRR in LAECM process. But from the literature survey, we have selected the energy approach, since it is more relevant in this context. A novel expression has been deduced in this study which clearly shows that the MRR is a direct function of, Inter-electrode Gap (IEG), Initial Current Density and End Machining Time.

References

1. Module 9, Electro chemical machining version 2, Me, I. I. T. Kharagpur.
2. http://www.substech.com/dokuwiki/lib/exe/detail.php?id=electrochemical_machining&cache=cache&media=electrochemical_machining_equipment.png
3. Dubey, A. K., & Yadava, V. (2008). Laser beam machining—A review. *International Journal of Machine Tools and Manufacture*, 48(6), 609–628.
4. [http://www.mechanicaldesignforum.com/content.php?18-Laser-beam-machining-\(LBM\)](http://www.mechanicaldesignforum.com/content.php?18-Laser-beam-machining-(LBM))
5. Zhang, H., & Xu, J. (2012). Laser drilling assisted with jet electrochemical machining for the minimization of recast and spatter. *International Journal of Advanced Manufacturing Technology*, 62(9–12), 1055–1062.

6. De Silva, A. K., Pajak, P. T., Harrison, D. K., & McGeough, J. A. (2004). Modelling and experimental investigation of laser assisted jet electrochemical machining. *CIRP Annals*, 53(1), 179–182.
7. Pajak, P. T., De Silva, A. K. M., McGeough, J. A., & Harrison, D. K. (2004). Modelling the aspects of precision and efficiency in laser-assisted jet electrochemical machining (LAJECM). *Journal of Materials Processing Technology*, 149(1–3), 512–518.
8. Zhang, H. (2012). Laser drilling assisted with jet electrochemical machining, Nd. In Y. Laser & D. C. Dumitras (Eds.). Tech, ISBN: 978-953-51-0105-5. <http://www.intechopen.com/books/nd-yag-laser/laser-drilling-assisted-with-jet-electrochemical-machining>
9. Wyszynski, D., Skoczypiec, S., Grabowski, M., Ruszaj, A., & Lipiec, P. (2012). Electrochemical microprocessing assisted by diode pumped solid state nd:yag pulse laser. *Journal of Machine Engineering*, 12(1).
10. [http://vedyadhara.ignou.ac.in/wiki/images/9/9b/BME-008_B-1\(Unit_11\).pdf](http://vedyadhara.ignou.ac.in/wiki/images/9/9b/BME-008_B-1(Unit_11).pdf)
11. <http://nptel.iitm.ac.in/courses/Webcourse-contents/IIT%20Kharagpur/Manuf%20Proc%20II/pdf/LM-39.pdf>
12. Jain, V. K. (2002). Advanced machining processes. Allied.
13. Zhang, H., Xu, J., & Wang, J. (2009). Investigation of a novel hybrid process of laser drilling assisted with jet electrochemical machining. *Optics and Lasers in Engineering*, 47(11), 1242–1249.
14. Pajak, P. T., Desilva, A. K. M., Harrison, D. K., & Mcgeough, J. A. (2006). Precision and efficiency of laser assisted jet electrochemical machining. *Precision Engineering*, 30(3), 288–298.

Design and Development of a Metal Jet Print-Head



Gurudev N. Mhetre, Vijay S. Jadhav, and Suhas P. Deshmukh

Abstract Additive manufacturing or 3D printing is a novel and fast-evolving technology in the manufacturing industry. Fused Deposition Modeling is a widely used 3D printing technology that produces objects by continuously extruding melted filament and adding it layer by layer onto the substrate. This method allows for more flexibility in the design of the parts and their structural complexity. The majority of FDM printers use plastic filaments since it is very challenging to print with metals. This research work focuses on the design and development of a metal jet print head for the FDM printer which can melt and extrude metal filaments and build metal parts. This study gives an idea about developing a high-temperature metal jet print-head that can print aluminium metal using less power consumption and less time. Additionally, factors including the heating method, target temperature, heating time, consumed electrical power, and materials required for the development of the print-head are discussed.

Keywords Additive manufacturing · Fused deposition modeling · Metal 3D printing · Metal extrusion

1 Introduction

Additive manufacturing is rapidly evolving technology in the manufacturing industry. Additive manufacturing creates the objects building it by layer-on-layer technique. 3D printer requires the 3D CAD model which is sliced in small layers in slicing software and then prints each layer one by one [1]. Additive manufacturing technique mostly use wire and powder as raw materials, which are melted and then cooled to make a component. Additive manufacturing technique may generate three-dimensional items with any geometrical shape without the need for a subsequent procedure or the formation of trash or waste. In recent few years researchers have investigated and optimized many process parameters of 3D printing by changing

G. N. Mhetre (✉) · V. S. Jadhav · S. P. Deshmukh
Government College of Engineering, Karad, India
e-mail: gurudevnmhetre@gmail.com

© The Author(s), under exclusive license to Springer Nature Switzerland AG 2024
P. M. Pawar et al. (eds.), *Techno-societal 2022*,
https://doi.org/10.1007/978-3-031-34644-6_72

697

material properties, operating conditions and material reinforcement. Murr et al. found that multiple metal wires or powder feed systems may be integrated into processes such as wire feed and powder feed to allow functional deposit grading or the fabrication and integration of various metal component in the manufacturing of a product [2]. Casati et al. found aging generated a considerable improvement in strength over the as-built state in the selective laser-sintered 18-Ni 300 alloy while decreasing tensile ductility [3]. Tang et al. concluded that results of the compression tests show that process faults have no impact on the mechanical properties when the minimum structural size is greater than 1.5 mm manufactured using SLM [4]. Manakari et al. found that metallurgical defects in magnesium alloys processed by SLM include porosity, oxide inclusions, thermal cracking and alloying element loss [5]. Yusuf et al. examined the samples of 316 L stainless steel generated by selective laser melting differ in porosity and microhardness (SLM). The presence of microscopic TiC particles greatly improved the wear performance and microhardness of the manufactured components [6]. Bambach et al. discussed two circumstances when laser metal deposition is utilised to reinforce sheet metal locally. Limited formability was found to be the main obstacle to using personalised laser-cladded blocks as moderately finished items [7]. Troy Y. Ansell focused on liquid metal printing; a family of metal jetting processes used in the additive manufacturing of metal items [8]. Murr discussed applications and illustrations of microstructures describing metallurgical occurrences in 3D printing and additive fabrication of metal and alloy components and products are provided [9]. In this research aluminium wire is used as feeding material for fused deposition modeling 3D printer. The heating method, heating time, input power and output temperature parameters are investigated.

2 Experimentation

2.1 *Selection of Machine and Material*

This is the Fused deposition modelling type 3D printer manufactured by Creality Ltd. It has highest temperature limit of 200 °C. It used resistance cartridge heater to heat the nozzle and it used aluminum material for heating block and radiator. We are going to modify in the extruder of this machine which is suitable for printing aluminium material. Aluminum components used in aeronautical applications have intricate shapes and structures. Traditional manufacturing methods are tough to use to produce these intricate shapes. However, since 3D printing allows for a great deal of customisation and flexibility when producing complicated structures, aluminium metal was chosen as the printing medium (Fig. 1).

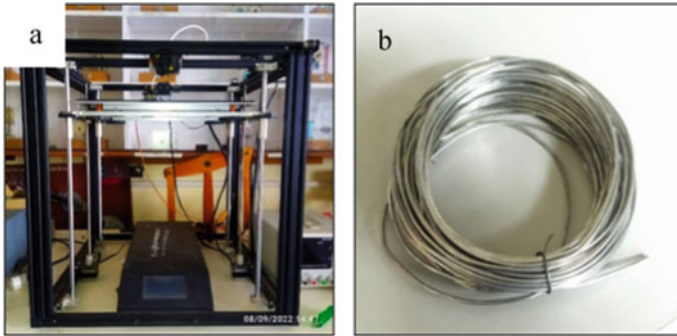


Fig. 1 a Creality Ender 5 Plus and b aluminium wire

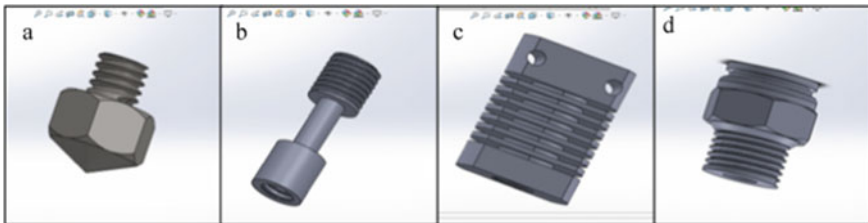


Fig. 2 CAD Model of a nozzle, b throat, c radiator and d fitting nut

2.2 Design and Modelling of Extruder

The extruder is regarded as one of a 3D printer’s crucial parts. Extruder is in charge of feeding in, melting, and extruding the filament. It’s frequently described as a “fancy hot glue gun.” In some circumstances, it is used to deposit a bonding agent to harden the powdered substance. This is the area where the primary printing process takes place. Since the extruder is a 3D printer’s main component, the material for a 3D print is discharged from the extruder in liquid or semi-liquid state. The 3D printer’s extruder is made up of the following components: a nozzle, a throat, a radiator, and a fitting nut (Fig. 2).

2.3 Manufacturing and Assembly of Extruder

The extruder parts are manufactured according to the drawings of the CAD models. Radiator and induction coil are made up of copper. Nozzle and fitting nut are made up of stainless steel. The throat is made from EN8 Steel because it has high inductivity than stainless steel. The fins radiator is manufactured by EDM machining and other machining is done on CNC lathe machine and vertical drill machine. Thorat

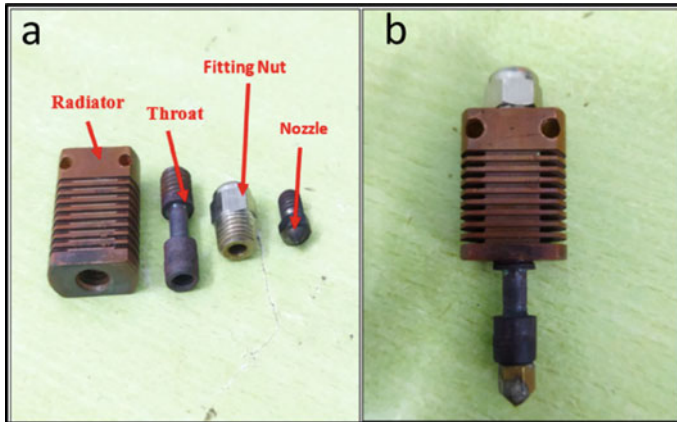


Fig. 3 a Manufactured extruder parts, b extruder assembly

is manufactured on CNC lathe and drilled on vertical drill. Solid Carbide tool is used for drilling the holes. The internal threads are cut by tap and drill method while external threads of throat are cut by die (Fig. 3).

2.4 Induction Heating Module and Power Supply

The induction Module is a high-quality module board for powering induction heaters. It is the compact induction heater suitable for low voltage applications. Its DC power supply voltage ranges from 5 to 12 V. Installation is very simple. It can deliver the output of 120W maximum power (12 V induction heating). It can be used from 0v to 20 V input voltage using cooling fan over the module, because heat can damage the circuit board. The SPD3303C power supply has a high resolution of 10 mV/10 mA and has 3 output modes: series/parallel/independent: The series–parallel function combines two power supply into one, making it ideal for a wide range of applications. The SPD3303C features three independent outputs that may be controlled independently and turned on or off individually or simultaneously (Fig. 4).

2.5 Experimental Setup and Temperature Measurement

All the manufactured extruder components are assembled together and mounted on the carriage of the 3D printer. The induction heater is mounted alongside the extruder in such a way that the throat and nozzle of the extruder should be at the centre of the induction coil. The induction coil is connected to the induction module and this module is connected to the DC power supply. The aluminium wire (feed

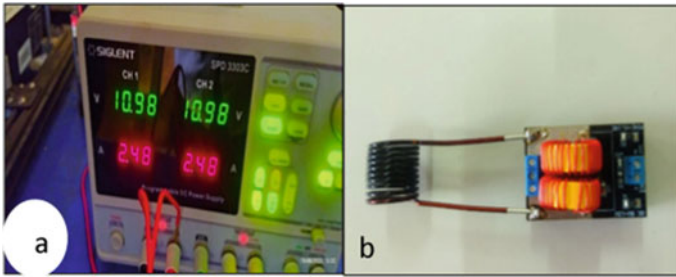


Fig. 4 a SIGLENT DC power supply and b Xcluma induction module

material) of SWG 16 (1.45 mm diameter) is supplied through the fitting nut. The FLIR E85 Thermal Imaging Camera is loaded with high-performance capabilities for quick and precise identification of hot spots and accurate temperature readings. It can measure the temperature of each part and generate the colourful image of the extruder according to the temperature readings. Later on, these images are analysed in FLIR Thermal Studio software and temperature readings of each part is taken. It has the temperature range between $- 20$ and $1200\text{ }^{\circ}\text{C}$ and the accuracy of this thermal camera is 99.99% (Fig. 5).

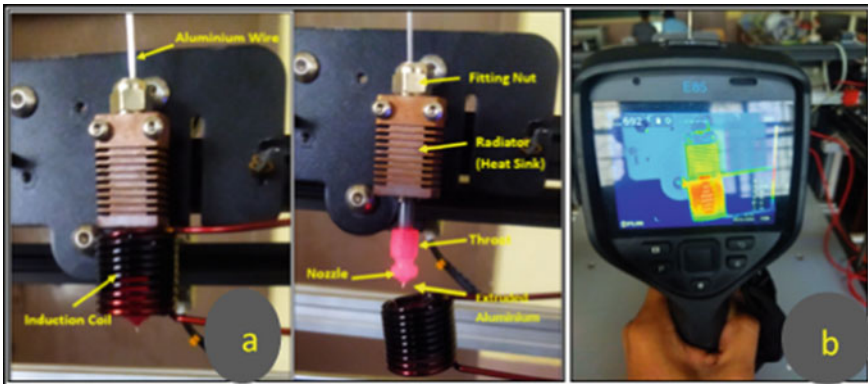


Fig. 5 a Experimental setup and b FLIR thermal camera E85

3 Results and Discussion

The experiments are conducted by varying the voltage input and how much current is drawn by the system is found. Again, the input voltage is varied and the output temperature is measured. Additionally, the time required to achieve the target temperature is also measured. Readings are taken with two different materials for throat i.e., EN8 Steel and Copper and two materials for nozzle Stainless Steel 202 and Brass.

3.1 Current Consumption and Temperature Output Between EN8 Steel and Copper Throat

The Fig. 6a shows the comparison between power consumed by the induction heater to achieve the maximum temperature using steel and copper material. The steel throat is consuming 3.2 A current at 16.6-V voltage input and copper throat is consuming 1.93 A current at 17.1-V voltage input, and steel throat is consuming 39.68% more current at 2.92% less voltage input than copper throat. The Fig. 6b shows the comparison between temperature output given by steel and copper throat. The steel throat is giving output temperature of 711.3 °C at 53.12 watts input power and copper throat is giving 329.3 °C temperature output at 33.03 watts input power, and Steel throat is giving 53.70% more temperature output than copper throat (Table 1).

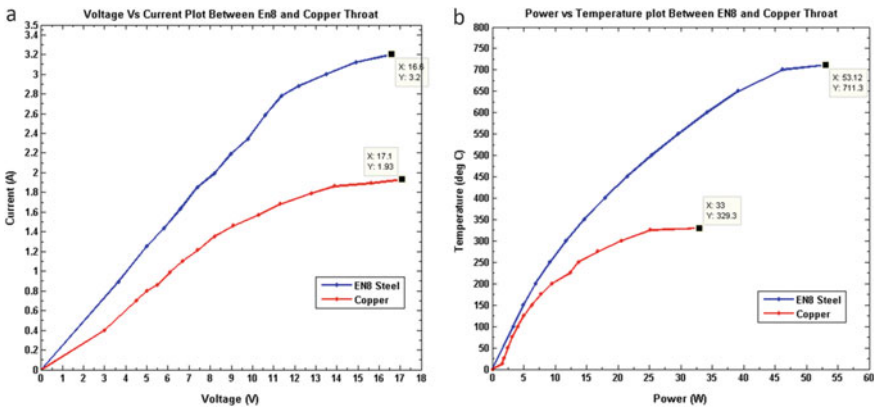


Fig. 6 Graph between EN8 steel and copper throat for **a** current consumption and **b** temperature output

Table 1 Experimental readings for EN8 steel and copper throat

EN8 steel throat						Copper throat					
Temperature (°C)	Voltage (V)	Current (A)	power (watts)	Time (s)	Temperature (°C)	Voltage (V)	Current (A)	Power (W)	Time (S)		
0	0	0	0	0	0	0	0	0	0		
100	4.19	0.79	3.31	2.74	100	12	1.24	14.88	35.4		
150	4.77	0.99	4.72	4.71	150	13.7	1.46	20	72.69		
200	6	1.32	7.92	8.31	200	14.09	1.53	21.56	131.5		
250	6.72	1.51	10.15	11.65	250	15.49	1.72	26.64	192.4		
300	7.32	1.65	12.08	14.71	300	16.29	1.84	29.97	238.4		
350	7.96	1.8	14.33	19.8	329.3	17.1	1.93	33	256.2		
400	8.76	1.98	17.34	24.75							
450	9.54	2.15	20.51	33.12							
500	10.31	2.32	23.92	38.85							
550	10.98	2.48	27.23	49.22							
600	12.7	2.98	37.85	70.09							
650	15.4	3.2	49.28	99.73							
700	16.2	3.2	51.84	140							
711.3	16.6	3.2	53.12	160.2							

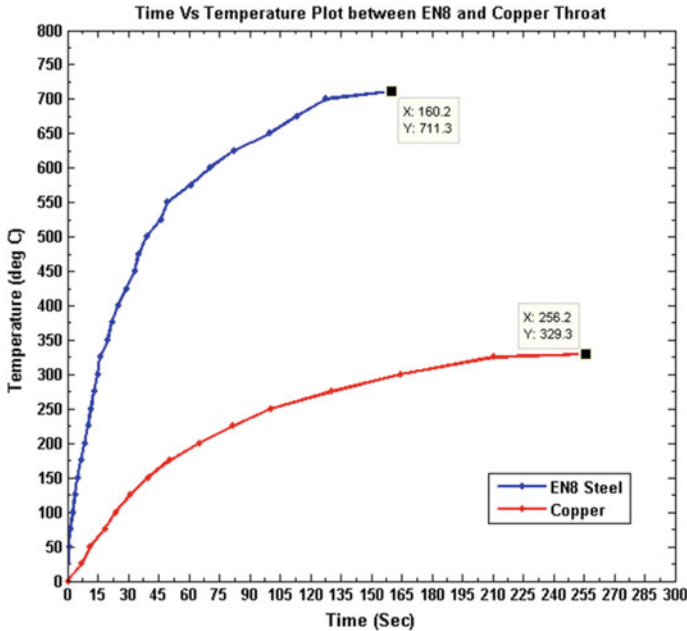


Fig. 7 Graph between EN8 steel and copper throat for time requirement

3.2 Time Requirement for EN8 Steel and Copper Throat

The following graph shows the comparison between time required to achieve the maximum temperature using steel and copper material. The steel throat is taking 160.2 s time to reach at the temperature of 711.3 °C and copper throat is taking 256.18 s time to reach at the temperature of 327 °C. Steel throat is taking 37.46% less time than copper throat to reach at 45.97% more temperature than copper throat (Fig. 7).

3.3 Temperature Output and Time Requirement Between Stainless Steel 202 and Brass Nozzle

Figure 8a shows the graph between brass and Stainless steel 202 nozzle temperature output. The maximum temperature achieved by stainless steel 202 nozzle is 652.5 °C at the input power of 53.12 watts. The maximum temperature achieved by brass nozzle is 312.5 °C at the input power of 33.03 watts. The stainless steel 202 nozzle has achieved 52.10% higher temperature than brass nozzle. Figure 8b shows the graph between brass and Stainless steel 202 nozzle time requirement for target temperature output. The time taken by stainless steel 202 nozzle to achieve 652.5 °C temperature is

160.2 s. The time taken by brass nozzle to achieve 312.5 °C is 256.18 s. The stainless steel 202 nozzle has achieved 52.10% higher temperature by taking 37.46% less time than brass nozzle (Table 2).

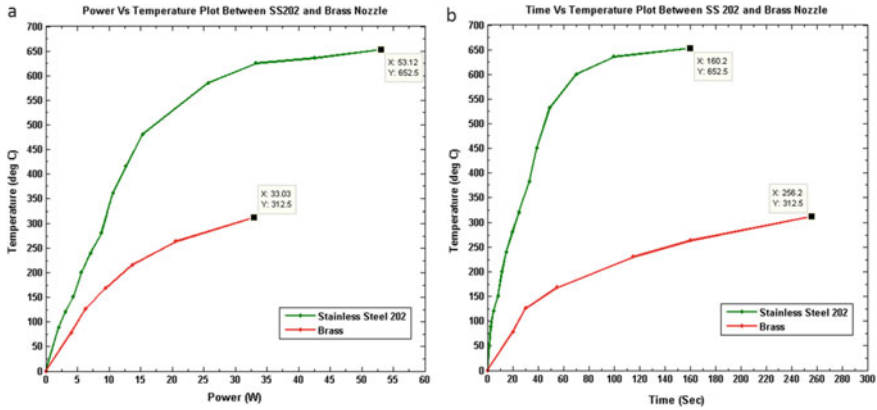


Fig. 8 Graph between stainless steel 202 and brass nozzle for **a** temperature output and **b** time requirement

Table 2 Experimental readings for stainless steel 202 and brass nozzle

Stainless Steel 202 nozzle				Brass nozzle		
Temperature (°C)	Temperature (°C)	Time (s)	Power (watts)	Temperature (°C)	Time (s)	Power (watt)
0	0	0	0	0	0	0
88.5	88.5	2.74	2	78.5	20	4.015
120	120	4.71	3.1	125.7	30	6.27
150	150	8.31	4.3	168.1	55	9.47
200	200	11.65	5.6	230.5	115	13.7
240	240	14.71	7.1	263.7	160	20.57
280	280	19.8	8.8	312.5	256.2	33.03
320	360.2	24.75	10.6			
381.3	415.1	33.12	12.7			
450	480	38.85	15.3			
531	585	49.22	25.68			
600	625	70.09	33.25			
635.5	635.5	99.73	42.55			
652.5	652.5	160.2	53.12			

4 Conclusion

From the experimental work carried out for developing a metal jet print head following conclusions are made. The steel throat is consuming 3.2 A current at 16.6-V voltage input and copper throat is consuming 1.93 A current at 17.1-V voltage input. Steel throat is consuming 39.68% more current at 2.92% less voltage input than copper throat. The steel throat is giving output temperature of 711.3 °C at 53.12 watts input power and copper throat is giving 329.3 °C temperature output at 33.03 watts input power. Steel throat is giving 53.70% more temperature output than copper throat. The steel throat is taking 160.2 s time to reach at the temperature of 711.3 °C and copper throat is taking 256.18 s time to reach at the temperature of 327 °C. Steel throat is taking 37.46% less time than copper throat to reach at 45.97% more temperature than copper throat. The stainless steel 202 nozzle has achieved 52.10% higher temperature than brass nozzle, and it has achieved this temperature by taking 37.46% less time than brass nozzle. The steel throat is giving 53.70% more efficiency by consuming 2.92% less voltage input and 37.46% less time than copper throat. Overall EN8 steel is best optimal material for the development of extruder throat and stainless steel 202 is best optimal material for the development of extruder nozzle for a metal jet print-head than the copper and brass materials.

References

1. Mhetre, G. N., Jadhav, V. S., Deshmukh, S. P., & Thakar, C. M. (2022). A review on additive manufacturing technology. *ECS Transactions*, 107(1). <https://doi.org/10.1149/10701.15355ecst>
2. Murr, L. E., & Johnson, W. L. (2017). 3D metal droplet printing development and advanced materials additive manufacturing. *Journal of Materials Research and Technology*, 6(1), 77–89 (Elsevier Editora Ltda). <https://doi.org/10.1016/j.jmrt.2016.11.002>
3. Casati, R., Lemke, J. N., Tuissi, A., & Vedani, M. (2016). Aging behaviour and mechanical performance of 18-Ni 300 steel processed by selective laser melting. *Metals*, 6(9). <https://doi.org/10.3390/met6090218>
4. Tang, L., Wu, C., Zhang, Z., Shang, J., & Yan, C. (2016). A lightweight structure redesign method based on selective laser melting. *Metals*, 6(11). <https://doi.org/10.3390/met6110280>
5. Manakari, V., Parande, G., & Gupta, M. (2017). Selective laser melting of magnesium and magnesium alloy powders: A review. *Metals*, 7(1) (MDPI AG). <https://doi.org/10.3390/met7010002>
6. Yusuf, S. M., Chen, Y., Boardman, R., Yang, S., & Gao, N. (2017). Investigation on porosity and microhardness of 316L stainless steel fabricated by selective laser melting. *Metals*, 7(2). <https://doi.org/10.3390/met7020064>
7. Bambach, M., Sviridov, A., Weisheit, A., & Schleifenbaum, J. H. (2017). Case studies on local reinforcement of sheet metal components by laser additive manufacturing. *Metals*, 7(4). <https://doi.org/10.3390/met7040113>
8. Ansell, T. Y. (2021). Current status of liquid metal printing. *Journal of Manufacturing and Materials Processing*, 5(2) (MDPI AG). <https://doi.org/10.3390/jmmp5020031>
9. Murr, L. E. (2018). A metallographic review of 3D printing/additive manufacturing of metal and alloy products and components. *Metallography, Microstructure, and Analysis*, 7(2), 103–132 (Springer New York LLC). <https://doi.org/10.1007/s13632-018-0433-6>

Innovative Design and Analysis of Plough for Vineyards



Pratik Katkade, Nikhil Joshi, and Puskaraj D Sonawwanay

Abstract Plough design development has been on the table for millennia, there is still room for improvement. This paper is an attempt to build and analyze a plough for a grape farm's complex terrain. Ploughing, which splits the top layer of soil, and mechanical weed elimination are two of the most basic tasks performed by farmers. Traditional plough designs were inefficient in covering complex regions, especially in grape vineyards. This paper details the design of a plough mounted on a 24/28 kW farming tractor. The primary goal of the design is to cover difficult areas in grape farms, which are generally gaps between two successive plants that aren't tilled by traditional plough designs. The optimized design is capable of Ploughing and weeding in complex areas of the farm by using a flexible plough arm on both sides working on an innovative mechanism thus providing aeration to the roots and being cost-efficient.

Keywords Plough · Vineyard · Innovation · Agriculture · FEA

1 Introduction

India is the world's second-largest agricultural producer. One of the primary contributing causes for the constant expansion is the arrival of farm machinery mechanization, which results to a consistent increase in farmer yield production [1, 2]. Tillage is the mechanical treatment of soil in order to prepare it for seed germination. The primary tillage operation serves various purposes. It's utilized for a variety of things, including soil cutting and seedbed preparation. The second step is to reduce breeding grounds and activities for insects and pests. The third purpose is to use crop waste to suppress weeds and create fertile soil. Finally, the goal is to improve soil aeration and infiltration while reducing water and wind erosion [3]. Tillage can directly damage soil organisms by disrupting their bodies, or indirectly by exposing

P. Katkade · N. Joshi · P. D Sonawwanay (✉)

School of Mechanical Engineering, Dr. Vishwanath Karad MIT World Peace University, Pune, India

e-mail: puskarajsonawwanay@gmail.com

© The Author(s), under exclusive license to Springer Nature Switzerland AG 2024

P. M. Pawar et al. (eds.), *Techno-societal 2022*,

https://doi.org/10.1007/978-3-031-34644-6_73

707

them to detrimental conditions, such as changing the distribution of organic matter in the soil, or changing soil moisture, temperature, aeration, or compaction. In comparison to an arable system, the potential effects of tillage on soil species in vineyards. Tractors, for example, are one of the most important components for maximum agricultural operations and tasks [4, 5]. Ploughing, uncovering the top layer of soil, and mechanical weed removal are only a few of the most basic chores that farmers perform. These chores are frequently completed with harrows and cultivators. Cultivators are available in a wide range of types, from tractor-mounted cultivators to the most common three-point linkage cultivators [6]. This research paper focuses on the innovative design and development of plough tilling in complex areas in between plants in vineyards (Compatible With farming tractor 24–28 kW) shown in Fig. 1. Hydraulic system to support the mechanism along with static structural, Modal Analysis of the parts designed to optimize design, save on material and so cost, also make the design more efficient and cost-saving. Traditional designs are not efficient enough to plough complex areas of vineyards shown in Fig. 2.

The ploughing process' outcome is mostly determined by the starting soil condition, plough body form and surface, and ploughing depth and speed. The intensity of soil loosening and breaking, ploughing uniformity, soil displacement and mixing, surface roughness, degree of furrow turning, the burial of weeds and crop wastes, and the quantity of soil smearing and compaction at the furrow bottom are all characteristics that might influence crop development.



Fig. 1 Ploughing area of farm

Fig. 2 Traditional plough used in grape farm



2 Design

The main components used in the plough design are the Supporting frame, Linear rails, Linear bearings, Plough teeth, Hydraulic components and Mechanical sensors are discussed below and presented in Fig. 3. The design of the frame is standard according to three-point hinge standards [7, 8].

Plough design has pair of flexible arms mounted at the rear side of the frame on linear rails with support of lubrication less linear bearings. A flexible plough has given motion with help of hydraulic cylinders connected to the hydraulic circuit.

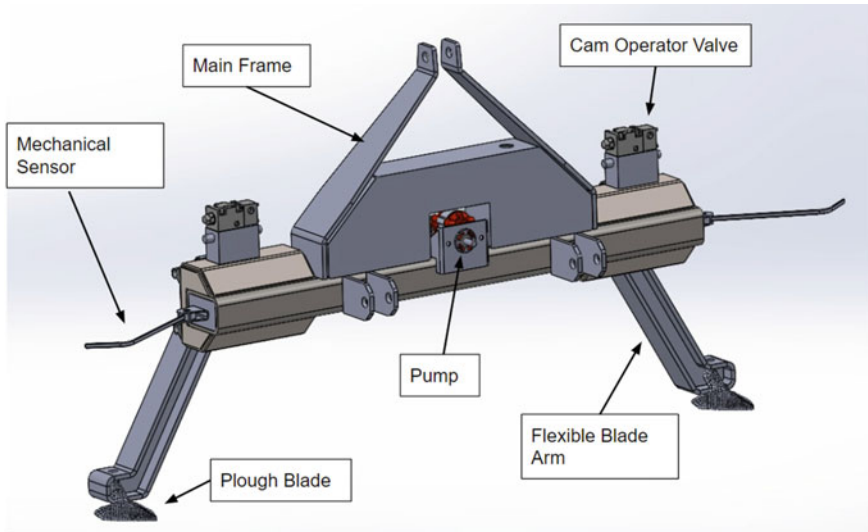


Fig. 3 Supporting frame with linear bearing

Table 1 Standard size categories for hitch design [6, 7, 9]

Tractor power	Top link pin diameter (mm)	Lift arm pin diameter (mm)	Lower hitch spacing (mm)
Up to 30 kW	16	16	510
20 to 45 kW	19	22	710
40 to 100 kW	25	29	860
80 to 225 kW	32	37	1000
More than 180 kW	44	51	1200

Other than this oil tank is there which is mounted in the middle of the frame above the Vane Pump.

Manifold, Direction control valves on both sides of the mainframe respectively. Table 1 shows three-point hinge standards followed by manufacturers (Fig. 4).

The optimized plough design works on a Linear mechanism. The pump is shown in Fig. 3 is connected to the PTO shaft of the tractor. A mechanical sensor is used for the detection of grape plants and is connected to the Cam operated valve through a brake wire, basically, the Mechanical sensor is in sync with the Cam of the Valve. As the mechanical sensor encounters the grape plant, the break wire connected to the cam operator valve activates the valve, thus the hydraulic circuit. In the Pressed position of the mechanical sensor, the hydraulic cylinder contracts so the flexible plough. As

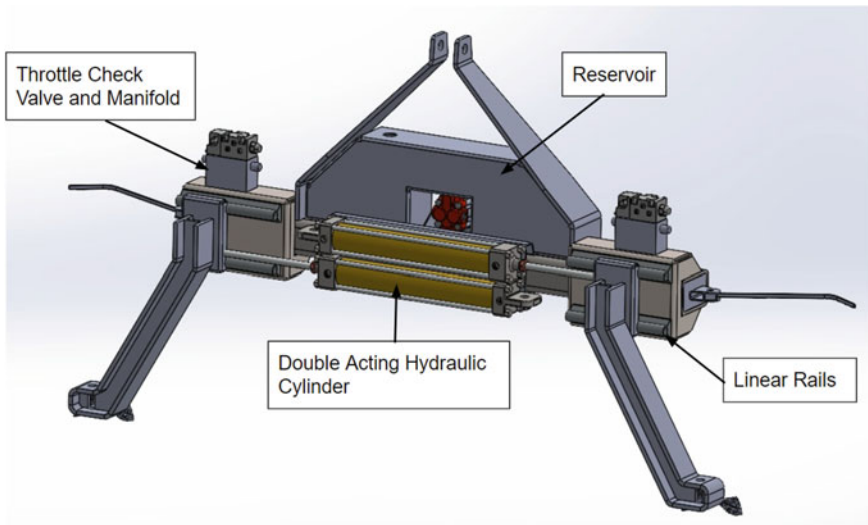


Fig. 4 CAD model of optimized design (rear side)

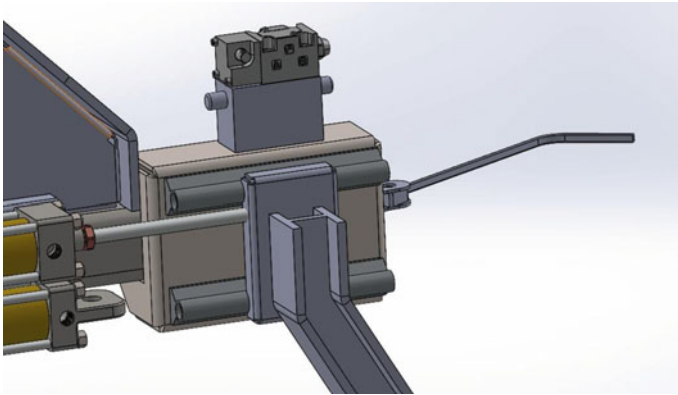


Fig. 5 Front and rear view of mechanical sensor

the cylinder compresses, the attached flexible arm moves inwards and returns to the initial position on disengagement of the mechanical sensor. The complete design of the Mechanism is shown in Fig. 5.

The linear rail used in the mechanism are Igus linear rails and Igus linear bearings, advantages of using the linear rail system are [10].

- They are not prone to corrosion
- No need for lubrication
- More accuracy
- More reliable in a dirt environment

2.1 Plough Teeth

Major goal of ploughing, according to popular perception, is to loosen the soil in preparation for additional seedbed preparation, root growth and labor, and improved water infiltration [9]. The furrow width, share shape, and mouldboard shape are all related to the body shape of the plough, as described here [11] and shown in Fig. 3.

2.2 Mechanical Sensor

Role of the mechanical sensor is to open the valve that controls the flexible plough, which is connected to the hydraulic cylinder. The mechanical sensor functions similarly to a motorcycle’s clutch lever. The mechanical sensor is connected to a cam operated valve with a break wire that initiates the working of hydraulic circuits, resulting in the compression of a double-acting hydraulic cylinder to slide the flexible arm from its initial position.

3 Hydraulic System

Flexible plough movement is regulated by a hydraulic system that is primarily controlled by a mechanical sensor that is in sync with the Cam operated valve [12] has been shown in Fig. 6.

Throttle check valves are connected after DCV to control the speed of extension and contraction of hydraulic cylinders according to needs [13]. A vane pump from the Yuken PVR1T series was selected with a max rpm of 1000, geometric displacement of 25.8 cc/rev, and flow rate of 25.8 LPM. The reason behind selecting the vane pump over the external gear pump is the vane pump has the ability to work bi-directionally. As the application needs TO and FRO motion, double-acting cylinders are used. With the use of a double-acting cylinder, a mechanically controlled 4/2 position cam operated DCV is used to manage flexible plough direction [14]. The Throttle check valve is used in the design to control the speed of extension and contraction of hydraulic cylinders, to counter different types of structures in vineyard planting. It will allow users to change the speed of cylinders with respect to, plant distance in different vineyard fields to achieve accurate weeding and flexibility in operation [15].

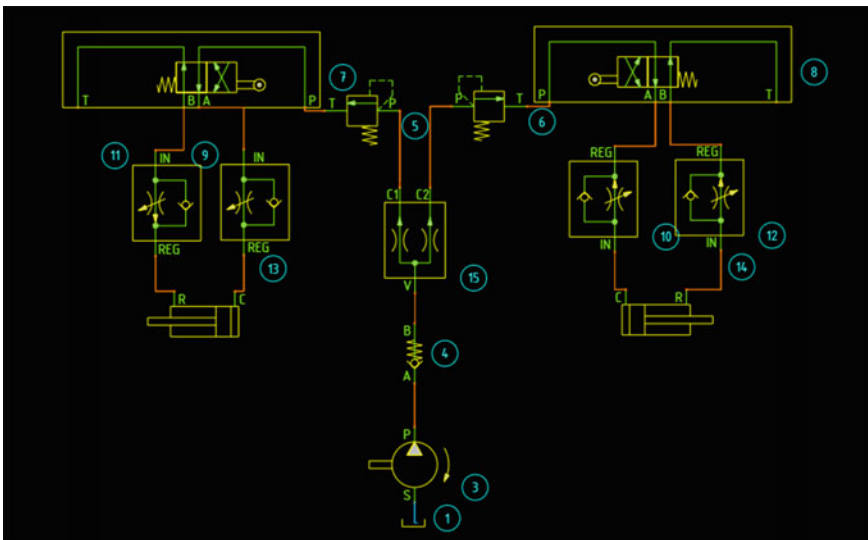


Fig. 6 Hydraulic circuit of complete system

Table 2 Materials used for components [15]

Component name	Mainframe	Plough	Mechanical sensor
Material name	ST-52	AISI 1095	AISI 1020
Modulus of elasticity (GPa)	205	190–210	205
Tensile ultimate strength (MPa)	520	685	294.75
Yield strength (MPa)	355	525	350
Poisson’s ratio	0.29	0.27–0.30	0.29
Density (kg/m ³)	7870	7850	7870

4 Materials

Components are assigned with specific material properties based on requirements. The following material qualities are allocated to the Mainframe, Plough, and Mechanical sensor. Materials have an important role to play especially in agriculture equipment because of harsh working conditions. Material properties are selected based on special requirements from specific components shown in Table 2.

5 Results and Discussions

The concept of a plough for weeding and ploughing in vineyards was studied and a model with a linear rail mechanism was developed. A plough was designed as shown in fig was designed and modelled in Solidworks. The study mainly focuses on Static and Modal analysis of frame, mouldboard and linear rail mechanism. So, all components in the assembly aren’t analyzed. The overall draft force magnitude on the plough is 3 kN and is distributed among 2 mouldboards. The draft force is applied in the opposite direction of the movement of the tractor and the approximate weight implement is. Considering the tractor speed during tilling at 3 km/h, medium black soil and mouldboard shape used in the study the horizontal force is taken as 19% of draft force which is 3 kN [16].

5.1 Meshing

Meshing is the most important tool for analysis, and depending on the mesh results, some big alterations can be expected. All components are delicately separated into numerous finite bits, and then each of these elements is subjected to a thorough analysis. As a result, meshing is regarded as a critical aspect of the component’s

analytical technique. The tetrahedral mesh is commonly used in the analysis because it produces the best results. Mesh convergence has been taken into consideration before doing both static and modal analysis. Ansys discovery is used for static and modal analysis of components with the highest fidelity for meshing [17–20].

5.2 Loads and Boundary Conditions

The amount of physical stress imparted to a mechanical system is referred to as a load. The three types of loads are static, dynamic, and fatigue (cyclic). Several loads are assessed during the study to determine deflection in the frame and mouldboard. Many forces are acting on the plough when it is running. These forces are primarily responsible for component deformation and fracture development, hence determining the highest stress locations is critical. Mainframe is applied with a fixed support on a three-point hinge, also two other forces from the front coming on a flexible arm and horizontal force because of to and fro movement of flexible plough on linear rails [6]. Forces are shown in Fig. 7. Material ST-52 is used for analysis with Young's modulus 205 MPa and Poisons ratio 0.29.

Figure 8 is showing results of displacement on the main frame solved in Ansys Discovery. Maximum displacement is observed at both ends of the mainframe because of mechanism is placed there. Displacement values are ranging from 0.01 to max 0.062 mm. The analysis helped in the optimization of design to save on material and make it more efficient.

Von Mises theory is used to achieve stress results on the main frame. As the mainframe is the most critical component in the design, Stress values are being used while doing design to make sure the safety of the overall component considering the factor of safety. Three-point hinges are fixed support and other forces applied are

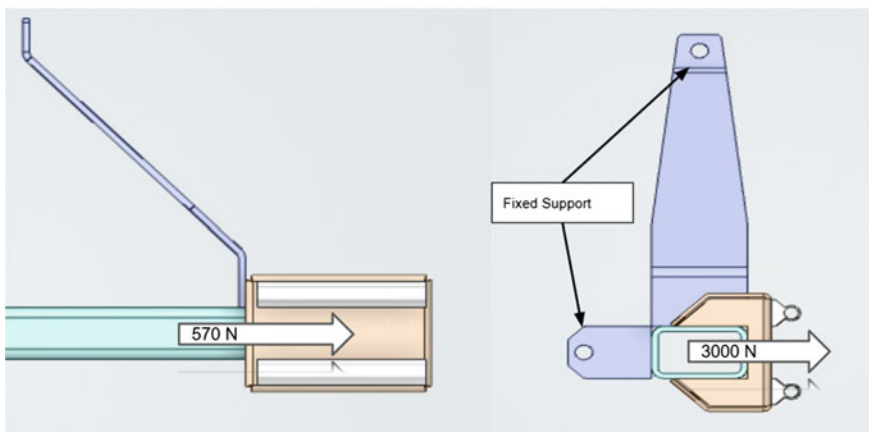


Fig. 7 Boundary conditions

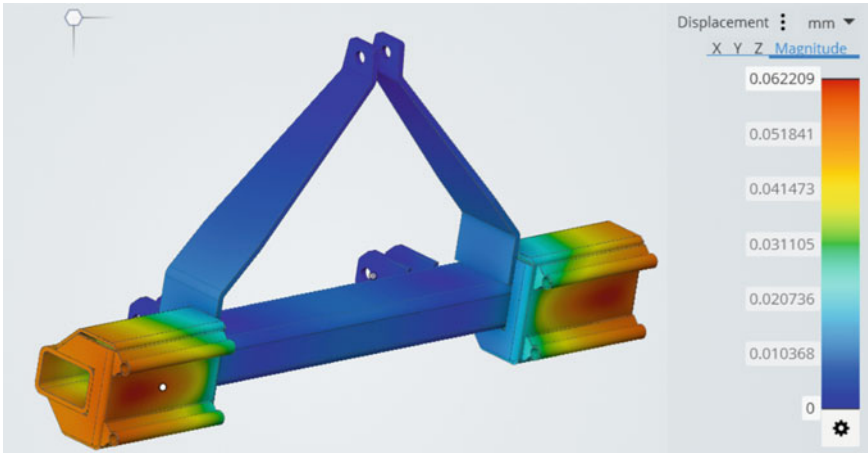


Fig. 8 Displacement result of the main frame

shown in Fig. 7. The maximum stress coming is 33.675 MPa and it is within the permissible limit considering the Factor of safety (Fig. 9).

Two modal studies, including local body stiffness and fixed boundary conditions, were used to investigate dynamic frequency responses and mode shapes. The acquired mode shapes of the developed model with localized stiffness are shown in Fig. 10. Modal analysis is conducted with fixed support and 6 modes are used from the results. Mode values are 38.696, 39.378, 207.03, 230.99, 127.62, 190.73 Hz respectively. Modal analysis has been conducted to be sure of possible design failures due to vibrations coming from the tractor [21]

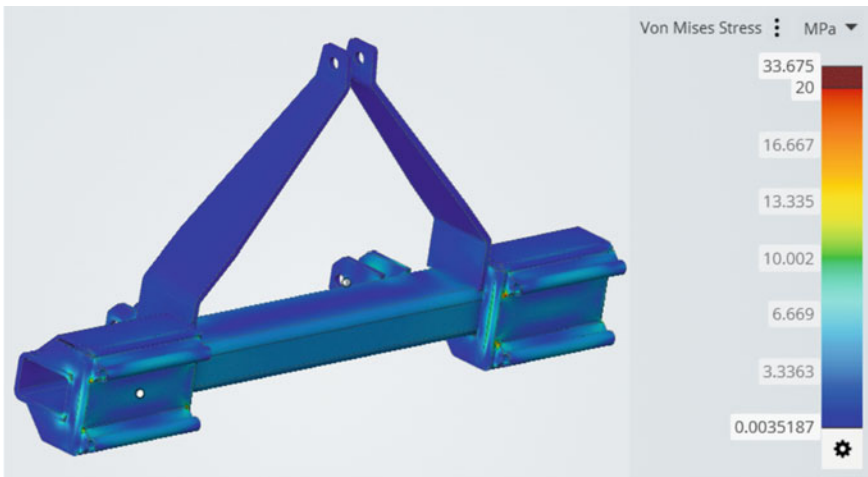


Fig. 9 Von Mises stresses

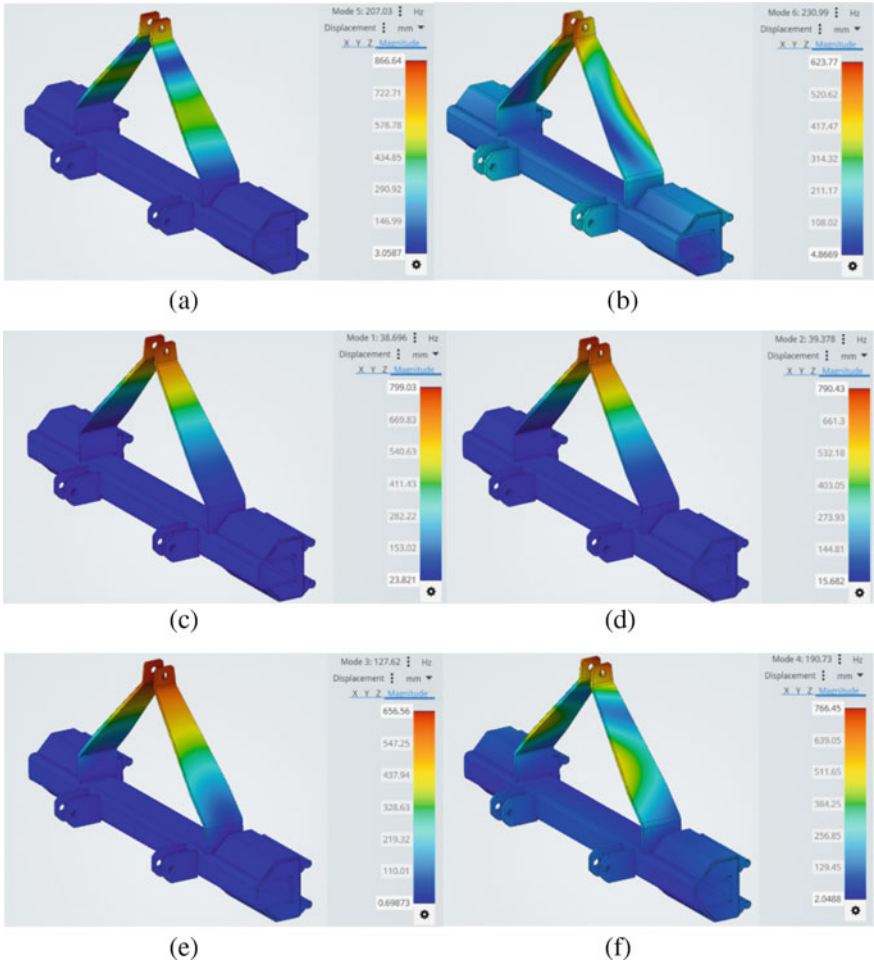


Fig. 10 Mode shapes of mainframe **a** mode 1, **b** mode 2, **c** mode 3, **d** mode 4, **e** mode 5 and **f** mode 6

The results of the study for plough and mouldboard, together with their ascribed material shows (Fig. 9) that, the maximum stress on the mainframe component is 33.675 MPa. ST-52 was chosen as the mainframe material. Design is safe and may be further enhanced compared to Ultimate tensile strength. Deformation is almost non-existent (0.06 mm). AISI 1095 Steel was used as the component mouldboard material. When maximum stress is compared to the material’s ultimate tensile strength, the design is found to be safe and may be further refined. To avoid any failure caused by vibrations, the frame’s natural frequencies and mode forms have been examined.

6 Conclusions

Design and analysis of plough for complicated terrain of the vineyard where traditional plough design has failed have been done. The proposed architecture in this research is capable of ploughing specific regions. To achieve the purpose, linear rails and linear bearings are employed in a unique mechanism design. Hydraulic systems have been created and integrated into designs to make things operate and move mechanisms. During the design process, the findings of static and modal analysis also aided in providing a clearer picture of the stresses imposed on the frame. To avoid vibration failures, Von Mises and displacement data are employed to reinforce the design and modal analysis. The innovative design discussed in this paper has been found more efficient for ploughing.

References

1. Uddhao, K., Dhiraj, K., Thakare, S., & Vivek, K. (2016). Performance evaluation of tractor operated rotavator in dry land and wet land field condition. *International Journal of Agricultural Science and research*, 6, 137–146.
2. Kareem, K., & Sven, P. (2019). Effect of ploughing depth, tractor forward speed, and plough types on the fuel consumption and tractor performance. *Polytechnic Journal*, 9, 43–49.
3. Selech, J., Ulbrich, D., Keška, W., Staszak, Z., Marcinkiewicz, J., Romek, D., & Rogoziński, P. (2019). *Design of a cultivator mounted on a tractor with a power of up to 20 kW*. MATEC Web of Conferences.
4. Faber, F., Wachter, E., & Zaller, J. G. (2019). *Effects of design of a cultivator mounted on a tractor with a power of up to 20 kW*. MATEC Web of Conferences.
5. Paoletti, M. G. (1988). Soil invertebrates in cultivated and uncultivated soils in Northeastern Italy. *Redia*, 71, 501–563.
6. Molari, G., Mattetti, M., & Guarnieri, A. (2014). Optimal three-point hitch design to maximize lifting performance. *American Society of Agricultural and Biological Engineers*, 57(2), 371–379.
7. Pripps, R. N. (1993). *Farmall tractors: history of international McCormick-deering farmall tractors*. Farm Tractor Color History Series.
8. Herguth, W. R., & Godfrey, D. (2010). Wear analysis of linear bearings. *Lubrication Engineering*, 60, 36–38.
9. Boxler, B. (1950). *Taschenbuch für Landmaschinen, I. Pflüge* (256 pp). Der staatliche Ingenieurschule.
10. Ayadi, I., Hatem, B., Elyes, H., Aref, M., & Abdul, M. (2017). Advanced analytical method of mouldboard Plough's design. *The International Journal of Advanced Manufacturing Technology*, 88, 781–788.
11. Mohammed, A., Nabil, M., Ahmed, E.-B., & Ashraf, H. (2018). Flow modelling and performance assessment of rotary sliding vane pump using CFD. *Journal of Al-Azhar University Engineering Sector*, 13, 1268–1288.
12. Duțu, I. C., Axinte, T., Maican, E., Nutu, C. S., & Diaconu, M. (2022). The use of double-acting cylinders in electro-hydraulic circuit. *Technium: Romanian Journal of Applied Sciences and Technology*, 4, 15–20.
13. Boye T. E., Adeyemi, O. I., & Emagbetere, E. (2017). Design and finite element analysis of double—Acting, cylinder for industrial automation application. *American Journal of Engineering Research (AJER)*, 6(3), 131–138.

14. Wang, G. R., Tao, S. Y., Liu, Q. Y., Fu, Y. K., Zhu, H., & Chu, F. (2015). Experimental validation on a new valve core of the throttle valve in managed pressure drilling. *Advances in Mechanical Engineering*, 6, 324219.
15. Makange, N., Parmar, R., & Tiwari, V. K. (2015). Stress analysis on Tyne of cultivator using finite element method. *Trends in Biosciences*, 8(15), 3919–3923.
16. Sarvesh, J., Rutuja, K., Aniruddha, J., Sumedh, J., & Pankaj, D. (2020). Design of helical gear with carbon reinforced EN36 steel for two stage constant mesh gearbox weight reduction. *Materials Today: Proceedings*, 46, 626–633.
17. Guul-Simonsen, F., Jørgensen, M. H., Have, H., & Håkansson, I. (2002). Studies of a Plough design and a ploughing relevant a to conditions in Northern Europe. *Acta Agriculturae Scandinavica, Section B—Soil & Plant Science*, 52(2), 57–77.
18. Chandravanshi, M., & Mukhopadhyay, A. (2017). Modal analysis of a vertically tapered frame. *International Journal of Structural Stability and Dynamics*, 17, 1771001
19. Yoshiharu, I., & Naohito, Y. (2015). Small high-efficiency vane pump based on vane pump theory. *SAE International Journal of Passenger Cars - Mechanical Systems*, 8, 614–623.
20. Mehta, C., & Badegaonkar, U. (2021). Farm mechanization in India. *Aperspective, Agricultural Research Journal*, 58, 1142–1146.
21. Cordesses, L., Poirier, J. P., & Veron, C. (2002). *Performance analysis of a three point hitch controller* (Vol. 3, pp. 2233–2238). IEEE.

Experimental Investigation of Ball Bearing for Vibration Analysis



Sunil Pondkule, Sachin Bhosle, and Pravin Dhandore

Abstract Vibration analysis is widely used for ball bearing prognostics to monitor the vibration signal. The measurement of vibration and their signal analysis plays an important role for identification of defect. Every defect gives characteristic vibration in the ball bearings. The careful observation of vibration spectra may provide worthwhile information about defects developed in the bearing. In this paper a test rig is used and a new two—wheeler front wheel axle bearing is installed. The bearings run under constant speed and various loading conditions. The effect of bearing conditions on the constant speed and various loading conditions are studied. When irregularities are detected in the statistical measures the vibration spectrum is obtained and examined to determine where the defect is on the running surfaces.

Keywords Ball bearing · Condition monitoring · Defects · Statistical analysis · Vibration analysis

1 Introduction

Rolling bearings are an essential part of rotating machines. A machine could be seriously harmful if faults occur in the bearings during the service. Their movement and dynamics contribute to the overall vibrations in the machine. Radially loaded rolling element bearings produces vibration even if they are geometrically perfect. This is because of the use of a finite number of rolling elements to carry the load [1–3]. There are two critical states in the condition monitoring of machine components the first is the detection of the fault and the second is the determination of the severity defects, i.e., the service life of the machine component [4]. Rolling bearing defects can be categorized as point or local defects and distributed defects. Distributed defects

S. Pondkule (✉)
BRACT's, VIIT, Pune, India
e-mail: sunilpondkule@gmail.com

S. Bhosle · P. Dhandore
VP's, KBIET, Baramati, India

include surface roughness, corrugations; misaligned grooves and rolling elements of a different size. They are usually caused by manufacturing error, improper installation or abrasive wear. Local defects include cracks, pitting and flaking on rolled surfaces. Most failures of rotating machines are often associated with bearing failures. Failures in rolling bearings often result in lengthy industrial downtime that has economic consequences [5]. Application procedures and the success of the techniques are discussed in several papers [6]. Prompt diagnostics of rolling element bearing fault is critical not only for the safe operation of machines, but also for the reduction of maintenance cost [7]. It is well known that ball bearings produce characteristic vibrations and when a defect develops in ball bearings, vibration characteristics and levels change [8]. Most of applications, entrenched accelerometers use to monitor the health of mechanical component [7, 8].

Although many studies are mentioned in the literature but reliability of the methodologies is ought to be increased. In this paper, a test rig was used and new ball bearings set installed in the test rig in order to investigate the vibration signature of the bearings. Bearing vibrations occur when radial loads are applied and high speeds affect bearing life and degrade component quality. The defects may be developed during longer runs of bearing under certain condition. Time domain is used for descriptive statistics such as the peak and RMS (Root Mean Square) of the time series signals, it identifies bearing faults. It is well known that ball bearings produce characteristic vibrations and when a defect develops in ball bearings, vibration characteristics and levels change. Statistical measures such as peak-to-peak amplitude, root mean square (RMS) and power spectrum value was monitored to predict the health of the bearings. The selected features are strategized to shows graph throughout the run to capture sudden changes in signals. This test was concluded as the statistical measures indicate failure evaluation in ball bearing and the frequency spectra of single defect and two defects are found to be identical.

1.1 Features of Defective Frequencies

The fundamental interaction of defects in ball bearings produces waves of very short duration whenever the defect strikes or is struck owing to the rotational motion of the system. These impulses will excite the natural frequencies of the bearing elements and housing construction, resulting in increased vibrational energy at these high frequencies. The defective frequencies of the individual bearing elements can be calculated theoretically as shown below:

The shaft rotational frequency (f_s) which is equal to the speed of shaft

$$f_s = \frac{N}{60} \quad (1)$$

The outer race defect frequency (f_o) is given by

$$f_o = \frac{n \times f_s}{2} \left[1 - \frac{bd}{pd} \cos \alpha \right] \quad (2)$$

The cage defect frequency (f_c) is given by

$$f_c = \frac{f_s}{2} \left[1 - \frac{bd}{pd} \cos \alpha \right] \quad (3)$$

The inner race defect frequency (f_i) is given by

$$f_i = \frac{n \times f_s}{2} \left[1 + \frac{bd}{pd} \cos \alpha \right] \quad (4)$$

The ball defect frequency (f_b) is given by

$$f_b = \frac{pd}{bd} \times f_s \left[1 - \left(\frac{bd}{pd} \cos \alpha \right)^2 \right] \quad (5)$$

2 Experimental Setup

The assembly consists of a shaft supported on healthy bearings and driven by a variable speed motor. The test bearing (Single row deep groove ball bearing) was placed end of two healthy bearings on the shaft. The drive to test rig was provided with DC motor through the coupling as shown in Fig. 1. A tensile loading arrangement was made to apply radial load on the healthy new bearing. The outer race of bearing was fixed with the help of special designed, easy removal and mounted housing. Housing installed at the free end of the spindle in order to apply load as well as to minimize speed oscillations of the spindle. A piezoelectric accelerometer with a magnetic sensitivity of 10 mV/s^2 has been used to measure the vibrations. It was mounted closer to the housing of the test bearing with the help of screws. The accelerometer was connected to the constant current source input and NI DAQ—9178 board is used with NI 9234 sound and vibration module the output of which was connected to a computer. The vibration response caused by a normal bearing and a defective bearing was investigated and analyzed.

2.1 Bearing Geometry

An investigation is carried out for new healthy 6301 bearing under different radial load, i.e., 50 N, 100 N, 150 N at 1200 rpm. Baring geometry is shown in Fig. 2.



Fig. 1 Experimental setup

In Table 1 shows a bearing dimensions and bearing defective frequencies which is calculated by above equations i.e. numerical results.

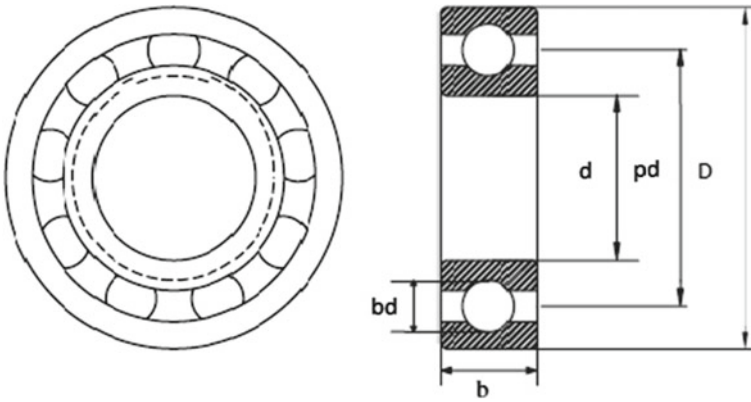


Fig. 2 Bearing geometry and bearing nomenclature

Table 1 Bearing nomenclature

Nomenclature	Values
Inner bore diameter (d)	12 mm
Outside diameter (D)	37 mm
Bearing width (b)	12 mm
Number of balls	6
Pitch diameter (pd)	25 mm
Ball diameter (bd)	7 mm
Mass	0.06 kg
Basic dynamic load rating	10.1 KN
Basic static load rating	4.15 KN
Limiting speed	14,000 r/min

3 Results and Discussions

An initiation and development of localized defect in the bearing is investigated and the test is conducted for new healthy ball bearings under Designed Test Rig (DTR). The vibration signals are captured at every 12 min for 5 s durations during the test. During the test, the temporarily results are calculated and analyze the data for judgment of incipient fault develop in bearing. Vibrational data are examined to detect the localized formation and propagation of defects. Scalar measures such as peak-to-peak value, root mean square and spectrum are calculated during the test.

3.1 Peak to Peak Level

Peak-to-Peak amplitude history of vibrations along with running time for the test of 6301 bearings at a speed of 1200 RPM and radial load of 50 N, 100 N, 150 N are given in Fig. 3 an initiative of wear in new healthy bearing are shown in Fig. 3 for the radial load 50 N at 123 h, 100 N at 96 h and 150 N at 76 h. For radial load 100 N, no observable trend in graphics after 130 h.

For radial load 150 N, the peak-to-peak level continuously changes with sudden fail after 85 h. The sudden increase/decrease and gradient fluctuations in the vibration level have been also observed other researcher [6, 8] and may attribute to a portent known as healing, the localized defect may be continued till rolls contact of the ball. When the failure time is reached, the vibration level suddenly increases. This has happened due to formation of defect in the bearing.

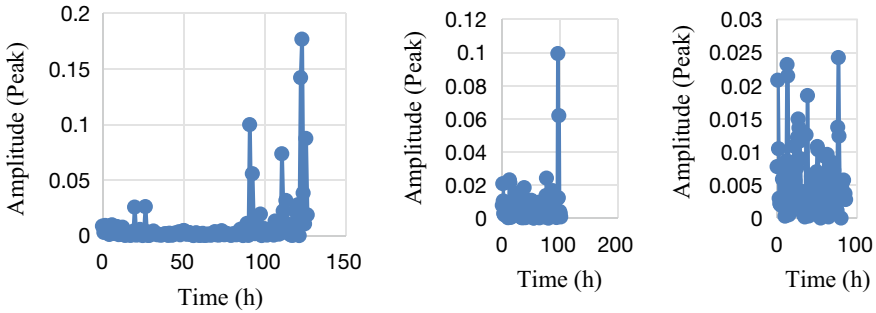


Fig. 3 Time versus peak graph for 6301 bearing at 1200 rpm, 50 N, 100 N, 150 N load

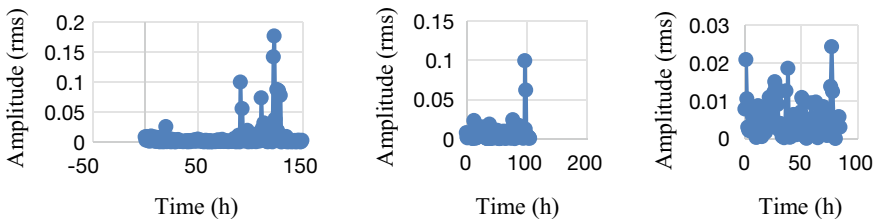


Fig. 4 Time versus RMS graph for 6301 bearing at 1200 rpm, 50 N, 100 N, 150 N load

3.2 RMS

The RMS history of vibrations in Fig. 4 is very similar to the peak-to-peak amplitude history at 1200 RPM at 50 N, 100 N and 150 N. The RMS figure appears to be a low-pass filtered form of peak-to-peak levels. The figure shows similar trends to peak levels, but sudden changes the RMS values are not observed clearly. Although the peak-to-peak level is increased up to 20 times, the maximum RMS value is only 4 times the level at the end of the running stage.

3.3 Spectrum

Scalar measures show experimental evaluation of the two-wheeler front wheel axle 6301 bearings for vibration analysis and statistical signals. However, they do not provide accurate information about the size and location of localized defects. In order to understand the characteristics of the vibration signals and detect the location and the relative size of the defects through vibration spectra (Fig. 5).

The scale measures indicate changes in the condition of the ball bearing for speed at 123 h (7380 min.) peak of frequency and amplitude spectrum are shown in Fig. 6, the value of peak frequencies is 43.3 Hz and 0.060 gRMS, and outer race defect

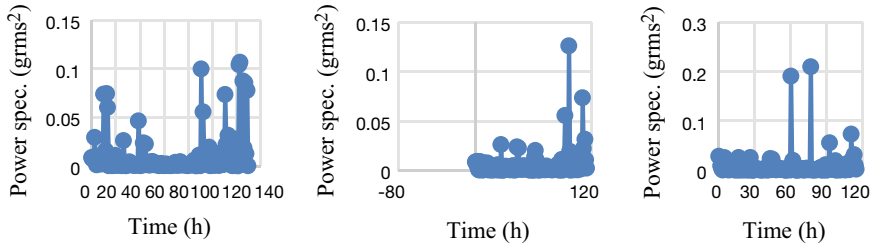


Fig. 5 Time versus power spec. graph for 6301 bearing at 1200 rpm, 50 N, 100 N, 150 N load

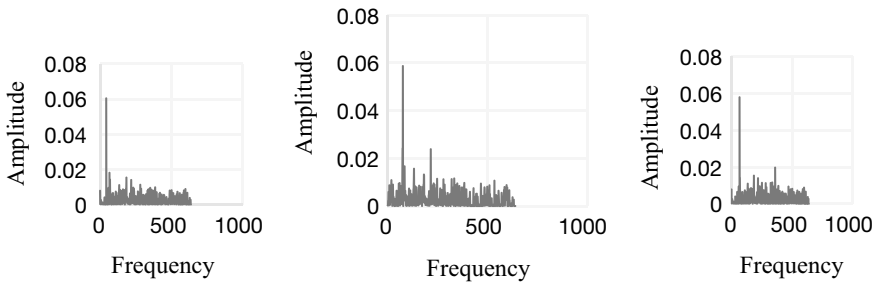


Fig. 6 Frequency versus amplitude graph for outer race defect, inner race defect, cage defect

develops in the bearing. The spectrum for speed 1200 RPM. The prominent peaks of frequency and spectrum amplitude are noted after 96 h (5760 min.) and values are frequented (78.6 Hz), spectrum amplitude (0.052 gRMS). It has observed defect developments in the inner race of the bearing. The spectrum for speed 1200 RPM. The prominent peaks of frequency and spectrum amplitude are noted after 76 h (4560 min.) and values are frequented (7.12 Hz), spectrum amplitude (0.049 gRMS). It has observed defect developments in the cage of the bearing.

The prominent peaks of frequency and spectrum amplitude are noted after 76 h (4560 min.) and values are frequented (66.53 Hz), spectrum amplitude (0.057 gRMS). It has observed defect developments in the ball of the bearing. The characteristics frequencies of 6301 bearing with its running times shown in Fig. 7. At 50 N load, bearing start the inner race defect at 112 h. And the outer race, cage, ball defects start at 123, 114, 115 h. Observed at 100 N load, bearing start the inner race defect at 96 h. And the outer race, cage, ball defects start at 115, 100, 98 h. At 150 N load, bearing start the inner race defect at 55 h. And the outer race, cage, ball defects start at 67, 76, 76 h. It has been also observed that when bearing run at constant speed at various loading conditions inner race defect earlier than other bearing parts like outer race, cage and ball.

The values of spectrum amplitude for defective bearing are observed to be at higher end than two parameters are shown in Fig. 7. It has been observed that peak to peak amplitude gives better detectability but spectrum gives defect location. That various load at 50 N, 100 N, 150 N get different defects size.

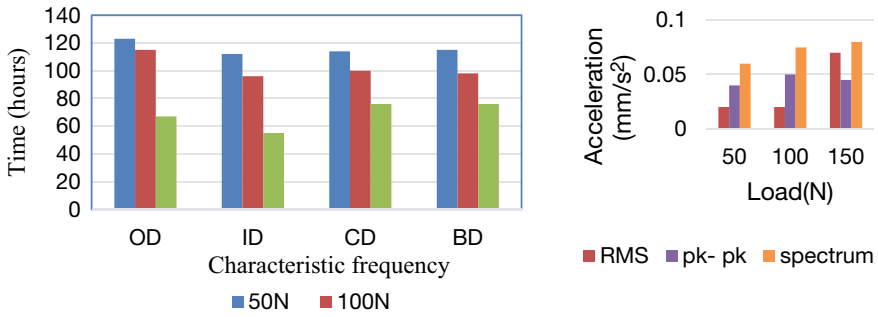


Fig. 7 Characteristic frequency versus time and load versus acceleration of various defects

In a Table 2 shows a comparison between experimental results and numerical results with percentage error.

Figure 8 shown that spectrum for healthy and defective bearing. Healthy bearings acceleration value is less and defective bearing amplitude acceleration is high at 78.6 Hz. and this point where inner race defect start and other bearing elements compare, inner race start earlier fast.

Table 2 Comparison between two results

Defective frequency	Experimental result (Hz)	Numerical percentage error (%) result (Hz)	Defective frequency
f_o	43.3	43.2	0.23
f_i	78.6	76.8	2.29
f_c	7.1	7.2	1.38
f_b	66.53	65.68	1.27

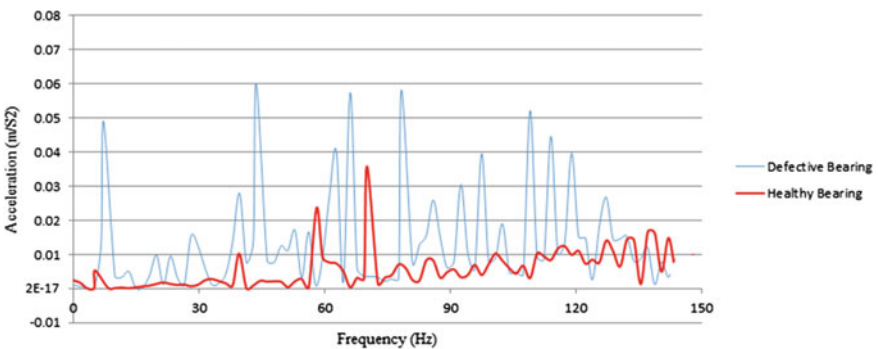


Fig. 8 Spectrum for healthy bearing versus defective bearing

4 Conclusion

- The defect size can be depending upon vibration magnitude and its severity.
- This is not possible to locate a general correlation between the defect size and the amplitude of the vibration.
- Scalar parameters clarify damage of ball bearing but they do not provide information about the location of defect.
- The spectrum analyses are investigated at running test durations in order to conceive defect locations.
- Although the system is under the influence of a relatively severe imbalance in the shaft and misalignment in the bearing supports, the analysis successfully shows the development of the localized defects in the ball bearing.
- Inner race defect gives better response to speed variation. However, outer race defect gives better response at high load. i.e., 1200 RPM and 150 N.

References

1. Tandon, N. (1994). A comparison of some vibration parameters for the condition monitoring of rolling element bearings. *Measurement*, 12, 285–289.
2. Kulkarni, S., & Wadkar, S. B. (2016). Experimental investigation for distributed defects in ball bearing using vibration signature analysis. *Procedia Engineering*, 144, 781–789.
3. Zarei, J., Tajeddini, M. A., & Karimi, H. R. (2014). Vibration analysis for bearing fault detection and classification using an intelligent filter. *Mechatronics*, 24, 151–157.
4. Kankar, P. K., Sharma, S. C., & Harsha, S. P. (2013). Fault diagnosis of rolling element bearing using cyclic autocorrelation and wavelet transform. *Neurocomputing*, 110 9–17.
5. Li, R., Sopon, P., & He, D. (2012). Fault features extraction for bearing prognostics. *Journal of Intelligent Manufacturing*, 23, 313–321.
6. Shakya, P., Darpe, A. K., & Kulkarni, M. S. (2016). Bearing diagnosis using proximity probe and accelerometer. *Measurement*, 80, 190–200.
7. Ahmer, M., Marklund, P., Gustaffson, M., & Berglund, K. (2022). An implementation framework for condition based maintenance in bearing ring grinder. *IRP, Procedia CIRP*, 107, 746–751.
8. Teixeira, H. N., Lopes, I., & Braga, A. C. (2020). Condition-based maintenance implementation: A literature review. *Procedia Manufacturing*, 51, 228–235.

Material Science and Composites

A Study on Mechanical Properties and Tribological Behaviour of Jute Filler Composites



Vijay Kumar Mahakur, Rajdeep Paul, Santosh Kumar, Promod Kumar Patowari, and Sumit Bhowmik

Abstract The present paper discusses the mechanical and tribological effect on the jute particles-based polymer composite. For the fabrication of the composite, several weight content of jute particles (0, 2.5, 5, 7.5, 10, and 12.5%) are reinforced into the epoxy. The mechanical and wear testing of the composite is done by considering the various input parameters. The composite with a lower filler weight percentage has produced satisfactory mechanical and wear characteristics. The highest tensile and flexural strength are achieved when the composite contains 5 wt.% of jute filler content. And the minimal wear is observed at the maximal load when the sample is fabricated with 2.5 wt.% filler content. For examining the surface of the composites, the microscopic analysis is done with the scanning electron microscope. The performance of the neat epoxy at lower load has produced minimal wear compared to the sample with high applied load.

Keywords Jute particulates · Epoxy resin · Mechanical characteristics · Tribology · Microscopic analysis

1 Introduction

During recent periods, the vast evolution of environmental problem because of plastics, metals and many more has become a prime issue throughout the world [1]. As a result, the researchers investigate the materials with a nature like 'biodegradable', 'economical', 'sustainable' and 'recyclable' are studied by the researchers [2]. The natural fibers are found to be the significant material that contains the above behaviour and are also observed to be the best substitution of artificial fibers [3, 4]. Because of significant features like sustainable mechanical characteristics, less weight, good

V. K. Mahakur (✉) · S. Kumar · P. K. Patowari · S. Bhowmik
Department of Mechanical Engineering, NIT Silchar, Silchar, Assam 788010, India
e-mail: vijay.mahakur0709@gmail.com

R. Paul
Department of Mechanical Engineering, Techno College of Engineering, Agartala, Tripura 799004, India

© The Author(s), under exclusive license to Springer Nature Switzerland AG 2024
P. M. Pawar et al. (eds.), *Techno-societal 2022*,
https://doi.org/10.1007/978-3-031-34644-6_75

toughness, etc., the natural fiber reinforced polymer composite (NFRC) can be used in multiple sectors like structural, automotive, marine and medical [5–9]. The bast fibers are utilized hugely among various natural fibres because of their good calorific value, better specific strength, and non-abrasive nature [10, 11]. And jute fiber with adequate strength and stiffness is considered one of the best fibres for fabricating the composite by reinforcing it into the matrix [12–14].

After cotton, jute is observed as the most important vegetable fibers globally regarding availability, consumption and production. Previously jute was used for furnishing and decorative items, but recently, these fibers have got a way towards construction, marine, automotive sectors etc., because of their easy availability and can be easily mingled with other natural and man-made fibers [15, 16]. The requirement for processing and its cheap, strong, rigid nature, jute is picked for reinforcing into the polymer matrix to create a composite [17]. During composite fabrication, these jute fibers behave as load-bearing parts and are supported by the matrix resin to endure the alignment in the proper position [18].

The researchers have already done a lot of work on jute fibre reinforced polymer composite, and their mechanical characterization was discussed earlier [19–25]. After finding an enormous research work on these fiber composites, little work has been absorbed on the basis of producing a jute particulate reinforced composite (JRC). In this paper, polymer composites are developed by contact layup method with different weight percentages of jute filler. These fabricated samples of different specifications are subjected to mechanical testing like tensile, flexural, and wear tests. The composite area after the testing is inspected and discussed using a scanning electron microscope (SEM).

2 Methodology

2.1 Materials

In this study, matrix (epoxy and hardener) is employed in a 10:1 ratio, as specified in the data sheet. Jute particulates are extracted from raw jute fiber, which is cleaned and dried at a temperature at 105 °C for approximately 6 h before being chopped into small pieces and sent through a mixer grinder, where the jute fillers are distributed using ball milling and a sieve shaker [26, 27].

2.2 Composite Fabrication

The typical particle size of the filler is less than 100 μm , and this particle is reinforced into the resin and hardener at varying weight contents (2.5, 5, 7.5, 10, and 12.5%) to make the composite. After proper stirring of filler and resin, these composites got

cured for 24 h in a mould which was made up of silicon rubber. Then these developed samples were set for some mechanical testing like tensile, flexural, and wear test.

2.3 Composite's Mechanical Characterization

The developed samples were put through various testing in according to ASTM standards and parallelly results were discussed. The tensile tests were carried out as per ASTM D638-5 standards in a universal testing machine (INSTRON) at a certain crosshead speed (1 mm/min). The flexural test of the specimen was processed in an INSTRON universal test machine. The dimension of the specimen was kept at $100 \times 15 \times 3 \text{ mm}^3$ as per the ASTM D790-81 standards and the tests were performed using 3-point loading test.

2.4 Wear Testing

At multi tribometer machine, the wear tests were performed keeping the specimen size as per the ASTM G-99 standard. By using Pin-On-Disk module, the specimens were tested by considering the load of 10 N, rubbing length of 1000 m and rubbing velocity of 1 m/s. With the help of Wensar electronic weight balance machine, the specimen's weight losses were observed.

3 Results and Discussions

3.1 Mechanical Characterization

According to the findings, the insertion of tiny particles into the matrix strengthened the sample when compared to the neat epoxy sample. At 5% of filler-based composite, the strength and modulus of the composite become high with 48.56 MPa and 2.9 GPa, respectively. The highest value of strength at 5% fine particle weight indicates excellent interfacial bonding and better stress transfer between the filler and matrix within the composite [14]. The lowest strength and modulus of 24.01 MPa and 1.46 GPa, respectively at 12.5 wt.% filler content is due to the filler agglomeration within the composite (Fig. 1).

According to the findings, the insertion of tiny particles into the matrix strengthened the flexural modulus and strength of the sample when compared to the neat epoxy sample. At 5% fraction of particles-based composite, the strength and modulus

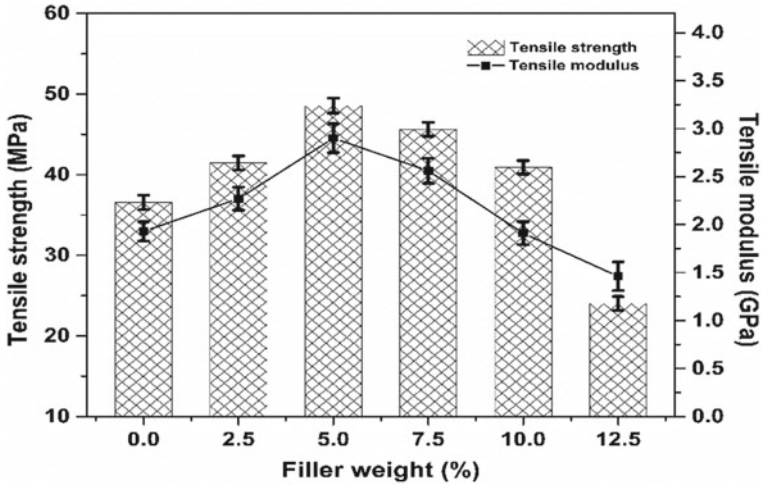


Fig. 1 Tensile strength and modulus at different filler weight percentage

of the composite become high with 64.28 MPa and 3.54 GPa, respectively. The highest value of strength at 5% particle content indicated excellent interfacial bonding within the composite (Fig. 2).

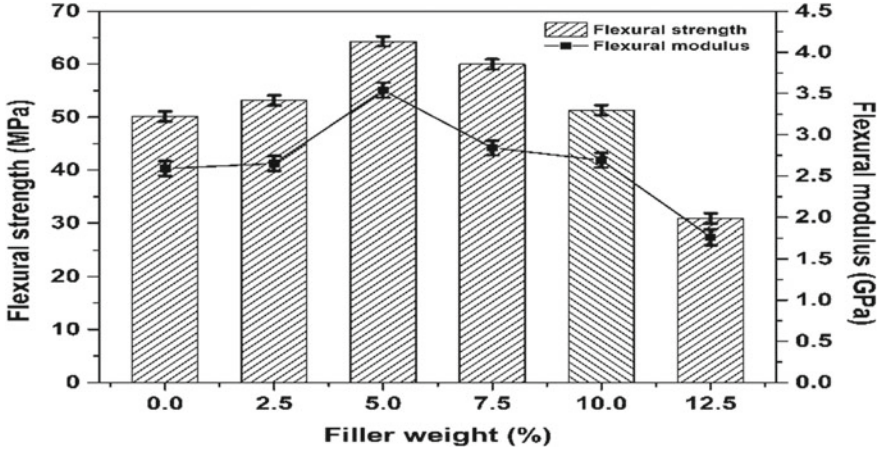


Fig. 2 Flexural strength and modulus at different filler weight percentage

3.2 Tribological Characterization

Figure 3, explains the variation in weight loss of the jute filler composite as per the applied load. The figure demonstrates that, when the load varies from 5 to 15 N, the weight loss of the composites is also started increasing gradually. At lower load values, the weight loss for all the composite become almost equal and low. Within multiple weight fractions, 2.5% of particle content produces the composite with minimum weight loss and the same become maximum at 12.5% of jute particles. The main reason behind the minimal and maximal weight loss is about the formation of interfacial interaction within the composite. Among all the composites, the sample with neat epoxy produces a highest weight loss at the maximum applied load of 15 N.

Coefficient of friction (CoF) is also one of the vital output factors which describes the wear properties of the composite. The impact of the applied load on the CoF is plotted in Fig. 4. From this figure, the increment in the CoF is noticed when the load varies from lower to higher values i.e., from 5 to 15 N. Also, the CoF goes on increasing when the percentage of filler content goes on raising. That's only because as the filler content raises, the surface roughness of the developed composites goes on increasing. Among multiple weight fraction composite, the sample with 12.5% of particle content produces the highest CoF which may be due to the formation of agglomeration of fillers within the composite and because of the proper interlocking between the fillers and matrix, the sample with 2.5 and 5% of particles have generated the minimal CoF at the maximal load of 15 N. The absence of filler in composite (neat epoxy sample) has the CoF of 0.48 at the maximal load which is almost equal with the sample having 12.5 wt.% fraction of filler content.

The evaluation of wear characteristics for the sample explains the tribological performance of the composite. The impact of the applied load on the amount of wear is plotted in Fig. 5. From the figure, it is clearly observed that due to very low penetration of load in the beginning, the wear of the samples is found less. However, by progressively increasing the applied stress on the composite, the wear of the samples began to increase, owing to the production of micro cracks and debonding in epoxy and filler composites, respectively. At 15 N, the sample with 2.5 wt.%

Fig. 3 Weight loss versus applied load of jute particulate reinforced composite

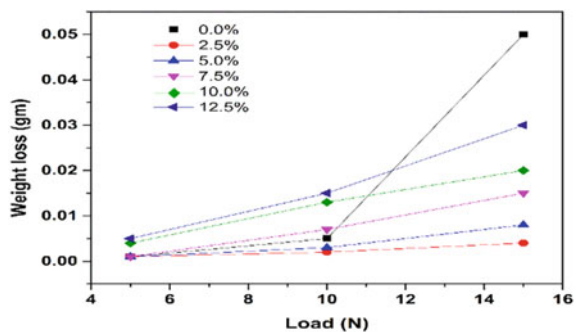


Fig. 4 Coefficient of friction versus applied load of jute particulate reinforced composite

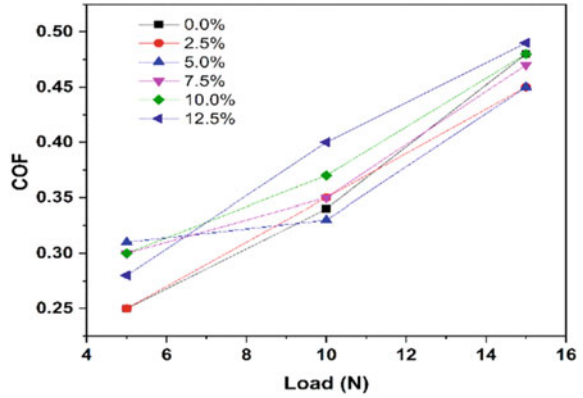
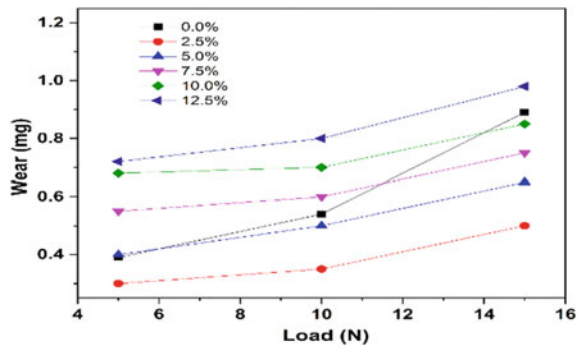


Fig. 5 Wear versus applied load of jute particulate reinforced composite



fraction of jute filler content has produced the minimal wear of 0.48 mg and the maximal wear of 0.99 mg is noticed when the composite contains 12.5 wt.% fraction of filler content.

3.3 SEM Observations

From the SEM image, it is observed that neat epoxy shows high plastic deformation and a high amount of wear debris are also present over the surface. This is due to a shortage of jute particles on the polymer material, which resulted in a decrease in composite strength and a significant volume loss. Compared to the higher filler reinforcement, weight loss and COF are likewise minimal when the filler reinforcement is low. The bonding within the sample is homogenous at 2.5% of particle-based composite, but at maximal particle concentrations, i.e., at 12.5%, the particles remain in a cluster shape, resulting in substantial material loss. Figure 6 demonstrates the worn surface of the various filler reinforced composite.

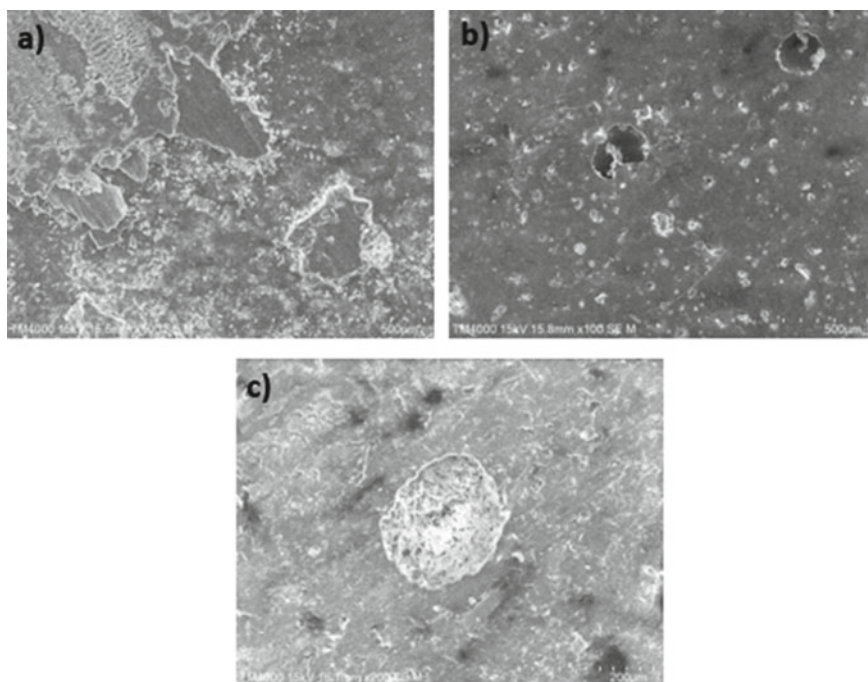


Fig. 6 Microscopic analysis of the tested surfaces of the various jute filler content composite **a** 0%, **b** 2.5% and **c** 12.5%

4 Conclusion

The paper explains the mechanical and wear characteristics of JRC. The process of fabricating the composites, which includes various filler weight content with epoxy resin, are found satisfactory. After various experimental tests, the results are observed and discussed below

- The interfacial interaction within the composite is excellent at reduced filler content, resulting in improved adhesion within the produced composites.
- At 5% jute filler content, the highest tensile strength of 48.56 MPa and modulus of 2.9 GPa is found. Also, the flexural strength of 64.28 MPa and modulus of 3.54 GPa is found maximal.
- Because of cluster formation at 12.5 wt.% jute filler content composites, the mechanical characteristics are observed very low.
- At the maximum load of 15 N, the weight loss and wear of the composites are noticed minimal at 2.5 wt.% jute filler composite. In comparison, 12.5 wt.% and neat epoxy composites have produced the maximal weight loss and wear, respectively.

- As the surface roughness of the developed composites for minimal filler content is low, the CoF of the same will also remain low and it becomes maximum with the composite containing higher percentage of filler content.
- After SEM analyzation, high amount of material loss and plastic deformation are observed at 12.5 wt.% of jute filler and neat epoxy composite, respectively.

References

1. Khan, G. A., Terano, M., Gafur, M. A., & Alam, M. S. (2016). Studies on the mechanical properties of woven jute fabric reinforced poly (l-lactic acid) composites. *Journal of King Saud University-Engineering Sciences*, 28(1), 69–74.
2. Parbin, S., Waghmare, N. K., Singh, S. K., & Khan, S. (2019). Mechanical properties of natural fiber reinforced epoxy composites: A review. *Procedia Computer Science*, 152, 375–379.
3. Sever, K., Sarikanat, M., Seki, Y., Erkan, G., & Erdoğan, Ü. H. (2010). The mechanical properties of γ -methacryloxypropyltrimethoxy silane-treated jute/polyester composites. *Journal of composite Materials*, 44(15), 1913–1924.
4. Karaduman, Y. E. K. T. A., Gokcan, D., & Onal, L. (2013). Effect of enzymatic pretreatment on the mechanical properties of jute fiber-reinforced polyester composites. *Journal of Composite Materials*, 47(10), 1293–1302.
5. Karnani, R., Krishnan, M., & Narayan, R. (1997). Biofiber-reinforced polypropylene composites. *Polymer Engineering & Science*, 37(2), 476–483.
6. Saheb, D. N., & Jog, J. P. (1999). Natural fiber polymer composites: A review. *Advances in Polymer Technology: Journal of the Polymer Processing Institute*, 18(4), 351–363.
7. Mahakur, V. K., Bhowmik, S., & Patowari, P. K. (2022). Machining parametric study on the natural fiber reinforced composites: A review. *Proceedings of the Institution of Mechanical Engineers, Part C: Journal of Mechanical Engineering Science*, 236(11), 6232–6249.
8. Averous, L., Fringant, C., & Moro, L. (2001). Starch-based biodegradable materials suitable for thermoforming packaging. *Starch-Stärke*, 53(8), 368–371.
9. Rowell, R. M., Sanadi, A. R., Caulfield, D. F., & Jacobson, R. E. (1997). Utilization of natural fibers in plastic composites: Problems and opportunities. *Lignocellulosic-plastics composites*, 13, 23–51.
10. Bledzki, A. K., & Gassan, J. (1999). Composites reinforced with cellulose based fibres. *Progress in polymer science*, 24(2), 221–274.
11. Mohanty, A. K., Misra, M. A., & Hinrichsen, G. I. (2000). Biofibres, biodegradable polymers and biocomposites: An overview. *Macromolecular materials and Engineering*, 276(1), 1–24.
12. Karmaker, A. C., & Schneider, J. P. (1996). Mechanical performance of short jute fibre reinforced polypropylene. *Journal of materials science letters*, 15(3), 201–202.
13. Mahakur, V. K., Bhowmik, S., Patowari, P. K., & Kumar, S. (2022). Effect of alkaline treatment on physical, mechanical, and thermal characteristics of jute filler reinforced epoxy composites. *Journal of Vinyl and Additive Technology*.
14. Pal, P. K. (1984). Jute reinforced plastics: A low cost composite material. *Plastics and Rubber Processing and Applications*, 4(3), 215–219.
15. Jacob, R., & Isac, J. (2017). Dynamic mechanical analysis and thermal degradation of jute fiber reinforced BSFT ($\text{Ba}_{0.6}\text{Sr}_{0.4}\text{Fe}_x\text{Ti}_{(1-x)}\text{O}_{3-\delta}$), ($x = 0.1$)-polypropylene composite. *Indian Journal of Pure and Applied Physics*, 55(7), 497–502.
16. Mohanty, A. K., & Misra, M. (1995). Studies on jute composites—A literature review. *Polymer-Plastics Technology and Engineering*, 34(5), 729–792.
17. Mahakur, V. K., Bhowmik, S., & Patowari, P. K. (2023). Tribo-informatics evaluation of dry sliding friction of silanized jute filler reinforced epoxy composites using machine learning techniques. *Tribology International*, 183, 108388.

18. Singha, K., Maity, S., Singha, M., Paul, P., & Gon, D. P. (2012). Effects of fiber diameter distribution of nonwoven fabrics on its properties. *International Journal of Textile Science*, *1*(1), 7–14.
19. Shah, A. N., & Lakkad, S. C. (1981). Mechanical properties of jute-reinforced plastics. *Fibre Science and Technology*, *15*(1), 41–46.
20. Roe, P. J., & Ansell, M. P. (1985). Jute-reinforced polyester composites. *Journal of Materials Science*, *20*(11), 4015–4020.
21. Gowda, T. M., Naidu, A. C. B., & Chhaya, R. (1999). Some mechanical properties of untreated jute fabric-reinforced polyester composites. *Composites Part A: Applied science and manufacturing*, *30*(3), 277–284.
22. Ahmed, K. S., & Vijayarangan, S. (2007). Experimental characterization of woven jute-fabric-reinforced isothalic polyester composites. *Journal of applied polymer science*, *104*(4), 2650–2662.
23. Mohanty, A. K., Khan, M. A., & Hinrichsen, G. (2000). Influence of chemical surface modification on the properties of biodegradable jute fabrics—Polyester amide composites. *Composites Part A: Applied Science and Manufacturing*, *31*(2), 143–150.
24. Acha, B. A., Marcovich, N. E., & Reboredo, M. M. (2005). Physical and mechanical characterization of jute fabric composites. *Journal of Applied Polymer Science*, *98*(2), 639–650.
25. Hong, C. K., Hwang, I., Kim, N., Park, D. H., Hwang, B. S., & Nah, C. (2008). Mechanical properties of silanized jute—Polypropylene composites. *Journal of Industrial and Engineering Chemistry*, *14*(1), 71–76.
26. Gouda, K., Bhowmik, S., & Das, B. (2020). Thermomechanical behavior of graphene nanoplatelets and bamboo micro filler incorporated epoxy hybrid composites. *Materials Research Express*, *7*(1), 015328.
27. Mahakur, V. K., Paul, R., Bhowmik, S., & Patowari, P. K. (2022). Influence of surface modification on mechanical and tribology performance of jute filler polymer composites and prediction of the performance using artificial neural network. *Polymer Bulletin*, 1–22.

A Review on Epoxy Polymer Matrix Composite, Its Mechanical and Thermal Properties



Basavraj R. Birajdar and R. T. Vyavahare

Abstract This paper is a concrete review on Polymer matrix composite materials and gives the reason why researchers are often attracted to the world of composite materials. Here we focus mostly on the fields of application of Polymer Matrix Composites (PMCs) and Polymers used in PMCs. Another objective of this state of art review is to study about the composite materials, its classification, application, and a comparative study of mechanical properties of metallic and composite materials. Here we carried out a detailed study on different types of reinforcement fibers of polymer matrix for tribological application. The increasing demand of high strength and light weight components has enhanced the use of E-glass composite in recent years. E-glass composite has been found extremely useful in many applications due to their strength, ease of processing, lightness, and availability. Number of industrial applications of E-glass composite can be found in automotive sector such as car body, brake pads, drive shaft, fuel tank, hoods etc., aerospace field, sports equipment and manufacturing industries etc. The behavior of E-glass composite is governed by various mechanical and thermal properties. One can achieve variation in density, specific wear rate by altering orientation of the fibers and volume percentage of filler material as well as young's modulus of the composite can also be altered with change in volume percentage of the filler material. On the other hand, thermal properties like thermal conductivity can be improved with increase in EGF content and specific heat capacity can also be increased with increase in temperature. Therefore, it has been proposed to select E-glass composite with brass filler for study. From the literature it has been found that there is scope of achieving better properties of E-glass composite by changing filler volume percentage and by changing grain size of the filler.

Keywords Polymer matrix composites · Thermosets · Thermoplastic · Mechanical properties

B. R. Birajdar (✉)
Walchand Institute of Technology, Sholapur, India
e-mail: birajdar.basav@gmail.com

R. T. Vyavahare
N. B. Navale Sinhgad College of Engineering, Kegaon-Solapur, Sholapur, India

1 Introduction

The extensive use of polymer based the composite have been found in many applications due to the fact of high strength, lightness, and ease of processing etc.

There are numerous industrial applications such as Bearing materials, Rollers, Seals, Gears, cams, Transmission belts and clutches. Where one can find the extensive use of polymer and their composites. However, to fit a polymer composite into particular application there is need of selecting appropriate values of mechanical and thermal properties.

Recent literature reveals that increased percentage of bronze with fixed volume of E glass fiber improves the tensile strength and modulus of elasticity of the composite. On the other hand, decreasing percentage of bronze leads to decrease in the density of composite [1]. It has also been investigated that flexural strength of the composite and flexural modulus can be enhanced with the increased percentage of graphite [2].

Suresha [3] have investigated the influence of two inorganic fillers, namely silicon carbide particle and graphite on wear of glass fabric reinforced epoxy composite subjected to dry sliding condition. Higher wear loss was recorded for increased load and sliding velocity situation. It was observed that there exists increasing trend of coefficient of frictional values with subsequent increase in load and sliding velocity.

1.1 Composite Materials

A composite material is a structural material produced from significantly different chemical or physical properties that are combined at a macroscopic level which are not soluble in each other. The ingredients of composite materials are Matrix and reinforcing element. The matrix is embedded in reinforcing phase. The reinforcing phase material are in the different forms like particles, fibre or flakes [4]. The matrix materials are generally continuous in phase. Concrete reinforced with steel and Epoxy reinforced with graphite fibres are few examples for composite materials [5] Composites materials have some more advantages over conventional materials are High strength, Light in weight, Optimum stiffness, fatigue resistance is high than metal, high corrosion resistance, ease of processing, lower overall system costs, thermal expansion and electrical conductivity are lesser than metal. Low radar visibility [6]. Figure 1 shows the comparison between conventional monolithic materials and Composite materials.

The Composite materials have got improved mechanical properties over conventional materials. Sometimes the properties of composite materials are unique [8].

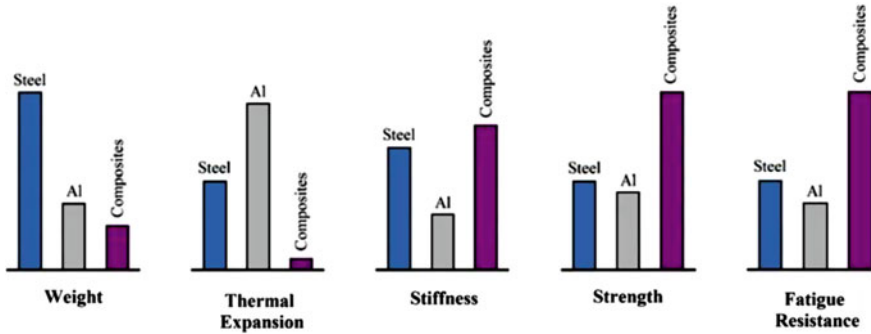


Fig. 1 Conventional monolithic materials and Composite materials, a comparison [7]

1.1.1 Polymer Matrix Composites (PMC)

PMCs are composed of different types of organic polymers containing of continuous or short fibers with the different reinforcing agents [9]. This improves the properties such as stiffness, high strength and fracture toughness of composite materials [10]. The reinforced fibers of PMCs support the mechanical load. The main objective of the matrix is to hold fibres together, transfer loads between the reinforcing fibers and protect the fibers from mechanical and environmental damages [11]. A polymer matrix reinforced with natural fibers contains a good resistance and interfacial bonding between them helps to maintain their mechanical and chemical identities. In general, the fibers are carriers of charge, while the matrix keeps them in position at the desired orientation, it acts as a means of protects them from environmental damage and transferring the charge between the fibre [12, 13]. From the viewpoint of easier fabrication, the production of PMC materials is desirable when compared to that of ceramic matrix composite, or metal matrix composites.

Thermoplastic polymers are very common because of their good mechanical properties, excellent resistance to chemical reaction and its lower cost compared to MMCs. But main disadvantage is they are non-biodegradable. After the end use which could be addressed to certain extent by making composite materials of polymers with natural fibres [14, 15]. Both, thermoplastics, and thermosets have certain advantages and disadvantages as matrix materials in composite preparation.

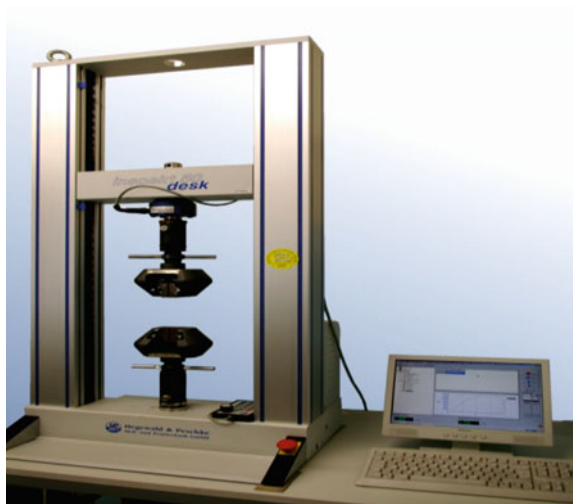
2 Mechanical Properties

2.1 Variation in Young's Modulus

Patil [1] carried out Tensile tests on rectangular specimens by using ASTM D 3039 standard at a crosshead speed of 1 mm/min. All the specimens were flat and rectangular in cross section having a thickness of 3 mm keeping tabs at the ends. Density, impact, and hardness were calculated by using ASTM: D 256 and ASTM: D 785 standards respectively. The tests were carried out for all specimens prepared and average results obtained were taken for each sample. Figure 2 show UTM used for the tests. He tested tensile properties of glass fiber reinforced graphite and bronze filled composite.

Results were plotted as shown in Fig. 3. From the graph, it can be seen that with increase in the graphite volume percentage from 10 to 20%, the tensile strength reduced from 4.8 to 3.67 GPa while young's modulus (E) was found to be lowest i.e. 39.58 MPa for G15/B15 composites. Also, it is found from the graph that with increased filler volume % of bronze from 10 to 20% both tensile strength and modulus indicated an increased trend. The increased tensile property of G10/B20 composite was recognized to the increased volume percentage of bronze and decreased volume percentage of graphite. It is seen that the decrease in graphite filler volume percentage has a positive effect on tensile properties. It might be because of the mechanical properties of the graphite and bronze filler.

Fig. 2 UTM used for tensile testing



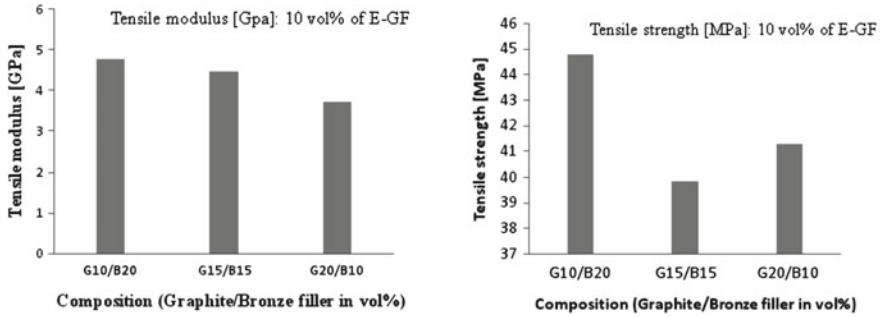


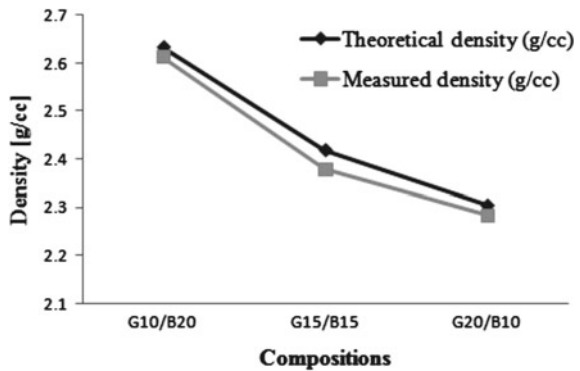
Fig. 3 Tensile modulus and strength of composite

2.2 Variation in Density

A comparison of theoretical value of density and measured value of density of glass fiber reinforced graphite and bronze filled epoxy composite was carried out. A rule of mixture has been used for the theoretical density measurement [16]. It is given by $\rho_{th} = \rho_m V_m + \rho_f V_f + \rho_g V_g + \rho_b V_b$, where ρ is the density and V is volume fraction and the suffix m, f, g and b refer to the matrix material, glass fiber, graphite and bronze fillers respectively. Archimedes Principle was used to calculate experimental density. It has been observed that the increased percentage of graphite filler or decreased percentage of bronze filler leads to fall in the value of density.

Glass fibers with graphite and bronze particulates in the epoxy matrix composite were observed under microscope and clustering of glass fiber was observed. Below Fig. 4 shows the variation in the theoretical and measured density with the variation in graphite and bronze percentage in the matrix of epoxy glass composite.

Fig. 4 Theoretical and measured density



2.3 Improvement in Wear Resistance

Kishore et al. [17] developed. Rubber bearing and graphite bearing containing glass epoxy composite. LY 556 epoxy was used as the resin for the matrix material with HY 951 grade room temperature curing hardener and diluent DY 021 (both supplied by Hindustan Ciba Geigy).

The designated rubber bearing laminate as ‘A’. Graphite-bearing laminate (i.e. 2.5 wt.%) is denoted by ‘B’ and the 4.5 wt.% graphite-bearing is designated ‘C’ were tested for characterizing friction and wear properties. Table 1 shows details of the sample regarding matrix reinforcement, material additive and wet percentage.

They designated and developed a test rig, consisting of Pin-on disc. Glass epoxy composite samples were tested or friction and wear by applying load on the sample and rotating the sample at various speeds. The tests were carried out by selecting various test parameters such as normal load, velocity and sliding distance (Fig. 5).

The sliding distance was maintained at 5 km for both the rubber and graphite bearing sample. A load and velocity range of 29 to 69 N and 2 to 5 m per second respectively where chosen. The weight loss of the sample was determined by noting the difference in the initial and final weight reading of the sample.

Table 1 Details of samples regarding the matrix, reinforcement material, additive and wt.%

Sample	Matrix	Reinforcement material	Additive	wt.%
A	Epoxy	E-glass fabric	HTBN rubber	3
B	Epoxy	E-glass fabric	Graphite powder	2.5
C	Epoxy	E-glass fabric	Graphite powder	4.5

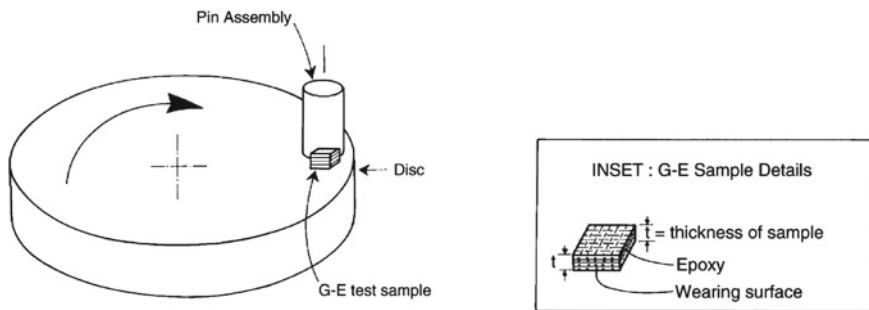


Fig. 5 Pin assembly showing location of the G–E test sample (inset: glass fabric details along with epoxy resin matrix showing the sample surface subjected to wear)

2.4 Wear Measurements

Figure 6 shows the details of the weight loss with respect to sliding velocity for the rubber-containing A type samples for different loads. The data show that weight loss increases with either increase in load or sliding velocity. Similar results are obtained for both B (Fig. 6) and C (Fig. 6) samples. To show the relative wear loss for differing loads and sliding velocities, the results are now represented in the form of bar diagram in Fig. 7 for a constant load (29 N) and sliding distance (5 km) but varying in sliding velocity. Similarly, Fig. 8 show the corresponding situations obtained at higher loads (i.e. 49 and 69 N, respectively). From such bar plots, it is noted that of the three filler bearing varieties tested, the C type exhibits the least wear and A variety the maximum for all conditions.

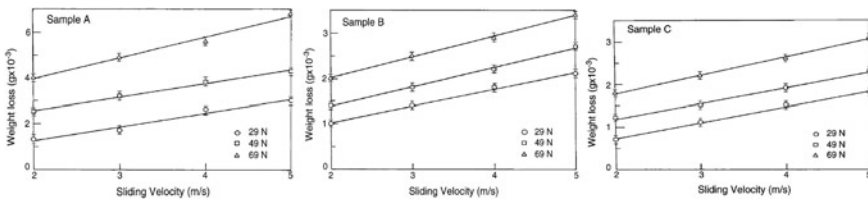


Fig. 6 Weight loss vs. sliding velocity for different loads in A–C type samples

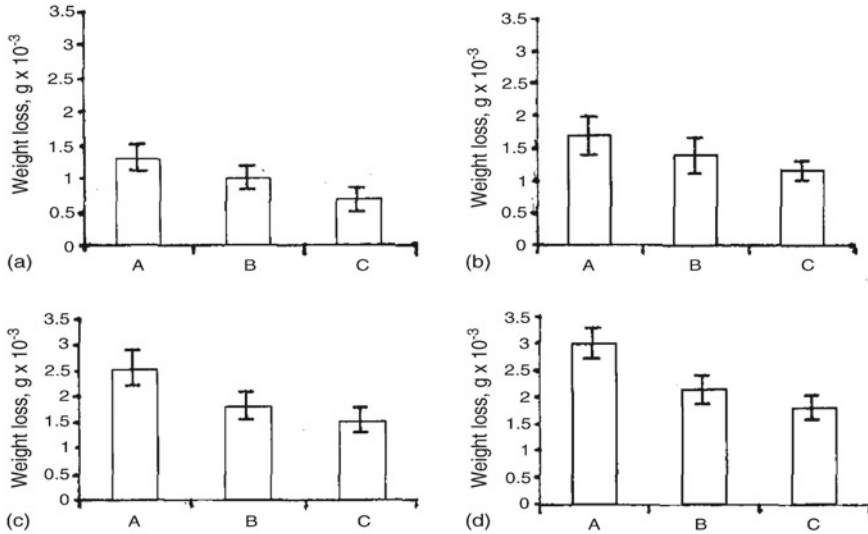


Fig. 7 Wear data of A–C samples at 29 N load application for sliding velocity of a 2 m/s; b 3 m/s; c 4 m/s; and d 5 m/s

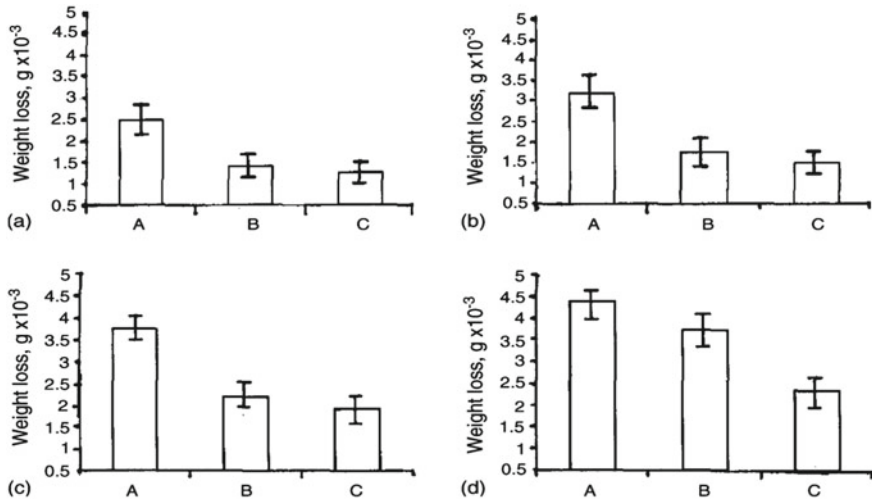


Fig. 8 Wear data of A–C samples at 49 N load application for sliding velocity of **a** 2 m/s; **b** 3 m/s; **c** 4 m/s; and **d** 5 m/s

2.5 Specific Wear Rate

Raju et al. [18] have investigated mechanical and tribological behavior of particulate filled glass fabric reinforced epoxy composite. They proposed that tensile strength and tensile modulus of glass epoxy composite can be improved by the inclusion of Al_2O_3 filler. They also claimed about reduction in specific wear rate of glass epoxy composite by the inclusion of Al_2O_3 filler. Decrease in wear volume was caused by increase in filler loading and excellent wear resistance was obtained for Al_2O_3 filled a glass epoxy composite. Above all, a very less wear loss was observed with 10% weight filler loading. Below Fig. 9 shows variation in specific wear rate of composite on 300 and 600 grit SiC papers at 10 N against abrading distance.

It is clear from Fig. 9a and b that increase in abrading distance causes increase in specific wear rate for Glass epoxy and Al_2O_3 filled composites. It is obvious from the figure that increase in grit size of SiC paper leads to decrease in specific wear rate.

3 Thermal Properties

Bertoncelly et al. [19] studied the effect of fraction of glass fiber weight content and its microstructure on thermal properties of the composites and investigated variation in thermal properties of polymer matrix composite reinforced with E glass fiber. A study on thermal properties of polymer matrix composite with CaCO_3 mineral fillers was carried out by changing the fraction of epoxy glass fiber reinforcement from

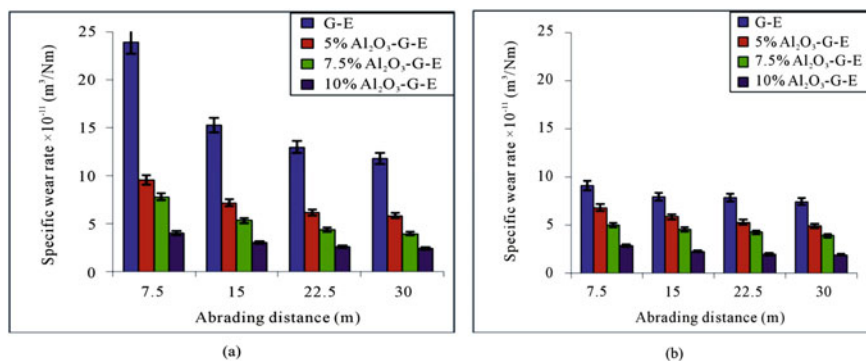


Fig. 9 Variation of specific wear rate with abrading distance for unfilled and Al_2O_3 filled G-E composites: **a** 320 and **b** 600 grit SiC paper

Table 2 Composition and density of the BMC composite samples

Sample	PM (wt%)	EGF (wt%)	MF (wt%)	P (g/cm^3)
BMC-0	21	0	79	1.96
BMC-5	21	5	74	1.91
BMC-10	21	10	69	1.87
BMC-15	21	15	64	1.86

zero to 15 weight percent. They determined thermal stability and thermal properties of fiber reinforced composite by microstructural changes induced by different fiber content. It has been found that even upon heating to 260°C composites are stable. Composites undergo thermal oxidation between 280 and 560°C . There is decrease in thermal conductivity of composite with increase in EGF content from 0.960 (6) w/mk to 0.878 (2) w/mk for 0 and 15 weight percentage EGF respectively. They prepared four sets of BMC (Bulk Molding Compounds) samples as shown in below table.

Table 2 below shows the composition and density of BMC composites samples.

Thermal conductivity of the composites with different weight proportions of EGF was calculated. The value of thermal conductivity decreases with increase in EGF content. It has also been observed that specific heat capacity (C_p) with mineral filler increased with increase in temperature.

4 Result and Discussion

It is clear from literature review that there exists a crucial role of composite material in the field of automobiles, aerospace, Sports, Transportation and Infrastructure and Agricultural equipment etc. One can achieve reduction in weight using composite

materials and in the case of aerospace and automobile this may lead to increase the fuel efficiency. Epoxy glass composites with filler material like Graphite, Bronze, CaCO_3 , and Al_2O_3 has major use in bush bearings, Agricultural equipment etc.

In the present era it is necessary to mitigate the friction resistance between sliding or rolling surfaces. This can be achieved by choosing appropriate filler material like graphite with desired % of weight. In addition to this specific heat capacity of composite material E-glass composite material can be increased by choosing appropriate % weight of mineral filler like CaCO_3 .

5 Conclusion

Extensive survey of literature reveals that properties of glass fiber epoxy composite can be improved by increasing the % of filler material like bronze. As well as inclusion of Al_2O_3 filler reduces specific wear rate of Epoxy glass composite. The results can be seen in abrasion mode and excellent wear resistance was obtained for Al_2O_3 filled epoxy glass composites. It is also presented in literature that inclusion of graphite in Epoxy glass composite makes lower coefficient of friction for any combination of load and velocity. Literature also reveals that the inclusion of mineral filler like CaCO_3 improves mechanical and thermal properties of epoxy glass fibers.

It is evident from the past that every industrial revolution comes with improvement in material ingredients and development of new materials to meet the current operational requirements. The above-mentioned survey points towards the scope for development of the new material model with better mechanical and thermal properties.

References

1. Patil, N., & Prasad, K. (2015). Effect of graphite and bronze on strength of chopped e-glass fiber reinforced epoxy composites. *American Journal of Materials Science*, 2, 121–125.
2. Patil, N., & Prasad, K. (2016). Characterization of short E-glass fiber reinforced graphite and bronze filled epoxy matrix composite. *Iranian Journal of Material Science and Engineering*, 13(1), 28–36.
3. Suresha, B., Chandramohan, G., Prakash, J. N., Balusamy, V., & Sankaranarayanan, K. (2006). The role of fillers on friction and slide wear characteristics in glass-epoxy composite system. *Journal of Minerals and Materials Characterization and Engineering*, 5(1), 87–101.
4. Clyne, T., & Hull, D. (2019). *An introduction to composite materials*. Cambridge University Press.
5. Kaw, A. K. (2005). *Mechanics of composite materials*. CRC Press.
6. Patel, M., Pardhi, B., Chopara, S., & Pal, M. (2018). Lightweight composite materials for automotive—A review. *Carbon*, 1(2500), 151.
7. Chawla, K. K. (2012). *Composite materials: Science and engineering*. Springer Science & Business Media.
8. Fan, J., & Njuguna, J. (2016). An introduction to lightweight composite materials and their use in transport structures. In *Lightweight composite structures in transport* (pp. 3–34). Elsevier.

9. Wang, R.-M., Zheng, S.-R., & Zheng, Y. G. (2011). *Polymer matrix composites and technology*. Elsevier.
10. Yashas Gowda, Y. G., Sanjay, M. R., Subrahmanya Bhat, K., Madhu, P., Senthamaraikannan, P., Yogesha, B., & Pham, D. (2018). Polymer matrix-natural fiber composites: An overview. *Cogent Engineering*, 5(1), 1446667. <https://doi.org/10.1080/23311916.2018.1446667>
11. Cao, Y., & Wu, Y.-Q. (2008). Evaluation of statistical strength of bamboo fiber and mechanical properties of fiber reinforced green composites. *Journal of Central South University of Technology*, 15(1), 564–567.
12. Akil, H. M., Omar, M. F., Mazuki, A. A. M., Safiee, S., Ishak, Z. A. M., & Abu Bakar, A. (2011). Kenaf fiber reinforced composites: A review. *Materials & Design*, 32(8–9), 4107–4121.
13. Ashori, A. (2013). Effects of nanoparticles on the mechanical properties of rice straw/polypropylene composites. *Journal of Composite Materials*, 47(2), 149–154.
14. Chung, D. (2007). Carbon fibers, nanofibers, and nanotubes. *Carbon Composites*, 2, 1– 87.
15. Hsieh, C.-Y., & Chung, S.-L. (2006). High thermal conductivity epoxy molding compound filled with a combustion synthesized aln powder. *Journal of Applied Polymer Science*, 102(5), 4734–4740.
16. Alger, M. S. M. (1997). *Polymer science dictionary* (2nd ed.). Springer Publishing. ISBN 0412608707.
17. Kishore, P., Sampathkumaran, S., Seetharamu, P. I. & Janardhana, M. (2005). A study on the effect of the type and content of filler in epoxy-glass composite system on the friction and slide wear characteristics. *Wear*, 2, 634–641.
18. Raju, B. R., Suresha, B., Swamy, R. P., & Kanthraju, B. S. G. (2013). Investigations on mechanical and tribological behaviour of particulate filled glass fabric reinforced epoxy composites. *Journal of Minerals and Materials Characterization and Engineering*, 1, 160–167.
19. Bertoneclj, B., Vojisavljevic, K., Vrabelj, M., & Malic, B. (2015). Thermal properties of polymer-matrix composites reinforced with E-glass fibers. *Journal of Microelectronics, Electronic Components and Materials*, 45(3), 216–221.

A Study on Mechanical Properties of Stainless Steel Welded Joints for Marine Applications



Kiran Lakkam, Chetankumar Jadhav, Sangamesh K. Sajjan, Ratan Patil, Anilkumar Shirahatti, and S. M. Kerur

Abstract Corrosion can be defined as a significant reason for structural failure in marine and offshore applications. Pitting corrosion is a savage and detrimental form of corrosion. It is a locally accelerated precipitation of metal that forms as a result of damage in the protective passive film on the material surface. From so many years it is being researched upon; yet, the actual nature of failure of susceptible materials due to pitting corrosion is still not completely comprehended. It penetrates deeply in the materials and weakens the material. More the carbon content, higher will be the risk of getting corroded. So mainly Stainless steel, that contains minimum amount of carbon, will display maximum resistance to this type of corrosion. In this paper, mechanical properties of stainless steel 304 are studied. Shielded metal arc welding is used to weld two SS304 plates and then tensile and impact specimens are prepared using AWS B4 standards. The test specimens are then subjected to accelerated corrosion as per ASTM G48 standards for 0, 48, 96, 144 and 192 h. Later, tensile test and impact test is carried out. The results obtained from testing shows that there is decrease in tensile strength of welded joints as the exposure time increases. The variation in the impact strength is not very prominent. However as compared to non-corroded SS304 material, the ones which are exposed to accelerated corrosion show slightly less impact strength. Microscopic study reveals that there is a change in phase to martensite at heat affected zone with higher carbon content compared to base metal, making the joint brittle compared to base metal.

K. Lakkam (✉)
SVERI's College of Engineering, Pandharpur, India
e-mail: klakkam@gmail.com

C. Jadhav · R. Patil
Jain College of Engineering, VTU, Belagavi, India

S. K. Sajjan
BLDEA's V. P. Dr. P. G. Halakatti College of Engineering & Technology, Vijayapur, India

A. Shirahatti
Jain Engineers, Belagavi, India

S. M. Kerur
Praavi Career Counselling Center, Belagavi, India

Keywords Pitting corrosion · Stainless steel · Welded joints · Mechanical properties · Hardness

1 Introduction

Stainless steel metals play a major role in applications where high resistance to corrosion is required. High chromium content in these stainless steel materials make them highly resistive to corrosion and makes a remarkable application in marine and offshore environments [1]. Many additives like nickel and molybdenum helps in enhancing the corrosion resistance capacity of stainless steel materials [2, 3]. Among the various types of corrosion, pitting corrosion plays a prime role towards the failure of structures which are exposed to corrosion atmosphere for a longer time period [4, 5]. These pits can make the structure weaken and reducing its strength carrying capability and in turn decreasing its life (Fig. 1).

To build structures, joining process plays a major role in which welding method is widely used for its high mechanical properties like strength [6, 7]. Different welding methods are used with respect to ease of fabrication to build huge structures [8].

When these welded joints of stainless steel material are exposed to corrosive atmosphere, weakening or failure of these joints may occur [9]. This is due to chloride ions present in these environments [10, 11]. This welded joint contains a part which is specified as Heat Affected Zone (HAZ) where phase transformation takes place

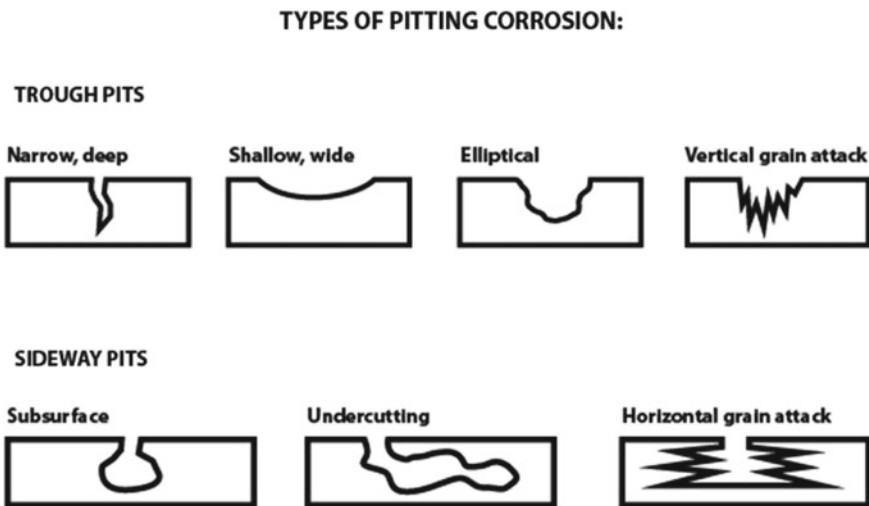


Fig. 1 Types of pitting corrosion

during welding and changes the properties of base metal at the joint area. These areas of the base metal where carbon content may get increased because of welding are prone to corrosion [12, 13].

The phenomenon of corrosion of these stainless steel welded joints was identified before decades. Lot of research is being carried, and several methods of welding and other parameters were tried for preventing corrosion [14].

2 Material and Methods

2.1 Material and Specimen Preparation

Stainless Steel 304 often known as Austenitic stainless steel (18Cr₈Ni) or “18/8” are in metastable state at room temperature. Nickel content present in this type of material makes it highly resistive to corrosion. It takes place in most of the corrosion resistance application in the production of steel. 0.4 wt.% Nitrogen is used to prepare special type of austenitic stainless steels. It influences as solid solution strengthened. Adding of nitrogen makes them still stronger and suitable for tougher applications. It also influences the resistance to corrosion mainly pitting and crevice corrosion. Tables 1 and 2. Shows the tabulation showing the chemical and mechanical properties of stainless steel 304 used in the research work.

Stainless steel 304 were purchased in the form of plates of thickness 10 mm. These plates were cut into two strips and welded in the form of butt joint, using shielded metal arc welding (SMAW) technique. After welding these stainless steel plates of all three types i.e. SS304, SS316, and SS430, to each other, finishing of welding joints was done.

According to AWS B4.0 2016 standards the tensile test specimens and ASTM E23-16b standards was used to prepare impact test specimens.

Using milling operation, the specimens were cut from welded strips of stainless steel according to the dimensions shows in Fig. 2 (Fig. 3).

Table 1 Composition specifications of 304 stainless steel

Grade	C	Mn	Si	P	S	Cr	Mo	Ni	N
SS304	0.015	2.0	0.34	0.045	0.03	19.5	–	10.5	0.10

Table 2 Tensile strength results of SS 304

Time period	0 h	48 h	96 h	144 h	192 h
Tensile strength in KN/mm ²	278.78	341.98	275.21	257.96	234.09

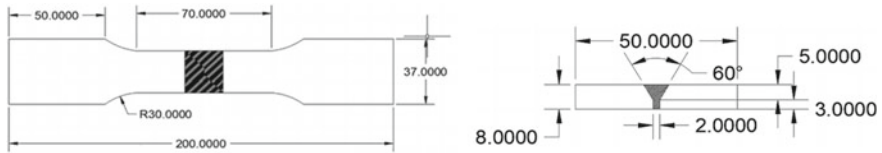


Fig. 2 Tensile and impact test specimen (all dimensions in mm)



Fig. 3 Specimen ready to dip into test solution

3 Methodology and Experimental Setup

3.1 Procedure for Pitting Corrosion

Corrosion test were carried out as per ASTM G48 standards. 100 mg of ferric chloride is added to 900 ml water and the solution is prepared. On the off chance that example bigger than the standard are utilized, give an answer volume of at any rate 5 ml/cm² (30 ml/in²) of explicit surface zone. Move the test measuring glass to a steady temperature shower and permit the test answer for go to the balance temperature of intrigue. Suggested temperatures for assessment are 22 ± 2 °C and 50 ± 2 °C.

Below is procedure of experiment.

- Place the sample in a glass support and submerge in the test arrangement after the solution has reached an ideal temperature. Keep test arrangement temperature constant throughout the test.
- Cover the test vessel with a watch glass. Specimens kept in a solution for 48, 96, 144, and 192 h.
- Remove the specimen after scheduled time from the solution. Wash with water and clean with a nylon bristle brush under running water to eliminate consumption items. Plunge in methanol and air-dry.

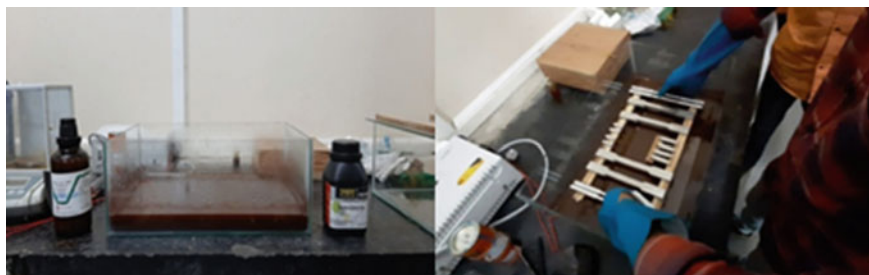


Fig. 4 Solution of ferric chloride and placing of specimens in ferric chloride solution [15]

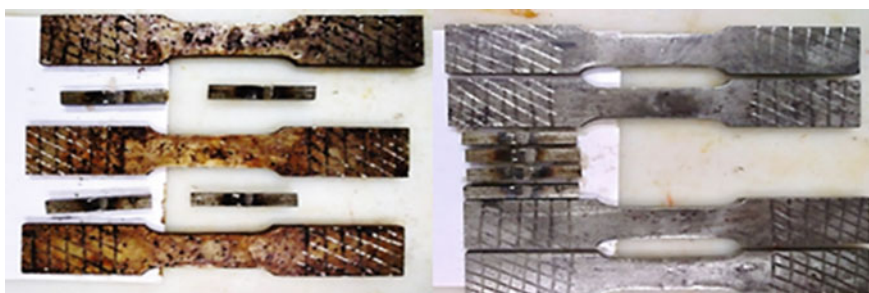


Fig. 5 Specimen before and after corrosion

- Weigh each specimen to 0.001 g or better and reserve for examination.

Figure 4 show the solution of ferric chloride and distilled water stirred well in which the specimens are dipped and kept for accelerated corrosion. The test temperature was maintained at room temperature throughout the experiment (Fig. 5).

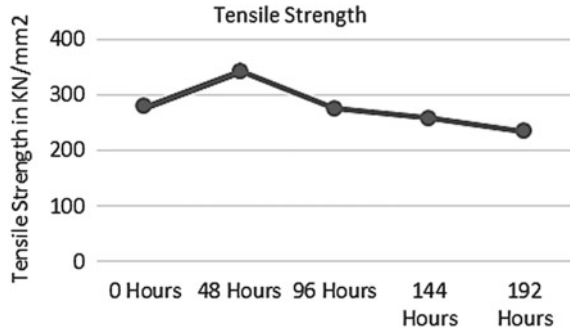
4 Results and Discussion

The results of Tensile strength and Impact test are discussed in the following sections.

4.1 Tensile Test

Tensile strength of the welded joint specimens was tested using Universal Testing Machine. Specimens of non-corroded, and cored with 48, 96, 144 and 192 were tested with three samples of each type and mean of it was considered.

Fig. 6 Plot of tensile strength in KN/mm² versus time of corrosion



Results show that when tensile strength is compared for 0 h i.e. without corrosion and for 48, 96, 144, and 192 h, for 48 h there is a slight increase in tensile strength. But further as corrosion time period increases tensile strength of the welded joint of stainless steel 304 decreases (Fig. 6).

4.2 Impact Test

Energy absorption capacity of the welded joints of stainless steel 304 was studied using Charpy impact test. A notched specimen is prepared according to ASTM standards shown in Fig. 2. Hammer is allowed to drop from an angle of 120°. As the hammer is released and hits the specimen placed as a simply supported beam position, some amount of impact energy is absorbed by the specimen. This deformation energy depends on the toughness of the specimen (Fig. 7 and Table 3).

Fig. 7 Impact strength versus Time period of corrosion

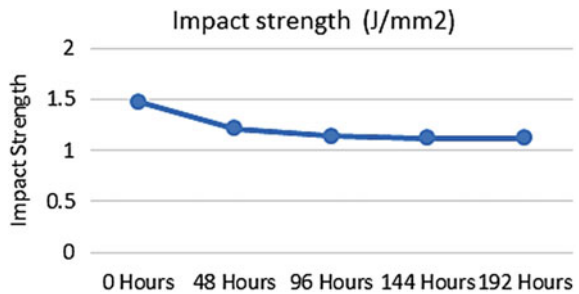


Table 3 Impact strength results of SS 304

Time period	0 h	48 h	96 h	144 h	192 h
Impact strength (J/mm ²)	1.475	1.2125	1.1375	1.1187	1.1155

Table 4 pH of ferric chloride solution

Time period	0 h	48 h	96 h	144 h	192 h
pH value	2.03	2.18	2.2	2.3	2.36

Results show that as time period of corrosion increases impact strength of welded joints of stainless steel decreases. Energy absorption capacity of welded joints of stainless steel 304 decreases with increase in time period of exposure to corrosion environment.

4.3 PH Values

pH level of ferric chloride solutions is also measured according to the time period. Table 4 shows the pH level of all the solutions used for different time period tests.

Above values show that there not must variation in pH values of all the solutions used for different time periods of corrosion.

4.4 Weight Loss

As the corrosion increases according increase in number of days, pits start growing and loss of material may occur which lead to loss in strength of the materials. Weights of test specimens were measured for before corrosion and after corrosion for different time intervals. Table 5 shows the weight loss of specimens with respect to increase in time period of corrosion.

We can observe that as corrosion time period increases there is not much remarkable weight loss in initial stages. But at 192 h of corrosion there is a weight loss, which indicates that material loss due to corrosion is effective for a longer time period of corrosion.

Table 5 Weight loss of tensile test specimens due to corrosion in grams

Time period	0 h	48 h	96 h	144 h	192 h
Average weight before corrosion	368.4	377.2	387.8	395.4	399
Average weight after corrosion	–	377.1	387.7	395.2	398.5
Weight loss of specimens	–	0.1	0.1	0.2	0.5

5 Conclusion and Future Work

Welding plays a major role in fabrication of stainless steel materials for marine and offshore applications. Based on the testing carried following conclusions can be given. Study of tensile strength of welded joints for different corrosion time periods reveal that as time with increase in time period of exposure to corrosion atmosphere tensile strength of welded joint of stainless steel 304 decreases. This may be due to creation of heat affected zone creation near the weld joints. At this area phase transformation takes place and affects the strength of the materials. Impact test also reveals that energy absorption capacity won't get affected at initial stage of corrosion i.e. at shorter time period, but for longer time periods impact strength decreases for the stainless steel 304 materials. Weight loss in specimens with respect to corrosion time period is not must remarkable. But at 192 h there is a slight difference which reveals that for longer period of corrosion material loss may occur.

Microstructure study may reveal still more clear idea regarding grains rearrangement at heat affected zone and effect of loss in strength.

References

1. Pérez-Quiroz, J. T., Alonso-Guzmán, E. M., Martínez-Molina, W., Chávez-García, H. L., Rendón-Belmonte, M., & Martínez-Madrid, M. (2014). Electrochemical behavior of the welded joint between carbon steel and stainless steel by means of electrochemical noise. *International Journal of Electrochemical Science*, *9*, 6734–6750.
2. Bhandari, J., Khan, F., Abbassi, R., Garaniya, V., & Ojeda, R. (2016). Reliability assessment of offshore asset under pitting corrosion using Bayesian network. *Corrosion NACE International*, *35*, 399–406.
3. Woldemedhin, M. T., & Kelly, R. G. (2014). Evaluation of maximum pit size model on stainless steel under atmospheric conditions. *ECS Transactions*, *58*, 41–50.
4. Ward, D. (2008). Correlation of accelerated corrosion testing with natural exposure after 6 years in a coastal environment. *Corrosion*.
5. Chaves, L., & Melchers, R. (2013). Long term localized corrosion of marine steel pilling welds. *Corrosion Engineering, Science and Technology*, *48*, 469–474.
6. Brytan, Z., & Niagaj, J. (2016). Corrosion resistance and mechanical properties of Tig and A-Tig welded joints of lean duplex stainless steel S82441/1.4662. *Archives of Metallurgy and Materials*, *61*(2), 771–784.
7. Laycock, N. J., Krouse, D. P., Hendy, S. C., & Williams, D. E. (2014). Computer simulation of pitting corrosion of stainless steels. *Electrochemical Society Interface*, *23*, 65–71.
8. Murariu, A. C., & Pleșu, N. (2015). Investigations on corrosion behaviour of welded joint in ASTM A355P5 alloy steel pipe. *International Journal of International Journal of Electrochemical Science*, *10*, 10832–10846.
9. Liu, D., Li, Y., Xie, X., & Zhao, J. (2019). Effect of pre-corrosion pits on residual fatigue life for 42CrMo steel. *Materials*, *12*, 2130. <https://doi.org/10.3390/ma12132130>
10. Mamat, M. F., Hamzah, E., Ibrahim, Z., & Majid, R. A. (2015). Effect of filler metals on the microstructures and mechanical properties of dissimilar low carbon steel and 316L stainless steel welded joints. *Materials Science Forum*, *819*, 57–62 (Trans Tech Publications, Switzerland). <https://doi.org/10.4028/www.scientific.net/MSF.819.57>

11. Otero, E., Pardo, A., Utrilla, M., Sáenz, E., & Perez, F. (1995). Influence of microstructure in the corrosion resistance of AISI type 304L and type 316L sintered stainless steels exposed to ferric chloride solution. *Materials Characterization*, 35, 145–151.
12. Ribeiro, R. B., Silva, J., Hein, L., Pereira, M., Corodo, E., & Matias, N. (2013). Morphology characterization of pitting corrosion on sensitized austenitic stainless steel by digital image analysis. *ISRN Corrosion* 2013.
13. Zatkaliková, V., Bulovina, M., _Skorik, V., & Petreková, L. (2010). Pitting corrosion AISI 316 steel with polished surface. *Materials Engineering*, 17, 135–147.
14. Caines, S., Khan, F., Shirokoff, J., & Qiu, W. (2012). Experimental design to study corrosion under insulation in harsh marine environments. *Journal of Loss Prevention in the Process Industries*, 33, 39–51.
15. ASTM G48. Standard test method for pitting and crevice corrosion resistance of stainless steels and related alloys by use of the ferric chloride solution—Methods E and F.

Formulation and Viscosity Evaluation of Copper Oxide Based Nanolubricants



Abhijeet G. Chavan and Y. P. Reddy

Abstract Energy wasted in friction can be reduced by adopting more effective lubrication strategy. Many studies reported improved friction performance of lubricants containing ultrafine additives. Present work deals with viscosity characterization of nanolubricants based on Copper oxide (CuO) nanoparticles. Nanolubricants are prepared by suspending commercially available Copper oxide nanoparticles in engine oil 15W40 in different proportions. A two step method was used for preparation of nanolubricants which involves mechanical agitation followed by ultrasonication. Kinematic viscosity of nanolubricant samples is measured as per IP 70. Comparative results are presented for different weight percentages of CuO nanoparticles. Dispersion stability of prepared nanolubricant samples is assessed by visual inspection over the time. Results implicate significant viscosity change due to addition of copper oxide nanoparticles.

Keywords Nanolubricant · Copper oxide nanoparticles · Viscosity measurement

1 Introduction

In order to meet today's ever increasing energy demand several methods are adopted by researchers and engineers. Energy saving is one of the effective ways to handle this critical issue. High amount of energy is lost in friction in almost every engineering application. This wastage of energy can be reduced by adopting more effective lubrication strategies. A machines ability to operate smoothly, reliably, and durably is

A. G. Chavan (✉) · Y. P. Reddy
Mechanical Engineering Department, Sinhgad College of Engineering, Vadgaon, Pune,
Maharashtra 411041, India
e-mail: abhijeetchavan101@gmail.com

Y. P. Reddy
e-mail: ypreddy.scoe@sinhgad.edu

A. G. Chavan
School of Engineering and Science, MIT ADT University, Pune, Maharashtra 412201, India

heavily dependent on how well wear and friction are handled on numerous interacting surfaces [1]. The application of lubricants at the interface of mating surfaces is one of the most efficient methods to reduce friction, wear, and to ensure the equipment has a longer service life. Due to their distinctive thermo physical properties, nano lubricants are one of the recently developed technologies that have caught the interest of researchers for use in lubrication [2]. For diverse mechanical systems like internal combustion engines [3], refrigeration systems, and radiator fluids nanolubricants with varying characteristics are being developed. Nanoparticles additives can be roughly divided into distinct groups as non metals, metals, metal oxides and metal dichalcogenide. Metal oxides are considered as one of the best alternative because of their chemically inert nature towards base lubricants [4].

Present work deals with preparation of copper oxide (CuO) based nanolubricant and its viscosity measurement. Nanolubricants are prepared by mixing CuO nanoparticles with 15W40 engine oil in different weight proportions. Prepared samples are tested for its viscosity at various temperatures.

2 Theory

Plain lubricant without any additive like engine oil 15W40 is considered as Newtonian fluid, for which general viscosity models like Walther, Barus are sufficient. These models can provide accurate predictions about change in viscosity of lubricants with reference to change in temperature and pressure. But inclusion of ultra-fine additives in lubricant can result into complete change in rheological behavior of lubricant. Many researchers reported that with addition of additives like nanoparticles, colloidal mixture of lubricant demonstrated Non-Newtonian behavior for higher shear rates and Newtonian behavior at lower shear rates [5]. There are different viscosity models proposed by researchers for prediction of viscosity of nanolubricants. Modified Krieger Dougherty Eq. (1) provides relationship between viscosity of nanolubricant and base lubricant. Here μ_n is viscosity of nanolubricant, μ_b viscosity of base fluid, ϕ is nanoparticle volume fraction, a_a is radii of aggregate nanoparticles in nm, a is radii of primary nanoparticles in nm [6].

$$\mu_n = \mu_b \left(1 - \frac{\phi}{0.5} \left(\frac{a_a}{a} \right)^{1.3} \right)^{-1.25} \quad (1)$$

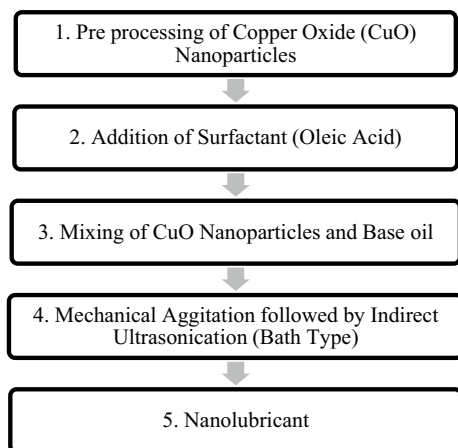
Many researchers have reported that this modified Krieger Dougherty approach holds good for nanolubricants prepared by mixing metal oxides in oils. This model involves effect of size of aggregate particles and primary particles as well as packing volume fraction [7].

3 Materials and Preparation of Nanolubricants

For present work, commercially available engine oil 15W40 is used as base lubricant. This particular engine oil is generally recommended for heavy duty diesel engines, that's why it is selected as base lubricant, because any reduction in friction can result in saving of huge amount of energy. Copper oxide nanoparticles are easily available commercially. It indicates neutral chemical behavior towards engine oil; few researchers have reported superior anti wear performance of CuO nanoparticles along with negative wear characteristics i.e. micro scratches are filled by deposition of CuO nanoparticles. The morphology of CuO nanoparticles is spherical in nature which can justify its selection as an additive. For obtaining dispersion stability of nanolubricants surfactant is used, it works on principle of micelle formation. For the present work Oleic acid is used as surfactant which results in more stable solution of nanolubricants.

There are two distinct methods for preparation of nanolubricants, single step method and two step method [8, 9]. In single step method synthesis of nanoparticles and preparation of mixture of base fluid and nanoparticles is carried out in single process. Although this method provides superior stability, consistent dispersion, and minimal agglomeration, it suffers from drawback of slow production rate hence limited quantity of production. In present work the two step method is used for preparation of nanolubricants. In two step method already prepared nanoparticles, generally in the powder form are mixed with the fluid using high shear and/or ultrasonication. This method is being adopted by researchers and commercial users because of its simplicity. The two step method has limitation of partial dispersion due to agglomeration; however agglomeration can be reduced by using suitable surfactant. Figure 1 shows the schematic representation of methodology adopted for preparation of CuO nanolubricants.

Fig. 1 Schematic of preparation methodology of CuO nanolubricants



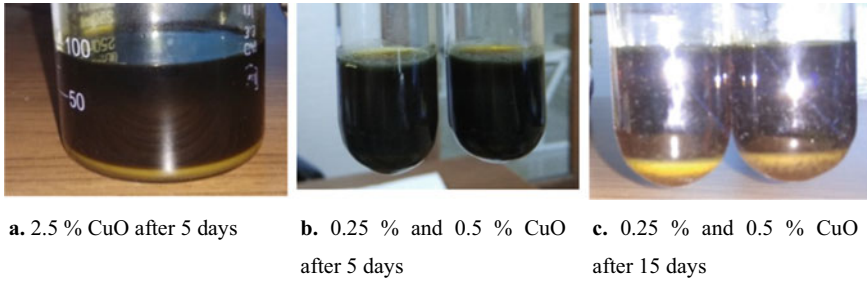


Fig. 2 Photographs of some nanolubricants samples representing settlement

Initially CuO nanoparticles were kept in surfactant (oleic acid) for 24 h, then the mixture of nanoparticles and surfactant is mixed with lubricant 15W40. This mixture is first agitated by mechanical stirrer and then placed in ultrasonic bath. Ultrasonicator was set for temperature of 50 °C and each sample was subjected to ultrasonic waves for 20 min i.e. 4 cycles of 5 min each. The same process was adopted for preparing different samples of nanolubricants.

4 Stability of Nanolubricants

Dispersion stability of nano lubricants is matter of concern as the nano particles tend to settle down after certain time. Oleic acid was used as surfactant. Surfactant and CuO nano particles forms polar and non polar pair and reduced the agglomeration. However due to gravitational force nano particles tend to settle down eventually. Stability of prepared nano particles is checked by keeping the solution undisturbed and observing it for any deposition or settlements, photographs of few samples are presented in Fig. 2 which shows settlement of nanoparticles over time.

After the duration of 5 days 2.5% CuO shows considerable settlement, while 0.25% and 0.5% didn't showed any remarkable settlement. After 15 days both 0.25 and 0.5% samples showed settlement. These settlements were mixed properly after mixing it in the ultrasonicator for 5 min.

5 Viscosity Testing

Viscosity is the one of the key parameter associated with lubricant performance. Many studies reveal that there is significant increase in the viscosity of base medium with the addition of nano particles. Therefore it is essential to measure the viscosity of nano lubricants. There are different standards available for measurement of viscosity of petroleum products and lubricants.

Table 1 Kinematic viscosity of prepared samples at various temperatures

Kinematic viscosity of lubricant sample (cSt)					
Temperature (°C)	Base oil	0.25% CuO	0.5% CuO	1% CuO	1.5% CuO
35	114.3	200.7	207.3	156.9	168.3
40	96.9	143.7	133.5	118.8	121.5
45	77.7	112.8	98.4	87.9	101.9
50	65.9	85.8	88.5	79.8	70.5
55	52.5	77.4	74.1	52.2	58.2
60	44.9	67.5	64.2	46.5	49.2

According standard IP 70, Redwood viscometer can be used for measurement of kinematic viscosity of liquid petroleum products like lubricating oils. For present work viscosity measurement was carried out according to IP 70 by using Redwood viscometer. Temperature range of 35–60 °C in the steps of 5 °C was used for determining viscosity. For each temperature experiment was repeated for three times and average of three values was used for determining kinematic viscosity. Table 1 represents the experimental data obtained by testing prepared nanolubricants. Viscosity variation at various temperatures is presented, for every lubricant there is decrement in viscosity with rise in temperature.

6 Results

Kinematic viscosity for base oil as well as prepared nano lubricants is calculated. Standard formula was used for converting Redwood seconds to kinematic viscosity in centistokes. The temperature vs kinematic viscosity values are plotted in Fig. 3. All samples shows gradual decrement in viscosity with rise in temperature. For the base oil the effect of variation in viscosity is almost linear while for few nano lubricant samples it is non linear.

At lower temperatures there is huge rise in viscosity of lubricant and with the increase in the temperature the rise in the viscosity reduced. Percentage rise in viscosity of nanolubricant as compared to base oil is plotted in Fig. 4, for calculating this percentage rise viscosity of base oil is taken as reference value.

It is observed that 0.25% CuO sample shows highest rise at almost all temperatures, which can be attributed to more stable, evenly dispersed mixture of nanoparticles.

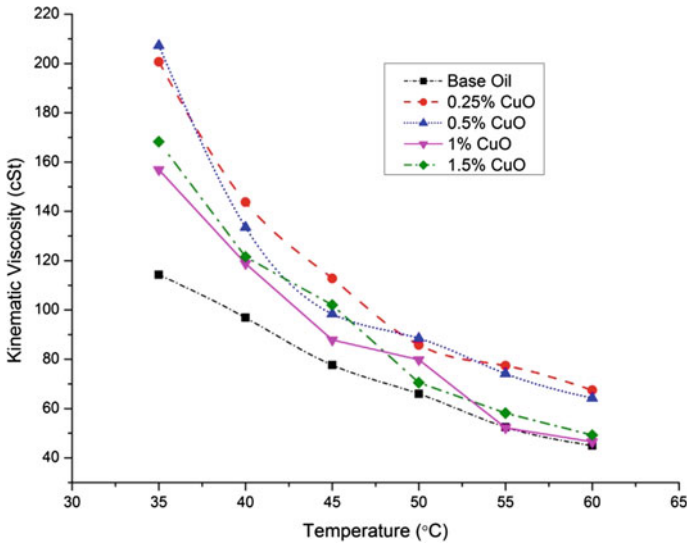


Fig. 3 Graph of Kinematic viscosity vs. temperature for various nanolubricant samples

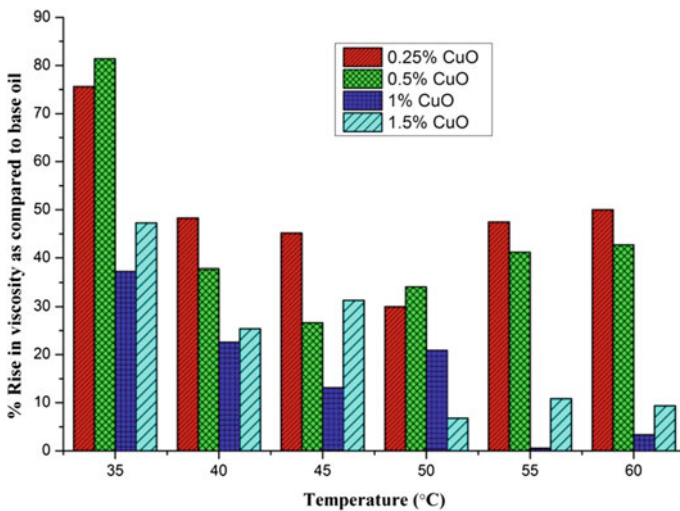


Fig. 4 Graph showing percentage rise in viscosity of nanolubricant samples w.r.t. base oil

7 Conclusion

Different nano lubricant samples containing base oil 15 W 40 and copper oxide nanoparticles in different weight proportions i.e. 0.25, 0.5, 1, 1.5% were prepared and checked for viscosity and dispersion stability. Addition of nanoparticles in base

oil demonstrates significant rise in the viscosity of base oil. However the increment in viscosity and weight proportion is not linear. Small amount of nano particles weight proportions i.e. 0.25 and 0.5% shows considerable rise in viscosity, while 1 and 1.5% samples show comparatively less increment in viscosity. The change in viscosity is more significant at lower temperatures. Thus it is concluded that small fractions of nano particles i.e. 0.25 and 0.5% are suitable for improving the viscosity of base oil. Maximum value of viscosity rise is 82% for 0.5% CuO sample at 35 °C as compared to base oil. Dispersion stability of samples containing 1 and 1.5% weight proportion of CuO Nano particles is poor. While the samples containing 0.25 and 0.5% weight proportions exhibit fairly good dispersion stability. Experimentation was carried out for measurement of flow viscosity; further, instruments like rheometer can be used for measurement of shear viscosity of nanolubricants to assess the effects of nanoparticle additives on shear behavior of nanolubricant. Besides viscosity, thermal properties of nanolubricants must be tested to gain insight in the lubrication mechanism offered by nanolubricants.

References

1. Kumar, H., & Harsha, A. P. (2021). Taguchi optimization of various parameters for tribological performance of polyalphaolefins based nanolubricants. *Proceedings of the Institution of Mechanical Engineers, Part J: Journal of Engineering Tribology*, 235, 1262–1280.
2. Ranjbarzadeh, R., & Chaabane, R. (2021). Experimental study of thermal properties and dynamic viscosity of graphene oxide/oil nano-lubricant. *Energies*, 14, 2886.
3. Akl, S., Elsoudy, S., Abdel-Rehim, A. A., Salem, S., & Ellis, M. (2021). Recent advances in preparation and testing methods of engine-based nanolubricants: A state-of-the-art review. *Lubricants*, 9, 85.
4. Zawawi, N. N. M., Azmi, W. H., Redhwan, A. A. M., Sharif, M. Z., & Samykano, M. (2018). Experimental investigation on thermo-physical properties of metal oxide composite nanolubricants. *International Journal of Refrigeration*, 89, 11–21.
5. Kedzierski, M. A., Brignoli, R., Quine, K. T., & Brown, J. S. (2017). Viscosity, density, and thermal conductivity of aluminum oxide and zinc oxide nanolubricants. *International Journal of Refrigeration*, 74, 3–11.
6. Chen, H., Ding, Y., & Tan, C. (2007). Rheological behaviour of nanofluids. *New Journal of Physics*, 9, 367.
7. Kole, M., & Dey, T. K. (2013). Enhanced thermophysical properties of copper nanoparticles dispersed in gear oil. *Applied Thermal Engineering*, 56, 45–53.
8. Mahbulul, I. M. (2019). 2-Preparation of nanofluid. In I. M. Mahbulul (Ed.), *Preparation, characterization, properties and application of nanofluid* (pp. 15–45). William Andrew Publishing.
9. Das, S. K., Choi, S. U., Yu, W., & Pradeep, T. (2007). *Nanofluids: Science and technology*. John Wiley & Sons.

Thermal Management of Electric Power Unit Using Phase Change Cooling Materials: Review, Classification, and Comparison



Roshan Mathew and Sateesh Patil

Abstract Electric Vehicles (EVs) are the latest transportation discoveries. Though EVs are very reliable there are a few factors that decrease their efficiency one of which is excess heat generation in the battery pack. Because of this, the thermal management system of batteries, have become crucial in electric vehicles to manage the heat produced by the battery and to increase the efficiency and performance for the vehicle. Battery thermal management can be done using different cooling methods which will be discussed further in the paper. In this review work, several Phase Change Materials used in earlier literature have been classified, compared, and studied.

Keywords Battery thermal management system · Phase change material · Electric vehicles

1 Introduction

The battery pack's thermal performance at various discharge rates is what determines how efficient an EV is. Two of the biggest issues with EVs are thermal runaway and electrolyte explosion. Typically, higher energy-related costs are needed when using an active approach that involves forced air movement or liquid circulation. Expectations are raised for this thermal control strategy because the BTM system operates passively without using external energy. The use of phase change material is one of the most successful passive methods. The phase transition process allows it to absorb a significant quantity of latent heat without raising the temperature. The benefits of using a PCM-based BTM system include passively lowering the maximum temperature rise and battery inconsistency because of this superior thermal control characteristic.

R. Mathew (✉) · S. Patil

Department of Mechanical Engineering, MIT School of Engineering, MIT Art, Design & Technology University, Pune, Maharashtra 412201, India

e-mail: roshanrobust@gmail.com

2 Battery Thermal Management System

Due to performance, lifespan, and high temperature sensitivity, maintaining the proper temperature range in Li-ion batteries is essential. The usage of a two-phase or three-phase material also known as a phase change material (PCM), which will be discussed as we move forward, can also be used to cool and regulate the temperature of batteries among all the battery thermal management systems that are now being utilised and researched.

3 Phase Change Materials

A phase change material is frequently employed in the field of battery thermal management because of its unique properties. It can either absorb or release latent heat to maintain temperatures that are nearly constant. A PCM is a substance which has the capacity to save thermal energy in sensible forms and latent forms reversibly and subsequently leave it by the opposite mechanism. In actuality, the PCM absorbs and stores the energy as the temperature rises, first in perceptible form and then in latent form when it reaches the phase transition temperature. The PCM will transition back to its starting phase and release the energy trapped throughout the operation when the temperature falls below the phase change temperature.

3.1 *Classification of Solid–Liquid Phase Change Materials*

See Fig. 1.

3.1.1 Organic Type of PCMs

A variety of substances make up organic PCMs. Table 1 displays the different compounds together with a number of their thermophysical characteristics.

3.1.2 In-organic Phase Change Materials

Table 2 lists the few inorganic compounds, eutectic mixtures and non-eutectic mixtures that have been thought as viable PCMs that can be used in low temperatures and high temperature applications. These include melting point, heat of fusion and other thermophysical characteristics (Table 3).

Fig. 1 PCM in general

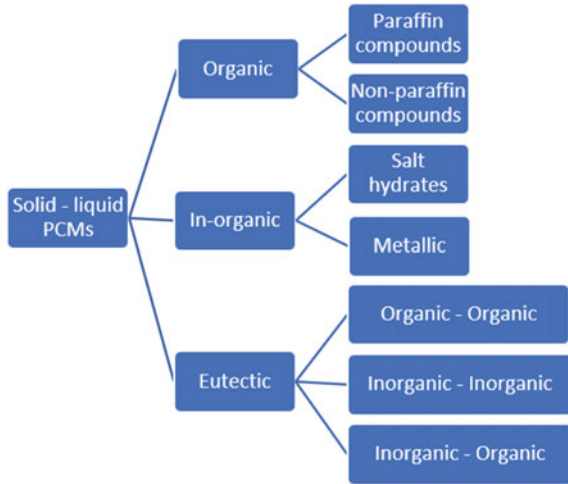


Table 1 Few types of organic materials that can be used as PCM [1–5]

Types	Compounds	Melting temperature (°C)	Fusion heat (J/g)
Paraffins	Tetradecane	5.8–6.0	227–229
	Pentadecane	9.9–10.0	206
	Hexadecane	18.0–20.0	216–236
	Heptadecane	22–22.6	164–214
Fatty acids	Caprylic acid	16.3	148
	CA	31.3–31.6	163
	LA	41–44	183–212
	MA	51.5–53.6	190–204.5
Fatty acid eutectic mixtures	CA or LA	17–21	143
	CA or PA	21.8	171.2
	LA or MA	34.2	166.8
	LA or PA	35.2	166.3

3.2 Conditions to Select Phase Change Materials

The following are the primary components of the selection rules:

1. Stability to chemical resistance and resistance to corrosion.
2. Easily available, not very costly and leak proof.
3. Good thermal conductivity.
4. Low degree of supercooling.
5. Ability to absorb heat.

Table 2 Few types of In-organic materials that can be used as PCM [6–9]

Types	Compounds	Melting temperature (°C)	Heat of fusion (J/g)
Salt hydrates	$\text{LiClO}_3 \cdot 3\text{H}_2\text{O}$	8	253
	$\text{KF} \cdot 4\text{H}_2\text{O}$	18.5–19	231
	$\text{Mn}(\text{NO}_3)_2 \cdot 6\text{H}_2\text{O}$	25.3	125.9
	$\text{CaCl}_2 \cdot 6\text{H}_2\text{O}$	28.0–30.0	190–200
Other compounds	AlCl_3	192	280
	LiNO_3	250	370
	NaNO_3	307	172
	KNO_3	333	266
Other eutectic mixtures			
	H_2O + polyacrylamide	0	292
	50% $\text{Na}(\text{CH}_3\text{COO}) \cdot 0.3\text{H}_2\text{O}$ + 50% HCONH_2	40	255

3.3 Phase Change Materials Specifications

It's crucial to consider the PCMs' many qualities, including their thermal, physical, kinetic, chemical, and economic characteristics, in order to select one that is appropriate for the system under study [10–13].

3.3.1 Thermal Properties

The temperature of the PCM must be equal to the system's operational temperature. It is between 20 and 25 °C for Li-ion battery systems. To hold all the heat generated by the system, its latent heat should be sufficiently large. It must have a high enough thermal conductivity which causes rapid heat storage and transmission. Some material having high conductivity, such as graphene or other similar materials like expanded graphite etc. along with metallic fins and nanomaterials is used to increase the low thermal conductivity.

3.3.2 Physical Properties

The change between the volume of the liquid and solid phases, should be kept to a minimum to prevent the PCM from damaging its surroundings as it expands. To achieve a high energy density storage, it is good for the PCM to have the ability to store a great energy during phase transition so that it may store a large energy in a small space.

Table 3 The benefits and drawbacks of eutectic, inorganic, and organic PCM

	Organic materials	Inorganic materials	Eutectic materials
Examples	1. Paraffin	1. Salt hydrates	1. Inorganic–organic
	2. Fatty acids	2. Metallics	2. Inorganic–inorganic
	3. Alcohol		3. Organic–organic
	4. Ester		
	5. Polyethylene glycol		
Advantages	1. Non-corrosiveness	1. Non-flammable	1. Wide variation for phase change temperatures
	2. Good chemical and thermal stability	2. Inexpensive	2. Great chemical and great thermal stability
	3. Zero supercooling	3. High fusion heat	3. High heat capacity
	4. High fusion heat	4. Great thermal conductivity	4. Zero supercooling
	5. Low vapour pressure		
	6. Nontoxic		
Disadvantages	1. Low thermal conductivity	1. Corrosion	1. Leakage during phase change
	2. Low phase change enthalpy	2. Phase decomposition	2. Low thermal conductivity
	3. High changes in volume	3. High super cooling effect	
		4. Loss of hydrate throughout the process	
		5. Insufficient thermal stability	

3.3.3 Chemical Properties

To prevent the degradation of its shell, the PCM should ideally be stable, should not be toxic, and should not be corrosive. The PCM must be widely accessible and inexpensive.

4 Battery Thermal Management Using Phase Change Materials

The PCM cooling technique has steadily supplanted aforementioned three conventional cooling techniques as the main choice for BTMS due to its benefits of requiring no extra equipment, simplicity, and very less cost. Because of PCM’s capacity to absorb and release heat as a result of the significant phase change in latent heat,

the group can maintain a secure range of operating temperature for an amount of time. To support the benefits of BTMS with PCM, Sabbah [14] looked into the effects of passive cooling centered on PCM with force air cooling. Unlike force air cooling, which utilizes fans for those reasons, passive cooling based on PCM uses graphite composite PCM to cool and spread heat all around item. The test findings demonstrated that, under conditions of high discharge rates and high temperatures, BTMS utilizing PCM was much more efficient at cooling and diffusing heat. These experiments suggest that the PCM battery temperature of the BTMS was operating normally.

Kizilel [15] investigated the effectiveness of BTMS using PA/graphite composite PCM as the lithium battery module, and results revealed the system was able to successfully address the issue of battery overheating and could control the temperature within 45 °C when the battery was discharged [15–17]. PCM components give BTMS enhanced compactness over the complex conventional cooling system while also reducing weight and production costs. If PCM-based passive components were used, the cost of design would be substantially cheaper and more affordable. Inside a battery, heat can be produced in three different ways chemically, internally, through internal resistance, and polarisation [18]. In experimental research, Mills et al. [19] found that the use of PCM infused with EG can significantly reduce the lack of heat transmission. The entire heat produced in the battery is calculated as the product of the heating power and the time, as per the temperature control period and the heat that the battery can produce. The battery generates heat which can be calculated as the addition of the PCM's sensible heat and the latent heat and convective heat dissipation. Because convective heat loss is so little, it may be skipped. The following mathematical equation might be used to express the definition above:

$$Q = m \text{ cp } \Delta T + mH \quad (1)$$

Q = amount of heat given out by the battery,

m = required mass of the PCM,

cp = capacity for specific heat,

T = internal temperature difference, H = phase change enthalpy.

5 Conclusion

When compared to organic PCMs as well as the inorganic PCMs have a greater latent heat capacity when calculated as per volume and also a higher thermal conductivity. Although, these tend to be more corrosive when in contact with metallic materials and supercooling effects might have a negative impact on their phase-change characteristics. Being chemically stable, noncorrosive, and having a high phase transition heat capacity, organic PCMs are most promising materials to provide best results due to their chemical and thermal properties. They also exhibit consistent liquifying and freezing behaviour after a large number of thermal cycles.

Furthermore, there are numerous approaches to improve the PCMs' performances:

- by boosting the PCM's thermal conductivity by using high conductivity parts like fins, by encasing the coolant using expanded graphite matrices, metallic foam, etc.
- by performing experiments with the properties of the extended graphite or the foam's density.
- by increasing PCM surface or bulk.

References

1. Paris, J., Falardeau, M., & Villeneuve, C. (1993). Thermal storage by latent heat: A viable option for energy conservation in buildings. *Energy Sources*, *15*, 85–93.
2. Nagano, K., Mochida, T., Takeda, S., Domanski, R., & Rebow, M. (2003). Thermal characteristics of manganese (II) nitrate hexahydrate as a phase change material for cooling systems. *Applied Thermal Engineering*, *23*, 229–241.
3. He, B., Gustafsson, E. M., Setterwall, F. (1999). Tetradecane and hexadecane binary mixtures as phase change materials (PCMs) for cool storage in district cooling system. *Energy*, *24*, 1015–1028.
4. Feldman, D., Shapiro, M. M., Banu, D., & Fuks, C. J. (1989). Fatty acids and their mixtures as phase-change materials for thermal energy storage. *Solar Energy Materials*, *18*, 201–216.
5. Sari, A., & Kaygusuz, K. (2002). Thermal and heat transfer characteristics in a latent heat storage system using lauric acid. *Energy Conversion and Management*, *43*, 2493–2507.
6. Khudhair, A. M., & Farid, M. M. (2004). A review on energy conservation in building applications with thermal storage by latent heat using phase change materials. *Energy Conversion and Management*, *45*, 263–275.
7. Hasanain, S. (1998). Review on sustainable thermal energy storage technologies. Part I. Heat storage materials and technologies. *Energy Conversion and Management*, *39*, 1127–1138.
8. Heine, D., & Heess, F. (Eds.). (1980). Chemische und physikalische Eigenschaften von Latentwärmespeichermaterialien für Solarkraftwerke. In *3rd International Solarforum*, Hamburg, Germany (in German).
9. Bilen, K., Takgil, F., & Kaygusuz, K. (2008). Thermal energy storage behavior of $\text{CaCl}_2 \cdot 6\text{H}_2\text{O}$ during melting and solidification. *Energy Sources, Part A: Recovery, Utilization, and Environmental Effects*, *30*, 775–787.
10. Faraj, K., Khaled, M., Faraj, J., Hachem, F., & Castelain, C. (2020). A review on phase change materials for thermal energy storage in buildings: Heating and hybrid applications. *Journal of Energy Storage*.
11. Khan, Z., Khan, Z. A., & Ghafoor, A. (2016). A review of performance enhancement of PCM-based latent heat storage system within the context of materials, thermal stability, and compatibility. *Energy Conversion and Management*, *115*, 132–158.
12. Achard, P., & Mayer, D. (1989). Heat Sink Material, US4816173 A.
13. Eddahech, A. (2013). Modélisation du vieillissement et détermination de l'état de santé de batteries lithium-ion pour application véhicule électrique et hybride (PhD thesis). Université Sciences et Technologies - Bordeaux I (in French).
14. Qi, G.-Q., Yang, J., Bao, R.-Y., Liu, Z.-Y., Yang, W., Xie, B.-H., & Yang, M.-B. (2015). Enhanced comprehensive performance of polyethylene glycol based phase change material with hybrid graphene nanomaterials for thermal energy storage. *Carbon*, *88*, 196–205.
15. Salunkhe, P. B., & Shembekar, P. S. (2012). A review on effect of phase change material encapsulation on the thermal performance of a system. *Renewable and Sustainable Energy Reviews*, *16*, 5603–5616.

16. Kizilel, R., Lateef, A., Sabbah, R., Farid, M., Selman, J., & Al-Hallaj, S. (2008). Passive control of temperature excursion and uniformity in high-energy Li-ion battery packs at high current and ambient temperature. *Journal of Power Sources*, *183*, 370–375.
17. Duan, X., & Naterer, G. (2010). Heat transfer in phase change materials for thermal management of electric vehicle battery modules. *International Journal of Heat and Mass Transfer*, *53*, 5176–5182.
18. Zhang, X. (2011). Thermal analysis of a cylindrical lithium-ion battery. *Electrochimica Acta*, *56*, 1246–1255.
19. Mills, A., & Al-Hallaj, S. (2005). Simulation of passive thermal management system for lithium-ion battery packs. *Journal of Power Sources*, *141*, 307–315.

Polyaniline Nanofibers Based Freestanding Electrode with High Electrochemical Performance for Supercapacitors



A. C. Molane, S. S. Gavande, A. S. Salunkhe, R. N. Dhanawade, R. N. Mulik, and V. B. Patil

Abstract High-performance supercapacitors grasp great potential for applications like portable electronic gadgets, electric vehicles etc. Effective flexible morphology is an important aspect for supercapacitors. Here, we present a novel electrospinning technique to fabricate flexible supercapacitive electrodes based on polyaniline (PAni) nanofibers. The structural relevance of PAni was evidenced by XPS, the thin nanofibrous morphology was confirmed through SEM. The contact angle was found to be 40° which reveals hydrophilic nature. The electrode revealed an excellent 204 F/g specific capacitance at 1 mV/s scan rate. Moreover, the electrode delivers specific energy up to 52.43 Wh/kg along with specific power of 12.78 kW/kg for corresponding current density of 1 mA/cm², tested in aq. 1 M KOH electrolyte. The retention of 92.03% of opening capacitance over 1000 cycles offered outstanding electrochemical stability. Thus, polyaniline nanofibers based electrode signifies great practical applicability in flexible devices for storing energy.

Keywords Supercapacitor · Electrospinning · Polyaniline · Nanofibers · Wettability · Cyclic voltammetry · Cyclic stability

1 Introduction

Flexible supercapacitors have recently grabbed tremendous attention as a smart energy source for portable electronics applications by virtue of efficient harvesting, storage and energy management [1, 2]. The most studied charge storage mechanism

A. C. Molane · S. S. Gavande · A. S. Salunkhe · R. N. Dhanawade · V. B. Patil (✉)
Functional Materials Research Laboratory, School of Physical Sciences, Punyashlok Ahilyadevi Holkar Solapur University, Solapur, Maharashtra, India
e-mail: drvbpatil@gmail.com

R. N. Mulik
Department of Physics, D. B. F. Dayanand College of Arts and Science, Solapur, Maharashtra, India

dependent electrode materials for electrochemical supercapacitors can be classified into three categories; including nano-carbon materials based electric double layer capacitors (EDLC) which utilize the electrochemical performance arising from electrostatic charges separation at electrode/electrolyte interface. Besides, metal oxide as well as conducting polymer based pseudocapacitors present reversible redox reaction (faradic reaction) occurring at or near the electrode surface, whereas the hybrid type involves both the mechanisms [3, 4].

Amongst the electrically conducting polymers, polyaniline (PAni) based electrodes mostly investigated for electrochemical properties and it has gained significant interest as a pseudocapacitor material due to simple and cost effective synthesis process, retaining environmental stability, unique electronic properties, high conductivity, and good redox behavior [5, 6]. However, comparing to bulk structure and dense packed PAni materials, the 1D nanomaterials exhibit higher surface area and surface-to-volume ratio which can improve ion diffusion capability within electrode, and the orientation of electron along 1D structure and ion transport within material facilitates fast electrochemical strategy. Consequently, it is an urgently required to develop an effective 1D nanomaterials-based electrode with an improved charge transfer as well as storage properties [7]. Doing so, a versatile top-down approach i.e. electrospinning technique offers to fabricate 1D nanofibers with dimensions of nanometers scale by electrostatic forces.

In the present work, we report polyaniline (PAni) based flexible electrode by simple and facile electrospinning technique with superior electrochemical properties. The structural relevance and morphological analysis are characterized by XPS and SEM. Further, wettability of electrode surface is studied by water contact angle measurement. The electrochemical study of flexible nanofiberous electrode was done by Chronopotentiometry technique and cyclic voltammetry using three-electrode system (CHI608E) in 1 M KOH electrolyte. The cyclic stability of electrode for 1000 cycles was tested, so as to make it applicable in long-term durable energy storage mechanism.

2 Experimental Details

In-situ polymerization method is employed for synthesis of PAni powder. Aniline and Ammonium persulfate (APS) were chosen as monomer and an oxidant solution respectively. For the polymerization process, 4.998 g of APS was added in 2 ml Aniline and 1 M HCl mixture, then resultant mixture was stirred for 7 h at room temperature. After polymerization, the green colored yield was filtered and washed with the help of 1 M HCl and distilled water for several times. Finally, from emeraldine salt (ES) form, PAni is obtained. The PAni/PVA solution for electrospinning process was prepared by dissolving 22 wt% of ES PAni powder and 8 wt% of PVA in 20 ml distilled water was stirred for 5 h and then transferred into plastic syringe. In a typical electrospinning process; Potential difference—14 kV, collector-to-needle

tip distance—14 cm and flow rate of 0.5 mL per hour. Lastly, the continuous as-spun PANi nanofibers network were obtained on flexible collector. The elemental analysis of PANi NFs was examined using XPS (VG, Multilab 2000), whereas, by SEM (Model JEOL-6300F), morphology of the surface of electrode was studied. To explore electrode's wettability, the CA measurement (Ramehart, USA instrument with CCD camera) was carried out. All the electrochemical studies were examined by a three-electrode system using electrochemical workstation (CHI608E) in 1 M KOH aqueous electrolyte.

3 Results and Discussion

3.1 Structural and Surface Morphological Elucidation

The chemical states of nanofibers based PANi material along with binding energy were found out by X-ray photoelectron spectroscopy with results been displayed in Fig. 1a. The wide range survey spectrum evidences the presence of carbon (C-1s), oxygen (O-1s) and nitrogen (N-1s) elemental peaks, which inferred the formation of PANi. The key characteristic (located at binding energy of 284.8 eV) of C-1 s spectrum on account of C–C bond, the core level spectrums i.e. N-1s located at binding energy of 399.42 eV (existence of single benzenoid amine) and O-1s at 531.54 eV (revealing the presence of absorbed water as well as C–O group due to unavoidable surface contamination owned by carbon hydrates) [8, 9]. The morphology of fabricated PANi nanofibers was analyzed by SEM. Figure 1b displays the SEM image of electrospun PANi nanofibers which demonstrated randomly oriented, continuous and bulk morphology of fibers with diameter around 220 nm. The 1-D structured nanofibers are so significantly oriented that they help in achieving fast electrons/ions penetration during electrochemical process and thus improve supercapacitive performance [7].

3.2 Wettability Study

The wetting ability of electrolyte with solid surface electrode was estimated by contact angle measurement. Figure 1c demonstrates the digital photograph of contact angle with surface of nanofibers based PANi Electrode, which exhibited 40° of water contact angle value i.e. more wettability with hydrophilic behavior (< 90°). The hydrophilic nature is considerably beneficial property for making better interfacial contact of an aqueous electrolyte with surface of an electrode during the electrochemical process [10] and is regarded as a key factor to improve supercapacitive performance.

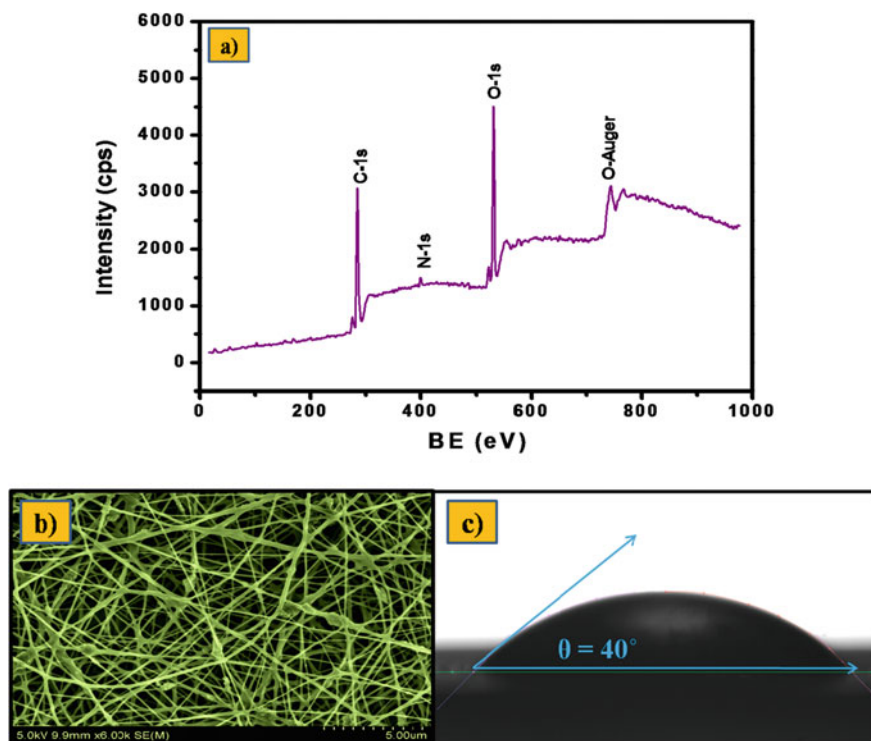


Fig. 1 a XPS survey spectra, b SEM image, c CA measurement of PANi electrode

3.3 Cyclic Voltammetry

The electrochemical study of nanofibrous PANi electrode was done by cyclic voltammetry analysis in 1 M KOH electrolyte at various scan rates. Figure 2a displays cyclic voltammetry plot for scan rate 1–100 mV/s in the -1.3 to -0.3 V potential window. It demonstrated an ideal capacitive behaviour i.e. current under the curve steadily enhances with respect to scan rate and the decrement in specific capacitance value is due to slow diffusion of ions to accessible sites of active material [11, 12]. The change in specific capacitance value with scan rate is shown in Fig. 2b.

The cycleability of PANi electrode was taken by repeating cyclic voltammetry for 1000 cycles for scan rate of 100 mV/s 1 M aqueous KOH electrolyte are shown in Fig. 2c, and it demonstrated to be chemically stable over the entire cycles. The nanofibers based PANi electrode retained 92.03% of opening capacity even after 1000 cycles which is presented by specific capacitance variation vs. cyclic number in Fig. 2d. Thus, stability study suggests the electrode to be potentially applied in the energy-storage devices with an outstanding cyclic life [13].

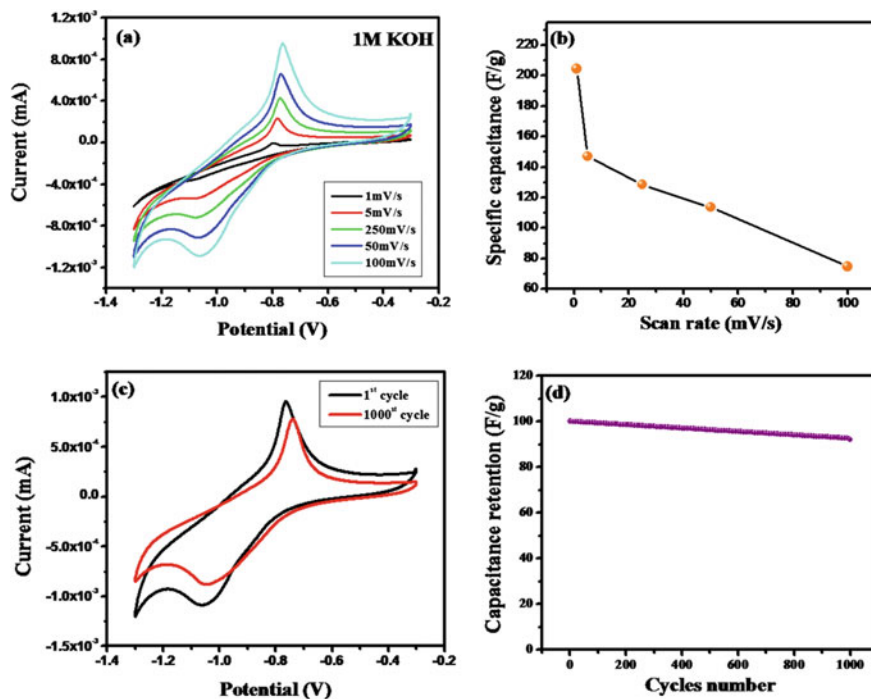


Fig. 2 a Cyclic voltammograms for different scan rates, b specific capacitance versus scan rate (1–100 mV/s), c cyclic stability for 1000 cycles at 100 mV/s scan rate, d specific capacitance retention of nanofibers based PANi electrode tested in aq. 1 M KOH electrolyte

3.4 Galvanostatic Charge–Discharge Study

The galvanostatic charging–discharging behaviour of PANi electrode was examined at 1 mA/cm² current density for the voltage window of – 1.3 to – 0.3 V in 1 M KOH. Figure 3a displays the typical charge–discharge plot. The charging–discharging profile is close to non-linear, isosceles triangle, which indicates common pseudo-capacitive behaviour. The discharging curve usually shows two parts; first one belongs to capacitive component i.e. potential ΔV_1 falls hurriedly because of an equivalent series resistance (ESR) and change in the energy values of electrochemical capacitor, whereas, voltage decrement ΔV_2 caused by internal resistance as in Fig. 3b [14, 15]. The specific energy and specific power were calculated from charging discharging curve and took values 52.43 Wh/kg and 12.78 kW/kg respectively, at 1 mA/cm² current density.

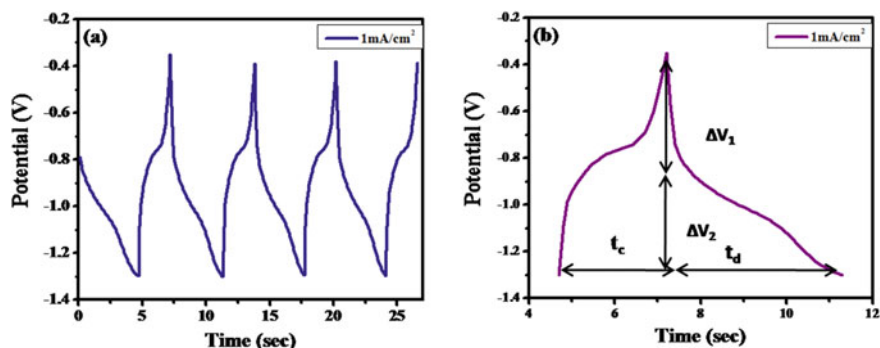


Fig. 3 a Galvanostatic charge–discharge cycles at 1 mA/cm^2 , b a representative cycle of nanofibers based PANi electrode tested in 1 M KOH aqueous electrolyte at 1 mA/cm^2

4 Conclusion

In this work, we have successfully fabricated nanofibers based polyaniline flexible electrode by electrospinning route. The presence of characteristic bands of expected chemical states are confirmed through X-ray photoelectron spectroscopy analysis. The continuous and thin nanofiber structure formation was observed by scanning electron micrograph image. The PANi electrode surface showed hydrophilic nature with contact angle 40° . The nanofibers based polyaniline electrode exhibits specific capacitance 204 F/g for the scan rate of 1 mV/s tested in 1 M KOH and capacity retention about 92.03% of over 1000 CV cycles indicating good cyclic stability. The charge–discharge time dependent electrochemical parameters include specific energy and specific power were found to be 52.43 Wh/kg and 12.78 kW/kg respectively, at 1 mA/cm^2 current density. The freestanding format of the nanofibers based polyaniline sheds light on flexible electrode material for supercapacitor with long-life stability.

Acknowledgements Prof. V. B. Patil is thankful to Rajiv Gandhi Science and Technology Commission for their financial support, Grant Id: RGSTC/file-2019/PAHSUS/CR-91 dated 23/12/2019. Also the authors are thankful to Chhatrapati Shahu Maharaj Research Training and Human Development Institute (SARTHI), Pune for their financial support.

References

1. More, P. D., Jadhav, P. R., Ingole, S. M., Navale, Y. H., & Patil, V. B. (2017). *Journal of Materials Science: Materials in Electronics*, 28, 707–714.
2. Gavande, S. S., Kulkarni, P. S., Karche, B. R., Gavande, S. S., & Patil, V. B. (2021). *Macromolecular Symposium*, 393, 2000169–2000175.
3. Kaur, M., Chand, P., & Ananda, H. (2022). *Chemical Physics Letters*, 786, 181.

4. Navale, Y. H., Navale, S. T., Chougule, M. A., Ingole, S. M., Stadler, F. J., Mane, R. S., Naushad, M., & Patil, V. B. (2017). *Journal of Colloid and Interface Science*, 487, 458.
5. Yang, R., Bai, X., Guo, X., Song, K., Jia, L., Chen, X., & Wang, J. (2022). *Applied Surface Science*, 586, 152574.
6. Gavande, S. S., Salunkhe, A. S., Navale, Y. H., Gavande, S., Kulkarni, P. S., & Karche, B. R. (2020). *AIP Conference Proceedings*, 2265, 030615.
7. Cheng, J., Wang, B., Gong, S., Wang, X., Sun, Q., & Liu, F. (2021). *Ceramics International*, 47, 32727.
8. Dhole, I. A., Navale, Y. H., Pawar, C. S., Navale, S. T., & Patil, V. B. (2018). *Journal of Materials Science: Materials in Electronics*, 29, 5675.
9. Bandgar, D. K., Navale, S. T., Nalage, S. R., Mane, R. S., Stadler, F. J., Aswal, D. K., Gupta, S. K., & Patil, V. B. (2015). *Journal of Materials Chemistry C*, 3, 9461–9468.
10. Dhavale, S., Patil, V., Beknalkar, S., Teli, A., Patil, A., Patil, A., Patil, P., & Shin, J. (2020). *Journal of Colloid and Interface Science*, 588, 589.
11. Navale, Y. H., Navale, S. T., Chougule, M. A., Ingole, S. M., Stadler, F. J., Mane, R. S., Naushad, M., & Patil, V. B. (2017). *Journal of Colloid and Interface Science*, 487, 458–464.
12. Wang, G., Zhan, L., & Zhang, J. (2012). *Chemical Society Reviews*, 41, 797.
13. Simotwo, S. K., DelRe, C., & Kalra, V. (2016). *ACS Applied Materials & Interfaces*, 8, 21261–21269.
14. Navale, S. T., Mali, V. V., Pawar, S. A., Mane, R. S., Naushad, M., Stadler, F. J., & Patil, V. B. (2015). *RSC Advances*, 5, 51961–51965.
15. Acharya, J., Park, M., Koa, T., & Kim, B. (2021). *Journal of Alloys and Compounds*, 884, 161165.

Dynamic Analysis of Rotating Composite Beam and Their Numerical Analysis Using COMSOL



Avinash K. Parkhe, Prashant M. Pawar, Sandeep S. Wangikar,
Digambar T. Kashid, and Pradnya K. Patil

Abstract Rotary beams play a significant role in engineering structures such as turbine blades, aircraft propellers and robotic manipulators. In this paper we have studied the analytical and numerical analysis of composite beam in dynamic condition. Centrifugal Force acts on the beam while rotating it at different RPM. By using this concept the analytical study is carried out for this rotating beam in which centrifugal forces are calculated for different RPM. Due to this force stress is induced in the beam at different locations. Also the elongation of the beam will take place in rotating condition. The analytical study has been carried out for measurement of stresses and elongation of beam. For the measurement of elongation of beam we have used the Finite Element Method (FEM). The analysis of beam is also carried out using COMSOL. In this software, the test specimens were modeled in accordance to analytical specimens. The numerical study is concerned with stresses induced and elongation of rotating composite beams for different rpm. This study is important to understand the effect of RPM on Stress, Elongation. After this study we have observed that there is no much difference between in the both analysis. The study of beam has been carried out at various end conditions of the beam.

Keywords Composite box beam · Centrifugal force · Stress · Elongation · FEM · COMSOL

A. K. Parkhe (✉) · S. S. Wangikar · D. T. Kashid · P. K. Patil
Department of Mechanical Engineering, SVERI's College of Engineering, Pandharpur,
MH 413304, India
e-mail: akparkhe@coe.sveri.ac.in

P. M. Pawar
Department of Civil Engineering, SVERI's College of Engineering, Pandharpur, MH 413304,
India

1 Introduction

The use of composite materials has continued to grow in a number of industries such as civil engineering, mechanical engineering and aeronautics. One of the most striking properties of the composite structure is its very high rigidity in relation to weight. Composite accounts are strong performers. In helicopter rotor applications, composites offer additional features such as a dramatic reduction in parts count and bulk, especially for the rotor hub system, which is typically a large source of profile thrust.

The analytical and numerical study is carried out on rotating beam for various rpm. It has been observed that the centrifugal force acts on in rotating condition and it get increases also with increase in rpm. Therefore, rpm of beam is varying from 50 to 400 rpm and for each rpm centrifugal forces are calculated. During stress analysis centrifugal forces are calculated by assuming that mass is concentrated at center of beam. Once the centrifugal forces and cross area of composite beam is known, the stresses induced in beam are calculated and it maximum near fixed end of the rotating beam. For axial deformation or elongation centrifugal forces are calculated by assuming that mass is concentrated at free end of the rotating beam and due to the application of deformation of beam will take place in axial direction. The analytical study is carrying out using Finite Element Method (FEM). Also the analysis has been carried out for same parameters by using COMSOL and the results obtained results are compared with analytical results.

Investigations were carried out on rotating box girders made of composite materials. Rao [1] studied the dynamic analysis of a rotating cantilever using the finite element method to calculate the time response and distribution of strain and stress as the rotational speed dictates. The effect of rotational velocity profile on beam vibration has also been studied. Yao et al. [2] to investigate the nonlinear vibration of blades with varying rotational speeds. Various rotational speeds and centrifugal forces are taken into account during the creation of the analytical model of the rotating blades. Otsuka et al. in [3], the deformation and stress of the rotor blades of an axial compressor under centrifugal force loading were discussed for the elimination of the rotor twist. Sina et al. [4] an axial torsional vibration rotating pre-twisted thin-walled composite beams. Ramazan-Ali Jafari-Talookolaei, Christian Della, et al. [5] dynamic behavior of rotational detachment composite beams including rotational inertia and shear deformation effects [7, 8].

In this paper, effect of increasing RPM of rotating beam on parameters like Stresses induced in beam and deformation of beam in axial direction due to centrifugal is studied. Dynamic analysis of beam has been carried out by using COMSOL [3, 6].

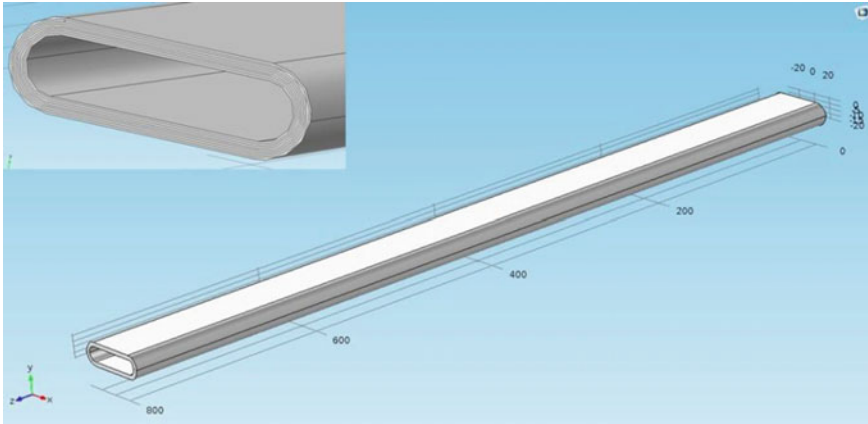


Fig. 1 Model of composite box beam in COMSOL

2 Introduction Composite Box Beam

The composite beam having cross-section area of $800 \times 60 \times 22$ mm. This beam is made of eight layers. The geometry of beam used for the analysis is shown in Fig. 1.

3 Stress Analysis of Composite Beam in Dynamic Condition

3.1 Analytical Analysis of Beam

The theoretical analysis has been carried out on composite beam which is rotating for different rpm. During rotating condition centrifugal force acts on beam and it will vary with different rpm. The Forces are calculated for different rpm (i.e. 50–400 rpm) by assuming that mass is concentrated at center. By using this forces and cross section area of beam we can calculate the stresses induced in beam and it is assumed that stress will remain constant to all cross section of beam for that particular force. Figure 2 indicates that, how centrifugal force is acts on rotating composite beam.

3.1.1 Introduction to Centrifugal Force

The concept of centrifugal force can be applied to rotating equipment such as centrifuges, centrifugal pumps, centrifugal governors, and centrifugal clutches, as well as centrifugal orbits, planetary orbits, and tilt curves when analyzed in a rotating

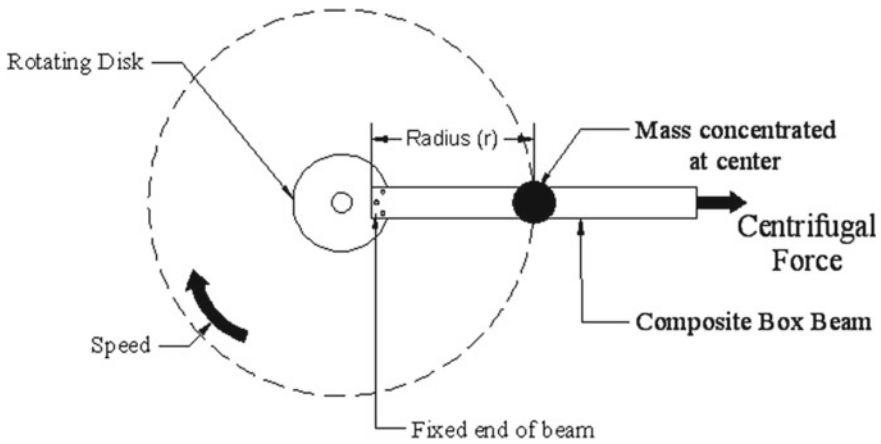


Fig. 2 Centrifugal force on rotating composite beam (mass concentrated center)

coordinate system. Centrifugal force is the outward force seen in a rotating coordinate system. Not present if measurements are taken in the inertial frame of reference. The formula of centrifugal force and centrifugal stress for rotating beam along with figure is given below.

$$\text{Centrifugal Force } (F_c) = m\omega^2r$$

where

m = mass,

ω = angular velocity = $\frac{2\pi N}{60}$,

r = radius,

Stress $(\sigma) = \frac{F_c}{Area}$.

The cross sectional area, mass and radius of composite box beam are given below.

$$Area = 618.19 \text{ mm}^2 = 0.00061819 \text{ m}^2 \quad m = 1.6 \text{ kg} = 1600 \text{ g}$$

$$r = 400 \text{ mm} = 0.4 \text{ m} \quad (\text{due mass is concentrated at center}).$$

The sample calculations for stress induced in beam due to centrifugal force of that particular rpm are given below and stresses for other rpm are presented in tabular form with its forces (Table 1).

(1) 50 RPM

$$\text{Angular velocity } (\omega) = \frac{2\pi N}{60} = \frac{2 \times \pi \times 50}{60} = 5.23 \tag{1}$$

$$\text{Centrifugal Force } (F_c) = m\omega^2r = 1.6 \times 5.23^2 \times 0.4 \tag{2}$$

$$F_c = 17.50 \text{ N}$$

Table 1 Stresses in rotating beam (analytical results)

Sr. No.	RPM	Centrifugal force (N)	Analytical stress (N/m ²)
1	50	17.50	2.83×10^4
2	100	73.82	1.19×10^5
3	150	157.75	2.55×10^5
4	200	280.62	4.53×10^5
5	250	438.31	7.09×10^5
6	300	631.41	1.02×10^6

$$\text{Stress } (\sigma) = \frac{Fc}{Area} = \frac{17.50}{0.00061819}$$

$$\sigma = 2.83 \times 10^4 \text{ N/m}^2 \tag{3}$$

3.2 Numerical Analysis Using COMSOL

Simulations were performed using the software package COMSOL Multiphysics. COMSOL Multiphysics is a powerful interactive environment for modeling and solving all kinds of scientific and engineering problems. It is used for composite box girder modeling and girder stress calculations.

Simulations are run for composite beams with different velocities and different forces and the stresses are calculated. Numerical stress results are measured at the fixed end of the beam. This is similar to the analysis result. The simulated results are presented below in numerical and tabular form (Fig. 3; Table 2).

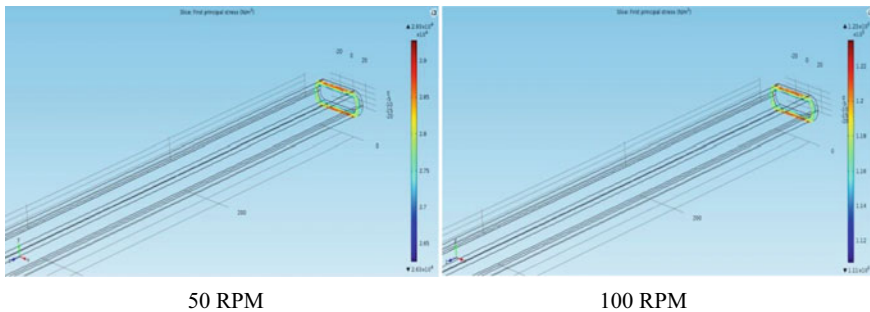


Fig. 3 Numerical results of stress for different RPM of beam

Table 2 Stresses in rotating beam (numerical results)

Sr. No.	RPM	Centrifugal force (N)	Numerical stress (N/m ²)
1	50	17.50	2.93×10^4
2	100	73.82	1.23×10^5
3	150	157.75	2.64×10^5
4	200	280.62	4.69×10^5
5	250	438.31	7.33×10^5
6	300	631.41	1.06×10^6

From above results, as RPM of beam is increases with its force then stress value are also increases. The graph of RPM versus analytical and numerical stress is shown in Fig. 4.

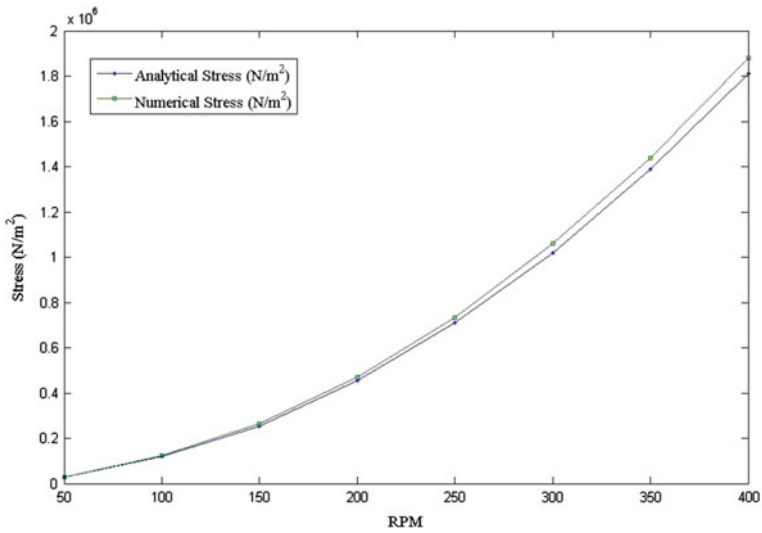


Fig. 4 Graph of RPM versus stress

4 Elongation or Displacement of Composite Box Beam in Rotating Condition

4.1 Analytical Study

We have studied above about centrifugal force on rotating composite beam. Due this force the deformation or elongation of beam take place at its free end and it is vary with increase in rpm. Therefore, the centrifugal forces are calculated for different rpm of beam by assuming that mass is concentrated at free end of beam. Due to increasing in rpm, the axial deformation or elongation will take place at its free end and it is in negligible quantity. The analytical study is carrying out using Finite Element Method (FEM) by considering it as 1D Problem (Fig. 5).

4.1.1 Deformation of Beam Using FEM

As discussed above the centrifugal forces are calculated for different rpm of beam. These forces are applied on beam to find its axial deformation is shown by Fig. 6. Therefore, beam is considered as 1D element during analytical analysis.

Let, as shown in above figure beam is considered as 1D problem having two nodes. u_1 and u_2 are displacement of beam at two nodes. There is no deformation at fixed end so u_1 becomes zero and our purpose is to find u_2 at free end of the beam. The u_2 is considered as axial deformation or elongation of beam for that particular rpm and force. The element equations are assembled to obtain the system equation, which describe the behavior of the body as a whole. These generally take the form.

$$\{F\} = [k]\{U\}$$

(1) 50 RPM

First we calculate force (F) acting on beam for given rpm.

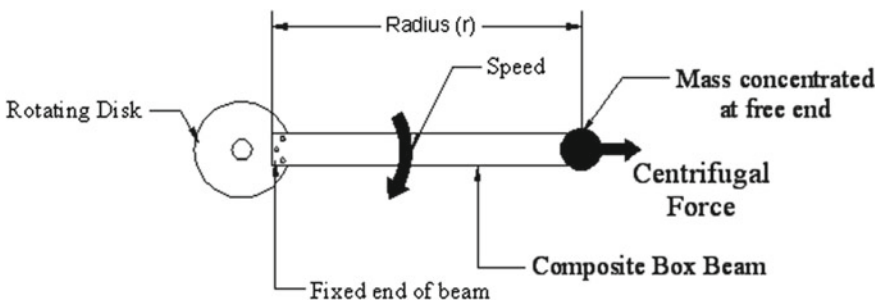


Fig. 5 Centrifugal force on rotating composite beam

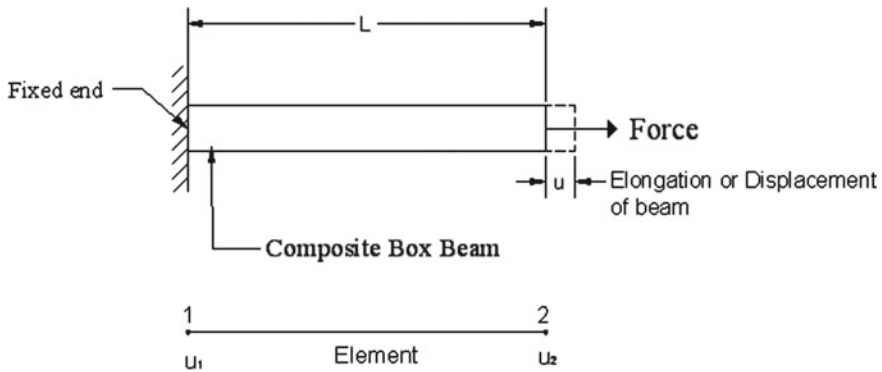


Fig. 6 Finite Element Method for beam deformation

$$\text{Centrifugal Force } (F_c) = m\omega^2 r = 1.6 \times 5.23^2 \times 0.8$$

$$F_c = F = 35.01 \text{ N} \tag{4}$$

Then, calculate the stiffness matrix $[k]$.

$$k = \frac{AE}{L} [1 \quad -1 \quad -1 \quad 1]$$

$$k = \frac{10 \times 10^3 \times 618.19}{800} [1 \quad -1 \quad -1 \quad 1]$$

$$k = 10^3 [7.72 \quad -7.72 \quad -7.72 \quad 7.72] \tag{5}$$

$$\{F\} = [k]\{U\}$$

$$35.01 = 10^3 [7.72 \quad -7.72 \quad -7.72 \quad 7.72] \begin{pmatrix} u_1 \\ u_2 \end{pmatrix}$$

There is zero deformation at node 1 due to fixed end, therefore, $u_1 = 0$.

$$35.01 = 10^3 [7.72 \quad -7.72 \quad -7.72 \quad 7.72] \begin{pmatrix} 0 \\ u_2 \end{pmatrix}$$

$$35.01 = 7.72 \times 10 \times 10^3 \times u_2 \tag{6}$$

Therefore, Deformation of beam = $u_2 = 4.53 \times 10^{-3} \text{ mm}$ (Table 3).

Table 3 Axial deformation of beam for different RPM (analytical results)

Sr. No.	RPM	Force (N)	Analytical deformation (mm)
1	50	35.01	4.53×10^{-3}
2	100	147.64	0.019
3	150	315.50	0.040
4	200	561.24	0.072
5	250	876.62	0.1135
6	300	1262.82	0.1635

Table 4 Axial deformation of beam for different RPM (numerical results)

Sr. No.	RPM	Force (N)	Numerical deformation (mm)
1	50	35.01	4.52×10^{-3}
2	100	147.64	0.02
3	150	315.50	0.04
4	200	561.24	0.07
5	250	876.62	0.11
6	300	1262.82	0.16

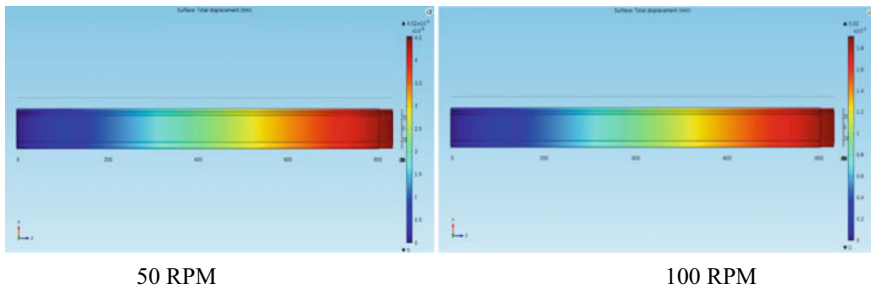


Fig. 7 Numerical results of deformation for different RPM

4.2 Numerical Study

The elongation of beam for different RPM along with its forces on beam is shown by Table 4. Also the graph of RPM versus analytical and numerical elongation is shown by Fig. 8 (Fig. 7).

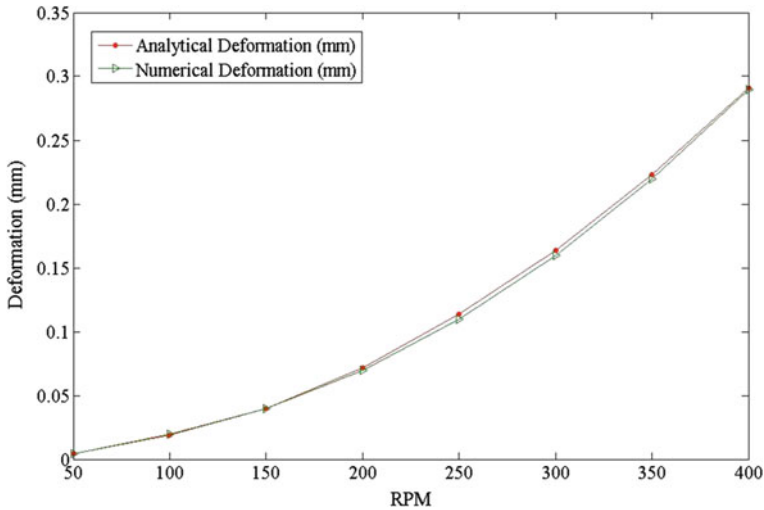


Fig. 8 Graph of RPM versus deformation

5 Conclusion

Rotating beams play an important role in man-made structures such as turbine blades, aircraft propellers, and robotic manipulators. This paper aims at analytical and numerical analysis of composite box girders in rotating conditions. From the above study on rotating composite beam following conclusions are drawn:

- As rpm of composite beam is increases with centrifugal force stresses is induced in the beam and it is maximum near fixed end of rotating beam.
- Axial Deformation of beam is take place at free end of the beam and it increases with increase in rpm.
- The magnitude of deformation is increases with negligible quantity.
- After comparison there is no much more difference both the obtained results.

Then, the simulated results are compared with the analytical results and the percentage error between them is observed within 10%.

References

1. Rao, S. S. (2001). Finite element vibration analysis of rotating Timoshenko beams. *Journal of Sound and Vibration*, 242(1), 103–124.
2. Deepak, B. P., & Ganguli, R. (2012). Dynamics of rotating composite beams: A comparative study between CNT reinforced polymer composite beams and laminated composite beams using spectral finite elements. *International Journal of Mechanical Sciences*, 64, 110–126.

3. Hake, A. A., Ronge, N. S., Bhingare, V. A., Parkhe, A. K., Bhuse, P. K., & More, S. N. (2019). Static & dynamic research of composite blade using condition monitoring method. *International Journal of Recent Technology and Engineering (IJRTE)*, 8(2S11). ISSN: 2277-3878.
4. Parkhe, A. K., Shinde, A. B., Sawant, N. S., Pawar, P. M., & Haridas, P. (2018). Experimental estimation of material uncertainty of composite beam using hall effect sensor. In *Techno-Societal 2018*.
5. Parkhe, A. K., Wangikar, S. S., Patil, P. K., Vhare, C. K., Kashid, D. T., & Pawar, P. M. (2020). Analytical and numerical stress analysis of composite box beam in dynamic condition and validation with COMSOL multiphysics software. *Aegaeum Journal*.
6. Parkhe, A. K., Haridas, P. D., Kapurkar, R. B., & Pawar, P. M. (2015). Experimental study on natural frequency of composite box beam for multiple. *International Journal of Research in Aeronautical and Mechanical Engineering*, 3(12).
7. Kachare, P. S., Parkhe, A. K., Utpat, A. A., & Salunkhe, S. Y. (2019). Health monitoring of static composite beam for material uncertainty and its numerical validation. *International Journal of New Technology and Research (IJNTR)*, 5(3), 79–83. ISSN: 2454-4116.
8. Kachare, P. S., Parkhe, A. K., & Utpat, A. A. (2019). Free vibration analysis of rotating composite box beam using GY-521 accelerometer. *International Journal of Scientific and Research Publications*, 9(2).

Study of Mechanical Properties and Water Absorption Behavior of TiO₂ Nanofiller-Enhanced Glass Fiber-Reinforced Polymer Composites: A Review



Sandeep Kumar Singh and Thingujam Jackson Singh

Abstract In the present scenario, glass fabric polymer is playing a significant role in the field of structural and aerospace industries due to its lightweight, high tensile strength, and corrosion resistance. The GFRP laminate composite is fabricated by hand lay-up process and subsequently submerged in a seawater bath at a certain time and temperature. We observed that tensile strength, flexural strength, and modulus have all properties decreased due to the absorption of water via capillary action inside the laminate composite. The development of mechanical and physical properties of nanofiller incorporated (with the help of mechanical stirring and prob ultrasonication) into polymer matrix composite strongly depends on the elemental composition of filler materials and the size of its particles. To increase the mechanical properties, varying quantities of TiO₂ nanofiller were combined with the polymer epoxy matrix in the current study. The results demonstrated that the flexural and interlaminar shear strengths of water-aged nanocomposites are improved with the inclusion of a fraction weight percent of TiO₂ nanofiller into the polymer epoxy matrix.

Keywords Glass fiber · TiO₂ filler · Glass fiber reinforced polymer (GFRP) composite · Mechanical property · Water absorption

1 Introduction

A composite material is created by a microscopic fusion of two or more materials having different physical and chemical properties. When they are combined, a brand-new substance is created that is specifically made to perform a given duty, like being stronger, lighter, or electrically resistant. They can also strengthen and stiffen things up [1]. Attraction toward GFRP composite is due to the advanced properties offered by reinforced polymer composite over traditional metallic materials because

S. Kumar Singh (✉) · T. Jackson Singh
National Institute of Technology Nagaland, Chumukedima, Nagaland 797103, India
e-mail: Sandeepsingh15july@gmail.com

of lightweight, high tensile strength and low density, ease of processing, high toughness, and damping. Composite materials have some crucial applications such as in racing car bodies, swimming pool panels, aircraft, marines, automobiles and sports industries, transportation and other infrastructures etc. [2]. Mechanical properties of laminate composite depend upon the strength, modulus, and chemical stability and depend upon the orientation of fibers, while in the case of matrix depend on the tensile, flexural strength, and interfacial bonding among matrix and fiber [3]. The characteristic of GFRP composite is equal to steel. Therefore, the strength and stiffness of the constituent fibers govern the strength and stiffness of such composites [4]. The optimal properties of GFRP composite are depending on the characteristic of the material's ingredient (quantity, type, orientation, void content, and fiber distribution). As is well known, material anisotropy is mostly caused by complex fiber orientation distribution. Nanofillers were recognized as a viable remedy to enhance the mechanical characteristics of FRP composites. Investigations found that the type, size, form, and type of the link between the matrix and the fillers all affected how effective they were [5]. The preparation of GFPR composite without the use of nanofiller leads to delamination in composite because of indigent interfacial bonding among fiber and matrix. Due to this, restricts its structural applications such as sports industries, aerospace, automobile etc. [6]. Several researched have been carried out to resolve the delamination problem by the use of different types of nanofiller in pure epoxy resin for improving the mechanical and thermal properties. Finally, these difficulties are overcome by the introduction of organic or inorganic nanofiller in GFRP laminate composites. The various types of inorganic fillers such as Al_2O_3 [7], SiO_2 [8], TiO_2 [9], ZrO_2 [10], MWCNTs and clay [11] and graphene [12], etc. Among the most investigated metal-oxide, TiO_2 presumably is very interesting because of its peerless properties such as Refractive index, Non-toxic, non-corrosive, low cost, Self-cleaning mechanism, anti-bacterial, Dielectric and catalytic properties [13]. Nanofiller like TiO_2 have also the capability to reduce the delamination in FRP composite if they are properly surface functionalized to enhance the interfacial interaction with the matrix system, and ultimately reduce the cost of fabrication and production of composite [14]. The current research work attempted to discuss the effect of water absorption, especially for GFRP laminate composites at control. However, these types of composite deal with a lot of challenges and intimidation in various atmospheres like water, hydrothermal, low and high temperature, alkaline, corrosive, UV light, etc. In the case of a hydrothermal environment, glass fiber-reinforced polymer composites typically absorb moisture. The polymer composites' absorbed water molecules come in two ways: bound water and free water. Free water is typically gathered in the epoxy's free volume/voids or at the matrix-fiber interface, where bound water is typically chemically attached to the hydroxyl group of the epoxy [15, 16]. Composites that have absorbed moisture lose their properties. Chemical and physical changes in epoxy are mostly brought on by chain scission and hydrolysis, whereas physical changes are primarily brought on by plasticization and swelling [17, 18]. Observed that in a hydrothermal environment, osmotic cracking, differential swelling, and interfacial debonding caused matrix microcracks to occur at the interphase [19] observed that the damage at the matrix and fiber matrix interface

is amplified by water temperature. This may be caused by either matrix plasticization or polymer hydrolysis of the glass fiber interface layer. It has been found that the momentum of water absorption rises with increased immersion duration due to capillary action and the uptake of hydrophilic groups by unsaturated polyester and glass fiber [20]. It was mentioned that one of the likely options to seal holes and voids and improve interface and interphase strength in GFRP composites is adding TiO₂ nanofillers [21]. The dispersed nanofiller inside the resin matrix closed the pore/void inside the matrix and thus interfacial bonding is increased between fiber-matrix and reduces the swelling, osmotic cracking at the interface, and water absorption into composite materials [22]. In the current research work we discussed the influence of TiO₂ nanofiller on tensile and flexural properties of polymer composite, when GFRP composite immersed in seawater as well as dry condition.

2 Materials and Methods

2.1 Fiber

The fiber in the polymer matrix composite provides strength and stiffness to the matrix. In current research work selecting the reinforcement as a glass fiber because of the larger strength-to-weight ratio, high percentage strain, ease of handling and cost-effectiveness, good surface completion, and low cost, it gets extended when it breaks.

2.2 Fillers

When nanofiller is used in polymer matrix composite, enhances the crosslinking density of epoxy resin and also improved the mechanical properties of GFRP polymer composite, and reduces the expense of composite. It increased the stiffness of the matrix, crack resistance, and fracture toughness of the matrix. But the degree of improvement due to the addition of nanofiller are depend on the type of filler, particle size, shape, amount of filler, dispersion characteristic, and compatibility with other components. The most important parameter is dispersion for good interfacial bonding between fiber reinforcement and matrix during the fabrication of GFRP composite [23].

Table 1 Physical and mechanical properties of glass fibers, epoxy resin, and TiO₂ nanofiller

Materials	Density (g/cm ³)	Tensile strength (GPa)	Young's modulus (GPa)	Elongation (%)	Coeff. of th. expansion (10 ⁻⁷ /°C)	Poisson's ratio	Refractive index	References
E-glass	2.58	3.445	72.3	4.8	54	0.2	1.558	[24]
TiO ₂	4	51.6	288	–	0.85	0.27	2.7	[25]
Epoxy	1.15	0.070	3.6	1.8	1.0–1.3	0.030	1.50–1.56	[26]

2.3 Matrix

The function of the matrix is to bond the fiber together and transfer the load between them. The role of the matrix is such as Protect the fiber from the environment, Improve the impact and fracture resistance of the composite. Matrix is a different type such as organic, metal, and ceramic matrix. Organic matrix composite was classified into polymer matrix composite (PMC). Polymer matrix composites are two types of thermosetting polymer, a thermoplastic polymer. Examples of thermosetting—are epoxy, phenolic, polyester, polyimide, resin, etc., and e.g., of thermoplastic polypropylene, polyamide, polyethylene, nylon, polycarbonate, polystyrene, etc. (Table 1).

3 Methods

3.1 Preparation of Matrix Mixture with Nanofiller and Fabrication of GFRP Laminate Composite

Preparation of the matrix mixture for making GFRP composite with TiO₂ nanofiller, for these, were used as resin, hardener, and accelerator with stoichiometric ratio. The weight ratio of resin and hardener is 1:0.23 and the accelerator is taken as 2% of resin weight. After 20 min of mechanical stirring slurry of (resin + TiO₂ nanoparticle) was processed by probe ultrasonication dual mixing process (UDM) with simultaneous stirring by impeller for up to 15 min with 10-s pules on and 30-s pules off. For effective nanoparticle prevalence into resin, followed by the addition of hardener plus accelerator again mechanical stirring at 3000 rpm for 10 min, after that finally we got a highly dispersed epoxy resin mixture [23]. During the probe ultrasonication process localized heat generated at the horn immersed into epoxy resin can impair the characteristics of based materials, to overcome this difficulty putting the ice cube surrounding the solution or recycling water from the chiller device because that temperature was maintained [6].

After preparing the mixture of epoxy resin and TiO₂ filler directly used for the fabrication of GFRP laminate composite by hand layup process. First of all, used peel ply for the easy removal of composite from steel plate at which stacking

Table 2 Comparison of the mechanical properties of different types of neat epoxy polymer composite in seawater aging

Materials type	Aging situation	Deterioration of properties	References
Glass/polyester	810 days of seawater aging at 30 °C	Modulus declined by 6% while flexural strength fell by 17%	[27]
Glass/vinyl ester	810 days of seawater aging at 30 °C	Modulus declined by 10% and flexural strength fell by 15%	[28]
Glass/vinyl ester	350 days of aging in a basic solution with a pH of 11.5	Tensile modulus loss as temperature increases	[19]
E-glass/epoxy	300 days were spent submerged in seawater and (1.6% NaCl) at 20 °C	All the mechanical properties decreased as a result of seawater aging, decreasing by 13.6%, 21.9%, and 8.9%, respectively. And by water aging by 39.8%, 36.1%, and 22.0%, respectively	[29]
Basalt/CNT/epoxy	Seawater aging	20% less fracture toughness now exists	[30]
Carbon/epoxy	Drenched with saltwater	Failure strength is now 20–40% lower	[28]

number of glass fiber with matrix materials as shown in Fig. 1. Then composite was put in a side air oven for pre-curing at 120 °C for 2 h. After that, the post-curing for 6 h at 160 °C and finally obtained the desired size of the laminate composite [24] (Table 2).

4 Result and Discussion

4.1 Void Content

Voids are nothing more than closed pores that are found in composite materials. They are crucial to first penetrate water inside the materials and the subsequent loss of mechanical qualities. It has been found that the percentage of voids rises as the weight percentage of nano-TiO₂ content increases shown in Fig. 2a. Because the tendency of agglomeration of TiO₂ nanoparticles is increased, it means that a stronger bond between particle-to-particle as compared to the matrix-to-particle forms larger air bubbles throughout the blending of matrix and filler. That is why, agglomeration of nano-TiO₂ particles weakens the bond between the fiber-matrix interface, rising the amount of water absorbed by capillary action. When compared to pure epoxy matrix

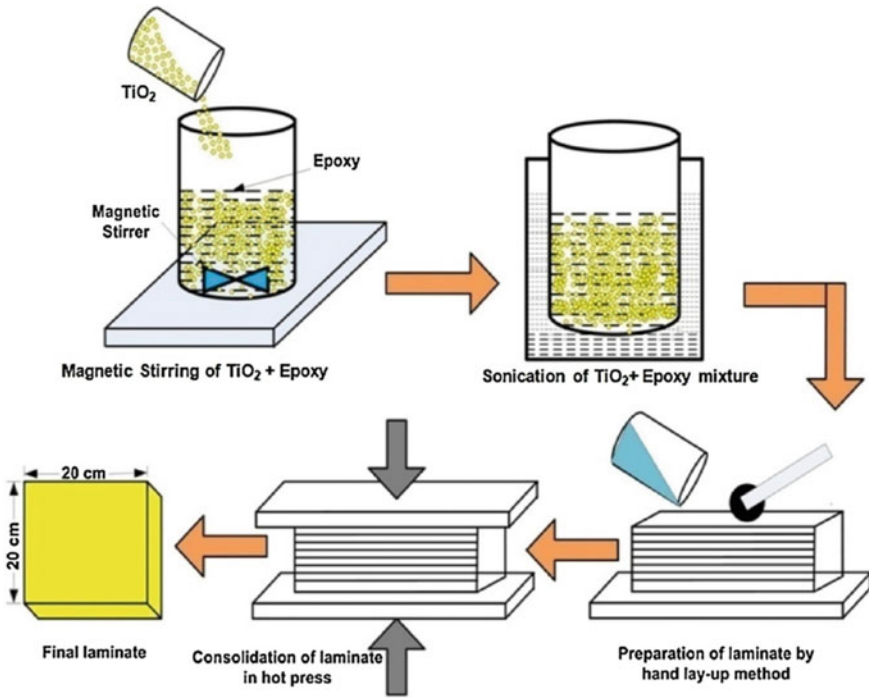


Fig. 1 Schematic diagram of fabrication of laminate composite by hand lay-up process [16]

polymer glass fiber reinforced polymer laminate composite, the seawater diffusivity of the nanocomposite at 0.1 wt.% of titanium dioxide nanofiller decreased by 15%.

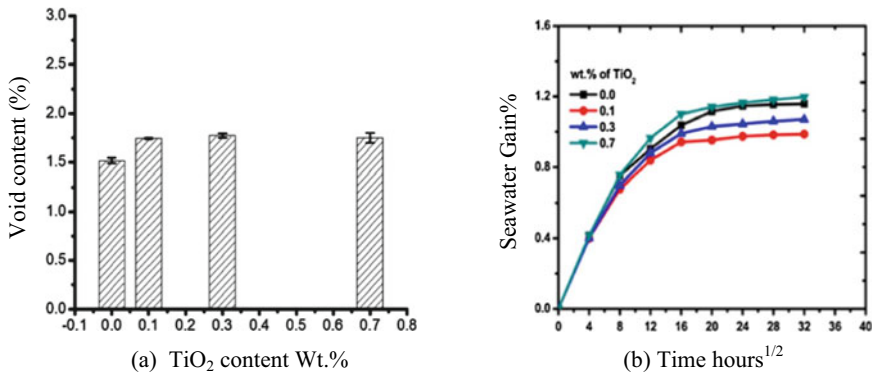


Fig. 2 a Influence on the void concentration of TiO₂ wt.% in composite b influence on seawater gain of the square root of time [16]

4.2 Accelerated Seawater Aging

Moisture absorption significantly contributes to the deterioration of the mechanical qualities of GFRP composites. Polymer Composite matrix materials frequently take in moisture inside the hydrothermal or hydrophilic atmosphere. The square root of seawater aging time and seawater gain weight percentage. The results showed that the percentage of water gain rises with time during the early stages of aging and then decreases as time goes on. It can be because the composite's surface has voids or open pores that speed up the absorption tendency shown in Fig. 2a. However, when the amount of nano-TiO₂ rises, it also increases water absorption. According to Fig. 2b minimum seawater absorption of nanocomposite at 0.1% of TiO₂ filler. It could be beneficial interfacial bonding among the fiber and matrix at 0.1% filler which reduced the seawater diffusion in composite through capillary action and then the seawater diffusivity reduced by 15%.

4.3 Mechanical Properties

The mechanical qualities and durability of a product's component should be developed and chosen in accordance with the design. To determine the materials' reliability and durability, the mechanical properties must be assessed in various environments.

The ILSS test can evaluate the strength of the interface, which is the core of GFRP composites. However, the flexural test may be able to detect bending and compressive stress [16].

4.4 Flexural Strength

The figure shows the relation between flexural strength and modulus versus Weight percentage of titanium dioxide filler content in composite. The result reveals that increase in the wt.% of TiO₂ filler decrease the flexural strength of nanocomposite. According to Fig. 3a maximum increment in flexural strength was seen for nanocomposites containing 0.1 wt.% of TiO₂ nanofiller from 330 to 366 MPa. After that further addition of Titanium dioxide nanofiller, then decrease the flexural strength of seawater as well as dry nanocomposite. For a composite with a 0.1 wt.% nano-TiO₂ content, the enhancement in flexural strength following wet condition is about 15% while 11% is in dry condition [31]. However, furthermore added TiO₂ filler content, then agglomeration has been occurring in matrix materials, and the van der Waal's force of attraction between particle to the particle is larger as compared to the particle-to-matrix interface shown in Fig. 3a. The agglomeration of nanoparticles in polymer composite reduces the mechanical properties due to the decrease in the dynamic specific surface area which interacts with the polymer matrix. Because of

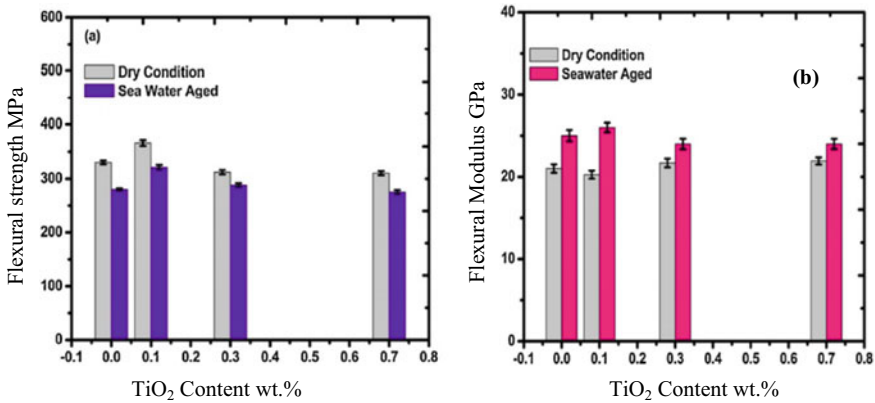


Fig. 3 Graph between flexural strength vs TiO₂ wt.% (a) and flexural modulus vs TiO₂ wt.% (b) in composite [19]

that insufficient load transfer between the fiber and matrix interphase of the nanocomposite. Void concentration in the composite is nearby responsible for decreasing flexural strength. The mechanical characteristic of composites that have undergone hydrothermal aging has decreased because of the fiber, epoxy, and nanoparticles' uneven thermal expansion, which results in interface swelling and the hydrolysis of the epoxy matrix [19].

Figure 3b demonstrated the relation between flexural modulus and titanium dioxide nanofiller content in composite. With an increase in TiO₂ nanofiller content in dry conditions, the flexural modulus rises. It might be caused by the composites' high modulus TiO₂ nanofiller content. But as the amount of TiO₂ nanofiller in seawater-aged composites rises, the flexural modulus of those materials decreases.

4.5 Interlaminar Shear Strength (ILSS)

The result reveals that Comparing the TiO₂ nanofiller content in polymer composite to other nanocomposites and pure epoxy composites in both (water and dry) conditions, the greatest ILSS is discovered to be at 0.1 wt.%. The addition of 0.1 wt.% ILSS has enhanced by 19% and 23% in dry and seawater aging, respectively, following the incorporation of TiO₂ nanofiller into the epoxy matrix.

The improvement or decline of mechanical characteristics may be connected to the fracture surface's structure analysis to back up the discoveries. Show in Fig. 4a the strengthening mechanism of nanocomposite at 0.1 wt.% of TiO₂ filler. It observed an effective interfacial bonding between fiber and matrix, because of the proper dispersion of TiO₂ nanofiller in an epoxy slurry with the help of Ultrasonication. Good dispersion means bonding between particle to matrix/fibers is stronger than particle to particle, which enhances the mechanical quality of both dry and wet conditions

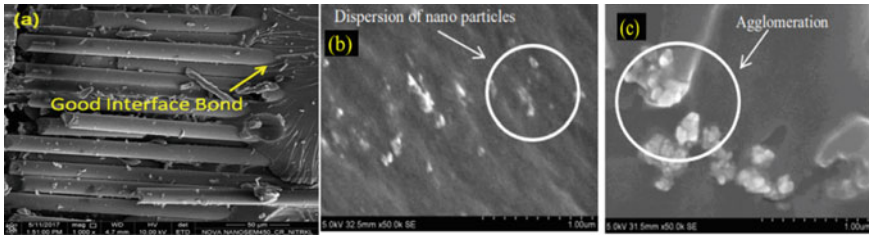


Fig. 4 FESEM picture of the bond interface at 0.1 wt.% of TiO₂ filler (a), Dispersion of TiO₂ (b) agglomeration at 0.9 wt.% of TiO₂ filler (c) [21]

[21]. However, Fig. 4c demonstrated the agglomeration of 0.9 wt.% nanofiller content in the composite which reduced the mechanical properties in dry as well as seawater conditions because of higher weight percentage of nanofillers is typically associated with the creation of voids during matrix modification and the agglomeration of TiO₂ nanofiller above a certain wt.% [13].

5 Conclusion

This current research work discussed the mechanical properties and water absorption of GFRP laminate composite with or without filler matrix. In the case of pure epoxy resin matrix had been reducing the mechanical properties due to the delamination of composite, these difficulties were overcome by the introduction of TiO₂ nanofiller into the polymer matrix. Surface modification of TiO₂ nanoparticles is also possible which allowed enhancing the interface region properties, dispersion, homogeneity with ultrasonic dual mixing (UDM), and mechanical properties. Maximum improvement of flexural strength at the addition of a certain amount of nanofiller in seawater condition, whereas further increase nanofiller then fall down the flexural strength. When compared to control GFRP composites, the ILSS of the nanocomposite with a certain weight percentage of TiO₂ nanofiller enhances under both dry and seawater-aged conditions. When the addition of TiO₂ nano-filler in composite, initially increases the flexural modulus. Aging matrix stiffening components in seawater and improved interfacial adhesion between the matrix and fiber are to blame. After that further increase the TiO₂ nanofiller in the composite, an adverse effect on mechanical properties.

References

1. Sathishkumar, T. P., Satheeshkumar, S., & Naveen, J. (2014). Glass fiber-reinforced polymer composites—A review. *Journal of Reinforced Plastics and Composites*, 33, 1258–1275. <https://doi.org/10.1177/0731684414530790>
2. Aydin, F. (2016). Effects of various temperatures on the mechanical strength of GFRP box profiles. *Construction and Building Materials*, 127, 843–849. <https://doi.org/10.1016/j.conbuildmat.2016.09.130>
3. Erden, S., Sever, K., Seki, Y., & Sarikanat, M. (2010). Enhancement of the mechanical properties of glass/polyester composites via matrix modification glass/polyester composite siloxane matrix modification. *Fibers and Polymers*, 11(5), 732–737. <https://doi.org/10.1007/s12221-010-0732-2>
4. EL-Wazery, M. S., EL-Elamy, M. I., & Zoalfakar, S. H. (2017). Mechanical properties of glass fiber reinforced polyester composites. *International Journal of Applied Science and Engineering*, 14(3), 121–131. [https://doi.org/10.6703/IJASE.2017.14\(3\).121](https://doi.org/10.6703/IJASE.2017.14(3).121)
5. Zahrouni, A., Bendaoued, A., & Salhi, R. (2021). Effect of sol-gel derived TiO₂ nanopowders on the mechanical and structural properties of a polymer matrix nanocomposites developed by vacuum-assisted resin transfer molding (VARTM). *Ceramics International*, 47(7), 9755–9762. <https://doi.org/10.1016/j.ceramint.2020.12.115>
6. Kumar, K., Ghosh, P. K., & Kumar, A. (2016). Improving mechanical and thermal properties of TiO₂-epoxy nanocomposite. *Composites Part B: Engineering*, 97, 353–360. <https://doi.org/10.1016/j.compositesb.2016.04.080>
7. Alam, M. S., & Chowdhury, M. A. (2020). Characterization of epoxy composites reinforced with CaCO₃-Al₂O₃-MgO-TiO₂/CuO filler materials. *Alexandria Engineering Journal*, 59(6), 4121–4137. <https://doi.org/10.1016/j.aej.2020.07.017>
8. Taylor, P., Halder, S., Ghosh, P. K., Goyat, M. S., & Ray, S. (2013). Ultrasonic dual mode mixing and its effect on tensile properties of SiO₂-epoxy nanocomposite. *Journal of Adhesion Science and Technology*, 37–41.
9. Maloth, B., Srinivasulu, N. V., Rajendra, R., Sathishkumar, T. P., Satheeshkumar, S., & Naveen, J. (2014). Glass fiber-reinforced polymer composites—A review. *Journal of Reinforced Plastics and Composites*, 33(13), 1258–1275. <https://doi.org/10.1177/0731684414530790>
10. Halder, S., Ghosh, P. K., & Goyat, M. S. (2012). Influence of ultrasonic dual mode mixing on morphology and mechanical properties of ZrO₂-epoxy nanocomposite. *High Performance Polymers*, 24(4), 331–341. <https://doi.org/10.1177/0954008312440714>
11. Hu, Y., Ji, W. M., & Zhang, L. W. (2020). Water-induced damage revolution of the carbon nanotube reinforced poly (methyl methacrylate) composites. *Composites Part A: Applied Science and Manufacturing*, 136, 105954. <https://doi.org/10.1016/j.compositesa.2020.105954>
12. Nayab-Ul-Hossain, A. K. M., Sela, S. K., Hasib, M. A., Alam, M. M., & Shetu, H. R. (2022). Preparation of graphene based natural fiber (Jute)-synthetic fiber (Glass) composite and evaluation of its multifunctional properties. *Composites Part C Open Access*, 9, 100308. <https://doi.org/10.1016/j.jcomc.2022.100308>
13. Nayak, R. K., Mahato, K. K., & Ray, B. C. (2016). Water absorption behavior, mechanical and thermal properties of nano TiO₂ enhanced glass fiber reinforced polymer composites. *Composites Part A: Applied Science and Manufacturing*, 90, 736–774. <https://doi.org/10.1016/j.compositesa.2016.09.003>
14. Zhai, W., Wu, Z. M., Wang, X., Song, P., He, Y., & Wang, R. M. (2015). Preparation of epoxy-acrylate copolymer@nano-TiO₂ Pickering emulsion and its antibacterial activity. *Progress in Organic Coatings*, 87, 122–128. <https://doi.org/10.1016/j.porgcoat.2015.05.019>
15. Visco, A. M., Calabrese, L., & Cianciafara, P. (2008). Modification of polyester resin based composites induced by seawater absorption. *Composites Part A: Applied Science and Manufacturing*, 39(5), 805–814. <https://doi.org/10.1016/j.compositesa.2008.01.008>
16. Nayak, R. K., & Ray, B. C. (2018). Influence of seawater absorption on retention of mechanical properties of nano-TiO₂ embedded glass fiber reinforced epoxy polymer matrix composites.

- Archives of Civil and Mechanical Engineering*, 18(4), 1597–1607. <https://doi.org/10.1016/j.acme.2018.07.002>
17. De'Nève, B., & Shanahan, M. E. R. (1993). Water absorption by an epoxy resin and its effect on the mechanical properties and infra-red spectra. *Polymer (Guildf)*, 34(24), 5099–5105. [https://doi.org/10.1016/0032-3861\(93\)90254-8](https://doi.org/10.1016/0032-3861(93)90254-8)
 18. Sridhar, I., & Venkatesha, C. S. (2013). Variation of damping property of polymer composite under saline water treatment. *International Journal of Innovations in Engineering and Technology*, 2(1), 420–423.
 19. Hodzic, A., Kim, J. K., Lowe, A. E., & Stachurski, Z. H. (2004). The effects of water aging on the interphase region and interlaminar fracture toughness in polymer-glass composites. *Composites Science and Technology*, 64(13–14), 2185–2195. <https://doi.org/10.1016/j.compscitech.2004.03.011>
 20. Yan, L., & Chouw, N. (2015). Effect of water, seawater and alkaline solution ageing on mechanical properties of flax fabric/epoxy composites used for civil engineering applications. *Construction and Building Materials*, 99, 118–127. <https://doi.org/10.1016/j.conbuildmat.2015.09.025>
 21. Prasad, V., Joseph, M. A., & Sekar, K. (2018). Investigation of mechanical, thermal and water absorption properties of flax fibre reinforced epoxy composite with nano TiO₂ addition. *Composites Part A: Applied Science and Manufacturing*, 115. <https://doi.org/10.1016/j.compositesa.2018.09.031>
 22. Ghosh, P. K., Pathak, A., Goyat, M. S., & Halder, S. (2012). Influence of nanoparticle weight fraction on morphology and thermal properties of epoxy/TiO₂ nanocomposite. *Journal of Reinforced Plastics and Composites*, 31(17), 1180–1188. <https://doi.org/10.1177/0731684412455955>
 23. Goyat, M. S., & Ghosh, P. K. (2018). Impact of ultrasonic assisted triangular lattice like arranged dispersion of nanoparticles on physical and mechanical properties of epoxy-TiO₂ nanocomposites. *Ultrasonics Sonochemistry*, 42, 141–154. <https://doi.org/10.1016/j.ultsonch.2017.11.019>
 24. Kuppusamy, R. R. P., Rout, S., & Kumar, K. (2020). Advanced manufacturing techniques for composite structures used in aerospace industries. *Modern Manufacturing Processes*. <https://doi.org/10.1016/b978-0-12-819496-6.00001-4>
 25. Tekin, D., Birhan, D., & Kiziltas, H. (2020). Thermal, photocatalytic, and antibacterial properties of calcinated nano-TiO₂/polymer composites. *Materials Chemistry and Physics*, 251, 123067. <https://doi.org/10.1016/j.matchemphys.2020.123067>
 26. Rathore, D. K., Prusty, R. K., Kumar, D. S., & Ray, B. C. (2016). Mechanical performance of CNT-filled glass fiber/epoxy composite in in-situ elevated temperature environments emphasizing the role of CNT content. *Composites Part A: Applied Science and Manufacturing*, 84, 364–376. <https://doi.org/10.1016/j.compositesa.2016.02.020>
 27. Gellert, E. P., & Turley, D. M. (1999). Seawater immersion ageing of glass-fibre reinforced polymer laminates for marine applications. *Composites Part A: Applied Science and Manufacturing*, 30(11), 1259–1265. [https://doi.org/10.1016/S1359-835X\(99\)00037-8](https://doi.org/10.1016/S1359-835X(99)00037-8)
 28. Tual, N., Carrere, N., Davies, P., Bonnemains, T., & Lolive, E. (2015). Characterization of sea water ageing effects on mechanical properties of carbon/epoxy composites for tidal turbine blades. *Composites Part A: Applied Science and Manufacturing*, 78, 380–389. <https://doi.org/10.1016/j.compositesa.2015.08.035>
 29. Cerbu, C. (2010). Effects of the long-time immersion on the mechanical behaviour in case of some E-glass/resin composite materials. *Woven fabric engineering*. <https://doi.org/10.5772/10462>
 30. Kim, H. Y., Park, Y. H., You, Y. J., & Moon, C. K. (2008). Short-term durability test for GFRP rods under various environmental conditions. *Composite Structure*, 83(1), 37–47. <https://doi.org/10.1016/j.compstruct.2007.03.005>
 31. Carlsson, L., Adams, D., & Pipes, R. (2014). Analysis of composite materials. *Experimental characterization of advanced composite materials* (4th ed., Vol. 50, pp. 11–34). <https://doi.org/10.1201/b16618-3>

Strengthening and Retrofitting of Reinforced Concrete Beam by Using Composite Materials



Priyanka S. Mirajkar, P. M. Pawar, and Sonali P. Patil

Abstract The strength and flexural behavior of RCC beams strengthened and retrofitted with glass fiber sheet (GFRP) and carbon fiber sheet (CFRP) with two layers of jacketing, were investigated experimentally. For strengthening and retrofitting, we created two RCC beam groups were tested under single point load. One group of beams was evaluated in their natural state and use for retrofitting, while another group was examined for strengthened with FRP. A vacuum bagging machine was used to airtight bond and beams are tested under loading frame; deflection is monitoring by LVDT. In the result of 2 methods, retrofitted beams have a large load carrying capacity as compare to strengthened beams. The experimental results indicated jacketing beams with CFRP got greater strength and less deflection as compare with control beam and jacketing beam with GFRP in both the methods. Jacketed beams with FRP sheets have less cracks and fiber damage is also negligible.

Keywords Glass fiber sheet (GFRP) · Carbon fiber sheet (CFRP) · Strengthening · Retrofitting · Jacketing · Reinforced concrete beam · Loading frame machine · LVDT

1 Introduction

Composite materials are being used worldwide for the strengthening and retrofitting of deficient and old infrastructures. Over the years, these structures have suffered severe weakness and stiffness because of aggressive environmental conditions like humidity, saltwater, and alkali solutions. Advanced fibrous composite materials like GFRP, CFRP, etc. can substantially increase the strength and stiffness of reinforced concrete beams. In the case of Reinforced Concrete (RCC) beams, remove deflection and repair with filling crack and expose them to aggressive environmental conditions. The bond between the composite material sheets and the surface of the RCC beam

P. S. Mirajkar (✉) · P. M. Pawar · S. P. Patil
SVERI's College of Engineering, Pandharpur, India
e-mail: piyamirajkar884@gmail.com

significantly affects the strength of externally reinforced RC beams. Thus, it's essential to analyze the overall response of the RCC beams when externally strengthened with composite material sheets and fabrics and exposed to different environmental conditions. Because it offers high strength, low weight, corrosion resistance, high fatigue resistance, easy and rapid installation, and minimal change in structural geometry, strengthening concrete structures with jacketing of composite materials sheets is a more economical and technically superior alternative to the old technique used in many situations. This technique has been largely used because of the high specific stiffness and strength of these materials. External bonding of high-strength Fiber Reinforced Polymers (FRP) to structural concrete members has grown in popularity in recent years, especially in rehabilitation and new construction projects. Experimental analysis conducted in the past has shown that this strengthening method has several advantages over the making of new, especially due to its corrosion resistance, high stiffness-to-weight ratio, improved durability, and flexibility in its use over steel plates. The use of fiber Reinforced Polymer (FRP) materials in civil infrastructure for the repair and strengthening of reinforced concrete structures and also for new construction has become stronger [1, 2]

2 Objective

- To design various approaches of strengthening techniques using composite materials.
- To analyze the performance of beam strengthened using composite materials.
- To design various approaches of retrofitting techniques using composite material for partially damaged beams.
- To analyze the performance of beam retrofitting techniques using composite materials for partially damaged beams.
- To understand the failure pattern of the RCC beams.

3 Methodology

3.1 Basic Terminology

Strengthening: To enhance resistance to aggressive environmental conditions of a building by strengthening. This method adds higher strength and ductility to any part of current building than the primary building. Strengthening can be done for seismically weak building.

Retrofitting: Resistance to aggressive environmental conditions can be upgraded to level of the present-day by adequate retrofitting techniques. Enhancing the strength of a damaged building is called retrofitting. It has been found that the retrofitting costs are much lower than constructing a new building.

3.2 *Material Used*

1. **Cement**

Ordinary Portland cement (OPC)-43, Wonder Cement Grade adhering to IS: 8112-1989, was used in the current experiment. In accordance with Indian Standard Specifications, physical properties were tested.

2. **Coarse Aggregate**

Aggregates with a size range of 10–20 mm and a coarse aggregate specific gravity of 2.8 are obtained from authorized quarries. According to IS 2386-1963, tests on coarse aggregate are carried out.

3. **Fine Aggregate**

M sand with a specific gravity of 2.65 that passes through a 4.75 mm sieve is employed. Zone II is the fine aggregate grading zone. Per IS 383-1970, the physical characteristics of fine aggregates were determined.

4. **Water**

The water on the college campus complies with the IS: 456-2000 criteria for water for curing and concreting.

5. **Reinforcement**

HYSB bars made of Fe 415 with a diameter of 12 mm were employed as longitudinal reinforcements, while bars with a diameter of 10 mm were used as hanger bars. Fe 250 mild steel bars with an 8 mm diameter were used to make the stirrups.

6. **Epoxy Resin**

Essentially, epoxy resins are low-molecular-weight pre-polymers that can be treated in a variety of ways. It is a thermosetting polymer produced by the interaction of polyamine “hardener” and epoxy “resins.”

7. **Glass Fiber Sheet**

A popular type of fiber-reinforced plastic that uses glass fiber is fiberglass. The fibers can either be braided into glass cloth or alternately arranged before being flattened into a sheet known as a chopped strand mat. The thermoset polymer matrix, which is most frequently built on thermosetting polymers like epoxy and polyester resin, may make up the plastic matrix (Table 1).

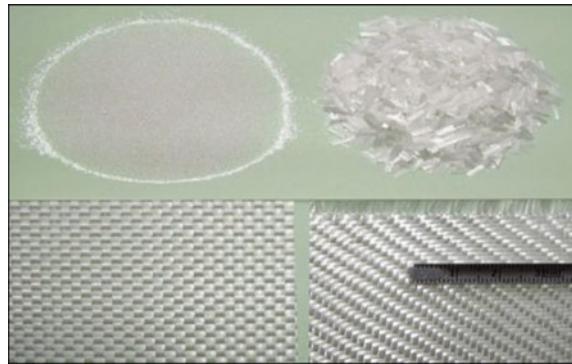
Table 1 GFRP sheet properties

Fiber type	Tensile strength (MPa)	Compressive strength (MPa)	Young’s modulus E (GPa)	Density (g/cm ³)	Thermal expansion (μm/m °C)	Softening T (°C)
GFRP	3445	1080	76.0	2.58	5	1000

Table 2 CFRP sheet properties

Fiber type	Tensile strength (MPa)	Compressive strength (MPa)	Young’s modulus E (GPa)	Density (g/cm ³)	Thermal expansion (μm/m °C)	Softening T (°C)
CFRP sheet	4900	896	230	1.78	1.7	1000

Fig. 1 GFRP sheet



8. Carbon Fiber Sheet

The carbon atoms are bonded each other’s in crystals that are more aligned parallel to the fiber is long axis as the crystal alignment gets the fiber a high strength-to-volume ratio (in other words, it is strong for its size). Several more carbon fibers are bundled together to form a tow, which may be used by itself or woven into a fabric (Table 2).

3.3 Mix Proportion of Concrete

M 20 grade concrete was proportioned in line with Indian Standards 10262:1982 and 10262:2019. A concrete mix design was carried out based on the results of components. For mix design, a water to cement ratio of 0.47 was used Proportion of M20 mix (Table 3).

Fig. 2 CFRP sheet

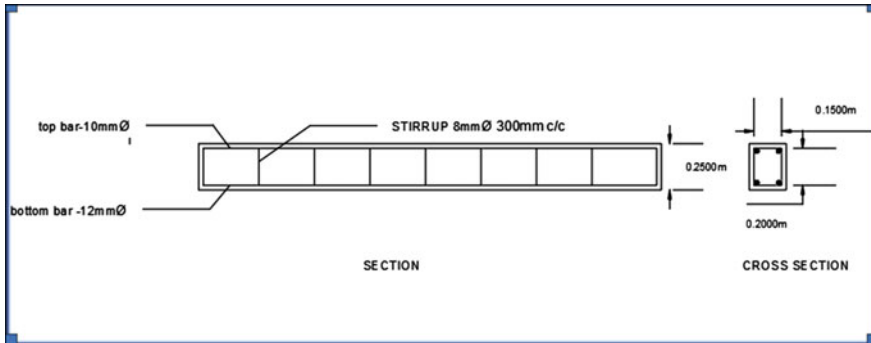
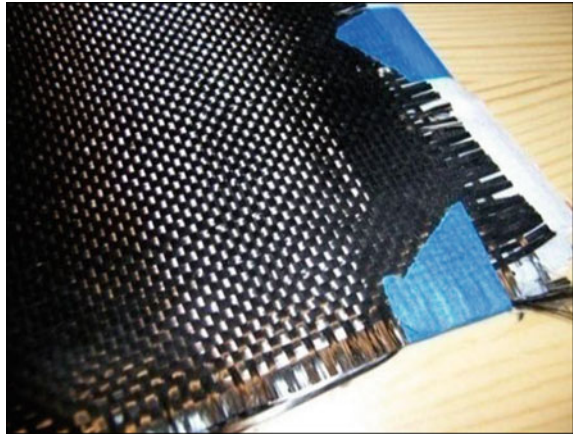


Fig. 3 Beam design

Table 3 Material required for 1M³ concrete

Content	Quantity	
Cement	350.64 kg	
Water	164.8 kg	
Fine aggregate	M sand—414.36 kg Dust sand—276.24 kg	Total—690.60 kg
Coarse aggregate	20 mm dia—760.35 kg 10 mm dia—536.88 kg	Total—1279.23 kg
Water cement ratio	0.47	

3.4 Casting of Beams

All four beams were created in accordance with the IS: 456-2000 standards utilizing the limit state technique, with the section being under-reinforced. Molds with dimensions of 2500 × 200 × 250 mm were made out of plywood. The machine-mixed concrete was made in accordance with IS10262-1982 and had a 1:2.1:2.95 mix ratio. (Cement:sand:coarse aggregate). The following methods were employed for casting beams:

- All of the mould was first lubricated. After 24 h, the beams can be easily removed from the mould.
- To provide uniform covering after the reinforcing bars have been fitted, cover blocks of 20 mm are used.
- The concrete mix was poured in layers and crushed with a vibrator and tamping rods until the mould was entirely filled. This process was completed with no voids.
- After a 24-h period, the beams were taken out of the moulds. The beams were then left to cure for 28 days.

3.5 Jacketing of FRP Sheet on the RCC Beam

FRP sheets were jacketed on RCC beams using the brush layup procedure. For optimal bonding with FRP sheets, the surface of the beams was roughened after curing and then wiped with water to eliminate all dirt. After that, the beams were left to cure for two hours. For the over-round part of the beams, the FRP sheets were cut to a width of 1 m for two layers and a length of 0.9 m. After that, the epoxy resin primers are correctly taken in a plastic container at a ratio of 1:2 (hardener:resin) to generate a homogeneous mix. Then, with the help of brush, it was painted on the surface of beams for good bonding of FRP sheets with the beams. Then FRP sheets were placed on the top of the epoxy resin layer, and another coating of epoxy resin was applied on the top of the FRP sheets. Another layer of FRP sheet was applied over it, and the final coating was done with epoxy resin. This procedure is performed at room temperature (Figs. 4, 5 and 6 [3]).

3.6 Vacuuming of FRP Sheet Jacket with Vacuum Bagging Machine

After doing jacketing immediately apply the cloth on the jacket of the FRP sheet on the beams and plastic paper is airtight attach overall with the help of a double-stick like an airtight bag. Attach vacuum bagging machine pipe in plastic airtight bag system and start the machine for 1 h to remove all air and make all bond of beams, FRP sheets layer with each other stronger. Make bond stronger with epoxy resin.

Fig. 4 Applying Epoxy Resin on beam



Fig. 5 Jacketing



Fig. 6 Vacuum machine



3.7 *Testing of Control Beam and FRP Sheet Strengthened Beams*

Testing of control beam and FRP sheet strengthened beams under loading frame machine of 200 kN capacity with data acquisition program system and flexural strength is also recorded during the testing with the help of LVDT (Figs. 7 and 8) [4, 5].



Fig. 7 GFRP jacketing beam test



Fig. 8 CFRP jacketing beam test

3.8 *Repair of the Pre-cracked Beam Using Mortar*

This methodology is useful for retrofitting method (for the 3rd objective) for repairing pre-cracked beams pre-cracked. The cracked beams were clean with polished paper. The loose parts of the beams are removed from the beams and wash the crack with water. Take it 2 h to dry and after that fill the crack with mortar (cement:sand) and attach the jack to the bottom of the beam to remove the bend of the beam for 1 day (Figs. 9 and 10) [6, 7].

Fig. 9 Cleaning of crack



Fig. 10 Filling of crack



Table 4 Compressive strength of the beams

Beams	Load taken by the beam (kN)	Increased load caring capacity
Control beam	58	0
<i>Strengthened beams</i>		
Strengthened beam by GFRP sheet	60.1	2.1
Strengthened beam by CFRP sheet	63.4	5.4
<i>Retrofitted beam</i>		
Retrofitted beam by GFRP sheet	75.6	17.6
Retrofitted beam by CFRP sheet	77.8	19.8

4 Result

4.1 Compressive Strength

Strengthened beams and retrofitted beams with GFRP and CFRP sheet are compared with Control beam (Table 4).

4.2 Deflection

Strengthened beams and retrofitted beams with GFRP and CFRP sheet are compared with Control beam (Table 5).

Table 5 Flexural strength of the beams

Beam	Deflection (mm)	Flexural strength (N/mm ²)	Failure effect
Control beam	43	11.6	Concrete fracture
<i>Strengthened beams</i>			
Strengthened beam by GFRP sheet	39	12.2	GFRP sheet fracture is very less
Strengthened beam by CFRP sheet	33.58	12.68	CFRP sheet fracture is very less
<i>Retrofitted beam</i>			
Retrofitted beam by GFRP sheet	44.68	15.12	GFRP sheet fracture is very less
Retrofitted beam by CFRP sheet	41.2	15.56	CFRP sheet fracture is very less

5 Conclusion

- In this research paper one point bending test were carried on the RCC beam (control beam) and strengthened as well as retrofitted beam with GFRP and CFRP sheet Jacketing with 2-layer Jacketing configuration.
- GFRP sheet and CFRP sheet strengthened beam have a more load caring capacity up to 5% to 10% respectively as compare to control beam and flexural behavior is also improved 10% and 21.9% respectively with compare to control beam. Deflection of GFRP and CFRP is less and fiber damage is negligible.
- GFRP sheet and CFRP sheet retrofitted beam have a more load caring capacity up to 2.5% and 2% respectively as compare to control beam and flexural behavior is also improved 30% to 34% respectively with compare to control beam. Deflection of GFRP and CFRP is less and fiber damage is negligible.
- The flexural behavior is also improved in of strengthened beams and retrofitted beams with GFRP and CFRP sheet.
- Failure of the material of the beam is also less as compare to the strengthened beams and retrofitted beams, fiber damage also less (negligible).

References

1. Ramachandra Murthy, A., & Meikandaan, T. (2017). Study of damaged RC beams repaired by bonding of CFRP laminates. *International Journal of Civil Engineering and Technology*, 8(2), 470–486.
2. Jain, A. K., & Padole, D. S. (2016). Comparative study on strengthening of RC beam in flexure using CFRP & GFRP: A review.

3. Ezz-Eldeen, H. A. (2015). An experimental study on strengthening and retrofitting of damaged reinforced concrete beams using steel wire mesh and steel angles. *International Journal of Engineering Research and Technology*, 4(5), 164–173.
4. Nayak, A. N., et al. (2014). Strengthening of square RC columns using externally bonded FRP sheets. In *Proceedings of the Second International Conference on Advances in Civil, Structural and Mechanical Engineering—CSM*.
5. Jaya, K. P., & Mathai, J. (2012). Strengthening of RC column using GFRP and CFRP. In *15WCEE Lisboa 2012*.
6. Vasudeva, R., & Kaur, M. (2016). Retrofitting of RC beams using glass fiber reinforced polymer sheets: An experimental study. *Indian Journal of Science & Technology*, 9, 44.
7. Karzad, A. S., et al. (2017). Repair of reinforced concrete beams using carbon fiber reinforced polymer. *MATEC Web Conferences*, 120.

A Study on Effect of Severe Plastic Deformation Process on Hardness of Aluminum Alloys



Mansi Chavan, Mayuri Abhangrao, Kiran Lakkam, and Sandeep Wangikar

Abstract Aluminum alloys have a wide range of applications mainly because of its high specific strength, easy to process, anti-erosion, and eco-friendly in nature. These properties make it highly applicable in many sectors like packaging, automotive industries, electronics industries, etc. in this study commercially available AA8011 is considered for study which has higher tensile strength, hardness and better wear resistance. Many methods are adopted to improve hardness of these materials where it is directly proportional to rise in weight of the material. Hardening the material without increasing the weight can be done by Severe Plastic Deformation (SPD) processes. Among many SPD processes, Continuous Repetitive Corrosion & Strengthening (CRCS) method is being adopted for the present study. In this method, grain structure of material can be reformed and this in turn increases the mechanical properties. Study reveals that after processing of AA8011 sheets through CRCS method, increase in number of passes increases grain refinement leading to increase in hardness of the material.

Keywords CRCS · Mechanical properties · Micro hardness · Corrugation

1 Introduction

From the last few years study on Severe Plastic Deformation (SPD) process for ultra-fine refinement of grains and enhancement of hardness has been done. Different technologies of SPD process are studied which are mainly classified as discontinuous and continuous methods. Discontinuous methods are Equal channel angular extrusion (ECAE) [1], High pressure Torsion (HPT) [2], Repetitive Corrugation and Straightening (RCS) [3], Twist Extrusion (TE) and Multipass Coin Forging (MCF) [4]. Continuous methods include Accumulative Roll Bonding (ARB), Continuous

M. Chavan (✉) · M. Abhangrao · K. Lakkam · S. Wangikar
Department of Mechanical Engineering, SVERI's College of Engineering, Pandharpur, India
e-mail: chavanmansi46@gmail.com

combined drawing and Rolling (CCDR), and Continuous repetitive Corrugation and Straightening (CRCS) [5]. In this study we have adopted CRCS process which consists of a significant feature that the external dimensions of the work piece do not change significantly during the processing.

SPD is mainly used for the Grain refinement of metals & alloys from micrometer into sub micrometer range [6]. For producing of Ultra-fine grain refinement in our study, we are using Continuous Repetitive Corrugation and Straightening method in which commercially available Aluminum 8011 sheet of 1 mm thickness is being processed. The influence of number of passes on mechanical properties like Micro hardness due to grain refinement by microstructure changes has been studied. As the specific material properties are being important in the present fast growing Scenario, requirement of high strength metals and alloys is also increasing. These applications cover Aerospace, Automobile, Transportation, Food and Chemical processing, and defense industries. In this CRCS method, a work piece is continuously repeatedly corrugated and straightened without significant change in thickness of AA8011 material [7]. This process can be easily adapted to large-scale production.

The main objective of this work is to study the changes of hardness properties with number of passes of AA8011 sheet metal of 1 mm thickness.

2 Experimental Set Up and Procedure

Aluminum 8011 sheet metal of 1 mm thickness with chemical composition as mentioned in Table 1 is taken as the material. Strips of 50 mm width, 100 mm length, and 1 mm thickness are considered. In CRCS method, a set of gears for sheet to get corrugate and set of rollers for straightening the sheet are arranged and set up for CRCS process is developed as shown in Fig. 1. The setup is designed for different thicknesses by adjusting upper gear and upper roller, up and down. The strip of AA8011 is first passed through gears where it get Corrugated and then passed through rollers which straighten the sheet metal. For passing one time in gears and rollers will be considered as one pass. Similarly repeating the same strip again for number of passes is carried out. The AA8011 strips of CRCS processed are cleaned and tested for Vickers Micro hardness (Hv), with a load of 200 g for duration of 20 s.

Rockwell Hardness test is conducted according to ASTM E10 standard test for determining hardness of Aluminum Alloys, in which 5 mm diameter steel ball indenter is used with a 100 kg load and the hardness is read on the B scale. Brinell

Table 1 Chemical composition of AA8011

Alloy	Si	Fe	Cu	Mn	Mg	Cr	Ni	Zn	Ti	Others	
										Each	Total
8011	0.5–0.9	0.6–1.0	0.1	0.2	0.05	0.05	–	0.1	0.08	0.1	0.15

Fig. 1 Set up of CRCS system



Hardness test is conducted according to ASTM E10 in which 10 mm diameter hardened steel ball indenter is used to indent into the surface of the AA 8011 specimens load applied is 250 kg then by measuring the diameter of indentation and using the formula BHN is calculated.

3 Results and Discussion

Figure 2 shows the changes in Micro hardness with respect to number of passes of the AA8011 alloy sheet material. The increase in Micro hardness (H_v) continues through subsequent cycles and this is due to the grain size reduction occurred as the number of passes increased in CRCS process. Homogeneity of grains in the material is increased by more number of passes at the higher constant strain. The hardness values are increased by number of passes till 12 passes and then it is decreased. Initially without passing the H_v was 59 and at 12th pass the H_v obtained was 86. With further increase in number of passes hardness value decreased and further more remained constant till 15 passes. Similarly Rockwell hardness tests and Brinell hardness test were conducted and the change in hardness with respect to number of passes is shown in Fig. 3 for BHN and Fig. 4 for HRB.

Fig. 2 Variation of micro hardness of Al alloy with number of CRCS passes

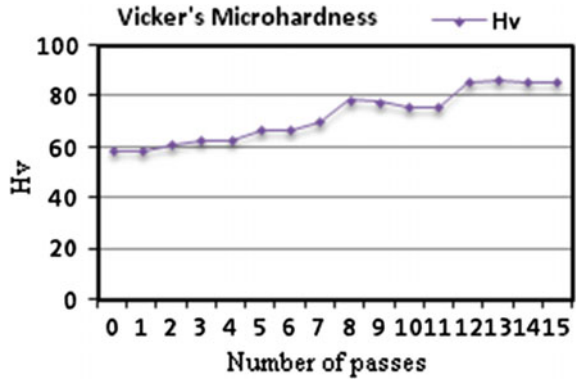


Fig. 3 Variation of BHN of Al alloy with number of CRCS passes

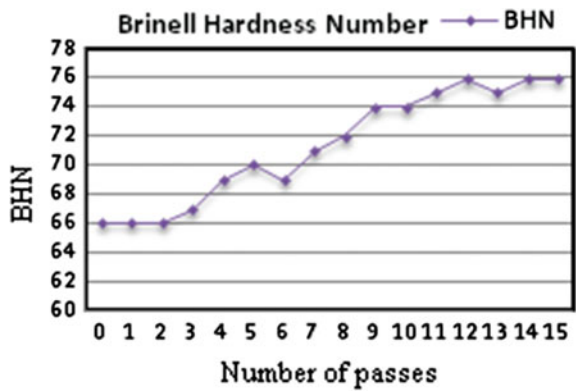
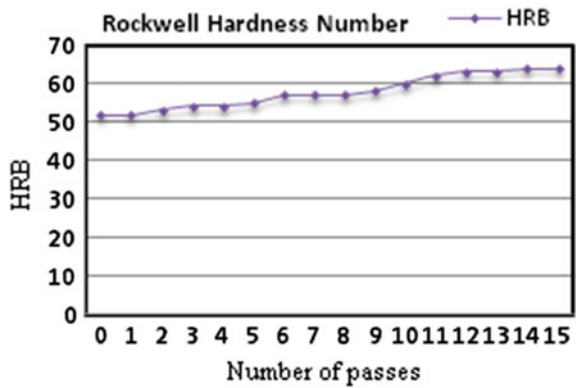


Fig. 4 Variation of HRB of Al alloy with number of CRCS passes



4 Conclusion

This study was carried out to inspect mechanical properties of AA 8011 alloy sheets processed by CRCS method. Based on the obtained results we can conclude that Micro hardness values of AA8011 alloy sheet before processing by CRCS method was 59 Hv, it increased to about 86 Hv after processing by CRCS method. Similarly HRB and BHN also increased. This increase in hardness is mainly due to strain induced and formation of ultra-fine grain refinement in the Al sheet material.

References

1. Mishra, A., & Richard, V. (2005). Micro structural evolution in copper processed in severe plastic deformation. *Materials Science and Engineering: A*, 410–411, 290–298.
2. Zhao, Y. H., & Zhu, Y. T. (2007). Influence of stacking fault energy on the minimum grain size achieved in severe plastic deformation torsion. *Materials Science and Engineering*, 463, 22–26.
3. Zhu, Y., & Jiang, H. (2001). A new route to bulk nano structured materials. *Metallurgical and Materials Transaction A: Physical Metallurgy and Material Science*, 32(6), 1559–1562.
4. Beygenzimer, Y., & Orlov, D. (2006). Futures of twist extrusion: Method, structures and material properties.
5. Vijapur, S. K., & Krishna, M. (2012). Effect of number of cycles on mechanical properties of aluminium sheet using corrugative and straightening methods. *IJMER*, 2(4), 2497–2499.
6. Krishnaiah, A., & Chakkiangal, U. (2005). Production of ultra fine grain sizes in aluminium sheets by severe plastic deformation using the technique of groove pressing. *Scripta Materialia*, 52, 1229–1233.
7. Siddesha, H. S., & Shantaraja, M. (2012). Investigation of micro structure and mechanical properties of commercially pure aluminium produced by RCS process. *IJERA*, 2(5), 333–341.

Effect of Extrusion Process on Mechanical Properties of Al-MWCNT Composites Synthesized by Powder Metallurgy Route



Vijaykumar S. Jatti, Nitin K. Khedkar, Vinaykumar S. Jatti, Ashwini V. Jatti, and Ajay S. Athare

Abstract Powder Metallurgy (PM) technique was employed in this study to synthesis aluminum reinforced with multi-walled carbon nano-tube (Al-MWCNT) composites. Composites are fabricated by varying CNT as 0.33, 0.66, and 0.99 wt.%. And the fabricated Al-MWCNT composites were extruded at 500 °C. Based on experimental results it was found an increase in ultimate tensile strength, yield strength, compression strength and hardness by 26.6%, 15.92%, 114.55%, and 36%, respectively at 0.99 wt.% MWCNT composites compared to pure aluminum. Scanning electron microscopy images shows the uniform distribution of MWCNT in the aluminum matrix.

Keywords Aluminum powder · Multi-walled carbon nanotube · Extrusion process · Powder metallurgy · Scanning electron microscopy

1 Introduction

In this era of modern technology, lightweight materials play an important role in technology development in the field of defense, energy, automotive, space, etc. The importance of lightweight material in these fields is driven largely by their role in achieving greater energy efficiency and contributing to energy independence. Aluminium has striking properties and the only demerit is low strength in comparison to steel. To enhance the properties of pure aluminum, reinforcement is done in aluminum matrix, which is known as metal matrix composites (MMC's). Over several decades

V. S. Jatti (✉) · N. K. Khedkar · V. S. Jatti · A. V. Jatti
Symbiosis Institute of Technology, Symbiosis International University (Deemed University),
Pune, Maharashtra, India
e-mail: vijaykumar.jatti@sitpune.edu.in

A. S. Athare
JSPM's Jayawantrao Sawant College of Engineering, Savitribai Phule Pune University, Hadapsar,
Pune, Maharashtra, India

researchers are working on MMC's and these composites are providing promising outcomes. Researchers have used reinforcement materials like carbides, carbon fiber, grapheme and carbon nanotubes (CNT's) to enhance the composite properties. CNT's were first discovered in 1991 by scientist Sumio Iijima [1]. Choi et al. [2] synthesized Al-CNT nano composites with multi, double and single walled CNT's using powder metallurgy route. Authors concluded that multi-walled CNT's showed higher mechanical properties in comparison to other two. Bakshi and Agarwal [3] studied the effect of processing method, CNT-matrix interface, degree of deformation and CNT dispersion on the toughness, strength and elastic modulus during production of Al-CNT composites. Manjunatha and Dinesh [4] synthesized the Al6061-CNT composite by employing powder metallurgical route and studied the effect of multi-walled CNT weight percentage on tensile strength, young's modulus and compression strength. Saravanan et al. [5] manufactured Al4032-CNT composite through powder metallurgy route and studied the effect of ball milling process on synthesized composite. Liao et al. [6] synthesized Al-CNT composite and understood the effect of powder mixing method and secondary method on the produced composite. Kim et al. [7] fabricated the CNT composites by varying the weight percentage of CNT and sintering temperature. Authors identified the effect of sintering temperature on the mechanical properties of composite. Chu et al. [8] manufactured the Cu-CNT composites using powder metallurgy route and identified the effect of weight percentage of CNT on the synthesized composite. Dong and Zhang [9] manufacturing Cu-CNT composite and found that hardness and tensile strength of Cu-CNT composite is higher than pure copper. Pham et al. [10] synthesized Cu-CNT composite and studied the effect of weight percentage of CNT on hardness of fabricated composite. Zhang et al. [11] synthesized two types of composite namely, Al-SiC-Graphite composite and Al-SiC-Graphene using powder metallurgical route. Daha et al. [12] manufactured Al-Al₂O₃-RGO composite and estimated hardness of composite and tribological performance of composite. Manohar et al. [13] synthesized Al7075-SiC-Graphite composite and estimated the mechanical and microstructural properties of composite. Aim of this study was to synthesize Al-MWCNT by varying the different weight fraction of MWCNTs and study the effect of weight fraction of MWCNTs on mechanical properties of composites.

2 Material and Methods

In this study Al composite with MWCNT as reinforcement material was synthesized through the powder metallurgy process which is a leading manufacturing process for Auto components. Aim of this work is improving the mechanical properties of light weight material without increasing the density of the material. Aluminium is better material whose density is one third of steel and availability is huge. MWCNT's were purchased from Sigma Aldrich, Pune. Composites were fabricated with three weight fractions of MWCNT i.e. 0.33, 0.66, and 1 wt.%. Planetary ball milling was used to get a homogeneous and uniform mixture of Al and MWCNT's powders. Mixture

of Al and MWCNT's was compacted into cylindrical billets of 30 mm diameter by using a 100 ton hydraulic press under ambient conditions. For compaction special purpose compaction set up i.e. die, and punch was developed. The compacted green billets were sintered in a tubular sintering furnace at 600 °C temperature for 120 min to convert into hard billets. The sinter billets were extruded at 500 °C temperature by using an extrusion set up which was fabricated especially for this work. Then the specimens were prepared for further mechanical testing. The density was measured before and after extrusion by using the Archimedeian principle at room temperature using water as an auxiliary liquid using Eq. 1. Hardness was checked before and after extrusion using Rockwell hardness tester B-scale. Tensile and compressive test was performed using universal testing machine. Tensile strength was measured as per the ISO-6892-1:2009 standard. As per the standard gauge length of specimen is 30 mm and gauge diameter is 6 mm and holding diameter is 12 mm.

$$Density = \frac{W_a \times \rho_a - W_w \times \rho_w}{W_a - W_w} \quad (1)$$

where, W_a —weight of sample in air, ρ_a —density of air, W_w —weight of sample in water, ρ_w —density of water.

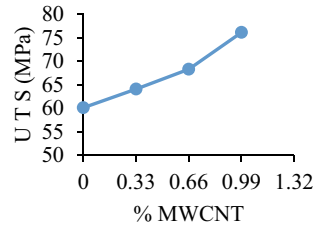
Microstructure was observed using Scanning electron microscopy (SEM). And the properties of Al-MWCNT's metal matrix composites were compared with pure Al material.

3 Results and Discussion

This study shows the mechanical behavior of Al-MWCNT composites. The specimens were synthesized by powder metallurgical route and further extruded using extrusion setup. Mechanical tests were carried out as per the ISO standards. This section discusses the results of mechanical, physical and microstructural properties of developed composites. Based on the results it was observed that ultimate tensile strength of Al increases with increases in MWCNT's. It's due to hard reinforcement into the soft matrix composite. It can be observed from Fig. 1, in addition to MWCNT's tensile strength increase with increase up to 26% without changing density of material which is desirable for light weight material similar results observed by [3].

It was observed Fig. 2, in addition to MWCNT's yield strength increase. This is due to the proper dispersion of MWCNT's in Al matrix and strong bonding between MWCNT's and Al matrix. For 0.99 wt.% of MWCNT's yield strength was 54.73 MPa which is 15% more than the plain Al. From Fig. 3 it can be observed that there is an appreciable increment in the compressive load on adding the MWCNT's. For 0.99 wt.% of MWCNT's compressive strength is 188 MPa. At lower percentage of MWCNT's the specimen fails by cracking but at 0.99 wt.% of MWCNT's there is no cracks on specimens. This is due to the proper and homogeneous dispersion

Fig. 1 Ultimate tensile strength versus percentage of MWCNT



of MWCNT's in Al matrix. From Fig. 4 it has been observed that, hardness of the extruded samples is increasing with increase in the wt.% of MWCNT. It is due to the decrease in porosity after extrusion. If we compared the hardness of pure Al before extrusion with Al-MWCNT's composite with 0.99 wt.% MWCNT's after extrusion there is 48% increment in hardness. Theoretical density decreases with increasing quantity of MWCNT's due to addition of light weight reinforcement material (1.7 g/cc), as depicted from Fig. 5 and Table 1. Density achieved through powder metallurgy is 94.80% of the actual density of Al material. From Fig. 6 and Table 1 it is clear that experimental density is less than the theoretical density, but experimental value is more correct because we get the correct volume of composites which is equal to the volume of water displaced. Experimental density also decreases with increasing quantity of MWCNT's due to addition of light weight reinforcement material (1.7 g/cc). Experimental Density achieved through powder metallurgy is 90% of the actual density of Al material.

When microstructure was investigated for the fracture part after tensile test, it was observed that the percentage of MWCNT is very less at fracture location. Because of MWCNT's homogeneously mixed with Al partials. At a higher percentage of

Fig. 2 Yield strength versus percentage of MWCNT

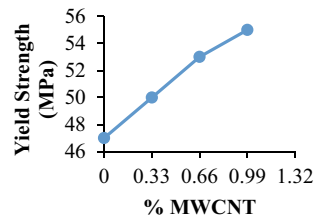


Fig. 3 Compression strength versus percentage of MWCNT

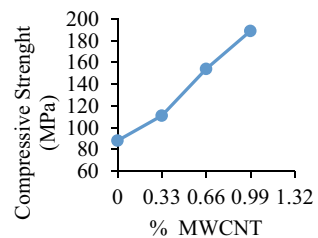


Fig. 4 Hardness versus percentage of MWCNT

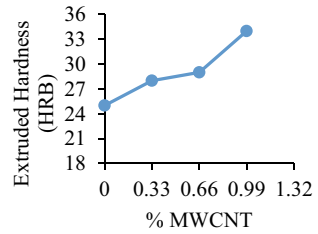


Fig. 5 Theoretical density versus percentage of MWCNT

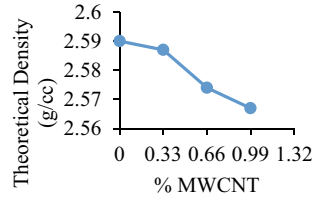
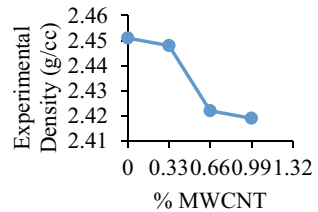


Table 1 Comparison between theoretical and experimental density

MWCNT (%)	Theoretical density (g/cc)	Experimental density (g/cc)	Deviation	Percentage error
0	2.59	2.45	0.14	5.41
0.33	2.588	2.446	0.142	5.49
0.66	2.575	2.42	0.155	6.02
0.99	2.57	2.415	0.155	6.03

Fig. 6 Experimental density versus percentage of MWCNT



MWCNT there is the problem of agglomeration which is overcome by planetary ball milling process in the present study. ED's image shows that percentage of carbon at the fractured location. In the microstructure of Al + 0.33 weight% MCNT's very less amount of MWCNT's are observed. This is because of the proper dispersion of MWCNT's in the Al matrix. In the microstructure of Al + 0.66 weight% MCNT's, it can be observed that uniform grains are fused in Al atoms. Again the very least amount of MWCNT's is observed. This is because of the proper dispersion of MWCNT's in the Al matrix. In the microstructure of Al + 0.99 weight% MCNT's, it can be observed that uniform grains are fused in Al atoms. Porosity between the grains was

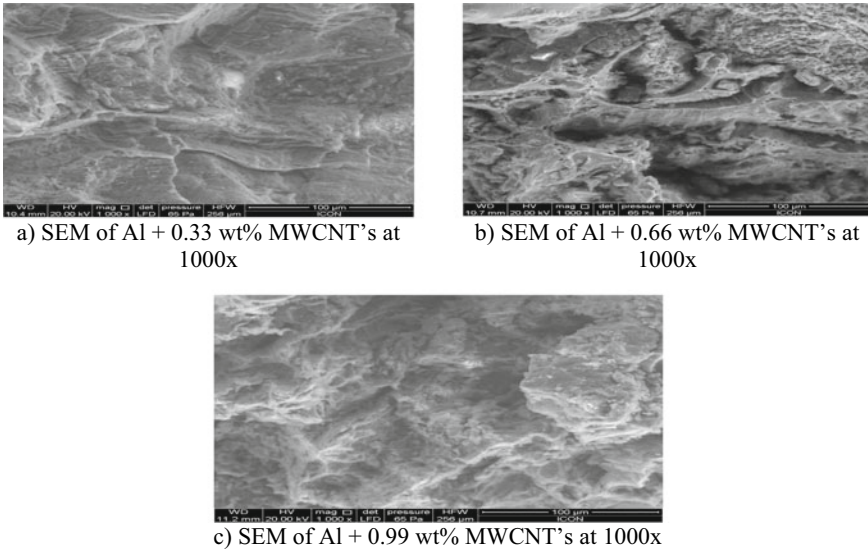


Fig. 7 Microstructure of composites

observed. Since grain boundary along the porosity and fused aluminium grains make the components brittle SEM shows that black portion is porosity, Fig. 7. Fusion of Al grains is uniform. Figure 8 shows the EDS image of composites. Amount of Al is more than the amount of carbon i.e. MWCNT's in case of Al + 0.33 weight% MCNT's composite. In case of Al + 0.66 weight% MCNT's composites, quantity of carbon was increased and Al + 0.99 weight% MCNT's composite shows further increase in carbon at the fracture tensile surface.

4 Conclusions

This study depicted the synthesis of Al alloy and Multi walled CNT composite using powder metallurgical technique. Study showed successfully synthesized composite. Following are the findings of the study:

- Hardness of Al-MWCNT composites is greater than pure aluminium.
- Hardness increases without increase in density of composites.
- Ultimate and yield strength increased with the addition of MWCNT'S.
- Due to the proper dispersion of MWCNT'S there is an increase in compressive strength of the composites without increase in brittleness.

Ultimate tensile strength, yield strength, compression strength and hardness of the composites at 0.99 wt.% MWCNT were 26.6, 15.92, 114.55, and 36%, more than

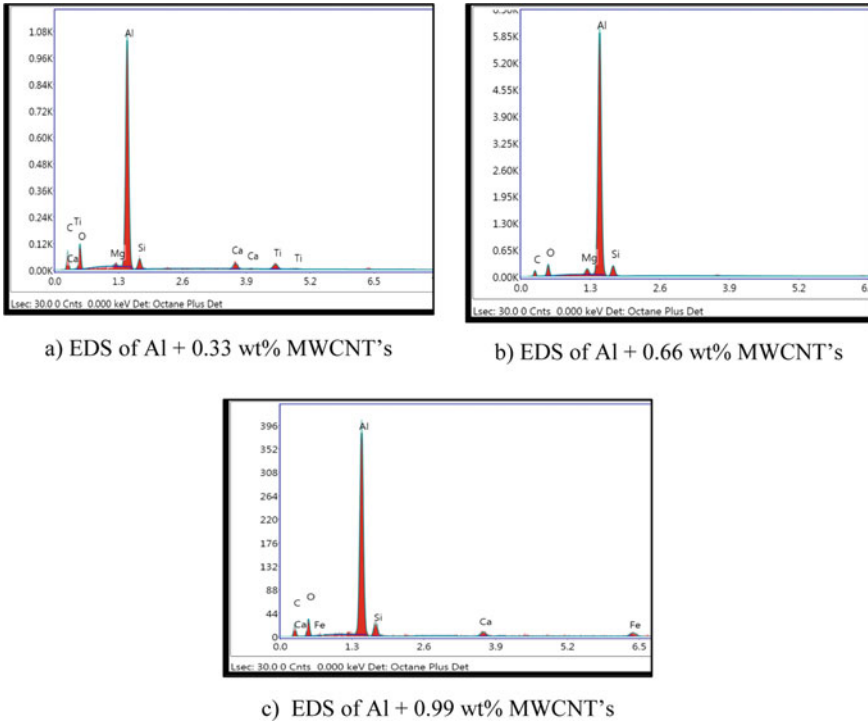


Fig. 8 EDS images of composites

the pure aluminum. Uniform distribution of MWCNT was observed in the aluminum matrix.

References

1. Iijima, S. (1991). Helical microtubules of graphitic carbon. *Nature*, 354, 56–58.
2. Choi, H., Wang, L., Cheon, D., & Lee, W. (2013). Preparation by mechanical alloying of Al powders with single, double, and multi-walled carbon nanotubes for carbon/metal nanocomposites. *Composites Science and Technology*, 74, 91–98.
3. Bakshi, S. R., & Agarwal, A. (2011). An analysis of the factors affecting strengthening in carbon nanotube reinforced aluminum composites. *Carbon*, 49, 533–544.
4. Manjunatha, L. H., & Dinesh, P. (2013). Fabrication and properties of dispersed carbon nanotube-Al6061 composites. *International Journal of Innovative Research in Science, Engineering and Technology*, 2(2).
5. Saravanan, M. S. S., Babu, S. P. K., & Sivaprasad, K. (2010). Mechanically alloyed carbon nanotubes (CNT) reinforced nanocrystalline AA 4032: synthesis and characterization. *Journal of Minerals and Materials Characterization and Engineering*, 9(11), 1027–1035.
6. Liao, J., Tan, M., Ramanujan, R. V., & Shukla, S. (2011). Carbon nanotube evolution in the aluminum matrix during the composite fabrication process. *Materials Science Forum*, 690, 294–297.

7. Kim, G.-N., Kim, H.-J., & Huh, S.-C. (2015). A study on the mechanical characteristics of Cu-CNT composites by extrusion process. *Applied Mechanics and Materials*, 764–765.
8. Chu, K., Cheng, J., Li-kun, J., & Wensheng, L. (2013). Improvement of interface and mechanical properties in carbon nanotube reinforced Cu-Cr matrix composites. *Materials and Design*, 45, 407–411.
9. Dong, S. R., & Zhang, X. B. (2001). An investigation of the sliding wear behavior of Cu-matrix composite reinforced by carbon nanotubes. *Materials Science and Engineering*, 131, 83–87.
10. Pham, V. M., Bui, H. T., Tran, B. T., Than, X. T., Nguyen, V. C., Doan, D. P., & Phan, N. M. (2011). The effect of sintering temperature on the mechanical properties of a Cu/CNT nanocomposite prepared via a powder metallurgy method. *Advances in Natural Sciences: Nanoscience and Nanotechnology*, 2.
11. Zhang, J., Liu, Q., Yang, S., Chen, Z., Liu, Q., & Jiang, Z. (2020). Microstructural evolution of hybrid aluminum matrix composites reinforced with SiC nanoparticles and graphene/graphite prepared by powder metallurgy. *Progress in Natural Science: Materials International*, 30, 192–199.
12. Daha, M. A., Nassef, B. G., & Nassef, M. G. A. (2021). Mechanical and tribological characterization of a novel hybrid aluminum/Al₂O₃/RGO composite synthesized using powder metallurgy. *Journal of Materials Engineering and Performance*, 30, 2473–2481.
13. Manohar, G., Maity, S. R., & Pandey, K. M. (2022). Microstructural and mechanical properties of microwave sintered AA7075/graphite/SiC hybrid composite fabricated by powder metallurgy techniques. *SILICON*, 14, 5179–5189.

Effect of Section Thickness on Solidification and Microstructure of Ductile Cast Iron



Bahubali B. Sangame and Y. Prasannatha Reddy

Abstract In the current situation, where the energy crisis is continuously worsening, industries and researchers are vigorously working toward a common energy savings objective through various techniques. The usage of lightweight components is increasingly prioritized by manufacturing sectors to reduce total energy consumption. Ductile cast iron is one of the leading alloys in structural and automotive applications. The solidification of ductile iron castings with both thick and thin walls has drawn more attention in recent years. However, it is challenging to produce thin-walled ductile cast iron items due to their intricacy. The morphology of the cooling curves and the microstructure of variable thickness (both thick and thin) ductile iron casting are explored in this study. According to the findings of the solidification and cooling curve study of the variable thickness step casting, thick portions show a prolonged eutectic reaction compared to the thin portion of step casting.

Keywords Ductile cast iron · Graphite nodule count · Solidification · Thermal analysis

1 Introduction

Controlling emissions, increasing fuel economy, and cutting prices are the three main issues facing the transportation sector. Reducing the weight of the vehicle is one way to increase fuel economy; a lowering of 100 kg corresponds to an increase in fuel efficiency of 0.4 km per litre [1]. The transportation sector will access alternative,

B. B. Sangame (✉) · Y. Prasannatha Reddy
Mechanical Engineering Department, Sinhgad College of Engineering Vadgaon, Pune,
Maharashtra 411041, India
e-mail: bahubali2010@gmail.com

Y. Prasannatha Reddy
e-mail: ypreddy.scoe@sinhgad.edu

B. B. Sangame
Mechanical Engineering Department, Sharad Institute of Technology College of Engineering,
Yadav, Maharashtra 416115, India

more affordable weight-reduction methods thanks to thin wall ductile iron castings. Additionally, the cost of melting is decreased due to the less iron used. Lower emissions of carbon dioxide into the atmosphere are the result of both of these factors. Many processing innovations have been achieved over time, and production capacity has significantly grown. However, occasionally defective castings are still produced using even the most modern ductile iron production techniques [2]. Experiences on the production floor have revealed that heats with similar compositions, modified and inoculated using the same techniques, and cast in identical moulds can vary significantly regarding graphite nodule count, carbide formation, and integrity [3]. These problems are frequently caused by differences in melt processing variables like superheating temperature, metal holding time, and input material quality [4]. Production deadlines and financial concerns constrain the ability to manage every aspect of production strictly. Additionally, there are still a lot of variables regarding the ductile iron's kinetics of nucleation and solidification [2, 5, 6]. As a result, different process monitoring tools have been designed to date to investigate these process control factors. One of these tools that can provide extremely precise information about the behavior of metals during solidification is thermal analysis [7].

The effect of important parameters such as section thickness and solidification rate on the ductile cast iron microstructure was investigated in this study. In this regard, the primary goal of this research is to analyse the solidification process of variable thickness ductile cast iron in order to comprehend graphite nucleation in variable thickness ductile iron castings.

2 Experimental Procedure

In order to produce defect-free sound castings of varied thickness, the current work involves developing, modelling, and simulating a variable thickness step casting. A five-step pattern with thicknesses of 3, 7, 12, 18, and 25 mm is fabricated and mould is prepared by using green sand. To avoid the consequences of end freezing on each step, the width is 100 mm. The overall length of the casting is 200 mm, with each step measuring 50 mm. Each step has a gate to allow for the obstruction-free proper filling of liquid metal (Fig. 1).

Fig. 1 Wooden pattern of step casting



2.1 Melting of Cast Iron and Magnesium Treatment

In a 150 kg medium frequency induction furnace, the raw material was melted. The charge consists of 30% pig iron, 25–30% cold-rolled steel scrap, and 30–40% foundry runner riser return. Ductile iron is treated at the foundry using a 5% ferrosilicon alloy with a 1.8 wt% addition rate. A preheated ladle with 10–15 mm of Ferro-silicon-magnesium alloy at its bottom and scrap stainless steel around it has been used to tap the molten metal, which is at a temperature of 1450 °C. Following the application of magnesium, the melt was immediately moved to 20 kg ladles, where the inoculant was mixed with the flowing metal. In the experiment, metal was inoculated with an inoculant of Ca, Ce-FeSi that contained 73.2% Si, 1.03% Ca, 1.67% Ce, and 0.94% Al, remaining Fe. The prepared melt is poured in the mould of variable thickness step casting mould. Metal samples were taken during the pouring to determine the final chemistry of the casting for spectroscopic investigation. Table 1 represents the composition of melt before and after magnesium and inoculation treatment.

3 Results and Discussion

The 3D model for the step casting of section thicknesses 3, 7, 12, 18 and 25 mm, length 50 mm and width 100 mm was prepared using CATIA software as shown in Fig. 2a. The variable thickness step casting model was used as a test model in AutoCAST software for simulation. In this study, the pouring temperature for the simulation was 1400 °C, while the average pouring temperature for ductile cast irons is between 1350 and 1400 °C.

Carbon and silicon content significantly influence the solidification of ductile cast iron. Ductile iron comes in three different compositions based on the carbon equivalent: hypoeutectic, eutectic, and hypereutectic. But hypereutectic ductile iron (C.E. > 4.3) is preferable because of its reduced propensity for shrinkage.

A simulation of the solidification process revealed that it begins with a plate of 3 mm thickness, as shown in Fig. 3. So the first plate to freeze was 3 mm thick. This indicates that compared to the other thicknesses, 3 mm plate cools at a faster rate. The cooling curves of the various portions of a step casting were produced by simulating a model of ductile iron casting with variable section thickness. Point TC1 represents the cooling curves for sections with a thickness of 25 mm, whereas points TC2, TC3, TC4, and TC5 reflect the cooling curves for sections 18, 12, 7, and 3 mm. Figure 4 shows the corresponding cooling curve for various section thicknesses.

According to simulation data, the solidification times for 3, 7, 12, 18, and 25 mm sections are 12, 30, 62, 112, and 178 s, respectively. With these data then TC5 has the highest cooling rate and TC1 has the lowest one from Fig. 4.

Table 1 Composition of molten metal in furnace before and after magnesium + inoculation treatment (final)

	C	Si	Mn	S	P	Cr	Ni	Cu	Mg
Before Mg treatment (wt.%)	3.70–3.72	1.70–1.85	0.22–0.28	0.012–0.015	0.010–0.015	0.010–0.020	0.02–0.03	0.015–0.02	Nil
Final composition (wt.%)	3.65–3.70	2.45–2.5	0.22–0.28	0.012–0.015	0.010–0.015	0.010–0.020	0.02–0.03	0.015–0.02	0.038–0.045

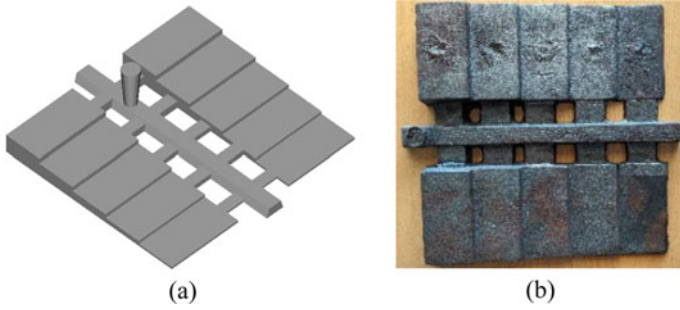


Fig. 2 a CAD model of variable thickness step casting b variable thickness step casting of ductile cast iron

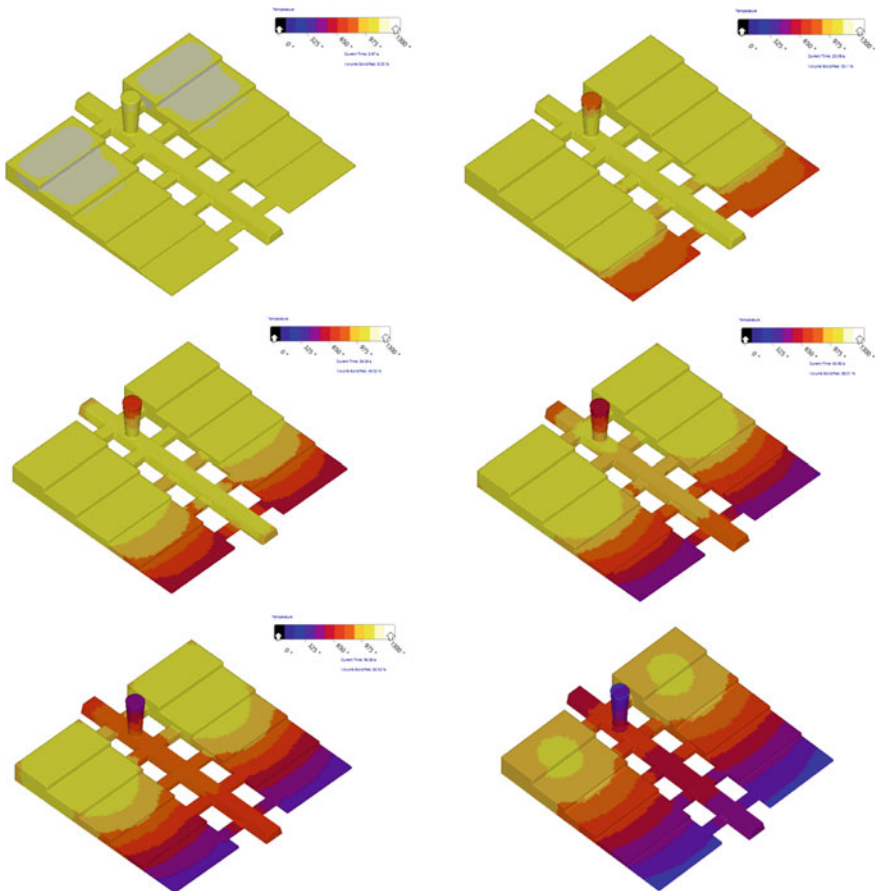


Fig. 3 Effect of section thickness on solidification sequence of step casting

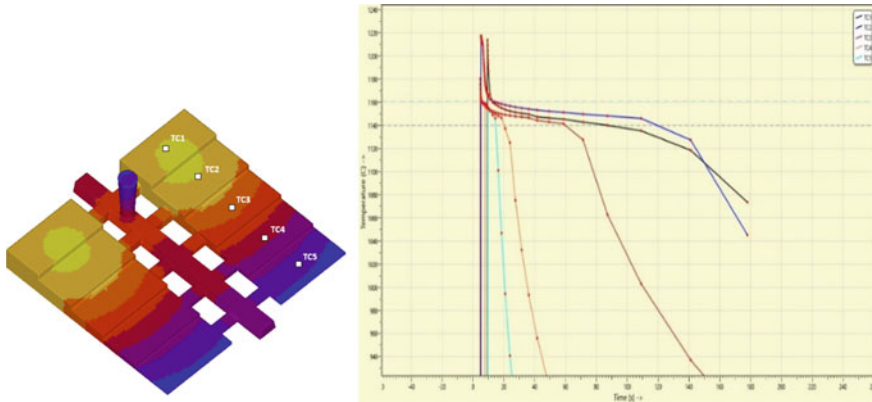


Fig. 4 Cooling curve comparison of ductile cast iron with varying section thickness

3.1 Effect of Section Thickness on Microstructure

The step casting was cut and prepared for a microstructure inspection to determine the nodule count and nodule size distribution. Microstructure study revealed that the nodule count is 341, 243, 228, 211, and 195 for sections with thicknesses of 3, 7, 12, 18, and 25 mm in step casting, respectively as shown in Fig. 5.

The higher nodule count in the 3 mm part can be correlated with forming of more nucleation sites due to higher cooling rates. However, in 3 mm and 7 mm sections as compared to 12, 18, and 25 mm sections, nodules are smaller in size. This is due to a prolonged eutectic reaction in thick parts, and as a results, the size of the nodules is larger in thick parts compared to thin ones. It is made clear in this study how important variables like section thickness and solidification rate greatly affected the ductile cast iron metallurgy and how these parameters are believed to effect the microstructure. In ductile cast iron, the association between thickness of casting and microstructure was taken into consideration. Based on casting thickness, the solidification rate is determined. The solidification rate is the most significant factor that affects the nodule count and nodule size of ductile cast iron. As section thickness increased, the rate of solidification reduced. The experimental study shows ductile cast iron exhibits growing nodule size and reduced nodule count with higher section thickness as shown in Fig. 5.

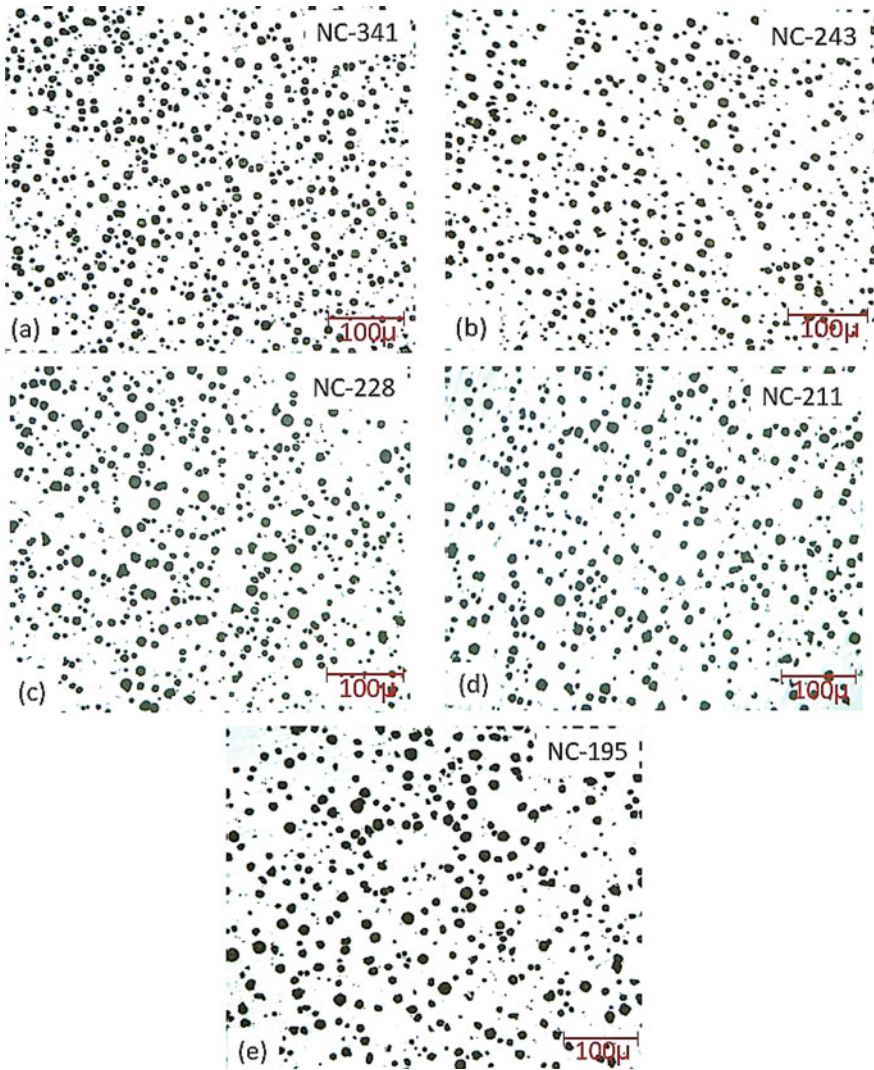


Fig. 5 Optical microstructure and phase distribution of samples having a 3 mm, b 7 mm and c 12 mm d 18 mm and e 25 mm section thickness

4 Conclusion

- Ductile cast iron cooling curve analysis is an important approach for forecasting casting quality since it analyses the behaviour of liquid metal during solidification.
- Casting wall thickness significantly affects the shape of the ductile iron solidification curve. In comparison to thick portions, thinner sections exhibit a smaller eutectic interval.

- Smaller graphite nodules are found in thinner areas of ductile iron casting, while large graphite nodules are found in thicker sections.
- The rate of graphite nucleation increases as casting thickness reduces, but nodule size grows as casting thickness increases.

References

1. Fraś, E., Górny, M., & Kapturkiewicz, W. (2013). Thin wall ductile iron castings: Technological aspects. *Archives of Foundry Engineering*, 13, 23–28. <https://doi.org/10.2478/afe-2013-0005>
2. Kapturkiewicz, W., Burbelko, A., & Górny, M. (2014). Undercooling, cooling curves and nodule count for near-eutectic thin-walled ductile iron castings. *ISIJ International*, 54, 288–293. <https://doi.org/10.2355/isijinternational.54.288>
3. Ochulor, E. F., Adeosun, S. O., & Balogun, S. A. (2015). Effect of gating sprue height on mechanical properties of thin wall ductile iron. *World Academy of Science, Engineering and Technology*, 9, 360–367.
4. Górny, M., Kawalec, M., Sikora, G., Olejnik, E., & Lopez, H. (2018). Primary structure and graphite nodules in thin-walled high-nickel ductile iron castings. *Metals (Basel)*, 8, 4–7. <https://doi.org/10.3390/met8080649>
5. Bhat, M. N., Mushtaq, S., & Mohbe, M. (2021). Impact of section thickness on cooling curve morphology, structure and properties of spheroidal graphite cast iron. *Sadhana—Academy Proceedings in Engineering Sciences*, 46. <https://doi.org/10.1007/s12046-020-01541-9>
6. Muhmond, H. M., & Fredriksson, H. (2018). Effect of the cooling rate on the graphite nodule count and size distribution in nodular cast iron. *Materials Science Forum*, 925, 45–53. <https://doi.org/10.4028/www.scientific.net/MSF.925.45>
7. Stefanescu, D. M. (2015). Thermal analysis-theory and applications in metalcasting. *International Journal of Metalcasting*, 9, 7–22. <https://doi.org/10.1007/BF03355598>

Analysis of Progressive Collapse of Moment Resisting Steel Frames for Failure Performance Improvement



Nishigandha Mahamuni, S. A. Gosavi, C. R. Abhangrao, S. P. Patil,
and G. K. Koshti

Abstract A moment-resisting steel frame's progressive collapse analysis is presented. Using STAAD PRO V8 for three distinct threat-independent column removal situations, the structural model was analyzed, and the alternative load path approach was used. The General Service Administration (GSA-2003) criteria for calculating the likelihood for progressive collapse are being followed when removing columns. Results for leisure that removes a crucial structural member are displayed.

Keywords GSA (2003) · Progressive collapse

1 Introduction

Progressive Collapse is the eventual collapse of an entire structure as a result of the spread of a primary local defeat from a structural section. Progressive collapse refers to the perception of the gradual loss of a portion of the structure or the entire structure brought on by the abrupt loss of a vertical load-carrying member, such as a column. When a member in the initial load-resisting system is lost, forces are transferred to the adjacent members, and if the transferred forces are greater than a member's capacity, the member collapses. A "skeleton frame" of vertical members and horizontal members made of various I-beams is constructed in modern steel frame structures (buildings) to support the floors, roof, and other elements linked to the frame.

1.1 Alternate Load Path Method

After excluding the column, the structure is examined for a probable collapse using the alternate load path approach. In this research work whole structure is designed

N. Mahamuni (✉) · S. A. Gosavi · C. R. Abhangrao · S. P. Patil · G. K. Koshti
Civil Engineering Department, SVERI'S College of Engineering, Pandharpur, Maharashtra, India
e-mail: nvmahamuni@coe.sveri.ac.in

These figures shows structure before and after progressive collapse.

Fig (1) - Structure Without Failure

Fig (2) - Removal Of Column

Fig (3) - Initial Structural Failure

Fig (4) - Progressive Collapse Of Structure.

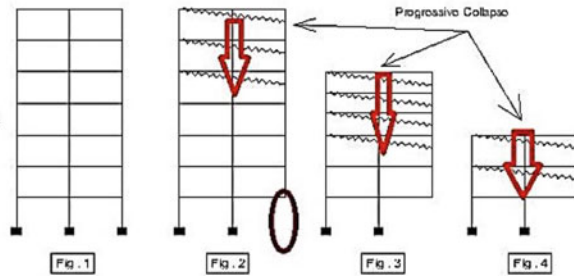


Fig. 1 Progressive collapse of structure

and analyzed, bending moment results of vertical structural member were taken in consideration. The member who observes lowest bending moment should be removed this in result gives the lowest number of failed structural member after reanalyzing (Fig. 1).

2 Recent Research Work

Vikas Tiwari and Sambhav Gangwal delivered a paper in 2019 titled “Progressive Collapse Study for Asymmetrical G + 11 Story Tall Building Using STAAD PRO.” GSA (2003) recommendations for progressive collapse analysis were taken into consideration. According to analysis, structural members close to a damaged or removed column joint sustain higher damage than structural members farther away from the joint. Critical in the incidence of progressive collapse is the corner column case. It has also been noted that appropriate reinforcing can be effective in keeping the DCR within the acceptable range in order to prevent the progressive failure of structural members following the failure of a column due to excessive blast loading. In order to assess the demand capacity ratio and the safety of the structure, Jain and Patil [1] devised a linear static analysis approach for progressive collapse analysis to test strength against local failure and accidental occurrences for an RC framed structure. In order to assess the exposure to progressive collapse of a representative RC framed structure, a finite element model for the G + 9 storey building had been taken into consideration and analyzed. The analysis was then conducted under critical column removal consequence in accordance with the guidelines provided in GSA (2003) while taking the provisions of IS 1893:2002 into consideration. This was done using ETABS software version 16.2.1 (software for modelling or analysis of structures). Observations of earthquake-damaged structures have demonstrated that an earthquake load may also cause local partial or complete failure of crucial components as well as progressive failure. The unusual dual system steel frame constructions with concentrically braced frames and entire loss of vital elements that were calculated to withstand earthquakes served as the foundation for this

study's three- and two-dimensional forming and push-over analyses [2]. Example of a probabilistic-based method for calculating structural systems' collapse potential can help us quantify earthquake-related losses more precisely. Equations and examples are used to illustrate how this methodology can be applied to the assessment of the collapse potential of existing structures and the design of structures that are safe from collapse. The likelihood of collapse at different danger levels and on an annually basis serves as a measure of the potential for collapse (mean annual frequency). A "collapse fragility curve," which expresses the likelihood of collapse as a function of the chosen ground motion intensity metric, serves as the fundamental component of the proposed methodology. The purpose of the execution encounters is to identify structural characteristics that could affect a structure's ability to collapse and to construct mathematical models for structural systems that can simulate performance close to collapse.

3 Structural Modeling

To determine the realistic behavior of the building during an earthquake, three models of steel frame buildings with (G + 10) floors were created for the analysis task. The steel frame construction is 12 m long and 8 m wide. The average story is 3.5 m tall. The first modifications in column size occur at five, eight, and nine stories. The structure is asymmetrical. Steel Fe 250 (mild steel) is utilized instead of concrete grade M20. Modeling using all the analytical variables that affect mass, strength, and stiffness. The non-structural element and the parts that barely affect how the structure behaves weren't modeled. The vertical and horizontal structural members, beams and columns, are modeled as frame elements and connected node to node. Analysis ignores the impact of soil structure interaction. It is believed that the vertical structural elements are fixed at the ground level.

4 Details of the Building Plan, Member Size and Materials

4.1 Plan

Figure 2 shows the plan of G + 10 steel frames depicts the steel building plan that was used for the study.

4.2 Size of Beam, Column, and Bracing Members

Table 1 displays the member sizes utilized for beams, columns, and bracing.

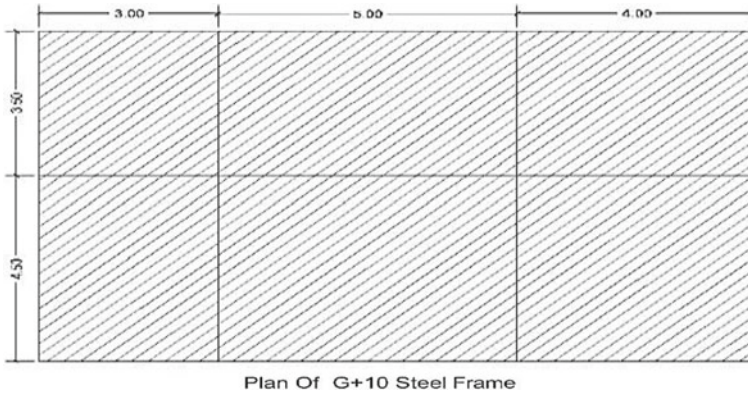


Fig. 2 Plan of G + 10 building

Table 1 Size of beams, columns and bracings

Level storey	Schedule of column		Schedule of beam	
	No. of column	Size	No. of beam	Size
G + 4	C1	ISMB 350	B1	ISMB 300
5–8	C2	ISMB 300	B2	ISMB 250
9–11	C3	ISMB 250	B3	ISMB 200

4.3 Material Analytical Properties

Concrete—M 20, Density—2400 kg/m³, Young’s Modulus E = 22,360 N/mm², Shear Modulus 8000 N/mm², Poisson’s Ratio—0.2.

Structural steel—Fe 250, Density—7850 kg/m³, Young’s Modulus E = 2.1 × 10⁵ N/mm², Shear Modulus 80,000 N/mm² Poisson’s Ratio—0.3.

4.4 Load Combinations

DL = 1.5 kN/m², LL = 3.5 kN/m².

Figure 3 shows Model Asymmetrical G + 11 Structure (2D) and (3D).

Load Combinations

1.5 × dl: 1.5 × L1

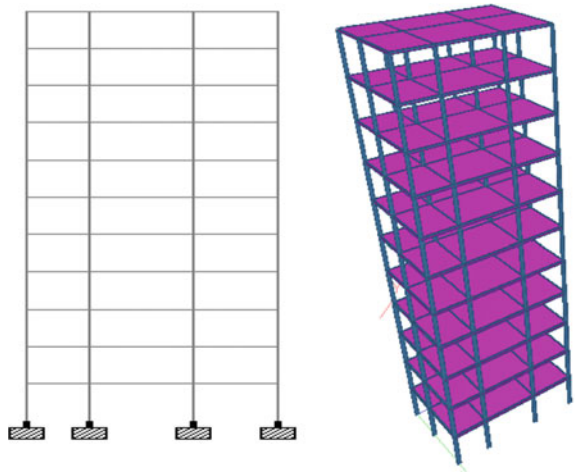
2 × dl: 1.2 × L1

1.5 × DL

0.9 × L1

(E = ZONE – NON SEISMIC ZONE).

Fig. 3 Model asymmetrical G + 11 structures (2D) and (3D)



Analysis of above structure shows zero member failure which indicates structure observed safe in linear static analysis.

For Progressive Collapse of above structure any load carrying element should be removed, for these vertical members of ground story are taken consideration.

4.5 Structural Member Removal and Analysis of Structure

Case 1: Vertical member near to shortest side of structure which is shown by Fig. 4.

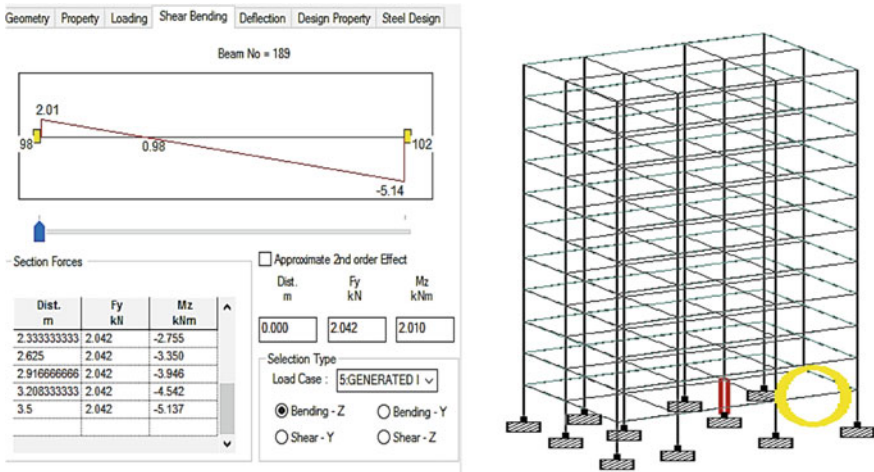


Fig. 4 Vertical member near to shortest side of structure

4.6 Overcome Failure and Improving Performance of Structure

After finding location of failure to achieve this objective different remedial measures for improving performance of structure like removal of failure causing member, strengthening structure are adopted. Figure 5 shows strengthening of column by increasing its size.

Strengthening can be done in different ways.

Two Adopted Methods

- (1) Strengthening of column by increasing its size.

Figures 6 and 7 show type of bracing and Inverted V bracing used in the structure.

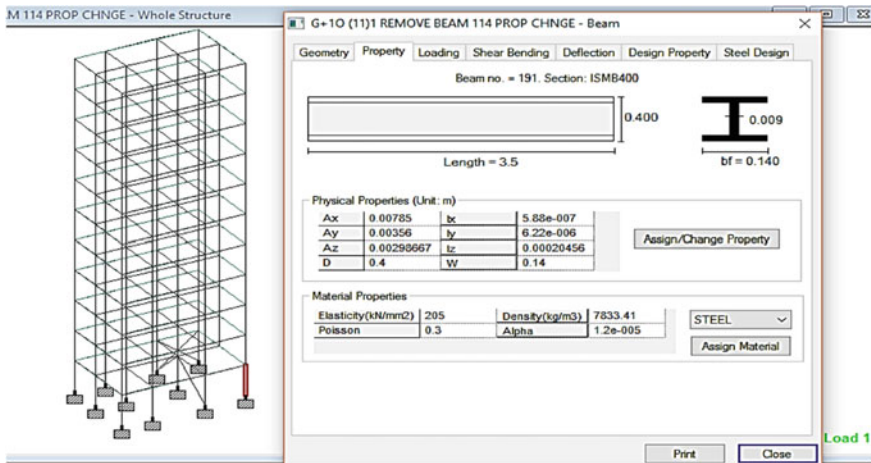
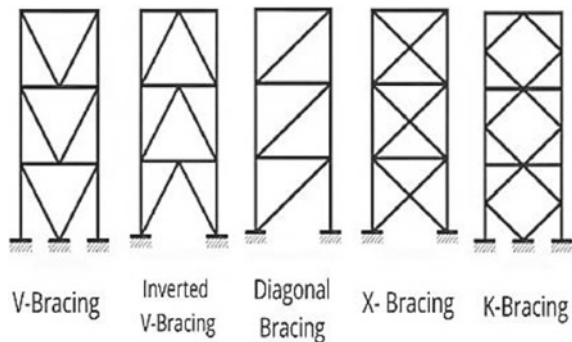


Fig. 5 Strengthening of column

Fig. 6 Type of bracing



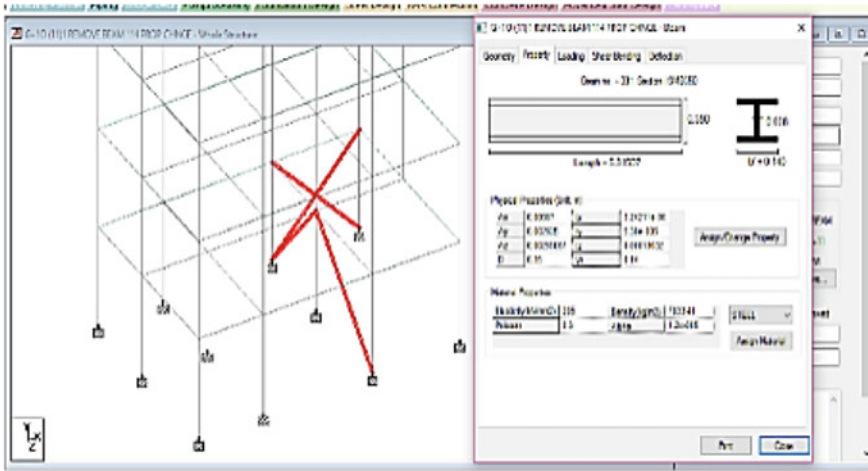


Fig. 7 Inverted V-bracing

4.7 Graphs of STAAD Pro Results

Bending moments of ground story are taken in consideration (Fig. 8).

5 Conclusions

Explanation of the findings from the 3D study of the steel frame of the asymmetrical G + 11 narrative. The ideal outcomes are based on stepwise analysis and procedures that adhere to GSA 2003 guidelines. By taking vertical member removal scenarios into consideration, a structure’s propensity for progressive collapse is determined. The outcomes are described below as.

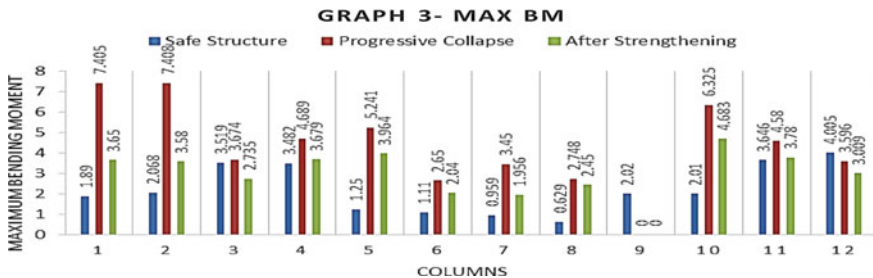


Fig. 8 Maximum BM of safe structure versus progressive collapse versus after strengthening

According to the current investigation, beams that are farther from the removed vertical member joint than the damaged or removed vertical member joint experienced higher destruction. The incidence of progressive collapse is revealed to have involved corner column removal (case 3). For structures with more than one failing member and for floor to floor failure, reinforcing a column becomes more challenging in order to reduce the effect of progressive collapse. A useful corrective measure to stop progressive collapse is a bracing element.

References

1. Patil, A. S., & Kumbhar, P. D. (2013). Time history analysis of multistore. *International Journal of Structural and Civil Engineering Research*, 2(3).
2. Zareian, F., et al. (2007). Assessment of probability of collapse and design for collapse safety. *Earthquake Engineering Structural Dynamics*, 36, 1901–1914. <https://doi.org/10.1002/eqe.702>

Comparative Study of Seismic Analysis and Design of Different Types of Bridge Abutments



Santosh K. Kumbar, Jyoti P. Bhusari, Anil Panjwani, and M. V. Bhogone

Abstract An essential component of the economics of the entire bridge project is choosing the right kind of abutment given the site characteristics. This study involves the seismic analysis and design of several non-submersible bridge abutment types, such as the box type, counter fort type, C-attached, C-type detached, and gravity type. The abutments under consideration are associated with the active project of the high-level bridge over the Venna River at Jawali, Satara, India (between Sawali and Mhate). Comparative analysis employing IRC requirements of several bridge abutments under dynamic earth pressure, superstructure loading, and live surcharge. The deck slab, girders, and abutments measurements have been specified in accordance with the PWD standard manual for two-lane traffic. STAAD PRO software is used to simulate the chosen bridge abutments in order to test the structural behaviour of eight HFL and OFL load combinations. On the basis of the abutments' design, cost analysis is performed. The box-type abutment has demonstrated reasonably stable structural performance with favourable economic cost effects. The box-type abutment has outperformed other types in a comparison of all abutments based on the bending moment, shear force, and deflection. Despite attracting less bending moment than the box-type abutment, the gravity-type abutment failed the stability test for the seismic situation.

Keywords Abutment modeling · Seismic performance · Box type abutment

S. K. Kumbar (✉) · J. P. Bhusari · M. V. Bhogone
Department of Civil Engineering, Sinhgad College of Engineering, Vadgaon (Bk), Pune, India
e-mail: kumbarsantosh194@gmail.com

A. Panjwani
ACME Structural Consultants, Pune, India

1 Introduction

An abutment should be designed to withstand damage from the earth pressure, gravity loads of the bridge superstructure and abutment, live load on the superstructure or the approach fill, wind loads, and the transitional loads transferred through the connection between the superstructure and the abutment. Any possible combinations of those forces which produce the most severe condition of loading should be investigated in the abutment design [1]. An approximate method for dynamic analyses of skewed bridges with continuous rigid decks was proposed by Kalantari and Amjadian [2]. They developed a three-degree-of-freedom analytical model to determine the natural frequencies, mode shapes, and internal forces for short-skewed bridges. Dimitrakopoulos [3] investigated the seismic response of short-skewed bridges with pounding deck-abutment joints and proposed a non-smooth rigid-body approach to analyze their response. Dimitrakopoulos concluded that the tendency of skewed bridges to rotate after deck-abutment collisions is a factor of the skew angle, deck geometry, and friction between the deck and abutment.

In a subsequent study [4], they used a dual-beam stick model to represent the bridge deck and showed that in-plane deck rotations are mostly due to abutment reactions. Related to seismic behavior some of the authors' have studied the seismic behavior of reinforced concrete bridges with skew-angled gravity-type abutments, and some studies are focused on an experimental study of the seismic behavior of an existing bridge abutment located on soft clay deposits.

Based on the area decided and the literature review carried out in detail, the aim and objectives of this study have been decided. The aim is to carry out a comparative study on the design and estimation of gravity type, counter fort type, box type, cantilever (C) attached type, and cantilever (C) detached type abutments (detached type means there is 20 mm gap between abutment wall and return wall) as shown in Figs. 1, 2, 3, 4 and 5.

Fig. 1 Gravity-type abutment

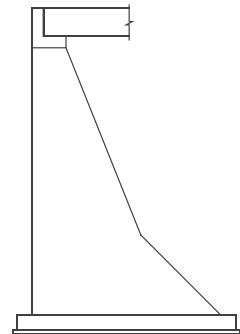


Fig. 2 Plan of counter-fort type abutment

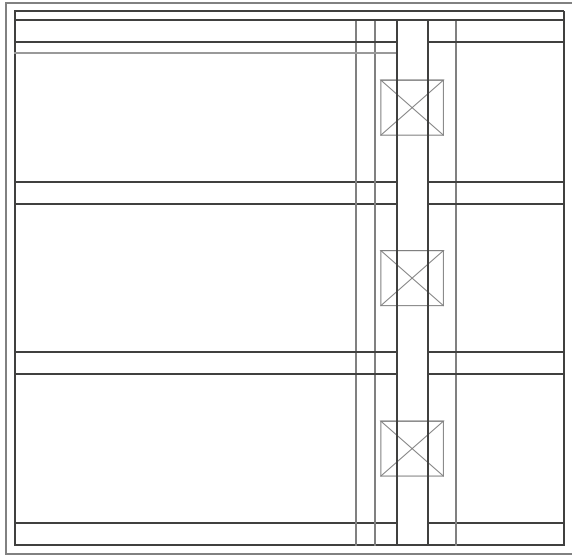
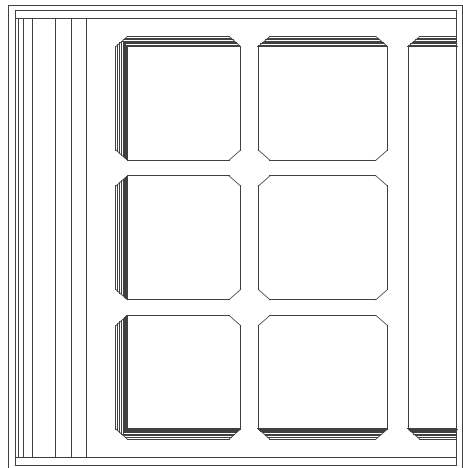


Fig. 3 Plan of box type abutment



2 Methodology

The high-level bridge project on the Venna River (between Sawali and Mhate), Taluka—Jawali, and Dist—Satara, which is part of the Pune PWD region, is connected to the abutments that were taken into consideration for the seismic study and design. The main focus of this study will be on the analysis and design of several bridge abutments that are suitable for this bridge under seismic zone IV, in compliance with the tender document. Since the geological study indicates that the

Fig. 4 Plan of C-type attached abutment

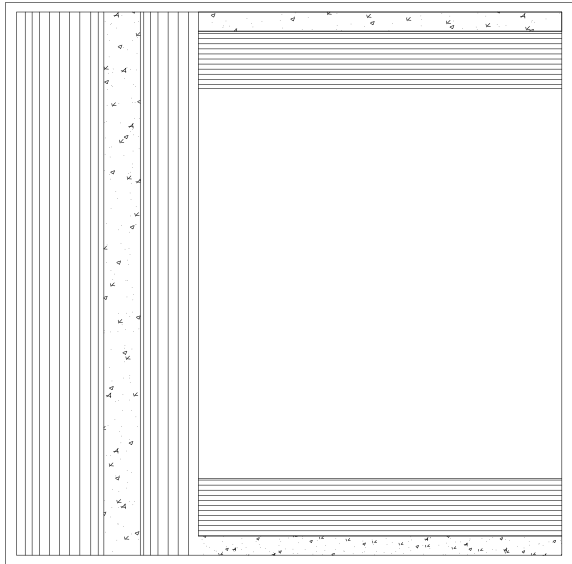
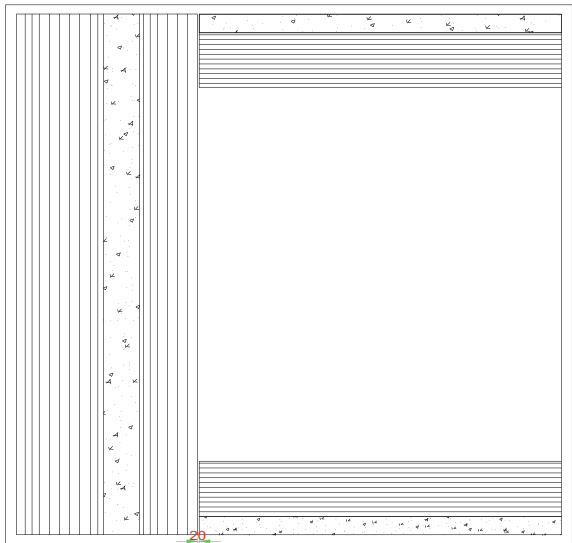


Fig. 5 Plan of C-type detached abutment



hard strata are accessible up to 2 m below the riverbed, an open raft foundation is suggested. The peak water current speed on this river during the rainy season is 5.25 km/h, and the high flood level (HFL) is below the soffit level of the bridge. The design therefore belongs to the non-submersible class. The analysis and design of the abutments for the bridge, including those of the gravity type, counterfort type, box type, cantilever attached type, and cantilever detached type, will be finished.

The steel grade utilised is Fe500, and the covers used are 75 mm on the earthy side and 40 mm on the other face. For the abutment wall, the grade of concrete used is M30, and for a pedestrian, it is M35. The references to IRC-112:2019: Standard standard and code of practise for concrete road bridges and IRC-6: 2017: Load and load combinations It is recommended to use both IRC-SP-114:2016: Guidelines for Seismic Design of Road Bridge and IRC-78:2014: Sub-structure and Foundation.

All abutments have undergone stability and base pressure inspections for various load combinations at HFL and OFL (observed flood level). There are three load combinations at HFL (i) Condition normal with live load (ii) Condition normal without live load (iii) There are five load combinations at the OFL condition with no superstructure, including the three mentioned above. The fourth and fifth load combinations are seismic condition with live load and seismic condition without live load, respectively.

3 Three Dimensional Modeling and Analysis

Using the finite element method, the analytical abutments create the 3D model in the STAAD pro software. The superstructure and abutments' dimensions are listed in Tables 1 and 2 [2]. Since the bottom node has a raft foundation, all sorts of abutments have been modelled utilising plate components with meshing for abutment walls, return walls, and tie walls. The STAAD model has been used to apply the predicted seismic ground pressure load and horizontal superstructure load. The seismic earth pressure is applied as a trapezoidal load per square metre area on the plate element and the superstructure loads are applied as a uniformly distributed load on top of the abutment cap in a negative Y-direction. All different kinds of abutments are subjected to these loads, and analysis is done. According to Figs. 6, 7, 8, 9, and 10, the bottom side of the abutment wall will experience the highest bending and shear loads. The self-weight of the deck slab, girders, wearing coat, etc., as well as vehicle live load, are included in the superstructure load. For the superstructure, the STAAD pro programme created a grillage model of the deck slab and girder. The static loads of the overlaid surface dead load and worn coat load were then applied to the grillage model to obtain the dead load reactions. Prepare a line model in STAAD Pro for a vehicle live load, create moving loads according to a live load combination on it, and measure the responses.

4 Results and Discussion

The abutments listed above have undergone systematic analysis and are created for various load combinations. Safety against sliding and overturning stability checks with the permitted values of 1.5 and 2. These FOSs decrease to 1.25 and 1.5 for

Table 1 Superstructure data

Sr. No.	Description	Input
1	Type of superstructure	RCC wide beam
2	Bearing center to center of the pier	19.15
3	Skew angle	'0' degree
4	Overall width of bridge (normal)	8.5 m
5	Carriageway width (normal)	7.5 m
6	Overall depth of superstructure including wearing coat	1.786 m
7	Type of wearing coat	Bituminous
8	The thickness of wearing coat	80 mm
9	Type of railing	Crash barrier
10	Type of bearings	Neoprene bearings

Table 2 Substructure data

Sr. No.	Description	Input
1	Length of the abutment wall	8.5 m
2	Width of abutment	6.75 m
3	Thickness of raft	450 mm
4	Width of abutment cap	1.25 m
5	Depth of abutment cap	0.3 m

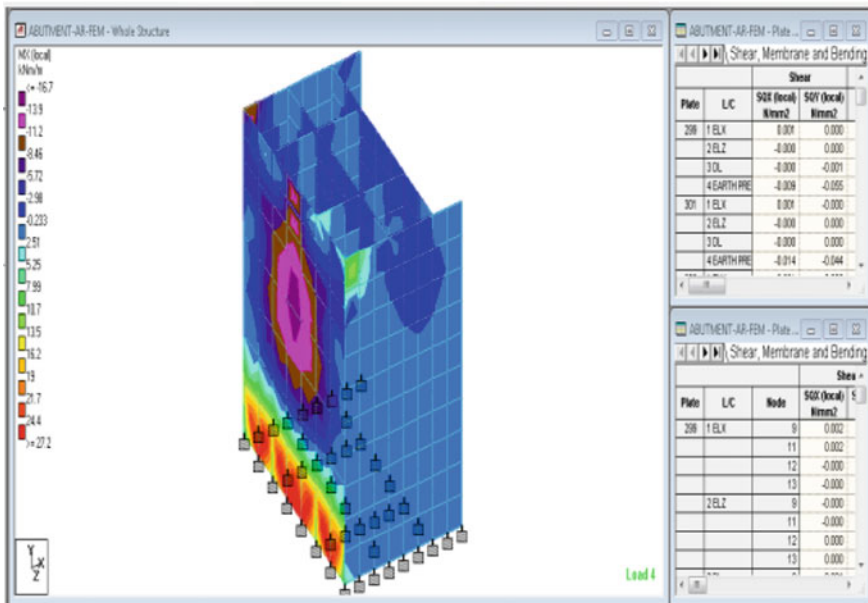


Fig. 6 Box type abutment (STAAD model)

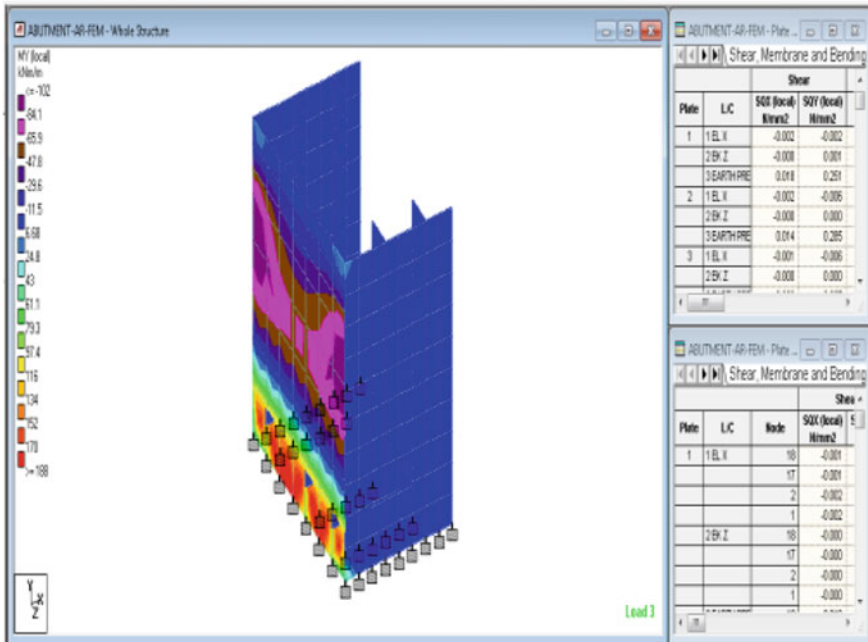


Fig. 7 Counter fort type abutment (STAAD model)

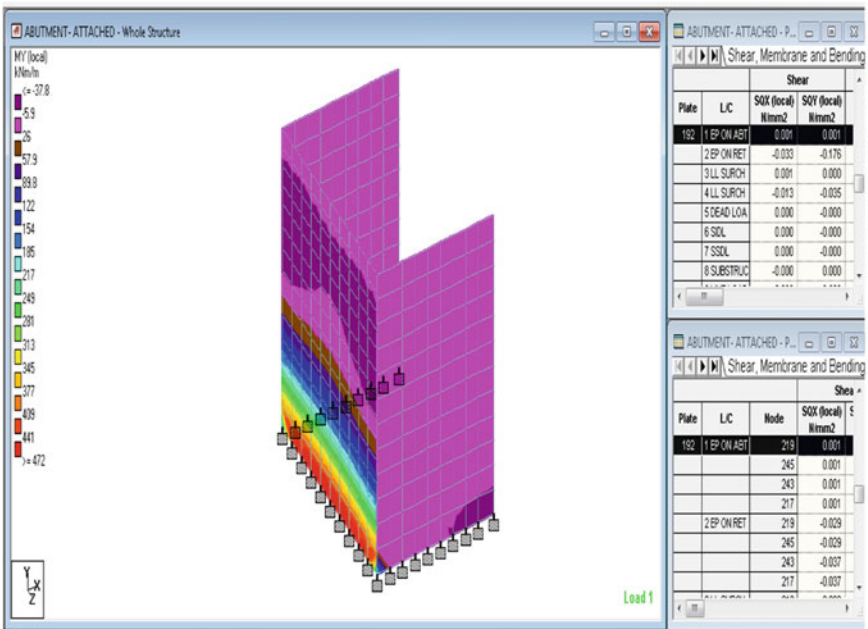


Fig. 8 C-type attached abutment (STAAD model)

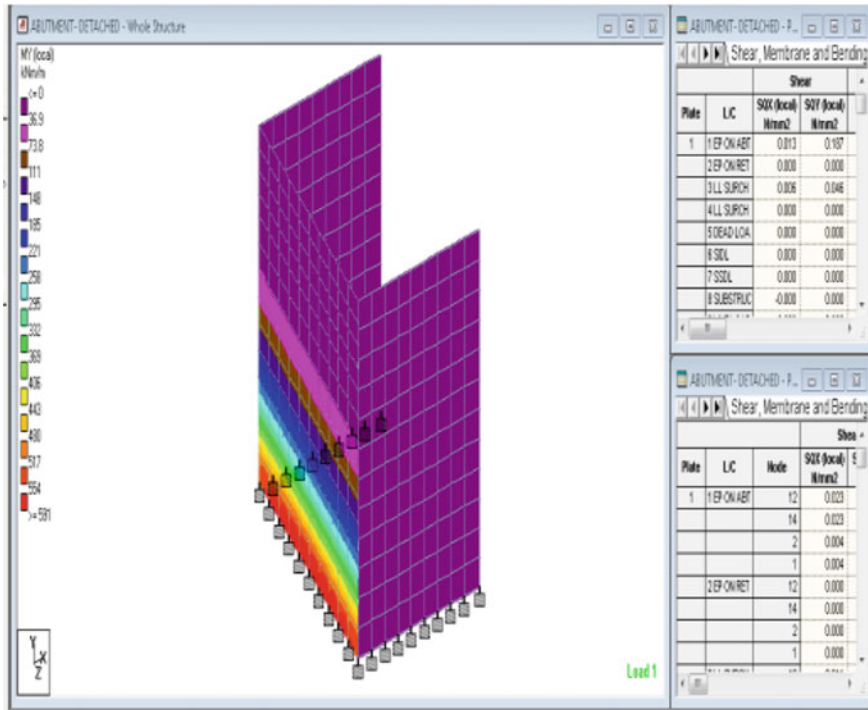


Fig. 9 C-type detached abutment (STAAD model)

seismic combinations. Cases for bending moment, shear force, deflection, and cost of abutments are shown in Figs. 11, 12, 13, and 14.

5 Results and Discussion

Based on the results and discussion regarding a comparative study of abutments, the following concluding remarks have been made.

- The box-type abutment has clearly outperformed other types of abutments in a comparison of abutments based on bending moment. Although the gravity-type abutment has a lower bending moment than the box type, the stability test for seismic conditions found it to be unstable.
- With an average abutment wall thickness of 500 mm and a tie wall thickness of 300 mm, the box-type abutment displayed good shear force behaviour and withstood shear failure.

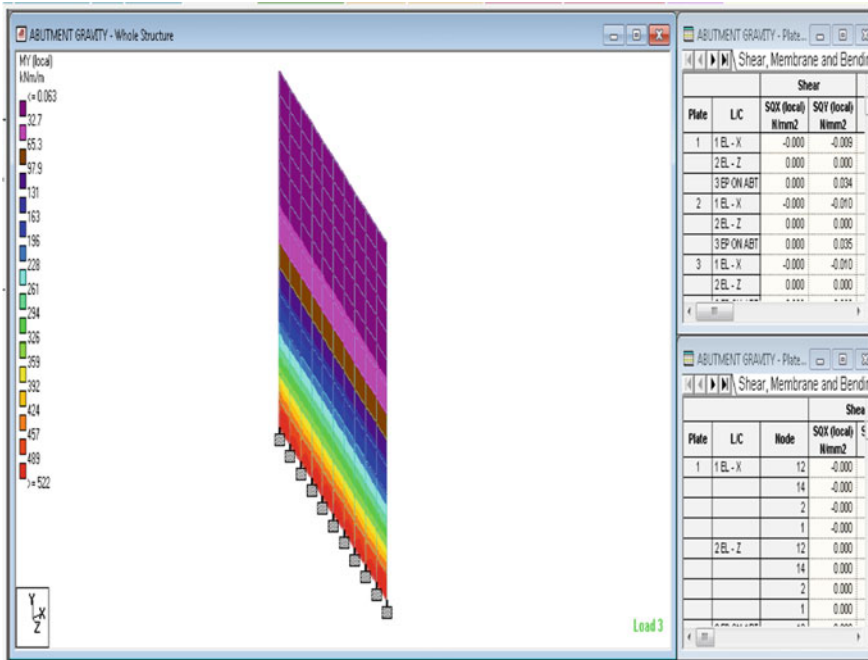


Fig. 10 Gravity type abutment (STAAD model)

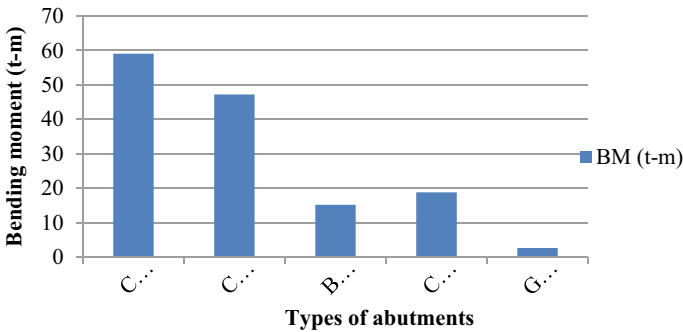


Fig. 11 Bending moments

- The box type abutment has a lower deflection (preferably zero) in the deflection criteria, and the deflection has decreased as a result of the provision of tie walls for the abutment wall and return wall.

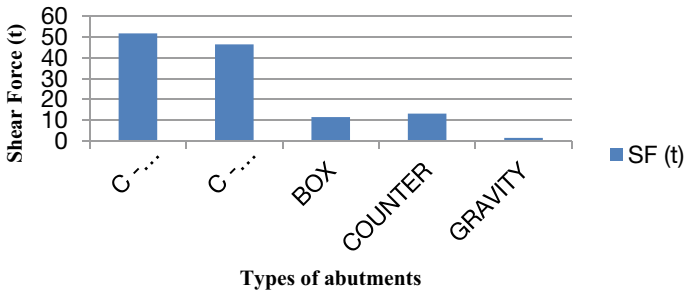


Fig. 12 Shear force

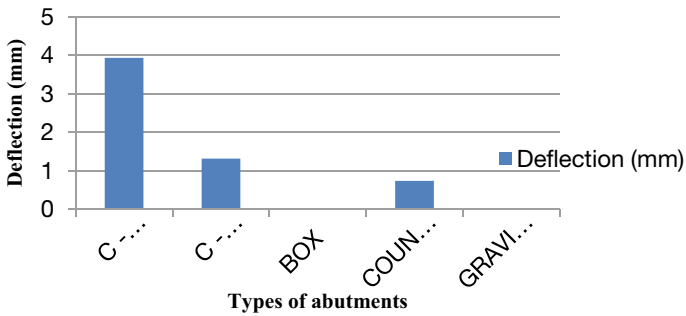


Fig. 13 Deflection

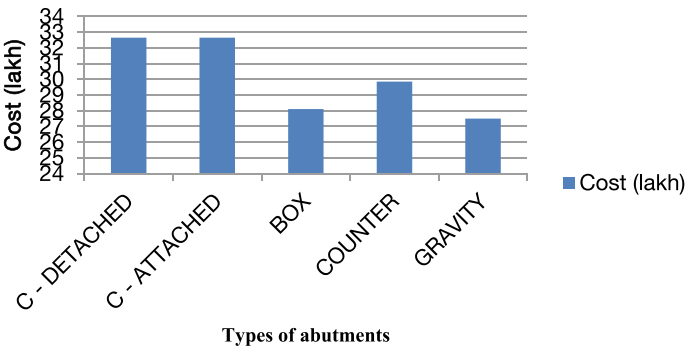


Fig. 14 Cost of abutments

- The box-type abutment is less expensive than the alternative abutment type. Summarizing the conclusion, the box-type abutment has shown better structural behavior considering all the load cases including the seismic effect. It has also turned out to be cost-effective.

References

1. Kalantari, A., & Amjadian, M. (2010). An approximate method for dynamic analysis of skewed highway bridges with continuous rigid deck. *Engineering Structures*.
2. Kalantari, A., & Amjadian, M. (2010). An approximate method for dynamic analysis of skewed highway bridges with continuous rigid deck. *Engineering Structures*, 32(9), 2850–2860.
3. Dimitrakopoulos, E. G. (2011). Seismic response analysis of skew bridges with pounding deck-abutment joints. *Engineering Structures*, 33(3), 813–826.
4. Meng, J. Y., & Lui, E. M. (2000). Seismic analysis and assessment of a skew highway bridge. *Engineering Structures*, 22(11), 1433–1452.
5. Meng, J. Y., & Lui, E. M. (2002). Refined stick model for dynamic analysis of skew highway bridges. *Journal of Bridge Engineering (ASCE)*, 7(3), 184–194.

Different Approaches for Optimising the Micro-machining Quality Parameters of Composite Materials Using Electrochemical Discharge Machining (ECDM) for Societal Application—A Review



Nikhil P. Ambole, Vijay K. Kurkute, and Mukund L. Harugade

Abstract Electrochemical discharge machining (ECDM) is a nonconventional machining process used to make micro features on composites, glass, and ceramics. Different composite materials have been studied during the ECDM process, such as silicon carbide, fibre composites, ceramic composite, polymer composite, etc. Composites are very useful in aerospace, automotive, medical, and electronics due to their hard, brittle and better strength-to-weight ratio. Consequently, the micro-machining of composites by conventional machining is challenging due to its hard and brittle nature. To overcome these challenges, ECDM is a promising option. ECDM is a hybrid machining process based on electrical discharge machining (EDM) and electrochemical machining (ECM). In this paper, different hybrid techniques have been reviewed, which are employed to enhance the machining performance of ECDM. Magnetic field (MF), ultrasonic vibrations (UV), stirring effect, LASER assistance, and rotary motion of the tool are some examples of hybrid techniques. Two or more hybrid techniques will be a novel approach to enhance the performance of ECDM.

Keywords ECDM · Micro-machining · Composites · Hybrid techniques

N. P. Ambole (✉) · V. K. Kurkute

Department of Mechanical Engineering, Bharati Vidyapeeth (Deemed to be University) College of Engineering, Pune, India

e-mail: nikhilambole@gmail.com

M. L. Harugade

Department of Mechanical Engineering, Padmabhooshan Vasantraodada Patil Institute of Technology, Budhgaon, Sangli, India

© The Author(s), under exclusive license to Springer Nature Switzerland AG 2024

P. M. Pawar et al. (eds.), *Techno-societal 2022*,

https://doi.org/10.1007/978-3-031-34644-6_89

865

1 Introduction

The micro-machining of composite materials, such as silicon carbide, borosilicate glass, ceramic composite, polymer composite, etc., are required in aerospace, automotive, medical, and electronics [1]. Composites have a better strength-to-weight ratio and better physical properties such as mechanical, thermal, electrical, and chemical. However, processing the composite is challenging [2]. To overcome these challenges, the ECDM process was studied by the researchers. ECDM is a recent process for micro-machining composites. Additionally, ECDM can be performed on both conductive and non-conducting materials. Silica glass (Quartz) [3], silicon carbide [4], carbon fiber [5, 6], soda lime glass [7–9], borosilicate glass [10, 11], metal matrix composites (MMC) [12] are some examples that were studied during the ECDM process.

1.1 Machining of Si-Based Composites

Micro-machining of silicon composites by using a conventional machining process is complicated, as composites are hard and brittle. However, nonconventional machining processes are relatively expensive for machining such composites. Yet, both conventional and non-conventional machining processes were used for composites. Figure 1 shows the application of conventional and nonconventional machining processes for composites. Different conventional processes (70%) are employed for machining composites, such as turning, milling, grinding, drilling, etc. These were performed with the help of computer numerical control (CNC), vertical machining centre (VMC), and horizontal machining centre (HMC). Comparatively, 30% of the machining of composites has been carried out by non-conventional machining processes. It includes EDM, ECM, wire electrical discharge machining (WEDM), arc-dimensional machining (ADM), LASER-assisted machining (LAM), ultrasonic assisted machining (UAM), abrasive water jet machining (AWJM), etc. [2].

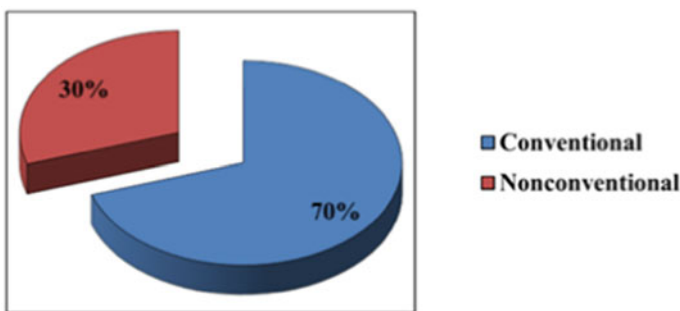


Fig. 1 Machining methods of composites

Though conventional machining is more used in silicon-based composite machining, it has drawbacks such as low material removal, poor surface finishing, high tool wear rate (TWR), low efficiency, and many other micro-machining difficulties. Some nonconventional machining processes, especially EDM and ECM, employ composites, but their machining efficiency is still limited. To overcome these issues, researchers have employed different hybrid machining techniques, and ECDM is one of them emerging and high-efficiency machining process [13]. Researchers successfully studied the ECDM process during conductive and non-conductive composite materials.

1.2 Principle of ECDM

The material removal in ECDM is done through thermal erosion and chemical dissolution [14]. Thermal erosion occurs due to spark generation, and chemical dissolution is the effect of a chemical reaction. Figure 2 shows the working principle of ECDM, which includes a cathode (tool electrode), anode (auxiliary electrode), power supply, electrolyte, and workpiece. The direct current (DC) supply develops potential differences between the tool and auxiliary electrodes. Firstly, the hydrogen bubbles are formed due to an electrochemical reaction. Then these bubbles accumulate at the tip of the tool electrode and form a gas film. After that, a momentary spark is produced due to electric breakdown, which generates localised heat energy. The combined effect of heat and dissolution removes the materials from the workpiece.

The ECDM is a promising option for micro-machining the composites, but still, some improvements are required to optimise the machining performance. In this paper, different hybrid techniques are reviewed for improving the machining performance of ECDM by optimising quality parameters. Different input parameters, such as tool feed rate (TFR) [15], wire feed rate (WFR), applied voltage (AV), number of tool contacts (NTC), inter-electrode gap (IEG) [14], electrode immersion depths (EID), electrolyte concentration (EC), type of electrolyte, tool material, etc., as well as the output quality parameters such as material removal rate (MRR), tool wear rate (TWR), overcut (OC), heat affected zone (HAZ), surface roughness (SR), surface finish (SF), depth of penetration (DOP) have been considered in this study. There are different methods have been studied to find the optimal quality parameter. However, in this paper, the magnetic field [4, 7, 16], ultrasonic vibrations [17, 18], stirring effect [19], and LASER [20] have been considered to enhance the machining performance of the ECDM.

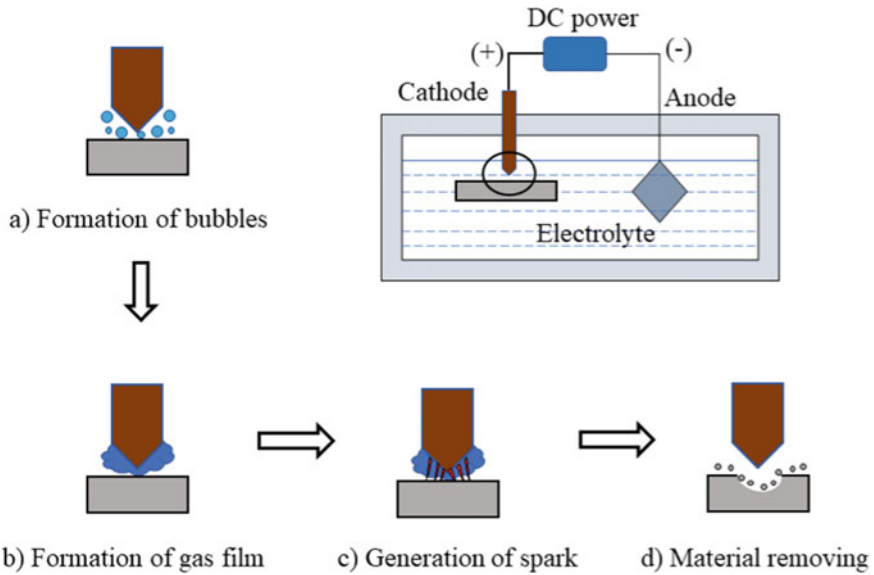


Fig. 2 Working principle of ECDM

1.3 Societal Applications of Si-Based Composites

Si-based composite material has many applications in the aerospace, automotive, medical, and electronics sectors. Some of the important applications of Si-based composite materials are mentioned in Table 1.

Table 1 Societal applications of Si-based composites [1]

Sectors	Application
Automotive	Brake discs, valves, spark plugs, nozzle parts, engine parts, and gas turbine parts
Aerospace	Aircraft engine parts, nose caps, leading edges, nozzles, space vehicle parts, and hypersonic aerospace parts
Medical	Dental ceramics, biomedical devices
Industrial	Furnace parts, heat exchanger parts, industrial pump sealings and bearings
Military	Supersonic vehicles parts, bulletproof jackets
Electronics	Resistors, capacitors, resonators, radio frequency identification (RFID) shielding parts

2 Review of Literature

Researchers are engaged in improving the machining efficiency of ECDM by developing mathematical modelling and using FEM simulation. Rajput et al. developed FEM thermal model for predicting the MRR in ECDM drilling on silica glass. The FEM results agreed with the experimental results. The optimum values are applied voltage as 51.22 V, electrolyte concentration as 25 wt.% of NaOH, tool feed rate as 4 mm/min, and tool material as tungsten carbide. The overall desirability is 0.8646 [3]. Paul and Hiremath conducted a 2D FEM thermal model analysis of the ECDM process in the discharge area, and MRR is characterised. The result of FEM (MRR 0.373 mg/min) is validated with the experimental result (MRR 0.414 mg/min) with a 9.9% error variation [21]. Leyva-Bravo et al. developed a mathematical model for the prediction of MRR using a fuzzy logic model, a backpropagation network model, and a radial basis function network model. Experimentation is carried out to validate results. It was found that the results are more than 90% accurate. The radial basis function model showed 97.25% accuracy with 2.75% mean absolute percentage error [22]. Rajput et al. developed FEM based transient thermal model for predicting MRR in the ECDM process. The experimentation is conducted to validate FEA results with soda lime glass material. The electrolyte concentration and the applied voltage are considered input process parameters, and it is observed that experimental results validate the FEM results [23]. Rajput et al. developed a thermal model for predicting MRR with different electrolytes viz, NaOH, KOH and NaCl. Experimentation is carried out to validate simulation results with AV, EC, spark radius, and duty ratio as input process parameters. The results show that 60 wt.% NaOH electrolyte gives higher MRR, and the KOH electrolyte gives the least OC and improved circularity of the hole [24]. Rathore and Divedi developed a mathematical model using the dimensional analysis method to predict MRR and tool electrode wear (TEW). Also, the effect of process parameters such as vibrational amplitude, pulse on time, AP, EC on TEW and MRR was investigated using ultrasonic-assisted ECDM. The results show that MRR increases by 12% and TEW reduces by 73% [17].

The design of the experiment (DOE) is an important stage before experimentation to avoid exhaustive work by limiting the number of experiments. There are different methods of DOE. Rajput et al. used a response surface methodology (RSM) based mathematical model derived for input variables with response parameters. They studied the effect of input variables (AV, TFR, EC, electrolyte type, tool material) on response parameters (MRR, TWR, NTC) using the analysis of variance (ANOVA). The multi-response optimisation is carried out to increase the MRR and decrease the TWR and NTC [3]. Kumar et al. used wired-ECDM for micro-slicing SiC composites. The experimentation is designed with the L_9 orthogonal array of Taguchi's methodology. The grey relational analysis (GRA) with AV, WFR, duty cycle as input process parameters and OC, MRR as output quality parameters. The results show that OC decreases from 71.87 to 60.2 μm and MRR decreases from 34.2 to 32.3 mg/min [25]. Rajput et al. also used the GRA for optimising the input process parameters such as AV, EC, IEG to improve the machining efficiency of ECDM. The

optimum values are 35 V AV, 15% EC, and the 25 mm IEG for maximising MRR and minimising HAZ, OC. The ANOVA results show that EC contributes more than other input process parameters, with a 68.34% contribution for controlling all the responses [14].

The efficiency of ECDM is improved by adopting different hybrid techniques with ECDM. This novel approach improves the machining performance of ECDM by optimising quality parameters. Mohitkar et al. used the travelling-wire electrochemical spark machining (TW-ECSM) method under magneto-hydrodynamic (MHD) convection for the machining of silicon carbide. They concluded that during the magnetic field induction, the MRR improved from 19.15 to 200%, SR was reduced from 16.86 to 48.58% and OC was reduced from 11.37 to 21.27% [4]. Xu and Jiang introduced the MHD effect in ECDM deep micro drilling to optimise the machining parameters such as AV, magnetic density, etc., and ultimately enhance machining performance. The MHD effect enhanced machining efficiency. The voltage and magnetic field play a vital role. The results show that machining time reduced from 200 to 95 s with a 55% reduction [16]. Singh et al. investigated the behaviours of ECDM with ultrasonic vibration. Ultrasonic vibration reduces energy consumption in ECDM by 2.23 times, improves the energy channelisation index by five times, reduces the HAZ, and increases MRR and depth-to-diameter ratio [18]. Charak and Jawalkar discussed the effect of electrode depths with electrolytic stirring in ECDM. They conducted experiments with input parameters (AV, EC, EID) and studied its effect on the output parameters (TWR, MRR, SF). They found that MRR improves when an applied voltage is higher than 53 V, the tool wears decrease at 50 and 60 V, MRR is good up to 20% EC, SF improved from 20 to 79%, with stirring the electrolyte [19]. Arab et al. investigated the effect of different tool electrode materials on the machining of soda lime glass using pulsed-ECDM. Molybdenum and High carbon steel (HCS) tools are used with 10% KOH. The considered machining input parameters are AV, TFR, pulse frequency, and output parameters are hole OC, taper angle, and HAZ. For molybdenum tool, hole OC was reduced by 30%, the taper angle was reduced by 55%, and the HAZ was reduced by 58%, respectively. Molybdenum had less tool wear than the HCS tool [26]. Ho et al. investigated the effect of adding micro-nano bubbles in electrolytes and using hollow electrodes on the machining performance of ECDM. The processing time is reduced by 31% for glass processing with micro-nano bubble electrolyte. With hollow electrodes time of replenishing electrolyte is reduced by 34.5%, and the gas film thickness is decreased by 54%. The combined effect of micro-nano bubble electrolyte and hollow electrodes on sapphire is that the machining depth is increased by 3.8 times [27]. Singh and Dvivedi investigated the combined effect of electrolyte flow and pressurised feeding for micro-holing using ECDM on Ytria-stabilised zirconia (YSZ) material. The conclusion is that introducing electrolyte flow and pressurised feeding increases the efficiency of ECDM. The hole depth is increased by 42%, the hole diameter is reduced by 33%, and tool wear is also reduced [28]. Harugade et al. investigated the hybrid effect of magnetic flux density (MFD) and high-speed tool rotation on the machining performance of the ECD-Drilling process for soda lime glass. In experimentation, the process variables are the AV, TFR, tool rotation speed, and the quality

variables are MRR and OC. In the presence of MFD, the MRR increases by 61%, and the OC increases by 46%. Also, it is observed that HAZ, micro-cracks, and uneven surface damage were reduced [7]. Rathore and Dvivedi investigated the effect of sonication of tool electrodes during the micro-drilling of borosilicate glass using ECDM. The comparative study is carried out for ECDM and UA-ECDM with AV and EC as input parameters and MRR, DOP, HOC as quality parameters. The results show that MRR improved by 11.13%, DOP improved by 27.17%, and reduction in HOC by 23.10% with UA-ECDM [29]. Singh and Dvivedi introduce titrated flow of electrolytes in ECDM for micro holes drilling on borosilicate glass. The electrolyte flow rate, AV, pulse on time, and EC are optimized for improving the penetration rate and diameter of the hole entrance (HED) by using the multi-criteria optimization method. The introduction of the titrated flow of electrolytes results in a reduction in machining time by seven times, an improvement in penetration rate by 4.5 times, reduction in HED by 1.25 times [10]. Elhami and Razfar introduced the nanoparticles in the electrolyte to enhance its electrical and thermal properties and improve the machining efficiency of ECDM. The comparative study between Cu nanoparticles and Al_2O_3 nanoparticles shows that hole depth improved by 21.1% for Cu and 18.7% for Al_2O_3 particles, while entrance overcut raised by 8.3% for Cu and 10.7% for Al_2O_3 particles. Also, the large molten material accumulated on the tool edge is undesirable [9]. Wang et al. proposed the use of a non-metallic backing layer and electrochemical reaming to improve the machining performance and quality of the holes in ECDM. The experimentation is carried out with and without a backing layer on cobalt-based super alloy and the surface of the hole wall and the OC were analysed. They found that the shape of the hole at the exit is improved and the taper of the hole is reduced. They noticed that optimal electrochemical reaming values are EC 1.5 g/L and AV is 60 V [30]. Singh et al. investigated the effect of LASER-assisted ECDM on output quality parameters such as OC and taper of the hole on carbon fibre composite. They conducted the experiments along with input parameters such as travel rate, rotation of tool, and duty cycle. They concluded that OC and taper of the hole decrease by 10 to 12% [20].

In another study conducted by Zhang et al. analysed the surface integrity, such as the surface morphology, element composition, residual stress, micro-hardness, and recast layer properties of micro holes. They compared performance of EDM and ECD-Drilling during the machining of nickel-based super-alloys. The results show there is improvement in surface integrity with ECD-Drilling with no recast layer, no melted debris, and no tensile residual stress [31]. Verma et al. investigated the effect of the duty cycle and EC on the surface topography of soda lime glass using pulsed-ECDM. They studied input parameters duty cycle (30, 50, and 70%) and KOH concentrations (10, 20, and 30%) while testing the micro-channel depth and HAZ. The study shows that micro-channel depth and HAZ increase with the increase in pulse cycle and EC [8]. Singh and Singh presented the study of environmental aspects such as fumes emission analysis and its impact on human health during ECDM. The input parameters are AV and EC. The results show that the fume mass concentration increases with an increase in AV and EC. The optimal values for less FMC are EC of 20% and AV of 40 V [6]. Arab and Dixit investigated the tool electrode feed rate

(TEFR) on the machining performance of ECD-drilling. They considered micro-hole size, hole circularity, HAZ, hole eccentricity, and TEFR as quality parameters. The results show that TEFR in the 3–4 $\mu\text{m/s}$ range gives the best results [15].

2.1 Key Points of Review

See Table 2.

Table 2 Use of hybrid techniques for improvements in quality parameters

Author	Hybrid techniques	Improvements in quality parameters
Mohitkar et al. [4]	Magnetohydrodynamic (MHD) convection	MRR improved from 19.15 to 200%, SR reduced from 16.86 to 48.58%, OS reduced from 11.37 to 21.27%
Harugade et al. [7]	MFD and high-speed tool rotation	MRR increased by 61%
Singh and Dvivedi [10]	Titrated flow of electrolyte	Machining time was reduced by 7 times, penetration rate improved by 4.5 times, and HED was reduced by 1.25 times
Rathore and Dvivedi [17]	Ultrasonic-assisted	MRR increased by 12% and TEW reduced by 73%
Xu and Jiang [16]	MHD effect	Machining time was reduced by 55%
Singh et al. [18]	Ultrasonic assisted	Energy consumption was reduced by 2.23 times; the energy channelisation index improved by 5 times
Charak and Jawalkar [19]	Electrolytic stirring	The surface finish improved from 20 to 79%
Arab et al. [26]	Pulsed-ECDM and tool materials	Molybdenum tool HOC was reduced by 30%, and the taper angle was reduced by 55%, HAZ was reduced by 58%
Ho et al. [27]	Addition of micro-nano bubbles in electrolyte and hollow electrodes	The depth of machining is increased by 3.8 times
Singh and Dvivedi [28]	Electrolyte flow and pressurised feeding	Hole depth improved by 42%, and hole diameter was reduced by 33%
Rathore and Dvivedi [29]	Sonication of tool electrode	MRR improved by 11.13%, DOP improved by 27.17% and HOC reduced by 23.10%
Wang et al. [30]	Non-metallic backing layer	The shape of hole at the exit improved, and the taper of the hole was reduced
Singh et al. [20]	LASER-assisted	OC and taper of hole decrease by 10 to 12%

2.2 Literature Gap

From the above study of literature following gap is found:

- No work has been found in the micro-machining of silicon-based composites with ECDM and hybrid techniques.
- The machining efficiency of ECDM can be improved by hybridizing two or more hybrid techniques.
- The hybridization of magnetic effect and ultrasonic vibration with high-speed tool rotation in ECDM will be the novel approach for micro-machining silicon-based composites.
- The optimization of micro-machining parameters of ECDM for silicon-based composite can be achieved with the above novel approach.

3 Conclusions

Electrochemical discharge machining (ECDM) is one of the emerging and promising techniques for micromachining composites. The following conclusions have been drawn from the reviewed literature:

- The machining efficiency of ECDM is higher than that of EDM/ECM, and it can be used for micro-machine composites.
- The machining efficiency of ECDM can be improved by using hybrid techniques.
- There is scope for improving the machining efficiency of ECDM by optimising quality parameters using the hybridization of two or more hybrid techniques.
- Combining the magnetic field, ultrasonic vibration, and high-speed tool rotation is possible during the ECDM.

References

1. Radhika, N., & Sathish, M. (2022). A review on Si-based ceramic matrix composites and their infiltration based techniques. *Silicon*. <https://doi.org/10.1007/s12633-022-01763-y>
2. Chen, J. P., Gu, L., & He, G. J. (2020). A review on conventional and nonconventional machining of SiC particle-reinforced aluminium matrix composites. *Advances in Manufacturing*, 8(3), 279–315. <https://doi.org/10.1007/s40436-020-00313-2>
3. Rajput, V., Goud, M., & Suri, N. M. (2021). Three-dimensional finite element modeling and response surface based multi-response optimization during silica drilling with closed-loop ECDM. *SILICON*, 13(10), 3583–3609. <https://doi.org/10.1007/s12633-020-00867-7>
4. Mohitkar, A. D., Rattan, N., & Mulik, R. S. (2022). Improvement in machining performances of SiC workpiece using TW-electro chemical spark machining. *SILICON*, 14(4), 1369–1379. <https://doi.org/10.1007/s12633-020-00892-6>

5. Harugade, M., Waigaonkar, S., & Dhawale, N. (2021). A novel approach for removal of delaminated fibers of a reinforced composites using electrochemical discharge machining. *Proceedings of the Institution of Mechanical Engineers—Part B: Journal of Engineering Manufacture*, 235(12), 1949–1960. <https://doi.org/10.1177/095440542111014483>
6. Singh, M., & Singh, S. (2020). Sustainable electrochemical discharge machining process: characterization of emission products and occupational risks to operator. *Machining Science and Technology*, 24(5), 739–757. <https://doi.org/10.1080/10910344.2020.1752238>
7. Harugade, M., Waigaonkar, S., Kulkarni, G., & Diering, M. (2021). Experimental investigations of magnetic field-assisted high-speed electrochemical discharge drilling. *Materials and Manufacturing Processes*. <https://doi.org/10.1080/10426914.2021.2016814>
8. Verma, A. K., Mishra, D. K., Pawar, K., & Dixit, P. (2020). Investigations into surface topography of glass microfeatures formed by pulsed electrochemical discharge milling for microsystem applications. *Microsystem Technologies*, 26(6), 2105–2116. <https://doi.org/10.1007/s00542-020-04770-4>
9. Elhami, S., & Razfar, M. R. (2020). Application of nano electrolyte in the electrochemical discharge machining process. *Precision Engineering*, 64, 34–44. <https://doi.org/10.1016/j.precisioneng.2020.03.010>
10. Singh, T., & Dvivedi, A. (2020). On prolongation of discharge regime during ECDM by titrated flow of electrolyte. *International Journal of Advanced Manufacturing Technology*, 107(3–4), 1819–1834. <https://doi.org/10.1007/s00170-020-05126-y>
11. Kumar, G., & Sharma, A. K. (2020). On processing strategy to minimize defects while drilling borosilicate glass with microwave energy. *International Journal of Advanced Manufacturing Technology*, 108(11–12), 3517–3536. <https://doi.org/10.1007/s00170-020-05563-9>
12. Shamim, F. A., Dvivedi, A., & Kumar, P. (2021). On near-dry wire ECDM of Al6063/SiC/10p MMC. *Materials and Manufacturing Processes*, 36(1), 122–134. <https://doi.org/10.1080/10426914.2020.1802044>
13. Kumar, M., Vaishya, R. O., Suri, N. M., & Manna, A. (2021). An experimental investigation of surface characterization for zirconia ceramic using electrochemical discharge machining process. *Arabian Journal for Science and Engineering*, 46(3), 2269–2281. <https://doi.org/10.1007/s13369-020-05059-4>
14. Rajput, V., Pundir, S. S., Goud, M., & Suri, N. M. (2021). Multi-response optimization of ECDM parameters for silica (quartz) using grey relational analysis. *SILICON*, 13(5), 1619–1640. <https://doi.org/10.1007/s12633-020-00538-7>
15. Arab, J., & Dixit, P. (2020). Influence of tool electrode feed rate in the electrochemical discharge drilling of a glass substrate. *Materials and Manufacturing Processes*, 1749–1760. <https://doi.org/10.1080/10426914.2020.1784936>
16. Xu, Y., & Jiang, B. (2021). Machining performance enhancement of deep micro drilling using electrochemical discharge machining under magnetohydrodynamic effect. *The International Journal of Advanced Manufacturing Technology*, 113(3–4), 883–892. <https://doi.org/10.1007/s00170-021-06657-8>
17. Rathore, R. S., & Dvivedi, A. (2020). Experimental investigations and its dimensional analysis-based modeling of the UAECDM process. *The International Journal of Advanced Manufacturing Technology*, 111(11–12), 3241–3257. <https://doi.org/10.1007/s00170-020-06320-8>
18. Singh, T., Dvivedi, A., Shanu, A., & Dixit, P. (2021). Experimental investigations of energy channelization behavior in ultrasonic assisted electrochemical discharge machining. *Journal of Materials Processing Technology*, 293. <https://doi.org/10.1016/j.jmatprotec.2021.117084>
19. Charak, A., & Jawalkar, C. S. (2022). Experimental investigation and analysis on borosilicate glass using electrochemical discharge machining process. *SILICON*, 14(4), 1823–1829. <https://doi.org/10.1007/s12633-021-00980-1>
20. Singh, M., Singh, S., & Kumar, S. (2020). Investigating the impact of LASER assistance on the accuracy of micro-holes generated in carbon fiber reinforced polymer composite by electrochemical discharge machining. *Journal of Manufacturing Processes*, 60, 586–595. <https://doi.org/10.1016/j.jmapro.2020.10.056>

21. Paul, L., & Hiremath, S. S. (2022). Model prediction and experimental study of material removal rate in micro ECDM process on borosilicate glass. *SILICON*, 14(4), 1497–1510. <https://doi.org/10.1007/s12633-021-00948-1>
22. Leyva-Bravo, J., Chifias-Sanchez, P., Hernandez-Rodriguez, A., & Hernandez-Alba, G. G. (2020). Electrochemical discharge machining modeling through different soft computing approaches. *International Journal of Advanced Manufacturing Technology*, 106(7–8), 3587–3596. <https://doi.org/10.1007/s00170-019-04766-z>
23. Rajput, V., Goud, M., & Suri, N. M. (2020). Finite element modeling for analyzing material removal rate in ECDM process. *Journal of Advanced Manufacturing Systems*, 19(4), 815–835. <https://doi.org/10.1142/S0219686720500365>
24. Rajput, V., Goud, M., & Suri, N. M. (2021). Finite element modeling for comparing the machining performance of different electrolytes in ECDM. *Arabian Journal for Science and Engineering*, 46(3), 2097–2119. <https://doi.org/10.1007/s13369-020-05009-0>
25. Kumar, U., Singh, M., & Singh, S. (2021). Wire-electrochemical discharge machining of SiC reinforced Z-pinned polymer matrix composite using grey relational analysis. *SILICON*, 13(3), 777–786. <https://doi.org/10.1007/s12633-020-00484-4>
26. Arab, J., Pawar, K., & Dixit, P. (2021). Effect of tool-electrode material in through-hole formation using ECDM process. *Materials and Manufacturing Processes*, 36(9), 1019–1027. <https://doi.org/10.1080/10426914.2021.1885700>
27. Ho, C. C., Huang, B. H., & Chu, P. C. (2021). A study based on electrochemical discharge assisted by hollow electrode and micro-nano bubble to process transparent non-conductive brittle materials. *International Journal of Advanced Manufacturing Technology*, 115(1–2), 367–382. <https://doi.org/10.1007/s00170-021-07170-8>
28. Singh, T., & Dvivedi, A. (2021). Fabrication of micro holes in Ytria-stabilized zirconia (Y-SZ) by hybrid process of electrochemical discharge machining (ECDM). *Ceramics International*, 47(16), 23677–23681. <https://doi.org/10.1016/j.ceramint.2021.05.017>
29. Rathore, R. S., & Dvivedi, A. (2020). Sonication of tool electrode for utilizing high discharge energy during ECDM. *Materials and Manufacturing Processes*, 35(4), 415–429. <https://doi.org/10.1080/10426914.2020.1718699>
30. Wang, C., Zhang, Y., Ji, L., Yang, W., & Wang, J. (2021). Improvement of machining accuracy in EDCM by enhanced electrochemical reaming based on a non-metallic backing layer. *Chinese Journal of Aeronautics*, 34(12), 251–264. <https://doi.org/10.1016/j.cja.2020.06.019>
31. Zhang, C., Xu, Z., Zhang, X., & Zhang, J. (2020). Surface integrity of holes machined by electrochemical discharge drilling method. *CIRP Journal of Manufacturing Science and Technology*, 31, 643–651. <https://doi.org/10.1016/j.cirpj.2020.09.004>

Numerical Simulation of Reinforced Granular Blanket over Granular Pile Under Vertical Loading



Himanshu Gupta, Jitendra Kumar Sharma, and Ravikant S. Sathe

Abstract Granular pile installation is a typical method for treating soft clay soils. In the current study, Mohr–Coulomb failure criteria were considered for the granular pile, granular blanket, expansive soil, and geogrid layers as reinforcement. Finite-element analyses were carried out to simulate the behaviour of multilayer geosynthetic-reinforced granular beds over granular pile-reinforced soft soil using the PLAXIS 2D. Those from the experiments strongly validate the findings of the current review. To better understand the mechanism of the load settlement curve in cases of regular granular piles (OGPs) and Reinforced Granular Blanket (RGB) over Granular Pile (GP) under Vertical Loading, significant research was undertaken. Additionally, parametric analyses were performed to examine the effects of variables like the number of variations in the reinforcing geogrid and its placement in the granular blanket over the granular pile. The findings showed that reducing the maximum settlement is not as successful when using multiple geosynthetic reinforcements with granular piles. However, when granular piles are not employed, a multilayer reinforcement system effectively reduces the maximum settling. Additionally, it demonstrated that the amount of stress concentration proportion increases significantly in the presence of geosynthetic reinforcement compared to the amount when it is absent. According to numerical results, placing a GB over a granular pile with a geogrid layer accelerates stress transformation to the depth of OGP. Thus, the higher zone of the OGP experiences a reduction in stress concentration.

Keywords Granular pile · Granular blanket · Geogrid · Soft soil

Abbreviations

OGP	Ordinary granular pile
GB	Granular blanket
GGB	Geogrid granular blanket

H. Gupta (✉) · J. K. Sharma · R. S. Sathe
Department of Civil Engineering, RTU, Kota, India
e-mail: him_kota@yahoo.com

GGBB	Geogrid at bottom in granular blanket
GGBM	Geogrid at mid in granular blanket
IF	Improvement factor
FEM	Finite element method
SLG	Single layer of geogrid
DLG	Double layer of geogrid
dia.	Diameter
Fig.	Figure
D	Diameter of granular pile
L	Length of granular pile
t	Thickness of granular blanket
VESC	Vertical encased granular piles
HRSC	Horizontal reinforced granular piles
LSR	Load settlement response

1 Introduction

The world is covered in soft soil deposits frequently found around major towns, rivers and coastal areas. The deposit's higher compressibility and lower shear strength are significant problems for geotechnical engineers. Structures are built on a soft clay layer, leading to several issues, including large settlements, mainly if the soft clay layer is up to a more significant depth below the foundation. Therefore, the most suitable ground improvement technique has to be adopted, although the processes are expensive and time-consuming. Numerous methods improve the ground's state, including preloading, lime stabilization, compaction, granular piles, grouting, etc. However, before adopting such techniques, it is necessary to understand the nearby ground conditions thoroughly. Then, a different approach of providing Granular piles can be adopted, which improves soil strength characteristics such as bearing capacity and shear strength. This approach also reduces vertical and lateral displacement, which overcomes the challenges in dealing with soft soils.

We feel the need for better soil management techniques more than ever today because of urban development and construction on unsuitable soils. Methods for in-ground improvement, effectiveness, and economic rationale have always been offered. Granular piles are an excellent ground improvement technology that is thought to be cost-effective and eco-friendly. They are referred to as thick, granular columnar components that can be generated in soft soil in various approaches. This method's benefits include boosting bearing capacity, lowering the risk of liquefaction, and minimizing settlement, and they can also provide reinforcement to the structures. Numerous investigations on the behavior of improved ground with granular piles have been conducted so far, such as experimental [1, 2], analytical [3–5],

and numerical [6–11]. Using geotextile and geo-grids decreases the pile's bulging and the granular blanket's deformation, respectively [12, 13]. Furthermore, using OGP improves the soft soil's bearing capacity [14]. Using a granular blanket increases, the ultimate bearing capacity of soft soil.

The bearing capacity of reinforced stone columns increases as the reinforcement's strength rises in both "VESC and HRSC." Additionally, the lateral bulging decreases due to the application of geotextiles. Additionally, the "stress concentration ratio" of the columns rises for both "VESC and HRSC" performed research on geosynthetic-encased stone columns that were both unreinforced and reinforced. [15]. The variation of GB thickness and stress concentration ratio of granular piles is analyzed by Ambily and Gandhi [16]. The stress concentration ratio of single and grouped un-reinforced and reinforced piles, bulging and Murugesan and Rajagopal [17] investigated load-bearing capacity. They discovered that the increasing axial load capacity of the granular pile affects the role of the encasement's modulus and the diameter of the granular pile. Madhav and Vitkar [18] illustrated using plane strain as a granular trench or pile failure mechanism. They concluded that using a granular trench or pile increased the bearing capability of weak clay deposits. In order to analyze the behavior of soft soil ground supported by granular piles with a Granular blanket beneath and on top of a rigid foundation, a formula in the form of simple hypotheses is given [19]. They understood that the GB's position on the OGP resulted in more developed soil, a decrease in the stress concentration factor on top of the granular pile, and a reduction in settling. In the present work, different geogrid layers, their placements, and "load-settlement response" were studied by numerical simulation.

2 Methods and Materials

The FEM "PLAXIS 2D" is used to model the single floating OGP. The granular pile with a 100 and 80 mm dia. was updated using the axisymmetric model. In all circumstances, OGP is considered 5 times their diameter. However, because of symmetry, the soil model is replicated by taking into account the OGP's half from its center, as illustrated in Fig. 1. Triangular elements are now used in the FEM model with 15 nodes to increase data generating accuracy. The analysis has been conducted using a medium mesh. The boundary influence will be negligible when the geometric model's depth and width are maintained at 4 times the footing diameter (4D) [20]. In this study, horizontal and vertical limits were allocated a larger value than the OGP's 4 times dia. to prevent the geometry model results from influencing the findings. In addition, the model's boundary conditions are strictly constrained at the vertical boundaries and completely controlled at the model's base. A uniform displacement of 50 mm in a downward direction was applied on a rigid circular steel plate. The rigid plate has an elastic modulus of $2 \times 10^5 \text{ N/mm}^2$ and shows elastoplastic behavior. The current investigation avoided the soil-granular pile interaction by using rigid plates

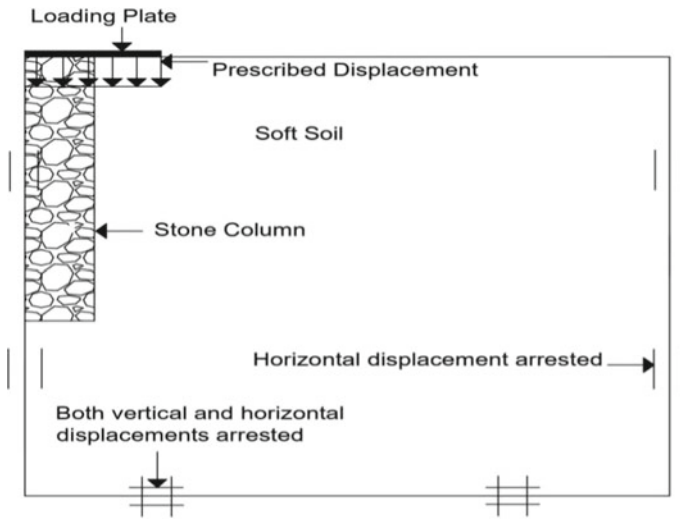


Fig. 1 Soil parameters

with a 200 mm dia. for each scenario. Nodal locations near the loading surface's center were chosen to measure the settlement and corresponding stress.

The soil, granular pile, and GB are all modeled using the Mohr–Coulomb method, with the soil being assumed undrained and the OGP and GB having drained behaviors. As shown in Fig. 2, the GB is placed on top of the OGP. The granular blanket is thought to have the same cross-section as soil but is measured in increments of 30, 40, and 50 mm. Additionally, a geogrid layer is put in various locations atop OGP and soft clay in a GB to enhance the response to load settlement. When GB is laid over OGP or soft clay, the position of the geogrid layer is at the bottom and midpoint of GB, respectively. For all of the materials, the “Mohr–Coulomb failure criterion” and “drained behavior” were taken into consideration. Table 1 introduces material attributes.

3 Results and Discussion

The results of the numerical analysis were validated with the results obtained by Rezaei et al. [21]. It exhibits the strong agreement shown in Fig. 3. The typical granular pile was evaluated for validity without encasement and granular blanket. The OGP was adopted with a 100 mm diameter and a length of 5 times that of the OGP.

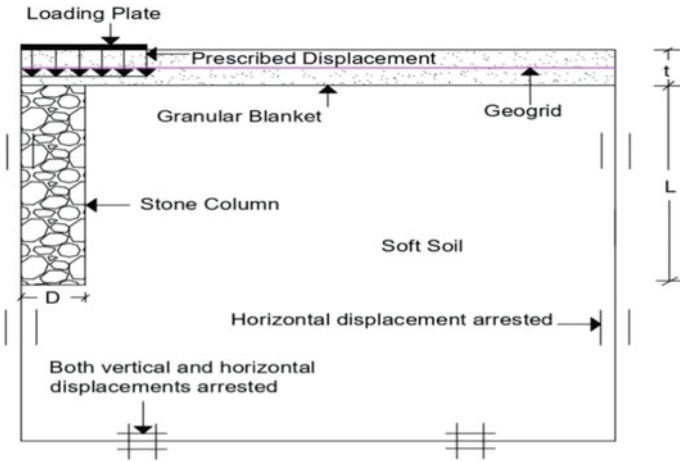


Fig. 2 Schematic diagram of a geogrid GB over OGP

Table 1 Properties of soft clay, granular pile, and granular blanket

Parameter	Soft clay	Granular pile	Granular blanket	Unit
γ_{unsat}	15.50	14.30	15.5	kN/m^3
γ_{sat}	19.10	16.90	15.5	kN/m^3
E	50	40,500	20,000	kN/m^2
N	0.45	0.3	0.3	-
C	6.5	0	0	kN/m^2
Φ	0	46	30	0
Ψ	0	7	4	0

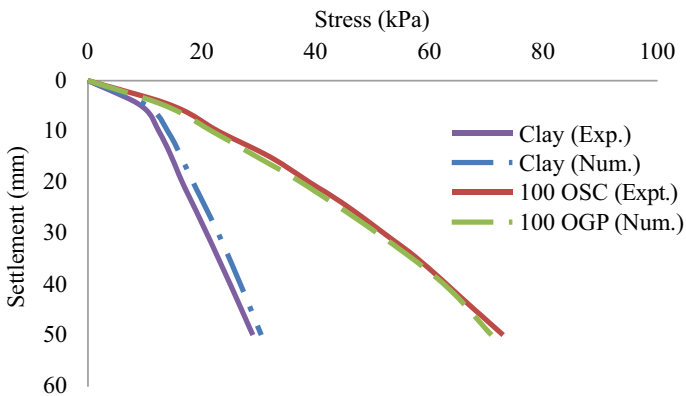
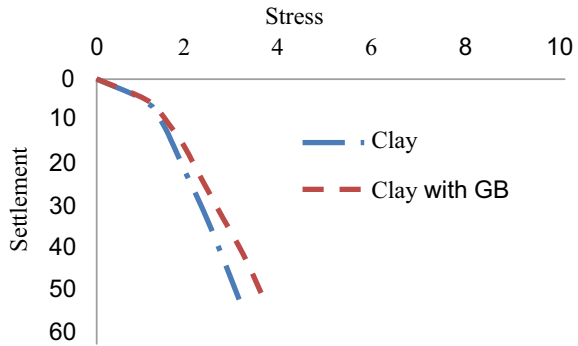


Fig. 3 Validation of results

Fig. 4 Effect of a granular blanket over soft clay



3.1 Impact of the GB Resting over Soft Clay Bed

The impact of granular blankets on soft clay can be evaluated by placing a GB of the same width as the soft clay. The load-settlement response of soft clay with the GB over soft clay is shown in Fig. 4. It is determined what happens when soft clay is covered in a granular layer of load-settlement response. The GB was kept about 30 mm thick for the same reason. It demonstrates that the load settlement response increased by 11.74% when a GB of thickness 30 mm was added over soft clay compared to soft clay. It was found that when a GB is placed over soft clay, the load settlement response increases.

3.2 Effect of the Geogrid in a Granular Blanket over Soft Clay

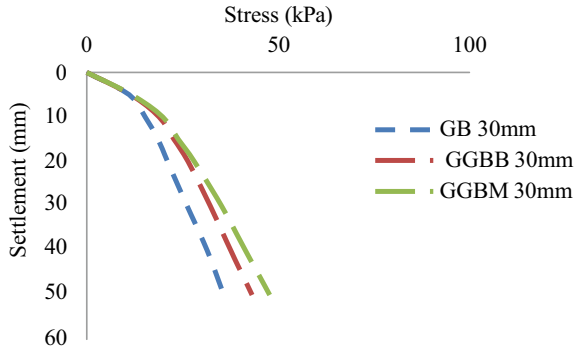
The effect of adding geogrid in a GB over the soft clay is analyzed in the form of LSR. GB is considered to have a 30 mm thickness. Therefore, the geogrid is positioned beneath the granular blanket that covers the soft clay. The load settlement response of the geogrid in a GB over soft clay is shown in Fig. 5, demonstrating that the LSR has increased compared to the GB over soft clay. According to Fig. 5, the geogrid placed at the bottom of GB enhances “load-settlement response” by 20.66%, and when geogrid placed at middle of GB raises the response by 33.51%.

3.3 Effect of with and Without a Geogrid GB over OGP

D = 100 mm Granular Pile

The LSR for OGP with unreinforced GB is depicted in Fig. 6a which is greater than LSR of OGP by 12.02%. The addition of GB improves the LSR in comparison to

Fig. 5 Effect of geogrid in a GB over soft clay



soft clay only. The effect of reinforcing the GB with geogrid is also shown in Fig. 6a. The geogrid is placed at bottom of the GB, and placement of the geogrid improved the LSR of OGP.

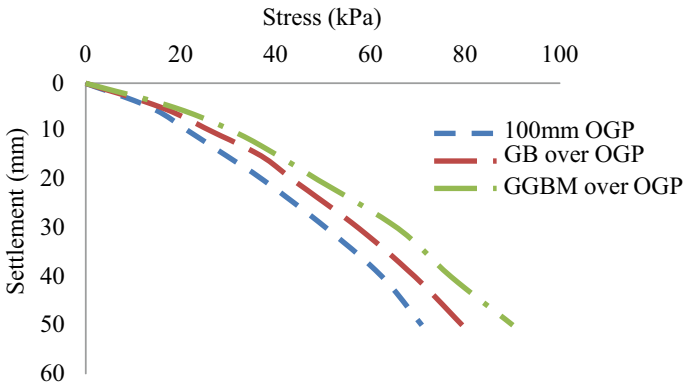
D = 80 mm Granular Pile

Figure 6b shows that the LSR can be improved by introducing the OGP in a soft clay bed. It increases the LSR of soft clay bed up to 10.27%. The LSR can be further enhanced by introducing geogrid within the GB. By placing the geogrid at the bottom of the GB, LSR is improved 28.12% compared to OGP. The LSR of the unreinforced GB can also be enhanced by introducing geogrid within the GB. Figure 6b shows that the LSR of GB with geogrid is 16.18% improved compared to GB. There is a considerable improvement in the LSR of soft clay bed by using GB with geogrid, and introducing the GB with geogrid improved the LSR by 238%.

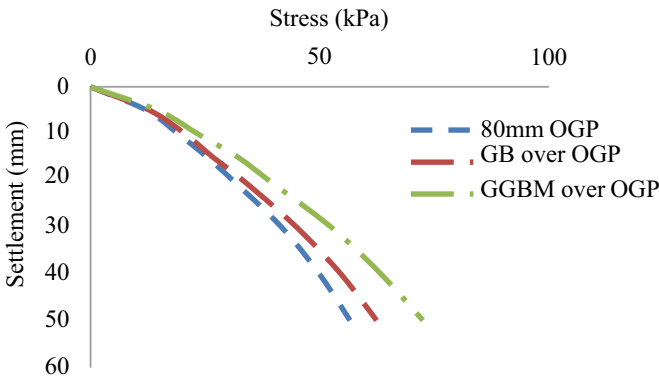
From Fig. 6a and b, it can be inferred that the GB over the granular pile provides better results for LSR, increases its strength and decreases OGP bulging because the load transformation is correctly performed. Also, it indicates that the placement of reinforced geogrids in a granular blanket over a granular pile gives a better effect than an unreinforced GB over a granular pile.

3.4 Impact of the Number of Geogrid Layers in a Granular Blanket over OGP

The effect of the number of geogrid layers in a granular blanket over OGP is determined in load settlement response. The same single and double number of geogrid layers has been used in a granular blanket over OGP. A single layer of geogrid is placed at a distance of 10 mm above the bottom level of GB. And when a double number of geogrid layers are used, the first layer is placed at 10 mm and the second



(a) D=100mm



(b) D=80mm

Fig. 6 Impact of GB and GGB over OGP

layer is placed at 20 mm above the bottom level of GB. Also determined was the effect of length of geogrid layers concerning diameter of granular piles such as on 2D, 4D, 6D and 8D.

D = 100 mm Granular Pile

Figure 7a and b depicts the load settlement response when single and double layers of geogrids are used in GB over OGP of 100 mm dia. First, the effect of single layer geogrid in GB is determined and found that the load settlement response gets increased by 17%, 21%, 23%, and 26% compared with the OGP without GB and RGB over OGP for 2D, 4D, 6D and 8D respectively. On the other hand, the effect of double-layer geogrids in GB is determined and found that the load settlement response gets increased by 24%, 31%, 35%, and 40% when compared with the OGP without GB and RGB over OGP for 2D, 4D, 6D and 8D respectively. Also noted is

that using double layers of geogrid will be more beneficial than the single layer of geogrid in GB. Furthermore, the load settlement response increases as we increase the numbers and length of geogrid in terms of diameter of OGP, i.e. by 2D, 4D, 6D and 8D.

D = 80 mm Granular Pile

Figure 8a and b shows the load settlement response when single and double layers of geogrids are used in GB over OGP of 80 mm dia. The load settlement response increases when a single layer of geogrid is placed in GB at a 10 mm distance above the bottom level of GB over OGP. Compared with the OGP, without GB and GGB over OGP increased by 15%, 18%, 21%, and 24% for 2D, 4D, 6D and 8D, respectively. And double layer geogrid in GB over OGP load settlement response get in- creased by 23%, 31%, 35%, and 39% for 2D, 4D, 6D and 8D respectively.

Figures 7 and 8 concluded that if we increase the number of geogrid layers in GB, the load settlement response of OGP gets increases. Also, if we increase the length

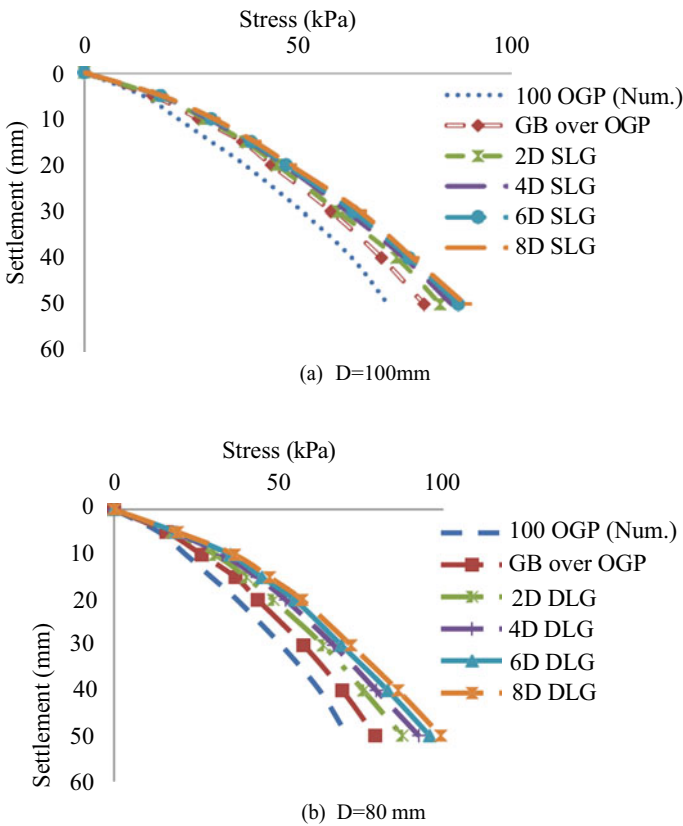


Fig. 7 a Effect of the number of geogrid layers in GB over 100 mm OGP. **b** Effect of the number of geogrid layers in GB over 80 mm OGP

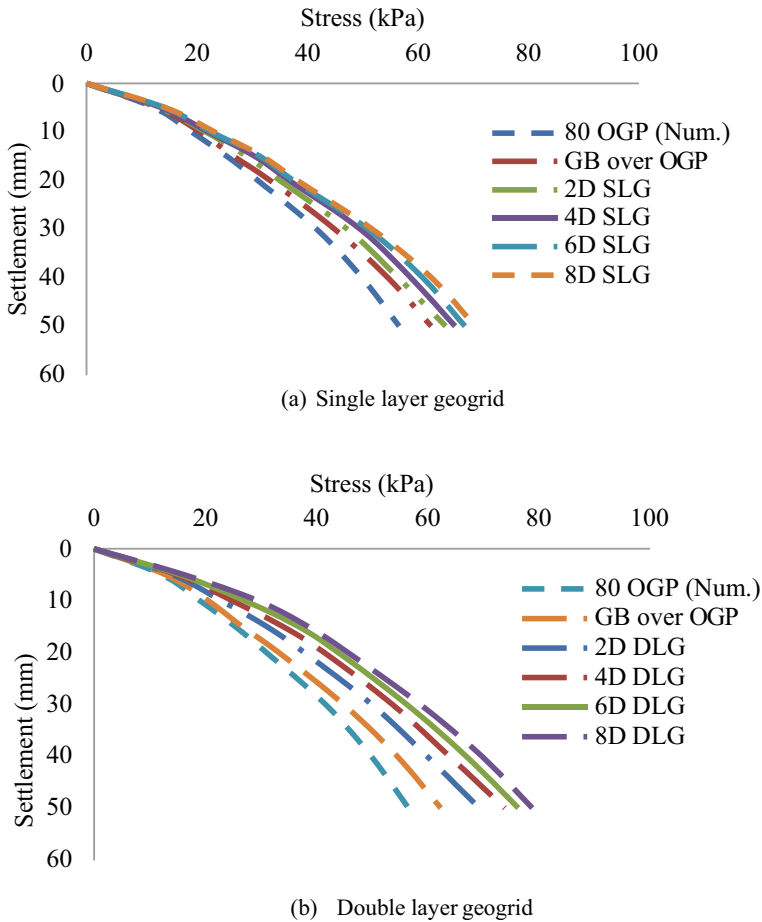


Fig. 8 a Effect of the number of geogrid layers in GB over 80 mm OGP. b Effect of the number of geogrid layers in GB over 80 mm OGP

of the geogrid, load settlement response rises to 6 times the diameter of OGP. Still, the rate of increment of load settlement response gets reduced.

Results show that using reinforced geogrids in a granular blanket over a granular pile produces better results than using an unreinforced granular blanket.

4 Conclusions

The following conclusions are drawn based on the performed numerical analyses:

- There is significant improvement in the properties of the soft ground when the GB is placed over the OGP. It improves the bearing capacity as well and reduces the settlement of OGP.
- The load settlement response increases when the number of geogrid layers increases in GB over OGP.
- A granular layer plays a vital role in the distribution of stresses and transformation of the applied pressures to a considerable depth of the OGP, where the surrounding soil provides additional support.
- The rate of load settlement response increases more as we increase length of geogrid compared to the diameter of the pile up to 6D, and then after that, the rate of load settlement response increases, but its rate goes down and down.

References

1. Ghazavi, M., & Afshar, J. N. (2013). Bearing capacity of geosynthetic encased stone columns. *Geotextiles and Geomembranes*, 38, 26–36. <https://doi.org/10.1016/j.geotexmem.2013.04.003>
2. Hasan, M., & Samadhiya, N. K. (2016). Experimental and numerical analysis of geosynthetic-reinforced floating granular piles in soft clays. *International Journal of Geosynthetics and Ground Engineering*, 2(3), 1–13. <https://doi.org/10.1007/s40891-016-0062-6>
3. Pulko, B., Majes, B., & Logar, J. (2011). Geosynthetic-encased stone columns: Analytical calculation model. *Geotextiles and Geomembranes*, 29(1), 29–39. <https://doi.org/10.1016/j.geotexmem.2010.06.005>
4. Deb, K., & Mohapatra, S. R. (2013). Analysis of stone column-supported geosynthetic-reinforced embankments. *Applied Mathematical Modelling*, 37(5), 2943–2960. <https://doi.org/10.1016/j.apm.2012.07.002>
5. Nazari Afshar, J., & Ghazavi, M. (2014). A simple analytical method for calculation of bearing capacity of stone-column. *International Journal of Civil Engineering*, 12(1), 15–25.
6. Chakraborty, M., & Kumar, J. (2014). Bearing capacity of circular foundations reinforced with geogrid sheets. *Soils and Foundations*, 54(4), 820–832. <https://doi.org/10.1016/j.sandf.2014.06.013>
7. Han, J., & Gabr, M. A. (2002). Numerical analysis of geosynthetic-reinforced and pile-supported earth platforms over soft soil. *Journal of Geotechnical and Geoenvironmental Engineering*, 128(1), 44–53. [https://doi.org/10.1061/\(ASCE\)1090-0241\(2002\)128:1\(44\)](https://doi.org/10.1061/(ASCE)1090-0241(2002)128:1(44))
8. Sathe, R. S., Sharma, J. K., & Suneja, B. P. (2020). Top settlement analysis of single circular floating stepped pile. In *Techno-Societal 2018*. https://doi.org/10.1007/978-3-030-16848-3_52
9. Sathe, R. S., Sharma, J. K., & Suneja, B. P. (2020). Settlement analysis of single circular hollow pile. *Construction in geotechnical engineering*. Lecture Notes in Civil Engineering (Vol. 84, pp. 703–712). https://doi.org/10.1007/978-981-15-6090-3_52
10. Sathe, R. S., Sharma, J. K., & Suneja, B. P. (2021). Estimation of settlement of stepped pile in granular soil. In *Indian Geotechnical Conference 2019*. Lecture Notes in Civil Engineering (Vol. 137, pp. 537–544). https://doi.org/10.1007/978-981-33-6466-0_49
11. Hanna, A. M., Etezad, M., & Ayadat, T. (2013). Mode of failure of a group of stone columns in soft soil. *International Journal of Geomechanics*, 13(1), 87–96. [https://doi.org/10.1061/\(ASCE\)GM.1943-5622.0000175](https://doi.org/10.1061/(ASCE)GM.1943-5622.0000175)

12. Mehrannia, N., Kalantary, F., & Ganjian, N. (2018). Experimental study on soil improvement with stone columns and granular blankets. *Journal of Central South University*, 25(4), 866–878. <https://doi.org/10.1007/s11771-018-3790-z>
13. Nazariafshar, J., Mehrannia, N., Kalantary, F., & Ganjian, N. (2019). Bearing capacity of group of stone columns with granular blankets. *International Journal of Civil Engineering*, 17(2), 253–263. <https://doi.org/10.1007/s40999-017-0271-y>
14. Hamed, N., Khairul, A. K., & Yah, C. (2011). Soil improvement by reinforced stone columns based on experiments works. *Electronic Journal of Environmental, Agricultural and Food Chemistry*, 10(7), 2460–2478.
15. Nazari Afshar, J., & Ghazavi, M. (2014). Experimental studies on bearing capacity of geosynthetic reinforced stone columns. *Arabian Journal for Science and Engineering*, 39(3), 1559–1571. <https://doi.org/10.1007/s13369-013-0709-8>
16. Ambily, A. P., & Gandhi, S. R. (2007). Behavior of stone columns based on experimental and FEM analysis. *Journal of Geotechnical and Geoenvironmental Engineering*, 133(4), 405–415. [https://doi.org/10.1061/\(ASCE\)1090-0241\(2007\)133:4\(405\)](https://doi.org/10.1061/(ASCE)1090-0241(2007)133:4(405))
17. Murugesan, S., & Rajagopal, K. (2009). Studies on the behavior of single and group of geosynthetic encased granular piles. *Journal of Geotechnical and Geoenvironmental Engineering*, 136(1), 129–139. [https://doi.org/10.1061/\(ASCE\)GT.1943-5606.0000187](https://doi.org/10.1061/(ASCE)GT.1943-5606.0000187)
18. Madhav, M. R., & Vitkar, R. P. (1978). Strip footing on weak clay stabilized with a granular trench or pile. *Canadian Geotechnical Journal*, 15(4), 605–609. <https://doi.org/10.1139/t78-066>
19. Shahu, J., Madhav, M., & Hayashi, S. (2000). Analysis of soft ground-granular pile-granular mat system. *Computers and Geotechnics*, 27, 45–62. [https://doi.org/10.1016/S0266-352X\(00\)00004-5](https://doi.org/10.1016/S0266-352X(00)00004-5)
20. Tan, X., Zhao, M., & Chen, w. (2018). Numerical simulation of a single granular pile in soft clay using the discrete element method. *International Journal of Geomechanics*, 18(12), 0401817-1. [https://doi.org/10.1061/\(ASCE\)GM.1943-5622.0001308](https://doi.org/10.1061/(ASCE)GM.1943-5622.0001308)
21. Rezaei, M. M., Lajevardi, S. H., Saba, H., Ghalandarzadeh, A., & Zeighami, E. (2019). Laboratory study on single columns reinforced with steel bars and discs. *International Journal of Geosynthetics and Ground Engineering*, 5, 2. <https://doi.org/10.1007/s40891-019-0154-1>

Application of Modern Waste Materials for Stabilizing the Cohesive Soil



Amit Kumar Jangid and Kamaldeep Singh Grover

Abstract Improving the soil's characteristics is still continuous and probably never ends because there is still so much room for research and development. The most popular technique for improving soil characteristics is stabilization. The main use of soil stabilization in geotechnical engineering is soil strengthening, which can be used for pavement design, slope stability, and ground improvement. This article reveals the application of a few modern waste materials to enhance the geotechnical characteristics of cohesive soils. The waste materials produced from the heavy industries are listed in this article, i.e., iron slag, copper slag, steel slag, sea garnet sand, and by-products from steel plants (GGBFS). The experiments have been conducted for cohesive soil available in Kota, Rajasthan, to study the impact of sea garnet sand waste materials. The experimental study demonstrates that sea garnet sand controls the consistency limits and enhances the dry density of the cohesive soils.

Keywords Expansive soil · Stabilization · Geotechnical properties · Sea garnet sand

1 Introduction

Several soil types are available in nature and used for any Civil Engineering construction project. However, all soils are not useful for construction projects because of their nature. Soils have been classified into non-cohesive and cohesive soils based on their nature. The geotechnical characteristics of soil define the behaviour of soil. The problematic expansive soils are also known as cohesive soils. These kinds of soils are required to be treated before their use. Geotechnical engineers and designers call BCS as PBCS because it changes behaviour in the absence and presence of water [1]. The PBCS is typically very expansive, and the structures constructed over the soils suffer considerably due to seasonal moisture content variations. When the amount of water in the PBCS increases, the particles disperse and rearrange. Due to this phenomenon,

A. K. Jangid (✉) · K. S. Grover
Department of Civil Engineering, RTU, Kota, Rajasthan 324010, India
e-mail: amitjangid92@gmail.com

© The Author(s), under exclusive license to Springer Nature Switzerland AG 2024
P. M. Pawar et al. (eds.), *Techno-societal 2022*,
https://doi.org/10.1007/978-3-031-34644-6_91

889

a differential settlement arises in the soil, showing the treatment requirement. The stabilization process is used to enhance the geotechnical characteristics of problematic soils. Lime, cement, bitumen, and chemical are conventional methods for stabilizing soil. As we know that modern problems require instant solutions; therefore, many different advanced stabilization methods have been introduced, such as thermal, electrical, grouting, geotextile, and reinforced earth. On the other side, it has been observed that industrial waste is increasing every day, which impacts the environment drastically. Numerous researchers and investigators have reported a serious concern for reusing industrial waste in geotechnical engineering.

Non-traditional substances are admixtures that interact chemically with the soil frequently in the existence of sufficient moisture to cause physicochemical reactions in the soil matrix. These materials also provide, but are not constrained to, heavy industry by-products (such as steel slag, waste paper sludge ash, pulverized coal bottom ash, wastes from cement, lime, steel manufacturing plants, and others), ionic compounds, polymers, and sulphonated oils [2, 3]. The changes in clay surface charge polarity and alignment of clay particles, which increases the cohesive strength of inter-particle, modify the clay lattice, and coat the diffuse double-layer influence zone, are the mechanisms involved in using sulphonated oils and polymers [4]. Kumar et al. researched the characteristics of PBCS that contained varying amounts of FA and CS [5]. The findings showed that the inclusion of FA (10%) and CS (30%) (by soil weight) enhanced the soil's dry density and CBR values and reduced swelling. Michael et al. investigated the uses of industrial solid waste for stabilization [6]. The investigators used sawdust, fly ash, brick dust, polyvinyl waste, red mud, copper slag, and ceramic dust and partially replaced them with soil. According to the test results, practically all types of wastes from different type of heavy industries, have the potential to enhance expansive soil at a lower cost than traditional soil. Chandrashekher et al. studied the effect of CS on the geotechnical characteristics of soil [7]. The soil specimen underwent tests for CP, SG, CBR, PSD, and FSI. The results revealed that the subgrade, subbase, and engineering behavior of the soil were enhanced by including 60% copper slag in PBCS. GGBFS, a by-product of the production of iron which is used as stabilizing waste material [8, 10]. Lime, alumina, and silicate comprise most of their composition [10, 11]. Additionally, GGBFS material helps stabilize soil as a cement alternative in concrete mixtures [9, 11]. The compressive strength, permeability, and durability of soil increase with the addition of GGBFS [8, 10, 11]. The compacted clay soil demonstrates high strength in the presence of steel slag. It was noticed that the UCS of PBC soil improved by 200% after adding 12% steel slag [12]. The varied PSD of basic oxygen furnace slag have a considerable influence on the strength expansion of the stabilized marine dredging clay under similar conditions of free lime concentration and initial clay moisture [13].

Sani et al. used garnet waste material for the road shoulders [14]. For this purpose, the authors have investigated to find the effect of garnet waste on soil characteristics. As a result, the authors found that the CBR and MDD were increased with increasing garnet waste (to 80%). Muttashar et al. (mixed garnet waste material as a

partial replacement with geopolymer in concrete and obtained that the waste material enhances the strength characteristics of concrete [15]. Also, Sukmak et al. improved the mechanical characteristics of stabilized soft clay by adding crumb rubber and garnet sand [16].

Gaps in the Literature Survey—The published work illustrates that waste materials improve the geotechnical characteristics of cohesive soil. It can be seen that very few research has been done to stabilize the cohesive soil using the sea garnet sand. Also, it has been found that the behaviour of cohesive soil available in Kota, Rajasthan, has not been studied with sea garnet sand.

Objectives of the Present Research—The present research shows the applicability of sea garnet sand to stabilize the PBCS. The focus of this study has been conducted to study the impact of sea garnet sand on the PBCS available in Kota, Rajasthan. For that purpose, the influence of sea garnet sand has been determined on the CP and consistency limits of soil.

Research Significance—The present research helps to reduce and consume industrial waste by stabilizing the cohesive soils. Also, the present research introduces a potent waste material to geotechnical engineers/designers to stabilize the PBCS available in Kota, Rajasthan.

2 Materials and Methodology

2.1 Materials

The PBCS changes their behaviour in the presence and absence of water. In Kota, Rajasthan, several places have cohesive soil, which requires stabilization. The soil specimens have been collected from Rangpur, Kota, for the present research. The sea garnet waste material has been collected from VKI, Jaipur. Table 1 shows the geotechnical characteristics of the sea garnet sand and soil specimen.

2.2 Methodology

In this research, the impact of the sea garnet sand on the cohesive soil available at Rangpur, Kota, Rajasthan, has been determined by performing laboratory tests, namely PSD (wet and dry), OMC, MDD, consistency limits (PI, LI, and PI). The laboratory procedures have been performed as per IS 2720: 1984 (P4), IS 2720: 1985 (P5), IS 2720: 1977 (P40), and IS 2720:1980 (P7). This research has stabilized the PBCS by mixing 5–30% sea garnet sand at 5% variations. A comparative study has been mapped wrt to the geotechnical characteristics of different soil. Also, the percentage variation has been computed for stabilized soil wrt to virgin soil.

Table 1 Geotechnical characteristics of soil

Particular	Soil	Sea garnet sand
Gravel content (%)	0.0	0
Fine content (%)	80.08	0
Sand content (%)	3.72	100
OMC (%)	16	4.6
MDD (g/cc)	1.76	2.39
SG	2.70	4.05
FSI (%)	30.56	0
PL (%)	20.87	NP
LL (%)	40.60	26.54
PI (%)	19.73	NP

2.3 Design of Research

In the present research, each experimental value of the soil sample has been obtained by performing the test on two samples. Table 2 shows the design of research.

3 Discussion and Results

In this section, the consistency limits, PSD curve, and SPT of soil and garnet sand mixed soil have been calculated, discussed, and presented.

Table 2 Design of research

Experiment title	No. of samples	Code provisions
Grain size distribution	1	IS 2720: 1984 (P4)
Standard proctor test	2 (4–6 attempts)	IS 2720:1980 (P7)
Specific gravity	2	IS 2720: 1980 (P3/sec 1)
Consistency limits	2	IS 2720: 1985 (P5)
Free Swell Index	2	IS 2720: 1977 (P40)

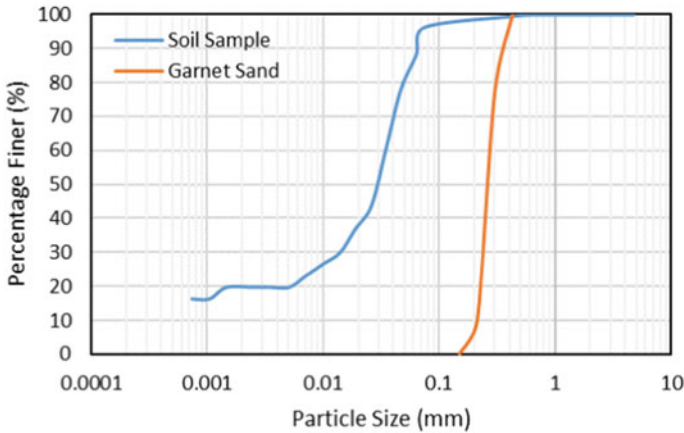


Fig. 1 PSD for soil and sea garnet sand samples

3.1 Grain Size Distribution

In this work, the PSD test has been performed for sea garnet sand and soil samples. Figure 1 shows the graphically representation for PSD test results.

Figure 1 demonstrates that the soil sample contains 3.72% sand and 80.08% fine content. Also, the sea garnet sand has medium and fine sand.

3.2 Consistency Limits

The consistency limits, such as PL, PI, and LL of soil, have been determined experimentally to study the effect of sea garnet sand. For this purpose, 5–30% sea garnet sand at 5% variations has been mixed in collected soil samples. The consistency limit results of PBCS and mixed soil samples are following:

Table 3 shows that virgin soil has 20.87%, 40.6% and 19.73% PL, LL, and PI, respectively. The sea garnet sand has been mixed in the soil to improve the LL, PL, and PI. It can be noticed that decrement of the LL of soil is 32.9% by adding 30% sea garnet sand. Also, the PL has decreased to 14.5% by adding 30% sea garnet sand. An interesting phenomenon has been observed in the case of the PI. The PI has been decreased to 17.60% by adding 10% sea garnet sand. Further increasing the percentage of sea garnet sand, the PI has started increasing. By adding 30% sea garnet sand, the PI of PBCS has been increased to 18.4%. Still, it can be found that the PI is lower than the PI of virgin soil. From the basis on the consistency limits, the soil has been categorised as “Inorganic clay of low to medium plasticity.” In addition, the percentage variation in consistency limits has been calculated and graphically presented in Fig. 2.

Table 3 Consistency limits of PBCS and mixed samples

Sample designation	PL (%)	LL (%)	PI (%)
PBCS	20.87	40.60	19.73
PBCS + 5% SG sand	19.65	37.90	18.25
PBCS + 10% SG sand	18.80	36.40	17.60
PBCS + 15% SG sand	17.75	35.70	17.95
PBCS + 20% SG sand	16.10	34.10	18.00
PBCS + 25% SG sand	15.30	33.53	18.23
PBCS + 30% SG sand	14.50	32.90	18.40

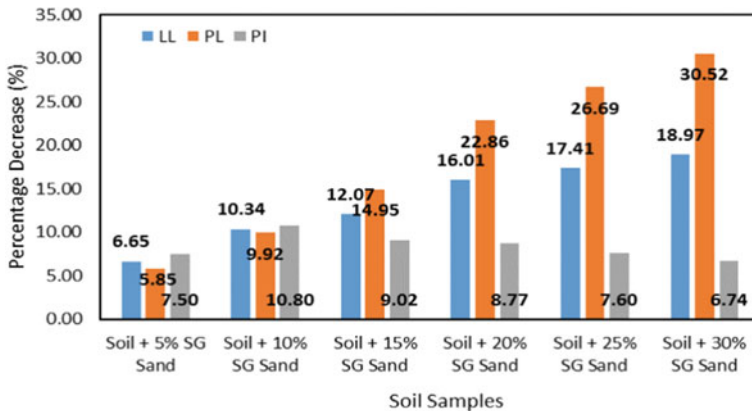


Fig. 2 Percentage variation in SG of PBCS

Figure 2 presents that the LL of the PBCS is decrease from 6.65 to 18.97% by adding 5–30% sea garnet sand. Similarly, the PL of soil is decrease from 5.85 to 30.52% by mixing 5–30% sea garnet sand. In the case of the PI, the maximum decrease in the PI of PBCS has been found at 10% sea garnet sand. Still, the PI of the 30% sea garnet mixed soil sample is 6.74% lower than the virgin soil.

3.3 Standard Proctor Test

Similarly, the SPT has been conducted in the geotechnical laboratory to find the MDD and OMC of PBCS and sea garnet sand mixed soil samples. The results acquired from the SPT and the values of OMC and MDD are given in Table 4.

Table 4 illustrates that the OMC content and MDD content of PBCS are determined experimentally as 16.0 and 1.760 g/cc, respectively. By adding 5% sea garnet sand, the MDD and OMC virgin soil have been increased to 1.820 g/cc and 14.8, respectively. The MDD of soil is increase to 1.999 g/cc by adding 20% sea garnet sand, and the

Table 4 MDD and OMC of PBCS and mixed samples

Sample designation	MDD (g/cc)	OMC (%)
PBCS	1.760	16.0
PBCS + 5% SG sand	1.820	14.8
PBCS + 10% SG sand	1.838	14.2
PBCS + 15% SG sand	1.910	13.8
PBCS + 20% SG sand	1.999	13.2
PBCS + 25% SG sand	1.950	14.4
PBCS + 30% SG sand	1.930	14.9

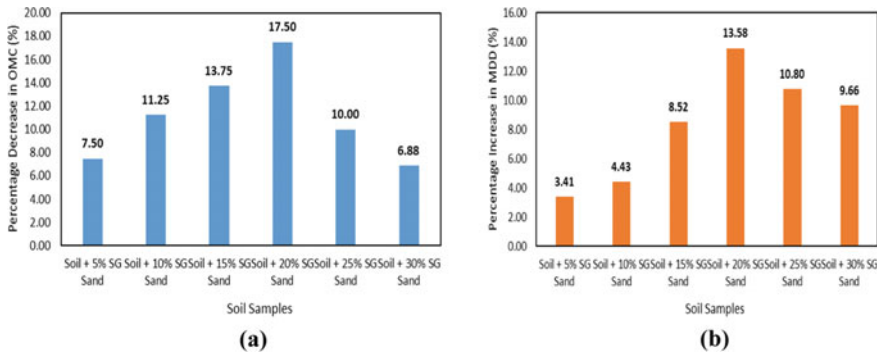


Fig. 3 Illustration of the effect of sea garnet sand on **a** OMC and **b** MDD

OMC is decrease to 13.2% by adding 20% sea garnet sand. Further addition of sea garnet sand shows that MDD has begun to fall. The percentage variation in the MDD and OMC of PBCS has been calculated, as shown in Fig. 3.

Figure 3a and b illustrates that the maximum decrease in OMC and maximum increase in MDD of soil have been determined by adding 20% sea garnet sand. The optimum percentage of sea garnet sand was found about 20% for the PBCS.

4 Conclusions

The present research has been conducted to stabilize the PBCS of Rangpur, Kota. For this purpose, the sea garnet sand waste material has been added in the range of 5–30% at 5% variations to the soil samples. During this research, the PSD, SPT, and consistency limits tests done at the Department of Civil Engineering, RTU, Kota. From the summary of the obtained results, the following outcomes are mapped: (1) The sea garnet sand contains the maximum amount of fine sand particles; (2) The

PL and LL of the PBCS (Rangpur) can be controlled by adding sea garnet sand; (3) The PBCS can be densified by adding 20% sea garnet sand.

To sum up, the present research demonstrates that sea garnet sand is a new stabilizing waste material that can be used to stabilize the PBCS. The present study may be extended by performing strength tests for the same soil specimens. Also, 1% of free lime can be added to the existing soil samples to study the impacts of free lime on the geotechnical characteristics of Rangpur soil. As stated by authors, the sea garnet sand waste material has been utilized to stabilize the Ranpur soil for the first time.

Nomenclature

GGBFS	Ground Granulated Blast Furnace Slag
PBCS	Problematic Black Cotton Soil
BCS	Black Cotton Soil
FA	Fly Ash
CS	Copper Slag
SPT	Standard Proctor Test
PSD	Particle Size Distribution
FSI	Free Swell Index
CP	Compaction Parameter
CBR	California Bearing Ratio
UCS	Unconfined Compressive Strength
MDD	Maximum Dry Density
OMC	Optimum Moisture Content
LL	Liquid Limit
PL	Plastic Limit
PI	Plasticity Index

References

1. Steinberg, M. (2000). Expansive soils and the geomembrane remedy. In *Advances in unsaturated geotechnics* (pp. 456–466).
2. Petry, T. M., & Little, D. N. (2002). Review of stabilization of clays and expansive soils in pavements and lightly loaded structures—History, practice, and future. *Journal of Materials in Civil Engineering*, 14(6), 447–460.
3. Estabragh, A. R., Soltani, A., & Javadi, A. A. (2020). Effect of pore water chemistry on the behaviour of a kaolin–bentonite mixture during drying and wetting cycles. *European Journal of Environmental and Civil Engineering*, 24(7), 895–914.
4. Onyejekwe, S., & Ghataora, G. S. (2015). Soil stabilization using proprietary liquid chemical stabilizers: Sulphonated oil and a polymer. *Bulletin of Engineering Geology and the Environment*, 74(2), 651–665.

5. Kumar, P. R., Kumar, P. S. P., & Maheswari, G. (2017). Laboratory study of black cotton soil blended with copper slag and fly ash. *International Journal of Innovative Research in Science, Engineering and Technology*, 6(2), 1960–1967.
6. Michael, T., Singh, S. K., & Kumar, A. (2016). Expansive soil stabilization using industrial solid wastes a review. *International Journal of Advanced Technology in Engineering and Science* 4(9).
7. Chandrshekhar, J., Chokshi, T. A., & Chauhan, D. V. (2015). A review on utilization of waste material “Copper Slag” in geotechnical applications. *International Journal for Innovative Research in Science & Technology*, 1, 2349.
8. Neeladharan, C., Muralidharan, A., Mohan, K., Sayeed, M., Azeed, A., Faizan, M., & Arafath, Y. (2019). Stabilization of soil using fly ash with ground granulated blast furnace slag (GGBS) as binder. *Suraj Punj Journal*, 9, 23.
9. Ghaffoori, F. K., & Arbili, M. M. (2019). Effects of fly ash and granulated ground blast furnace slag on stabilization of crude oil contamination sandy soil. *Polytechnic Journal*, 9(2), 80–85.
10. Mandal, S., & Singh, J. P. (2016). Stabilization of soil using ground granulated blast furnace slag and fly ash. *IJIRSET*, 5, 21121–21126.
11. Dayalan, J., & Dayalan, J. (2016). Comparative study on stabilization of soil with ground granulated blast furnace slag (GGBS) and fly ash. *International Research Journal of Engineering and Technology*, 3(5), 5.
12. Mozejko, C. A., & Francisca, F. M. (2020). Enhanced mechanical behavior of compacted clayey silts stabilized by reusing steel slag. *Construction and Building Materials*, 239, 117901.
13. Cikmit, A. A., Tsuchida, T., Kang, G., Hashimoto, R., & Honda, H. (2019). Particle-size effect of basic oxygen furnace steel slag in stabilization of dredged marine clay. *Soils and Foundations*, 59(5), 1385–1398.
14. Sani, W. M., Mohamed, A., Nor, H. M., Kamarudin, N. A. S., Khalid, N. H. A., Sam, A. M., & Ab Rashid, R. (2019). Characterization of soil mixed with garnet waste for road shoulder. In *IOP Conference Series: Earth and Environmental Science* (Vol. 220, No. 1, p. 012052). IOP Publishing.
15. Muttashar, H. L., Ariffin, M. A. M., Hussein, M. N., Hussin, M. W., & Ishaq, S. B. (2018). Self-compacting geopolymer concrete with spend garnet as sand replacement. *Journal of Building Engineering*, 15, 85–94.
16. Sukmak, P., Sukmak, G., Horpibulsuk, S., Kassawat, S., Suddepong, A., & Arulrajah, A. (2021). Improved mechanical properties of cement-stabilized soft clay using garnet residues and tire-derived aggregates for subgrade applications. *Sustainability*, 13(21), 11692.

Sensor, Image and Data-Driven Societal Technologies

Face Sketch to Image Generation and Verification Using Adversarial and Discrimination Network



Mokshada S. Bhandare and Anup S. Vibhute

Abstract In this paper, we propose a solution to transforming the human face sketch into the original photo. In this area many of the researches are done before, some of them got very good results and some of them observed the drawbacks in their research. The drawbacks observed are blurry boundaries, color mixing and color spreading. But these results are mostly observed from the basics of the GAN that is convolutional networks. To avoid this problem and to produce realistic output we are going to use the conditional generative adversarial networks. By using this we can obtain the output as we want, for that we require converting the original image into sketch and applied as input. And the output is we got more realistic output as compared to CNN. We overcome the problem of mixing of colors and got the different colors for hair, lips, and skin using conditional GAN as compared to CNN state-of-the-art with improved accuracy and performance.

Keywords CNN · GAN · Conditional GAN

1 Introduction

If anyone wants to describe their mind ideas, thoughts or any seen object the easiest method is to draw a sketch. Drawing is a very easy method to represent your thought in minimum time. It does not require any object and it's free. In recent days the conversion of sketch to image is very interesting and hot topic on internet. This is used in machine learning [1]. There are lots of applications of sketch to image conversion. One of them is in police station. If anyone seen a thief or a suspect but the person is unable to describe it that time the sketch to image conversion is used [2]. It is also used in editing of a photo [3] another application of this is in public security

M. S. Bhandare (✉)

Department of Electronics and Communication, SVERI's College of Engineering, Pandharpur, Maharashtra, India

e-mail: b.mokshada1996@gmail.com

A. S. Vibhute

Dr. D.Y. Patil, Institute of Technology, Pune, India

© The Author(s), under exclusive license to Springer Nature Switzerland AG 2024

P. M. Pawar et al. (eds.), *Techno-societal 2022*,

https://doi.org/10.1007/978-3-031-34644-6_92

901

system and image processing [4–7]. To build a conditional GAN we took 500 images of face sketch and then done the conversion of them the each image is of $200 * 200$ dimension. Out of 500 the 400 images are used for the testing. The input is of sketch and reference image is original image of sketch. We compared our network with the basic of GAN that is convolutional neural network. we are going to understand existing approaches, identify the limitations of existing approaches and according to that will design a novel neural network for generating a good quality face images from sketches and comparing the generated face images with ground truth images to increase the accuracy and SSIM (Structural Similarity Index). In this paper, we propose a novel human face sketch to color image conversion that allows all types of skin tones between the age group of 50to80. We overcome the problem of mixing of colors and got the different colors for hair, lips, and skin using conditional GAN as compared to CNN state-of-the-art with improved accuracy and performance.

2 Related Works

2.1 Existing Approaches

Liu et al. [1] in recent years many of the researchers trying to generate an original image with the help of deep neural networks. These researches are comes under the machine learning and the computer vision. By using the large amount of data set the generation of the image is takes place. They also were trying to learn for color images of cartoon. By using CGAN they are working on sketch to image synthesis problem. For that they produced the auto painter model. And their model is successful in painting the colors automatically and also gives the chance to user for showing the preferred colors. Instead of image to image method their auto painter model works best for showing the realistic outputs.

Chen et al. [2] by combining the various original images with the hand drawn sketches is very interesting topic in computer vision and graphics. The previous research needs the accurate mapping functions or relies to recover the photographs. For their research they took the various kinds of data sets like horses, couches and the motorcycles. They derived the data augmentation method for their sketches. To provide an image on the multiple scales they form a block for the gan models that is generator and the discriminator. And this theory is helpful for improving the flow of information.

2.2 Gan

GAN is a generative algorithm introduced by Ian Good fellow and other researchers in 2014. To train a generative model the generative adversarial networks are developed.

In recent years using original GAN different kinds of network models are derived [8] They consists of two generative models first is generator as G, and the discriminator as D [9]. The data diffusion is done by the generator, and the discriminator is works as classifier. It shows the probability of showing the sample is generated by G or from training. The generator and discriminator models are non-linear mapping functions. Such as multi-layer perceptron. The GANs are used generating of image [10–15] image translation from one to other [16, 17] To study how the generator distribution pg over data X, it helps to build the mapping function from noise distribution pz(z) to data space as G(z; θg). And the discriminator, D(x; θd), outputs a single scalar representing the probability that x came from training data rather than pg. G and D are both trained simultaneously: we adjust parameters for G to minimize log (1 – D (G (z))) and adjust parameters for D to minimize logD(X), as if they are following the two-player min–max game with value function V (G, D):

$$\begin{aligned} \text{Min G Max D V (D, G) = } & E_{x \sim p_{\text{data}}(x)} [\log D(x)] \\ & + E_{z \sim p_z(z)} [\log(1 - D(G(z)))] \end{aligned} \tag{1}$$

2.3 DCGAN

The DCGAN stands for deep convolution gan. These DCGAN’s are the basics of conditional GAN. In the conditional GAN there are various types of conditions are known as class labels. The class labels are male, female, and many more depends upon the project. But in the deep convolution GAN there is not any specific condition to produce a desired output that is any specific image. In the DCGAN there is no any criterion to develop an image in serial manner, and they don’t know which image is generated first or which is last. But in the conditional GAN this problem can be overcome. GAN means there is a generator and the discriminator network. The input given to the generator is the condition that is class labels. The generator takes an input and encodes it and transfer output towards the discriminator. The properties are if we are going to produce the sketch conversion of an animal into an image the properties are their legs, teeth’s, tail skin etc. are the class labels. In above figure the input is sketch and the output is the conversion of sketch into an image. The generator consists of encoder and decoder block. The detailed information of this block is given below (Fig. 1).

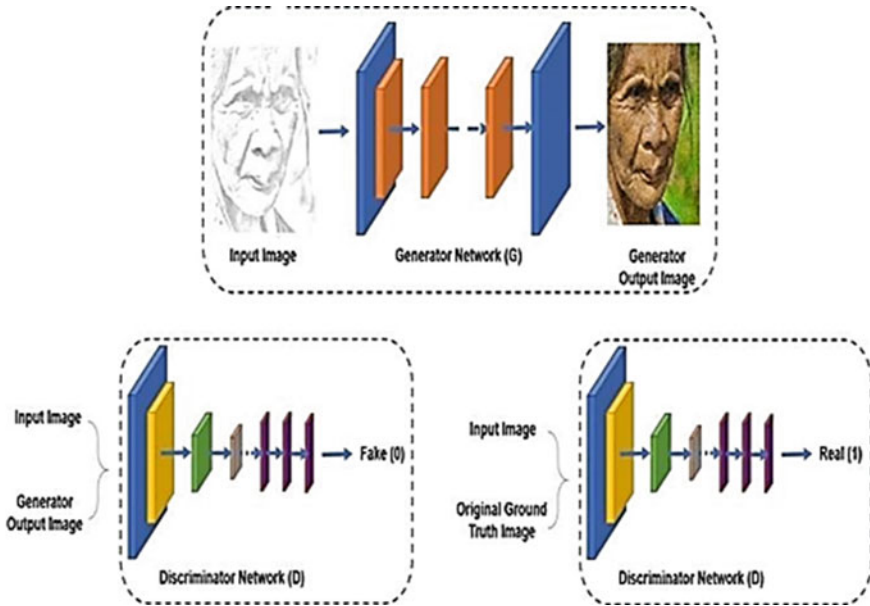


Fig. 1 Architecture of image colorization

3 Methodology

In GANs, the input of the generator network consists of noise vector which are randomly generated. But in the task of Image colorization problem, such GANs will not work as our GAN is not designed to generate images from random vectors but instead add colors to already existing photos having only one channel (Black and white). So the basic task for our GAN is to add three channels (RGB) with relevant intensities of each color channel. Hence, to address this problem, we use a special flavor of GAN called Conditional GANs which accepts gray scale images that is our input sketch (with one intensity channel) as input (i.e. $G(\theta_z | x)$, mathematically). The discriminator input is also changed to be compatible with the conditional GANs. Our final cost functions are as follows with above modifications (Fig. 2).

$$\begin{aligned} \text{MinTj G}(\theta_D, \theta_G) = \min E_z [\log(D(G(\theta_z|x)))] \\ + \lambda \|G(\theta_z|x) - y\|_1 \end{aligned} \tag{2}$$

$$\begin{aligned} \text{maxTj G}(\theta_D, \theta_G) = \max(E_y [\log(D(y|x))] \\ + E_z[\log(1 - D(G(\theta_z|x)|x))]) \end{aligned} \tag{3}$$

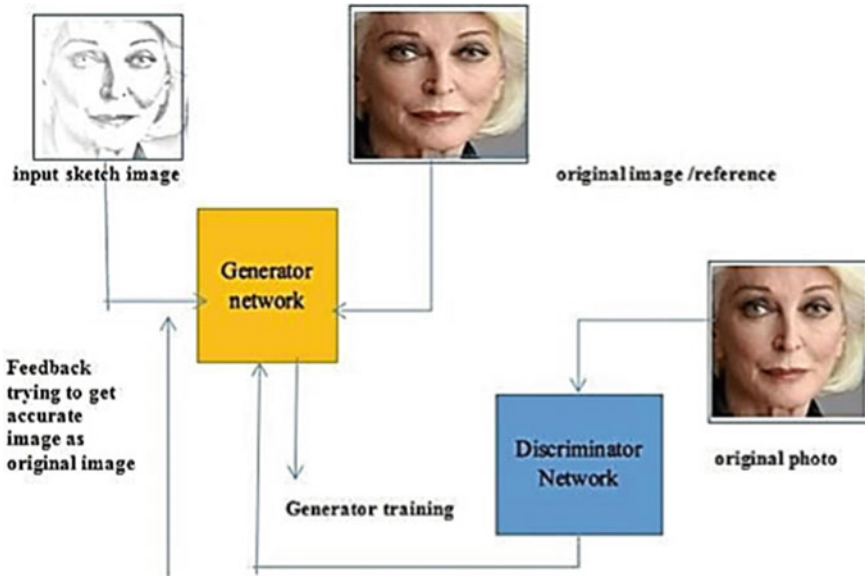


Fig. 2 Proposed architecture

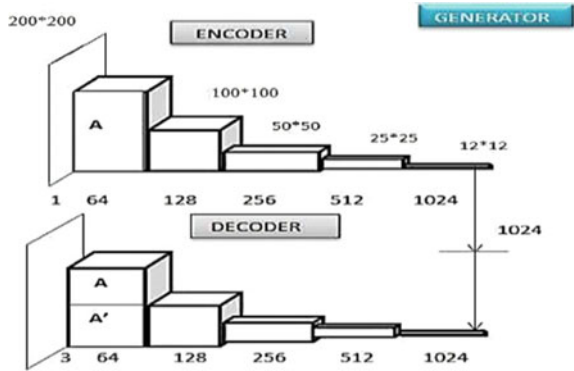
3.1 Method

The problem we are trying to solve comes under the category of Image to Image translation with mapping from high dimension input to high dimension output. It is actually regression on pixel level with a condition of output having structure similar to the input. Hence the network needs to have very high similarity of spatial dimensions of input and output and also provide information regarding the color to each pixel in the original gray scale image.

3.2 GAN Architecture

The network for this model is based on “fully connected networks”. We use layers of convolutions in Generator. But instead of pooling layers, down sampling of the image is done till it becomes vector of size 2×2 pixels. Then up sampling is done to expand the compressed part and making it to the size of the input sample (i.e. 200×200 pixels). This strategy is motivated by special types of deep networks called Encoder-Decoder networks containing encoding and decoding networks for contracting and then expanding and hence reconstructing the input. This strategy helps in training the network without consuming large amount of memory. It is initially down sampled with kernel of size 1 and stride 1. After this layer, it is subsequently compressed to image to size (12×12) with kernel of size 2 and strides 2. This is done five times after

Fig. 3 Proposed generator architecture for image colorization



the initial layer, making the matrix of dimensions $(12 \times 12 \times 1024)$. The expansion stages consists of up sampling of the matrix with kernel size 2 and strides 2 except the last layer. Concatenation of I and n-I layers are done to preserve the structural integrity of the image. In the first and second expansive layers, drop out of scale 0.2 is done to introduce noise for robust training of Generator. Batch normalization is done for better training. In our model, we used Leaky ReL U with slope of 0.2 as it has shown better performance than ReLU activation function. In the last layer convolution with kernel size 1 and strides 1 is done to construct image of dimension $(200 \times 200 \times 3)$. “tanh” activation function is used as it has shown to have better performance than linear activation functions. It gives output in the form of matrix containing values from -1 to 1. We train the model to minimize the cosine distance between predicted and the original image. After this layer, it is subsequently compressed to image to size (12×12) with kernel of size 2 and strides 2. This is done five times after the initial layer, making the matrix of dimensions $(2 \times 2 \times 1024)$ (Fig. 3).

3.3 Discriminator Network

For discriminator, we first concatenate the grayscale image and the predicted or the grayscale image and the ground truth image on the channel axis (axis = 3), hence it forms a colored image. We perform down sampling of the matrix successively using convolution layer with filter size of (2×2) and strides equal to 2. Each layer has Leaky ReLU activation function with slope 0.2 and Batch Normalization is performed at every layer. The last layer is flattened followed by a hidden layer containing 12 units, which are connected to output layer containing 1 unit. The activation function which is used in the last layer is “sigmoid”, which gives the probability of the input image to belong to predicted one or the ground truth (Fig. 4).

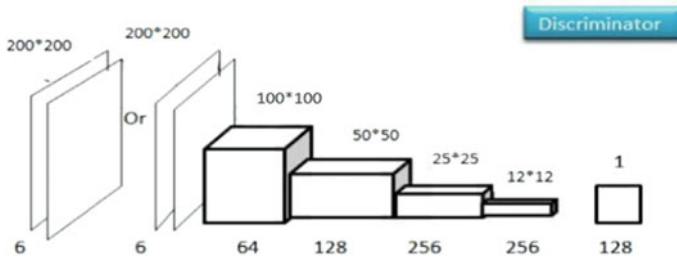


Fig. 4 Proposed discriminator architecture for image colorization

4 Experiments

To train our model the software we are going to use is Google’s Collaborators. For this the Google’s Collaborators uses the GPU of Tesla P100-PCI-E-16GB. To train our model for we require 10 h and for testing 20 min. The initial learning rate for generator and discriminator is 0.0002. We used the Adam optimizer [18]. We used STL-10 dataset. We took the 500 images for dataset, and converted these images in sketch. We used 500 images for training and out of these 400 images for the testing purpose. For each image the dimension is 200 * 200 for the input setup we converted the images in sketch. After conversion we got the dataset of original image and their sketches for input.

5 Results

Figure 5a is original image as reference image, (b) is the sketch conversion; (c) is the testing image as output.

Fig. 5 **a** Original image as reference image, **b** sketch conversion, **c** testing image as output



References

1. Liu, Y., Qin, Z., Wan, T., & Luo, Z. (2018). Auto-painter: Cartoon image generation from sketch by using conditional Wasserstein generative adversarial networks. *Neurocomputing*, 311, 78–87.
2. Hu, M., & Guo, J. (2020). Facial attribute-controlled sketch-to-image translation with generative adversarial networks. *EURASIP Journal on Image and Video Processing*, 2020(1), 1–13.
3. Liu, Q., Tang, X., Jin, H., Lu, H., & Ma, S. (2005, June). A nonlinear approach for face sketch synthesis and recognition. In 2005 IEEE Computer Society conference on computer vision and pattern recognition (CVPR'05) (Vol. 1, pp. 1005–1010). IEEE.
4. Wang, N., Tao, D., Gao, X., Li, X., & Li, J. (2014). A comprehensive survey to face hallucination. *International Journal of Computer Vision*, 106, 9–30.
5. Kazemi, H., Iranmanesh, M., Dabouei, A., Soleymani, S., & Nasrabadi, N. M. (2018, March). Facial attributes guided deep sketch-to-photo synthesis. In 2018 IEEE Winter Applications of Computer Vision Workshops (WACVW) (pp. 1–8). IEEE.
6. Peng, C., Gao, X., Wang, N., & Li, J. (2015). Superpixel-based face sketch-photo synthesis. *IEEE Transactions on Circuits and Systems for Video Technology*, 27(2), 288–299.
7. Liu, R., Yu, Q., & Yu, S. X. (2020). Unsupervised sketch to photo synthesis. In Computer Vision–ECCV 2020: 16th European Conference, Glasgow, UK, August 23–28, 2020, Proceedings, Part III 16 (pp. 36–52). Springer International Publishing.
8. Goodfellow, I., Pouget-Abadie, J., Mirza, M., Xu, B., Warde-Farley, D., Ozair, S., & Bengio, Y. (2014). *Generative adversarial nets in advances in neural information processing systems (NIPS)* (pp. 2672–2680). Red Hook, NY, USA: Curran Associates, Inc.

9. Chang, J., & Scherer, S. (2017, March). Learning representations of emotional speech with deep convolutional generative adversarial networks. In 2017 IEEE International Conference on Acoustics, Speech and Signal Processing (ICASSP) (pp. 2746–2750). IEEE.
10. Zhang, L., Lin, L., Wu, X., Ding, S., & Zhang, L. (2015, June). End-to-end photo-sketch generation via fully convolutional representation learning. In Proceedings of the 5th ACM on International Conference on Multimedia Retrieval (pp. 627–634).
11. Zhang, M., Li, Y., Wang, N., Chi, Y., & Gao, X. (2019). Cascaded face sketch synthesis under various illuminations. *IEEE Transactions on Image Processing*, 29, 1507–1521.
12. Dosovitskiy, A. (2016). Generating images with perceptual similarity based on deep networks, Feb 2016.
13. Gulrajani, I., Ahmed, F., Arjovsky, M., Dumoulin, V., & Courville, A. C. (2017). Improved training of Wasserstein GANs. *Advances in Neural Information Processing Systems*, 30.
14. Zhu, J. Y., Park, T., Isola, P., & Efros, A. A. (2017). Unpaired image-to-image translation using cycle-consistent adversarial networks. In *Proceedings of the IEEE international conference on computer vision* (pp. 2223–2232).
15. Song, M., Chen, C., Bu, J., & Sha, T. (2012). Image-based facial sketch-to-photo synthesis via online coupled dictionary learning. *Information Sciences*, 193, 233–246.
16. Efros, A. A., & Freeman, W. T. (2001, August). Image quilting for texture synthesis and transfer. In *Proceedings of the 28th annual conference on Computer graphics and interactive techniques* (pp. 341–346).
17. Nazeri, K., Ng, E., & Ebrahimi, M. (2018). Image colorization using generative adversarial networks. In *Articulated Motion and Deformable Objects: 10th International Conference, AMDO 2018, Palma de Mallorca, Spain, July 12–13, 2018, Proceedings 10* (pp. 85–94). Springer International Publishing.
18. Levin, A., Lischinski, D., & Weiss, Y. (2004). Colorization using optimization. In *ACM SIGGRAPH 2004 papers* (pp. 689–694).

Touchless Fingerprint Recognition System



Sujit A. Inamdar, Mahesh M. Zade, and Snehal Y. Abhangrao

Abstract A new approach to the traditional touch-based fingerprint recognition method is the touchless fingerprint recognition system. Offline processes improve processes and produce better results. Instead of the outdated conventional systems, touchless systems uses digital camera to acquire the fingerprint image. This article offers a brand-new, excellent answer to the issues with latent fingerprints, maintenance, and hygiene. In this paper, we have added a novel fingerprint minutiae matching algorithm-based fingerprint identification system. It includes the three key steps as Preprocessing, feature extraction, and matching stage. The preprocessing phase is crucial since it calls for positive outcomes in terms of core point recognition, segmentation, and enhancement. The Principal Component Analysis yields favourable recognition findings.

Keywords Image preprocessing · Minutiae core extraction · Local ridge orientation · Principle component analysis

1 Introduction

The use of biometric technology for identification and verification is possible. In these situations, a database containing the biometric data of a group of people should exist. In an identification task, the system's job is to compare an input image with every entry in the database and check for matches, determining whether the person is present in the database. Using traditional touch-based sensors has a number of drawbacks, including image distortion, changes in rotation and displacement, wet/

S. A. Inamdar (✉) · S. Y. Abhangrao
SVERI's College of Engineering, Pandharpur, MH, India
e-mail: sainamdar@coe.sveri.ac.in

M. M. Zade
S.B. Patil College of Engineering, Indapur, India

dry impressions, and the need for the user to apply a particular amount of pressure to get adequate image quality. However, this pressure causes physical deformation that cannot be avoided in all directions. The practical substitute is to utilize a high-resolution image capture device such as Rapid-i for acquisition of touchless images [1]. It takes a direct image of the fingertip using cameras. It benefits from cleanliness, the absence of latent prints, and the absence of pressure-related distortion.

2 Proposed System

2.1 Proposed System Overview

Figure 1 depicts the system flow of the new touchless fingerprint recognition system. The system's primary supporting modules are as follows:

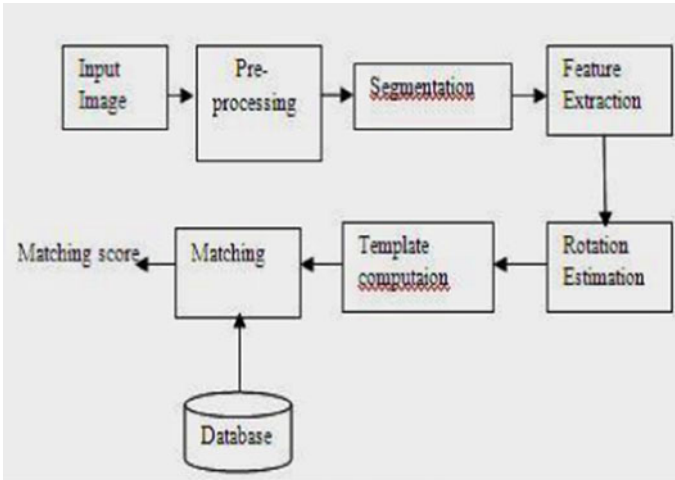


Fig. 1 System operation flow

(1) Preparation

Using the suggested method, which includes core point detection, image enhancement, fingerprint segmentation, and normalization, the fingerprint pictures are preprocessed.

(2) The extraction of features

Following preprocessing, the feature vectors are retrieved using the Novel technique.

(3) PCA

By removing the later principal components, it is possible to maintain the feature vectors' dimensionality while keeping the traits that account for the majority of their variance.

(4) Matching

The fingerprint matching is carried out by using the Euclidean distance method, Principal Component Analysis [2].

2.2 Preprocessing

First, a grayscale [0–255] conversion of the RGB fingerprint image takes place. The image is then normalized by altering the dynamic values of the pixel intensity to improve the quality brought on by the illumination. It must then be changed from black and white to grayscale and finally into a logical image. After applying Gaussian filters to normalize the image's local mean and variance, the Gaussian filters' sigma value is set to 4, and the formula used to calculate their size is:

$$\text{Size} = 2 * \text{Hori_size} \text{ plus one};$$

Fig. 2 RGB to Gray image conversion

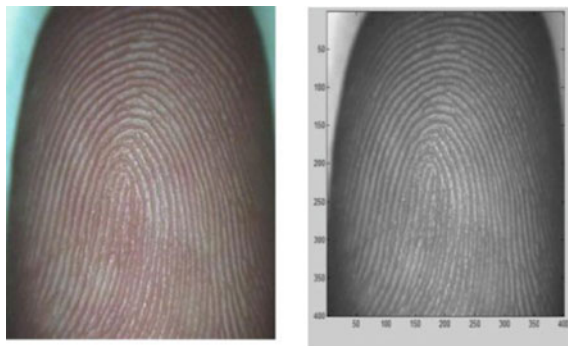
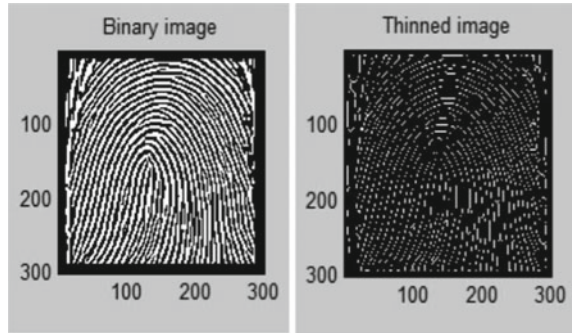


Fig. 3 Thinning process



When using the corresponding mean, “Hori_size” will be the inverse of the normal CDF (cumulative distribution function).

“mu=0” and standard deviation “sigma = 4” at the corresponding probabilities in “P = epsilon/2”

$$\text{Hori_size} = \text{ceil}(-\text{norminv}(\text{epsilon}/2), 0, 0, \text{sigma});$$

$$\text{Epsilon} = 1^{e-1} \text{ in this case.}$$

The output is the result of applying the local mean and standard deviation to the input image to normalize it locally.

The grayscale image must be converted to a logical image after normalization in order to accurately extract the ridges. This procedure is known as binarization. Additionally, an adaptive thresholding is required algorithm; followed by the morphological processing for thinning purposes: The ridge orientations are used to remove minute particles. The current black-and-white image consists of wide ridges beyond a pixel. This makes it impossible for us to extract the finer points, so the ridges must be thinned.

The “bwmorph” function is available in the MATLAB toolbox is used for thinning process.

$$\text{Bwmorph}(\text{img_in}, \text{“Inf”}, \text{“thin”})$$

The input binary image img_in needs to be thinned. Thinning is required to get rid of picture spikes and H-breaks. Pointless noise bridges called H-breaks, which join two or more ridges as shown in Fig. 3.

2.3 Feature Extraction

After capturing both the frequency and orientation information from a fingerprint image, the Minutiae points are the unique identification points such as “bifurcation”,

“termination” points. Initial step in extracting the minutiae points is to find the central point of a 3 * 3 sliding filter block. Connected parts of each block are determined by using the “bwlabel” function. “centerp” for termination and bifurcation are separately determined by assigning 1 and 3 respectively to the nonlinear filter.

```
Li = nlfiter(img_in,[3 3],fun2);
```

```
Lterm = (Li == 1);  
LTermb = bwlabel(Lterm);
```

```
Pterm = regionprops(LTermb, 'centerp');
```

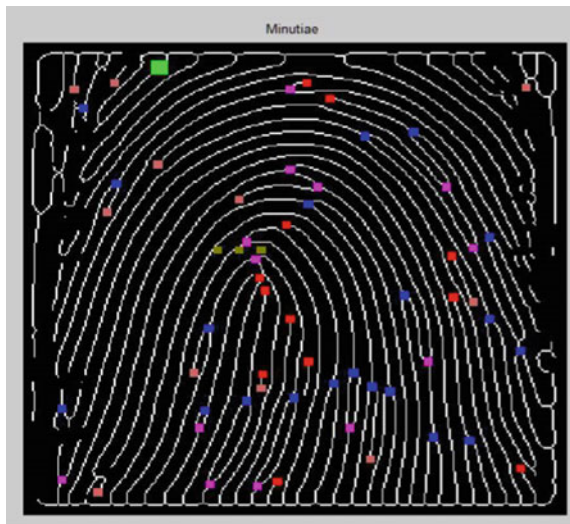
where `img_in` is the input image and “fun2” is a function called “minutiae” which provides `x` and `y` values of the image. For bifurcation, `L_bif = (L == 3)` is implemented to get the “centerp”. These centerp are nothing but the actual minutiae points in the image. In order to remove unwanted minutiae, Euclidean distance (`L`) estimation is been used. We give a threshold = 6 and measure the distance between the termination and bifurcation points. Input arguments for distance measurement are `x1` and `x2` consisting of termination and bifurcation central points respectively [3].

We remove the minutiae if,

- (a) If the distance between a termination and a bifurcation < `L`.
- (b) If the distance between two terminations < `L`.
- (c) If the distance between two bifurcations < `L`.

The above conditions remove the spurious minutiae points present on the image. These conditions were based on the Euclidean distance [4] between the minutiae points. Refer (Fig. 4).

Fig. 4 Minutiae extraction process



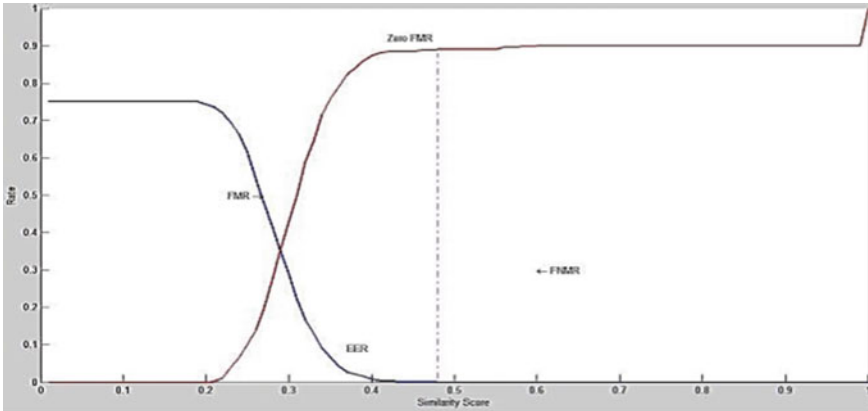


Fig. 5 Minutiae matching method [7]

3 Experimental Results

In the recognition system, false acceptance rate (FAR) [5] and false reject rate (FRR) are the two main terms of mismatch/fault finding. The Equal Error Rate (EER), or $FAR = FRR$, is used to assess the performance of our system. Here, we have contrasted our findings with those of the correlation approach, another mathematic algorithm. Our approach for minutiae matching produces superior results, or less EER [6] (Fig. 5).

4 Conclusion

A touchless approach for acquiring fingerprint images was suggested in this paper. While the benefits of touchless imaging include cleanliness, preventing fingerprint distortion, and not creating latent prints. Low ridge-valley contrast and minor distortion between images from various perspectives do, however, effect on result in touchless imaging. From the experimental findings, the correlation method’s results are inferior to those of EERs obtained with test images with our Novel algorithm.

References

1. Hiew, B. Y., & Teoh, A. B. J. (2007). Digital camera based fingerprint recognition. In Y. H. Pang (Ed.), *Proceedings of the 2007 IEEE international conference on telecommunications and Malaysia international conference on communications*, 14–17 May 2007. IEEE, Penang, Malaysia.
2. Principal component analysis for minutiae verification on fingerprint image. In *Proceedings of the 7th WSEAS international conference on multimedia systems & signal processing*, Hangzhou, China, April 15–17, 2007 CHING-TANG HSIEH, SHYS-RONG SHYU.
3. Ravi, J., Raja, K. B., & Venugopal, K. R. (2009). Fingerprint recognition using minutia score matching. *International Journal of Engineering Science and Technology*, 1(2), 35–42. ISSN: 0975-5462.
4. Jadhav, S.D., Barbadekar, A. B., & Patil S. P. (2009). *Euclidean distance based fingerprint matching*. ISBN: 978-960-474-276-9.
5. Johal, N. K., & Kamra, A. (2011). A novel method for fingerprint core point detection. *International Journal of Scientific & Engineering Research*, 2. ISSN 2229-5518, Apr 2011.
6. Ravi, H., & Sivanath, S. K. (2013). *A novel method for touch-less finger print authentication*. IEEE. 978-1-4799-1535-4/13©2013.
7. Choi, H., Choi, K., & Kim, J. (2011). Fingerprint matching incorporating ridge features with minutiae. *IEEE Transactions on Information Forensics and Security*, 6(2), 338–345.

Reducing Clock Power by Using the Clock Gating Technique



Garad Ashutosh, Musale Jivan, Garad Shraddha, and Pawar Rahul

Abstract The clock signal is always a significant way of mouse and is a worst issue in any synchronous circuit. Clock gates are a successive method of minimize positive power dissipation in digital circuits. A general-purpose microprocessor is a typical synchronous circuit, which is active. To avoid unnecessary power consumption of the circuit by closing the inactive portion of the circuit. One method is to hide the pulse that drives the torpid part of the circuit. I will present a review of existing clock triggering methods as well as a comparative analysis of these clock triggering techniques on a variety of synchronous digital designs such as ALU and FIFO.

Keywords Signal chime · Digital watermark · LCG · Clock power · Dynamic power

1 Introduction

The demand for energy-efficient designs has skyrocketed in recent years. We see that now-a-days there is rapid growth in portable battery-operated devices that is laptops, notebooks and mobiles these devices are primarily responsible for this massive demand [1]. Other mobile communications with each technology generation, semi-conductor devices are aggressively expanded to get excessive presentation as well as excessive unification substance. Power consumption in the chip with each technology generation due to increased transistor density and higher operating frequency. If we want to put power consumption within a permissible range, we need to adjust the supply voltage proportionally a result power voltage scaling alone may not be enough to keep power density within acceptable limits [2]. If power consumptions are

G. Ashutosh (✉) · M. Jivan · P. Rahul
Department of Electronics and Telecommunication Engineering, SVERIs COE Pandharpur,
Pandharpur, Maharashtra, India
e-mail: aagarad@coe.sveri.ac.in

G. Shraddha
Department of Electrical Engineering, SVERIs COE Pandharpur, Pandharpur, Maharashtra, India
e-mail: aagarad@coe.sveri.ac.in

increased, system on chips design has become a major impediment to achieve excessive presentation. Microprocessor system consumes more power which is consumed by highly synchronous system.

1.1 Electronic Design Automation (EDA)

EDA is a software program used to design electronic systems such as printed circuit boards [3]. On chips there is number of components mounted which makes design complexity. All electronics components got in library of this software. If we want to design the PCB of any circuits first up all we draw a schematic diagram of circuit. By using this tool collaborate on necessary process and analysis of the design and its results bringing together designers working at all levels of semiconductor chip abstraction tools has become a synonymous with design automation tools. To reduce the PCB design time, develop a EDA tools with more features. To design a chip designer requires most important chip design parameters such as area, power and performance.

2 Power Dissipation in VLSI Circuits

In VLSI circuits that are CMOS circuits are very power efficient because it dissipates zero power. Because of number of transistors clock frequency is increased that's why power dissipation becomes a primary constraint.

Power dissipation is categorized in to two ways that is static power dissipation and dynamic power dissipation.

2.1 Sources of Motivation

There are two components to dynamic energy dissipation. The first is energy conversion because of charging as well as discharging of load capacitance. The second one is the short-circuit power caused by the input waveform. A single port's switching power is derived as [4]

$$PD = C_L V_{DD}^2 f$$

f operational frequency

C_L load capacitance

V_{DD} supply voltage

An unloaded inverter's short circuit power can be approximated by

$$\frac{(V_{DD} - V_{th})^3}{12T} = PSC$$

where α is the transistor coefficient, t_r is the rise/fall time, and the delay $T = (1/f)$.

2.2 *Electrical Leakage*

A nanoscale mode MOSFETs consists of:

- (1) The leakage below the threshold (I_{sub}).
- (2) Electron and holes gate to gate inherit barricades.

2.3 *Techniques for Dynamic Power Reduction*

Even if technology scaling causes the leakage power to rise fiercely with each generation, the dynamic power still accounts for the majority of the combine power dissolution of multi-purpose microprocessors. Using gated clocks, multiple supply voltages, optimized transistor size and interconnects, many supply voltages, and positive supply voltage sway are all effective circuit strategies to lower dynamic power usage. The positive power dissolution of nanoscale circuits is greatly reduced by incorporating the aforementioned methods. Other way exists to lessen the positive power dissolution in both logic and evocations, including as instruction set optimization, memory access reduction, and low complexity algorithms. Optimizing the transistor size is the greatest strategy to lower the intersection capacitance as well as the gate capacitance; classified mostly into two categories.

- (a) Static inflation
- (b) Root-based inflation.

The root-based inflation, the complicated ways gates are enlarged to get the results, and in non-critical paths' gates are shrunk to save energy. Static inflation involves inflating every gate in a circuit for a specific delay.

2.4 *Clock Gating*

Digital circuits can effectively use clock gating to lower their dynamic power dissipation. Only a fraction of a typical synchronous circuit, like a general-purpose microprocessor, is active at any given moment [5]. Therefore, it is possible to avoid the unneeded power consumption by turning off the circuit's inactive section. One method for doing this is to hide the clock that runs to the circuit's idle area.

To avoiding needless input switching to the idle circuit block, this lowers dynamic power. The registers, they are typically made up of consecutive components that is

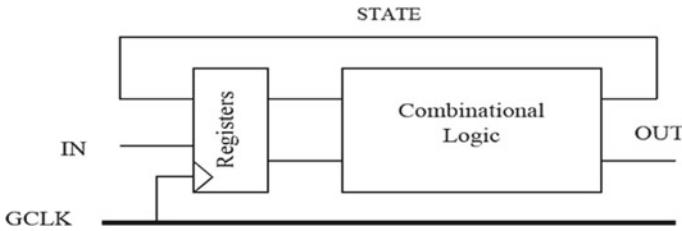


Fig. 1 Flip-flop-based FSM, one clock

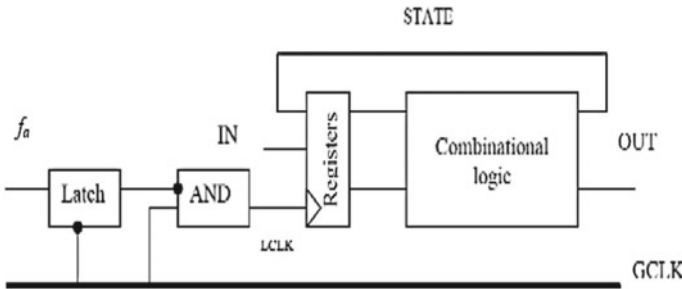


Fig. 2 Design of a gated clock schematic diagram

DFF depicted in Fig. 1, provide the input to the combining logic. The clocking structure in Fig. 1 can be changed to create a gated clock design [6]. When the combining block is not in use, the LCLK was selectively stopped using controlling signals (f_a). When f_a is high, the local clock is disabled. When the global clock (GCLK) is on, the clip in Fig. 2 is required to prevent any bugs in controlling signal from spreading. The circuit functions as shown below. Only before to the rising edge is the signal f_a valid.

A mechanism that decides circuit diagrams created by using gating techniques are necessary for effective clock gating. Clock-gating techniques that either cause the clock-gating circuit to often switch betwixt the authorized and non-authorized conditions, or pulse to such tiny modules results in significant overhead because pulses are big as a tiny module. This aloft could cause power dissipation to be more than it would be in the absence of clock gating.

3 Problem Definition

Power management and power optimization remain essential as CMOS technology range out with forty-five nm, not only due to strict power grants but also because of two reliability issues, packaging costs, and cooling requirements. The development of tools infusion to maximize positive power and, most critically, minimize wasted deluge power is primarily responsibility process technologists.

3.1 Trends in Technology Scaling

Technology ranging has an impact on a number of characteristics, including delay, size, capacitance, etc.

1. Decrease gate up to 30%, which will lead to an enhancement in operational frequency of approximately forty three percent.
2. Increasing the transistor substance.
3. About 65% less energy is used during each transition, snatching fifty percent of energy (with forty three percent enhancement in frequency), as indicated in Table 1 [7].

Frequency-Scaling Trends (Performance): Every generation, the frequency has doubled thanks to the architecture becomes more pipelined in the first place by reducing the amount of gate delay used throughout a clock period. Gate latency is decreased by design procedure by more than 30%. According to scaling theory, transistor count will increase by 50%. Transistor substance is the number of logic transistors in a total circumference.

Interconnect scaling: This tendency occurs as designs get more complicated, leading to increasingly complex interconnect routing, which is the restriction. As a result, additional interconnects are introduced with each generation, increasing parasitic.

Power: Dynamic and leakage power are added to determine total power [8]. Switching power and short-circuit power are added together to create dynamic power as depicted in Fig. 3. When intramural and total capacitor is imposed, there is a loss

Table 1 Scale of technology’s effects

Particular	Change (%)	Decreases
Delay	– 30	0.7
Frequency	+ 43	1.43
W, L, tox	– 30	0.7
Area capacitance	– 30	0.7
Fringing capacitance	– 30	0.7
Total capacitance	– 30	0.7

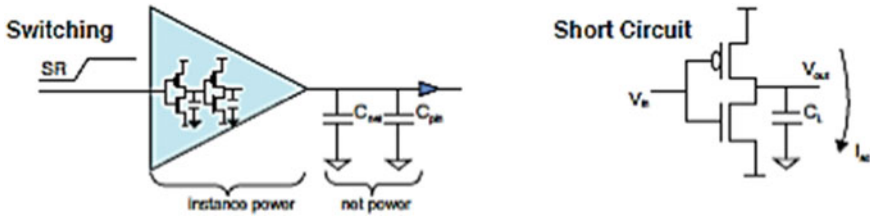


Fig. 3 Dynamic power in CMOS

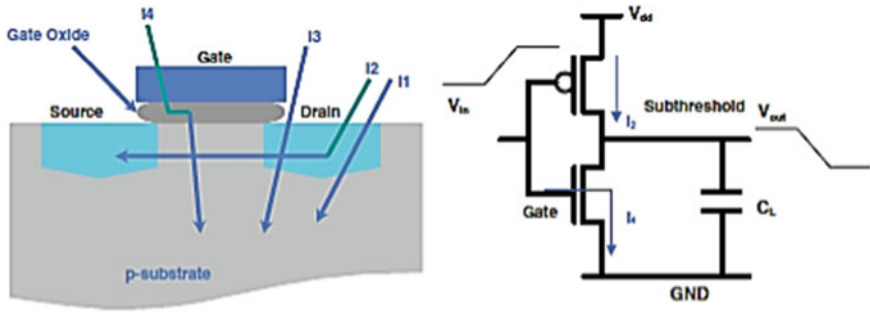


Fig. 4 Leakage power in CMOS

of switching power. Short-circuit power is the power lost when there is a momentary short circuit between the source voltage and the ground when the gate changes states [9].

Figure 4 illustrates the relationship between leakage power and the VDD, threshold leakage predominates among the remaining leakage components. Diode reverse I_b , I_{sb} , gate-induced drain leakage and I_1 are some examples.

4 Implementation Results and Details

This uses a variety of designs to implement various clock gated approaches. We are using clock gating techniques on an 8bit ALU in this application. All the methods are carried out at various technologies with temp., voltage, and frequency fluctuation and their positive, global, and total power have been enumerated [10, 11]. Verilog HDL is used to implement the current clock gating. Table 2 displays the findings. Xilinx14.1 is the EDA tool used for all tests. SIM for Mentor Graphics. We are using XPOWER to calculate power. For results and analysis, the Spartan-3(90 nm), Virtex-5(65 nm), and Spartan-6(45 nm) FPGA platforms are employed. The previous chapter’s techniques are all intended for an 8 Bit ALU. The SPA analysis at various temperatures is displayed in the tables below.

Table 2 Positive power comparison of several pulse gated methods of various

Clock gating technique	90 nm	65 nm	45 nm
Without clock gating	0.220	0.223	0.212
AND gate based	0.137	0.209	0.202
Latch based	0.115	0.209	0.201
MUX based	0.146	0.220	0.217
Flip flop based	0.137	0.209	0.201
Positive level sensitive latch based	0.136	0.209	0.202
T-FF based	0.149	0.225	0.216
Double gated based	0.203	0.209	0.138
Negative latch based	0.125	0.210	0.202

4.1 Analysis

See Table 2.

5 Conclusion

The aforementioned findings show that an ALU operating in pulsed modes consumes little electricity. But each designed methods have a benefit as well as drawbacks. The AND gated clock uses less room compared to typical ALU, requiring just one gate, and its power consumption is also quite low. The dynamic FF has a tremendous clock power, but it requires large space. Another problem with those methods is their flaws and risks. We can infer from the pulse power as well as gate count a new design with a small pulse power as well as less circumferences is required.

References

1. Garcia, O. N., Glass, H., & Hames, S. C. (1978). An approximate and empirical study of the distribution of adder inputs and maximum carry length propagation. In *1978 IEEE 4th symposium on computer arithmetic (ARITH)*, pp. 97, 103, 25–27 October 1978.
2. Zhu, N., Goh, W.-L., Yeo, K.-S. (2009). An enhanced low-power high-speed adder for error-tolerant application. In *ISIC'09. Proceedings of the 2009 12th international symposium on integrated circuits*, pp. 69, 72, 14–16 December 2009.
3. Leem, L., Cho, H., Bau, J., Jacobson, Q. A., & Mitra, S. (2010). ERSA: Error resilient system architecture for probabilistic applications. In *Design, automation & test in europe conference & exhibition (DATE)*, pp. 1560, 1565, 8–12 March 2010.
4. Surekha, N., Porselvi, R., & Kumuthapriya, K. (2013). An efficient high speed Wallace tree multiplier. In *2013 international conference on information communication and embedded systems (ICICES)*, pp. 1023, 1026, 21–22 February 2013.

5. Kaung, A. B., & Kang, S. H. (2012). Accuracy-configurable adder for approximate arithmetic designs. In *Design automation conference (DAC), 2012 49th ACM/EDAC/IEEE*, pp. 820, 825, 3–7 June 2012.
6. Kim, K., & Kim, T. (2012). Algorithm for synthesizing design context-aware fast carry-skip adders. In *Design automation conference (ASP-DAC), 2012 17th Asia and South Pacific*, pp. 795, 800, January 30, 2012–February 2, 2012.
7. Prakash, A. R., & Kirubaveni, S. (2013). Performance evaluation of FFT processor using conventional and Vedic algorithm. In *2013 international conference on emerging trends in computing, communication and nanotechnology (ICE-CCN)*, pp. 89, 94, 25–26 March 2013.
8. Pedram, M., & Abdollahi, A. *Low power RT-level synthesis techniques: A tutorial*. Department of Electrical Engineering, University of Southern California.
9. Gandhi, D. R., & Shah, N. N. (2013). Comparative analysis for hardware circuit architecture of Wallace tree multiplier. In *2013 international conference on intelligent systems and signal processing (ISSP)*, pp. 1, 6, 1–2 March 2013.
10. Rudge, J. M., Amble, V. M., Ravindra, P., & Vijaykumar, S. (2011). *Design and implementation of efficient multiplier using Vedic mathematics* (pp. 162, 166), 14–15 November 2011.
11. Gupta, A., Malviya, U., & Kasper, V. (2012). Design of speed, energy and power efficient reversible logic-based Vedic ALU for digital processors. In *2012 Niram University international conference on engineering (Nicoma)*, pp. 1, 6, 6–8 December 2012.

Generation of Isometric Projections in MATLAB



Janhavi Saklecha, Swanand Pachpore, and Omkar Kulkarni

Abstract The research paper aids in comprehending and creating isometric projections using MATLAB. There are various inaccuracies while creating isometric projections on paper, and the resulting drawing may not give us the exact coordinates of the given object. To eliminate such errors and enhance accuracy while also minimizing the solving time, we created a MATLAB algorithm that projects an isometric view of an object. When we execute the produced algorithm, we are asked to enter the number of vertices, followed by the original coordinates of the vertices of the supplied object. And once you enter the data, it prompts you to define the edge, which results in the development of the final view, i.e., an isometric projection on the x - y plane. Two transformations are used to achieve the ultimate orientation of an object in order to obtain isometric projection. The findings were obtained after removing all mistakes with MATLAB R2021b.

Keywords Isometric projection · MATLAB · Plane geometric projections

1 Introduction

The name MATLAB stands for MATRIX Laboratory. MATLAB is an interactive program for numerical computation and data visualization. Furthermore, MATLAB is a contemporary programming language and problem-working terrain. It has important erected- routines comprising of data structures, editing, and debugging tools and supports object-acquainted programming [1, 2].

The accessibility of such a specialized computing environment is reshaping the part of computer-grounded systems to involve the stoner in a more intense problem-solving experience. This accessibility further enables openings to conduct numerical trials effortlessly and tackle realistic and more complicated problems. Matrices are the introductory rudiments of the MATLAB terrain. An array with two dimensions consisting of m rows and n columns is called a matrix.

J. Saklecha (✉) · S. Pachpore · O. Kulkarni
Dr. Vishwanath Karad MIT World Peace University, Pune, Maharashtra, India
e-mail: janhavisaklecha14@gmail.com

© The Author(s), under exclusive license to Springer Nature Switzerland AG 2024
P. M. Pawar et al. (eds.), *Techno-societal 2022*,
https://doi.org/10.1007/978-3-031-34644-6_95

927

An orthographic perspective is a vertical perspective from infinity with parallel rays. Computation of orthogonal projections of a 3D model is necessary for a wide array of analyses playing an essential part in traditional engineering. Numerous products are still designed by means of orthographic perspectives [3–9].

The aim of the present work is to give experimenters and interpreters an orderly and automatic procedure enabling a straightforward implementation of constructing a wireframe model of an object in the MATLAB terrain. The proposed system, though inspired by a number of studies (), makes use of an original approach acquainted with the perpetration task mentioned over. In the paper, after the description of the said procedure, attained results are presented using the MATLAB terrain. Eventually, some hints about possible future work are provided.

2 Understanding Isometric Projections on MATLAB

2.1 Isometric Projection

It is a special case of Axonometric Projections. Wherein the projectors are not parallel to the principle axis. Many faces of the model are visible in this case. This kind of projection preserves the parallelism of the lines but not the angles. In Isometric projections, all three principle axes are equally reduced, which allows the measurements along the axes with the same scale. Principle axes are equispaced at an angle of 120° in the viewing plane. The final orientation of its object to obtain isometric projection is obtained with two transformations (Figs. 1 and 2) [5, 8, 10–12].

- To obtain the most common orientation in the viewing plane (i.e. XY plane and $Z = 0$), consider an example of the cube;
- This is done by first looking straight toward one face. Next, the cube is rotated -45° about the perpendicular axis, followed by a rotation of roughly 35.264° about the horizontal axis.

Fig. 1 Isometric projection of the cube [1]

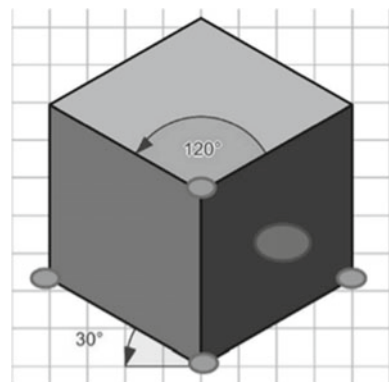
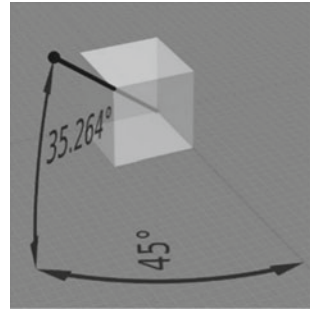


Fig. 2 Rotation of the cube with mentioned angles [2]



2.2 Methodology

To generate an Isometric projection matrix $\{P_i\}$, the concatenated matrix is multiplied by the object matrix which is written in the homogeneous coordinate system [13, 14].

CT stands for Concatenated Transformation matrix, and it is used to acquire new coordinates on isometric projections.

$$\{P_i\} = O_z * [R_x] * [R_y] * \{P\} \tag{1}$$

$\{P_i\}$ = Object matrix ($Z = 0$) * $[R_x]$ * $[R_y]$ * $\{P\}$.

Where $\{P_i\}$ is the transformed matrix.

$\{P\}$ is the Matrix in which the coordinates of given object are written in matrix form i.e., Homogenous coordinate system.

$[R_x]$ is rotation matrix for rotation about x axis.

$[R_z]$ is rotation matrix for rotation about z axis.

$\{\text{Object matrix } (Z = 0) * [R_x] * [R_y]\}$ is Transformation matrix for Isometric Projection.

$$[R_x] = \begin{bmatrix} 1 & 0 & 0 & 0 \\ 0 & \cos \theta & -\sin \theta & 0 \\ 0 & \sin \theta & \cos \theta & 0 \\ 0 & 0 & 0 & 1 \end{bmatrix} \tag{2}$$

$$[R_y] = \begin{bmatrix} \cos \theta & 0 & \sin \theta & 0 \\ 0 & 1 & 0 & 0 \\ -\sin \theta & 0 & \cos \theta & 0 \\ 0 & 0 & 0 & 1 \end{bmatrix} \tag{3}$$

$$[CT] = O_z * [R_x] * [R_y] \tag{4}$$

$$\begin{aligned}
&= \begin{bmatrix} 1 & 0 & 0 & 0 \\ 0 & 1 & 0 & 0 \\ 0 & 0 & 0 & 0 \\ 0 & 0 & 0 & 1 \end{bmatrix} * \begin{bmatrix} 1 & 0 & 0 & 0 \\ 0 & \cos(35.26^\circ) & -\sin(35.26^\circ) & 0 \\ 0 & \sin(35.26^\circ) & \cos(35.26^\circ) & 0 \\ 0 & 0 & 0 & 1 \end{bmatrix} \\
&\quad * \begin{bmatrix} \cos(-45^\circ) & 0 & \sin(-45^\circ) & 0 \\ 0 & 1 & 0 & 0 \\ -\sin(-45^\circ) & 0 & \cos(-45^\circ) & 0 \\ 0 & 0 & 0 & 1 \end{bmatrix} \\
&= \begin{bmatrix} 0.707 & 0 & -0.707 & 0 \\ -0.408 & 0.817 & -0.408 & 0 \\ 0 & 0 & 0 & 0 \\ 0 & 0 & 0 & 1 \end{bmatrix} \tag{5}
\end{aligned}$$

2.3 MATLAB Code

To generate isometric projection matrix, MATLAB Code has been developed. Each step is further explained for the better understanding of the given code.

```
clc
clear all
```

`clear`—Removes everything from the workspace, which frees up system memory. `clc` removes all text from the Command Window, leaving a blank screen. You can't utilize the scroll bar in the Command Window to see previously shown text after running `clc`.

However, you may recall statements from the command history by using the up-arrow key in the Command Window.

To always display output in the same beginning location on the screen, use `clc` in a MATLAB® code file.

```
fprintf('Enter No of vertices: \n');
```

`fprintf(fileID, formatSpec, A1, ..., An)` applies the `formatSpec` to all array elements `A1, ... ,An` in column order and writes the results to a text file. `fprintf` implements the encoding method supplied in the `open` call.

```
n=input("");
```

Here `n` is number of vertices of the object/figure to be projected. “`x = input(prompt)`” Waits for the user to enter a value and press the Return key before displaying the text in a prompt.

```
for i=1:n
    fprintf('Enter x coordinate of point: %d \n', i);
```



```

x(i)=input("");
fprintf('Enter y coordinate of point: %d \n', i);
y(i)=input("");
fprintf('Enter z coordinate of point: %d \n', i);
z(i)=input("");
end

```

Above syntax allows the user to enter the co-ordinates. This step repeats n times to enter the co-ordinates of the n number of vertices. Every for loop has to be closed by using syntax “end”. $Y = \text{double}(X)$ converts the values in X to double accuracy. While expression is true, while statements are being executed, while expression is being evaluated, while statements are being evaluated, while end. When an expression’s result is nonempty and solely contains nonzero rudiments, it is said to be true (logical or real numeric). Otherwise, the expression is false.

```

h=double(0);A=[];ctr=0;
while h==0
    ctr = ctr + 1;
    x1=input('Enter 1st point:\n');
    x2=input('Enter 2nd point:\n');
    A=[A;x1 x2 ctr];
    fprintf("Are these the only edges?");
    h=input("Press 1 if yes, 0 if no :\n");
end
old_obj=ones(4,n);
old_obj(1,:)=x;
old_obj(2,:)=y;
old_obj(3,:)=z;

```

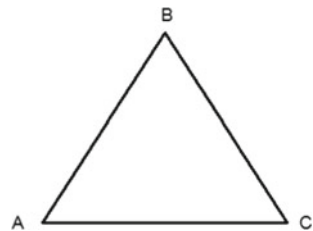
In the syntax above, we input the edge end points. The edge’s end points are x1 and x2. Consider it an ABC triangle. If x1 = A, then x2 = B. Further, the programme asks the user if this is the single edge. As seen in the illustration, A is also connected to be, thus the user must enter “0” and then x1 = A and x2 = C. Similarly, input the remaining edges, i.e., x1 = B, x2 = A, and so on (Fig. 3).

```

CT=[ 0.707 0 -0.707 0 ; -0.408 0.817 -0.408 0 ; 0 0 0 0 ; 0 0 0 1 ];
new_obj=CT*old_obj;
for i=1:ctr
    Pt1=A(i,1);
    Pt2=A(i,2);
    x3=[new_obj(1,Pt1),new_obj(1,Pt2)];

```

Fig. 3 Sample specimen



```

y3=[new_obj(2,Pt1),new_obj(2,Pt2)];
plot(x3,y3);
hold on
end

```

2.4 Test Cases

- For the given Fig. 4, find the data for the isometric view of the object in the viewing plane. The vertices are

A(2,3,4) B(6,3,4) C(2,5,4) D(4,4,10)

i. User Inputs

```

Enter No of vertices: 4
Enter x coordinate of point:1 2
Enter y coordinate of point:1 3
Enter z coordinate of point:1 4
Enter x coordinate of point:2 6
Enter y coordinate of point:2 3
Enter z coordinate of point:2 4
Enter x coordinate of point:3 2
Enter y coordinate of point:3 5
Enter z coordinate of point:3 4
Enter x coordinate of point:4 4
Enter y coordinate of point:4 4
Enter z coordinate of point:4 10
Enter 1st point: 1
Enter 2nd point: 2
Are these the only edges? Press 1 if yes, 0 if no: 0
Enter 1st point: 1
Enter 2nd point: 4
Are these the only edges? Press 1 if yes, 0 if no: 0
Enter 1st point: 2
Enter 2nd point: 1
Are these the only edges? Press 1 if yes, 0 if no: 0
Enter 1st point: 2
Enter 2nd point: 3
Are these the only edges? Press 1 if yes, 0 if no: 0
Enter 1st point: 3

```

Fig. 4 Test specimen

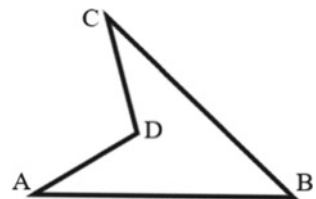
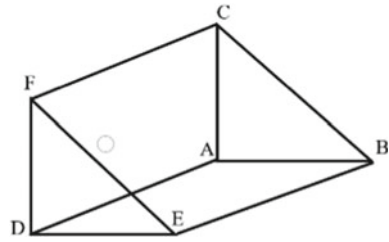


Fig. 5 Triangular prism specimen



```

Enter 2nd point: 2
Are these the only edges? Press 1 if yes, 0 if no: 0
Enter 1st point: 3
Enter 2nd point: 4
Are these the only edges? Press 1 if yes, 0 if no: 0
Enter 1st point: 4
Enter 2nd point: 1
Are these the only edges? Press 1 if yes, 0 if no: 0
Enter 1st point: 4
Enter 2nd point: 3
Are these the only edges? Press 1 if yes, 0 if no: 1
    
```

Here, the user input contains all possible edges through each and every point, and user can also see that 1–4 and 4–1 are the same edge. User can skip one step if it is more convenient. Similarly, data is entered into the MATLAB Command Window for each of the remaining test cases, and results are obtained for the same which is shown in the findings. In the first case, the co-ordinates entered by the user are saved in “old_obj,” which can be found in the workspace. When you click on old_obj in the workspace, a popup window with this arrangement of co-ordinates in the homogeneous system matrix appears.

2. Generate the data for the isometric view of the object in the viewing plane for a triangular prism shown in Fig. 5. Plot the results obtained. The vertices are A(2, 3, 4) B(5, 3, 4) C (2,5,4) D(2, 3, 10) E(5, 3, 10) F(2,5,10)
3. Find the data for the isometric view of the object in the viewing plane for the given fig. The vertices are (Fig. 6)
 A(4,10,5) B(2,4,5) C(6,4,5) D(6,4,-5) E(2,4,-5)
4. Establish the data for the isometric view of the object in the viewing plane for the triangular prism represented in Fig. 7. The vertices are (Fig. 7)
 A(5,5,15) B(15,5,15) C (15,15,15) D(5,15,15) E(5,5,10) F(15,5,10) G(15,15,10) H(5,15,10)

2.5 Result Table

The output is computed using the inputs entered in the MATLAB command window (Tables 1 and 2).

2.6 Isometric Projection of the Tested Cases

The new coordinates obtained after performing the isometric projection are shown in given figures. First is projection of test case 1 and second figure is projection of test case 4 (Figs. 8 and 9).

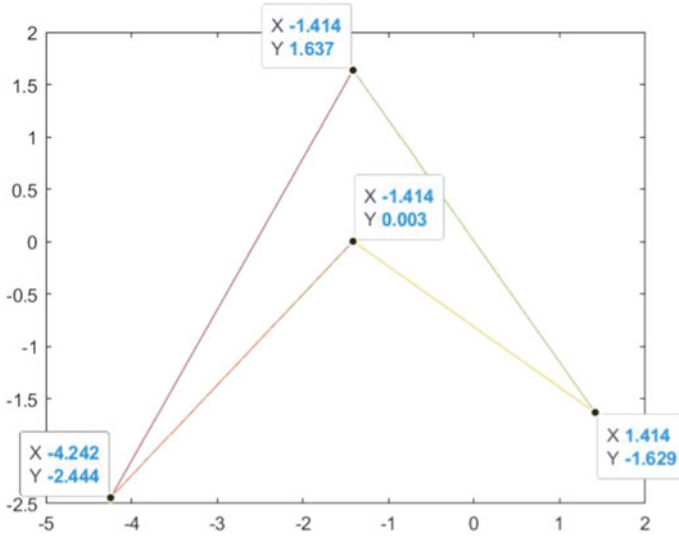


Fig. 8 First projection of test case 1

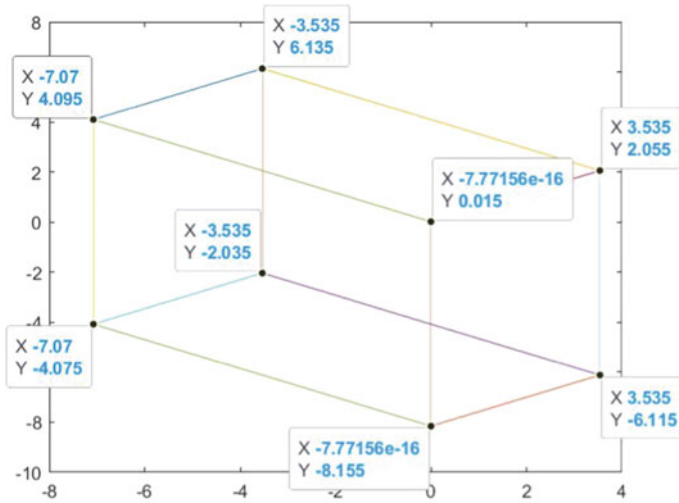


Fig. 9 First projection of test case 4

2.7 Conclusion

Two transformations are used to achieve the ultimate orientation of an object in order to obtain isometric projection. MATLAB allows users to plot accurate results while also minimizing the solving time, whereas manual solutions may result in inaccuracies.

References

1. TATA McGRAW-Hill ISRD Group. (2008). *Computer graphics* (Third print 2008).
2. Foley, J. D. (1942). *Introduction to computer graphics*. Georgia Institute of Technology, Andries van DAM, Brown University, Steven K. FEINER, Columbia University, John F. HUGHES, Brown University, Richard L. PHILLIPS, Los Alamos National Laboratory, and the University of Michigan.
3. Press, CRC. (2008). *Solving applied mathematical problems with MATLAB* (p. 6). CRC Press. ISBN 978-1-4200-8251-7. Retrieved September 16, 2020
4. Cai, D., He, X., & Han, J. (2006). Isometric projection. Technical report, Computer Science Department, UIUC, UIUCDCS-R2006-2747.
5. Pusparini, N. N. (2019) Education Games To Learn Basic Algorithm With Near Isometric Projection Method, 26-Sep-2019. [Online]. Available: <https://osf.io/preprints/inarxiv/yuzn7>
6. Patel, G., Ganesh M, K., & Kulkarni, O. (2022) Experimental and numerical investigations on forming limit curves in micro forming Advances in Materials and Processing Technologies, 8(1), 33–44. <https://doi.org/10.1080/2374068X.2020.1793268>
7. Abhishek, G., Neve Ganesh, M., Kakandikar Omkar, Kulkarni V. M., Nandedkar, K. Srujan, Raju Roman, Senkerik Satya Prasad, Lanka V., Rajagopal. (2020)Data Engineering and Communication Technology Proceedings of 3rd ICDECT-2K19 Optimization of Railway Bogie Snubber Spring with Grasshopper Algorithm Springer Singapore Singapore, 941–952.
8. Sushant P. M., Ganesh M. K., Omkar K. K., Vilas M. N., Kaushik K., Paulo Davim, J. (2019) Optimization for Engineering Problems Development of a Multi-objective Salp Swarm Algorithm for Benchmark Functions and Real-world Problems Wiley, 101–130.
9. Rishil S. S., Swapnil R., Tushar E., Shubham B., & Swanand S. P., (2020) Development of API for Estimating Torsional Strength of Shaft through Knowledge-Based Engineering Approach, *International Research Journal of Engineering and Technology (IRJET)*,7(7).
10. Kakandikar, G. M., Kulkarni, O., Patekar, S., & Bhoskar, T. (2020). Optimising fracture in automotive tail cap by firefly algorithm. *International Journal of Swarm Intelligence*, 5(1), 136–150. <https://doi.org/10.1504/IJSI.2020.106396>
11. Gawande, J. S., Kale, S. S., & Pachpore, S. S. (2017). Failure investigation of badminton racket using modal analysis. *International Journal for Scientific Research & Development*, 5(2), 1849–1856.
12. Yang, Q., Chen, H., Ma, Z., Xu, Y., Tang, R., & Sun, J. (2021) Predicting the Perceptual Quality of Point Cloud: A 3D-to-2D Projection-Based Exploration IEEE Transactions on Multimedia 23, 3877–3891. <https://doi.org/10.1109/TMM.2020.3033117>
13. Bober, W. (2020). *Introduction to numerical and analytical methods with MATLAB for engineers and scientists* (p. 517). CRC Press. ISBN 978-1-4665-7609-4. Retrieved October 15, 2020.
14. Oai, D. C., He, X., & Han, J. (2007). *Isometric projection*. January 2007.

Non-intrusive Torque Measurement System



Amruta V. Adwant, Suhas Dehmukh, and Vijay Kumar Singh

Abstract The design, development, and demonstration of a portable dynamic torque measuring system based on lasers with the ability to alter resolution by varying the distance between laser probes is the primary emphasis of this research. The proposed system also measures vibrations, a crucial metric for determining the health of a vibrating machine. The suggested smart sensory system will be helpful for a variety of tasks, including: (1) Monitoring Applications (2) Application of feedback control.

Keywords Non instructive · Sensor · Torque measurement

1 Introduction

Real-time torque measurement is a crucial component in the industrial and automotive sectors where feedback management is required for accurate regulation of equipment power consumption. Numerous academics have attempted to measure the dynamic torque, but the industry is still waiting for answers that are financially feasible. In the automotive industry, where real-time torque response control is required to lower fuel feeding and enhance ride comfort, there is a high need for such measures.

To properly assemble machines, enhance machine presentation, and manage power conduction systems, a spinning shaft's torque must be measured. Obtaining this data from a moving shaft without intrusive with it is the fundamental difficulty

A. V. Adwant (✉) · V. K. Singh
Department of Mechanical Engineering, Lovely Professional University, Phagwara, India
e-mail: amruta.adwant@gmail.com

A. V. Adwant · S. Dehmukh
Department of Mechanical Engineering, Karad, India

in measuring the torque on rotating shafts. The dynamic torque on rotating shafts can be measured in three different methods in real time.

- (1) Passive sensors (based on capacitive, inductive, resistive (strain gauge), etc.)
- (2) Active Sensors, second (piezoelectric materials, magneto-strictive sensors etc.)
- (3) Calculating the Turning angle (capacitive, magnetic, or optical sensors).

These techniques have advantages and disadvantages. The torque signal is preconditioned by a circuit incorporated in the revolving shaft in the passive technique. This circuit, particularly those that use contact pairing with a stationary device, can be a source of noise. Torsion angle sensors typically offer better noise immunity and do not need electrical systems coupled to the spinning shafts. These transducers can only measure the time difference between two distant probes, which is most suited for measuring torsion angles in long axes. Since these sensors have a low resolution and precision and are still in the early stages of development, there isn't a commercial version available. The proposed smart sensor can measure speed, torque, and vibrations with a level of accuracy that is comparable to that of instruments that are currently on the market. The proposed smart sensory system, however, will be helpful in a variety of applications, including (1) monitoring (situations where rotating shafts of large DG sets, LIS pumping stations in irrigation, rolling mills, wind power generators, and other heavy industries are frequently damaged by fatigue cracks and are primarily caused by torque overload), (2) feedback control applications, and (3) feedback monitoring applications (situations where precise feedback control of torque transmission is important such as precise control of fuel consumption, power consumption in automotive applications).

2 Literature Survey

The accurate measure of mechanical torques, both static and dynamic, is essential for many applications [1]. The main dispute in calculating torque on rotation of shafts is obtaining this indication from a rotating shaft without affecting it. There are now three main ways to calculate the torque on moving shafts: by using passive sensors, active sensors, and calculating the torsion angle. Figure 2 depicts a common scheme for strain gauge-based torque sensing. Torque is measured via resistive, capacitive, or the inductive Surface acoustic wave which is SAW or surface transverse wave which is STW resonators in passive sensors [2, 3]. Here, an electrical source is necessary, and power can be transferred from a stationary source using slip rings or batteries. These sensors are used nowadays in industry for torque monitoring and control applications and are commercially accessible (Fig. 1).

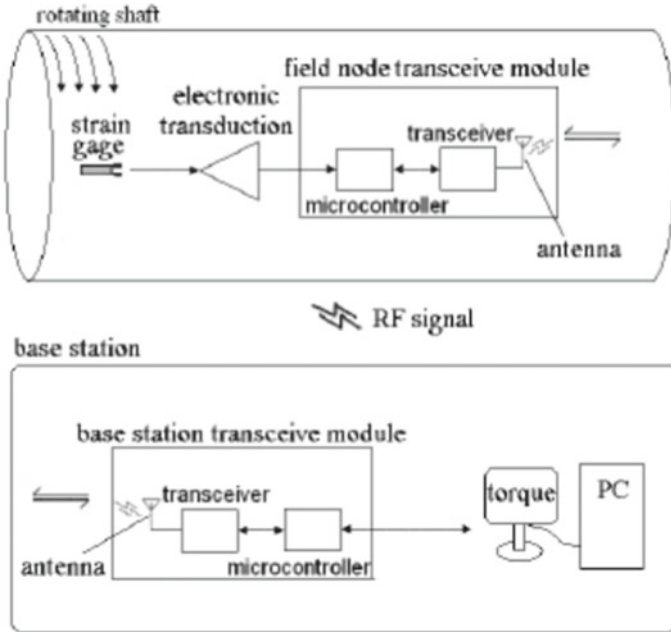


Fig. 1 Illustration of the rf instrumentation system [3]

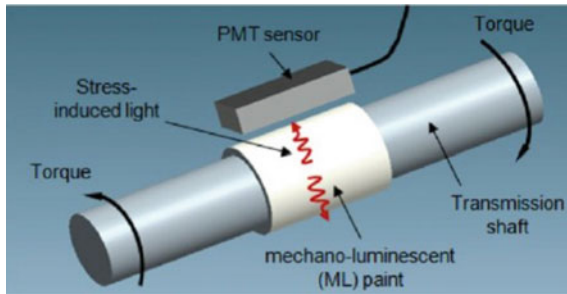


Fig. 2 Dynamic Torque Sensor using mechano-luminescence

The disadvantage of this technology is that it relies on a rotating shaft-mounted circuit or information transfer and torque signal processing; this circuit can introduce noise and couple to a stationary unit through slip rings. Torque is monitored in Active Sensors employing piezoelectric materials, magnetostrictive sensors, and mechanoluminescence (Fig. 2).

Transducers can detect torque with the torsion angle using capacitive or magnetic, or the optical sensors. Active sensors and torque transducers that measure torsion angle don't require electrical systems to be connected to rotating shafts and often have more noise intensity. These transducers, e.g., can evaluate the torsion angle

by assessing the displacement of the magnets under the gravity of torque; which is more effective with longer axes. They can also measure the time gap in two distant magnets passing by the Hall sensor at time of rotation. One drawback of these transducers is their less resolution. Additionally, magneto-strictive sensors frequently have significant hysteresis and implementation complexity. Mechanoluminescence sensors don't yet have a commercial version because the measured values they take are still in the early stages.

The sensor configuration for non-contact torque calculations of a mechanically burdened shaft utilizing a thin, soft ferromagnetic film is shown in Fig. 3. By using a ferromagnetic film using an in-plane uniaxial anisotropy and a stress-dependent on ferromagnetic resonance or a cut-off frequency shift, the system of sensor enables the characterization of torque. A vector network analyzer that outputs the frequency-dependent scattering parameter can be used in conjunction with a trip late strip line to measure this. To identify variations in the frequency dependent handful parameter S11 brought on by mechanically tempted stress in the ferromagnetic film, a short circuited triplet strip line was created. When a torque between 0 and 100 N m is applied, the cut-off frequency rises by around 37% due to compression stress in the ferromagnetic film that results from the shaft's torsion.

The torque sensor in Fig. 4 is a multi-hall sensor device that detects the magnetic field strength of permanent magnets positioned on the surface of a rotating shaft by comparing the phase differences of two induction signals from individual magnetic sensors. The torque magnitude is measured using a real-time measuring technique that uses filtering and calibration. This novel torque sensor has demonstrated good performance at rotational speeds between 300 and 500 rpm. This paper illustrates the viability of noncontact torque measuring by magnetic field monitoring. The outcome displays an inaccuracy of under 2% over the whole test range, which is a competitive performance for commercial sensors.

Figure 5 illustrates torque measurements by keeping track of their roughness. This uses the traditional laser speckle contrast sensing approach. A cross-correlation function is used to process the intensity that is output after being scattered by the rough

Fig. 3 Scheme of the distorted shaft. Distorting the shaft by an angle of ϕ the sensor surface is sheared by the angle γ [4]

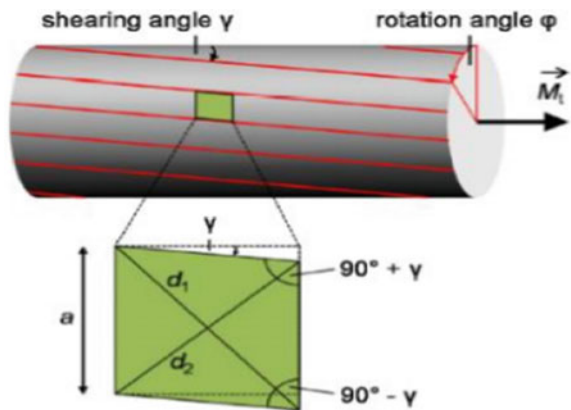
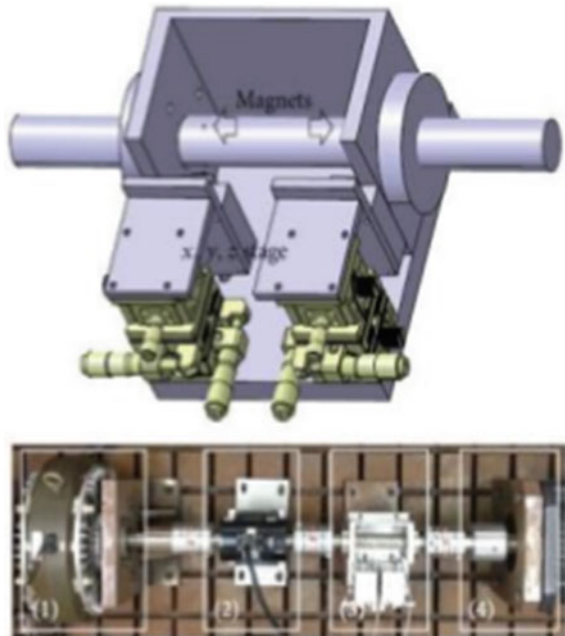


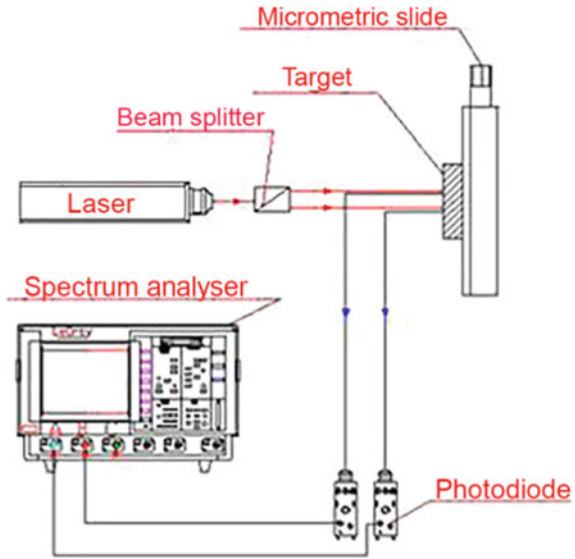
Fig. 4 Schematic of torque sensor with multiple hall sensors [5]



surface. This method yields the angular torsion of two separate sections. Knowing the shaft torsional stiffness makes it easy to identify the applied torque. The light source’s wavelength, the distance between the emitting and receiving fibres, and the optical alignment made possible by fiber-coupled components all affect how accurately torque measurements are made.

For the measurements of static and dynamic torque, there is a wealth of literature. The creation of the sensors described above involved numerous researchers. Only a few sensors are now employed in industry for monitoring and control since they are commercially available. The following is a list of these applications: By automating and carrying out repeated activities, versatile and adaptable robotic arms offer the advantage of enhancing production output. Servo or stepper motors operate the joints in these arms. Engineers must monitor joint torque output in addition to shaft position in order to manage robot mobility smoothly and steadily. These motors can be used in conjunction with a reaction torque sensor to build control loops for seamless, autonomous operation. Measuring the power input, voltage, and current in the power line controlling the servo drive is a reasonably easy way to assess the torque of a DC servo motor. For the majority of motors, torque is directly proportional to current and can be calculated from it by knowing the motor efficiency and shaft speed. Since the relationship between the electrical power amounts and the theoretical and estimated torque value is not the actual mechanical torque, this is regarded as an indirect measurement of torque. However, a reaction torque sensor is the suggested technique for a precise and accurate shaft output torque measurement. Servo motors

Fig. 5 Schematic of non-contact torque transducer based on the laser speckle contrast method [6]



are used in automated systems in many different sectors to track linear and rotational motion.

A closed loop control system must be used due to frictional loss and motor speed variation. To do this, attach a reaction torque sensor between the mounting site and the servo gearbox to gauge the generated torque. In conclusion, the development of static and dynamic real-time torque sensors must take into account the following crucial factors.

- To embed the sensors on the shaft, passive torque sensors (such as strain gauge-based ones) are required, and noise, the environment, and other factors can impair measurement accuracy.
- Active sensors are also installed on shafts and have less impact on measurement, but it is challenging to power the sensors using slip rings and there is a chance of failure because of direct contact.
- Twist angle measurement-based sensors offer more precision at long shafts but are less suitable for non-contact measurements due to the distance between two probes (optical, magnetic, etc.). But creating reliable encoding that can attain acceptable sensitivity to minor torsion angles remain a difficult task.

Different types of force or torque sensors which have been created for these varied force and torque measurement applications. Due to their great accuracy, the most representative strain gauge type torque sensors are frequently utilized. Non-contact displacement sensors used for force/torque measurement, such as optical and the capacitive, and the inductive sensors, need a significant displacement to achieve high sensitivity, which invariably reduces the stiffness of the sensor. The FBG sensor has the advantage of a small size, sterilizability, and accurate calculation of strain on

an object similar to a standard electronic strain gauge. However, due to the sensor system's complexity and expensive price, its application is restricted. As a result, simple strain gauge load cells or force/torque sensors based on electronic strain gauges have primarily been used in robotic applications because of their excellent measurement accuracy and inexpensive cost. The literature review mentioned above shows that there is much room for developing dynamic torque sensors that are simple to use, have high resolution and accuracy, and can withstand hard environments (Figs. 6 and 7).

Every aspect of the sectors, including the automotive, power generation [4], heavy industries, the agricultural sector, and heavy irrigation equipment, need force, torque, and vibration. Monitoring these factors in rotating machinery will enable failure patterns to be predicted and sufficient warning signals to be generated prior to severe failure, preventing major accidents and reducing breakdown-related costs. Similar technological contributions can be seen at the national level. Professors and researchers from prestigious universities are creating technologies that require mechanical system monitoring. Microelectronics systems and sensors are being developed in order to provide accurate monitoring and control. For the purpose of real-time monitoring of the friction stir welding process, Bipul Das et al. attempted to design a force and torque measurement setup [1]. Here, a torque monitoring system based on strain gauges is created. The difficulty in measuring torque and force in

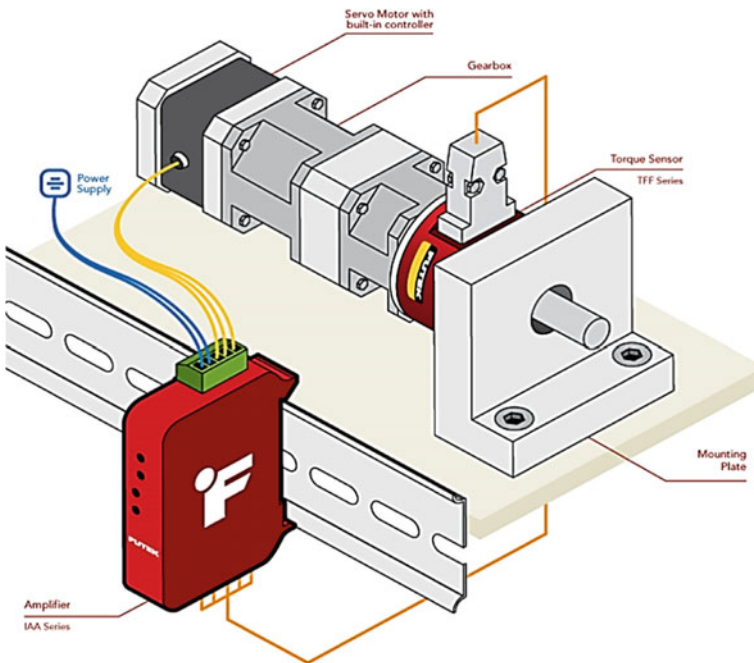


Fig. 6 Static and dynamic torque measurement at robotic arms for precise position control [7]

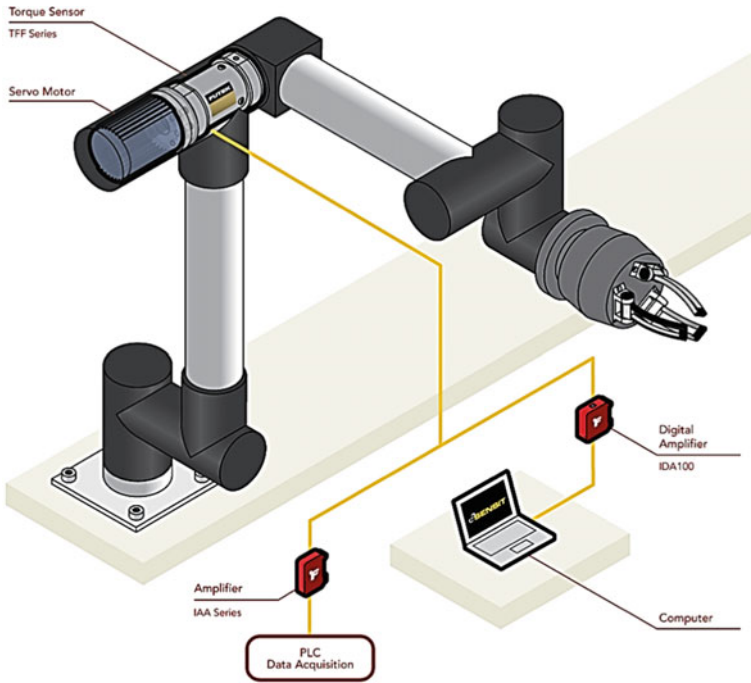


Fig. 7 Torque control of servo motor [8]

the FSW process is addressed, and the developed system is calibrated and compared with available standard force measurement systems for its accuracy and found to be in considerable agreement.

Quality, accuracy, and time for machining operations are key issues in industry. Monitoring and controlling production processes like CNC, robotic systems, and intensive machining activities are in high demand. Small variations in the input torque and force have an impact on both process quality and productivity in this process, which mostly involves rotating apparatus. Therefore, real-time monitoring and control of the machining processes are necessary to achieve the desired quality and productivity. A closed-loop hydraulic drive utilized in mining equipment is presented in the work as a segmented pump-motor control scheme. It uses simulation and modelling to analyse the drive's dynamics. The system model incorporates a control strategy for varying the pump and hydro-motor of the hydraulic drive's displacement [4] (Fig. 8).

The developed Unscented Kalman Filter (UKF) was a promising approach that could replace the torque sensor in the bicycle to save costs [9].

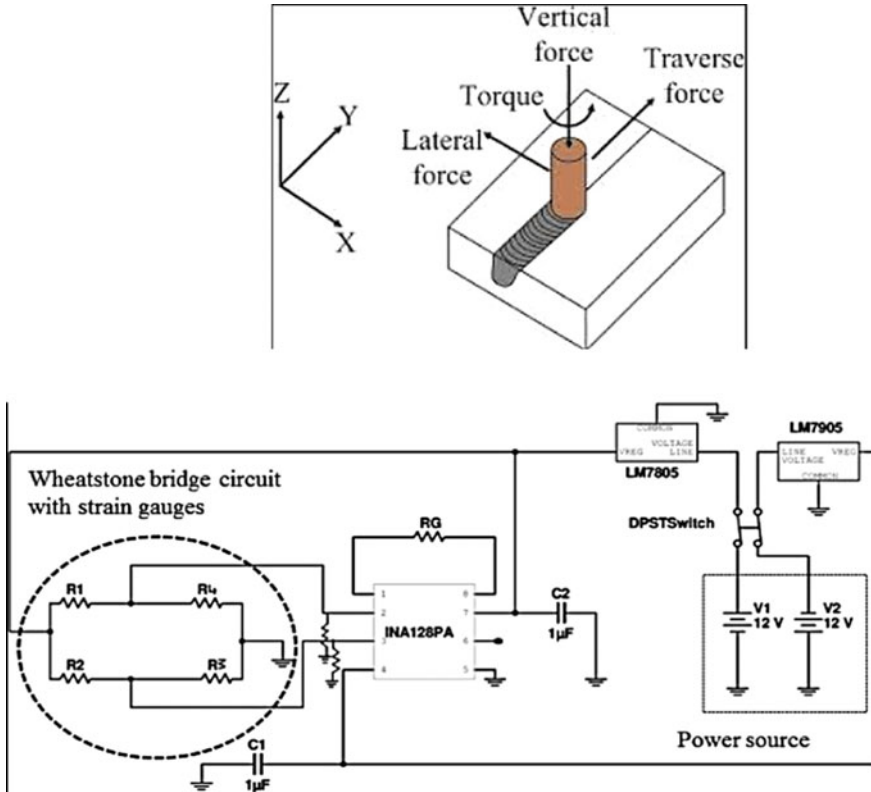


Fig. 8 Schematic of force and torque measurement in FSW process and DAQ system (Wheatstone Bridge) [9]

3 Measurement of Torque

Our desire to build and create a portable smart sensor that can track force, torque, and vibration in rotating machinery is sparked by the literature review indicated in the previous section. Further uses of sensor data include signal pattern prediction and early failure warning detection. Basically, the research’s main focus is on creating a portable contact-less torque measuring system. The remaining parameters are either geometrical or material characteristics that are constant for a given shaft, measuring either the angle of twist or shear forces created in the shaft. Using a strain gauge to measure shear stress has a few drawbacks, is substantially impacted by noise, and requires slip rings to transfer the data from a rotating shaft to a stationary DAQ system. The best technique to gauge torque is to gauge the angle of twist. We may measure this angle of twist in a variety of ways, but each method has advantages and disadvantages that were previously discussed. In this proposal, a laser beam is produced by two laser probes, and after the beam is reflected by reflecting tape

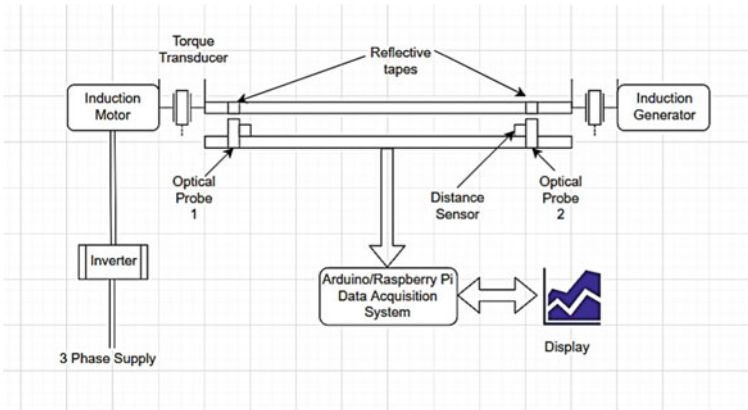


Fig. 9 Recommended representation diagram of torque test rig. [1]

installed on the shaft, a detector mounted at the laser probe picks up the light and produces the pulse depicted schematically in Fig. 9. The shaft depicted in Fig. 9 will have a torque applied to it by a torque generating system, and a load will be applied to it by a mechanical loading/dynamometer unit. Induction motor, induction generator, test shaft, frame, portable torque sensor made up of two optical probes, a distance sensor, and microcontroller unit (as DATA collection and processing unit) for sensing and data manipulation make up the experimental test setup as illustrated in Fig. 10. The calibration of the calibrated torque sensor fitted in the test setup is used to validate the portable torque sensor for use in experimental measurements.

4 Results and Discussion

A torque sensor calculates the forces needed to twist or spin an object. They can be static or dynamic and can measure turning forces in both clockwise and counter-clockwise directions. Torque sensors are used to measure the reaction force generated by a torque-producing device. It can measure torque by positioning itself in relation to something that generates or is impacted by torque, like a motor and its static mounts. Such torque sensors are not intended to spin. The concept of contactless torque is tested experimentally using optical encoders positioned at two different locations on a revolving shaft. Due to the usage of the Arduino microcontroller and the low-resolution optical encoders, the accuracy of the torque measurement is reduced (Fig. 11).

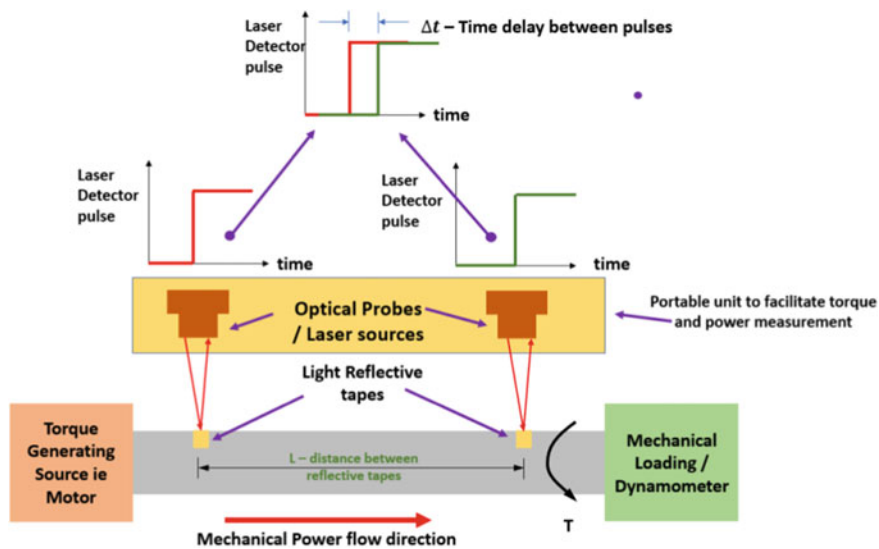


Fig. 10 Schematic of proposed laser probe methodology for detecting angle twist and ultimately real-time dynamic torque measurement [1]

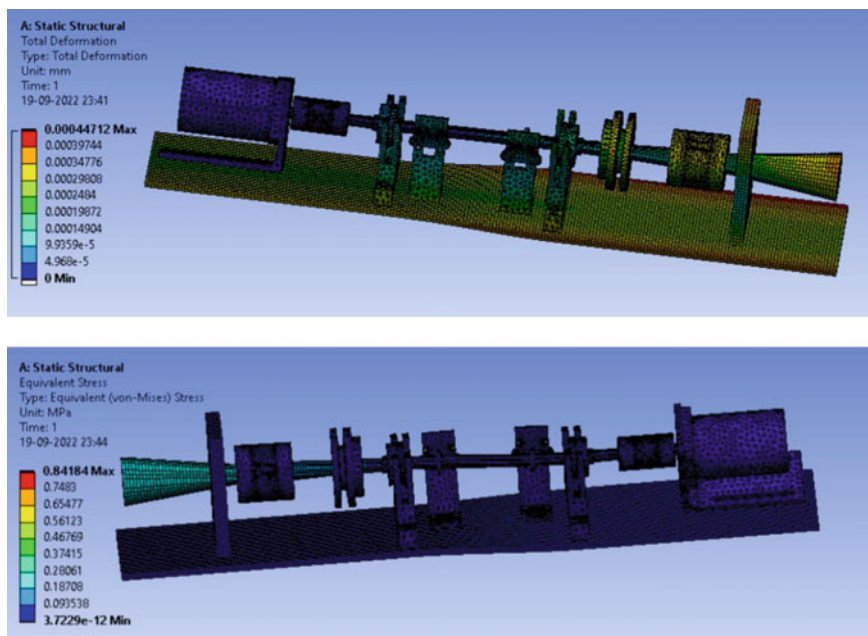


Fig. 11 FEA analysis of torque sensor as per the theoretical calculations

5 Conclusion

- In accordance with the amount of light emitted by the zebra tape patterns as the shaft revolve, each optical sensor will generate a pulse train signal. The timings of the rising edges of the pulse trains were used to determine the shaft's rotational rate.
- By calculating the twist angle starting the pulse train time shift data and using cross-correlation and rising edge detection techniques, torque has been calculated.
- The effectiveness of the contactless, monitoring system with optical torque has been measured by comparing the outcomes from the two approaches with the standard readings from an in-line torque transducer installed on the test bench shaft.
- Experimental quantities made under stable state settings to authorize the contactless system show a right connection between torque and twist, exactly in line with theoretical predictions.
- The recommended zebra tape torque meter removes the need for expensive surrounded sensors, electronics, or wires on the revolving shaft, in contrast to classic in-line torque transducers and the conservative strain gauge method. The proposed methodology is less intrusive, simpler, and more affordable to apply than traditional twist angle measurement methods, making it appropriate for a wider range of technical applications. By carefully configuring the zebra tapes and their parting along the shaft, quantity accuracy and resolution may be readily adjusted to the field application needs.

References

1. Zappalá, D., Bezziccheri, M., Crabtree, C.J., & Paone, N. (2018). Non-intrusive torque measurement for rotating shafts using optical sensing of zebra-tapes. *Measurement Science and Technology*, 29, 065207 (18pp.). <https://doi.org/10.1088/1361-6501/aab74a>
2. Lee, K., & Cho, C. (2015). Study of noncontact torque measurement method with magnetic sensor band. *Journal of Mechanical Science and Technology*, 29(9), 3897–3903. [www.springerlink.com/content/1738-494x\(Print\)/1976-3824\(Online\)](http://www.springerlink.com/content/1738-494x(Print)/1976-3824(Online)). <https://doi.org/10.1007/s12206-015-0835-1>
3. Mateev, V., & Marinova, I. (2021). Magnetic elastomer sensor for dynamic torque and speed measurements. *Electronics*, 10, 309. <https://doi.org/10.3390/electronics10030309>
4. Garinei, A., & Marsili, R. (2017). Development of a non-contact torque transducer based on the laser speckle contrast method. *Journal of Sensors and Sensor Systems*, 6, 253–258. <https://doi.org/10.5194/jsss-6-253-2017>
5. Wu, Y., Liu, Y., Li, F., Zhou, Y., Ding, J., & Lia, R. A novel approach based on magneto-electric torque sensor for non-contact biomarkers detection. <https://www.sciencedirect.com/science/article/abs/pii/S0925400518315211>
6. Shia G., Wang, N., & Cho, C. (2011). Design of a new non-contact torque sensor for rotating stepped shaft by monitoring magnetic field. *Applied Mechanics and Materials*, 44–47, 547–551. Online available since 2010/Dec/06 at www.scientific.net© (2011). Trans Tech Publications, Switzerland.<https://doi.org/10.4028/www.scientific.net/AMM.44-47.547>

7. Kakaley, D. E., Altieri, R. E., & Buckner, G. D. (2020). Non-contacting measurement of torque and axial translation in high-speed rotating shafts *Mechanical Systems and Signal Processing*, 138, 106520.
8. Lee, K., & Cho, C. (2015). A feasibility study of a noncontact torque sensor with multiple hall sensors. *Hindawi Publishing Corporation Journal of Sensors*, 2015, 126935, 6 p. <https://doi.org/10.1155/2015/126935>
9. Lee, K.-E., Kim, J.-W., Kim, C.-Y., & Ahn, S.-H. (2009) Development of micro torque measurement device using strain gauge. In *Proceedings of IEEE international symposium on assembly and manufacturing* (pp. 101–106). ISAM 2009. Suwon, Korea, 17–20 November 2009.

Development and Implementation of a Smart Agriculture System Based on LORA



Manoj A. Deshmukh, Seema A. Atole, Avinash A. Mote,
and Vikram R. Chavan

Abstract The availability of electrical energy of days is a major concern for framers. The primary cause is the significant demand from industrial sectors and the variety of electrically powered locomotives. Farmers from many regions struggle to obtain continuous electricity for farming. Electricity is available; however, it fluctuates and switches on and off at random. Due to these factors, electrical pumps break down, and farmers must constantly visit pumping stations to turn on pumps. In this study, we present a gadget that will help farmers operate irrigation pumps with less effort and time. Longer battery life, cheap cost, and reliable transmission of information and control signals over great distances characterize this technology. For communication between the farmer and the pump control, we use long-range technology (LoRa).

Keywords LoRa (long range technology) · Irrigation · Arduino nano

1 Introduction

We are now all heavily reliant on atomized electronics and electrical products today. These goods provide comfort while also assisting us in reducing our physical effort. The vast majority of these products rely on electricity to operate. The supply of electrical energy for the agricultural sector is suffering from frequent power outages due to the rise in demand for electricity from big populations. This will have an impact on farmers' daylight working hours, when they must operate numerous pumps for farm irrigation. Especially for farmers who live further from farms, this will result in a shortage of water needed to process the fields. We developed this product with the intention of helping these farmers by using a remotely controlled system that will turn pumps ON/OFF via Lora Communication. A wireless communication protocol from the physical layer is called LoRa (Long Range). Developed by Semtech, LoRa is a WAN that modifies signals using spread spectrum. A protocol stack called LoRa WAN was created by "Lora Alliances" and is available at the data-link layer. Radio

M. A. Deshmukh (✉) · S. A. Atole · A. A. Mote · V. R. Chavan
SVRI's College of Engineering, Pandharpur, Maharashtra, India
e-mail: madeshmukh@coe.sveri.ac.in

Table 1 LoRa Ra-02

Specifications	Rated values
Power supply	2.5–3.7 V
Model	Ra-02
Interface	spi
Antenna	IPEX
Programmable bit rate	UP to 300 kbps
Max transmit power	18 ± 1 dBm
Package	SMD
Frequency range	410–525 MHz

chipsets like the SX1272/SX1278 make up LoRa. Lora is present in the Physical layer of the OSI model. Additionally, Media Access Control (MAC) features from the Data-link layer are supported by LoRa WAN. Lora is mostly used to automate irrigation farms by reducing labor costs and human effort requirements.

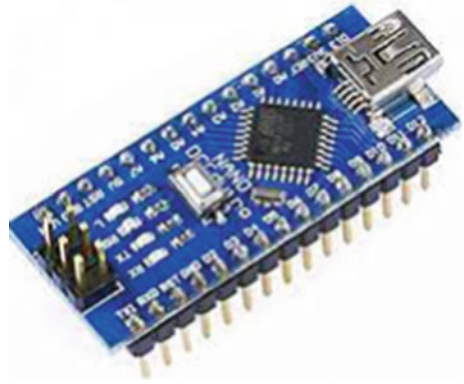
2 Components of System

2.1 LoRa Module Ra-02

To effectively resolve the issues with conventional wireless technology, Ra-02 will be used to measure ultra-long distance with spread spectrum communication, compatible to FSK remote modulation as well as demodulation. Design cannot account for distance or opposition. Power consumption and interference Ra-02 is the best option for things networking applications since it can be utilized in a wide range of networking along with automatic metering, automation of homes, smart security based systems and remotely operated irrigation systems [1]. Ra-02 is offered in an SMD packaging and can be manufactured quickly using typical SMT machinery. Ra-02 is available in an SMD packaging so that manufacturing will be faster using SMT machinery (Table 1).

2.2 Controller Arduino Nano

The Controller is one of major component. It serves as the main nervous system for all connected parts, including relays, motors, and LoRa. Monitoring the signals from electrical components and determining the course of action needed to complete a certain task are the primary duties of an electric Arduino controller. The Arduino board is made in such a way that learning how to use microcontrollers is relatively

Fig. 1 Arduino nano

simple for beginners. The connectors on this board, in particular, are quite simple to manage (Fig. 1).

3 Proposed System

3.1 *LoRa Technology*

The ultimate goal of all cutting-edge technologies today is to automate human behavior. Controlling electrical pumps on farms poses a challenge, especially if there are few individuals in charge of or engaged in the labor of managing vast tracts of land. There are some areas where the agricultural industry experiences frequent power outages, particularly during the daytime when farmers irrigate their fields. This causes a shortage of water to process the crops, especially for farmers who live far from their farms. So, we put into practice a Lora-based system that has two main components, a transmitter and a receiver [2]. All transmission and reception operations are handled by the transmitter and receiver sections, respectively. The green LED must first turn ON and the LCD must display the command “Motor ON” before the transmitter can be turned on. Here, the Arduino Nano is instructing the LoRa module, which is transmitting a signal, to turn on the motor. Currently, the receiver’s primary function is to receive signals and to apply them to electric motors. After the receiver receives the signal, the motor turns ON. When the switch is pressed to the OFF position, the Red LED turns on and “Motor OFF” message will be showing on the LCD 16 * 2 Display. Simultaneously the relay is triggered and GSM 800L begins sending SMS. The LORA Transmitter motor is then given the command to “Stop” by Arduino Nano [3]. The LORA receiver then picks up the signal. Additionally, the motor is “STOP” and GSM 800L is sending SMS (Fig. 2).

Fig. 2 Module name-LoRa
Ra-02



Specification of Product

- Wireless Frequency Standard: 433 MHz
- Frequency: 420–450 MHz
- Available Ports: SPI/GPIO
- Supply Voltage: 1.8–3.7 V, (Typically: 3.3 V)
- Operating Current: less than 10.8 mA, Current for transmission less than 120 mA (+ 20 dBm), Sleep model: 0.2 uA
- Temperature range: – 40 to + 85°
- Pin size: 2.0 mm.

3.2 Arduino Nano Board

The Arduino Nano is a compact beard board with ATmega328. It has only a DC power slot and operates via Mini-B USB connector.

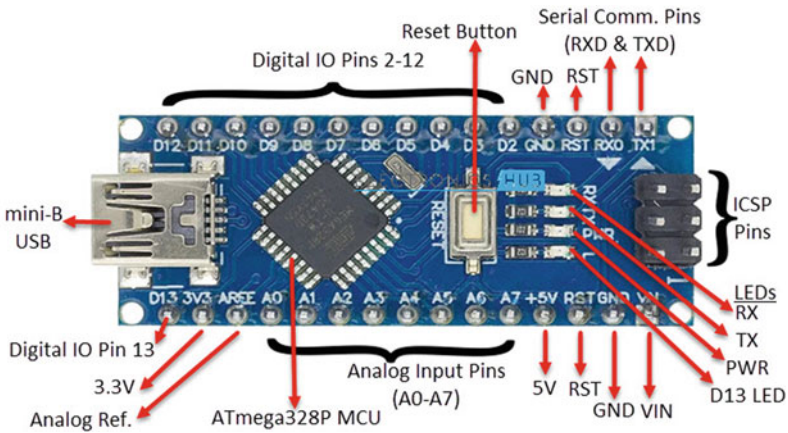
3.2.1 Arduino Major Specifications

Following are the major specifications of the Arduino used in this study (Table 2).

Table 2 Arduino major specifications

Controller used in nano	ATmega328 microcontroller
Working voltage	5 VDC
General range of input voltage	7VDC-12 VDC
Cut-off input voltage	6VDC-20 VDC
Digital input/output pins	14 (of which 6 provide PWM output)
Analog inputs	8
Maximum current per I/O pin	40 mA
Storage flash memory	16 kB (ATmega168) or 32 kB (ATmega328) of which 2 kB used by bootloader
Available SRAM	1 kB (ATmega168) or 2 kB (ATmega328)
Typical EEPROM	1 kB (ATmega328)
Clock rate	16 MHz
Dimensions	0.73" × 1.70"

3.2.2 Pin Diagram of Arduino Nano



3.3 Working of Transmitter Section

The signals (“Motor ON”) are received by the LORA receiver when the Arduino Nano instructs the LORA Transmitter to do so. The motor then turns on. Both the relay and the GSM 800L send SMS motor are turned on at the same time (“START”).

Fig. 3 Transmitter section



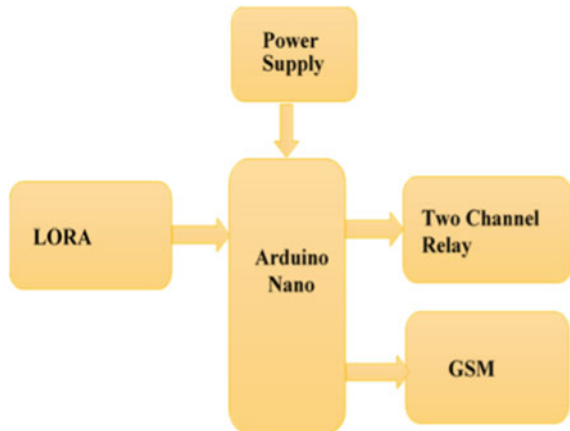
When a LORA transmitter broadcasts a signal to provide feedback regarding power, a LORA receiver receives the signal and at that moment, the receiver turns on an LED continuously [4]. When power is off, the LED turns off (Fig. 3).

3.4 Working of Receiver Part

When the LORA Transmitter Receives the Command from the Arduino Nano. The signals are then received by the LORA receiver (“Motor ON”). Then Motor is turned ON. At the same instant Relay is ON and GSM 800L is send SMS to motor is (“START”). The Red LED turns ON when the switch is depressed to the OFF position and the LCD 16 * 2 Display shows “Motor OFF.” Next, Arduino.

Nano directs LORA’s transmitter motor. The LORA receiver then receives the signal (“Stop”). Next, the GSM 800L is sending SMS while the motor is OFF. (“STOP”) (Fig. 4).

Fig. 4 Receiver section



4 Implementation of System

As per connections LoRa transmitter is connected to Arduino Nano along with LCD display. Arduino analyses the input from the Transmitter Circuit and outputs the appropriate data to the Receiver Circuit. This completes the motor control (ON/OFF condition). When a LoRa transmitter transmits a signal, a LoRa receiver receives it at the same instant. The receiver then provides feedback for power testing, and the LED is continuously ON, when the power is on, and it is OFF, when the power is off. The device can be monitored and managed using a specialized program created for this purpose. Additionally, GSM sends an SMS with the motor and power conditions. Once control signal is received LoRa receiver send these signals to Arduino Nano to control motor (Figs. 5 and 6).

Receive Sensitivity of an LoRa receiver is as Table 3.

Fig. 5 LoRa based transmitter section

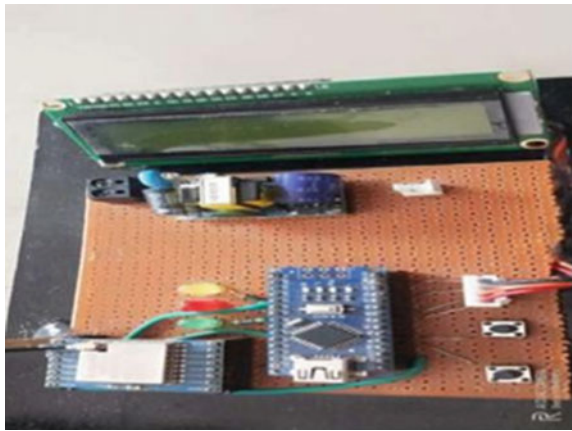


Fig. 6 LoRa based receiver section

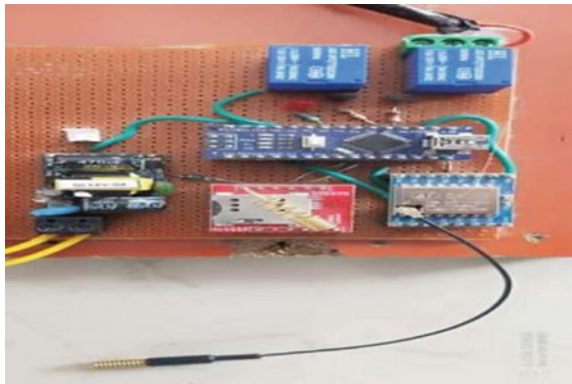


Table 3 Sensitivity of an LoRa receiver

Frequency	Spread factor	SNR	Sensitivity
433 MHz	7	- 7	- 125
	10	- 15	- 134
	12	- 20	- 141
470 MHz	7	- 7	- 126
	10	- 15	- 135
	12	- 20	- 141

5 Results and Conclusions

This proposed system reduces human efforts and saves time as well. LoRa based system provides connectivity between framers (Transmitter Section) and irrigation control room/panel (Receiver Section). The basic model does not require any internet connectivity and supports up to 10,000 m due to this a cost-effective solution will be provided. For LoRa Ra-02 module we are not compromise for the balance of range, interference immunity, or energy consumption.

6 Future Scope

LoRa Transceiver Module and Node MCU Microcontroller are used in the design of LoRa Gateway. It is put in place at the spot on the campus where the gateway has a direct Wi-Fi connection to the internet. Data is sent to the Thing Speak cloud platform via LoRa Receiver after it receives it from the LoRa client. MathWorks has registered Thing Speak as a trademark. A cloud-based IoT platform that enables users to gather, displays, and analyze real-time data. As demonstrated in Fig. 7, LoRa Gateway can deliver data directly to the Thing Speak.

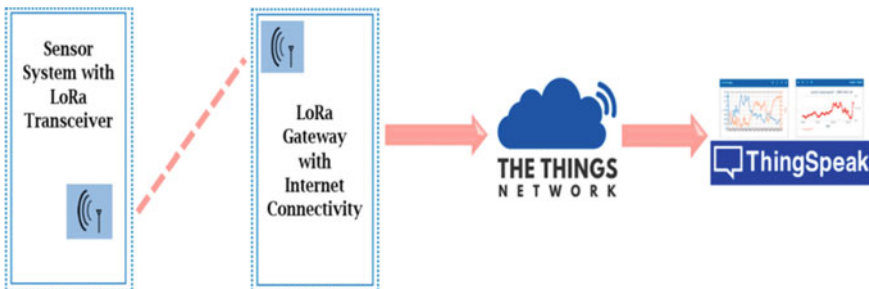


Fig. 7 LoRa connecting with IOT platform

References

1. Prade, L., Mores, J., de Albuquerque, E., Rosário, D. (2022). *Multi-radio and multi-hop LoRa communication architecture for large scale IoT deployment*. 0045-7906. Elsevier.
2. Alahmadiy, H., & Bouabdallah, F. (2022). *A novel time-slotted LoRa MAC protocol for scalable IoT networks*. 0167-739X, Elsevier.
3. Bathre, M., & Das, P. K. (2022). *Water supply monitoring system with self-powered LoRa based wireless sensor system powered by solar and hydroelectric energy harvester*. 0920-5489. Elsevier.
4. Nakamura, K., & Manzoni, P. (2022). *A LoRa-based protocol for connecting IoT edge computing nodes to provide small-data-based services*. 2352-8648. Elsevier.
5. Florita, N. J. B., & Senatin, A. N. M. (2020) *Opportunistic LoRa-based gateways for delay-tolerant sensor data collection in urban settings*. 0140-3664. Elsevier.
6. Leonardi, L., Bello, L. L., & Patti, G. (2022). *MRT-LoRa: A multi-hop real-time communication protocol for industrial IoT applications over LoRa networks*. 16 December 2022, Version of Record.
7. Triantafyllou, A., Zorbas, D., & Sarigiannidis, P. (2022). *Time-slotted LoRa MAC with variable payload support*. 0140-3664. Elsevier B.V.
8. Aarif, L., Tabaa, M., & Hachimi, H. (2022). *Experimental test and performance of RSSI-based indoor localization in LoRa networks*. 1877-0509. Elsevier B.V.
9. Osorio, A., Calle, M., Soto, J., & Candelo-Becerra, J. E. (2022). *Routing in LoRa for smart cities—a gossip study*. 0167-739X. Elsevier B.V.
10. Anzum, R. (2021). *Factors that affect LoRa propagation in foliage medium*. 1877-0509. Elsevier B.V.

Fruit Weight Measurement and Categorization Using Convolution Neural Network



Amol Chounde, Anuja Lotake, and Satish Lendave

Abstract In India, annual fruit production is within the range of 98 million metric tons. Before being exported, all fruits are subjected to look at for internal control purpose and are graded in step with their maturity, size, and presence of a defect. The scale of fruit is usually defined by its mass because it is relatively simple to live. Within the paper, we propose a fruit weight measurement approach named as FWNet using a convolution neural network. The fruit image (input) is processed through the proposed FWNet to anticipate the fruit weight. We use pre-trained weight parameters of the prevailing VGG-16 to initialize the parameters of the proposed FWNet. The proposed FWNet is validated for fruit weight measurement using the COFILAB fruit image dataset. Image processing techniques proposed for the measurement of area and perimeter to map the scale of pomegranates shows the coefficient of determination R^2 up to 0.7529. CNN is proposed for evaluating Mean Absolute Error and Mean Square Error; the experimental analysis witnessed the prevalence of the proposed FWNet over the opposite existing approaches like Inception V3, ResetNet and Mobile Net for fruit weight measurement. Comparative analysis is formed between actual and estimated weight, which shows an average accuracy of 95.67 percentages. Thus image processing and CNN combination can provide a beneficiary result for weight estimation and classification of pomegranate consistent with weight.

Keywords Convolution neural network · Fruit weight measurement · Processing techniques · Features extraction

A. Chounde (✉) · A. Lotake · S. Lendave
Department of Electronics and Telecommunication Engineering, SVERI's College of Engineering, Pandharpur, India
e-mail: abchounde@coe.sveri.ac.in

1 Introduction

India is a vast fruit production country and annual fruit production in India is in the range of 98 million metric tons. It is necessary that before being exported, fruits need to go through inspection regarding quality, size and defect. Among this parameter, the size of the fruit is directly proportional to its weight. Measuring the weight of individual fruit is a laborious task as well as time-consuming. Therefore an automatic fruit weight measurement is essential to speed up this process. In this paper, we propose a fruit weight measurement approach named as FWNNet using a convolution neural network. The proposed approach processes the input fruit image and outputs its weight. The next section describes the existing approaches for fruit weight measurement using image processing techniques.

2 Literature Survey

The major physical characteristics of fruits are shape, thickness, density porosity, strength, mass and friction against various surfaces, which are the most critical criteria in deciding the correct quality requirement for marking, manufacturing, packing and conveying processes. For agricultural products such as onion, breadfruit, terebinth fruit, almond, caper, and pomegranate, these properties were analyzed. There are many cases where the definition of relationships between geometrical measurements is beneficiary for e. g. sometimes fruit graded by weight, but designing a computer vision system that is graded by its weight could be much more feasible. Researchers' define agricultural products such as apricot, apple, mango and pomegranate in terms of equations for mass estimation. The use of digital caliper for measuring parameter however is prone to human error and may not be an elective and practical solution to volume measurement, especially when processing large amounts of agricultural goods or measuring yields during harvest. It is well-known fact that mass, volume and density are correlated when dealing with vegetable and fruits. Fruit volume can be used to calculate the harvest period. For e.g. the volume used as a vegetable and fruit sorting function shows a correlation coefficient of 0.91 with length on the gradation of jalapeno chili. Density variations were often used for consistency testing, such as the test for citrus granulation and the test for seed viability. Various mathematical expression and techniques of numerical analysis were implemented to derive a volume representation. The most widely used methods for calculating volume include a geometric mean diameter (GMD), a method for displacing carbon and a method for displacing water. Indeed, computer vision is the most powerful method for assessing exterior characteristics such as intensity and uniformity of color, bruising, scale, form and recognition of stems. Computer vision has been found to be increasingly important in the agri-food industries in recent years, especially for applications in compliance with quality requirements, quality inspection, and

growing consumer demand. The usage of computer vision is also increasing in popularity in estimating the physical characteristics of fruit and unusual artifacts because it is a non-destructive tool. Particularly in [1]. Authors proposed volume measurement of non-circular shaped carrots. To estimate volume of ax-symmetric fruits, image processing based techniques were proposed in [2]. In [3] authors proposed an approach for volume estimation from 2-D images using machine vision techniques. The approach based on machine learning techniques for fruit weight measurement is proposed in [4]. Recently, extensive research has been carried out on automatic fruit quality measurement using image classifiers. The online color recognition of the lentil using a neural classifier was used and developed by [5]. In the authors proposed an online fruit grading system based on quadratic discriminant analysis and ANN. This approach for image grading includes six stages: acquisition of fruit image; surface color identification; calyx and stem recognition; defect-recognition; defect clustering and the fruit grading. For online fruit quality check, Blasco et al. [6]. Utilized Bayesian discriminant analysis. The majority of approaches discussed above make use of hand-crafted features to define the shape, size, color and fruit defect. Further some of the discussed approaches used machine vision-based techniques for volume measurement, fruit weight as well as fruit grading. However, hand-crafted features are insufficient to describe the fruit volume, size, shape when there is large interclass and intra-class variations. In the area of computer vision and artificial intelligence research, researchers make use of convolution neural networks (CNN) for feature extraction as well as to overcome the intra and inter-class variation. Nowadays, CNN is a state-of-the-art technique for most computer vision applications such as apple flower detection [7], brain tumour grading [8] leaf disease detection [9], image regression [10].

3 Proposed Method for Fruit Weight Measurement

In this section, the proposed approach for fruit weight measurement using CNN is discussed. We propose an end-to-end regression network named as FWNet for fruit weight measurement. Figure 1 shows a block diagram of the proposed Fruit weight network. As shown in Fig. 1, the proposed fruit weight network consists of the trail of convolution, rectified linear unit and pooling layers. To have non-linearity in the fruit weight network, each convolution layer is followed by a Rectified Linear Unit (ReLU). These basic building blocks of the CNN are used to extract the robust features. Further, extracted feature maps are passed through the global average pooling layer to approximate feature maps and to prepare the proposed network for the regression task. We placed two fully connected layers on learning the fruit weight through the extracted features. Finally, the regression layer is placed after the fully connected layers to anticipate the fruit weight. Input fruit image to the proposed FWNet is of size $128 \times 128 \times 3$. As shown in Fig. 1, a trail of CNN layers are applied to the input image, and it reduces to the size $7 \times 7 \times 512$. On top of these learned feature maps, we applied a global average pooling operation. Finally, to anticipate

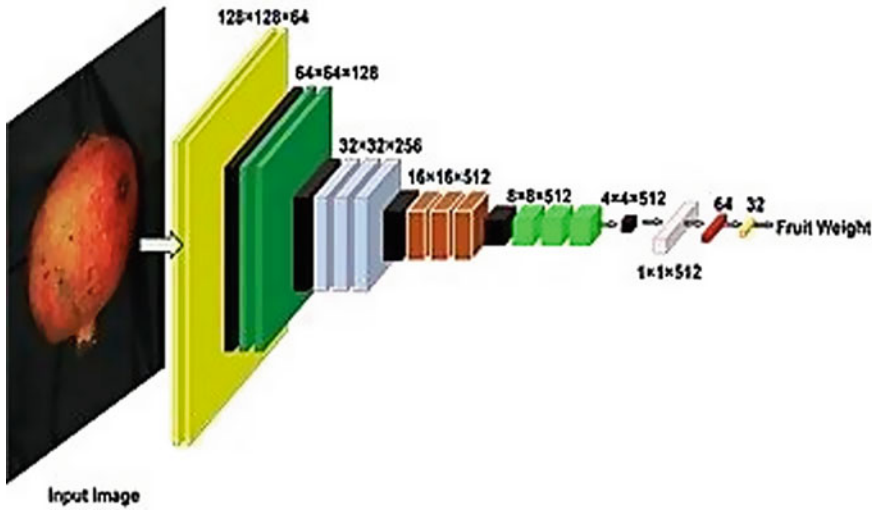


Fig. 1 Proposed (FWNet) fruit weight measurement network

the fruit weight, the regression layer is placed on top of the fully connected layers. The network architecture detailed is given in Table 1. Due to the unavailability of the large-scale labelled fruit image dataset, instead of optimizing the weight parameters of the FWNNet from scratch, we make use of pre-trained weight parameters of the existing VGG16 network. We initialized the weight parameters of the FWNNet by pre-trained weight parameters of the VGG16. VGG16 is a benchmark network proposed for the image recognition task. It is trained over a large scale database consisting of millions of labelled images. Also, it is a popular choice of many researchers for feature extraction from an input image. Due to these facts, within the paper, we utilize the pre-trained weight parameters of the VGG16 to train the FWNNet for the fruit weight measurement task.

Note: Conv = convolution layer, Pool = spatial pooling layer, GAP = global average pooling, FC = fully connected layer. In the case of the pooling layer, “Filter size” indicates the pooling window. Each convolution layer is followed by a Rectified Linear Unit (ReLU) to introduce non-linearity in the network (Fig. 2).

4 Experimental Analysis

We have carried out the experimental analysis, and an existing benchmark pomegranate fruit image database is used for the experimentation. This analysis is divided into six parts which is explained below.

Table 1 Detailed network architecture of the FWNet for fruit weight measurement

Input size	Type	Stride filter shape	Output size
128 × 128 × 3 128 × 128 × 64 128 × 128 × 64	Conv/1 Conv/1 Pool/2	3 × 3 × 3 × 64 3 × 3 × 64 × 64 3 × 3	128 × 128 × 64 128 × 128 × 64 64 × 64 × 64
64 × 64 × 64	Conv/1	3 × 3 × 64 × 128	64 × 64 × 128
64 × 64 × 128	Conv/1	3 × 3 × 128 × 128	64 × 64 × 128
64 × 64 × 128	Pool/2	3 × 3	32 × 32 × 128
32 × 32 × 128	Conv/1	3 × 3 × 128 × 256	32 × 32 × 256
32 × 32 × 256	Conv/1	3 × 3 × 256 × 256	32 × 32 × 256
32 × 32 × 256	Conv/1	3 × 3 × 256 × 256	32 × 32 × 256
32 × 32 × 256	Pool/2	3 × 3	16 × 16 × 256
16 × 16 × 256	Conv/1	3 × 3 × 256 × 512	16 × 16 × 512
16 × 16 × 512	Conv/1	3 × 3 × 512 × 512	16 × 16 × 512
16 × 16 × 512	Conv/1	3 × 3 × 512 × 512	16 × 16 × 512
16 × 16 × 512	Pool/2	3 × 3	8 × 8 × 512
8 × 8 × 512	Conv/1	3 × 3 × 512 × 512	8 × 8 × 512
8 × 8 × 512	Conv/1	3 × 3 × 512 × 512	8 × 8 × 512
8 × 8 × 512	Conv/1	3 × 3 × 512 × 512	8 × 8 × 512
8 × 8 × 512	Pool/2	3 × 3	4 × 4 × 512
4 × 4 × 512	GAP	–	512
1 × 1 × 512	FC	512 × 512	1 × 1 × 512
1 × 1 × 512	FC	512 × 64	1 × 1 × 64
1 × 1 × 64	FC	64 × 32	1 × 1 × 32
1 × 1 × 32	FC	32 × 1	1 × 1

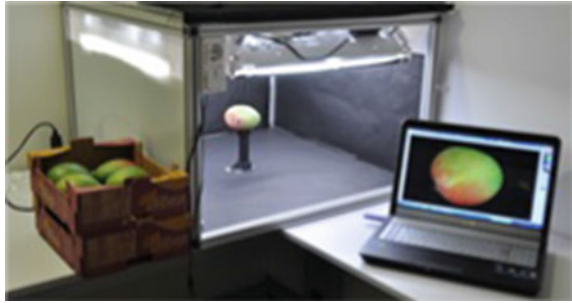


Fig. 2 Pomegranates images sample

4.1 Database Information

In this, we make use of the existing pomegranates image dataset acquired by the COFILAB team [11, 12]. The image capturing system makes use of a digital camera (EOS 550D, Canon Inc., Japan) to acquire a high-resolution image of size 3456 ×

Fig. 3 Inspection chamber for capturing fruit images



2304. The photographs were taken by putting each input sample within an examination chamber in which the proper lighting device was located. The camera had been placed 20 cm away from the input samples. Four lamps, each having two fluorescent lights, were used for illumination (Fig. 3).

The angle between both the fluorescent lamps and the lens axis was about 45°, as the diffuse reflection responsible for the color appearance from the incident light energy at 45°. The input samples, even so, have a curved shape that can still yield bright spots impacting measurements of color. Placing polarizing filters next to the lamps and in the camera, lenses have been used to minimize the effect of the specular reflection cross-polarization. The fluorescent tubes were functioned by the electrical ball with high frequency to prevent the flickering effect of the alternating current (ac) and to create a steadier glow. They also weighed the fruits as well as recorded the perimeter.

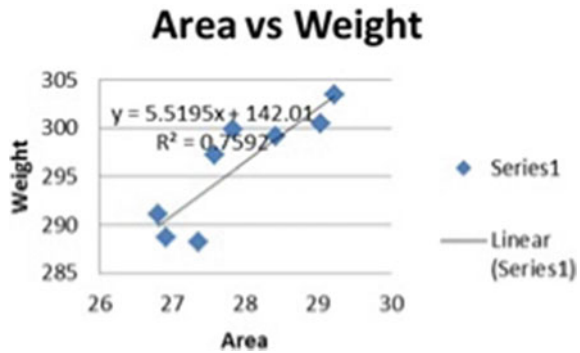
4.2 Image Processing Technique to Calculate the Size (Area) of Pomegranate

Firstly input image is preprocessed, i.e. RGB to gray scale format. Wavelet transform techniques are used to separate low and high-frequency component. Segmentation is applied on a low-frequency band of wavelet. Canny edge detection is used to identification of shape of the pomegranate, and from the edge segmented image, we count no white pixels and use the formula $(\sqrt{P} * 0.264)$ to calculate the area of pomegranate where P is total no white pixels. Table 2 shows the calculated area and actual weight and graph showing coefficient of determination (R^2) and correlation (0.871) between area and weight of pomegranate (Fig. 4).

Table 2 Area calculated from image processing and actual weight

S. No.	Area x-axis	Weight y-axis
1	29.034	300.4
2	26.9099	288.7
3	27.5826	297.2
4	28.4239	299.1
5	27.3606	288.2
6	29.2314	303.4
7	26.797	291.1
8	27.8417	299.8

Fig. 4 Graph of area and weight



4.3 Training Details of the Proposed FWNet

In total, the COFILAB database [11, 12] consists of 328 pomegranates input images along with their weight. We have divided the entire data set into validation and training sets. We consider 80% images for training while the remaining 20% images are considered to validate the proposed Fruit weight network for fruit weight measurement. Due to the limited reduced number of images, we utilize the pre-trained weight parameters of the VGG16 to initialize the weight parameters of the proposed FWNet. We have used an RMS prop optimizer to optimize the proposed Fruit weight network. The proposed Fruit weight network is trained for 20 epochs with a learning rate of 0.001. Tensor flow library is used to design and train the proposed Fruit weight network for fruit weight measurement. Figure 5 shows the MSE and MAE plots of the training and validation phase.

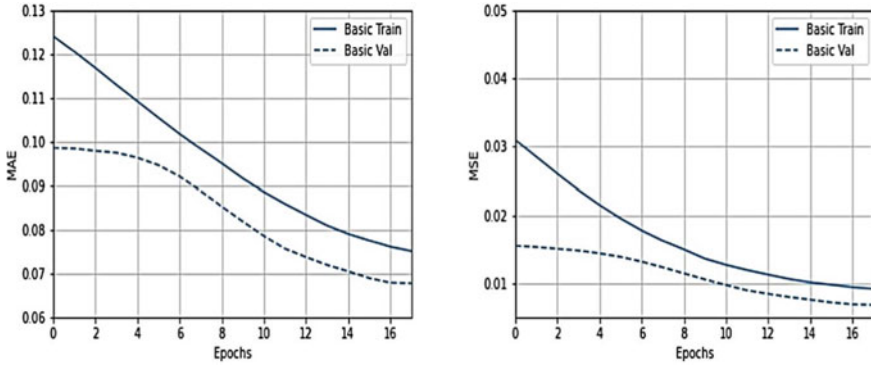


Fig. 5 MAE and MSE plot (graph)

Table 3 Performance evaluation metrics of the proposed fruit weight network and existing deep networks for fruit weight measurement

Method	MAE	MSE
InceptionV3	0.1201	0.0297
ResNet	0.2165	0.0665
Mobile net	0.0964	0.0148
Proposed FWNet	0.0771	0.008

4.4 Quantitative Results of Fruit Weight Measurement

In this, we have discussed the performance of the proposed Fruit weight network for fruit weight measurement. Mean square error (MSE) and mean absolute error (MAE) are used as performance evaluation metrics. We have made a comparison of the performance of the proposed FWNet with existing approaches. For unbiased comparison, we have compared other existing deep networks like ResNet50 [13], AlexNet [14], MobileNet2 [15] with the proposed Fruit weight network for fruit weight measurement. For a fair comparison, we fine-tuned these deep networks for fruit weight measurement using the same training set on which the proposed Fruit weight measurement is trained.

It is clear from Table 3; the proposed fruit weight network (FWNet) outperforms the other existing deep networks for fruit weight measurement.

4.5 Comparative Analysis

Comparative analysis is done with actual and estimated weight, and related accuracy in percentage is calculated with an average accuracy of 95.67 percentages (Table 4).

Table 4 Comparative analysis is done with actual weight and estimated weight with related accuracy in percentage

Image number	Actual weight	Estimated weight	Accuracy
1	274.5	256.451	93.424
2	306.8	281.925	91.892
3	279.1	270.282	96.840
4	358.2	346.449	96.719
5	262.7	263.474	100.29
6	264.4	250.727	94.721
7	270.7	256.177	94.63
8	266.1	257.713	96.848
Average accuracy			95.67

4.6 Categorization of Pomegranate

From the weight of above eight pomegranates, six pomegranate weights comes under category B (150–300 g), two pomegranates weight comes under category C (300–450 g).

5 Conclusion

The proposed Fruit Weight measurement Network (FWNet) processes the input fruit image and output its weight. Due to the unavailability of the large-scale fruit weight dataset, pre-trained weight parameters of the existing VGG16 network are used to initialize the weight parameters of the proposed Fruit Weight network (FWNet). We utilized the existing COFILAB fruit weight dataset to validate the proposed Fruit weight network for fruit weight measurement.

Image processing technique proposed for the measurement of area and perimeter to map the size of pomegranate, shows the coefficient of determination R^2 equal to 0.7529 and correlation coefficient (R) of 0.87 with weight. CNN is proposed for evaluating Mean Absolute Error and Mean Square Error; the experimental analysis witnessed the superiority of the proposed FWNet over the other existing approaches such as Inception V3, ResNet and Mobile Net for fruit weight measurement. Comparative analysis is made between Actual and estimated weight, which shows the average accuracy of 95.67 percentage and related error percentage represented graphically with low and high error percentage. Also, the proposed CNN can be used for the categorization of pomegranate according to weight. Thus Image processing techniques and CNN combination can provide a beneficiary result for weight estimation and classification of pomegranates according to weight in four categories A(0–150 g), B(151–300 g), C(301–450 g) and D(451 and above) with reliable accuracy.

References

1. Hahn, F., & Sanchez, S. (2000). Carrot volume evaluation using imaging algorithms. *Journal of Agricultural Engineering Research*, 243–249.
2. Sabliov, C. M., Boldor, D., Keener, K. M., & Farkas, B. E. (2002). Image processing method to determine surface area and volume of axisymmetric agricultural products. *International Journal of Food Properties*, 5(3), 641–653.
3. Chaithanya, C., & Priya, S. (2015). Object weight estimation from 2D images. *APRN Journal of Engineering and Applied Sciences*, 10, 7574–7578.
4. Cömert, O., Hekim, M., & Kemal, A. D. E. M. (2017). Weight and diameter estimation using image processing and machine learning techniques on apple images. *International Journal of Engineering Research and Development*, 9(3), 147–154.
5. Dae-Hyun, J., & Klim, H.-J. (2015). Image processing method for measurement of lettuce fresh weight. *Journal of Biosystem Engineering*, 40, 89–93.
6. Blasco, J., Aleixos, N., & Molto, E. (2003). Machine vision system for automatic quality grading of fruit. *Biosystems Engineering*, 85(4), 415–423.
7. Dias, P. A., Tabb, A., & Medeiros, H. (2018). Apple flower detection using deep convolution networks. *Computers in Industry*, 99, 17–28.
8. Pan, Y., Huang, W., Lin, Z., Zhu, W., Zhou, J., Wong, J., & Ding, Z. (2015). Brain tumour Grading based on neural networks and convolution neural networks. In *37th annual international conference of the IEEE engineering in medicine and biology society (EMBC)*, 699–702.
9. Sladojevic, S., Arsenovic, M., Anderla, A., Culibrk, D., & Stefanovic, D. (2016). Deep neural networks based recognition of plant diseases by leaf image classification. *Computational Intelligence and Neuroscience*, 2016.
10. Lee, D. J., Eifert, J. D., Zhan, P., & Westover, B. P. (2003). Fast surface approximation for volume and surface area measurements using distance transform. *Optical Engineering*, 42(10), 2947–2955.
11. Vidal, A., Talens, P., Prats-Montalbán, J. M., Cubero, S., Albert, F., & Blasco, J. (2013). In-line estimation of the standard colour index of citrus fruits using a computer vision system developed for a mobile platform. *Food and Bioprocess Technology*, 6(12), 3412–3419.
12. Cubero, S., Diago, M. P., Blasco, J., Tardáguila, J., Millán, B., & Aleixos, N. (2014). A new method for pedicel/peduncle detection and size assessment of grapevine berries and other fruits by image analysis. *Biosystems Engineering*, 117, 62–72. Image Analysis in Agriculture [Online]. Available: <http://www.sciencedirect.com/science/article/pii/S1537511013000950>
13. He, K., Zhang, X., Ren, S., & Sun, J. (2016). Deep residual learning for image recognition. In *Proceedings of the IEEE conference on computer vision and pattern recognition* (pp. 770–778).
14. Krizhevsky, A., Sutskever, I., & Hinton, G. E. (2012). Image net classification with deep convolution neural networks. In Pereira, F., Burges, C. J. C., Bottou, L., & Weinberger, K. Q. (Eds.), *Advances in neural information processing systems* (Vol. 25, pp. 1097–1105). Curran Associates, Inc.
15. Howard, A. G., Zhu, M., Chen, B., Kalenichenko, D., Wang, W., Weyand, T., ... & Adam, H. (2017). Mobilenets: Efficient convolutional neural networks for mobile vision applications. arXiv preprint [arXiv:1704.04861](https://arxiv.org/abs/1704.04861)

IOT-Based Waste Management for Smart Cities



Nirmala T. Pujari, Shital S. Pawar, and Vrushali V. Gore

Abstract The environment needs to be sanitary and clean due to the rising population. Most cities overflowing trash cans contribute to an unclean environment. This will also contribute to the emergence of several unidentified diseases. An effective smart trash management strategy must be created to address these issues. Environmental measurement tools have improved and this plainly shows that the demand on the planet's resources is unsustainable and needs to be handled right away. Garbage management is evolving into a global issue due to rapid population increase, city government dysfunction, a lack of public knowledge and inadequate money for programmers. The garbage cans frequently appear to be full due to the authorities lack of care and attention. Three IR sensors are positioned in this project's garbage tank and are connected to it in three different ways.

Keywords Environment · Central server · Infrared sensor · Internet of things · Motor driver

1 Introduction

In all areas of real life, the practice of making things automatic is being exploited. Making processes automatic lightens the workload for humans. Physically operated devices are substantially more expensive and require more effort than electronic systems. Given that the problem of effective waste management is one of the most pressing ones in contemporary conditions, it is imperative that this problem be resolved. For the globe as a whole and for the majority of sterile societies, the best waste management framework is required. Strong waste, one of the sources and causes of ecological contamination, is defined by the Resource Conservation and Recovery Act as any strong, semi-strong fluid or enclosed vaporous material dumped from group exercises, mechanical, commercial, mining or agricultural

N. T. Pujari (✉) · S. S. Pawar · V. V. Gore
Department of Electronics and Telecommunication Engineering, SVERI's COE Pandharpur,
Pandharpur, India
e-mail: ntpujari@coe.sveri.ac.in

operations. Strong waste also includes rubbish, construction debris, business refuse, oozing from waste water treatment facilities or air pollution, control offices and other discarded materials. A carefully regulated and controlled treatment of these wastes is necessary to protect human health and the environment from the potential risks of delayed waste transfer and ecological pollution. The type of wastes that constitute natural contamination and are the focus of this work are residential wastes, which include food wastes that decompose naturally, such as leaves and dead animals as well as non-biodegradable wastes like plastics, bottles and nylon that are generated in households, hospitals, businesses and other commercial settings.

2 Problem Statement

The management of solid waste is currently a major issue in both developed and developing countries main cities. Garbage production grows along with the population. This enormous uncontrolled buildup of trash is endangering the ecosystem, destroying the area natural attractiveness and posing a health risk. For the purpose of maintaining a clean and trash-free city, the challenges and potential of waste management in IOT-enabled smart cities are proposed.

3 Objectives

The objective of the proposed system is given below:

- To put forth a system that can effectively manage the city's trash.
- A successful Internet of Things solution that is utilized to monitor smart city components in the city.
- The garbage tank's condition is monitored using IR sensors. Regularly checking the garbage level enhances the city's cleanliness and environment.
- The primary goal is to find a workable, affordable, and efficient garbage management solution for the city.

4 Literature Survey

The issue and the earlier methods of detecting smart cities are described in literature.

Swachh Bharat Abhiyaan is a government-led initiative that spans 4041 urban regions and towns in India with the goal of sanitizing the country's lanes, streets, and fundamental structures. Covering the entire rural and urban spectrum of the country is the main goal of the mission. The powerful dry and wet earth gathering using Embedded System is depicted in this research using the proliferation of Web of Things (IoT) devices, such as Smartphone sensors. The application main witticism

is the separate collection of dry and wet waste, which is set up in a transport line with the dry trash collected in clean containers placed on the left side and the wet garbage collected in containers on the right side. The clean container cover automatically closes when the belt starts to pivot in a clockwise direction and the waste is deposited into the underground waste compartment located on the first floor. Here an IoT module is used to monitor and control the waste and the information will be provided to the relevant organization and the average person [1]. Innovative Internet of Things-based Waste Management: A Survey Strong waste management is currently a major concern in the urban centers of the developing and developed worlds. This enormous, uncontrolled accumulation of rubbish is polluting the environment, destroying the area beauty and endangering public health. IOT (Internet of Things) can be used effectively in this era of the Internet to cope with this strong waste. In this essay, we discussed the definition of the Internet of Things as well as its components, testing, and prototyping tools. Cooja test platform the analysis of many works on smart waste management systems using IOT is the final step [2]. By providing the civil web server with a ready flag for momentary dustbin cleaning with the proper check in view of the level of waste filling, this study provides a clever ready framework for refuse freedom. This process is aided by an ultrasonic sensor connected to an Arduino UNO that measures the amount of trash in the trash can and alerts the metropolitan web server when it is full. After emptying the trash can, the driver confirms that he will remove the waste using an RFID tag as guidance. An installed module with RFID and IOT Facilitation keeps the entire process running. With the use of this framework, the district expert could monitor and track the ongoing status of how waste collection is being carried out. Despite this, the crucial therapeutic/exchange measures could be changed. In order to play out the remote monitoring of the cleaning procedure performed by the labourers and to insinuate the alarms from the microcontroller to the urban office, an Android application is created and connected to a web server, thereby reducing the manual procedure of observing and verifying. Using a Wi-Fi module, the notifications are relayed to the Android application [3]. The use of an automatic unloading robot in a smart waste management and monitoring system Dustbins placed in public areas of our city are overflowing. It creates unsanitary circumstances for the people. Additionally, it brings offensiveness to that location. Meanwhile, a terrible odor is also being transmitted. There are many technologies being developed today that are specifically used for the proper management of trash or strong waste. To avoid situations of this nature, we will put into practice an initiative named A Smart Waste Management also, Monitoring System with programmed Unloading Robot. For a quick explanation, the sensors are installed in the typical trash canisters where they belong in normal society. The PIC microcontroller will receive the signal when the waste reaches the sensor's threshold. Robots were utilized to collect the losses after obtaining significant levels of waste. Using a DC motor, remove the robot from the waste area and empty the trash. Through the GSM modem interface, the microcontroller receives messages containing the garbage fill level and air contamination level. This method produces insightful and practical results that may be applied to automate the administration of any powerful waste canister system [4].

One of the most important issues of the present is the finding, inspection, and management of wastes. The traditional approach of physically examining the losses in waste canisters is a difficult process that requires more human effort, time, and money, none of which are compatible with modern advancements. This research suggests a sophisticated method for automating waste management. The most encouraging and anticipated advancements in recent years are without a doubt those involving radio frequency identification (RFID). The system takes use of online support and radio recurrence (RF) labels. Unquestionably, the work presented here offers a novel method for managing and disposing of the regular strong wastes in a straightforward and efficient manner. The four main subsystems of the framework are the Smart Trash System (STS), Local Base Station (LBS), Smart Vehicle System (SVS), and Smart Monitoring and Controlling Hut (SMCH) [5]. It includes a deluge of trash that contaminates the environment and spreads disease. It also creates offensiveness and unclean situations for those there. So that the container can be cleaned promptly and the ground can be protected, a system that can monitor the container and transmit information about its fill level to the area using remote sensor technology is required. The Brilliant waste management system is described in this paper. It uses a remote sensor network (WSN) and a Linux board to detect when a canister is full and instruct the designated person to clean it. The system provides the cleaning professional with a web interface so they can screen and clean the trash canister. The Raspberry Pi is used as an embedded Linux board in this study, and it is built using arm 11 microcontroller designs. The inserted Linux board uses the ZigBee protocol to communicate with every distributed sensor hub installed in the test area and functions as a planned hub for the remote sensor network. The goal of the facilitator hub is to remotely collect parameters like the container's level and fragrance. Each sensor hub is equipped with a level sensor, a gas sensor, and a ZigBee RF radio wire device for communication with the organizer hub. Raspberry Pi collects collected data in a database and analyses the data that has been stored. The board runs the essential information web server and has an Ethernet interface. As a result, the organizer collects the data using a ZigBee remote communication protocol and enables the client to view the data through a web application. An experienced cleaner can collect the waste promptly [6].

5 System Design

This system's primary goal is to control urban waste. The level of trash in the garbage tank is detected by this method using an infrared sensor. When the waste tank's level is detected, the motor immediately turns on to handle the garbage there. We are keeping track of the level of waste present at two places using the proposed technique. The amount of trash dumped on the trashcan is measured by three sensors. The waste will be pushed forward in the tank by the motor1 if IR1 detects it at the first level. The waste will be pushed downward in the tank by the motor2 if IR2 detects it at the second level. Similar to this, IR3 can predict when a tank will be full by detecting third-level junk. When the garbage tank is completely full, the message

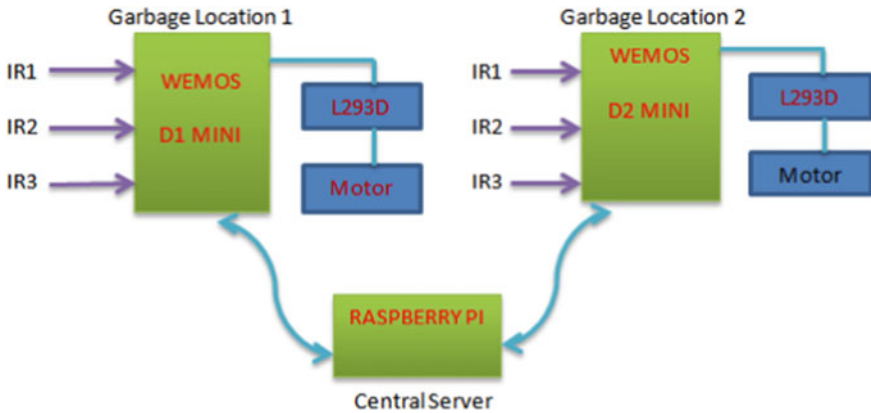


Fig. 1 Diagram of planned design

“tank is full” is sent to the main central unit (a Raspberry Pi), and the homepage is displayed. The waste management committee immediately took action in response to this information (Fig. 1).

6 Experimental Results

Above result shows the interfacing of different hardware like IR sensors, motor, Wemos d1 mini, mouse and keyboard with Raspberry pi and the OS of Raspberry is, as shown in Figs. 2, 3, 4 and 5, running on the monitor.

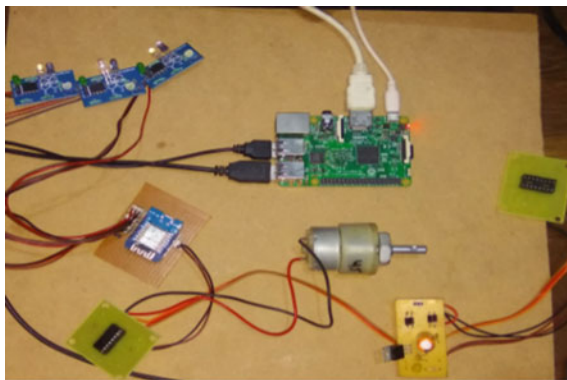


Fig. 2 Hardware of proposed system

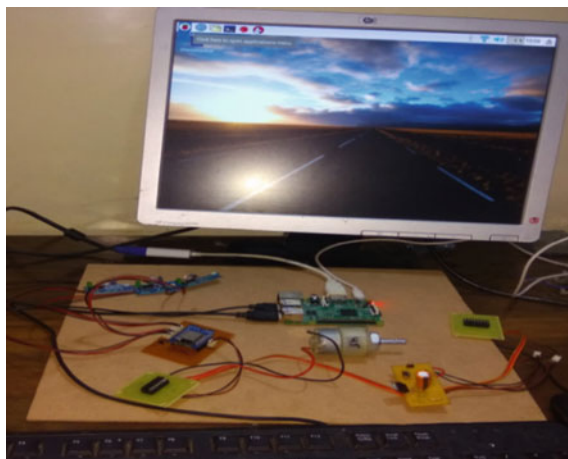


Fig. 3 Proposed system

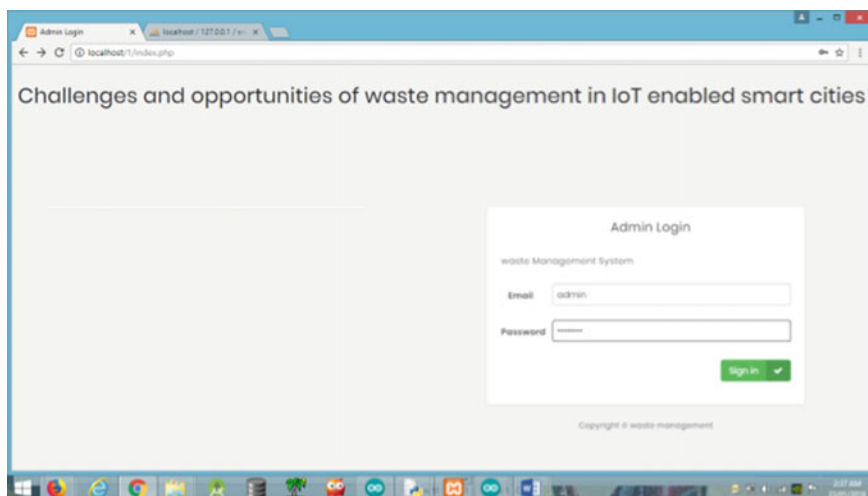


Fig. 4 Webpage showing admin login

7 Advantages

- Keeps the atmosphere fresh and tidy
- Reduces pollution to the environment
- Preserves energy and the environment.

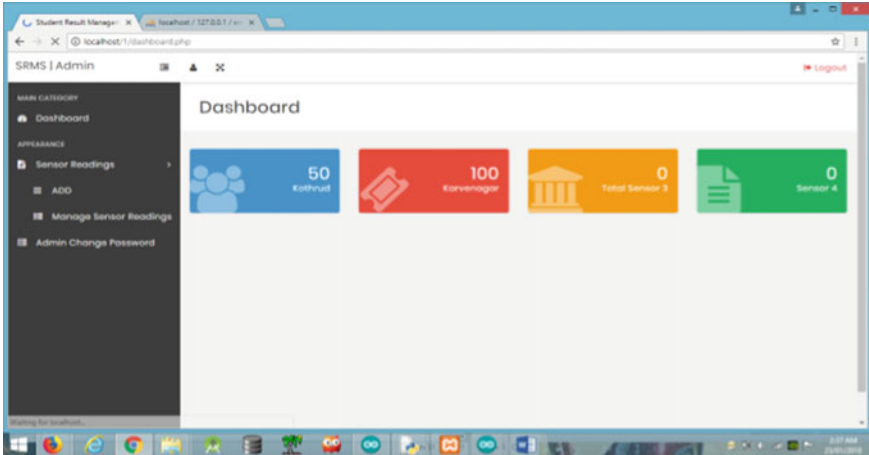


Fig. 5 Webpage displays condition of dustbin

8 Limitations

- High Initial Cost
- The tools utilised are expensive
- Needs a skilled individual.

9 Conclusion

A step toward automating the manual collection and identification of wastes is the installation of a garbage management system. The current technique in use requires the concerned municipal employee to manually search for the filled trash cans in various locations around a neighborhoods or street to regularly check whether the trash can is filled or not, which is a difficult and time-consuming task. Additionally, by automating trash management, less labor is required overall, which lowers costs. IOT can be used to track garbage/bin location, load, missing/stolen bins, the level of waste in garbage bins, and to advise the quickest route for rapid collection of solid waste with no human interaction or with little human involvement.

References

1. Xenya, M. C., D'souza, E., Woelorm, K. O. D., Adjei-Laryea, R. N., & Baah-Nyarkoh, E. (2020). A proposed IoT based smart waste bin management system with an optimized route: a case study of ghana. In *2020 conference on information communications technology and society (ICTAS)* (1–5). IEEE.
2. Kumar, S., Kaur, M., & Rakesh, N. (2021). IoT-based smart waste management system. In *2021 innovations in information and communication technologies (IICT-2020)* (133–139). Springer.
3. Soh, Z. H. C., Husa, M. A. A. H., Abdullah, S. A. C., & Shafie, M. A. (2019). Smart waste collection monitoring and alert system via IoT. In *2019 IEEE 9th symposium on computer applications & industrial electronics (ISCAIE)* (50–54). IEEE.
4. Parkash, P. V. (2016). IoT based waste management for smart city. *International Journal of Innovative Research in Computer and Communication Engineering*, 4(2), 1267–1274.
5. Gawad, H. A., Suraj Kadam, D. J., & Patel, N. (2017). An IOT based dynamic garbage level monitoring system using raspberry-pi. *International Journal of Engineering Research and Application*. www.ijera.com ISSN. 2248-9622.
6. Bashir, A., Banday, S. A., Khan, A. R., & Shafi, M. (2013). Concept, design and implementation of automatic waste management system. *International Journal on Recent and Innovation Trends in Computing and Communication*, 1(7), 604–609.

Design of Narrow Band Pass Filter Using Open Loop Circular Resonator



Akhilesh Kumar Pandey, Meenakshi M. Pawar, and Mohammad Mushaib

Abstract The paper proposes a compact and planar narrow band bandpass filter. The filter structure is formed by using two concentric open loop circular resonators structure. The basic structure of open loop circular resonator is inside coupled to another open loop to have the required passband performance. The filter does not comprise of defected ground structure and via that makes the fabrication easy. The narrow band associated with center frequency at 5.76 GHz. The s-parameter characteristic performance shows. A passband with a minimum value of insertion loss .99 dB and maximum value of return loss 17.16 dB. The passband has good selectivity and rejection performance on its both sides. The upper stop band extended from 5.88 GHz. The design parameter shows a filter of small size that is 4.7 mm × 4.6 mm. The proposed filter is designed and simulated in Key sight ADS.

Keywords Bands pass filter · Open loop circular resonator · Split-ring stubs and selectivity

1 Introduction

A recent development in wireless communication system, narrow band pass filters play key roles in several applications like WLAN, WIMAX, Satellite communication etc. Now day filters have single narrow pass band and wide stop band are commonly used to transmission frequency to pass it. RF filter mostly used in receiver with some specification for rejection in the band of consecutive transmitted frequency so that damages are not possible due high transmission power [1]. Resonators are mostly important devices to design the filters and open loop resonators. This micro strip canonical filter with open loop resonator has ability to identify electric and

A. K. Pandey (✉) · M. M. Pawar
SVERI's College of Engineering, Pandharpur, India
e-mail: akpandey@coe.sveri.ac.in

M. Mushaib
Sam Higginbottom University of Agriculture Technology and Sciences, Uttar Pradesh, Allahabad, India

magnetic coupling [2]. In micro strip resonators filter is simple has no grounding and coupling aperture using mutual coupling. The nature of fringing field decides strength of coupling. In open loop resonator have maximum electric field density at the side of open loop gap and maximum magnetic field density opposite to open loop gap. The nature of fringe field is exponential decay hence maximum electric field density at near the side having maximum electric disturbance and maximum magnetic field density at near side having maximum magnetic disturbance stronger. Coupling effects could enhance and reduce the storage energy and splitting the resonance mode [3]. The dual band resonator characteristics are achieved using two open loop stubs. An incorporating the shunt stub and series stub shows undesired pass band and better rejection performance are achieved [2–6]. The corrugate coupled micro strip filter is proposed to suppressions of spurious pass band at second harmonics [7]. In parallel coupled line micro strip band pass filter desired pass band response maintained and harmonics in pass band is modulated [8]. A continuous effort of researchers to design a filter with high rejection performance is a challenging and try to overcome it, applying various technique such as cascading open loop triangular resonator and embedded with rectangular ring is used to improve and achieved wide stop band at both side of pass band [9]. In triangular patch resonator has high power handling capability and filtering characteristics is achieved with simple structure of cascading triangular resonator [10]. A Simple structure circular ring resonator using pair of shorted and open stubs, frequency bandwidth and wide bandwidth is achieved [11]. Resonators having harmonic response degrade the system performance. There are various methods in the past for harmonic reduction in open ended resonator and the harmonic suppression in band pass filter is achieved [7, 8, 12–17]. In this paper, Narrow band pass filter using open loop circular ring resonator is presented. Proposed filters designed on, the dielectric material Rogers RT Duroid 6010 having dielectric constant 10.2 and thickness of 1.277 mm.

2 Design of Single Narrow Band Bandpass Filter

The design of narrow band pass filter has pass band and wide stop band, both side of pass band. Circular resonator is used since circular resonator has strong electrical and magnetic coupling when compared with triangular and rectangular resonators.

Figure 1 shows closed loop circular ring resonator as single mode band pass filter. Various responses can be obtained with different position and size of desperateness can be achieved for band pass filter. Using the slow wave and resonant mode theory, cutting in a circular patch structure that change in electric field and magnetic field coupling and existed higher mode of harmonics and generate attenuation due to cross coupling, is achieved abbreviated band pass filter design technique.

The fundamental resonance is occurs when λ_g (Perimeter of circular ring resonator) is equals to guided wavelength, the resonant frequency of a resonator depends on its electrical length $\lambda_g/2$ and

Defined as

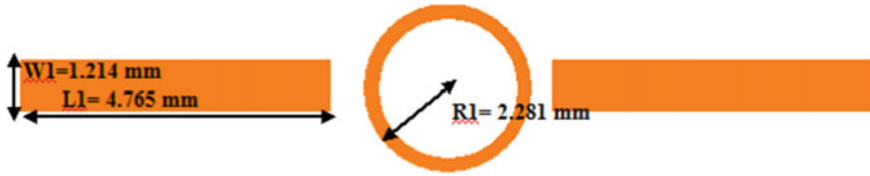


Fig. 1 Configuration of the circular ring resonator filter

$$\lambda_g = \frac{c}{f_r \sqrt{\epsilon_{eff}}} \tag{1}$$

where

- f_r is resonant frequency
- c Velocity of light in m/s
- ϵ_{eff} is effective permittivity of the medium.

When resonant frequency of circular ring is fixed, on reducing the perimeter of circular ring resonator is increasing in effective dielectric constant. On other hand effective dielectric constant is fixed, on reducing the perimeter of circular ring resonator is increasing the resonance frequency. An open loop resonator is play significant role in coupling in the electromagnetic structures. Open loop resonator has electrical and magnetic coupling both hence shows minimum insertion loss and better coupling. Perimeter of Open loop circular ring resonator, relative dielectric constant ϵ_r and height h of the material decide the coupling coefficient of the open loop circular resonator. The nature, extent of the field and the perimeter of circular ring resonator decides the coupling strength and its characteristics of open loop resonators.

The basic structure is converted into Open loop circular loop resonator with shoe increase in electric and magnetic coupling so overall coupling effects increase, the s-parameter characteristics show the increase in insertion loss and return loss value with the harmonics in the upper stop band. The value of insertion loss and return loss is 0.99 and 17.16 dB, see Fig. 3. Resonant frequency defined as.

$$f_r = \frac{c}{2L\sqrt{\epsilon_e}} \tag{2}$$

- ϵ_e is effective permittivity of the medium
- c Velocity of light in m/s
- f_r Resonating frequency in Hz
- L Total perimeter of open loop circular ring resonator.

3 Dimension of Proposed Filter

The optimized dimensions of the proposed design are as follows: $L1 = 4.765$ mm, $W1 = 1.214$ mm, $R1 = 2.281$ mm, the overall size of the proposed filter is 4.7 mm \times 4.6 mm, see Fig. 2. The s-parameter characteristic performance shows narrow band centered at 5.76 GHz. The lower value of insertion loss is 0.99 dB and maximum return loss is 17.16 dB. The fractional bandwidth of the narrow pass band is 2.02% , see Fig. 3.

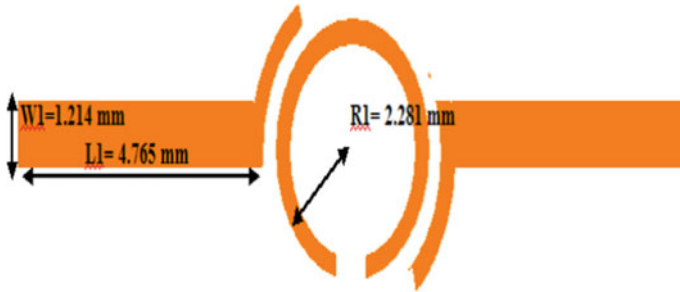


Fig. 2 Structure of open loop circular resonator coupled in series with transmission line with shoe

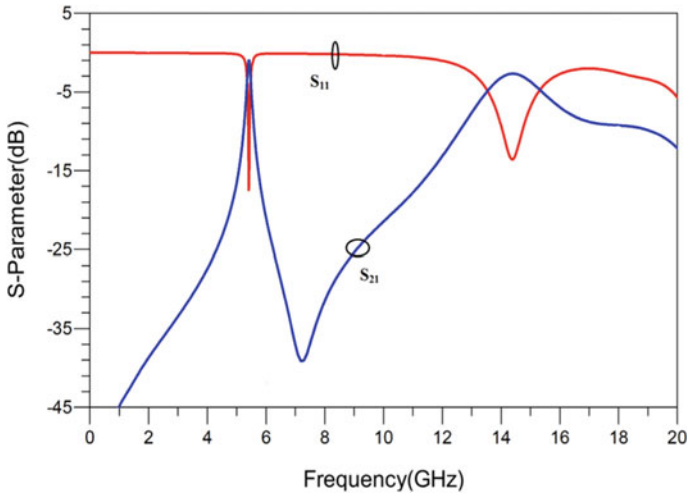


Fig. 3 S-parameters versus frequency (GHz)

4 Conclusion

A compact and planar single narrow-band band pass filter using two open concentric circular loops is proposed. Frequency response clearly shows that coupled resonator theory is being used. The proposed structure generates single narrow-band band pass filter centered at 5.88 GHz with good rejection performance and selectivity. The proposed structure shows various applications in C- band of communication system.

References

1. Hunter, I. (2000). *Theory and design of microwave filters*. IEE Press.
2. Hong, J. S., & Lancaster, M. J. (1995). Canonical micro strip filter using square open-loop resonators. *Electronics Letters*, 3(23), 2020–2022.
3. Hong, J.-S., & Lancaster, M. J. (1996). Coupling of microstrip square open-loop resonators for cross-coupled planar microwave filters. *IEEE Transactions on Microwave Theory and Techniques*, 44(12), 2099–2109.
4. Hsieh, L. H., & Chang, K. (2003). Tunable microstrip band pass filters with two transmission zeros. *IEEE Transactions on Microwave Theory and Techniques*, 51(2), 520–525.
5. Mondal, P., & Mandal, M. K. (2008). Design of dual-band band pass filters using stub-loaded open-loop resonators. *IEEE Transactions on Microwave Theory and Techniques*, 56(2), 150–155.
6. Zhang, X. Y., Chen, J.-X., Xue, Q., & Li, S.-M. (2007). Dual-band band pass filters using stub loaded resonators. *IEEE Microwave Wireless Components Letter*, 17(8), 583–585.
7. Kuo, J. T., Hsu, W. H., & Huang, W. J. (2002). Parallel coupled microstrip filters with suppression of harmonic response. *IEEE Microwave Wireless Components Letter*, 12(10), 383–385.
8. Lopetegi, T., Laso, M. A. G., Hernandez, J., Bacaicoa, M., Benito, D., Garde, M. J., Sorolla, M., & Guglielmi, M. (2001). New microstrip wiggly line filters with spurious pass band suppression. *IEEE Transactions on Microwave Theory Technique*, 49(9), 1593–1598.
9. Gaurav, Y., & Chauhan, R. K. (2017). Design of single narrow band pass filter using cascaded open loop triangular ring resonators embedded with rectangular ring. *Journal of Telecommunication, Electronic and Computer Engineering*, 9(2), 119–123.
10. Hong, J. S., & Lancaster, M. J. (2000). Microstrip triangular patch resonator filters. In *IEEE MTT-S international symposium on digestive* (pp. 331–334), June 2000.
11. Wang, W., Cao, Q., Yang, C., Wang, Y., & Chen, Y. (2015). Design of dual-band pass filters using stepped-impedance circular ring resonator. *Electronics Letters*, 51(25), 2117–2119.
12. Tu, W. H., & Chang, K. (2005). Compact microstrip bandstop filter using open stub and spurline. *IEEE Microwave Wireless Components Letter*, 15(4), 268–270.
13. Kim, I. K., Kingsley, N., Morton, M., Bairavasubramanian, R., Papapolymerou, J., Tentzeris, M. M., & Yook, J. G.: Fractal-shaped microstrip coupled-line bandpass filters for suppression of second harmonic. *IEEE Transactions on Microwave Theory Technique*, 53(9), 2943–2948.
14. Kim, B. S., Lee, J. W., & Song, M. S. (2004). An implementation of harmonic suppression microstrip filters with periodic grooves. *IEEE Microwave Wireless Components Letter*, 14(9), 413–415.
15. Moradian, M., & Tayarani, M. (2008). Spurious-response suppression in microstrip parallel-coupled band pass filters by grooved substrates. *IEEE Microwave Theory Technique*, 56(7), 1707–1713.

16. Chen, C. F., Huang, J. Y., & Wu, R. B. (2005). Design of microstrip bandpass filters with multiovermode spurious-mode suppression. *IEEE Microwave Theory and Techniques*, 53(12), 3788–3793.
17. Lin, S. C., Deng, P. H., Lin, Y. H., Wang, D. H., & Chen, C. H. (2006). Wide stop band microstrip band pass filters using dissimilar quarter-wavelength stepped-impedance resonators. *IEEE Transactions on Microwave Theory and Techniques*, 54(3), 1011–1018.

Review of Obstacle Detection by Ultrasonic and Laser Sensor for Automated Guided Vehicles



Mahesh G. Sonawane and Nishigandha S. Patel

Abstract In this twenty-first century, industries are using automated guided vehicles for material handling. The wide usage is because AGVs can easily customize per application requirements. One of the areas of concern is obstacle detection, as AGVs operated in highly congested industrial environments. While working with automated guided vehicles on the production floor, these vehicles come across human operators and manufacturing equipment. In such events, the collision of automated guided vehicles with human operators or manufacturing equipment can occur. These accidents on the production floor can cause loss of human life or damage manufacturing equipment. To avoid such circumstances, AGVs must be able to detect obstacles and avoid them. This paper reviewed obstacle detection techniques using ultrasonic and laser sensors. This study shall help the researchers to understand the advantages, limitations, applications and future scopes of ultrasonic and laser sensors for obstacle detection.

Keywords Obstacle detection · Ultrasonic sensor · Laser sensor

1 Introduction

Automated Guided Vehicles, popularly called as AGVs. A. M Barrett Jr. invented “Guide-O-Matic” a towing tractor. This tractor follows an overhead wire. Valvo company used AGVs and 280 computer controlled vehicles in their automobile plant. Since then, enormous research has been done on the AGVs to customize them to particular application requirements, hence increasing usage of AGVs in industries like manufacturing, healthcare & pharma, logistic, packaging, automotive, and paper printing [1, 2]. Several aspects of AGVs require improvements, like navigation, drive, safety, power, and vehicle control systems. AGVs are classified into five generations. The first generation AGVs are AGV systems guided using cables or guiding rails; the second generation AGVs are guided using a fixed system. The

M. G. Sonawane (✉) · N. S. Patel
MIT Art, Design and Technology University, Pune, India
e-mail: maheshsonawane437t@gmail.com

first and second generations AGVs couldn't detect and avoid obstacles. The third generation AGVs use a laser system for navigation. The Inertial Navigation System (INS) is implemented in fourth generation AGVs. Advance distance sensor systems such as cameras, and sensors can be integrated with INS. Advancements like gyroscope for positioning, automatic navigation, static and dynamic obstacle detection through processing software modules are used in the central control unit. The fifth generation AGVs, called Autonomous Mobile Robots (AMR), has high speed data processing capability. The third, fourth, and fifth generation AGVs can detect and avoid obstacles coming across their path [3]. The AGVs must, among other things, have the ability to detect obstacles in their path and create a path to avoid running into them. Otherwise, these crashes may cause damage to the vehicle, injury to nearby personnel, and damage to the items being delivered. The ultrasonic sensors are used for obstacle detection in AGVs in early models when the AGVs are guided using a colour line or magnetic line. Also, ultrasonic sensors are cost effective, which makes them the perfect choice for low cost obstacle detection systems; this is the reason behind the study of ultrasonic sensors for obstacle detection. Laser technology in the twenty-first century is capable of both obstacle detection and navigation purpose. Due to this reason, the use of lasers for obstacle detection and navigation increased. As per market research, the use of laser based AGVs is increased due to the high accuracy and ability of laser sensors to use combinedly with vision systems. In 2021, the market was dominated by the laser guidance industry, which had a global revenue share of about 35% [4].

2 Ultrasonic Sensor Based Obstacle Detection

The ultrasonic sensors work on the principle of ultrasonic sound waves. The sensor consists of an emitter and a receiver. The emitter emits ultrasonic sound waves which reflect from the obstacle and are received at the sensor receiver, and the obstacle is said to be detected. Ultrasonic waves are longitudinal waves travelling as a series of compresses and extensions. The ultrasonic sensor is used to find the distance of the obstacle from the sensor. The main aspect of this sensor is its cost effectiveness which makes it used in autonomous vehicles. In [5], the authors used an ultrasonic sensor as the cheapest, most reliable, and most widely used. They discussed the use of ultrasonic sensor in distance measurement in a vehicle application. The authors also described the features of the ultrasonic sensor and its working principle. For this experiment, HC-SR04 ultrasonic sensor used has a maximum range of 400 cm. Also, the microcontroller used is Raspberry Pi. The performance evaluation of ultrasonic sensors in relation to the real distance of the obstacle from the sensor and the obstacle's measured distance was also demonstrated in this paper. The authors successfully used HC-SR04 in the automobile prototype system. In [6], the authors performed performance evaluation on ultrasonic sensors to find the accuracy of the ultrasonic sensor in measuring the distance of obstacles from sensors and how accurately the ultrasonic sensor identifies the direction of obstacles. The

experimental setup uses an Arduino Uno microcontroller for data collection. The test results showed that the ultrasonic sensor has above 90% accuracy in measuring the distance of obstacles and their direction. The authors of [7] suggested an ultrasonic sensor-based obstacle detection and avoidance system for unmanned ground vehicles. The ultrasonic sensor implemented is SRF05. They developed a testing rig using five ultrasonic sensors to test a method for object recognition and found a beam pattern from the test. They identify that the simultaneous use of five ultrasonic sensors causes a false reading. They developed a neural network using supervised machine learning for object recognition. In [8], the authors presented low cost obstacle detection and obstacle avoidance method that can be used for autonomous robots. Their objectives are to minimise vehicle deviation from a predefined path and develop an algorithm that uses the low cost ultrasonic sensor. This low-cost system can be used as a backup in the event of the primary ranging sensor malfunctioning. The triangulation method is used for measuring the exact angles and distances of the obstacle. A single ultrasonic sensor is used by the authors' obstacle avoidance system to estimate shape and avoid collisions. Various experiments are performed in [9] to find the accuracy of the ultrasonic sensor in detecting moving obstacles. They used the ultrasonic sensor HC-SR04 and the servo motor SG90. The authors investigated the real distance of the obstacle from a sensor as well as distance measurements made by an ultrasonic sensor. This experiment performed is for both metal and nonmetal obstacles. For both experiments, ultrasonic sensor gives 94% average accuracy for metal obstacles and 90% average accuracy for nonmetal obstacles. The accuracy measurement of direction of ultrasonic sensor performed is by comparing the actual direction of obstacles to servo indicated direction mechanism measurements. The average accuracy measurement of direction of the ultrasonic sensor is 99%. The authors in [10] developed an autonomous robot for obstacle detection and avoidance using an ultrasonic sensor. In the design, the ultrasonic sensors serve as the eye of the robot to aid its autonomous movement. This robot uses two motors, L293D motor driver, a servo motor, an Arduino board, an ultrasonic sensor, a Bluetooth module and a control app. This research paper also showed the circuit diagram and its simulation outputs. In this research paper, the robot working principle is also presented carefully as its flowchart. This paper evaluated robot performance in environments such as well-lighted, dark, semi-lighted, clear, semi-clear, and unclear terrain. This performance evaluation is about the ability of the robot to avoid obstacles in different environments. This research concluded that a working robot is successfully developed for avoiding obstacles on its path at a distance range of 30 cm. Also, a robot uses manoeuvres to avoid obstacles autonomously. The accuracy recorded from several testing trials shows that the robot performed excellently, scoring 87.5%. The authors of [11] suggested using an ultrasonic sensor to detect obstacles for mobile robot navigation. The system in use makes use of a motor shield driver, an Arduino Uno development board, and a Wi-Fi module. A 2400 mAh lithium polymer battery powers this robot. The ultrasonic sensor used is HC-SR04. This research shows the robot's performance analysis in different environments, such as well-lit and dimly lit, corresponding to different obstacles, such as single solid obstacles, double solid obstacles, and uniform shaped surfaces. This research concluded that the ultrasonic sensor for a

mobile robot is a helpful tool that improves the ability of the mobile robots to detect obstacles successfully. Additionally, the findings of the performance analysis demonstrated the ultrasonic sensor's high degree of accuracy in detecting obstacles. In [12], the automated guided vehicle is created for the warehouse for logistic purposes. The main focus is making effective routing, obstacle detection, and avoidance systems. The ultrasonic sensor and infrared ray sensor are for obstacle detection. The process of interfacing sensors and actuators with the Raspberry Pi microcontroller is explained.

3 Laser Sensor Based Obstacle Detection

Light amplification by stimulated emission of radiation is known as laser. It is a monochromatic, coherent, and convergent beam of light. Laser sensors have been used for obstacle detection as well as for navigation. Laser range sensors transmit light beams to the interested area and measure the time taken by the light beam to leave and return to the sensor. The laser sensor is a popular choice for many researchers and applied projects because of its perfect performance in real time applications and high measurement accuracy. The laser range finder (LRF) sensors are used for moving obstacle detection and tracking. The authors in [1] described data fusion methodologies for obstacle detection in an automated factory. For obstacle detection, the authors used multisensor data fusion technique. In order to produce an accurate and reliable representation of an environment, the multisensor data fusion approach merges data from many sensors. This fusion technology is used in robotics, military applications, biomedicines, and image processing. The authors used multisensor fusion technology in forklifts to avoid accidents. They used medium-level and high-level data fusion. They discovered that data fusion can be used well for obstacle detection in automated systems for logistics in modern factories. This paper [2] presented novel sensing and control technologies that aim to enhance the efficiency of groups of AGVs used in logistics sector. The adoption of AGV systems for factory logistics was examined in this article. The authors give two main reasons that prevent from applying advanced control strategies. First of all, commonly used sensing devices are laser scanners, these devices are very effective in improving the safety of AGVs, but they are not suitable for distinguishing between humans and other kinds of obstacles. Second, these sensor systems cannot acquire global information about the surrounding environment. The data fusion technique is applied for a laser scanner and omnidirectional stereovision system. The data fusion is applied at two levels medium level and high level. The authors concluded that advanced sensing technologies, together with a centralised data fusion system, are an effective tool for improving the efficiency of multi-AGV systems. In [13], several works done on detecting and tracking multiple objects using laser sensors are shown. The authors addressed two issues; how to detect and extract mobile objects and how to track their motion and predict their future position. The laser sensor LMS200 is placed in the front part of the vehicle. They used geometric transformations to convert laser data to the global two dimensional cartesian system. As a LRF generates a large amount

of data, grouping measurements that belong to the same object allows dimension reduction in data to improve the efficiency of object detection and tracking. The data collected goes through the process of segmentation, feature extraction and line fitting. The Extended Kalman Filter algorithm was also designed to track mobile obstacles. The authors in [14] presented an implementation methodology for typical obstacle detection and recognition with LRF. The implementation process of detecting the obstacle and recognizing the ditches and the platforms; is divided into five steps. The first step is clustering, which finds suspect obstacles from rough scan data. For the clustering process, the Euclidean distance is calculated between two adjacent points in the scan, which is used to partition different clusters. The second step is line segment extraction from the cluster to achieve intensive description. In the third step, line segments from the two dimensional scanner coordinate system are converted to the three dimensional global coordinate system to fulfil the object recognition task and use the height information to detect and recognize the obstacle. In the fourth step, matching of the corresponding lines in the scans of adjacent time stamps is performed; the authors used the parameters of the space line segment to find the corresponding line segments. Recognizing the obstacles and delivering the dimensional descriptions is the last step. In [15], the authors presented obstacle detection using a data fusion between two dimensional laser scanner and a stereovision. This work aims to present new techniques and tools to design a robust, accurate and reliable obstacle detection system for outdoor environments using a minimum number of sensors. The authors explained the stereovision framework, laser scanner raw data processing, fusion and multi objects association. The authors concluded that the laser points' altitude is not sufficiently reliable to be exploited alone. Hence a systematic architecture for the application consists in using the laser points' altitude to invalidate some false laser targets before the tracking step. Then only the tracked obstacles are confirmed using the obstacle pixels criterion. A long-range obstacle detection system using data fusion between a laser scanner and stereo vision is the approach suggested in [16]. The detection and tracking of obstacles are done using a laser sensor, and stereo vision is used for confirming the detection of obstacles. The paper described the geometrical configuration of the used sensors, an overview of the application, and stereo based confirmation of an obstacle. The paper presented three obstacle confirmation criteria: number of obstacle pixels, prevailing alignment orientation, and laser points altitude. The range enhancement technique using numerical zoom can use higher resolution images without increasing the computation time. In [17], the authors presented a method for obstacle detection as well as tracking using two dimensional laser and Kalman filter algorithm. Kalman filter is a recursive algorithm used for tracking moving obstacles. It is used to estimate the state variables of given systems represented by linear equations. The system needs to be considered linear and disturbed by Gaussian noise to use the Kalman filter. This filter increases computational cost and isn't efficient in case of disturbances in the measured position of the obstacle. This work suggested the use of the Corrector of Discrepancies algorithm to avoid interrupting the laser beam when the object track is behind a barrier. The experiment results show that using the Kalman filter with Corrector of Discrepancies provides effective results when the vehicle track is behind a barrier.

In [18], the authors presented a method to improve the system's performance with low cost sensors and fusion between stereo vision and laser rangefinder. The laser range finders read the two dimensional plane which is in front of the vehicle using laser beams. Each laser beam is addressed by an incident angle and the distance of the nearest obstacle. All results are analysed to generate a local map considering the vehicle's real-time location and the field of view of the laser range finder. Simultaneously, a stereo vision camera can also obtain a local map from visual perception. The authors concluded that having multiple data sources for detection of obstacles is an advantage. The authors in [19] proposed using laser intensity based obstacle detection. This paper showed that laser intensity is better for detecting long range obstacles. The laser intensity-based obstacle detection technique worked well for detecting small obstacles over long distances and at high speeds. Additionally, this approach has the benefit that laser intensity sensors are less expensive and use less power than laser range sensors.

4 Discussion, Identifying Research Gaps and Future Research Directions

The ultrasonic sensors have been used in many projects due to their cost effectiveness, but their range for obstacle detection is very less compared to the laser sensor. and thus can be used within small and medium distances. The authors in [5–10] successfully detected static and dynamic obstacles using ultrasonic sensors. By comparing the work of [5–10], we can say that the average accuracy of the ultrasonic sensor to measure the distance of the obstacle from the ultrasonic sensor and average directional accuracy is very good but not good as laser sensor. The main limitation of ultrasonic sensors is that they cannot detect small obstacles and obstacles very close to the sensor. The shape and size of the obstacle play a very important role in obstacle detection by ultrasonic sensors. The big size obstacles and square shape obstacles are easy to detect. The round obstacles and very small obstacles are difficult to detect. The cylindrical shape obstacles are very difficult to detect using the ultrasonic sensor as a very small portion of the waves is reflected back towards the sensor from the cylindrical obstacle. At current conditions, ultrasonic sensors are very effective in detecting static obstacles. Further studies in the area of radar using ultrasonic sensors can increase the efficiency of detecting and tracking static and moving obstacles. Laser sensors are widely used for navigation as well as obstacle detection. The main reason for large usage is laser sensors are highly accurate and have a large range of 100 m. Also, using effective algorithms on laser scan data, easy identification and tracking of the obstacle are possible. The commonly used algorithms for obstacle detection are clustering and segmentation. For obstacle tracking Corrector of Discrepancies, Kalman filter algorithms are used. The use of the Kalman filter algorithm increases computational cost [16]. The higher computational cost of the algorithm comes with high processing power processor and

high energy consumption of processor which makes electronics system expensive and complex. To mitigate this drawback in [16], authors used the parameters of the space line segment to find the corresponding line segments. Hence, further studies in obstacle tracking algorithms can reduce the computational cost of the algorithms. Also, data collected from different sensors is not correctly combined to represent the surrounding environment; hence the use of data fusion techniques is essential. Many times only a laser sensor is used for obstacle detection but in the case of obstacle recognition using a vision system, data fusion proved very efficient. Further studies in data fusion using heuristics can lower the computational cost [1]. The obstacle recognition system proved helpful for recognizing and confirming obstacles as sometimes the primary obstacle detection sensor gives false readings. The stereo vision system is appropriate for obstacle recognition as it is efficient for monitoring and cost effective. Further studies in data fusion of laser sensor and stereo vision can make an efficient navigation system for AGVs.

5 Conclusion

This paper presents literature review of ultrasonic and laser sensors for obstacle detection. This study concluded that ultrasonic sensors could be used effectively for obstacle detection of obstacles present at small and medium distances i.e. from 1 to 400 cm. At a very small distance of less than 1 cm, the ultrasonic sensor is unable to detect obstacles. Also, by applying machine learning models to the sensor's data, the object detection capability of an ultrasonic sensor can be further increased. Further studies in obstacle recognition system for ultrasonic sensor makes it the best choice for low cost obstacle detection system. For laser sensors, this study concluded that laser sensors have more capability to detect obstacles at a long range than ultrasonic sensors up to 100 m. However, another obstacle recognition system, mainly vision systems, plays a important role in confirming the obstacle. The combination of obstacle detection and confirmation plays a crucial role in navigating AGVs. This combination of obstacle detection and confirmation can be easily achieved using data fusion techniques. Further studies in data fusion may help current multisensor systems to reduce computational cost and use them as navigation systems.

References

1. Cardarelli, E., Sabattini, L., Secchi, C., & Fantuzzi, C. (2014). Multisensor data fusion for obstacle detection in automated factory logistics. In *IEEE 10th international conference on intelligent computer communication and processing*, Romania.
2. Sabattini, L., Cardarelli, E., Digani, V., Secchi, C., Fantuzzi, C., & Fuerstenberg, K. (2015). Advanced sensing and control techniques for multi AGV systems in shared industrial environments. In *IEEE 20th conference on emerging technologies & factory automation*, Luxembourg.

3. Thai, N., Khanh Ly, T., & Dzung, L. Q. (2021). Roadmap, routing, and obstacle avoidance of AGV robot in the static environment of the flexible manufacturing system with matrix devices layout. *VNUHCM Journal of Science and Technology Development*, 24(3), 2091–2099.
4. Grand View Research, Automated Guided Vehicle Market Size Report. (2030). Report ID: GVR-1-68038-153-5. <https://www.grandviewresearch.com/industry-analysis/automated-guided-vehicle-agv-market>
5. Vidhya, D. S., Rebelo, D., D'Silva, C., & Fernandes, L. (2016). Obstacle detection using ultrasonic sensors. *International Journal for Innovative Research in Science and Technology*, 2, 11.
6. Faisal, M., Reddy, G., Kumar, B. A., & Ajitha, D. (2021). Object detection using ultrasonic sensor. *IJMTST*, 7, 7010.
7. De Simone, M., Rivera, Z., & Guida, D. (2018). Obstacle avoidance system for unmanned ground vehicles by using ultrasonic sensors. *Machines*, 6(2).
8. Yasin, J. N., Mohamed, S. A. S., Haghbayan, M. H., Heikkonen, J., Tenhunen, H., & Plosila, J. (2021). Low-cost ultrasonic based object detection and collision avoidance method for autonomous robots. *International Journal of Information Technology*, 13(1), 97–107.
9. Biswas, A., Abedin, S., & Kabir, A. (2020). Moving object detection using ultrasonic radar with proper distance, direction, and object shape analysis. *Journal of Information Systems Engineering and Business Intelligence*, 6(2).
10. Agbeyangi, A. O., Alashiri, O., Odieta, J. O., & Adenekan, O. A. (2020). An autonomous obstacle avoidance robot using ultrasonic sensor. *Journal of Computer Science and Its Application*, 27.
11. Azeta, J., Bolu, C., Hinvi, D., & Abioye, A. (2019). Obstacle detection using ultrasonic sensor for a mobile robot. *8th International Conference on Mechatronics and Control Engineering, IOP Conference Series: Materials Science and Engineering*, 707.
12. Khedkar, A., Kajani, K., Ipkal, P., Banthia, S., Jagdale, B., & Kulkarni, M. (2020). Automated guided vehicle system with collision avoidance and navigation in warehouse environments. *International Research Journal of Engineering and Technology*, 07(05).
13. Rebai, K., Benabderahmane, A., Azouaoui, O., & Ouadah, N. (2009). Moving obstacles detection and tracking with laser range finder. In *International conference on advanced robotics 2009*, Munich, Germany.
14. Qiu, Q., & Han, S. J. (2009). An implementation of typical obstacle detection and recognition with laser range finder. In *IEEE international conference on intelligent computing and intelligent systems*, Shanghai.
15. Labayrade, R., Gruyer, D., Royere, C., Perrollaz, M., & Aubert, D. (2007). Obstacle detection based on fusion between stereovision and 2D laser scanner. *Mobile Robots: Perception & Navigation*.
16. Perrollaz, M., Labayrade, R., Roy, C., Hauti, N., & Aubert, D. (2006). Long range obstacle detection using laser scanner and stereovision. In *IEEE intelligent vehicles symposium*, Japan.
17. Habermann, D., & Garcia, C. (2010). Obstacle detection and tracking using laser 2D. In *Latin American robotics symposium and intelligent robotics meeting*, Brazil.
18. Hussein, A., Plaza, P., Martin, D., Escalera, A., & Armingol, J. (2016). Autonomous off-road navigation using stereo-vision and laser-rangefinder fusion for outdoor obstacles detection. In *IEEE intelligent vehicles symposium (IV)*, Sweden.
19. Hancock, J., Hebert, M., & Thorpe, C. (1998). Laser intensity-based obstacle detection. In *IEEE/RSJ international conference on intelligent robots and systems. Innovations in theory, practice and applications (Cat. No.98CH36190)*, Canada.

Establishing a Relationship Between Soil Erodibility and NDVI in the Urmodi River Watershed of Maharashtra Using GIS



Wasim Ayub Bagwan 

Abstract In this study, the two important bio-physical factors that plays a key role in understanding the nature of soil erosion takes place on terrain has been investigated. Numerous Remote Sensing (RS)-based indicators are used to show the state of the vegetation. A typical slope-based vegetation factor used to attain the canopy condition is the Normalized Difference Vegetation Index (NDVI), which is one of the RS-based indices. One of the most popular techniques for calculating soil erosion all across the world is the Revised Universal Soil Loss Equation (RUSLE). The soil texture and SOM parameters were calculated using field-based soil samples. K factor values ranged from 0.02 to 0.75 $\text{ton/ha}^{-1} \text{ h}^{-1} \text{ ha}^{-1} \text{ MJ mm}^{-1}$ when calculated using the Stone and Hillborn method. A higher propensity for soil erosion is indicated by a high erodibility factor. High values on an NDVI raster map indicate decreased susceptibility to soil erosion. The amount of vegetation and water-induced soil loss are inversely related. It was found that there was a positive association between these variables, which basically means that there is a lot of land degradation activities in the current study area.

Keywords Soil erosion · Soil erodibility (K factor) · RUSLE · NDVI · Pixel correlation

1 Introduction

The soil degradation phenomena do not only relate to fragility of the ecosystem but also indicate the imbalance of the resistivity of soil to loss with respect to its vegetation cover. Such degradation activity makes the current soil to become more vulnerable to degradation along with loss of future carrying capacity [1]. Soil erosion due to water is also a land degradation activity. Erosion can be classified according

W. A. Bagwan (✉)

School of Rural Development, Tata Institute of Social Sciences, Tuljapur 413601, Maharashtra, India

e-mail: wasim.bagwan16@gmail.com

to the agencies by which it occurs like wind, water, glacial. The detachment of soil from the rocks and mass movement takes place over the down slopes [2]. Soil erosion over the terrain occupies large tracts and it shows adverse effect on the natural and artificial ecosystems which includes the forests and crop lands. The erosion occurs due to energy contained in the raindrop which hits exposed soil. Especially in the developing countries higher population densities and cultivation activities leads to loss of vegetation cover [3]. Vegetation is possibly the chief component in the soil erosion activity and its management. The Normalized Difference Vegetation Index (NDVI) is an essential tool for execution of environmental analysis of biomes and specifically of its application in water erosion as it protects against surface soil erosion [4]. Erosion of soil is precursor of loss of fertility of soil and has adverse impacts on environmental factors and threat to cropland [5]. At catchment scale it has its implication in the conservation of soil and water [6]. The absence of vegetation cover is known factor responsible for fast erosion and perturbations along with other side effects; high rate of soil loss leads to denuded vegetation which turns to exposure of more soil surface [7]. Cover of vegetation shields the soil by the raindrop energy before hitting the soil surface [8]. The objectives of the study were, to compute the field based soil texture characteristic and Remote Sensing (RS) based vegetation factor that is, NDVI. Also, to find the relationship between these two raster datasets and find relationship between them.

2 Study Area

The Urmodi river watershed (Fig. 1) is located in Satara and Jaoli block of Satara district, which covers an area of 412.44 km². The coordinates of location is 73° 47' 37.235" E to 74° 6' 59.555" E longitude and 17° 28' 32.329" N to 17° 44' 34.352" N latitude. The Urmodi River originates at the elevation of 1264 m from mean sea level in Kaas pond and the whole basin lies in Humid Equatorial Climate-Long Dry Season [9]. The world heritage site of 'Kaas Plateau' is present in the same watershed; this is one of the main touristic place during the monsoon season. This river is tributary of Krishna River and located on its right bank on the Deccan plateau.

3 Material and Methodology

3.1 Dataset Used

For the present study, Landsat 8 imagery has been used with path: 147 row: 48. The image was cloud free; and acquired on 18 November 2015. From the available bands NIR and Red band was basically used for the present analysis. For the analysis of



Fig. 1 Location of Urmodi River watershed

soil erodibility conditions, primary data i.e. field based soil sampling was carried out. Based on the soil data, soil erodibility status was determined.

3.2 Soil Erodibility (*K* Factor)

In the determination of *K* factor, the soil physical property i.e. the texture determination is necessary. The soil texture was determined using the soil texture classification method of USDA, where sand (2.0–0.05 mm), silt (0.05–0.002 mm) and clay (< 0.002 mm) particles of soil samples were physically analyzed by sieve method on mechanical shaker with the run of 10 min. The percentage of sand, silt and clay which further used to draw the texture triangle using online tool: <https://www.nrcs.usda.gov/resources/education-and-teaching-materials/soil-texture-calculator>. The texture class is used as a sub-factor to integrate with Soil Organic Matter (SOM). This factor is also known *K*-factor of RUSLE, this is totally based on the soil characteristics. It

Table 1 Soil erodibility (K-factor) values of soil samples [11]

S. No.	Soil texture class	K if (OM < 2%)	K if (OM > 2%)
1	Clay loam	0.74	0.63
2	Fine sand	0.2	0.13
3	Loam	0.76	0.58
4	Loamy fine sand	0.34	0.2
5	Sandy clay loam	0.45	0.45
6	Sandy loam	0.31	0.27
7	Sand	0.07	0.02

is measurement unit is $\text{ton/ha}^{-1} \text{ h}^{-1} \text{ ha}^{-1} \text{ MJ mm}^{-1}$ (ton hectare hour hectare mega joule⁻¹ mm⁻¹). The mathematical equation developed by Wischmeier and Smith [10] shows that, it has strong influence of soil structure, texture, permeability and organic matter. The soil erodibility factor is crucial spatial layer while modeling and assessing the soil erosion, and such map is very helpful in managing and proper planning at watershed scale. Stone and Hillborn [11] method deals with soil texture and Soil Organic Matter (SOM) present in soil, based on that K-factor value can be computed. In the present study, soil samples were analysed using sieves to categorize its soil texture and also the SOM was analyzed. For estimation of SOM firstly we have estimated the Soil organic carbon using Walkley and Black [12] method and by multiplying it by 1.74 we get SOM. Table 1 Shows the soil erodibility values of soil sample based on texture class and SOM. The K-factor value was interpolated using Inverse Distance Weighted (IDW) method using Geographical Information System (GIS) platform with the help of ArcGIS 10.2.2 software.

3.3 Normalized Difference Vegetation Index

It is an indicator of vegetation condition over terrain. This has direct connection with vegetation and soil transportation. This is calculated using band 4 (Red), and band 5(NIR) of Landsat 8. The range of $\text{NDVI} = (\text{NIR} - \text{RED})/(\text{NIR} + \text{RED})$, is always between $- 1.0$ and $+ 1.0$. It shows the health status of vegetation [13]. It has a huge significance in managing and controlling loss of water by runoff and soil, the value greater than 0.5 represents denser vegetation [14]. For the assessment of soil erosion traditional land use land cover based thematic layer has been replaced by NDVI based cover management factor of Revised Universal Soil Loss Equation proposed by Renard et al. [6, 14, 15]. This also indicated the robustness of NDVI output. Many researchers from the India have used the NDVI based cover management factor for the soil loss assessment. In the current analysis final NDVI map was reclassified by natural break method into five classes as shown in Table 2.

Table 2 Classification of zones of K factor and NDVI by natural jenk (break) method

Categories	K factor with range	Area (km ²)	Proportion (%)	NDVI with range	Area (km ²)	Proportion (%)
Very low	0.02–0.26	49.96	12.11	– 0.15–0.05	16.49	4.00
Low	0.27–0.32	249.31	60.45	0.06–0.18	76.89	18.64
Moderate	0.33–0.40	63.86	15.48	0.19–0.24	125.22	30.36
High	0.41–0.53	34.89	8.46	0.25–0.31	127.82	30.99
Very high	0.54–0.76	14.42	3.50	0.32–0.51	66.02	16.01

3.4 Relationship Between Soil Erodibility and NDVI Using Scatterplot

A scatterplot is a graph which depicts point symbol to show the corresponding value of pair in the Cartesian plane. In case of two raster grid layer, point cloud and local/global fitted lines plot reveals the different association between two grid variables. The investigation based on such statistical approach helps the researchers to find more realistic models [16]. The General Public License (GPL) package named System for Automated Geoscientific Analyses (SAGA) [17] was employed to plot the graph. The GIS and RS approach has been used in the current analysis. It is an essential tool in the assessment of natural resources and found to be a cost effective tool having ability to provide timely, accurate and up to date information [18]. According to, Nunes et al. [19] soil erodibility is high in soils with sandy texture and less organic matter. Tree and shrub cover has been found to be agents having role in increment of the organic matter in top soil. The vegetation cover has crucial role in supporting the soil structure thus, arresting the soil erosion by water flow activity. The lower vegetation coverage enhances the risks of water induced soil loss [20].

4 Results and Discussion

4.1 Soil Erodibility (K Factor)

The USDA soil texture classification map of each sub component of texture class i.e. sand, silt and clay in percent is depicted in Fig. 2. The chemical characteristic of soil that is Soil Organic Matter (SOM) was also determined. With the help of these two parameters K factor value assessed using Inverse Distance Weighted (IDW) performed in ArcMap 10.2.2. The output raster map is show below. Figure 3a shows the soil erodibility condition of the Urmodi River catchment, it is clear from the output that, soil erodibility is low at the upper catchment, and high at lower catchment.

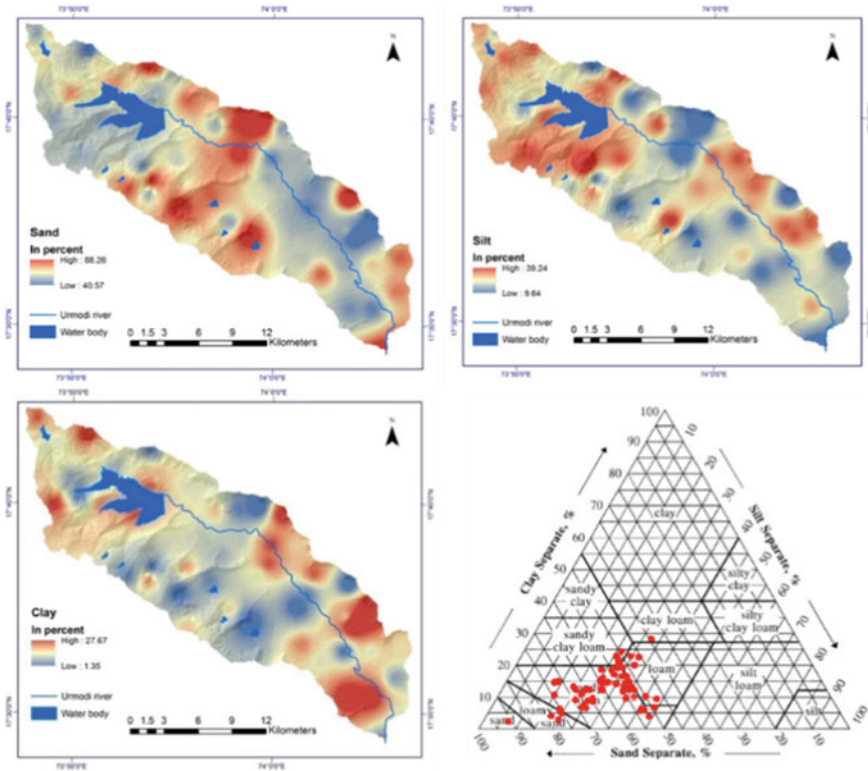


Fig. 2 Soil particle classification by USDA method with texture triangle

According to K-factor map, on the left side of river is more susceptibility to erosion than right bank.

4.2 Normalized Difference Vegetation Index (NDVI)

According the Fig. 3b, which indicated the Landsat 8 based NDVI condition of Urmodi River watershed. The index value ranges between -0.15 and 0.52 . The average vegetation condition value was found to be 0.24 . Hence we can consider that, in the entire watershed low vegetation cover was exist. The high value of NDVI represents the more greenness and healthy canopy cover and vice versa. Near the origin of the Urmodi River, surrounding to Kaas pond has shown high vegetation coverage. The value of NDVI was found to be more than 0.4 . And for the proper conservation of the vegetation there is need to focus on the improvement of canopy cover within the watershed. This could help in the soil and water conservation. In

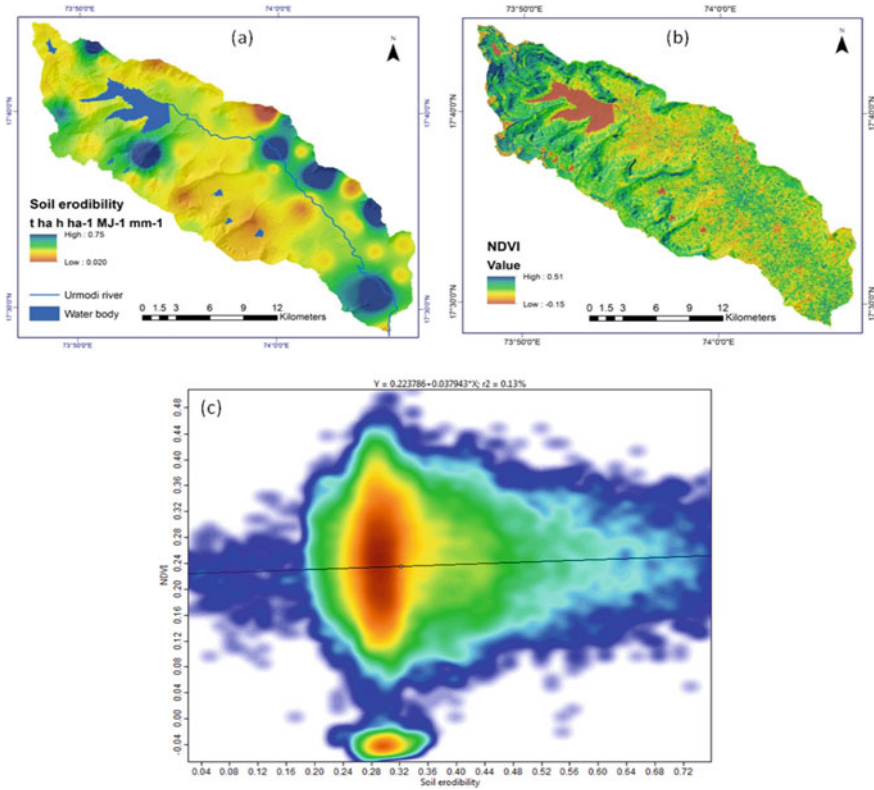


Fig. 3 a K factor of RUSLE, b Landsat 8 imagery based NDVI map, c correlation of pixel values of (a, b)

the present study area, reservoir and other small water conservation structures shows negative NDVI value.

4.3 Assessment of Relationship of K Factor and NDVI

It has been stated that, good vegetation cover boosts the organic matter in the soil and has dual role in protecting the land against the water induced soil erosion [2]. In the current study, we found the same results which also confirm the role of healthy canopy in controlling the soil wash out. While dealing with RS based vegetation index; it has been reported that increase in canopy density could reduce the water induced soil loss [21]. This statement simply shows that, how vegetation plays the role of barrier to soil loss at catchment level. The scatterplot has shown $r^2 = 0.13\%$ after the assessing the correlation of 41,657 pixels of two grids. Figure 3c shows the scatter diagram of the two thematic layers i.e. K factor and RS based NDVI. Here,

as the level of relationship between the two raster data sets tend to get negatively correlated is a good indication of the reduction in the loss of soil. As the value is going to tend positive correlation, that means the soil erosion is very active and having severe impact on the land resource. Thus the positive value is the symbol of more land degradation is occurring the given area.

5 Conclusion

In case of erosion susceptibility, and NDVI must be negatively correlate with the K-factor of RUSLE; this is the good symbol of the healthy condition of land resources. Such negative value indicates the less proneness to soil erosion at the catchment level. The positive value of r^2 is an indication pixel value of one factors for soil degradation are active with its particular cell or grid. The analysis shows that, the use of GIS for natural resource management like soil and vegetation saves the time and it is one of the purely scientific method. To protect the catchment for sustainable soil resource management; more emphasis would to be given to vegetation canopy on hill slopes basically along the boundary of the Urmodi River catchment. The research has great help in the investigation of spatio-temporal analysis soil condition with the vegetation condition prevailing there. From the point of view of Integrated Watershed Management Plan (IWMP) the soil and vegetation resource mapping can have great impact for the natural resource management.

Conflict of Interest The author declares no competing or conflict of interest.

References

1. Oldeman, L. R. (1992). *Global extent of soil degradation. Soil resilience and sustainable land use.*
2. Stoorvogel, J. J., Bakkenes, M., Temme, A. J. A. M., Batjes, N. H., & ten Brink, B. J. E. (2017). S-world: A global soil map for environmental modelling. *Land Degradation and Development.* <https://doi.org/10.1002/ldr.2656>
3. Pimentel, D., & Kounang, N. (1998). Ecology of soil erosion in ecosystems. *Ecosystems.* <https://doi.org/10.1007/s100219900035>
4. Durigon, V. L., Carvalho, D. F., Antunes, M. A. H., Oliveira, P. T. S., & Fernandes, M. M. (2014). NDVI time series for monitoring RUSLE cover management factor in a tropical watershed. *International Journal of Remote Sensing.* <https://doi.org/10.1080/01431161.2013.871081>
5. Mondal, A., Khare, D., & Kundu, S. (2016). Impact assessment of climate change on future soil erosion and SOC loss. *Natural Hazards.* <https://doi.org/10.1007/s11069-016-2255-7>
6. Renard, K., Foster, G., Weesies, G., McCool, D., & Yoder, D. (1997). Predicting soil erosion by water: A guide to conservation planning with the revised universal soil loss equation (RUSLE). *Agricultural Handbook No. 703.*

7. Burg, D., Malkinson, D., Katriel, G., & Wittenberg, L. (2014). Modeling the dynamics of soil erosion and vegetative control—Catastrophe and hysteresis. *Theoretical Ecology*. <https://doi.org/10.1007/s12080-014-0233-9>
8. Karaburun, A. (2010). Estimation of C factor for soil erosion modeling using NDVI in Buyukcekmece watershed. *Ozean Journal of Applied Sciences*.
9. National Geographic MapMaker Interactive. (2018). Retrieved from <https://mapmaker.nationalgeographic.org/#>
10. Wischmeier, W. H., & Smith, D. D. (1978). Predicting rainfall erosion losses. *Agriculture Handbook No. 537*.
11. Stone, R. P., & Hillborn, D. (2012). *Universal soil loss equation (USLE) factsheet*. Ministry of Agriculture, Food and Rural Affairs, Ontario. Retrieved from <http://www.omafra.gov.on.ca/english/engineer/facts/12-051.htm>
12. Walkley, A., & Black, I. A. (1934). An examination of the degtjareff method for determining soil organic matter, and a proposed modification of the chromic acid titration method. *Soil Science*. <https://doi.org/10.1097/00010694-193401000-00003>
13. Prasannakumar, V., Vijith, H., Geetha, N., & Shiny, R. (2011). Regional scale erosion assessment of a sub-tropical highland segment in the western Ghats of Kerala, South India. *Water Resources Management*. <https://doi.org/10.1007/s11269-011-9878-y>
14. Sharma, A. (2010). Integrating terrain and vegetation indices for identifying potential soil erosion risk area. *Geo-Spatial Information Science*. <https://doi.org/10.1007/s11806-010-0342-6>
15. Demirci, A., & Karaburun, A. (2012). Estimation of soil erosion using RUSLE in a GIS framework: A case study in the Buyukcekmece Lake watershed, northwest Turkey. *Environmental Earth Sciences*. <https://doi.org/10.1007/s12665-011-1300-9>
16. Li, B., Griffith, D. A., & Becker, B. (2016). Spatially simplified scatterplots for large raster datasets. *Geo-spatial Information Science*, 19(2), 81–93. <https://doi.org/10.1080/10095020.2016.1179441>
17. Conrad, O., Bechtel, B., Bock, M., Dietrich, H., Fischer, E., Gerlitz, L., Wehberg, J., Wichmann, V., & Böhner, J. (2015). System for automated geoscientific analyses (SAGA) v. 2.1.4. *Geoscientific Model Development*. <https://doi.org/10.5194/gmd-8-1991-2015>
18. Javed, A., Jamal, S., & Khandey, M. Y. (2012). Climate change induced land degradation and socio-economic deterioration: A remote sensing and GIS based case study from Rajasthan, India. *Journal of Geographic Information System*. <https://doi.org/10.4236/jgis.2012.43026>
19. Nunes, A. N., de Almeida, A. C., & Coelho, C. O. A. (2011). Impacts of land use and cover type on runoff and soil erosion in a marginal area of Portugal. *Applied Geography*, 31(2), 687–699. <https://doi.org/10.1016/j.apgeog.2010.12.006>
20. Issaka, S., & Ashraf, M. A. (2017). Impact of soil erosion and degradation on water quality: A review. *Geology, Ecology, and Landscapes*, 1(1), 1–11. <https://doi.org/10.1080/24749508.2017.1301053>
21. de Carvalho, D. F., Durigon, V. L., Antunes, M. A. H., de Almeida, W. S., & de Oliveira, P. T. S. (2014). Predicting soil erosion using Rusle and NDVI time series from TM Landsat 5. *Pesquisa Agropecuaria Brasileira*. <https://doi.org/10.1590/S0100-204X2014000300008>

Self-biased Cascade Current Mirror with Wide Range Level Shifter



Tejas S. Joshi, Mohua Biswas, Smita Gawade, and Rahul B. Pawar

Abstract Wide-range position shifters are very necessary components of ultra-low-voltage circuits and components. State-of-the-art position shifters will convert a sub threshold voltage to the standard voltage; their operating ranges will be limits to ranges, limiting the flexibility of dynamic voltage ranges. As a result, our paper proposed a new position shifter with an operating range of sub threshold voltage to standard force voltage and overhead and over position conversion. The edited Wilson current glass and general CMOS sense gates are used in the proposed position shifter, which is a cold-blooded structure. Using 65-nm technology, the simulation and dimension results were validated. According to the dimension results, the proposed position shifter's minimum operating voltage was less than 200 mV. Using a 22-nm technology, the modeling and measurement results were confirmed.

Keywords Ultra-low-voltage · CMOS · Threshold voltage · Wilson current

1 Introduction

While designing SOC for size optimization we are facing challenges with power consumption. As we reduce size of device, the number of transistors used in that device is goes on very close to each other and then frequency also goes on increasing. In case of SOC devices dynamic power is cubically proportional to voltage supplied, this supplied voltage is reduced then power is also reduced. This leads to reduce frequency to increase performance of device. To improve the performance a solution is to reduce power consumption from multiple voltages. The components having critical path will operate at VDD range and Non-Critical Path devices will operate at a reduced VDD level. This mitigates the negative impact on performance by keeping critical path components at VDD levels while reducing down non-critical path components. When a DC current flows from a gate having lower voltage to a gate

T. S. Joshi (✉) · M. Biswas · S. Gawade · R. B. Pawar
Department of Electronics and Communication, SVERI's College of Engineering, Pandharpur,
Maharashtra, India
e-mail: tsjoshi@coe.sveri.ac.in

having higher voltage in case of a multi-VDD system, the voltage is not sufficient to “ON” the PMOS and the PMOS conducts static current from supply to the ground.

The static current will be removed by the level shifters, restoring the full voltage swing from VDDL to VDDH. Various types of gates available chip structure use different levels of voltages. The output generated by higher voltage gate will be connected to the input of a lower voltage gate and reverse also. The Level shifter plays important role in CMOS devices [1]. The unlikely variation between the voltage levels of circuits from various ranges of voltage devices, where major blocks operate with different range of voltage range is another reason to use level shifter circuits. To move signal from block to block are used.

The use of level shifters (LS) in a multi-VDD system presents a number of difficulties that make the design of such a system fundamentally complex. They waste energy and increase propagation latency. To reap the potential benefits of having numerous power supply domains, the LS circuit must be optimized for the smallest energy-delay product. LS will need additional space and routing resources because it has both high voltage and low voltage gates [2].

For instance, the quantity of level converters can readily increase and turn into a design space overhead, each functional block requires a different voltages for its expected performance. In order to reduce energy usage, techniques like Dynamic Voltage Scaling (DVS) are frequently utilized in digital signal processing components. Another approach is to use data driven dynamic logic for CMOS OR gates to lower the circuit’s power consumption. The synchronization clock has been removed in this logic approach, and correct sequencing is now produced through wise usage of data instances. Therefore, compared to traditional dynamic logic, replacing the clock for input data results into reduction in power dissipation with maintaining speed.

This study describes a new level shifter that makes use of a PTL-based buffer along with self-biased cascade current mirror design. The deep sub threshold working voltage of these is near to minimum supply voltage of the circuit, and the rated voltage to be supplied, which is determined from transistor based design, is the maximum operating voltage. Both bidirectional level conversion and full range conversion are intended uses for this level shifter.

The remainder of the essay is structured as follows. Different forms of level shifters are introduced in part 2 along with comparisons to the level shifter circuits. Part 3 describes the level shifter’s construction. Part 4 presents simulation and measurement findings of expected power utilized by the circuit, and lastly concludes.

2 Surveys and Qualitative Comparisons Using Sub Threshold Level Shifter

In this section, sub threshold level shifters are explained. Five distinct level shifters have been compared to the proposed level shifter [3]. Five characteristics are necessary to use LS in a variety of DVS applications, as shown in Table 1. All five criteria

are satisfied by the suggested LS. According to the level shifter, the next paragraph describes each characteristic and the comparison [4].

Two cross-coupled stages are shown in Fig. 1. In first level a switched logic gate with differential cascade voltage that connected to a cross-coupled PMOS. This will works at a higher voltage level. Driving capabilities of NMOS based transistor is increased to reduce leakage of weak density of conducting PMOS type transistor. Low input voltage (V_{in}) input voltage activates mn1, this will lead to down fall level of node A to ground which turns on mp2. The output voltage of Node B will be low because it will be pulled up to VDDH. When V_{in} is asserted, mn2 and mp1 are activated, raising the output voltage level up to VDDH. To overcome latch action driven by a higher supply voltage, the driving capability of the pull-down transistors should be higher than that of the PMOS transistors. It is a straight forward design which is suitable to super-threshold level transformation. The Moto of the next level is to get maximum voltage swing. The internal circuit which carries diode which is connected to NMOS is used to reduce strength of the pull-up circuit, to allow variable input supply voltage to increase.

The working range is calculated by the dimensions of transistor and the threshold required voltage. A cross-coupled arrangement for level shifting is depicted in Fig. 1a. The Differential cascade voltage level switch logic for boosting a lower supply voltage level is known as a cross-coupled level shifter. The driving capabilities of NMOS transistor are increased to combat the leakage of lower conducting PMOS transistors. The operational range of CC LSs is only dependent on the transistor threshold voltage (V_t) and size; however, it is crucial to expand operating range of CC-LSs to the sub threshold area, due to the exponential decline in NMOS driving capabilities. For CC-LSs to convert a sub threshold supply voltage, the size of the NMOS transistor should increases, which is not expected. So, for small regions, sub threshold level conversion is not possible [5]. Even though full range bidirectional level conversion is critical, this level shifter gives bidirectional level conversion. To analyze various possible combinations of levels of input and output it is must be considered when analyzing pull-up and pull-down strength. As a result of the pull-up and pull-down capabilities being out of balance, it has few bidirectional regions.

The Level Shifter in Fig. 1 showed a fundamental current mirror configuration (CM) [6]. Because PMOS transistors' high drain-to-source voltages make it easier to build a stabilized current mirror and provide an efficient ON-OFF current differentiation at the output, this can convert a deep sub threshold level. A significant

Table 1 A comparison between results obtained by reverse ANN

Parameter	CC	CM	WCM	TSCC	MWCM	Proposed
1. Limited space		✓	✓	✓	✓	✓
2. Minimal power	✓		✓	✓		✓
3. Bilateral LC	✓	✓		✓	✓	✓
4. Dimension and VT intensity		✓	✓		✓	✓
5. Equally distributed raising and falling delays	✓	✓		✓	✓	✓

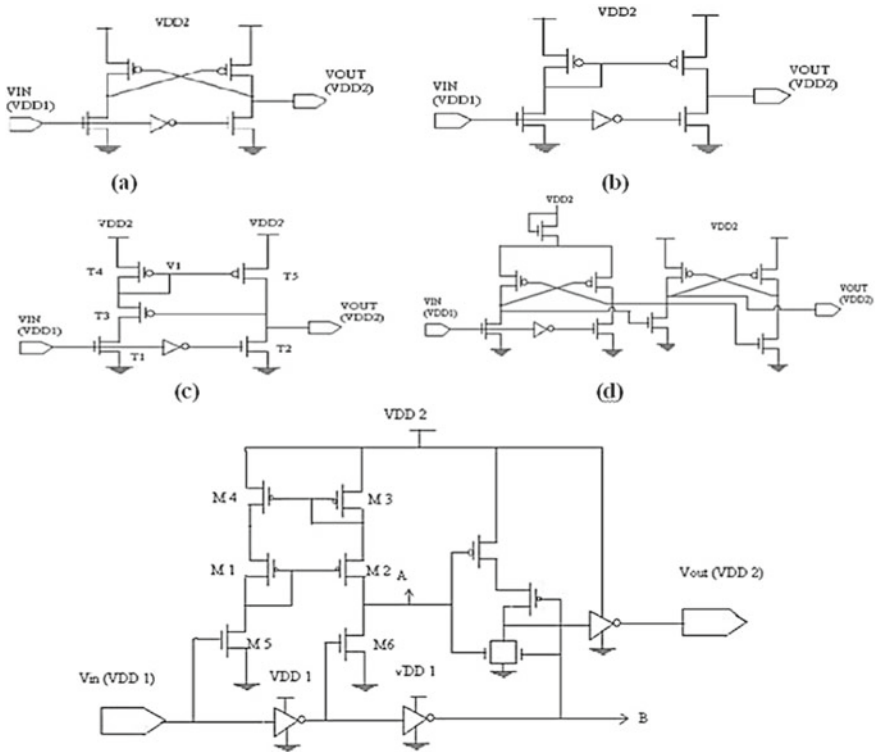


Fig. 1 Circuit for various structures

measurable quiescent current generates when the supply input voltage is above the minimum expected. The use of the traditional CM LS is constrained by its high power consumption. Bias currents produce a high quiescent current for CM-LS.

Here A 50% signal duty cycle is ensured by a balanced rising and falling delay. The monitoring duty cycle of WCM LS is crucial, when supply of input and output are near to one another. Due to a poor pull-up network, the WCM LS has a long rising edge of delay which is 100 times greater than the falling edge delay. So, signal skew develops [4].

Figure 1 represents TSCC, where a header NMOS decreases the pull-up driving intensity while increasing the convertible input voltage. The transistor size and V_t influence the LS's operating range. Given that this is a two-stage cross-coupling arrangement, the size inevitably grows.

Wilson current mirror structure that has been modified is depicted in Fig. 1. This design is also complies with the fundamental requirement of having a limited region for threshold level conversion. It is possible to convert levels in both directions, meaning that input and output levels can be adjusted separately. The rising and declining delays are likewise balanced by this arrangement. Less power is used as a result.

3 Design of Level Shifter

The design consists of a hybrid construction made up of CMOS logic gates, PTL-based buffers, and a self-biased cascade circuit of current mirror. The ranges of voltages as well as currents can be increased more quickly than with a mirror circuit by using a self-biased cascade current mirror. Low voltage analogue and mixed mode circuits can also benefit from it. The channel length modulation can be effectively suppressed using the cascade connection. Additionally, it lessens ratio mistakes brought on by a disparity between input and output voltages. The cascade design has the benefits of higher output impedance and a diminished impact of miller capacitance on the input. In order to maintain the high precision and high output impedance throughout a wide working range, the biasing mechanism is used to maintain the cascade transistor in the saturation region constantly.

Compared to CMOS levels of logic, the pass transistor based logical type is more power-efficient method. The source side of the logic transistor is connected to some input signals rather than the power supply, which are the primary distinction in-between pass transistor logic level and the CMOS logic level. The number of transistors is reduced in these logical levels since one pass transistor is enough to carry out the whole logic operation. In CMOS inverters, the input determines when the inverter trips. The output of invert is HIGH when the input is LOW. The inverter's output is LOW when the input is HIGH. However, with pass transistor logic, the inverter's output is dependent both on the input and the circuit input.

The fundamental building component that is extensively employed in analogue VLSI architecture is the current mirror. Applications requiring high performance analogue circuits should have extremely little sensitivity and temperature change. Additionally, it has a broad variety of operating frequencies. Figure 2 depicts the level shifter structure that has been suggested.

Transistors M1, M2, M3, and M4 are used to locate a cascade current mirror. Three major components make up the level shifter: a modified Wilsons current mirror, a delay circuit, and a OR gate of CMOS. A revised Wilson's circuit of current mirror

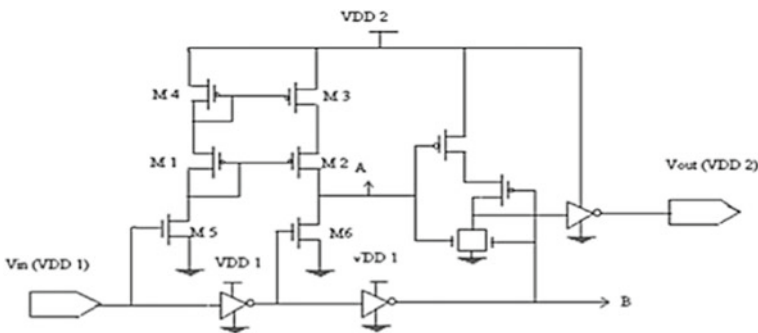


Fig. 2 Proposed circuit diagram

maintains the rising as well as falling down edge delays, but when the input and output levels are close to one another, a problem called skews occurs because the driving currents in the cascade PMOS are insufficient, which lengthens the rising delay [2]. A delay path is created to lessen the increasing latency. With the aid of inverters, which serve as a buffer, this delay path was created. The CMOS OR gate, which provides the right output and restricts leakage current, is finally present in the output stage. The cascade current mirror structure maintains the rising edge and falling edge delays at Node A when VDD1 is sub-threshold and VDD2 is high, preserving the initial static bias. The complementary OR gate's stacked PMOS transistors help to reduce leakage current while the CM-type structure provides a wide operating range.

In this circuit, two different kinds of OR gates are employed. One is a straightforward CMOS OR gate that uses static logic, and the other is a CMOS OR gate that uses dynamic logic, specifically Data Driven Dynamic Logic. When building traditional dynamic logic gates, one of the static logic's PDNs or PUNs must be removed, and a number of requirements must be placed on the inputs. All of the inputs of a Domino logic block must be low during the pre-charge period, whereas during the pre-charge phase of a P-block in NP-CMOS, all inputs must be high. There is no requirement for a clock signal because the relevant gate is pre-charged with a combination of input data. Data pre-charging may be utilized in place of clock pre-charging in this situation. As a result, this type of reasoning is known as D3L, or Data-Driven Dynamic Logic. One or more inputs are used in place of the clock signal in D3L. While D3L style only needs $n + 2$ transistors, n -input CMOS logic gates require $2n$ transistors. The OR gate is illustrated in Fig. 3 utilizing two different logic designs. It is obvious from this that employing D3L logic results in fewer transistors and, consequently, a smaller silicon surface area.

The expected technique reduces size and reduced capacitance, which increases speed and power dissipation. The increasing signal generated from Node A as well as Node B that reaches the cut off-point voltage rapidly causes VOUT to climb as input voltage rises. The voltage applied at point A leads to increases when applied VDD2 is greater than applied VDD1. The voltage applied at point B increases when applied

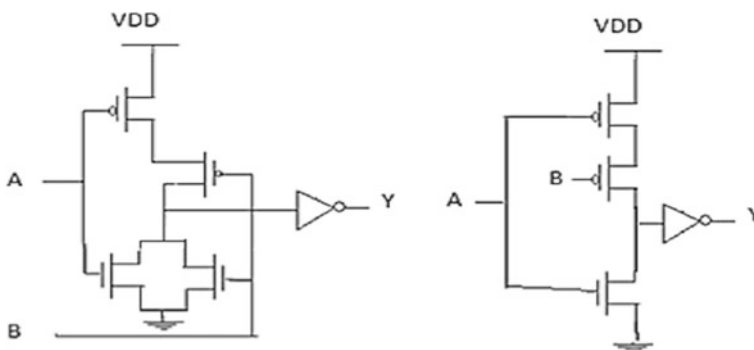


Fig. 3 CMOS logic level

VDD2 is lower than applied VDD1. The rising and falling delays of the cascade current mirror are comparable when VDD2 is significantly bigger than VDD1. When value of VDD2 is less than value of VDD1, two long channel length VDD1 inverters are employed to balance the rising and falling delays. For performance analysis, only low-Vt transistors (LVTs) were utilized. Circuit latency and power consumption are decreased while using these LVTs. High short circuit power is present when the input level is extremely low and the slew rate is slow. While PMOS LVTs lower the rising delay and voltage drop in this level shifter, NMOS LVTs reduce the required transition time to get output and also short-circuit which leads to power consumption from a circuit.

4 Simulation and Measurement Results

The suggested level shifter circuit's simulation is done using the Tanner tool. Using 22-nm technology, the modeling and measurement results were confirmed. The proposed level shifter circuit's minimum operating range is 200 mV or less.

The suggested level shifter circuit's four waveforms are shown on the basis of results in Fig. 4. The level shifter's input in this case is fixed at 200 mV. According to Fig. 4a–c, the VDD2 levels are 1200 mV, 800 mV, 500 mV respectively and 400 mV (d). The voltage drop, or V , in 22-nm technology is 100 mV.

5 Conclusion

A self-biased cascade current mirror wide range level shifter using PTL buffer is proposed in this paper. This design is useful for ultra-low power applications as well as full range and bidirectional level conversions. Minimum working voltage is sub-threshold voltage, which is close to the digital circuit's minimum supply voltage, and the maximum working supply voltage is rated working voltage specified for transistor based technic. The designed level shifter's power consumption is confirmed using transistor technology. Data-driven dynamic logic, or D3L, is a novel approach to dynamic logic discussed in this work. D3L is a more advanced form of D-logic consists of the pre charge and analyzing phases are performed without the use of an explicit clock and under the control of incoming data. Inverting functions are also included in this logic-style implementation. As a result, our proposed designs for D-D Dynamic Logic will be opted in the future to create OR gates that is faster and use less power.

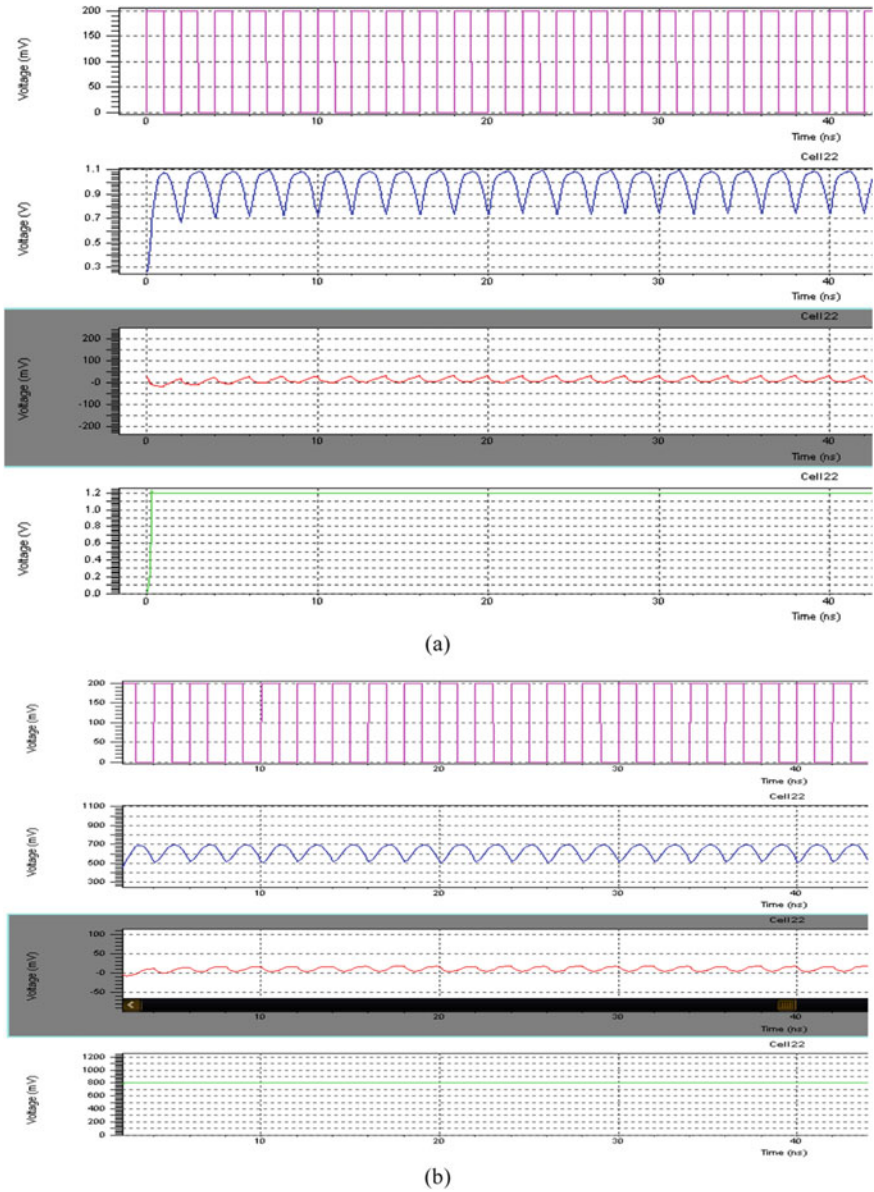
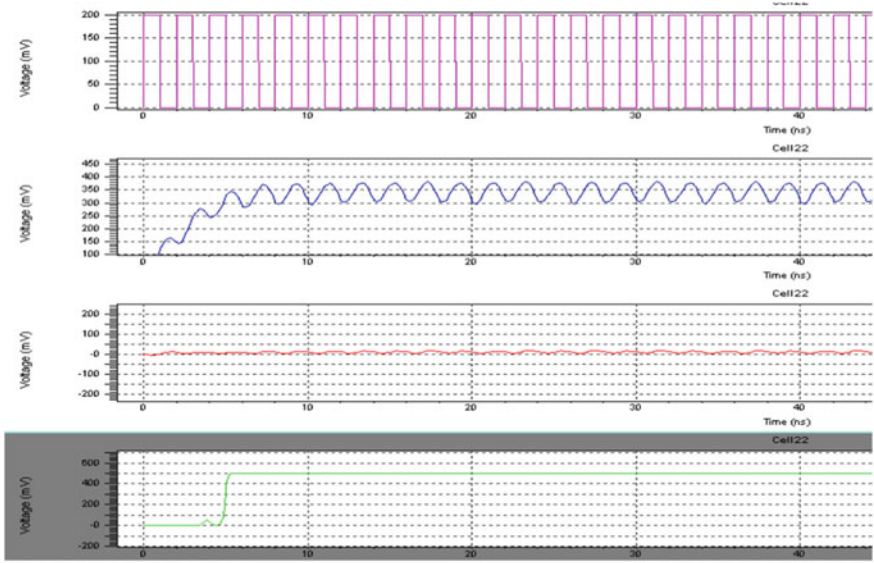
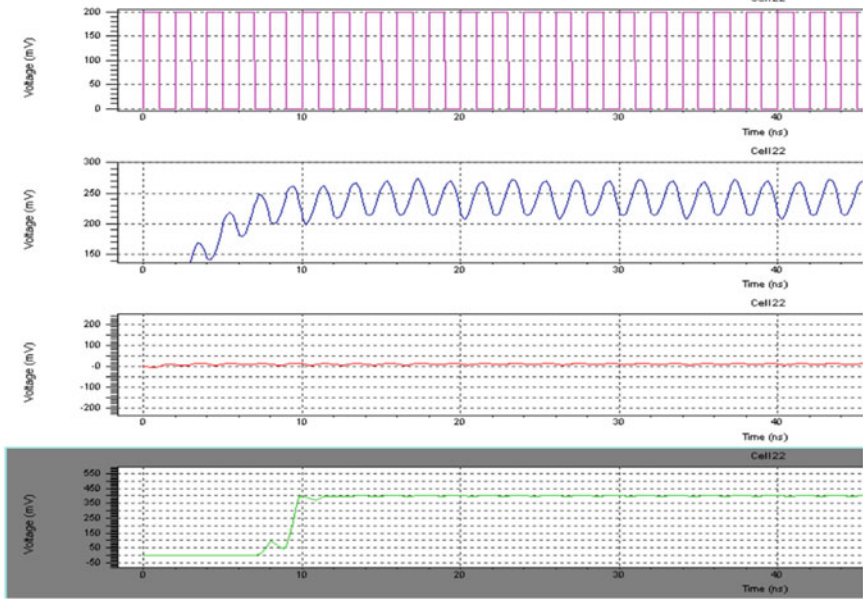


Fig. 4 Simulation waveform and corresponding power consumption: **a** 200–1200 mV, **b** 200–800 mV, **c** 200–500 mV, **d** 200–400 mV



(c)



(d)

Fig. 4 (continued)

References

1. Lanuzza, M., Corsonello, P., & Perri, S. (2012). Low-power level shifter for multi-supply voltage designs. *IEEE Transactions on Circuits and Systems II: Express Briefs*, 59(12), 922–926.
2. Lütkeemeier, S., & Rückert, U. (2010). A sub threshold to above-threshold level shifter comprising a Wilson current mirror. *IEEE Transactions on Circuits and Systems II: Express Briefs*, 57(9), 721–724.
3. Luo, S. C., Huang, C. J., & Chu, Y. H. (2014). A wide-range level shifter using a modified Wilson current mirror hybrid buffer. *IEEE Transactions on Circuits and Systems I: Regular Papers*, 61(6), 1656–1665.
4. Sugimoto, K. H. J., & Ino, F. (2013). Performance analysis of various level shifters using lecc. *International Journal of Advanced Research in Electrical, Electronics and Instrumentation Engineering*, 2(4).
5. Rafati, R., Fakhraie, S. M., & Smith, K. C. (2000, May). Low-power data-driven dynamic logic (D/sup 3/L) [CMOS devices]. In *2000 IEEE international symposium on circuits and systems (ISCAS)* (Vol. 1, pp. 752–755). IEEE.
6. Wooters, S. N., Calhoun, B. H., & Blalock, T. N. (2010). An energy-efficient sub threshold level converter in 130-nm CMOS. *IEEE Transactions on Circuits and Systems II: Express Briefs*, 57(4), 290–294.

Free Vibration Analysis of Functionally Graded Skew Sandwiched Plates by Using a New Discrete Kirchhoff Quadrilateral Element



G. A. Deshpande and R. S. Parekar

Abstract In the present work, a four-node quadrilateral element is developed for the free vibration analysis of functionally graded moderately thick skew sandwich plates. The element has seven degrees of freedom per node namely, two in-plane displacements, the transverse displacement, two rotations of mid plane and two transverse shear strain components at the mid plane. In the present study, Rule of Mixture model is considered. The results for skew sandwich plates with different thickness configurations and with different boundary conditions are compared with the finite element ANSYS results. It is observed that the performance of the present element is quite satisfactory for the sandwich plates considered in this study.

Keywords Functionally graded material · Finite element · Quadrilateral element · Third order theory · Skew sandwich plates

1 Introduction

Functionally graded materials (FGM) are being increasingly used in aeronautical and aerospace industry as well as in other fields of modern technology, especially where structures are subjected to high temperatures. Functionally graded materials normally consist of two phases, namely; the metal phase and the ceramic phase. Ceramic acts as thermal barrier and the metal gives required ductility. The FGM have advantage over the laminated composites. The delamination problem which is normally observed in laminated composites is totally absent in FGM because of the smooth variation of material properties through the thickness. This material is mainly used as thermal barrier material. In 1984 Japanese scientists invented the novel concept of FGM. Since then FGMs are being increasingly used in the aeronautical and aerospace industry as well as in other fields of modern technology. In propulsion systems and airframe of the space planes lot of heat and thermal stresses are induces,

G. A. Deshpande (✉) · R. S. Parekar
Department of Civil Engineering, Rajarshi Shahu College of Engineering, Tathawade, Pune, India
e-mail: girijadeshpande2@gmail.com

therefor FGM is used in space planes for decrease these thermal stresses and also for protection from heat. FGM composition can vary from ceramic rich material to metal rich material by varying the volume fractions of the two materials. Thermal conductivity of ceramic is very low and metal is good in reducing tensile stresses this together can help in enhancing the properties of thermal barrier. Several studies have been performed to analyze the behaviour of functionally graded Plates and Shells. In this work the four-node quadrilateral element having seven degrees of freedom per node, developed earlier by the first author for FG sandwich plates is used for free vibration analysis of functionally graded skew sandwich plates.

The FGM structures are normally modelled as plates and shells and determination of their natural frequencies is essential in many applications. Many researchers have presented 3D exact as well as 3D approximate solutions for the free vibration response of FG plates. 3D exact solution is presented for free and forced vibration of simply supported functionally graded rectangular plates by Vel and Batra [1]. Results are also computed for a functionally graded plate that has a varying microstructure in the thickness direction using a combination of the Mori–Tanaka and the self-consistent methods.

Many researchers have also developed 2D analytical solutions based on 2D theories. Kalhori et al. [2] have analysed FG rectangular plates based on Mori–Tanaka homogenization scheme for vibration response using first order shear deformation theory (FSDT). Zenkour [3] has also studied buckling and free vibration analysis of functionally graded sandwich plates using sinusoidal shear deformation plate theory. Exact free vibration analysis of Levy FG plates using higher-order shear and normal deformation theories is given by Dozio [4].

2D analytical solutions also are not available for complex geometries and for complicated boundary conditions, therefore many researchers have employed 2D finite element technique. Natarajan and Manickam [5] used an eight-node finite element with 13 DOF per node based on their accurate theory for bending and vibration analysis of FGM sandwich plates. A continuous Lagrangian quadrilateral nine-noded element with eight degrees of freedom per node based on a new hyperbolic higher-order shear and normal deformation theory (HHSNDT) is employed by Gupta and Talha [6] for the large amplitude vibration analysis of FGM plates. An eight-noded C^0 isoparametric element with 13 degrees of freedom per node based on Layer wise theory is used by Pandey and Pradyumna [7] to develop the finite element model to determine thermally induced vibrations of FGM sandwich plates and shell panels.

Reddy's third order shear deformation theory (TOT) [8] is one of the best available 2D theories for the analysis of moderately thick FG plates but the finite element formulation based on this theory faces a problem of C^1 continuity. Thus it is difficult to develop a four node quadrilateral element based on Reddy's theory. Kulkarni and Kapuriya [9, 10] earlier developed a four node discrete Kirchhoff quadrilateral element for the analysis of laminated composite and sandwich plates wherein the problem of C^1 continuity was successfully circumvented. The present author modifying the four node discrete Kirchhoff quadrilateral element of [10] have analysed a single layer FG plate for free vibration response under thermal environment [11].

In the present work the four node discrete Kirchhoff quadrilateral element of [11] is modified for the analysis of FG skew sandwich plates. The element has seven degrees of freedom per node namely, two in-plane displacements, the transverse displacement, two rotations of mid-plane and two transverse shear strain components at the mid plane. The results of the non-dimensionalised frequencies for a square, all round simply supported, FG skew sandwich plates are validated by comparing them with the 2D FE results obtained using ANSYS. It is observed that the performance of the present element is excellent and its use is recommended.

2 Formulation

Consider a FGM sandwich plate (Fig. 1) of total thickness h with the top and the bottom layers made of functionally graded material. The middle layer is of ceramic. Mid surface of the plate is considered as reference plane where $z = 0$ and the top and the bottom surfaces are at $z = \frac{h}{2}$ and $z = -\frac{h}{2}$, respectively.

2.1 Material Properties

The functionally graded sandwich plates where variation of material properties is as per power law.

$$P(z) = P_b + (P_t - P_b) \left(\frac{2z + h}{2h} \right)^n \tag{1}$$

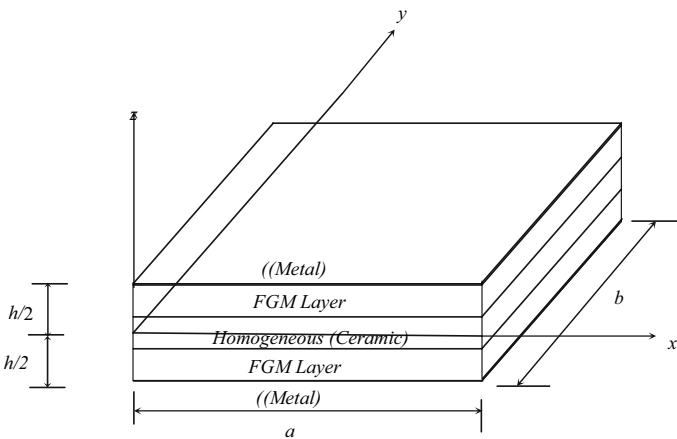


Fig. 1 Geometry of a FGM sandwich plate

where n is the volume fraction index, P_b and P_t are the material properties at the bottom and the top of the layer respectively and h is the thickness of the layer. Poissons ratio is assumed to be same for both the materials.

2.2 Displacement Field Approximation for Reddy's Third Order Theory

Let $u_x, u_y; w$ be the in-plane and transverse displacements. The normal strain components $\varepsilon_x, \varepsilon_y, \varepsilon_z$, and shear strain components γ_{xy}, γ_{yz} and γ_{zx} are related to the displacements by

$$\begin{aligned}\varepsilon_x &= u_{x,x}, \varepsilon_y = u_{y,y}, \\ \varepsilon_z &= w_z, \gamma_{xy} = u_{x,y} + u_{y,x}, \\ \gamma_{yz} &= u_{y,z} + w_y, \gamma_{zx} = u_{x,z} + w_x\end{aligned}\quad (2)$$

where a subscript comma denotes differentiation. Like most other 2D plate theories, the transverse normal stress σ_z is neglected ($\sigma_z \simeq 0$) in comparison with other stress components. In the third order theory of Reddy [8], the deflection w is approximated to be independent of z and the in plane displacements u_x, u_y are approximated as a cubic variation in z across the thickness:

$$w(x, y, z, t) = w_0(x, y, t), \quad (3)$$

$$\begin{aligned}u(x, y, z, t) &= u_0(x, y, t) - zw_{0d} + z\psi_0(x, y, t) \\ &\quad + z^2\xi(x, y, t) + z^3\eta(x, y, t),\end{aligned}\quad (4)$$

$$\begin{aligned}u &= \begin{bmatrix} u_x \\ u_y \end{bmatrix}, \omega_{0d} = \begin{bmatrix} \omega_{0,x} \\ \omega_{0,y} \end{bmatrix}, \\ u_0 &= \begin{bmatrix} u_{0,x} \\ u_{0,y} \end{bmatrix}, \Psi_0 = \begin{bmatrix} \Psi_{0,x} \\ \Psi_{0,y} \end{bmatrix}, \\ \xi &= \begin{bmatrix} \xi_x \\ \xi_y \end{bmatrix}, \eta = \begin{bmatrix} \eta_x \\ \eta_y \end{bmatrix}\end{aligned}\quad (5)$$

ξ, η are obtained by satisfying the shear traction-free conditions $T_{zx} = T_{yz} = 0$ at $z = \frac{h}{2}$ and $z = -\frac{h}{2}$.

$$\begin{aligned}\xi_x &= 0, \quad \xi_y = 0, \\ \eta_x &= R(z)\psi_0 \quad \eta_y = R(z)\psi_{0y},\end{aligned}\quad (6)$$

Substituting values for ξ , η from Eq. (6) into Eq. (4) yields

$$u(x, y, z, t) = u_0(x, y, t) - zw_{0d} + R(z)\psi_0(x, y, t). \quad (7)$$

where, $R(z)$ is defined as

$$R(z) = z - \frac{4z^3}{3h^2} \quad (8)$$

2.3 Finite Element Formulation

The four node quadrilateral element formulation is based on Reddy's third order theory. Stiffness coefficients \bar{Q}_{ij} are defined as:

$$\begin{aligned} \bar{Q}_{11} = \bar{Q}_{22} &= \frac{E(z)}{1 - \nu^2} \\ \bar{Q}_{12} = \bar{Q}_{21} &= \frac{\nu E(z)}{1 - \nu^2} \\ \bar{Q}_{16} = \bar{Q}_{26} &= 0 \\ \bar{Q}_{44} = \bar{Q}_{55} = \bar{Q}_{66} &= \frac{E(z)}{2(1 + \nu)} \end{aligned}$$

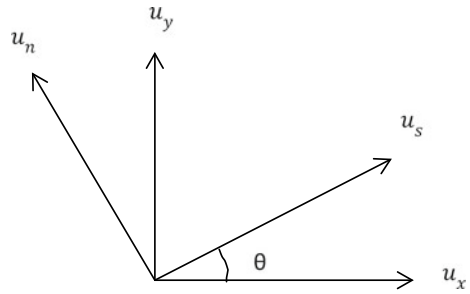
Principle of virtual work is used for obtaining stiffness matrix and mass matrix. Details regarding the interpolation functions are given in [12].

2.4 Transformations of Generalized Displacements

In case of skew plates, for assigning boundary conditions to simply-supported edge which is not parallel to the global axis, transformation of displacements from global to local axes is necessary. To achieve this, the following procedure is used for relating the displacement variables in (s, n) coordinates are related to those in (x, y) coordinates. Let (x, y) be the global axes and (s, n) be the local axes. Let the in-plane displacements u_x and u_y be positive as shown in (Fig. 2). Let θ be the angle made by the s axis with the x as shown. Then the displacement variables u_s and u_n in (s, n) co-ordinates are related to those in (x, y) co-ordinates by:

$$\begin{bmatrix} u_s \\ u_n \end{bmatrix} = \begin{bmatrix} s_x & s_y \\ -s_y & s_x \end{bmatrix} \begin{bmatrix} u_x \\ u_y \end{bmatrix} \quad (9)$$

Fig. 2 Local and global in-plane displacement



where $s_x = \cos\theta$ and $s_y = \sin\theta$.

Similarly let the rotation variables $w_{0,x}$, $w_{0,y}$ and the shear strains $\psi_{0,x}$ and $\psi_{0,y}$ be considered positive. Then these displacement variables in (s, n) co-ordinates are related to those in (x, y)

$$\begin{bmatrix} w_{0,s} \\ w_{0,n} \end{bmatrix} = \begin{bmatrix} s_x & s_y \\ -s_y & s_x \end{bmatrix} \begin{bmatrix} w_{0,x} \\ w_{0,y} \end{bmatrix} \tag{10}$$

$$\begin{bmatrix} \varphi_{0,s} \\ \varphi_{0,n} \end{bmatrix} = \begin{bmatrix} s_x & s_y \\ -s_y & s_x \end{bmatrix} \begin{bmatrix} \varphi_{0,x} \\ \varphi_{0,y} \end{bmatrix} \tag{11}$$

3 Numerical Results

A typical skew plate is shown in (Fig. 3). In order to assess the performance of the developed element for non-rectangular plates, square sandwich FG skew Plates, where core is made up of ceramic with functionally graded face sheet. Thickness configuration 1-1-1 and 2-1-2 are analysed for two different skew angles $\alpha = 15^\circ$ and 30° , with side to thickness ratio as $S = 10$. Comparison of results obtained from present element for skew sandwich plates with 2D ANSYS are shown in the following tables. Material properties for skew sandwich plate are as below.

Aluminum (metal) and Alumina (ceramic)

$$E_m = 70 \text{ GPa,}$$

$$\rho_m = 2707 \text{ kg/m}^3$$

$$E_c = 380 \text{ GPa,}$$

$$\rho_c = 3800 \text{ kg/m}^3$$

Poissons ratio = 0.3 (aluminum and alumina).

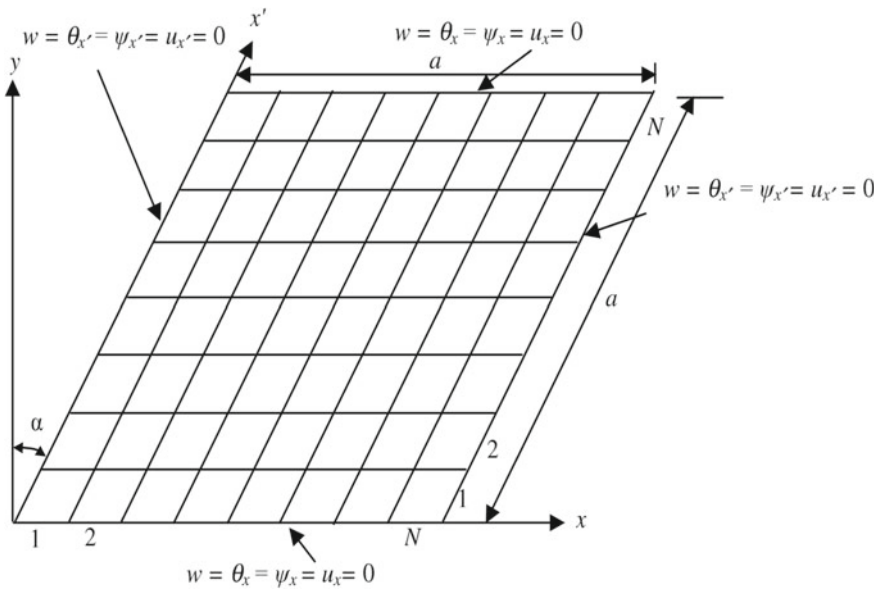


Fig. 3 A simply-supported skew plate with $N \times N$ mesh

3.1 Convergence Study

The results of present element for non-dimensionlised frequencies obtained by discretising the full plate with following three mesh sizes $N \times N = 12 \times 12, 16 \times 16$ and 20×20 , are compared with the 2D finite element (FE) results obtained using the commercial software ANSYS [13]. The results of the first five non-dimensionlised natural frequencies for all edges simply supported and all edges clamped square FG skew sandwich plates with $a/h = 10$ and thickness configurations 1-1-1 and $n = 5$ are presented in Table 1. Two different skew angles 15 and 30 are considered here.

The results are compared with the 2D finite element (FE) results obtained using the commercial software ANSYS [13]. ANSYS [13] results are obtained by dividing the top and the bottom FG layers of plate each into 25 layers in the thickness direction. And the central homogeneous core part is considered as one single layer. Thus a complete sandwich plate is split into 51 layers in the thickness direction. It is assumed that the material properties are different in the different layers but in a layer they are assumed to be constant and are obtained at the midpoint of each layer. The Shell 181 element with a mesh size of 20×20 is used for obtaining the ANSYS [13] results. It appears that though the results are quite close to the results obtained by ANSYS, they are not converging to ANSYS results, as ANSYS results are based of FSDT.

Table 1 First five frequencies in Hz for Al/Al₂O₃ sandwich square plate with configuration 1-1-1 and n = 5

Skew angle	Boundary condition	Mesh size	$\bar{\omega}_1$	$\bar{\omega}_2$	$\bar{\omega}_3$	$\bar{\omega}_4$	$\bar{\omega}_5$
15	SSSS	12 × 12	3487.15	7857.13	9092.50	12,538.07	14,432.45
		16 × 16	3488.23	7865.03	9100.03	12,565.92	14,395.10
		20 × 20	3488.67	7868.89	9103.49	12,579.55	14,376.21
		2D ANSYS	3364.70	7723.14	8898.76	12,261.70	14,982.82
	CCCC	12 × 12	6200.56	11,475.58	12,908.96	16,714.90	20,853.67
		16 × 16	6201.24	11,469.52	12,902.31	16,715.11	20,808.40
		20 × 20	6200.73	11,464.33	12,896.14	16,710.33	20,781.67
		2D ANSYS	6160.33	11,460.96	12,868.38	16,693.11	20,970.18
30	SSSS	12 × 12	4185.29	8550.95	11,564.24	13,278.48	13,940.16
		16 × 16	4175.53	8558.37	11,549.58	13,296.58	13,793.43
		20 × 20	4169.56	8562.15	11,539.95	13,305.63	13,707.81
		2D ANSYS	3999.92	8449.74	11,265.69	13,115.15	17,656.22
	CCCC	12 × 12	7414.89	12,716.05	16,104.86	18,018.15	24,135.44
		16 × 16	7416.45	12,710.49	16,098.01	18,015.64	24,126.46
		20 × 20	7416.05	12,705.25	16,090.26	18,009.64	24,116.63
		2D ANSYS	7345.72	12,683.09	15,993.90	18,023.60	24,298.58

3.2 Comparisons with Different Skew Angles

The results of the first four non-dimensionalised natural frequencies for all edges simply supported square FG skew sandwich plates with skew angle 15° and 30° are presented in Tables 2 and 3 respectively. The a/h = 10 and thickness configurations, 1-1-1 and 2-1-2 are presented for n = 1, 2 are presented in Tables 2 and 3. It is also observed that for this case of ROM, as the value of volume fraction index n increases the non-dimensionalised frequencies decrease for all the thickness configurations. It is also observed that the results obtained for skew sandwich FGM plates with different skew angles and with two different boundary conditions are quite close to the 2D FE results of ANSYS. With the increase in skew angle the natural frequencies increases.

Table 2 First four frequencies in Hz for Al/Al₂O₃ all-round simply supported sandwich square plate with skew angle = 15°

Thickness configuration	Volume fraction	Results	$\bar{\omega}_1$	$\bar{\omega}_2$	$\bar{\omega}_3$	$\bar{\omega}_4$
1-1-1	1	Present	4517.96	10,119.37	11,685.08	15,991.98
		2D ANSYS	4401.28	10,071.24	11,584.72	15,921.06
		% difference	2.651	0.478	0.866	0.445
	2	Present	3968.20	8922.83	10,314.14	14,220.38
		2D ANSYS	3875.01	8888.08	10,233.89	14,109.28
		% difference	2.405	0.391	0.784	0.787
2-1-2	1	Present	4340.48	9729.89	11,237.81	15,459.88
		ANSYS	4212.81	9634.15	11,084.20	15,144.85
		% difference	3.031	0.994	1.386	2.080
	2	Present	3747.87	8434.09	9751.30	13,452.21
		ANSYS	3661.11	8398.87	9671.83	13,339.98
		% difference	2.370	0.419	0.822	0.841

Table 3 First four frequencies in Hz for Al/Al₂O₃ all-round simply supported sandwich square plate with skew angle = 30°

Thickness configuration	Volume fraction	Results	$\bar{\omega}_1$	$\bar{\omega}_2$	$\bar{\omega}_3$	$\bar{\omega}_4$
1-1-1	1	Present	5392.21	10,999.28	14,756.68	15,248.46
		2D ANSYS	5261.32	11,067.24	14,699.60	17,013.78
		% difference	2.488	-0.614	0.388	-10.376
	2	Present	4739.70	9704.38	13,052.45	14,526.77
		2D ANSYS	4583.71	9667.43	12,869.60	14,943.26
		% difference	3.403	0.382	1.421	-2.787
2-1-2	1	Present	5181.23	10,577.24	14,198.10	14,825.95
		ANSYS	5003.46	10,532.82	13,997.49	16,216.22
		% difference	3.553	0.422	1.433	-8.573
	2	Present	4477.26	9173.94	12,345.61	13,880.50
		ANSYS	4331.25	9136.77	12,166.24	14,131.26
		% difference	3.371	0.407	1.474	-1.774

4 Conclusions

The results for the non-dimensionalised natural frequencies obtained with the developed four node discrete kirchhoff quadrilateral element, based on Reddy’s third order theory, for free vibration response of FG skew sandwich plates are compared in this work with 2D finite element results of ANSYS. It is observed that for different

thickness configuration, with two different skew angles, the present element is giving excellent performance for all the cases considered in this study. Maximum percentage difference between the present results obtained with mesh size 20×20 and 2D FE results of ANSYS is less than 3.6% for fundamental natural frequency. This percentage difference is observed because the present results are based on Third Order Theory and ANSYS results are based on First order shear deformation theory. Till date commercial software packages do not provide the facility for the analysis of functionally graded plates and shell. There library of element does not support such element. In present work ANSYS results are obtained by dividing the plate in 25 or 50 layers in thickness direction. It is assumed that the material properties are different in different layers but in a layer they are assumed to be constant and are obtained at the midpoint of each layer. This is quite tedious and time consuming job. On the other hand programming with current developed element gives quick results with less computational efforts. Hence present developed technique which is completely innovative can be used in aerospace industry for finite element analysis of functionally graded plates and shell.

References

1. Li, Q., Iu, V. P., & Kou, K. P. (2008). Three-dimensional vibration analysis of functionally graded material sandwich plates. *Journal of Sound and Vibration*, 311(12), 498–515.
2. Kalhori, H., Akhavan, H., Hossein Rokni, D. T., & Alibeigloo, A. (2009). Vibration analysis of functionally graded rectangular plates based on Mori-Tanaka homogenization scheme. In *7th EUROMECH solid mechanics conference (ESMC/7)*, Lisbon, Portugal, 7–11 September 2009.
3. Zenkour, A. M. (1819). A comprehensive analysis of functionally graded sandwich plates: Part 2 Buckling and free vibration. *International Journal of Solids and Structures*, 2005(42), 5224–5242.
4. Dozio, L. (2014). Exact free vibration analysis of Lvy FGM plates with higher-order shear and normal deformation theories. *Composite Structures*, 111, 415–425.
5. Natarajan, S., & Manickam, G. (2012). Bending and vibration of functionally graded material sandwich plates using accurate theory. *Finite Elements in Analysis and Design*, 57, 32–42.
6. Gupta, A., & Talha, M. (2017). Large amplitude free flexural vibration analysis of finite element modeled FGM plates using new hyperbolic shear and normal deformation theory. *Aerospace Science and Technology*, 67, 287–308.
7. Pandey, S., & Pradymna, S. (2017). A finite element formulation for thermally induced vibrations of functionally graded material sandwich plates and shell panels. *Composite Structures*, 160, 877–886.
8. Reddy, J. N. (1984). A simple higher order theory for laminated composite plates. *ASME Journal of Applied Mechanics*, 51, 745–752.
9. Kulkarni, S. D., & Kapuriya, S. (2007). An improved discrete Kirchhoff quadrilateral element based on third-order zigzag theory for static analysis of composite and sandwich plates. *International Journal of Numerical Methods in Engineering*, 69(9), 1948–1981.
10. Kulkarni, S. D., & Kapuriya, S. (2008). Free vibration analysis of composite and sandwich plates using an improved discrete Kirchhoff quadrilateral element based on third-order zigzag theory. *Computational Mechanics*, 42, 803–824.
11. Deshpande, G. A., & Kulkarni, S. D. (2019). Free vibration analysis of functionally graded plates under uniform and linear thermal environment. *Acta Mechanica*, 230(4), 1347–1354.

12. Kulkarni, S. D., Trivedi, C. J., & Ishi, R. G. (2015). Static and free vibration analysis of functionally graded skew plates using a four node quadrilateral element. In *Advances in structural engineering*. Springer India Publications, 15–24.
13. ANSYS, Academic Research, Release 17.2.

Wideband MIMO Antenna Design for Ku Band Application



Aditi Bhardwaj, Mohammad Mushaib, Mohd. Gulman Siddiqui, and Poonam Tiwari

Abstract The design of a multiple-input, multiple-output (MIMO) antenna is presented in this paper for Ku band application. There will be two unfilled L-shaped slot (LS) antenna elements plus a small ground plane slots include the antenna. The suggested MIMO antenna uses an RT duroid substrate and has a small dimension of 32 mm² at high frequency. The findings indicate that for frequencies between 8 and 14 GHz, the return loss is 10 dB.

Keywords Wideband · Patch antenna · Ku band · MIMO · HFSS

1 Introduction

In wireless communication systems, the use of a microstrip antenna is a success that satisfies a need created by fresh invention and the era of wireless communication technology that is currently in use. Because of their many benefits [1], including their extremely low weight, flat construction, and extremely high efficiency, microstrip antennas are used in each of these systems. Its disadvantage is a small operational bandwidth, which limits how it may be used in wireless systems [2]. Wireless devices and broadband programmers that perform a variety of activities have become an essential component of our daily correspondence lives. As a result, the requirement for discrete wideband has decreased [3]. Most criteria for mobile and satellite are met by microstrip antennas equipment, and their use allows for the fulfillment of many commercial needs. The microstrip is useful because it can reduce the amount of electronic circuits needed for wireless applications. The dimensions

A. Bhardwaj (✉) · Mohd. G. Siddiqui · P. Tiwari
Department of Physical Sciences, Banasthali Vidyapith, Aliyabad, Rajasthan, India
e-mail: aditibhardwaj1602@gmail.com

M. Mushaib
Department of Electronics and Communication, University of Agriculture Technology and Sciences, Sam Higginbottom, Prayagraj, Uttar Pradesh, India

of the antennas utilized for majority of applications is also substantially decreasing. Microstrip antennas match these requirements with design fulfillment. The correct bandwidth of the microstrip antenna's impedance was discovered to be one factor for enhancement when various strategies were taken into account [4–6].

The following equations are used to determine the antenna's length, L , and width, W .

$$W = \frac{c}{2f} x \frac{\sqrt{2}}{\epsilon_r + 1} \quad (1)$$

$$L = \frac{c}{2f} \left[\frac{\epsilon_r + 1}{2} + \frac{\epsilon_r - 1}{2} \sqrt{\left(1 + 12 \frac{h}{w}\right)} \right]^{\frac{-1}{2}} - 2\Delta L \quad (2)$$

The substrate's dielectric constant ϵ_r is given here.

For wireless local area networks and 5G communications, MIMO communication techniques there have developed in response to the expanding demands for big communication capacity and high data speeds. MIMO antennas have undergone substantial research as a key technology [7–11].

2 Proposed MIMO Antenna Design

2.1 Design of Antennas

The geometry of both the proposed $32 \times 32 \text{ mm}^2$ Ku-band MIMO antenna is illustrated in Fig. 1. It is printed on a Rogers RT/Duroid substrate with a 2.2 relative permittivity which is 0.8 mm thick. The dimensions of a Ku-band open L-shaped slot antenna described in [12] are used as a model and are modified to achieve a smaller size. Two L-shaped slot antenna elements, denoted LS1 and LS2, form up the proposed MIMO antenna. It is constructed so that the two LSs are perpendicular to one another to provide adequate isolation between the two antenna elements. An L-shaped slot and a rectangular patch that are both fed by a 50 microstrip line make the element antenna. To increase Ku band bandwidth, the rectangular patch is attached to a T-shaped stub.

Figure 1 illustrates the design and accurate measurements of the proposed MIMO antenna. The above are the different antenna model which includes: 35 mm is width, 35 mm in length, 1mm in slot width, and 13 mm is slot length. For versatility, a Rogers RT/Duroid 5880 substrate with a 0.8 mm thickness and a 2.2 r value is used.

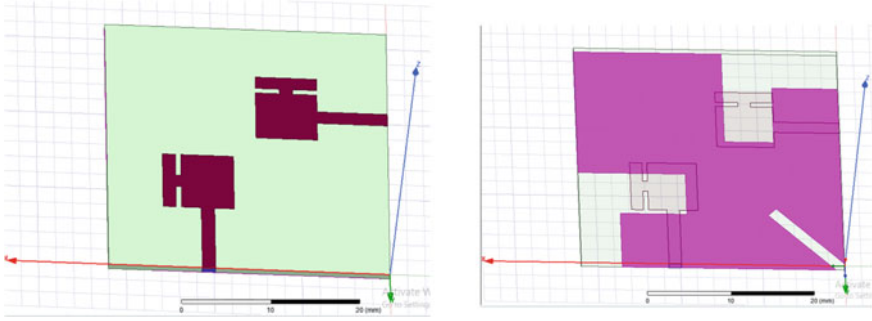


Fig. 1 Top view of the proposed antenna's geometry

3 Results and Discussion

3.1 Loss of Return and Port Isolation

The L-slot MIMO antenna described in Section II has a working model. The ANYSS Hfss is used to assess the proposed antenna's bandwidth performance. Figure 2a, b show the suggested antenna's computed parameters (b). Both the LS1 and LS2 have a bandwidth of more than 8–14 GHz for dB and dB, as shown in Fig. 2a. The antenna complies with the Ku band's impedance matching criterion. Figure 2 depicts the mutual connection between the two input ports for simulation and measurement. (b). That is apparent across the entire Ku band. The antenna is suited for MIMO applications since Ku Band applications only call for mutual coupling of less than 14 dB.

3.2 Gain

See Fig. 3.

3.3 VSWR

See Fig. 4.

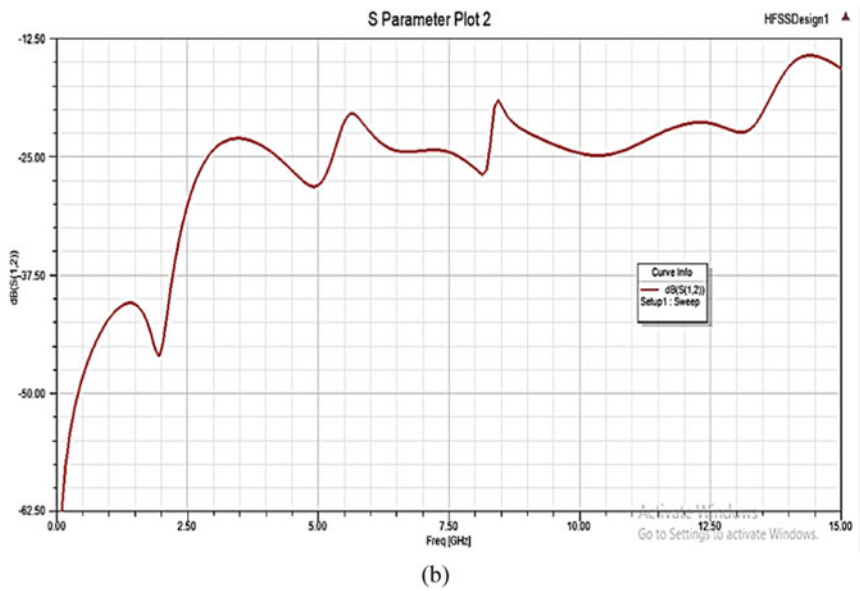
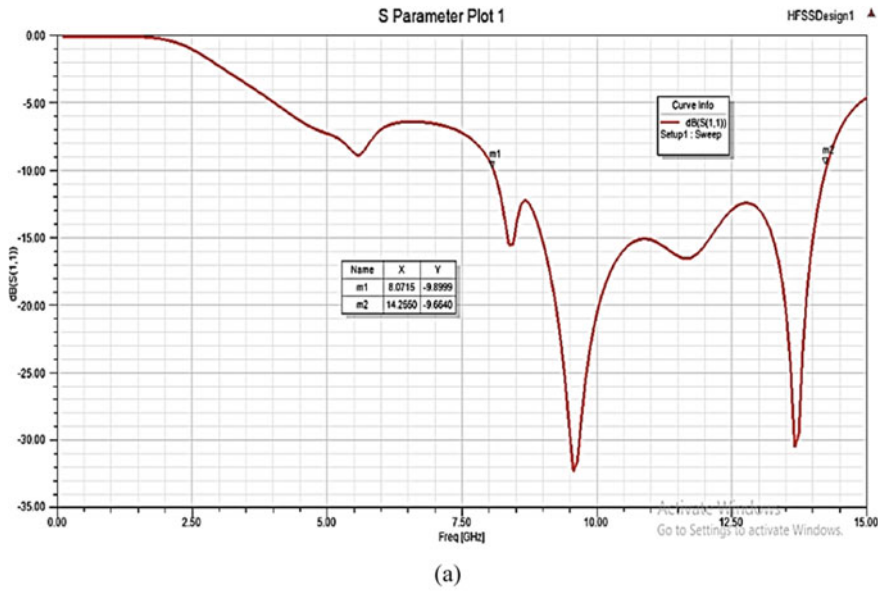


Fig. 2 a Simulated S11 parameters, b simulated S12 parameters

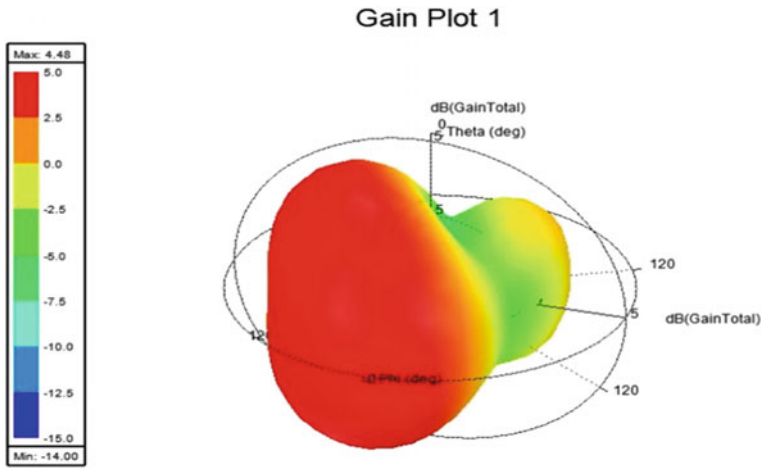


Fig. 3 Polar plot of gain

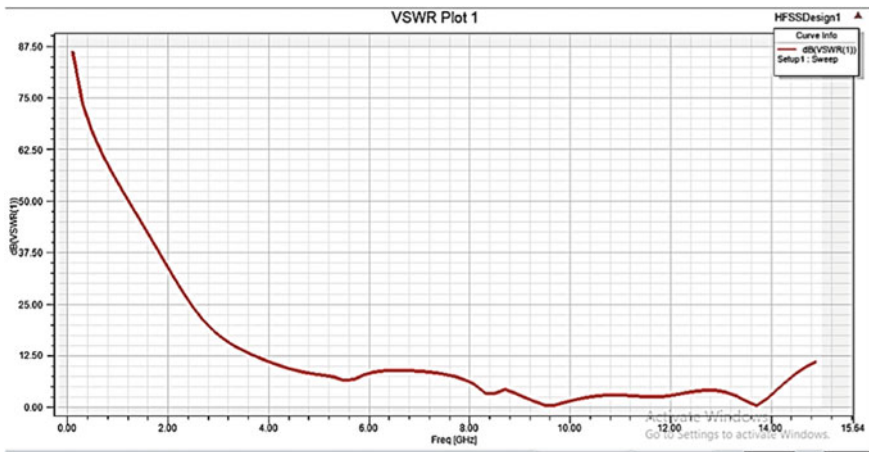


Fig. 4 VSWR

3.4 Radiation Pattern

See Fig. 5.

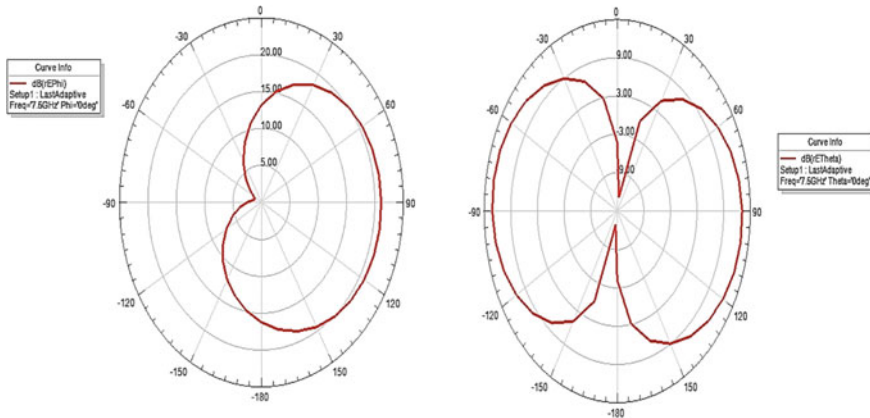


Fig. 5 The proposed antenna's measured radiation pattern

4 Conclusion

For use in Ku band applications, a compact MIMO antenna with two open L-shaped slot elements is shown. A tiny slit is provided to the ground plane to decrease contact between both the antenna parts. Using the simulation results, the suggested antenna achieves a low mutual coupling of less than 14 dB across the entire Ku band and an impedance bandwidth of greater than 8–14 GHz. The outcomes of the tests indicate that the suggested antenna is a promising choice for Ku band uses.

References

1. Garg, R., Bhartia, P., Bahl, I. J., & Ittipiboon, A. (2001). *Microstrip antenna design handbook*. Artech House.
2. Mishra, R., Mishra, R. G., Chaurasia, R. K., & Shrivastava, A. K. (2019). Design and analysis of microstrip patch antenna for wireless communication. *International Journal of Innovative Technology and Exploring Engineering*, 8(7), 663–666.
3. Coulibaly, Y., Denidni, T. A., & Boutayeb, H. (2008). Broadband microstrip-fed dielectric resonator antenna for X-band applications. *IEEE Antennas and Wireless Propagation Letters*, 7, 341–345.
4. Kim, D. Z., Son, W. I., Lim, W. G., Lee, H. L., & Yu, J. W. (2010). Integrated planar monopole antenna with microstrip resonators having band-notched characteristics. *IEEE Transactions on Antennas and Propagation*, 58(9), 2837–2842.
5. Mishra, R., Jayasinghe, J., Mishra, R. G., & Kuchhal, P. (2016). Design and performance analysis of a rectangular microstrip line feed ultra-wide band antenna. *International Journal of Signal Processing, Image Processing and Pattern Recognition*, 9(6), 419–426.
6. Kuchhal, P., Ramful, G. H., Mishra, R. G., & Mishra, R. (2020, September). Design and analysis of CPW-fed microstrip patch antenna for ISM band applications. In *2020 international conference on smart electronics and communication (ICOSEC)* (pp. 955–960). IEEE.

7. Wong, K. L., Jian, M. F., Chen, C. J., & Chen, J. Z. (2021). Two-port same-polarized patch antenna based on two out-of-phase TM₁₀ modes for access-point MIMO antenna application. *IEEE Antennas and Wireless Propagation Letters*, 20(4), 572–576.
8. Kishor, K. K., & Hum, S. V. (2013). A two-port chassis-mode MIMO antenna. *IEEE Antennas and Wireless Propagation Letters*, 12, 690–693.
9. Yetisir, E., Chen, C. C., & Volakis, J. L. (2013). Low-profile UWB 2-port antenna with high isolation. *IEEE Antennas and Wireless Propagation Letters*, 13, 55–58.
10. Tao, J., & Feng, Q. (2016). Compact ultrawideband MIMO antenna with half-slot structure. *IEEE Antennas and Wireless Propagation Letters*, 16, 792–795.
11. Nie, L. Y., Lin, X. Q., Xiang, S., Wang, B., Xiao, L., & Ye, J. Y. (2020). High-isolation two-port UWB antenna based on shared structure. *IEEE Transactions on Antennas and Propagation*, 68(12), 8186–8191.
12. Liu, L., Cheung, S. W., & Yuk, T. I. (2013). Compact MIMO antenna for portable devices in UWB applications. *IEEE Transactions on Antennas and Propagation*, 61(8), 4257–4264.

Electronic Shoe to Assist Visually Challenged People



Salma S. Shahpur, Mahanthgouda Patil, Vikas Bandi, Kiran Patil, and Gopal Lamani

Abstract This paper serves the intention to help visually challenged people by contributing a model which includes the latest technologies to serve systematic and smart electronic tools in the shoe of those who are in need. We have implemented ultrasonic technology. It works with GPS technology and will send an alarm in the form of SMS to the enrolled mobile number in unease situations. The core purpose of this is to serve an easy and comfortable navigation tool for the or visually disabled which help with them in unreal vision by giving instruction about the environment out sketches living and nonliving objects present in the surrounding. The evolution in wearable devices with its latest inventions and growth in technology has brought innovation and has revolted the smart shoe technology. These are sometimes cited as computer-based or intelligent shoes. Even smart shoes have the potential to identify and keep an account on day to day task of the user. To pull up the extra work, such shoes are built with sensors, vibrating motors, GPS. In this paper, we have analyzed the different technologies that have been put into practice in smart shoes.

Keywords Obstacle detection · Fall detection · Sending SMS to the registered number

1 Introduction

Darkness, Myopia, low imagination and prescience, visible disfigurement, and lack of imagination and prescient have sizable influences on a man or woman stricken by this type of disabilities [1]. These holds the mental, physical, social and financial results, finally this incapacity impacts the first-class in their lifestyles and motive downside for a person from performing daily task and one of the essential undertaking is to transport from one vicinity to any other vicinity [2]. Blindness is an approximate time period which reviews the medical conditions, wherein people are stricken by incapability to stumble upon light, is a final result of absolute blindness [3]. It is

S. S. Shahpur (✉) · M. Patil · V. Bandi · K. Patil · G. Lamani
Department of Electronics and Communication, Jain College of Engineering, Belagavi, India
e-mail: salma.jce@gmail.com

(blindness) additionally cited to low imaginative and prescient that the person has to rely totally on different senses for eye sight accomplishment. Moreover, visible disfigurement is only a partial time period used to explain lack of visible circumstance and is ready aside through imaginative and prescient loss, performing at an organ level, probably as a lack of eager sight and lack of scope [4]. This undertaking serves the cause of offering a smart digital device for visually challenged humans. The purpose of this device is to offer a universal item identification, and supply a statistic to the individual that is the use of it. This device is made from microcontroller, ultrasonic sensor, flex sensor, piezo electronic plate, buzzer, battery, GPS, GSM and panic button. The intention of this undertaking is to offer an Electronic Travelling Aid (ETA) device to assist visually challenged humans to detect on an impediment on their path. This ETA is implied on footwear. When it detects an item close to it, on its path, it indicators its owner with the assist of higher functions indicators via the headphones or audio system. The major goal in that is electricity supply, since it has built with unit of self-power generation (piezo electronic plate), it doesn't need any power backup [5].

2 Literature Survey

In [6] author designed an inventive stick for blind which may deliver early warning of associate impediment the utilization of Infrared (IR) sensors. once figuring out the obstacles, the stick signals the visually impaired lineage the utilization of vibration signals. but the clever stick centered handiest for impediment finding, however it isn't serving to for emergency functions required with the assistance of victimization the blind. And additionally the IR sensors aren't simply inexperienced ample because of the actual fact it might detect handiest the closest impediment in quick distance.

In [7] author proposed Blind Spot, a complicated white cane that mixes GPS technology, social networking, and ultrasonic sensors to assist visually impaired humans navigate public settings. With the assist of ultrasonic sensors, the GPS determines the impediment's region and warns individuals who are unaware to live far from it. However, due to the fact ultrasonic suggests the distance of the obstruction, GPS now not displayed the overall performance in tracing the location of the barriers.

In [8] author had proposed superior smart assistive shoes for the blind in this article. We introduce smart assistive shoes for blind humans to assist them in their desired activities. The shoe detects nearby policies and at the identical time sends a message with inside the form of audio and vibration to the recipient. Ultrasonic sensor reveals obstacles for blind humans. The Arduino microcontroller maintains to drag the ultrasonic sensor and provide the feedback thru the vibrator. The Arduino microcontroller maintains to drag the ultrasonic sensor and provide feedback thru the vibrator. Arduino is used for the sensor take a look at technique. The trouble of this record is a concept that addresses the issues faced thru manner of method of a

visually impaired man or woman thru a beneficial aid with inside the form of shoes. And the forestall cease end result is that the ultrasonic sensor has been truly applied to decorate the blind person's mobility [9].

In [10] author had proposed superior a smart stick the usage of laser sensors to find out the obstacles and down curbs. Obstacle detection modified into signaled via an immoderate pitch "BEEP" the usage of a microphone. The format of the laser cane is pretty easy and intuitive. The stick can simplest find out obstacle, but cannot provide cognitive and intellectual support. There exists simplest beep sound that triggers any obstacle and there is no any assist to direct them.

3 Methodology

This task is meant to be advanced as tool or useful resource with the intention to help blind humans in moving or travelling. The dependency on others is reduced and people humans can end up more self-reliant. The task is built spherical AVR controller. The task has abilities to find limitations the usage of ultrasonic module in conjunction. These sensors are established on the shoes of the blind individual. The individual is alerted and will records on the environment. Buzzer sound is used to alert the blind individual if there are any limitations in his path. Flex sensor is used to find whether or not or now no longer the individual is able to balance at the same time as he is waling. In case he is losing the stableness the individual is alerted. This artwork seeks to triumph over the way navigation records is relayed through using smart phones through manner of way of implementing it proper right into a wearable device which in this case is a shoe. A prototype is advanced the usage of the block diagram in figure. That is, the shoes will offer signs and symptoms through manner of way of alarming to inform the wearer. Electronic Shoe and Android Smart phones to the Aid of Blindly Disabled Individuals, targets at offering a proper navigation for human beings affected by blurred vision and blindness, which takes place due to growing old and absolutely disabled individual. Many embedded systems have substantially unique designs in step with their capabilities and utilities. In this task format, primarily based totally modular format concept is accompanied and the system is mainly composed of a microcontroller, Flex sensor, GPS module, GSM Module, Ultrasonic sensor. The microcontroller placed at the center of the block diagram office work the control unit of the entire task. Once the entire unit (comprising of microcontroller and sensors) is worn thru manner of way of the affected individual the sensors begin to show the encircling environment conditions. The output of the sensors is a voltage that corresponds to the encircling environmental conditions. This voltage generated through the manner of way of the sensors is fed to the inputs of the microcontroller. In this case ultrasonic sensor input to the microcontroller. Based upon this gadget embedded within the controller an output is generated and transmitted to the Android-based Smartphone via a GPS module (Fig. 1).

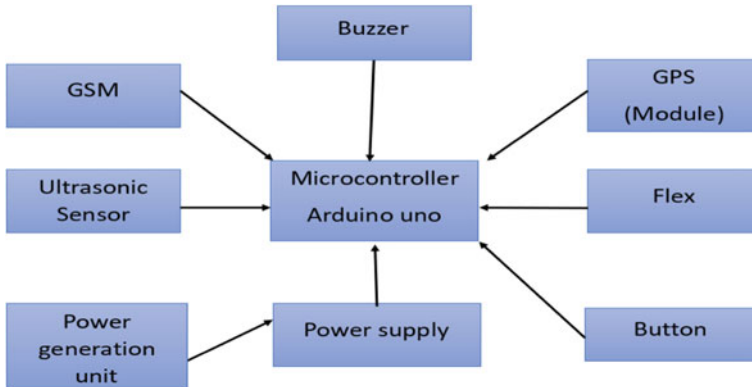


Fig. 1 Block diagram

3.1 Arduino UNO

An Arduino UNO is employed in this setup. The ATmega328P microprocessor is used by the Arduino UNO microcontroller board (datasheet). It has 14 digital input/output pins, including a USB port, a 16 MHz quartz crystal, six analogue input pins, six PWM output pins, and a reset button [5]. A low-power microcontroller is required for this gadget, and Arduino is the best choice. The Arduino microcontroller offers features like low power consumption and excellent performance in a range of packages. An Arduino UNO is employed in this setup. The ATmega328P microprocessor is used by the Arduino UNO microcontroller board (datasheet). It has six PWM output pins, six analogue input pins, a 16 MHz quartz crystal, a USB connection, and a reset button among its 14 digital input/output pins.

3.2 GSM Module

Dual Band GSM engine SIM900A, used in the GSM Modem-RS232, operates on frequencies 900 and 1800 MHz [6]. The modem has an RS232 interface that lets you link a PC and a microcontroller that has an RS232 chip (MAX232). With the help of the AT command, the baud rate can be changed from 9600 to 115,200. To enable you to connect with the internet through GPRS, the GSM/GPRS Modem has an inbuilt TCP/IP stack. It is appropriate for M2M interface applications involving SMS, voice, and data transfer.

3.3 *GPS*

The GPS module is the primary part of our project. Each and every second, together with the time and date, this device receives the coordinates from the satellite. The real-time data for tracking position is sent by the GPS module.

3.4 *Flex Sensor*

A flex sensor is a type of sensor that gauges how much deflection or, alternatively, bending has occurred [7]. Materials like plastic and carbon can be used to build this sensor. The sensor's resistance will alter when the plastic strip holding the carbon surface is turned aside. It is also known as a bend sensor as a result. It can also be used as a goniometer because the amount of turn immediately correlates with the variation in resistance.

3.5 *Ultrasonic Sensor*

An ultrasonic sensor is a piece of technology that uses ultrasonic sound waves to measure a target object's distance and then turns the sound that is reflected back into an electrical signal. Audible sound cannot match the speed of ultrasonic waves.

3.6 *Battery*

Six single cells are connected in series to form a 12-V battery, which has an output voltage of 12.6 V when completely charged. A battery cell is made up of two lead plates, one of which is covered in a negative constructed of sponge lead and a paste of lead dioxide, with a separator in between.

3.7 *Embedded C*

One of the most well-liked and frequently employed programming languages in the creation of embedded systems is embedded C. Consequently, we will observe some of programming and the fundamentals of embedded C program composition of Embedded C.

3.8 Arduino IDE

It is necessary to download and install the Arduino software on a computer in order to be able to program Arduino boards. This program is referred to as the Arduino IDE. Environment for integrated development. Motorists must be installed to allow you to control in Arduino from the IDE for Arduino.

3.9 Flowchart

If any obstacles are detected with inside the shape of 20 cm or 30 cm, and it will warn its owner about the obstacles, and the owner notices the obstacle present in front and this completes the observation. Also the person can use the mechanical component smart phone to get an SMS from the blind person stuck in an undesirable situation by using an emergency button or panic button. The receiver receives the message along with the coordinates. Whenever a person goes unwittingly for the extend distance in such times he can send alert message to the guardians by using panic button via GPS and GSM. Likewise, it has flex sensor, if a blind person falls or become unbalanced the flex sensor (bends) and it alerts its owner by alarming. Likewise, it helps a blind human in every victimized situation (Fig. 2).

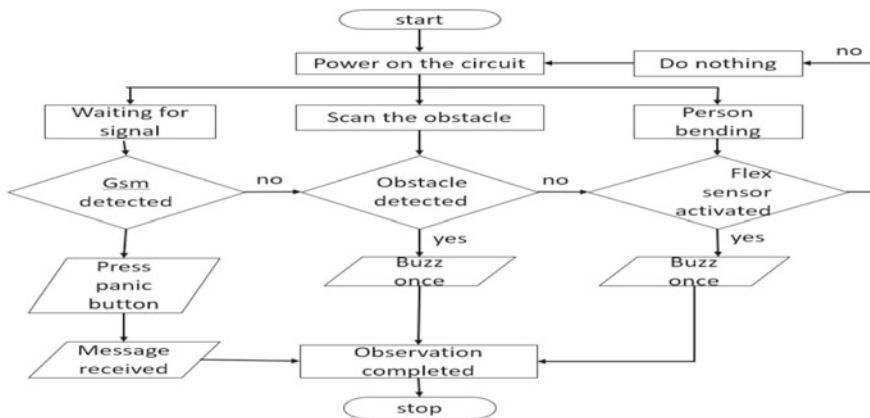


Fig. 2 Main flow diagram

4 Result

The result obtained in our project is shown in below steps:

- Step 1. Alerts the blind through different vibration pattern depending upon distance of the obstacle, as we can see from the below image the obstacle has been detected and hence it will alert its owner by alarming as in Fig. 3.
- Step 2. It also has bending sensor or flex sensor; it will detect the falling of the (blind) person. From the below picture we can see that upon bending to certain extent it starts making sound and alert its owner as in Fig. 4.
- Step 3. If a person is stuck in an emergency situation he can use the Panic button, the message is sent to the enrolled number upon pressing this panic button. The below image depicts the using of panic button or an emergency button as in Fig. 5.
- Step 4. By pressing the panic button, the message is sent to guardian when there's distress for the blind person in the form of SMS, it also includes location details in it. With the help of GPS and GSM user can be tracked by using location details sent over GSM network as in Fig. 6. In this fashion this technology becomes a reliable partner for the visually impaired folks in each situation.

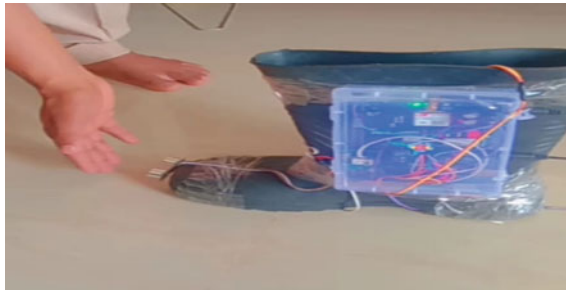


Fig. 3 Obstacle detected



Fig. 4 Falling detection

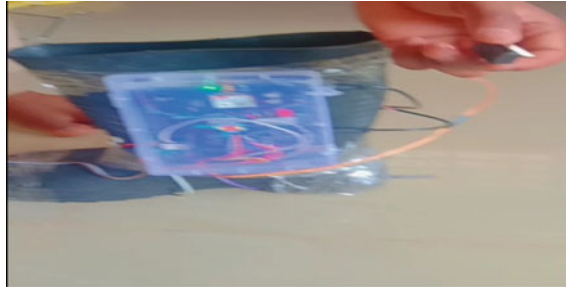


Fig. 5 Using of panic button

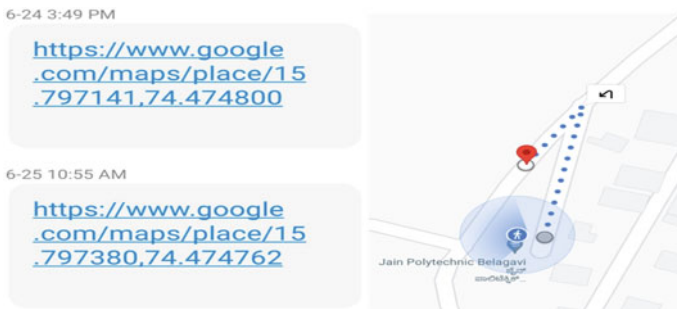


Fig. 6 Location details

5 Conclusion

Smart electronic shoes project is designed using structured modelling and is capable of giving the desired results. This system is built using various components namely ultrasonic sensor, buzzer is some, and has battery for power backup. It detects the obstacles on the way and alerts its owner of it. It also has panic button which is used when the user is stuck in an undesirable situation. Panic button alerts the enrolled number by sending SMS to it, basically it works like a SOS (save our souls or simply emergency) button for the user. It works through android application. The idea behind this project is to support the visually disabled to navigate. This helps the user to know the better out sketch of the surrounding area. The user can rely on this tool and feel less disabled. The aim of this project is to provide a virtual eye for the blind and help them in mobility.

References

1. Smart Shoe Gadget for Visually Impaired People. (2022). *Advances in Image and Video Processing*, 10(2). <https://doi.org/10.14738/aivp.102.11975>
2. Shajahan, S., Kalpana, M., & Ali, M. S. (2018). Designing a flexible device to assist visually challenged people. *Indian Journal of Public Health Research & Development*, 9(10).
3. Sumathi, G., Dharshan, V., Monishkumar, M., & Raj, A. T. (2022, April). A dynamic system to assist vision for visually challenged. In *2022 8th international conference on smart structures and systems (ICSSS)* (pp. 1–5). IEEE.
4. Prathyush Raj, R. (2022). How visually challenged people understand the film with audio description. *Journal of Advanced Research in Journalism & Mass Communication*, 09(03), 11–14. <https://doi.org/10.24321/2395.3810.202203>
5. Xia, K., Li, X., Liu, H., Zhou, M., & Zhu, K. (2022). IBGS: A wearable smart system to assist visually challenged. *IEEE Access*, 10, 77810–77825.
6. Mandal, S., & Chandran, A. B. (2020). Low-cost ultrasonic-based shoe for visually impaired people. In *Smart healthcare for disease diagnosis and prevention* (pp. 103–114). Academic Press.
7. Raval, V. J. (2019). *Design and development of a computer vision algorithm and tool for currency recognition in Indian vernacular languages for visually challenged people* (Doctoral dissertation, Maharaja Sayajirao University of Baroda, India).
8. Ramaiah, N. S. (2019). *IoT based route assistance for visually challenged*.
9. Chinmay, L., & Gururaja, H. S. (2021, December). Currency detection for visually challenged people using convolutional neural network model. In *2021 international conference on forensics, analytics, big data, security (FABS)* (Vol. 1, pp. 1–4). IEEE.
10. Devi, A., Therese, M. J., & Ganesh, R. S. (2020, September). Smart navigation guidance system for visually challenged people. In *2020 international conference on smart electronics and communication (ICOSEC)* (pp. 615–619). IEEE.

A Review of 6G Technologies and Its Advantages Over 5G Technology



Suhas Khadake, Sagar Kawade, Shreya Moholkar, and Madhuri Pawar

Abstract Shortly, 6G technology will replace 5G as the standard. The primary goal of 6G network technology is communication with a delay of 1 microsecond, and it achieves this by using higher-bandwidth frequencies over longer distances than the previous technique (5G). We require faster signal transmission and low-latency connectivity to advance the state of the art. Thanks to the proliferation of IoT gadgets, the next generation of communication systems must meet stringent requirements for spectrum and energy economy, low latency, and high throughput. These IoT gadgets will pave the way for novel services like telemedicine, virtual reality (VR), and virtual guidance; environmental telemetry and condition tracking; and linked drones and robots capable of transmitting high definition (HD) and full HD video.

Keywords Virtual reality (VR) · Technology for communications · Internet of Things (IoT) · 6G & 5G technology

S. Khadake (✉)

Department of Electronics and Telecommunication Engineering, SVERI's College of Engineering, Pandharpur, Solapur, M.S, India
e-mail: suhaskhadake@gmail.com

S. Kawade · S. Moholkar · M. Pawar

Department of Electrical Engineering, SVERI's College of Engineering, Pandharpur, Solapur, M.S, India
e-mail: sskawade@cod.sveri.ac.in

S. Moholkar

e-mail: moholkarshreya@gmail.com

M. Pawar

e-mail: mkpawar@coe.sveri.ac.in

S. Khadake · S. Kawade · S. Moholkar · M. Pawar
SVERI's College of Engineering, Pandharpur, Solapur, M.S, India

1 Introduction

The 5G technologies are standardized and even used globally. Global 5G enterprise network maps (5G field trials, 5G studies, and 5G research). beginning in April 2019 [1]. South Korea pioneered 5G. A distributed approach using a 3.5 GHz (sub-6) spectrum showed data rates around 193 and 430 Mbit/s, although 85% of 5G ground stations have been spread across 6 cities like Seoul, Busan, and Daegu [2].

By 2025, 65% of the world will have 5G ultrafast Internet 5G networks will offer enhanced mobile broadband (eMBB), ultra-reliable, low-latency communications (URLLC), with massive machine-type connectivity (mMTC). 5G wireless cellular communications system aims, standards, and key aspects are available [3]. Nevertheless, mobile internet traffic as well as the internet of things (IoT will increase 100-fold per m³). The mm-wave spectrum can't even handle data-intensive programs such as holographic film transmissions. The region as well as frequency.

Mobile apps, especially those using AI, are also sparking a passionate debate about wireless communications' potential [4]. 6G wireless communications networks will meet upcoming corporate and educational communication needs due to these problems. The process requires continuous wireless networks competitive until 2030 [5]. 6G communications networks' unique features, such as an utterly gigantic bandwidth (THz waves) and increasing AI that covers operational and environmental factors as well as network support, will allow consumers to interact with one another anywhere with a high data rate speed.

The 6G technology is expected to advance imaging and involvement techniques. 6G tech chooses the optimum processing site and stores, processes, and shares data. AI will assist this talent. It's important to understand that 6G remains emerging. Although numerous companies have expenditures in the 6th wireless technology, higher data a speed have been needed over generations. 6G wireless should replace 5G cellular. 6G networks can have wide throughput and latency over 5G technology because of their greater bandwidth. 6G internet communications aim for one-microsecond latency. 1/1000th the latency and 1000 times faster than millisecond throughput. Given the rapid rate of technological progress and the equal technologies for the Internet of Things, wireless communication networks have become major new inventions. The latest wireless mobile communications network is 5G. Since 1980, a new wireless cellular generation has arisen every decade. In 1981, analog FM cellular networks were developed, followed by the second generation in 1992, the third generation in 2001, and the fourth generation (LTE) in 2011. Over the past decade, cellular communication has grown, leading to information applications.

2 6-G Network Technologies

The 5G network spectrum cannot provide ultrahigh data transfer rates and integrity of information for sophisticated approaches. The evolution of connectivity must have superior efficiency, reliability, and reduced latency. The next stage wants to expand worldwide coverage via below-sea-level and high-altitude data transfer. The current mobile service framework particularly includes 5G infrastructures, cannot meet the foreseeable expectations of high elevations and deep-sea connectivity. The non-terrestrial network can enhance 6G coverage for image processing [6]. Satellite, land-based, and marine system enables 3D surveillance. HTS is comparable to terrestrial internet in pricing and bandwidth.

Satellite systems in geostationary orbit (GEO) were delayed and unlikely to link to the earth's natural mobile network. The non-geostationary orbit (NGSO) satellite may give global internet access with low latency and excellent data rates. While mobile networks can employ NGSO technology, they must be commercially deployed.

Radiofrequency (RF), lasers, and low-altitude satellites can communicate faster than fibre optic networks. Communications consider distances over 18–20 k-miles [7]. Space-based networks could cover more land while keeping in touch with space. Numerous technological advances mix local and satellite networks. The space terrestrial integrated network (STIN) uses SDN and ICN for flexible network control, effective network architecture, and reduced demand latency [8]. Scaling, network availability, latency, and customization will result. Platform for High and Low Altitude (HAP & LAP) Aerial-based systems LAP and HAP operate at a few kilometres as well as the stratosphere, accordingly. HAP-based networks provide better network reach [9]. Unmanned aircraft drones might help local and intergalactic LAP systems communicate. When building the 6G cellular network, this UAV function is crucial. UAV-based mobile networks maintain required cellular communication even when technology is insufficient.

UAVs are occasionally employed, especially in emergencies. However, there are still challenges and obstacles that limit its wider adoption [10]. UAV-based networks require energy-efficient route design [11]. Second, increasing data flow causes periodic network nodes, requiring more efficient and advanced protocols. Mixed protocol communication patterns may overcome current cellular network challenges. There are various considerations for implementing a 6G network under the ocean's surface as a potential underwater development effectiveness. The subsea network is mostly RF, acoustic, and optical. The largest issue of submarine implementation is equipment degradation.

On the low-depth OBS connected in blue, the data transfer from deeper sea-level stations to the surface-level stations is relayed. This indicates that the deeper-level OBSs are not in direct communication with those at or above the surface level. Submarines and autonomous underwater vehicles (AUUV) are other options that can further create a communication hub with the OBS. Therefore, via radio frequency transmission, information may be sent from the surface to the coastal station. A very high-speed link may be created through an optical connection, and minimal latency

may show promise. To build a connection that won't be interrupted by things like ocean turbulence, optical waves, or waves under the sea, physical connectivity is essential. Artificial Intelligence Concept Researchers and academics are becoming interested in using artificial intelligence (AI), more specifically Machine Learning, in cellular networks.

The cellular 5G network [12] has included ML features at several TCP/IP model levels. Higher efficiency, cost savings, and Qi may be attained by combining AI with edge computing technologies [13]. The use of AI in 5G is limited because it only entails improving existing network infrastructure; nonetheless, the full potential of AI technology was initially disregarded while designing the 5G architecture. The 6G network architecture should include a more thorough approach to the possible use of AI to address the flaw in 5G. There is a need for an AI-based system that is capable of offering a self-aware and self-adaptive solution when the network complexity increases due to the variety of system and application needs [14].

The intelligence system's application is not restricted to the network as a whole. However, it also incorporates the application of artificial intelligence (AI) in network structures, which may be able to understand the situations and adapt respective solutions to them. The main objective of AI-based network design is to use machine learning techniques to modify the autonomous aspects on which the decision is based.

3 Challenges Available 3G to 5G and Potential Solutions in 6G

Accomplishing a value strategic plan for a quick access system as well as expansion with a focus on rural and stand-alone areas; reducing the cost of mobile network utilization; pursuing strategies to increase the battery life durability of mobile equipment; and achieving a higher data rate aided by edge, super-duper low-latency communications are the five primary factors that create barriers for 6G correspondence. It's important to note that it's challenging to achieve all needs, thus a strategy must be established to deftly strike a balance between them. These sections focus on the projected challenges and possible solutions for 6G communications. Superior cognition versus opaqueness and anonymity, Sect. 3.1 6G networks, to be considered human-friendly, would need to strike a fine balance between intelligence and privacy.

However, to improve network performance, alter network statistics, and provide better services, Ai technologies need to interact with and modify private data [15]. That's why we'd sacrifice privacy for the sake of progress in the realm of ideas. An example of such a strategy would be to use a mediator to act as a go-between for user input and AI processing.

Such a negotiator should be an impartial third party who is geographically distributed. With the help of a neutral third-party mediation service, all sensitive data will be rendered anonymous. Additionally, the increasing intelligence provided by AI algorithms as well as intelligent nodes restricts individual agency. Users' tastes may not always align with the optimal solution recommended by AI. When multiple users are taken into account, the contradictory condition becomes more problematic. It may mimic this problem by looking for the sweet spot between customization and comprehension in 6G communication [16].

The focus is undoubtedly more on individualization, and smart nodes and AI algorithms necessitate intelligence rather than costly procedures and intelligence above subroutines [17]. Such procedures and sub-procedures ought to be part of the bare minimum of 6G networks operation. With this strategy, it's simple to provide smart portfolios inside the allotted space. Network operators and equipment makers may face increased expenses as a result of the high cost of intelligence in light of the network's complexity [18]. These innovations would drive up the price of consumer products, defeating the purpose of making technology affordable for everyone.

Improvements in intelligent structure technologies are essential to finding a remedy for this issue. Furthermore, original concepts and strategies are crucial for the success of any organization [19]. Once privacy, security, and trust have been established, consumers can trade their easily available anonymized data for a lower data rate. Similar to the smart grid concept, this approach would use 6G communications networks to let people trade their excess electricity generation with utilities. Avoiding Spectral Efficiency Loss Finally, many spectrum bandwidth protective measures are needed to guarantee strike wireless data connection, all of which reduce the amount of frequency that may be used for data transmission. Third, AI algorithms can detect network vulnerabilities with pinpoint accuracy, making them ideal for use in developing early warning systems for bolstering 6G networks' security. The primary goal of most studies in wireless communication has been to discover methods that do not have to choose between spectral efficiency and energy savings. As we have seen in the literature, its optimization challenge has dominated each succeeding wireless generation, and it will continue to do so in 6G communications. The 6G alternative to the current 1–5G communications can offer a novel, energy-harvesting, ground-breaking technology to significantly reduce this cost [20].

It's important to control for things like high power, high sensitivity, and a high degree of noise figure. Transmission power and distance need more study. Designing for the limited power improvements in mobile networks does not preclude the use of silicon germanium, gallium nitride, gallium arsenide, and indium phosphide-based technologies in THz frequency ranges. As a result, the distance across which such technologies can transmit is limited. Since the modulation index, phase noise, and nonlinear amplifier all play a role, a specialized transceiver design is necessary. Finally, because current transceiver architectures can't deal with THz sources, new transceiver architectures are required, particularly for the medium-to-high section of the THz bands (> 300 GHz).

Complementary metal oxide semiconductor technologies and newly discovered Nanomaterials, like graphene, can be utilized in the construction of new transceiver

architectures for THz-enabled devices. Possible Harm to Health the THz band's wide availability and high data rate (terabits per second) could be used by lightning-fast communication networks [21]. Experts believe that 6G could benefit from the very high-frequency bands, despite estimates that 6G networks and applications are still in their infancy (100 GHz–1 THz) [22]. It is crucial to think about how THz wave propagation could affect human health and safety. According to Nokia Bell Labs, 6G will be divided into six distinct technological subsets.

4 Future Scope of 6G Networks

About a decade ago, the phrase “Beyond 4G” (B4G) was coined to describe the pressing need to accelerate the development of 4G networks beyond the LTE standard [23, 24]. Before standards were finalized, only research and development (R&D) prototypes were available, leaving the potential features of 5G a mystery. For a long, people relied on B4G. It alluded to what might come after 4G. Contrary to expectations, 5G will make use of some components originally developed for the LTE standard. 6G technologies, like B4G, are expected to supplant those of the previous generation.

Multiple private 5G wireless communications deployments for businesses and industries that leverage LTE, 5G, and edge computing have paved the way for the next generation of mobile networking [25]. Future 6G wireless networks will improve upon this in a significant way. As solar PV power has led to cogeneration within the smart grid, so too will they construct a network of communication service providers, many of which will act as self-providers. As a result of conceptual and practical improvements made for 6G, mesh networks can extend coverage beyond what was possible with traditional cell towers. Data centres are already feeling the effects of the big changes brought about by 5G [26]. These include issues that arise when trying to handle many networks at once, such as both public and private kinds, as well as virtualization, programmable networks, computing, and so on. Some business customers, for instance, may choose to combine data center-hosted core network components for private company networks or ASPs with on-premises RAN at the edge.

The data collecting and transmission capabilities offered by 6G radio networks will be useful in this endeavour. Data analytics, artificial intelligence, high-performance computing (HPC), and quantum computing are all integral parts of the systems approach required by the 6G technology field. As an outcome of the integration of various novel technologies, 6G will cause profound adjustments to the underlying structure of telecommunications networks, including the RAN [27]. One notable aspect of 6G is how much emphasis it will place on AI.

5 Detailed Analysis of Communication Technologies

To guide the needs and requirements for the next generational transformation, use cases that seek to foresee important trends in use scenarios are being identified as part of the road to 6G. The ITU-R IMT Vision for 2030 and beyond, which outlines future connectivity requirements, will be informed by these demand forecasts. Thereafter, standards development groups will create and standardize the necessary technologies [28].

For 5G, a similar strategy was employed, which resulted in the deployment of capabilities that satisfy industry and user forecasted needs. For instance, both the radio access network and the core network now have additional capabilities thanks to 5G. First off, the 5G radio access network was created to be adaptable and forward-thinking to handle new frequency bands and a variety of new applications that need more stringent KPIs; second, a service-based architecture, access independence, and a converged framework were used in the design of the 5G core network to accommodate a broad range of services [29] (Fig. 1).

The 5G technology can last beyond this decade because of its cleverer cloud-native architecture. When identifying unique potential for future 6G capabilities, it is crucial to take the drivers and needs into account. With this context in mind, NGMN asked its membership operators, technology providers, and academic advisors to share their predictions for the demands and use cases that will materialize over the next ten years [30]. The strategy adopted consists of several processes, including methodology design, use case collecting, high-level classification, generic use case abstraction, and use case analysis.

There were 50 total contributed use cases, which were divided into 4 types and then translated into 14 generic use cases. These use cases are currently being investigated

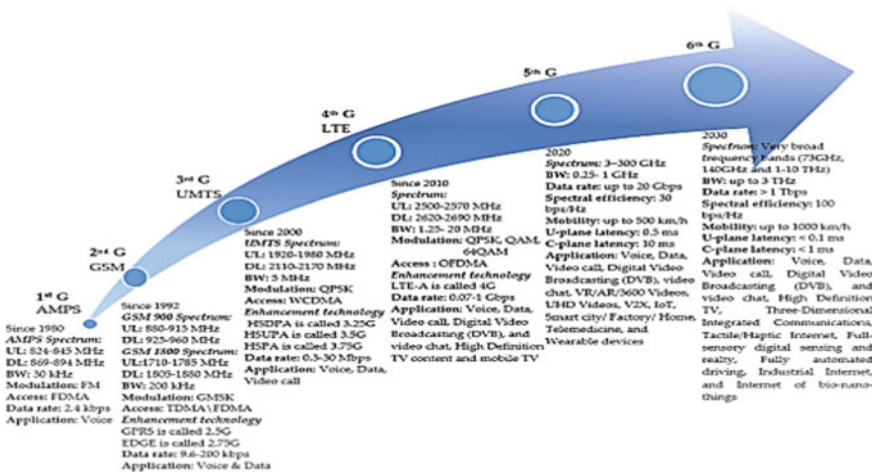


Fig. 1 Graph of development of communication technologies

further and given more priority. Some of these use cases are related to 5G and 5G advanced at first sight. A rudimentary investigation of 5G differentiation has been done by the project due to time and depth restrictions. While several use scenarios have been predicted (for the 6G time horizon), many of them may also be supported by cutting-edge 5G networks. Finding use cases that will be specially addressed after 2030 and that are compatible with 6G is difficult.

6 Conclusion

From what has been said previously, it is apparent that our society stands to benefit much from the implementation of 6G. Future 6G wireless networks will improve upon this in a significant way. As PV power has led to cogeneration within the smart grid, so too will they construct a network of communication service providers, many of which will act as self-providers. 6G's theoretical and practical improvements may help mesh networks by allowing coverage to be stretched beyond the restrictions of older cell towers, providing an innovative, energy-harvesting, ground-breaking innovation that can significantly mitigate such exchange.

The implementation of 6G will overcome the major drawback of society regarding network strength and speed than the previous technologies used for wireless communications, as the 6G may use greater frequency with much more capacity than the previous 3G to 5G technology.

References

1. Soldani, D., & Manzalini, A. (2015). Horizon 2020 and beyond: On the 5G operating system for a true digital society. *IEEE Vehicular Technology Magazine*, 10(1), 32–42.
2. Gómez Escobar, J. A. (2019). *Design of a reference architecture for an IoT sensor network*.
3. Barakabitze, A. A., & Walshe, R. (2022). SDN and NFV for QoE-driven multimedia services delivery: The road towards 6G and beyond networks. *Computer Networks*, 214, 109133.
4. Stone, P., Brooks, R., Brynjolfsson, E., Calo, R., Etzioni, O., Hager, G., & Teller, A. (2022). *Artificial intelligence and life in 2030: The one-hundred-year study on artificial intelligence*. [arXiv:2211.06318](https://arxiv.org/abs/2211.06318)
5. Hakeem, S. A. A., Hussein, H. H., & Kim, H. (2022). Vision and research directions of 6G technologies and applications. *Journal of King Saud University-Computer and Information Sciences*.
6. Khadake, S. B. (2021). Detecting salient objects of a natural scene in a video's usspatiotemporal saliency & colour mAP. *Journal NX -A Multidisciplinary Peer Reviewed Journal*, 2(08), 30–35.
7. Weisser, A., Miles, K., Richardson, M. J., & Buchholz, J. M. (2021). Conversational distance adaptation in noise and its effect on signal-to-noise ratio in realistic listening environments. *The Journal of the Acoustical Society of America*, 149(4), 2896–2907.
8. Oubbati, O. S., Atiquzzaman, M., Ahanger, T. A., & Ibrahim, A. (2020). Softwarization of UAV networks: A survey of applications and future trends. *IEEE Access*, 8, 98073–98125.
9. Mershad, K., Dahrouj, H., Sareddeen, H., Shihada, B., Al-Naffouri, T., & Alouini, M. S. (2021). Cloud-enabled high-altitude platform systems: Challenges and opportunities. *Frontiers in Communications and Networks*, 30.

10. Karaca, Y., Cicek, M., Tatli, O., Sahin, A., Pasli, S., Beser, M. F., & Turedi, S. (2018). The potential use of unmanned aircraft systems (drones) in mountain search and rescue operations. *The American Journal of Emergency Medicine*, 36(4), 583–588.
11. Jawhar, I., Mohamed, N., & Al-Jaroodi, J. (2015, June). UAV-based data communication in wireless sensor networks: Models and strategies. In *2015 international conference on unmanned aircraft systems (ICUAS)* (pp. 687–694). IEEE.
12. Gupta, A., & Jha, R. K. (2015). A survey of 5G network: Architecture and emerging technologies. *IEEE access*, 3, 1206–1232.
13. Qi, Q., & Tao, F. (2019). A smart manufacturing service system based on edge computing, fog computing, and cloud computing. *IEEE Access*, 7, 86769–86777.
14. Arzo, S. T., Naiga, C., Granelli, F., Bassoli, R., Devetsikiotis, M., & Fitzek, F. H. (2021). A theoretical discussion and survey of network automation for IoT: Challenges and opportunity. *IEEE Internet of Things Journal*, 8(15), 12021–12045.
15. Kibria, M. G., Nguyen, K., Villardi, G. P., Zhao, O., Ishizu, K., & Kojima, F. (2018). Big data analytics, machine learning, and artificial intelligence in next-generation wireless networks. *IEEE Access*, 6, 32328–32338.
16. Aledhari, M., Razzak, R., Parizi, R. M., & Saeed, F. (2020). Federated learning: A survey on enabling technologies, protocols, and applications. *IEEE Access*, 8, 140699–140725.
17. Selwyn, N. (2019). *Should robots replace teachers?* Wiley.
18. Mahdavian, A., Shojaei, A., McCormick, S., Papandreou, T., Eluru, N., & Oloufa, A. A. (2021). Drivers and barriers to implementation of connected, automated, shared, and electric vehicles: An agenda for future research. *IEEE Access*, 9, 22195–22213.
19. Kraus, S., Palmer, C., Kailer, N., Kallinger, F. L., & Spitzer, J. (2019). Digital entrepreneurship: A research agenda on new business models for the twenty-first century. *International Journal of Entrepreneurial Behavior & Research*, 25(2), 353–375.
20. Božanić, M., & Sinha, S. (2021). *Mobile communication networks: 5G and a vision of 6G*. Springer.
21. Huq, K. M. S., Busari, S. A., Rodriguez, J., Frascolla, V., Bazzi, W., & Sicker, D. C. (2019). Terahertz-enabled wireless system for beyond-5G ultra-fast networks: A brief survey. *IEEE Network*, 33(4), 89–95.
22. Banafaa, M., Shayea, I., Din, J., Azmi, M. H., Alashbi, A., Daradkeh, Y. I., & Alhammedi, A. (2022). 6G mobile communication technology: Requirements, targets, applications, challenges, advantages, and opportunities. *Alexandria Engineering Journal*.
23. Breakfast, B., Lunch, L. L., & Coffee, C. Monday Friday 8-December 12-December.
24. Rangan, S., Rappaport, T. S., & Erkip, E. (2014). Millimeter-wave cellular wireless networks: Potentials and challenges. *Proceedings of the IEEE*, 102(3), 366–385.
25. Cau, E., Corici, M., Bellavista, P., Foschini, L., Carella, G., Edmonds, A., & Bohnert, T. M. (2016, March). Efficient exploitation of mobile edge computing for virtualized 5G in EPC architectures. In *2016 4th IEEE international conference on mobile cloud computing, services, and engineering (MobileCloud)* (pp. 100–109). IEEE.
26. Guo, F., Yu, F. R., Zhang, H., Li, X., Ji, H., & Leung, V. C. (2021). Enabling massive IoT toward 6G: A comprehensive survey. *IEEE Internet of Things Journal*, 8(15), 11891–11915.
27. Sivaramakrishnan, S., Rathish, C. R., Lingasamy, V., & Premalatha, S. (2022). Augmentation of terahertz communication in 6G and its dependency for future state-of-the-art technology. In *Challenges and risks involved in deploying 6G and NextGen networks* (pp. 91–105). IGI Global.
28. Pana, V. S., Babalola, O. P., & Balyan, V. (2022). 5G radio access networks: A survey. *Array*, 100170.
29. Ramakrishnan, R., & Gaur, L. (2019). *Internet of things: Approach and applicability in manufacturing*. CRC Press.
30. Wang, N., Xiao, P., Khalily, M., Heliot, F., Foh, C. H., Ma, Y., & Tafazolli, R. *IEEE future networks*.

Monitoring and Controlling of Field Pond Parameters Using an IOT



Smita Gawade, Seema Atole, Snehal Marab, and Tejas Joshi

Abstract The Internet of Things (IoT) is a worldwide network that plays an important role in “smart devices” that can sense and interact with the environment through the internet for communication and interaction with users and other systems. Agriculture-related issues have been trying to suppress the nation’s development consistently. Utilizing modern technologies and agriculture to use water sustainably will help overcome this challenge. This real-time application uses ultrasonic sensors for sensing the percentage of water level to determine on/off the motors automatically. Two motors are used for the suction and discharge of water. To provide the security pi camera is used to capture images of the presence of obstacles, if any the message will be sent to Gmail of the user. The biggest benefits of the suggested method are its low cost and lack of direct human involvement. Saving time and resources will increase production for all parties involved.

Keywords Pump · Cloud and Internet

1 Introduction

In world there is 71% of water and 29% of land, out of 71% of water, only 3% is used for drinking purpose. Remaining water is not used for any purpose as it is in alkali medium. Many regions in Maharashtra are drought-prone zones [1]. Our ministry is contributing a lot of resources to help with that issue, as well as establishing new government rules through which farmers can gain more beefiness. To fulfill the need of water for farming farmers uses deep well System for efficient use of water. Digging field ponds is affordable to the farmers, but in recent days, the depth of field pond has led to an increase death of human beings so, that for the security it is useful. Wireless systems can be of great help for automation systems [2]. Wireless systems are utilized daily and everywhere thanks to new technologies including Wi-Fi and cloud networks in the latest years. Water conservation and efficient use of water is

S. Gawade (✉) · S. Atole · S. Marab · T. Joshi
SVRI’s College of Engineering, Pandharpur, Pandharpur, India
e-mail: smitagawade21entc@gmail.com

becoming prime objective in region of drought prone area. The scarcity of water can be overcome by efficient utilization monitoring of stored water for agriculture as well as residential areas. By monitoring and controlling field pond parameter such as water level [3], water discharge, human intervention, fish cultivation and feeding, benefits can be enhanced and reuse can be excelled. This will enhance over all proficiency of system. IOT based electronic system is suggested in proposed system for monitoring and controlling above parameter.

2 Proposed System Design

I incorporated a camera, servo motors, and DC motors into the system I had created. It serves as both an input and an output [4]. When an introducer enters the field pond area, the camera utilized here for input purposes takes a picture of them and sends it through mail to the introducer's owner. We also receive security breach SMS in our link system [5]. Which form of entrance occurs in this system is easily understood through email. Accordingly, the user takes an appropriate decision. And the feeding of fish is done two times a day using a servo motor [6]. The information has finally been transmitted as a notification over Wi-Fi to a PC and a mobile device. The Introducer could be a person, an animal, or something else that is simple to recognize, in which case we react right away to the situation. Therefore, this technique offered security for field pond parameters (Fig. 1).

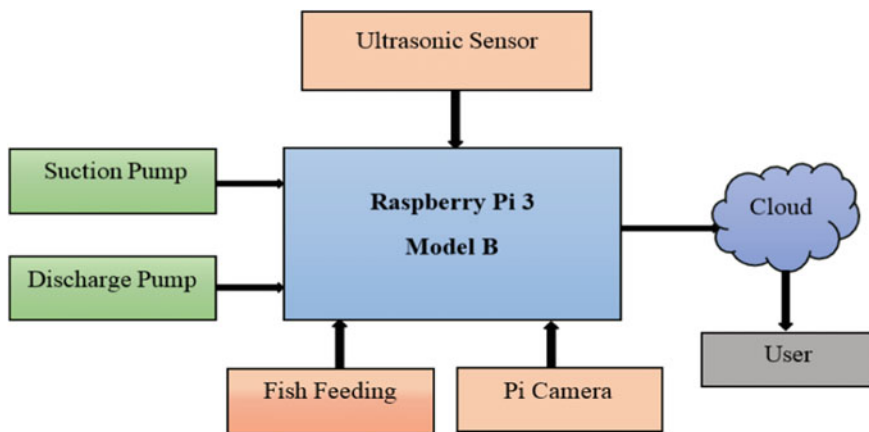


Fig. 1 Proposed system diagram

2.1 Cloud Communication

In our project, we employed the cloud computing concept, which enables on-demand network access to a common pool of quickly deployable, un-configurable computing resources. There are various features accessible. We made use of the cloud’s on-demand self-service functionality. The cloud offers a wide network access, allowing us to quickly access the network anywhere in the world [7]. Users can provision computing capabilities as needed without requiring human contact with each service provided [8].

We bought a cloud for our project that offers services to people. On a web page, we created one HTML link just for communication [9]. We uploaded this link to the cloud. Our programming made use of the link. The Raspberry Pi’s IP address is used throughout the system, which is useful for us (Figs. 2 and 3).

Fig. 2 PCB layout of relay circuit

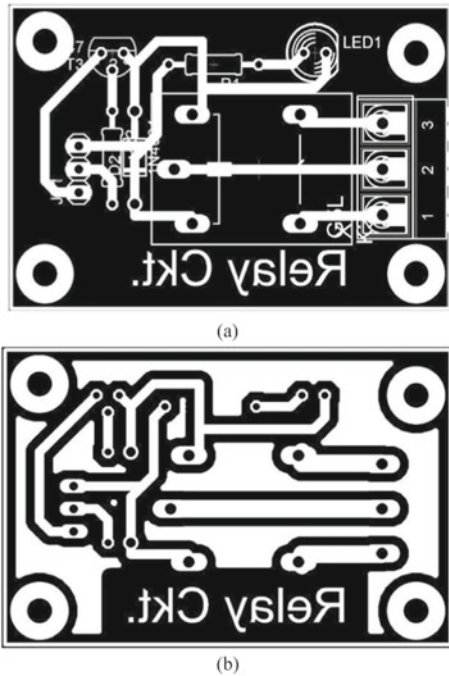
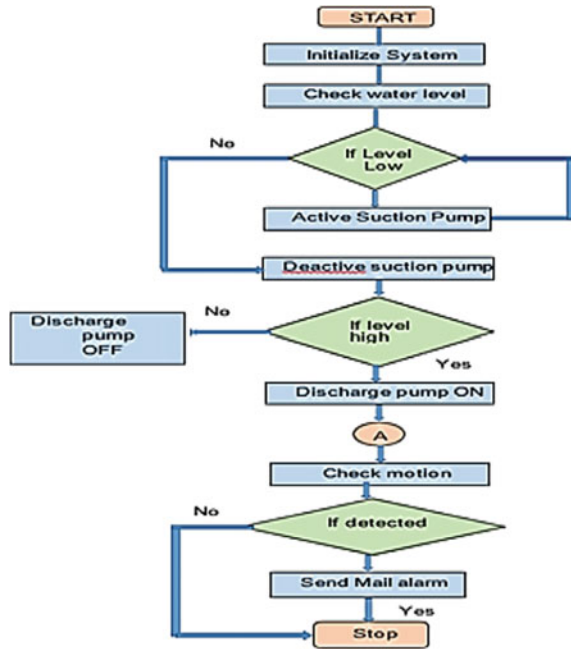


Fig. 3 Flowchart of proposed system



2.2 Description of Flow Chart

This flow chart gives the information regarding various parameters like water level, pump status, security, suction pump, discharge pump, food feed.

1. Security Algorithm

- Step 1: Start Application.
- Step 2: Capture Image Using Pi Camera.
- Step 3: Face Detection.
- Step 4: Sending mail to user with accurate time and obstacle.
- Step 5: Status of various parameter are displayed after clicking on that link <https://world4.tech/fsecure/>

2. Water Level-Sensor Algorithm

- Step 1: Start Process.
- Step 2: Capture inputs from sensor.
- Step 3: Using Formula detect the water level percentage.
- Step 4: Display value on Web-server <https://world4.tech/fsecure/>

3. Motor Control Algorithm

- Step 1: Start process.
- Step 2: When Water level is 0% then main motor ON and Drain motor off.

- Step 3: When water level is more than 90% then drain motor is on and Main motor is off.
- Step 4: Display the state of motor on web browser <https://world4.tech/fsecure/> As a control parameter.

Figure 5 shows the email sends immediately for security alert with date and time when the introducer is presents in surrounding area of the pond.

3 Result and Discussion

As the introducer is present in area surrounding of the pond, the status shown in Fig. 6a as security breached under the security status and (b) shows security status as all secured due to the absence of introducer (Figs. 4 and 5; Tables 1 and 2).

In this security alert table when introducer is occurred at field pond area that time pi camera captured the image of introducer. User get security alert mail and also user see the status of security breached on web page [10]. If introducer is not occurred, then user can get security alert Status on web page all secured.

4 Conclusion

The monitoring and controlling of field pond is done with the help of various parameters such as water level, motor parameter unit, fish feeding and security. From this the main summarized conclusions obtained are as follows:

1. Through the developed link, user can easily get the information regarding the real time status of water reservoir/field pond in the form of percentage. Wherever the user is, he will get the status of water level which can be known by laptop, computer or mobile device etc. through this link.
2. The various field pond parameters like water level, water discharge, human intervention and fish feeding are studied and analyzed. From study it is clear that if water level is 0–90 %then main motor is operating and drains motor is on off mode. And if water level is greater 90% then drain motor is on and main motor is off.
3. The fish feeding is done automatically or manually twice in a day as per the requirement of the fish by using servomotor.
4. Relay card and pushup resister are used for the development of electronic platform which are electrically operated switch/resister that allows user to turn on or off a circuit using voltage or current much higher than raspberry pi could handle.
5. With the help of camera situated nearby pond area user can easily get the information about introducer after getting the mail.

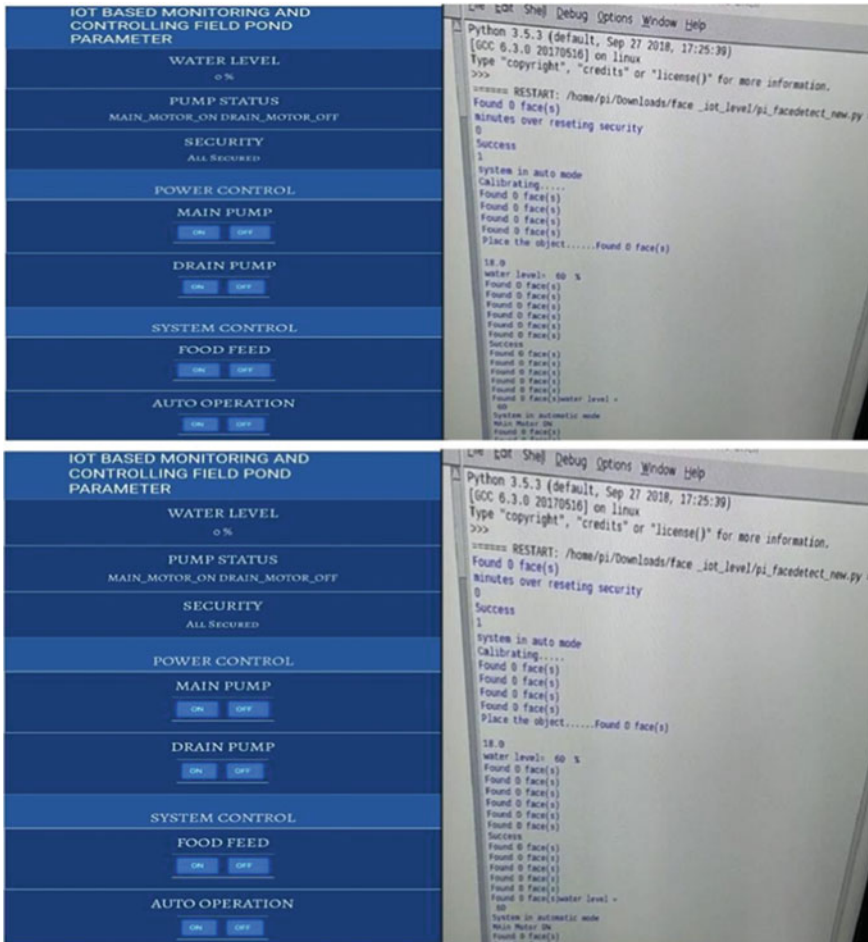


Fig. 4 Software webpage

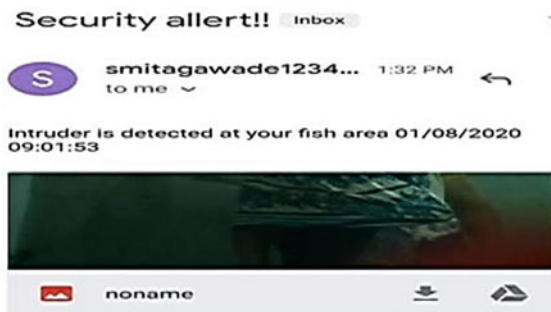


Fig. 5 Security alert mail

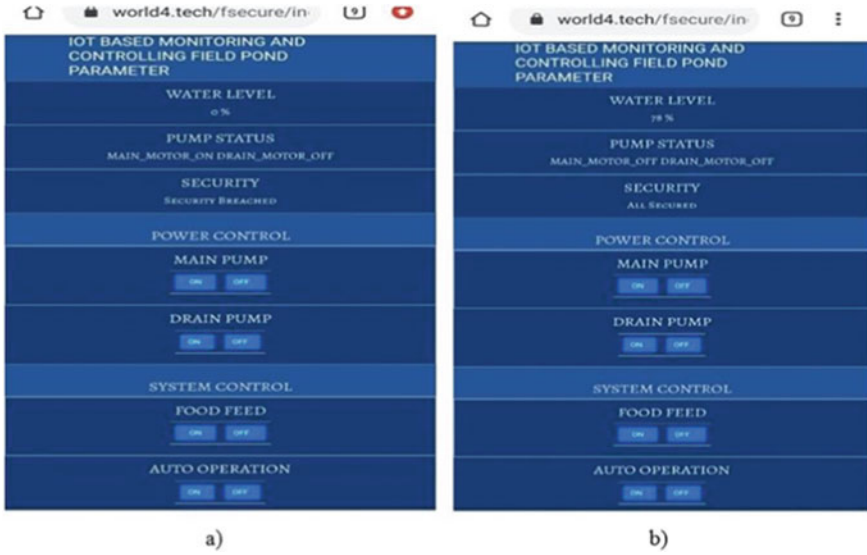


Fig. 6 a As security breached under the security status, b shows security status

Table 1 Security alert

S. No.	User information	Alert SMS
1	Introducer occurred	Security breached
2	Introducer not occurred	All secured

Table 2 Motor parameter and water level status

S. No.	Motor parameter	Water level (%)
1	Main on, drain off	0
2	Main on, drain off	25
3	Main on, drain off	50
4	Main on, drain off	75
5	Main on, drain off	80
6	Main off, drain on	90
7	Main off, drain on	100
8	Main off, drain on	110
9	Main off, drain on	122
10	Main off, drain on	125

References

1. Farooq, M. S., Riaz, S., Abid, A., Abid, K., & Naeem, M. A. (2019). A survey on the role of IoT in agriculture for the implementation of smart farming. *IEEE Access*, 7, 156237–156271.
2. Putjaika, N., Phusae, S., Chen-Im, A., Phunchongharn, P., & Akkarajitsakul, K. (2016, May). A control system in an intelligent farming by using arduino technology. In *2016 fifth ICT international student project conference (ICT-ISPC)* (pp. 53–56). IEEE.
3. Carullo, A., & Parvis, M. (2001). An ultrasonic sensor for distance measurement in automotive applications. *IEEE Sensors Journal*, 1(2), 143.
4. Lanuzza, M., Corsonello, P., & Perri, S. (2012). Low-power level shifter for multi-supply voltage designs. *IEEE Transactions on Circuits and Systems II: Express Briefs*, 59(12), 922–926.
5. Mateen, A., Zhu, Q., & Afsar, S. (2019). IoT based real time agriculture farming. *International Journal of Advanced Smart Convergence*, 8(4), 16–25.
6. Idachaba, F. E., Olowoleni, J. O., Ibhaze, A. E., & Oni, O. O. (2017, October). IoT enabled real-time fishpond management system. In *Proceedings of the world congress on engineering and computer science* (Vol. 1, pp. 25–27).
7. Mekala, M. S., & Viswanathan, P. (2017, February). A novel technology for smart agriculture based on IoT with cloud computing. In *2017 international conference on I-SMAC (IoT in social, mobile, analytics and cloud) (I-SMAC)* (pp. 75–82). IEEE.
8. Jiang, P., Xia, H., He, Z., & Wang, Z. (2009). Design of a water environment monitoring system based on wireless sensor networks. *Sensors*, 9(8), 6411–6434.
9. Saraf, S. B., & Gawali, D. H. (2017, May). IoT based smart irrigation monitoring and controlling system. In *2017 2nd IEEE international conference on recent trends in electronics, information & communication technology (RTEICT)* (pp. 815–819). IEEE.
10. Preetham, K., Mallikarjun, B. C., Umesha, K., Mahesh, F. M., & Neethan, S. (2019). Aquaculture monitoring and control system: An IoT based approach. *International Journal of Advance Research, Ideas and Innovations in Technology*, 5(2).

Development of Smart Strips in the House for Safety Monitoring



Devyani Kadgaye, Rahul Chaudhari, and Manish Narkhede

Abstract Safety monitoring of residential premises has been a topic of keen interest to many researchers. Moreover, this monitoring and control are greatly facilitated these days with the advancement in wireless data transmission technology. A smart Wireless sensor network is the key to the Internet of things (IoT) as it can detect moisture, sense fire, gas, water leakage, and seismic vibration present in the house. In the proposed work, the development of a smart strip using wireless sensor networks for health and safety monitoring in the house is done. Through this system, sensors are deployed at various places inside the wall for monitoring parameters including humidity moisture content, seismic vibration, and fire. The sensed data is collected using a microcontroller board and then processed and sent to the concerned people.

Keywords Safety · Health and safety monitoring · Wireless sensor network · Smart house · ESP32 board · DHT22

1 Introduction

In recent years, many research papers have been published related to safety monitoring with the help of wireless sensor technology with their functionality. The development of wireless sensor technology is important in the evolution because it can be more useful for health and safety monitoring as it can reduce the possibility of accidents inside the house due to gas leakage, increase in temperature, water leakages, etc. Accidents may cause permanent disablement to any family member. So, a system can be developed which shall detect such types of leakage or mis-happenings cause accidents.

D. Kadgaye (✉) · R. Chaudhari · M. Narkhede
Pimpri Chinchwad College of Engineering, Pune 411044, India
e-mail: devyani.kadgaye20@pccoepune.org

R. Chaudhari
e-mail: rahul.chaudhari@pccoepune.org

1.1 Health and Safety Monitoring

The process of health and safety monitoring includes the installation of sensors, data collection, analysis of data, transfer of data, and diagnostics through which the performance is monitored for the health and safety of the house. Health and safety monitoring gives valuable information such as the house's condition, enabling residents to make decisions regarding maintenance, and it can help to give surety of the safety of family members.

A sensor is used to detect and collect some type of input like light, heat, motion, moisture, pressure, or anything from the physical environment. The output is converted to a human-readable display. The WSN is used in various areas such as healthcare, residential and commercial projects occupancy information, human behavior, personal safety, and health monitoring of structures.

The industrial sector will initially deploy wireless sensor networks (WSN) for manufacturing control, equipment monitoring and control, and structural health monitoring. Low-power embedded sensor nodes that are coupled by self-forming, self-healing wireless networks with adaptable topologies make up wireless sensor networks.

2 Methodology

See Fig. 1.

Fig. 1 Methodology of project



3 Literature Survey

This chapter deals with a literature survey carried out related to health and safety monitoring. This study was all about a broad survey and analysis of relevant research articles about sensing technologies for structural health monitoring (SHM). The subject of structural engineering is starting to take into consideration the developing sensing paradigms of wireless sensors and sensor networks as alternatives to conventional tethered monitoring methods [1].

Industrial health and safety monitoring system and issues which causes accidents are highlighted. In this work, they demonstrate the main relationship between organization and technology in the concrete industry accordingly they designed a system that reduces the number of accidents by using the wireless sensor for monitoring workers. Formulation of risk behaviour and risk perception and rules are formed for health and safety [2].

Hazardous gas is dangerous to health hence, improving construction safety management is important. WSN is a key technology in the Internet of Things (IoT). Building information modelling (BIM) technology is used for the digital modelling of databases and geometry that gives visualized way of the lifecycle of construction management. They developed a unique system using BIM and WSN which visually monitors construction site safety and automatically removes hazardous gas if present [3].

The Internet of Things (IoT) application uses a sensor with the help of cloud computing. They mainly focused on health care monitoring using network sensors either worn on the body or in a living environment. Challenges and opportunities for IoT in the future of healthcare monitoring are highlighted [4].

They introduce IoT-based indoor safety monitoring for COVID-19 parameters like sensing temperature without contact, mask detection, and social distancing check. They used raspberry Pi. In this research, they used MQTT (Message queuing telemetry transport) the machine-to-machine communication between devices like Raspberry Pi, Arduino and smartphones [5].

Portable healthcare monitoring systems in hospitals are designed using IoT technology which is the process of healthcare from face-to-face consulting to telemedicine. The system is used to monitor the patient's basic health simultaneously room condition is also monitored. They were using five sensor heartbeat sensor, body temperature sensor, room temperature sensor, CO sensor and CO₂ sensor to capture the data and data is conveyed by portal to medical staff accordingly they can analyze the patients' current situation [6].

Low-cost wireless sensors are used for the development of civil infrastructure systems. Methods of structural health monitoring for bridges and buildings. Wireless monitoring with their prototypes and embedded data processing are discussed in detail with the help of case studies [7].

The methods are discussed to detect, locate, and damage detection of structural and deck systems using measured vibration. Various criteria are developed such as level of damage detection, model non-based methods and linear and non-linear

methods. Damage identification methods are classified at different levels. They also used the unity check method, and stiffness error matrix method and their effects and changes [8]. Monitoring based on the sensor LRFD designed Girder Bridge. They analyzed lightweight bridge decks on star city bridge in Morgantown. They used a total of 700 sensors which can record superstructure elements to various loading parameters and record data every 20 min which can continuously monitor data and evaluation of the performance of the bridge since construction in 2003–2004 [9].

Health monitoring based on the IoT can provide remote monitoring of patient health to doctors to access the data. This system is low power consumption, is cost-effective and has access to doctors for collecting information about the patient health that can help doctors to monitor the patients easily. This system is cost-effective, can be accessed from anywhere via the internet and is time-saving in critical conditions [10].

Indoor air quality is important for the health and safety of passengers everywhere. This study is related control and monitoring of IAQ in subway stations with the help of WSN. They suggested the framework was designed to monitor IAQ and used twisted pair local network, ZigBee wireless network to collect and transmission of data. This system is used for safety in subway stations to increase the efficiency and productivity of operations [11].

Worker safety is a very major problem in the construction industry. Fall detection and monitoring of their health are proposed to ensure the safety of the worker system. This system overcomes all issues and injuries of the worker. It can provide alert the responsible person to provide medical attention [12].

Structural health monitoring can also be monitored with the help of a wireless sensor network is discussed in this research paper based on ZigBee Technology. ZigBee technology is used for structural health monitoring of buildings bridges and roads and analysis is done with the help of multi-hop network technology is used for effective time synchronization. (Xiang-dong JIANG, Yu-Liang TANG, Ying LEI).

Smart home and a smart city which is very popular in this generation. The smart home concept includes video monitoring of apartments or separate waste bins with the help of an internet network. They introduced Augmented Reality, Smart City and Smart Home technologies which can save time, and improve the security and quality of life of people.

4 Development System Design

4.1 Operations

A system should be developed to monitor parameters like gas leakages, shock and vibration, and fire detection that cause accidents in the house with help of a wireless sensor network. The sensor gets the information from the surroundings data sensing

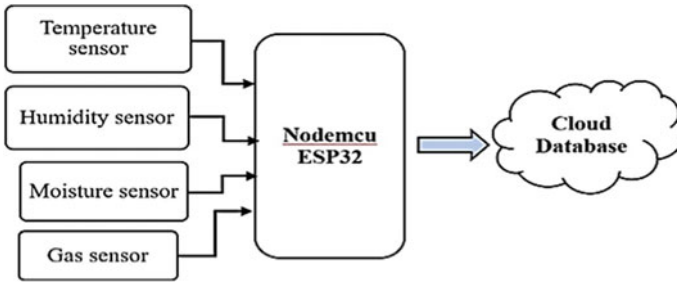


Fig. 2 Block diagram for the system

is done and after sensing the data the transmission is to be done with the help of cloud computing data analysis is done (Fig. 2).

4.2 Major Components Used

The following components are used to develop a system:

1. ESP32 development board
2. DHT22
3. Moisture sensor
4. Shock sensor
5. Gas sensor.

4.2.1 ESP32 Development Board

ESP32 is a development board for WIFI and Bluetooth IoT-based applications. This board chip has a Tensilica Xtensa LX6 microprocessor in both dual and single-core variations. It has a 240 MHz clock rate.

Functions

1. ESP32 has many applications in IoT but it is mainly used for networking, data processing, P2P connectivity and web servers.
2. In the networking module, a WIFI antenna and dual-core enable embedded devices and then connect to routers and it can transmit data.
3. Data processing deals with the basic input from an analog and digital sensor for critical calculations with a real-time operating system (RTOS).

Table 1 DHT22 sensor module

S. No.	Pins	Description
1	Vcc	Power supply 3.5–5.5 V
2	Data	Outputs both temperature and humidity through serial data
3	Ground	Connected to the ground of the circuit

4. P2P connectivity directly makes communication between the ESP board and other devices.

Applications

ESP32 is used for the following devices

1. It can use in Industrial devices with programmable logic controllers.
2. Medical devices include monitoring of health.
3. It can use in Energy devices like HVAC and thermostats.
4. It can use for Security devices including surveillance cameras and smart locks and monitoring for security purposes.

4.2.2 DHT22

DHT22 is a low-cost humidity and temperature sensor which has a microcontroller of 8-bit which gives output values of humidity and temperature properly. It is a more accurate sensor and it can work in a higher range of temperature and humidity (Table 1).

DHT22 Technical Details

1. 3.5–5.5 V operating voltage.
2. 0.3 mA (for measurement) and 60 uA for operating current (standby).
3. Serial data output.
4. – 40 to 80 °C in the temperature range.
5. 0–100% humidity.
6. Resolution: Humidity and temperature are both 16-bit values.
7. Accuracy: 1% and 0.5 °C.

Applications

1. It can measure humidity and temperature.
2. Local weather stations can benefit, and automatic control is possible.
3. Environment monitoring is a possibility (Figs. 3 and 4).

4.2.3 Moisture Sensor

A moisture sensor is used for the detection of the amount of moisture present in the wall. This sensor measures the volumetric content of water inside.

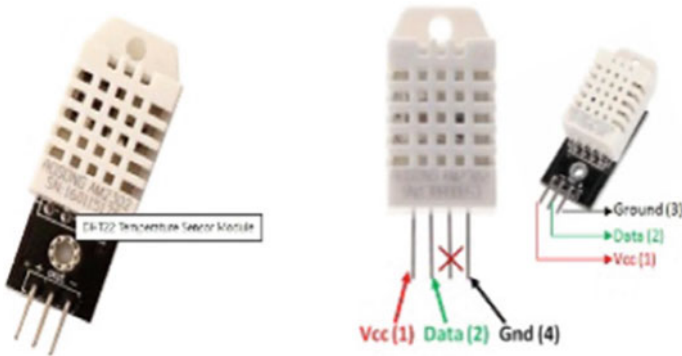


Fig. 3 DHT22 sensor module with pinout

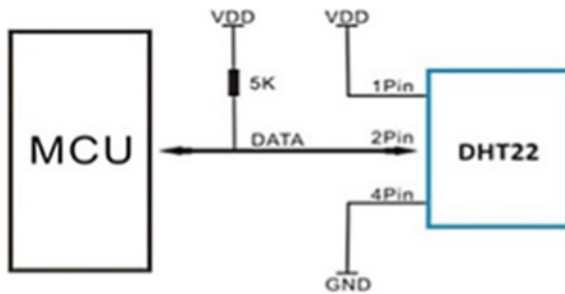


Fig. 4 Connection diagram for DHT22

4.2.4 Shock Sensor

A shock sensor is used to detect shocks, vibrations, and impacts. It can be used for health and safety monitoring in the health care centre and infrastructure.

4.2.5 Gas Sensor

A gas sensor is a device that senses the presence of gas and its concentration. If the concentration of hazardous gases such as toxic, explosive gas or hazardous substance is increased then it may cause accidents (Fig. 5).

4.3 ThinkSpeak

Thinkspeak is an IoT-based cloud platform that sends data from sensors to the cloud. It can analyze and visualize all collected data with MATLAB or any other software,

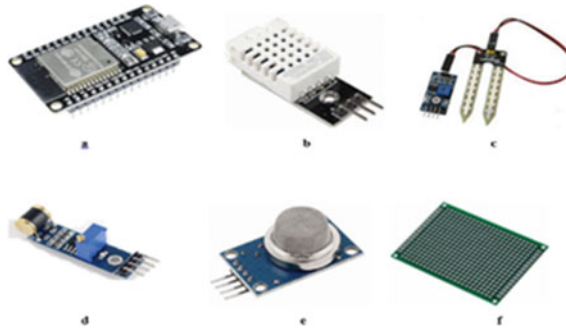


Fig. 5 Components used **a** ESP32, **b** DHT22, **c** moisture sensor, **d** shock sensor, **e** gas sensor, **f** PCB board

including making its application. It is used for real-time data collection and data processing. Channels are used for data storage; each channel includes 8 fields for any type of data, 3 location fields, and 1 status field.

5 Conclusion

1. Thermal field, magnetic field, acoustic or ultrasonic, radiography, and eddy-current methods can be used for damage identification.
2. Health and safety monitoring can detect accidents caused and can reduce the accident rate therefore, Health and safety monitoring is as important as SHM.
3. By installing smart strips in the house, gas leakage can also be identified, preventing possible hazardous accidents.
4. This smart strip can sense and control the following parameter:
 - (a) Humidity (b) Temperature (c) Moisture (d) Vibration

Future Scope There is some future development in our system to use the idea more fluently with the help of tiles.

References

1. Lynch, J. P. (2006). A summary review of wireless sensors and sensor networks for structural health monitoring. *The Shock and Vibration Digest*, 38(2), 91–128. <https://doi.org/10.1177/0583102406061499>
2. Kortuem, G., et al. (2007). *Sensor networks or smart artifacts? An exploration of organizational issues of an industrial health and safety monitoring system*. Lecture notes computer science (including subseries lecture notes artificial intelligence lecture notes bioinformatics) (Vol. 4717, pp. 465–482). LNCS. https://doi.org/10.1007/978-3-540-74853-3_27
3. Cheung, W. F., Lin, T. H., & Lin, Y. C. (2018). A real-time construction safety monitoring system for hazardous gas integrating wireless sensor network and building information modelling technologies. *Sensors (Switzerland)*, 18(2). <https://doi.org/10.3390/s18020436>
4. Hassanaliheragh, M., et al. (2015). Health monitoring and management using internet-of-things (IoT) sensing with cloud-based processing: Opportunities and challenges. In *Proceedings of 2015 IEEE international conference on service computing SCC 2015* (pp. 285–292). <https://doi.org/10.1109/SCC.2015.47>
5. Petrovic, N., & Kocić, Đ. (2020). IoT-based system for COVID-19 indoor safety monitoring SCOR (semantic coordination for Rawfie) view project, September 2020 [online]. Available <http://mqtt.org/>
6. Islam, M. M., Rahaman, A., & Islam, M. R. (2020). Development of smart healthcare monitoring system in IoT environment. *SN Computer Science*, 1(3), 1–11. <https://doi.org/10.1007/s42979-020-00195-y>
7. Swartz, R. A., & Lynch, J. P. (2009). *Wireless sensors and networks for structural health monitoring of civil infrastructure systems*. Woodhead Publishing Limited. <https://doi.org/10.1533/9781845696825.1.72>
8. Doebling, S. W., Farrar, C. R., & Prime, M. B. (1998). A summary review of vibration-based damage identification methods. *The Shock and Vibration Digest*, 30(2), 91–105. <https://doi.org/10.1177/058310249803000201>
9. Shoukry, S. N., Riad, M. Y., & William, G. W. (2009). Longterm sensor-based monitoring of an LRFD designed steel girder bridge. *Engineering Structures*, 31(12), 2954–2965. <https://doi.org/10.1016/j.engstruct.2009.07.023>
10. Ahmed, Z. U., Mortuza, M. G., Uddin, M. J., Kabir, M. H., Mahiuddin, M., & Hoque, M. J. (2018). Internet of things based patient health monitoring system using wearable biomedical device. In *2018 international conference on innovation engineering technology*. ICIET 2018, December, pp. 1–5. <https://doi.org/10.1109/CIET.2018.8660846>
11. Choi, G. H., Choi, G. S., & Jang, J. H. (2009). A framework for a wireless sensor network in web-based monitoring and control of indoor air quality (IAQ) in subway stations. In *Proceedings of 2009 2nd IEEE international conference on computer science information technology*. ICCSIT 2009, pp. 378–382. <https://doi.org/10.1109/ICCSIT.2009.5234728>
12. Mehata, K. M., Shankar, S. K., Karthikeyan, N., Nandhinee, K., & Robin Hedwig, P. (2019). IoT based safety and health monitoring for construction workers. In *Proceedings of 1st international conference on innovation information communication technology*. ICIICT 2019, pp. 1–7. <https://doi.org/10.1109/ICIICT.2019.8741478>

New Approaches for a Reconfigurable Microstrip Patch Antenna Using Inverse Artificial Neural Networks



Mohammad Mushaib, Meenakshi Mukund Pawar, Akhilesh Kumar Pandey, and Mohd Gulman Siddiqui

Abstract Inverse artificial neural networks (ANNs) are used in this study to design and improve a reconfigurable 5-fingers-shaped microstrip patch antenna. Utilizing three precise prior knowledge inverse ANNs and a sizable quantity of training data, new solutions are created by including frequency information into the design of the ANNs. The recommended antenna resonates at frequencies that range from 2 to 7 GHz and may configure in four modes, each of which is controllable by two PIN diode switches featuring ON/OFF states. Utilizing prior knowledge mitigates the complexity of the input/output collaboration. With a multilayer perceptron (MLP) as the first phase of the training process, three separate techniques of knowledge incorporation are illustrated, and their outcomes are compared to those of an EM simulation.

Keywords Artificial neural networks · Reconfigurable microstrip antenna · Prior knowledge input

1 Introduction

Satellites, MIMO systems, radar, and portable computers are just a few case studies of wireless communication applications that are steadily increasing [1]. Reconfigurable antennas are available in a wide range of varied shapes and structural configurations. Reconfigurable antennas' architecture can be altered to provide alternative characteristics (desired operation) (Jiajie & Anguo, 2018; Allayioti & Kelly, 2017).

M. Mushaib (✉)

Department of Electronics and Communication, Sam Higginbottom University of Agriculture Technology and Sciences, Prayagraj, Uttarpradesh, India
e-mail: er.mushaib007@gmail.com

M. M. Pawar · A. K. Pandey

Shri Vitthal Education and Research Institute (College of Engineering, Pandharpur), Pandharpur, Maharashtra, India

M. G. Siddiqui

Banasthali Vidyapith, Aliyabad, Rajasthan, India

Additionally, according to Aoad et al. [2], they possess the characteristics of the reconfiguration mechanism. Only the ON-ON state of PIN diode switches is examined in this application [1, 2]. The design and outcomes of a prior research were different [3].

For the purpose of creating new solutions for the suggested antenna, ANN models have been chosen. They can model and improve non-linear interactions between a wide range of inputs and outcomes (Huff & Bernhard, 2008). In order to build, develop, and optimize antennas, integrated circuit-antenna modules, and microwave circuits, ANNs can be utilized [2, 4]. Ample training data that is supplied during the training process is necessary for accuracy training data for this application is produces using CST-EM simulator.

In this study, a two-stage EM-ANN model is processed, with the first step utilising MLP to model the geometrical dimensions (response) of the suggested antenna, and the second step using additional information to correct the response obtained from the first phase. Finally, EM simulator will rework the results of the second stage to create the newly produced solution.

2 Design of Reconfigurable Antennas

The researched antenna is a microstrip patch antenna with five adjustable fingers (R5SMPA). This R5SMPA features three layers and a feeding mechanism in the middle patch. Radiating conductors in the first layer are made up of three strips of varied dimensions.

On the other side, where L_3 (1.05 cm) is the center strip, the parameters of L_1 (1.35 cm) and L_2 (0.75 cm) are mirrored. All strips are connected by the widths W_1 (3.3 cm) and W_2 (0.3 cm). The ground plane (third layer) is printed on the back of the FR-4 dielectric board, which is the second layer and has a thickness of 0.2 cm (substrate). The vacant region W_3 (0.15 cm) contains two PIN diodes (D_1 and D_2). According to the bias state of the microstrips, they are positioned as illustrated in Fig. 1 to spread the current courses on the microstrips. Two resistors are utilized with the PIN diodes to achieve the ON-ON condition. The resistance of each resistor is 5 ohms.

3 Inverse Artificial Neural Network

For evaluating the efficiency of the techniques employed in [3]. The suggested antenna, which has a different construction as depicted in Fig. 1, has the same techniques employed. The two phases that comprise the postulated inverse ANNs are known as knowledge-based response correction (KBRC) and an EM simulator, which is employed to redesign the KBRC outcomes in order to formulate new R5SMPA solutions. The KBRC framework involves just frequency sample points as input

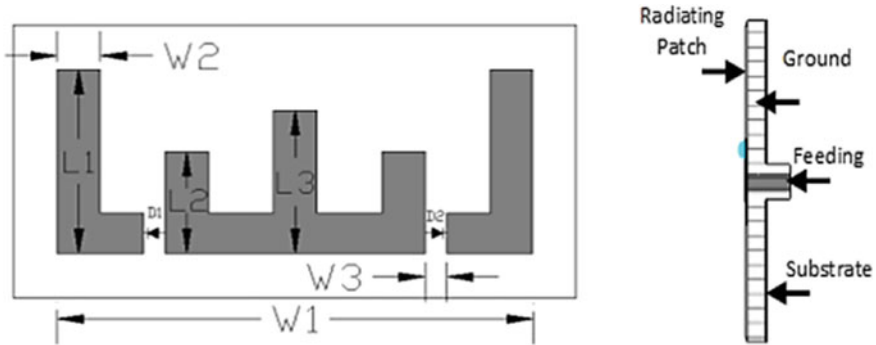


Fig. 1 Reconfigurable antenna top view and side view

and outputs the overhauled geometrical dimensions of the R5SMPA. It is significant to note that the MLP response from the KBRC model’s first step has not yet been adjusted. The second step’s SD, PKI-D, and PKI models, however, rectify that reaction.

3.1 Multilayer Perceptron

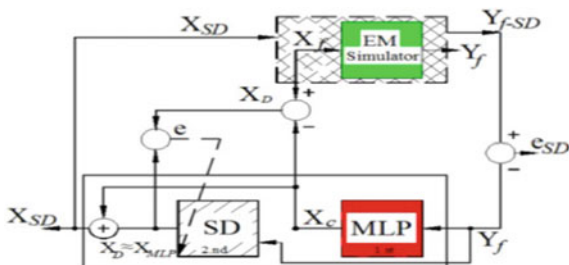
According to Zhang and Gupta (2000), MLP is the first phase of the KBRC model and corresponds to the model Y and X variables. It is made up of three perceptron layers, lined up as an input layer, one or more hidden layers, and finally an output layer. $X = f(Y)$ can be used to represent the relationship between the input and output vectors. In this investigation, the anticipated output is $X_c = [L_1, L_2, L_3]^T$ and the input parameter is $Y_f = [f]^T$ (Y_f displays 200 samples of S-parameters).

3.2 Source Difference Method

The concept behind SD [5] (Zhang & Gupta, 2000) is the network’s objective being created by mixing two training data sets. The fine data and the output response of MLP (X_c) from the first phase are shown in these data sets, which are the results of the EM simulation of $X_f = [L_1, L_2, L_3]^T$. As a result, the SD’s only input parameter is a set of frequency samples, or $Y_f = [f]^T$; its projected output is $X_{SD} = X_c + X_{MLP}$; and its intended output is $X_{SD} = X_{RL} - X_c$. According to Fig. 2, SD is situated in the second phase of the KBRC. The redesign case of EM-input simulations and output function is stated as

$$Y_{f-SD} = f_{EM}(SD) \tag{1}$$

Fig. 2 Two steps of KBRC model when SD is in 2nd step of processing



where Y_{f-SD} is the outcome of redesigning the second step's expected output (X_{SD}), and the error measure, e_{SD} can be used to quantify the absolute difference between Y_{f-SD} and Y_f calculated by

$$e_{SD} = Y_{f-SD} - Y_f \tag{2}$$

3.3 Prior Knowledge Input Method (PKI)

In this approach (Zhang & Gupta, 2000), in addition to the initial input of Y_f , the output response of MLP (X_c) is employed as input to PKI. The fine output (X_f) is the desired output. As a result, the input/output mapping (in the first phase) is between the MLP's (X_c) and (Y_f) output responses.

$Y_{PKI} = [Y_f, X_c]^T$ is the input parameter for PKI as a result. According to Fig. 3, PKI is situated in the second phase of KBRC.

Fig. 3 Two steps of KBRC model when PKI is in 2nd step of processing

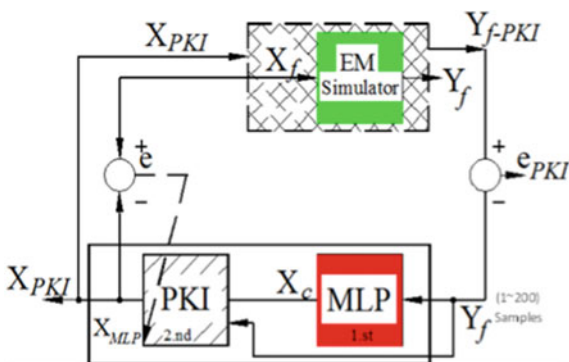
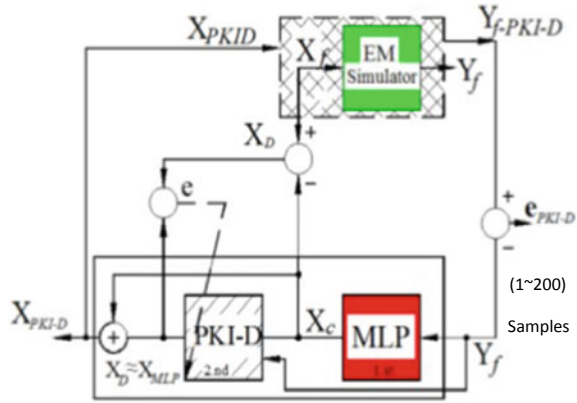


Fig. 4 When PKI-D is at the second phase of processing, there are two steps of the KBRC model



3.4 Prior Knowledge Input with Different

PKI-D [2] (Zhang & Gupta, 2000) is a knowledge-based strategy that combines the benefits of the two previously mentioned knowledge-based approaches (PKI and SD). The input of the fine model (Y_f) and the previous knowledge received from the output response of the MLP (X_C) are combined to form the input of PKI-D (Y_{PKI-D}). The intended output is $\Delta X_{PKI-D} = X_f - X_C$, hence the input parameter is $Y_{PKI-D} = [Y_f, X_C]^T$. According to Fig. 4, PKI-D is situated in the second stage of KBRC.

4 Parameters of ANN Model

The first two data sets that are proposed are training data and extrapolation testing data sets. 24800 samples were used to create the training data for the EM simulator three geometric antenna parameters ($L_k^i, i = 1, 2, 3$ and $k = 5$), k depicts number of *samples* shown below:

$$N_{tr} = f_s \prod_{i=1}^3 L_i^k \tag{3}$$

where f_s is the frequency samples count, which is equal to 200, and N_{tr} is the number of training data samples. Only 27 samples out of the previously vast quantity of training data have been used (Bataineh & Marler, 2017). The choice of resonant frequency samples from the training data determines the reduction process. The analyzed models' inputs are 200 frequency sample points, and their outputs are three parameters representing the geometrical dimensions of the R5SMPA. Two testing data sets are chosen throughout the testing phase. The extrapolation accuracy of the models is evaluated using testing data sets that are chosen from outside of the

training data [5]. For all approaches, there are two hidden levels. However, for MLP and knowledge-based neural networks, the number of neurons is (20–20) and (30–20), respectively (KBNNs). Tangent-sigmoid transfer functions (TFs) are used in the hidden layers of inverse ANN models trained using the Levenberg-Marguardt technique, while a linear function is used in the output layer (Beale et al., 2013). By setting the learning rate (η) to 0.1 for MLP and 0.05 for KBNNs, the performance target to 0.000001 for MLP and KBNNs, and the momentum coefficient (μ) to 0.2 for MLP and 0.1 for others, the model's training parameters are realized. The network's denoising coefficient is set at 0.2.

5 Result and Discussion

New geometrical dimensions of R5SMPA are produced after 50 iterations of training the neural network models. The best resonant frequency and return loss of the S-parameter curves, which are the outcomes of modelling the new geometrical parameters derived by inverse ANN models for extrapolation testing data, demonstrate the models' correctness. Without training any ANNs, as described in Sect. 2 and demonstrated in Figs. 1a and 5 displays the R5SMPA result. Inverse ANNs are then used to produce the subsequent results (Fig. 6).

The results of the revised physical parameters generated using inverse ANN models, along with the optimal frequencies and their return losses, are displayed in Tables 1 and 2. The newly created solutions differ from the original R5SMPA, which is depicted in Fig. 1a, and the outcome of Fig. 5, in terms of new values and forms for R5SMPA. As seen in Figs. 7 and 9, every result from ANNs performs

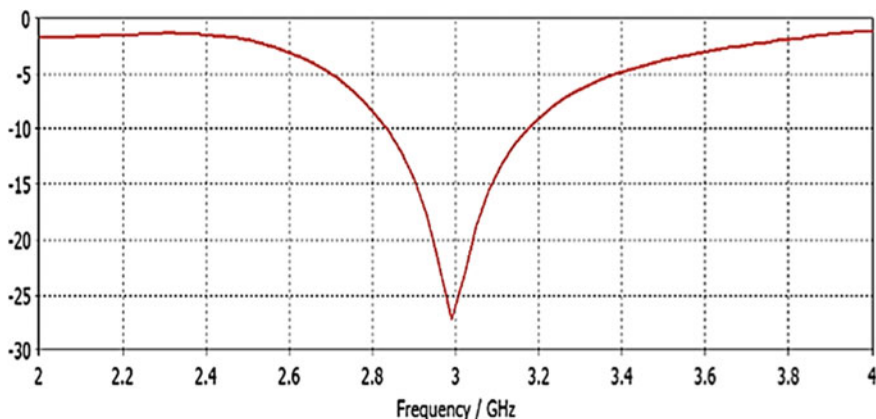


Fig. 5 S-parameter for R5SMPA modeled by EM-Simulator, at 3 GHz

Fig. 6 Top view of the developed solution for MLP only at 2.44 GHz

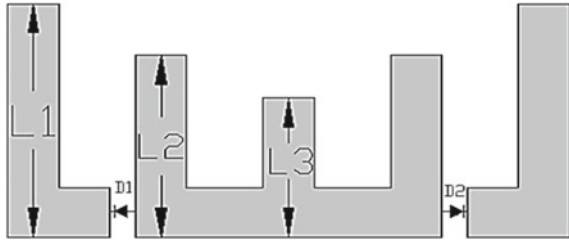


Table 1 A comparison between results obtained by reverse ANN

Parameters	Test	MLP	SD	PKI	PKI-D
L_1 (cm)	–	1.4271	1.4738	1.3960	1.4377
L_2 (cm)	–	1.1115	1.0995	1.0818	1.1184
L_3 (cm)	–	0.8535	0.8496	0.8578	0.8340
f_{op} (GHz)	2.44	2.71	2.68	2.74	2.71
RL (dB)	–	– 26.89	– 32.00	– 25.91	– 25.73

Table 2 A comparison between results obtained by inverse ANNs at 3.74 GHz extrapolation testing data

Parameters	Test	MLP	SD	PKI	PKI-D
L_1 (cm)	–	0.5521	0.5445	0.5905	0.5466
L_2 (cm)	–	0.7800	0.7923	0.7745	0.7900
L_3 (cm)	–	0.9486	0.9618	0.9647	0.9689
f_{op} (GHz)	3.74	3.77	3.74	3.77	3.77
RL (dB)	–	– 21.05	– 21.11	– 22.47	– 22.05

well in a small resonant frequency region. The bandwidths are also approximately 0.32 GHz and 0.41 GHz, respectively, with a goal of return loss of $S_{11} \leq -10$ dB, as shown in Figs. 7, 8 and 9.

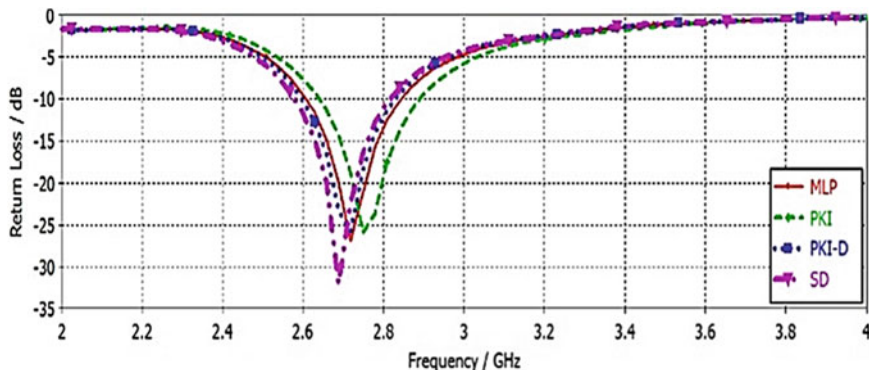


Fig. 7 Comparison of S-parameters. The plots show results obtained by ANNs then designed by EM simulator, at 2.44 GHz

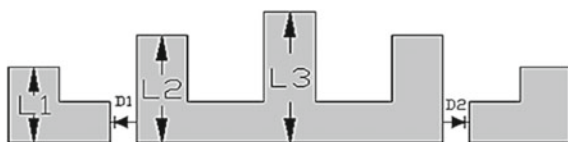


Fig. 8 Top view of the developed solution for MLP only, at 3.74 GHz

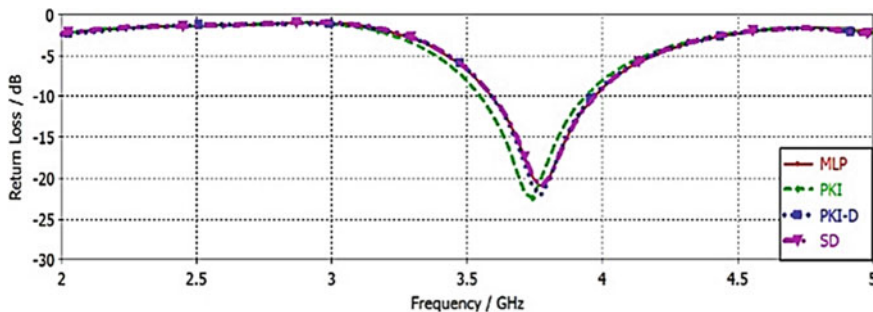


Fig. 9 Comparison of S-parameters. The plots show results obtained by ANNs then designed by EM simulator, at 3.74 GHz

6 Conclusion

Inverse ANN techniques have been suggested and used to provide novel reconfigurable antenna systems. Two phases of processing are involved in them. To rectify the answer from MLP, SD, PKI-D, and PKI are used in the first step, the second step uses PKI, PKI-D, and PKI, and the third step uses an EM simulator to redesign the findings from the second step. For the two hidden layers, all approaches work.

The development of novel solutions for two variously shaped reconfigurable antennas was completed after using the suggested inverse ANN algorithms. To create antennas that are reconfigurable and offer great precision, the same design techniques may be used.

References

1. Costantine, J., Tawk, Y., Barbin, S. E., & Christodoulou, C. G.: Reconfigurable antennas: Design and applications. *Proceedings of the IEEE*, 103(3), 424–437.
2. Aoad, A., Simsek, M., & Aydin, Z. (2014). Design of a reconfigurable 5-fingers shaped microstrip patch antenna by artificial neural networks. *International Journal of Advanced Research in Computer Science and Software Engineering (IJARCSSE)*, 4(10), 61–70.
3. Aoad, A., Simsek, M., & Aydin, Z. (2015). Development of knowledge based response correction for a reconfigurable N-shaped microstrip antenna design. In *IEEE MTT-S international conference*. Ottawa.
4. Wang, F., & Zhang, Q. J. (1997). Knowledge-based neural models for microwave design. *IEEE Transaction on Microwave Theory and Techniques*, 45(12), 2333–2343.
5. Simsek, M., Zhang, Q., Kabir, H., & Sengor, N. (2010). The recent developments in knowledge based neural modelling. *Elsevier-Science Direct*, 1(1), 1321–1330.
6. Jiajie, Z., Anguo, W., & Peng, W. (2008). A survey on reconfigurable antennas. *IEEE ICMMT Proceedings*.
7. Balanis. (2008) *Modern antenna handbook*. Wiley (369–395).
8. Jiajie, Z., Anguo, W., & Peng, W. (2008) A survey on reconfigurable antennas. *IEEE ICMMT Proceedings*.
9. Allayiti, M., & Kelly, J. R. (2017). Multiple parameter reconfigurable microstrip patch antenna. In *IEEE international symposium*, San Diego.
10. Lebbar, S., Guennoun, Z., Drissi, M., & Riouch, F. (2006). A compact and broadband microstrip antenna design using geometrical-methodology-based artificial neural network. *IEEE Antennas and Propagation Magazine*, 48(2), 146–154.
11. Langoni, D. (2005). Gallium-arsenide MESFET small-signal modeling using backpropagation & RBF neural networks, thesis (M.S.), Florida State University.
12. Boualleg, A., & Merabtine, N. (2005). Analysis of radiation patterns of rectangular microstrip antennas with uniform substrate. *Semiconductor Physics, Quantum Electronics & Optoelectronics*, 8(3), 88–91.
13. Deshmukh, A. A., & Ray, K. P. (2011). Broadband proximity-fed modified rectangular microstrip antennas. *IEEE Antennas & Propagation Magazine*, 3(5), 41–56.
14. Neog, D. K., Patnaik, S. S., Panda, D. C., Devi, S., Khuntia, B., & Dutta, M. (2005). Design of a wideband microstrip antenna and the use of artificial neural networks in parameter calculation. *IEEE Antennas and Propagation Magazine*, 47(3), 60–65.